Czech University of Life Sciences Prague

Faculty of Engineering

2016

Proceeding of
6th International Conference on

Trends in Agricultural Engineering 2016

Czech University of Life Sciences Prague - Faculty of Engineering

Sept. 7th - Sept. 9th 2016

TAE 2016

CZECH UNIVERSITY OF LIFE SCIENCES PRAGUE

Faculty of Engineering

6th International Conference on Trends in Agricultural Engineering 2016

Proceeding of 6th International Conference on Trends in Agricultural Engineering 2016

September 7th 2016 – September 9th 2016

Prague

Czech Republic

Editor in chief: David Herák

Editors: Rostislav Chotěborský, Stanislav Kovář, Václav Křepčík

Online version is available at http://www.tae-conference.cz/

ISBN 978-80-213-2683-5

6th International Conference on Trends in Agricultural Engineering 2016

September 7th 2016 – September 9th 2016

Conference TAE 2016 publishes research in engineering and physical sciences that represent advances in understanding or modelling of the performance of biological and physical systems for sustainable developments in land use and the environment, agriculture and amenity, bioproduction processes and the food chain, logistics systems in agriculture, manufacturing and material systems in design of agriculture engineering.

Conference venue:

Faculty of Engineering, Czech University of Life Sciences Prague, Kamýcká 129, Praha 6, Prague, 16521, Czech Republic

Scientific committee:

All manuscripts in conference proceedings have been reviewed by peer review process.

Reviewers:

Adamovský R.; Aldoshin N.; Aleš Z.; Bakti M.; Berisso F.; Beyhan M.; Dajbych O.; D'Amato R.; Didmadidze O.; Gurdil A. K. G.; Herák D.; Hrabě P.; Chotěborský R.; Jankauskas V. ; Jasinskas A.; Jurča V.; Kabutey A.; Kučera M.; Kumhála F.; Libra M.; Lisowski A.; Machado J.; Mašek J.; Moltot Z.; Müller M.; Napitupulu R.; Neuberger P.; Pandiangan S.; Petrů M.; Popescu S.; Poulek V.; Rataj V.; Ruggiero A.; Růžička M.; Selvi K. C.; Sigalingging R.; Simanjuntak S.; Ševčík L.; Valášek P.; Valickas J.

Welcome to Trends in Agriculture Engineering 2016

The progressive prestige that Trends in Agriculture Engineering has attained has made it a world-wide reference on fast developments in agriculture from its engineering point of view and a meeting point for professionals with responsibilities in the improvement of this fundamental area devoted to meeting diverse human needs. 117 papers have been selected for TAE 2016 by the Technical Committee of the conference to be presented in a wide thematic spectrum, covering the newest and most relevant aspects of agricultural engineering.

The Faculty of Engineering, Czech University of Life Sciences Prague, organizer of this 6th TAE conference, welcomes you to this event.

Prague, the largest city of the Czech Republic and the historical capital of Bohemia, cordially welcomes you and looks forward to making your stay with us the most pleasant possible.

Cordially,

prof. Ing. Vladimír Jurča, CSc.
Dean of Faculty of Engineering
Czech University of Life Sciences Prague

Contents

PARAMETERS JUSTIFICATION OF PICKUP MECHANISM FOR FORAGE HARVESTER

D.T. Abilzhanov[1], T. Abilzhanuly[1], F. Kumhála[2], A.S. Alshurina[2], A.S. Adilsheev[1]

[1]Kazakh scientific - research institute of mechanization and electrification of agriculture, Almaty, Republic of Kazakhstan
[2]Department of Agricultural Machines, Faculty of Engineering, Czech University of Life Sciences Prague, Czech Republic

Abstract
In the article, new pickup mechanism for forage pickup choppers, balers, and forage harvesters has been suggested. In developing PIK-1.8 universal forage pickup chopper was installed a new pickup mechanism with high reliability. Results of theoretical and experimental research on pickup mechanism were given. Here, the main structure of the pickup mechanism was developed by the obtaining patent №9472 Republic of Kazakhstan andits main novelty is pickup fingers mounted to the reel rigidly, i.e., no treadmills, cranks, rollers, bearings and further without profiled attachments (as pickup reel of the company Krone). In this case, within the angle 180° of rotation of the fingers, i.e while lifting it through ring-rays its radius while turning to the angle $\Delta\varphi$ angle increases to a certain length ΔR. In the proposed pickup mechanism, the fingers will gradually move under the ring-rays. Here, when selecting the parameters of the pickup mechanism must take into account that the value of the angle γ between a finger and a tangent to the circle of the ring-rays must be more than or equal to 70°. As a result of laboratory and field tests were found that new pickup mechanism with the above parameters works well. In picking up and cutting dry mas the forage pickup cutter with new pick up mechanism worked with performance 6.0 - 9.0 t/h, in harvesting wet hay 3.2 - 5.0 t/h. During the testing of experimental model of the forage pickup cutter were checked theoretical determined parameters of pickup mechanism. Results of testing showed that all parameters have rational values. During laboratory and field tests the reliability of the new pick mechanism were proved.

Key words: pickup fingers, ring-rays, pickup reel, making hay, balers, harvesting alfalfa.

INTRODUCTION

Currently for picking up hay and grain mass conveyor and reel types balers are used (LISTOPAD ET AL., 1986; KARPENKO ET AL., 1983). In the design of existing forage harvesters pickup reel with controllable fingers and driven fingers are used (Fig. 1).

In designs of balers with control fingers on one side at the end of the tubular shaft are fitted cranks with rollers. During the technological process, these rollers rotate in the profiled treadmill. In this case, the profile of the treadmill provides finger rotation while leaving them under the ring -rays. In this case, on the horizontal section of the ring-rays, fingers almost in the vertical position omitted under the ring-rays. In this case, the capture of the stems by pickup fingers inside the ring-rays is excluded.

In the construction of the header also pickup reel with driven fingers are mounted, and it is intended to transfer the grain mass from the header to the inclined conveyor, which transfers the mass to the threshing drums hearer.

In the construction of combine, harvesters for picking the grain mass chain- slatted balers are used (Fig. 3). In design of combine harvesters, as well as in the pickup truck and chopper-spreader trailer conveyor type balers are used (LISTOPAD ET AL., 1986; ASTAFJEVS ET AL., 2011).

Last few years, due to the easy design paid attention to improve the design of reel pickup devices (PAT. KAZ, 2011; PAT.RU, 2009).

In these inventions providing the pickup reel with clamping device are offered, fastening of the fingers is perfected and also using the fingers of variable section are proposed. However, in these inventions a treadmill turning fingers are used.

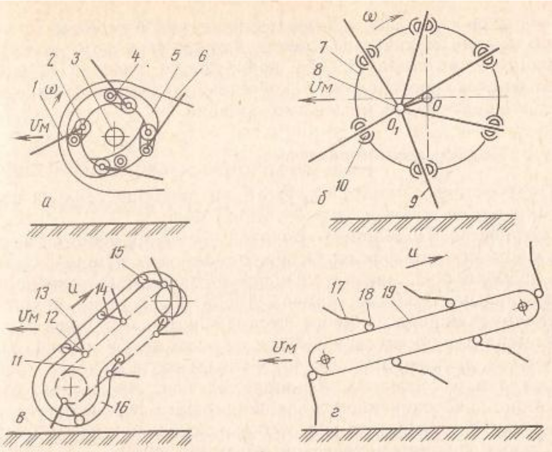

Fig. 1. – Scheme of the pickup devices

a – reel with controlled fingers; b – reel with driven fingers; *в* - chain-and-slat with controlled fingers; g – polotenno-slat; 1, 9, 13 and 17 - fingers; 2, 12 and 18 - tubular shaft; 3 - pickup shaft; 4 and 14 -cranks; 5 and 16 - track guide; 6 and 7 – the fixed and rotating housings; 8 – an eccentric shaft; 10 - peephole; 11 - chain; 15 - crank pulley; 19 - conveyor

The pickup reel that designed with controllable fingers has many fast wearing parts (roller, treadmill). In addition, the treadmill cannot be repaired and manufactured in economic conditions. Drum baler with a driven finger also has a complex structure and many wear parts.

Analysis of modern designs of pickup mechanisms shows that these balers have a complex structure and low maintainability details. All this reduces the reliability in terms of quality forage harvesting in agronomic terms.

In this regard, reliable operation provide pickers of the «Krone» company. These balers have not the treadmill rollers and cranks. This smooth movement of finger under the ring-rays carried out with the installation on the horizontal section of the ring- rays profiled attachment (Fig. 2).

Hence, it is clear that the world's leading firms phasing out from the production of balers with treadmills, i.e. development of balers designs implemented in the direction of simplification of design of modern of pickup mechanisms. The aim of study is development of a simple design pick mechanism which increased reliability of pickup work and productivity of the forage harvesters and grain harvesters.

Fig. 2. – Constant pickup device for many models of Krone Easy Flow

MATERIALS AND METHODS

Government Grant (State registration №0112PK01402) at LLP «Kazakh Research Institute of Mechanization and Electrification of Agriculture» supported development of forage pickup-cutter for preparing roughage and silage in 2012-2014.

For a theoretical justification of the parameters of the new pick mechanism applied methods of theoretical mechanics and construction of agricultural machinery.

Refinement of theoretical founded parameters exercised by conducting laboratory and field test on the forage pickup cutter with the proposed pickup mechanism.

New pickup mechanism without the treadmill, cranks, rollers and bearings (patent of RK №9472 and innovative patent RK №27286) is installed in the machine based on the zoo technical requirements for cutting roughage (17% to 22% of moisture content).

Hammers remade from steel (65G) plate 160 x 50 x 10 mm, they create a strong air flow, through the deflector can load crushed mass directly into vehicles. Cutting mechanism, which comprises a drum with knives and the shear bar. Depending on the required degree of cutting, on the drum it can be set 6, 9 or 18 knives. Shear bar has 6 working edges and it can be rearranged in the process of exploitation of harvester, which increases its service life.

Laboratory and field tests of experimental model of forage pickup-cutter equipped with a new pick-up mechanism were conducted using first, second and third crop alfalfa at the family farm that occupy 40 ha of fields, called "Zhaniko" Ili district of Almaty region. The crop was harvested and cut with forage pickup cutter which was mounted on the MTZ-80 (59.7 kW) and chopped material was conveyed into a trailer 2PTS-4. Stopwatch, tachometer, dynamometer and thermometer also were used during the experiment. Other devices were express moisture meter VLK-01, scales VLKT-500m, Express analyzer Infra Hast (for determination quality of chopped hay) of firm Foss.

15 samples (each weigh is about 60-80 g) of the chopped material were gathered to determine moisture content using the oven dry method (GOST 31640-2012). Another set of 15 samples was periodically gathered to determine the material practical size using GOST 27262-87.

The first experiment was conducted over five days, harvesting either first or second alfalfa crop. Second experiment was conducted over three days, harvesting either second or third alfalfa crop. All test were conducted with forage pickup cutter.

A subsequent experiment was conducted to determine the main technical parameters of the machine. In all the laboratory and field tests of the forage pickup cutter has been defined its power requirement by the torque meter. The value of torque and propeller shaft rotational speed were registrated on an oscillographic paper.

RESULTS AND DISCUSSION

Theoretical studies

In the proposed forage pickup cutter design pickup reel design were simplified and expanded operational capabilities of the machine.

In the proposed pickup mechanism (PATENT №9472 KAZ) fingers fixed inflexibly to the drum, and the ring-rays are made variable radius (PAT. KAZ№9472). Starting from a lower position to an angle Δφ of turning fingers, lower radius of ring-rays $R_i$and the next higher radius$R_{i+1}$is more than the lower radius for length ΔR (Fig. 3).

This gradual change in radius of ring rays provides a gradual withdrawal of fingers under the ring-rays. When choosing the length ΔR should be noted that the angle between the finger and a tangent to the circumference of the rings γ-slope should not be less than 70° (BASOI ET AL., 1977).

To determine the value of the angle γ considering the circuit shown in Fig. 4. For clearer explanation of the theoretical determination of the angle γ Fig. 4 shows separately the position of two adjacent rows of ring-rays.

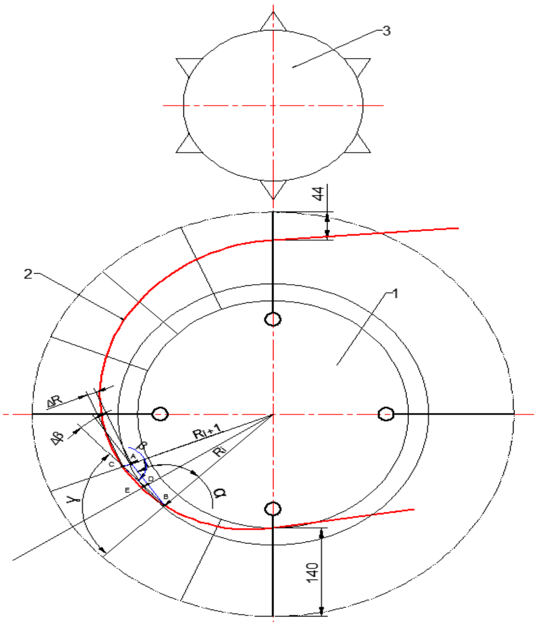

Fig. 3. – Scheme of the pickup mechanism
1- Pickup reel; 2 - ring-rays; 3- precompression reel

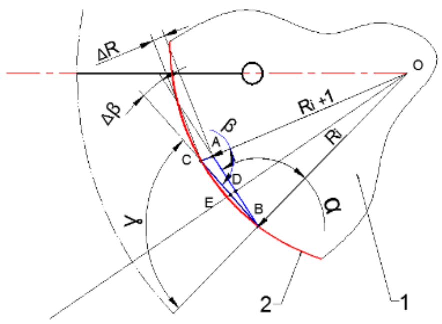

Fig. 4. – Diagram of changing radius of ring-rays for determination angle γ
1- Pickup reel; 2 ring-rays

Tab. 1. – Results of calculated data from telematics systems – John Deere

Number of tractors	Type of tractors	Operational hours (hrs)	Average values of fuel consumption CAN-BUS (l/hrs)	Average values of fuel consumption capacitance probe (l/hrs)	Difference of fuel consumption (l/hrs)
1	**John Deere 6630**	**1,028**	**7.3559**	**7.9606**	**0.6047**
2	John Deere 6630	1,158	11.594	12.377	0.783
3	John Deere 6630	1,257	8.807	9.986	1.179
4	John Deere 6630	1,023	7.247	7.776	0.529
5	John Deere 6630	1,268	10.58	11.392	0.812
6	John Deere 6530	1,087	11.698	12.61	0.912
7	John Deere 6530	1,587	8.837	9.903	1.066
8	John Deere 6530	1,698	8.356	8.929	0.573
9	John Deere 6430	1,147	12.546	13.259	0.713
10	John Deere 6430	1,158	10.458	11.431	0.973
11	John Deere 6430	1,236	7.549	8.623	1.074

* - measured and calculated data of fuel consumption (Fig. 2)

Here, due to the small value of the angle $\Delta\varphi$, the angle between the finger and a tangent to a circle of the ring-rays, which held between the radii R_i and R_{i+1}, approximately equal to the angle between the chord of the circle, which limited within the turning radius of the ring-rays to the angle $\Delta\varphi$, and by pickup finger, disposed in the middle chord (γ). Here the triangle BDE:

$$\gamma = 90 - \Delta\beta = 90 - \alpha - \beta = 90 - \left(\frac{180-\Delta\varphi}{2} - \beta\right) \qquad (1)$$

where$\Delta\beta$–the angle CDEwithinthechangingof radius-ring-raystoΔR;

α- from triangleAOB angleABO;

β – from triangleBOC angleBAO;

$\Delta\varphi$ – angle of turning ring-rays radii.

To calculate the value of the angle γ by the obtained expressions, it is necessary to determine the angle β. To determine the angle β consider the triangle COB. Fromthis triangle:

$$R_i^2 = R^2{}_{i+1} + CB^2 - 2R_{i+1} \cdot CB \cdot \cos\beta$$

Fromthis expression:

$$\cos\beta = \frac{R_{i+1}^2 + CB^2 - R_i^2}{2R_{i+1} \cdot CB} \qquad (2)$$

From the considered triangle COB:

$$CB^2 = R_i^2 + R_{i+1}^2 - 2R_i R_{i+1} \cos\Delta\varphi.$$

Inputting these values CB andCB^2 in the formula (2) we obtain an expression for determination an angle β.

$$\beta = \arccos\frac{R_{i+1} - R_i\cos\Delta\varphi}{\sqrt{R_i^2 + R_{i+1}^2 - 2R_i R_{i+1}\cos\Delta\varphi}} \qquad (3)$$

Inputting these values into the angle β in the formula (1) and taking into account that the limiting value of the angleγ must be at least 70°, for the determination of this angle, following expression is obtained:

$$\gamma = 90 - \left(\frac{180-\Delta\varphi}{2} - arccos\frac{R_{i+1} - R_i cos\Delta\varphi}{\sqrt{R_i^2 + R_{i+1}^2 - 2R_iR_{i+1}cos\Delta\varphi}}\right) \geq 70° (4)$$

Thus, according to this formula define a radius increment of ring-rays depending on the length of the longest dimension of fingers extending over the circumference of the rings-rays, given the fact that the angle between the circumference of the rings and finger-rays was not less than 70°, i.e. ensure the removal of stems capture by fingers inside the circle ring-rays.

The pickup reel’s finger is arranged so as its front surface extending beyond the circumference of the rings-rays when fingers are in the top of the ring-rays have a slope or bevel in the direction of the reel opposite rotation.

This solution provides an increase of the angle γ when stems of plant are in the upper part of the ring-rays, i.e. at the moment, when a maximum opportunity is appeared to pull stem by fingers inside the circle of ring-rays. This solution provides a reduction or elimination of force, which pulls the stem inside the circle of ring-rays.

To use this solution into practice, you can perform the front surface of the fingers end with a slope or it can be sharpened.

Production of ring-rays circle on the proposed form and fingers with a slope or bevel is not difficult. This eliminates the need for a mechanism that ensures turning of the fingers during rotation of reel, i.e. simplified production of the pickup reel and reduces the cost of its manufacture.

An example of the definition the variable radius circle of ring-rays.

During the work, the pickup fingers must pick up swath by ring-rays circle until the place, where the swath can catch precompression drum. It means the value of the angle when pickup fingers turning (from a short distance between the ends of the fingers and the ground, i.e. when they are arranged perpendicular to the ground) until full entrance into the ring-rays circle may be taken as in 225°.

In the pickup reel of existing machines when fingers are close to the ground the largest dimension of the length of the fingers, projecting over ring-rays is equal to 120-140 mm (BASOI ET AL., 1977).

, therefore, will take the value of the maximum size of the length of fingers, extending over the rings-rays circle to 140 mm.

As shown in Fig. 3, the operating angle of rotation of the pickup reel fingers weredivided into 8 parts, i.e. Δφ=22,5°. Thus $\Delta R = 12$ mm.

If use prepared serial spring as a pickup fingers and install them on the axis, as shown in Fig. 14, then we can take the value of the minimum radius ring-rays to 120 mm, and the radius of the fingers – 260 mm, i.e. $R_i = 120$ mm, $R_{i+1} = 132$ mm, $\Delta R = 12$ mm, $\Delta\varphi = 22{,}5^0$.

Now we determine the value of the angle between the chord of the circle, limited within the turning radius of the rings-rays to the angle $\Delta\varphi$ and the pickup finger, placed in the middle of the chord.

$$\gamma = 90 - \left(\frac{180-\Delta\varphi}{2} - arccos\frac{R_{i+1} - R_i cos\Delta\varphi}{\sqrt{R_i^2 + R_{i+1}^2 - 2R_iR_{i+1}cos\Delta\varphi}}\right) \geq 70° = 90 - \left(\frac{180-22{,}5}{2} - arccos\frac{132 - 120\cdot 0{,}9239}{\sqrt{120^2 + 132^2 - 2\cdot 120\cdot 132\cdot 0{,}9239}}\right) = 76{,}5°$$

Thus, according to the calculation of the angle γ is more than 70°, i.e., the value of the radius increment of the ring-rays circle is determined correctly. If the angle γ less than 70°, it is necessary to increase the value of diameters of pickup reel and ring-rays.

From these calculations, it is known that the diameter of the Pickup reel – 520 mm, minimum radius – 120 mm and a maximum radius of ring-rays – 216 mm, ΔR -12 mm, γ - 76,5°, in the vertical position of the fingers, the maximum length of the projecting part of fingers under the ring-rays – 140 mm and the minimum length of the fingers protruding under the ring-rays – 44 mm.

Pickup mechanism with above parameters is set to forage pickup chopper PIC-1.8. Laboratory and field tests of experimental model of pickup-chopper equipped with a new pick-up mechanism have been carried out in the family farm "Zhaniko", Ili district of Almaty region. As part of this machine developed new pickup mechanism showed a highly reliable operation, and not observed process shutdown due to a failure of the pickup mechanism.

When picking up and chopping herbs with humidity 18-20% pickup chopper has a capacity - 6.0- 9.0 t/h, and it provides pickup andgrinding of roughage in humidity of 45-55% for making silage. In making silage its performance is in the range of 3.2 - 5.0 t/h (ABILZHANULY ET AL., 2014).

Fig. 5. – Forage pickup chopper PIK-1,8 with new pickup mechanism (Pickup and cuttinghay with moistur econtent 18-20%)

Currently, the pickup mechanism is mounted on a prototype square baler PT-160, and there is an interest to this pickup mechanism of "Bobruiskagromash" (Republic of Belarus), which develops baler PT-165. The technical novelty of the pick mechanism is proved by obtaining a patent Republic of Kazakhstan №9472 «Pickup-chopper for cattle" and innovative patent RK №24471 «Pickup reel for harvesting agricultural machinery» (PAT. KAZ№19961;PAT. KAZ№24471).

CONCLUSIONS

1. As a result of theoretical research the radius increment of ring-rays is determined, depending on the longest length dimension of fingers extending over the rings-rays circle, given the fact that the angle between the rings-rays circle rings and fingers was less than 70°, i.e. ensure the removal of stems capture by fingers inside ring-rays circle.

According to the calculation of the angle γ more than 70°, i.e., correctly determined the value increment of the radius circle ring-rays. If the angle γ less than 70°, it is necessary to increase the value of diameter of pickup reel and ring-rays.

2. As a result of laboratory and field tests were found that the pickup mechanism with the above parameters works well, and there was not stopping the technological process due to a failure of the pickup mechanism.In picking up and cutting dry mas the forage pickup cutter with new pick up mechanism worked with performance 6.0 - 9.0 t/h, in harvesting wet hay 3.2 - 5.0 t/h.

3. In testing an experimental sample of forage pickup chopper were tested theoretically certain parameters of the picking mechanism. Test results showed that all the parameters of the new pick mechanism have rational values. Also proved the reliability of the pickup mechanism during laboratory and field tests.

ACKNOWLEDGEMENTS

The authors are highly thankful to the Erasmus Mundus CASIA program and Technical faculty of the Czech University Life Sciences for the opportunity to present this study.

REFERENCES

1. BASOI, E.S., VERNIAIEV, O.V., SMIRNOV, P.P., SULTAN SHAH, E.G.: Theory, design and calculation of agricultural machinery: Textbook for higher educational institutions of agricultural engineering. p. 568. Moscow. Kausr. 1977.
2. LISTOPAD, G.E., DEMIDOV, G.K.: Agricultural and reclamation machines: Textbooks and learning manuals for Executive. p. 688. Moscow. Agropromizdat, 1986.
3. KARPENKO, A.H., KHALANSKY, V.M.: Agricultural machinery: Textbooks and teaching aids for higher educational institutions. 495 p. Moscow. Kolos, 1983.
4. ASTAFJEVS V.L., BOBKOV S.I.: Parameters pneumatic pick-up-truck. Tractors and farm machinery. №7. Moscow.185, 2011: 10-11.
5. PAT. KAZ №25513 Republic of Kazakhstan A01F 29/00, A01D 87/10. Trailed chopper-spreader rolls of straw / Laptev NV, SvetlakovAY.; patent RSE "Kostanay State University im.A.Baytursynova" MES. - №2011 / 0239.1; appl. 11.03.11; publ. 15.03.12, Bul. No. 3.
6. PAT. RU №2438292 C1 Russian Federation, A01D 89/00. Drum Baler / Kopchenov A. A .; patent FSEIHPE "Chelyabinsk State Academy of Agricultural Engineering". - №2010144730 / 02; appl. 01.11.10; publ. 10.01.12, Bul. №1.
7. PAT. RU №2420946 Russian Federation, A01D 89/00. Gatherer device for harvesting agricultural / Getty Christophe Lionel Haas, Fabien Mey, Thierry Bonhomme; patent Uzyn CLAAS France SAS (FR). - №2006140852 / 21; appl. 27.05.08; publ. 20.06.2011, Bull. №17.
8. PAT. RU№125018, A01D. Node fastening fingers drum picker. / KOPCHENOV A. A.; patentees FSEIHPE "Chelyabinsk State Academy of Agricultural Engineering". - № 000000; appl. 19.10.11; publ. 02.27.13, Bul. №6.
9. PAT. EP2342967 A1 Germany, A01D 89/00. Pick-protected winding / FreitagAloys; patent FreitagAloys. - №EP20110000016; appl. 03.01.11; publ. 13.07.11.
10. PAT. RU №2409018 C2 Russian Federation, A01D 89/00. Pick drum stems of crops / Smirnov N.A, Sokolov VN, Lobachyov AA, Smirnov B.; patent FSEIHPE "Kostroma State Agricultural Academy." - №2009108868 / 21; appl. 10.03.09; publ. 20.01.11, Bul. №2.

11. PAT. KAZ№9472, MPK6 AO1D 89/00. Pick-cutter feed for livestock / T. ABILZHANULY SEITBEKOV, L., RZALIEV, AS, ZHORTUYLOV, O.ZH. The applicant and patentee of State Enterprise "Kazakh Research Institute of Mechanization and Electrification of Agriculture» - № 990408.1; appl. 07.04.99 was published. 16.10.2000; Bull. Number 10. - P.75.
12. ABILZHANULY, T., ABILZHANOV, D.T: Development of a universal feed pickup cutter. Agricultural Science - Agricultural Production in Siberia, Mongolia, Kazakhstan and Bulgaria. In: Proceedings of XVII International Scientific and Practical conference. 13 November 2014, pp.133-135, Novosibirsk.
13. ABILZHANULY, T., ABILZHANOV, D.T.: Determination of the air flow velocity in the deflector of forage pick up cutter. In: Proceedings of II International Scientific and Technical Conference "Agricultural machinery".2014.Varna, Bulgaria,
14. ABILZHANULY, T.: Machines other agricultural formations: a manual for agricultural engineering specialties of higher educational institutions. Publishers S.Seifullin, Astana. 200. 2007 (Inrus).
15. PAT. KAZ№19961, A01D89100. Crushing and cleaning device for cattle feed / Abilzhanuly T. 0318.1., 16.03.2006. Publ. 27.06.2007.
16. PAT. KAZ№24471, A01D 89/00. Drum pick for harvesting agricultural machines / Abilzhanuly T., Zhortuylov, O., Evtifeev, A.G., Alekseek, A.A. Soldatov V.T., Bekenov C.U., Smagulov T.A. The applicant and the patentee; "Kazakh Research Institute of Mechanization and Electrification of Agriculture» .- №2010 / 1371.1; appl. 08.11.2010 of Publ. 15.09.2011.
17. PAT. KAZ №27286, A01D 89/00 Pick for forage and grain harvesters / Abilzhanuly T., Zhortuylov O, Uteshev V.L., Abilzhanov D.T. The applicant and the patentee: "Kazakh Research Institute of Mechanization and Electrification of Agriculture»- №2012 / 1113.1; appl. 24.10.2012 r .; publ. 09/16/2013.

Corresponding author:
Assem Alshurina, Department of Agricultural Machines, Faculty of Engineering, Czech University of Life Sciences Prague,Kamýcká 129, Praha 6, Prague, 16521, Czech Republic,

ENERGY EXTRACTION FROM ROCK MASS USING VERTICAL HEAT EXCHANGERS

R. Adamovský[1], P. Neuberger[1], D. Adamovský[2]

[1]*Department of Mechanical Engineering, Faculty of Engineering, Czech University of Life Sciences Prague*
[2]*University Centre for Energy Efficient Buildings, Czech Technical University in Prague*

Abstract
The aim of the verification study was to determine and analyse the temperatures of the rock mass, specific heat capacities and specific energies extracted from the rock mass by two types of vertical heat exchangers namely single U-tube heat exchanger (U1) and double U-tube heat exchanger (U2). The exchangers were used as low-potential energy source for heat pumps. Design and operating parameters influencing the process of heat transfer between the rock mass and the heat-transfer fluid were also evaluated. The results demonstrated the advantages of using double U-tube heat exchanger U2 both in terms of its impact on the performance factor of the heat pump, and in terms of specific heat outputs and specific energies extracted from the rock mass. The average daily temperatures of the heat-transfer fluid in heat exchanger U2, specific heat outputs and specific energies extracted from the rock mass were higher by 4.5%, 26.8% and 25.6%, respectively than in the heat exchanger U1.

Key words: thermal energy; thermal power; ground loop heat exchanger; heat pump; rock mass.

INTRODUCTION

We can efficiently gain low potential energy contained in the rock mass, usable as low-temperature energy source for heat pumps evaporators, via vertical rock mass heat exchangers. These exchangers, using geothermal heat of the rock mass are usually installed in Central Europe at depths of 50-150 m. Effective usability and service life of these relatively investment-costly low-potential energy sources are considered in dozens years. It is therefore realistic to expect that after the end of life of one heat pump energy system there will be a new modern one connected to the vertical heat exchanger. This concept increases the efficiency of the entire system in terms of return of the investment on heat exchanger implementation. These reasons have led us to operational verification of vertical heat exchangers, the aim of which was to monitor and analyse:

- Differences of operating parameters of U1 and U2 heat exchangers;
- Rock mass temperatures and temperature changes during the heating period and the period of heat exchangers stagnation;
- Specific heat flows and specific energies extracted from the rock mass during the heating period.

PLATELL (2006) identified, according to the configuration, four main types of vertical rock heat exchangers: GLHE (Ground Loop Heat Exchangers) U-shaped exchangers with one or two loops; TIL (Thermal Insulated Leg) coaxial heat exchangers with several loops and a common thermally insulated centre; coaxial tube heat exchanger, and coaxial heat exchangers with reduced permeability of a rock wall; SCW (Stab Water Column) coaxial heat exchangers with permanent water column. In Central Europe, GLHEs with one or two U-shaped loops is mostly used.

BANKS (2012) analysed the process of heat transfer between the rock mass and the heat-transfer fluid on a base of a thermal resistance of the rock mass and a thermal resistance of the borehole; the border between the two resistors being the borehole wall. The volume of the rock mass thermal resistance is dependent on the rock mass thermal characteristics: coefficient of thermal conductivity λ ($W \cdot m^{-1} \cdot K^{-1}$), volumetric thermal capacity C ($J \cdot m^{-3} \cdot K^{-1}$) and coefficient of temperature conductivity (thermal diffusivity) a ($m^2 \cdot s^{-1}$). The thermal characteristics have a dominant influence on temperatures and temperature distribution across the rock mass, vertical heat exchanger capacity and the duration of use of the exchanger.

Heat exchanger configuration, pipe size and material, diameter of the borehole, grouting material and type of heat-transfer fluid flow determine the thermal resistance of the borehole. The influence of the heat exchanger configuration and other parameters on the thermal borehole resistance was addressed by HUANG ET AL. (2015). SELÇUK AND BERTRAND (2014) evaluated thermal hydraulic and mechanic properties of the grouting material. SANNER AND MANDS (2003) and SANNER ET AL. (2000) reported on the basis of performed thermal response tests in Germany, borehole thermal resistance values between 0.06 and 0.50 K·m·W^{-1}. All tests except two of them have proved values of 0.12 K·m·W^{-1} or less. Therefore they consider thermal resistance being appropriate < 0.11 K·m·W^{-1} and unsatisfactory > 0.14 K·m·W^{-1}. Analysis of temperature areas and heat transfer in the rock mass with a single and double U-tube heat exchanger was carried out by CARLI ET AL. (2010). They also evaluated types of flow and temperatures of heat-transfer fluid. GEHLIN AND HELLSTRÖM (2003) focused on temperature distribution and heat accumulation into the rock mass by vertical heat exchanger. MARCOTTE AND PASQUIER (2009) have proved that a slight inclination of the borehole has a positive influence on heat exchanger capacity. BANKS (2012) indicated a specific energy extracted from the rock mass of 159 kWh·m^{-1} at an annual heat exchanger performance of 1 666-2 400 hours and an average value of specific heat output for Europe of 62 W·m^{-1}. However, he emphasized that the values of specific energies and specific heat outputs can be only the initial information for the design of a heat exchanger.

MATERIALS AND METHODS

The vertical rock mass heat exchangers U1 and U2 were power sources for 1×IVT PremiumLine EQ E13 heat pump and 2×Green Line HT Plus E17 heat pumps (Industriell Värme Teknik, Tnanas, Sweden) used for heating the administration building and manufacturing halls of the company VESKOM Ltd. based in Prague, Dolní Měcholupy. The heat pumps were used only for heating of the buildings, but not for their cooling.

The measurements were carried out on two types of heat exchangers placed in boreholes at depth of 113 m. There is a single U-tube heat exchanger in one borehole (U1) made from polyethylene piping PE 100RC 2×40×3.7 mm (LUNA PLAST Inc., Hořín, Czech Republic) resistant to point loads and cracking. The outer surface of the heat exchanger per 1 m length is 0.2512 m^2·m^{-1}, inner 0.2047 m^2·m^{-1}. A double U-tube heat exchanger (U2) is placed in the other borehole, made from polyethylene piping PE 100RC 4×32×2.9 mm. The outer surface of the heat exchanger per 1 m length is 0.4019 m^2·m^{-1}, inner 0.3291 m^2·m^{-1}.

There were 5 temperature sensors of type Pt 1000 A (GREISINGER electronic GmbH, Regenstauf, Germany) in each borehole placed between the pipes at depths 0.2 m, 9 m, 20 m, 50 m and 100 m. The air temperature t_e above the ground was monitored by sensor ATF 2 KTY 81.210 (S+S Regeltechnik, Nürnberg, Germany) placed at a height of 2.5 m above the ground. Temperature sensors of type Pt100 were installed at the inlet and outlet pipelines of the boreholes, measuring temperature of the heat-transfer fluid. All temperatures were recorded at quarter-hour intervals. Heat exchanger outputs and energy values extracted from the rock mass were determined by an electronic heat consumption meter MTW3 (Itron Inc. Liberty Lake, USA). The heat-transfer fluid flowing through the vertical heat exchangers was a mixture of 33% ethanol and 67% water.

The upper part of the geological profile of the rock mass was made up of detritus; its thickness ranged from 4.0 to 9.5 m. The subsoil of the detritus was composed of grey-black clay slate of the Letná formation. There was solid rock mass in the deeper parts, heavily cracked in some places, as indicated by strong inflows of underground water into the boreholes. Cracked profiles were found at depths of 30 to approximately 80 m below ground. The level of underground water in all boreholes was encountered at depth of 10-12 m below ground. The results of the thermal response tests indicated the average value of coefficient of thermal conductivity of the rock mass $\lambda_{r.m.}$ = 2.9 W·m^{-1}·K^{-1} and total thermal resistance of the boreholes 0.137 K·m·W^{-1}.

The verification of the vertical heat exchangers was performed between 19 September 2012 and 17 September 2013 and it covers the heating period (19 September 2012-22 April 2013, 216 days) and the stagnation period of the heat exchangers (23 April 2013-17 September 2013, 148 days) following the heating period.

RESULTS AND DISCUSSION

Rock mass temperatures in the area of the heat exchangers

a) Temperatures during the heating period.

In Tab. 1, the average daily temperatures of the rock mass $t_{Ø}$ are summarized, the minimum temperatures of the rock mass $t_{min.}$ in individual depth levels, the average temperatures of the rock mass along the entire length of the borehole t_C, the average air temperatures t_e and the minimum air temperatures.

Tab. 1. – Average daily and minimum temperatures of the rock mass and air temperatures during the heating periods.

		Depth (m)				t_C (°C)	t_e (°C)
		9	20	50	100		
U1	$t_{Ø}$	6.26±2.98	6.27±2.78	6.24±2.45	6.48±2.41	6.31	5.34
	$t_{min.}$	0.53	0.31	0.71	0.65	-	-15.80
U2	$t_{Ø}$	6.96±2.86	6.42±2.69	6.34±2.46	6.60±2.33	6.58	5.34
	$t_{min.}$	0.59	0.75	0.49	0.78	-	-15.80

The verification results show that the rock mass temperatures in all monitored depths in the heating period were positive. This is an important point in terms of heating factor as well as the heat pump operation. It was also found that in all monitored depths of the rock mass the average daily temperatures were lower at the single U-tube heat exchanger U1 than at the double U-tube heat exchanger U2. The greatest temperature difference in the area of the heat exchangers U1 and U2, of Δt_U = 0.69 ± 0.24 K occurred at a depth of 9 m. On the contrary, at a depth of 100 m the temperature difference of Δt_U = 0.12 ± 0.13 K was significantly the smallest. The diagram in Fig. 1 shows the monitored values and regression curves of the average daily rock mass temperatures t_C and the ambient air temperatures t_e in the heating period running between 19 September 2012 and 22 April 2013, 216 days.

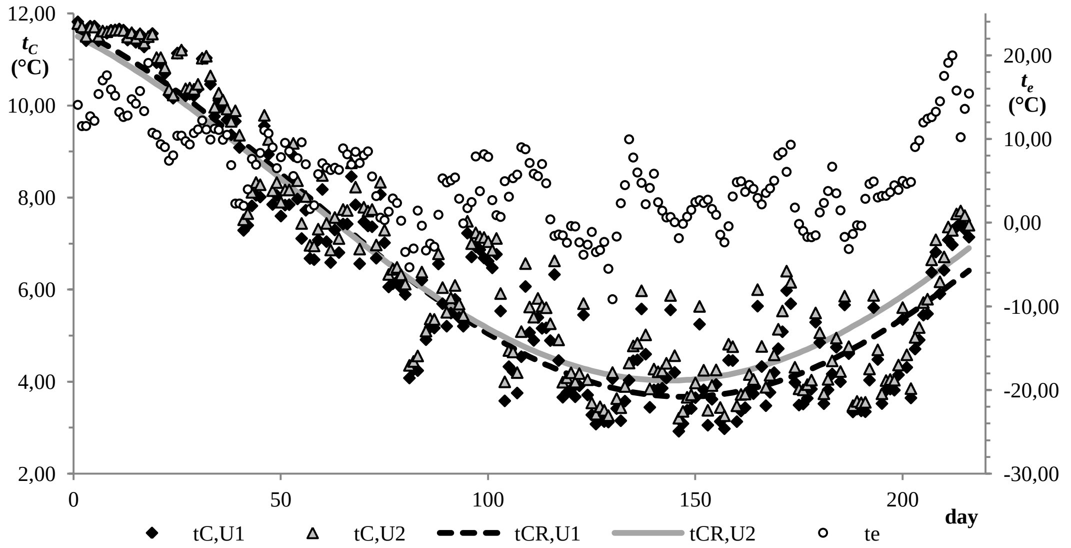

Fig. 1. – Average daily rock mass temperatures in the heating period and ambient air temperatures

At the beginning of the heating period, the average daily rock mass temperatures t_C in the area of the exchangers consistently decline with respect to increasing heat output extracted from the rock mass due to decreasing ambient air temperature. The drop in temperatures occurred approximately for 150 days with an intensity of 1 K per 18.36 days (U1 heat exchanger) and 19.20 days (U2 heat exchanger).

In the next stage of the heating period, due to rising ambient air temperatures and decreasing heat consumption the rock mass temperatures increased with the same intensity as there was in the case of a decline. At the end of the heating period (on day 216), the average daily rock mass temperature reached the value of 60.40% (U1), and 62.81% (U2) of the rock mass temperature at the beginning of the heating period. The average daily rock mass temperatures during the heating period were higher than the average daily ambient air temperatures in 59.72% of the heating period in the area of the U1 heat exchanger and 62.96% in the area of the U2 heat exchanger. The course of the average daily rock mass temperatures in the heating period was expressed by NEUBERGER ET AL. (2014) by an equation based on the equation of free, undamped oscillation of the mass point:

$$t_{CR} = \bar{t}_C + \Delta t_{am.}.\sin(\Omega.\tau + \varphi) \quad (°C) \quad (1)$$

Where:

t_{CR} - rock mass temperature (°C); $\bar{t}_C$ - mean rock mass temperature (°C);

$\Delta t_{am.}$ - oscillation amplitude around the temperature $\bar{t}$ (K); τ - number of days from the start of measurement (day);

φ - initial phase of oscillation (rad); Ω – angular velocity ($2 \cdot \pi/365$ rad · day^{-1}).

It is a non-linear regression of y on x, therefore a determination index I_{yx}^2 (-) was used according to BOWERMAN ET AL. (1997) to determine the degree of tightness in the relation between both random quantities.

The course of the average daily rock mass temperatures $t_{C,U}$ in the monitored heating period can be in terms of equation (1) expressed by equations (2) and (3).

$$t_{CR,U1} = 8.072 + 4.399 \cdot \sin(\Omega.\tau + 2.179) \quad (°C)$$

$$I^2_{CR,U1} = 0.897 \quad (2)$$

$$t_{CR,U2} = 8.241 + 4.216 \cdot \sin(\Omega.\tau + 2.241) \quad (°C)$$

$$I^2_{CR,U2} = 0.888 \quad (3)$$

b) Course of temperatures in the period of the rock mass energy potential recovery

The ability of the rock mass energy potential to regenerate during the exchangers stagnation period, or only its partial use, can be evaluated by the rock mass temperatures at the beginning and the end of successive heating periods. The average daily rock mass temperatures at the beginning and the end of the heating periods I. (19 September 2012-22 April 2013) and II. (18 September 2013-23 May 2014) are summarized in Tab. 2.

The results show that the rock mass temperatures at the beginning of the heating periods did not change significantly. Therefore, it can be assumed that the vertical rock mass heat exchangers were stable long lasting sources of low-potential energy. Similar conclusions were reached by LUA ET AL. (2013) during operational testing of vertical heat exchangers and DARKWA ET AL. (2013) in his study °C.

Tab. 2. – Average daily rock mass temperatures at the beginning and the end of the heating period.

		Heating period	Depth (m) 9	20	50	100	Average temperature (°C)	Average temperature difference (°C)
Beginning of the heating period	U 1	I.	13.06	12.31	11.02	10.89	11.82	-0.61
		II.	12.28	11.60	10.41	10,53	11.21	
	U 2	I.	13.43	12.04	10.94	10.72	11.78	-0.49
		II.	12.67	11.51	10.53	10.44	11.29	
End of the heating period	U 1	I.	6.90	7.13	7.12	7.40	7.14	2.98
		II	10.67	10.41	9.60	9.80	10.12	
	U 2	I.	7.38	7.30	7.28	7.64	7.40	2.78
		II.	10.87	10.32	9.72	9.80	10.18	

Higher temperature difference at the end of the heating periods I. and II. emanated from lower ambient air temperatures in the heating period I. and thus increased heat consumption by both heat exchangers.

The course of the average daily rock mass temperatures t_C in the period of heat exchangers stagnation, following the heating period between 23 April 2013 and 17 September 2013, 148 days, are displayed in Fig. 2.

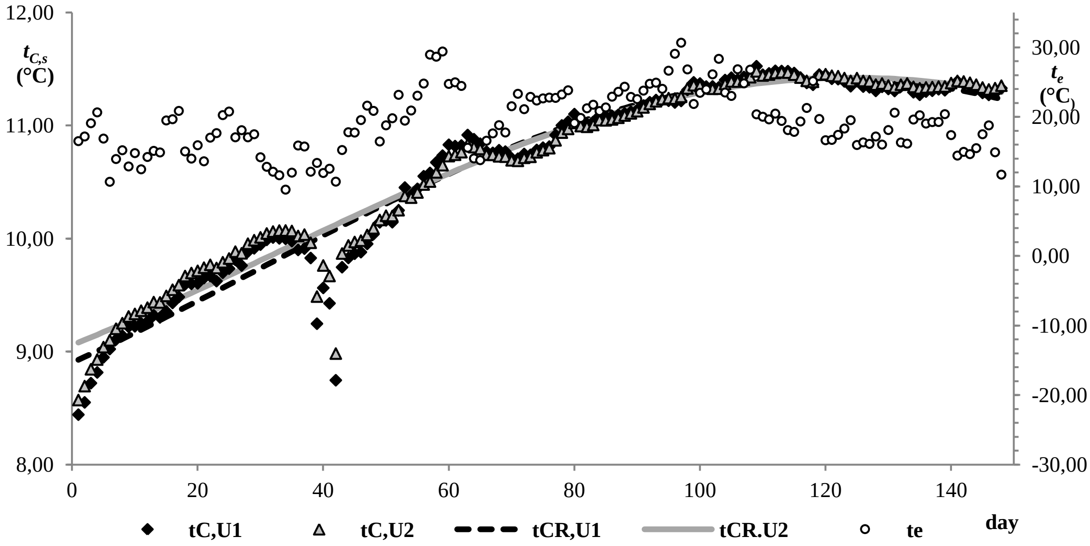

Fig. 2. – Average daily rock mass temperatures in the stagnation period and air temperatures

The diagram in Fig. 2 shows that the differences in the average daily temperatures t_C in the area of the U1 and U2 heat exchangers were not significant in the stagnation period. They were in the range of Δt_U = 0.03 ± 0.07 K. The rock mass temperatures increased approximately until day 120 of the stagnation period with an intensity of 1 K per 40 days; then it slightly decreased. The sharp drop in the rock mass temperature (day 39-42) responds to a decrease in ambient air temperature t_e and putting the heating system into operation.

The course of the average daily rock mass temperatures $t_{C,U,s}$ in the heat exchangers stagnation period can be expressed within the meaning of equation (1) by equations (4) and (5).

$$t_{C,U1,s} = 9.725 + 1.692 \cdot \sin(\Omega.\tau + 5.774) \quad (°C)$$

$$I^2_{U1,s} = 0.948 \tag{4}$$

$$t_{C,U2,s} = 9.885 + 1.538 \cdot \sin(\Omega.\tau + 5.715) \quad (°C)$$

$$I^2_{U2,s} = 0.958 \tag{5}$$

Temperatures, hydrodynamic and thermokinetic parameters of the heat-transfer fluid.

Configuration differences of U1 and U2 heat exchangers affected the mass flows of the heat-transfer fluids m_τ, temperatures of the heat-transfer fluids at the inlet t_1 and the outlet t_2 of the heat pump evaporator, temperature differences $\Delta t = t_1 - t_2$ and the minimum temperatures of the heat-transfer fluid $t_{2,min}$. The average temperatures and the mass flows of the heat-transfer fluid are presented in Tab. 3.

Tab. 3. – Average mass flows and heat-transfer fluid temperatures.

	m_τ (kg.s^{-1})	t_1 (°C)	t_2 (°C)	Δt (K)	$t_{2,min.}$ (°C)
U1	0.122 ± 0.04	7.73 ± 0.7	6.12 ± 2.2	2.49 ± 0.75	-1.76
U2	0.141 ± 0.04	8.08 ± 0.4	6.28 ± 2.2	2.61 ± 0.79	-1.60

The results in Tab. 3. indicated that the U2 heat exchanger had better thermokinetic and hydrodynamic parameters than U1 heat exchanger. Higher heat-transfer fluid temperatures of the U2 heat exchanger showed a positive effect also on the heating factor of the heat pump.

During the verifications within several heating periods, the temperatures of the heat-transfer fluids did not drop below -2 °C. Still a mixture of 33% ethanol and 67% water has been most commonly used heat-transfer fluid in the Czech Republic. At this concentration of ethanol, the freezing point according to the Engineering ToolBox (2015), is -17.4 °C. BANKS (2012) as well as BRANDL (2006) stated that higher concentration makes the hydrodynamic and thermokinetic parameters of the heat-transfer fluid more unfavourable. Based on these facts, the type of heat-transfer fluid flow and heat transfer coefficient

α ($W \cdot m^{-2} \cdot K^{-1}$) between the inner exchanger pipe wall and the heat-transfer fluid was determined. According to BRANDL (2006), the heat transfer coefficient can significantly affect the process of heat transfer between the rock mass and the heat-transfer fluid. On the basis of the facts given it is apparent that satisfactory concentration for the verified vertical rock mass heat exchangers would be 20% of ethanol, when the freezing point is -9.0 °C. The results of the verifications and calculations have shown that lowering the concentration of the heat-transfer fluid would have significant positive effect on the Reynolds criteria and the heat transfer coefficient α, but the flow rates of the heat transfer fluid were low in both heat exchangers. They were in range of w = 0.03-0.34 $m.s^{-1}$ for the U1 heat exchanger and w = 0.02-0.32 $m.s^{-1}$ for the U2 heat exchanger. Thermokinetically favourable turbulent flow (Re > 2 500) would be achieved at a concentration of 20% and a heat-transfer fluid flow speed of w > 0.39 $m.s^{-1}$ for the U1 heat exchanger and w > 0.49 $m.s^{-1}$ for the U1 heat exchanger. According to BANKS (2006), it is not necessary to achieve a turbulent flow. However, laminar flow was not effective in terms of heat transfer.

Specific heat outputs and specific energies transferred by the heat exchangers.

The average q_τ and maximum $q_{\tau,max}$ heat outputs ($W \cdot m^{-1}$), specific energies q, q_{max} transferred by the heat exchangers per day ($Wh \cdot m^{-1} \cdot day$) and total energy q_Σ transferred by 1m length of the heat exchanger in the heating period ($kWh.m^{-1}$) at an average daily ambient air temperature t_e = 5.34 °C are given in Tab. 4.

Tab. 4. – Average and maximum specific heat outputs and specific energies extracted from the rock mass

	q_τ ($W \cdot m^{-1}$)	$q_{\tau,max}$ ($W \cdot m^{-1}$)	q ($Wh \cdot m^{-1} \cdot day$)	q_{max} ($Wh \cdot m^{-1} \cdot day$)	q_Σ ($kWh \cdot m^{-1}$)
U1	6.46±2.19	20.66	125.48±72.17	262.77	27.16
U2	8.19±2.73	26.57	157.54±90.73	353.16	34.10

The results of the verification summarized in Tab. 4. show that specific heat outputs q_τ, $q_{\tau,max}$ for the U2 heat exchanger as well as the specific energies q, $q_{max.}$, q_Σ extracted from the rock mass were higher than for the U1 heat exchanger. The results also showed that the maximum specific heat outputs of the heat exchangers $q_{\tau,max}$ and the total energy extracted from the rock mass q_Σ did not reach its limits as stated by BANKS (2006) and VDI 4640 (2001).

Higher specific heat outputs as well as specific energies extracted from the rock mass by the U2 heat exchanger were caused by its larger heat exchanger surface. External heat exchanger surface per 1 m length at the U2 heat exchanger was bigger by 60% than at the U1 heat exchanger. Heat outputs together with their transferred energies were in our verifications most probably limited by low value of heat transfer coefficient α caused mainly by purely laminar heat-transfer fluid flow.

The diagram in Fig. 3 shows the course of specific heat outputs of the heat exchangers extracted from the rock mass in the coolest day of the heating season (26.1.2013) when the average daily ambient air temperature was t_e = -9.15 ± 5.03 °C. The courses of the outputs reacted to the ambient air temperatures and the working time of the company's employees. The average specific heat outputs of the heat exchangers were higher than the average outputs for the entire heating period, but lower than that stated by the standard VDI 4640 (2001). They reached values in the range of 7.58 ± 2.54 $W.m^{-1}$ (U1 heat exchanger) and 9.82 ± 4.06 $W.m^{-1}$ (U2 heat exchanger). Also the specific energies transferred by the heat exchangers on this day were 186.95 $Wh \cdot m^{-1}$ (U1) and 241.50 $Wh \cdot m^{-1}$ (U2) being higher than the average values for the entire heating period.

The bar diagram in Fig. 4 illustrates the specific heat energy transferred by the heat exchangers on individual days of the entire heating period.

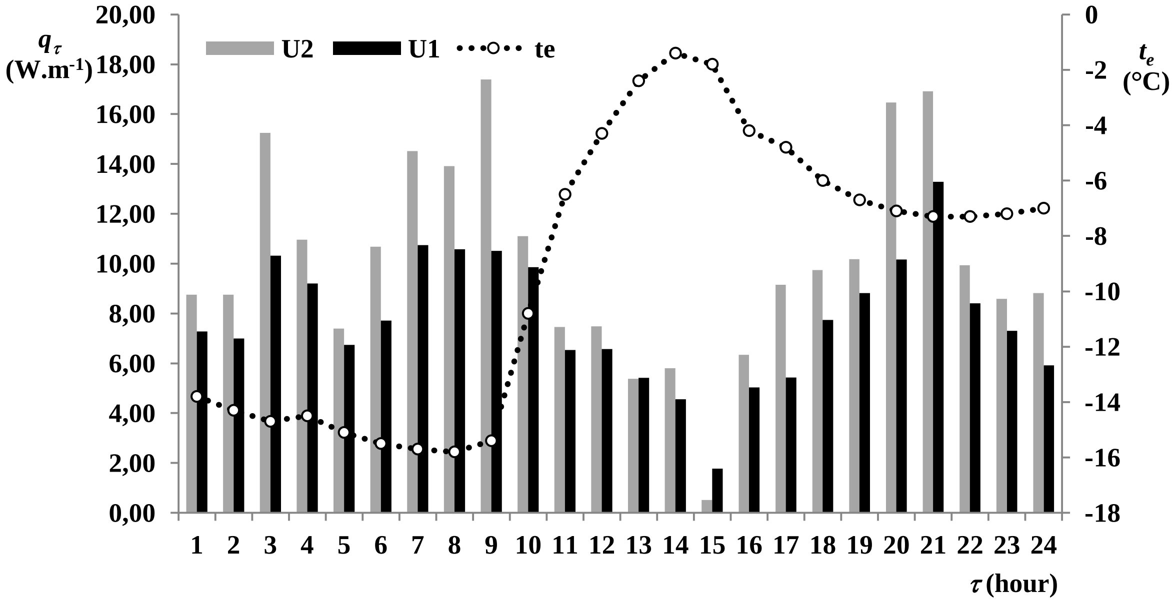

Fig. 3. – Heat outputs extracted from the rock mass in the coolest day of the heating season

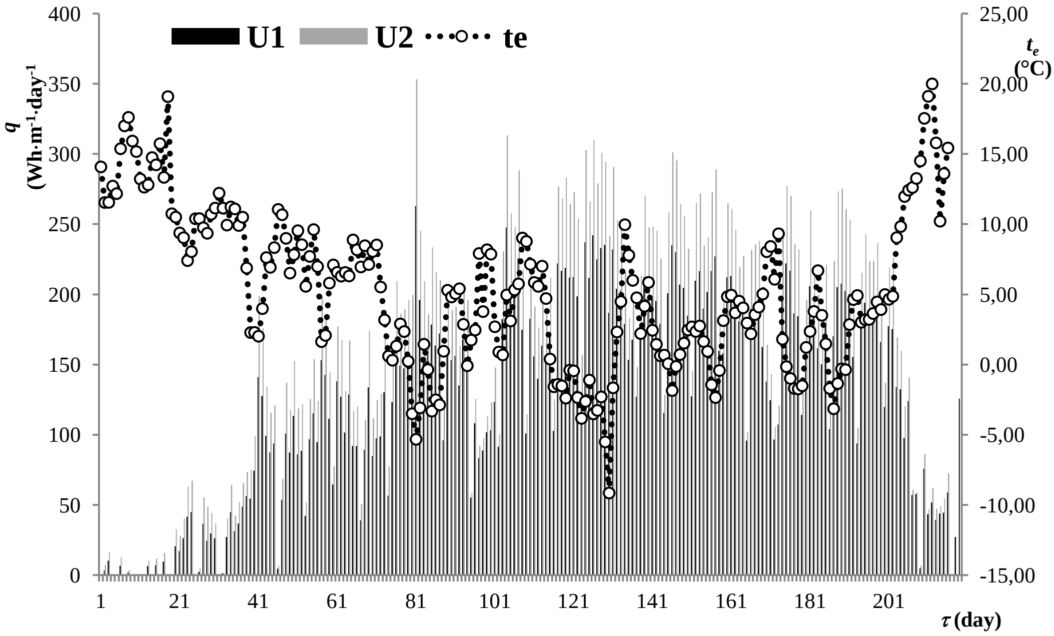

Fig. 4. – Specific energies extracted from the rock mass in the heating period

The response of the heat exchanger operation to the ambient air temperatures resulted from the course of specific energies extracted from the rock mass on individual days.

CONCLUSIONS

The study provided knowledge that can be useful for design and realization of the vertical rock mass heat exchangers. Based on the verification and monitoring the temperatures, heat outputs and heat energies extracted from the rock mass, the following conclusions were made:

- Cooling of the rock mass in the area of the U2 heat exchanger was smaller than in the case of U1. The rock mass temperatures in the area of both heat exchangers were positive.
- The courses of the average daily rock mass temperatures t_C in the heating and the stagnation period can be expressed, with sufficient accuracy, using simple equations (2), (3) and (4), (5). Knowledge of the rock mass temperature courses together with knowledge of its thermal

characteristics and ambient air temperatures revealed the important basis for controlling the energy systems with heat pumps.

- The average daily rock mass temperatures in the areas of both heat exchangers for the greater part of the heating period were higher than the ambient air temperatures (59.72% for U1; 62.96% for U2). The verification confirms the advantages of GLHEs as low-potential energy sources for heat pumps compared to the outside air.
- Rock mass temperature differences in the area of the heat exchangers at the beginning and at the end of the heating periods were not significant. The verification results thus indicated that the vertical rock mass exchangers can be considered a long-term stable source of low-potential energy.
- Specific heat outputs and specific energies extracted from the rock mass by the U2 heat exchanger were higher than at the U1 heat exchanger.
- The average and the minimum temperatures of the heat-transfer fluid in the U2 heat exchanger were higher than in the U1 heat exchanger.
- In both types of the heat exchangers U1 and U2, only laminar flow of the heat-transfer fluid was obtained. A significant cause of the disadvantageous laminar flow was a high concentration of ethanol, which does not correspond to the operating temperatures of the heat-transfer fluid.
- Decreasing the ethanol concentration had a positive influence on the type of heat-transfer fluid flow and the heat transfer coefficient between the heat-transfer fluid and the exchanger pipe walls.

Further studies will analyze and verify the possibilities of increasing the specific heat outputs of the heat exchangers by obtaining at least temporary turbulent flow of the heat-transfer fluid. The acquisition of knowledge about the impact of using GLHEs for heating and cooling buildings on a temperature field, heat outputs and specific energies extracted from the rock mass will be considered.

REFERENCES

1. BANKS, D.: An Introduction to Thermogeology: Ground Source Heating and Cooling. 2 nd ed., Oxford, UK, John Wiley &Sons, Ltd. 2012.
2. BOWERMAN, B. L., O´CONNELL, R. T.: Applied statistics: improving business processes. 1nd ed., Boston, United States of America, Richard D. Irvin Inc. 1997.
3. BRANDL, H.: Energy foundations and other thermo-active ground structures. Géotechnique, 56, 2006: 81 – 122.
4. DARKWA, J., SU, W., CHOW, D. H. C.: Heat dissipation effect on a borehole heat exchanger coupled with a heat pump. Appl. Therm. Eng., 60, 2013: 234–241.
5. DE CARLI, M., M. TONON, M., A. ZARRELEA, A.: A computational capacity resistance model (CaRM) for vertical ground-coupled heat exchangers. Renewable Energy, 35, 2010: 1537–1550.
6. GEHLIN, S. E. A., HELLSTRÖM, G. H.: Influence on Thermal Response Tests by Groundwater Flow in Vertical Fractures in Hard Rock. Renewable Energy, 28, 2003: 2221-2238.
7. HUANG, S., MA, Z., WANG, F.: A multi-objective design optimization strategy for vertical groundheat exchangers. Energy and Buildings, 87, 2015: 233–242.
8. LUO, J., ROHN, J., BAYER, M., PRIESS, A.: Thermal performance and economic evaluation of double U-tube borehole heat exchanger with three different borehole diameters. Energy and Buildings, 67, 2013: 217–224.
9. MARCOTTE, D., PASQUIER, P.: The effect of borehole inclination on fluid and ground temperature for GLHE systems. Geothermics, 38, 2009: 392–398.
10. NEUBERGER, P., ADAMOVSKÝ, R., ŠEĎOVÁ, M.: Temperatures and Heat Flows in a Soil Enclosing a Slinky Horizontal Heat Exchanger. Energies, 7, 2014: 972-978.
11. PLATELL, P.: Developing Work on Ground Heat Exchangers. In: Conference Proceedings ECOSTOCK 2006, 31 May – 2. June, 2006, 7A-1, Pomona, New Jersey, USA.
12. SANNER, B., MANDS, E.: Larger geothermal heat pump plants in the central region of Germany. Geothermics, 32, 2003: 589–602.
13. SANNER, B., REUSS, M., MANDS, E., MUELLER, J.: Thermal response test – Experiences in Germany. In: Proceedings of TERRASTOCK 2000, 28 August 2000, pp.177 – 182, Stuttgart, Germany.
14. SELÇUK, E., BERTRAND, F.: Efficiency of various grouting materials for borehole heat exchangers. Appl. Therm. Eng., 70, 2014: 788–799.
15. The Engineering ToolBox: Ethanol Freeze Protected Water Solutions, Available online http://www.engineeringtoolbox.com/ethanol-water-d_989.html. (accessed 2 July 2015).
16. VDI 4640- Part 2, Thermal use of the underground – Ground source heat pump systems. Verein Deutscher Ingenieure, Düsseldorf, (2001).

Corresponding author:
prof. Ing. Radomír Adamovský, DrSc., Department of Mechanical Engineering, Faculty of Engineering, Czech University of Life Sciences Prague, Kamýcká 129, Praha 6, Prague, 16521, Czech Republic, phone: +420 22438 4176, e-mail: adamovsky@tf.czu.cz

POTENTIAL OF VILLAGE HOUSE FOR SUSTAINABLE ENERGY PRODUCTION

V. Adomavičius[1], J. Valickas[2], G. Petrauskas[1], L. Pušinaitis[1]

[1]*Kaunas University of Technology, Studentų 48–205, LT-51367 Kaunas, Lithuania*
[2]*Panevėžys Institute at Kaunas University of Technology, S. Daukanto 12–113, LT– 35212 Panevėžys, Lithuania*

Abstract
Concept of energetically self-sufficient one-family house and study of its feasible technical potential for energy production from renewable energy sources are presented. Urgent necessity of eco-friendly buildings development is explained and substantiated. Scheme of the building's microgrid is proposed, its equipment used for power and heat production and local universally available free from payment renewable energy resources are described. Monthly power production by the microgrid is computed and compared with demands of the building. Main findings of this study are presented and discussed. They confirmed that one-family house can produce more power and heat energy than it is necessary. Results of this study allow designing of pilot building and to perform further researches in the natural conditions.

Key words: microgrid, solar energy, wind energy, renewable energy, efficiency.

INTRODUCTION

Rates of eco-friendly buildings development in the world are not sufficient and adequate to the current level of knowledge in ecology and climatology sciences. Therefore necessity of rapid development in this area must be well explained and substantiated. Many arguments can be given in favour of self-sufficient RES-based energy production in the buildings of various types. First of them should be mentioned protection of environment pollution by the greenhouse gases (GHG) and the climate change. The updated mental picture of the greenhouse effect is explained well enough by BENESTAD (2016) and other authors. Reasons of this phenomenon, environmental damages and other negative consequences of these processes are described in thousands of scientific papers, monographs, scientific reports and books. Available information on this subject makes up a solid scientific background, which allows accepting the decision to take urgent actions in order to phase out environment pollution by the GHG. This can be done by the transition from fossil fuels to the renewable energy sources as soon as possible. Such and similar proposals are strongly expressed in many reports by IPCC WGIII (2014), IEA (2013), documents – COP21 (2015) and many other sources of information.

Renewable energy sources have many advantages against fossil fuels. Primarily, as it is depicted in Fig. 1 presented by ADOMAVICIUS AND KAMINICKAS (2014), RES-based power plants (and nuclear power plants – NPP) have a huge superiority regarding the carbon intensity of power generation: amounts of CO2 equivalent emissions in grams per kWh of produced electricity for hydroelectric power plants (HPP), oceanic hydroelectric power plants (OHPP), wind power plants (WPP), concentrated solar power plants (CSPP), geothermal power plants (GTPP) and photovoltaic power plants (PVPP) are from tenths to hundreds times less than emissions from power plants based on fossil fuels, which are natural gas power plants (NGPP1 and NGPP2), running on the ecologically best (1) and worst (2) natural gas, furnace oil power plants (FOPP), coal power plants (CPP) and lignite power plants (LPP). Low carbon intensity of the RES-based power plants is one of the strongest drivers accelerating development of the clean power production technologies.

Second important driver of RES-based power production development is economic: costs of solar and wind power production and costs of batteries used for power storage are rapidly falling down. Impact of only ecological and economic drivers is the main factor in the powerful breakthrough of RES-based power production technologies what is evidently indicated in Fig. 2, where indicators of growth are compiled on basis of data found in report of REN21 (2014) and in EPI DATA CENTER (2015). The first five positions in Fig. 2 have photovoltaic, wind, biomass, hydro energy and geothermal power plants. Growing awareness about destructive impact of fossil fuels on biosphere and global climate change is inducing growing opposition of the world population to the dirty fuels. More and more people understand and support the necessity to leave the fossil fuels underground. It is supposed that this generation is the last, which still can solve or mitigate the climate change problem before it is not too late, but the time for actions is short. And this is another important driver (social) of green revolution, which is in process from the first years of 21-st century and up to now.

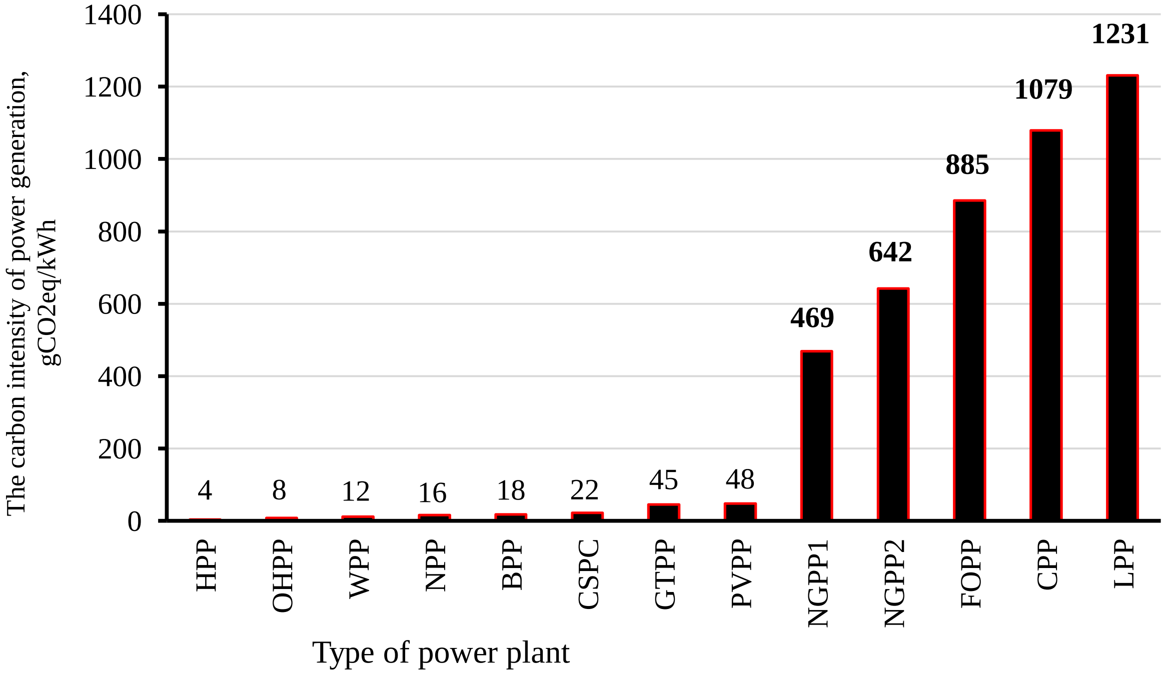

Fig. 1. – Comparison of power generation technologies by carbon intensity

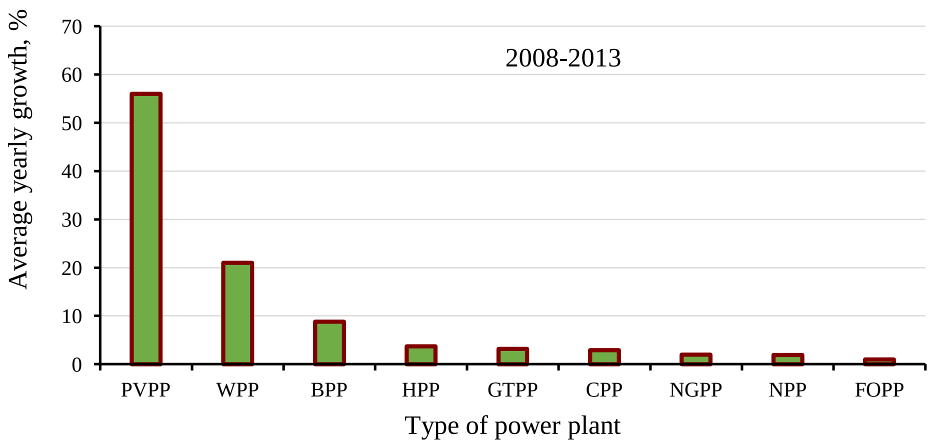

Fig.2. – Global annual growth of electricity production by type of power plant

Buildings consume about 41 % of energy in the EU countries. They have a huge potential for reduction of GHG emissions. It can be achieved in many ways in all types of buildings:

- ✓ by reducing of energy demands necessary for space heating or cooling in buildings (relevant thermal insulation of buildings);
- ✓ by using smokeless heat energy generation equipment (heat pumps, electric heaters);
- ✓ by installing local microgrid based on solar, wind, hydro energy sources and low temperature heat energy sources for power and heat production in buildings;

- ✓ by using of highly efficient domestic electric appliances (energy class A+) and efficient well controlled lighting system.

In this paper we present a concept and case study of energy self-sufficiency feasibility of one-family house. Presently majority of traditional houses already existing in towns and cities of many countries have three energy inlets – electric power, natural gas and district heating, or at least one or two inlets in a majority of villages (electricity, natural gas). In our case study we are exploring a variant of house, which in principle need not outside energy input and can function self-dependently. In this study all power and heat energy necessary for the house, including charging of electric vehicle batteries, is designed to produce in local microgrid running on free from payment and self-delivering renewable energy sources.

MATERIALS AND METHODS

In general case resources of renewable energy depends on the geographic coordinates of locality under consideration and on the time. Resources of renewable energy in any locality can be evaluated approximately by the average perennial data of variable energetic parameters of the energy source. It can be sum of average perennial global irradiation on the conventional planes per squire meter for solar energy, average perennial wind speed per year together with parameters of Weibull distribution of wind speed for wind energy and average perennial outdoor temperature of air in shadow for the certain period of time (e.g., month, week, day), when renewable energy source is the mass of low temperature air existing around the house under investigation. Resources of the chosen renewable energy sources in the chosen locality are presented in Tab. 1. Their potential possibilities will be checked in this study in regard of their capability to cover all necessary power and heat needs of the experimental house.

Tab. 1. – Resources of self-delivering renewable energy in the locality of building

Conditions	**Months**												**Per year**
	01	**02**	**03**	**04**	**05**	**06**	**07**	**08**	**09**	**10**	**11**	**12**	
Geographic coordinates of locality													
55˚18’46” North; 22˚01’52” East (in Lithuania)													
Average perennial monthly sum of global solar irradiation, kWh/m^2													
Inclination 35˚	23.9	43.1	112	152	176	168	167	149	113	66.4	27.2	17.2	1120
Inclination 90˚	25.6	42.1	98.1	108	103	90.8	94.2	97.1	91.2	62.5	28.5	18.7	860
Average perennial outdoor temperature of air, ºC													
In shadow	–4.0	–3.7	–0.4	5.1	11.3	14.9	16.3	15.9	11.9	7.6	2.5	–1.5	6.3
Average annual parameters of wind speed													
Hub height 25 m	v = 5.7 m/s; Weibull parameters: a = 6.4 m/s; K = 2.07												

Data in the Tab. 1 show rather good wind energy resources in the chosen locality, however solar energy and low temperature heat energy resources of atmosphere air are moderate. But it is worthy to note that during the years of 21-st century average temperatures of air of all months of entire Earth planet are significantly higher than perennial average of the 20-th century due to the climate change. Therefore average temperatures of air in February, March and December in Lithuania already are positive and exceed zero degree very significantly.

Overall view of the house under investigation is depicted in Fig.3 and short description of its characteristics is presented below in Tab. 2. The building is designed and oriented in line with principles of solar architecture – slope of the roof is turned southward (azimuth – 0 deg.). Roof-top photovoltaic (PV) array is mounted on the building’s roof on the plane, which has optimal inclination to the horizontal plane for this geographic latitude (35 deg.). A small-scale wind turbine is mounted on the ground from the west side of the building (the main direction of wind). The glassed-in added greenhouse is designed mainly for the preheating of air in order to have a higher efficiency of heat pump intended to use for space heating and producing of domestic hot water. In this case it is operating as the collector for air heating. Additionally, in some periods of year it also can be used as a greenhouse – for growing of early vegetables, or for drying of wet wash.

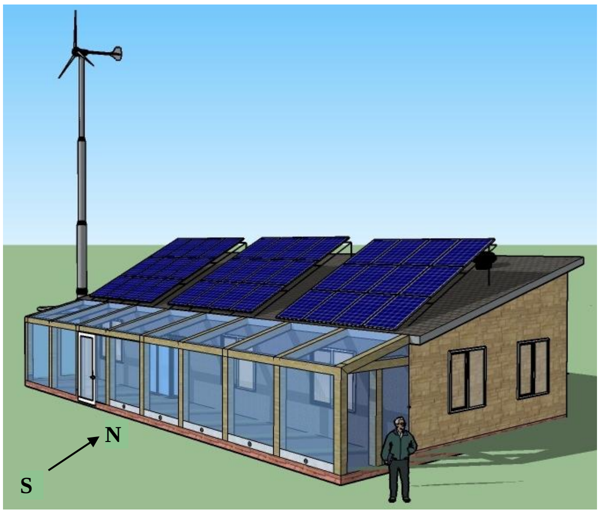

Fig. 3. – Overall view of energy independent one-family house

Benefit of air preheating in the added greenhouse can be explained using Fig. 4, where typical curves of power demand and heat energy output of heat pump "air to water" are depicted. The curve of heat energy output (the upper one) clearly shows that efficiency of heat pump operation is significantly higher at higher temperatures of the ambient air: the power demand curve remains approximately stable, but the heat energy output is increasing together with increase of the ambient air temperature. In our case outdoor module of the heat pump is intended to install in the loft of the house. Preheated air finds the way from the greenhouse to the outdoor module via the specially designed air ducts.

Tab. 2. – Characteristics of the one-family house

Parameters of the building	Unit	Value	Note
Building's energy class	–	A+	15 kWh/m^2 annually
Total living area	m^2	105	
Total heating area	m^2	95	
Temperature of air in heating spaces	ºC	18–22	Lithuanian standard
Number of inhabitants	–	4	
Temperature of domestic hot water (DHW)	ºC	50	
Consumption of DHW per month per inhabitant	m^3	2	Average data
Consumption of DHW per month per building	m^3	8	Average data
Roof area	m^2	120	
Area of glassed-in wall of the added greenhouse	m^2	~30	Vertical windows
Area of glassed-in roof of the added greenhouse	m^2	~28	Roof windows
Number of electric vehicles	units	1	

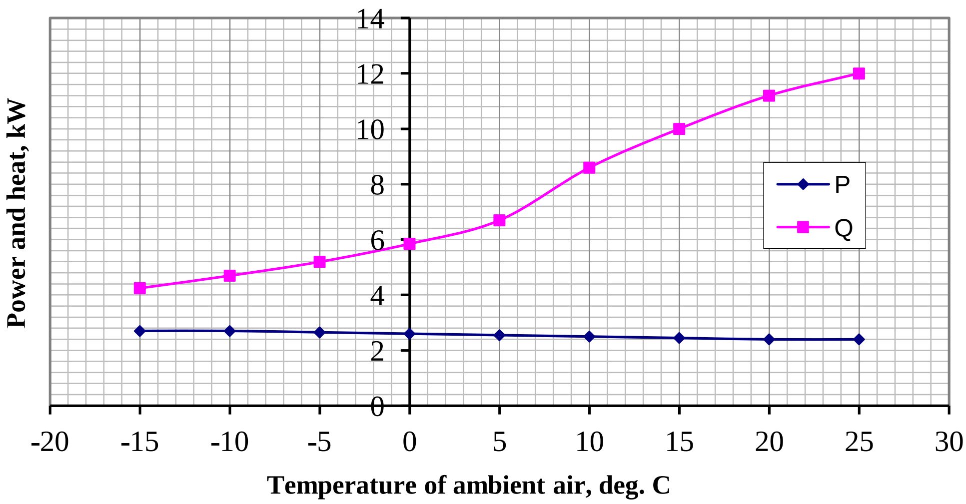

Fig. 4. – Typical curves of power demand and heat energy production by the heat pump

The greenhouse will operate efficiently in sunny and half-sunny days of autumn, winter and spring. Increment of inside air temperature can be achieved approximately up to 30–40 º C in sunny winter days at negative outdoor temperatures, if the greenhouse has perfect thermal insulation. Thus, the greenhouse added to the house will allow saving of electric energy used by the heat pump. Operation of the greenhouse as solar collector for air heating is not essential in summer but it also will help save energy in colder days.

The main parameters of power and heat generating equipment designed to use in the experimental microgrid are shortly described in Tab. 3. Apart from the RES-base power generation system, it would be expedient to have connection of the building's microgrid to the distribution grid of electric power system. It allows increasing of power supply flexibility and reliability. It also enables cooperation between the microgrid and the distribution grid. Microgrid can perform some functions useful for the distribution grid (e.g., function of power storage, support of the power distribution grid during the peak demand hours, when surplus of electric power produced and stored in the microgrid can be supplied into the power system). The distribution grid also can support microgrid at emergency.

Tab. 3. – Main parameters of energy generators in the building's microgrid

Parameters of power and heat generators	Unit	Value	Note
Small-scale wind turbine of horizontal axes			
Rated capacity of wind turbine	kW	9.5	At wind speed 10 m/s
Maximum capacity of wind turbine	kW	12	At wind speed ≥ 12 m/s
Hub height	m	24	
Rated wind speed	m/s	10	
Diameter of wind rotor	m	6.5	3 blades x 14 kg
Swept area of wind rotor	m^2	20.4	
Weight of wind turbine	kg	~160	Without tower
Roof-top photovoltaic power plant			
Rated capacity of one module	Wp	300	Crystalline Silicon
Number of PV modules	–	36	
Rated capacity of PV power plant	kWp	10.8	At irradiance 1 kW/m^2
Optimal inclination angle of PV array	deg.	35	
Azimuth of PV array	deg.	0	Oriented to South
Heat pump „air to water" for space heating and domestic hot water			
Rated power demand by the heat pump (HP)	kW	~ 2.3	
Range of heat generation capacity	kW	4.4–12.0	(Fig. 5)
Lowest average ambient temperature of month	º C	– 4.0	January
Highest average ambient temperature of month	º C	16,3	July
Rated temperature of water in output of HP	º C	50	

Possible variant of electrical scheme of the building's microgrid power conversion system is presented in Fig. 5. The system comprises the following subsystems:

1) the small-scale wind turbine SWT includes the generator G, the rectifier R, the step up chopper DC/DC–1, the switch S1 and the charger Ch1 of the battery B;
2) the small-scale photovoltaic power plant consists of the PV array, the step up chopper DC/DC–2, the switch S2 and the charger Ch2 of the battery B;
3) the electric power storage subsystem consists of the battery B, the step up chopper DC/DC–3 and the switch of the battery Sb;
4) mutual for the microgrid power conversion system consists of the grid-tied inverter GTI, the capacitor for short-time power storage C, the switch Si and

the inverters control system, which is included in the united control system of the microgrid CS;
5) the united control system of the building's microgrid has the unit of the control system CS and the switch Sc.

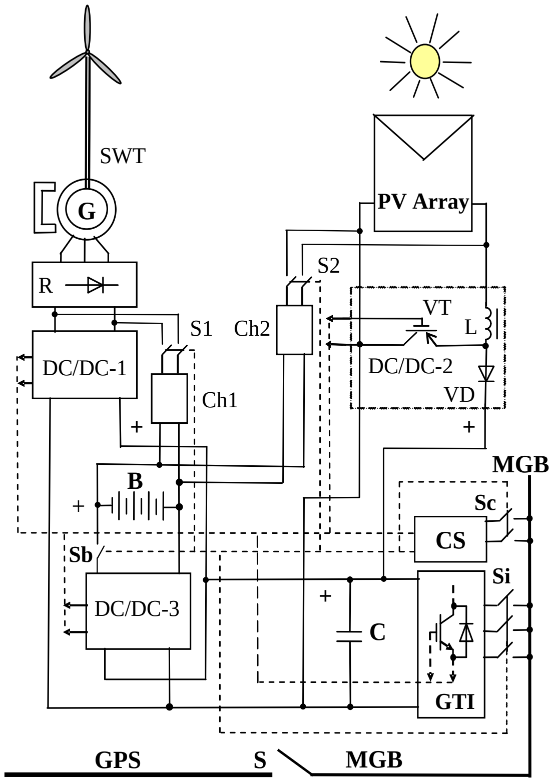

Fig. 5. – Electrical scheme of the house microgrid power conversion system

Microgrid's bus MGB can be connected to the distribution grid of power system GPS through the switch S. The microgrid can function both in grid-connected and stand-alone (islanded) modes of operation.
All three DC/DC choppers have the same electrical scheme, which is revealed in Fig. 5 and depicted under the PV array. It consists of the shorting transistor VT, the inductor L and the flyback diode VD. The DC/DC choppers are used for stepping up the input voltages of the GTI inverter. Three phase grid-tied bridge inverter with short-time power storage capacitor C is used for the power supply into the bus of microgrid MGB for feeding of all electricity users in the building. The main elements of the inverter are six transistors connected with six diodes as it is shown in this figure. Inverters of this type can be exploited in any power sources having variable DC voltage in the inlet. Specific feature of this type converter is the possibility to have a few inlets from different and intermittent power sources connected through the DC/DC converters to one mutual DC/AC inverter.
Battery B of electric power storage subsystem is important part of the building's microgrid, when high reliability of power supply is required and operation in stand-alone mode during long periods is probable. A huge progress made in power storage technologies during the last decade paved the way not only for rapid development of electric vehicles but also for breakthrough of installations of RES-based power plants and microgrids. Significant improvements of batteries and rapid decrease of their prices are described by LUO ET AL. (2015), WANG ET AL. (2014), JOHN (2015), AMBRI (2015) and by many other authors.
Batteries of electric vehicles also can be used in microgrids for power storage in two ways:
- ✓ second use of batteries retired from electric vehicles;
- ✓ according to the vehicle-to grid (microgrid) concept.

Technical, economic and commercial viability of these implementations is analysed by MULLAN ET AL. (2013), PETERSON ET AL. (2013), STANDRIDGE AND CORNEAL (2014) and by many other authors.
Control pulses for the inverter, for all DC/DC choppers and switches are generated in the microgrid's control system CS. There are many versions of micrigrids control and energy management systems design, which are reviewed by MENG ET AL. (2016). Aspects of optimal control and stability of operation are among the main problems for designers of microgrids. They were analysed by MAJUMDER (2013) and many other authors. It has to be taken into consideration in order to design optimal and efficient microgrids for feeding all necessary domestic electrical appliances.

RESULTS AND DISCUSSION

Probable monthly power amounts of power production in the building's microgrid were computed on basis of data presented in Tab. 1 and Tab. 3. Results of the computations are presented in Tab. 4, where *Ewi* is the power produced by the small-scale wind turbine per month "*i*"; *Esi* is the power produced by the rooftop photovoltaic power plant per month "*i*" and *Ei* is the total power amount produced in the microgrid by both small-scale power plants.

Tab. 4. – Monthly power production and power demands in the building's microgrid

Month	*Ewi*	*Esi*	*Ei*	*Edi*	*Edai*	*Eshi*	*Ehwi*	*Eevi*
	kWh							
1	2356	270	2626	1200	700	200	80	220
2	2008	454	2462	1170	700	170	80	220
3	2282	1080	3362	1140	700	140	80	220
4	1710	1318	3028	1070	700	70	80	220
5	1340	1473	2813	1000	700	0	80	220
6	1226	1391	2616	1000	700	0	80	220
7	1149	1365	2514	1000	700	0	80	220
8	1428	1262	2690	1000	700	0	80	220
9	1739	998	2736	1000	700	0	80	220
10	2062	635	2697	1070	700	70	80	220
11	2075	261	2336	1130	700	130	80	220
12	3210	180	3390	1160	700	160	80	220
Year	22 584	10 686	33 270	12 940	8 400	940	960	2 640

Total power demands in the building *Edi* per month "*i*" comprises of the power expenditures by the domestic appliances *Edai*, by the heat pump for space heating *Eshi* and domestic hot water *Ehwi* and by the charger of electric vehicle batteries *Eevi*. Power demands for domestic appliances are assumed above the average demands of a typical house. Demands for space heating depend mostly on the size of heating area, energy class of building and local meteorological conditions. High energy class of building and energy saving measures are extremely important for substantial reducing of energy demands for space heating and simultaneously for reducing emissions of the greenhouse gases because presently in many cases heat energy is generated using fossil fuels.

Electricity consumption by the electric vehicles is not considerable. It mostly depends on the mileage, size, speed, aerodynamic characteristics of the car, and on the quality of roads. Approximately it was assumed that average daily mileage of the electric vehicle in Lithuania is 35 km. Power consumption rate for middle-sized electric vehicle is about 200 $Wh \cdot km^{-1}$.

Total monthly power production, total power demand and their balance in the building's microgrid under investigation are shown in Fig. 6.

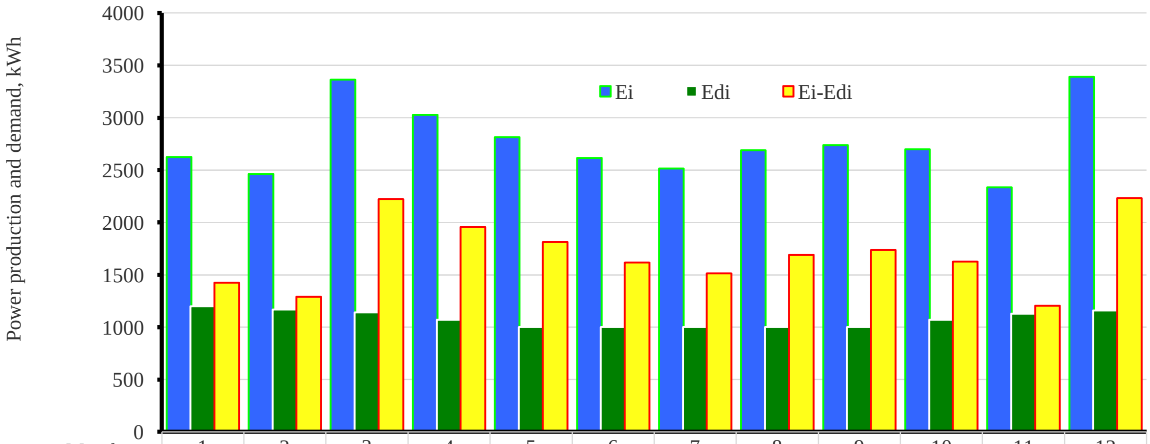

Months	1	2	3	4	5	6	7	8	9	10	11	12
Ei	2626	2462	3362	3028	2813	2616	2514	2690	2736	2697	2336	3390
Edi	1200	1170	1140	1070	1000	1000	1000	1000	1000	1070	1130	1160
Ei-Edi	1426	1292	2222	1958	1813	1616	1514	1690	1736	1627	1206	2230

Fig. 6. – Monthly power production by the microgrid, total power demand and power balance

Analysis of information depicted in this chart evidently shows that potential of power production in the buildings microgrid at the mentioned above local renewable energy resources covers all electricity demands (including electric vehicle) more than two times. Thus, this microgrid could feed one more house having the same power demands, or to supply electricity into the distribution grid of power system. Secondly, it is not the limit of power production potential for this house: under the necessity it would be possible to choose higher capacity of the turbine, to install additional wind turbine or to install additional (ground mounted) photovoltaic power plant.

A wide variety of microgrids and small-scale power plants based on renewable energy sources exists in practice or are described in papers. Advantages of the microgrid of energetically self-sufficient house proposed in this paper are following:

- ✓ convenience and almost universal availability of chosen self-delivering renewable energy sources (solar, wind and low temperature heat energy source of ambient air),
- ✓ exploitation of the loggias for enhancing efficiency of heat energy production,
- ✓ low operation and maintenance expenditures (no expenses for fuel and fuel supply, no ash and other waste materials, water is not used for power production),
- ✓ versatility of the microgrid (covers all power and heat energy demands of the house for electrical appliances, space heating, domestic hot water and electric vehicle),
- ✓ power conversion system based on innovative converter (it has three inlets from intermittent solar, wind power sources and power storage battery, all connected through the DC/DC converters to one mutual DC/AC inverter).

Results of researches of power conversion systems with mutual inverter are described in papers by RAMONAS ET AL. (2009), RAMONAS AND ADOMAVICIUS (2013) and in their other publications. As a rule, traditionally every electricity generating or storing unit in the microgrids has their own inverter and majority of domestic RES-based power plants are roof-top solar (in this case shortage of electricity in winter is unavoidable). Other renewable and non-renewable energy sources are also used. It is described in the report performed by MARNAY ET AL. (2012) and in other references. But it makes the system more expensive.

Previously many hopes and expectations in transport sector were related with biofuels. It was believed that biofuels is the main way of transport sector to the green future. However, production of biofuels in many cases is linked with considerable use of land, which preferably is necessary for agriculture, and usage of soil polluting chemical materials as pesticides, fertilizers and other. Thus, possibilities of biofuel production are limited and this type of fuel is rather expensive. Presently it is clear that, most probably, the main way of transport sector to the green future will be through the electric power. Batteries of electric vehicles can be charged from the RES-based power plants without any combustion of fuels, which release the GHG. Additionally, according to the United Nations Framework Convention on Climate Change and other documents, our way to the sustainable future goes directly towards the zero emissions of GHG and it is not a matter of far future – it is happening now. Transition to the epoch of clean energy production is ongoing now rather rapidly and smoothly: total capacity of wind turbines installed in the world in 2015 made up 63 GW (2014 – 50.2 GW), solar power plants – about 50 GW (2014 – 40 GW) and hydroelectric power plants – 33 GW (2014 – 39 GW). Meanwhile increases of total capacities of power plants based on fossil fuels during the same years are few times lesser at the best case (natural gas power plants) or even are shrinking (coal, lignite, furnace oil, nuclear) because of their decommissioning. So, public electric grid is becoming greener and greener every year. Most probably, biofuels in transport sector will be used in future in cases when usage of electricity is hardly applicable. It could be sectors of maritime and aviation.

CONCLUSIONS

The necessity of urgent development of eco-buildings can be easily substantiated on basis of scientific information proved by the ecologists and climatologist of the world. Pollution of environment by massive long-term burning of fossil fuels is inducing frequent and strengthening catastrophic disasters and dangerous climate change. The main remedy for solving this problem is sustainable development by the decisive, urgent and deep reduction of the greenhouse gases emissions into the atmosphere. There are many ways to do this in every sector of economy and it must be done as soon as possible. All sectors of world‘s economy must be reconsidered in this aspect and agriculture as well.

A huge untapped potential for reduction of the greenhouse gases emissions have buildings. A permanent decline of costs of photovoltaic modules, batteries and photovoltaic systems caused unprecedented growth of their markets and paved the way for economically reasonable implementation of RES-based microgrids in buildings. Principles of renewable energy systems implementation in buildings are energy conservation (perfect thermal insulation), efficient exploitation of the primary source (wind, solar irradiance) and efficient usage of the produced energy (energy efficient equipment). Microgrids have very good environmental characteristics of energy production and they are attractive for possibilities to exploit local, free, non-fuel and non-emitting greenhouse gases primary energy sources in high extent.

The presented microgrid has not any expenses for fuels and fuels supply, because it is running on a free local primary energy sources. Therefore maintenance and operation of this system do not require much expenditure and time. Besides, the system does not produce any waste (ash), does not use water for power production, and solar power plant has not moving parts.

The main finding in this study is justified conclusion that potential of this experimental house for power production significantly exceeds all intentionally enhanced power demands of the building. Results of this study allow taking further steps: to implement a pilot experimental project of the house fed by the power generated in its own microgrid, which is based exclusively on local, free, self-delivering and smokeless renewable energy sources. The microgrid operating in natural conditions will be useful as basis for researches to be carried out in order to enhance efficiency of power production, to find optimal sizes of wind and solar power plants, heat pump and added greenhouse, and to find optimal algorithm of overall system control for microgrids of this type.

REFERENCES

1. ADOMAVICIUS, V., KAMINICKAS, M.: Analysis of PV power future development possibilities. Energetika, T. 60, Nr. 4, 2014: 233–248.
2. AMBRI: Storing Electricity for our Future. July 27 2015, 19 p. Available at: http://www.nga.org/files/live/sites/NGA/files/pdf/2015/1507LearningLabAmbriOverview_Giudice.pdf. Accessed 18 March 2016.
3. BENESTAD, R. E.: A mental picture of the greenhouse effect. Theoretical and Applied Climatology, January 2016, 10 p.
4. EPI (EARTH POLICY INSTITUTE) Data Center. Available at: http://www.earth-policy.org/data_center/C23. Accessed 11 March 2016.
5. IEA (INTERNATIONAL ENERGY AGENCY): Redrawing the Energy-Climate Map. World Energy Outlook Special Report. Paris, Corlet, June 2013, 124 p.
6. JOHN, J. S.: 24M Unveils the Reinvented Lithium-Ion Battery. Greentech Media, June 22 2015. Available at: http://www.greentechmedia.com/articles/read/24m-unveils-the-reinvented-lithium-ion-battery. Accessed 24 February 2016.
7. LUO, X., WANG, J., DOONER, M., CLARKE, J.: Overview of Current Development in Electric Energy Storage Technologies and the Application Potential in Power Systems Operation. Applied Energy, vol. 137, 2015: 511–536.
8. MAJUMDER, R. Some aspects of stability in microgrids. IEEE Transactions on Power Systems, vol. 28, no. 3, 2013: 3243–3252.
9. MARNAY, CH., ZHOU, N., QU, M., ROMANKIEWICZ, J.: Lessons Learned from Microgrid Demonstrations Worldwide. Report LBNL–5825E, Lawrence Berkeley National Laboratory, CA, USA, 2012, 39 p.
10. MENG, L., LUNA, A., DRAGICEVIC, T., VASQUEZ, J. C., GUERRERO, J. M.: Microgrid supervisory controllers and energy management systems: a literature review. Renewable and Sustainable Energy Reviews, vol. 60, 2016: 1263–1273.
11. MULLAN, J., HARRIES, D., BRAUN, T., WHITELY, S.: The technical, economic and commercial viability of the vehicle-to-grid concept. Energy Policy, vol. 48, 2013: 394–406.
12. PETERSON, S. B., WHITACRE, J. F., APT, J.: The economics of using plug-in hybrid electric vehicle battery packs for grid storage. Journal of Power Sources, vol. 195, 2013: 2377–2384.
13. RAMONAS, Č., ADOMAVIČIUS, V.: Research of the reactive power control possibilities in the grid-tied PV power plant. Elektronika ir Elektrotechnika (Electronics and Electrical Engineering), vol. 19, no. 1, 2013: 31–34.
14. RAMONAS, Č., ADOMAVIČIUS, V., KEPALAS, V.: Research of the power conversion processes in the system of power supply from a number of wind turbines over the one grid-tird inverter. In: Proceedings of International Conference Electrical and Control Technologies, 7–8 May 2009, pp. 368-373, KTU, Kaunas, Lithuania.
15. REN21: Global Status Report, Paris, 2014, 216 p.
16. STANDRIDGE, CH. R. – CORNEAL, L.: Remanufacturing, Repurposing and Recycling of Post-Vehicle-Application Lithium-Ion Batteries. Report 12–20, San Jose State University, CA, USA, June 2014, 74 p.
17. UN COP21: Framework Convention on Climate Change. Paris, 2015, 32 p. Available at: https://unfccc.int/resource/docs/2015/cop21/eng/l09r01.pdf. Accessed 17 February 2016.
18. UN IPCC WGIII: Summary for Policy Makers. Fifth Assessment Report, 2014, 31 p.
19. WANG, K., JIANG, K., CHUNG, B., OUCHI, T., BURKE, P. J., BOYSEN, D. A., BRADWELL, D. J., KIM, H., MUECKE, U., SADOWAY, D. R.: Lithium–antimony–lead liquid metal battery for grid-level energy storage. Nature, vol. 514, October 16, 2014: 348–350.

Corresponding author:

Jonas Valickas,, Panevėžys Institute at Kaunas University of Technology, S. Daukanto 12–113, LT– 35212 Panevėžys, Lithuania; e-mail: jonas.valickas@ktu.lt

METHODS OF HARVESTING OF MIXED CROPS

N. Aldoshin

The Russian state agricultural university – the Moscow agricultural academy named after K. A. Timiryazev, Russia

Abstract
The mixed crops of grain grains and leguminous crops can promote receiving bigger quantity of production from each hectare of a cultivated area. Now combines which could fully provide high-quality harvesting of the mixed crops completely aren't issued. When using combine harvesters with the classical scheme of the threshing and separating device the way of harvesting of the mixed crops for two passes of the combine is offered. An example of harvesting of the mixed crops is reviewed: triticale – a white lupine.
In rotor combines process of the threshing and separation happens in one body which at the same time threshes and separates the grain. In such solution rather big technological gaps between a rotor and a separation unit are established. Because of repeated impact on harvested material process of the thresh turns out rather effective, and the area of separation several times is more, than in classical scheme. When using combine harvesters with axial rotor on harvesting of the mixed crops, various schemes of modernization of their design are offered that allows making harvesting of crops with different technological properties.

Key words: mixed crops, grain crops, legumes, method of harvesting, combine harvester, threshing-separating device.

INTRODUCTION

Agricultural producers are faced with a problem of receiving bigger quantity of production from each hectare of crops. One of ways of the solution of this task can be the use of the mixed crops. In this case, productivity of each of the cultures entering the mixed crops decreases in relation to their pure crops, but the general exit of production from each hectare can increase.

Cultivation of various mixed crops of grain grains and leguminous cultures is possible. For example, barley – a narrow-leaved lupine, oats – a narrow-leaved lupine, wheat – a narrow-leaved lupine, oats – peas, oats – Vika, triticale – a white lupine, etc. In addition to the direct benefits of such crops may be present and other positive aspects. In the mixed crops of a lupines albus and triticale, we have a natural way of fight against weeds. Such mixed crops aren't littered with weed plants and at the same time we save on herbicides. Given that lupines albus in their biological features metabolizes nitrogen from the air and stores it, it improves the quality of cereal crops. Such crops are good predecessors for any other cultures which are grown up in crop rotations together with them.

One of the most difficult stages of cultivation of grain crops in the mixed crops is their harvesting. It is connected with the fact that it is at the same time necessary to clean cultures with absolutely various technological properties. Legumes easily threshed their grain larger and more susceptible to damage. Conversely, cereal crops require a more "hard" mode of threshing, grain finer and less prone to injury. Readiness for harvesting of mixed crops is determined by degree of a maturity of plants of a lupine when more than 90% of beans at moisture content of seeds grow brown in them 16-18% - (ALDOSHIN, 2015).

Designs of modern combines according to the technological scheme of the threshing and separating device (TSD) can be divided into three main types: classical, rotor and combined. In combines of the classical scheme the threshing and separation of grain harvested material is carried out by a threshing drum and a keyboard straw separator (ALDOSHIN, 2015).

For harvesting of unevenly ripening cultures various designs of threshing mechanism which are carrying out the differentiated thresh have been offered. Heterogeneity of mechanical communications of seeds with a maternal plant demands differential impact on vegetable harvested material at the threshing. The essence of a design of such devices is that at first there is a threshing of more mature grain, and then intensity of a thrashing for less mature increases.

The idea of the two-phase thresh of grain has formed the basis of production of models of two drum combines of the Rostselmash, Krasnoyarsk and Taganrog the of plants for the production of combines in the Russian Federation, firms "John-Deere", "New Holland", "Case". On the basis of a two-phase method also rotor combines have been created subsequently (ALDOSHIN, 2015).

In threshers of a new series of LEXION combines of CLAAS firm the advanced threshing -separating APS device which the firm has for the first time used in MEGA series combines is used. Such device provides acceleration of the movement of grain harvested material thanks to the additional bitter located in front of a threshing drum. APS system increases the speed of the movement of grain harvested material because of what her giving becomes more uniform. At the same time the centrifugal forces operating on grain increase, his separation through lattices of a concave which area is doubled almost, in comparison with one-drum threshing devices improves.

Threshing and separating device with a rotational separator is used in combines of NEW HOLLAND, MASSEY FERGUSON firms and combines of other firms, similar on a class. In new classical combines of the ACTIVA, BETA and CEREA series of MASSEY FERGUSON firm the threshing mechanism of different designs which basis is the 8-bilny threshing drum are applied. For an intensification of process of separation in combines of the CEREA series the advanced design of a concave with the doubled sizes of the separating openings on the last four levels is used.

As it follows from above, combine harvesters suitable for mixed crops harvesting are not available now despite of its need. That is why the main aim of this article is to evaluate the possibilities of its development and to offer its possible design solutions.

MATERIALS AND METHODS

Experiments were done with combine harvesters with classic threshing and separating device (TSD). Triticale crop mixed with white lupine *(lupines albus)* was harvested during our experiments. The dependences between triticale threshing losses and the gap between threshing drum and threshing concave were studied at the first part of the experiments. Consequently, micro and macro damages of threshed white lupine grains were observed.

Another part of experiments were done with two phase harvesting. Harvesting was carried out by two passes of the combine. The example of performance of this way of harvesting has been carried out in September, 2014 on skilled fields in educational economy of Kalinin of the Tambov region of the Michurinsk area.

Harvesting of the mixed crops of a white lupine *(lupinus albus)* and triticale has been carried out. At the first pass technological settings corresponded to harvesting of a white lupine. In the bunker collecting grain of a white lupine and partially triticale was carried out. The harvested material threshed for the first pass was stacked in a row. At the second pass of the combine made selection of rows with the threshing at the technological settings corresponding to triticale harvesting. After harvesting of the mixed crops threshing losses and free grain, macrodamages (crushing, crush, a collapse) and microdamages (a jointing, damages of a germ, endosperm, covers, etc.) grains were defined.

RESULTS AND DISCUSSION

Qualitative indicators of performance combine harvesters with classic TSD are shown in Fig. 1 - 3.

From the analysis of the data presented in Fig. 1 - 3 follows that an increase in the gap at the outlet of the threshing drum device for different speeds when harvesting mixed crops triticale thrashing losses increased and the damage of white lupine are reduced on the contrary. This condition does not allow both to perform agro-technical requirements for both the mixed harvested crops (ALDOSHIN, 2016, ALDOSHIN, 2015).

For example, to make triticale harvesting by a combine harvester with the classical the threshing and separating device (TSD) according to agrotechnical requirements it is necessary to set:

• linear speed of scourges of a threshing drum to 30-32 m/s;

• a gap between a threshing drum and a concave at the exit to 2-4 mm.

And respectively for a white lupine:

• linear speed of scourges of a threshing drum to 15 - 18 m/s;

• a gap between a threshing drum and a concave at the exit to 14 - 18 mm.

Now combine harvesters which could fully provide high-quality harvesting of the mixed crops completely aren't issued. Actually we need two combines which are consistently working one after another. In this case the next way of harvesting of the mixed crops for combines with classical threshing mechanisms can be offered.

These designs of threshing mechanism for the differential thresh can't solve a problem of harvesting of the mixed crops of grains and leguminous cultures, for example, of a lupine and triticale as technological properties of cultures are too various. Therefore, technological settings of threshing mechanism of a combine harvester for harvesting of these cultures have to be various. In addition, after threshing legumes we have to select it completely out of the grain heap (separate out), and only then proceed to the threshing and separating of grain crops, although some of it we already threshed and separated with leguminous. Actually we need two combines which are consistently working one after another. In this case the next way of harvesting of the mixed crops for combines with classical threshing mechanisms can be offered.

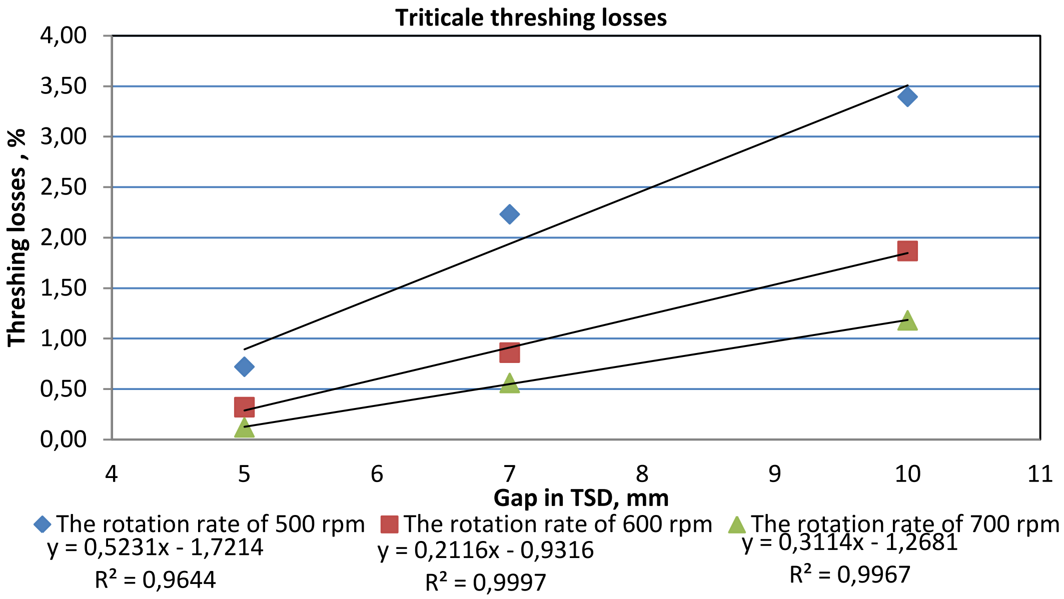

Fig. 1. – Dependence of triticale thrashing losses on the gap at the outlet of the threshing and separating device for different speeds when harvesting mixed crops

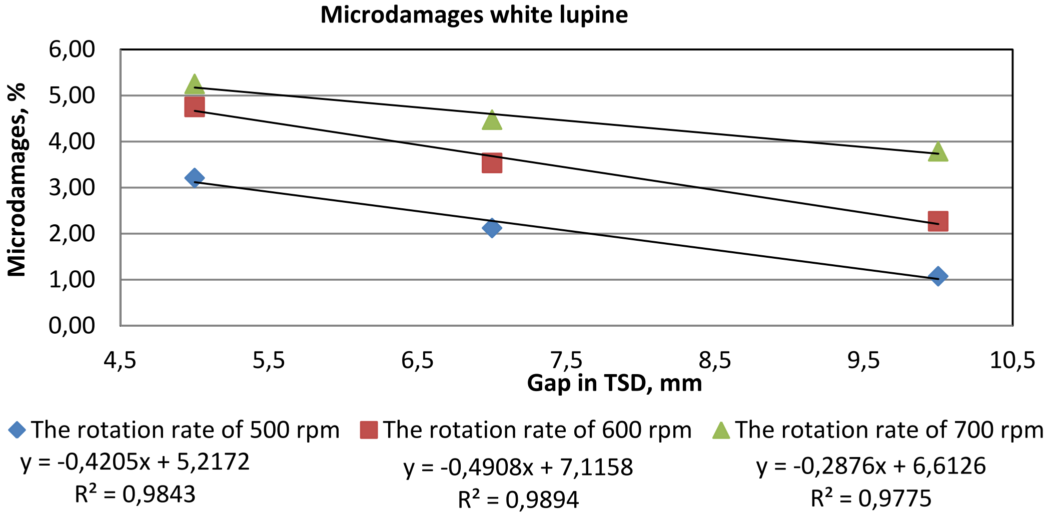

Fig. 2. – Dependence of microdamages of a white lupine *(lupinusalbus)* on a gap at the exit of the threshing and separating device for different speeds of a drum when harvesting of the mixed crops

During two phases threshing, at the first pass threshing losses of white lupine was absent, damages have made 3%. Triticale – not threshed 65%, damages were absent. At the second pass white lupine grain in the threshed harvested material wasn't. Triticale threshing losses have made 0.5%, triticale grain damages – 1.5%. This conformed to agro technical requirements of harvesting of grain grains and leguminous cultures. When harvesting of the mixed crops of such cultures for one pass there is no opportunity to receive losses

and grain damage at the level of agro technical requirements.
In rotor combines, the process of threshing and separation happens in one body which at the same time threshes and separates grain (SRIVASTAVA ET AL., 1993; STOUT AND CHEZE, 1999). Due to intensity of process of separation in rotor working bodies the minimum losses of grain even are provided at high productivity of cultures, at the increased moisture content and at the presence of weeds.

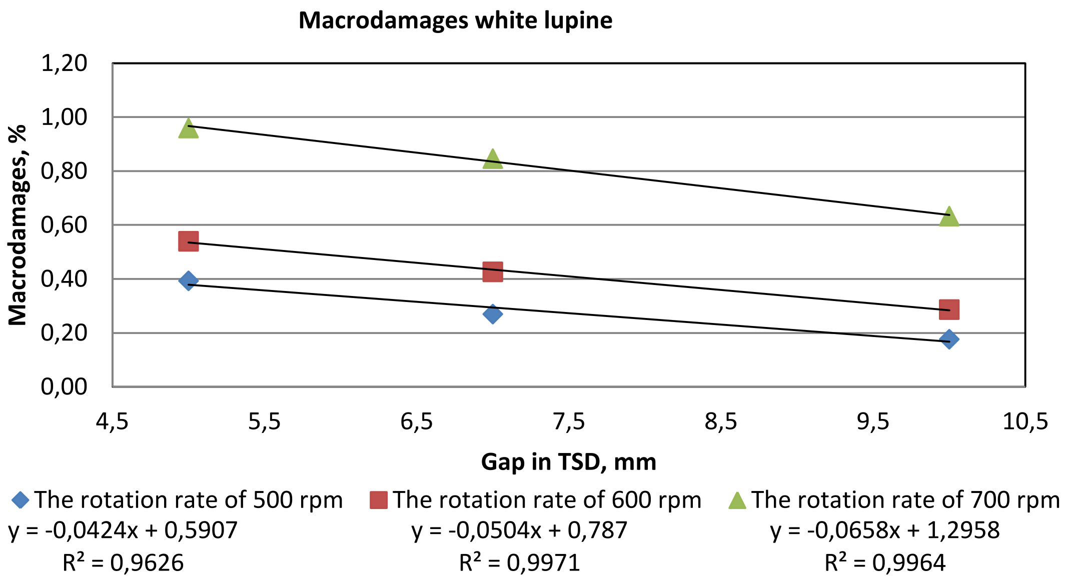

Fig. 3. – Dependence of macro damages of a white lupine *(lupinusalbus)* on a gap at the exit of the threshing and separating device for different speeds of a drum when harvesting of the mixed crops

On the basis of rotor combines various options of harvesting of the mixed crops can be also realized. For example it is possible to use a consecutive combination of axial and rotor threshing mechanisms with tangential feeding of the harvested material (Fig. 4).

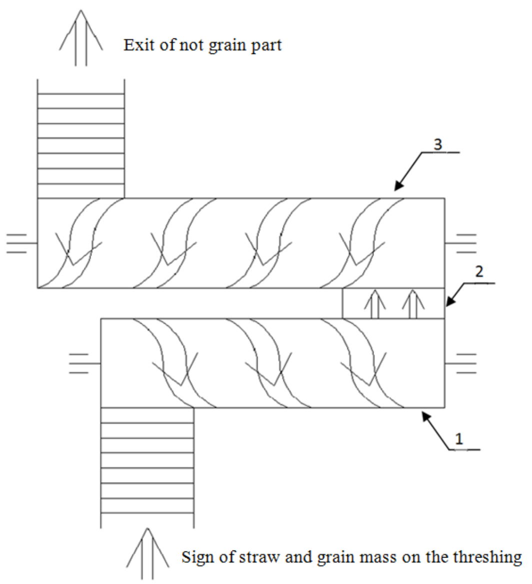

Fig. 4. – A consecutive combination of two axial rotor threshing mechanisms with tangential feeding of harvested material for harvesting of the mixed crops

The combined device works as follows. The conveyor of an inclined chamber, tangential gives the processed harvested material to a rotor of the first threshing-separating device 1 which is adjusted on a "soft" operating mode where grain of easily threshing bean culture not only threshing completely but also is completely separated at the movement of harvested material on a screw trajectory. Full release of grain of bean culture is provided with the big area of the threshing and separation in the first device 1. At the same time part of cereal grain is also threshed and separated.
The remained harvested material is tangentially transmitted through the sending device 2, in the second threshing - separating device 3 which works in the "rigid" mode that provides full threshing of the remained cereal material. Considerable length of a screw trajectory of the movement of the processed harvested material in threshing space, at continuous intensive shock influence promotes full release of grain according to agro technical requirements.
Other option of use of axial threshing mechanisms on harvesting of the mixed crops can be realized due to its division into two parts, each of which provides the threshing and separation of one of cultures. The threshing mechanism with the body divided into two

parts is offered. Each of parts of a body has a possibility of rotation (Fig. 5) different from each other.

The device works as follows. Processed harvested material of the feeder enters the lead-area of threshing mechanism. Under the influence of the rotor blades and the guide casing (1) it acquires spiral motion. At the same time the considerable part of bean culture is threshed. At the same time process of separation of free grain of bean culture through openings of conic part of a casing in a zone "A" begins that reduces grain damage. The remained grain is threshed by scourges (4) rotors of the first zone. Full release of free grain of bean culture through openings of a casing of a zone "A" happens at shock influence of the separating levels of the rotor (5). As the direction of rotation of a rotor and a casing of the first zone coincide that and intensity of shock influence is insignificant that excludes damage of grains of bean culture. Besides gaps between a rotor and a threshing concave are increased, i.e. correspond to the modes of harvesting of leguminous cultures. Speed of blow of scourges of a rotor to the threshed harvested material decreases by size corresponding to the speed of rotation of a threshing concave. Such technological parameters for the first part of threshing mechanism provide agro technical admissible requirements for harvesting of leguminous cultures, and also the partial thresh and separation of grain culture grains.

In a zone "B" the casing has opposite rotation concerning a rotor. At the expense of it the speed of blow of scourges (6) and the separating levels of the rotor (7) on the threshed harvested material increases at a size corresponding to the speed of rotation of a concave. At the same time gaps between scourges and levels of a rotor and the separating concave are reduced. Such technological parameters of axial TSD provide complete threshing and separation of grain cereal crops. The remained part of straw is brought out of the device through straw separator part (8) of the device.

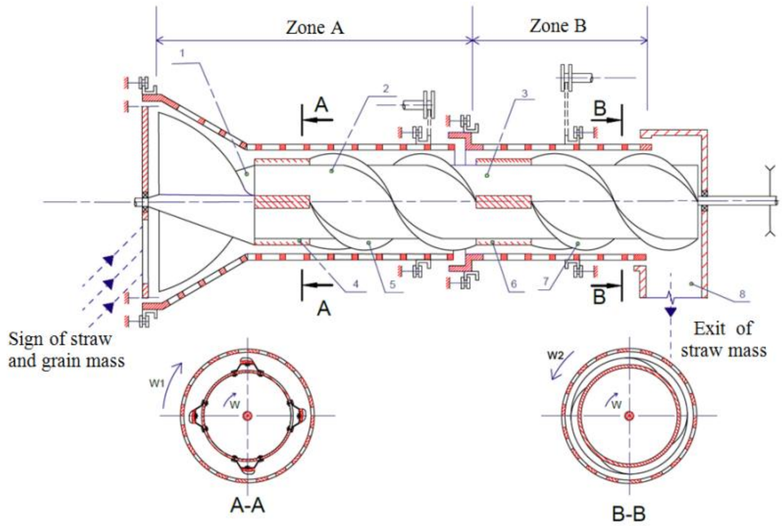

Fig. 5. – Axial threshing mechanism for harvesting of the mixed crops with separately rotating parts of a body

Also for harvesting of the mixed crops of grain crops the axial threshing mechanism having a two-section rotor (Fig. 6) can be offered. It consists of a two-part rotor with a tangential lead-in part. Each of parts of a rotor includes the threshing and separating parts. The separating casing clasps a rotor on all his extent. Section "A" of a rotor has the low speed of rotation corresponding to the threshing of leguminous culture. The threshing part provides the threshing of leguminous culture and the separating part its separation.

The section "B" of a rotor has the increased rotation speed corresponding to threshing of cereal crop. At the expense of it there is a hauling of a layer of the threshed harvested material that improves grain separation process. At the same time the threshing part of section "B" of a rotor provides the final thresh of cereal crop, and the separating part its full allocation.

The device works as follows. Harvested material, lead-through part of the housing (1), is captured pests threshing part (2) of the section "A" of the rotor and threshed in a "soft" mode, typical of legumes. At the same time the threshed vegetable harvested material receives spiral three-dimensional motion between a rotor and a concave (4). After release of grains from beans in the separating part of a rotor (3) there is their final allocation through openings of a concave (4).

The rotor section "A" at the expense of the drive (7) has the low speed of rotation corresponding to the threshing of leguminous crop.

The remained grain harvested material, moving, gets to an area of coverage of section "B" of a rotor. The full thresh and separation of cereal crop is provided at the expense of the increased speed, the movement of scourges (5) and the separating levels of rotors (6) located on section "B". The rotor section "B" also has the independent drive (8). After threshing and separation of grain grains of cultures crop is derived from the device through of the housing (9).

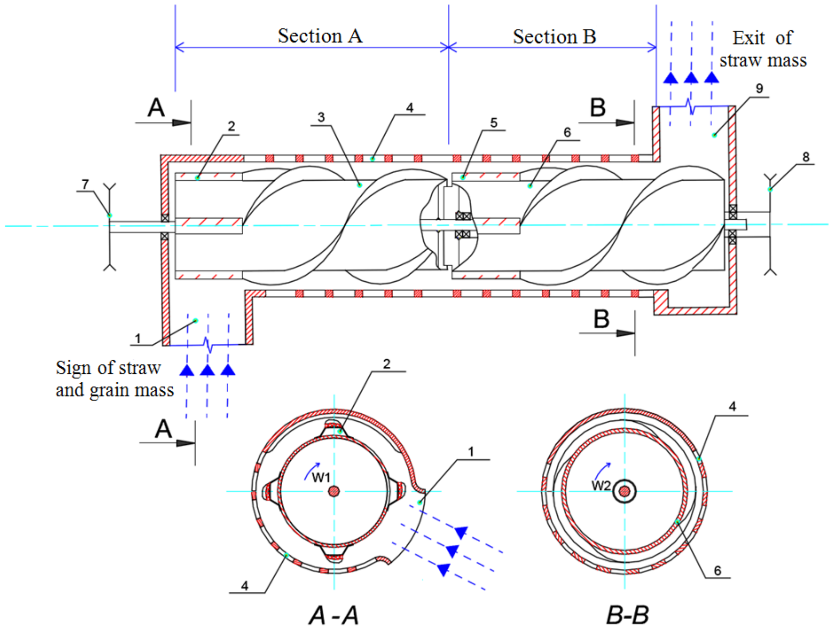

Fig. 6. – Axial threshing mechanism for harvesting of the mixed crops consisted from two sections of rotor

CONCLUSIONS

1. For harvesting of the mixed crops of grain and leguminous crops the combine harvesters with the classical threshing-separating system it is possible to use by the way based on two passes of a combine. At the first pass, harvested material is mown with the thresh, at technological settings of the leguminous crops corresponding to harvesting, then the lots is stacked in a row and at the second pass carry out selection of a row with the final thresh of harvested material at technological adjustments corresponding to harvesting grain crops.

2. On the basis of rotor combines, various options of harvesting of the mixed crops can be also realized. It is possible to use a consecutive combination of axial threshing mechanisms with tangential feeding of harvested material.

3. Advanced designs of axial and rotor threshing mechanisms with separately rotating parts of a concave or from a two section rotor can be also applied to harvest of the mixed crops.

REFERENCES

1. ALDOSHIN, N. V.: Justification of technological parameters of combines on harvesting of a lupinusalbus/ N. V. Aldoshin, A.A.. Zolotov, A.S. Tsygutkin, In, D. Suleev, A.E. Kuznetsov, N. A. Aladyev, Mull Bakhaa // Achievements of science and technology of agrarian and industrial complex, – ISSN. 0235-2451, No. 1, T. 29, 2015: p. 64 - 66.
2. ALDOSHIN, N. V.: Definition of damages of grain of a lupinusalbus while harvesting / N. V. Aldoshin, A.A. Zolotov, A.S. Tsygutkin, V.D. Suleev, A.E. Kuznetsov, N. A. Aladyev, Mull Bakhaa // Tractors and agricultural cars, ISSN 0235-8573, No. 2, 2015: p. 26-29.
3. ALDOSHIN, N. V.:Harvesting of mixed crops of cereals by stripper header / N. V. Aldoshin, A.A. Zolotov, A.S. Tsygutkin, N. A. Lylin, MallaaBakhaa // the Bulletin of federal public educational institution of higher education "The Moscow state agroengineering university of V.P. Goryachkin". No. 1 (71). 2016: p. 7-13.
4. ALDOSHIN, N. V.: Technical ensuring quality of the mechanized works: Monograph / N. V. Aldoshin, R. N. Didmanidze. M.: RGAU publishing house – MSHA, 2015: p. 188.
5. ALDOSHIN, N. V.: A comparative assessment of combines on harvesting of a lupinusalbus / N. V. Aldoshin // the Rural machine operator, ISSN 0131-7393, No. 11, 2015: p. 10-13.
6. ALDOSHIN, N. V.: Mechanization of harvesting of the mixed crops of grain crops / N. V. Aldoshin, A.A. Zolotov, A.S. Tsy-

gutkin, MallaaBakhaa // Tractors and agricultural cars, ISSN 0235-8573, No. 10, 2015: p. 41-45.
7. SRIVASTAVA, A. K., GOERING, C. E., ROHRBACH, R. P.: Engineering Principles of Agricultural Machines, ASAE Textbook No. 6, ASAE 2950 Niles Road, St Joseph, Michigan 49085-9659, USA, 1993, ISBN 0-929355-33-4, pp.601.
8. STOUT, B. A., CHEZE, B: CIGR Handbook of Agricultural Engineering, Volume III – Plant Production Engineering. ASAE 2950 Niles Road, St Joseph, Michigan 49085-9659, USA, 1999, ISBN 1-892769-02-6, pp.632.

Corresponding author:
Nikolay V. ALDOSHIN, PhD (Doct. Techn. Sci.), professor, Head of Department of Agricultural Machines Russian State Agrarian University – Moscow Agricultural Academy named after K.A. Timiryazev, e-mail: naldoshin@yandex.ru

INFLUENCE OF BIOBUTANOL ON WEAR OF FUEL INJECTION SYSTEM

Z. Aleš[1], J. Pavlů[1], M. Pexa[1], J. Svobodová[2], M. Kučera[3], B. Peterka[1], J. Pošta[1]

[1]Department for Quality and Dependability of Machines, Faculty of Engineering, Czech University of Life Sciences Prague, Czech Republic
[2]Faculty of production technology and management, Jan Evangelista Purkyně University in Ústí nad Labem, Czech Republic
[3]Department of Mechanics, Mechanical Engineering and Design, Faculty of Environmental and Manufacturing Technology, Technical University in Zvolen, Slovak Republic

Abstract
Effort to reduce the consumption of fossil energy sources leads to their replacement by renewable sources. In the automotive industry it is substitution of diesel and petrol with biofuels based on bio-oils and bioethanol, mainly from crop production. Fuel injection systems of modern combustion engines work with high operational pressures. This is possible because of precise manufacture of individual parts of fuel injection system. Fuel quality has a vital impact on the wear of these important components. The aim of this paper is to compare the impact of biofuels on the wear of the fuel injection system. During the experiment were examined mixtures of diesel oil and biobutanol. For analysis was used tribometer Reichert tester M2. Part of real fuel injector was used as a test roller. Paper proved the hypothesis that greater share of biofuels in conventional fuels increases wear of parts of fuel injection system.

Key words: reichert tester, wear, bioethanol, fuel injection system.

INTRODUCTION

Surface preparation is an important factor for the practical application of machine components, particularly in situations such as the precise alignment and high strength applications. It is necessary to pay attention to optimization of machining process. Influence of machining is a significant factor affecting the life of machine components within various applications (MÜLLER ET AL., 2013).

Parts of fuel injection system are very difficult in terms of surface preparation and choice of proper materials. Fuel injection systems of modern combustion engines also work with high operational pressures. Fuel quality has a vital impact on the wear of these important components. Effort to reduce the consumption of fossil energy sources leads to their replacement by renewable sources (MAŘÍK ET AL., 2014). In the automotive industry it is the substitution of diesel and petrol with biofuels based on bio-oils and bioethanol, mainly from crop production (HÖNIG ET AL., 2015).

Newly produced biofuels can lead to increased wear of the fuel injection system due to reduced lubrication capability compared to conventional fuel. Increased wear of the fuel injection system leads to failures and reduces durability of the entire fuel injection system. Increased wear of the fuel system is associated with the formation of the wear particles, which consequently accelerate the process and the intensity of wear (HÖNIG ET AL., 2014).

Wear is a permanent adverse change on the surface or dimensions of rigid bodies, caused by the interaction of functional surfaces, or functional surface and medium which causes wear. Wear occurs as a removal or relocation of particular matter from the surface by mechanical effects, sometimes accompanied by other factors, such as chemical or electrochemical. Generally, there can be classified six basic types of wear: adhesive, abrasive, erosive, cavitation, vibration and fatigue (VALÁŠEK, MÜLLER, 2015).

Adhesive wear is typical for cases where there is a slip of two rigid bodies, together forced down with normal force. As a result of contact between them there occurs the rupture of adsorption layers and surface oxide layers and creation of the interfacial micro-junctions, which are subsequently disarranged. Such a process generates particles having the shape of flakes with a diameter of 5 to 10 μm and a thickness of 0.25 – 0.75 μm, the size should not exceed 15 μm. The shape of adhesive particle is shown in Fig. 1. Adhesively worn surface is smooth, polished (PEXA ET AL., 2015).

Abrasive wear is typical for cases when two surfaces are in contact and that one or both are rough and hard, or in case when there are presented free particles between two hard surfaces. The abrasive particles have shape of wires, spirals, chips with a length of tens to hundreds of micron and tenth micron of thickness. Abrasively worn surface is rough, scratched (MÜLLER ET AL., 2015).

Fatigue wear is characterized by progressive accumulation of defects in the functional surface layer during repeated contact stress (roller bearings, gear wheels, etc.). Fatigue wear particles may have a spherical (round) shape with a diameter of 2 – 5 µm, laminar as a result of pressing laminar spherical particles in the path of the bearing roller and may have the shape of triangles of size up to tens of µm (MÜLLER ET AL., 2010).

The aim of this paper is to prove or disprove the hypothesis that biofuels increase wear of parts of fuel injection system.

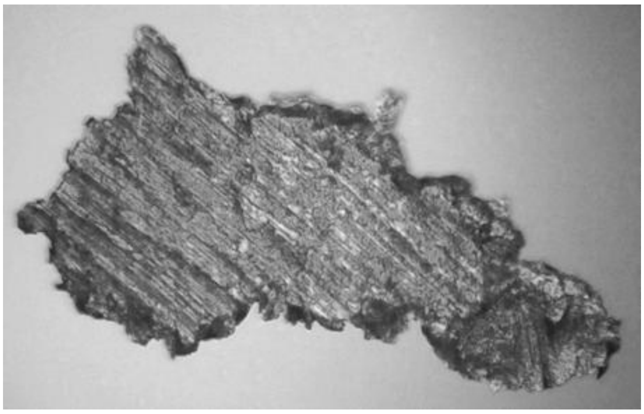

Fig. 1. – Example of shape of adhesive particle (ALEŠ ET AL., 2016)

MATERIALS AND METHODS

The aim of the measurements was to assess the impact of biobutanol (according to different share of biobutanol in diesel fuel) on wear of fuel injection system. Standard ISO 12156-1:2006 is used as a test method using the high-frequency reciprocating rig (HFRR), for assessing the lubricating property of diesel fuels. Test method according to EN ISO 12156-1 is not available at workplace of authors and therefore test device Reichert tester M2 was used. Reichert tester (Fig. 2) belongs to a group of devices which simulates real frictional contact. Frictional contact is evaluated by load carrying capacity of lubricating film. Test roller is firmly clamped and pushed by a weight on the rotating slip ring (made of specially alloyed steel) through a lever mechanism during a defined distance. The lower third of the slip ring is immersed in the oil bath. Sufficient quantity of oil is fed into contact with the test roller during rotation of slip ring. The better lubricity of the fuel is, the smaller elliptical area on the test roller is formed. The size of elliptical area *A* is calculated according to Equation 1.

$$A = \pi \cdot \frac{l}{2} \cdot \frac{d}{2} = 0.785 \cdot l \cdot d \qquad (1)$$

Where: A - elliptical wear area (mm^2); l - length of elliptical wear area (mm); d - width of elliptical wear area (mm)

For the purpose of the experiment there were prepared 10 test rollers (plungers of line high-pressure pump) of material used to produce components of fuel injection systems (element EA8Pg-35). Test rollers were cut using a cutter metallurgical Struers Discotom using a liquid coolant. Test rollers were shortened to the desired length, diameter was not machined. Hardness HV1 and HRC was measured at 30 points equally spaced on the surface of test roller. Vickers hardness at a low load i.e. HV1 (9.807 N) was measured on the surface of test roller. Hardness value HV1 was 839.4 ± 9.4, i.e. variation coefficient was 1.12%. Additionally, Rockwell hardness measurements using a scale HRC was done. The result of HRC value was 65.24 ± 0.31, i.e. variation coefficient was 0.47%. From the measurement results it is obvious an even hardness on the surface of the test samples.

Each test roller was used three times to test lubricating properties of the fuels at laboratory device Reichert tester. Tested fuels were as follows: pure diesel, diesel with a share of 25%, 50%, 75% of biobutanol and 100% biobutanol. Each fuel was subjected to tests of lubricating properties 6 times. Reichert tester was set to the following parameters: 50 m trajectory, 500 rpm and 1.5 kg weight load. Set parameters were lowered compare to standard parameters (100 m trajectory, 980 rpm and 1.5 kg weight load) due to safety reasons.

Elliptical wear area can be evaluated by use of the scanning electron microscopy (SEM) (HEINRICHS ET AL., 2014). There is a clearly recognizable difference between the machined surface and elliptical wear area (Fig. 3).

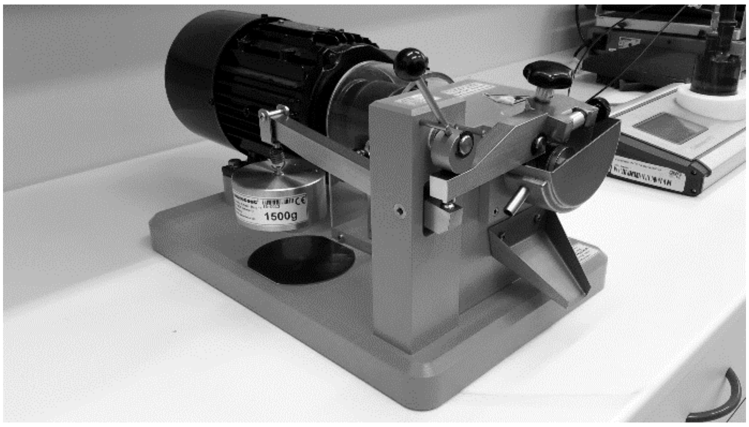

Fig. 2. – Reichert Tester M2

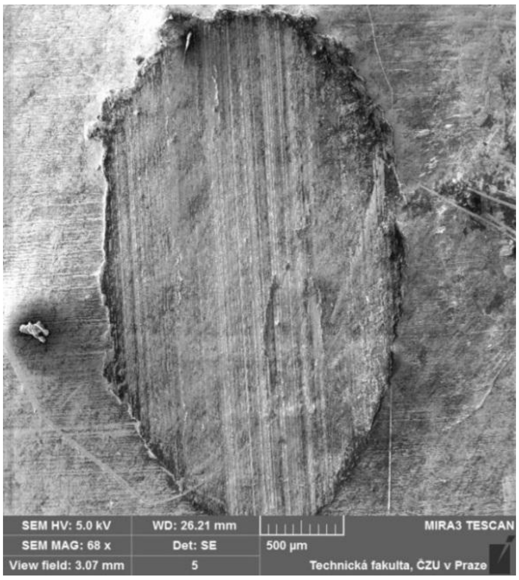

Fig. 3. – SEM image – Elliptical wear area after Reichert test (ALEŠ ET AL., 2016)

RESULTS AND DISCUSSION

Altogether of 30 measurements were performed on the device Reichert tester M2. Results of sizes of elliptical wear area are shown in Tab. 1.

Tab. 1. – Size of elliptical wear area after Reichert test according to different fuels

Number of Elliptical wear area	Size of elliptical wear area (mm^2)				
	Diesel	Share of biobutanol in diesel			Biobutanol
	100 %	25 %	50 %	75 %	100 %
1	22.9975	26.6084	25.0723	27.8678	26.2954
2	24.1769	26.2990	26.9214	25.3781	27.2345
3	25.0723	25.9896	27.8678	27.2345	28.1736
4	23.3557	26.2961	25.8518	26.7255	27.2586
5	23.6095	26.4011	27.7834	26.9239	27.2446
6	24.5855	26.4290	25.9985	26.1202	27.8052

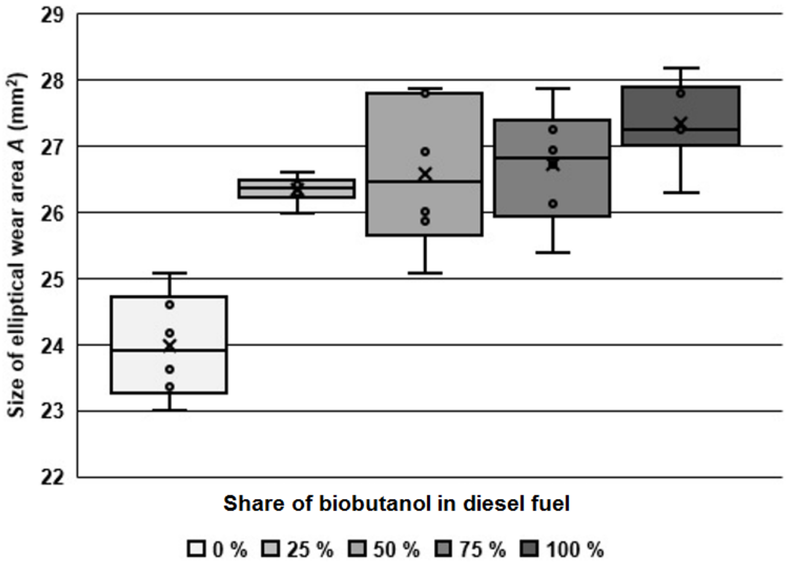

Fig. 4. – Size of elliptical wear area dependent on share of biobutanol in diesel fuel

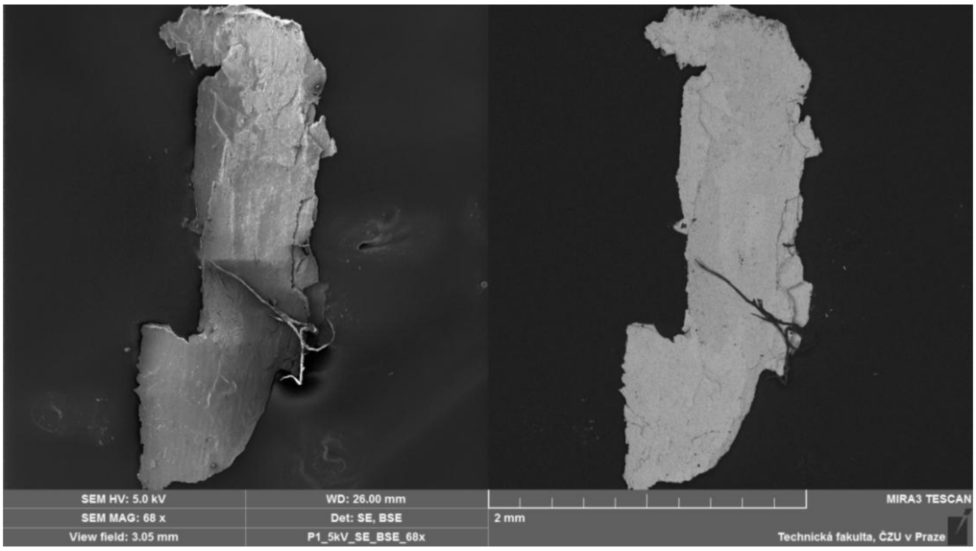

Fig. 5. – Abrasive wear particle generated during Reichert test with 100 % biobutanol

Box plot (Fig. 4) was created from the data in Tab. 1. From displayed data is obvious that a relatively small proportion of biobutanol in diesel causes a decline of lubricity, which affects the size of elliptical wear area. On average biobutanol has 12% larger elliptical wear area than pure diesel. Lower lubricity relate to the generation of wear particles. Loose wear particles can cause intense abrasive wear in the fuel systems particularly in the injector. These generated wear particles (Fig. 5) significantly reduces durability of the entire fuel system. Besides that, when the biobutanol dilute lubricating engine oil it often leads to a shortening of the recommended oil drains (between 30% and 60%) and an increase in wear (GILI ET AL., 2014).

CONCLUSIONS

Designed of used materials, surface finishing and precision of manufacturing are essential for a properly functioning system fuel system. Development of biofuels often raises the question of their ability to ensure proper lubrication capabilities in fuel systems. Described experiment was focused on measuring of lubricating properties of biobutanol as an alternative to diesel fuel. Reichert Tester M2 was used to verify this assumption. Results show that even a relatively low share of bioethanol in diesel has a significant influence on the size of elliptical wear area. Presence of biobutanol in diesel increases the size elliptical wear area on average by 12 %. Increase of the size of elliptical wear area comparing pure Diesel and pure biobutanol was even 14 %. The results show that biobutanol has a lower lubricating ability and it would be appropriate to verify this assumption in real operation. Other solution might be to consider possibility to suggest a suitable type of additive to enhance lubricating abilities of biobutanol.

ACKNOWLEDGEMENTS

Paper was created with the grant support – IGA CULS Prague 2016: 31190/1312/3117 Effect of mixtures of biofuels on production of nitrogen oxide and smoke of combustion engine during NRSC.

REFERENCES

1. ALEŠ, Z., PAVLŮ, J., MÜLLER, M., SVOBODOVÁ, J., LEBEDEV, A., YUROV, A., PEXA, M., LINDA, M.: Influence of Abrasive - Free Ultrasonic Finishing Process of Steel on Wear. Manufacturing Technology, 16 (1), 2016: pp. 4-12.
2. HEINRICHS, J., OLSSON, M., JENEI, I. Z., JACOBSON, S.: Transfer of titanium in sliding contacts-new discoveries and insights revealed by in situ studies in the SEM. Wear, 315 (1-2), 2014: pp. 87-94.
3. HÖNIG, V., HORNÍČKOVÁ, Š., HROMÁDKO, J.: Analysis of the distillation curves of mixtures of biobutanol with gasoline. Advanced Materials Research, Volume 1030-1032, 2014: pp. 25–28.
4. HÖNIG, V., KOTEK, M., MAŘÍK, J.: Use of butanol as a fuel for internal combustion engines. Agronomy Research 13, 2015: pp. 333–340.
5. GILI, F., IGARTUA, A., LUTHER, R., WOYDT, M.: The impact of biofuels on engine oil performance. Lubrication Science, 23 (7), 2011: pp. 313-330.
6. MAŘÍK, J., PEXA, M., KOTEK, M., HÖNIG, V.: Comparison of the effect of gasoline - ethanol E85 - butanol on the performance and emission characteristics of the engine Saab. Agronomy Research 12, 2014: pp. 359–366.
7. MÜLLER, M., CHOTĚBORSKÝ, R., HRABĚ, P.: Application of Overlay Material on Soil Processing Tools for Purpose of Increasing their Abrasive Wear Resistance. Czech Sugar and Sugar Beet Journal, 131 (9-10), 2015: pp. 279 -283.
8. MÜLLER, M., CHOTĚBORSKÝ, R., VALÁŠEK, P., HLOCH, S.: Unusual possibility of wear resistance increase research in the sphere of soil cultivation. Tehnicki Vjesnik - Technical Gazette, 20 (4), 2013: pp. 641-646.
9. MÜLLER, M., RUŽBARSKÝ, J., PAŠKO, J., ŽARNOVSKÝ, J., HRABĚ, P.: The quality of cut surface without cooling. In: Trends in Agricultural Engineering 2010, Prague, Czech University of Life Sciences Prague, Faculty of Engineering, 2010: pp. 459-462.
10. PEXA, M., ČEDÍK, J., MAŘÍK, J., HÖNIG, V., HORNÍČKOVÁ, Š., KUBÍN, K.: Comparison of the operating characteristics of the internal combustion engine using rapeseed oil methyl ester and hydrogenated oil. Agronomy Research, 13, 2015: pp. 613–620.
11. VALÁŠEK, P., MÜLLER, M.: Abrasive wear in three-phase waste-based polymeric particle composites. Tehnicki Vjesnik - Technical Gazette, 12 (2), 2015: pp. 257-262.

Corresponding author:

Ing. Zdeněk Aleš, Ph.D., Department for Quality and Dependability of Machines, Faculty of Engineering, Czech University of Life Sciences Prague, Kamýcká 129, Praha 6, Prague, 16521, Czech Republic, phone: +420 22438 3254, e-mail: ales@tf.czu.cz

MATERIAL FLOW ANALYSIS OF BIMETALLIC HOLLOW DISC UPSETTING

Ö. Ayer

Department of Mechanical, Faculty of Engineering, Engineering, Trakya University, Edirne/ Turkey

Abstract

Bimetallic materials have a growing area of usage and named a type of composite materials with combining advantageous features of two different materials. Upsetting of discs obtained by aluminum and copper was studied. The FEM method was used to simulate the process and results were compared with experiments by taking material flow into account. It was determined that material flow increased with height and reduction rates and on the middle axis the material flow was highest. On the interfaces of sleeve and core materials separation after forming was not observed. Also, it was understood that simulation results of bimetallic disc sample obtained with FEM based DEFORM-3D software in upsetting procedure were in concordance with experimental results and FEM model can be useful for future studies.

Key words: bimetallic materials, upsetting, DEFORM-3D, material flow, load analysis, finite element method.

INTRODUCTION

As the time goes on and different needs emerge composite materials' areas of usage are steadily increasing. Bimetallic materials are named as composite materials because of acting like a single material with combining different alloys of the same material or a new material by bringing two types of different materials together physically. Bimetallic materials can have superior properties by composing of two different materials. Bimetallic materials are commonly selected for their corrosion resistance, low costs, weight disposition and fatigue strength. For example a bimetallic material which was obtained by using aluminum in inner part and steel in outer part shall be lighter than whole steel material and more durable than whole aluminum material. Manufacturing methods of bimetallic materials are mostly limited with coating, close fitting and casting, even though, the first examples of bimetallic materials produced by upsetting method were dating back to old times. Nowadays, application area of bimetallic materials is getting bigger and bigger. Nevertheless there are not too many studies regarding forming bimetallic materials.

CHITKARA AND ALEEM (2001) compared the obtained experimental results with analyses for axisymmetric extrusion of bimetallic tubes**.** HAGHIGHAT AND ASGARI (2011) proposed a new spherical velocity field for extrusion of bi-metallic materials and obtained numerical results. KAZANOWSKI, EPLER, AND MISIOLEK (2004) investigated the relation between initial geometries and the quality of the product with the influence of the initial billet geometry on the product geometry during bi-material rod extrusion. HAGHIGHAT AND MAHDAVI (2013) offered a kinematically admissible velocity field for bimetal tube extrusion process through rotating conical dies. YEH AND WU (2005) investigated the upsetting rings. They used variational upper bound method to evaluate the bulge profile of the upset ring and compared the results with upper bound and FEM results. WIFI ET AL. (1996) selected an updated Lagrangian, elasto-plastic large strain finite element code for mathematical approach to the upsetting disc problem. PLANCAK ET.AL.(2011) investigated the forming of two different geometries in closed die by using two different materials as a bimetallic material and also obtained the forming load, material flow. KACMARCIK ET AL. (2013) obtained experimental and numerical results from backward extrusion of bimetallic materials for gear like profiles. EIVANI AND TAHERI (2007) studied ECAE process for a new method for producing bimetallic. BARATA MARQUES AND MARTINS (1991) made simulations for the joint of a bi-metal coin to obtain forming load and strain field. ESSA ET AL. (2012) investigated interface of these two components using cylindrical samples with different H/D ratios by using C15E as softer material for core and stronger material C45E as sleeve for upsetting experiments.

In the presented study; upsetting of bimetallic hollow discs was investigated by using commercially pure aluminum as sleeve material and electrolytic copper as core material. Material flow was selected as main parameters for the analyses. The FEM model was built for disc upsetting process and results were compared with experimental results. Material flow was investigated by comparing cross sectional views of simulations and upsetting products of the experiments. Both experimental and FEM results agree well each other and the obtained model can be expand to further studies for the different process parameters.

MATERIALS AND METHODS

Commercially pure aluminum (Al 1070) and electrolytic copper was selected as bimetallic material. Al 1070 aluminum was sleeve material in view of its higher mechanical properties comparing to core material which was electrolytic copper. Stress-strain curves of the materials were given in Eq. 1 and Eq. 2.

$$\sigma_{al} = 144\varepsilon^{0.162} \quad (1)$$

$$\sigma_{cu} = 319\varepsilon^{0.583} \quad (2)$$

The dimensions of the bimetallic samples can be seen in the Fig. 1.

Experiments were carried out by Universal test machine which has 600 kN capacity. The press was controlled by software to obtain the load-displacement curves. Experimental setup was given in Fig. 2. Billets were compressed using flat faced platens. The surfaces of the platens were cleaned with acetone to ensure the same friction conditions for all specimens for each test. The cylindrical specimens were centered on the lower die and were upset at different deformation ratios. Height in reductions for 10%, 20%, 30% ratios were calculated and selected for the experimental study.

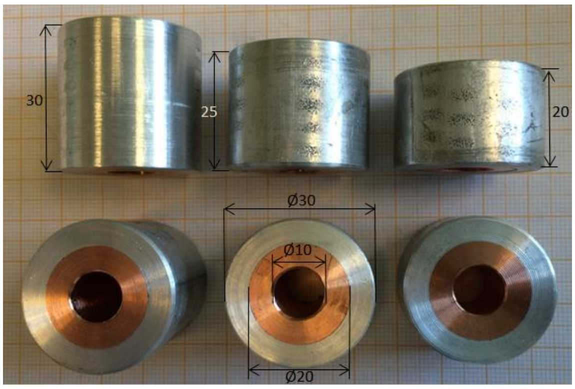

Fig. 1. – Photographical views of workpieces and dimensions

The load-displacement diagram was obtained by data taken from the software. After upsetting, the specimens were cut into two parts from the midsection with MICROCUT 1050 machine to observe material flow of the samples.

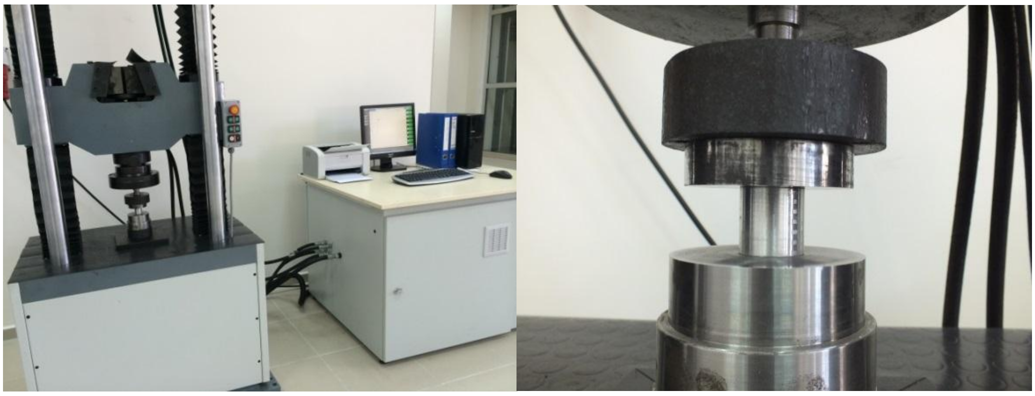

Fig. 2. – Experimental setup

Finite element method was commonly preferred for complex engineering problems. DEFORM is a FEM based software which was specialized for metal forming processes. DEFORM-3D v10.2 was used for simulations. Geometries were modeled in a CAD system, and exported to DEFORM-3D software. The model can be seen in Fig. 3. Mesh distribution in the FEM method is very important to obtain accurate results from the simulations. Environment temperature is defined as room temperature same as experiments. Press velocity was selected as 0.1 mm/sec to correspond with experiments. The friction type considered as shear and the friction factors (m) between workpiece and the dies are assumed as constant and it was selected as m=0.4 for Aluminum/Die contact surfaces and m=0.4 was selected for Copper/Die contact surfaces obtained from the ring compression test. Friction was assumed as zero at the aluminum and copper interface. The iteration method selected as direct and the type of the simulation was Lagrangian Incremental. The dies are selected as rigid bodies and all elastic and plastic deformations of the dies are neglected. H13 steel was selected as a die material from the software library.

CDA 110 was selected for core material and ALUMINIUM 1070A was for sleeve material in the FEM simulations. 35.000 elements was used for both workpiece materials' were models for accurate FEM results. The convergence error limit for velocity and force were 0.005 and 0.05 respectively. The global remeshing was chosen and the type of interference depth selected as relative and its value considered as 0.7. The Conjugate-Gradient solver has been used to solve the problem.

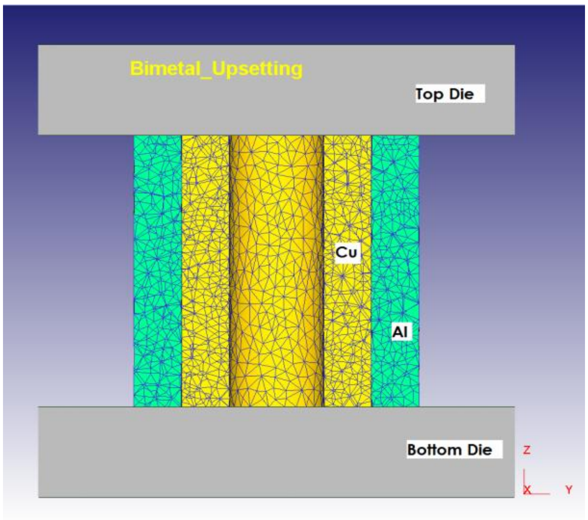

Fig. 3. – View of the FEM model of the die assembly and the bimetallic material

RESULTS AND DISCUSSION

In this study, effective parameter for upsetting of bimetallic disc was firstly investigated and analysis parameters were decided as upsetting load and material flow. FEM model was constructed by DEFORM-3D software and the simulation results were compared with experimental ones.

Material Flow Analysis

After the forming bimetal samples processed with upsetting procedure were cut through axis of symmetry by using MICROCUT 1050 sensitive cutting machine. Flow of materials composing sleeve and core parts are examined. Behavior of material flow is related with height and friction. Since friction factor is the same for the study, reduction in height is investigated for the study and for this purpose; real samples were compared with material flow profiles in the simulations. Samples are processed such in a manner that their lengths are 30 mm, 25 mm. and 20 mm. in the experiments. They are formed in the rates of 10 %, 20 % and 30 % reduction. In order to examine product material's flow middle axis is used as base, inner diameter and outer diameter values of the disc from middle axis are measured on products and simulations as it is given in Fig. 4.

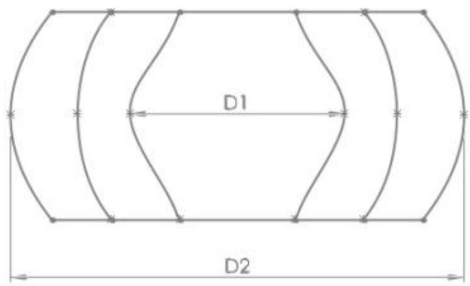

Fig. 4. - Measurement points of the samples

The workpieces was measured from the middle axis of the samples after upsetting according to Fig. 4 and the material flow of the samples was analyzed with reference to the Tab. 1 results.

For 10% reduction; the differences between the measured values of the simulations and products for the outer diameter are getting higher when the initial height increases.

Tab. 1. – Measurement values of simulation and experimental results

Product	D1 (mm)	D2 (mm)	
H30%10	*10.44*	*31.79*	**Exp.**
	10.53	*31.65*	**FEM**
H30%20	*11.26*	*33.56*	**Exp.**
	11.31	*33.78*	**FEM**
H30%30	*12.24*	*36.07*	**Exp.**
	12.33	*36.23*	**FEM**
H25%10	*10.41*	*31.68*	**Exp.**
	10.50	*31.60*	**FEM**
H25%20	*11.17*	*33.24*	**Exp.**
	11.26	*33.49*	**FEM**
H25%30	*12.16*	*36.08*	**Exp.**
	12.28	*35.83*	**FEM**
H20%10	*10.36*	*31.44*	**Exp.**
	10.48	*31.51*	**FEM**
H20%20	*11.08*	*32.52*	**Exp.**
	11.21	*32.86*	**FEM**
H20%30	*11.82*	*35.68*	**Exp.**
	11.89	*35.39*	**FEM**

When the reduction in height increases for the outer profiles, the simulation and experimental measured values converge. The difference for the inner profile does not change entirely for all reduction rates. Visual comparisons regarding to material flow after upsetting are given in Fig. 5, Fig. 6 and Fig. 7.

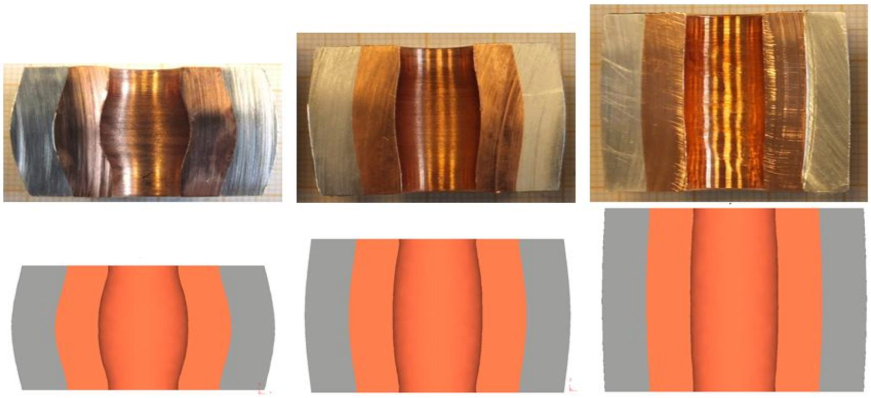

Fig. 5. – Cross section views of the midplane of experimental products and FEM models for the 30 mm. initial height. (A= 30% red., B= 20% red., C= 10% red.)

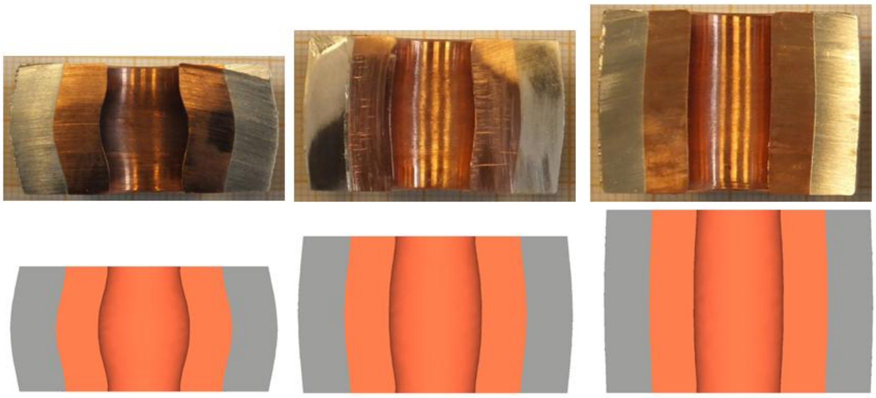

Fig. 6. – Cross section views of the midplane of experimental products and FEM models for the 25 mm. initial height. (A= 30% red., B= 20% red., C= 10% red.)

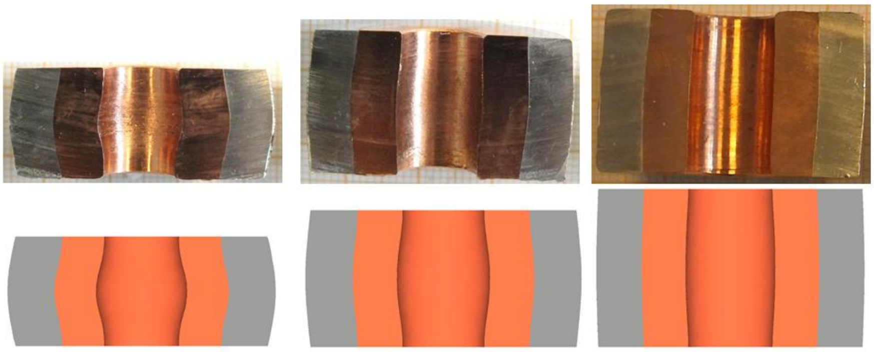

Fig. 7. – Cross section views of the midplane of experimental products and FEM models for the 20 mm. initial height. (A= 30% red., B= 20% red., C= 10% red.)

When 30 mm. height samples are examined after forming, it was observed that for 10% reduction the highest similarity is obtained in the comparison of product and simulation profiles. It was observed that material flows on the core/sleeve material interfaces are rather similar. And for 20% and 30% reduction, it was also observed outer profiles of the products are quite familiar but in the inner side, similarity is not fit with simulations.

For 25 mm. initial height, it is clear that sleeve material's outer diameter flow profile is similar to the product. In addition to that it was determined that at each % reduction rate increase material flow on core/sleeve material interfaces is in concordance with simulation. Similarly, it was observed that profile on the inner surface of the core material on the disc where there is hole was in concordance with simulations.

Like after forming samples with 20 mm. initial length for 30% reduction; it was observed that material flow is match with real product profiles on both on core material inner diameter middle axis and on the sleeve material outer diameter profile and it can be seen that material flow modeling was in concordance with actual experiments.

After upsetting the disc it was observed that core material flowed out to middle axis. The highest material flow appears at the highest reduction value of the sample with highest initial length (h / d = 1). The reason for this is the increase of stress at the center area of work piece and being this stress distribution not homogenous and material flow's being higher at the middle axis due to accumulation of the tension at the middle axis.

CONCLUSIONS

The paper presents experimental and mathematical approach for the bimetallic ring upsetting. The material flow in the upsetting process was investigated. The copper was used as core material and aluminum was used for sleeve material. Following observations are obtained with the regard to detailed analysis and experimental results;

- It was seen that material flow modeling was in concordance with transverse sections obtained after experiments. Core material shows an outer flow at the middle axis. With higher h / d rate the deformation clearly concentrates at the middle axis.

- It is seen that on the top and bottom surfaces where material makes contact with dies the material flow is low and on the middle axis the material flow is high because of there is no contact.
- Owing to aluminum and copper are soft materials and have high plasticity, it can be seen that flow profiles are similar and because of this reason no separate on the core / sleeve material interfaces occurs.
- Based on data obtained from the model it was determined that the model gives a product profile and material flow in concordance with experiments and because of this reason this model can be used for future studies which will be performed with different process parameters.

REFERENCES

1. BARATA MARQUES, M. J. M., MARTINS, P. A. F.: A Study of Bi-Metal Coins by the Finite Element Method. Journal of Materials Processing Tech., 26(3), 1991: 337–48.
2. CHITKARA, N. R., ALEEM, A.: Extrusion of Axi-Symmetric Bi-Metallic Tubes: Some Experiments Using Hollow Billets and the Application of a Generalised Slab Method of Analysis. International Journal of Mechanical Sciences, 43(12), 2001: 2857–82.
3. EIVANI, A. R., KARIMI TAHERI, A.: A New Method for Producing Bimetallic Rods. Materials Letters, 61(19-20), 2007: 4110–13.
4. ESSA, K. ET. AL.: Upsetting of Bi-Metallic Ring Billets. Journal of Materials Processing Technology, 212(4), 2012: 817–24. http://dx.doi.org/10.1016/j.jmatprotec.2011.11.005.
5. HAGHIGHAT, H., ASGARI., G. R.: A Generalized Spherical Velocity Field for Bi-Metallic Tube Extrusion through Dies of Any Shape. International Journal of Mechanical Sciences, 53(4), 2011: 248–53. http://dx.doi.org/10.1016/j.ijmecsci.2011.01.005.
6. HAGHIGHAT, H., MAHDAVI, M. M.: Analysis and FEM Simulation of Extrusion Process of Bimetal Tubes through Rotating Conical Dies. Transactions of Nonferrous Metals Society of China (English Edition), 23(11), 2013: 3392–99.
7. KACMARCIK, I ET.AL.: Bi-Metallic Extrusion of Gear-Like Components. The 6th PSU-UNS International Conference on Engineering and Technology (ICET-2013), 2013: 1–4.
8. KAZANOWSKI, P., MARIO E. E., WOJCIECH Z. M.: Bi-Metal Rod Extrusion-Process and Product Optimization. Materials Science and Engineering, A 369(1-2), 2004: 170–80.
9. PLANCAK, M., CAR, Z., VILOTIC, D., MOVRIN, D., KRSULJA, M.: Upsetting of Bimetallic Components in Closed Die. Engineering review 31(2), 2011: 105–9.
10. WIFI, A. S., ABDEL-HAMID, A., EL-MONAYRI, H., AND EL-ABBASI, N.: Finite Element Determination of Workability Limits for Disks and Rings under Different Upsetting Conditions. Journal of Materials Processing Technology 56(1–4), 1996: 918–32. http://www.sciencedirect.com/science/article/pii/0924013695019049.
11. YEH, W.C., WU, M.C.: A Variational Upper-Bound Method for Analysis of Upset Forging of Rings. Journal of Materials Processing Technology 170(1-2), 2005: 392–402.

Corresponding author:

Önder Ayer, , Department of Mechanical, Faculty of Engineering, Engineering, Trakya University, Edirne/ Turkey

EFFECT OF DIFFRECT DOSES OF COMPOST ON SOIL PROPERTIES

B. Badalíková[1], J. Novotná[1],V. Altmann[2], I. Balada[2]

[1]*Agricultural Research, Ltd., Zahradní 1, Troubsko, Czech Republic*
[2]*Department of Machinery Utilization, Faculty of Engineering, Czech University of Life Sciences Prague, Czech Republic*

Abstract
The paper is the result of experiments carried out within the research project on the application of compost biodegradable waste for erosion-affected soils. Measurements were carried out at two sites: on permanent grassland (PG) and arable land (AL,) and batches of compost were on three sites: 0 T.H.$^{-1}$ as a control batch, 80 T.H.$^{-1}$ and 150 T.H.$^{-1}$. From the gained results a positive effect on the incorporation of compost retention capacity of the soil was proved, as well as the reduction in penetration resistance.

Key words: experiment, compost, retention, penetration resistance.

INTRODUCTION

The quality and quantity of compost incorporation into the soil affect the physical, chemical and biological properties of the soil. Among the important features of soil belong the retention capacity, which also varies according to a habitat, crops and tillage, and a total penetration resistance, which has got a favorable effect on the soil regime too.

HEJDUK (2009) found out that there is a higher retention on farmed soils than the one on permanent grassland. There was a faster reduced retention rate on soils without plowing, and this reduction was more intense than on mellow soil after plowing. CROHN (2011) also dealt with the retention capacity of the soil using compost and he demonstrated the connection between different kinds of compost and retention. LUKAS ET AL. (2009) were in their experiments concerned with the processing of soil and how it effects the retention capacity, and recorded higher water infiltration when using minimization technologies for tillage and also when measuring after harvesting crops.

The aim of this study is to find out, effect of compost of biodegradable waste to the erosion affected soils.

MATERIALS AND METHODS

In addressing the issue over a period of five years the retention capacity of the soil at two different sites was monitored, namely on the permanent grassland (PG) in the village of Ocmanice, and on the arable land (AL) of town Náměšťˇnad Oslavou. Monitoring was done as an experiment on a pilot scale stationary.

Measurement of the retention properties of the soil were performed at the beginning and at the end of the vegetation with a concentric cylinder, 28 and 54 cm in diameter. The outer cylinder eliminates spilling of water in the soil to the sides, and the principle of measuring don in the inner cylinder was to monitor the volume of a water loss over time. The measurements were performed for at least 2 hour period on the surface layer of soil. From the measured values of cumulative infiltration it was subsequently calculated the speed of retention rate expressed in mm.min^{-1} (l.h^{-1} m^{-2}).

The same period of time needed for the retention measurement was dedicated to a soil cementation thanks to a mechanical compaction penetrometer. The measurements were performed in five to ten repetitions. The measurement was based on detecting the force required to push a standard steel cone into the soil. Its advantage was the high expedition with instant evaluation of the results for the reference profile.

There were established three variants of the experiment with comparative doses of compost at both sites:

stand A - permanent grassland (PG):

Option 1 - breaking the sod without incorporation of compost,

Option 2 - disposable incorporation of compost at 80 T. H^{-1},

Option 3 - disposable incorporation of compost at 150 T. H^{-1}

stand B - arable land (AL):

Option 1 - stubble without incorporation of compost,

Option 2 - stubble, disposable incorporation of compost at 80 T. H^{-1},

Option 3 - stubble, disposable incorporation of compost at 150 T. H^{-1}

The compost made to ensure the experiment was produced with a controlled microbial composting technology in the belt heaps on the loose, on water secure area. The main raw materials in compost fillings were a cut grass from the maintenance of municipal green and the airport, biological waste from gardens and vegetable scraps.

Arable crops packages were sown under the following **crop rotation:**

1. year - rye tufted (Secalecereale) - spring sowing,
2. 2nd year - winter pea (Pisumsativumsubsp. Arvense) + triticale (Triticale)
3. 3rd year - Oats (Avenasativa)
4. 4th year - spelled (Triticumspelta)
5. 5th year - clover mixed bag

Soil and climatic characteristics of the stands:

stand A - permanent grassland (TTP) is characterized as soil type cambisol litica with a compact solid - reinforced rock, grain composition of loamy, with a high content of skeleton, tread depth of topsoil reaches max. 0.20 m. Located at an altitude of 320 m.

stand B - arable land is soil type cambisol modal grain composition sandy loam, containing less skeletal depth of humus horizon is max. 0.40 m. Located at an altitude of 365 m.

Both units belong to a slightly warm and humid region, with the long-term average rainfall of 594.4 mm long and a long-term average temperature of 7.2 °C.

RESULTS AND DISCUSSION

Infiltration

The speed of infiltration was detected in the amount of water seeped per unit area for each repetition, and subsequently averaged for the individual variants. Infiltration was calculated as infiltration coefficient in liter per hour per m^2. This way the quantity of water that had soaked into the soil and its speed was determined Tab. 1 shows that the infiltration capacity of the soil was dependent on the reference year, a date of the measuring, and the measurement station. The results from the Tab. 1 are shown in Fig. 1 and Fig. 2.

Tab. 1. – Infiltration water at different sites in variants with comparative doses of compost in monitored years

Term of measurement	Stand	Variant	Infiltration [$l.h^{-1}.m^{-2}$]				
			1. year	2nd year	3rd year	4th year	5th year
Start of vegetation	**PG**	1	0,61	0,82	1,21	1,60	2,31
		2	0,67	1,70	1,58	1,45	1,88
		3	0,70	2,20	1,81	4,87	2,50
		average	0,66	1,57	1,53	2,64	2,23
	AL	1	4,92	0,63	4,10	2,04	1,36
		2	6,86	1,08	5,17	2,62	2,83
		3	6,78	1,35	5,26	3,30	2,28
		average	6,19	1,02	4,84	2,65	2,16
End of vegetation	**PG**	1	0,75	1,32	0,75	3,15	2,85
		2	1,00	3,22	2,07	4,83	2,43
		3	2,10	5,13	1,31	4,98	2,85
		average	1,28	3,22	1,38	4,32	2,71
	AG	1	1,24	1,60	1,08	2,35	2,66
		2	2,76	2,21	1,31	5,36	1,70
		3	3,00	1,89	3,28	7,98	2,36
		average	2,33	1,90	1,89	5,23	2,24

During the five-year monitoring of soaking water at different sites was found out that there it was mostly lower retention capacity at the station of permanent grassland compared to arable land. This was due, among other things, to a different soil type and profile of habitat. At the station with the PG there were on average higher values of retention factor at the end of the growing season, except the 3rd year of monitoring, which was atypical in rainfall and temperature. A strong soil compaction was found on grassland this year at the end of the growing season due to prolonged drought that affected the infiltration of the soil. Resulted variants with varying amounts of compost indicate that it was significantly higher infiltration in the variant with the highest amount of incorporated compost (variant 3), at the beginning and end of the growing season and at both sites. The differences among variants decreased by and by monitored years, namely in the fifth year at the end of the PG and vegetation on AL and at the beginning of vegetation.

At the station of arable land the values of the infiltration coefficient were higher at the beginning of the growing season in the first and the third year of tracking, and in the following years, the values were higher at the end of vegetation. According to the size of water infiltration into the soil and other factors, the retention capacity of the soil is estimated. Retention at this habitat was affected by a crop grown in a given year, which was also found out by other authors (HEJDUK AND KASPRZAK, 2010; BEVEN AND GERMANN, 1982; BLACKWELL, GREEN AND MASON, 1990). Otherwise, the retention is caused by a number of factors, which can be classified into four groups - soil characteristics, characteristics of the soil surface, the method of land management and natural conditions (Lal, 2002).

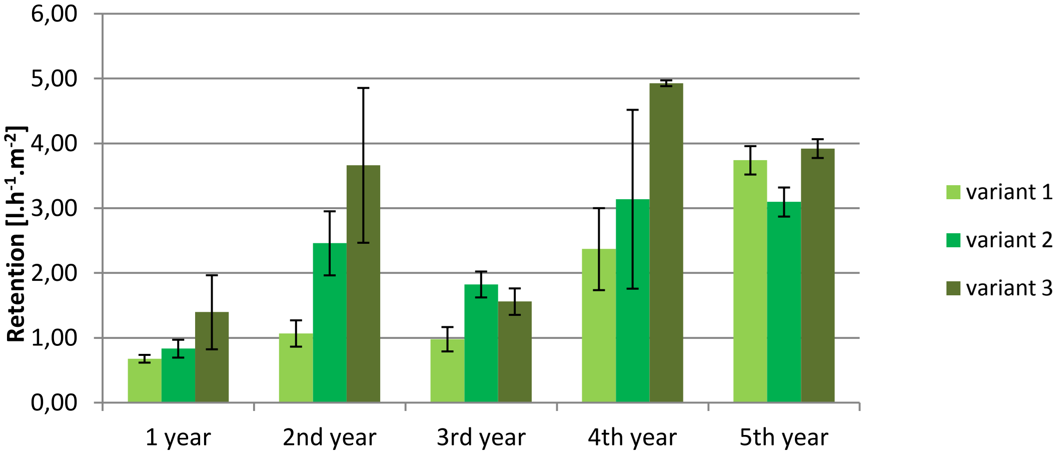

Fig. 1. – Infiltration of water on permanent grassland

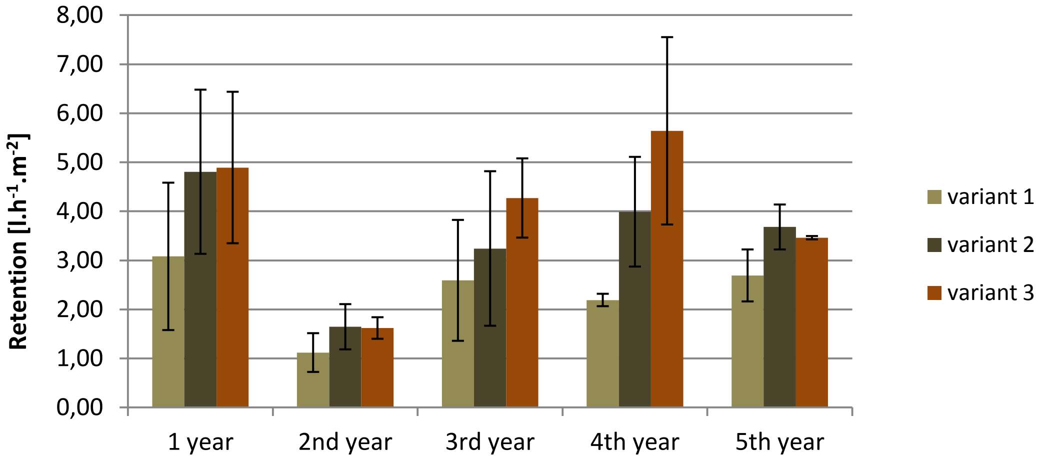

Fig. 2. – Infiltration of water on arable land

Penetration

As showed in previous measurements, infiltration was influenced not only by saturation of soil water, but also by its compaction. In this context, the penetration resistance of the soil was measured. The results for the five year monitoring of two field trials are presented in Tab. 2.

Tab. 2. – Penetration resistance at different sites in variants with increasing doses of compost over monitored years

Stand	**Variant**	**Deep [m]**	Penetration resistance [**MPa**]				
			1. year	2nd year	3rd year	4th year	5th year
PG	**1**	0 – 0,05	0,776	1,034	1,112	1,086	2,28
		0,05 – 0,10	1,293	1,189	1,525	1,525	2,80
		0,10 – 0,20	1,344	1,499	1,810	1,965	3,06
	2	0 – 0,05	1,034	0,776	1,163	1,112	2,53
		0,05 – 0,10	1,344	0,931	1,396	1,654	3,29
		0,10 – 0,20	1,654	1,241	1,551	1,965	3,81
	3	0 – 0,05	1,189	0,776	1,034	1,086	2,28
		0,05 – 0,10	1,189	0,742	1,551	1,551	3,30
		0,10 – 0,20	1,706	1,241	1,706	1,810	3,56
AL	**1**	0 – 0,10	0,517	0,827	1,086	1,034	3,03
		0,10 – 0,20	0,517	1,137	1,189	1,706	2,79
		0,20 – 0,30	0,724	1,213	1,086	2,016	3,31
		0,30 – 0,40	0,931	1,654	1,189	2,016	3,31
	2	0 – 0,10	0,517	1,034	0,827	1,034	2,78
		0,10 – 0,20	0,517	1,052	0,931	1,370	2,54
		0,20 – 0,30	0,672	1,448	1,189	2,016	3,06
		0,30 – 0,40	0,982	1,810	1,293	2,016	3,06
	3	0 – 0,10	0,517	0,776	0,879	1,034	2,53
		0,10 – 0,20	0,517	0,845	0,879	1,344	2,54
		0,20 – 0,30	0,672	1,551	1,034	1,810	2,80
		0,30 – 0,40	0,982	1,551	1,241	1,913	3,06

Tab. 3. – Measured values of electrical conductivity of LAD 27 fertilizer for the air stream of 115 $m^3.h^{-1}$

Time [h]	**Electrical conductivity[$m^{-2}.kg^{-1}s^3.A^2$]**						**Average**
	Sieve 2.00 mm			**Sieve 3.15 mm**			
0,5	46,80	47,80	45,40	46,80	47,80	45,40	46,67
1,5	74,10	76,20	78,70	74,10	76,20	78,70	76,33
2,5	85,70	84,50	86,40	85,70	84,50	86,40	85,53
3,5	88,60	89,80	91,50	88,60	89,80	91,50	89,97
4,5	94,40	95,00	95,70	94,40	95,00	95,70	95,03
5,5	95,70	95,30	96,70	95,70	95,30	96,70	95,90
6,5	96,40	96,10	97,80	96,40	96,10	97,80	96,77
7,5	99,40	99,70	99,80	99,40	99,70	99,80	99,63
8,5	99,80	100,50	100,20	99,80	100,50	100,20	100,17
9,5	101,30	102,20	102,10	101,30	102,20	102,10	101,87

Penetration resistance values from Tab. 2 are plotted in Fig. 3 to 7 on a permanent grassland, and in the in Fig. 8 to12 on arable land. It all applies again for the variants 1 to 3.

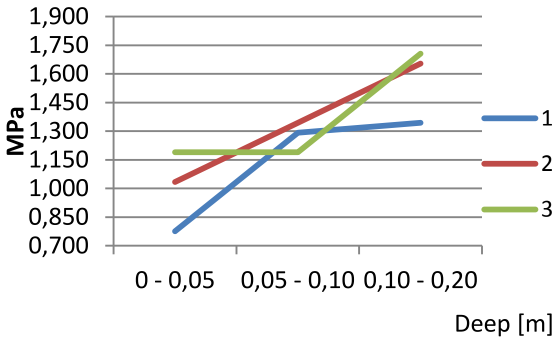

Fig. 3. – Penetration resistance of the soil to PG in the 1st year

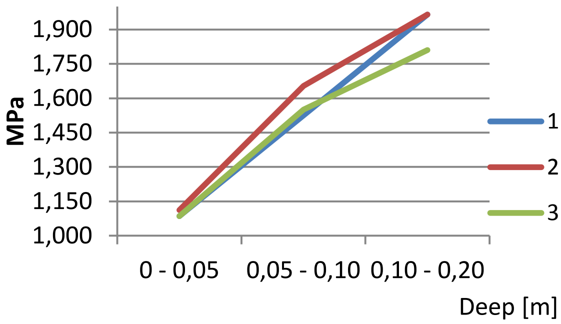

Fig. 6. – Penetration resistance of the soil to PG in the4th yearr

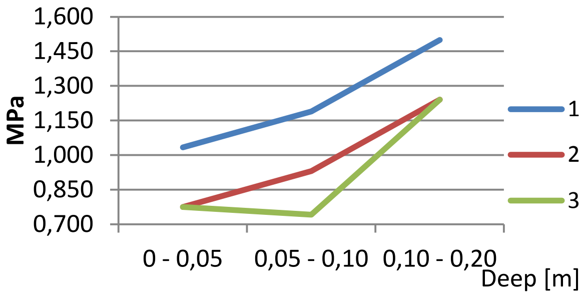

Fig. 4. – Penetration resistance of the soil to PG in the 2nd year

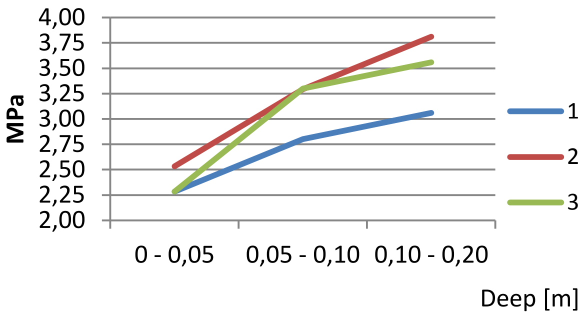

Fig. 7. – Penetration resistance of the soil to PG in the 5th year

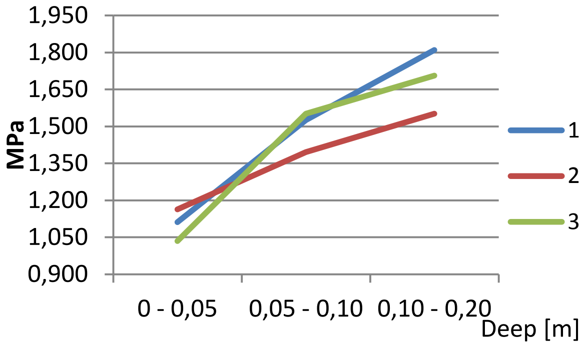

Fig. 5. – Penetration resistance of the soil to PG in the3rd year

From the curves shown in Fig. 3 to 7 of the station PG it is apparent the increasing soil compaction with increasing depth. Also, of the measurement showed the highest soil compaction in the fifth year of measurement. Outside of the initial values of the first year of the experiment, there was a clear effect of the variants with sunk mulch to reduce soil penetration resistance. No measurement in the first four years exceeded the critical value indicating compaction (above 3 MPa). That was exceeded for the fifth year in all variants in the deeper layer of soil.

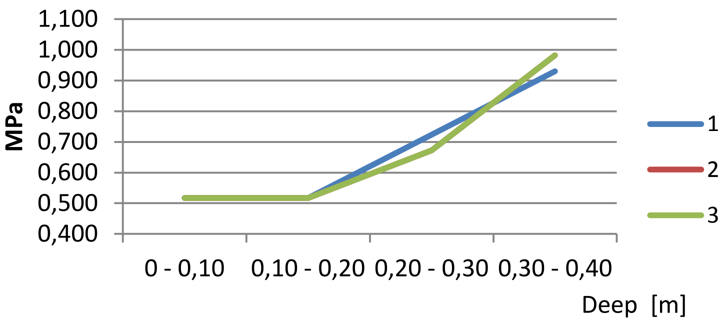

Fig. 8. – Penetration resistance of the soil to AL in the 1st year

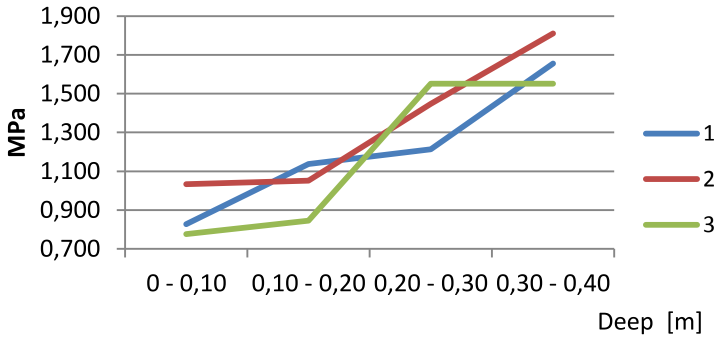

Fig. 9. – Penetration resistance of the soil to AL in the 2nd year

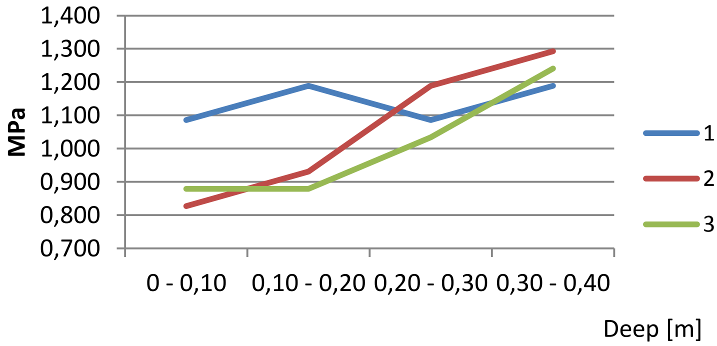

Fig. 10. - Penetration resistance of the soil to AL in the3rd year

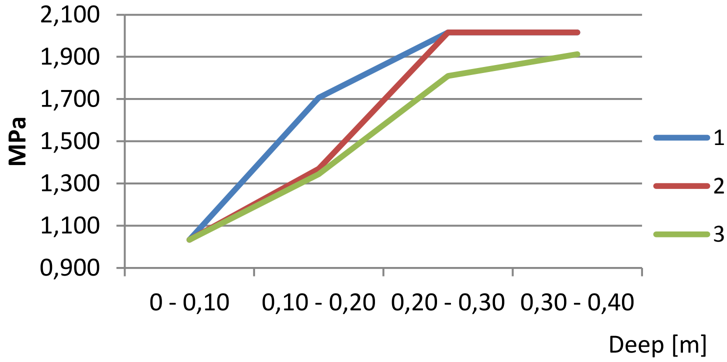

Fig. 11. - Penetration resistance of the soil to AL in the 4th year

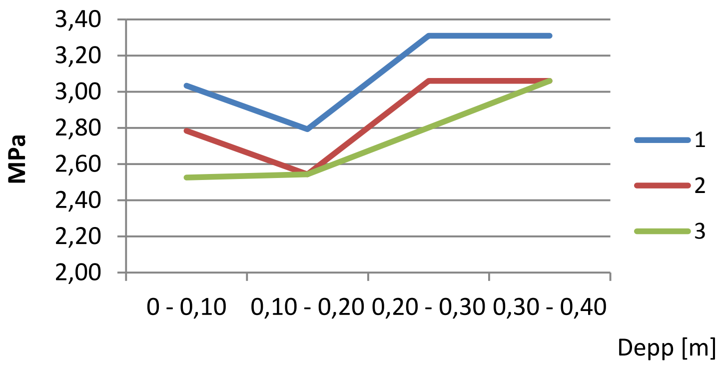

Fig. 12. - Penetration resistance of the soil to AL in the 5th year

The curves in Fig. 8-12 show the progress of penetration resistance values in the soil profile on arable land. In the first year of the experiment the values of options 2 and 3 were almost identical, therefore, there are shown only two curves. As at the previous station, the lowest resistance while measuring the soil profile at the surface layer of soil was found at the variation 3 with the highest dose compost. The highest values for the entire period were measured at all variants in the fifth year of measurement, when there was an apparent a deficiency of organic matter in the soil leading to a reduction in the infiltration capacity of the soil in the upper layers of the soil. Again, as in the pasture soil, the critical value indicating compaction was exceeded (above 3 MPa) only in the fifth year of measurement. In the first four years the value was not exceeded.

DISCUSSION

From the example of both stations it is clear that incorporation of compost has got its purpose in terms of increasing the organic matter in the soil and thereby lightening the topsoil profile. There are known cases where the compost is being applied on the sandy soil with humus deficiency in order to improve the water regime and sorption properties. It is also the main measure in changing the culture to arable land, which is applied in the reclamation (HORN ET AL., 2006; STOFFEL AND KAHN, 2001), or in the protection and creation of permanent grassland. Morse also used compost as void material to improve the structure of heavy soils. KROULÍK ET AL (2010) also found out that application of compost increases the amount of organic matter in soil which has a long-lasting beneficial effect on infiltration and water retention in the soil.

Supplying well matured compost into the soil it delivers prepared humus creating material, and thus making the process of restoring soil fertility much faster. To ensure a level balance of humus in the soil we must annually supply about 1.5 tons of pure organic matter by fertilizing on average 1ha of arable land equivalent to 9 t of medium-quality manure.

Usefulness of incorporation of compost into the soil was commented on by many authors abroad. Depositing compost as an organic matter not only has a positive effect on preserving moisture in the soil, on soil structure (KUTÍLEK, 1978), on a gradual release of nutrients, and on a biological activity in the soil, but it is also important for soil protection against water erosion especially from the point of view of a higher retention water in soil.

CONCLUSIONS

The results obtained showed the positive impact of incorporation of compost on the soil infiltration rate while lowering soil penetration resistance. There were found significant differences in permanent grassland in a case of incorporation of a higher dose of compost. Embedding medium and even higher doses of compost into the soil (80, 150 T. H^{-1}) resulted in a higher retention capacity, where the soil incepted more water compared to the control variant without a compost, on permanent grassland and on arable land. It is therefore concluded that the organic material incorporated into the soil as compost is beneficial in terms of absorption capacity of the soil and reducing its consolidation, as well as erosion protection. It is important to provide soil with well matured quality compost at regular intervals.

ACKNOWLEDGEMENTS

These results were obtained within the framework of the project of CULS Prague IGA No. 2015:31180/1312/3115 and QJ1210263 supported by National Agency of Agricultural Research, Ministry of Agriculture of the Czech Republic.

REFERENCES

1. BADALÍKOVÁ, B., HRUBÝ, J.: Following of erosive wash of soil in variants with different intercrops. In: ACTA Universitatis Agriculturae et Silvicultarae Mendelianae Brunensis, roč. LVIII, no. 2, 2010: p. 27-33.
2. BROWN, S., COTTON, M.: Changes in Soil Properties and Carbon Content Following Compost Application: Results of On-farm Sampling. Compost Science & Utilization, Volume: 19 Issue: 2, 2011: p. 87-96.
3. CROHN, D. M.: Compost Best Management Practices and Benefits [online]. 2011, [cit. 2012-12-03]. <http://www.calrecycle.ca.gov/publications/Detail.aspx?PublicationID=1377>.
4. HEJDUK, S.: Comparison of surface runoffs from grasslands and arable land. Grassland Science in Europe, 15, 2009: p. 63–67.
5. HEJDUK, S., KASPRZAK, K.: Zvláštnosti vodního režimu zemědělských půd v zimě a v předjaří. J. Hydrol. Hydromech., *58*, 3, 2011: 175–180.
6. HORN, R., FLEIGE, H., PETH, S., ET AL.: Soil management for sustainability. Reiskirchen, Catena Verlag GMBH, 2006: p. 497.
7. KUTÍLEK M.: Soil Science in Water Management. SNTL, Praha. 1978.
8. KROULÍK, M., BRANT, V., MAŠEK, J., KOVAŘÍČEK, P.: Influence of soil tillage treatment and compost application on soil properties and water infiltration. Trends in Agricultural Engineering 2010, 4th International Conference TAE 2010, Prague, 2010: 343-349.
9. LAL, R.: Encyclopedia of soil science. New York: Marcel Dekker, s. 1476. 2002.
10. LUKAS, V., NEUDERT, L., PROCHÁZKOVÁ, B., MIKUŠOVÁ, Z., HARTMAN, I., ILLEK, F.: Vliv technologie zpracování půdy na fyzikální a infiltrační vlastnosti půdy. Úroda, 12/2009, vědecká příloha časopisu, 2009: s. 375-378.
11. PLÍVA, P., ALTMANN, V., JELÍNEK, A., KOLLÁROVÁ, M., STOLAŘOVÁ, M.: Technika pro kompostování v pásových hromadách. Praha: VÚZT, č. 1, 2005: s. 72.
12. STOFFELA, P. J., KAHN, B. A.: Compost Utilization in Horticulture cropping system, Lewis Publisher, USA. 2001.

Corresponding author:

doc. Ing. Vlastimil Altmann, Ph.D., Department of Machinery Utilization, Faculty of Engineering, Czech University of Life Sciences Prague, Kamýcká 129, Praha 6, Prague, 16521, Czech Republic, phone: +420 22438 3144, e-mail: altv@tf.czu.cz

PRODUCTION OF BRIQUETTES FROM WASTE PAPER

I. Balada, V. Altmann

Department of Machinery Utilization, Faculty of Engineering, Czech University of Life Sciences in Prague, Czech Republic

Abstract
The article focuses on the possibility of recycling waste paper, which has become one of the major commodities collecting raw materials for its wide use in many economic areas. In the introduction to the description of the overview of the development segment of waste paper in the Czech Republic. The article presents information about the opportunities of new products and materials from processed recycled paper. In another part of the article presents practical information from the process to produce briquettes from three kinds of waste paper with a description technology and obtained a description of the physical characteristics of produced briquettes.

Key words: biodegradable municipal waste, material recycling, composting, production of briquettes.

INTRODUCTION

In the Czech Republic, 800,000 tons of waste paper is collected annually in average via separate sorting, but out of this amount only 315,000 tons is processed, and the rest, i.e. approx. 60% out of the mentioned total amount, is being exported abroad at the expense of the environment and the Czech economy. Although a paper consumption in the Czech Republic is estimated at 1.5 million tons, only 900,000 tons of paper is produced there. Out of this quantity, 700,000 tons is exported simultaneously, which means that it is necessary to import 1.3 mil. tons of new paper (BARTÁK, 2010). These figures clearly confirm that 85 % of the paper intended for consumption must be imported to the Czech Republic.

Today the comfortable life is paid with the expressive consumption of energy in all its forms. The non-renewable energy source reserves are limited and they are to exhaust. Nevertheless, they supply about four fifths of energy consumption. In last decades, the renewable energy sources have been preferred. One of alternative forms of fuel, made from renewable sources, is the fuel on the basis of paper waste. First of all, it is recommended to recycle this raw material – to use it as a material (MCKINNEY, 1995).

From the results of works published before (BROŽEK 2013; BROŽEK, NOVÁKOVÁ, 2013), it follows that compared to briquettes from wood waste, briquettes made from recovered paper and board are of low moisture content, high density, high mechanical durability and relatively high force is necessary for their rupture. But at the same time, they have high ash amount and low gross calorific value.

The constant industrial activity rise and world population growth are directly related to the increase of overall energy consumption, and it is estimated that in 2025, energy demand will surpass by 50 % the current needs (RAGAUSKAS ET AL., 2006). Nowadays, almost 80% of the world's energy supply is provided by fossil fuels (SIMS ET AL., 2007) with harmful impacts to the environment.

The goal of research is to obtain the heating value of paper briquettes and to compare with available fuels on the Czech market. Part of the research is to calculate the bulk density of briquettes made of paper. Result of research can help to find a new fuel from recycled paper.

MATERIALS AND METHODS

Determining the volume of shredded paper using measuring cylinders of known volume and weight of the material.

There were chosen 3 kinds of waste paper for the experiment:

- Office paper shredded with the Fellowes MS 450Ms paper shredder,
- Shredded paperboard (see Fig. 1),
- Shredded waste paper (a mixture of magazines, newspapers and other paper packaging), shredded with the HSM DuoShredder 5750 at WEGA recycling Ltd.

The materials were scattered into a 1000 ml measuring cylinder. The material was not compacted, just sprinkled into the measuring cylinder of the same height. Subsequently, the material was sprinkled on a scale and the weight of the material was measured in [g]. There were performed 10 measurements for each material and the mean value was determined, from which the specific weight of input shredded material was calculated.

Other devices:

- The measuring cylinder with a volume of 2000 ml, Laboratory scale KERN PFB 2000-2 with weighing range up to 2 000 g with a 0.01 g accuracy.

Briquetting of three kinds of shredded waste paper.

The material was inserted into the reservoir of briquetting machine BrinkStar CS25 with a matrix of 65 mm, and three types of briquettes were produced depending on a waste paper. Maximum operating pressure of the briquetting machine was 18 MPa (180 bar). Materials for pressing had to meet the following conditions: moisture content from 8 to 15 %, dimensions smaller than 15 mm and bulk density of at least 70 kg.m^{-3}. Briquette height was measured in two spots and the average value was calculated. Using the matrix diameter 65 mm, the height and the weight of the briquettes, the resulting bulk density was calculated.

Calculation of density of the produced briquettes.

Briquettes were measured in height in two places and the average value was calculated. Due to the matrix diameter 65 mm, the height and weight of the briquettes the resulting bulk density was calculated. The compression coefficient was calculated as the ratio between the density of the material prior to entering the briquetting facility and the density of the resulting briquettes.

Calculation of heating value by using the norm ISO 1928.

The briquettes were also analyzed to obtain a combustion heat and heating value according to ISO 1928. According to the manual of the briquetting machine, the briquettes should have had a shape of a cylinder of diameter 65 mm, length from 30 to up to 50 mm, and the heating value from 15 to 18 MJ.kg^{-1}.

RESULTS AND DISCUSSION

The density of selected materials (Tab. 1) was calculated in the first part of the research, and it was found out that a cardboard has the highest density. It is due to a higher proportion of pulp after multiple recycling, which is contained in the cardboard compared to other kinds of waste paper.

Tab. 1. – Measurement of density of selected paper waste in a vessel of volume 1000 ml

Number measurement	Separate paper [g]	Cardboard [g]	Office paper [g]
1.	55.263	76.120	73.820
2.	56.760	75.820	68.200
3.	51.774	74.280	62.000
4.	56.113	80.020	64.200
5.	57.906	79.458	63.220
6.	52.821	74.120	64.680
7.	56.219	71.720	68.400
8.	58.066	78.860	66.000
9.	54.017	73.520	67.100
10.	57.323	78.102	65.600
Average	55.626	76.202	66.322

In the next part of the experiment the production of briquettes of cylindrical shape with a diameter of 65 mm (Fig. 1 a, b, c) using a briquetting press was performed. The test waste material was gradually inserted into the reservoir and after the creation of briquettes the entire reservoir was cleaned before being used again for another test material. 20 pieces of produced briquettes were tested for each measured commodity of the paper waste. Each briquette was measured at two points to calculate the height and its average value. Furthermore, the volume of the briquettes was calculated and so was its weight and the bulk density. At the end it was calculated the compression ratio of mentioned kinds of waste paper (Tab. 2).

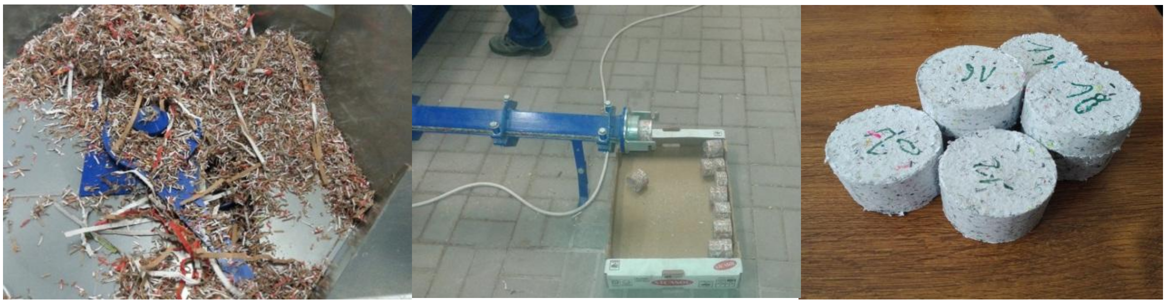

a) b) c)

Fig. 1. – **a, b, c** – Briquette manufacturing process: a) a container with the material, b) conveyor of the briquettes c) manufactured briquette

Tab. 2. – Calculation of compression ratio of measured kinds of waste paper

Input material	Bulk density of measured commodities [kg.m^{-3}]	Bulk density of briquettes [kg.m^{-3}]	Pressing coefficient [-]
Separate paper	66.322	278.343	4.20
Cardboard	76.202	252.322	3.31
Office paper	55.622	258.126	4.64

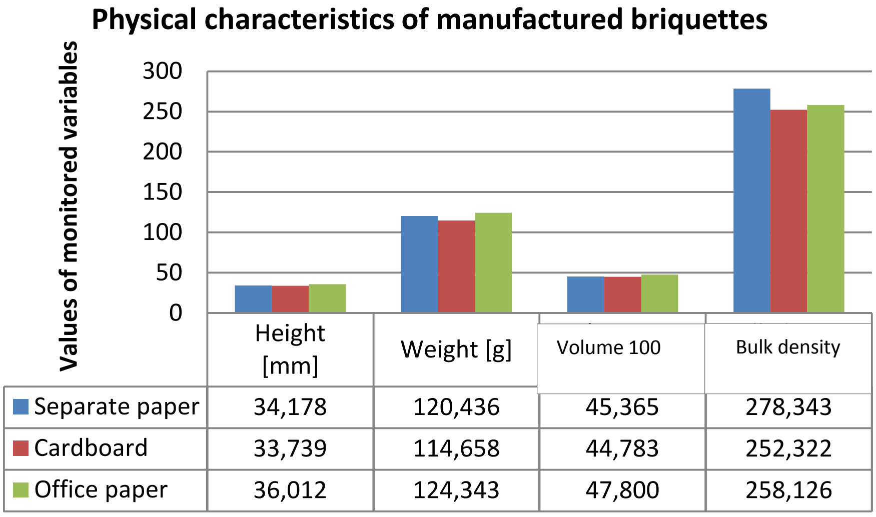

Fig. 2 – Chart with evaluation of measured physical characteristics of manufactured briquettes

Fig. 2 shows a relationship of measured values for the individual measured commodities of waste paper. For the visibility of the value of volume in Fig. 2 the value is stated as 100 pcs briquettes dm^3.

The briquettes were analyzed to obtain a combustion heat and heating value according to ISO 1928 (Tab. 3). The heating value of briquettes made of paper fell bellow the interval indicated by the manual of the briquetting machine. The cardboard briquettes demonstrated the highest heating value, probably because of the content of chemical binders.

The aim of the experiment where briquettes were produced by pressing three types of waste paper was to assess quality of the compression and possibility of further material use after its shredding. It is well known that there is a large amount shredded waste paper in office buildings that is according to current practice disposed of mainly together with a mixed municipal waste to a landfill. The briquettes produced can be used both in the process of energy production via combustion, and in the compost production process where they can significantly reduce the cost of transportation thanks to the compression ratio.

Tab. 3 – Chemical analysis, heating vaue and combustion heat of the briquettes

Materials		office paper	separate paper	cardboard
Parameter	units			
Humidity	[% weight]	4.13	4.23	4.82
Ash	[% weight]	12.63	20.41	11.58
C	[% weight]	36.17	35.31	39.35
H	[% weight]	5.11	4.77	5.41
N	[% weight]	0.06	0.09	0.14
S	[% weight]	0.04	0.03	0.05
O	[% weight]	44.15	37.22	41.18
Combustion Heat	[MJ.kg^{-1}]	12.94	13.19	14.72
Heating value	[MJ.kg^{-1}]	11.82	12.15	13.54

This is going to be the subject of further reflection and experimentation. The size of manufactured briquettes is in accordance with data reporting the size of wood chip material from various wood chippers (EPSTEIN ET AL., 1997), and corresponds to the commonly used sizes exploited in composting plants as mentioned by SOUCEK & BURG (2009).

The bulk density of the paper briquettes is up to 4 times lower than the density of briquettes made from herbaceous phytomass, and there is no problem of increased level of nitrogen that is generated by energy utilization of herbal phytomass as indicated by e.g. ZAJONC & FRYDRYCH (2012) or THEERARATTANANOON ET AL. (2011).

The most important indicator of quality briquettes is heating value. The produced briquettes reached heating value values ranging from 11.82 to 13.54 MJ.kg^{-1}. Comparison of results produced briquettes from waste paper with the other, freely available briquettes that are used today as the fuel, and are available on the Czech market, is shown in (Tab. 4).

Tab. 4 – Higher heating value and lower heating value of sewage sludge (MIKLUŠ, 2007)

Materials	**Humidity**	**Ash**	**Heating**	**Notes**
	[% units]	[% units]	[MJ.kg^{-1}]	
office paper	4.13	12.63	11.82	
separate paper	4.23	20.41	12.15	
cardboard	4.82	11.58	13.54	
EKO briquettes	10	5	13	sawdust made of soft wood
Briquettes Rekord	9	0.4	18	without bark and other binders
brown coal	5-20	10	13,3	assorted
black coal	1	6,5	20-29	

From Tab. 4 it can be observed significant differences between paper briquettes and available fuel for Czech households. It is evident that the paper briquettes have a very small percentage of moisture extruded material against the wooden briquettes and brown coal. Deficiencies in the paper briquettes on the other hand a higher percentage of ash to the total weight of the original produced briquettes. During the test Burning and obtaining the percentage of ash in paper briquettes it was already evident after the briquettes have a high ash content (see Fig. 3a, b). It was also noticeable that the paper even after burning left input material characteristics, whether of briquettes or shredded cardboard. It can however noted that the ash after incineration of paper or paper briquettes is not hazardous and can be further processed like ash after the combustion of wood, ie. for example composted.

Heating value of waste paper from different kinds of waste paper approached the heating value of the graded brown coal heating value and cardboard were higher for both graded brown coal as well as exceed the heating value of eco briquettes It can therefore be concluded that there is potential, therefore, as an alternative fuel, according to the results is possible.

Fig. 3. – a) Ash from incineration briquette, b) the ash from burning of input materials for the production of briquettes

CONCLUSIONS

The research contained four parts of the research. The main objective was to obtain a heating value of paper briquettes and compared with available fuels on the Czech market. Calculated a heating value briquettes was between 11.82 to 13.54 MJ.kg^{-1}. From these results, it can be argued that the briquettes which reach heating value over 13 MJ.kg^{-1} are high-quality fuel. For example, brown coal reaches in average 13 MJ.kg^{-1}. The difference of the ash content in the briquettes and brown coal is 1.58 %. This difference is negligible. According to the results of research it can be argued that the paper briquettes are a suitable substitute for brown coal. The question is the cost against the price of brown coal, but it can be a topic of follow-up article.

ACKNOWLEDGEMENT

The work was supported by the internal research project of the Faculty of Engineering IGA 2015:31180/1312/3116.

REFERENCES

1. BARTÁK, V.: Paper and paper waste. World Press.4. 2010.
2. BROŽEK M., NOVÁKOVÁ A.: Briquettes from recovered paper and board. In: Engineering for Rural Development. Jelgava, Latvia University of Agriculture: 488–493, 2013.
3. BROŽEK M.: Properties of briquettes from paper waste. Manufacturing Technology, 13, 2013a: 138–142.
4. EPSTEIN, E.: The Science of Composting. Technomic Publishing. Co INC, Pensylvania, 1997.ISBN No. 1-56676-478-5.
5. MCKINNEY, R.: Technology of paper recycling. New York: Chapman & Hall, 1995. ISBN 0751400173.
6. MIKLUŠ, M.: Spalné teplo a výhřevnost čistírenských kalů: Higher heating value and lower heating value of sewage sludge [CD-ROM]. Brno: Vysoké učení technické, Fakulta strojního inženýrství, 2007.
7. RAGAUSKAS, A.J., WILLIAMS, C.K., DAVISON, B.H., BRITOVSEK, G., CAIRNEY, J., ECKERT, C.A., FREDERICK, W.J. , HALLETT, J.P., LEAK, D.J., LIOTTA, C.L.: The path forward for biofuels and biomaterials. Science, 311 (5760), 2006: 484–489.
8. SIMS, R.E.H., SCHOCK, R.N., ADEGBULULGBE, A. FENHANN, J., KONSTANTINAVICIUTE, I., MOOMAW, W., NIMIR, H.B., SCHLAMADINGER, B., TORRES-MARTÍNEZ, J., TURNER, C., UCHIYAMA, Y., VUORI, S.J.V., WAMUKONYA, N., ZHANG, X., METZ, B., DAVIDSON, O.R., BOSCH, P.R., DAVE, R., MEYER, L.A.: Climate Change 2007: Mitigation. Contribution of Working Group III to the Fourth Assessment Report of the Intergovernmental Panel on Climate Change, Cambridge University Press, Cambridge, United Kingdom and New York, NY, USA (2007).
9. SOUČEK, J., BURG, P.: The amount and opportunities of using material generated during maintenance of trees. Yearbook of Lawn, vol. 5, n.1, Olomouc, Publisher Baštan, 2009: 89-92. ISBN 978-80-87091-08-1.
10. THEERARATTANANOON, K., XU, F., WILSON, J., BALLARD, R., MCKINNEY, L., STAGGENBORG, S.: Physical properties of pellets made from sorghum stalk, corn stover, wheat straw, and big bluestem. Industrial Crops and Products, vol. 33, 2011: 325–332.
11. ZAJONC, O., FRYDRYCH, J.: The Mechanical Properties Of Pellets From Energy Grasses, Agritech Science, VÚZT, Praha, roč. 6, č. 2, 2013: 1-4. ISSN 1802-8942.

Corresponding author:

Ing. Ivo Balada, Department of Machinery Utilization, Faculty of Engineering, Faculty of Engineering, Czech University of Life Sciences in Prague, Kamýcká 129, Praha 6, Prague, 16521, Czech Republic, e-mail: baladai@tf.czu.cz

SOIL PHYSICAL PROPERTIES AS AFFECTED BY REPEATED WHEELING

F. E. Berisso

Institute of Technology, School of Biosystems and Environmental Engineering, Hawassa University, Hawassa Ethiopia

Abstract

A field experiment was carried out in the spring of 2015 to analyse the effect of field traffic on soil physical properties. A tractor used for wheeling and the experiment had a randomized block design with four replicate plots. Control and four repeated wheeling were used as treatments. Intact cores of 100 cm^3 were collected from and used for determination of soil mechanical and physical properties. The inflicted compaction was significantly increased bulk density at 10 and 20 cm depths, whereas the saturated hydraulic conductivity was reduced. At -6 and -30 hPa, the air-filled porosities were consistently lower for compacted soil than for control soil; whereas for most soil the values were higher than value proposed as the critical lower limit for plant growth. Our study hence documents that commonly used agricultural machinery may compact the soil to 0.3 m and even deeper with effect on important soil functions.

Key words: soil compaction, bulk density air –filled porosity, saturated hydraulic conductivity.

INTRODUCTION

In recent years, a growth in agricultural economy of Ethiopia has increased the dependence of agricultural operations on modern machineries such as tractors and combines harvesters. An increasing number of farmers are purchasing these machineries and associated drudgeries with farm operation are eased. On the other hand, high costs of these machineries, combined with timeliness of agricultural operations, force the owners to hire these equipments and operate even in wet soil condition, which increases high risk of soil compaction.

Compaction is a major problem affecting agricultural soil structure and this consequently leads to a reduction to crop production. Direct cause and effect relations appear to exist between the use of machinery and soil compaction, between soil compaction and a plant root environment, and between a plant root environment and crop production (HAMZA AND ANDERSSON, 2005). Compaction by wheel traffic, cultivation equipment, animals or natural processes can affect soil water movement by increasing bulk density and decreasing porosity and infiltration (ARVIDSSON, 2001). These changes can result in less soil water storage, poor nutrient movement, slowed gas exchange and restricted root growth, all of which can cause a reduction in crop yields (LIPIEC AND HATANO, 2003).

Due to these deleterious effects, soil compaction has received greater attention from different stakeholders, including public authorities and international policy makers, especially in developed countries. For instance, the European Union (EU) proposed an EU Soil Framework Directive to protect soil against threats that undermine its capacity to perform environmental, economic, social and cultural functions (COMMISSION OF THE EUROPEAN COMMUNITIES, 2006). Soil compaction has also been the subject of many studies, which are reported in books, research articles and review papers. Many international series of field experiments and projects have also been initiated at different times in order to address compaction effects on soil and crop yield, for example the Working Group on Soil Compaction by Vehicles with High Axle Load in 1980 (HÅKANSSON ET AL., 1987) and the POSEIDON project in 2009 (WWW.POSEIDON-NORDIC.DK).

Compared with these numerous studies and efforts worldwide, there are few reports from Ethiopia. Moreover, most of the data concerns the primitive agriculture or few estate farms alone. For instance, TADDESE ET AL. (2002) conducted study in primitive agriculture and reported higher bulk density in heavily grazed than in nongrazed medium grazed plots. TESHOME AND KIBRETE (2009) characterized soils of soil in one of the estate farms in terms of their physical and hydraulic properties and reported variation in soil bulk density. They attribute the observed differences entirely to soil management classes by disregarding the effect of agricultural machinery.

In Ethiopian context, there are a lack of studies that focus on the effect stresses due to agricultural machinery on soil compaction. The aim of this project was to analyse how soil compaction during field traffic effects soil pore structure and associated transport processes. The project was focused on immediate effect of agricultural machinery on water flow, soil air filled porosity, and bulk density. It was hypothesize that soil compaction affects the structure and functioning of soil pores.

MATERIALS AND METHODS

New compaction experiment was established in spring 2015 at Hawassa University Farm, which is located 260 km from capital city Addis Ababa. The field has been used for maize growth for many year and then used as experimental site for agronomy crops since 2007. Some physical and mechanical characteristics of the soil are shown in Tab. 1. Also listed is the soil water content during field sampling. Methods used to determine these properties are briefly described below.

Tab. 1. – Soil water content at sampling, soil texture, cohesion and angle of internal friction of the soils

Depth [m]	Water content [cm^3 cm^{-3}]	Clay <0.002 mm [g g^{-1}]	Silt 0.002-0.02 mm [g g^{-1}]	Sand 0.02-0.2 mm [g g^{-1}]	Cohesion kPa	Angle of internal friction (^{0})
0.10	0.36	0.17	0.21	0.62	54.0	36.1
0.20	0.34	0.19	0.24	0.57	54.2	34.5
0.30	0.37	0.20	0.24	0.56	58.0	33.8

Traffic experiment and machinery

The experiment had four replicate plots and wheeling was carried by a tractor, which was commonly used in the farm for tillage and harrowing operations. The front and rear wheel loads of the tractor were 750 and 3250 kg, respectively. The inflation pressure of the front tyres was of the tractor was 150 kPa, whereas that of the rear tyres 250 kPa. Wheeling was done by driving the tractor on the same track and the experiment had two treatments: 1) control treatments, which was not exposed to experimental traffic; 2) four repeated wheeling in single track by driving the tractor back and forth twice.

Field measurement and soil sampling

Penetrometer resistance was measured to a depth of 35 cm in the track before and immediately after wheeling. The outer area of the front and back tyres (footprint) was marked with sand while the tractor was stationary and photographed. The area was determined from image analysis of the footprint and used as an input in the *Soilflex* model by KELLER ET AL. (2007). Rut depth was measured after each wheeling at three different location of each plots.

After wheeling, access pits was carefully opened in each plot, and horizontal planes was sequentially prepared for sampling intact cores of 100 cm^3 at 10, 20 and 30 cm depth. Six replicate cores were collected from each plot and used to characterize physical and mechanical properties of the soil by a range of standard measurements in the laboratory as indicated below. Bulk soils of 1 kg were collected from each sampling plots at three depths (10, 20 and 30 cm) and used for determination of soil textural class.

The complete stress state in the soil profile beneath the machinery was predicted using the *SoilFlex* model presented by (KELLER ET AL., 2007). Soil deformation (change in soil volume, rut depth) was calculated according to the (O'SULLIVAN AND ROBERTSON, 1996) model, which is included in the SoilFlex.

Laboratory analyses

Prior to the experiment, all soil cores were carefully trimmed with a sharp-edged knife, covered with fine nylon cloth. Two replicate cores, at field moisture contents, were used to determine initial mechanical properties of the soil. The precompression stress and other mechanical properties (see Tab. 2) were derived by fitting Gompertz equation to stress-strain curve obtained from uniaxial confined compression test with odometer.

Soil cores used for measurement of saturated hydraulic conductivity (two replicate for each treatments) were saturated bottom with a distilled water containing 0.01 M $CaCl_2$. The saturation was done in three steps within 24 hours and the samples were kept in distilled water for a week in order to assure fully saturation. Samples used for measurement of water retention were transferred to sandboxes, where they sequentially drained to -6 and -30, hPa matric potentials. The cores were weighed at each matric potential and after oven-dried (105 ºC) for 24 hours. Bulk density (BD) was calculated from weight of oven-dried soil and total volume of the soil cores. Total porosity (θs) was calculated from BD and particle density (2.65 gm.cm^{-3} was used in this study). Gravimetric water content (w) was calculated as a difference between the weight of the samples at a given matric potential and at an oven dry. Volumetric water content at a given matric potential (θ) was calculated from w and BD. Air-filled porosity (ε_a) was calculated as a difference between θs and θ.

Tab. 2. – Soil parameters used for the simulations

Parameter	Symbol (unit)	Soil depth		
		10 cm	20 cm	30 cm
Specific volume[a] at p = 1 kPa	n (-)	2.335	2.382	2.383
Compression index[b]	λ_n (ln (kPa^{-1}))	0.114	0.131	0.130
Swelling index[a]	κ (ln (kPa^{-1}))	0.0040	0.0042	0.0026
Slope of the ‘steeper recompression line’[a]	κ' (ln (kPa^{-1}))	0.0214	0.0235	0.0020
Separation between yield line and virgin compression line[a]	M (-)	0.92	1.22	0.8600
Initial bulk density	ρ (Mg m^{-3})	1.31	1.33	1.36

[a] The soil depth refers to the midpoint depth of a sample of 3.8 cm height
[b] Calculated from oedometer tests by assuming s2 =s3 = 0.5 s1 (KOOLEN AND KUIPERS, 1983; KELLER ET AL., 2007)

The saturated hydraulic conductivity, K_{sat}, was measured using constant head method as described by KULTE AND DIRKSEN (1986). The measurements of average value of water discharge (Q), soil length (L), cross-sectional area of the soil sample (A), and hydraulic head (H), were used to determine the Ksat using (Equation 1).

$$q = K_{sat} \frac{\Delta H}{L} \tag{1}$$

Where q is Darcy flux density and given by q=Q/A. K_{sat} was then calculated as:

$$K_{sat} = \frac{QL}{AH} \tag{2}$$

Before analyses, the bulk samples were kept in the laboratory at room temperature (25 °C) and used for the analysis of soil textural class. The standard sieve-hydrometer method was used for this purpose.

Statistical analysis

In new compaction experiment, statistical analysis of all variables was performed using the MIXED procedure in SAS by assuming the effect of treatment and blocks as fixed and random, respectively. The Kenward and Roger method was used for calculating the degrees of freedom in the statistical tests (KENWARD AND ROGER, 1997). The normality of residuals was tested after fitting a linear mixed model to the data in order to ensure that the normality assumption of the model was satisfied.

RESULTS AND DISCUSSION

Predicted soil stress

Predicted mean normal stresses under front and rear wheels after four repeated wheeling are shown in Fig. 1. Research finding from Scandnevian (E.G. KELLER, 2004; KELLER ET AL., 2012) have been shown the occurrence of plastic deformation (irreversible compaction) when the vertical stress exceeds 50 kPa at water contents close to field capacity and this value has been suggested as a critical threshold for sustainable traffic in the field (SCHJØNNING ET AL., 2012). It can be note from Fig. 1 that the predicted vertical stress of front and rear wheels were exceeded this value at depths shallower than 25 and 50 cm, respectively. Based on this, one can assume that soil deformation has actually took place to approximately that depth during wheeling event.

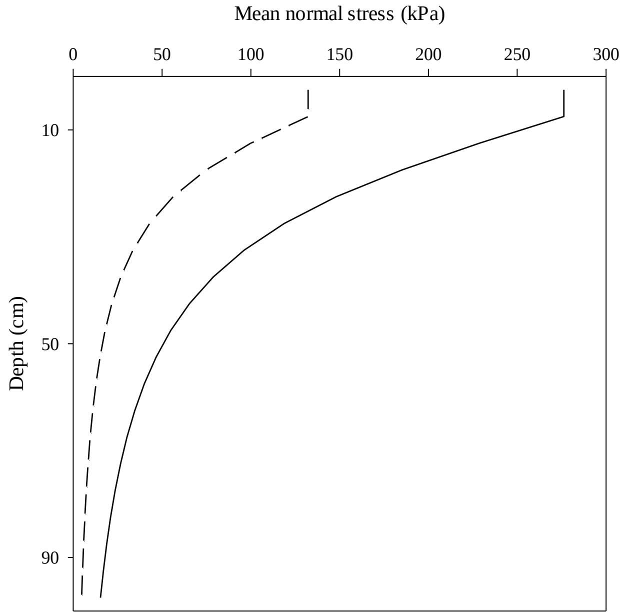

Fig. 1. – Calculated mean normal stress under the center line of the wheel rut (dotted line for front wheel; solid line for rear wheel)

Penetration resistance

Four repeated wheelings, during field experiment, had increased the penetration resistance of the soil at all depths down to 30 cm (Fig. 2), whereas significant differences were observed from 10-30 cm depth. In general, the penetration resistance was sharply increased from 0-10 cm depth for both control and wheeled plots. Similar trends were reported by ANSORGE AND GODWIN (2006),who measured penetration resistance immediately after wheel passes. However, such measurements should not be taken as a conservative estimate of compaction effect.

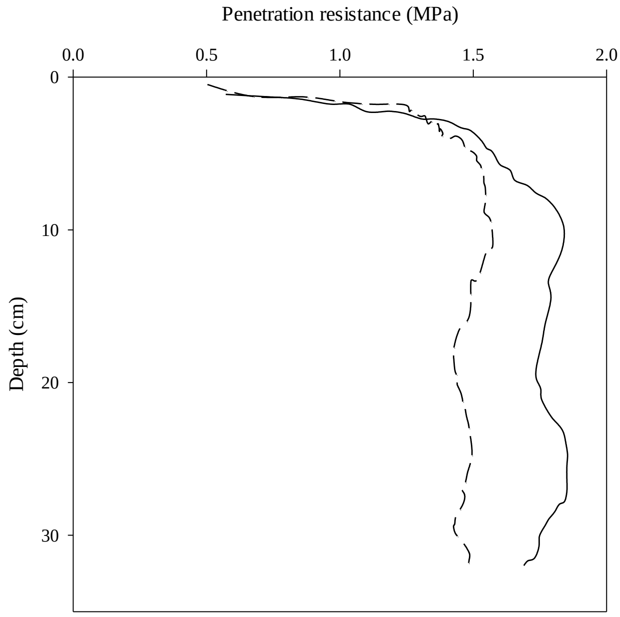

Fig. 2. – Penetration resistance measured before (dotted line) and after (solid line) four repeated wheelings

In control plots, this increase could be attributed to the residual effect of traffic from previous management or repeated traffic imposed during annual agricultural operations. Since there were no tillage activities during the time of wheeling, which can partially or fully alleviate compaction from preceding traffic, natural regeneration must occur by biological and abiotic activities in this soil, which might require much more time. However, no such activities were observed during sampling event.

Measured soil physical properties

Bulk density, air-filled porosity at -6 and -30 hPa, and saturated hydraulic conductivity for both control and compacted soils are shown Tab. 3. Results of the statistical analysis are also included in the figure. In general, four repeated wheelings increased the bulk density at all sampling depths, whereas significant differences were observed in the two upper sampling depth (Tab. 3).

Tab. 3. – Bulk density, air-filled pore space at -6(e_{a6}) and -30 (e_{a30}) hPa and saturated hydraulic conductivity for compacted and control treatments. The values shown are least squares means observed in four replicate blocks. P-values show the results of the linear mixed model tests on the differences between control and compacted treatments.

Depth (cm)		BD	Air filled porosity $m^3\ m^{-3}$ ε_{a6}	ε_{a30}	Saturated hydraulic conductivity cm day^{-1}
10	Control	1.28	0.06	0.11	182
	Compacted	1.35	0.04	0.09	74
	P-value	<0.01	<0.01	<0.01	<0.01
20	Control	1.33	0.08	0.14	166
	Compacted	1.36	0.04	0.12	124
	P-value	0.02	0.04	0.01	0.04
30	Control	1.36	0.07	0.17	143
	Compacted	1.37	0.05	0.15	123
	P-value	0.08	0.09	0.62	<0.01

Several researchers obtained similar results. For instance, from nine different six experiments in Sweden on soils with clay contents ranging from 19 to 256 g kg^{-1} of soil, ARVIDSSON (2001) observed significant increase in bulk density up to 50 cm depth in the compacted plots as compared to the control one. Despite this changes, bulk density observed in this study, both in compacted and control plots, was lower than the typical minimum bulk density at which root-restricting conditions occur according to USDA-NCRS (1996; CIT. KAUFMANN ET AL., 2010) for sandy clay loam (1.70 $g.cm^{-3}$) soil.

The air-filled porosity values, ε_a, measured at -6 and -30 hPa were lower in the compacted treatment than in the control treatment at all four soil depths (except at 30 cm depth). Our observed reductions in volume of ε_a at both matric potentials are similar to the findings of BERISSO ET AL. (2013). For soils from compacted treatment, the εa_6 values were below 10 % (0.1 $m^3\ m^{-3}$), the value which has been proposed as the critical lower limit for plant growth (GRABLE AND SIEMER, 1968). The low ε_a values in control soils indicate that the Hawassa soil was generally less dense and favourable for crop growth.

The function of soil pores can be evaluated from their ability to conduct water. At all three depths, the saturated hydraulic conductivity was lower in compacted than in control treatments at (Tab. 3). The finding is in agreement with HORTON ET AL. (1994), who reported a reduction in saturated hydraulic conductivity from 1437 to 224 cm day^{-1}in a no-till treatment and from 1892 to 291 cm day^{-1} in a chisel plough treatment due to field traffic.

In general, for both soils from compacted and control plots, the saturated hydraulic conductivity values of the Hawassa soil were considerably higher than

8.6 cm day^{-1}, which was established by MCQUEEN AND SHEPHERD (2002) as the critical limit for adequate hydraulic conductivity for crop growth. However, the saturated hydraulic conductivity values for compacted soil at 0.3 m depth was rather low compared with the extreme precipitation events in recent days. This situation inevitably increases the risk of surface ponding, which eventually leads to soil erosion and leaching of agro chemical to receiving water bodies.

Estimated and measured soil compaction

For soil considered in this study, the mean normal stresses (σ_m) were calculated from the principal stress components, and converted to total rut depth using O'SULLIVAN AND ROBERTSON, (1996) model. The calculated values are plotted against measured values in Fig. 4. Different researchers made similar attempts: for instance GUPTA AND RAPER (1994) used the major principal stress (σ_1) and predicted changes in bulk density across the wheel rut. In another study, BERISSO ET AL. (2013), predicted changes in total porosity from mean normal stress and reported good agreement between measured and predicted values. The results in these studies confirmed the validity of different component of stresses to predict volume change in the soil during deformation.

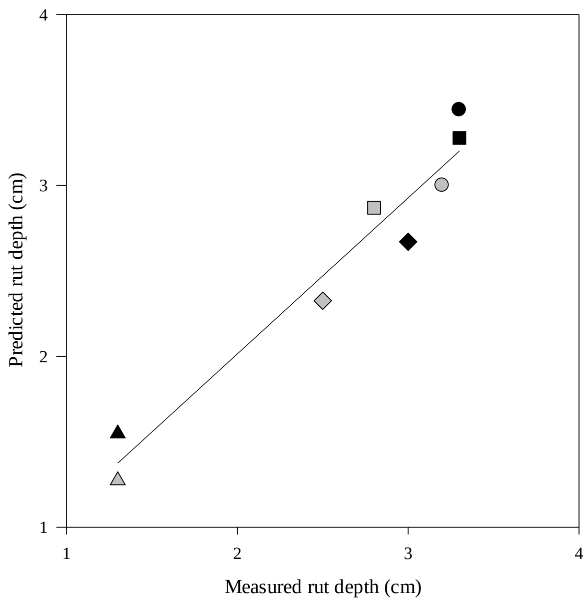

Fig. 3. – Measured and predicted rut depth for soils collected at 0 (circle), 10 (rectangle), 20 (diamond), and 30 (triangle) cm from center of wheel rut after two times (gray shaded) and four times (black shaded) wheeling

CONCLUSIONS

This study provides clear evidence that the top 0.3 m of agricultural soils may be mechanically compacted by traffic with heavy machinery. Our results further document that the compaction had immediate and negative effects on soil bulk density, air filled porosity and saturated hydraulic conductivity of the soil. The documented low hydraulic conductivity in the compacted soil may increase the risk of preferential convective flow of water in periods with high precipitation and may carry contaminants to receiving water bodies.

ACKNOWLEDGEMENTS

The author would like to thank Czech university of life science for financial support and Hawassa University farm for allowing him to use the farm plot.

REFERENCES

1. ANSORGE, D., GODWIN, R., 2006. High axle load - track - tire comparison In: R. Horn, H. Fleige, P. Stephan, X. Peng (Eds.), Soil management for sustainability. Advances in Geoecology 38. Catena verlahg GMBH, Reiskirchen, Germany, pp. 9-14.
2. ARVIDSSON, J., 2001. Subsoil compaction caused by heavy sugarbeet harvesters in southern Sweden: I. Soil physical properties and crop yield in six field experiments. Soil and Tillage Research 60(1-2), 67-78.
3. COMMISSION OF THE EUROPEAN COMMUNITIES., 2006. Proposal for a Directive of the European Parliament and of the Council establishing a framework for the protection of soil and amending Directive 2004/35/EC, Brussels, Belgium.

4. GRABLE, A.R., SIEMER, E.G., 1968. Effects of Bulk Density, Aggregate Size, and Soil Water Suction on Oxygen Diffusion, Redox Potentials, and Elongation of Corn Roots. Soil Sci. Soc. Am. J. 32(2), 180-186.
5. GUPTA, S.C., RAPER, R.L., 1994. Prediction of soil compaction under vehicles. In: B.D. Soane, C. van Ouwerkerk (Eds.), Soil compaction in crop production. Developments in Agricultural Engineering II. Elsevier Science B.V., pp. 71-90.
6. HÅKANSSON, I., VOORHEES, W.B., ELONEN, P., RAGHAVAN, G.S.V., LOWERY, B., VAN WIJK, A.L.M., RASMUSSEN, K., RILEY, H., 1987. Effect of high axle-load traffic on subsoil compaction and crop yield in humid regions with annual freezing. Soil and Tillage Research 10(3), 259-267.
7. HAMZA, M.A., ANDERSON, W.K., 2005. Soil compaction in cropping systems – a review of the nature, causes and possible solutions. Soil Tillage Res. 82, 121–145.
8. HORTON, R., ANKENY, M.D., ALLMARAS, R.R., 1994. Effects of compaction on soil hydraulic properties In: B.D. Soane, C. van Ouwerkerk (Eds.), Developments in agricultural engineering II: Soil compaction in crop production. Elsevier, Amsterdam-London-New York-Tokyo, pp. 141-165.
9. KELLER, T., 2004. Soil compaction and soil tillage studies in agricultural soil mechanics, Swedish University of Agricultural Sciences, Uppsala.
10. KELLER, T., DEFOSSEZ, P., WEISSKOPF, P., ARVIDSSON, J., RICHARD, G., 2007. SoilFlex: A model for prediction of soil stresses and soil compaction due to agricultural field traffic including a synthesis of analytical approaches. Soil Till Res 93(2), 391-411.
11. KENWARD, M.G., ROGER, J.H., 1997. Small sample inference for fixed effects from restricted maximum likelihood. Biometrics 53, 983-997.
12. KLUTE, A., DIRKSEN, C., 1986. Hydraulic conductivity and diffusivity: Laboratory Methods. In: A. Klute (Ed.), Method of soil analysis, Part 1. Physical and mineralogical methods. American Society of Agronomy-Soil Science Society of America, pp. 687-734.
13. LIPIEC, J., HATANO, R., 2003. Quantification of compaction effects on soil physical properties and crop growth. Geoderma 116, 107– 136.
14. MCQUEEN, D.J., SHEPHERD, T.G., 2002. Physical changes and compaction sensitivity of a fine-textured, poorly drained soil (Typic Endoaquept) under varying durations of cropping, Manawatu Region, New Zealand. Soil and Tillage Research 63(3–4), 93-107.
15. O'SULLIVAN, M.F., ROBERTSON, E.A.G., 1996. Critical state parameters from intact samples of two agricultural topsoils. Soil and Tillage Research 39(3-4), 161-173.
16. SCHJØNNING, P., LAMANDE, M., KELLER, T., PEDERSEN, J., STETTLER, M., 2012. Rules of thumb for minimizing subsoil compaction. Soil Use and Management 28(3), 378-393.
17. TADESSE, G., MOHAMMED SALEEM, M.A., ABIYE, A., WAGENEW, A., 2002. Impact og grazing on plant species richness, plant biomass, plant attribute, and soil physical and hydrological prpperties of vertisol in East Africa highlands. Environmental Management 29 (2), 279-289.
18. USDA-NCRS, 1996. Soil quality resource concerns: Compaction. USDA-NRCS Soil Quality Inst., Ames, IA.
19. TESHOME, Z., KIBRET, K., 2015. Charaterization of soil management groups of Metahara sugar estate in terms of their physical and hydraulic properties. Advances in Crop Science and Technology. 3:159.

Corresponding author:
Feto Berisso., Institute of Technology, School of Biosystems and Environmental Engineering, Hawassa University, Hawassa Ethiopia

CULTIVATION OF TALL WHEATGRASS AND REED CANARY GRASS FOR ENERGY PURPOSES IN TERMS OF ENVIRONMENTAL IMPACTS

J. Bernas, M. Kopecký, J. Moudrý Jr., Z. Jelínková, J. Moudrý, K Suchý

Faculty of Agriculture, University of South Bohemia in České Budějovice, Czech Republic

Abstract

Cultivation of energy crops for the production of thermal energy through direct combustion has become one of the trends within the ecological energetics. A number of perennial plants is grown in the conditions of the Czech Republic, too, for this purposes. One of them is reed canary grass (RCG). This species might gradually be replaced by another grass, better-performing tall wheatgrass (*Elymus elongatus* subsp. *ponticus* cv. Szarvasi-1). Greenhouse gas emission savings may be achieved due to the higher yield potential and energy yield when growing it. This article presents the results of emission load monitoring resulting from the RCG and Szarvasi-1cultivation for energy purposes. The simplified LCA method, respectively its Climate change impact category is used as a tool for emission load measuring. The results show that the emission savings of up to 45% per 1 GJ can be achieved when growing Szarvasi-1 for energy purposes in comparison with RCG.

Key words: energy grasses, greenhouse gases emissions, Life Cycle Assessment.

INTRODUCTION

Global energy demand increases in the context of demographic transition (HO AND SHOW, 2015). Fossil fuels represent a major source (VOSTRACKÝ ET AL., 2009). However, their combustion contributes to environmental pollution (NICOLETTI ET AL., 2015) and is responsible for a significant share of greenhouse gas emissions (GHG) (MOUTINHO ET AL., 2015). Moreover, they are not renewable (MASTNÝ ET AL., 2011) and thus their use is not sustainable (LIBRA AND POULEK, 2007). The importance of renewable energy sources (RES) increases in relation to the finite nature of fossil fuels (GÜRDIL ET AL., 2009). RES are considered as "clean" sources of energy (PANWAR ET AL., 2011). The most important renewable energy source is BIOMASS (JASINSKAS AND ŠATEIKIS, 2009) and the combustion of biomass, in particular (MALAŤÁK ET AL., 2008). The production of biogas is also widespread (JASINSKAS ET AL., 2008). Switching to biomass offers a range of economic, social and environmental benefits (SAIDUR ET AL., 2011), including the reduction in carbon dioxide emissions within the energy sector (LIND ET AL., 2016). The importance of the emission reduction, as well as fight against the climate change has been widely acknowledged (HOEL, 2011).

Many agricultural products may be used, inter alia, for energy purposes (ROBBINS ET AL., 2012). However, some plants are grown specifically for this purpose (LEWANDOWSKI ET AL., 2003). Their suitability has been examined to the present day (MAST ET AL., 2014) and, in the context of a changing climate, the special emphasis has been placed on the drought tolerance (KONVALINA ET AL., 2010). Perennial plants appear to be more suitable from an environmental point of view (KOPECKÝ ET AL., 2015). Grasslands perform a range of non-productive functions (SKLÁDANKA, 2007) and may also be recommended for the areas with high erosion risk (DUMBROVSKÝ ET AL., 2014). In addition, fewer fertilisers are required (LEWANDOWSKI ET AL., 2003) and grasslands have lower requirements for the pest and disease management (LEWANDOWSKI ET AL., 2000) in comparison with annual plants. For instance, RCG (*Phalaris arundinacea* L.) (TAHIR ET AL., 2011) or *Elymus elongatus* subsp. ponticus cv. Szarvasi-1 (CSETE ET AL., 2011) may be included into energy crops.

Although energy plants offer many advantages compared to fossil fuels, it is necessary to determine the impacts on all components of the environment that may be affected by their production (SAIDUR ET AL., 2011) or operation of the facilities using biomass for energy production (MALAŤÁK AND VACULÍK, 2008). Combustion of biomass in the combustion chambers intended for fossil fuels is technically possible, but very inefficient and high emissions of carcinogenic substances and aromatic hydrocarbons are produced. This also applies under unfavorable combustion conditions, as may be the low temperature combustion (OCHODEK ET AL., 2006). Many authors (i.e. DAS ET AL., 2010; OCHODEK ET AL., 2006) point out that energy plants compete with food crops for arable land. Therefore, it is recommended to grow energy crops on

marginal lands (LEWANDOWSKI ET AL., 2003) or degraded lands (VASSILEV ET AL., 2012).
For the quantification of specific emission loads in different farming systems, the LCA (Life Cycle Assessment) study (KOČÍ, 2009) or the simplified LCA (HOCHSCHORNER AND FINNVEDEN, 2003), evaluating environmental impacts of a product based on the assessment of the impact of material and energy flows that the monitored system exchanges with the environment (BISWAS ET AL., 2010), may be used. LCA is a transparent scientific tool (WEINZETTEL, 2008) which evaluates the environmental impact on the basis of inputs and outputs within the production system (O'BRIEN ET AL., 2014).
The aim of this study was to draw up models of technological processes during the practical cultivation of RCG (the Chrastava variety) and Szarvasi-1 and determine their emission load impact on the environment.

MATERIALS AND METHODS

The simplified method of Life Cycle Assessment (LCA), defined by the international standards of ČSN EN ISO 14 040 (CNI, 2006A) and ČSN EN ISO 14 044 (CNI, 2006B) was used as a tool to calculate the emission load. The results of the study were related to *the Climate Change Impact Category* expressed as an indicator of carbon dioxide equivalent (CO_2e). The SIMA Pro software and the ReCiPe Midpoint (H) method was used for the calculations. The functional unit of the system was 1 kg of the final product - dry matter (hereinafter referred to as DM) and 1 GJ obtained through combustion of the final product. Technological processes of the cultivation of RCG and Szarvasi-1 intended for the direct combustion was compiled based on primary data (field experiments at ZF JU in České Budějovice), as well as secondary data (acquired from the *Ecoinvent 2010* database, literature search and normative data on agricultural production technologies). The database uses data geographically related to central Europe. The primary data were collected between 2013 - 2016 and the secondary data between 2000 - 2015. The data selected for modelling are based on the average of commonly applied intensive farming technologies (KAVKA, 2006; WROBEL, 2009; CSETE ET AL., 2011; STRAŠIL, 2012). Agrotechnical operations from seedbed preparation, the amount of seeds and seedlings, the use of plant protection products, production and application of fertilizers, etc., to harvesting the main product and transport were included into the model system. Infrastructure was not included into the system processes.
Besides the emissions arising from the inputs mentioned above, so called field emissions (N_2O emissions) are also produced after the application of nitrogen fertilizers. The IPCC methodology (*Intergovernmental Panel on Climate Change*) is used to quantify them (DE KLEIN ET AL., 2008).
Furthermore, the CHNS analysis (elemental composition of phytomass) was carried out using the Vario EL CUBE within the BBOT Standard. The heat of combustion was calculated using the Mendeleev's Formula $Q_s^r = [81 \cdot C + 300 \cdot H - 26 \cdot (0 - S)] \cdot 4.187$ (kJ·kg^{-1}), as well as calorific value from the formula $Q_u = Q_v - 5.85 \cdot (W + 8.94 \cdot H) \cdot 4.186$ (kJ·kg^{-1}), where Q_v is the heat of combustion in kcal·kg^{-1} (HUBÁČEK ET AL., 1962).

RESULTS AND DISCUSSION

This paper evaluates the results of the 3-year cultivation of RCG and *Elymus elongatus* subsp. ponticus cv. Szarvasi-1 for the direct combustion purposes using the intensive farming technologies under one cut treatment. Based on the methodology and acquired data (DM yields, inputs and outputs of the growing cycle, heat of combustion and calorific value calculated from the elemental composition), it was possible to compile the life cycle of chosen energy plants and quantify their impact on the environment. As already mentioned, the results of the study were related to the *Climate Change Impact Category* expressed in the carbon dioxide equivalent where CO_2e = 1x CO_2; 23x CH_4; 298x N_2O, based on the difference in the effectiveness of these greenhouse gases (FORSTER ET AL., 2007; SOLOMON, 2007).
Fig. 1 shows the amount of phytomass harvested during each season The grasslands always underwent a one-phase harvest in late winter or early spring. In this period, the plants contain the highest amount of DM (Ø>75%) (STRAŠIL ET AL., 2011) which is favourable for the direct combustion.process. In this case, the harvest took place from 17.3. - 1.4. , when RCG contained on average 80.6% of DM and Srazvasi-1 78% of DM. The CHNS analysis (elemental composition) was carried out and the heat of combustion (Q_s^r) and calorific value (Q_u) was calculated in DM samples. Values are reported in Fig. 2.

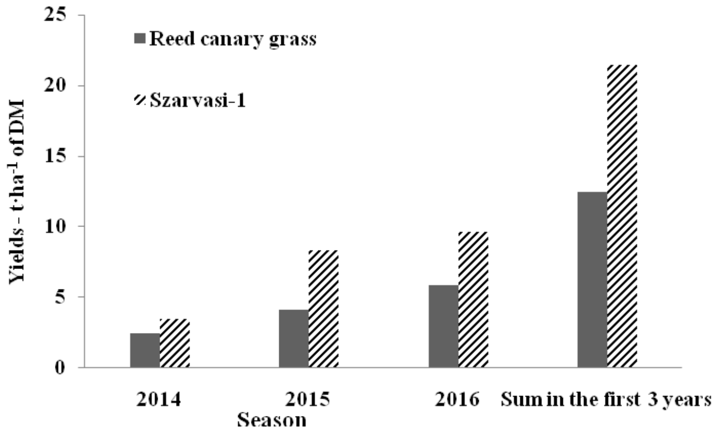

Fig. 1. – DM yields in particular years

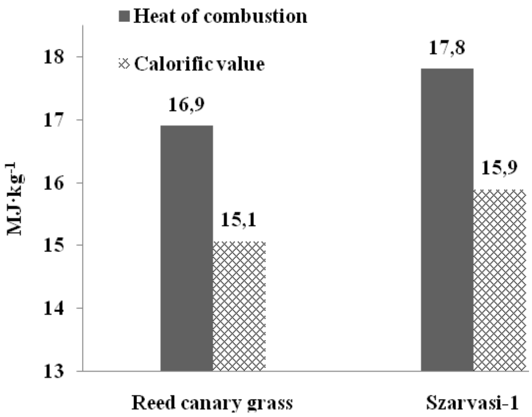

Fig. 2. – Heat of combustion and calorific value of chosen grasses calculated from the elemental analysis (MJ·kg^{-1})

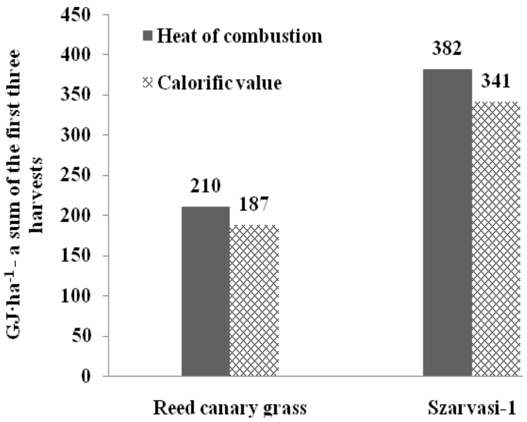

Fig. 3. – Net energy gain (a sum of the first three harvests) (GJ·kg^{-1})

The heat of combustion values of RCG (Q_s^r) are in accordance with ŠTINDL ET AL. (2006). He notes that the value is 16.6 ±0.20 (MJ·kg^{-1}) (calculated according to the Mendeleev's Formula). The heat of combustion of Szarvasi-1 is, according to the obtained data, on Ø 7% higher [Q_s^r = 17.8 (MJ·kg^{-1})], as well as the calorific value (Q_u Szarvasi-1 > Q_u RCG) in comparison with RCG (see Fig. 2). Q_u value is variable depending on the current moisture content of harvested phytomass. Fig. 3 presents the values of the total net energy gain (GJ·ha^{-1}) for the first three years. Szarvasi-1 can be regarded as more energy efficient due to the higher energy yield per production unit and higher production of phytomass per area unit. The total net energy gain of Szarvasi-1 (GJ·ha^{-1}) is almost $^1/_2$ higher in comparison with RCG on the basis of three-year monitoring. Based on these values, the emission load (in the form of CO_2e) per 1 kg DM and 1 GJ of the phytomass intended for direct combustion was then quantified (see Fig. 4).

Due to the identical farming technologies used for both species, the total net energy gain and yield is crucial in order to determine the difference between the emission loads at a profit of 1 GJ . As shown in Fig. 4, the difference in the total emission load in Szarvasi-1 cultivation (11.1 kg CO_2e·GJ^{-1}) and RCG cultivation (20.2 kg CO_2e·GJ^{-1}) is about 45%. A share of particular inputs and outputs of the growing cycle, making up the total emission load, is shown in Fig. 5.

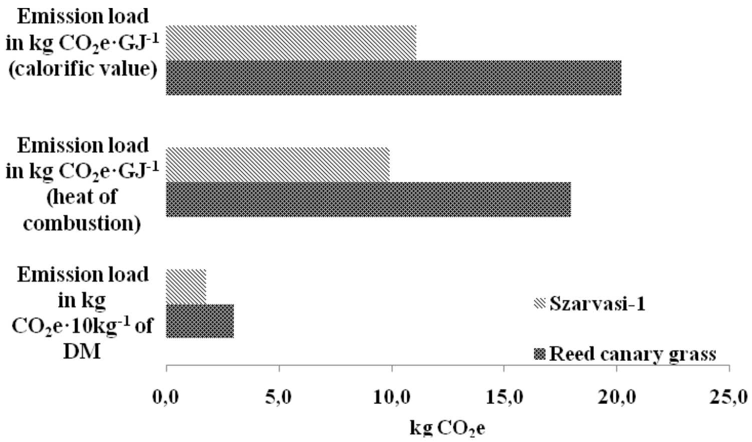

Fig. 4 - Emission load (kg CO_2e) per the production unit (1 GJ and 10 kg of DM)

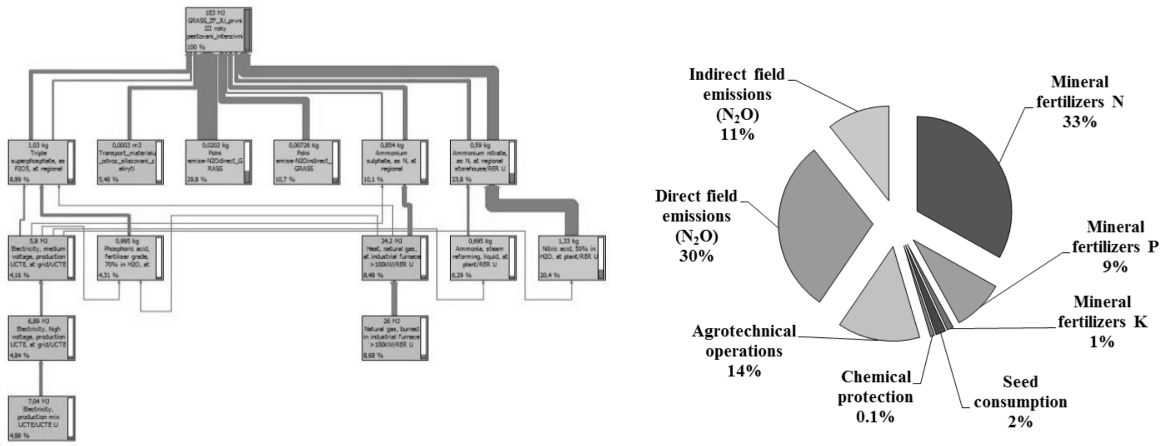

Fig. 5. – A share of particular inputs (in %) contributing to GHM emissions

Legend: Percentage of individual inputs is identical for both monitored grasses owing to the same farming technologies used.

The largest sources of GHG emissions from the crop production are fertilizers and their application (GATTINGER ET AL., 2012). In this case, the emissions arising from the use of mineral nitrogen fertilisers (33%) and the emissions resulting from their application represent the largest share of total emissions. These are known as field emission and can be divided into two categories: direct (30%) and indirect (11%). Agrotechnical operations (14%), particularly characterized by the consumption of fossil fuels, have a significant impact on the emission load. However, their consumption in the agricultural sector is, according to SAUERBECK (2002), considered less significant in comparison with the overall fuel consumption (in agriculturally advanced countries it is only about 3-4.5%).

Speaking of reductions in CO_2e production within the chosen cultivation process, it is necessary to focus especially on two of the strongest sources (application of nitrogen fertilizers and field emissions arising after the application of nitrogen fertilizers). For example, SMITH (2008) provides a variety of options of GHG mitigation within crop production In this regard, the issue of reduction in the dose of fertilizers or the total change of the agricultural system is often discussed (PAUSTIAN ET AL., 1998; MOUDRÝ ET AL., 2013). Also, the amount of emissions from agriculture is influenced to a great extent by farming systems. Conventional farming systems use more inputs in the form of fertilizers (organic and mineral), which are key factors in the mitigation of N_2O a NO emissions from soil. N_2O may be considered as the main greenhouse gas and organic farming systems generally produce less N_2O, as well as CO_2emissions due to lower inputs (BOS ET AL., 2007) and more close production cycle (KONVALINA ET AL. 2014A,B).

This paper points out the possibility of GHG mitigation per production unit (GJ) when growing different, more efficient energy grasses (Szarvasi-1) for direct combustion with the identical farming technologies. As the results show, Szarvasi-1 appears to produce more DM (21.4:12.4 $t \cdot ha^{-1}$ - (a sum of three harvests). It also has a higher heat of combustion (Q_s^r) (17.8:16.9 $MJ \cdot kg^{-1}$ of DM), as well as calorific value (Q_u) (15.9:15.1 ($MJ \cdot kg^{-1}$ of harvested material) and, in connection with this, a lower emission load per energy unit (11.1:20.2 kg CO2e·GJ-1). Therefore, Szarvasi-1 has a potential to gradually replace RCG, which has been grown for energy purposes last few years and, for example, has covered almost 70 thousand hectares in Finland (GHICA AND SAMFIRA, 2011).

CONCLUSIONS

The emission load per energy unit was quantified based on a three-year monitoring of selected energy grasses (RCG and *Elymus elongatus* subsp. ponticus cv.Szarvasi-1) grown for direct combustion. Based on the measured values, Szarvasi-1 appears to be more environmentally friendly alternative in comparison with RCG (11.1: 20.2 kg $CO_2e \cdot GJ^{-1}$). According to the monitoring, the difference is 45% per kg $CO_2e \cdot GJ^{-1}$. The article shows that GHG mitigation (related to a production unit) may be achieved through the replacement of existing plants by a more energy and yield efficient plant while maintaining the identical farming technologies. Further, mitigation could be initiated through the better management of mineral nitrogen fertilisers, extensive farming methods or a change of farming technology. Besides, cultivation of these perennial energy grasses brings extra benefits, such as the soil erosion protection, promotion of biodiversity and, when achieving appropriate yields of dry matter (> 12 $t \cdot ha^{-1}$ DM), economic efficiency.

ACKNOWLEDGEMENTS

This work was supported by the University of South Bohemia in České Budějovice research project GAJU 094/2016/Z.

REFERENCES

1. BISWAS, W. K., GRAHAM, J., KELLY, K., JOHN, M. B.: Global warming contributions from wheat, sheep meat and wool production in Victoria, Australia - A life cycle assessment. J. Cleaner Prod., 30, 2010: p. 1-7.
2. BOS, J. F. F. P., DE HAAN, J. J., SUKKEL, W., SCHILS, R. L. M.: Comparing energy use and greenhouse gas emissions in organic and conventional farming systems in the Netherlands. In: 3rd QLIF Congress: Improving Sustainability in Organic and Low Input Food Production Systems, March 20 – 23, 2007: pp. 439-443. University of Hohenheim, Germany.
3. CSETE, S., STRANCZINGER, S. , SZALONTAI, B., FARKAS, Á., PÁL, R. W., SALAMON-ALBERT, É., KOCSIS, M., TÓVÁRI, P. ,VOJTELA, T., DEZSŐ, J., WALCZ, I., JANOWSZKY, Z., JANOWSZKY, J., BORHIDI, A.: Tall Wheatgrass Cultivar Szarvasi-1 (*Elymus elongatus* subsp. ponticus cv. Szarvasi-1) as a Potential Energy Crop for Semi-Arid Lands of Eastern Europe. In: NAYERIPOUR (Ed): Sustainable Growth and Applications in Renewable Energy Sources. pp. 269–295. Rijeka, Croatia, InTech 2011.
4. CSN EN International Organisation for Standardisation (ISO) 14040 Environmental Management – Life Cycle Assessment – Principles and Framework. Czech Office for Standard, Prague, Czech Republic, 2006a.
5. CSN EN International Organisation for Standardisation (ISO) 14040 Environmental management – Life Cycle Assessment – Requirements and Guidelines. Czech Office for Standard, Prague, Czech Republic, 2006b.
6. DAS, S., PRIESS, J. A., SCHWEITZER, CH.: Biofuel Options for India-Perspectives on Land Availability, Land Management and Land-Use Change. J BIOBASED MATER BIO, 13, 2010: 243-255.
7. DE KLEIN, C., NOVOA, R. S. A., OGLE-SMITH, K. A., ROCHETTE-WIRTH, T. C., MCCONKEY, B. G., MOSIER, A., RYPDAL, K.: N_2O emissions from managed soils, and CO_2 emissions managed from lime and urea aplications. In EGGLESTON, S. et al. (Eds.): 2006 IPCC Guidelines for National Greenhouse Gas Inventories. Volume: Agriculture, Forestry and Other Land Use. IGES, 2006, pp. 11.1-11.54. Japan.
8. DHILLON, R. S., VON WUEHLISCH, G.: Mitigation of Global Warming Through Renewable Biomass. Biomass Bioenergy, 48, 2013: 75–89.
9. DUMBROVSKÝ, M., SOBOTKOVÁ, V., ŠARAPATKA, B., CHLUBNA, L., VÁCHALOVÁ, R.: Cost-effectiveness evaluation of model design variants of broad-base terrace in soil erosion control. Ecol. Eng., 68, 2014: 260–269.
10. FORSTER, P., RAMASWAMY, V., ARTAXO, P., BERNTSEN, T., BETTS, R., FAHEY, D. W., HAYWOOD, J., LEAN, J., LOWE, D. C., MYHRE, G., NGANGA, J., PRINN, R., RAGA, G., SCHULZ M., VAN DORLAND, R.: Changes in atmospheric constituents and in radiative forcing. In: SOLOMON, S., QIN, D., MANNING, M., CHEN, Z., MARQUIS, M., AVERYT, K. B., TIGNOR, M., MILLER, H. L. (EDS.): Climate Change 2007: The physical science basis. Contribution of working group i to the fourth assessment report of the Intergovernmental panel on climate change. United Kingdom and New York, USA, Cambridge University Press, Cambridge 2007.
11. GATTINGER, A., MULLER, M., HAENI, C., SKINNER, A., FLIESSBACH, N., BUCHMANN, U., NIGGLI, U.: Enhanced Top Soil Carbon Stocks under Organic Farming. Proc. Natl. Acad. Sci., 109 (44), 2012: 18226–18231.

12. GHICA, A., SAMFIRA, I.: Bibliographic study of genetic process in *Phalaris arundinacea*. Research Journal of Agricultural Science, 43, 2011: 65-71.
13. GÜRDIL, G. A., MALAT'ÁK, J., SEIVI, K. Ç., PINAR, Y.: Biomass utilization for thermal energy. AMA-AGR MECH ASIA AF, 40, 2009: 80–85.
14. HO, Y. C., SHOW, K. Y.: A perspective in renewable energy production from biomass pyrolysis-challenges and prospects. Curr. Org. Chem., 19, 2015: 423-436.
15. HOEL, M.: The green paradox and greenhouse gas reducing investments. International Review of Environmental and Resource Economics, 5, 2011: 353–379.
16. HUBÁČEK, J., KESSLER, F., LUDMILA, J., TEJNICKÝ, B.: Coalchemistry. SNTL, Prague and SVTL Bratislava 1962. (in Czech).
17. JASINSKAS, A., ZALTAUSKAS, A., KRYZEVICIENE, A.: The investigation of growing and using of tall perennial grasses as energy crops. Biomass Bioenergy, 32, 2008: 981–987.
18. JASINSKAS, A., ŠATEIKIS, I.: Evaluation of plant biomass potential and technologies of biomass preparation and utilization for energy purposes in Lithuania. In: The fourth international scientific conference Rural Development 2009: pp. 327–332.
19. KAVKA, M.: Norms of agricultural production technologies: cultivation and breeding technology and normative calculation. 1st Ed., Prague, Czech Republic, ÚZPI 2006. (in Czech).
20. KOČÍ, V.: Life cycle assessment LCA. 1st Ed., Ekomonitor, Chrudim 2009. (in Czech).
21. KONVALINA, P., MOUDRÝ, J., DOTLAČIL, L., STEHNO, Z., MOUDRÝ, J. JR.: Drought tolerance of land races of emmer wheat in comparison to soft wheat. Cereal Res. Commun., 38, 2010: 429–439.
22. KONVALINA, P., MOUDRÝ, J., UCHÝ, K., CAPOUCHOVÁ, I., JANOVSKÁ, D.: Diversity of carbon isotope discrimination in genetics resources of wheat. Cereal Res. Commun., 42, 2014: 687–699.
23. KONVALINA, P., STEHNO, Z., CAPOUCHOVÁ, I., ZECHNER, E., BERGER, S., GRAUSGRUBER, H., JANOVSKÁ, D., MOUDRY, J.: Differences in grain/straw ratio, protein content and yieldin landraces and modern varieties of different wheat species under organic farming. Euphytica 199, 2014a: 31–40.
24. KOPECKÝ, M., BERNAS, J., MOUDRÝ, J. JR., KOBES, M.: Germination of selected grass species in water stress conditions. In: SEED AND SEEDLINGS: XII. Scientific and technical seminar. Prague: Czech University of Life Sciences Prague, 2015, pp. 216–221. (in Czech).
25. LEWANDOWSKI, I., CLIFTON-BROWN, J. C., SCURLOCK, J. M. O., HUISMAN, W.: Miscanthus: European experience with a novel energy crop. Biomass Bioenergy, 19, 2000: 209–227.
26. LEWANDOWSKI, I., SCURLOCK, J. M. O., LINDVALL, E., CHRISTOU, M.: The development and current status of perennial rhizomatous grasses as energy crops in the US and Europe. Biomass Bioenergy, 25, 2003: 335–361.
27. LIBRA, M., POULEK, V.: Resources and energy use. 1st ed., Prague, Czech republic, Czech University of Life Sciences Prague 2007 (in Czech).
28. LIND, S. E., SHURPALI, N. J., PELTOLA, O., MAMMARELLA, I., HYVÖNEN, N., MALJANEN, M., RÄTY, M., VIRKAJÄRVI, P., MARTIKAINEN, P. J.: Carbon dioxide exchange of a perennial bioenergy crop cultivation on a mineral soil, Biogeosciences, 13, 2016: 1255–1268.
29. MALAŤÁK, J., GURDIL, G. A., JEVIČ, P., SELVI, K. Ç.: Biomass Heat-Emission Characteristics of Energy Plants. AMA-AGR MECH ASIA AF, 39, 2008: 9–13.
30. MALAŤÁK, J., VACULÍK, P.: Biomass for energy production. 1st ed., Prague, Czech republic, Czech University of Life Sciences Prague 2008 (in Czech).
31. MAST, B., LEMMER, A., OECHSNER, H., REINHARDT-HANISCH, A., CLAUPEIN, W., GRAEFF-HÖNNINGER, S.: Methane yield potential of novel perennial biogas crops influenced by harvest date. Ind Crops Prod, 58, 2014: 194-203.
32. MASTNÝ, P., DRÁPELA, J., MIŠÁK, S., MACHÁČEK, J., PTÁČEK, M., RADIL, L., BARTOŠÍK, T., PAVELKA, T.: Renewable sources of electricity. 1st ed., Prague, Czech republic, Czech technical university in Prague 2011 (in Czech).
33. MOSIER, A., KROEZE, C., NEVISON, C., OENEMA, O., SEITZINGER, S., VAN CLEEMPUT, O.: Closing the global N2O budget: Nitrous oxide emissions through the agricultural nitrogen cycle. Nutrient Cycling in Agroecosystems, 52, 1998: 25-248.
34. MOUDRÝ, J. JR., JELÍNKOVÁ, Z., MOUDRÝ, J., KOPECKÝ, M., BERNAS, J.: Production of greenhouse gases within cultivation of garlic in conventional and organic farming system production of greenhouse gases within cultivation of garlic in conventional and organic farming system. Lucrări Ştiinţifice: seria Agronomie. 53, 2013: 1-4.
35. MOUTINHO, V., MADALENO, M., SILVA, P. M.: Which factors drive CO2 emissions in EU-15? Decomposition and innovative accounting. Energy Efficiency, 2015: 1–27.
36. NICOLETTI, G., ARCURI, N., NICOLETTI, G., BRUNO, R.: A technical and environmental comparison between hydrogen and some fossil fuels. ENERG CONVERS MANAGE, 89, 2015: 205–213.
37. O'BRIEN, D., SHALLOO, L., CROSSON, P., DONNELLAN, T., FARRELLY, N., FINNAN, J., SCHULTE, R.: An evaluation of the effect of greenhouse gas accounting methods on a marginal abatement cost curve for irish agricultural greenhouse gas emissions. Environ. Sci. Policy, 39, 2014: 107–118.
38. OCHODEK, T., KOLONIČNÝ, J., JANÁSEK, P. The potential of biomass, species balance and fuel properties of biomass. 1st ed., Ostrava, Czech republic, Energy Research Center 2006 (in Czech).
39. PANWAR, N. L., KAUSHIK, S. C., KOTHARI, S.: Role of renewable energy sources in environmental protection: A review. Renew. Sustainable Energy Rev., 15, 2011: 1513–1524.
40. PAUSTIAN, K., COLE, C. V., SAUERBECK, D., SAMPSON, N.: CO_2 Mitigation by agriculture: an Overview. Climatic Change, 40, 1998: 135–162.
41. ROBBINS, M. P., EVANS, G., VALENTINE, J., DONNISON, I. S., ALLISON, G. G.: New opportunities for the exploitation of energy crops by thermochemical conversion in Northern Europe and the UK. Prog. Energ. Combust., 38, 2012:138–155.
42. SAIDUR, R., ABDELAZIZ, E. A., DEMIRBAS, A., HOSSAIN, M. S., MEKHILEF, S.: A review on biomass as a fuel for boilers. Renew. Sustain. Energy Rev., 15, 2011: 2262–2289.
43. SAUERBECK, D. R.: CO2 emissions and C sequestration by agriculture perspectives and limitations. Agric., Ecosyst. Environ., 91, 2002: 175-189.
44. SIMAPro 8.1: LCA software produced by PRe Consultants B.V., Netherlands, 2015.
45. SKLÁDANKA, J.,: Species diversity of grassland and its relationship to production and non-production functions. In: SKLÁDANKA, J., VESELÝ, P. (Ed.): The grassland as landscaping element, pp. 24–32. Brno, Czech Republic, Mendel University in Brno 2007 (in Czech).

46. SMITH, P., MARTINO, D., CAI, Z., GWARY, D., JANZEN, H., KUMAR, P., SCHOLES, B.: Greenhouse gas mitigation in agriculture. philosophical transactions of the royal society B: Biological Sciences, 363, 2008: 789–813.
47. SOLOMON, S.: Climate change 2007–The physical science basis: Working group I contribution to the fourth assessment report of the IPCC. 4nd ed., Cambridge University, UK, Solomon 2007.
48. ŠTINDL, P., KOLÁŘ, L., KUŽEL, S.: Combustion heat of biomass and its calculation from elementary composition. In: Agroregion 2006 – Increasing competitiveness in agriculture (soil - the basis for the competitiveness of agriculture), 2006, pp. 136–140, České Budějovice, Czech Republic. (in Czech).
49. STRAŠIL, Z., KOHOUTEK, A., DIVIŠ, J., KAJAN, M., MOUDRÝ, J., MOUDRÝ, J. JR.: Grasses as a source of energy. 1st ed., Prague, Czech Republic, Crop research institute 2011 (in Czech).
50. STRAŠIL, Z.: Evaluation of reed canary grass (*Phalaris arundinacea* L.) grown for energy use. Res. Agric. Eng., 58, 2012: 119-130.
51. SZABÓ, G., FAZEKAS, I., SZABÓ, S., SZABÓ, G., BUDAY, T., M PALÁDI, M., KERÉNYI, A.: The Carbon Footprint of a Biogas Power Plant. Environ. Eng. Manage. J., 13, 2014: 2867–2874.
52. TAHIR, M. H. N., CASLER, M. D., MOORE, K. J., BRUMMER, E. CH.: Biomass yield and quality of reed canary-grass under five harvest management systems for bioenergy production. BIOENERG RES., 4, 2011: 111–119.
53. TOMA, Y., KIMURA, S. D., HIROSE, I., KUSA, K., HATANO, R.: Variation in the emission factor of N2O derived from chemical nitrogen fertilizer and organic matter: A case study of onion fields in Mikasa, Hokkaido, Japan. Soil Sci. Plant Nutr., 53, 2007: 692-703.
54. VASSILEV, S. V., BAXTER, D., ANDERSEN, L. K., VASSILEVA, CH. G., MORGAN, T. J.: An overview of the organic and inorganic phase composition of biomass. Fuel, 94, 2012: 1–33.
55. VOSTRACKÝ, Z., JEŽEK, V., KORECKÝ, M., POLÍVKA, J.: Electrical energy is the key to the harmonious development of world. In: Proceedings of the 5th international scientific symposium on electric power engineering – Electroenergetics, 2009, pp. 20-25, Košice, Slovakia, Technical University (in Czech).
56. WROBEL, C., COULMAN, B. E., SMITH, D. L.: The potential use of reed canary grass (P*halaris arundinacea* L.) as a biofuel crop. Acta Agr. Scand. B - S. P., 59, 2009: 1–18.

Corresponding author:
Jaroslav Bernas, Faculty of Agriculture, University of South Bohemia in České Budějovice, Studentská 1668, České Budějovice, 370 05, Czech Republic, e-mail: bernas@zf.jcu.cz

THERMAL ANALYSIS OF ROOT VEGETABLE AT 30 – 90 °C

J. Blahovec

Department of Physics, Faculty of Engineering, Czech University of Life Sciences, Prague, Czech Republic

Abstract

Roots of carrot, parsley and black radish were studied by DMA in temperature range 30 – 90 °C using vibrations with frequency 1 Hz and temperature increase 1 °C/minute. From directed measured quantities the storage modulus and the loss modulus were determined and the relative temperature slopes (SMR and LMR) were calculated. These new quantities have a characteristic minimum at temperatures T_m at 50 – 70 °C. It was shown that with increasing T_m the observed minima of SMR and LRM are deeper. The observed behavior is discussed in relation with thermal destruction of the cell membranes; initially due to cell pore proteins denaturation and lately by direct destruction of the cell wall membrane. Deeper knowledge of the thermal stimulated processes in the cell walls of vegetable is important for their optimal processing as food components.

Key words: DMA, modulus of elasticity, cell membrane, destruction, cooking.

INTRODUCTION

Thermal processing of fruits and vegetables is a frequent operation in every kitchen. In last years (E.G. IMAIZUMI ET AL., 2015; FUENTES ET AL., 2014) it is more and more clear that quality of the product of thermal processing in this case sensitively depends on details of the whole process. Although the role of temperature as an important external parameter for living organisms is generally known (GARRET AND GRISHAM, 2010), there is still a lack of information on the details of the parallel processes taking place in living cells and tissues as well as in some foods during their heating. The group of methods applied in this area for indirect study of the processes includes the methods of thermal analysis (PRICE, 2002). The modulus of elasticity of a tested specimen is the main recorded parameter in a DMA test during the specimen heating (GEORGET ET AL., 2002; PRICE, 2002). The DMA test makes possible the measurement of two components of the complex modulus: the real part (storage modulus, SM) expressing the elastic part of the material toughness, and the imaginary part (loss modulus, LM) describing the inelastic (fluid) part of the toughness. The modulus of elasticity of cellular walls decreases with increasing temperature in the same way as the modulus of elasticity of other substances (WARD, 1983). This decrease, as well as the changes in the intracellular pressure during the specimen heating, can be displayed in DMA's modulus-temperature plots.

Equilibrium between the tissue symplast and its apoplast plays an important role in the temperature controlled tissue properties (PERSONIUS AND SHARP, 1938; SAKURAI, 2002): changes in this equilibrium can be well detected also by electric means (IMAIZUMI ET AL., 2015; FUENTES ET AL., 2014).

In previous papers (BLAHOVEC AND LAHODOVÁ, 2011, 2012; BLAHOVEC ET AL., 2012) we used DMA for the detection of starch swelling in cells of potato parenchyma under conditions of high humidity. The observed characteristic peaks at temperatures above 70 °C, i.e. close to the temperature of starch gelatinization in potato tubers (KARLSSON AND ELIASSON, 2003 A,B) were explained by the cell starch swelling pressure (BLAHOVEC AND LAHODOVÁ, 2011). Similar role can be played also by the cellular turgor pressure as an important source of the tissue toughness (NILSSON ET AL., 1958). The turgor pressure sensitively depends on the temperature stimulated changes in the cellular plasmodesma (e.g. the changes in the pore protein conformation – folding - caused e.g. by the protein denaturation - MAULE, 2008; MINETTI AND REMETA, 2006; SEIDI ET AL., 2009; TSONG AND SU, 1999). The pore proteins have very complicated structures; thus, for the structure of plasmodesma, MAULE (2008) gave more than 20 components and different proteins including of cytoskeletal components, such as actin, and dynamic motor proteins such as myosin. The temperature stimulated folding in the conformed components can cause deep changes in pore function (KUBELKA ET AL., 2004) and may be also a source of the plasmodesma stability (DE WEER, 2000). The changes in the plant tissue rigidity during heating at temperatures 40-80 °C, i.e. at protein denaturation temperatures, were observed in previous DMA experiments (for carrot see BLAHOVEC AND LAHODOVÁ, 2012A; XU AND LI, 2014).

Trying to detect the basic changes in the vegetable cell membrane during its heating, we applied standard DMA to three vegetable products. We supposed under the standard hypothesis that the heating process causes the same and/or similar changes in the plasmodesma. The main aim of the experiments is to detect the possible differences in the resulting changes caused by the standard heating process in the DMA temperature scan.

MATERIALS AND METHODS

Fresh roots of carrot (Daucus carota, subsp. Sativa, diameter about 4 cm and length about 15 cm), parsley (diameter also about 4 cm), and black radish (diameter about 10 cm) were bought from the local market and stored in cold and wet conditions (4 °C, 85% relative humidity). After a short storage (less than 2 weeks), the roots were washed in cold water. The selected defect-free roots of medium size were then left at room temperature for testing the next day.

Rectangular specimens measuring 8 (width) × 3 (thickness) × 22 (length) mm with the long axis parallel to the root axis were cut from the myzoderma (outer part of the tested roots) using special cutting jigs. From one root, four specimens were prepared. In case of carrot and black radish the specimens of the same dimensions were also prepared from the central part of the roots. In these cases we distinguished outer and central parts.

The DMA experiment was performed with a special DMA instrument, constructed by RMI company (Pardubice, Czech Republic), model DX04TC. Each specimen was mechanically fixed in two points so that the longitudinal axis was perpendicular to the fixing jaws. The free length of the specimen between the jaws was 10.8 mm. The height of the fixed specimen was approx. 3 mm. One of the jaws was fixed, while the other moved up and down with a constant amplitude = 1 mm at a frequency = 1 Hz. The force connected with the oscillation was recorded, being the basis for the complex modulus determination (storage - SM and loss - LM). The moduli values (originally in Pa) are sensitive to the form of the tested specimen. To prevent this source of variation we calculated the resulting SM and LM values as a ratio of the corresponding value obtained for SM at 30 °C. This method is suitable for the determination of peak positions and the slope analysis. Every experiment started at a temperature of 30 °C and 90% air humidity in the test chamber. The humidity was kept constant during the whole experiment, while the temperature increased up to 90 °C with constant rate 1 °C/minute. Every test was repeated ten times using fresh specimens.

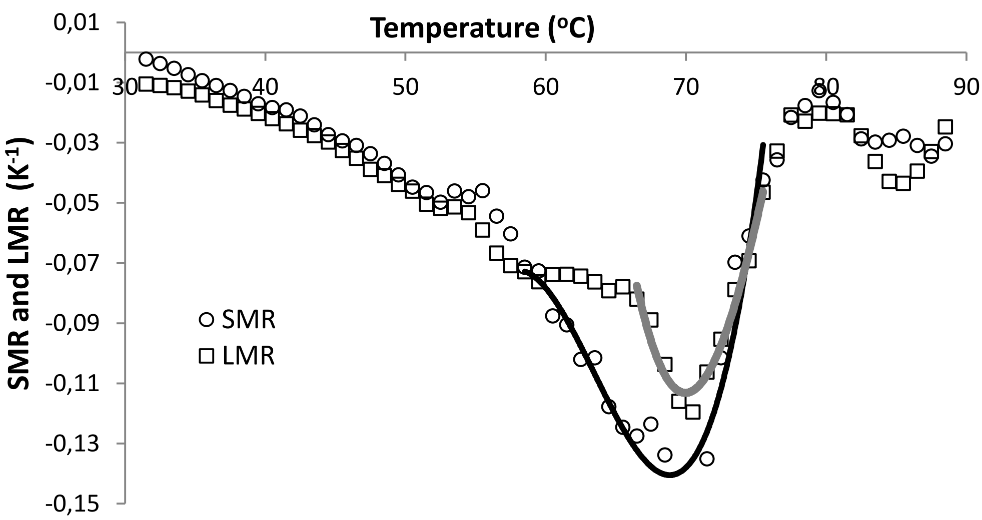

Fig. 1. – Typical temperature plots of SMR and LMR. The data were obtained for central parts of carrot. Approximation by cubic polynomials (Eq. (2)) is given by thick lines (black for SRM and grey for LMR)

The experimental results were analyzed using the standard laboratory software OriginPro Ver. 7 (Origin Lab, Northampton, MA, USA). The analysis was focused on the temperature slopes of SM and LM that are expressed in logarithmic scale. The resulting parameters denoted as SMR and LMR defined by the following formula (BLAHOVEC AND LAHODOVA, 2013):

$$SMR = \frac{1}{SM}\frac{\mathrm{d}SM}{\mathrm{d}T} = \frac{\mathrm{d}\ln(SM)}{\mathrm{d}T} \quad (1a)$$

$$LMR = \frac{1}{LM}\frac{\mathrm{d}LM}{\mathrm{d}T} = \frac{\mathrm{d}\ln(LM)}{\mathrm{d}T} \quad (1b)$$

where T is temperature. Both SMR and LMR have the same dimension: K^{-1}. The data were analysed using the software Origin® with smoothing the data initially by averaging every 5 neighbouring points, followed by differentiating the smoothed data. The data obtained from the analysis of the slopes of the individual plots were then unified and classified into classes of 1 °C wide. The basic statistical analysis of the individual classes was then done using a special FORTRAN program made for this purpose.

RESULTS AND DISCUSSION

Examples of the measured thermal scans are given in Fig. 1, where are plotted SMR and LMR (see Eq. (1 a,b)) for the central part of carrot. This figure contains typical minima in range 50-70 °C. The experimental scans were approximated close to their minima by cubic polynomials (see Fig. 1):

$$y = a + bT + cT^2 + eT^3 \quad (2)$$

and positions of the minima T_m were then found by solving the quadratic equation:

$$\frac{\mathrm{d}y}{\mathrm{d}T} = 3eT_m^2 + 2cT_m + b = 0 \quad (2a)$$

Tab. 1. – Results obtained by analysis of SMR minima from Fig. 1. Eqs. (1) and (1a) are used

	Carrot O	Carrot C	Parsley	Radish O	Radish C
e/0.00001	8.18	10.83	-22.32	-6.05	-7.47
c	-0.0152	-0.0206	0.0433	0.0108	0.0131
b	0.936	1.299	-2.794	-0.640	-0.759
a	-19.04	-27.18	59.75	12.50	14.54
R^2	0.913	0.893	0.839	0.862	0.915
T_m	68.6	68.8	60.9	55.0	54.4
SMR_m	-0.149	-0.139	-0.119	-0.076	-0.092

Symbol O and C mean the outer part of root and the central part of root, respectively

Tab. 2. – Results obtained by analysis of LMR minima from Fig. 1. Eqs. (1) and (1a) are used

	Carrot O	Carrot C	Parsley	Radish O	Radish C
e/0.00001	-0.36032	-8.7658	-5.4488	-8.0803	-3.6397
c	0.0014	0.0211	0.0112	0.0141	0.0066
b	-0.140	-1.661	-0.760	-0.812	-0.396
a	3.97	42.96	17.05	15.54	7.80
R^2	0.930	0.961	0.843	0.902	0.913
T_m	65.4	70.0	63.2	54.7	55.4
LMR_m	-0.114	-0.115	-0.094	-0.069	-0.079

Symbol O and C mean the outer part of root and the central part of root, respectively

Analysis of all minima was performed and resulting values are concentrated in Tab. 1 and 2. These tables show that the obtained values for T_m differ for different analyzed roots and they are also different for SRM and LRM. It means that the processes detected in the heated roots are not spontaneous and well defined by temperature only. Its character is rather kinetic, i.e. they depend not only on temperature but also on time; temperature scans depend on rate of heating as it was observed previously (BLAHOVEC AND LAHODOVA, 2012A). Both SMR_m and LMR_m in Tab. 1 and 2 decrease with increasing T_m. More exactly it is described in Fig. 2 where the relations between both characteristic quantities SMR_m and LRM_m and the temperatures in the observed minima were approximated by lines.

The corresponding linear equations have a common point at T_{mm} = 44.26 °C with SMR_{mm} = LRM_{mm} = -0.0423 K^{-1}. It seems that at this temperature begins the thermal range in which the vegetable cells are opened by the thermally activated denaturation of cell pore proteins (BLAHOVEC AND LAHODOVA, 2012A; IMAIZUMI ET AL., 2015). This process is very complicated and can be influenced either by the type of plant, the conditions of cultivation, the variety, the conditions of storing, and of cause the details of heating. BLAHOVEC AND LAHODOVA (2012A) observed that for carrot the quicker heating leads to higher T_m values, sometimes higher than 70 °C.

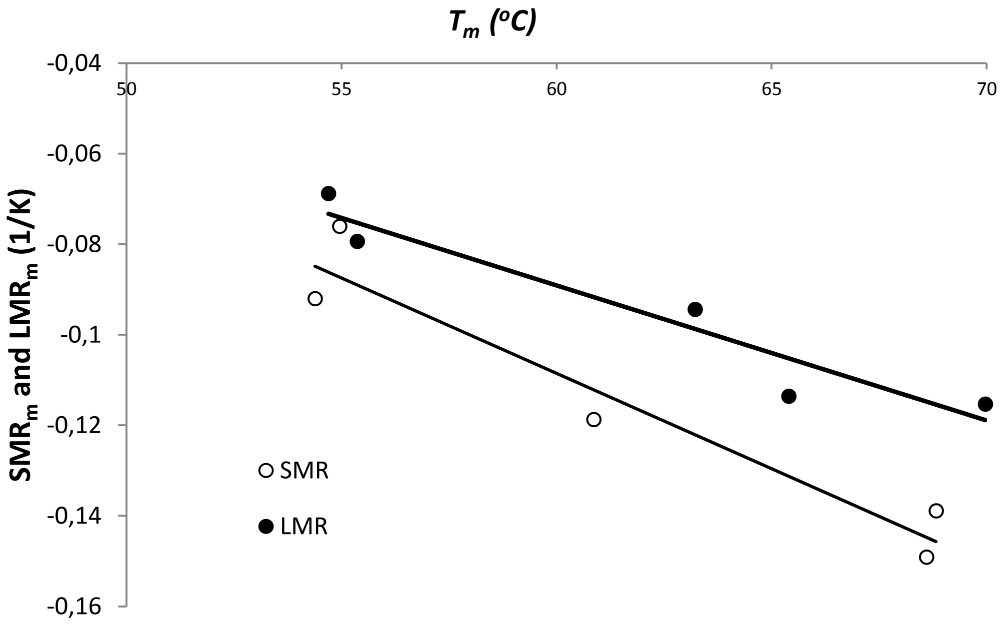

Fig. 2. – Relations between positions of minima (T_m) and their values (SMR_m and LMR_m)

Data were taken from Tab. 1 and 2 and were approximated by linear relations:
$SMR_m = 0.14404 – 0.00421T_m$; $R^2 = 0.924$
$LMR_m = 0.09004 – 0.00299T_m$; $R^2 = 0.918$

For the common point at T_{mm}, the relative differential activation energy (RDAE – see BLAHOVEC AND LAHODOVA, 2012A IN EQ. (2A) AND (2B)) was determined as 686.54 K. It has to be lowest value of this quantity for our vegetables – this value could be reached at very slow heating. New mechanism of direct destruction of cellular membrane starts to operate at temperatures close to or above 70 °C (BLAHOVEC ET AL., 2015; BLAHOVEC AND KOUŘÍM, 2016). The effect of the new mechanism is more effective when activity of the previously mentioned mechanism controlled by pores was lower.

CONCLUSIONS

Cell membrane is destructed during heating of root vegetable. The process starts at temperatures just above 40 °C. Its mechanism consists probably in denaturation of proteins in the cell wall pores. Role of this mechanism increases with decreasing heating rate and it is also different in different roots. At temperatures close and/or above 70 °C the role of pore is finished and it is replaced by thermally induced destruction of the whole cell membrane.

REFERENCES

1. BLAHOVEC, J., KOUŘÍM, P.: Combined mechanical (DMA) and dielectric (DETA) thermal analysis of carrot at temperatures 30–90 °C. J. Food Eng. 168, 2016: 245-250.
2. BLAHOVEC, J., KOUŘÍM, P., KINDL, M.: Low temperature carrot cooking supported by pulsed electric field - DMA and DETA thermal analysis. Food and Bioprocess Technology, 8, 2015:2027-2035.
3. BLAHOVEC, J., LAHODOVÁ, M.: DMA peaks in potato cork tissue of different mealiness. J. Food Eng. 103, 2011: 273-278.
4. BLAHOVEC, J., LAHODOVA, M.: DMA thermal analysis of different parts of potato tubers, Food Chem. 133, 2012: 1101-1106.
5. BLAHOVEC, J, LAHODOVA, M.: Changes in carrot (*Daucus carota)* parenchyma at higher temperatures detected in vivo by dynamic mechanical (thermal) analysis. Biorhelogy 49, 2012a: 289-298.
6. BLAHOVEC, J., LAHODOVA, M.: Storage induced changes of potato properties as detected by DMA. LWT - Food Science and Technology 50, 2013: 444-450.
7. BLAHOVEC, J., LAHODOVÁ, M., ZÁMEČNÍK, J.: Potato DMA analysis in area of starch gelatinization. Food Bioprocess Technology, 5, 2012: 929–938.
8. DE WEER, P.: A century of thinking about cell membranes. Annual Review of Physiology. 62, 2000: 919–926.
9. FUENTES, A., VAZQUEZ-GUTIERREZ, J.L., PEREZ-GAGO, M.B., VONASEK, E., NITIN, N., BARRETT, D.M.: Application of non-destructive impedance spectroscopy to determination of the effect to temperature on potato microstructure and texture. J. Food Eng. 133, 2014:16-22.
10. GARRET, R.H. - GRISHAM C.M.: Biochemistry. 4th edition. Brooks/Cole, Boston 2010.
11. GEORGET, D.M.R.- SMITH, A.C. - WALDRON, K.W.: Dynamic mechanical thermal analysis of cell wall polysaccharides extracted from lyophylised carrot *Daucus carota.* Carbohydr. Polym. 48, 2002: 277-286.
12. IMAIZUMI, T., TANAKA, F., HAMANAKA, D., SATU, Y., UCHINO, T.: Effects of hot water treatment on electrical properties, cell membrane structure and texture of potato tubers. J. Food Eng. 162, 2015: 56-62.
13. KARLSSON, M.E., ELIASSON, A.-C.: Gelatinization and retrogradation of potato (*Solanum tuberosum*) starch *in situ* as assessed by differential scanning calorimetry (DSC*)*. Lebensmittel-Wissenschaft und-Technologie 36, 2003a: 735-741.
14. KARLSSON, M.E., ELIASSON, A-C.: Effects of time-temperature treatments on potato (*Solanum tuberosum*) starch: a comparison of isolated starch and starch *in situ.* J. Sci. Food Agriculture 83,2003b:1587-1592.
15. KUBELKA, J., HOFRICHTER, J., EATON, W.A.: The protein folding 'speed limit'. Curr. Opin. Struct. Biol. 14, 2004: 76-88.
16. MAULE, A.J.: Plasmodesmata: structure, function and biogenesis. Curr. Opin, Plant Biol. 11, 2008: 680-686.
17. MINETTI, C.A.S.A. - REMETA, D.P.: Energetics of membrane protein folding and stability. Arch. Biochem. Biophys. 453, 2006: 32-53.
18. NILSSON, S.B., HERTZ, C.H., FALK, S.: On relation between turgor pressure and tissue rigidity. II. Theoretical calculations on model systems. Physiologica Plantarum 11, 1958: 818-837.
19. PERSONIUS, C., SHARP P.F.: Permeability of potato-tuber tissue as influenced by heat. Food Res. 3, 1938: 525–541.
20. PRICE, D.M.: Thermomechanical, dynamic mechanical and dielectric methods. In: Principles of thermal analysis and calorimetry, P.J. Haines ed., The Royal Society of Chemistry, Cambridge 2002, pp. 94-128.
21. SAKURAI, N.: Physical properties of fruit firmness and chemical structure of cell walls during fruit softening. In; Physical Methods in Agriculture – Approach to Precision and Quality, eds. Jiri Blahovec and Miroslav Kutilek, Kluwer, Academic/Plenum Press, New York 2002: pp. 311-342.
22. SEIDI, Y., FINKA, A., MURISET, M., BROMBERG, Z., WEISS, Y.G., MAATHUIS, F.J.M., GOLOUBINOFF, P.: The heat shock response in moss plants is regulated by specific calcium-permeable channels in the plasma membrane. Plant Cell 21, 2009: 2829-2843.
23. TSONG, T.Y., SU, Z.–D.: Biological effects of electric shock and heat denaturation and oxidation of molecules, membranes, and cellular functions. Ann. N.Y. Acad. Sci. 888, 1999: 211-232.
24. WARD, I.M.: Mechanical properties of solid polymers. John Wiley & Sons New York 1983.
25. XU, C., LI, Y.: Development of carrot parenchyma softening during heating detected *in vivo* by dynamic mechanical analysis. Food Control 44, 2014: 214-219.

Corresponding author:

prof. Ing. RNDr. Jiří Blahovec, DrSc., Department of Physics, Faculty of Engineering, Czech University of Life Sciences Prague, Kamýcká 129, Praha 6, Prague, 16521, Czech Republic, phone: +420224383281, e-mail: blahovec@tf.czu.cz

ASSESSMENT OF TRANSPORT SUBSTRATES FOR SELECTED AGRICULTURAL BIOGAS PLANT

S. Borowski[1], L. Knopik[2], M Markiewicz-Patalon[1], A. Brzostek[1]

[1]*Institute of Machine Operation and Transport, Faculty of Mechanical Engineering, UTP University of Science and Technology in Bydgoszcz*
[2]*Faculty of Management, UTP University of Science and Technology in Bydgoszcz*

Abstract
The paper presents transportation problem the biomass to biogas plants. An assessment real data from the area of the selected agricultural biogas plant. We analyzed the number of shipments executed by the transport units and established a theoretical transport set capacity of 17300 kg. For such a set of defined theoretical number of shipments and the theoretical amount of kilometers.

Key words: calorific biomass, transport, biogas plant.

INTRODUCTION

The use of fossil fuels is the biggest source of pollution and greenhouse gases' emission. Last years the European Union countries' leaders have accepted a comprehensive package of activities aiming at prevention of climate changes and providing Europe with reliable and sufficient energy supplies. The package constituting the widest so far ranging reform of the European energy policy aims at assuring the Union the world leader's position in the field of renewable energy and low-emission technologies. The result of these arrangements there is to be limitation of greenhouse gases' emission by 20% by the year 2020, as compared to 1990. The European Union is planning to obtain the above goal most of all limiting of energy's consumption and increasing of the use of energy originating from renewable sources. Such a state of affairs drove to the increase of use of energy production's technologies based on renewable sources, including among the others to the dynamic increase of biomass use for energy purposes, in particular as the raw material for bio-fuels production.

The energy use of biomass as a raw material for biofuels production is justified when it makes it possible to obtain a positive ecological effect (reduction of greenhouse gases), with a desire to reach the highest production and economical efficiency as compared to the use of conventional fuels. In many literature sources, as the sources influencing the bio-fuels' production, there are mentioned appropriate location of biofuels' production, considering among the others the areas richness in biomass as well as efficient production's organization with reference to the raw material's transport and storage (MAJ ET AL., 2014; DUDA-KĘKUŚ, 2011). From the point of an appropriate location of bio-fuels' production, important is correct identification of raw material resources as well as the trends of their use, pursuant to the balanced development rules. At present, more and more often techniques based on spatial information GIS (PANICHELLI, GNANSOUNOU, 2008; JANOWICZ, KUNIKOWSKI 2008) systems are used while looking for favorable location.

Acceptance of an appropriate logistic strategy of raw-material's supplies – biomass, is a very important aspect while planning bio-fuels' production. Logistics means planning of demand, efficiency in time and space as well as controlling and use of the planned stream, mass and energy having regard to the cost optimum. In case of already existing biomass processing installations, the logistic activities change most often as regards planning of raw materials' sourcing. There are attempts aiming at reduction of their sourcing's costs by sourcing of the cheapest raw materials The cost of raw materials transport most often incurred by a customer is the second important factor.

With the growing use of biomass for purposes connected with energy's generation, optimization of supplies logistics requires correct planning, organization and management of raw materials' base and means of transport (ROGULSKA ET AL., 2011).

The use of biomass for energy purposes is connected with the following production processes: biomass production, biofuels production from biomass and energy generation from biomass or biofuels. There should be stressed the fact, that these processes are usually performed by separate economic entities. Production of biofuels seems to be particularly advantageous locally, for the purposes of local communities.

Such a manner of biomass' use has many advantages, among the others it decreases the costs connected with transport of raw materials and distribution of biofuels and bioenergy, may contribute to create new places of work, makes it possible to manage wastes and raw material surpluses from agrarian production, wood and food industry, and also increases the local energy safety (ŻARSKI 2012).

Energy intensity of its generation and processing (ZASTEMPOWSKI 2014) is one of the main aspects of biomass production for energy purposes. However, transport of the harvested material to the place of destination is the element which may be controlled in a deliberate manner. It is caused by low density of energy included in biomass. Application of optimum solutions in this field may generate sizeable benefits.

Raw material's availability is one of the more important information which should be taken into consideration while designing installation for biomass processing. Prior to the investment's commencement, the analysis of the processing plant's functioning area with biomass abundance should be conducted.

The evaluation of abundance is performed on the basis of the method of biomass' energy potential assessment, otherwise referred to as "cascade method." (IEO, 2007). It consists in determination of energy's volume possible to be generated from biomass, taking into account different criteria limiting the opportunities of its use. We can distinguish the following levels of energy potential (JASIULEWICZ 2010):

- Theoretical potential – volume of energy possible to be used from biomass on condition of having appropriate installations efficient in 100% (process defects are not taken into consideration), and also assuming that the complete available potential is used for energy purposes only.
- Technical potential – it is that part of theoretical potential, which may be used, decreased due to technical restrictions, (efficiency of machines now available on the market , sometimes the process's own needs, geographical location, energy storage). Usually determined on the basis of detailed technical analyses.
- Economical potential – determined as a part of the technical potential defined above which may be used with consideration of economic criteria.

MATERIALS AND METHODS

The agrarian biogas producer has been buying raw material from farmers from the area around Rypin on the contracting rules. The biogas plant purchases sowable material and guarantees transport of substrate to the biogas plant. Slurry is collected from pigs producers, management of which is difficult due to arduous smell and problems with excessive, harmful fields' manuring. Farmers delivering products for biogas generation may in exchange receive post-fermentation substance free from harmful substances which can also be used for fields' fertilizations. Corn for biogas generation, is harvested from about 500 hectares. On average, from 1ha of corn cultivation about 50 tons of green fodder may be harvested what gives the total sum of about 25000 tons. The raw material is stored at the turn of September and October. Then, ensilage is prepared at the territory of the plant. Corn ensilage is prepared by green fodder's shredding and pressing. The process of ensilage's forming lasts for about 6 weeks, when by appropriate coverage and cutting off air, earlier prepared corn undergoes the process of ensilaging. Each day about 56 tons of corn ensilage is used in the process of biogas generation. The annual demand amounts to approx. 20000 tons of corn ensilage. Moreover, about 20% of raw-material reserve that a plant should have, has to be taken into consideration. Slurry delivered by farmers specializing in pigs' breeding is the second raw material in the process of biogas generation. Slurry in whole is delivered by the local farmers. The daily demand for slurry in the plant amounts to approx. 24 tons. The results of the energy potential's assessment on the economic level for green fodder from corn show, that in the commune it shall be possible to acquire raw material for that purpose from the area amounting to approx. 500 ha. For the Rypin poviat, that area is estimated to be about 1500 ha.

The study analyzed data on transport costs of biomass in 2013. The aim of analysis was to determine the cost-transport due to its transport sets.

As a basis for research was adopted the actual shipments of biomass. Determined the average weight of the transported material for individual transport sets. The vehicle with the largest capacity has been recognized as a model. The vehicle model was used to determine the theoretical amount of travel and the theoretical amount of kilometers. The results obtained are presented in the form of graphs.

RESULTS AND DISCUSSION

For the analysis the field of which was collected biomass was divided because of the distance from the biogas plant. Determined ranges about the size of 5 km. The amount of the collected biomass and percentage of the total weight is shown in Fig. 1.

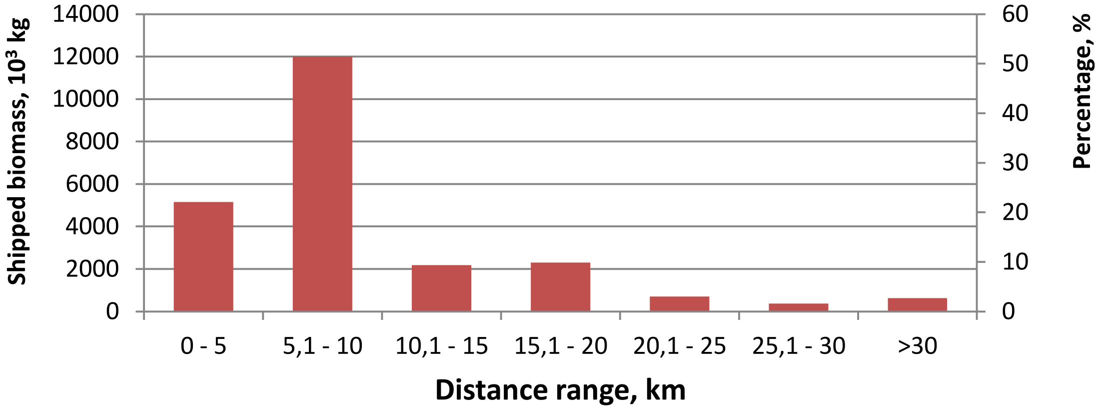

Fig. 1. – The amount of the collected biomass and percentage of the total weight

As can be seen from Figure the largest biomass was collected in the range 5.1 – 10 km. Whereas the last two ranges are not of interest to the Management Board of the biogas plant and the decision to use them was a result of considerations beyond the economic. As a model set of a transport was adopted farm tractor with a trailer of medium capacity of 17300 kg (item 13 on the Fig. 2).

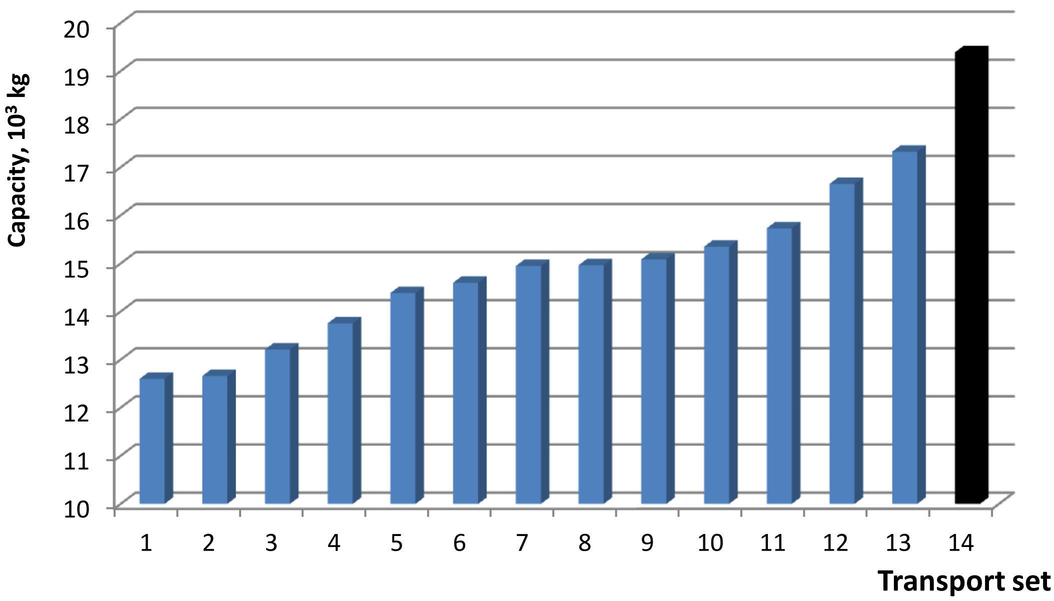

Fig. 2. – Comparison of the capacity of transport sets

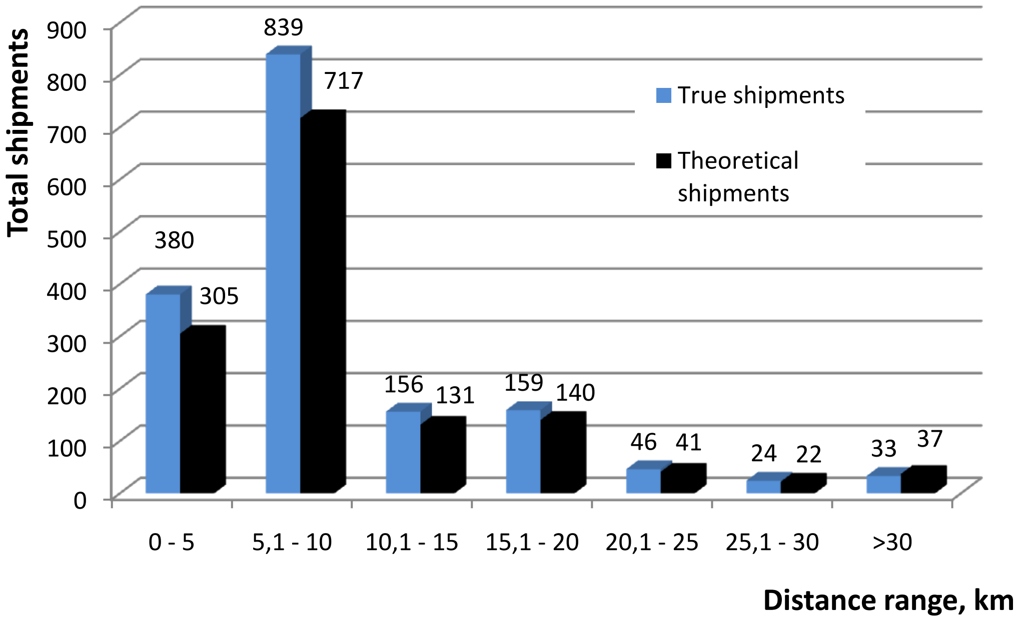

Fig. 3. – Comparison of the number true and theoretical shipments

For a set of model calculated the theoretical number of shipments for the real yield obtained from the data fields. Fig. 3 presents a summary of real and theoretical shipments.

As can be seen from the graph the theoretical amount of shipments sniffed from 80% (0 – 5 km) to 90% (25 – 30 km). This is caused by a better selection of transport sets and more care during loading of biomass for transport sets. For the range of > 30 km obtained more theoretical shipments (item 14 on the the Fig. 1). However, this is caused by using a set of enhanced capacity. The set consisted of a tractor and two trailers. It was designed for long-distance transport.

Similar summary was prepared for the distance which was realized transport. However, this statement also included only road transport set with a cargo of biomass. Summary of results is shown in Fig. 4.

As is apparent from Fig. 4, a similar relationship was obtained in an amount of real of kilometers as compared to theoretical as in Fig. 3.

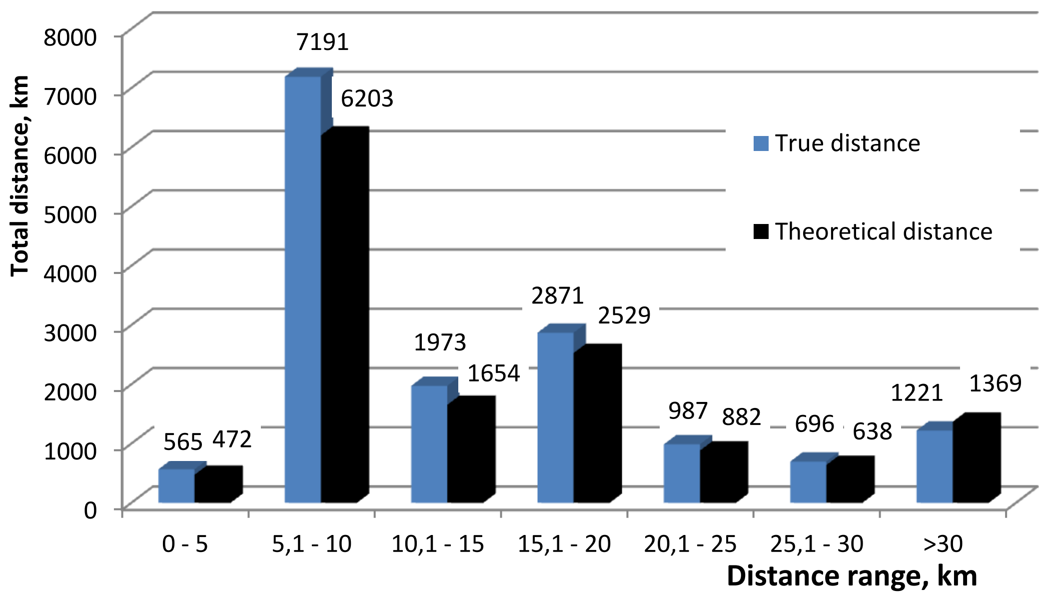

Fig. 4. – Comparison of the true and theoretical distance

CONCLUSIONS

As shown in the research transport of biomass to biogas plants in 2013 was carried out incorrectly. It should determine the economically justified the maximum distance at that can be transport the biomass.

The use of transport sets with a high capacity can reduce 10% to 20% of the number of passes. This value a direct impact on number of people employed in the transport and reducing transport sets.

In the same way to reduce the number of of kilometers. Unfortunately, no data are available on fuel consumption during transportation. They are not possible to estimate the fuel savings. It should in the coming yearcarry out necessary research to estimate the size.

REFERENCES

1. DUDA-KĘKUŚ, A.: Transport logistics of biomass fuel supply for power plants implementing the program of green energy. (pol) Transport biomasy w logistyce dostaw paliw dla elektrowni systemowych realizujących program zielonej energetyki. Logistyka 2, 2011.
2. IOZ: The possibilities of using renewable energy sources in Poland until 2020, (pol) Możliwości wykorzystania odnawialnych źródeł energii w Polsce do roku 2020, Instytut Energetyki Odnawialnej, Warszawa 2007: 5-15.
3. JANOWICZ, L., KUNIKOWSKI, G.: Assessment of renewable resources based on the geographic information system (GIS), (pol) Ocena zasobów odnawialnych w oparciu o system informacji geograficznej. Inżynieria Rolnicza, 102(4), 2008: 329-335.
4. JASIULEWICZ, M.: The biomass potential in Poland, (pol) Potencjał biomasy w Polsce, Wydawnictwo Politechniki Koszalińskiej, Koszalin, 2010.
5. MAJ, G., PIEKARSKI, W., KOWALCZYK-JUŚKO, A.: Logistics supplies to agricultural biogas plant, (pol) Logistyka dostaw surowca do biogazowi rolniczej. Logistyka, 6, 2014.
6. PANICHELLI, L., GNANSOUNOU, E.: GIS-based approach for defining bioenergy facilities location: A case study in Northern Spain based on marginal delivery costs and resources competition between facilities, Biomass and Bioenergy 32, 2008: 289-300.
7. ROGULSKA, M., GRZYBEK, A., SZLACHTA, J., TYS, J., KRASUSKA, E., BIERNAT, K., BAJDOR, K.: Linking agriculture and energy in the context of achieving the objectives of low-carbon economy in Poland. (pol) Powiązanie rolnictwa i energetyki w kontekście realizacji celów gospodarki niskoemisyjnej w Polsce. Polish Journal of Agronomy, *7*, 2011: 92-101.
8. Siejka, K. – Tańczuk, M. – Trinczek, K.: The concept of estimating biomass energy potential on the example of selected municipalities Opole Province (pol) Koncepcja szacowania potencjału energetycznego biomasy na przykładzie wybranej gminy województwa opolskiego. Inżynieria Rolnicza, 12, 2008: 167-174.
9. ZASTEMPOWSKI, M., BOCHAT, A.: Modeling of cutting process by the shear-finger cutting block. ASABE Applied Engineering in Agriculture. Vol. 30, No. 3, 2014, pp. 347-353.
10. ŻARSKI W.: Utilization of biomass for energy production purposes in the Kujawsko-Pomorskie Province. Examples and development prospects, Studia i Materiały Polskiego Stowarzyszenia Zarządzania Wiedzą 61, Bydgoszcz 2012: 150-159.

Corresponding author:

Sylwester Borowski, Institute of Machine Operation and Transport, Faculty of Mechanical Engineering, UTP University of Science and Technology in Bydgoszcz, ul. Prof. S. Kaliskiego 7, 85-789 Bydgoszcz, Poland, phone: +485 23408208, e-mail: sylwa@utp.edu.pl

SELECTED THERMAL AND RHEOLOGIC PARAMETERS OF LIQUID FUELS

M. Božíková[1], P. Hlaváč[1], M. Valach[1], Ľ. Híreš[1], Ľ. Krišťák[2], M. Malínek[1], T. Regrút[1]

[1]*Department of Physics, Faculty of Engineering, Slovak University of Agriculture in Nitra, Slovak Republic*
[2]*Department of Physics, Electrotechnics and Applied Mechanics, Faculty of Wood Sciences and Technology, Technical University in Zvolen, Slovak Republic*

Abstract
This article deals with thermal and rheologic properties of selected liquid fuels (diesel with different content of RME – Rapeseed Methyl Esters). Fuel samples had RME content 3 %, 7 %, 10 %, 15 %, 20 %. There were measured basic thermophysical parameters as: thermal conductivity, thermal diffusivity, volume specific heat and effusivity. Thermal conductivity and thermal diffusivity of samples were measured by two different transient method – Hot wire (HW) method and Dynamic plane source (DPS) method. The values of volume specific heat and effusivity were calculated from obtained experimental results. All results were statistically processed. Rheologic parameter – dynamic viscosity was measured during heating process in temperature range (20 - 80) °C. For dynamic viscosity detection was used digital rotational viscometer DV 2T. For every dependency were obtained decreasing exponential relations with high coefficients of determination. The results of physical properties measurement showed on significant influence of RME concentration in diesel.

Key words: thermophysical parameter, viscosity, diesel, method, component.

INTRODUCTION

The main advantages of biofuels are that these fuels are nontoxic, biodegradable and renewable with potential to reduce engine exhaust emissions. In Europe is one of the most important biofuel FAME – Fatty Acid Methyl Esters manufactured mainly as Rapeseed Methyl Esters – RME. RME is added to regular diesel fuels in amount of up to 7 % (MERKISZ ET AL., 2016). For biofuels quality determination is necessary to know basic chemical and physical parameters. From physical parameters are very important rheologic parameters and thermal parameters. These parameters could be supplemented with others physical parameters. Methods and results of direct thermal properties measurements of biofuels are presented by authors SNOWSTORM ET AL. (2011), MACHADO ET AL. (2012). YAMANE ET AL. (2001), VOZÁROVÁ ET AL. (2015) presented general oil, biooil, fuel and biofuel characteristics and their influence on thermal and rheologic properties. Selected mechanical properties of biofuels were examined by KUBÍK AND KAŽIMÍROVÁ (2015) and rheologic properties as kinematic and dynamic viscosity were measured by TRÁVNÍČEK ET AL. (2013). Temperature dependences of density and kinematic viscosity for petrol, bioethanol and their blends were measured by KUMBÁR AND DOSTÁL (2014).

This article presents selected physical properties of diesel with RME component in relation to conventional diesel. The aim of the research was to determine changes of selected physical properties with increasing content of RME in diesel.

MATERIALS AND METHODS

In modern physical research are often used dynamic methods of measurements, which are quicker than static methods. By using dynamic methods we can get characteristics of material in the short time. This fact is very important for the practice. In this part are defined measured parameters and there are described theoretical basics from thermal and rheology measurement methods which were used for physical parameters detection.

Thermal conductivity λ is the property of a material which relates its ability to conduct heat. Thermal conductivity is defined as the quantity of heat transmitted through a unit surface to a unit temperature gradient in unit time. This thermophysical parameter depends on many factors as: material structure, pressure, chemical content, temperature etc. Energy is transferred from the more energetic to the less energetic molecules when neighbouring molecules collide (SAHIN AND SUMNU, 2006). Thermal conductivity is mathematically defined by Furier´s law (1):

$$\vec{q} = -\lambda \left(\frac{\partial T}{\partial x} \vec{i} + \frac{\partial T}{\partial y} \vec{j} + \frac{\partial T}{\partial z} \vec{k} \right) \quad (1)$$

Where $\vec{q}$ is the vector of heat flow and $\frac{\partial T}{\partial x}\vec{i}+\frac{\partial T}{\partial y}\vec{j}+\frac{\partial T}{\partial z}\vec{k}$ is temperature gradient. The unit of thermal conductivity is $W.m^{-1}.K^{-1}$.

Thermal diffusivity *a* characterizes the velocity of the temperature equalization in material during non-stationary processes. In numeric view it is equal to temperature change of unit volume caused by heat, which is transferred in unit time, by unit surface of coat with unit thickness, in unit temperature difference on her facing side. The unit of thermal diffusivity is *1* $m^2.s^{-1}$. Definition equation (2) for thermal diffusivity is:

$$a=\frac{\lambda}{c\,\rho} \tag{2}$$

Where λ is thermal conductivity and $c\ \rho$ is volume specific heat. The meaning of *c* is mass specific heat and ρ is density of material.

We could define effusivity of sample by equation (3).

$$e=\frac{\lambda}{\sqrt{a}}=\sqrt{\rho\,c\,\lambda} \tag{3}$$

The parameters in last equation were defined in the previous text.

Thermal parameters were measured by two transient methods HW and DPS method because of methods comparison. In literature HW method is preferred but in convenient arrangement of experimental apparatus it can be used DPS method.

The HW (Hot wire) method is a transient dynamic technique based on the measurement of the temperature rise of a linear heat source (hot wire) embedded in the tested material (ASSAEL ET AL., 2008; KADJO ET AL., 2008). For an infinitely long metallic wire (length/radius ratio >> 200) heated at time t > 0 with a constant heat flux per length unit *q* and immersed in an infinite homogeneous medium (thermal conductivity and diffusivity: λ and *a* with uniform initial temperature, the temperature rise $\Delta T(t)$ of the wire is given by (4) (CARSLAW AND JAEGER, 1959):

$$\Delta T(t)=\frac{q}{4\pi\lambda}\ln\frac{4F_0}{C}, \tag{4}$$

$C = e^{\gamma} = 1.781$ where γ is Euler's constant ($\gamma = 0.5772$) and *Fo* the Fourier number defined by:

$$F_0=\frac{a\,t}{r_0^2} \tag{5}$$

Equation (4) is the analytical solution of an ideal thermal conductive model valid for $F_0 >> 1$ nd without convective transfers (WAKEHAM AND NAGASHIMA, 1991; TAVMAN, 1996). From this ideal model and with known *q* values, the thermal conductivity can be calculated by (6):

$$\lambda=\frac{q}{4\pi}\left(\frac{dT}{d(\ln t)}\right)^{-1} \tag{6}$$

Where $dT/d(\ln t)$ is a numerical constant deduced from experimental data for t values which satisfy the condition $F_0 >> 1$. For practical applications of the HW method, wire and material sample dimensions, among other ideal model hypothesis, are finite and the deviations from the ideal model have then to be evaluated. In fact, the *e(t)* answer to the wire heating $\Delta T(t)$ resultant of the Joule effect due to an electrical current *i* is (7):

$$R(t)=R_0\left(1+\beta_0\left(T(t)-T_0\right)\right) \tag{7}$$

where *R(t)* – is the instantaneous electrical resistance of the wire, R_0 – is the resistance of the wire at the T_0 reference temperature, and β_0 the temperature coefficient of the wire at 22 °C. Taking into account (6) and (7), the thermal conductivity λ may be calculated as follows:

$$\lambda=\frac{q\,R_0\,\beta_0\,i}{4\pi}\left(\frac{d\,e(t)}{d(\ln t)}\right)^{-1} \tag{8}$$

where $de(t)/d(\ln t)$ is a numerical constant deduced from the experimental data and from the linear part of the $e(t) = f(\ln(t))$ curve.

The DPS (Dynamic Plane Source) method is based on using an ideal plane sensor. The plane sensor acts both as heat source and temperature detector. The plane source method is arranged for a one dimensional heat flow into a finite sample. The theory considers ideal experimental conditions – ideal heater (negligible thickness and mass), perfect thermal contact between PS sensor and the sample, zero thermal resistance between the sample and the material surrounding sample, zero heat losses from the lateral surfaces of the sample (KARAWACKI ET AL., 1992). If *q* is the total output of power per unit area dissipated by the heater, then the temperature increase as function of time is given by (9):

$$\Delta T(x,t)=2\frac{q\sqrt{at}}{\lambda}ierf\left(\frac{x}{2\sqrt{at}}\right) \tag{9}$$

Where *a* - is thermal diffusivity, λ - is thermal conductivity of the sample and *ierfc* is the error function (BECK AND ARNOLD, 2003). The principle of method resides in fitting of the theoretical temperature function given by theoretical equation over the experimental points. In case of the best fit, both parameters λ and *a* can be determined. The method of fitting based on least-squares procedure was described in detail (KARAWACKI ET AL., 1992; MALINARIČ, 2004).

We could define effusivity of sample by equation (10).

$$e = \frac{\lambda}{\sqrt{a}} = \sqrt{\rho c \lambda} \qquad (10)$$

From rheologic parameters was measured dynamic viscosity η. Dynamic viscosity is very important rheologic parameter of liquids which can be defined as the resistance of a fluid to flow. The unit of dynamic viscosity in SI units is Pa.s. Viscosity of the liquids usually decreases with increasing temperature. The difference in the effect of temperature on viscosity of fluids is related to the difference in their molecular structure (BIRD ET AL., 1960). The temperature effect on dynamic viscosity can be described by an Arrhenius type equation (11):

$$\eta = \eta_0 \, e^{-\frac{E_A}{RT}} \qquad (11)$$

where η_0 is reference value of dynamic viscosity, E_A is activation energy, R is gas constant and T is absolute temperature (FIGURA AND TEIXEIRA, 2007). Measuring of dynamic viscosity was performed by digital viscosimeter Anton Paar DV 2P. Principle of measuring by rotational viscosimeter is based on dependency of sample resistance against the probe rotation. Probe with signification ULA0 was used in our measurements. The frequency of probe rotation was 120 rpm.

RESULTS AND DISCUSSION

Measured samples of diesel were with different RME content. The first sample was pure diesel and next measured samples had concentration of RME 3 %, 7 %, 10 %, 15 % and 20 %.

Results for thermal parameters measurements – there were measured parameters as thermal conductivity and thermal diffusivity at laboratory temperature 22 °C. Samples were stabilised 24 hours before measurement. All measured samples were stored in special bottles. For data reliability protection were realized series of one hundred measurements for every sample of diesel with RME and every thermal parameter was measured by HW and DPS method. Results presented in Tab. 1 were obtained as valued averages. For every series of measurements were calculated probable error and relative probable average error in %.

Thermal parameters measurements showed that increasing concentration of bio-components in the fuel had significant influence of all investigated physical parameters. For sample of pure diesel were detected by Hot wire method the smallest values of thermal parameters. Thermal conductivity of pure diesel was $\lambda = (0.1472 \pm 0.0002)$ W.m^{-1}.K^{-1} and thermal diffusivity of pure diesel was $a = (0.7897 \pm 0.0011)$ 10^{-7}m^2.s^{-1}. From basic thermal parameters and density of samples was calculated value of volume specific heat $c\rho = (0.1864 \pm 0.0004)$ 10^7 J.m^{-3}.K^{-1} and effusivity $e = (5.2381 \pm 0.0099)$ 10^{-5} W.m^{-2}.K^{-1}.s$^{-0,5}$. The highest values of thermal parameters had sample of diesel with the addition of 20 % RME – thermal conductivity was $\lambda = (0.1725 \pm 0.0009)$ W.m^{-1}.K^{-1}, thermal diffusivity of the sample was $a = (0.8297 \pm 0.0007)$ 10^{-7} m^2.s^{-1}. Presented results are in good agreement with values presented in literature (GUIMARÃES ET AL., 2012). Thermal effusivity of sample was $e = (5.9886 \pm 0.0510)$. 10^{-5} W.m^{-2}.K^{-1}.s$^{-0,5}$ and the volume specific heat was $c\rho = (0.2079 \pm 0.0006)$ 10^7 J.m^{-3}.K^{-1}. Values of volume specific heat and effusivity for diesel samples with different RME content were not compared with results in the literature, because they had not been published yet.

Tab. 1. – Results of thermal parameters measurements by HW method for samples of diesel with different RME content

Sample	Thermal conductivity $W.m^{-1}.K^{-1}$	Thermal diffusivity $. 10^{-7}\ m^2.s^{-1}$	Volume specific heat $. 10^7\ J.m^{-3}.K^{-1}$	Effusivity $. 10^{-5}\ W.m^{-2}.K^{-1}.s^{-0.5}$
	Probable error			
	$W.m^{-1}.K^{-1}$	$. 10^{-7}\ m^2.s^{-1}$	$. 10^7\ J.m^{-3}.K^{-1}$	$. 10^{-5}\ W.m^{-2}.K^{-1}.s^{-0.5}$
	Relative probable error %			
Diesel	0.1472	0.7897	0.1864	5.2381
	± 0.0002	± 0.0011	± 0.0004	± 0.0099
	± 0.1600	± 0.1400	± 0.2300	± 0.1900
Diesel with 3 % RME	0.1526	0.8034	0.1899	5.3832
	± 0.0004	± 0.0005	± 0.0005	± 0.0140
	± 0.2700	± 0.0600	± 0.2500	± 0.2600
Diesel with 7 % RME	0.1581	0.8153	0.1939	5.5367
	± 0.0004	± 0.0008	± 0.0004	± 0.0110
	± 0.2300	± 0.1000	± 0.1900	± 0.2000
Diesel with 10 % RME	0.1620	0.8199	0.1977	5.6593
	± 0.0003	± 0.0003	± 0.0004	± 0.0120
	± 0.2000	± 0.0300	± 0.2200	± 0.2100
Diesel with 15 % RME	0.1662	0.8217	0.2022	5.7970
	± 0.0004	± 0.0004	± 0.0005	± 0.0140
	± 0.2400	± 0.0400	± 0.2300	± 0.2400
Diesel with 20 % RME	0.1716	0.8278	0.2073	5.9643
	± 0.0004	± 0.0005	± 0.0005	± 0.0140
	± 0.2400	± 0.0600	± 0.2300	± 0.2300

One of the main aims of the thermal parameters measurements was comparison of two different types of thermophysical parameters measurement methods. From results presented in Tab. 1 and 2 is evident, that relative probable error of thermal parameters measurement for Hot wire method was from ± 0.03 % to ± 0.27 % and the same relative probable errors for Dynamic plane source method were in range (± 0.06 % – ± 0.86 %). The results of two measurement methods comparison confirmed that for the liquid materials is more appropriate to use Hot wire method. This fact was presented in literature (RODER, 1981), but detected small differences between basic thermal parameters values showed that at appropriate arrangement of the measuring apparatus there can be used both thermophysical measurement methods.

Results for rheologic parameter measurements - there was measured dynamic viscosity as one of the basic rheologic parameters. All samples were measured during heating process in the temperature range (20 – 80) °C. Every point in graphical dependencies on Fig. 1 was obtained as average from ten measured values for sample of diesel with different RME content.

Tab. 2. – Results of thermal parameters measurements by DPS method for samples of diesel with different RME content

Sample	Thermal conductivity $W.m^{-1}.K^{-1}$	Thermal diffusivity $. 10^{-7}\ m^2.s^{-1}$	Volume specific heat $. 10^7\ J.m^{-3}.K^{-1}$	Effusivity $. 10^{-5}\ W.m^{-2}.K^{-1}.s^{-0.5}$
	Probable error			
	$W.m^{-1}.K^{-1}$	$. 10^{-7}\ m^2.s^{-1}$	$. 10^7\ J.m^{-3}.K^{-1}$	$. 10^{-5}\ W.m^{-2}.K^{-1}.s^{-0.5}$
	Relative probable error %			
Diesel	0.1480	0.7902	0.1873	5.2650
	± 0.0005	± 0.0039	± 0.0011	± 0.0122
	± 0.3600	± 0.4900	± 0.5800	± 0.2300
Diesel with 3 % RME	0.1530	0.8045	0.1902	5.3945
	± 0.0007	± 0.0016	± 0.0009	± 0.0360
	± 0.4300	± 0.2000	± 0.4900	± 0.6700
Diesel with 7 % RME	0.1593	0.8170	0.1950	5.5735
	± 0.0006	± 0.0011	± 0.0010	± 0.0280
	± 0.3600	± 0.1300	± 0.5100	± 0.5020
Diesel with 10 % RME	0.1650	0.8208	0.201	5.7589
	± 0.0004	± 0.0005	± 0.0008	± 0.0340
	± 0.2500	± 0.0600	± 0.41	± 0.5900
Diesel with 15 % RME	0.1681	0.8226	0.2044	5.8617
	± 0.0007	± 0.0008	± 0.0008	± 0.0440
	± 0.4300	± 0.1000	± 0.37	± 0.7500
Diesel with 20 % RME	0.1725	0.8297	0.2079	5.9886
	± 0.0009	± 0.0007	± 0.0006	± 0.0510
	± 0.5100	± 0.0800	± 0.31	± 0.8600

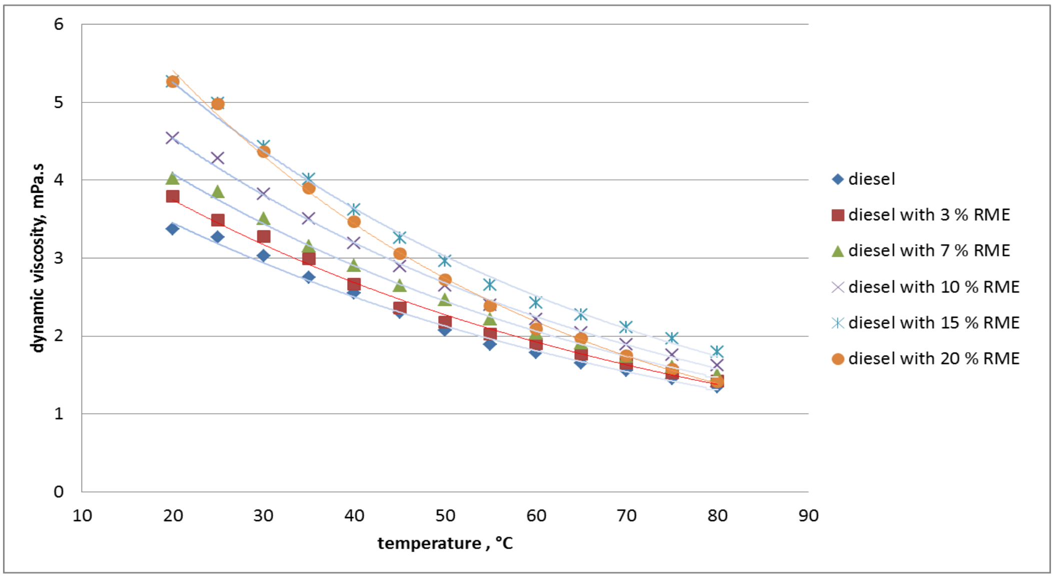

Fig. 1. – Temperature dependencies of dynamic viscosity for samples of diesel with different RME content

Measured values of dynamic viscosities for all measured samples are shown on Fig. 1. It is possible to observe from Fig. 1 that dynamic viscosity of diesel is decreasing with increasing of temperature. The progress can be described by decreasing exponential function (12), which is in accordance with Arrhenius equation (11) (MUNSON ET AL., 1994).

$$\eta = A\,e^{-B\left(\frac{t}{t_0}\right)} \qquad (12)$$

Regression coefficients and coefficients of determination are shown in Tab. 3. On the base on presented results is clear that coefficients of determination are in range (0.9932 – 0.9983).

Tab. 3. – Coefficients A, B of regression equation (12) and coefficients of determinations for relations of dynamic viscosity to the temperature

sample	Regression equation (12)		Coefficient of determination R^2 (-)
	Coefficients		
	A (mPa.s)	B (1)	
Diesel	4.7715	0.016	0.9944
Diesel with 3 % RME	5.2328	0.017	0.9932
Diesel with 7 % RME	5.7492	0.017	0.9983
Diesel with 10 % RME	6.4549	0.018	0.998
Diesel with 15 % RME	7.6053	0.018	0.9952
Diesel with 20 % RME	8.5145	0.023	0.9978

From Fig. 1 can be seen that dynamic viscosity of diesel with RME component is higher than pure diesel. This proportion should be caused by the RME content. In general, dynamic viscosity of diesel increasing with higher concentration of bio component RME, which is evident from Fig. 1. There was detected difference only for diesel sample with 20 % RME content, but this change could be caused by too high proportion of bio-components.

CONCLUSIONS

Thermal parameters, such as temperature, thermal conductivity, thermal diffusivity, volume specific heat and effusivity characterize heat transfer ability of material, velocity of the temperature equalization and the intensity of the temperature changes in the material. Dynamic viscosity is very important rheologic parameter defined as the resistance of a fluid to flow. Accurate values of these properties are critical for practical design as well as theoretical studies and analysis, especially in the fields of heat transfer and thermal processing. The knowledge of thermophysical and rheologic properties of the materials are especially significant in the context of liquid bio-based materials or materials which obtained bio components. These materials are often thermally processed or they are exposed to natural changes of temperature conditions.

The results obtained by the implementation of Hot wire method and Dynamic plane source method on the fuels samples (pure diesel and diesel with 3 %, 5 %, 7 %, 10 %, 15 % and 20 % content of RME) can be compared only with ranges of thermal parameters presented in the literature because of the fuels products variety. Usually are presented thermal parameters for diesel sample with 7 % content of bio-components, because this concentration of bio-components is recommended by EU standards. Results of selected thermal parameters were presented by authors SADROLHOSSEINI ET AL. (2011) and GUIMARÃES ET AL. (2012), for thermal conductivity of fuels were determined values from range λ = (0.143–0.175) W.m^{-1}.K^{-1} and thermal diffusivity was in range a = (0.784 – 0.835) 10^{-7} m^2.s^{-1}. Examined samples of fuels have thermal conductivity and thermal diffusivity from these ranges.

Rheological properties as dynamic viscosity, kinematic viscosity and fluidity were measured by many authors. Temperature dependencies of examined fuels dynamic viscosity had decreasing exponential shape for all measurements (Fig. 1). Coefficients of determination are very high (Tab. 3). Arrhenius equation (11) has decreasing exponential shape, so the dependency of dynamic viscosity on temperature can be described by it.

Nowadays we know many types of fuels and biofuels which differ in their composition and consistency and their chemical properties too, but for their quality evaluation is necessary to know their physical parameters.

ACKNOWLEDGEMENT

This work was supported by Research Project of the Technology Agency of the Czech Republic no. TA04021390 and by the project of CULS Prague IGA No. 2015:31180/1312/3116.

REFERENCES

1. ASSAEL, M. J., ANTONIADIS, K. D., WU J.: New measurements of the thermal conductivity of PMMA, BK7, and Pyrex 7740 up to 450 K. Int. J. Thermoph., 29 (4), 2008: 1257–1266.
2. BECK, J. V., ARNOLD, K. J.: Parameter Estimation in Engineering and Science. 1st ed., New York, USA, Wiley 1977.
3. BIRD, R. B., STEWART, W. E., LIHGTFOOT, E. N.: Transport Phenomena. 1st ed., New York, USA, John Wilie & Sons 1960.
4. CARSLAW, H. S., JEAGER, J. C.: Conduction of heat in solids. 1st ed., Oxford, United Kingdom Oxford University Press 1959.
5. FIGURA, L. O., TEIXEIRA, A. A.: Food Physics, Physical properties – measurement and applications. New York, USA, Springer 2007.
6. GUIMARÃES, A. O., MACHADO, F. A. L., DA SILVA, E. C., MANSANARES, A. M.: Thermal Effusivity and Thermal Conductivity of Biodiesel/Diesel and Alcohol/Water Mixtures. Int. J. Thermoph., 33 (10), 2012: 1842 – 1847.
7. KADJO, A., GARNIER, J. P., MAYE, J. P., MARTEMIANOV, S.: A new transient two-wire method for measuring the thermal diffusivity of electrically conducting and highly corrosive liquids using small samples. Int. J. Thermoph., 29 (4), 2008: 1267 – 1277.
8. KARAWACKI, E., SULEIMAN, B. M., UL-HANG, I., NHI, B. T.: An extension to the dynamic plane source technique for measuring thermal conductivity, thermal diffusivity and specific heat of Sol. I Rev. Sci. Instrum., 63, 1992: 4390 – 4397.
9. KUBÍK, Ľ., KAŽIMÍROVÁ, V.: Mechanical properties of pellets in compression. Res. Agr. Eng. 61(special iss.): 2015, S1–S8.
10. KUMBÁR, V., DOSTÁL, P.: Temperature dependence density and kinematic viscosity of petrol, bioethanol and their blends. Pak. J. Agri. Sci. 51(1): 2014, 175 – 179.
11. MACHADO, F. A. L., ZANELATO, E. B., GUIMARÃES, A. O., E DA SILVA. C., MANSANARES, A. M.: Thermal Properties of Biodiesel and Their Corresponding Precursor Vegetable Oils Obtained by Photopyroelectric Methodology. Int. J. Thermoph., 33 (10), 2012: 1848 – 1851.
12. MALINARIČ, S.: Parameter Estimation in Dynamic Plane Source Method. Meas. Sci. Technol., 15(4), 2004: 807 – 813.
13. MERKISZ, J., FUĆ, P., LIJEWSKI, P., KOZAK, M.: Rapeseed O il Methyl Esters (RME) as Fuel for Urban Transport. Environmental Sciences "Alternative Fuels, Technical and Environmental Conditions", book edited by Krzysztof Biernat, 3.0 license CC BY 2016.
14. MUNSON, B. R., YOUNG, D. F., OKIISHI, T. H.: Fundamentals of fluid mechanics. New York, USA, John Wilie & Sons 1994.
15. RODER, H. M.: A Transient Hot Wire Thermal Conductivity Apparatus for Fluids. J. Res. Nat. Bur. St., 86(5), 1981. The national Bureau of Standards. Boulder, CO 80303, 1981.
16. SADROLHOSSEINI, A. R., MOKSIN, M. M., NANG, H. L. L., NOROZI, M., YUNUS, W., MAHMOOD, M., ZAKARIA, A.: Physical Properties of Normal Grade Biodiesel and Winter Grade Biodiesel. Int. J. Mol. Sci., 11, 2011: 2100 – 2111.
17. SAHIN, S., SUMNU, S. G.: Physical properties of foods. 2006. New York, USA, Springer 2006.
18. TAVMAN, I. H.: Effective thermal conductivity of granular porous materials. Int. Commun. Heat Mass, 23(2), 1996: 169 – 176.
19. TRÁVNÍČEK, P., VALACH, M., HLAVÁČOVÁ, Z., MAREČEK, J., VÍTĚZ, T., JUNGA, P.: Selected physical properties of liquid biofuels. Res. Agr. Eng., 59(4), 2013: 121–127.
20. VOZÁROVÁ, V., KARDJILOVA, K., HÍREŠ, Ľ., VALACH, M., WOLLNER, A.: Temperature dependence of dynamic viscosity and DSC analysis of the plantohyd samples. JCEA, 16 (2): 2015, 221–230, (online). Published 2015 (cit. 2016-05-10) URL: https://jcea.agr.hr/artic/774195_Temperature_Dependence of_Dynamic_Viscosity_and_DSC_ Analysis_of_the_Plantohyd_samples .pdf.
21. WAKEHAM, W. A., NAGASHIMA, A., SENGERS, V. J.: Measurement of the transport properties of fluids. Exp. Thermodynamics. London, United Kingdom, Blackwell Scientific Publications, 1991.
22. YAMANE, K., UETA, A., SHIMAMOTO, Y.: Influence of physical and chemical properties of biodiesel fuels on injection, combustion and exhaust emission characteristics in a direct injection compression ignition engine. Int. J. Eng. Res., 2, 2001: 4249 – 4261.

Corresponding author:

Monika Božíková, Department of Physics, Faculty of Engineering, Slovak University of Agriculture in Nitra, Tr. A. Hlinku 2, SK - 949 76 Nitra, Slovak Republic, e-mail: Monika.Bozikova@uniag.sk

WOOD WEAR RESISTANCE TO BONDED ABRASIVE PARTICLES

M. Brožek

Department of Material Science and Manufacturing Technology, Faculty of Engineering, Czech University of Life Sciences Prague, Czech Republic

Abstract
In this contribution the results of the wear resistance study of twelve types of wood commonly growing in the Czech Republic are published. The laboratory tests were carried out using the pin-on-disk machine with abrasive cloth according to the modified standard ČSN 01 5084. The abrasive track length and the abrasive clothes of three different grits were used. The wear intensity was assessed by the volume, weight and length losses of tested samples. The technical-economical evaluation was the part of the carried out tests. The samples from spruce and pine were the cheapest. The samples from locust and walnut were the most expensive. From the point of view of wear the most favourable results were determined at the samples from oak. Regardless of the criterion of assessment the wood of oak was keenly priced and it had the smallest wear without regard to the used abrasive cloth grit.

Key words: DMA wood, abrasive wear, bonded abrasive particles, wear resistance, laboratory tests.

INTRODUCTION

Wood is a natural material, which our ancient ancestors have learned to utilize very early. The first use of wood was evidently energy utilization with the aim to gain heat by its combustion. Later wood has been utilized to construction of buildings and fortifications, building of means of transport (ships and wagons) and tools.

In contrast to other used materials (metals, plastics, aggregate, limestone, glass, ceramics) wood has one exceptional property – it is a case of a renewable material. From statistical sources it follows that in the Czech Republic the one-year wood growth is in the long term higher than logging. So the wood supplies increase.

Compared to other materials the properties of wood are different (KAFKA, 1989; KETTUNEN, 2006; PESCHEL, 2002; PLUHAŘ ET AL., 1989). Some differences can be seen at first sight, e,g, colour, gleam or texture.In contrast to many other materials wood has a specific aroma. From physical properties let us specify e.g. density, moisture (shrinkage, swelling) and thermal, electric and acoustic properties. From mechanical properties let us specify at least elasticity, strength (tensile, pressure, bending, shear, torsion), hardness, toughness. Technological properties of wood are also exceptional, e.g. machinability, bending ability, loading capacity of metallic binders, wear resistance or various defects. For some applications, e.g. floors and staircases, the wear resistance is very important (KRÁL AND HRÁZSKÝ, 2008; LIU ET AL, 2012; OHTANI ET AL, 2001; OHTANI ET AL, 2002; OHTANI ET AL, 2003; ČSN 01 5050, 1969; ČSN 49 0134, 1984; ČSN EN 13696, 2009; ČSN 91 0276, 1989).

Even today wood is considered for a very good building material. The greatest consumer of wood is therefore building industry, followed by cellulosic-paper industry (FAHERTY AND WILLIAMSON, 1995; SLAVID, 2009; TSOUMIS, 1991; ZAHRADNÍČEK AND HORÁK, 2007). Production of furniture, musical instruments, works of art, sports equipment or of toys for children represent an interesting utilization of wood. A part of wood is consumed in form of firewood.

The aim of this study is to determine woods wear resistance of selected woods.

MATERIALS AND METHODS

In the contribution the results of abrasive wear resistance study of twelve types of wood (ash, birch, cherry, larch, lime, locust, maple, oak, pine, poplar, spruce and walnut) are published. The laboratory tests were carried out using the pin-on-disk machine with abrasive cloth, when the abrasive clothes of three different grits were used. The wear intensity of all test samples was assessed by volume, weight and length losses at different conditions.

The part of carried out tests was the technical-economical evaluation, too. The prices of test samples from wood were calculated from the actual price of semi-finished products (board, balk, trunk) used for

their production. The used prices are the average prices of wood in the Czech Republic at January 2014.
For the materials wear resistance determination against single wear types (ČSN 01 5050, 1969) in principle field tests, pilot tests and laboratory tests are used. Each of mentioned tests is of advantages, but also of disadvantages. Therefore each of test types is most suitable for other field of application. The wear resistance test type is always necessary to be chosen with regard to the in wear process dominant conditions and to the demanded test results (BROŽEK, 2007).
The wear intensity can be expressed by the directly measured values or by the relative values. The directly measured value can be abrasion specified in length (cm), weight (g) or volume (cm^3). The other possible way is the expression by the dimensionless quantity, when wear intensity of the tested sample is compared to the wear intensity of the standard (VOCEL, 1993; VOCEL AND DUFEK, 1976).
In literature a sufficient number of wear resistance testers for various types of wear is mentioned (BLAU, 1992; FRICTION AND WEAR TESTING, 1987; LEVER AND RHYS, 1968; VOCEL, 1993). Testing equipment for abrasive wear resistance determination is usually classified according to the contact mode of the sample with free or bonded abrasives. In practice the testing machines with abrasives bonded to cloth (Fig. 1) are used most often. They are simple and reliable, with small variance in results. Their disadvantage is the variable quality of abrasive cloth. In Czech Republic this testing method is standardised according to standard ČSN 01 5084 (similar foreign standards: STN 01 5084, ASTM G 132).

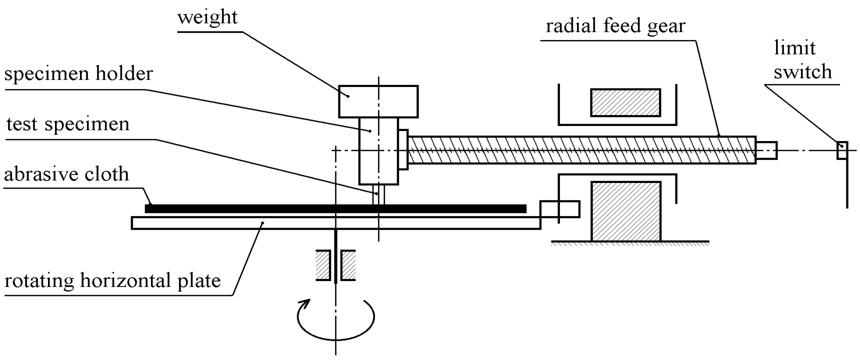

Fig. 1. – Scheme of the abrasion testing machine (pin-on-disk)

The principle of an abrasive wear test using the pin-on-disk machine with abrasive cloth (ČSN 01 5084; Fig. 1) is to wear the specimen under pre-determined conditions. Using the apparatus with abrasive cloth the samples were of 10 mm diameter and 70 mm length. The test sample is pressed against an abrasive surface using the prescribed normal force. The wear path is a spiral on the disk, caused by a disk rotation and a radial feed of a sample, so the sample progressively moves over the unused abrasive along the prescribed track length.
As abrasive cloth the corundum twill type A 99 – G, S 25, trade mark Globus, grit 120, was used. In addition tests using grits 60 and 240 were carried out, too. It corresponds to the average abrasive grain sizes of 44.5 µm (grit 240), 115.5 µm (grit 120) and 275 µm (grit 60) (BROŽEK ET AL., 2010). During the test the test sample was pressed to the abrasive cloth by the pressure of 0.1 MPa. The wear path total length was 250 m.
The above mentioned pin-on-disk machine with abrasive cloth (bonded abrasive) is primarily destined for the determination of abrasive wear resistance of metallic materials (BROŽEK, 2012; BROŽEK AND NOVÁKOVÁ, 2008; CIESLAR ET AL., 2013). By the carried out tests it was proved that this machine is suitable and applicable for wear resistance tests of plastics (BROŽEK, 2015) and wood, too.
In practice also machines of other design are used, e.g. machine with rubber cylinder. In this case the test sample is worn out by free abrasive, which is poured between the sample surface and the slowly rotating cylinder, which touches the sample surface. The rubber cylinder pushes the free abrasive grains against the tested sample surface. The used grains fall in a container (BUDINSKI, 1997).
The summary of the used materials, their density and price of test samples are stated in Tab. 1. Moisture of tested woods ranged from 8.3 to 9.1 %.

Tab. 1. – Summary of tested materials

Tested material	Density g·cm^{-3}	Price of test sample CZK	Price of test sample EUR	Price of test sample USD
ash	0.688	0.403	0.015	0.017
birch	0.695	0.516	0.019	0.021
cherry	0.804	0.901	0.033	0.037
larch	0.888	0.379	0.014	0.016
lime	0.542	0.282	0.010	0.012
locust	0.751	1.378	0.051	0.057
maple	0.726	0.426	0.016	0.018
oak	0.798	0.581	0.021	0.024
pine	0.584	0.228	0.008	0.009
poplar	0.553	0.402	0.015	0.017
spruce	0.427	0.222	0.008	0.009
walnut	0.638	1.199	0.044	0.049

For information: 1 EUR = 27.0650 CZK; 1 USD = 24.2670 (24 March 2016)

Before the abrasive wear test the density (ρ) of all tested materials was determined. Using a dial balance the sample weight (g) before (m_1) and after (m_2) the test was determined with the accuracy of 0.0001 g.
At the preparatory tests it was determined that at grinding of wood using abrasive cloth no abrasiveness reducing occurs, as it is known at metallic materials. Therefore at metallic materials it is by the standard prescribed to use for the next test new cloth. At tested woods the dependence between weight loss and track length was always linear with the high value of the coefficient of determination R^2 (from 0.998 to 1.000). Therefore the test procedure prescribed by the standard (ČSN 50 0184, 1974) could be adapted.
After the abrasive path of 50 m completion the abrasive cloth was carefully cleaned from the tested material worn out particles and again used. The test was repeated five times. By this way the weight losses of all tested samples after the wear path of 50 m, 100 m, 150 m, 200 m and 250 m were determined. For the next material test the new abrasive cloth was used.
The weight loss Δm (g) is calculated using the equation:

$$\Delta m = m_1 - m_2 \tag{1}$$

The volume loss ΔV (cm^3) is calculated from the weight loss Δm (g) and the density ρ (g·cm^{-3}) (Tab. 1) from the equation:

$$\Delta V = \frac{\Delta m}{\rho} \tag{2}$$

The length loss Δl (cm) is calculated from the volume loss ΔV (cm^3) and from the worn out sample front surface from the equation:

$$\Delta l = \frac{4.\Delta V}{\pi.d^2} \tag{3}$$

RESULTS AND DISCUSSION

In next Figures the woods are arranged according to the decreasing weight loss using the abrasive cloth of grit 240 (the average abrasive grain size 44.5 µm).
From the test results shown in Fig. 2 (weight loss) and in Fig. 3 (volume loss/length loss) it follows that different woods have different abrasive wear resistance. The order of tested woods arranged according to the decreasing weight/volume loss is identical. It is logical owing to the same worn out front surface diameter of all tested samples.
At the test using the pin-on-disk machine the highest wear was determined at the wood lime (Fig. 2). The wear intensity of next woods decreased in order birch, locust, larch, walnut, poplar, pine, ash, spruce, cherry and maple. The minimum wear was determined at the wood oak.
Concurrently the wood of oak showed 51 % wear of the wood of lime. At the wear using the abrasive cloth of grit 120 (115.5 µm) the woods placing changed. The highest wear was determined at lime. The next placing in descending order was larch, pine, locust, birch, walnut, spruce, poplar, maple, ash, cherry and oak. Concurrently the wood of oak showed 46 % wear of the wood of lime. At the wear using the abrasive cloth of grit 60 (275 µm) the woods wear placing in ascending order was larch, locust, lime, walnut, poplar, ash, maple, pine, birch, cherry, spruce and oak. Concurrently the wood of oak showed 42 % wear of

the wood of larch. So from the results it follows that at the increasing size of abrasive particles the ratio between the wear rate of the least and most wear resistant woods decreases. It means that the properties of the concrete wood influence less its wear. From the carried out tests it also follows that the average wear of wood samples regardless of their type is the greatest using the abrasive cloth of grit 120 (1.165 ± 0.260 g), smaller using the abrasive cloth of grit 60 (1.033 ± 0.262 g) and the smallest using the abrasive cloth of grit 240 (0.698 ± 0.155 g). From this fact it follows that the wear of wood depends significantly on the abrasive particles size. The greatest wear is caused by particles of medium size, small and big particles cause a smaller wear.

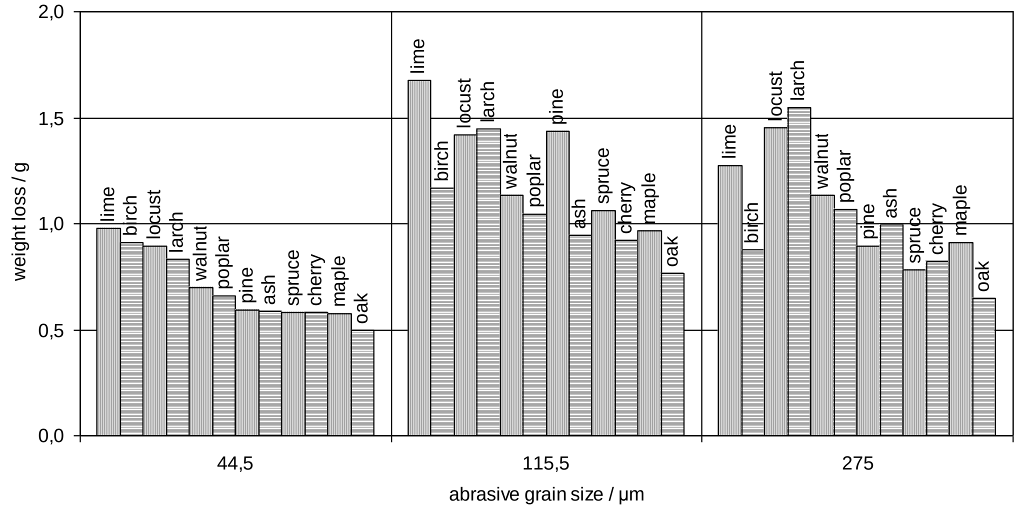

Fig. 2. – Weight loss

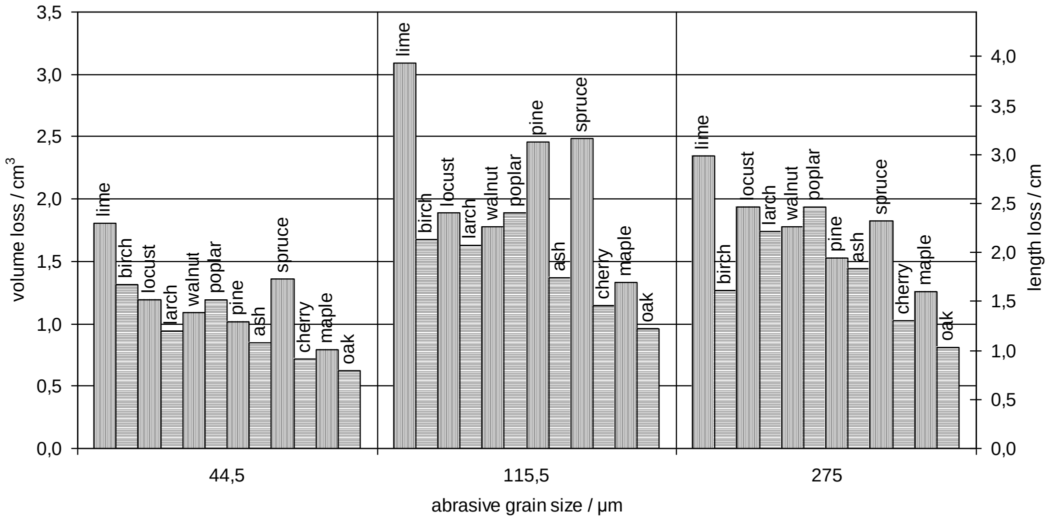

Fig. 3. – Volume/length loss

In comparison with Fig. 2 to Fig. 3 it is evident that the order of tested woods wear intensity expressed by volume/length loss does not correspond to the order expressed by weight loss. It is caused by the considerably different density of the tested woods (Tab. 1). The greatest volume/length wear using the abrasive cloth of grit 240 was determined at lime and it decreased in order of woods spruce, birch, locust, poplar, walnut, pine, larch, ash, maple, cherry and oak. Using the abrasive cloth of grit 60 the order of woods was lime, poplar, locust, spruce, walnut, larch, pine, ash, birch, maple, cherry and oak. From the point of view of volume/length loss the wood of lime was the least wear resistant, the wood of oak the most wear resistant. At the use of all abrasive cloth grits the volume/length loss of the wood oak ranged from 31 % to 34 % of the wood lime.

The graphical illustration of the technical-economical evaluation of the carried out tests is evident from Fig. 4 (according to weight loss) and Fig. 5 (according to volume/length loss). Both of diagrams represent the results of the tests carried out using the abrasive cloth of grit 120 (average abrasive grain size 115.5 µm).

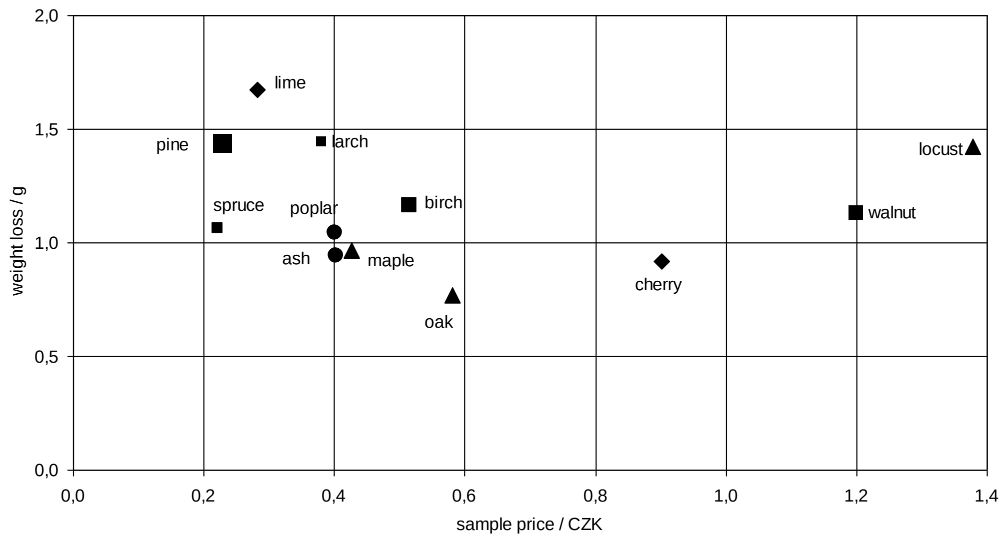

Fig. 4 – Relationship between weight loss and sample price

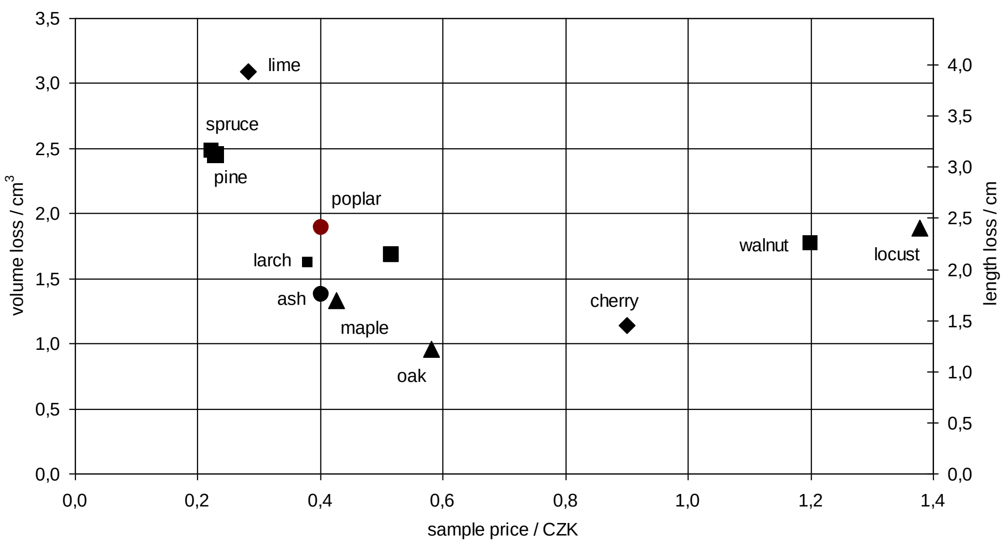

Fig. 5 – Relationship between volume/length loss and sample price

In Figs 4 (weight loss) and 5 (volume/length loss) the results of for practice most suitable woods from the technical-economical point of view are located left at the bottom. It is a case of keenly priced materials of relatively small wear. On the contrary the results of woods located right on the top are not suitable for use in conditions of abrasive wear. It is a case of material low wear resistance and high price.

As it is evident from Fig. 4 the greatest weight loss is shown by the woods of lime, pine, larch and locust. The first mentioned woods are cheap. The wood from locust is multiple expensive (Tab. 1). On the contrary the smallest weight loss is shown by the wood of oak, cherry, maple and ash. The woods of ash and maple are at the same time keenly priced.

From the point of view of wear expressed by volume/length loss (Fig. 5) the greatest wear was determined at the woods of lime, spruce and pine, the smallest wear was determined at the woods of oak, cherry and maple. The medium wear was determined at the woods of walnut and locust, but which are the most expensive. The price of the samples ranged from 0.222 to 1.378 CZK (from 0.008 to 0.051 EUR or from 0.009 to 0.057 USD) per unit.

On the basis of the carried out tests the wood of oak proved to be the abrasive wear most resistant. It has the smallest wear regardless in the way of the wear resistance definition (weight loss, volume/length loss) and it is relatively keenly priced.

From the results summarization of the carried out tests it follows that at the different materials wear resistance evaluation it is necessary to give the parameter of loss. As it is showed in above mentioned figures, the results expressed by volume or length loss (Fig. 3) are at the same size of test samples identical, while results expressed by weight loss (Fig. 2) differ.

CONCLUSIONS

The contribution contains the laboratory tests results of abrasive wear resistance of selected wood using the pin-on-disk machine with abrasive cloth. In total twelve types of wood commonly growing in the Czech Republic (ash, birch, cherry, larch, lime, locust, maple, oak, pine, poplar, spruce and walnut) were tested. The aim of the carried out tests was to assess the possibility of their use for products, which are intensively worn out, e.g. terraces or staircases.

All samples were of cylindrical shape of 10 mm diameter and 70 mm length. For the test samples wear three abrasive clothes of different grit, namely 240 (average abrasive grain size 44.5 μm), 120 (average abrasive grain size 115.5 μm) and 60 (average abrasive grain size 275 μm) were used. The test of all materials was carried out according to the modified standard ČSN 01 5084 except that using the same abrasive cloth the sample was worn out five times, which means using the path 50 m 100 m, 150 m, 200 m and 250 m. After each test of one material the abrasive cloth was carefully cleaned from the material rests and used again. For the next material the new abrasive cloth was always used.

The wear intensity was evaluated by weight loss, volume loss and length loss at all tested samples. From the evaluation of the carried out tests it follows that the greatest difference between the most and the least wear resistant woods (oak/lime) was determined at the use of the abrasive cloth of grit 240 having the smallest abrasive particles. The difference is put by the ratio of 0.51. With the increasing size of abrasive particles this ratio decreases. Using the abrasive cloth of grit 120 it is 0.46 and of grit 60 having the greatest abrasive particles it is 0.42 (oak/larch). It was also found that the greatest wear regardless to the sort of wood are caused by the particles of the medium size (grit 120, weight loss 1.165 ± 0.260 g), the minor wear by the great particles (grit 60, weight loss 1.033 ± 0.262 g) and the smallest wear by the small particles (grit 240, weight loss 0.698 ± 0.155 g).

The technical-economical evaluation was the part of the carried out tests. At the same time it was proved that on the Czech market the price of wood is very different. The samples of spruce and pine were the cheapest; the samples of locust and walnut were the most expensive. From the point of view of wear resistance the most favourable results were determined at the wood of oak. Oak was relatively keenly priced and regardless of the evaluation criterion (weight loss, volume loss, length loss) and of the used abrasive cloth grit (240, 120 and 60) it had the smallest wear.

From the results of carried out tests it follows that for applications, where wood is intensively abrasively worn out, from domestic woods it is possible to recommend only oak. The other tested woods are no so wear resistant and as the case may be more expensive.

REFERENCES

1. BLAU, P. J.: ASM Handbook. Volume 18 – Friction, Lubrication, and Wear Technology (online). ASM International. 1992. available at: http://app.knovel.com/hotlink/toc/id:kpASMHVFL2/asm-handbook-volume-18. Accessed 10 November 2013.
2. BROŽEK, M.: Wear resistance of multi-layer overlays. In: 11th International Scientific Conference Engineering for Rural Development, 24-25 May 2012, Jelgava, Latvia University of Agriculture, pp. 210-215.
3. BROŽEK, M.: Technicko-ekonomické hodnoceni aplikace návarů u plužních čepelí (Technical-economical evaluation of the overlays application on plough shares). Acta Univ. Agric. et Silvic. Mendel. Brun., 55, 2007: 129-136. (In Czech).
4. BROŽEK, M.: Selected plastics wear resistance to bonded abrasive particles compared to some ferrous materials. Acta Univ. Agric. et Silvic. Mendel. Brun., 63, 2015: 387-393.
5. BROŽEK, M., NOVÁKOVÁ, A.: Evaluation of sintered carbides wear resistance. In: 7th International Scientific Conference Engineering for Rural Development, 29-30 May 2008. Jelgava, Latvia University of Agriculture, pp. 209-213.
6. BROŽEK, M., NOVÁKOVÁ, A., MIKUŠ, R.: Study of wear resistance of hard facings using welding powders on the NiCrBSi basis. In: 4th International Conference Trends in Agri-

cultural Engineering 2010. 7-10 September 2010. Prague, Czech University of Life Sciences Prague, pp. 115-118.
7. BUDINSKI, K. G.: Resistance to particle abrasion of selected plastics. Wear, 203-204, 1997: pp. 302-309.
8. CIESLAR, J. – BROŽEK, M. – BEDNÁŘ, B.: An experimental assessment of special metal castings in reducing abrasive wear. Manufacturing Technology, 13, 2013: 423-428.
9. FAHERTY, K. F., WILLIAMSON, T. G.: Wood engineering and construction handbook. 2nd ed., New York, Osborne-McGraw-Hill 1995.
10. Friction and Wear Testing. American Society for Testing and Materials. West Conshohocken, PA, American Society for Testing and Materials 1987.
11. KAFKA, E.: Dřevařská příručka (Woodworking guide). Praha, Nakladatelství technické literatury. 1989. (In Czech).
12. KETTUNEN, P. O.: Wood: Structure and properties. Uetikon-Zuerich, Enfield, Trans. Tech. Publication 2006.
13. KRÁL, P., HRÁZSKÝ, J.: A contribution to the resistance of combined plywood materials to abrasion. Journal of Forest Science, 54, 2008: 31-39.
14. LEVER, A. E., RHYS, J. A.: The properties and testing of plastic materials. 3rd ed., Bristol, Wright Temple Press Books. 1968.
15. LIU, Z. D., WANG, W. B., CAI, L., GUO, D. J., DAI, Z. D.: Friction and wear properties of commercial solid wood floorings. Mocaxue Xuebao (Tribology), 32, 2012: 557-562.
16. OHTANI, T., YAKOU, T., KITAYAMA, S.: Two-body and three-body abrasive wear properties of Katsura wood. J. Wood Sci., 47, 2001: 87-93.
17. OHTANI, T., YAKOU, T., KITAYAMA, S.: Effect of annual rings on abrasive wear property of wood. J. Wood Sci., 48, 2002: 264-269.
18. OHTANI, T., KAMASAKI, K., TANAKA, C.: On abrasive wear property during three-body abrasion of wood. Wear, 255, 2003: 60-66.
19. PESCHEL, P.: Dřevařská příručka. Tabulky. Technické údaje (Woodworking guide. Tables. Technical data). Praha, Sobotáles 2002. (In Czech).
20. PLUHAŘ, J. ET AL.: Nauka o materiálech (Material Science). Praha, SNTL 1989.
21. SLAVID, R.: Wood architecture. Paperback ed. London, Laurence King 2009.
22. TSOUMIS, G.: Science and technology of wood: Structure, properties, utilization. New York, Chapman & Hall 1991.
23. VOCEL, M.: Experimentální metody hodnocení tření a opotřebení (Experimental Methods of Friction and Wear Evaluation). Kovové materiály, 21, 1993. (In Czech).
24. VOCEL, M. – DUFEK, V. ET AL.: Tření a opotřebení strojních součástí (Friction and Wear of Machine Parts). Praha, SNTL 1976.
25. ZAHRADNÍČEK, V., HORÁK, P.: Moderní dřevostavby (Modern wooden houses). Brno, ERA 2007.
26. ČSN 01 5050. Opotřebení materiálu. Názvosloví. (Wear of materials. Terminology). 1969. (In Czech).
27. ČSN 01 5084. Stanovení odolnosti kovových materiálů proti abrazívnímu opotřebení na brusném plátně (Determination of metal material resistance against wear by abrasive cloth). 1974. (In Czech).
28. ČSN 49 0134. Drevo. Metóda zisťovania odolnosti proti oderu (Wood. Determination of abrasion resistance). 1984. (In Slovak).
29. ČSN EN 13696. Wood flooring - Test methods to determine elasticity and resistance to wear and impact resistance. 2009.
30. ČSN 91 0276. Nábytek. Metoda zjišťování odolnosti povrchu proti otěru (Furniture. Method of determining the surface resistance to abrasion). 1989. (In Czech).

Corresponding author:
prof. Ing. Milan Brožek, CSc., Department of Material Science and Manufacturing Technology, Faculty of Engineering, Czech University of Life Sciences Prague, Kamýcká 129, Praha 6, Prague, 16521, Czech Republic, phone: +420 22438 3265, e-mail: brozek@tf.czu.cz

OPTIMAL FEEDSTOCK PARTICLE SIZE AND ITS INFLUENCE ON FINAL BRIQUETTE QUALITY

A. Brunerová, M. Brožek

Department of Material Science and Manufacturing, Faculty of Engineering, Czech University of Life Sciences Prague, Czech Republic

Abstract

Present paper monitored one of most important feedstock property, specifically particle size, and its influence on briquette quality. Six different types of briquettes were produced; two conifer tree barks (pine and spruce) with three different particle sizes (<6; 6 – 12; >12 mm) were used as feedstock materials. Investigated briquettes were subjected to gross calorific value, ash content, volume density, mechanical durability and rupture force determination. Evaluation of measured values stated particle size 6 – 12 mm as most suitable for spruce bark briquettes, followed by <6 mm and >12 mm. Within pine bark briquettes a particle size equal to <6 mm exhibited best results, then 6 – 12 mm and >12 mm. Generally, most suitable particle size was attributed to 6 – 12 mm, however, results did not prove one unambiguous optimal particle size. In conclusion, results values did not support prevailing opinion that smaller particle sizes are more suitable for briquette production.

Key words: solid biofuel, mechanical durability, rupture force, quality testing, particle size.

INTRODUCTION

Until recently, the biomass has not been widely utilized as renewable source of energy due to its relatively low energy efficiency when compared to fossil fuels. However, concern over climate changes and global inappropriate waste management caused increasing effort to use biomass and waste materials for energy production (McKendry, 2002). Currently, briquetting is one of suitable evolving technologies of waste materials conversion to solid biofuels for energy purposes. Great amount of waste materials proper for briquette production are produced every day and one of them is tree bark. Bark is ordinarily used as a mulching material for greater soil evaporation (Zribi et al., 2015), nevertheless, there is a potential to use it as a feedstock for briquette production (Kesley et al., 1979).

Two most important feedstock properties are particle size and moisture content (Mitchual et al., 2013). Optimal level of moisture content is defined by mandatory technical standard EN 18134–2 (2016): Solid biofuels – Determination of moisture content – Oven dry method – Part 2: Total moisture – Simplified method and it ranges between 8 – 12% (EN 18134–2, 2016). Despite the fact that particle size is also considered as great influencer of final briquette quality (Saptoadi, 2008) there is no mandatory technical standard to define optimal range of particle size. According to previous researches, there is prevailing opinion that finer grind of feedstock material causes higher quality of solid biofuels (Kaliyan and Morey, 2009; Karunanithy et al., 2012). MacBain (1966) asserted that larger particles accept less moisture which causes fractures in solid biofuels in contrast with finer particles.

Thus, according to previous researches briquette quality increases with decreasing of feedstock particle size, but this trend is limited. Extremely small particles exhibit negative influence and decreasing of mechanical durability, which is main indicator of mechanical quality of briquettes, as well as disproportionately large particles (Kaliyan and Morey, 2009). Previous research of Mitchual et al. (2013) focused on briquettes produced from tropical hardwood sawdust proved that best particle size ranges between 1 – 2 mm. However, other authors exhibited that suitable particle size ranges between 10 – 15 mm for briquettes from municipal solid waste (Young and Kennas, 2003) or ranges between 6 – 8 mm size for briquettes made from combination of three hardwood species (Emerhi, 2011). Different research done by Tumuluru et al. (2015) which was focused on briquettes produced from wheat, oat, canola, and barley straw proved best particle size between 25 – 32 mm (Tumuluru et al., 2015). Choice of optimal particle size apparently partially depends on concrete feedstock material but in general, it is not disputed that overall optimal particle size is not defined yet.

Main aim of this paper is to determine optimal particle size (fraction) of two feedstock materials – pine and spruce bark - used for the briquette samples production to optimize briquetting process by preventing material loose during briquette production, transportation and storage which can be directly caused by inappropriate particle size.

MATERIALS AND METHODS

Two different types of barks which were used as feedstock material for briquette sample production originated from pine tree and spruce tree. Both materials were acquired by cooperation with the Arboretum FFWS Kostelec nad Černými lesy. Raw unprocessed materials occurred in an unacceptable form for briquette production (moisture content above 40%, particle size above 100 mm) therefore preproduction preparation was executed. Material was primarily dehydrated in heated laboratory followed by drying in laboratory dryer LAC type S100/03 (LAC, Czech Republic) to proper moisture content in accordance to mandatory technical standard EN 18134–2 (2016): Solid biofuels – Determination of moisture content – Oven dry method – Part 2: Total moisture – Simplified method (EN 18134–2, 2016). Dried material exhibited following values of moisture content: pine bark equal to 14.02% and spruce bark equal to 11.91%. In next step were two mentioned feedstock materials crushed by shredder AL–KO New Tec 2400 R (Dolpima, Czech Republic) and subsequently divided by sieves according three different fraction size: <6 mm, 6 – 12 mm and >12mm.

Thus three different types of each bark feedstock materials were made within what six different types of briquettes were produced by hydraulic piston press Briklis type BrikStar type 30–12 (Malšice city, Czech Republic) under the same manufacturing conditions into cylindrical shape with diameter equal to 50 mm. Used briquetting press operates with pressure equal to 18 MPa, temperature equal to 60°C and proper feedstock moisture content varieties between 8–15%. Feedstock preparation and subsequent briquette samples production were performed according to mandatory technical standard EN ISO 17225–1 (2015): Solid biofuels – Fuel specifications and classes – Part 1: General requirements (EN ISO 17225–1, 2015).

< 6 mm 6 – 12 mm > 12 mm

Fig. 1. – Briquette samples produced from different particle size feedstocks

Length of produced briquette samples was equal to 55.86 mm in average (min. 38.41 mm; max. 73.57 mm) for pine bark and equal to 55.62 mm (min. 40.87 mm; max. 68.61 mm) for spruce bark. Variety of briquette weights exhibited following values: pine bark briquettes equal to 116.32 g (min. 74.20 g; max. 146.10 g) and spruce bark briquettes equal to 110.56 g (min. 63.40 g; max. 137.40 g). Volume density which is considered as important indicator of densification process efficiency was monitored and calculated within overall briquette quality. Detail ranges of volume density of all briquette samples are exhibited in Fig. 2 and Fig. 3.

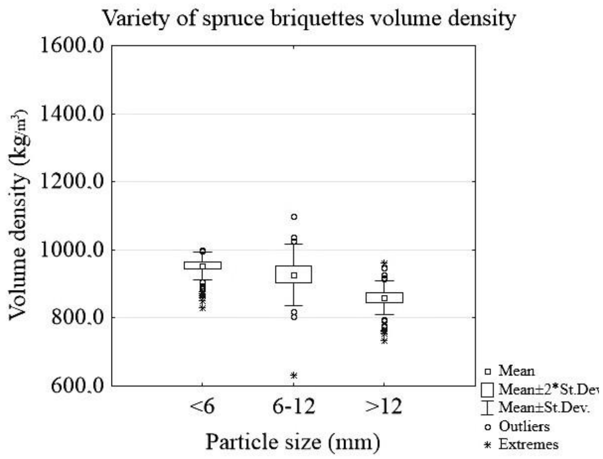

Fig. 2. – BoxPlot of volume density varieties within different particle sizes

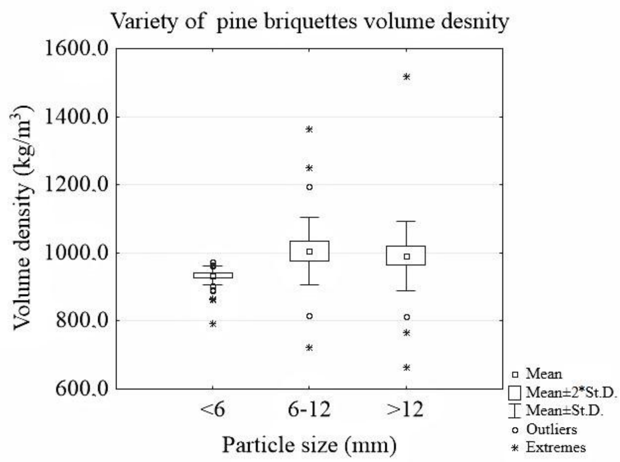

Fig. 3. – BoxPlot of volume density varieties within different particle sizes

Experimental methods

Experimental testing performed within briquette samples quality determination was conducted to mandatory technical standard EN 15234–1 (2011): Solid biofuels – Fuel quality assurance – Part 1: General requirements (EN 15234–1, 2011). Within analysis of chemical properties of mentioned feedstock a gross calorific value (GCV) and ash content (A_c) were determined. Measurements of GCV were performed according to mandatory technical standard EN 14918 (2010): Solid biofuels – Determination of calorific value (EN 14918, 2010). Adiabatic calorimeter Laget MS – 10 A (Laget, Germany) was used for experimental testing and subsequent result values were calculated by using of following formula (1):

$$GCV = \frac{dTk \times Tk - (c_1 + c_2)}{m} \tag{1}$$

Where:
GCV – Gross calorific value (J·g^{-1})
dTk – Temperature jump (°C)
Tk – Heat capacity of calorimeter (J·°C^{-1})
c_1 – Repair of benzoic acid (J)
c_2 – Repair of burning spark wire heat (J)
m – Weight of material sample (g).

Content of ash was investigated by using of laboratory muffle furnace LMH (LAC, Czech Republic) in accordance to mandatory technical standard EN 14775 (2009): Solid biofuels – Determination of ash content. Final result values were calculated by formula (2):

$$A_c = \frac{(m_3 - m_1)}{(m_2 - m_1)} \times 100 \times \frac{100}{100 - M_{ad}} \tag{2}$$

Where:
A_c – Ash content (%)
m_1 – Mass of empty crucible (g)
m_2 – Mass of crucible + sample (g)
m_3 – Mass of crucible + ash (g)
M_{ad} – Water content in a sample (%) (EN 14775, 2009).

Within mechanical quality determination a mechanical durability of all specific briquette types was tested. Whole preparation, testing and used equipment were conducted to mandatory technical standard EN 15210–2 (2011): Solid biofuels – Determination of mechanical durability of pellets and briquettes – Part 2: Briquettes (EN 15210–2, 2011). Experimental measurements was performed in special dustproof rotating drum (see in Fig. 4) and for subsequent mechanical durability calculation following formula was used (3):

$$DU = \frac{m_A}{m_E} \cdot 100 \tag{3}$$

Where:
DU – Mechanical durability (%)
m_A – Mass of sieved briquettes after the drum treatment (g)
m_E – Mass of pre-sieved briquettes before the drum treatment (g).

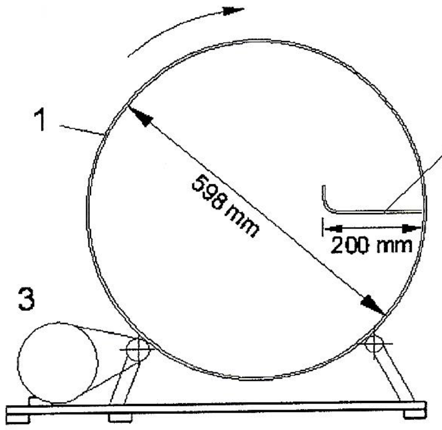

Fig. 4. – Special dustproof rotating drum: 1 – drum, 2 – partition, 3 – motor

A hydraulic universal tensile compression testing machine type ZDM 50 (VEB, Dresden, Germany) which operates with loading speed 20 mm/min. and maximal force 500 kN was used for performance of second mentioned quality test. Drawing of machine ZDM 50 and used principle of special plate-loading test are expressed in Fig. 5. There are no mandatory technical standards to define process of rupture force determination and evaluation of result values. Nevertheless, investigated briquette samples were loaded by application of force produced by ZDM 50 machine and maximal force which briquette sample was able tolerated before it broke down was measured and noted as a rupture force in Newton.

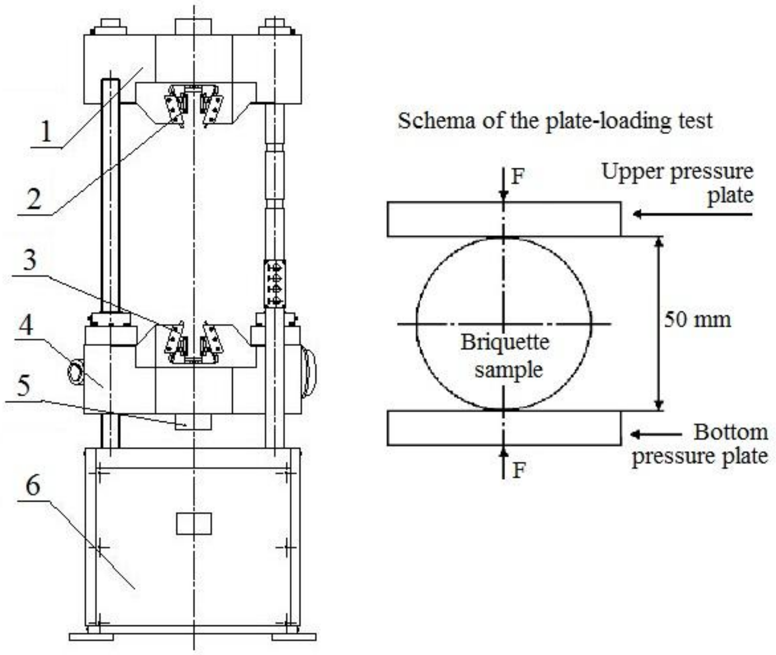

1 – up crossbeam, 2 – up jaw, 3 – down jaw, 4 – down crossbeam, 5 – platen, 6 – configuring

Fig. 5. – Schema and principle of rupture force testing machine

RESULTS AND DISCUSSION

Level of briquette samples volume density expressed efficiency of briquetting process and appropriateness of used feedstock material for briquette production. Fig. 2 and Fig. 3 shows result values proving highest volume density for fraction <6 mm for spruce briquette samples. If compared differences between individually fractions of spruce feedstock, very small differences were proved. However, decreasing trend was observed with increasing of particle size. This trend corresponds with the common opinion that biofuel quality increases with decreasing of particle size as stated by SAPTOADI (2008). On the contrary, result values of pine briquette samples testing did not confirmed this trend. If compare differences between individually fractions of pine feedstock the highest level of volume density was observed for middle fraction 6 – 12 mm, following by largest fraction >12 mm and then lowest level was observed for fraction <6 mm. It implies that it cannot be represented that smaller particle size always indicated higher briquette quality.

Result values of GCV were stated equal to 18.6 MJ kg^{-1} in average for pine bark material and equal to 19.3 MJ kg^{-1} for spruce bark material. Present result values corresponded to mandatory minimal requirement (>17 MJ·kg^{-1}) according to appropriate standard. In compare with wood of those conifer trees, previous researches proved GCV of pine wood equal to 16.3 MJ·kg^{-1} and equal to 20.5 MJ·kg^{-1} for spruce wood (KRATZEISEN ET AL., 2010; RHEN ET AL., 2007). Ash content determination exhibited following result values: 1.87% for pine bark material and 5.15% for spruce bark material. Mentioned values presented very high level of ash content if compare with pine wood (0.31%) and spruce wood (0.48%). This inequality could be caused by external contamination and pollution of bark during tree lifetime (RHEN ET AL., 2007).

Evaluation of mechanical durability result values proved that feedstock material which contains smallest particle size not always ensures best briquette quality results. Briquette samples produced from pine bark exhibited best result for middle particle size briquette samples (6 – 12 mm), following by smallest particle size briquette samples (<6 mm) and worst result was achieved by largest particle size briquette samples (>12 mm). Result values obtained for spruce bark briquette samples corresponded to prevalent opinion about improving of briquette quality with decreasing of particle size as visible from Fig. 6 (SAPTOADI, 2008). Overall evaluation of mechanical durability determination proved positive influence of decreasing of particle size on briquette quality. However, this evaluation is not unambiguous for all investigated briquette types as well as volume density result values indicated. In any case, overall evaluation of mechanical durability of all investigated briquettes samples indicated high level of this quality indicator (>90%) according to appropriate mandatory technical standard (EN 15210-2, 2011).

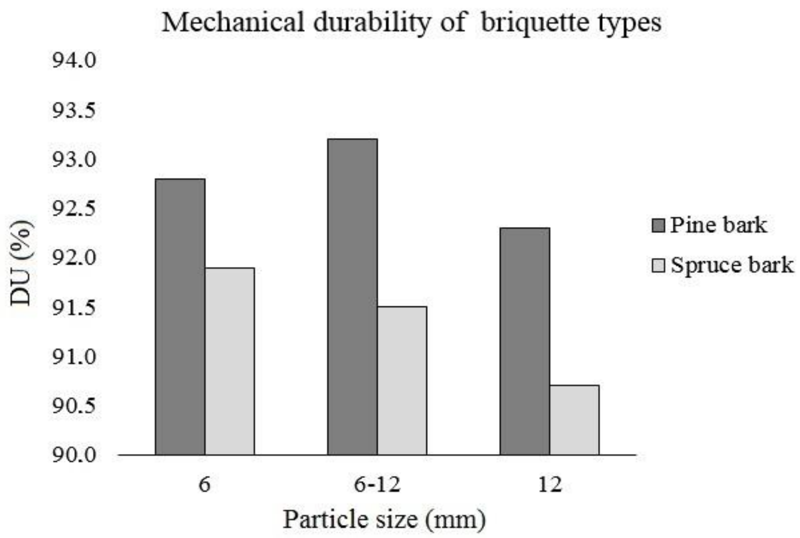

Fig. 6. – Comparison of mechanical durability of investigated briquette sample types

Within rupture force testing a highest level of this mechanical quality indicator was proved by pine bark briquette samples with largest particle size (>12 mm), followed by middle particle size (6 – 12 mm) and worst result exhibited briquette samples with smallest particle size (<6 mm).

Investigated spruce bark briquette samples exhibited best result for middle particle size (6 – 12 mm), then for smallest particle size (<6 mm) and worst results proved briquette samples with largest particle size (>12 mm). Comparisons between specific particle sizes of concrete feedstock materials are expressed in Fig. 7 and Fig. 8.

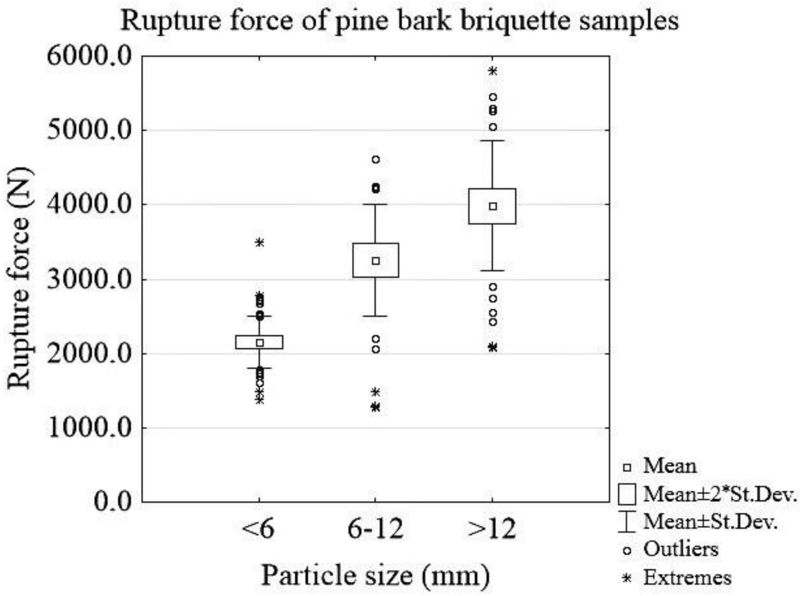

Fig. 7. – Boxplot of rupture force variety within different fractions of pine bark feedstock

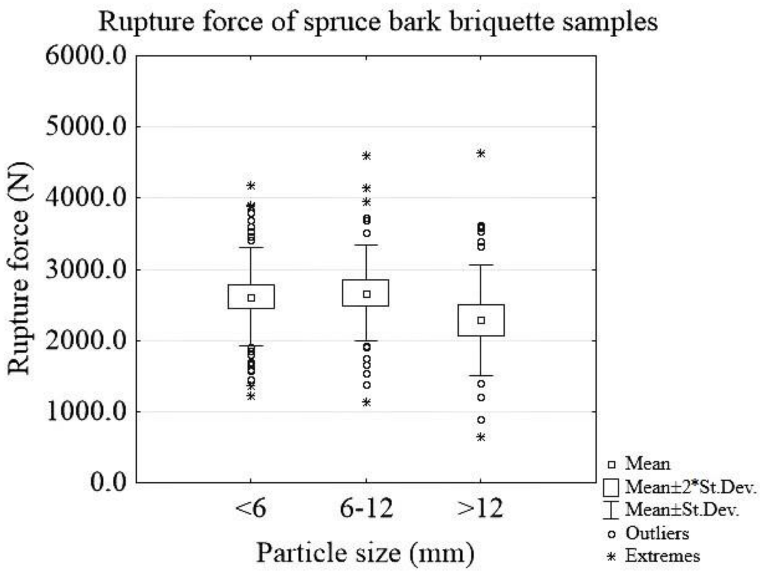

Fig. 8. – Boxplot of rupture force variety within different fractions of spruce bark feedstock

As is visible from Fig. 7 and Fig. 8 in neither case was highest result values reached by briquette samples made from smallest particle size. It can be concluded that smallest particle size (<6 mm) influences rupture force negatively.

CONCLUSIONS

Overall evaluation of investigated quality indicators did not prove unambiguous result. According to the Tab. 1 which expressed all result values (best results are emphasize by bold font) there was low difference between specific feedstock material and in case of specific particle size the results exhibited best values out of sequence.

Thus it can be concluded that one unique optimal particle size was not proved but if compare all best result values the middle particle size (6 – 12 mm) expressed most of them. Within explored influence of different particle size on final briquette quality it can be recommended to continue in future researches in attempt to define unique optimal particle size for different types of biomass.

Tab. 1. – Result values of quality indicators of different feedstock briquette samples

	Pine bark			Spruce bark		
Particle size (mm)	<6	6 – 12	>12	<6	6 – 12	>12
Volume density (kg/m^3)	933.9	**1005.6**	991.1	**953.3**	926.7	859.7
Mechanical durability (%)	92.8	**93.2**	92.3	**91.9**	91.5	90.7
Rupture force (N)	2155.54	3248.41	**3984.53**	2613.6	**2663.0**	2287.2

ACKNOWLEDGEMENTS.
The research was supported by Internal Grant Agency of the Faculty of Engineering, Czech University of Life Sciences Prague, grant number 2016:31140/1312/3107 and further by Internal Grant Agency of the Czech University of Life Sciences Prague, grant number 20165003.

REFERENCES

1. EMERHI, E. A.: Physical and combustion properties of briquettes produced from sawdust of three hardwood species and different organic binders. Pelagie Research Library, 2, 2011: 236–246.
2. EN 14775: Solid biofuels – Determination of ash content, 2009: 1–12.
3. EN 14918: Solid biofuels – Determination of calorific value, 2009: 1–52.
4. EN 15210–2: Solid biofuels – Determination of mechanical durability of pellets and briquettes – Part 2: Briquettes. 2011: 1–12.
5. EN 15234–1: Solid biofuels – Fuel quality assurance – Part 1: General requirements, 2011: 1–24.
6. EN 18134–2: Solid biofuels – Determination of moisture content – Oven dry method – Part 2: Total moisture – Simplified method, 2016: 1–12.
7. EN ISO 17225–1: Solid biofuels - Fuel specifications and classes – Part 1: General requirements. 2015: 1–64.
8. KALIYAN, N., MOREY, R. V.: Factors affecting strength and durability of densified biomass products. Biomass and Bioenergy, 33, 2009: 337–359.
9. KARUNANITHY, C., WANG, Y., MUTHUKUMARAPPAN, K., PUGALENDHI, S.: Physiochemical characterization of briquettes made from different feedstocks. Biotechnology research international, 2012:1–12.
10. KESLEY, R. G., SHAFIZADEH, F., LOWERY, D. P.: Heat Content of bark, twigs, and foliage of nine species of western conifers. Forestry, 69, 1979:1–8.
11. KRATZEISEN, M., STARCEVIC, N., MARTINOV, M., MAURER, C., MÜLLER, J.:. Applicability of biogas digestate as solid fuel. Fuel, 89, 2010:2544–2548.
12. MCKENDRY, P.: Energy production from biomass (Part 1): Overview of biomass. Bioresource technology, 83, 2002:37–46.
13. MITCHUAL, S. J., FRIMPONG-MENSAH, K., DARKWA, N. A.: Effect of species, particle size and compacting pressure on relaxed density and compressive strength of fuel briquettes. International Journal of Energy and Environmental Engineering, 4, 2013:1–6.
14. RHEN, C., OHMAN, M., GREF, R., WASTERLUND, I.: Effect of raw material composition in woody biomass pellets on combustion characteristics. Biomass and Bioenergy, roč. 31, 2007:66–72.
15. SAPTOADI, H.: The Best Biobriquette Dimension and its Particle Size. Asian Journal Energy Environment, 9, 2008:161–175.
16. TUMULURU, J. S., TABIL, L. G., SONG, Y., IROBA, K. L., MEDA, V.: Impact of process conditions on the density and durability of wheat, oat, canola, and barley straw briquettes. Bio-Energy Research, 8, 2015:388–401.
17. YOUNG, P., KENNAS, S.: Feasibility and Impact Assessment of a Proposed Project to Briquette Municipal Solid Waste for Use as a Cooking Fuel in Rwanda. Intermediate Technology Consultants, 1, 2003:1–59.
18. ZRIBI, W., ARAGÜÉS, R., MEDINA, E., FACI, J. M.: Efficiency of inorganic and organic mulching materials for soil evaporation control. Soil and Tillage Research, 148, 2015:40–45.

Corresponding author:
Ing. Anna Brunerová, Department of Material Science and Manufacturing Technology, Faculty of Engineering, Czech University of Life Sciences Prague, Kamýcká 129, Praha 6, Prague, 16521, Czech Republic, phone: +420 22438 3271, e-mail: brunerova@tf.czu.cz

PROPERTIES OF THE SUGAR BEET TOPS DURING THE HARVEST

V. M. Bulgakov[1], V. V. Adamchuk[2], L. Nozdrovicky[3], M. Boris[4], Y. I. Ihnatiev[5]

[1]*National University of Life and Environmental Sciences of Ukraine*
[2]*National Scientific Centre "Institute of Agricultural Engineering and Electrification" NAASU*
[3]*Slovak University of Agriculture in Nitra, Slovak Republic*
[4]*Podolsky State Agricultural and Technical University of Ukraine*
[5]*Tavria State Agrotechnological University of Ukraine*

Abstract
All methods of sugar beet tops separation from the roots are based on the difference in the placement tops and root crops relative to the soil surface and their relative placement. Separation of tops residues after cutting is based on the various strength of sugar beet heads and leaves. The aim of the study is to determine the optimal method of mechanical impact on the beet tops in order to improve the quality of its harvest process. To study the form and structure of the sugar beet stalks there was used cuttings used photo-shoot overlaid by coordinate grids. For determine the hardness of various zones was used specially designed hardness tester. Impact action on the root crops head was investigated by a special laboratory facility. As a result of experimental studies there were obtained a new data characterizing the structure, shape and strength of the various zones of the root crops head and leaves with the aim to study the possibilities of effective mechanical destruction of leaves and subsequent separation of them from the head.

Key words: sugar beet, sugar beet tops, structure and properties, harvesting, hardness.

INTRODUCTION

Among the urgent scientific and production task belongs the development of the new high effective working mechanisms for the separation of the sugar beet leaves from the sugar beet root allowing to decrease the losses of the sugar containing part of the sugar beet root and increase the forward speed of the sugar beet topper. The process of the sugar beet topping is focused on the separation of sugar beet top from the sugar beet root. All this process is effected by the different properties of the sugar beet tops and sugar beet roots material. When analysing the current level of the development of technological process and used machines, it is possible to define the following ways of the sugar beet topping: cutting of the leaves with the sensing or without sensing with the additional cleaning of the root tops after the topping and separation of the leaves by using of the dynamic action with the help of the defoliators - rotors with the elastic working elements. All types of the sugar beet topping manners are based on the differences in the location of the sugar beet leaves and sugar beet roots in relation to the soil surface and their joint distribution. Separation of the sugar beet leaves residues after the cut by using of the dynamic action of the cleaning elements on the sugar beet root head is based on the different firmness of the sugar beet root head and leaves. Therefore, it is very important to study such properties of the sugar beet leaves and sugar beet heads, which allow to separate them.

Agro-physical characteristics of the sugar beet crop stands and mechanical-technological properties sugar beet roots and top leaves very studied by VASILENKO (1984); POGORELYJ L. AND TATJANKO (2004); BULGAKOV (2005); ZUEV (1971); VOVK (1936); KHELEMENDIK (1996); MARTINENKO (1997); TOPOROVSKIJ (1988); POGORELIJ M. (2001).

The height of the sugar beet root heads above the soil surface can be considered as a very significant indicator effecting the separation of the leaves from root head. It is the top of the head located above the soil surface which is used for orientation of the sensing mechanism of the sugar beet toppers. According to the distribution of the height values of the sugar beet root heads it is possible to determine the location of the sugar-containing matter in relation to the soil surface and subsequently to determine the height of the sensing-less topping. Based on the research results obtained by POGORELIJ L., TATJANKO (2004) AND TOPOROVSKIJ (1988) it can be stated that the distribution of the heads of sugar beet roots relative to the surface of the soil is described in most cases by the normal law, only in rare cases by lognormal law and Erlang law. The results of the study of morphological structures of roots of sugar beet are presented in scientific papers. POGORELIJ L., TATJANKO (2004); ZUEV (1971) in their research has obtained the values of size and weight characteristics of roots and leaves of the sugar beet. They had obtained also the correlation relations between the diameter of the sugar beet root and height of the root top over the soil surface. The research of the physical and mechanical properties of the sugar beet roots and leaves is presented in the scientific papers BULGAKOV (2005); POGORELIJ L., TATJANKO (2004) and there are evident the variability of the mechanical and technological characteristics, such as: bulk density, specific resistivity coefficient, specific cutting resistivity. MARTINENKO (1997) investigated the characteristics of tensile strength, compression strength and bending strength. It was found that the hardness of the sugar beet leaves and roots, in relation to the depth of penetration of the conical indenter, is different in 2 – 3 times. Anyway, there are not mentioned the zones where the hardness of the sugar beet leaves and roots were measured. The research provided by POGORELIJ M. (2001) had confirmed that the values of hardness of the heads of sugar beet root significantly vary in different points of measuring. The strength of the top the sugar beet root head is lower when compared with other zones. Investigation of the other physical properties, during the process of the leaves separation, and also study of the given process is presented in the scientific papers VISKHOM (1970); KHELEMENDIK (1996); CARENCO ET AL. (2000); ROLLER (2010); MERKES (2001), KOPF (2010). Based on the results obtained it can be stated, that due to the biological specifics of the plants, strength properties in different zones of the sugar beet root and leaves can significantly vary. It is important to provide additional comparative research: to analyze a mechanical structure of the sugar beet root heads and leaves, to compare the strength in different zones of the heads and leaves stalks. It is also very important to formulate conclusions regarding potential possibilities of the separation sugar beet tops by dynamic interactions.

Main aim of the research was to determine the optimal way of the mechanical action on the sugar beet leaves in order to increase the quality of its separation from the root crops.

MATERIALS AND METHODS

During our research our attention was focused on the structure, shape and strength of the different zones on the sugar beet root head and leaves with the aim to study the possibilities of the mechanical destruction of the leaves and their subsequent separation from the root head. The spatial structure of the leaves stalks was investigated by imposing on them cross-sections of the grid (Fig. 1) and the definition of geometric cross-section dimensions and its area. Combining on a certain distance all the sections there have been derived 3D model of a single stalk, which allowed to determine by calculation its mass-centering characteristic.

Studies of spatial distribution on the root head of the individual leaves stalks and the geometric shape of the head itself was carried out by the photos at different times of the growing season (Fig. 6). Impact resistance and stress resistance were determined by application of mechanical shock and stress (Fig. 5).

The experiment was based on laboratory device in order to determine the effect of the convexity of the head of root crops on the process of purification from the leaves residues. To do this, on a place of the root there was consolidated a cylindrical wooden model by setting the cylinder axis parallel to the axis of rotation of the rotor. With multiple camera there was filmed the action of the blade rubber on the model.

It was determined the hardness of the head of root crop in different areas of the placing of green leaves and hardness of the leaves stalks at the surface and in the inner part at different distances from the head. The hardness of the inner part was determined in a direction perpendicular to the cross-sectional plane.

Before hardness measurement of root crop head the stalks were removed a knife prior to disappearance of borders between their bases. Hardness characteristic in this case was considered as an amount of deformation of the spring hardness tester in millimetres at which the indenter penetration occurred into the body of the leaves or head of root. The spring rate was regulated by its previous compression. In order to compare the hardness of the leaves and head of root the pre-compression of the spring was the same in both cases.

RESULTS AND DISCUSSION

Stalks of the leaves significantly change the shape of their cross-section, depending on a distance from the top of the head of root (Fig. 1). Especially intensive there is changed shape in the distance of 0 – 20 mm from the surface of the head, it turns sharply from the vane segment to hexagon shape, one corner of which is directed into the apex section. The biologists use to call such cross-sectional shape of the stalk as a dissected. The cross section of the stalk in the form of a hexagon form further retained throughout a leaf lamina. This form of leaf stalk gives it the rigidity to maintain a massive leaf.

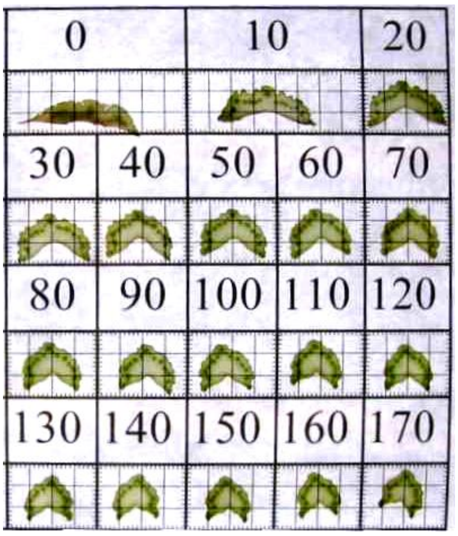

Fig. 1. – The shape of the cross section of the sugar beet leaf stalk

During research we have focused our attention to the area of the cross section of the different leaf stalks from the top part, centre part and down part of the root head (Fig. 2).

At the head of the root, the cross-sectional area of the external (outer) stalks is maximal. They do not set on other stalks. Biologically it leads to an increase of the sectional area and stiffness which is needed to hold the leaf blade. Sectional area of the base of the central rows is close to the outer cross-sectional area of the outer stalks. Much less is the area at the base of the internal (upper) stalks.

If the cross-sectional area of the stalks in the external and middle rows has the maximum value at the base and it is reducing to the direction of leaf blade, the section of the internal cuttings at a distance 0 – 20 mm from the ground is increasing and then decreases. According to the mechanical structure, the surface layer of the stalk is characterized by a large concentration of fibro-vascular tissues and it is strong enough (Fig. 3).

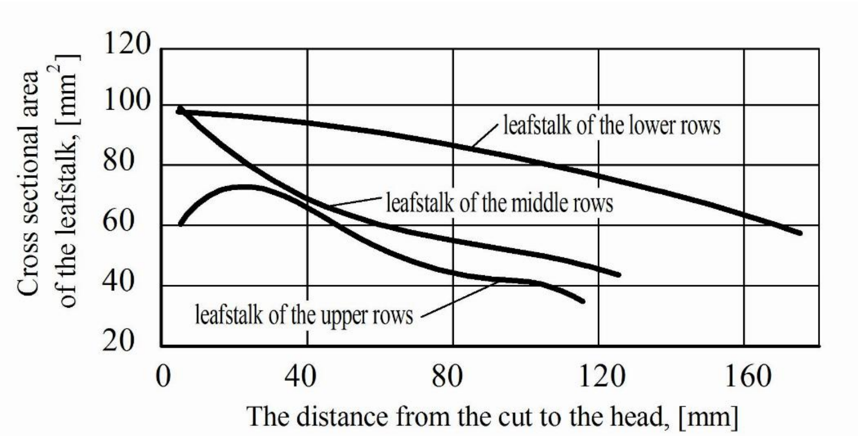

Fig. 2. – Effect of the distance from the root head cutting on the cross section area of the leaf stalk

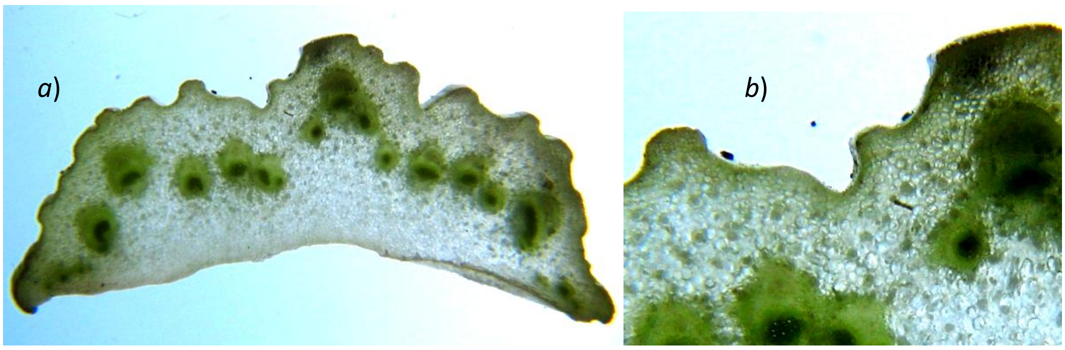

Fig. 3. – Cross-section of the leaf stalk and its mechanical structure

The inner layer is less durable, since the concentration of the mechanical tissues is much less. Thus, the stalk from the point of mechanical structure is anisotropic composite variable cross-section body, it can be characterized by different elastic modules in the longitudinal and transverse directions. At high turgor of the plant (the high osmotic pressure in the cells) significantly, it increases the stress state of the mechanical stiffness of the tissues and the strength of the stalk is necessary to keep the leaf blade. It is well-known that sheaf of sugar beet leaves has a form of cone, rosette and semi-rosette, Fig. 4.

Fig. 4. – The shape of the leaves sheaf at the base and typical stalks disruption

The form of the leaves on top of the root is largely dependent on a turgor, maturation period, fertilizing regime, and plants density on a field. Segment shape of the stalk at the surface of the head creates the preconditions for tight placement of stalks, creating a sufficiently dense and durable package that is difficult to completely destroy during a short-term effect of the cleaner of the heads of the sugar beet roots.

When removing from the head, due to the peculiarities of leaves shapes, the sprout becomes less dense and therefore easily destroyed. Under the influence of gravity force of the leaves the stalk is in the initial state of stress and due high turgor of the plant it becomes fragile and easily destroyed by minor efforts.

External stalks can be easily cracked almost at their base, and internal once at a distance of 10-20 mm from the head, due to the dense placing the stalks in the sprout (Fig. 4).

Often under the influence of the working body on the sprout tops, towards the centre of the root, it occurs quite effective shock damping by internal stalks. In this, outer stalks close to the base are destroyed, and subsequently, when approaching the centre of the sprout passes there occurs the combing only of the upper part (Fig. 5). Due to the conical structure of the root, with the approach to the centre, the length of the destruction and splitting of the stalks into the fibres, is reduced.

On the side of the root head, located opposite to the direction of rotation of the rotor shaft, stalks are not sufficiently destroyed, necessitating the use of two treatment counter-rotating shafts. Root crops with the small head height above ground or in which heads are placed below a soil surface are especially badly cleaned.

Fig. 5. **–** The view of the head of a sugar beet root with low extend from the soil after cleaning

The shape of the head of root varies during the growing season from spherically flattened at the beginning of the growing season to the spherical at the beginning of autumn and convex cone-shaped at the end of the growing season for the period of harvesting of the crops (Fig. 6). The development of this form of the head depends upon the biological characteristics of crop - the head of the sugar beet root can be considered as a modified stem.

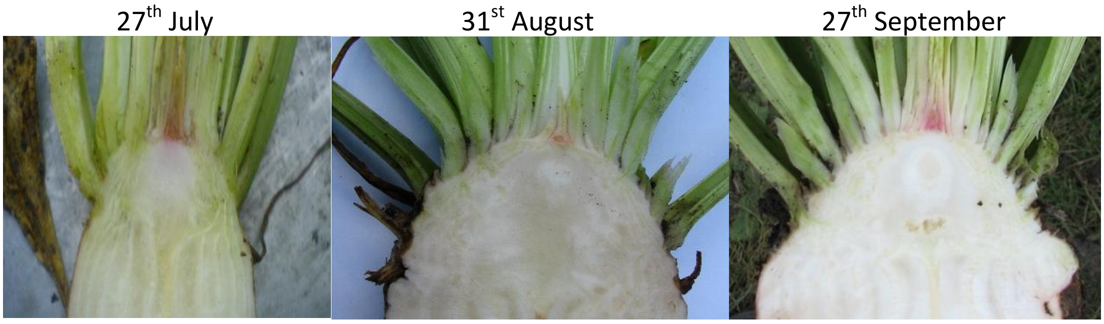

Fig. 6. – The shapes of the heads of sugar beet root during growing season (beginning, middle, end of the growing season)

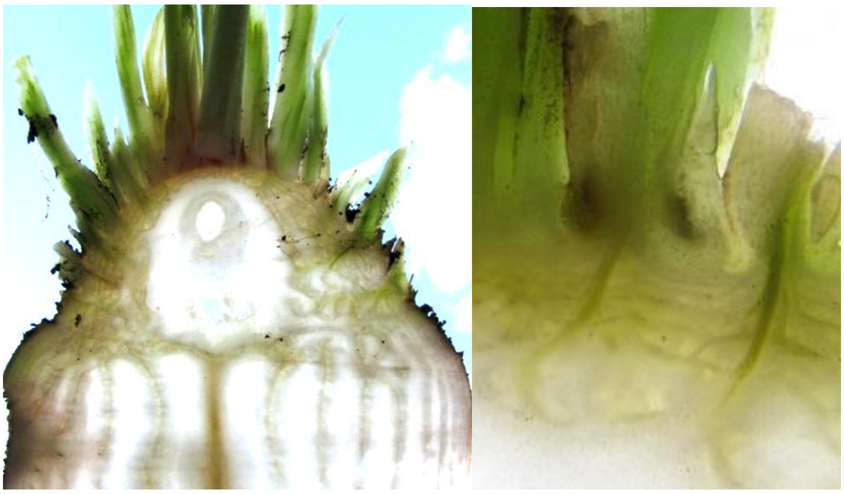

Fig. 7. – The morphological structure of the head of the sugar beet root

Individual heads may have a nearly spherical shape, flattened conical. However, their number in the total number of roots is small.

If we analyse the photo of the cross section of the head, it can be seen that the area of green leaves has a fibrous structure and relatively smoothly penetrates into the head (Fig. 7). Analyzing the morphological structure of the head, it is possible to conclude that perhaps there is a small difference in the strength of the stalks and heads in zone of their delineation. Due to the convex shape of the head of root the cleaning is very poor on the opposite side to the direction of rotation of the rotor cleaner.

On a trace of the action of the blade on the model it is clearly visible the spot on the part of the surface from the side of the rotation of the rotor. It is the evidence of the impossibility of the application of effective efforts to the head from the opposite side of the rotor rotation. In addition, this type of contact area indicates the absence of an effective working body sliding across the head and confirms that the normal load is applied to the head of sugar beet root.

The results of the determination of a hardness of the different zones of the head of the sugar beet root are shown on Fig. 8.

Hardness of the heads was measured both on the surface of the head in different zones, and in layers of these zones up to a depth of 15 mm. Maximum hardness of the head was measured in the area of green leaves in the layer at a depth of 5 – 10 mm, minimum hardness on top of the head in a layer of 0 – 5 mm.

Hardness zone of the sleeping cells was less than the hardness of the zone of green leaves, but the difference is negligible. The hardness of the top of head differs significantly from the other zones of hardness at a depth of 0 – 10 mm, and in a smaller extent – at a depth of 10 – 15 mm.

The hardness of the surface of the cuttings on the base is almost equal to the hardness of the top of head, and is 20 – 30% different from the hardness of the surface areas of green leaves and sleeping cells. However, at the depth 20 – 30 mm from the surface of the head, the hardness of the stalk surface is almost halved. With an increase of up to 30 – 40 mm distance from the surface, the hardness of the stalk head of root decreases and then increases. The hardness of the inner part of the stalks is significantly smaller than the hardness of all zones of the root head. During laboratory research of the process of separation of leaves residues it was observed a light separation of the sugar beet leaves at a distance of 20 – 30 mm from the surface of the sugar beet root. It is very difficult to separate, and sometimes not at all to separate the leaves at a distance of less than 10 mm. These quality indicators are easily explained by a slight difference in the hardness of leaves and root.

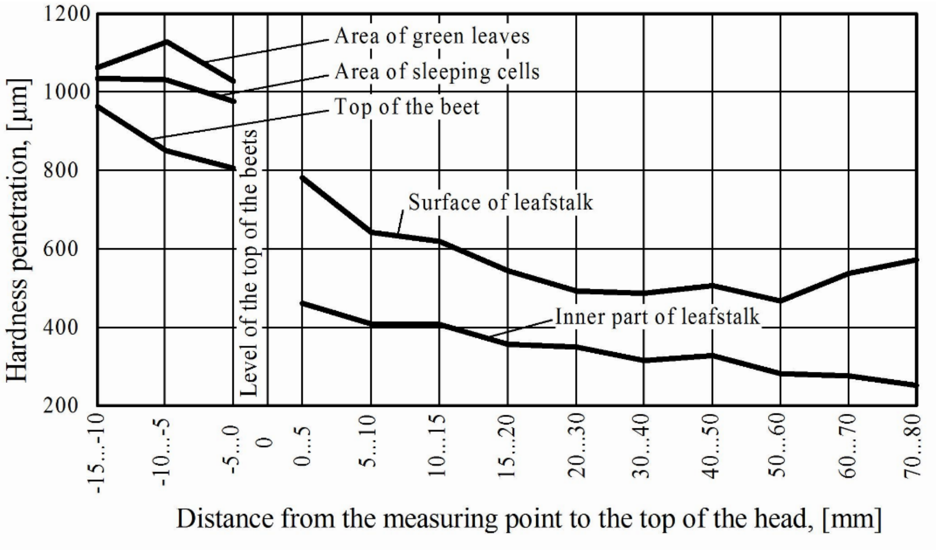

Fig. 8. – Hardness of the stalks and zones on the head of the sugar beet root

CONCLUSIONS

1. Results of the conducted research of physical-mechanical and agrophysical properties of the head and leaves of the sugar beet root allowed to receive their new properties which can be used for definition of an optimum way of mechanical impact on a sugar beet tops for improvement of its separation quality.
2. As a result of the conducted experimental research by determination of hardness of the leaves at the head of the root and hardness of the head in the areas of green leaves and sleeping cells, and also to the hardness of top of head of the sugar beet it is defined that head hardness on 30 - 40% are higher, than root crop hardness.
3. Repeated measurements confirm that the leafstalk considerably changes the form and the cross-sectional area depending on the distance to the head top. Thus in a zone of mechanical separation of leafstalks from a head of the sugar beet root during harvesting it has the greatest cross-sectional area and the most elongated form.
4. The results of multiple measurements cross-sectional area of the upper, middle and lower rows of the stalks allowed to find that the sugar beet stalk is anisotropic composite variable cross-sectional body. It can be characterized by different elastic modules in the longitudinal and transverse directions.
5. The typical form of the sheaf of sugar beet leaves was studied. The shape and morphological structure of the sugar beet head in different periods of vegetation were considered as well.
6. A number of repeated measurements of hardness of stalks and areas of root head enabled to define new dependences of their hardness on the location upon the head of sugar beet root. The received data indicate that the maximum hardness of the head appeared in the area of green leaves in the layer at 5 – 10 mm depth. Minimum hardness was on top of the head in a 0 – 5 mm layer. The hardness of the stalks surface at the base is almost equal to the hardness of the top of head, and is 20 – 30 % different comparing with the hardness of the surface areas of green leaves and sleeping cells.
7. Set of the received physical-mechanical and agrophysical properties of the head and leaves of the sugar beet root allowed to establish that the separation of the sugar beet leaves takes place most easily at a distance of 20 – 30 mm from the surface of the sugar beet root.

REFERENCES

1. BULGAKOV, V.M.: Theory of beet harvesting machinery (In Russian language), Kiev, Ukraine, Izdatelskij centr NAU 2005.
2. CARENKO, O.M. – JACUN, S.S. ET AL.: Mechanical and technological properties of agricultural materials: practicum (In Russian language), Kiev, Ukraine, Agrarnoe obrazovanie 2000.
3. KHELEMENDIK, N.M.: Increasing the mechanical-technological efficiency of labor-intensive processes in the sugar beet production (In Russian language) [Ph.D. thesis.], TPI, Ternopol, Ukraine, 1996, 48 p.
4. MARTINENKO, V.JA.: Machines for harvest the beet tops (In Russian language), Ternopol, Ukraine, Polygrafist 1997.
5. MERKES R.: 50 Jahre Prodaktionstechnik im Zuckerrübenbau in Deutchland. J. Zuckerrübe №4., 2001: 214–217.
6. POGORELIJ, M.L.: Increasing the technological efficiency of machines for harvest beets (In Russian language) [Ph.D. thesis.], NAU, Kiev, Ukraine, 2001, 21 p.
7. POGORELIJ, L.V. – TATJANKO N.V.: Machines for harvest beets: history, design theory, forecast (In Russian language), Kiev, Ukraine, Feniks 2004.
8. ROLLER O.: Entblatten statt Köpfen. J. Zuckerrüben № 2., 2010: 14–15.
9. TOPOROVSKIJ, S.A.: Substantiation process and basic parameters of the working body for cleaning the tops of sugar beet without copying heads of root crops (In Russian language) [Ph.D. thesis.], USKhA, Kiev, USSR, 1988, 19 p.
10. VASILENKO, P.M. – POGORELIJ L.V.: Basics of scientific research (Mechanization of agricultural production) (In Russian language), Kiev, USSR, Vysshaja shkola 1984.
11. VISKHOM.: Physical and mechanical properties of plants, soils and fertilizers: research methods, equipment, specifications (In Russian language), Moscow, USSR, Kolos 1970.
12. VOVK, P.F.: Agrophysical properties of sugar beet roots in connection with the mechanization of harvesting. In: Theory, design and manufacture of agricultural machinery: collection of scientific papers. Tome II (In Russian language). pp. 269-284. Moscow, USSR, Selkhozgiz 1936.
13. ZUEV, N.M.: Research of quality of sugar beet harvesters, depending on the agrophysical properties of sugar beet at different ways of forming of planting of plants (In Russian language) [Ph.D. thesis.], Kharkov, USSR, 1971, 33 p.

Corresponding author:
prof. Volodymyr Bulgakov, DrSc.,National University of Life and Environmental Sciences of Ukraine

THEORETICAL INVESTIGATIONS OF MINERAL FERTILISER DISTRIBUTION BY MEANS OF AN INCLINED CENTRIFUGAL TOOL

V. Bulgakov[1], O. Adamchuk[2], S. Ivanovs[3]

[1]*National University of Life and Environmental Sciences of Ukraine*
[2]*National Scientific Centre of Ukraine "Institute for Agricultural Engineering"*
[3]*Latvia University of Agriculture*

Abstract

At present a great part of mineral fertilisers is introduced by means of machines equipped with centrifugal spreading tools. One of possible solutions of their improvement towards uniform fertiliser distribution around the surface of the field is the use of centrifugal spreading tools with their axes of rotation being inclined at an angle to the horizontal plane. Theoretical investigations have been conducted and a new equation obtained describing the movement of a material particle of a fertiliser along the blade of the centrifugal tool, taking into account the inclination angle of the spreading disk; and its solution is given in a closed form. The research was carried out with the use of the methods of theoretical mechanics and numerical estimations on the PC. Theoretical dependencies have been determined in order to find out absolute velocity of the particles of fertilisers at the moment they leave the spreading disk. The use of the revealed dependencies and their subsequent numerical solution on the PC provided a possibility to establish the impact of the design and kinematic parameters, the operational conditions of the inclined centrifugal distributor, particularly, the value of absolute velocity of the fertiliser particles leaving the distributor disk and their acceleration angle.

Key words: differential fertiliser, centrifugal spreading, absolute velocity.

INTRODUCTION

The production efficiency of various agricultural crops depends to a considerable degree on the application of mineral fertilisers, most often introduced on the field by the surface method – spreading them using machines equipped with centrifugal spreading tools, were described by BIOCCA (2013). The use of these machines has indisputable advantages over the other similar machines. Yet they need further improvement, which concerns, first of all, the uniformity of fertiliser distribution around the surface of the field and depends on the design and kinematic parameters of their operating tools.

It is well-known that the working width of the machine for the application of mineral fertilisers by a centrifugal method depends on the value of absolute velocity V_{AC} of fertilisers leaving the surface of its spreading tool and angle α_{AC} between the vector of the latter and the horizontal plane. Value V_{AC} depends on the geometric parameters and the kinematic conditions of the operation of the centrifugal spreading tool, as well as on physical and mechanical properties of mineral fertilisers.

As a result of earlier conducted investigations, optimisation of the geometric parameters of the centrifugal spreading tool was carried out, taking into account the physical and mechanical properties of mineral fertilisers, were described by ADAMCHUK (2004). Besides, it was established that increase in the kinematic conditions of the operation of the centrifugal spreading tool is limited by the strength of the granules of the fertilisers. Therefore, when using the common construction materials and kinds of fertilisers, the possibility to increase the working width of the machines by increasing velocity V_{AC} is exhausted.

In order to optimise the centrifugal spreading tool with an inclined axis of rotation, it is necessary to have a methodology which would ensure determination of absolute velocity of fertilisers leaving its surface and the angle between the vector of the latter and the horizontal plane depending on the parameters and conditions of operation of the centrifugal spreading tool, as well as the physical and mechanical properties of mineral fertilisers. It is known that an increase in the distribution width of mineral fertilisers using the centrifugal spreading tool is possible by reaching rational values of angle α_{AC}, were described by ADAMCHUK (2005). The obtained results of research witness that the rational values of angle α_{AC} are situated within the limits $30^{o}…35^{o}$. At the same time it was established that the existing centrifugal spreading tools can reach the values of angle α_{AC} not higher than 15.7°, were described by ADAMCHUK (2002). The centrifugal spreading tools with an inclined axis of rotation ensure higher optimal values of angle α_{AC}, were described by ADAMCHUK (2005). The familiar methodologies by using of which one can determine absolute velocity of a fertiliser particle leaving the centrifugal spreading tool with a vertical axis of rotation, were described by ADAMCHUK (2010) and the methodology which allows determination of absolute velocity of a fertiliser particle leaving the centrifugal spreading tool with a horizontal axis of rotation, were described by VASILENKO (1960, 1996), BULGAKOV (2014) do not consider determination of absolute velocity of a fertiliser particle leaving the centrifugal spreading tool with an inclined axis of rotation to the horizontal plane.

The aim of the investigation is to obtain new analytical dependencies in order to discover the impact of the design and kinematic parameters and modes of operation of an inclined centrifugal distributor of mineral fertilisers, particularly, the value of absolute velocity of the fertiliser particles leaving the distributor disk, as well as their acceleration angle.

MATERIALS AND METHODS

The design of the centrifugal spreading tool developed by us with an inclined axis of rotation comprises a flat disk which has blades radially installed on its working surface and is cinematically joined with the drive unit of rotary movement. Besides, the axis of rotation of the centrifugal spreading tool is arranged at an angle α to the horizontal plane.

For such a centrifugal distributor of mineral fertilisers we will build an estimated mathematical model of the movement of a material particle along its radially installed blade so that the axis of rotation of the spreading tool has an inclination. For this purpose, first of all, we will compose an equivalent scheme in which we will show the material particle moving along the blade of the inclined spreading disk, and we will show the forces acting upon it (Fig. 1). There: M – the initial position of the fertiliser particle on the blade, point S – the current position of the fertiliser particle on the blade, point O – the centre of rotation of the centrifugal spreading tool.

Further, to simplify the analytical solution of the present task, we make the following assumptions:

– the coefficient of friction of the fertiliser particles against the surface of the blade has a constant value;

– the character of the movement of each fertiliser particle is the same, and it corresponds to the character of the movement of the entire mass of fertilisers along the blade;

– the fertiliser particle is moving along a section of the blade which is common for the vertical wall of the blade and its bottom, without a rolling motion;

– the thickness of the blade and the diameter of the fertiliser particle are neglected.

An essential difference of dispersion of the particles of mineral fertilisers using the centrifugal spreading tool with an inclined axis of rotation, in contrast to the horizontal one, is that here there are basic differences in the position of vectors of forces applied to the material particle depending on at which place of the inclined disk mineral fertilisers are supplied and gripped by the blades: at the upper part of the inclined disk or its lower part, at the right side of the axis of rotation or at its left side. This circumstance should also be considered in analytical solution of the present task.

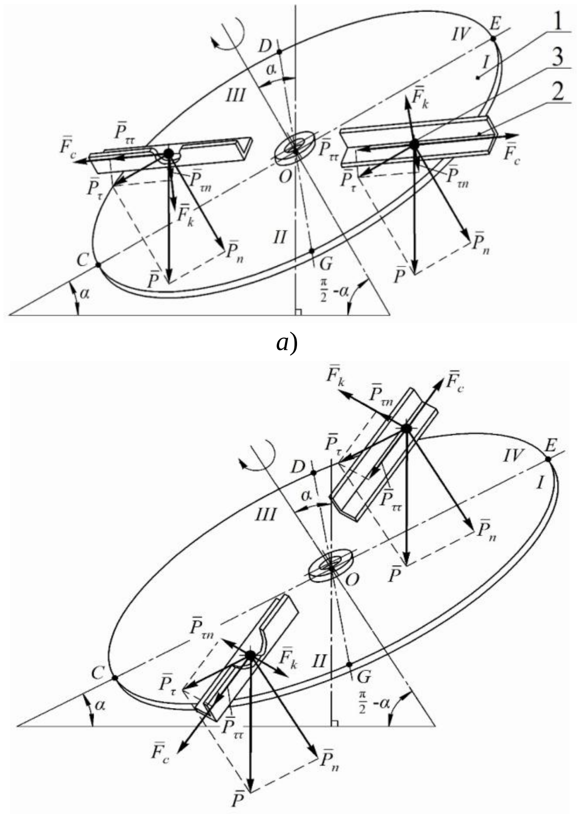

a)

b)

Fig. 1. – An equivalent scheme of the movement of a fertiliser particle along the blade of the spreading disk inclined at angle α to the horizon (*a*, *b* – respectively, a fertiliser particle is moving along the blade within the limits of sectors I, III and II, IV): 1 – the disk; 2 – the blade; 3 – a fertiliser particle

At first let us write an equation in order to determine absolute velocity V_{AC} of a fertiliser particle leaving the centrifugal spreading tool. It will be equal to:

$$V_{AC} = \sqrt{V_{rc}^2 + V_{NC}^2}\,, \tag{1}$$

where: V_{rc} – relative velocity of the movement of a fertiliser particle at the moment it leaves the surface of the centrifugal spreading tool m·s^{-1}; V_{NC} – transportation velocity of the movement of a fertiliser particle at the moment it leaves the surface of the centrifugal spreading tool m·s^{-1}.

In this case the transportation velocity V_{NC} of the movement of a fertiliser particle at the moment it leaves the surface of the centrifugal spreading tool can be determined by means of such a dependency:

$$V_{NC} = \omega R\,, \tag{2}$$

where ω – angular velocity of the centrifugal spreading tool, s^{-1}; R – the radius of the centrifugal spreading tool, m.

In order to determine V_{AC}, it is necessary, first of all, to have a dependency for the estimation of relative velocity V_{rc}. Due to the fact that the projection of the component of force $\bar{P}$ of weight of the fertiliser particle upon segment *AB* in the process of its movement along the blade changes the direction of the vector, it is purposeful to divide the centrifugal spreading tool into sectors in such a way that the direction of the vector in the process of its movement did not change within the limits of each sector. Fulfilling this, we obtain four mutually equal sectors: *EOG* – I; *GOC* – II; *COD* – III; *DOE* – IV (Fig. 2).

Segments *EC* and *DG* are mutually perpendicular diameters of the flat disk but segment *EC* forms angle α with the horizontal plane.

Let us determine the values of forces acting upon the fertiliser particle M and write an equation for the resultant force F_r under the impact of which this particle will move along the blade (Fig. 1, 2).

Since the movement of the material particle of the mineral fertiliser proceeds in a rectilinear direction along the surface of the blade, we will write this equation in the form of projections upon the axis which coincides with the surface of the blade itself:

$$F_r = F_c \pm P_{\tau\tau} - f_f F_k - f_f P_n - f_f P_{\tau n}\,, \tag{3}$$

where: f_f – the friction coefficient of the fertiliser particle M against the surface of the blade.

Let us determine the values of forces applied to particle M, which constitute expression (3).

The resultant force under the impact of which the fertiliser particle M is moving along the blade is defined as:

$$F_r = m\frac{d^2L}{dt^2}\,, \tag{4}$$

where: m – the mass of the fertiliser particle, kg; L – the path covered by the fertiliser particle moving along the blade, m; t – the time (duration) of the movement of the fertiliser particle along the blade, s.

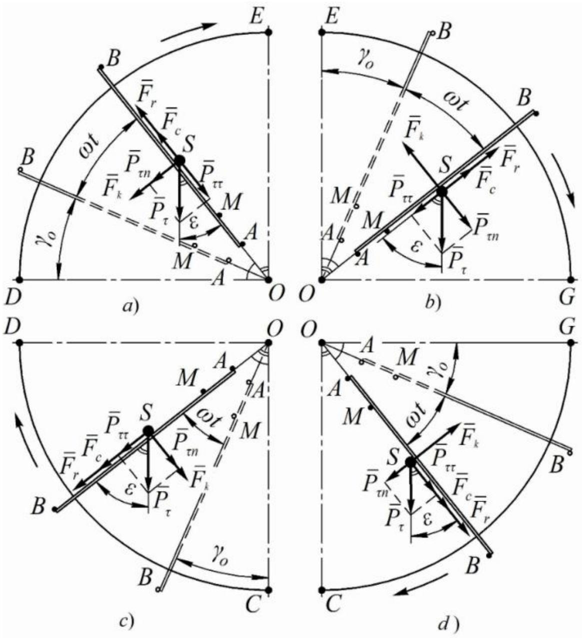

Fig. 2. – A scheme of the distribution of the resultant force under the impact of which the fertiliser particle is moving along the blade of the centrifugal spreading tool: *a*, *b*, *c*, *d* – respectively, the fertiliser particle is moving along the blade within the limits of sectors IV, I, III and II

The centrifugal force $\bar{F}_c$ of inertia is determined by means of the expression:

$$F_c = mr\omega^2\,, \tag{5}$$

where: r – the distance from the centre of rotation of the centrifugal spreading tool before the current position of the fertiliser particle on the blade, m; ω – angular velocity of the centrifugal spreading tool, s^{-1}.

The projection of the component of force $\bar{P}_\tau$ of the weight of the fertiliser particle upon segment *AB* is defined as:

$$P_{\tau\tau} = P_\tau \cos\varepsilon\,, \tag{6}$$

where: ε – the angle between the component of the force of weight $\bar{P}_\tau$ and its projection upon segment *AB*, rad.

The component of force $\bar{P}_\tau$ of the weight of the fertiliser particle acting along the surface of the disk, parallel to segment *EC*, will be defined by such an expression:

$$P_\tau = P\sin\alpha, \tag{7}$$

where: α – the angle between the axis of rotation of the centrifugal spreading tool and the vertical plane, rad.

Force $\bar{P}$ of the weight of the fertiliser particle will be equal to:

$$P = mg, \tag{8}$$

where: g – the free fall acceleration, m·s^{-2}.

The Coriolis force of inertia is defined by the expression:

$$F_k = 2m\omega\frac{dL}{dt}. \tag{9}$$

The component of the force of the weight of the fertiliser particle acting along the normal to the bottom of the blade has such an appearance:

$$P_n = P\cos\alpha. \tag{10}$$

The projection of the component of force P_τ of the weight of the fertiliser particle upon the normal to segment *AB* will be equal to:

$$P_{\tau n} = P_\tau \sin\varepsilon. \tag{11}$$

It should be remarked that in case the particles (the flow) of fertilisers come onto the surface of the centrifugal spreading tool within the limits of sector I or IV, then into expression (3) before force $P_{\tau\tau}$ one should put the sign “ – ”, if within the limits of sector II or III, then it is necessary to put the sign “ + ” before the symbol of this force.

By substituting the values of forces defined by expressions (4) – (11) into equation (3) we will obtain a differential equation of the movement of the fertiliser particle M along the blade of the centrifugal spreading tool, inclined at angle α to the horizon:

$$m\frac{d^2L}{dt^2} = mr\omega^2 \pm mg\sin\alpha\cdot\cos\varepsilon - f_f\left(2m\omega\frac{dL}{dt} + mg\cos\alpha + mg\sin\alpha\cdot\sin\varepsilon\right) \tag{12}$$

As it follows from Fig. 2, depending on the sector in which fertilisers are supplied onto the surface of the centrifugal spreading tool, the values of angle ε between the component of the vector of the force of weight $\bar{P}_\tau$ and its projection onto segment *AB* will be different, and the values of this angle are defined by such four expressions:

$\varepsilon = \gamma_o + \omega t$ – for the case when fertilisers come onto the surface of the centrifugal spreading tool within the limits of sector I,

where: γ_o – the angle formed by segments *OE* and *OB* at the contact moment of the fertiliser particle with the blade, rad;

$\varepsilon = \frac{\pi}{2} - (\gamma_o + \omega t)$ – for the case when fertilisers come onto the surface of the centrifugal spreading tool within the limits of sector II,

where: γ_o – the angle formed by segments *OG* and *OB* at the contact moment of the fertiliser particle with the blade, rad;

$\varepsilon = \gamma_o + \omega t$ – for the case when fertilisers come onto the surface of the centrifugal spreading tool within the limits of sector III,

where: γ_o – the angle formed by segments *OC* and *OB* at the contact moment of the fertiliser particle with the blade, rad;

$\varepsilon = \frac{\pi}{2} - (\gamma_o + \omega t)$ – for the case when fertilisers come onto the surface of the centrifugal spreading tool within the limits of sector IV,

where: γ_o – the angle formed by segments *OD* and *OB* at the contact moment of the fertiliser particle with the blade, rad.

Further we will write an equation for distance r from the centre of rotation of the centrifugal spreading tool to the current position of the fertiliser particle S on the blade. It is defined by means of the expression:

$$r = r_o + L, \tag{13}$$

where: r_o – the radius of the supply of the fertiliser particle onto the centrifugal spreading tool, m.

By substituting into expression (12) the value of distance r and making a series of transformations we will obtain:

$$\frac{d^2L}{dt^2} = \omega^2 r_o + \omega^2 L \pm g\sin\alpha\cdot\cos\varepsilon - 2f_f\omega\frac{dL}{dt} - f_f g\cos\alpha - f_f g\sin\alpha\cdot\sin\varepsilon. \tag{14}$$

Let us consider a case when the fertilisers are supplied onto the surface of the centrifugal spreading tool within the limits of sector II (*GOC*). Then equation (14) will have the appearance:

$$\frac{d^2L}{dt^2}+2f_f\omega\frac{dL}{dt}-\omega^2L=\left(\omega^2r_o-f_fg\cos\alpha\right)+$$
$$+g\sin\alpha\cdot\sin\left(\gamma_o+\omega t\right)-f_fg\sin\alpha\cdot\cos\left(\gamma_o+\omega t\right).\quad(15)$$

In such a way a linear differential equation of the second order is obtained with constant coefficients and the right-side part.

Let us solve the obtained differential equation (15). Its characteristic equation will look like this:

$$\lambda^2+2f_f\omega\lambda-\omega^2=0,\quad(16)$$

but its roots will correspondingly be equal:

$$\lambda_1=\omega\left(\sqrt{f_f^2+1}-f_f\right),\quad \lambda_2=\omega\left(-\sqrt{f_f^2+1}-f_f\right).\quad(17)$$

Let us write a general solution $\bar{L}$ of equation (15) without the right side:

$$\bar{L}=C_1e^{\lambda_1t}+C_2e^{\lambda_2t},\quad(18)$$

where: C_1 and C_2 – arbitrary constants.

Further we will find a specific solution L^* of equation (15).

Let us introduce the following designations:

$$\omega^2r_o-f_fg\cos\alpha=K,\quad g\sin\alpha=U.\quad(19)$$

Then, taking into account the accepted designations, the right side of the differential equation (15) will have such an appearance:

$$K+U\sin\left(\gamma_o+\omega t\right)-f_fU\cos\left(\gamma_o+\omega t\right)\quad(20)$$

In this case we will look for the specific solution of the heterogeneous equation in the following way:

$$L^*=W\sin\left(\gamma_o+\omega t\right)+Z\cos\left(\gamma_o+\omega t\right)+J\quad(21)$$

where: W, Z and J – the unknown coefficients.

These unknown coefficients are defined using the method of indefinite coefficients. For this, we will twice differentiate the specific solution (21). We have:

$$\frac{dL^*}{dt}=\omega W\cos\left(\gamma_o+\omega t\right)-\omega Z\sin\left(\gamma_o+\omega t\right)\quad(22)$$

$$\frac{d^2L^*}{d^2t}=-\omega^2W\sin\left(\gamma_o+\omega t\right)-\omega^2Z\cos\left(\gamma_o+\omega t\right)\quad(23)$$

Let us substitute the obtained expressions (22) and (23) into equation (15). We will have:

$$-\omega^2W\sin\left(\gamma_o+\omega t\right)-\omega^2Z\cos\left(\gamma_o+\omega t\right)+$$
$$+2f_f\omega\left[\omega W\cos\left(\gamma_o+\omega t\right)-\omega Z\sin\left(\gamma_o+\omega t\right)\right]-$$
$$-\omega^2\left[W\sin\left(\gamma_o+\omega t\right)+Z\cos\left(\gamma_o+\omega t\right)+J\right]=$$
$$=K+U\sin\left(\gamma_o+\omega t\right)-f_fU\cos\left(\gamma_o+\omega t\right).\quad(24)$$

Performing the necessary transformations of expression (24), we will obtain:

$$-\omega^2W\sin\left(\gamma_o+\omega t\right)-\omega^2Z\cos\left(\gamma_o+\omega t\right)+$$
$$+2f_f\omega^2W\cos\left(\gamma_o+\omega t\right)-2f_f\omega^2Z\sin\left(\gamma_o+\omega t\right)-$$
$$-\omega^2W\sin\left(\gamma_o+\omega t\right)-\omega^2Z\cos\left(\gamma_o+\omega t\right)-\omega^2J=$$
$$=K+U\sin\left(\gamma_o+\omega t\right)-f_fU\cos\left(\gamma_o+\omega t\right).\quad(25)$$

Further we equate the coefficients at the corresponding trigonometric functions. We have:

$$\left.\begin{aligned}&-\omega^2W-2f_f\omega^2Z-\omega^2W=U,\\&-\omega^2Z+2f_f\omega^2W-\omega^2Z=-f_fU,\\&-\omega^2J=K,\end{aligned}\right\}\quad(26)$$

or

$$\left.\begin{aligned}&-2\omega^2W-2f_f\omega^2Z=U,\\&-2\omega^2Z+2f_f\omega^2W=-f_fU,\\&-\omega^2J=K.\end{aligned}\right\}\quad(27)$$

From the obtained system of linear equations (27) in relation to unknowns R, S and T we find the values of these unknown coefficients:

$$J=-\frac{K}{\omega^2},\quad Z=0,\quad W=-\frac{U}{2\omega^2}.\quad(28)$$

Substituting the values of the obtained coefficients (28) into expression (21), we obtain a specific solution of the heterogeneous differential equation:

$$L^*=-\frac{U}{2\omega^2}\sin\left(\gamma_o+\omega t\right)-\frac{K}{\omega^2}.\quad(29)$$

The general solution of the differential equation (15) can be written like this:

$$L=\bar{L}+L^*=C_1e^{\lambda_1t}+C_2e^{\lambda_2t}-\frac{U}{2\omega^2}\sin\left(\gamma_o+\omega t\right)-\frac{K}{\omega^2}.\quad(30)$$

The arbitrary constants C_1 and C_2 are found from the following initial conditions:

at $t=0$: $L=0$, $\frac{dL}{dt}=0$.

For this, we differentiate by t expression (30). We will have:

$$\frac{dL}{dt} = \lambda_1 C_1 e^{\lambda_1 t} + \lambda_2 C_2 e^{\lambda_2 t} - \frac{U}{2\omega}\cos(\gamma_o + \omega t) \quad (31)$$

Using the presented initial conditions, we obtain the following system of algebraic equations in relation to unknowns C_1 and C_2:

$$\left.\begin{aligned} &C_1 + C_2 - \frac{U}{2\omega^2}\sin\gamma_o - \frac{K}{\omega^2} = 0, \\ &\lambda_1 C_1 + \lambda_2 C_2 - \frac{U}{2\omega}\cos\gamma_o = 0. \end{aligned}\right\} \quad (32)$$

By solving the system of equations (32) we find the values of the arbitrary constants C_1, C_2:

$$C_1 = \frac{U\cos\gamma_o}{2\omega(\lambda_1 - \lambda_2)} - \frac{U\lambda_2 \sin\gamma_o}{2\omega^2(\lambda_1 - \lambda_2)} - \frac{K\lambda_2}{\omega^2(\lambda_1 - \lambda_2)} \quad (33)$$

And

$$C_2 = -\frac{U\cos\gamma_o}{2\omega(\lambda_1 - \lambda_2)} + \frac{U\lambda_2 \sin\gamma_o}{2\omega^2(\lambda_1 - \lambda_2)} + \frac{K\lambda_2}{\omega^2(\lambda_1 - \lambda_2)} + \frac{U\sin\gamma_o}{2\omega^2} + \frac{K}{\omega^2} \quad (34)$$

RESULTS AND DISCUSSION

In order to arrive at a final solution of the differential equation (15) and to establish the rule of the movement of a fertiliser particle along the blade of the centrifugal spreading tool, inclined at α to the horizon (35), we substitute the obtained values (33) and (34) of the arbitrary constants C_1 and C_2 into expression (30):

$$\begin{aligned} L = &\left[\frac{U\cos\gamma_o}{2\omega(\lambda_1 - \lambda_2)} - \frac{U\lambda_2 \sin\gamma_o}{2\omega^2(\lambda_1 - \lambda_2)} - \frac{K\lambda_2}{\omega^2(\lambda_1 - \lambda_2)}\right] e^{\lambda_1 t} + \\ &+ \left[-\frac{U\cos\gamma_o}{2\omega(\lambda_1 - \lambda_2)} + \frac{U\lambda_2 \sin\gamma_o}{2\omega^2(\lambda_1 - \lambda_2)} + \frac{K\lambda_2}{\omega^2(\lambda_1 - \lambda_2)} + \right. \\ &\left. + \frac{U\sin\gamma_o}{2\omega^2} + \frac{K}{\omega^2}\right] e^{\lambda_2 t} - \frac{U\sin(\gamma_o + \omega t)}{2\omega^2} - \frac{K}{\omega^2}. \end{aligned} \quad (35)$$

After substitution of expressions (33) and (34) into expression (31), we obtain the rule about the change of velocity V_r in relation to the movement of the fertiliser particle along the blade at an arbitrary moment of time t:

$$\begin{aligned} V_r = \frac{dL}{dt} = &\left[\frac{U\cos\gamma_o}{2\omega(\lambda_1 - \lambda_2)} - \frac{U\lambda_2 \sin\gamma_o}{2\omega^2(\lambda_1 - \lambda_2)} - \frac{K\lambda_2}{\omega^2(\lambda_1 - \lambda_2)}\right] \lambda_1 e^{\lambda_1 t} + \\ &+ \left[-\frac{U\cos\gamma_o}{2\omega(\lambda_1 - \lambda_2)} + \frac{U\lambda_2 \sin\gamma_o}{2\omega^2(\lambda_1 - \lambda_2)} + \frac{K\lambda_2}{\omega^2(\lambda_1 - \lambda_2)} + \right. \\ &\left. + \frac{U\sin\gamma_o}{2\omega^2} + \frac{K}{\omega^2}\right] \lambda_2 e^{\lambda_2 t} - \frac{U}{2\omega}\cos(\gamma_o + \omega t). \end{aligned} \quad (36)$$

In order to determine the time t_1 of the movement of a fertiliser particle along the blade from the point of its supply (point M) to the point of its leaving the blade (point B), it is necessary to replace L in expression (35) by its value $L = R - r_o$, which determines the distance between points M and B, and to solve the obtained equation in relation to time t_1. By substituting the obtained value of time t_1 into equation (36), we obtain value V_{rc} of the relative velocity of the movement of the fertiliser particle at the moment when it leaves the surface of the spreading disk.

In such a way, taking into account expression (1), we have a possibility to determine the value of absolute velocity V_{AC} at the moment it leaves the surface of the spreading disk, when fertilisers are supplied onto the surface of the disk within the limits of sector II (*GOC*).

Using the obtained analytical expressions, in accordance with the worked out programme, numerical estimations were performed on the PC, which provided a possibility to determine the impact of ω, r_o and α upon V_{AC}.

It has been established that increase in the value of α from 0° to 90° leads to the change of V_{AC} not more than by 0.1 m·s^{-1}. The impact of ω and r_o upon V_{AC} is presented in Fig. 3.

As it is evident from the graphs in Fig. 3, at ω = 104.6 s^{-1} increase of r_o from 0.1 m to 0.3 m leads to a decrease of V_{AC} from 41.32 m·s^{-1} to 38.21 m·s^{-1}. Besides, increasing ω from 26.2 s^{-1} to 104.6 s^{-1} at r_o = 0.1 m results in the increase of V_{AC} from 10.33 m·s^{-1} to 41.32 m·s^{-1}.

The choice of the sector for the supply of fertilisers onto the spreading disk affects but little the value of V_{AC}. Thus, at R = 0.34 m, f_f = 0.55, $\alpha = 90^o$, r_o = 0.2 m, $\gamma_o = 1^o$, ω = 104.6 s^{-1} the values of V_{AC} will be the following: sector I – V_{AC} = 40.74 m·s^{-1}; sector II – V_{AC} = 40.78 m·s^{-1}; sector III – V_{AC} = 40.75 m·s^{-1}; sector IV – V_{AC} = 40.74 m·s^{-1}.

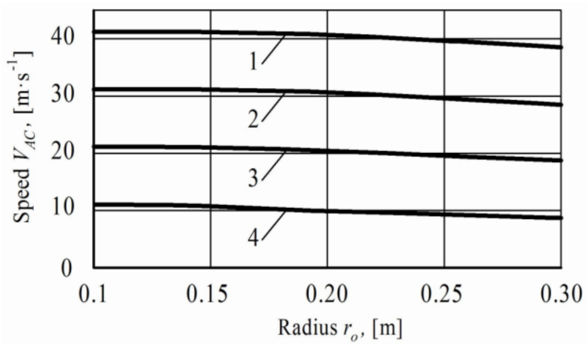

Fig. 3. – Dependence of absolute velocity V_{AC} of a fertiliser particle leaving the surface of the spreading disk on the radius r_o of its supply (fertilisers are supplied onto the surface of the disk in sector II at R = 0.34 m, f_f = 0.55, $\alpha = 30^o$, $\gamma_o = 1^o$):1 – ω = 104.6 s^{-1}; 2 – ω = 78.5 s^{-1}; 3 – ω = 52.3 s^{-1}; 4 – ω = 26.2 s^{-1}.

In order to determine the value of the angle at which fertilisers leave the spreading disk, at first it is necessary to find out the place of their leaving. Considering that the position of the blade at the moment of its contact with the fertiliser particle is known, it is expedient to use angle β_a of its acceleration in order to determine the place from which fertilisers leave the spreading disk. The angle of acceleration is an angle between the positions of the blade at the moment of its contact with the fertiliser particle and the same blade at the moment when fertilisers leave the disk. Let us write an equation to determine angle β_a:

$$\beta_a = \omega t \,. \tag{37}$$

Using expressions (35), (36) and equation (37) the impact of parameters ω, r_o and α upon β_a was studied. The obtained results are presented in Fig. 4 and 5.

On the basis of the graphs in Fig. 4 one can draw a conclusion that at high values of ω the impact of the inclination angle α of the axis of rotation of the spreading disk upon the acceleration angle β_a of the fertiliser particle is insignificant. Thus, at ω = 104.6 s^{-1} increasing α from 0° to 90° results in decreased values of β_a from 79.13° to 78.86°.

It has been established that increasing r_o from 0.1 m to 0.3 m leads to decreased values of β_a from 147.53° to 32.24°. Besides, the choice of the sector for the fertiliser supply onto the surface of the disk affects a little the value of angle β_a. Thus, at R = 0.34 m, f_f = 0.55, $\alpha = 90^o$, r_o = 0.2 m, $\gamma_o = 1^o$, ω = 104.6 s^{-1} the values of β_a will be: sector I – β_α = 79.16°; sector II – β_α = 78.86°; sector III – β_α = 79.09°; sector IV – β_α = 79.23°.

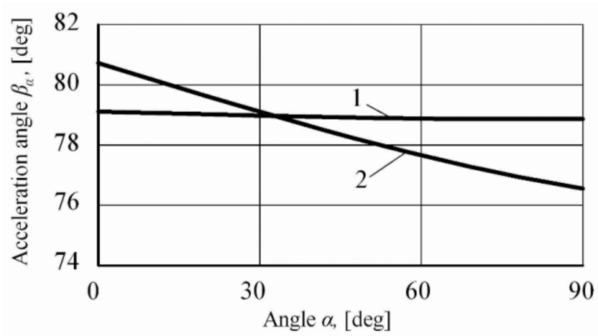

Fig. 4. – Dependence of the acceleration angle β_a of a fertiliser particle on angle α (fertilisers are supplied onto the surface of the disk in sector II, at R = 0.34 m, f_f = 0.55, r_o = 0.2 m, $\gamma_o = 1^o$): 1 – ω = 104.6 s^{-1}; 2 – ω = 26.2 s^{-1}.

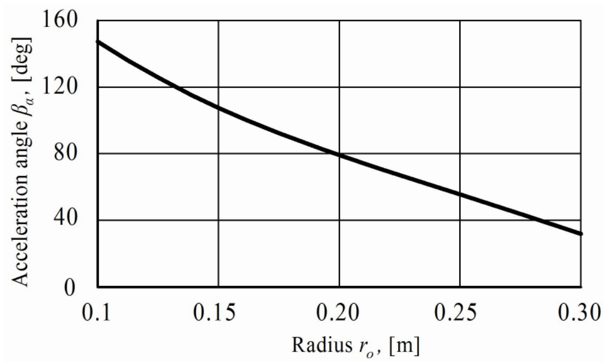

Fig. 5. – Dependence of the acceleration angle β_a of a fertiliser particle on radius r_o of its supply onto the disk (fertilisers are supplied onto the surface of the disk in sector II, R = 0.34 m, f_f = 0.55, ω = 104.6 s^{-1}, $\alpha = 30^o$, $\gamma_o = 1^o$).

The use of the revealed dependencies and the methodology for the determination of the angle at which the fertiliser particle leaves the surface of the spreading disk provides a possibility to obtain initial data for the estimation of the distribution distance of a fertiliser particle by the spreading disk. In its turn, determination of the distribution distance of the fertiliser particle from the centrifugal spreading tool makes it possible to substantiate other rational parameters and modes of operation of the centrifugal spreading tool.

CONCLUSIONS

1. New theoretical dependencies have been revealed which describe the movement of a particle of mineral fertilisers along the radially situated blade of the centrifugal spreading tool the axis of rotation of which is arranged at an angle to the horizontal plane.
2. The results of numerical estimations on the basis of the newly obtained formulae allow to evaluate the degree of impact of individual parameters of the inclined centrifugal spreading tool for the distribution of fertilisers by the value of absolute velocity of the particle leaving the disk and to obtain initial data for the estimation of the distribution distance of mineral fertilisers.

REFERENCES

1. BIOCCA, M. ET AL.: Aerodynamic properties of six organo-mineral fertiliser particles. In: Journal of Agricultural Engineering. No 44 (e83), 2013: pp. 411-414.
2. ADAMCHUK, V.: Impact of the parameters and modes of operation of the spreading tool upon its leaving by the mineral fertiliser particles. In: Herald of Agrarian Science. Kiev, No 12, 2004: pp. 42-45. (In Ukrainian).
3. ADAMCHUK, O.: Raising labour efficiency of the machine for the distribution of mineral fertilisers. In: Mechanisation and Electrification of Agriculture. Glevaha: “IMESH”, No 89, 2005: pp. 207-212. (In Ukrainian).
4. ADAMCHUK, V.: Substantiation of a model for the application of mineral fertilisers // Interdepartmental subject collection. In: Mechanisation and Electrification of Agriculture. Glevaha, “IMESH”, No 86, 2002: pp. 90-99. (In Ukrainian).
5. ADAMCHUK, V.: Theory of centrifugal tools for the distribution of mineral fertilisers. Kiev: Agrarian Science, 2010: pp. 89-117. (In Ukrainian).
6. VASILENKO, P.: Theory of the movement of a particle along rough surfaces of agricultural machines. Kiev: UASHN, 1960: 283 p. (In Russian).
7. VASILENKO, P.: Introduction into terramechanics. Kiev, Selhozobrazovaniye, 1996: 252 p. (In Russian).
8. BULGAKOV, V. ET AL.: Theory of motion of a material point along a plane curve with a constant pressure and velocity. Agronomy Research. Vol. 12. No 3, Estonian university of Life sciences. 2014: pp. 937-948.

Corresponding author:
Semjons Ivanovs, Latvia University of Agriculture, Latvia, e-mail: semjons@apollo.lv

APPLICATION OF ORGANIC AND INORGANIC AMENDMENTS ON SOIL PHYSICAL PROPERTIES OF A XEROFLUVENT SOIL

M. Çercioglu

Vocational College of Simav, Dumlupinar University, Kutahya, TURKEY

Abstract
The aim of this study was to investigate the impacts of application of different amendments as composted tobacco waste (CTW), poultry manure (PM), bio-humus (BH), zeolite (Z) and lime (L) on soil physical properties. This research was performed in the experimental fields of the Agriculture Faculty's research farm at Ege University in Menemen, Izmir, Turkey from 2009 to 2011. In this study, tobacco wastes gathered from the cigarette industry were composted and bio-humus (composted plant residuals), poultry manure were obtained from organic manure industry for this study. It has been analyzed that application of organic amendments (CTW, BH, PM) increased porosity, field capacity, available water content, wilting point, sturucture stability index between the rates of 14% and 26.4%; decreased bulk density, particle density of soil samples between 3.4% and 15.8% rates when compared with the variation of the control. The results show that these organic wastes were determined as the most effective amendments on soil physical properties.

Key words: bio-humus, lime, physical properties of soil, poultry manure, tobacco waste, zeolite.

INTRODUCTION

The addition of agricultural wastes with high OM content to soil is a current environmental and agricultural practice for maintaining soil OM, reclaiming degraded soils and supplying plant nutrients (AGGELIDES AND LONDRA, 2000). Tobacco waste material might be reused as an OM source in agriculture to improve soil quality. The measurable minimum data set needed to evaluate soil quality includes physical, chemical and biological properties such as texture, structural stability, organic matter (DORAN AND PARKIN, 1994). Direct use of tobacco waste could create an unfavorable soil environment; however, composting tobacco waste could accelerate the breakdown of nicotine and result in the production of a less toxic and more useful organic amendment (ADEDIRAN ET AL., 2004). A considerable increase in crop yields can also be achieved with lime application (HAYNES AND NAIDU, 1998). Zeolite is used as a soil conditioner in organic farming. It has been estimated that zeolite provides using fertilizers economically on soils which are sandy or have less organic matter content (ERTIFTIK, 1998).

In the present study, composted tobacco waste (CTW), bio-humus (BH), poultry manure (PM), lime (L) and zeolite (Z) combined with mineral fertilizer at different ratios were applied to soil and the influences of these amendments on some physical properties of a Xerofluvent soil were compared.

MATERIALS AND METHODS

Site and organic waste description

This research was performed in the experimental fields of the Agriculture Faculty's research farm at Ege University in Menemen region (Western Anatolia) of Izmir, Turkey between the years of 2009-2011. The experiment was arranged in a randomized block design with four replicates. The soil was a sandy loam, classified as a Xerofluvent with pH of 7.62. Organic matter (OM), total N and total soluble salt contents of soil were analyzed that 1.11 g kg^{-1}, 0.07 g kg^{-1} and 0.046 g kg^{-1}, respectively. In this study, tobacco wastes gathered from the cigarette industry were composted and bio-humus (composted plant residuals), chicken manure were obtained from organic manure industry for this study. Treatments were as follows: (1) 1 t ha^{-1} Z+NPK, (2) 4 t ha^{-1} PM+NPK, (3) 1 t ha^{-1} L+NPK, (4) 300 kg ha^{-1} NPK, (5) 50 t ha^{-1} CTW, (6) 10 t ha^{-1} BH+NPK and (7) control. During the research, soil samples were taken six times in three years. (I, 3 June 2009; II, 23 October 2009; III, 1 June 2010; IV, 5 November 2010; V, 13 July 2011; VI, 21 October 2011). Tab. 1 and Tab. 2 show that the composition of different soil amendments in the study.

Tab. 1. – The composition of composted tobacco waste (CTW); poultry manure (PM); bio-humus from composted plant residues (BH); zeolite (Z)

Material	OM (%)	C:N	pH	EC (ds m^{-1})
CTW	33.6	22.41	9.18	49.5
PM	44.9	25.84	8.60	54.5
Z	-	-	7.33	0.065
BH	46.5	29.35	7.88	9.20

Tab. 2. – Macro and micro element status of the amendments

Material	N (%)	P (ppm)	K (ppm)	Ca (ppm)	Mg (ppm)	Na (ppm)	Fe (ppm)	Cu (ppm)	Mn (ppm)	Zn (ppm)
CTW	0.87	2770	19486	74440	635	794.8	14500	119	442	124
PM	1.01	3470	21985	94424	12000	5663	2200	72.2	536.3	648.6
Z	0.01	0.378	11205	3454	80.86	3185	0.928	0.298	2.422	0.690
BH	0.92	2050	6995	117656	9200	993.5	12400	34.8	433.8	86.14

Soil sampling and analysis

During the research, soil samples were taken as disturbed and undisturbed (0-20 cm) from the center of each plot in planting and harvest periods. The samples were air-dried and sieved through 2 and 8 mm sieves. Particle-size distribution was determined according to BOUYOUCOS (1951). Bulk density was determined from undisturbed soil samples that were taken by using a steel cylinder of 100 cm^3 volume (BLACK, 1965). Porosity was determined according to DANİELSON ET AL., (1986). Field capacity, wilting point, and available water content were determined using disturbed soil samples sieved through a 2 mm-mesh utensil (U.S. SALINITY LABORATORY STAFF., 1954). Total salt, OM concentration, calcium carbonate and pH were all determined according to PAGE ET AL., (1982). Some characteristics of the soil are given in Tab. 3.

Statistical analysis

ANOVA and Duncan tests were performed according to 0.05 significance level ($p \leq 0.05$) and 95% confidence interval by using the statistical package, SPSS Statistics 19 (SPSS 19, 2010). The experimental design was performed three factors and mixed-level factorial randomized block as shown in Tab. 4.

Tab. 3. – Initial soil characteristics

Clay (%)	8.72
Silt (%)	36
Sand (%)	55.28
$CaCO_3$ (%)	4.70
BD (g cm^{-3})	1.46
PD (g cm^{-3})	2.65
PO (%)	50.66
FC (%)	17.77
WP (%)	10.26
AWC (%)	7.51

(BD: Bulk density PD: Particle density PO: Porosity FC: Field capacity WP: Wilting Point AWC: Available water content).

Tab. 4. – Mixed-level experimental design

Factor	Parameter	Level 1	Level 2	Level 3	Level 4	Level 5	Level 6	Level 7
A	Year	2009	2010	2011	-	-	-	-
B	Sampling	I	II	-	-	-	-	-
C	Treatment	1	2	3	4	5	6	7

(1) Zeolite at 1 t ha^{-1} + NPK, (2) poultry manure at 4 t ha^{-1} + NPK, (3) lime at 1 t ha^{-1} + NPK, (4) NPK at 300 kg ha^{-1}, (5) composted tobacco waste at 50 t ha^{-1}, (6) bio-humus at 10 t ha^{-1} + NPK and (7) control (Duncan test, $p \leq 0.05$).

RESULTS AND DISCUSSION

Changes in physical properties of soil samples

By the addition of amendments, physical properties of soil samples were analyzed statistically significant when compared with the control (Tab. 5, 6, 7). All the applications were ensured a significant ($p \leq 0.05$) decrease on bulk density compared to the control plots. The lowest bulk density was analyzed last year of the experiment by the treatment of PM as 1.05 g cm^{-3}. Maximum porosity values were found last year of the study by application of PM compared to the control plots. MBAGWU (1989), noted that organic wastes incorporated into the soil at the rate of 10% increased the total porosity by 23%. MARİNARİ ET AL. (2000), also found that total soil porosity increased with organic fertilizers and compost, depending on the amount of materials applied. The water holding capacity of soils at field capacity (FC), wilting point (WP) and available water content (AWC) were significantly ($p \leq 0.05$) effected by additions of organic wastes. Plots amended with bio-humus resulted in the highest values in FC each year of experiment. FC values varied as 21.89%, 21.65% and 20.29% in BH treated soil samples according to years respectively. The highest wilting point (WP) results of each year were analyzed in PM plots. By addition of PM, wilting point (WP) was determined as high as 11.50% in 2010 (Tab. 6). AWC values varied between 7.36% and 10.83%. Second year of experiment, the maximum AWC was determined in L treated soil samples (Tab. 6). AGGELIDES AND LONDRA (2000) determined that porosity and water-retention capacity of loamy and clay soils increased with application of compost. However, HAYNES AND NAIDU (1998) concluded that water content at both field capacity and wilting point was generally increased by additions of manure applications but available water content was not significantly changed.

All the treatments were determined statistically significant ($p \leq 0.05$) on structure stability of soil. The highest structure stability values of all years were analyzed that by PM treatment compared with the variation of the control (Tab. 5, 6, 7). Since there is a strong correlation between SSI and amounts of high organic matter (OM) in PM, BH and CTW, the application of these materials increased soil aggregation and SSI. Additionally, our findings were in agreement with findings of CHENU ET AL. (2000), PUGET ET AL. (2000), and TEJADA AND GONZALEZ (2003, 2004), who found that soil structure depended on the content and nature of the OM added.

Tab. 5. – Changes in physical properties of soil by application of amendments in 2009

Treatments (t ha^{-1})	BD (g cm^{-3})	PO (%)	FC (%)	WP (%)	AWC (%)	SSI (%)
1	1.24	50.38	21.22	10.09	11.13	17.55
2	1.23	50.41	21.67	11.21	10.46	22.37
3	1.27	49.46	19.87	9.76	10.10	18.64
4	1.29	49.29	18.72	9.45	9.28	17.49
5	1.20	51.08	21.76	11.04	10.73	21.66
6	1.19	51.38	21.89	11.19	10.71	17.78
7	1.39	45.64	18.86	9.16	9.69	15.54

(1)Zeolite at 1 t ha^{-1} + NPK, (2) poultry manure at 4 t ha^{-1} + NPK, (3) lime at 1 t ha^{-1} + NPK, (4) NPK at 300 kg ha^{-1}, (5) composted tobacco waste at 50 t ha^{-1}, (6) bio-humus at 10 t ha^{-1} + NPK and (7) control. (Duncan test, $p \leq 0.05$)

Tab. 6. – Changes in physical properties of soil by application of amendments in 2010

Treatments ($t\ ha^{-1}$)	BD ($g\ cm^{-3}$)	PO (%)	FC (%)	WP (%)	AWC (%)	SSI (%)
1	1.31	49.42	20.46	10.57	9.89	20.06
2	1.26	51.11	21.20	11.50	9.69	22.47
3	1.34	48.51	21.14	10.31	10.83	19.87
4	1.37	47.85	18.50	9.95	8.54	19.68
5	1.23	52.46	20.99	11.18	9.81	21.44
6	1.24	51.08	21.65	11.27	10.38	20.83
7	1.43	45.88	17.97	9.73	8.23	18.68

(1)Zeolite at 1 t ha^{-1} + NPK, (2) poultry manure at 4 t ha^{-1} + NPK, (3) lime at 1 t ha^{-1} + NPK, (4) NPK at 300 kg ha^{-1}, (5) composted tobacco waste at 50 t ha^{-1}, (6) bio-humus at 10 t ha^{-1} + NPK and (7) control. (Duncan test, $p \leq 0.05$)

Tab. 7. – Changes in physical properties of soil by application of amendments in 2011

Treatments ($t\ ha^{-1}$)	BD ($g\ cm^{-3}$)	PO (%)	FC (%)	WP (%)	AWC (%)	SSI (%)
1	1.15	55.94	19.25	9.99	9.25	16.17
2	1.05	59.55	20.00	11.26	8.74	18.37
3	1.19	54.55	19.25	10.45	8.79	16.64
4	1.28	51.19	17.15	9.45	7.70	17.18
5	1.07	57.66	20.02	10.66	9.36	18.14
6	1.10	57.28	20.29	10.67	9.62	17.19
7	1.33	49.85	16.62	9.26	7.36	15.79

(1)Zeolite at 1 t ha^{-1} + NPK, (2) poultry manure at 4 t ha^{-1} + NPK, (3) lime at 1 t ha^{-1} + NPK, (4) NPK at 300 kg ha^{-1}, (5) composted tobacco waste at 50 t ha^{-1}, (6) bio-humus at 10 t ha^{-1} + NPK and (7) control. (Duncan test, $p \leq 0.05$)

CONCLUSIONS

It was observed that the use of organic wastes had a positive impact on physical characteristics of a Xerofluvent soil because of their high organic matter content which promotes flocculation of particles, the essential condition for the aggregation of soil particles. In the present study, application of 50 t ha^{-1} CTW, 4 t ha^{-1} PM and 10 t ha^{-1} BH with chemical fertilizers increase soil organic matter content and this results in decreased bulk density the rate of 16.5%; and increased porosity, field capacity, wilting point, available water content and structure stability index as 15.4%, 19.5%, 20.6%, 22.6% and 26.8% as compared to the average of the years and control plots. They can therefore be used at those rates for improving soil physical properties. Occasionally applying the organic and inorganic materials may cause some problems. For instance, high salinity of PM is the most important factor limiting the usage of it. It is therefore recommended to apply to the soil after analyzing the salt content of PM. In addition, due to the fact that experimental soil has high sand content, provides permeable structure and the applications do not cause any soil pollution problem. Nevertheless, they might cause pollution of groundwater. It is highly recommended that 50 t ha^{-1} CTW, 4 t ha^{-1} PM with NPK fertilizer and 10 t ha^{-1} BH with NPK fertilizer should be added to soils for improving soil physical properties.

ACKNOWLEDGEMENTS

The author thank Ege University for their financial support of this research as a scientific research project (09-ZRF-031).

REFERENCES

1. AGGELIDES, S. M., LONDRA, P. A.: Effect of compost produced from town wastes and sewage sludge on the physical characteristics. Bioresource Technology 71, 2000: 253-259.
2. ADEDIRAN, J. A., MNKENI, P. N. S., MAFU, N. C., MUYIMA, N. Y. O.: Changes in chemical properties and temperature during the composting of tobacco waste with other organic materials and effects of resulting composts on lettuce (*Lactuca sativa* L.) and spinach *Spinacea oleracea* L.). Biological Agriculture and Horticulture 22, 2004:101–119.

3. BLACK, C. A.: Methods of soil analysis, part II. Madison, Wisc.: ASA, 1965.
4. BOUYOUCOS, G. J.: A recalibration of the hydrometer method for making mechanical analysis of the soils. Agronomy Journal 43, 1951: 434-438.
5. CHENU, C., BISSONAIS LE, Y., ARROUAYS, D.: Organic matter on clay wettability and soil aggregate stability. Soil Science Society of America Journal 64, 2000: 1479–1486.
6. DANIELSON, R. E., SUTHERLAND, P. L.: Porosity. In Methods of Soil Analysis, part 1: Physical and mineralogical methods, 2nd ed., ed. A. Klute, 443-461. Madison, Wisc.: ASA-SSA 1986.
7. DORAN, J. W., PARKIN, T. B.: Defining and assessing soil quality. In Defining Soil Quality for a Sustainable Environment, Soil Science Society of America Special Publication *35*, eds. J. W. Doran, D. C. Coleman, D. F. Bezdicek, and B. A. Stewart, 3-21. Madison, WI: ASA-SSSA 1994.
8. ERTİFTİK, H. (1998). Tavuk dışkısının gübre olarak uygulanabilirliği üzerine bir araştırma, Yüksel Lisans Tezi, Selçuk Üniversitesi Fen Bilimleri Enstitüsü, Ziraat Fakültesi, Toprak Anabilim Dalı, Ankara.
9. HAYNES, R. J. - NAIDU, R. (1998). Influence of lime, fertilizer and manure applications on soil organic matter content and soil physical conditions: a review. Nutrient Cycle Agroeceosystem 51: 123-137.
10. MARINARI, S. - MASCIANDARO, G. - CECCANTI, B. - GREGO, S. (2000). Influence of organic and mineral fertilizers on soil biological and physical characteristics. Bioresource Technology 72: 9-17.
11. MBAGWU, J. S. C. (1989). Effects of organic amendments on some physical properties of tropical Utisol. Biol. Wastes 28, 1-13.
12. PAGE, A. L. - MILLER, R. H. - KEENEY, D. R. (Eds.), (1982). In: Methods of Soil Analysis. Part 2. Chemical and Microbiological Properties, 2nd ed. Agron. Monogr. 9. ASA-SSA, Madison, USA.
13. PUGET, P. - CHENU, C. - BALASDENT, J. (2000). Dynamics of soil organic matter associated with particle size fractions of water-stable aggregates. European Journal of Soil Science 51: 595–605.
14. TEJADA, M. - GONZALEZ, J. L. (2003). Effects of the application of a compost originating from crushed cotton gin residues on wheat yield under dryland conditions. European Journal of Agronomy 19: 357–368.
15. TEJADA, M. - GONZALEZ, J. L. (2004). Effects of application of a byproduct of the two-step olive oil mill process on maize yield. Agronomy Journal 96: 692–699.
16. U.S. SALINITY LAB. STAFF. (1954). Diagnosis and improvement of saline and alkali soils (U.S. Government Handbook No:60). Washington, D.C: U.S. Government Printing Office.

Corresponding author:
Melİs ÇERÇİOĞLU, Vocational College of Simav, Dumlupinar University, Kutahya, TURKEY

DIFFERENTIAL HARVESTING STRATEGY: TECHNICAL AND ECONOMIC FEASIBILITY

D. Cillis, A. Pezzuolo, F. Gasparini, F. Marinello, L. Sartori

TeSAF Department, University of Padova, Legnaro, PD, Italy

Abstract

Differential Harvesting (DH) is performed to differentiate the product according to a precise quality standard in order to gain an economic advantage from temporal and spatial field variability. In agriculture this technique has been extensively applied in grape harvesting. There are fewer examples for extensive crops, since DH is mostly used for products with a value at harvest that differs depending on their quality characteristics. DH can be achieved through the use of sensors applied on the combine or through qualitative yield maps.

The aim of this paper is to compare the technical and economic feasibility of five DH methods identified in the literature and a new technique proposed by the authors. The analysis was conducted using yield and protein maps obtained in two years of experimentation growing durum wheat. Results highlight how management zone harvesting allows an increase of about 28 % of high-protein wheat, with a subsequent growth in gross revenue.

Key words: differential Harvesting, selective harvest, harvesting management, precision agriculture.

INTRODUCTION

Differential Harvesting (DH) is a harvesting approach performed to differentiate products according to pre-defined quality standards and allowing exploitation of economic advantages from the temporal and spatial field variability (BRAMLEY ET AL., 2005).

The first applications of DH were in the fishery and forestry sectors. In the fishery sector it is applied to improve the quality of the product by reducing the unintentional catching of undersized fish. In forestry it is used to limit damages caused to the forest and preserve the wood quality (ZILBERMAN ET AL., 1997). In agriculture this technique has been applied extensively in grape harvesting, where DH is achieved by simultaneously conveying the harvested grape into two or more hoppers with specific harvesting machines or through fractional grape harvesting. In the latter, the different zones are harvested at different times after analysis of vegetation indices performed with multispectral images derived from satellites or other platforms.

Implementing scalar harvesting enables to obtain different grape quality classes, resulting in the delivery of a product with homogeneous features. There are fewer DH examples for extensive crops as their value mostly different depending on their quality parameters at harvest-time (MEYER-AURICH ET AL., 2008). On the other hand, extensive crops as cereals take up an important role to satisfy the food demand and the food quality (PEZZUOLO ET AL., 2014; BASSO ET AL., 2016). By way of example, Durum wheat (Triticum durum Desf.) is the main cereal crop in several countries of the Mediterranean basin mainly used for pasta, bread, and couscous production. Durum wheat market constantly demands a grain protein content of 13.5 % or higher (CLARKE, 2001), since this trait represents the most important factor affecting pasta-making properties. However, for the farmer point of view, produce wheat with high protein levels allow a high income thanks to major market value and the premium price established by food companies.

This led to the idea of segregating wheat in different quality classes, achieved through the use of sensors mounted on combines (TAYLOR ET AL., 2005; LONG ET AL., 2013; MARINELLO ET AL., 2015) or qualitative yield maps (TOZER ET AL., 2007).

The aim of this paper is to define the technical and economic feasibility of the application of DH based methods. Different DH methods found in the literature are compared with the one proposed here (on-combine differential harvesting). The methods are tested using yield and protein maps obtained in two years of experimentation on durum wheat.

MATERIALS AND METHODS

Experimental site and climatic data

The grain yield and protein maps used in the present analysis were collected during the 2010/2011 and 2011/2012 wheat crops in a farm in the Venice Lagoon Watershed – Veneto – Italy (45°23'N; 12°09'E). The experimental field measured 13.46 ha (520 m long and 260 m wide), with a soil defined as sandy according to the USDA classification. In terms of climate, most of the annual average rain falls in the months of April (90.6 mm), July (86.2 mm), October (119.4 mm) and November (82.8 mm). Temperatures peak in the summer months and daily average values are lower in the winter months (January and February), with mean values of 13 °C over the entire season. Durum wheat, cultivar Biensur (RAGT Semences – France), was managed with traditional agro-technical practices and the fertilization practice was applied using variable rate distribution techniques.

Homogeneous zone management

The three homogeneous zones were characterized by a different soil fertility (high, medium and low), on which different nitrogen fertilization levels were distributed (Fig. 1). In addition, each zone was split into two parts at flowering stage: one considered as control and the other treated with UAN (urea-ammonium-nitrate) solution (Tab. 1).

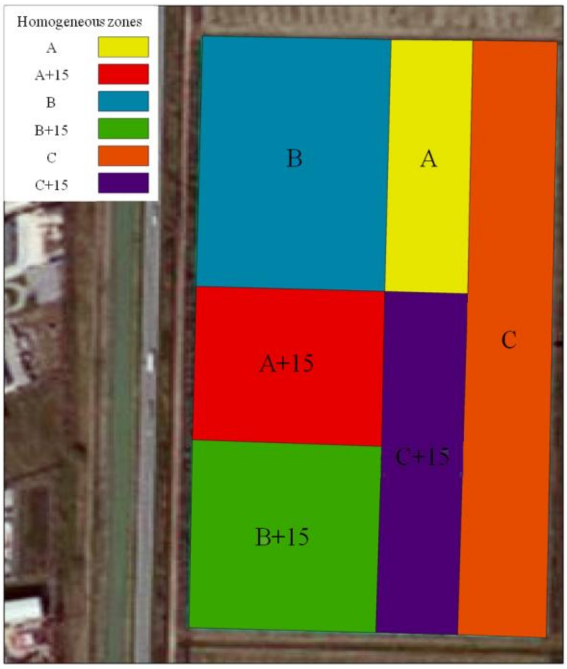

Fig. 1. – Homogeneous zones of the field trial during the wheat cropping seasons 2010/2011 and 2011/2012. The homogenous zones were identified according to soil fertility parameters.

Yield and protein mapping

Grain yield was recorded by a yield mapping system (Agrocom CL021) mounted on a combine harvester (Claas mbH *mod.* Lexion 460).

Consequently, protein content was measured with a Near Infrared Spectroscopy sensor (GraiNIT – RxGrains, Italy) associated to the mapping system GPS. As suggested by MORARI ET AL. (2013), NIRS accuracy was tested in 32 points of the field comparing the protein content measured by a NIRS used in laboratory and traditional Kjeldhal-method. Data were collected with a relatively high frequency (0.15-0.20 Hz), allowing high field resolution. Raw maps were post-processed in order to filter out points collected in correspondence of turn operations or in stationary combine conditions. Finally, data derived from maps were uploaded in a GIS software and interpolated using the Kriging-function (Fig. 2).

Differential harvesting strategy

Collected data were used in order to evaluate 4 different DH techniques (including a new method proposed by the authors) and compare with the uniform harvesting technique.

Uniform harvesting (UH): uniform harvesting of the field and undifferentiated unloading of wheat into the truck using a conventional combine without the possibility of segregating high-protein wheat.

Management zone harvesting (MZ): each homogeneous zone is harvested separately. Homogeneous areas within the field must be identified using GNSS (Global Navigation Satellite System) and the use of NIRS sensor is not necessary. Wheat yield is selected and unloaded on the basis of the protein content of the whole area.

On-truck differential harvesting (TD): the product is unloaded into two different trucks according to the average protein content found during the harvest. This strategy requires a NIRS sensor installed on the combine and information about the protein distribution in the field derived from the previous year protein maps.

On-combine differential harvesting (CD): the combine has two hoppers and the yield is differentiated on the basis of the indications of the NIRS sensor. Wheat with lower and higher protein concentrations falls into two different hoppers. This technique does not provide information about field protein, but it is important to check the right cut-off value. It is possible to assess the optimal cut-off value harvesting through a representative run of the field which allows to know the protein level present in the field. The basic requirement for successful application is a normal field distribution of protein. In this study a cut-off value of 13.5 % was considered.

Optimized on-combine differential harvesting (OCD): the hopper combine is divided into 8 equal parts of approximately 1 m^3 capacity. Each part is equipped with electrically controlled damper opening systems at the top and bottom. All the bottom openings convey into a pre-compartment where a screw allows the unloading operation. During the harvest operation wheat passes through the elevator and is conveyed into the different bins on the basis of protein content read by NIRS. In this way it is possible to know the protein level of each bin. In the unloading phase different bins are opened in order to mix the wheat and obtain a product with a protein content above the threshold. The control software is not limited to managing the protein content of the bin, but calculates the protein content of the truck at each unloading and determines the maximum quantity of low-protein wheat that can be mixed without falling below the threshold level.

Tab. 1. – Nitrogen fertilizer supply for each homogeneous zone

Fertilization practices (kg N·ha^{-1})	**Homogeneous zone**						**Date**		**Fertilizer**
	A	**A+15**	**B**	**B+15**	**C**	**C+15**	**2010/2011**	**2011/2012**	
	high	high	medium	medium	low	low			
Tillering fertilization	52	53	54	55	56	57	24/02/2011	02/03/2012	Ammonium nitrate (26%)
Stem extension fertilization	78	78	108	108	100	100	07/04/2011	06/04/2012	Urea (46%)
Stem extension fertilization					48	48	19/04/2011	27/04/2012	
Flowering stage fertilization		15		15		15	09/05/2011 17/05/2011	14/05/2012 24/05/2012	UAN
TOTAL	**130**	**145**	**160**	**175**	**200**	**215**			

Technical and economic analysis

Four parameters were calculated to evaluate the technical and economic feasibility of all the previously described DH strategies.

Combine working times: including turning and unloading times. It considers the working width and the average working speed. Turning and unloading time were monitored during harvesting time.

Machine operating costs: a model was built encompassing all the operating costs that were added to the combine working time in order to obtain the operating cost of different techniques.

Grain Protein Concentration: evaluates the amount of collected product with a protein level higher than 13.5 % and the relative gross saleable production thanks to the protein maps of previous years obtained with NIRS sensor. Using the first three parameters the operating income was calculated, considering all other farming operations as constant. The different nitrogen rates applied to the different homogeneous zones were considered during the farming operation costs calculation.

Payback period: period needed for each DH technique considering the different technologies applied in each method.

Operating costs of the harvest for each DH strategy have been calculated using the ASABE standards (ASABE, 2011A; 2011B). Costs related to buying seeds, insecticides, fungicides and their application are the same for all the scenarios. On the other hand, it is assumed that the harvesting machines suitable for each DH method are available on the market and are not intended as experimental prototypes.

Gross revenues were determined for each year using price schedules of durum wheat on the AGER corn exchange of Bologna - Italy during the first week of July for both experimental years. The bonus payment for high-protein wheat was 15 EUR·t^{-1}, the threshold that distinguishes the product quality was 13.5 % for both the years (Tab. 2). The results of the various DH methods were compared with those of traditional harvesting.

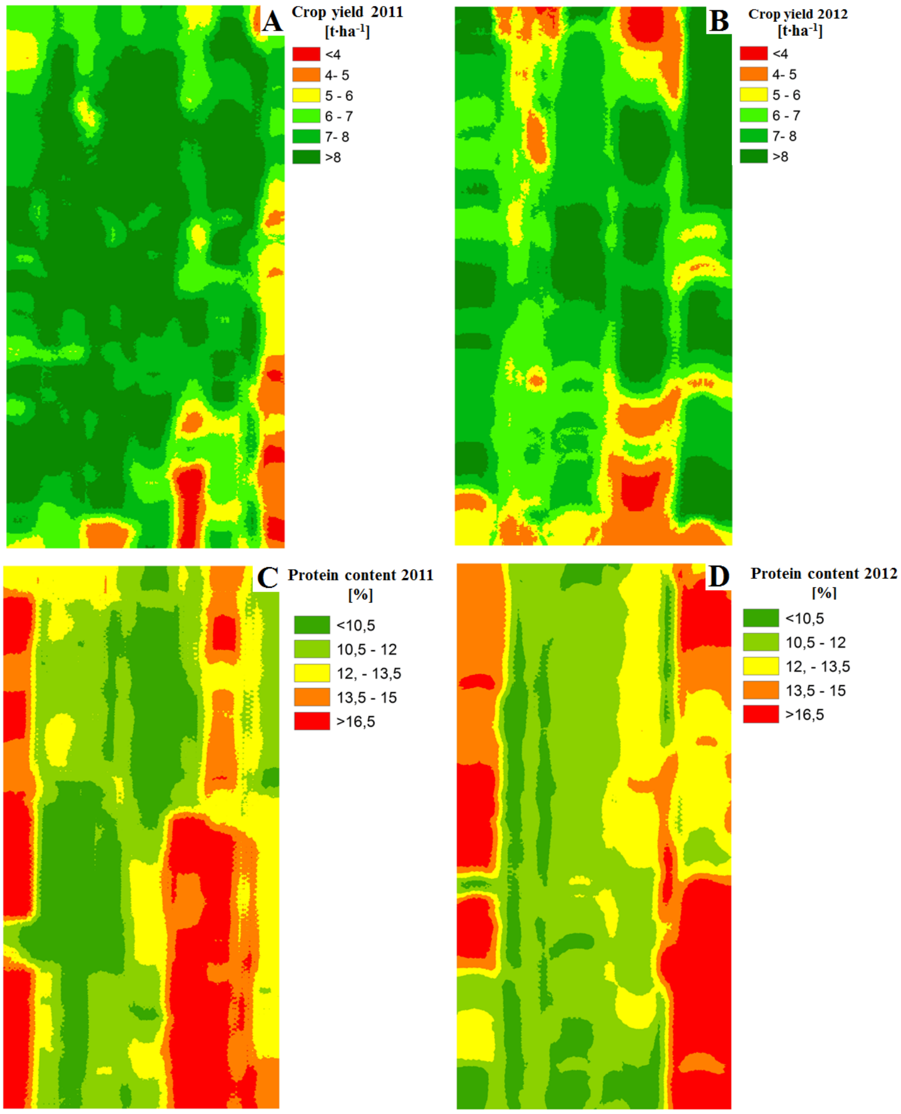

Fig. 2. – Grain yield and protein content maps of the field trial during the 2010/2011 (A; C) and 2011/2012 (B; D) wheat seasons

Tab. 2. – Wheat price at different protein content

Protein content (%)	Durum wheat market price (EUR·t^{-1})	
	2010/2011	2011/2012
< 13,5	297,5	256,5
≥ 13,5	312,5	271,5

RESULTS AND DISCUSSION

Harvesting costs

UH presents lower harvesting costs due to no need for additional investment, and greater field capacity of the combine (Tab. 4).

All DH methods have a low field capacity due to more turns or extra unloading times and the difference in price compared to a machine used for the UH ranges between EUR 10.000 (for the GNSS components required for MZ or for the installation of NIRS used by TD) and EUR 20.000 (required to install the additional bins necessary for CD and OCD).

Separating the combine bins leads to a reduction in the autonomy of the combine and an increase in the unloading time. All these factors affect the field capacity of the harvesting machine: field capacity for UH was

estimated to be 2.06 ha·h^{-1}, whereas there were reductions of 7 and 13 % respectively for MZ and OCD.
Harvesting costs were estimated to range from 141 EUR·ha^{-1} in the case of UH, to 188 EUR·ha^{-1} in the case of CD and automatic harvesting determines cost increases of 31.1 % compared to UH. Despite the higher initial investment, OCD does not determine significant cost increases (19.4 %) compared to UH.

Tab. 4. – Harvesting costs for the differential harvesting strategy

Economics parameters	UH		MZ		TD		CD		OCD	
Initial investment (EUR)	272.000		282.000		282.000		292.000		292.000	
Operating or turning time (h·ha^{-1})	0.03		0.07		0.03		0.03		0.03	
Unloading time (h·ha^{-1})	0.058		0.055		0.058		0.192		0.128	
Actual field capacity (ha·h^{-1})	2.06		1.92		1.84		1.61		1.80	
Harvesting cost (EUR·ha^{-1})	141		155		161		188		168	
Experimental year	**2011**	**2012**	**2011**	**2012**	**2011**	**2012**	**2011**	**2012**	**2011**	**2012**
Cultivation cost (EUR·ha^{-1})	667	673	667	673	666	673	666	673	666	673
Total cost (EUR·ha^{-1})	808	814	821	828	828	834	854	861	835	841

High-protein wheat segregation capacity
The amount of segregated high-quality wheat is related to different characteristics of the methods. Total wheat production was 90.2 tons in 2011 and 86.9 tons in 2012 year. The UH has supplied a product with an average protein content of 12.3 % in the first year and 12.4 % in the second, therefore below the threshold of 13.5 %.
All DH methods have allowed a high-protein product differentiation but at different levels. Because of the quantity and distribution of protein in the field, each scenario has segregated different quantities of wheat with high protein content (Tab. 5). OCD is the best technique in segregating wheat with a high protein content (47.2 % and 43.6 % in the two experimental years).
As reported by LONG ET AL. (2013), all other harvesting methods succeed in segregating approximately 30 % of high-protein product. Gross revenues have been calculated on the base of the high-protein wheat collected by each DH method.

Tab. 5. – Percentage of high-protein wheat segregated by each differential harvesting strategy

DH Strategy	2010/2011		2011/2012	
	Average yield (t·ha^{-1})	**Segregated fraction (%)**	**Average yield (t·ha^{-1})**	**Segregated fraction (%)**
UH	6.7	0	6.4	0
MZ	6.7	32.8	6.4	23.8
TD	6.7	30.2	6.4	35.7
CD	6.7	31.3	6.4	28.7
OCD	6.7	47.2	6.4	43.6

Gross revenues
Wheat with a protein content higher than 13.5 % obtains the bonus payment of 15 EUR·t^{-1}.
Gross revenues are therefore higher in the DH method that can collect a larger quantity of high-protein wheat. DH techniques allow to increase gross revenue of 28 EUR·ha^{-1} (+ 1.5 %) and 45 EUR·ha^{-1} (+ 2.5 %) respectively for MZ and OCD compared to UH.
Gross revenues obtained from different DH scenarios do not appear to be consistent. This is probably due to the “low bonus” awarded to the product with high protein content.

Income
As shown in Tab. 6, MZ allows higher operating profit compared to UH due to higher gross revenues. Despite this type of harvesting method requires a preliminary preparation of the field for each homogeneous zone, harvesting costs are slightly higher than UH one. The automatic DH methods using separate bins have high gross revenues, demonstrating how this is a viable technique to differentiate large quantities of wheat

with high protein content. On the other hand, the operating income of this scenario is lower than that of the UH due to high harvesting costs that undermine higher revenues.
High harvesting costs come from the lower capacity of the bin, due to its division into two sections. Consequently, a decrease of bins operative efficiency is observed with a consequent decrease in field capacity of the combine. OCD can partially lessen problems that characterize DH methods using separated bins. Indeed, OCD optimizes the segregation of high-protein wheat. The high flexibility of the hopper capacity, high gross revenues and moderate harvesting costs allow economic feasibility of this method.

Tab. 6. – Analysis of operating income deriving from DH scenarios examined

DH Strategy	Incomes ($EUR \cdot ha^{-1}$)			Operating income ($EUR \cdot ha^{-1}$)			Operating income gap (compared UH)		
	2011	2012	mean	2011	2012	mean	2011	2012	mean
UH	1994	1658	1826	1186	843	1015	-	-	-
MZ	2027	1681	1854	1205	853	1029	19.05	9.13	14.09
TD	2025	1693	1858	1197	858	1027	10.29	14.55	12.42
CD	2026	1686	1856	1171	824	998	-15.23	-18.92	-17.08
OCD	2042	1700	1871	1207	858	1032	20.31	14.96	17.63

Payback period

Considering a durum wheat harvesting season of 20 days and the field capacity of the different DH methods, the maximum harvestable area does not exceed 300 $ha \cdot year^{-1}$. In this situation the payback period is less than 2 years for MZ and TD and 3 and 4 for OCD and CD respectively.
If a payback period of 5 years is considered, the minimum annual areas to harvest are approximately 100 ha for TD MZ, 125 ha for OCD and 200 ha for CD (Fig. 5).

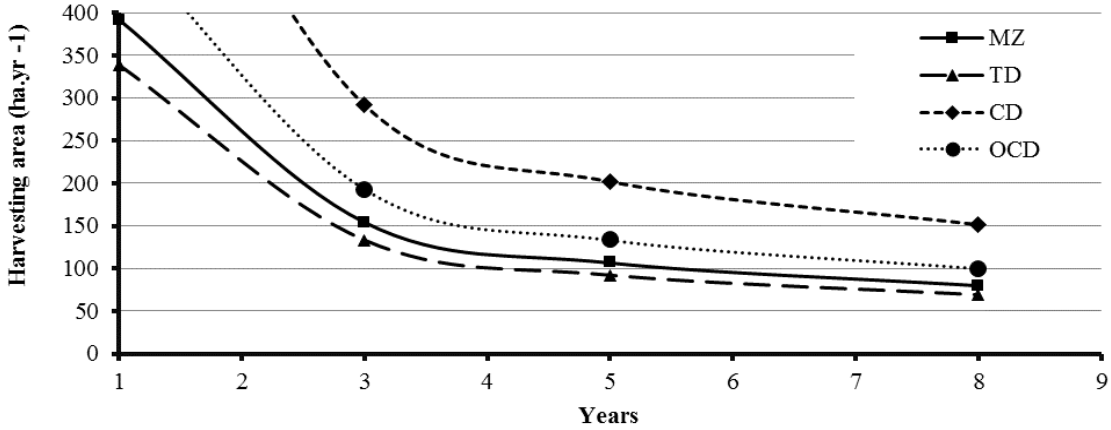

Fig. 5. – Minimum area harvested to pay off the technology applied to machines for the different DH strategy

CONCLUSIONS

The aim of this paper is to evaluate the technical and economic feasibility of DH methods found in the literature and the technique proposed by the authors for durum wheat harvesting, on the basis of protein content.
In this specific study case characterized by small field size, small homogeneous zones and a moderate bonus payment (15 $EUR \cdot t^{-1}$), a different behaviour distinguishing the different DH strategies was observed. MZ, as discussed also by TOZER ET AL. (2007), seems to be advantageous due to the regularity and size of the six zones found in the field. However, to obtain an economic advantage from this technique it is essential to have big differences in terms of potential protein between homogeneous zones. DH on-truck methods using NIRS can generate more profits if the distribution of the protein in the field and the field measures are adequate.
The high harvesting costs related to on-combine DH methods are moderated by OCD. The hopper divided

into 8 sections can be more effective that the one divided into 2. This allows to enhance the bin operative efficiency, and consequently an increase in the combine field capacity.

Moreover, the software able to optimize the truck protein content at each unloading can segregate large amounts of high-protein wheat obtaining higher income.

ACKNOWLEDGEMENTS

Research supported by Progetto AGER, GRANT N. 2010-C21J10000660002. Authors are grateful to Mr. Efrem Destro for the practical support given when conducting the experiment.

REFERENCES

1. ASABE: D497.7 - Agricultural machinery management data. 2011a. St. Joseph, Mich.
2. ASABE: EP496.3 - Agricultural machinery management. 2011b. St. Joseph, Mich.
3. BASSO, B., DUMONT, B., CAMMARANO, D., PEZZUOLO, A., MARINELLO, F.,, SARTORI, L.: Environmental and economic benefits of variable rate nitrogen fertilization in a nitrate vulnerable zone. Science of Total Environment, 545-546, 2016: 227-235.
4. BRAMLEY, R.G.V., PROFFITT, A.P.B., HINZE, C.J., PEARSE, B., HAMILTON, R.P.: Generating benefits from Precision Viticulture through selective harvesting, In: Stafford, J.V. (Ed) Proceedings of the 5th European Conference on Precision Agriculture 2005. Wageningen Academic Publishers, The Netherlands. 891-898.
5. CLARKE, J.M.: Improvement of durum wheat grain quality breeding. In: ABECASSIS, J., Autran, J.C., Feillet, P. (Eds.), Durum Wheat, Semolina and Pasta Quality. Recent Achievements and New Trends. INRA Paris, 2001.
6. LONG, D.S., MCCALLUM, J.D., SCHARF, P.A.: Optical-mechanical system for on-combine segregation of wheat by grain protein concentration, Agronomy Journal, 105, 2013: 1529-1535.
7. MARINELLO, F., PEZZUOLO, A., GASPARINI, F., ARVIDSSON, J., SARTORI, L.: Application of the Kinect sensor for dynamic soil surface characterization. Precision Agriculture, 5, 2015: 1-12.
8. MEYER-AURICH, A., GANDORFER, M., WEERSINK, A., WAGNER, P.: Economic analysis of site-specific wheat management with respect to grain quality and separation of the different quality fractions. In Proceedings of the 12th Congress of the European Association of Agricultural Economists – EAAE, 2008.
9. MORARI, F., LODDO, S., BERZAGHI, P., FERLITO, J.C., BERTI, A., SARTORI, L., VISIOLI, G., MARMIROLI, N., PIRAGNOLO, D., MOSCA, G.: Understanding the effects of site-specific fertilization on yield and protein content in durum wheat precision agriculture - Papers Presented at the 9th European Conference on Precision Agriculture ECPA, 2013.
10. PEZZUOLO, A., BASSO, B., MARINELLO, F., SARTORI, L.: Using SALUS model for medium and long term simulations of energy efficiency in different tillage systems. Applied Mathematical Sciences, 8, 2014: 129–132.
11. TAYLOR, J., WHELAN, B., THYLÉN, L., GILBERTSSON, M., HASSALL, J.: Monitoring wheat protein content on-harvester: Australian experiences. In: Proceedings of the 5th European Conference on Precision Agriculture, ed. J.V. Stafford, Wageningen Academic Publishers, 2005.
12. TOZER, P.R., ISBISTER, B.J.: Is it economically feasible to harvest by management zone, Precision Agric., 8, 2007:151–159.
13. ZILBERMAN, D., KHANNA, M., LIPPER, L.: Economics of new technologies for sustainable agriculture, The Australian Journal of Agricultural and Resource Economics, 41, 1997: 63-80.

Corresponding author:

Andrea Pezzuolo, TeSAF Department, University of Padova, Legnaro, PD, Italy, e-mail: andrea.pezzuolo@unipd.it

PRESSURE CONDITIONS INSIDE THE WORKSPACE OF MULCHER WITH VERTICAL AXIS OF ROTATION

J. Čedík[1], M. Pexa[1], J. Chyba[1], R. Pražan[2]

[1]*Faculty of Engineering, Czech University of Life Sciences Prague, Czech Republic*
[2]*Research Institute of Agricultural Engineering, p.r.i., Czech Republic*

Abstract
Maintenance and treatment of permanent grassland areas, areas left fallow and mulching in combination with other workflows (mowing, grazing) represent advantageous procedures. Conventional impact grass cutting and chopping is energy demanding. The energy demands and the quality of work is affected by air flow and pressure conditions inside the mulcher workspace. In this paper the pressure inside the workspace of the mulcher with vertical axis of rotation is measured and analyzed. The dependencies of pressure inside the workspace of mulcher on rotation speed and distance from the axis of rotation were examined. The torque and power input of the mulcher are also presented. It was found that inside the workspace the negative pressure is created due to centrifugal force and the pressure decreases with the square of rotation speed.

Key words: mulcher, pressure, torque, power.

INTRODUCTION

Currently, increasing importance on reducing the energy demands of agricultural operations is being put. This may be achieved in various ways, for example by reducing wear of the tools or by material or structural modifications. (MÜLLER ET AL., 2014; MULLER ET AL., 2013).

Mulching is a technological process during which crushed plant residues are left on the surface. It is primarily used for cutting and crushing green plant residues, old grass on permanent grasslands and for treatment of fallow lands. Mulching can also be used for crushing crop residues on the arable land (SYROVÝ ET AL., 2013; MAYER & VLÁŠKOVÁ, 2007; ANDREJS, 2006).

Mulcher with vertical axis of rotation is very similar to rotation mowers. Many authors tried to measure the energy demands of rotation mowers but their results differ significantly (Table 1).

Tab. 1. – Results of energy demands of rotation mowers, measured at different conditions

Source	Performance requirement (kW m^{-1})	Conditions
Čedík et al. (2015)	10–23	Mulcher working with mass performance of 10–35 t h^{-1}
ASABE D497.7 (2011)	5	Mower
	8	Mower with conditioner
Syrový et al. (2008)	6.67	Mower with the average mass performance 120 t h^{-1} and blunt blades.
	5.67	Mower with the average mass performance 120 t h^{-1} and sharp blades.
Srivastava et al. (2006)	11–16	Mower at a speed of 15 km h^{-1}
Tuck et al. (1991)	8–10	Mower with sharp blade
	10–12	Mower with worn blade
McRandal & McNulty (1978)	5	Mower
	3.5–6.5	Mower with conditioner

The typical cutting speed of the disc and rotary mowers ranges between 71–84 m s^{-1} (O'DOGHERTY, 1982). Optimization of the cutting speed, the knife shape, the blade oblique angle and the blade rake angle can significantly reduce the energy consumption

(KAKAHY ET AL., 2014; HOSSEINI & SHAMSI, 2012; JOHNSON ET AL., 2012).

Ventilation effect formed by working tools and air pressure in the workspace influence significantly the energy demands and work quality of mulcher with vertical axis of rotation. Direction and speed of air flow have an influence on relative speed of air and tool and thus influence aerodynamic resistance and also repeated contact of plant matter with tool, which lead to the perfect crushing of plant matter. Last but not least, air flow and pressure conditions in workspace of mulcher influence uniform dispersion of crushed plant matter in the whole working width of machine (JUN ET AL., 2008; CHON & AMANO, 2004; CHON & AMANO, 2003; CHON ET AL., 1999A,B).

Air flow, aerodynamic resistance and pressure conditions in workspace of mower are mainly influenced by the design of knife, cover of workspace and cutting speed (ČEDÍK ET AL., 2016; ZU ET AL., 2011; JUN ET AL., 2008; CHON & AMANO, 2004; CHON & AMANO, 2003; HAGEN ET AL., 2002). CHON & AMANO (2003) found out, that speed of air flow increases in direction from the centre of rotor towards its periphery and also, that the speed of air flow in areas of interaction of two rotors can be unstable.

The aim of the study was to determine the pressure conditions inside of workspace of the mulcher with vertical axis of rotation in radial direction to axis of rotation and create the dependencies of pressure in mulcher workspace on the cutting speed and distance from the rotor center.

MATERIALS AND METHODS

In order to determinate the pressure conditions in workspace of mulcher with vertical axis of rotation there was used a model of one rotor of mulcher. It was designed at Department of Agricultural Machines at Faculty of Engineering, Czech University of Life Sciences Prague. The basis of this model was formed by working mechanism of three-rotors mulcher MZ 6000 produced by the BEDNAR FMT company. The rotor diameter is 2 m and driving gear is ensured by electric motor MEZ with performance of 22 kW and equipped by frequency converter Siemens, 30 kW. This model is shown in the Fig. 1.

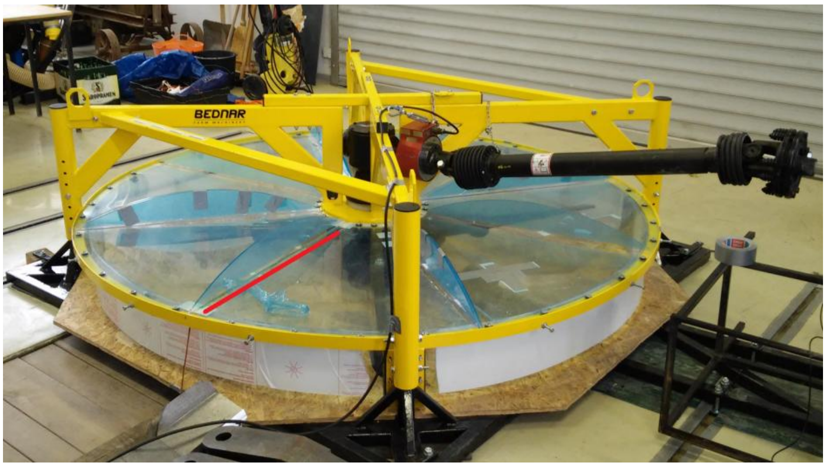

Fig. 1. – Used model of one mulcher rotor with highlighted location of the pressure sensors

Pressure scanning was carried out by means of pressure sensors in the form of pressure tapes produced by the Association for Research and Education, Ltd. (Fig. 2). These pressure tapes were placed inside the top cover of workspace, radially to the axis of rotation of the working tools (Fig. 1). Three pressure tapes were used for scanning. Data from pressure tapes were stored on the PC hard disc with a scanning frequency of 2.5 Hz. All the data were processed by means of MS Excel programme. Parameters of pressure sensors are given in Table 2.

Furthermore, there were scanned the torque and performance by means of torque sensor MANNER Mfi 2500 Nm_2000 U/min (accuracy 0.25 %). The revolutions were scanned by optical sensor Sick WL4-3N1330 with one pulse per revolution. These data were stored on hard disc of measuring computer HP mini 5103 with use of A/D converter LabJack U6 with 18 bit resolution and module for pulse sensors Papouch Quido 10/1. Frequency of data scanning was 5 Hz.

Measurements have been always carried out in a steady state at different revolutions. Working revolutions of mulcher are 1000 rpm. There were chosen the following measuring revolutions: 400, 600, 800 and 1000 rpm, which corresponds to the cutting speed about 42, 63, 84 and 105 m s^{-1}.

Fig. 2. – Pressure sensors

Tab. 1. – Parameters of the pressure sensors

Pressure range	93 – 107 kPa
Temperature range	15 – 40°C
Sampling frequency	10 Hz
Accuracy	<10 Pa
Nonlinearity and hysteresis	<8 Pa
Noise	±5 Pa

RESULTS AND DISCUSSION

In the Fig. 3 there is shown the course of torque and power in dependence on revolutions. It is obvious, that the torque rises with square power of speed of rotation, which is caused by resistance of air, which creates main part of produced energy. It means that power increases with cube power of revolutions, as it is obvious on the Fig. 3.

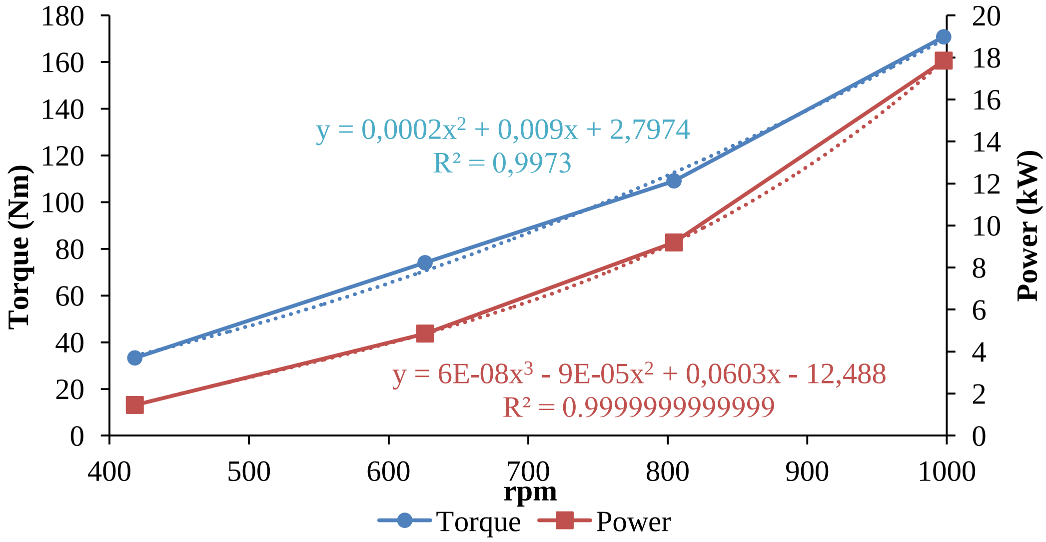

Fig. 3. – Torque and power of the mulcher model in dependence on rotation speed

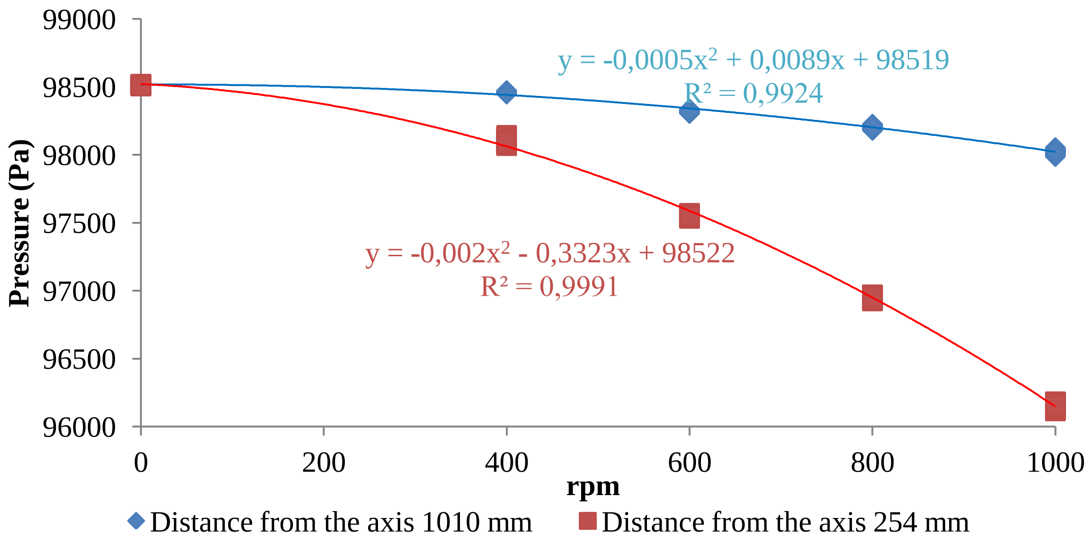

Fig. 4. – Pressure in workspace of the mulcher model in dependence on rotation speed

In the Fig. 4 there are shown dependences of pressure in workspace of mulcher model on revolutions in two distances from the axis of rotor. It is obvious, that in workspace of mulcher there is created negative pressure by movement of working tools and this negative pressure increases with square power of rotor revolutions. Under working revolutions (1000 rpm) there is created negative pressure on periphery of rotor around 0.49 kPa and in the distance of 254 mm from axis of rotor 2.36 kPa. The pressure difference makes about 1.87 kPa.

In the Fig. 5 there is shown the course of pressure from individual pressure sensors. We can see, that the pressure, depending on revolutions, decreases from periphery towards the centre of rotor almost linearly. During the comparison of pressure courses with drawing of working tool placed under graph, it is possible to see the effect of individual elements on working tool on course of pressure, for example tool cranking, cloth, fixing screw etc.

During the measurements there was determined the lowest pressure near to the centre of rotor. CHON & AMANO (2004) have also measured near to the centre of rotor of municipal mower the lowest pressure caused by centrifugal forces. This result is also in good accordance with the results of CHON & AMANO (2003), who state an increase of flow velocity from the centre of rotor towards its periphery.

The mulcher BEDNAR MZ 6000 equipped with three rotors, which driving mechanism was used as a basis of model, draws during the idle operation approx. 30 kW (ČEDÍK ET AL., 2016). In comparison with results achieved with the laboratory model, where the power of 17,8 kW is necessary for one rotor, it is obvious, that in the real mulcher there is an interaction between the individual rotors, which causes lower losses caused by the air resistance. This fact is in good agreement with findings determined by (CHON & AMANO, 2003), who stated unstable flow velocity in area of interaction of two rotors.

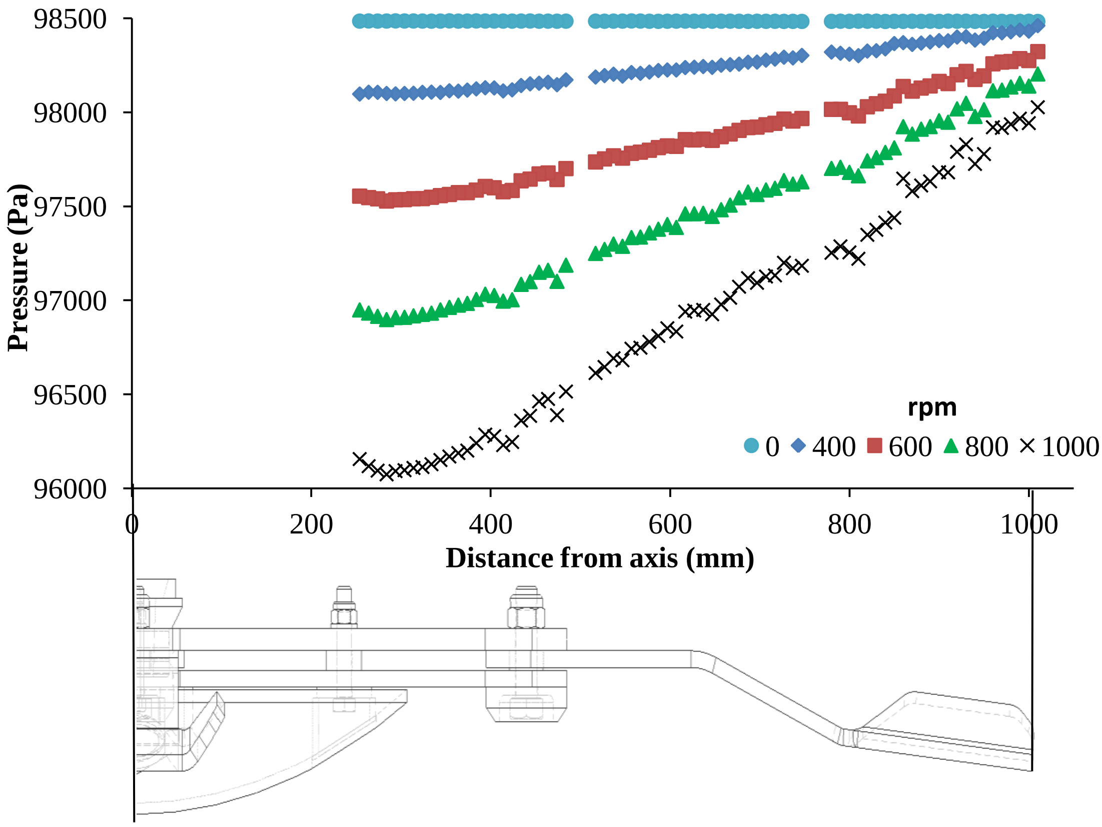

Fig. 5. – Course of the pressure in workspace of the mulcher model at different rotation speeds

CONCLUSIONS

It was determined, that negative pressure was created in mulcher workspace by the movement of working tools. This negative pressure is increasing from the periphery of rotor towards its centre. This negative pressure rising with square power of engine revolutions and the highest measured negative pressure was approx. 2.36 kPa. The decrease of pressure was almost linear across mulcher workspace section. The deviations are probably caused by the design of the working tool. This phenomenon is probably a consequence of centrifugal force.

Negative pressure in the centre of rotor can cause a suction of higher quantity of grass matter under the rotor and thus it can reduce the work quality. In order to increase the work quality there is desirable to carry out the measurements leading to an increase of negative pressure on the periphery of rotor, with the aim to prevent the grass matter or its part to penetrate into the space under centre of rotor.

ACKNOWLEDGEMENTS

The paper is developed with the grant support – 2016: 31190/1312/3116 – Effect of cutting tool shape on air flow in working area of mulcher with vertical axis of rotation.

REFERENCES

1. ANDREJS, V.: Possibilities to reduce energy intensity of mulching in dependence on quality of work. [Diploma thesis.], Department of agriculture machinery, Czech University of Life Sciences Prague, Prague, Czech Republic, 2006, 57 pp.
2. ASABE D497.7: Agricultural Machinery Management Data. The American Society of Agricultural and Biological Engineers. St. Joseph, 2011.
3. ČEDÍK, J., PEXA, M., CHYBA, J., VONDRÁŠEK, Z., PRAŽAN, R.: Influence of blade shape on mulcher blade air resistance. Agronomy Research 14(2), 2016: 337–344.
4. ČEDÍK, J., PEXA, M., PRAŽAN, R., KUBÍN, K., VONDŘIČKA, J.: Mulcher energy intensity measurement in dependence on performance. Agronomy Research 13(1), 2015: 46–52.
5. HAGEN, P. A., CHON, W., AMANO, R.S.: Experimental Study of Aerodynamics Around Rotating Blades in a Lawnmower Deck. American Society of Mechanical Engineers, Fluids Engineering Division (Publication) FED 257(1A), 2002: 67-76.

6. HOSSEINI, S.S., SHAMSI, M.: Performance optimization of a rotary mower using Taguchi method. Agronomy Research 10(spec. issue 1), 2012: 49–54.
7. CHON, W., AMANO, R. S.: Experimental and Computational Investigation of Triple-rotating Blades in a Mower Deck. JSME International Journal Series B: Fluids and Thermal Engineering 46(2), 2003: 229–243.
8. CHON, W., AMANO, R. S.: Experimental and computational studies on flow behavior around counter rotating blades in a double-spindle deck. KSME International Journal 18(8), 2004: 1401–1417.
9. CHON, W., JENSEN, M., AMANO, R.S., CACERES, D., SUNJIC, A., TETZLAFF, P.: Investigation of flows around a rotating blade in a lawn mower deck. In: Proceedings of the 1999 3rd ASME/JSME Joint Fluids Engineering Conference FEDSM'99, San Francisco, California, USA, 18-23 July 1999a. (CD-ROM).
10. CHON, W., TETZLAFF, P., AMANO, R. S., TRISCARI, A., TORRESIN, J., JOHNSON, K.: Experimental study of aerodynamics around co-rotating blades in a lawn mower deck. American Society of Mechanical Engineers, Fluids Engineering Division FED 250, 1999b: 57–64.
11. JUN, H., CHOI, Y., LEE, C., KANG, Y.: Development of Side-discharge Type Mid-mower Attached to a Tractor. Engineering in Agriculture, Environment and Food 1(1), 2008: 39–44
12. KAKAHY, A.N.N., AHMAD, D., AKHIR, M.D., SULAIMAN, S., ISHAK, A.: Effects of knife shapes and cutting speeds of a mower on the power consumption for pulverizing sweet potato vine. Key Engineering Materials 594, 2014: 1126–1130.
13. MAYER, V., VLÁŠKOVÁ, M.: Mulching on soils put to rest. Agritech Science 1(2), 2007: 1–5, http://www.agritech.cz/clanky/2007-2-1.pdf, Accessed 20.1.2015. (in Czech).
14. MCRANDAL, D.M.,MCNULTY, P.B.: Impact cutting behaviour of forage crops II. Field tests. Journal of Agricultural Engineering Research 23(3), 1978: 329–338.
15. MÜLLER, M., CHOTĚBORSKÝ, R., VALÁŠEK, P., HLOCH, S.: Unusual possibility of wear resistance increase research in the sphere of soil cultivation. Tehnicki Vjesnik-Technical Gazette 20(4), 2013: 641-646.
16. MÜLLER, M., NOVÁK, P., HRABĚ, P.: Innovation of material and design solutions of plough blade in the conventional tillage of soil during the cultivation of sugar beet. Listy cukrovarnické a řepařské 130(3), 2014: 94-99 (in Czech).
17. O'DOGHERTY, M.J.: A review of research on forage chopping. Journal of Agricultural Engineering Research. 27(4), 1982: 267–289.
18. JOHNSON, P.C., CLEMENTSON, C.L., MATHANKER, S.K., GRIFT, T.E., HANSEN, A.C.: Cutting energy characteristics of Miscanthus x giganteus stems with varying oblique angle and cutting speed. Biosystems Engineering 112(1), 2012: 42–48.
19. SRIVASTAVA, A.K., GOERING, C.E., ROHRBACH, R.P.: Engineering principles of agricultural machines. St Joseph, American Society of Agricultural Engineers 2006.
20. SYROVÝ, O., BAUER, F., GERNDTOVÁ, I., HOLUBOVÁ, V., HŮLA, J., KOVAŘÍČEK, P., KROUHLÍK, M., KUMHÁLA, F., KVÍZ, Z., MAŠEK, J., PASTOREK, Z., PODPĚRA, V., RYBKA, A., SEDLÁK, V., SKALICKÝ, J., ŠMERDA, T.: Energy saving in crop production technologies. Prague, Czech Republic, Research Institute of Agricultural Engineering, p.r.i. 2008. (in Czech).
21. SYROVÝ, O., SVĚTLÍK, M., PRAŽAN, R., PASTOREK, Z., KUBÍN, K., GERNDTOVÁ I.: Mobile energy devices and the approximate values of unit fuel and energy consumption, Prague, Czech Republic, Research Institute of Agricultural Engineering, p.r.i. 2013. (in Czech).
22. TUCK, C.R., O'DOGHERTY, M.J., BAKER, D.E., GALE, G.E.: Field Experiments to Study the Performance of Toothed Disk Mowing Mechanisms. Journal of Agricultural Engineering Research 50, 1991: 93–106.
23. ZU, L., ZHANG, L., WANG, H.K.: Optimization design of the lawn mowing vehicle's blade based on aerodynamics. Advanced Materials Research 199-200, 2011: 173-181.

Corresponding author:
Ing. Jakub Čedík, Department for Quality and Dependability of Machines, Faculty of Engineering, Czech University of Life Sciences Prague, Kamýcká 129, Praha 6, Prague, 16521, Czech Republic, phone: +420 22438 3321, e-mail: cedikj @tf.czu.cz

WIRE DIAMETER OF HELICAL COMPRESSION SPRINGS INITIAL ESTIMATION

O. Dajbych, A. Sedláček

Department of Mechanical Engineering, Faculty of Engineering, Czech University of Life Sciences, Czech Republic

Abstract
The article is focused on helical compression spring wire diameter estimation when the diameter is not specified or required. Formulae for initial estimation of minimal and maximal wire diameter based on amount and type of load and material properties were determined. Thus the diameter can be chosen from appropriate range.

Key words: helical spring, wire diameter; ultimate stress; spring index.

INTRODUCTION

In calculation process of helical compression springs the wire diameter is often fixedly given or estimated by guesswork or by experience (SCHMID, HAMROCK & JACOBSON, 2014; BUDYNAS & NISBETT, 2011). However, sometimes only load and deflection in selected spring positions are required and other dimensions of the spring including wire diameter are not defined. Whereby wire diameter is fundamental value for further calculation. It is useful to have some range of values for correct initial diameter estimation (ZACHARIÁŠ, 2002). Unfortunately, many of materials` mechanical properties vary with wire size what makes the estimation difficult. Aim of this article was to provide method for appropriate estimation of wire diameter based only on amount and type of load and spring material properties.

MATERIALS AND METHODS

Maximal operational tangential stress in helical compression spring can be calculated by Equation (1) (SCHMID, HAMROCK & JACOBSON, 2014; BUDYNAS & NISBETT, 2011; ZACHARIÁŠ, 2002).

$$\tau = \frac{8 \cdot F \cdot D}{\pi \cdot d^3} \cdot K \tag{1}$$

where F is maximal operational loading force in N, D is mean coil diameter in m, d is wire diameter in m and K is stress correction factor. There are more correction factors used around the globe. In this case Wahl's factor was used (SUHU, KUMAR & KUMAR, 2014). It can be determined by Equation (2) (WAHL, 1944). For easier evaluation several replacements for Wahl's factor are used. Equation (3) (ZACHARIÁŠ, 2002) was used in presented calculation.

$$K = \frac{4C - 1}{4C - 4} + \frac{0.615}{C} \tag{2}$$

$$K = 1 + \frac{1.53}{C} \tag{3}$$

where C is spring index which is calculated by Equation (4).

$$C = \frac{D}{d} \tag{4}$$

Different spring index ranges are recommended in the literature although they cover similar values, e.g. *4-12* (SCHMID, HAMROCK & JACOBSON, 2014; BUDYNAS & NISBETT, 2011) or *5-15* (ZACHARIÁŠ, 2002; SUHU, KUMAR & KUMAR, 2014). Values lower than the range are considered hard to manufacture and inclinable to fatigue. Higher values bring inconstant coil diameter, flimsiness and the springs more likely tangle when manipulated or transported.

Furthermore, the allowable shear stress is needed for the calculation. Generally, the tensile strength of the material is the value that is provided by manufacturer or by the standard. It is related to wire diameter and also the material processing. Its relation to wire diameter can be described by Equation (5) (SCHMID, HAMROCK & JACOBSON, 2014; BUDYNAS & NISBETT, 2011).

$$\sigma_{ut} = \frac{A_s}{d^{m_s}} \tag{5}$$

Where: A_s is constant in $MPa \cdot mm^{ms}$, d is wire diameter in mm and m_s is exponent.

These values are obtained by mechanical tests, they are valid for specific range of diameters and they can vary by different manufacturers or different literature. Obviously, the variation for standard materials should be minimal. E.g. the published values for Chrome-Silicon wire are $A_s = 1974\ MPa \cdot mm^{0.108}$ and $m_s = 0.108$ (valid for d = 1.6-9.5 mm) (Budynas & Nisbett, 2011) or $A_s = 2000\ MPa \cdot mm^{0.112}$ and

$m_s = 0.112$ (valid for d = 1.6-10 mm) (SCHMID, HAMROCK & JACOBSON, 2014). The relation between allowable shear stress and tensile strength of the material is also dependent on material and its processing. The correlation factor k_{all} values (ranges) are also slightly different across different sources and the correlation can be expressed by Equation (6).

$$\tau_{all} = k_{all} \cdot \sigma_{ut} \tag{6}$$

Maximal operational stress of the string must be lower than allowed shear stress, thus there must be a reserve for full string deflection – Eq. (7) (ZACHARIÁŠ, 2002).

$$\tau = k_d \cdot \tau_{all} \tag{7}$$

where τ_{all} is allowed shear stress and k_d is reserve factor.

By substitution Equations (3) to (7) into Eq. (1) full equation for maximal operational shear stress of the spring is derived. After evaluation the formula for wire diameter is obtained – Eq. (8).

$$d = \left[\frac{8 \cdot F}{\pi \cdot k_{all} \cdot k_d \cdot A_s} (C + 1.53) \right] \tag{8}$$

For wire diameter estimation range determination it is necessary to substitute appropriately minimal and maximal values for all constants that have ranges. Then the Equations (9) and (10) are obtained.

$$d_{\min} = \left[\frac{8 \cdot F}{\pi \cdot k_{all\max} \cdot k_{d\max} \cdot A_s} (C_{\min} + 1.53) \right]^{\frac{1}{2-m_s}} \tag{9}$$

$$d_{\max} = \left[\frac{8 \cdot F}{\pi \cdot k_{all\min} \cdot k_{d\min} \cdot A_s} (C_{\max} + 1.53) \right]^{\frac{1}{2-m_s}} \tag{10}$$

RESULTS AND DISCUSSION

Based on Equations (9) and (10) the final formulae for wire diameter estimation are derived – Eq. (11), (12) and (13).

$$d = (B_{s\min} \div B_{s\max}) \cdot F^{\frac{1}{2-m_s}} \tag{11}$$

$$B_{s\min} = \left[\frac{8 \cdot (C_{\min} + 1.53)}{\pi \cdot k_{all\max} \cdot k_{d\max} \cdot A_s} \right]^{\frac{1}{2-m_s}} \tag{12}$$

$$B_{s\max} = \left[\frac{8 \cdot (C_{\max} + 1.53)}{\pi \cdot k_{all\min} \cdot k_{d\min} \cdot A_s} \right]^{\frac{1}{2-m_s}} \tag{13}$$

where B_{min} and B_{max} are constants of diameter estimation range.

Constants values used for calculation can be obtained by any appropriate source. For illustration of described process selected values are shown in Tab. 1. The column *d* limits the validity of further constants.

For comfortable or repeated calculation the Tab. 1 could be enlarged by column B_s which represents the range of diameter choice – Tab. 2.

Example of calculation follows.

Input values:

Loading force F = 2000 N

Static load

Wire material – Chrome-Silicon

$A_s = 1974$ MPa · $mm^{0.108}$; $m_s = 0.108$; $C_{min} = 4$; $C_{max} = 12$; $k_{allmin} = 0.65$; $k_{allmax} = 0.75$; $k_{dmin} = 0.84$; $k_{dmax} = 0.94$

Result values:

$$d = (0.088 \div 0.162) \cdot F^{\frac{1}{2-0.108}}$$

Thus wire diameter should be chosen from range:

$d = 4.9 \div 9.0\,mm$

This range has to be compared to range of validity from *Tab. 1* and the final diameter must fit in both ranges. In this example, any available diameter from given range can be chosen and it is highly probable that it will not be necessary to change it afterwards due to strength check failure or other requirements miss.

Presented method allows the designer to choose the wire diameter from appropriate range based only on amount and type of load and selected material properties (ZACHARIÁŠ, 2002). It is different from generally used trial selection of wire diameter (SCHMID, HAMROCK & JACOBSON, 2014; BUDYNAS & NISBETT, 2011). There is also possibility to choose acceptable string index and calculate approximate wire diameter which is rounded to nearest available value (BUDYNAS & NISBETT, 2011).

Values for quick calculation based on selected information sources were provided (Tab. 1 and Tab. 2) so it is possible to use this article for spring design immediately. If different material properties, acceptable spring index range or safety factor is used, the method for obtaining custom constants was provided – Equations (11), (12) and (13).

Tab. 1. – Constants values for selected spring wire materials (BUDYNAS & NISBETT, 2011; ZACHARIÁŠ, 2002)

Material	d	A_s	m_s	C	k_{all}	k_d
	mm	$MPa \cdot mm^{ms}$	-	-	-	-
Music wire	0.1-6.5	2211	0.145	4-12	0.45-0.60	0.84-0.94
Oil-tempered wire	0.5-12.7	1855	0.187	4-12	0.45-0.50	0.84-0.94
Hard-drawn wire	0.7-12.7	1783	0.190	4-12	0.45-0.55	0.84-0.94
Chrome-Vanadium wire	0.8-11.1	2005	0.168	4-12	0.65-0.75	0.84-0.94
Chrome-Silicon wire	1.6-9.5	1974	0.108	4-12	0.65-0.75	0.84-0.94
302 Stainless steel	0.3-2.5	1867	0.146	4-12	0.45-0.55	0.84-0.94
	2.5-5.0	2065	0.263	4-12	0.45-0.55	0.84-0.94
	5.0-10.0	2911	0.478	4-12	0.45-0.55	0.84-0.94
Phosphor-bronze	0.1-0.6	1000	0.000	4-12	0.45-0.50	0.84-0.94
	0.6-2.0	913	0.028	4-12	0.45-0.50	0.84-0.94
	2.0-7.5	932	0.064	4-12	0.45-0.50	0.84-0.94

Tab. 2. – Wire diameter range values for selected spring wire materials

Material	d	B_s
	mm	$mm \cdot N^{-1/(2-ms)}$
Music wire	0.1-6.5	0.089-0.179
Oil-tempered wire	0.5-12.7	0.103-0.190
Hard-drawn wire	0.7-12.7	0.099-0.193
Chrome-Vanadium wire	0.8-11.1	0.081-0.151
Chrome-Silicon wire	1.6-9.5	0.088-0.162
302 Stainless steel	0.3-2.5	0.102-0.196
	2.5-5.0	0.083-0.166
	5.0-10.0	0.046-0.103
Phosphor-bronze	0.1-0.6	0.173-0.302
	0.6-2.0	0.177-0.311
	2.0-7.5	0.169-0.301

CONCLUSIONS

Universal method for appropriate estimation of wire diameter of helical compression spring was determined. The estimation can be based only on amount and type of load and selected wire material. This procedure can be useful when only force and deflection of spring are specified.

REFERENCES

1. BOLEK, A., KOCHMAN, J.: Části strojů, 2. svazek. SNTL, Praha 1990.
2. BUDYNAS, R. G., NISBETT, J. K.: Shigley's Mechanical Engineering Design, Ninth Edition. McGraw-Hill, New York 2011.
3. SAHU, V., KUMAR, S., KUMAR, R.: Simplified stress calculation method for helical spring. In IJIRT, Vol. 1, Issue 6, 2014: 1623-1631.
4. SCHMID, S. R., HAMROCK, B. J., JACOBSON, B. O.: Fundamentals of Machine Elements, Third Edition: SI Version. CRC Press, Boca Raton 2014.
5. WAHL, A. M.: Mechanical springs. The Penton pub., Cleveland 1944.
6. ZACHARIÁŠ, L.: Části strojů I. A II. díl. ČZU, Praha 2002.

Corresponding author:
Ing. Oldřich Dajbych, Ph.D., Department of Mechanical Engineering, Faculty of Engineering, Czech University of Life Sciences Prague, Kamýcká 129, Praha 6, Prague, 16521, Czech Republic, phone: +420 22438 3178, e-mail: dajbych@tf.czu.cz

THE DEVELOPMENT OF THE AUTOMOBILE TRANSPORT IN AGRICULTURE

O. N. Didmanidze, G. E. Mityagin, A. M. Karev

The Russian state agricultural university – the Moscow agricultural academy named after K. A. Timiryazev, Russia

Abstract
One among the factors for the increase of competitiveness and profitability of producers within the agricultural production is the stimulation of researches and the development of progressive technologies within transport processes as transport is an important component of agro - industrial complex and as for agriculture itself, it is one of the most transport-capacious branches within the national economy. The article is being devoted to the directions and the perspectives for the increase of efficiency of transport appliance due to the improvement of machine-park structure, the design and the organization of operation of vehicles.

Key words: automobile transport, machine-park structure, mobile electrical units, gas-balloon cars, systems of satellite navigation.

INTRODUCTION

The transport is the important component of the agro-industrial complex; its main purpose is to provide the movement of freights at the production stage for the plant farming and animal husbandry. The annual transport turnover for the goods within agricultural enterprises constitutes from 20 to 40 tons per hectare of the cultivated land and as for the overall volume of transport labour – 80 – 200 tons/km per hectare of the cultivated land. About 40 - 60% of all energy expenses within the agricultural enterprises are being regarded as those being spent on transportation: at seeding and planting phases – supplying grains, seeds and fertilizers; at harvesting phase – collecting and picking up of the crops; at the phases of preparation and application of fertilizers – transporting them to the storage points and then to the fields. The labour expenses within the transportation, taking into account the total sum of workforce applied for the cultivation and harvesting procedures, constitute for – 30%, for potatoes – 40%; corn on a silo – 70%. A quarter of all workers within the agricultural enterprise are being engaged in transportation (DIDMANIDZE, 2005).

The transportation process ensures the rhythmical functioning of the general technological process of the enterprises. Especially it belongs to the enterprises with the continuous processes of production, in which the strictly regulated movement of objects of the labour is required.

At the organization stage of transportation and the definition of carrying capacities of transport enterprise for a certain economic region the goods` turnover is initial. The characteristic and important features of the transport processes in agro-industrial complex are the wide range in accordance with the purpose and high unevenness of goods` turnover within a year (Fig. 1) (EVTJUSHENKOV, 2004).

The factors of no small importance, making the transport performance more complicated are the following: the exploitation of the rolling stock on the roads of low categories of pavement (III, IV, V), even often in cross-country conditions; the urgency caused by transportation of perishable production; the complexity of mechanization of loading and unloading works.

Depending on the distance and technology of the freights` movement, one can distinguish inner-farm, inner-economy and outer-economy types of transportation.

Inner-farm ones provide the movement of freights, for example, forages from warehouses on farmyards to the barnyards, the removal of manure from barnyards to the storage units etc. They are characterized by a big variety of freights and recurrence of transportations of the same freights in a day. The inner-farm means of transportation are presented by low-power tractors with special trailers or bodies, transport cranes, screws, pneumatic devices. It has to work all the year round irrespective of climatic and other conditions.

The inner-economy types of transportation (the removal of manure from the farm to the fields, the transportation of seed material, fertilizers, grains from combines, etc.) are being characterized by short distances (1-20 km). For this purpose cars and trailers on the tractor pull are being applied.

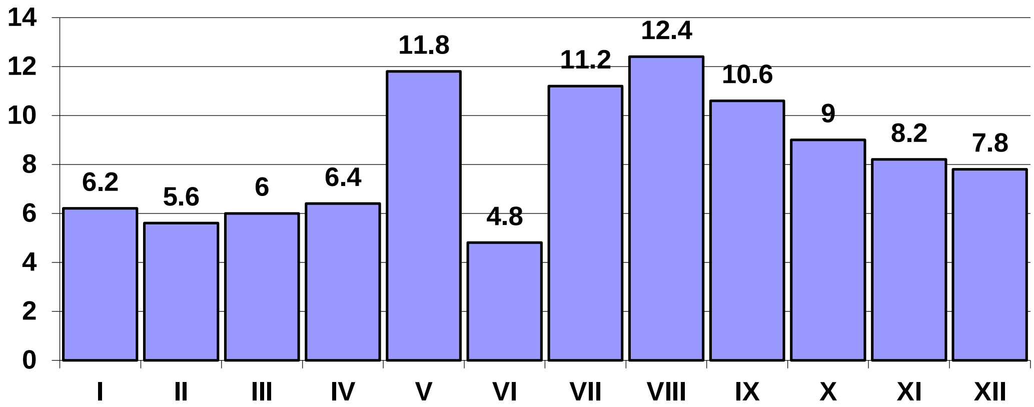

Fig. 1. – The share of the overall annual volume within the transportation works in Central part of RF in months – percentage

The outer-economy types of transportation are connected with the carrying of freights into the economy or from the economy: the movement of goods from the threshing floors, fields and warehouses to the places of further processing; the delivery of mineral fertilizers, oil products, construction materials, cars, the equipment to the economy. The distances for such transportations can be 40 – 60 km and more. For this the means of the big loading capacity and high technical speeds are being applied.

The work of transport becomes complicated because of high degree of wear of a rolling stock and means of loading at the simultaneous annual increase in load for them.

According to the Avtostat agency, the total number of trucks (a middle and big class) reaching in our country 3, 7 million copies, a share of cars with the age over 15 years reaches 2, 4 million. The share of the cars assembled in Russia makes 88% (Fig. 2) (WWW.AUTOSTAT.RU/INFOGRAPHICS/22363).

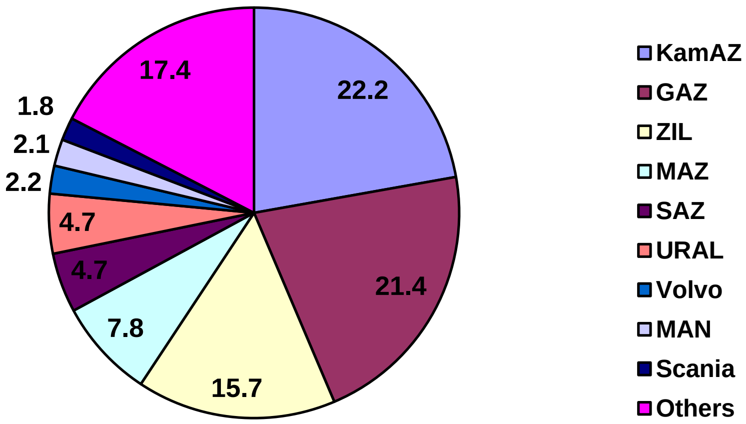

Fig. 2. – The park of trucks in Russia in accordance with the first of July, 2015: – KamAZ; – GAZ; – ZIL; – MAZ; –SAZ; – URAL; – Volvo; – MAN; – Scania; – Others

In 2015, KamAZ (22.2%) has come out on top, having moved on the second place GAS brand cars which share has decreased to 21,4% (from 22.2%). On the third place holds an essential share of ZIL park (15.7%) though actually several years these cars aren't made. Other marks have entered "five" of leading brands: MAZ (7.8%) and SAZ (4.7%). Among brands from more than 2% shares are the Ural (4.7%), Volvo (2.2%) and MAN (2.1%). In the long term rather intensive redistribution of shares of producers, first of all, because of reduction of a share of the brands which aren't letting out or not importing cars to Russia is expected. It is possible to carry cars of brands to them ZIL, SAZ, KRAZ.

As for the brands` distribution according to the age structure, it doesn't differ essentially from each other, the difference is only in number of rather new cars, speaking about success of work of car makers in the last decade (Fig. 3) (POLJAKOVA, 2013).

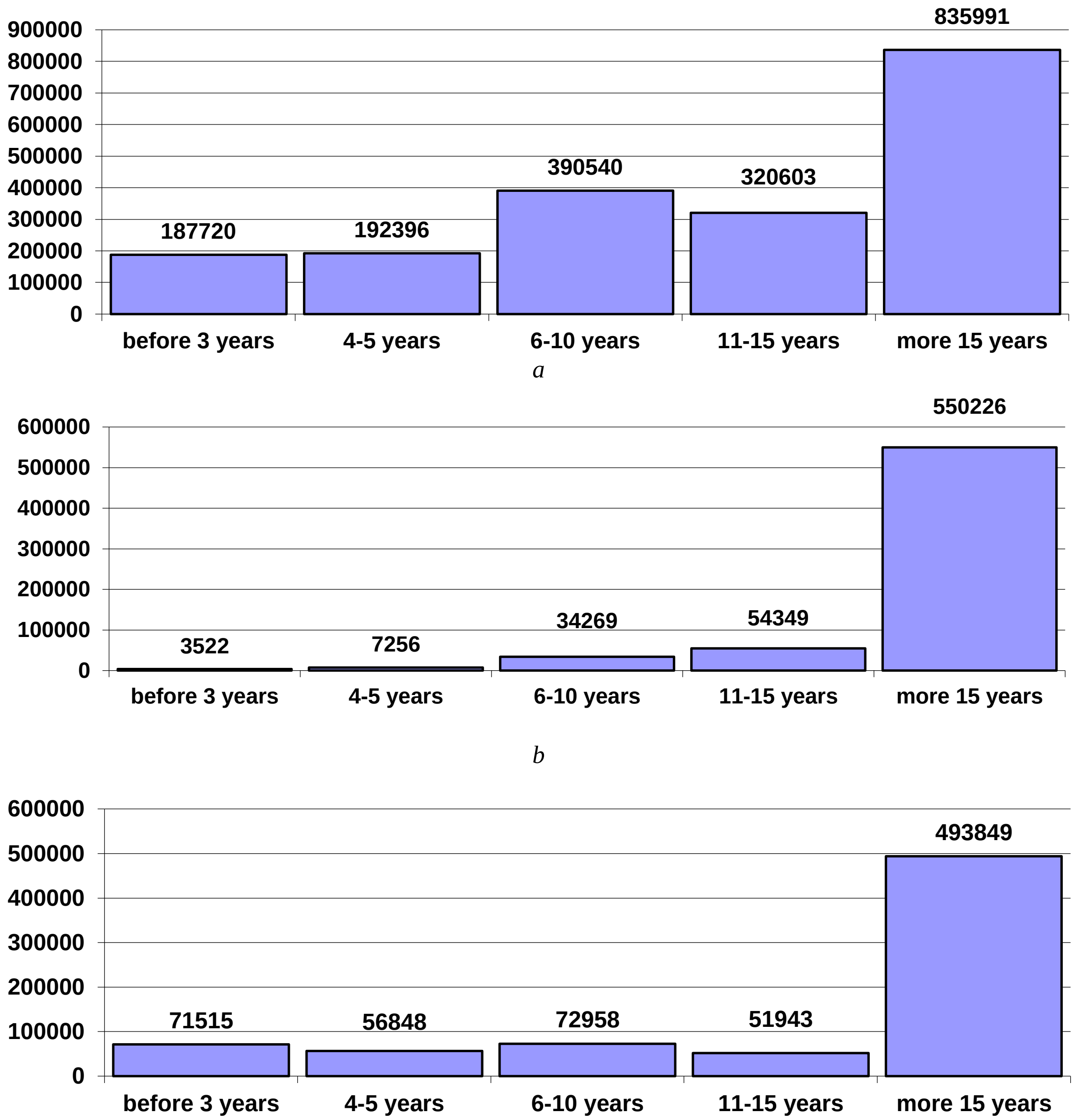

a

b

c

Fig. 3. – The age structure of trucks` brands: a – GAZ; b – ZIL; c – KamAZ

Nowadays it is possible to observe the sharping contrasts in the appliance of the equipment: on an equal footing machine operators receive absolutely different results of operation of machines. It is caused by the fact that on places modern means of the organization of transportations aren't used, work of separate services of the enterprises isn't sufficiently coordinated, the fleet of vehicles isn't fully adapted for transportation of agricultural freights, and the service regulations of equipment, its storage, maintenance and repair aren't followed.

In the conditions of the modern economy, the role of improvement of transport service of agro-industrial complex also raises. This is caused by the fact that in the spheres of agricultural production, the further processing and realization of goods, the large number of specialized branches and productions which are connected among them-selves, are being engaged both economically and quite often technologically.

In this regard, the importance of effective use of vehicles and loading- unloading equipment increases even more considerably. At the same time, the further improvement of the organization of transportation of goods in agriculture and branches serving it, the improvement of usage of transport and loading- unloading means, the reduction of expenses of work and funds for the transportation of goods is required.

The solution for these questions especially is important in the connection with the existence of small-scale country (farmer) enterprises and the overworking enterprises and the saturation of farms by new vehicles. The implementation in the country of necessary organizational and technical measures allows using rationally available material and technical resources of transport of agro- industrial complex, to improve the transport service of farms and the overworking enterprises.

The tasks connected with the increase of the efficiency of the automobile transport of agro-industrial complex needed to be solved in the complex are presented by several levels:

1. The determination of necessary productivity (decrease in prime cost) in connection with the planned growth of volume of transportations.
2. The definition of the sources for the gain coverage in volume of transportations (decrease in cost of transportations).
3. The definition of elements for the gain coverage in volume of transportations (depreciation of transport work) as a result of improvement of indicators of work.
4. The definition of necessary indicators (coefficients of release and technical readiness, etc.).

It is clear from the above that automobile transport in relatively small-scale farm level is important part of farm management and needs some improvement for future. That is why the main aim of this article is to highlight the ways for possible improvement of this sector.

MATERIALS AND METHODS

The activity for the improvement of work of park and in general work of transport in agro- industrial complex can be conducted with the usage of several indicators. At the first stage - they are set or the target indicators allowing to achieve the desirable objectives pay off (on the example of the region this is an increase in gross collecting production, respectively, growth of a cargo transportation, on the example of the enterprise – it can be the increase in load capacity or the decrease in the current costs (Fig. 4)).

At the second stage – the definition for the ways of growth of productivity, as a rule, it is the increase in park of cars (an extensive way), or change of indicators of work (an intensive way) that is more preferable. In the analysis of cost of transportations the decisive key - the change of structure of the park.

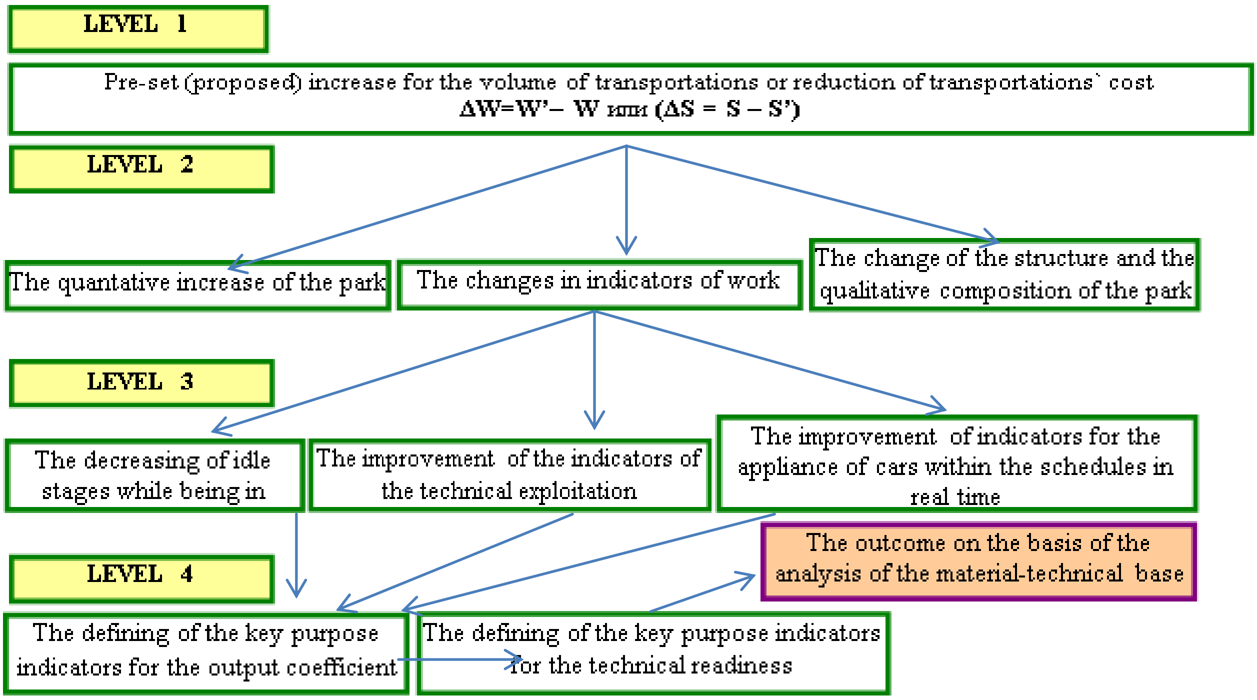

Fig. 4. – The stages for the improvement of work of the transport means` park

At the third stage the directions of improvement of indicators of work assuming the reduction of idle times, improvement of technical operation and improvement of indicators of the usage are being considered. All factors listed above at the fourth stage allow the reaching of the target values of coefficients of release and technical readiness.

RESULTS AND DISCUSSION

The majority of freights in agro-industrial complex require the appliance of specialized vehicles. Depending on the type of transport, the structure to be transported has its distinctive features, but at the same time the obvious domination of bulk cargoes (Fig. 5 and 6) is observed (DIDMANIDZE, 2005).

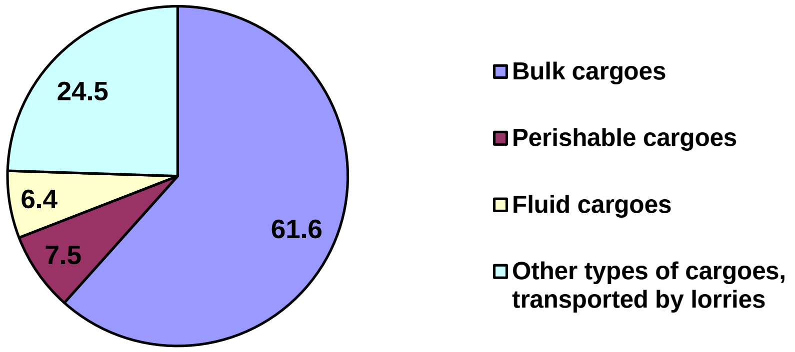

Fig. 5. – The structure of the cargoes, being transported in the outer-economy types of transportation, percentage – bulk cargoes; perishable cargoes; fluid cargoes and other types of cargoes, being transported by lorries

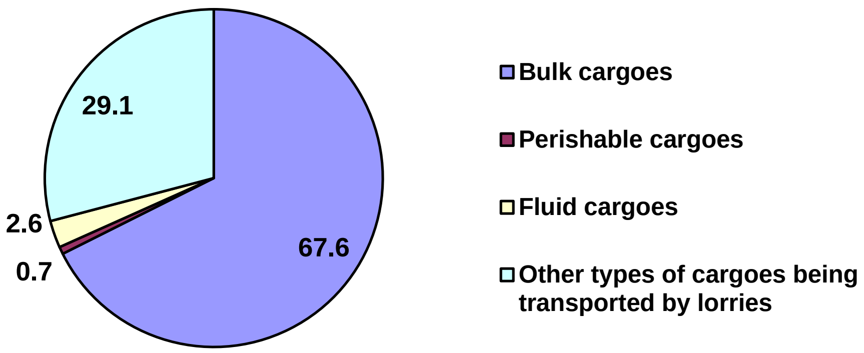

Fig. 6. – The structure of the cargoes, being transported in the inner-economy types of transportation, percentage – bulk cargoes; perishable cargoes; fluid cargoes and other types of cargoes, being transported by lorries

If to speak in general, the park of lorries or trucks in the country and the goal orientation of the native industry for the production of the basic resources have led to the fact that in the park the average weight in transportation is occupied by the dump trucks (Tab. 1, Fig. 7) (POLJAKOVA, 2011). The fact that it is necessary to carry cargoes along the long distances and their irrational organization, and also the low degree of their containerization may be referred to the distinctive features of the Russian road haulage. So such a big average weight is present in the park of lorries with sides.

Nearly 75% of freights in agro-industrial complex (AIC) require the presence of lorries with the specialized or dump bodies, however the real structure of the park within the AIC is far from the rational for both types of bodies, and as for the loading capacity of lorries see (Tab. 2) (EVTJUSHENKOV, 2004). Within the concrete enterprises this ratio can be another.

Tab. 1. – The Structure of the park of lorries with the full weight more than 3,5 tons in accordance with types of a body, %

Body type	All brands	GAZ	KamAZ	MAN	ISUZU
Dump trucks	21,5	5,2	32,1	5,2	7,7
Lorries with sides	18,5	29,6	17,6	6,5	33,1
Articulated lorries	12,3	–	17,5	57,3	1,7
Vans	10,5	19,2	4,4	15,2	27,4
Special vehicles	6,6	7,7	5,7	1,6	6,2
Tank-lorries (trucks)	3,3	6,4	1,9	0,4	0,7
Mobile or truck-based cranes	2,1	0,1	1,6	–	0,8
Others	25,1	31,8	19,3	13,9	22,4

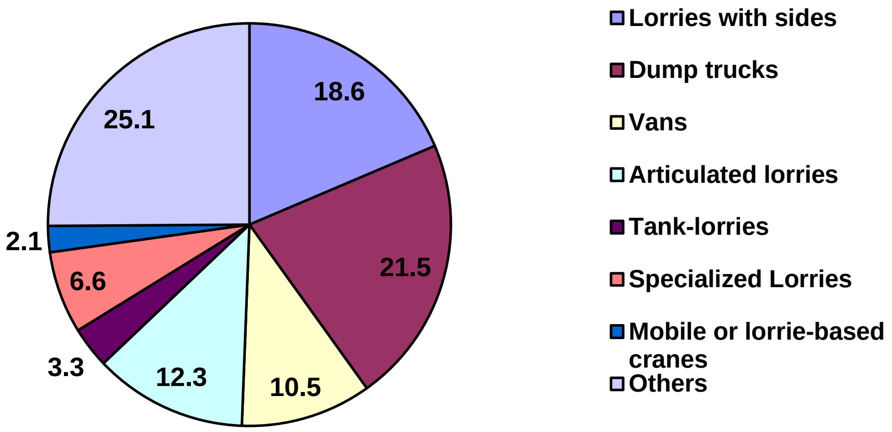

Fig. 7. – The distribution of lorries in the park according to the body type – percentage

Nowadays one can mention the certain movements in the field of the rationalization of the lorries` park structure, which can be easily seen on the example of the registration processes of new lorries and trucks in different regions; the specifics of their activity began to set up a distinctive imprint on the supply of the necessary body types. For example, let`s take Moscow oblast and the distinctive features of cargo freight – the prevailing of the already finished and packed production which has been received after final stages of processing (POLJAKOVA, 2012).

Tab. 2. – The lorries` park structure in accordance with the body types and the load capacities within the AIC (according to the data, provided by VIM)

Body type	Share, %	Load capacity	Share, %
Dump truck	39	to 2 т	5.9
Lorry with sides	42	from 2.1 to 5 т	65.6
Vans (of all types)	4	from 5.1 to 8 т	20.7
Tank-trucks	12.9	from 8 т	7.8
Others	2.1		

The other distinctive feature of the replenishment of modern park of a rolling stock is the obvious shift towards lorries of a big class that allow to improve the inter-economic external transportations, but doesn't improve the situation with the inner-economic as the purchased lorries are first of all prepared for the roads with the rigid improved coating (POLJAKOVA, 2012). According to the number of the researches which has been being carried out, during the previous 5 to 10 years, the creation of specialized transport technological machines can be a solution of the problem of transport service (IPATOV, 2008; DZOCENIDZE, 2011). However, the development and the deployment of new vehicles has seemed to the car-makers as the irrational and the Silant project has been developed at the level of the small-scale assembly, serving the needs of generally Novgorod region, and the multipurpose transport-technological machine has been developed on the modular base of lorry "Ural" has remained at the level of experimental cars as the factory has considered that this segment of equipment has bad market potential, having switched resources to the creation of a line of cars under the Urals-Next brand (CHERNJAVSKIJ, 2015).

The real perspectives for the nearest future – the creation of specialized cars on serial chassis as the recession consequences in the market of vehicles first of all have struck at perspective developments. On the new chassis "Gazon-Next" and "Ural-Next", the creation of scale of cars of middle class and a big class is possible. The scale of bodies like "Multilift" at present is very limited and serves as the municipal rather, than agriculture (CHERNJAVSKIJ, 2007).

As the option which is the most really embodied in practice, it is possible to consider the further development of hook-on equipment for the ordinary or modified bodies of articulated lorries for work with the hydro-fixated equipment, which in its turn is widespread in all regions of the country, and a large number of the equipment will be released from large infrastructure projects, especially after 2018. The perspectives of such a scheme still should be defined, as well as load capacities of modern serial cars in the conditions of agro-industrial complex.

Here it is necessary to allocate the two directions, the work on which has been being conducted for a long time, and the leading role belongs to the experts working at our university.

The first direction, of course, is the development of various schemes of mobile electrical units whose types are presented by hybrid schemes (DIDMANIDZE, 2015). As for the remote perspective – after 2030 one can be able to predict the intensive growth of number of cars equipped with fuel elements and working on the hydrogen (Fig. 8).

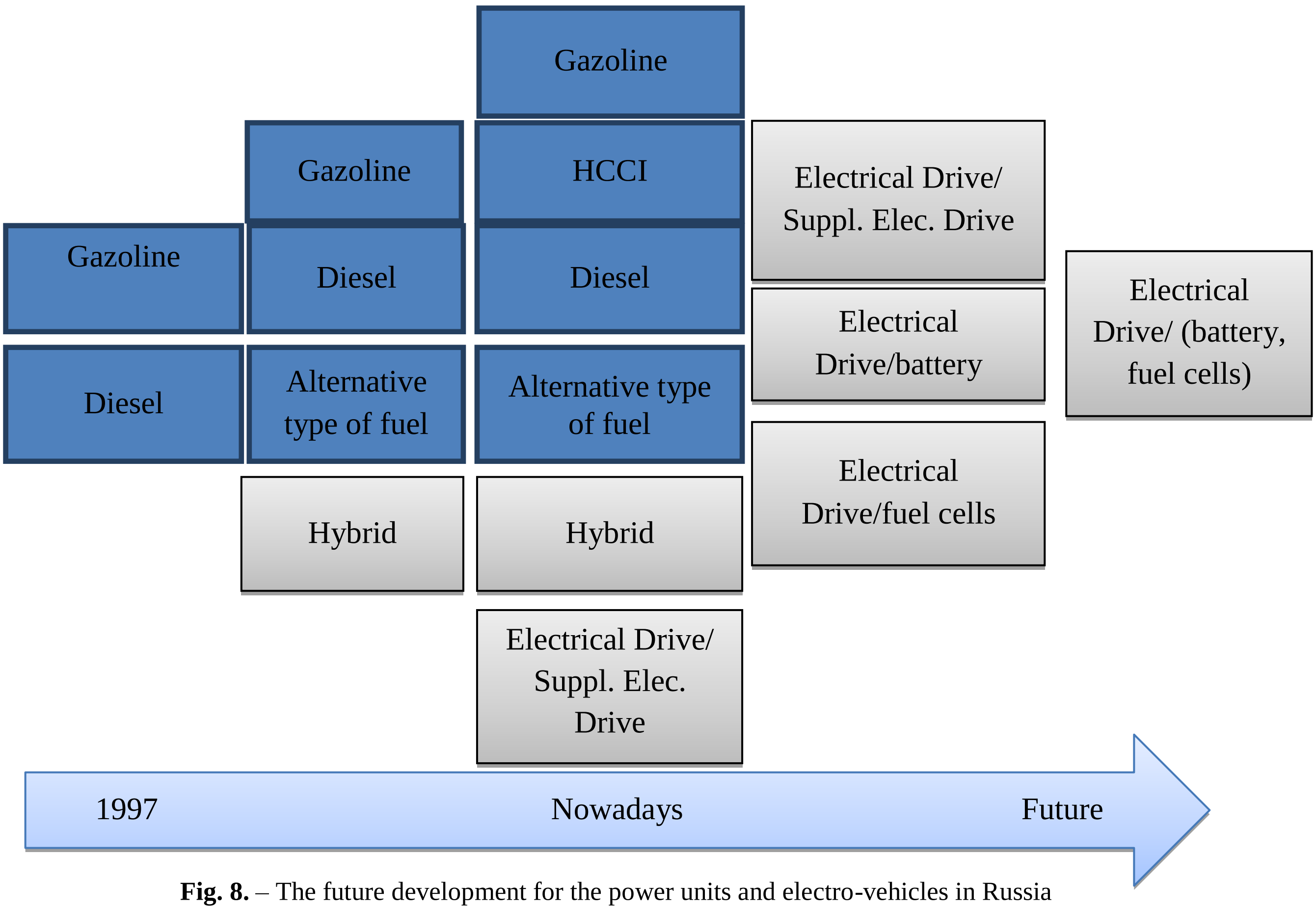

Fig. 8. – The future development for the power units and electro-vehicles in Russia

Nowadays there are four types of mobile electrical units with autonomous power supply, two of which – with the traction rechargeable batteries (TRB) and a combination of the internal combustion engine (ICE) and TRB – are the most widespread. Mobile electrical units with TRB have found mass application as inland transport of the enterprises of various types. Inter-economic transportations are rather complicated because of a small stock for the movement and lack of an opportunity for intermediate TRB charging on a route, i.e. due to the lack of a service network. Mobile electrical units with ICE and TRB are deprived of the main lack of electrical units of the first type, however their mass application, first of all, as vehicles, is restrained by the complexity of a design, and, respectively, unavailability of the existing enterprises of technical service for their maintenance and repair.

The research works which has been being carried out until recently in scientific divisions of higher education institutions and branch scientific research institutes, in the connection with that fact that they are not required by automobile construction enterprises, are rooting extremely slowly because of this, the lag in this area from foreign countries becomes more notable. On the practical level a lot of work in this direction has been performed in MSAU named after V. P. Goryachkin and some other higher education institutions (Fig. 9). In MSAU the concept of creation of the combined power stations has been developed for application in traction vehicles.

Fig. 9. – The mobile electric-powered units, having been developed in MSAU named after V.P. Goryachkin

The development of mobile electrical units for transportation purposes is being conducted worldwide. Foreign producers have created a line of vehicles of loading capacity on the basis of the serial and specially designed chassis, the Russian developers have planned the main characteristics of perspective electrical units for transportation purposes only on the basis of serial chassis (DIDMANIDZE, 2015).

The design of similar vehicles began with category M1 vehicles on classification of UNECE worldwide, having gradually extended to the categories M2 and M3. The work with the category N1, i.e. with trucks, has begun after receiving a certain effect (more often ecological in operation, but not in full life cycle) from operation of small-scale examples of category M.

The creation of equipment for inner-economic transportations on the basis of the Belarus-920 tractor and the recharged passenger vehicle of a small class (Tab. 3) (DIDMANIDZE, 2015) became the newest developments in a scope of mobile electrical units.

Tab. 3. – The technical features of the mobile electric units for the transportation purposes having been developed in Russia

Basic model	VW Caddy Maxi	Ford Transit	KamAZ-65115-Electro	Tractor Belarus
Electric motor	Siemens	Azure Dynamics	Trolleybus	Azure Dynamics
Power of electric motor, kWT	61	57	189	60
The capacity of one cell, A·h	160	300	300	160
The mass of one cell, kg.	5,6	9,6	9,6	5,6
The amount of cells, piec.	86	100	144	100
The overall mass of the batteries, kg.	481,6	960	1382,4	560
Maximum speed, km/h	130	75	75	Not available

Besides the application of hybrid transport technological machines, the perspective direction is the usage of gas fuel as one of the most really applicable amongst alternative ones. The problems, ecological orientation and an economic orientation are at his expense solved.

In recent years a number of important documents have come into force. First of all, It should be noted the Federal law "About energy saving..." and the order of the Prime Minister to the executive authorities and organizations about the preparation and providing the comprehensive program of the stimulation of application of the natural and liquefied hydro-carbonic gas as motor fuel. The law would become the basis for the formation of the state order for acquisition of the cars completed with the gas-balloon equipment (GBE) and transfer to the propane for the departmental transport of the organizations financed from the state budget that can give economy to 1 billion rubbles a year (VASIL'EV, 2015).

The transition of automobiles to the alternative types of fuel is, in fact, actual and essential. Domestic car makers began to release more willingly gas-balloon automobiles (GBA), but not all and not in the volumes demanded really. In leaders is KAMAZ with the RARITEK subsidiary which has mastered the release of several models of trucks and city buses NEFAZ, and also "GAZ Group" with "Gazelles" and LiAZ buses. In 2010 GAZ issued about 1, 2 thousand gas-balloon "Gazelles", and approximate output in 2016 – about 4 thousand cars have been let out. Many cars will be also turned on gas-balloon equipment by small firms, which are specializing on this. At the same time the total of gas-balloon cars will only grow, having reached half a million units only on trucks and buses without automobile transport (Fig. 10) (VASIL'EV, 2015; MORDOVCEV, 2011; PROHOROV, 2011).

The exploitation of gas-balloon cars is impossible without the creation of system of supply with fuel. The system of supply with the compressed natural gas (CNG) for GBA gas station is based on the available network of automobile gas-filling compressor stations (ACNG filling station) of various power or mobile refueling units (PAGZ - MRU).

Nowadays in Russia there are 211 ACNG filling stations making from 220 to 500 gas stations a day. ACNG filling station capacities are used for 25% so far.

Gas stations with the usage of the mobile refuellers located directly at the enterprise, on platforms near highways and on the highway on the platforms adjoining gas stations and also in field conditions, turns out to be economically for the consumer who is situated from the station on the distance 10 to 70 km (RYBAKOV, 2004).

The application of mobile gas-filling means in comparison with gas station of transport directly from the ACNG filling station increases the prime cost of CNG, but cuts transportation costs of consumers due to the elimination of single run of GBA that can be useful at the organization of work of agricultural machinery separated from the central estate.

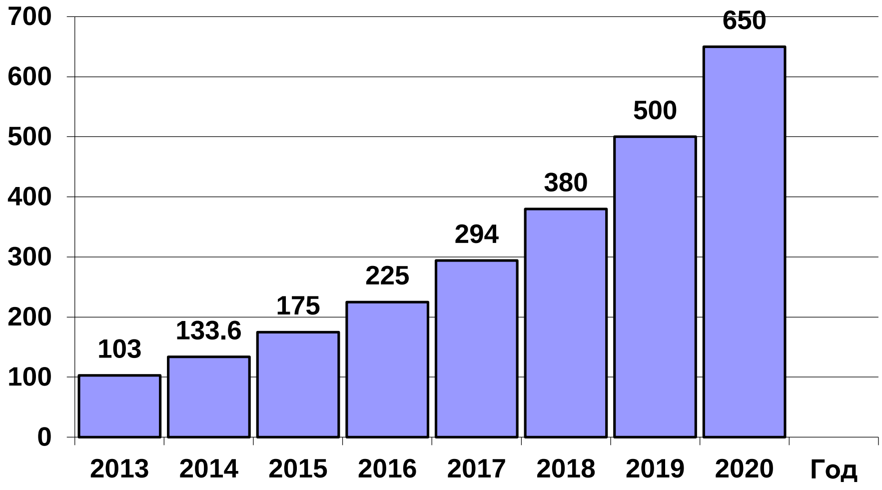

Fig. 10. – The total amount of automobile park using the gas as fuel, units

PAGZ or MRU can be applied as the transported gas-accumulators. At the same time on the platform of gas station the stationary gas-filling station (GFS) for 4 to 6 posts (as well as on the ACNG filling station) is equipped to which CNG is delivered by MRU, filled on powerful CNG filling stations. In this case the equipment of MRU considerably becomes simpler as the equipment for gas station of cars, the commercial accounting of the filled gas, difficult fittings of switching of sections (DIDMANIDZE, 2012) isn't required.

Thus, this technology of the MRU appliance gives the chance to solve the problem of mass gas station of cars at the enterprise, even taking into account the peak loadings on gas consumption, at an exit of cars to works. 18 technological schemes of supply with the usage of mobile and stationary gas-re-fuelling stations have been developed for providing machine and Tractor Park with natural gas in the GNU "VIM" still in the late nineties – the beginning of the 2000-th year. The garage gas-refuelling station, working from household gas networks has been developed for agricultural and transport enterprises in VNIIGAZ. At the beginning of the 2000th years more than five enterprises let out sets and separate units of the filling equipment, now their production is forced out by foreign producers, as a rule, the Italian. Domestic producers began to offer the container modules of storage and the CNG filling station (LLC RARITEK).

Having considered the features of the formation of park of vehicles, improvement and prospects of a transport design and transport technological machines on the basis of application of new power sources and new fuels, it is necessary to pass to the organizational stage of work of the automobile transport.

The comprehensive control and the effective usage of park of transport technological machines – an important condition in order that agricultural and transport enterprises to remain competitive in the Russian and foreign markets in the conditions of integration of the Russian Federation into the World Trade Organization.

The major factors defining an organizational technological level and efficiency of performance of these transport productions are:

- the reduction of duration of a cycle of process in connection with combination of operation of basic and transport cycles;
- the continuity and the threading of process;
- the rhythm of course of process;
- the reliability of the cars which are carrying out separate operations.

To give an essential impulse towards the improvement and optimization of transport productions can give the more active usage of modern hi-tech achievements to which the means of global satellite network belong (BOROVICKIJ, 2014). However, even taking into account that the appliance of means of satellite communication became recently considerably more available to the ordinary consumer, their application, especially in agro-industrial complex, is insufficiently active. The main reasons for the insufficient use of opportunities of system are:

- The lack of sufficient regulatory base for use of satellite technologies in agriculture;
- The lack of mechanisms of promoting and stimulation of use of satellite systems in agriculture;

- The absence of necessary number of the qualified users satellite systems;
- The lack of high-precision hardware elements of satellite system, available at cost (it is actual for systems of exact agriculture).

The usage of means of satellite communication can give synergetic effect in case of application in transport productions.

1 During the application of freight processes for the transportation of agricultural and food production the following tasks are being realized:

- The finding out the possible location of the car;
- The tracking of loading of the car with collecting and data transmission about the potential deliveries of freight to the consumer for the purpose of optimization of processes of reception and unloading, management of freight traffics;
- The tracking of a condition of freight, for example, temperatures in transit the cooled or frozen freights, providing the IFS and HACCP standards;
- The tracking of actions of the operator, in particular opening and closing of a body, raising of a body of the dump truck, etc.
- The control of technical condition of the car and the trailer with collection of data on fuel consumption, pressure in tires, a condition of brake system allowing to lower operational expenses.

2 The usage of means of satellite communication in production and technological processes of cultivation of agricultural and commercial crops allows the passing to the exact agriculture, using geo-information technologies and providing the adoption of optimal solutions on management of activity of the agricultural enterprise.

When using satellite technologies at cultivation of crops the following problems are solved:

- The automation of processes of management of equipment (parallel driving, auto-piloting) on the basis of systems of navigation when carrying out the technological operations providing high precision of crops, uniformity of rows etc.
- The drawing up soil cards of farms with use of automatic samplers;
- The monitoring of a condition of fields and crops;
- The differentiated application of fertilizers;
- The automatic monitoring of productivity and drawing up cards of productivity, and in the long term cards of profitability of sites of fields;
- The monitoring of technical condition of harvest and landing equipment, other power saturated cars;
- The planning of statement of cars on maintenance on loading;
- The accumulation and data storage, the processes and to carry out the multiple-factor analysis for the long period allowing to trace dynamics.

Finishing the consideration of prospects of development of the automobile transport, it is necessary to stop on the important direction without which the solution of those tasks and problems which have been designated above is impossible. This direction is training, and it is not only training of graduates with the high education, but also the preparation of the scientific personnel capable to realize and develop the designated directions.

CONCLUSIONS

The scientific work is being conducted in several directions reflecting all aspects of operation of transport technological machines.

The first direction considered the development of energy saving traction vehicles, meaning the development of designs and technologies of ensuring operability of new types of cars.

The second direction considered the improvement of methods of usage and management of work of transport technological machines. Here the mutual and beneficial work with VIM and other researching institutions is possible too for example the assessment of technological capabilities of the transport technological machines used in agro- industrial complex for the purpose of determination of the operational properties which are most adapted for transfer to gas without loss. The definition for the list of technological operations and transport works, where the usage of the installed gas-balloon equipment on cars is the most effective. The future perspectives of the appliance of serial cars in agro-industrial complex are being taken into consideration too.

The third direction considered the researches in the field of improvement of technical service of transport technological machines at all stages of their usage – from the delivery to the enterprise to the utilization upon the coming to the point of the destination. From the perspective researches it is possible to present, for example, an assessment of a condition of technological base of the enterprises and the choice of the preparatory activities which are most adapted for carrying out the ensuring filling and technical operation of TTM working at gas. Such difficult work can also be conducted together with VIM and STATE PLANTS. Consideration of technological processes of technical service of new types of transport technological machines can be conducted together with GOSNITI.

As authors considered, the fourth direction regards the researches in the field of improvement of quality of traditional types of fuel and the appliance of alternative fuels. From the perspective researches it is possible to allocate, for example, the creation of inter-economic associations' operators for the management of park of mobile funds of TTM gas station from GBO, the development of onboard and stationary means of improvement of quality of the fuels intended for the equipment used in the conditions of agro-industrial complex.

REFERENCES

1. AVTOTRANSPORTNYE I TRAKTORNYE PEREVOZKI: UCHEBNIK. / O. N. Didmanidze [i dr.] M.: UMC «Triada», 2005: 552 p.
2. EVTJUSHENKOV, N. E., HABATOV, R. SH.: Nauchnye osnovy razvitija perspektivnoj sistemy transportnogo obsluzhivanija sel'skohozjajstvennogo proizvodstva: monografija. M. : Put' Art, 2004: 192 p.
3. DVE TRETI GRUZOVYH AVTOMOBILEJ V ROSSII – starshe 15 let [Jelektronnyj resurs]. Rezhimdostupa: http://www.autostat.ru/infographics/22363/.
4. POLJAKOVA, I.: Gosprogramma i podderzhka // Rejs. 2013. № 6. pp. 12–21.
5. DIDMANIDZE, O. N., ESENOVSKIJ-LASHKOVJU, A., PIL'SHHIKOV, V. L.: Specializirovannyj podvizhnoj sostav avtomobilej agropromyshlennogo kompleksa. – M.: UMC «TRIADA», 2005: 200 p.
6. POLJAKOVA, I.: Nash staryj park // Rejs. 2011. № 6. pp. 6–10.
7. POLJAKOVA, I.: Markiiregiony // Rejs. 2012. № 5. pp. 6–10.
8. IPATOV, A. A., DZOCENIDZE, T. D.: Sozdanie novyh sredstv razvitija transportnoj infrastruktury. Problemy i reshenija. M. :Metallurgizdat, 2008: 272 p.
9. DZOCENIDZE, T. D., KOZLOVSKAJA, M. A., ZAGARIN, D. A., ZHURAVLEV, A. V., KABANIN, P. A.: Avtomobil'nyj transport dlja malyh form hozjajstvovanija. Konstrukcija i osobennosti jekspluatacii: monografija. – M.: Metallurgizdat, 2011: 288 p.
10. CHERNJAVSKIJ, M., KOLHOZNIKI // Avtorevju. 2015. № 24. pp. 58–59.
11. IZMAJLOV, A. JU.: Tehnologii i tehnicheskie reshenija po povysheniju jeffektivnosti transportnyh sistem APK. M.: FGNU «Rosinformagroteh», 2007: 200 p.
12. DIDMANIDZE, O. N., ASADOV, D. G., MITJAGIN, G. E., KAREV, A. M.: Tehnicheskaja jekspluatacija mobil'nyh jelektroagregatov: monografija. M.: OOO «UMC «Triada», 2015: 226 p.
13. PROIZVODSTVO I PRODUKCIJA KOMPANII: Drive Electro [Jelektronnyj resurs]. Rezhim dostupa: http://www.drivelectro.ru/views/production/.
14. VASIL'EV, V.: O perspektivah razvitija jelektronnyh pasportov, gazomotornoj tehniki i polnocennoj sistemy utilizacii vyshedshih iz jekspluatacii transportnyh sredstv // Avtomobil'nyj transport. 2015. № 8. pp. 32–40.
15. MORDOVCEV, N.: Pribav' gazu // Rejs. 2011. № 10. pp. 14–28.
16. PROHOROV, O.: Obdumannyj vybor // Rejs. 2011. № 11. pp. 16–27.
17. RYBAKOV, K. V., DIDMANIDZE, O. N., KARPEKINA, T. P., PULJAEV, N. N.: Avtozapravochnye processy i sistemy v polevyh uslovijah. M.: UMC «Triada», 2004: 292 p.
18. DIDMANIDZE, O. N., SOLNCEV, A. A., MITJAGIN, G. E.: Tehnicheskaja jekspluatacija avtomobilej. M.: OOO «UMC Triada», 2012: 455 p.
19. BOROVICKIJ, D.: Upravlenie parkom // Rejs. 2014. № 9. pp. 10–20.

Corresponding author:
prof. Didmanidze Otari Nazirovich Ph.D., member correspondent of the Russian Academy of Sciences, Russia, e-mail: didmanidze@timacad.ru

TIDAL EFFECTS ON SMALL CATCHMENTS

Š. Dvořáková, J. Zeman

Department of Mathematics, Faculty of Engineering, Czech University of Life Sciences in Prague, Czech Republic

Abstract
The content of this article is the analysis of the tidal effects on the flow which is measured on a long-term basis. Influence of the Moon gravity leads to a movement of fluid in the upper layer of the Earth's cover. As a result, a greater amount of water is expelled into the water flow periodically with a period of 12 hours. In this paper we deal with the analysis of this contribution. Size of the tidal contribution is changing with the time depending on the distance and position of the Moon and the Sun. We present the results of the analysis from few weeks data obtained during rainless period. The mean values of the tidal effects on the flow measured by us make 0,074 ± 0,069 l/s for Teply Brook and 0,012 ± 0,008 l/s for Starosuchdolsky Brook.

Key words: tides, Fourier analysis, water discharge, stream.

INTRODUCTION

While in the coastal areas the observation of the tide is relatively easy and applies to life of practically all the people in this area, in the conditions of the Czech Republic it is necessary to do the observation by using measuring techniques.

Usually, the observation of tidal effects is carried out in the undrawn wells. While the movement of free oceans fluid is causing a tidal wave with amplitude of normally a few meters, fluid flowing through the porous rock causes oscillation of just about several centimetres in the wells.

For example, the well KV1 oscillates at an amplitude of about 12.5 cm. However, from the wells observed so far, it is the highest value. It is interesting that the change of the gravitational acceleration is able to cause oscillation in some wells in the antiphase against the assumed monthly flow.

This effect is explained by the declination of the relatively freely stored plate in the vicinity of the well. Wells with antiphase are found, however, only very rarely (e.g. KV18). In most cases the classic tidal wave is observed. For this reason, the overall contribution of the tidal effects on the levels of surface flows is positive.

And so if the Moon is in the zenith and also 12 hours after, the amount of water flowing from the spring is higher. The tidal analysis of several streams is followed for example by RENSEL, FORSTER (2003). In addition to the Moon in some cases also the effect of the Sun position at the flow rate of the stream is evident. However, it is approximately 12 times weaker.

The biggest change of the gravitational acceleration and therefore, even the strongest tidal effects occurre always during the eclipse of the Moon or the Sun, because the effect of both elements adds together. The calculation is elegantly executed in the work by MOŠNA (2014). If, therefore, we monitor with a sufficiently fine resolution the flow rate of the unregulated water flow, there is a fair chance to detect the contributions of the tide.

We have chosen for the analysis of these effects two of the four catchments measured by our group, namely Teply Brook catchment and Starosuchdolsky Brook catchment.

MATERIALS AND METHODS

The **Teply Brook catchment** is located about 25 km south from the town of Žďár nad Sázavou, Czech Republic. The catchment characteristics were derived from a detailed GIS analysis, and they are summarised in Tab. 1. The elevation ranges from 417 m to 602 m, with a mean elevation slightly over 500 m. The mean catchment slope is about 22 %, with maximum slopes more than 55 % occurring in the middle part of the catchment. The geology of the catchment is composed mainly of metamorphic rocks (gneiss, amphibolite, migmatite). In the lower elevations of the catchment area it is composed mainly of peridotite and serpentinite. Alluvial deposits of loamy sands and gravels occur at the valley bottom.

As far as the soil composition is concerned, forms of cambisols and ceptosols are typical for the catchment area, and are present as haplic cambisols, alcalic or

cambic leptosols. In the valley of the stream we find fluvic cambisols and gleysols (FAO-WRB 2006).
The prevailing land use is a mixed semi-natural forest of spruce *(Picea abies)*, pine *(Pinus sylvestris)*, hornbeam *(Carpinus betulus)* and alder *(Alnus incana)*. Arable land is found only in the southern part of the catchment area. The climate is moderately warm and humid, with estimated mean annual precipitation of 650 – 750 mm, and mean annual temperature of 7 °C.

Tab. 1. – Characteristics of the Teply Brook catchment

A	Catchment area	1.56	km^2
L_{th}	Length of thalweg	1.41	km
L_{MF}	Length of main river	1.10	km
P	Length of water divide	5.13	km
B	Average width of catchment	1.10	km
I_R	Average slope of river	13.0	%
I_S	Average catchment slope	15.1	%
$H_{max.}$	Maximum catchment elevation	595	m a.s.l.
$H_{min.}$	Minimum catchment elevation (outlet)	417	m a.s.l.

The **Starosuchdolský Brook catchment** is located at the north side of Suchdol village, which is now part of the Prague Metropolitan area. The Starosuchdolsky brook rises at an elevation of 230 m The length of the stream (to the outlet) is 580 m, and the catchment area is 2.95 km^2. The brook forms a right side tributary to the Uneticky brook, which flows into the Vltava River. The catchment area characteristics have been derived from a detailed GIS analysis, and they are summarised in Tab. 2.
The morphology of the catchment area is mostly flat, with a slope of up to approximately 5 %. However, the slopes in the forested part of the catchment area are up to 36 %. The shape of the catchment area is elongated; in the South West part of the catchment, the highest point is at an elevation of 335 m and the outlet is located at an elevation of 211 m.
Geomorphologically, the site of the catchment area falls within the district of the Tursko plateau, which is formed mainly from upper proterozoic and cenomanian conglomerates, sandstones, clay stones and sponge-spicule rock (spiculites). The bedrock of the forested slopes near the Starosuchdolsky brook is formed by proterozoic siltstones and graywackes, which rise up on the surface in places with a higher slope. However, most of the base is formed by loess, loamy sands and debris, as a result of geological processes during the quaternary period.

Tab. 2. – Characteristics of the Starosuchdolsky Brook catchment

Catchment area/ basin	km^2	A	2.946
Maximum catchment elevation	m a.s.l.	H_{max}	335
Minimum catchment elevation (outlet)	m a.s.l.	H_{min}	211
Elevation of brook source	m a.s.l.	H_{pr}	230
Length of thalweg	km	L_{th}	3.7
Length of brook	km	L_b	0.58
Length of catchment divide	km	P	9.1
Average slope of brook	%	i_b	5.4
Shape of catchment	-	A	0.2

As the soils types are mostly haplic fluvisols, gleysols and cambisols, the prevailing land use is arable land (53 %) and urbanised areas (36 %). The forest area is a mix of semi-naturals. Besides arable land and an urbanized area, with a relatively high population density, the downstream part of the catchment is environmentally protected in its riparian belts by a valuable canopy. These river belts, situated on both sides, contain typical local forest species, represented by alder (*Alnus glutinosa*), ash (*Fraxinus excelsior*), oak (*Quercus robur*), and sporadically hornbeam (*Carpinus betulus*). The climate is moderately warm and semiarid, with an estimated mean annual precipitation of 350 – 400 mm, with a mean annual temperature of 8.8 °C.

The water column was measured at 1.0 m upstream by the Vegawell 71 submersible level gauge and the V-notched weir (Figs. 1a, 1b) with a sapphire membrane, having a range of application from 0.0 m to 1.0 m. The water levels were measured on both experimental catchment profiles. The Drak3 AD converter was used for digitization. The data was stored in a standard PC, installed in the Technical Maintenance building of the alternative storage for fuel from the Skalka Nuclear Power Plant (Teply Brook) and Spaleny Mlyn residence (Starosuchdolsky Brook), reported by ZEMAN (2007).

The discharges of the two catchment areas were determined from the water levels on the Thomson spillway, which was located at their outlets (Figs. 1a and 1b).

Fig. 1a – Hydrometric profile on the Teply Brook

Fig. 1b – Hydrometric profile on the Starosuchdolsky Brook

In the time series of the discharge data, a component with 12 hour period was found. This was realized by fitting data by function (1).

$$Q(t) = \sum_{i=1}^{3} V_i e^{-\frac{t}{\tau_i}} + \sum_{i=1}^{2} A_i \sin\frac{2i\pi t+\varphi_i}{86400} \qquad (1)$$

where

V_i … tributaries of individual soil zones (l/s)

τ_i … relaxation times of the depletion of soil zones (s)

A_i … the elements of the periodic expansion (l/s)

$Q(t)$ … discharge depending on the time (l/s)

t … time (s)

φ_i … phases of the day (s)

Eq. (1) corresponds to the zone depletion in DVOŘÁKOVÁ, ZEMAN (2014) and to the influence of evapotranspiration in the coefficient A_1, which represents the first member of the harmonic expansion. The second member of the harmonic expansion includes tidal and therefore double frequency. The intensity of this effect is given by the coefficient A_2.

To this component, for each day separately, also phase φ_2 of this signal and the moment of the maxima have been found. Sunrises and sunsets and moonrises and moonsets were found in the astronomical yearbooks. The moments of the maxima were correlated with the predicted maxima of the tide occurrence, therefore, with the moments when the Moon is in the zenith. From the difference of these times of maxima a delay has been found caused by the time of flow of expelled water through the porous rock and the time of flow of this already free surface water through the basin to the place of the closing profile.

RESULTS

The Fig. 2 shows an example of a well visible tides on Starosuchdolsky Brook on 26th July 2013. In the figure, the measured data and the best fitting by function (1) are shown.

Fig. 3 shows the phase φ_2 (eq. 1) on the moments of the tidal maxima. The coefficient of determination of these moments is $R_1^2 = 0{,}4755$ for Teply Brook.

Fig. 4 shows the phase φ_2 (eq. 1) on the moments of the tidal maxims. The correlation coefficient of these moments is $R_2^2 = 0{,}4261$ for Starosuchdolsky Brook.

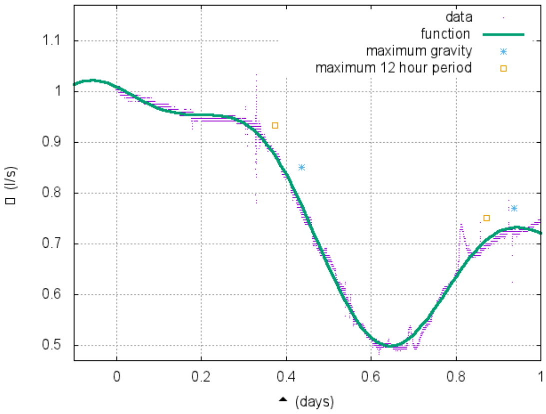

Fig. 2. – Example of tides on Starosuchdolsky Brook

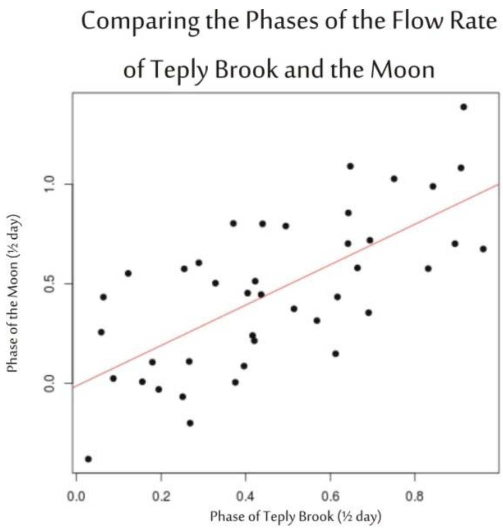

Fig. 3. – Dependence of discharge maxima of Teply Brook on the moments of gravitational acceleration maxima

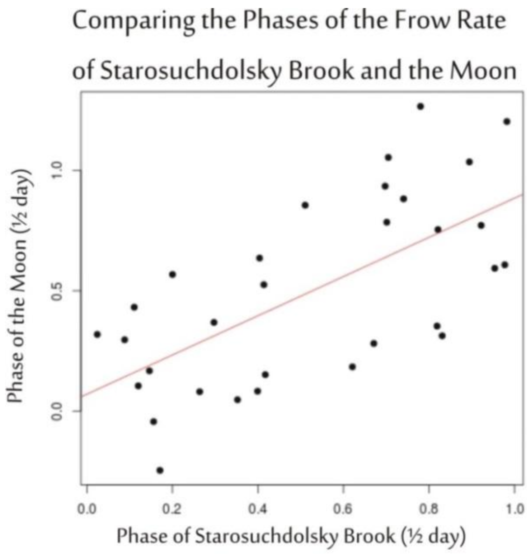

Fig. 4. – Dependence of discharge maxima of Starosuchdolsky Brook on the moments of gravitational acceleration maxima

Tab. 3. shows the comparison of the mean values of the moments of the maxima of the second members of the harmonic expansions according to the eq. (1) with the predicted maximum tidal effects according to the immediate astronomical constellation of the individual catchments, where $s_{\varphi 2}$ are standard deviations of mean values of time delay.

Tab. 3. – Mean values of discharge delay after gravitational acceleration maximum

	Teply Brook	Starosuchdolsky Brook
$\bar{\varphi}_2(s)$	4200	600
$s_{\varphi_2}(s)$	13000	14000

DISCUSSION

As we found out on the example of the two small catchments the tidal effect is still noticeable and demonstrable. The coefficient of determination R^2 is proving this. Generally, the more tributaries there are in the catchments, the possibility of detection of tidal effects in the resulting flow detect is worse. This is due to the fact that in the flow of the various tributaries tidal effects occure with different phases and the mutual uncoherency of these tributaries makes the detection of tidal effect less easy in summation of flow rates in the resulting bigger flow.

Tab. 3 shows that average delay of the maximum discharge after gravitational maximum is practically zero for Starosuchdolsky brook and therefore the increase of the gravitational acceleration causes a pressing out of water from the subsoil. In the case of Teply Brook the delay of the maximum discharge after gravitational maximum is negative, and thus pores in the Earth's layer are opening by the influence of gravity, they acquire water and this results the loss of the water flowing through the river basin.

The phase delay is given in accordance with GEORGAS (2001) from 17,5° to 355,1°for Stony Brook Harbor, Long Island, New York, which calculated to a time corresponding to a delay from 36 minutes 14 seconds to 12 hours 15 minutes 5 seconds. Our results are similar for both brooks, i.e., for Teply brook 1 hour 10 minutes and for Starosuchdolsky brook 10 minutes. However, it is important that the tidal influence on both of us measured brooks was approved, because the tidal signal is often immeasurable for many basins due to infiltration and the addition of tributaries.

A better correlation result could be reached when using the actual period of the tide, i.e. 12 hours, 25 minutes and 14 seconds. We, however, tried for the development of the series as the second harmonic frequency to 24 hourly cycle of evapotranspiration.

CONCLUSIONS

We managed to detect the influence of the tides on the flow rate through the basin by harmonic analysis of the flow on the two small catchments (1,5 km^2 and 3 km^2) by adding a second member. The coefficients of determination R_1^2 and R_2^2 showed that there really are tidal effects. These coefficients show a strong dependence between the moments of the phase maxima of the gravitational acceleration and the flow rate. The value of secondary delay between the maxima of these signals gives evidence about the mechanics of the bedrock of the catchments.

REFERENCES

1. DVOŘÁKOVÁ, Š. – ZEMAN, J.: Conditions of Physical Solvability of Two- and Three-zone Linear Storage Models. Scientia Agriculturae Bohemica, 2014, 45, 2, pp. 117-123. ISSN: 1211-3174, doi: 10.7160/sab.2014.450207.
2. FAO-WRB 2006 IUSS Working Group WRB: World reference base for soil resources 2006. 2nd edition. *World Soil Resources Reports* No. 103. FAO, Rome.
3. GEORGAS, N.: Tidal Hydrodynamics and Bedload Transport in a Shallow, Vegetated Harbor (Stony Brook Harbor, Long Island, New York): A Modeling Approach with Management Implications, State University of New York, 2001.
4. http://web.stevens.edu/ses/documents/fileadmin/documents/pdf/GeorgasThesis1.pdf.
5. MOŠNA, F.: From Newton to Kepler, Italian Journal of Pure and Applied Mathematics, 2014, 32, pp. 393 – 400. ISSN 2239-0227, http:// ijpam.uniud.it/online_issue/201432/35-mosna3.pdf.
6. RENSEL, J.E. – FORSTER, J.R.M.: Strait of Juan de Fuca, Offshore Finfish Mariculture: Feasibility Study , 2003, NOAA National Marine Fisheries Service.
7. http://www.lib.noaa.gov/retiredsites/docaqua/reports_noaaresearch/juandefucarept.htm. ZEMAN, J.: Nasazení kamer s vysokým rozlišením v meteorologii (Deploying high-resolution camera in meteorology), Jemná mechanika a optika, 2007, 52, 5, pp. 150–15.
8. ZEMAN, J.: Nasazení kamer s vysokým rozlišením v meteorologii (Deploying high-resolution camera in meteorology), Jemná mechanika a optika, 2007, 52, 5, pp. 150–15.

Corresponding author:
Ing. Šárka Dvořáková, Ph.D., Department of Mathematics, Faculty of Engineering, Czech University of Life Sciences in Prague, Kamýcká 129, 165 21 Prague 6, Prague, Czech Republic, phone: +420 22438 3240, e-mail: dvorakovas@tf.czu.cz

EDGE DETECTION IN FICUS CARICA TREE IMAGES USING FUZZY LOGIC

I. Gravalos, D. Kateris, T. Gialamas, P. Xyradakis, N. Alfieris, P. Pigis

Department of Biosystems Engineering, Technological Educational Institute of Thessaly, School of Agricultural Technology, Greece

Abstract
Edge detection is an essential part of image processing, computer and machine vision. Numerous edge detection methods have been developed in the last years that can be summarized into two basic categories: gradient based and zero-crossing. All classical operators identify a pixel as a particular class by carrying out some series of operations within a mask centered on the pixel under observation. Recent researches have concentrated on the most accurate classification methods that include fuzzy logic, artificial neural networks, etc. This study shows how to detect edges in ficuscarica tree images based on fuzzy set theory. The fuzzy logic for edge detection using membership functions define the degree to which a pixel belongs to an edge or uniform region. The results are compared to classical operators. The proposed fuzzy image-processing algorithm has shown greater accuracy compared to other edge detection techniques, and avoids obtaining double edges.

Key words: fuzzy logic, edge detection, image processing, ficuscarica tree.

INTRODUCTION

Edge detection is an essential part of image processing, computer and machine vision. Edges are changes in intensity values of neighboring pixels in an image that occur on the boundary between different regions (MAINI AND AGGARWAL, 2009). If an image is composed of objects and contrasting background, an edge is a transition from background to object or vice versa (GOSE ET AL., 1996).

Many edge detection methods have been developed in the last years and can be summarized into two basic categories: gradient based and zero-crossing. The gradient based methods detect edges by computing the maximum and minimum in the first derivative expression of an image. The zero-crossing methods search for zero crossings in the second derivative computed from the image. This is the basis for the gradient and zero-crossing edge detectors used to locate sharp changes in the intensity functions (SONKA ET AL., 1993). Here we will discuss some commonly used edge detectors. One of the early edge operators is the Roberts operator. It uses two 2x2 masks to compute the gradient across the edge in two diagonal directions. The disadvantage of the Roberts operator is its high sensitivity to noise. The Sobel operator is a discrete differential operator that utilizes two 3x3 masks, the first one estimates the gradient in the x-direction while the other estimates the gradient in the y-direction. It is less sensitive to noise but its smoothing affects the accuracy of edge detection. The Prewitt operator, similarly to the Sobel operator, uses the same equations except the constant, which is equal to 1 (HARALICK AND SHAPIRO, 1992).

The Laplacian operator searches for zero crossing in the second derivative of the image to find edges. As a second derivative, the Laplacian is unacceptably sensitive to noise. Its magnitude produces double edges and it is unable to detect the edge direction (GONZALEZ AND WOODS, 1992). Therefore an operator that combines both smoothing and differentiating in the same operator is desirable. This could be done in separate steps. Firstly, it may smooth an image with a binomial operator in order to reduce the noise, and then a discrete Laplacian operator can be applied to this smoothing image so as to detect the edges. A combination consisting of a Gaussian operator followed by a discrete Laplacian operator is called Laplacian of Gaussian operator (LOG operator) (SOLOMON AND BRECKON, 2010).

The Canny edge detector is an operator that can be implemented in the following steps: smooth image with a Gaussian filter, compute the gradient magnitude using partial derivative, remove pixels that are not part of an edge by applying non-maxima suppression to the gradient magnitude, and detect edges by double thresholding (CANNY, 1986). The Canny edge detector is generally acknowledged as the best edge detection method developed to date.

All the above classical operators identify a pixel as a particular class by carrying out a series of operations within a mask centered on the pixel under observation. The classic operators work well in circumstances where the area of the image is in high contrast. However, classic edge detectors tend to give poor results for labeling edge pixels, when an edge represents a small grayscale jump (ALSHENNAWY AND ALY, 2009).

Recent research projects have concentrated to the most accurate classification methods that include fuzzy logic, artificial neural networks, support vector machines, etc. Image information is a very complex process, so fuzzy set theory used in image analysis can give us better effect compared to other computing methods (HU AND TIAN, 2006). Fuzzy image processing has three main steps: image fuzzification, modification of membership values, and if necessary, image defuzzification. The fuzzification (coding of image data) and defuzzification (decoding of results) are steps that make it possible to process images with fuzzy techniques. The main power of fuzzy image processing is in the middle step (modification of membership values) (MONDAL ET AL., 2012). LIU ET AL. (2016) describe a fuzzy inference engine for detecting image edges. Some membership functions (Gaussian and triangle) were used for designing the fuzzy inference system. By applying fuzzification and defuzzification, the relationship between input and output values was identified.

This paper shows how to detect edges in ficuscarica tree images based on fuzzy set theory. It has created a fuzzy inference engine to detect image edges. On the inference engine step, two Gaussian membership functions in two directions (horizontal and vertical) are used for input signals. Triangular membership functions, white and black, are used for the defuzzification step. Finally, the results are compared to classical operators.

MATERIALS AND METHODS

Ficuscarica tree images were acquired in plantation at MarkopouloMesogaias (Attiki, Greece). For image acquisition, a digital camera (Canon Power Shot SX530 HS) was used. The digital camera was mounted on a tripod to maintain stability. Images were acquired during the daytime from August to September for a total of 250 images. Two of the original images are shown in Fig. 1.

Fuzzy logic image processing was performed in the MATLAB environment (Mathworks, MA, USA). The developed algorithm includes the below steps: a) The original RGB images converted in gray scale for fuzzy analysis, b) The image gradients calculated along the horizontal (x-axis) and vertical (y-axis) directions, c) A fuzzy inference system created for edge detection, d) The image gradients (I_x and I_y) specified as inputs of edge of fuzzy inference system, e) The intensity of edge detected image specified as an output of edge of fuzzy inference system, f) The rules for fuzzy inference system specified to make a pixel black or white, and g) The fuzzy inference system was evaluated.

Fig. 1. – Ficus Carica tree original images

The fuzzy logic for edge detection allows the use of membership functions to define the degree to which a pixel belongs to an edge or uniform region. A zero-mean Gaussian membership function is specified for each input of the designed edge fuzzy inference system (Fig. 2). If the gradient value for a pixel is ‘0’ then it belongs to the zero membership function with a degree of 1. Standard deviations for the zero membership can be changed to adjust the performance of the edge detector. Increasing the values makes the algorithm less sensitive to edges in the image and decreases the intensity of detected edges (SUDHAVANI ET AL., 2014). Triangular membership functions, ‘white’ and ‘black’ are specified for the output of edge of the fuzzy inference system. Membership function plot for outputs of edge of the fuzzy inference system is shown in Fig. 3.

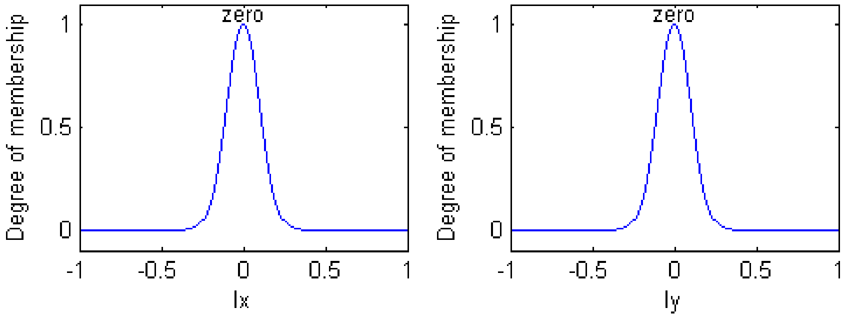

Fig. 2. – Gaussian membership functions in horizontal and vertical directions

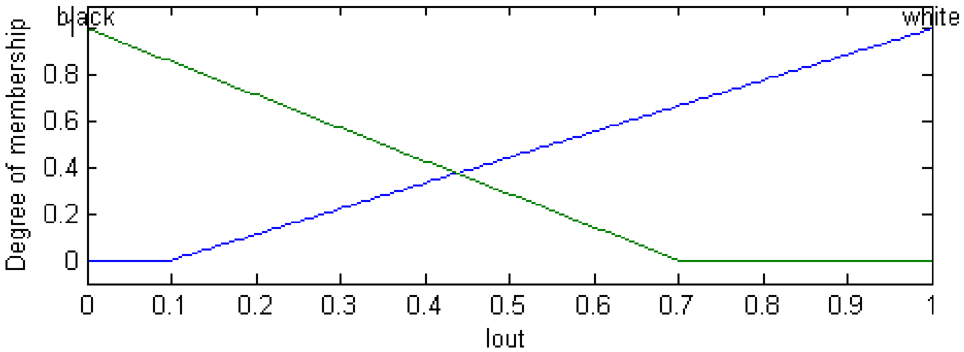

Fig. 3. – Output membership functions

The edges are detected using fuzzy inference system, by comparing the gradient of every pixel in horizontal and vertical directions. If the gradient for a pixel is not zero then the pixel belongs to an edge (black). The gradient is defined as zero using Gaussian membership functions for fuzzy inference system inputs. The edge detector performance is adjusted by changing the values of triangular membership functions in ‘white’ and ‘black’. The triplets specify the start, peak, and end of the triangles of the membership functions. These parameters influence the intensity of the detected edges.

RESULTS AND DISCUSSION

In this study, a simple fuzzy inference system is tested which has two fuzzy sets with Gaussian membership function for each input fuzzy variable and two fuzzy sets with triangular shape membership function as ‘white’ and ‘black’ for the output fuzzy variable while two fuzzy rules were simultaneously defined for it. Then according to the described fuzzy inference system, the edges of two ficuscarica tree images were detected.Fig. 4 shows the experiment results of the proposed edge detection algorithm. The input RGB original image converted in gray scale in Matlab (Fig. 4a) for fuzzy analysis. After specifying the image gradient along the horizontal (x-axis) and vertical (y-axis) directions, the fuzzy logic edge detection algorithm relied on the image gradient to find breaks in uniform regions. The outputs of the fuzzy inference system are shown in Fig. 4b and 4c. The fuzzy inference system allows edges to be detected even in the low contrast regions as shown in Fig. 4d. This is due to the different treatment given by the fuzzy rules to the regions with different contrast levels.

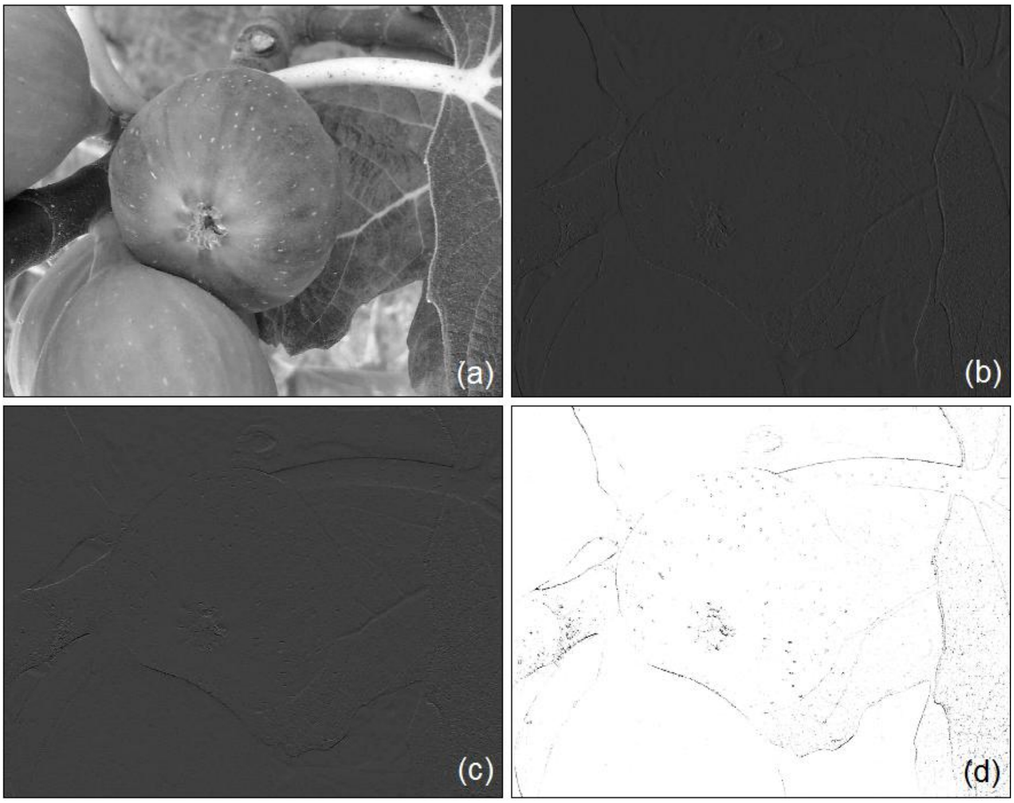

Fig. 4. – Proposed edge detection algorithm: a) Input grayscale image, b) Image gradient along horizontal direction, c) Image gradient along vertical direction, and d) Edge detected using fuzzy logic

The proposed fuzzy algorithm for image edge detection was tested for different values from the start, peak and end of the triangles of the membership functions. These values influence the intensity of the detected edges. The resulting images shown below in Fig. 5a and 5b compare the proposed fuzzy edge detection algorithm with triangular membership functions, white and black, for I_{out}: w_a=0.1; w_b=1; w_c=1; b_a=0; b_b=0; b_c=0.7 and w_a=0.6; w_b=1; w_c=1; b_a=0; b_b=0; b_c=0.99, respectively. It was observed that the output that has been generated by the I_{out}: w_a=0.6; w_b=1; w_c=1; b_a=0; b_b=0; b_c=0.99 has found out the edges of the image more distinctly as compared to the ones that have been found out by the I_{out}: w_a=0.1; w_b=1; w_c=1; b_a=0; b_b=0; b_c=0.7. In addition, it was tested for different standard deviations (s_x and s_y) for the zero membership functions for the image gradients (Ix and Iy) inputs. These values adjust the edge detector performance. The resulting images shown below in Fig. 5a and 5c compare the proposed fuzzy edge detection algorithm with standard deviations s_x=s_y=0.1 and s_x=s_y=0.01, respectively. It was observed that the output that has been generated by the standard deviation s_x=s_y=0.01 has found out the edges of the image more darkly as compared to the ones that have been found out by the standard deviation with s_x =s_y=0.1.

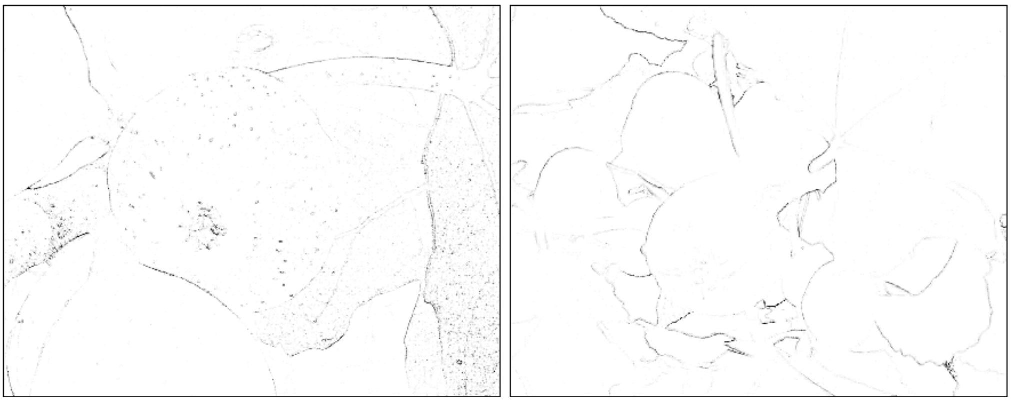

(a)

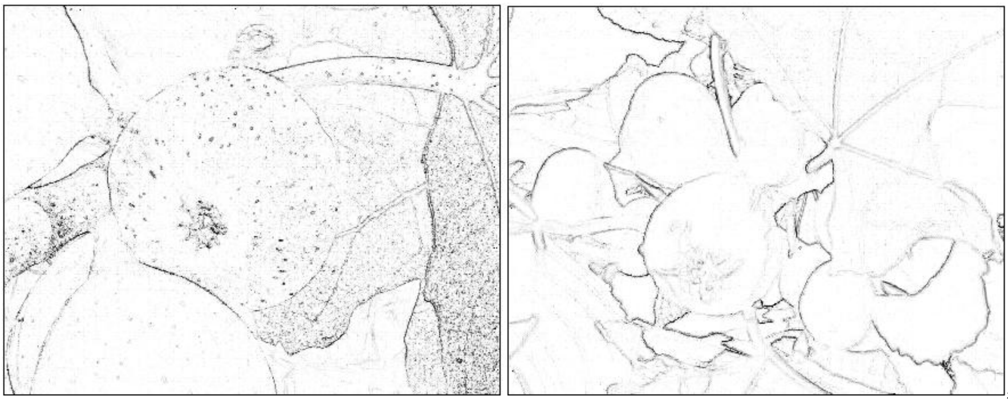

(b)

(c)

Fig. 5. – Resulting images of the proposed edge detected algorithm

The classical edge detection techniques (Roberts, Prewitt, Sobel, LOG, and Canny edge operators) of ficuscarica trees images are described in detail and tested on the article GRAVALOS (2013). As shown in Fig. 6, the resulting images of the proposed edge detected algorithm are compared with the existing classical edge operators.

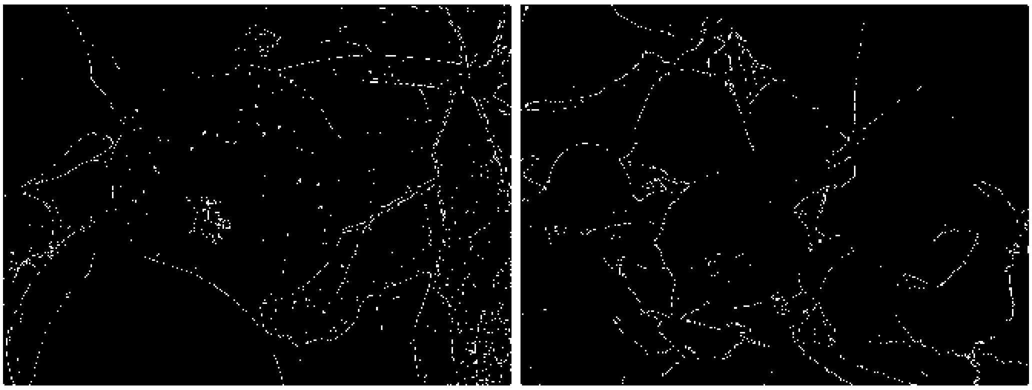

(a)

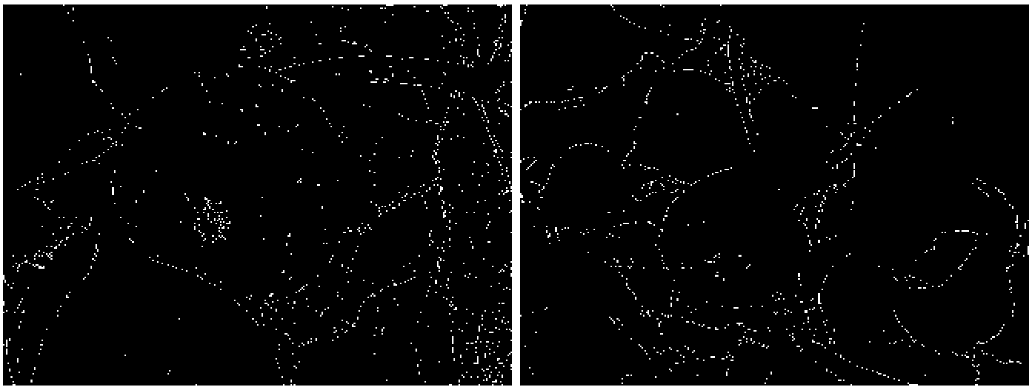
(b

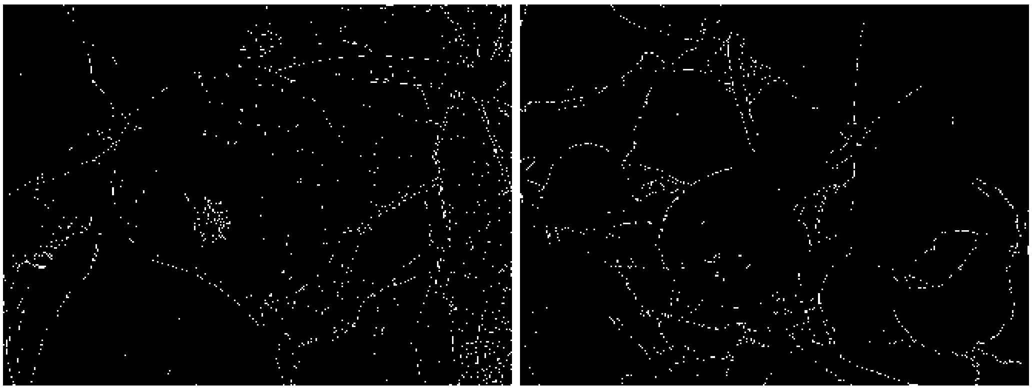
(c)

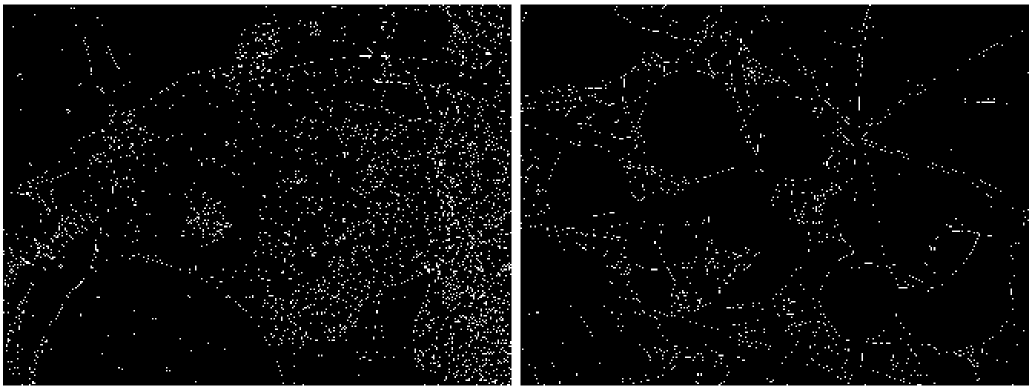
(d)

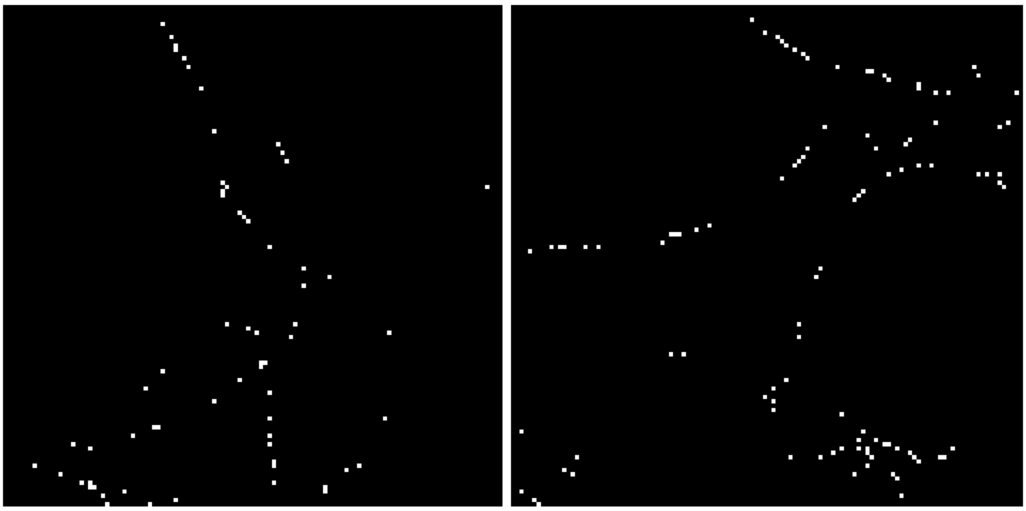
(e)

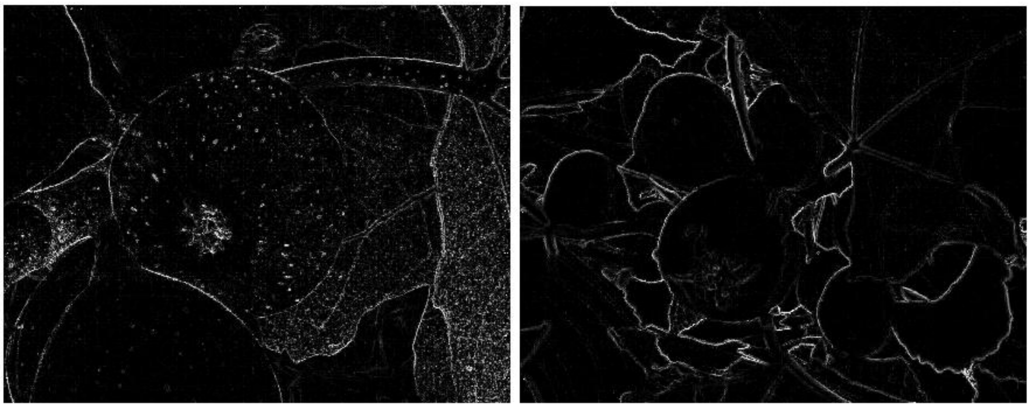

(f)

Fig. 6. – Resulting images: a) Edge detected using Roberts operator, b) Edge detected using Prewitt operator, c) Edge detected using Sobel operator, d) Edge detected using Laplacian of Gaussian (LOG) operator, e) Edge detected using Canny operator, and f) Edge detected using fuzzy logic

It is shown that the proposed fuzzy image processing algorithm improves the quality of edges as compared to Roberts, Prewitt, Sobel, LOG and Canny operators. It is observed that the output images that were generated by the fuzzy image processing algorithm has found out the edges of the images more distinctly as compared to the images that were found out by the classic edge detection operators. Therefore, the fuzzy rule based on the algorithm provides better edge detection and has a comprehensive set of fuzzy conditions, which helps to extract the edges with very high efficiency. This algorithm is suitable for applications in the area of digital image processing for agricultural imaging, where specific boundaries need to be specified for further image analysis.

CONCLUSIONS

The results allow us to conclude that: The proposed fuzzy image processing algorithm is an attractive solution to improve the quality of edges as much as possible. It shows greater accuracy compared to the other edge detection techniques (Roberts, Prewitt, Sobel, LOG, and Canny edge operators) avoiding double edges. This algorithm has the potential to be applied in various areas of digital image processing.

REFERENCES

1. ALSHENNAWY, A. A., ALY, A. A.: Edge detection in digital images using fuzzy logic technique. Word Academy of Science, Engineering and Technology, 53, 2009: 252 – 257.
2. CANNY, J.: A computational approach to edge detection. IEEE Transactions of pattern analysis and machine intelligence, 8(6), 1986: 679–698.
3. GONZALEZ, R. C., WOODS, R. E.: Digital image processing. 1st ed., Reading, MA, USA, Addison–Wesley 1992.
4. GOSE, E., JOHNSONBAUGH, R., JOST S.: Pattern recognition and image analysis. 1st ed., New Jersey, USA, Prentice Hall 1996.
5. GRAVALOS, I.: Image segmentation of ficuscarica trees during the harvesting season. In: Proceedings of the 8th National Conference on Agricultural Engineering, 25 – 26 September 2013, pp. 501 – 505, Volos, Thessalia, Greece. (In Greek with English abstract).
6. HARALICK, R. M., SHAPIRO, L. G.: Computer and robot vision. Volume I. 1st ed., Boston, MA, USA, Addison–Wesley 1992.
7. HU, D., TIAN, X.: A multi-directions algorithm for edge detection based on fuzzy mathematical morphology. In: Proceedings of the 16th International Conference on Artificial Reality and Telexistence – Workshops (ICAT'06), 29 November – 1 December 2006, pp. 361–364, Hangzhou, China.
8. LIU, G., BAI, B., JEON, G.: Fuzzy detection on color image. International Journal of Multimedia and Ubiquitous Engineering, 11 (2), 2016: 343–354.
9. MAINI, R., AGGARWAL, H.: Study and comparison of various image edge detection techniques. International Journal of Image Processing, 3(1), 2009: 1–12.
10. MONDAL, K., DUTTA, P., BHATTACHARYYA, S.: Gray image extraction using fuzzy logic. In: Proceedings of the 2nd International Conference on Advanced Computing & Communication Technologies (ACCT 2012), 7 – 8 January 2012, pp. 289–296, Rohtak, Haryana, India.
11. SOLOMON, C., BRECKON, T.: Fundamentals of digital image processing: A practical approach with examples in Matlab. 1st ed., Chichester, UK, John Wiley & Sons 2010.
12. SONKA, M., HLAVAC, V., BOYLE, R.: Image processing, analysis and machine vision. 1st ed., London, UK, Chapman & Hall 1993.
13. SUDHAVANI, G., SRAVANI, S., VENKATESWARA RAO, P., SATYA PRASAD, K.: Fuzzy edge linking process on fuzzy noise filtered image. International Journal of Computer Applications, 93 (15), 2014: 33–40.

Corresponding author:
Ioannis Gravalos, Department of Biosystems Engineering, Technological Educational Institute of Thessaly, School of Agricultural Technology, 41110 Larissa, , email: gravalos@teilar.gr

PELLETING HAZELNUT HUSK RESIDUES FOR BIOFUEL

G. Gürdil, B. Demirel, Y. Baz, Ç. Demirel

Department of Agricultural Machines and Technologies Engineering, Faculty of Agriculture, Ondokuz Mayıs University, Samsun Turkey

Abstract

In this study evaluation possibilities of hazelnut husk agricultural residue as a solid bio-fuel in the form of pellets were investigated, which comes out of hazelnut production every year in our country. Researches were done with the material at ≤ %12 moisture content and with 10 mm particle size. Optimum pelleting parameters for hazelnut husk residue regarding to physical-mechanical properties (pellet bulk density, pellet particle density, mechanical durability, and pellet moisture content), gas emissions, heating value, and ash content after burning were determined. In conclusion, hazelnut husk agricultural residue was found to be very suitable as a solid bio-fuel in the form of pellets both in environmental and in fuel properties aspects.

Key words: differential biofuel, pellet, renewable energy, hazelnut, agricultural residue.

INTRODUCTION

Hazelnut production is one of the major agricultural products for Turkey, especially in Black Sea region. The husk of hazelnut is outer part of the shell which binds it to the branch. The shelled hazelnut is taken out of husk during harvesting. It's reported that Turkey has produced more than 70 % of the world's hazelnut need with 549 000 tons in 2013 (FAO, 2013). Out of this production it's estimated that 200 000 tons of husks were obtained per year. But, this huge amount generally is not evaluated for any purpose, just a small amount of it is used as litter in animal barns and most of them are just burnt randomly on the field or left for natural deterioration. Therefore, this should be considered as a big economical and environmental loss.

Shaping the grinded material under pressure to smaller sizes (approx. 30 mm) is called pelleting (ÖZTÜRK, 2012). Pellets can be produced from sawdust, wood chips, tree barks, agricultural products, straw, hazelnut shell, almond shell, walnut shell and even from waste papers. The density of material is increased and the transportation and storing costs are decreased by pelleting process. Moreover, homogeneity is provided in size and shape which make them more suitable for automatic feeding systems and effective usage of material is provided (WERTHER ET AL., 2000; MANI ET AL., 2003; HOLM ET AL., 2006; NILSSON ET AL., 2011; THEERARATTANANOON ET AL., 2011; CELMA ET AL., 2012).

Fig. 1. – Arbitrarily burnt hazelnut husk in the village

Fig. 2. – Hazelnut harvester

Generally, hazelnut shells are used as a solid biofuel in our country. However, hazelnut husks with its big potential can be used as source of solid biofuel, also. For this reason, evaluation possibilities of hazelnut husk agricultural residue as source of solid biofuel in the form of pellets were investigated in this study. In this study, some physical-mechanical and thermal properties of hazelnut husk pellets were determined and their suitability as a solid biofuel was investigated.

MATERIALS AND METHODS

This study was carried out in the workshop and labs of Agricultural Machines and Technologies Engineering Department at Ondokuz Mayis University. Up to date European standard EN 14961-2 (Solid biofuels- Fuel specifications and classes- Part 2: Wood pellets for non-industrial use) was taken as a reference for this study.

Hazelnut husk agricultural residue which has a big potential in the Black Sea Region of Turkey was used a material for pelleting. The husks obtained after harvesting were brought to labs and they were left under sun during the day for natural drying. The moisture content of the material was decreased down to 12% and the dried materials were grinded by a 3 kW powered hammer mill having 8 blades and with 2850 r.min^{-1} rotation speed. For the homogenization of particle size a sieve having 10 mm sieve diameter was used during grinding.

Laboratory type pelleting machine was used for pelleting. Tests for determining physical-mechanical and thermal properties of pellets, chimney gas emission values were measured for determining the quality of pellets.

Volume density of pellets was calculated according to the EU norms EN 15103 in kg.m^{-3}, where the pellets were poured in a pot and the ratio of mass to the volume of the filled pot was calculated.

Pellet density of pellets were calculated by stereometric method according to EN 15150 EU standards in kg.m^{-3}, as well.

Fig. 3 – Hazelnut husk pellets

Fig. 4 – Laboratory type pelleting machine

Fig. 5 – Determining some physical properties of pellets

Mechanical durability of pellets was calculated according to EN 15210-1 EU standards. For this, 500 g sample was poured into the testing chamber and rotated with 50 r/min speed for 10 minutes. Then the pellets were sifted out by a sieve having 3.15 mm sieve holes and the oversized pellets were weighed and durability of pellets was calculated as follows:

$$D_U = \frac{M_A}{M_E} \times 100$$

Where,

D_U= Mechanical durability of pellets (%)

M_A= Pellet mass before testing (g)

M_E= Mass of oversized pellets (g)

Moisture content of pellets were defined as in EN 14961-2 EU standards by using a desiccators. Pellets were burnt in a pellet stove and the chimney gas emission values such as; O_2, CO, CO_2, NO and NO_x were measured by a gas emission device. Lower heating values of pellets were determined by a calorimeter device according to EN 14918 EU standards. Ash contents then calculated according to EN 14775 EU standards.

RESULTS AND DISCUSSION

The husks which were brought directly from the gardens were dried and the moisture content of the husks decreased down to 12 %. Some physical properties of grinded material are as shown in Tab. 1 and some physical-mechanical properties of hazelnut husk pellets are given in Tab. 2.

Tab. 1. – Some physical properties of grinded husk material

Particle size	Bulk density of material	Geometrical mean diameter of material
10 mm	211.94 $kg.m^{-3}$	2.28 mm

Tab. 2. – Some physical-mechanical properties of hazelnut husk pellets

Bulk Density ($kg.m^{-3}$)	Particle Density ($kg.m^{-3}$)	Mechanical Durability (%)	Moisture content of Pellet (%)
552.40	1309.87	89.57	11.54

It’s been reported that the volume density of pellets for EN plus-A1, EN plus-A2 and for EN-B classes must be ≥ 600 $kg.m^{-3}$ in EN 14961-2 European Union standards. However, the standards covers just the pelltes made from woodchips the volume density of hazelnut husk pellets were found to be lower than this amount. Besides, there were no definitions or limitations for particle density in EN 14961-2 EU standards. TABIL AND SOKHANSANJ (1996) and TABIL AND SOKHANSANJ (1997) reported that the pellet quality is higher when the pellet durability is 80% or higher. Mechanical durability of hazelnut husk pellets indicated that they are in high quality. But, the value of it was lower than the values suggested in EN 14961-2 EU standards for EN plus-A1, EN plus-A2 (≥ %97.5) and for EN-B classes (≥ %96.5).

Some amount of moisture absorbed in the material for pelleting evaporated due to heating up of mould caused by friction between the mould and disc. Hence, the moisture content of the pellets changes a little bit. It's been reported in EN 14961-2 EU standards that the moisture content of pellets for EN plus-A1, EN plus-A2 and for EN-B classes should be ≤%10. The moisture contents of pellets produced from hazelnut husk residues were lower than the value given in standard. Ash content, heating value and gas emissions of pellets are shown in table below.

Tab. 3. – Heating value, ash content and gas emissions of hazelnut husk pellets

Ash content dry (%)	Heating value dry ($MJ.kg^{-1}$)	CO (ppm)	CO_2 (%)	O_2 (%)	NO (ppm)	NOx (ppm)
7.19	18.35	1383.67	0.90	19.17	121	61.67

Ash content values in EN 14961-2 EU standard are given as ≤ %0.7 for EN plus-A1 class, ≤%1.5 for EN plus-A2 class and ≤ %3.0 for EN-B class. Ash content of pellets made from hazel husk residue was more than the values reported in the particular standard. The reason for this is the pellets given in EU standard is made from wood chips. But, the heating value of hazelnut husk pellets was conformable to the value ($Q \leq 19$ MJ.kg^{-1}) given in that standard.

Tab. 4. – Heating values of some residues

Residue	Heating value (MJ.kg^{-1})
Stem of wheat- barley	18.07
Stem of sunflower	16.90
Stem of rice	15.18
Stem of maize	17.86
Stem of tobacco	17.36
Hazelnut pruning residue	18.80
Kiwi pruning residue	18.36
Pruning residues of other fruits and vineyard	17.99
Paddy husk	15.14
Tea dust	19.37
Wood	17.57

Chimney gas emission values of hazelnut husk pellets after burning were found to be lower than the permitted limit according to the regulations for air pollution control due to heating.

CONCLUSIONS

Evaluation possibilities of hazelnut husk agricultural residue as source of solid biofuel in the form of pellets were investigated in this study. Some physical-mechanical and thermal properties of hazelnut husk pellets were determined. In conclusion, hazelnut husk agricultural residue was found to be very suitable as a solid biofuel in the form of pellets both in environmental and in fuel properties aspects. Many researches on this topic are needed to be done, especially from the point of view of search for an alternative renewable energy sources. We believe in that these kinds of studies will help agricultural engineers, scientific researches, farmers and even the policy makers to think more globally and wisely for the future and will definitely have a positive contribution to sustainable development in the world.

REFERENCES

1. CELMA, A.R., CUADROS, F., RODRIGUEZ, F.L.: Characterization of pellets from industrial tomato residues, Food and Bioproducts Processing, 90, 2012: 700-6.
2. EN 14961-2: Solid Biofuels-Fuel specifications and classes-Part 2: Wood pellets for non-industrial use, 2011.
3. EN 15103: Solid Biofuels-Determination of bulk density, 2009.
4. EN 15150: Solid Biofuels-Determination of particle density, 2011.
5. EN 15210-1: Solid Biofuels-Determination of mechanical durability of pellets and briquettes-Part 1: Pellets, 2011.
6. EN 14918: Solid Biofuels-Determination of calorific value, 2009.
7. EN 14775: Solid Biofuels-Determination of ash content, 2009.
8. HOLM, J.K., HENRIKSEN, U.B., HUSTAD, J.E., SORENSEN, L.H.: Toward an understanding of controlling parameters in softwood and hardwood pellet production, Energy and Fuel, 20, 2006: 2686-94.
9. MANI, S., TABIL, L.G., SOKHANSANJ, S.: An overview of compaction of biomass grinds, Power Handling and Process, 15, 2003: 160-8.
10. NILSSON, D., BERNESSON, S., HANSSON, P.A.: Pellet production from agricultural raw materials- a systems study, Biomass and Bioenergy, 35, 2011: 679-89.
11. ÖZTÜRK, H.H.: Enerji bitkileri ve biyoyakıt üretimi, Hasad yayıncılık Ltd. Şti, İstanbul, 2012, ss 272.
12. TABIL, L.G., SOKHANSANJ, S.: Process conditions affecting the physical quality of alfalfa pellets, Applied Engineering in Agriculture, 12, 1996: 345-50.
13. TABIL, L.G., SOKHANSAMJ, S.: Bulk properties of alfalfa grind in relation its compaction characteristic, Applied Engineering in Agriculture, 13, 1997: 499-05.
14. THEERARATTANANOON, K., XU, F., WILSON, J., BALLARD R., MCKINNEY, L., STAGGENBORG, S., VADLANI, P., PEI, Z.J., WANG, D.: Physical properties of pellets made from sorghum stalk, corn stoves, Wheat Straw and Big Bluesterm, Industrial Crops and Products, 33(2), 2001: 325-32.
15. WERTHER, J., SAENGER, M., HARTGE, E.U., OGADA, T., SIAGI, Z.: Combustion of agricultural residues, Progress in Energy and Combustion Science, 26, 2000: 1-27.
16. URL: http:/faostat.fao.org (last visited: January 31, 2016).

Corresponding author:
Bahadir Demirel, Department. of Agricultural Machines and Technologies Engineering, Faculty of Agriculture, Ondokuz Mayıs University, Samsun Turkey

DETERMINING ORGANIC WASTE POTENTIAL OF MOBILE PUBLIC BAZAARS IN SAMSUN (REVIEW)

G. Gürdil[1], B. Demirel[1], I. Balada[2], Y. Baz[1]

[1]*Department. of Agricultural Machines and Technologies Engineering, Faculty of Agriculture, Ondokuz Mayıs University, Samsun Turkey*
[2]*Faculty of Engineering, Czech University of Life Sciences, Prague, Czech Republic*

Abstract
Mobile public bazaar is an important part of our culture in Turkey. This bazaar settles down every day in a certain place of the towns or city districts in Turkey. Turkey has 81 provinces and 957 towns in total and a public bazaar settles down in a town every day. If you take into consideration the number of towns, theoretically 957 mobile public bazaars must be settling down every day in Turkey. This number is enough to imagine the size of this market in our country. These are mainly food markets for the local people. Mainly vegetables and fruits are sold in these mobile local markets but, you can also find olive, fish and some animal products such as cheese, egg, sausage, salami, etc. Textile products are also sold in these markets. In this study, the structure of a mobile public bazaar is analysed. Organic waste potential of this bazaar is determined and some advices for evaluation possibilities of this organic waste are given.

Key words: organic waste, compost, biogas, public bazaar, organic manure, energy.

INTRODUCTION

Solid waste is a serious environmental problem in both developed and developing countries. In recent years, most developing countries have started to improve their municipal solid waste management practices. The increasing amount of wastes generated by rapid urbanization in these countries is usually not properly managed. Solid waste management systems in developing countries must deal with many difficulties, including low technical experience and low financial resources which often cover only collection and transfer costs, leaving no resources for safe final disposal (COLLIVIGNARELLI ET AL., 2004; MOGHADAM ET AL., 2009). Inadequate management of solid waste in most cities of developing countries leads to problems that impair human and animal health and ultimately result in economic, environmental and biological losses (SHARHOLY ET AL., 2008).

Samsun is the biggest and more developed city of Black Sea region in Turkey. It's located in northern part of Turkey, on the Black Sea cost. Atakum is one of the three central districts of Samsun province with the population 156000 and spread over 34500 ha (URL 1, 2014).

Mobile public bazaar is an important part of our culture. A mobile public bazaar moves every day and settles down along a street in a district of a city. For example, the mobile public bazaar in Atakum tours fifteen different places in a week. The public bazaar settles down early in the morning and generally ends after sunset in the evening. This bazaar is generally a food market for the locals. Mainly different kinds of seasonal vegetables and fruits are sold in this market but, some animal products such as egg, butter, milk, yoghurt, honey, salami, etc. and some other products like textile, plastics, paper products are also sold in this every day mobile public market. In this study, the structure of the mobile public bazaar touring in Atakum district is analysed. Organic waste potential of this bazaar is determined and some advices for evaluation possibilities of this organic waste are given.

Structure of mobile public bazaar

Atakum central district has a very rich organic waste potential. The public bazaar tours 15 different places in a week in Atakum. The structure of public bazaar and average waste amounts are given in table below.

Tab.1. – The capacity of public bazaar and waste amount in Atakum distrcit

Bazaar Place	Days	Number of Stallholders	Average Waste Amount (kg/day)
Altınkum	Monday	25	400
Yeşildere	Monday	30	450
Salı	Tuesday	240	3500
Kurupelit	Tuesday	30	500
Denizevleri	Wednesday	40	500
KamalıToki	Wednesday	20	150
Çatalçam	Wednesday	30	600
Atakent	Thursday	85	1300
Cuma	Friday	160	6500
Cuma	Friday	170	4000
Çakırlar	Saturday	30	500
Kurupelit	Sunday	35	500
Atakent 2	Sunday	40	500
Kuleli	Sunday	100	2500
Taflan	Sunday	70	1000
Total		**1105**	**22900**

(URL 2, 2014)

Fig. 1. – Some views from the bazaar

Waste potential of bazaar

According to the results of this research it's found that a total of 22900 kg/week organic waste is extracted from public bazaar in Atakum. This waste contains mainly vegetable residues (60 %), and then 20 % residues from fruits, 10 % paper, textile and plastic wastes and the remaining 10 % is other kinds of wastes.

Fig. 2. – Public bazaar wastes at the end of the day

These wastes swept out by sanitation workers of Atakum municipal and they are transported to landfill by garbage trucks. These organic wastes from the bazaar are very suitable for composting and biogas production. However, they are not used for those purposes. Although, Samsun Metropolitan Municipality has waste management plant but, they just produce electricity from solid wastes. Organic wastes extracted from public bazaars could be a very good source for organic manure production or even for biogas production if they are combined with agricultural residues in this region (URL 2, 2014).

Evaluation possibilities for public bazaar wastes

Organic materials can positively affects physical, chemical and biological properties of soils (FLAIG ET AL., 1977) in dependence on organic matter content and quality of the materials (CLAPP ET AL., 1986). Agricultural production is intensively realized in Black Sea region. As a consequence of that this region has a very big potential of agricultural residues. The main products in this region are hazelnut, tea, maize, sunflower and cereals. Especially, hazelnut is the major agricultural product in Black Sea region with a yield of 660000 tons per year (FAO, 2012). The shelter of hazelnut is used as a solid fuel in the region (ANON., 1996; ZEYTIN AND BARAN, 2003). Hazelnut processing produces large quantities of husk and shell waste.

Husk is the green part of the hazelnut fruit after it's separated from the shelled hazelnuts. Husk generally holds 3 or more shelled hazelnut fruit. Unfortunately, this husk is not evaluated in any form and it's left in the hazelnut gardens as a waste or it's exterminated by burning it casually under uncontrolled conditions (Fig. 3). Approximately, it's assumed that 200 thousand tons hazelnut husk has been produced per year from the hazelnut production as an agricultural residue. Having that big potential of hazelnut husk as an agricultural residue in our country, made it unavoidable to utilize it in some way. It can be used for solid biofuel production, in the form of briquettes or pellets (GÜRDIL ET AL., 2014). In this way you just burn the material for heating purposes but, another better solution can be using this potential for composting purposes. It's been reported in some researches that hazelnut husk is very good material for composting (UZUN, 1996; ÖZÇELIK AND PEKŞEN, 2007) and for biogas production.

It's been observed from the literature search that generally the researches were focused on evaluating the shell of hazelnut plant but, no researches were come across for evaluation of hazelnut husk. Although there is a big potential of hazelnut husk residue in our country they are not utilized in any way and they are being removed by burning them randomly under uncontrolled conditions or they are left for decomposition. For this reason, utilization of hazelnut husk residue for composting purposes would be very useful for our country. The content of hazelnut husk is given in table below. The husk covering the shelled hazelnut fruit and random burning of husk on the field under uncontrolled conditions are given in the figures below.

Tab. 2. – The content of hazelnut husk

Content	Value
pH	6.05–7.37
$CaCO_3$ (%)	0.55–0.88
N, (%)	1.96–2.67
K, (%)	2.99–4.90
Mg, (%)	0.25–0.41
Mn, ppm	406–488
P (%)	0.15–0.37
Ca, (%)	0.46–1.21
Fe, ppm	4187–7314
Zn, ppm	46–78
Cu, ppm	28–46
O.M. (%)	65.5–74.9

(a) (b)

Fig. 3. – Hazelnut husk (a), random burning of hazelnut husk residue

RESULTS AND DISCUSSION

Atakum central district has a very rich organic waste potential. 144 tons of solid waste is collected daily in Atakum district. These wastes can be utilized as bio-compost or RDF (Refuse Derived Fuel). But, utilization of solid wastes for organic manure production will be more useful than burning and wiping it out without any purpose.

According to the results of this research just from the Atakum district a total of 22900 kg/week of organic residue is produced from the mobile public bazaars. It's observed that 20700 kg/week of this organic waste could be used for composting or even for biogas production purposes in Atakum district in Samsun Turkey.

CONCLUSIONS

A mobile public bazaars starts early in the morning and generally ends in the evening after the sun set and the stallholders move to the next bazaar place in that district for the next day. Of course, an important amount of organic residues is left after departing of the stallholders. In this study a research has been done to determine the organic waste potential of mobile public bazaars in Atakum district in Samsun Turkey. It's found that this public bazaar tours 15 different places in a week in Atakum district in Samsun and a total of 1105 stallholders involve in this event in a week. The amount of organic residue from these bazaars is estimated as 23000 kg per week. This residue consists of approximately 60 % vegetable wastes, 20 % fruit wastes, 10 % textile, paper and plastic wastes and the remaining 10 % is other kinds of wastes. This means 13800 kg/week of vegetable and 6900 kg/week fruit, paper and textile that is; 20700 kg per week of organic waste could be used for composting or even for biogas production purposes in Atakum district in Samsun Turkey. Implementing horizontal composter for organic manure production or tower bioreactors for biogas production in the public bazaar area could be another solution since they won't have transportation costs. But, this can be done only with the support of municipal and private sector.

REFERENCES

1. ANON: Annual Statistics of Turkey. State Institute of Statistics Prime Ministry Republic of Turkey, 1889, Ankara.
2. CLAPP, C.E., STARK, S.A., CLAY, D.E., LARSON, W.E.: Sewage sludge organic matter and soil properties. In: Chen, Y., Avnimelch, Y. (Eds.), The Role of Organic Matter in Modern Agriculture. MartinusNijhoff Publishers, Boston, 1986: pp. 209–253.
3. COLLIVIGNARELLI, C., SORLINI, S., VACCARI, M.: Solid Wastes Management in Developing Countries, CD-ROM of ISWA 2004 World Congress, October 17–21, Rome, Italy.
4. ÇALIŞKAN, N., KOÇ, N., KAYA, A., ŞENSES, T.: Compost Production from Hazelnut Husk, Fourth Int. Sym. Hazelnut, (Eds. A. I. Köksal, Y. Okay, N. T. Güneş), Acta Hort. 1997: 445 ISHS.
5. FAO: Food and Agriculture Organization of the United Nations, FAO Statistics Division. 2012.
6. FLAIG, W., NAGAR, B., SOCHTIG, H., TICTJEN, C.: Organic materials and soil productivity. FAO Soil Bulletin, 35, Rome, Italy, 1977.
7. GÜRDİL, G. A. K., DEMİREL, B., ACAR, M., DOK, M.: Samsun'da Tarımsal Faaliyetler Sonucu Açığa Çıkan Bazı Tarımsal Atıklardan Elde Edilen Briketlerin Özellikleri. Enerji Tarımı Ve Biyoyakıtlar 4. Ulusal Çalıştayı. Samsun, 2014.
8. MOGHADAM, M.R.A., MOKHTARANİ, N., MOKHTARANİ, B.: Municipal solid waste management in Rasht City, Waste Management 29, 2009: 485–489, Iran.
9. ÖZÇELIK, E., PEKŞEN, A.: Hazelnut husk as a substrate for the cultivation of shiitake mushroom (Lentinula edodes). Bioresource Technology 9, 2007: 2652–2658.
10. SHARHOLY, M., AHMAD, K., MAHMOOD, G., TRIVEDI, R.C.: Municipal solid waste management in Indian cities – A review. Waste Management 28 (2), 2008: 459–467.
11. URL 1: http://www.samsun.bel.tr. Erişim tarihi: Kasım 2014. Samsun.
12. URL 2: http://atakum.bel.tr. Erişim tarihi: Kasım 2014. Samsun.
13. UZUN, A.: Karadeniz Bölgesinde Kültür Mantarı Üretiminde Kullanılabilecek Organik Materyallerin Tespiti ile Bunların Mantarın Verim ve Kalitesine Etkisi Üzerine bir Araştırma. Ondokuz Mayıs Üniversitesi Fen Bilimleri Enstitüsü, Doktora Tezi, Samsun, 1996.
14. ZEYTİN, S., BARAN, A.: Influences of composted hazelnut husk on some physical properties of soils. Bioresource Technology 88, 2003: 241–244.

Corresponding author:

Gurkan Gürdil, Department. of Agricultural Machines and Technologies Engineering, Faculty of Agriculture, OndokuzMayıs University, Samsun Turkey

INTRUSION AND HOLD-UP ALARM SYSTEMS AND THEIR RELIABILITY GLASS BREAK DETECTION

J. Hart, V. Hartová, J. Bradna

Faculty of Engineering, Czech University of Life Sciences Prague, Czech Republic

Abstract
This article is focused on the evaluation of the reliability of glass break detectors in intrusion and hold-up alarm systems (I&HAS). I&HAS serve primarily for protecting buildings against unlawful conduct of third parties, and can be used as monitoring and control systems. Several security risks may arise during the installation of intrusion and hold-up alarm systems, which impair the security of the entire building. The risks which occur due to poor installation or various sabotage techniques are always a serious danger for the guarded premises. In a time of increasing property crime, it is highly important for detectors to be able to achieve efficiency, reliability and faultlessness. In the case of proposal for placement of detectors it is naturally important determine position of detector, the type of detector, but also to guarantee their capability of detection for using. The practical tests conducted on GB detectors brought an insight into their functionality and usability in practice. If a saboteur is instructed about the operation of these detectors, then they can be overcome.

Key words: building, security, control, monitoring, installation, protect, error.

INTRODUCTION

Intrusion and hold-up alarm systems serve primarily for protecting buildings against unlawful conduct of third parties, and can be used as monitoring and control systems. They are therefore primarily a tool for ensuring a state of security. They operate in the material realm (physical protection of property, life and health) and in the emotional realm (providing a feeling of peace, safety and a certain security). As a result it is important for them not to malfunction and for them to be sufficiently resistant to attack (HANACEK, 2015). The critical point of intrusion and hold-up alarm systems is predominantly elements of the building envelope protection (KRECEK, 2006; STAFF, 1999). These elements are highly susceptible to poor installation, and as a result it is very important to pay attention to this problem. One of the most widely used types of detector is the GB detector (glass break), which ranks amongst active detectors. On average, of all the types of the building envelope detectors used, the largest numbers of false alarms occur on these detectors. This high error rate is primarily caused by incorrect installation (MAGNANI, 2016). Thus the aim of this study is to evaluate the reliability of glass break detectors in intrusion and hold-up alarm systems (I&HAS). I&HAS serve primarily for protecting buildings against unlawful conduct of third parties, and can be used as monitoring and control systems.

MATERIALS AND METHODS

Several security risks may arise during the installation of intrusion and hold-up alarm systems, which impair the security of the entire building. The risks which occur due to poor installation or various sabotage techniques are always a serious danger for the guarded premises (CUMMING, 1994; URBANCOKOVA, 2015). They may jeopardise the guarded property or even the lives of the people who the intrusion and hold-up alarm systems are intended to protect (HANACEK, 2015). Above all, however, they have an influence on determining the security risks of buildings.

Upon installation of GB detectors it is necessary to take into account a number of fundamental prerequisites. The first prerequisite is for the detector must be installed on the opposite side than the guarded glass surface. The second prerequisite is for the cabling not to be visibly installed. In addition the relevant norms must be adhered to upon implementation of the cable distribution mechanisms (CAPEL, 1999; PETRUZZELLIS, 1993; UHLAR, 2005). If the cable distribution mechanisms are installed in such a manner that enables access to them, it is possible to sabotage these systems and thus attack the entire installation of the intrusion and hold-up alarm systems.

If no end of line (EOL) resistor is connected to the switchboard loop upon installation of the detector, the system is more vulnerable and can easily be bypassed.

If a resistor is connected, bypassing is far more difficult than in the case of a simple loop (it is not possible to use simple short-circuiting). Upon sabotage it is necessary to create a dual bypass and use it to replace the original loop at a single moment (Fig. 1).

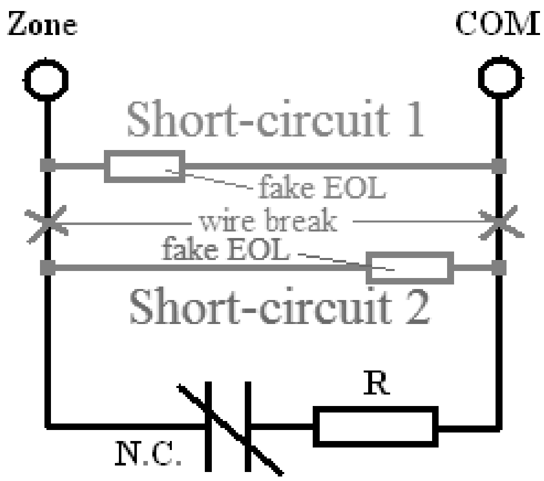

Fig. 1. – Short-circuit systems

Upon use of a bus bar (as wiring), sabotage is far more difficult than in the case of loop wiring. Successful sabotage would require for example the use of scanning communication (or decoding) across the bus bar, with subsequent replacement of this communication with false reports which correspond to the communication of the existing system.

Wireless systems for communication most frequently use two unlicensed bands which comply with the Federal Commission for Communication (FCC) and the European Telecommunications Standards Institute (ETSI) (POWEL & SHIM, 2012). These are the bands 433 MHz and 868 MHz. These wireless transmissions should be protected by detecting disturbance of the frequency band, which monitors the load on the communication frequency. In the case of overloading of the frequency, the switchboard evaluates this fact and responds according to the setting (malfunction, alarm etc.). The detectors are also mostly protected, namely by "wireless detector surveillance", which monitors the presence of the detector within the range of the switchboard (PETRUZZELLIS, 1993; URBANCOKOVA, 2015; STAFF, 1999).

The greatest risk upon use of wireless communication (between detectors and the switchboard) is a signal frequency jammer (HANACEK, 2015). This can overload the communication frequency by rendering the switchboard incapable of receiving the signal transmitted from the detector. This signal frequency jammer is dangerous above all because it can attack the system before the saboteur enters the guarded area, where he or she could be detected by one of the detectors (HANACEK, 2015).

Measurement of GB detectors should be focused primarily on tests which examine the capability of detection under more arduous conditions.

The GB detector detects pressure in the room and the characteristic sound of breaking glass.

The detectors GBS 210 and Glasstrek were used for measurement. These are frequently used detectors, which are installed in both small buildings and large firms.

All the tested GB detectors are loop detectors with a simple type of sending of alarm information, which are cheap in comparison with other types of GB detectors (using a different type of data transmission).

During these tests an intrusion into the building was simulated, and a window was broken. To initiate the alarm, 60 x 60 cm glass plates were used, which were modified for various types of sabotage.

The GBS 210 detector (Fig. 2) uses the dual method for detection, wherein negligible changes to the air pressure in the room are evaluated (impact to the glass panel) and the subsequent sounds of breaking glass. The sensitivity of the pressure component of the detector can be easily configured according to the distance and dimensions of the protected windows.

Like the GBS 210 detector, the Glasstrek Detector (Fig. 3) uses the dual method for detection, during which air pressure changes in the room are evaluated (impact to the glass panel) and the subsequent sounds of breaking glass. Although the sensitivity of the pressure component of the detector cannot be configured, the used installation distance (4 or 9 meters) can be configured. This configuration changes the evaluation characteristic of the breaking glass. The pressure compound of the detector is constant.

Six detection ability methods of the detectors were tested with differently-modified initialization materials – standard, with coating and a screen. Coating means that the initialization material is modified by being covered by foil on one side. This modification changes the characteristic of breaking glass, and thus it also affects the functions of the detector. A screen is a barrier between the detector and initialization material which dampens the characteristic of the broken glass arising during an attack.

Fig. 2. – Detector GBS 210

Fig. 3. – Detector Glasstrek

The testing was carried out on ten samples of each type, and testing it was repeated twenty times. During every detection method, both the classical breaking of the initialization material (using a metal rod) and the gradual denting of this material were tested. Through denting, the pressure component arising when the initialization material is punctured, is softened. The basic results from the measurements carried out are shown in Tab. 1, 2.

Tab. 1. – Measured results for the detector GLASSTREK

Method of meassurement	Alarms
Breaking the glass	94%
Breaking the glass with tape	82%
Dent glass	88%
Dent glass with tape	6%

Tab. 2. – Measured results for detector 210 GBS

Method of meassurement	Alarms
Breaking the glass	100%
Breaking the glass with tape	92%
Dent glass	98%
Dent glass with tape	34%

RESULTS AND DISCUSSION

The measured results and the overall comparison of GB detectors (Fig. 4) do not differ greatly, with the exception of the better elimination of false alarms. This is caused by the large demands of the building envelope detector, which leads a thorough checking during certification.

Until all the systems are tested, it is possible only to ask how many detectors and systems are at all secure. A further question is whether any system exists which could provide reliable protection for a reasonable price.

The present state of development of security systems is at a point of stagnation. Although manufacturers are constantly attempting to develop systems, the majority copy old errors in the technical design into new products of a higher class, even despite the endeavours of customers to ensure manufacture is modified. Without innovative approaches and user feedback, this array will career into a blind alley.

As stated in the article "Self-mixing digital closed-loop vibrometer for high accuracy vibration measurements", a mechanical wave is fully dependent on the environment (MAGNANI, 2016). Influencing or changing environment will affect even wave that spread the actual environment. From these foundations based on the structure of measuring glass break detectors. The same assumption affecting the environment was described in the article "The Methods of Testing and Possibility to Overcome the Protection Against Sabotage of Analog Intrusion Alarm Systems" (HANACEK, 2015).

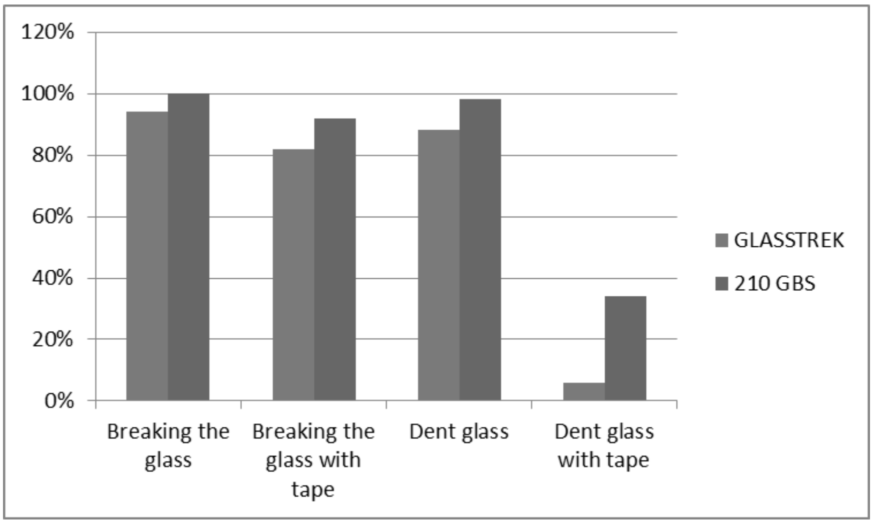

Fig. 4. – Comparison of GB detectors

CONCLUSIONS

The technical design of security systems is unique for the majority of manufacturers. In the case of every manufacturer it is possible to find some poor technical designs which require modification. This deficiency can be resolved by technical development of the given product and adaptation to customer requirements.

The practical tests conducted on GB detectors brought an insight into their functionality and usability in practice. If a saboteur is instructed about the operation of these detectors, then they can be overcome. At the same time the saboteur can also bypass the individual loops, and if skilled, can also bypass loops with an EOL resistor.

Tests have proved that a glass break detector GBS 210 better processing and evaluation of the situation caused alarm. Glass break detector Glasstrek not qualitatively adequate evaluation of alarm situations.The only protection which would be usable against current sabotage techniques is the development of new technologies. It is very important not to cast doubt on this development and to apply a constant endeavour to advance towards new technologies and greater security.

ACKNOWLEDGEMENTS

It is a project supported by the CULS IGA TF 2016 “The University Internal Grant Agency” (Innovation of systems for verification of a person according to his characteristic).

REFERENCES

1. CAPELL, V.: Security Systems & Intruder Alarms. Elsevier Science, 1999: 301 p.
2. CUMMING, N.: Security: A Guide to Security System Design and Equipment Selection and Installation. Elsevier Science, 1994: 338 p.
3. HANACEK, A., SYSEL, M.: The Methods of Testing and Possibility to Overcome the Protection against Sabotage of Analog Intrusion Alarm Systems. 4th Computer Science On-line Conference (CSOC). 2015: 119-128 p.
4. HANACEK, A., SYSEL, M.: Universal System Developed for Usage in Analog Intrusion Alarm Systems. 4th Computer Science On-line Conference (CSOC). 2015: 129-138 p.
5. KRECEK, S.: Manual security technology. Blatná: Circetus, 2006: 313 p. (in Czech).
6. MAGNANI, A., MELCHIONNI, D., PESATORI, A., NORGIA, M.: Self-mixing digital closed-loop vibrometer for high accuracy vibration measurements. OPTICS COMMUNICATIONS, 2016: 133-139 p.
7. PETRUZZELLIS, T.: Alarm Sensor and Security. McGraw-Hill Professional Publishing, 1993: 256 p.
8. STAFF, H., HONEY, G.: Electronic Security Systems Pocket Book. Elsevier Science, 1999: 226 p.
9. UHLÁŘ, J.: Technical protection of objects, Part II, electrical security systems II. Prague: PA ČR, 2005: 229 p. (in Czech).
10. URBANCOKOVA, H., VALOUCH, J., ADAMEK, M.: Testing of an intrusion and hold-up systems for electromagnetic susceptibility - EFT/B. International Journal of Circuits, Systems and Signal Processing. 2015: 40-46 p.

Corresponding author:

Ing. Jan Hart, Ph.D., Department of Technological Equipment of Buildings, Faculty of Engineering, Czech University of Life Sciences Prague, Kamýcká 129, Praha 6, Prague, 16521, Czech Republic, phone: +420 22438 3330, e-mail: jhart@tf.czu.cz

RELIABILITY OF FACE READERS IN DIFFICULT CONDITIONS

V. Hartová, J. Hart, J. Bradna

Faculty of Engineering, Czech University of Life Sciences Prague, Czech Republic

Abstract
This article is focused on the evaluation of biometric readers that identify a person based on facial features. Biometric user identification is a highly topical theme these days. The most widespread areas are identification of a person on the basis of fingerprints and identification on the basis of facial features. For testing, systems were selected that identify a person based on facial features. Testing showed errors in these readers under both standard and difficult conditions. Testing was focused on reliability of acceptance authorized user. Testing was performed on the 2 biometric systems. Wrong of user acceptance was based on unfavorable conditions. Unfavorable conditions were: pollution with dark oil, pollution with soil, pollution with makeup, pollution with soot, pollution with black coal, pollution with paints. The results of the measurements showed that the measured reliability values do not correspond to those of the manufacturers. It is necessary to adapt and perfect these biometric identification systems for use in industrial areas, as they are often used in these areas as access or attendance systems.

Key words: face, biometric, reader, reliability, difficult conditions.

INTRODUCTION

Modern biometric technologies offer an automated method of establishing or verifying the identity of living or dead persons on the basis of measurable and in commutable biometric characteristics. These characteristics are demonstrable, precise and unique for each individual and no confusion is possible. The initial use of these systems was very successful, but only until methods of sabotaging them were discovered. Since then, the focus is on developing safe technologies and when introducing them, measures must be taken to minimise the possibility of sabotaging biometric sensors (ABATE, 2005; DI MARTINO, 2016).

Biometric recognition systems are currently used mainly for identifying persons entering facilities (e.g. nuclear power stations, airports, research institutes, banks, state buildings).

Other common use is for recognition of persons (e.g. when searching for specific individuals from wanted persons databases) (DI MARTINO, 2016; STROICA, 2012).

One of the frequently-used methods of biometric recognition is identification on the basis of facial features. Systems working on this principle are already available at prices acceptable for the general public and now we can find them both in commercial and state institutions. These systems can be monocriterial or more. In this article we will be measured multicriterial systems. The reliability of this readers which identifying based on facial features should be investigated (NÍDLOVÁ, 2015).

The most commonly used readers, besides fingerprint readers are readers based on facial recognition. These systems are financially acceptable and therefore are used in many industries. They find their using in industrial areas. Therefore, it is necessary to test the readers in difficult conditions that may occur in industrial areas (NÍDLOVÁ, 2015). Therefore the aim of this study is to evaluate biometric readers that identify a person based on facial features.

MATERIALS AND METHODS

Each measurement comprised twenty repeats. 80 persons were measured (16 women and 64 men) with an age range of 21 – 62 years of age. It was essential to observe laboratory conditions when performing the 3D face scan, especially with respect to lighting (lighting required by the manufacturer is 0 – 800 lx). Measurements were performed on D-Station and IFace 800. All of these devices have optic sensors. These readers were chosen because manufacturers are recommended in difficult conditions. Both use a combination of recognition on the basis of codes, finger prints and sample facial features. Measurements took place under both normal and impaired conditions. The number of false acceptances or failure to capture the user was measured. In addition, the degree of confusion between persons was scrutinised, which to a large extent is expressed in the FAR values (JAIN, 2009; RAK, 2008).

Errors in the form of false rejection of the user do not occur with these readers; there just is the possibility that the user is not identified. The time limit for recognition was set at 5 minutes. If the reader does not manage to identify the user within this time limit, the situation is regarded as a false rejection.
The term standard recognition means recognition under laboratory conditions. Values for establishing the functionality and reliability of biometric recognition systems that work on the basis of 3D face scans were collated over the course of 27 months. The two most important values were the time span during which users were admitted to the facility and the related number of accepted/not accepted (identified, not identified).
Measurement under impaired conditions was intended to simulate situations in dusty operations where smears on faces are common, and also work with lubricants and other substances can lead to dirty faces. In everyday life too, smears can appear on people's faces, for instance smeared make-up in the rain.
Measurement occurred with a selected group of 20 subjects with five repeat measurements. Black coal, earth, soot, make-up, paint and dark oils were used as soiling (RAK, 2008; SVOZIL, 2009).
A hypothesis was set: Pollution of face significantly reduces the reliability of biometric systems identification of based on facial features.
For evaluation of the hypothesis a one-sample test of relative frequencies for the parameter π (SVATOŠOVÁ, 2012).

1. H0: $\pi 1 = \pi 2$
2. Ha: $\pi 1 \neq \pi 2$
3. The level of significance was determined $\alpha = 0{,}05$
4. Testing criterion (1):

$$u = \frac{\frac{m}{n} - \pi_0}{\sqrt{\frac{\pi_0 .(1-\pi_0)}{n}}} \quad (1)$$

where: m – the value of a successful acceptance of user under standard conditions, percent;
n – number of measurements;
π_0 – average values of reliability under adverse conditions, percent

5. Determination of the uα (from statistical tables according to the level of significance) $u\alpha = 1{,}96$
6. Critical field – K: ($|u| > u\alpha$)

RESULTS AND DISCUSSION

Fig. 1 show the percentual representation of recognitions in separate time intervals. The penultimate column of the graph shows user false rejection rate – FRR, which is stipulated to occur upon exceeding 5 minutes per attempt at recognition. The last specified value in the graphs represents user false recognition (false acceptance rate – FAR). This value appears on the graph to give the results more relevance and is taken from the total number of attempts at recognition. Fig. 1 shows measurements taken on the D-Station reader. 63 % of users were successfully enrolled into the system and were let into the facility. Also the value for both readers of just over 28 % successful recognitions within 5 minutes is very inconvenient for the user. Fig. 1 also shows measurements taken on the IFace 800 reader, and they are even less acceptable than those on the previous reader. Only 59 % of users were successfully enrolled into the system and were let into the facility. Also the value for both readers of just over 30 % successful recognitions within 5 minutes is very inconvenient for the user.
The calculations and the graphic expression thereof tell us that the percentage of false user rejections exceeds the percentage of false user acceptances by about 10 %. However, these values are extremely worrying and the question should be asked as to whether these systems are suitable for entrance security at important facilities. The results of our readings clearly demonstrate that with recognition systems based on facial features there is still considerable room for improvement.
Subjects with prominent facial features were no problem to identify. However, in contrast to standard recognition, the false rejection rate rose with the remaining subjects, see Tab. 1.

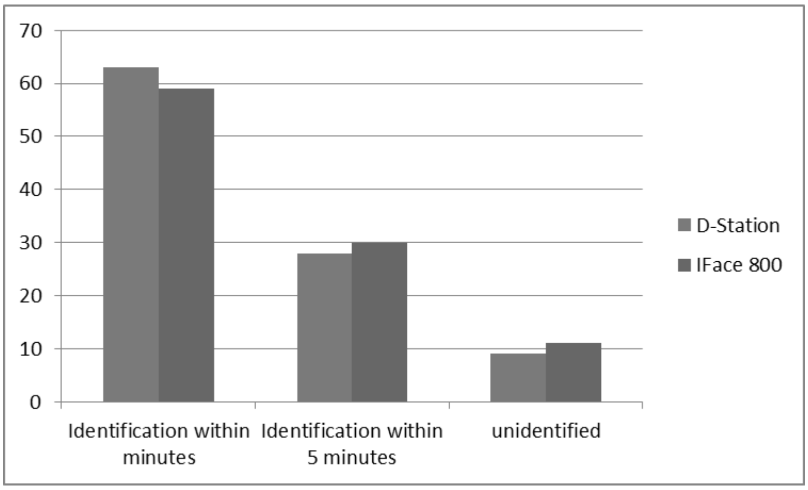

Fig. 1. – Recognition Capability of IFace 800 and D-Station Biometric Device

Tab. 1. – Percentual user acceptance with SD face readers with dirty faces

	IFace 800 – testing [%]	D-Station – testing [%]
Standard identification	84	89
Pollution with dark oil	73	82
Pollution with soil	77	79
Pollution with makeup	63	76
Pollution with soot	58	62
Pollution with black coal	48	58
Pollution with wall paint	40	51

Hypothesis: Pollution of face significantly reduces the reliability of biometric systems identification of based on facial features

Statistical calculation for IFace 800 biometric system

H0: $\pi 1 = \pi 2$

Ha: $\pi 1 \neq \pi 2$

A significance level has been set at: $\alpha = 0{,}05$

Testing criterion (1): u=4,93

Setting uα (from statistical tables, according to significance level): $u\alpha = 1{,}96$

Critical field: K: ($|u| > u\alpha$)

K: ($|4{,}93| > 1{,}96$)

H0 is rejected → pollution of face significantly reduces the reliability of biometric systems identification of based on facial features.

Statistical calculation for D-Station biometric system

H0: $\pi 1 = \pi 2$

Ha: $\pi 1 \neq \pi 2$

A significance level has been set at: $\alpha = 0{,}05$

Testing criterion: u=4,50

Setting uα (from statistical tables, according to significance level): $u\alpha = 1{,}96$

Critical field: K: ($|u| > u\alpha$)

K: ($|4{,}50| > 1{,}96$)

H0 is rejected → pollution of face significantly reduces the reliability of biometric systems identification of based on facial features.

In view of the results of the one-sample relative frequency test performed with IFace 800 a D-Station readers, the Hypothesis is rejected.

The matter of reliability of biometric systems that identify on the basis of face recognition is also being addressed by Di Martino, Luis D. et al. in their article "Face matching with an a contrario false detection control", where they pointed out the existence of two identical templates. Thanks to this, the reliability of the systems should increase distinctly. Also, in their article "Beard tolerant face recognition based on 3D geometry and color texture", authors Abate, Andrea F. et al. talk of the technology for recognition on the basis of facial features, where color texture was used in combination with 3D geometry as an innovation for increasing reliability. Constant innovation of these systems is important for increasing reliability which, as can be seen in the results of scans, is not user friendly (ABATE, 2005; DI MARTINO, 2016).

CONCLUSIONS

The measurements showed that reliability of the tested facial recognition systems differs from the values cited by the manufacturers. With such readers there are many aspects that can influence their reliability. One of these are light conditions, another is make-up in women or a moustache or beard in men; they are also very sensitive to face soiling and other circumstances. These readers can recognize a person both by fingerprints and by facial features. The question is whether or not the manufacturers concentrated more on the fingerprint option than on facial recognition capabilities. The results clearly show that the existing systems need more testing and improvement to make it possible to rely fully on the technology and to avoid unwanted confusion of persons that can lead to admission of unauthorized persons into restricted areas. It should also be borne in mind that companies will want to use these systems in industrial environments where soiling and dust nuisance is common. The results indicated that readers cannot deal with this type of problem and perform false recognitions or else recognition does not come about at all.

ACKNOWLEDGEMENTS

It is a project supported by the IGA 2016 “The University Internal Grant Agency” Innovation of systems for verification of a person according to his characteristic.

REFERENCES

1. ABATE, A.F., RICCARDI, S., SABATINO, G., TUCCI, M.: Beard tolerant face recognition based on 3D geometry and color texture, In:11th International Conference on Distributed Multimedia Systems, 2005: 202-207 p.
2. DI MARTINO, L., PRECIOZZI, J., LECUMBERRY, F., FERNÁNDEZ, A.: Face matching with an a contrario false detection control, In:Neurocomputing. 2016.: 64-71 p.
3. JAIN, A.K., FENG, J.J.: Latent Palmprint Matching, In:IEEE Transactions on pattern analysis and machine intelligence, 2009: 1032-1047 p.
4. NÍDLOVÁ, V., HART, J: Reliability of Identification Based on Fingerprints in Dual Biometric Identification Systems. In:Applied Mechanics and Materials, 2015: pp 1040-1044.
5. RAK,R., MATYÁŠ, V., ŘÍHA, Z.: Biometrics and identity of man - in forensic and commercial applications, 2008: 664 p (in Czech).
6. STROICA, P., VLADESCU, M.: Implementation of a multiple biometric identification system based on face, fingerprints and iris recognition. In:Advanced topics in optoelectronics, microelectronics, and nanotechnologies VI. , 2012
7. SVATOŠOVÁ, L., PRÁŠILOVÁ, M.: Statistical methods in Examples. 1st ed.,Prague, Czech University of Life Sciences Prague, 2012 (in Czech).
8. SVOZIL, L.: Aspects of biometric identification of persons using facial recognition. In:Bachelor thesis, Tomas Bata University in Zlín. 2009 (in Czech).

Corresponding author:

Ing. Veronika Hartová, Ph.D., Department of Vehicles and Ground Transport, Faculty of Engineering, Czech University of Life Sciences Prague, Kamýcká 129, Praha 6, Prague, 16521, Czech Republic, phone: +420 734 170 850, e-mail: nverca@seznam.cz

CONSTRUCTION AND VERIFICATION OF AN EXPERIMENTAL CHAMBER DRYER FOR DRYING HOPS

P. Heřmánek[1], A. Rybka[1], I. Honzík[1], D. Hoffmann[1], B. Jošt[1], J. Podsedník[2]

[1]*Department of Agricultural Machines, Faculty of Engineering, Czech University of Life Sciences Prague, Czech Republic*
[2]*CHMELAŘSTVÍ, cooperative Žatec, Czech Republic*

Abstract
Hop drying takes a significant part in growers' costs of the final product processing. The current drying technology is based on drying at the drying air temperature of 55-60°C for 6-9 hours to the final moisture content of about 10%. However, the process results in irreversible transformations and losses of, inter alia, heat labile substances contained in hops. The paper describes the design and builds an experimental chamber dryer. The experimental chamber drier was tested at harvest 2015. Assays hop drying were carried out at a temperature of the drying medium 40°C. The research results in the form of an experimental new experimental chamber dryer will be used for testing of drying technologies at lower temperatures of the drying medium.
This is what will make it possible to preserve the quality of aroma as well as other characteristics of the components contained in hops.

Key words: hops, drying, chamber dryer, moisture.

INTRODUCTION

The current state in the field of hop-drying and hop-conditioning technology is not ideal. The process of artificial drying proceeds at the air temperature of 55-60°C for 6-9 hours until the hop final moisture content is approximately 10 %.
Hop-cone drying below 10 % of moisture and following controlled conditioning requires roughly 1/3 of the overall energy requirements. Drying to the final moisture content of 10-12 % with subsequent uncontrolled and natural conditioning (resting chambers) to approximately balanced cone moisture can shorten the way of drying used so far, remove risks of mechanical changes of dried cones and effect positively the quality of brewing as well as other parameters.
Besides brewing parameters there are other heat labile substances contained in hops that are important and for which the current drying temperatures in the final stage of drying are too high. For some special aroma hop varieties, whose content and composition of essential oils are key qualitative parameters, such losses result in a reduced quality of the product. Aroma hops are applied by means of so called dry hopping technique that is widespread especially in the segment of small and restaurant breweries. Based on the above it is concluded that for special hop varieties it is necessary to develop technology and technique suitable for a careful (low-temperature) drying method that would to the extent possible preserve the original composition of hops.
According to the literature in the Czech Republic, no one had a problem hop drying at a lower temperature than 55°C. Drying hops at ambient temperature above 55°C, some authors have discussed (BERNÁŠEK 2007 AND MEJZR 2007). Both authors describe the drying curve and the energy consuption of the drying of hops, wherein the drying air has a temperature of about 60°C. In foreign sources only describe the drying temperature of the drying medium 65 to 68°C (MÜNSTERER, 2006).
The research objective was therefore to design and assemble the experimental chamber dryer including the heater, measurement devices and accessories, allowing hop drying at temperatures below 50°C.

MATERIALS AND METHODS

The aim was to assemble an experimental chamber hop dryer which would enable testing experiments with the drying air temperature, drying air speed or usage of moistened air for a careful drying method.

For the purpose of the experimental measurement, monitoring a drying process at a lower temperature (40 to 45°C) than it is used in current operating dryers, an experimental chamber dryer (Fig. 1) had been designed and produced.

The experimental chamber dryer is in the form of a self-supporting steel structure with inserted wooden boxes measuring 0.9 x 0.9 x 0.3 m for storing dried hops. It is possible to insert up to 3 boxes one above the other into the dryer. The weight of green hops inside one box may be approx. 20 kg.

The dryer is heated by electric hot air aggregate with a maximum thermal input of 18 kW, and the heated air temperature can be set by means of an indoor thermostat to 40-45°C. The heated air is blown into the dryer by a fan. The amount of blown air is possible to regulate through a change in the fan's rotation frequency by means of a frequency converter.

Under and over a layer of hops there are probes to measure the air temperature, relative humidity, excess pressure and speed. The electrical energy consumption is read from the electricity meter.

Over the layer of hops there are 2 axial fans placed to verify the possibility of exhaust (creation of underpressure) above the measured layer.

Fig. 1 clearly shows that the heated air is directed into the fan's intake. In between the fan outlet and the dryer there is a short supply pipe which directs and distributes the supplied air over the entire width of the dryer. The supply pipe is followed by a bottom-mount drying chamber that is fitted with flaps to direct the air stream. This way ensures a uniform circulation over the overall coverage area of the dryer. The air flow uniformity gets even better after inserting drying hops, for a layer of drying hops creates resistance to the air flow resulting in a slight overpressure under the layer.

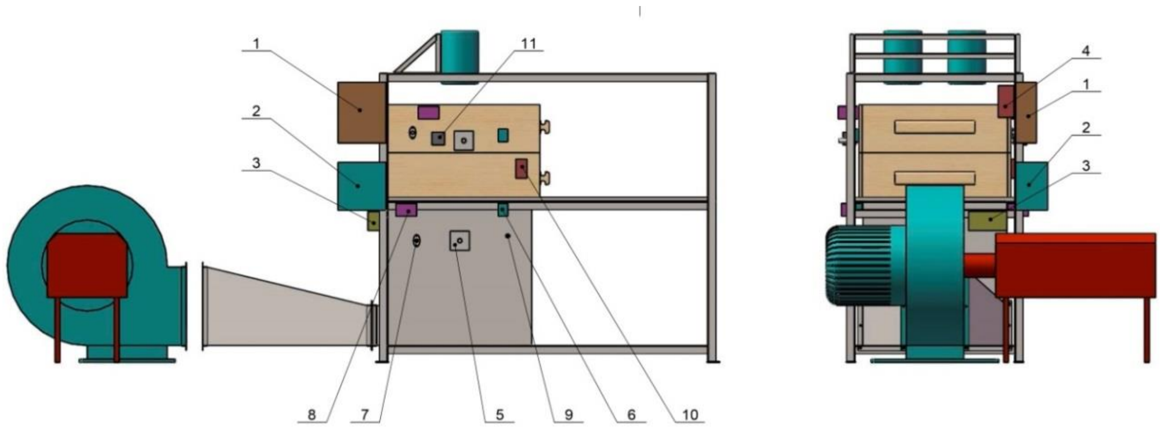

Fig. 1. – Distribution of control elements and sensors on the experimental chamber dryer
1-fuse box, 2-frequency converter, 3-electricity meter, 4-thermostat, 5-air temperature and relative humidity data logger probe, 6-display unit for the air temperature and relative humidity data logger, 7-air speed probe, 8-air speed probe display unit, 9-pressure gauge probe, 10-pressure gauge probe display unit, 11-hygrometer

By contrast, to create underpressure, thus reaching a forced drawing off of the air passing through the hop layer, there are two axial fans in the upper part of the dryer.

Measurement methodology

The thermostat of the hot-air aggregate was set to 45°C, and the radial fan rotation frequency was set by the frequency converter so that the drying air temperature was kept between 40 and 45°C.

Into one wooden box (Fig. 2) green hops were put of the total weight of approx. 20 kg. The box was inserted into the dryer and another empty box, which prevented hops from rising during the process of drying, was placed above it. At the same time, sensors of the air speed, temperature and humidity were placed on the walls of the upper box. The same sensors were placed also under the lower box with hops.

During the measurement we monitored:

- air temperature and relative humidity under the layer of hops – 2x data logger COMET R0110,
- air speed under the layer of hops – 2x probe GREISINGER GIA 2000/GIR 2002,
- air pressure under the layer of hops – pressure gauge GREISINGER 3100,
- air temperature and relative humidity over the layer of hops – 2x data logger COMET R0110,
- air speed over the layer of hops – 2x probe GREISINGER GIA 2000/GIR 2002,
- temperature of blown air – thermostat FAMATEL,
- energy consumption – electricity meter NOARK EDN 3412,

- radial fan rotation frequency– frequency converter.

The values read from individual sensors were recorded every 15 minutes, and every two hours a sample was taken to provide for the hop moisture detection and another samples for laboratory analyses.

Fig. 2. – A wooden box partially filled with hops

RESULTS AND DISCUSSION

The measurement was made on the premises of Chmelařství, Cooperative Žatec, the Machinery Plant. To verify the structure and measuring apparatus, varieties Vital and Kazbek had been selected. The measurement results for the variety Kazbek are presented below.

The product input and output values are presented in Tab. 1.

Tab. 1. – Input and output values for Kazbek variety

Parameter	Input values	Output values
weight of green hops in the box	19 kg	5.2 kg
layer height of green hops in the box	0.25 m	0.21 m
hop moisture content	75.0%	11.4%

The graph in Fig. 3 illustrates progress of drying including values from embedded sensors on the experimental chamber dryer, and hop moisture measured from the samples. Approximately at a time of 600 min the air inlet was cut and hops remained in the wooden box over the entire night. This procedure simulated a resting chamber to balance the moisture between hop bracts and spindle.

Hop moisture was determined through gravimetric analysis in the laboratory chamber dryer of Hop Research Institute Co., Ltd, Žatec with forced air circulation according to the EBC 7.2 method. Following this method, the weighed hops are dried at a temperature of 105°C for 1 h. Drying time for hops with moisture content over 30 % shall be extended to 1.5 h. With the samples we also monitored the hop storage index (HSI) which had been determined by the official EBC 7.13 spectrophotometric method from a hop toluene extract. Alpha bitter acid content was measured by means of liquid chromatography according to the EBC 7.7 method (KROFTA 2008; WEIHRAUCH ET AL., 2010). The measured value was then converted to an absolutely dry matrix for all the points of the drying curve.

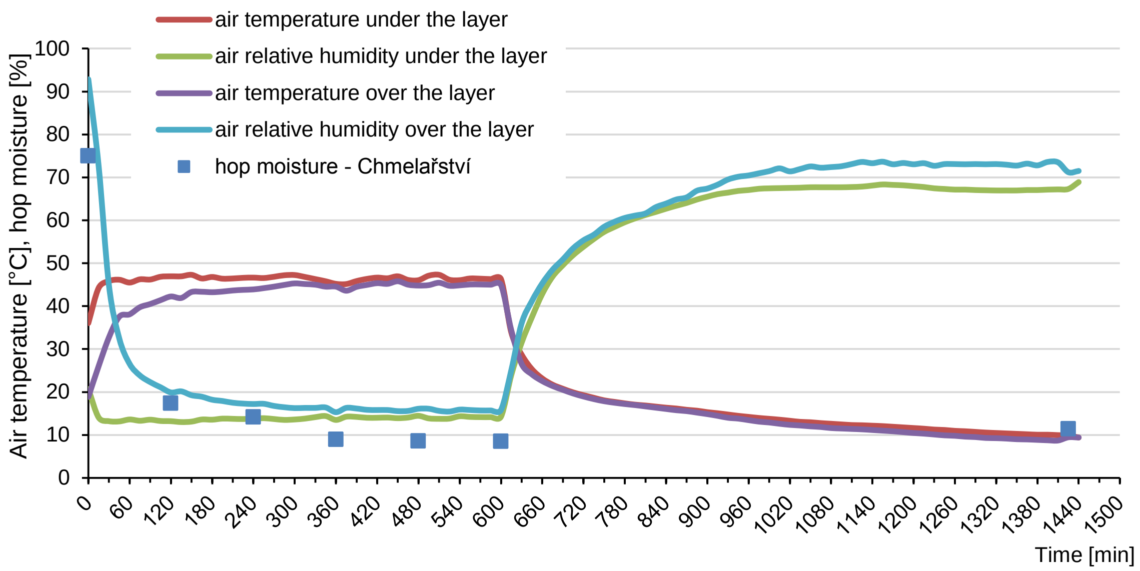

Fig. 3. – Air temperature and relative humidity and hop moisture during the drying process

At the start of the drying process, three data loggers VOLTCRAFT DL-121-TH had been inserted into approximately half of the hop layer (SRIVASTAVA ET AL., 2006). These are described in the article "RYBKA ET AL, 2015. Analysis of the technological process of hop drying in belt dryers". Since they were buried under a pile of hops, the values they recorded corresponded better to the progress of hop moisture in comparison with the probes placed under and over the layer. The graph in Fig. 4 depicts the average values obtained from data loggers.

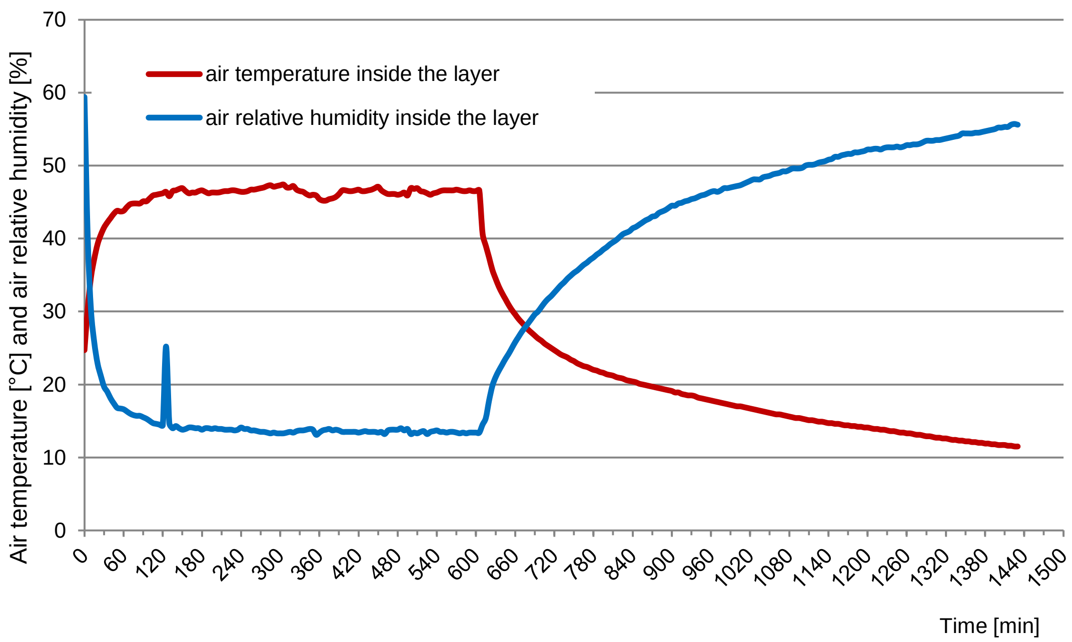

Fig. 4. – Air temperature and relative humidity measured by data logger DL-121-TH

The graph in Fig. 5 gathers all the values of the air temperature and relative humidity as well as hop moisture measured and determined by the analysis for Kazbek variety.

Another two graphs (Fig. 6 and 7) illustrate variability in the air speed under and above the dry hop layer on one hand, and cumulation of electric energy consumption during the process of drying.

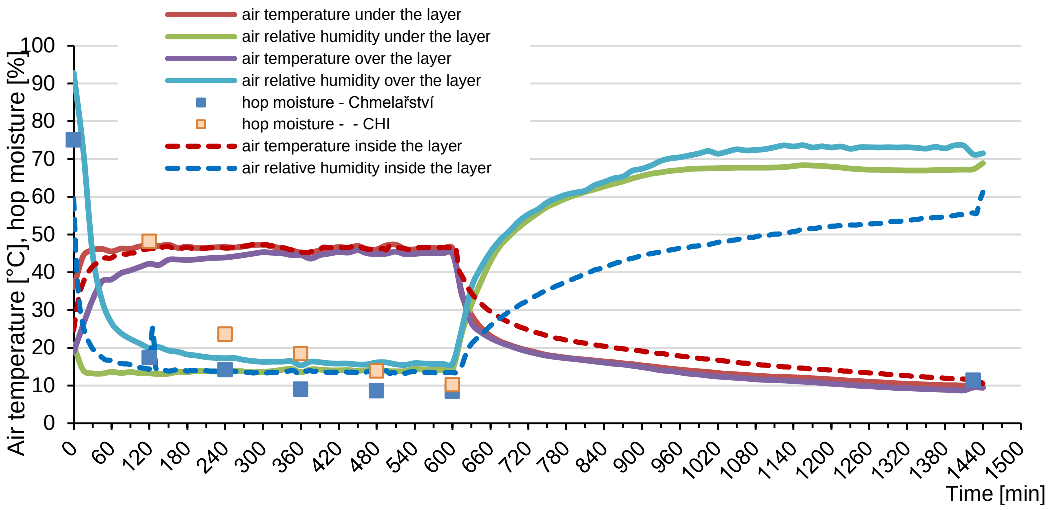

Fig. 5. – Cumulative graph for Kazbek variety

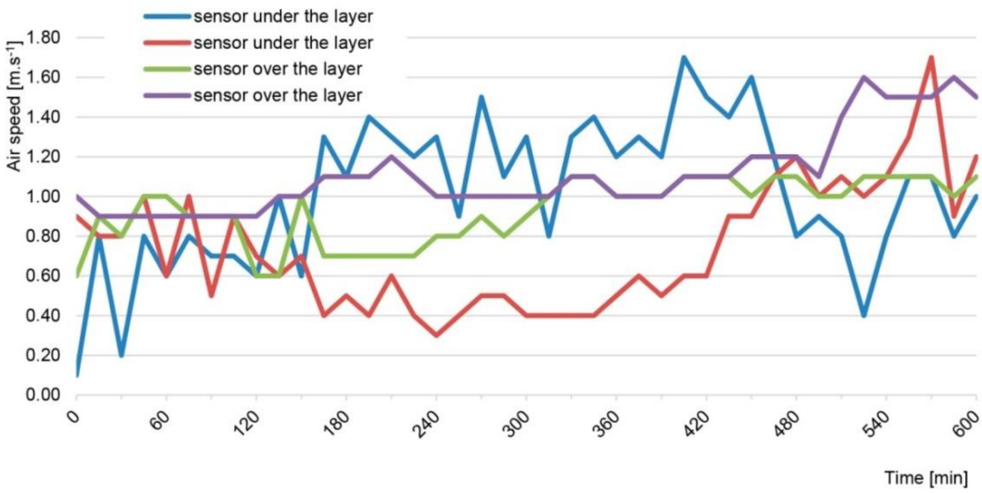

Fig. 6. – Air speed during the drying process

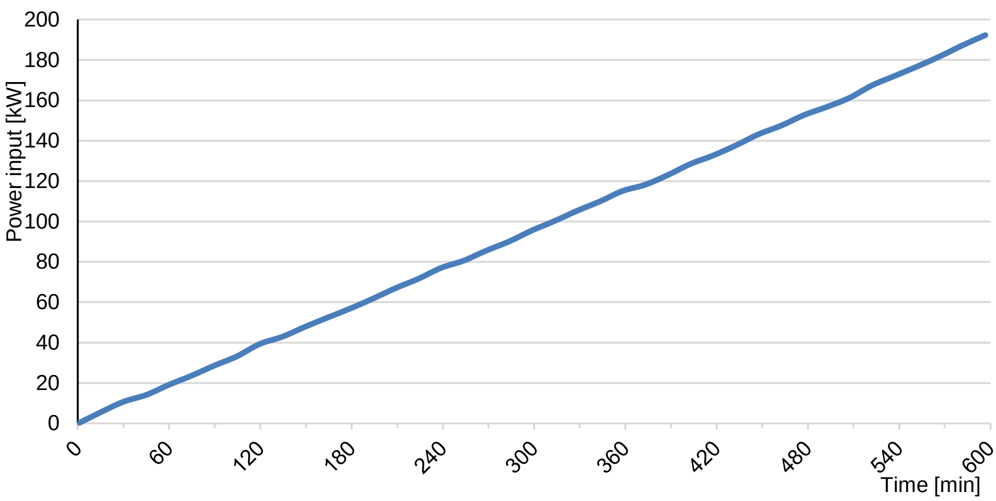

Fig. 7. – Cumulation of electric energy consumption during the process of drying

During the drying process samples were taken for purposes of laboratory analyses. Results of the sample laboratory analyses are presented in Tab. 2. The laboratory analyses focused, inter alia, also on essential oils, xanthohumol (X) and desmethylxanthohumol (DMX). High drying temperatures result in significant losses of the mentioned xanthohumol and desmethylxanthohumol. The analyses results are shown in Tab. 2.

Tab. 2. – Results of laboratory analyses of Kazbek variety samples during the drying process

Sampling time [min]	Hop moisture [% weight]		HSI	Alpha [%DM wgt]	X	DMX
	probe (Chmelařství)	gravim. (CHI Žatec)				
0	17.4	48.2	0.233	8.96	0.37	0.26
120	14.2	23.6	0.240	8.35	0.36	0.23
240	9.0	18.4	0.246	8.22	0.34	0.24
360	8.6	13.8	0.242	8.78	0.37	0.25
480	8.5	10.2	0.247	8.00	0.34	0.22

The task of research project (NAZV MZe) solution in its first year was to analyse the drying process in a designed experimental chamber dryer, which should result, in the following years of the project solution, in an optimal structural solution of the chamber dryer, leading to a design and development of a new line for gentle drying of selected hop varieties. Throughout the 2015 harvest season, continuous measurements of the drying process were being carried out, including verification of various measuring devices and methods in the experimental chamber dryer.

The air speed distribution both under and above the hop layer was very uneven and no correlations between patterns of the air relative humidity and hop moisture can be deduced from graphic waveforms.

The cumulation of electric energy consumption had linear progress.

Experiments in the laboratory chamber dryer showed that the drying time at the drying air temperature lower than 60°C is approximately 4 to 5 hours to reach cone moisture of 10 % needed for conservation of hops by pressing into sacks or square bales. This is approximately half the drying time compared to belt dryer. It follows that in belt dryer hops are exposed to allowable temperature for a very long time. Shortening the drying process to a half time would, inter alia, mean a considerable energy savings.

CONCLUSIONS

Hop drying at lower temperatures of the drying air (to 45°C) proved applicability of this concept in hop drying. A problem occurred in hop moisture measuring by means of a special probe supplied by Chmelařství, cooperative Žatec. A check determination of hop moisture in the laboratory of Hop Research Institute Co., Ltd., Žatec pointed to significant differences. As a consequence, the process was terminated early, since the special probe recorded an incorrect value of hop moisture (8.7 % of weight). The actual moisture value was almost 25 %. The cause of these false results in measuring hop moisture by the probe was an incorrect methodical procedure (the measurement was conducted too shortly after inserting the probe into a layer of pressed hops).

For practical use, and further experiments will be necessary to ensure:

- optimum ripeness hops depending on the variety,
- uniform distribution hops within the dryer including an optimal height of the layer of hops,
- temperature of the drying medium a maximum of 40 to 45°C,
- uniform distribution of the drying medium within the dryer,
- continuous monitoring of temperature and moisture of hops,
- continuous monitoring of temperature, humidity and velocity of the drying medium,
- control the speed and temperature of the drying medium,
- uniform final moisture of hop between 8-10 %,
- option air and moisture balancing hops,

documentation of the measured values.

ACKNOWLEDGEMENTS

This paper was created with the contribution of the Czech Ministry of Agriculture as a part of NAZV n° QJ1510004 research project. In the project solution, besides CULS Prague, are involved: Hop Research Institute Co., Ltd., Žatec, Chmelařství, cooperative Žatec, Rakochmel, Ltd., Kolešovice and Agrospol VelkáBystřice Ltd.

REFERENCES

1. BERNÁŠEK, K., HANOUSEK, B., RYBKA, A., KVÍZ, Z.: Drying curves shape for hop cones and energy consuption during different drying air flow rate and drying temperature. 2007, In: Conference Proceedings - 3rd International Conference, TAE 2007: Trends in Agricultural Engineering 2007, CULS Prague, 57-60 p.
2. DOE, P.E., MENARY, R.C.: Optimization of the Hop Drying Process with Respect to Alpha Acid Content. In: J. Agric. Engng Res. 24, 1979: pp. 233-248.
3. HANOUSEK, B., RYBKA, A., BERNÁŠEK, K.: Hodnocení práce česačky chmele PT 30/15 a sušení chmele v pásové a komorových sušárnách v r. 2007. Ekonomicko-technologický seminář k problematice pěstování chmele 27. 2. 2008. Hop Research Institute Co., Ltd., 2008: pp. 43-61 (In Czech).
4. HENDERSON, S.M., MILLER, G.E.: Hop Drying - Unique Problems and Some Solutions. In: J. Agric. Engng Res. 17, 1972: pp. 281-287.
5. JECH, J., ARTIM, J., ANGELOVIČ, M., ANGELOVIČOVÁ, M., BERNÁŠEK, K., HONZÍK, I. KRČÁLOVÁ, E., KVÍZ, Z., MAREČEK, J., POLÁK, P., PONIČAN, J., RUŽBARSKÝ, J., RYBKA, A., SLOBODA, A., SOSNOWSKI, S., SYPULA, M., ŽITŇÁK, M.: Stroje pre rastlinnú výrobu 3 - Stroje a zariadenia napozberovú úpravu rastlinných materiálov a nai chskladovanie. Profi Press s.r.o. Prague-Czech Republic, 2011 (In Czech and Slovak).
6. KROFTA, K.: Hodnocení kvality chmele. Metodika pro praxi. Hop Research Institute Co., Ltd., 2008: 50 p. (In Czech).
7. KROFTA, K., RYBKA, A.: Inovace sušení chmele je předmětem řešení nového výzkumného projektu. Chmelařství, roč. 88, č. 3, 2015: 31-33 p. (In Czech), ISSN 0373-403X.
8. MEJZR, J., HANOUSEK, B.: Drying of hop. Research in Agricultural Engineering, 53 (4), 2007: pp. 155-160.
9. MÜNSTERER, J.: Optimale Trocknung und Konditionierung von Hopfen. Bayerische Landesanstaltfür Landwirtschaft, Arbeitsgruppe Hopfenbau, Produktionstechnik, Wolnzach, 2006: 26 p.
10. RYBÁČEK, V.: Hop production. Development in Crop Science, 16. Elsevier, Amsterdam-Niederland and SZN, Prague-Czech Republic, 1991.
11. RYBKA, A., PATZAK, J., POKORNÝ, J.: Chmelařský den, 13. 8. 2015, Účelové hospodářství Stekník Chmelařského institutus.r.o. Žatec, 2015 (In Czech).
12. SRIVASTAVA, A. K., GOERING, C. E., ROHRBACH, R. P., BUCKMASTER, D. R.: Engineering Principles of Agricultural Machines. ASABE, 2nd Edition, Michigan, USA, 2006.
13. WEIHRAUCH, F., BAUMGARTNER, A., FELSL, M., KAMMHUBER, K., KNEIDL, J., LUTZ, A., NEUHOF, BUCKL, E., PETZINA, C., SPERR, B., WEIHRAUCH, S., WYSCHKON, B.: The influence of aphid infestation during the hop growing season on the quality of harvested cones. Programme, EBC Hop Symposium 2010, Wolnzach (Bavaria), 29, 12.-14. Sept. 2010.

Corresponding author:

doc. Ing. Petr Heřmánek, Ph.D.,Department of Agricultural Machines, Faculty of Engineering, Czech University of Life Sciences Prague, Kamýcká 129, Praha 6, Prague, 16521, Czech Republic, phone: +420 22438 3126, e-mail: hermanek@tf.czu.cz

TEMPERATURE EFFECT ON MILK SELECTED PHYSICAL PROPERTIES

P. Hlaváč, M. Božiková

Department of Physics, Faculty of Engineering, Slovak University of Agriculture in Nitra, Slovak Republic

Abstract
This article is focused on temperature dependencies of dynamic viscosity, density and activation energy of milk. Viscosity measurement was performed using a single-spindle viscometer and density was measured by pycnometric method. The measurements and calculations of mentioned physical properties were analysed in the temperature range (8–26) ºC. The relations of all physical parameters of milk to temperature showed the influence of relative fat content. Obtained relations of dynamic viscosity for milk during temperature stabilisation had an exponential decreasing progress (Fig. 1), which is in accordance with Arrhenius equation. Density of samples is decreasing linearly with the temperature (Fig. 2). Temperature dependencies of activation energy are described by linear increasing functions (Fig. 3). The mathematical description of the dependencies is summarised by regression equations Eq. (2, 4 and 5). Coefficients of regression equations and coefficients of determination are presented in Tab. 1.

Key words: milk, dynamic viscosity, density, activation energy, temperature, fat content.

INTRODUCTION

In the quality evaluation of food material, it is important to know the physical properties, particularly mechanical, rheological and thermophysical (HLAVÁČ AND BOŽIKOVÁ, 2013). Effect of composition on physical properties of milk was investigated by many authors (ROHM ET AL., 1996; CHEN ET AL., 2004; ALCANTARA, 2012; MONTANHOLI ET AL., 2013). Densities and viscosities of various milk were measured by OGUNTUNDE AND AKINTOYE (1991), DINKOV ET AL. (2008), ALCANTARA (2012), KUMBÁR AND NEDOMOVÁ (2015). The knowledge about physical properties of packaging materials is also important (KUBÍKAND, ZEMAN, 2014). Automatically controlled processes at manufacturing, handling and holding require exact knowledge about physical quantities of material. The knowledge of physical properties of food materials has a decisive importance for the implementation of many technological processes, especially for monitoring their quality (FIGURA AND TEIXEIRA, 2007). Very interesting is the monitoring of material quality in the food industry, especially it is very convenient for food materials with a short expiration time as dairy products. So, the presented research was oriented on selected dairy products – milk with different fat content. There are still detected new methods that are utilizing new modern apparatuses (HLAVÁČOVÁ, 2003). Because of the necessity to measure many series of measurements in a short time, scientists have preferred non-stationary methods for physical parameters measurements to stationary methods which take a long time. On the base of presented facts, there were created experimental apparatuses for determination of basic rheological parameters. The rheological parameters were measured by the rotational viscometer. Details of the experimental apparatus were selected according to the nature of the sample and according to the nature of measured parameters.
The aim of our research was oriented on finding the relations of selected physical properties of milk to the temperature.

MATERIALS AND METHODS

The viscosity measurement can be done by various devices. There are often used the following types of viscometers (SAHIN AND SUMNU, 2006): capillary flow viscometers, orifice type viscometers, falling ball viscometers, rotational viscometers, vibration viscometers, etc.
In rotational viscometers, the sample is sheared between two parts of the measuring device by means of rotation. Shear rate is proportional to rotational speed, so it is possible to measure the shear stress as shear rate is changed. The sample can be sheared as long as necessary; therefore, rotational viscometers are the best for non-Newtonian fluids and fluids with a time-dependent behaviour. Rotational viscometers can be divided into four groups: concentric cylinder (coaxial rotational) viscometers, cone and plate viscometers, parallel plate viscometers and single-spindleviscometers (STEFFE, 1996).

The rotational viscometer Anton Paar DV-3P was selected for our research. It works on the principle of single-spindle viscometer, which is based on measurement of torsion forces required to overcome the resistance of material at rotating spindle embedded in the measured material. The spinning spindle is interconnected through the spring to the engine shaft, which is rotating with defined velocity. The angle of angular rotation shaft is measured electronically. On the base of internal calculations, values of dynamic viscosity in mPa·s are directly displayed from measured values. This instrument works with several types of spindles and uses a wide area of velocity, which allows the measurement of viscosity in a wide area. For liquids with constant viscosity resistance to motion, it is growing proportionately with the velocity and dimension of the spindle. The combination of various spindles and velocities provides an optimal selection extent for viscosity measurement. The measuring range for determination of rheological properties of material can be changed by using other velocity with the same spindle. During our research we used spindle R2 and frequency of rotation was 200 min^{-1}. Temperatures higher than 20 °C were obtained by heating in the water bath and lower temperatures were obtained by cooling in the refrigerator.

It is evident from theory that viscosity is influenced by temperature. This dependency can be described by Arrhenius equation:

$$\eta = \eta_0 \, e^{-\frac{E_A}{RT}} \tag{1}$$

where η_0 is reference value of dynamic viscosity [Pa·s]; E_A is activation energy [J·mol^{-1}]; R is gas constant [J·mol^{-1}·K^{-1}]; T is absolute temperature [K] (MUNSON ET AL., 1994).

In our case, the identical type of exponential function (Eq. 2) was proved for every measured relation, which corresponds to Arrhenius equation

$$\eta = A e^{-B\left(\frac{t}{t_0}\right)} \tag{2}$$

where t is temperature [°C]; t_0 = 1 °C; A and B are constants dependent on the kind of material, and on ways of processing and storing [mPa·s; –].

Density of material ρ is defined as a ratio between mass of material m and its volume V at the same temperature

$$\rho = \frac{m}{V} \tag{3}$$

The definition is valid for solids, liquids, gases and disperses (FIGURA AND TEIXEIRA, 2007). The standard SI unit of density is kg.m^{-3}. Density of most solids and liquids can be calculated using this equation (Eq. 3). The accuracy of this method depends on precision of mass and volume determination. One of the most exact methods for measurement of liquid density is pycnometric method (SAHINANDSUMNU, 2006). Pycnometer is a closable glass jar with specified volume. Measured liquid material is filled into the pycnometer and after it the pycnometer is closed. All air bubbles must be removed before closing of the pycnometer. Pycnometer with the sample is weighted and the density of material can be calculated using Eq. (3). This process was repeated with all samples at different temperatures from measured temperature range.

For all samples the dependencies of density on temperature can be described by decreasing linear function:

$$\rho = C - D\left(\frac{t}{t_0}\right) \tag{4}$$

where C and D are constants dependent on kind of material, and on ways of processing and storing [kg·m^{-3}; kg·m^{-3}].

In chemistry, activation energy means the amount of energy that is required to activate atoms or molecules to a condition in which they can undergo chemical transformation or physical transport. In terms of the transition-state theory, activation energy is the difference in energy content between atoms or molecules in an activated or transition-state configuration and the corresponding atoms and molecules in their initial configuration. Activation energies are determined experimentally at different temperatures (MANSUR ET AL., 2014).

In case that $\eta_0 = A$, Eq. 1 and Eq. 2 can be used for calculation of activation energy at different temperatures. In our case, temperature dependencies of activation energy can be described by a linear increasing function:

$$E_A = F\left(\frac{t}{t_0}\right) - G \tag{5}$$

where F and G are constants dependent on the kind of material, and on ways of processing and storing [J·mol^{-1}; J·mol^{-1}].

Milk is an emulsion or colloid of butterfat globules within a water-based fluid. Each fat globule is surrounded by a membrane consisting of phospholipids and proteins; these emulsifiers keep the individual globules from joining together into noticeable grains of butterfat and also protect the globules from the fatdigesting activity of enzymes found in the fluid portion of the milk (MC GEE, 1984). In unhomogenized cow's milk, the fat globules average is about four micrometers across. The fat-soluble vitamins A, D, E, and K are found within the milk fat portion of the milk (JANZEN ET AL., 1982).

Samples of milk (RAJO) were purchased in local market. All measured samples of milk were provided in storage boxes at the temperature from 4 °C to 5 °C and 90 % of air moisture content during 24 hours before measurement, and relations of chosen parameters to temperature were measured during the temperature stabilization of samples. All measurements were made in laboratory settings. Measurements were performed for milks with relative fat content 0.5 %, 1.5 % and 3.5 % in the temperature range (8–26) ºC.

RESULTS AND DISCUSSION

Measured values of dynamic viscosity for milk with 0.5 %, 1.5 % and 3.5 % of fat content are shown in Fig. 1.

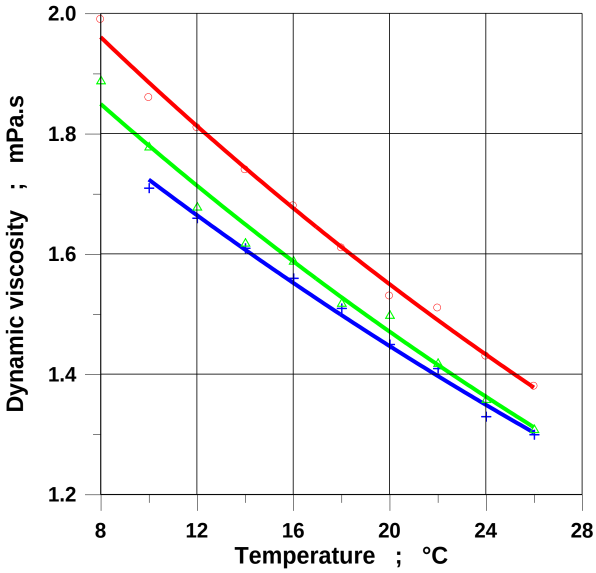

Fig. 1. – Relations of dynamic viscosity to temperature for the samples of milk with fat content (+) 0.5%; (Δ) 1.5 %; (○) 3.5 %

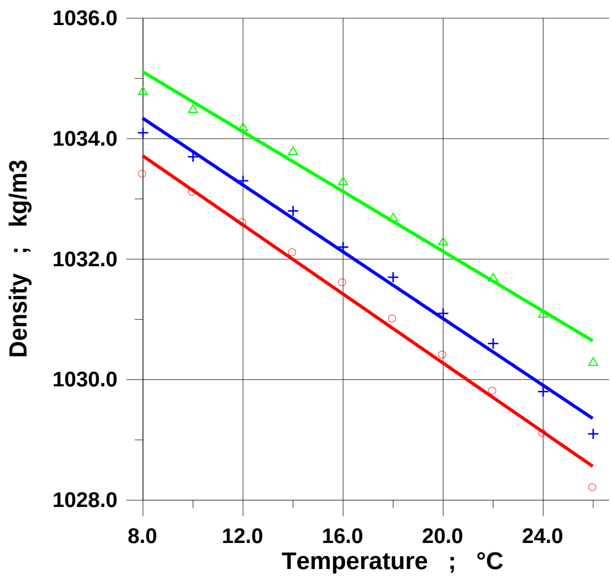

Fig. 2. – Relations of density to temperature for the samples of milk with fat content
(+) 0.5 %; (Δ) 1.5 %; (○) 3.5 %

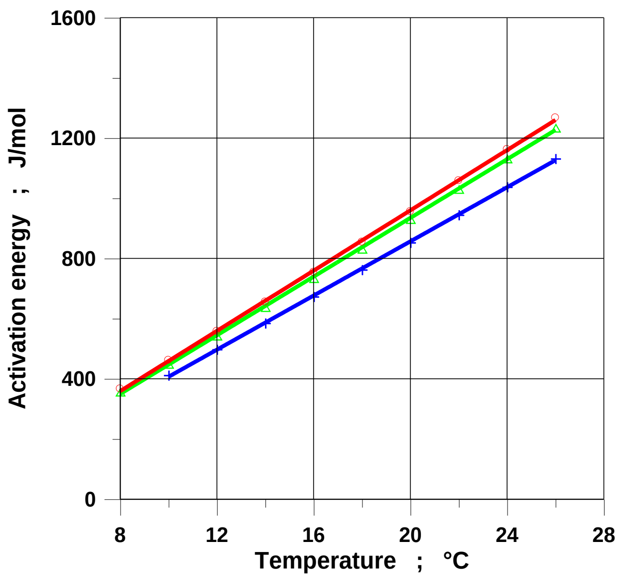

Fig. 3. – Relations of activation energy to temperature for the samples of milk with fat content (+) 0.5 %; (Δ) 1.5 %; (○) 3.5 %

It can be seen from Fig. 1 that the highest dynamic viscosity values were observed in the sample milk with 3.5 % of fat content and the lowest dynamic viscosity values were in the sample milk with 0.5 % of fat content. The highest viscosity of milk (with 3.5 % of fat content) 1.99 mPa·s was obtained at the lowest temperature from the measured temperature range. The lowest viscosity of milk (with 0.5 % of fat content) 1.30 mPa·s was obtained at the highest temperature from the measured temperature range. Similar results were obtained by KUMBÁR AND NEDOMOVÁ (2015). The progress can be described by decreasing exponential function, which is in accordance with Arrhenius equation (Eq. 1). All regression coefficients and coefficients of determination are shown in Tab. 1. Coefficients of determination had the highest values in the interval (0.987–0.994) for the exponential function, which is in accordance with Arrhenius equation (Eq. 1). Obtained results and temperature dependencies are in good agreement with results presented by KUMBÁR AND NEDOMOVÁ (2015), ALCANTARA (2012), DINKOV ET AL. (2008), FIGURAAND TEIXEIRA (2007), SAHIN AND SUMNU (2006), OGUNTUNDE AND AKINTOYE (1991).

Mass of pycnometer with sample of milk was weighted at each temperature with precision ± 0.0001 g. Density values were calculated from Eq. 3.Temperature dependencies of milks density are presented on Fig. 2. It is evident from Fig. 2 that milks density is decreasing linearly with temperature in measured temperature range. Density of milks is also influenced by amount of fat content. The highest fat content (3.5 %) had caused the lowest density (Fig. 2). But in case of lower fat contents (0.5 % and 1.5 %, which are very similar) this proportion does not proved. It could be due to the different amount of proteins in measured samples of milk. Coefficients of regression equation and coefficients of determination (0.984 – 0.992) are presented in Tab. 1. Similar values and decreasing progresses of milk density with increasing temperature were observed by other authors (KUMBÁR AND NEDOMOVÁ, 2015; ALCANTARA, 2012, DINKOV ET AL., 2008; OGUNTUNDE AND AKINTOYE, 1991).Temperature dependencies of activation energy for milk are shown in Fig. 3. All regression coefficients and coefficients of determination are shown in Tab. 1. Coefficients of determination are very high (not less than 0.9997) for linear function.

It can be seen from Fig. 3 that activation energy is increasing linearly with temperature increase. Fig. 3 clear indicates that the higher amount of fat caused higher activation energy values. It can be expressed by more difficult movement of fat molecules in milk. Lower values of activation energy were obtained for milk with lower fat content. The obtained results of milk activation energy and also its temperature dependencies are innovative. It is not possible to found comparable results.

Tab. 1. – Coefficients A, B, C, D, F, G of regression equations (Eq. 2, Eq. 4, Eq. 5) and coefficients of determination

	Regression equation (2)			**Regression equation (5)**		
Milk/ Fat content	**Coefficients**					
	A [mPa·s]	**B[1]**	**R^2**	**F[J·mol^{-1}]**	**G[J·mol^{-1}]**	**R^2**
0.5 %	2.05302	0.0174987	0.993841	44.9763	43.2551	0.999785
1.5 %	2.15451	0.0190892	0.986770	48.7468	40.6244	0.999729
3.5 %	2.29349	0.0196039	0.994037	50.0615	41.7257	0.999729
Milk/ Fat content	**Regression equation (4)**					
	Coefficients					
	C[kg·m^{-3}]		**D[kg·m^{-3}]**		**R^2**	
0.5 %	1036.55		0.276 969		0.991 812	
1.5 %	1037.09		0.248 183		0.983 792	
3.5 %	1036.00		0.286 364		0.988 326	

CONCLUSIONS

The main part of the presented paper is focused on experimental results for the samples of milk with different fat content. Presented results are relations of dynamic viscosity, density and activation energy to temperature. Relations were determined according to coefficients of determination. Temperature dependencies of dynamic viscosity of all samples are decreasing exponentially with increased temperature, which is in accordance with Arrhenius equation which has exponential shape. Values of dynamic viscosity are influenced by other factors, i.e. by the amount of fat content. Higher values of fat content caused higher values of dynamic viscosity, and a denser structure of sample caused an increase of dynamic viscosity. Density of samples was characterized by decreasing linear function in this temperature range. The highest fat content of milk had caused the lowest density. Lower fat contents did not confirm previous result, which may be due to the differences in protein content in measured samples of milk. The activation energy of all samples is increasing linearly with temperature increase. The higher amount of fat caused higher activation energy values. It can be expressed by more difficult movement of fat molecules in milk. Lower values of activation energy were obtained for milk with lower amount of fat.

ACKNOWLEDGEMENT

This work was supported by the project of VEGA 1/0854/14 of Ministry of Education, Science, Research, and Sport of the Slovakia and by Research Centre AgroBioTech built in accordance with the project Building Research Centre „AgroBioTech" ITMS 26220220180.

REFERENCES

1. ALCANTARA, L. A. P.: Density and viscosity of bovine milk affect by temperature and composition. IJFE, 8, 2012: 556 – 568.
2. DINKOV, K., DUSHKOVA, M., TOSHKOV, N.: Regression models for density and viscosity of ultrafiltration milk concentration. BJAS, 14: 542 – 548.
3. FIGURA, L. O., TEIXEIRA, A. A.: Food Physics, Physical properties – measurement and applications, Springer, USA, 2007.
4. HLAVÁČ, P., BOŽIKOVÁ, M.: Influence of storing and temperature on rheologic and thermophysical properties of whisky samples. JCEA, 14, 2013: 291–304.
5. HLAVÁČOVÁ, Z.: Low frequency electric properties utilization in agriculture and food treatment,Res. Agr. Eng., 49, 2003: 125–136.
6. CHEN, S., BOBE, G., ZIMMERMAN, S., HAMMOND, E. G., LUHMAN, C. M., BOYLSTON, T. D., BEITZ, D. C.: Physical and sensory properties of dairy products from cows with various milk fatty acid composition. J. Agric. Food Chem., 52, 2004: 3422 – 3428.
7. JANZEN, J. J., BISHOP, J. R., BODINE, A. B., CALDWELL, C. A.: Shelf-life pasteurized fluid milk as affected by age of raw milk.J. DairySci., 65(12), 1982: 2233–2236.
8. KUBÍK, Ľ., ZEMAN, S.: Mechanical properties of polyethylene foils, JCEA, 15, 2014: 138–145.
9. KUMBÁR, V., NEDOMOVÁ, Š.: Viscosity and analytical differences between raw milk and UHT milk of Czech cows. SAB, 46, 2015: 78 – 83.
10. MANSUR G. A. ET AL., Encyclopaedia Britannica, 2014, Available at: www.britannica.com/EBchecked/topic/4535/activation-energy. Accessed 10 January 2016.
11. MUNSON, B. R., YOUNG, D. F., OKIISHI, T. H.: Fundamentals of fluid mechanics, John Wiley & Sons, New York, 1994.
12. MC GEE, H.: "Milk and Dairy Products". On Food and Cooking: The Science and Lore of the Kitchen, Charles Scribner's Sons, New York, 1984: 3–53.
13. MONTANHOLI, Y. R., LAM, S., PERIPOLLI, V., VAN DER VOORT, G., MILLER, S. P.: Associations between chemical composition and physical properties of milk and colostrums with feed efficiency in beef cows. CJAS, 93, 2013: 487 – 492.
14. ROHM, H., MÜLLER, A., HEND-MILNERA, I.: Effect of composition on raw milk viscosity. Milchwissenschaft, 51, 1996: 259 – 261.
15. OGUNTUNDE, A. O., AKINTOYE, O. A.: Measurement and comparison of density, specific heat and viscosity of cow´s milk and soymilk. J. Food Eng., 13, 1991: 221 – 230.
16. SAHIN, S., SUMNU, S. G.: Physical properties of foods, Springer, USA, 2006.
17. STEFFE, J. F.: Rheological method in food process engineering, Freeman Press, East Lansing (USA), 1996.

Corresponding author:

Peter Hlaváč, Department of Physics, Faculty of Engineering, Slovak University of Agriculture in Nitra, Slovak Republic

DRYING CHARACTERISTICS AND ELECTRICAL PROPERTIES

Z. Hlaváčová, T. Regrut, M. Malínek

Department of Physics, Slovak University of Agriculture in Nitra, Slovakia

Abstract

The aim of the contribution was to find a correlation between drying characteristics and electrical properties. We measured electrical properties of some food materials by the bridge method. The frequency and moisture content dependencies of these properties were also determined. We investigated the time dependencies of dried samples mass, moisture ratio, and moisture content. We found out that the moisture ratio of samples decreases with time. During drying, the mass of the samples decreases according to fifth degree polynomic function. The impedance decreases with frequency. The resistivity decreases with increase of the moisture content according to the power function.

Key words: electrical properties, moisture ratio, moisture content, temperature.

INTRODUCTION

In the case of food materials storing, the moisture content and temperature are the most important parameters which influence the various processes in them. Food materials have limited durability in general because they are in instable or metastable states. The decrease of food materials stability during ageing is caused by mechanical deterioration, influence of water, transport of heat and humidity, metabolic processes, respiration, destructive processes caused by microorganism (BLAHOVEC, 2008). Water can be removed from food materials by various processes. On the beginning, we can name the mechanical treatment. The water removal is caused by the material compression or centrifugation. Second is the drying, it is the process of the removal of water (moisture) from hygroscopic materials at low to medium moisture contents (normally < 30 % wb) by means of evaporation. When the moisture content of the food products is high (usually > 50 % wb) the process of removal of moisture is referred as dehydration (JAYAS, SINGH, 2011). Drying and dehydration are high energy consumption process, because of very high latent heat of the water evaporation (BOŽIKOVÁ, HLAVÁČ, 2013). Only if we use aeration, it needs only low energy costs (RAGHAVAN, SOSLE, 2007). The aeration is usually carried out in a storage bin with ventilation. In hot, dry countries, they can use solar drying (MISHA ET AL., 2016). Quality assurance of the dried product, potential risks at convective drying, and quality of dried material protection are described by ŽITŇÁK ET AL. (2015), KUBÍK AND ZEMAN (2014). In the convective drying of food can be used power ultrasound, and the drying rate is affected in this case by both the drying temperature and the applied ultrasonic power. Power ultrasound brings mechanical effects both on the gas-solid interfaces and in the material being dried, which may facilitate water removal without introducing a high given amount of thermal energy. The ultrasound application induces an increase of both the effective diffusion and the mass transfer coefficients, although, this increment is more notorious at low temperatures than higher ones (RODRIGUES ET AL., 2014; CÁRSEL ET AL., 2011). Microwave, chemical, and pulsed electric field can be used as a pre-treatment processes on convective drying of food. In such cases, heat is transferred to the product by a heating medium usually hot air or superheated steam, on other hand heat could be applied through radiation, for example, in infrared dryers or through volumetric heating, for example, in microwave dryers. Depending on the heat source, operating pressure, and operating mechanism, dryers are classified as hot air, infrared, microwave, vacuum, freeze, flash, superheated steam, spouted bed, fluidized bed, and spray (JAYAS, SINGH, 2011). Other processes used at water removal from food materials are osmotic drying, lyophilization, and addition of water absorbing substances (e. g. silica gel).

Electrical properties of food materials have many applications in various branches (JHA ET AL., 2011). The measurement of electrical properties of food can be used to get information about many other characteristics of this material; in addition, there are some food processes which are based on electrical effects. An electric current flowing through a food material causes a temperature rise due to energy dissipation by the electric resistance of the food. Ohmic heating has several advantages. The heat is produced inside the food. On the other hand, high voltage electric pulses can damage cells and cause higher permeability of cell walls (FIGURA, TEIXEIRA, 2007). The dielectric properties of materials dictate, to a large extent, the behaviour of the materials when subjected to radio-frequency (RF) or microwave field for the purposes of heating, drying or processing the materials. The characterisation of dielectric properties is vital for understanding the response of a material to microwaves, since most useful quantities needed in the design of microwave thermal processes can be described in terms of them (JHA ET AL., 2011; VENKATESH, RAGHAVAN, 2004).

Many authors use mathematical models for describing the drying process. The effects of air temperature, air-flow rate and sample thickness on the drying kinetics of carrot cubes were investigated by DOYMAZ (2004). The Page model gave better prediction than the Henderson and Pabis model and satisfactorily described drying characteristics of carrot cubes. KERTÉSZ ET AL. (2015) confirmed this model also for carrot slices.

MATERIALS AND METHODS

The samples of carrots (*Daucus carota* L.) were procured from the local market. We used 50 slices for the measurement. Other samples: corn (*Zea mays* L.) grains hybrid, of CTF-8C, wheat (*Triticum aestivum* L.) grains variety, of Magister, Amaranth (*Amaranthus hypochondriacus* L. and *Amaranthus caudatus*L.) seeds we had from various departments of the Slovak University of Agriculture in Nitra. Samples were dried in cabinet dryer Venticell 111 (MMM group). Moisture analyser MAC 50NP (RADWAG) was also used for the drying of samples. The mass of samples was measured with a Sartorius Basic electronic analytical and precision balance (Sartorius AG). The moisture content of samples was determined according to standard by drying to constant mass. The moisture content wet basis was calculated from mass losses. Moisture ratio is defined as:

$$M_R = \frac{u - u_e}{u_0 - u_e} \tag{1}$$

where: M_R is moisture ratio, u, u_0 and u_e are local, initial and equilibrium moisture contents, respectively. The values of equilibrium moisture content, u_e, are relatively low compared to u or u_0. Thus Eq. 1 is simplified (DOYMAZ, 2004) to:

$$M_R = \frac{u}{u_0} \tag{2}$$

The electrical properties of samples were measured with precision LCR meter GoodWill 821(Good Will Instrument Co.) in frequency range from 100 Hz till 200 kHz, and also with precision LRC meters HP 4284A and 4285A (Keysight Technologies) at frequencies from 30 Hz to 30 MHz, at voltage of 1 V. Each electric property was measured at all frequencies three times. Average value and standard deviation has been computed from these ones. The measured values were loaded by PC.

RESULTS AND DISCUSSION

The moisture ratio versus time of drying curves for the carrot samples No 2, and 5 as influenced by temperature 50 °C are shown in Fig. 1.

Moisture ratio decreases with drying time, and after drying, moisture content (wb) ranged from about 7 % to 8 %. As we can see, the change in moisture ratio at the beginning of the drying period is significant, compared to the final stage of drying where very small changes in moisture ratio were reported. For approximation we used the exponential function:

$$M_R = M_{R0}\, e^{-c\tau} \tag{3}$$

where: M_{R0} - reference value of moisture ratio, c - constant (s^{-1}).

In Tab. 1, the coefficients of regression equation Eq. (3) and coefficient of determination are presented. The values of the coefficient of determination also for other slices range from 0.9865 to 0.9983. Eq. 3 is in good agreement with Henderson and Pabis model. We can also use the Page's model which has been widely advocated for the thin-layer drying of solids under constant drying conditions. This model has produced good fits in predicting the drying of sweet potato, garlic, apricot, seedless grapes, and mint leaves (DOYMAZ, 2004). The samples of corn and wheat were dried in Moisture analyzer MAC to constant mass. For corn grains the drying time 120 min and for wheat grains 150 min was appropriate. The drying curves can be approximated by polynomial function:

$$m = a_0 + a_1\tau + a_2\tau^2 + a_3\tau^3 + a_4\tau^4 + a_5\tau^5 \tag{4}$$

where: m – mass, a_i – coefficients of regression equation, τ – time.

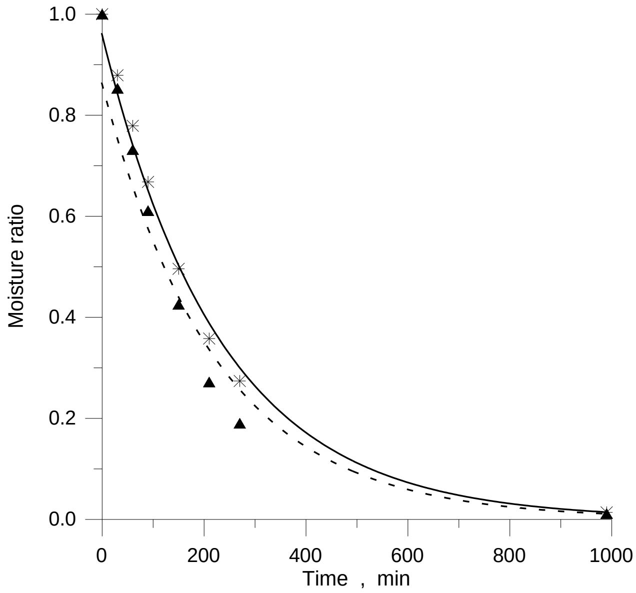

Fig. 1. – Drying time dependence of moisture ratio for carrot slices No 2 (△), 5 (∗)

Tab. 1. – Coefficients of regression equation Eq. (3) and coefficient of determination

Sample	M_{R0}	c (s^{-1})	R^2
Slice 2	0.8637	- 0.0045	0.9865
Slice 5	0.9611	- 0.0043	0.9983

The coefficient of regression equation Eq. (4) and coefficient of determination, which has high value, are in Tab. 2.

At the drying beginning, the change in mass is more notable as the end of drying. This fact is right also at lower moisture content as has carrot. We had used the fifth degree polynomial function as regression equation. For thin layer drying, Wang and Sing model can be used (KILIC, 2016), which is second degree polynomial function (quadratic function). But Eq. 4 for our samples has higher coefficient of determination. This may be due to the fact that the sample had a loose character.

Fig. 3 represents drying time dependency of the apparent moisture content for amaranth seeds. The drying temperature was (103 – 105) °C. Each hour after conditioning, samples were weighed and the moisture content was calculated.

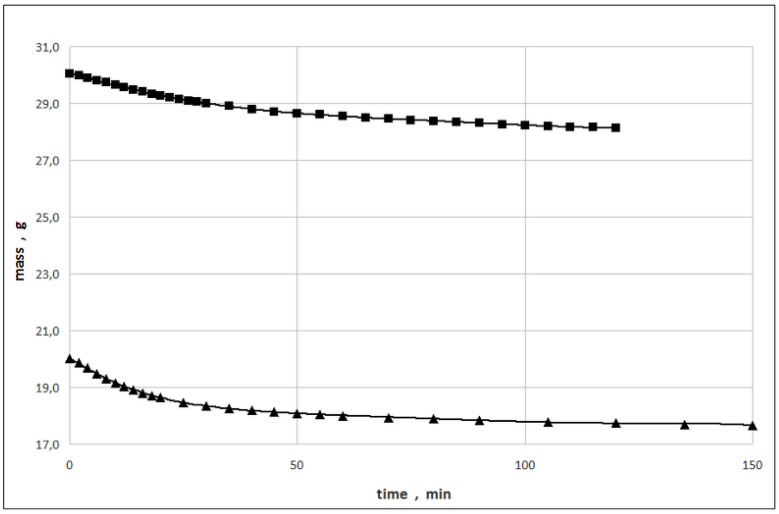

Fig. 2. – Time dependence of the sample mass, maize (CTF-8C) grains (■) and wheat (Magister) grains (▲)

Tab. 2. – Coefficients of regression equation Eq. (4) and coefficient of determination

Coef.	a_0 (g)	a_1 (g/min)	a_2 (g/min^2)	a_3 (g/min^3)	a_4 (g/min^4)	a_5 (g/min^5)	R^2
corn	30.067	- 0.0465	0.0003	4E-06	- 6E-08	2E-10	0.9996
wheat	20,043	- 0.11	0.0025	- 3E-05	2E-07	-4E-10	Higher

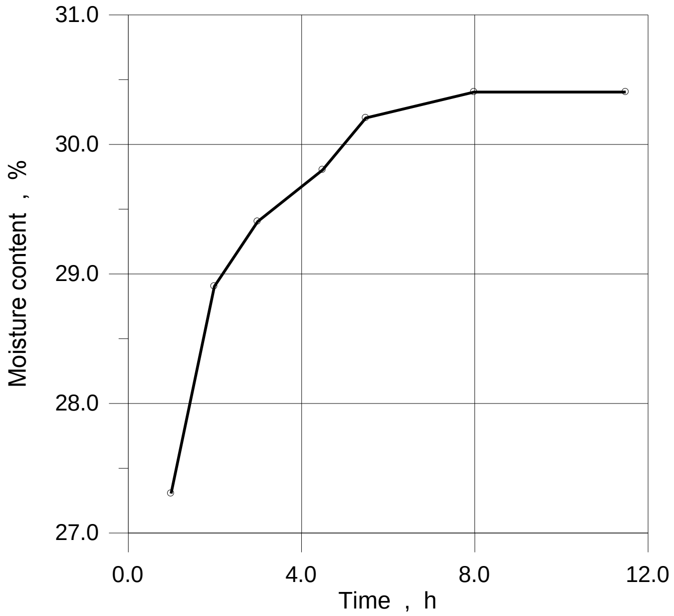

Fig. 3. – Drying time dependence of apparent moisture content (wb) for Amaranthushypochondriacus seeds (mass 10 g)

We can observe the changes in slope of the curve caused by different types of bound water evaporation. The stable (and thus correct) value of moisture content was reached after 8 hours. The standard for the amaranth seeds moisture content determination currently not exist, and according our measurement, we can recommend the required drying time, 8 hours.

Fig. 4 illustrates the frequency dependence of impedance for the sample of dried carrot slice No 16 after drying for 660 min, and 780 min.

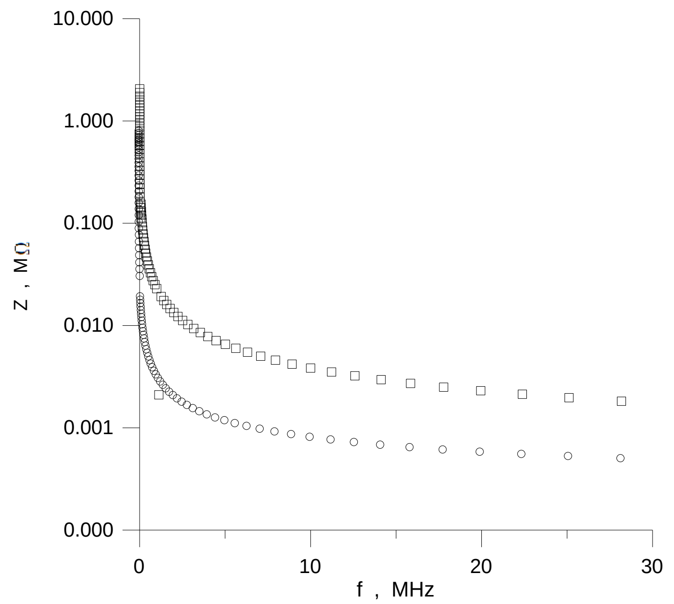

Fig. 4. – Frequency dependence of impedance for the sample of dried carrot slice No 16 (660 min - o, 780 min - □)

The following charts are described by power function

$$Z = Z_o \left(\frac{f}{f_o} \right)^{-k} \qquad (5)$$

where: Z - impedance, Z_0 - reference value of impedance, f - frequency, f_o = 1 Hz, k – constant. Tab. 3 contains the coefficients of regression equation Eq. (7) and coefficients of determination.

Tab. 3. – Coefficients of regression equation Eq. (5) and coefficient of determination for slice No 16

Time of drying	Z_0 (MΩ)	k	R^2
660 min	300 000	- 0.926	0.9931
780 min	200 000	- 0.9056	0.9893

The impedance of the sample 16 is increasing with drying time because the moisture content of the sample decreases with drying time. In the final stage of drying, there can be recorded a very little change in the values of moisture content of samples (KERTÉSZ ET AL., 2015). The impedance of these samples at this stage does not differ greatly from each other, as shown on Fig. 4.

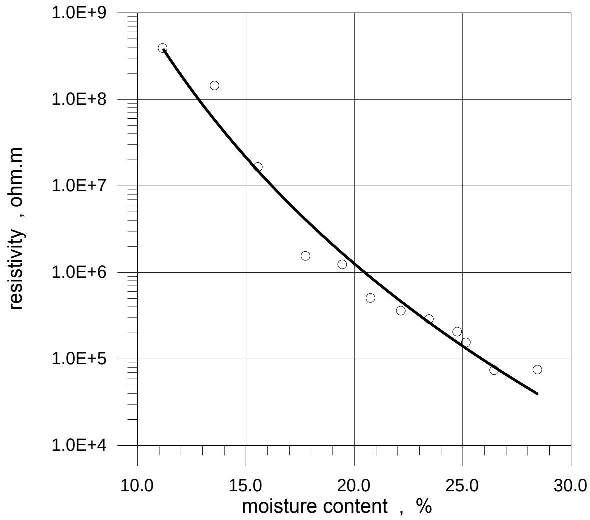

Fig. 5. – Moisture content dependency of resistivity for the sample of Amaranthuscaudatus at an average bulk density of 760.4 kg.m^{-3}

The resistivity decreases with moisture content, as is shown on Fig. 5. We can use once again the decreasing power function as the mathematical model to describe this dependence:

$$\rho = \rho_o \, \omega^{-d} \qquad (6)$$

where: ρ - resistivity, ρ_o = 8.00329 .10^{18} Ω.m – resistivity at the reference moisture content, ω - moisture content wet basis, and d = 9.8411 – constant. Regression equation (6) has high coefficient of determinations R^2 = 0.969244. This regression equation was used also by VERMA ET AL. (2001) for the conductivity of Brassica species.

CONCLUSIONS

We found out the connection between drying characteristics (as are change in mass, moisture ratio, moisture content) and electrical properties. Most significant factor influencing electrical properties is the moisture content, and this is the reason why correlation between drying characteristic and electrical properties exists.

The results of the measurements are time dependencies of sample mass, moisture ratio, apparent moisture content. First two characteristics decrease with drying time, apparent moisture content increasing with the time. We found out that the impedance of the measured samples decreases with frequency according to power function in measured frequency range. The impedance of the samples is increasing with drying time because the moisture content of the samples decreases with drying time. The resistivity decreases with moisture content according to power function. The regression equations coefficients of determination reached high values for all measured quantities and materials.

Drying characteristics of various agricultural and food materials are different and are also influenced by growing region, growing season, and weather conditions; therefore, it becomes necessary to study drying characteristics of the specific product for design of proper and efficient drying conditions. We can conclude that the measured electrical properties are investigated to reveal the quality of food materials and quality of drying as well.

ACKNOWLEDGEMENTS.

This work was supported by research project VEGA 1/0854/14 of Ministry of Education, Science, Research, and Sport of the Slovakia, and by Research Center AgroBioTech built in accordance with the project Building Research Centre „AgroBioTech" ITMS 26220220180.

REFERENCES

1. BLAHOVEC, J.: Agromaterials. 1st ed., Prague, Czech Republic, Czech University of Life Sciences 2008.
2. BOŽIKOVÁ, M., HLAVÁČ, P.: Comparison of thermal and rheologic properties of Slovak mixed flower honey and forest honey. Res. Agr. Eng. 59, 2013: 1-8.
3. CÁRCEL, J. A., GARCIA-PEREZ, J. V., RIERA, E., MULET A.: Improvement of convective drying of carrot by applying power ultrasound - Influence of mass load density. DRY TECHNOL, 29, 2011: 174–182.
4. DOYMAZ, I.: Convective air-drying characteristics of thin layer carrots. J Food Eng, 61, 2004: 359-364
5. FIGURA, L. O., TEIXEIRA, A. A.: Food Physics. 1st ed., Berlin, Germany, Springer 2007.
6. JAYAS, D. S., SINGH, C. B.: Drying of agricultural products. In: GLIŃSKI, J., HORABIK, J., LIPIEC, J. (Eds.): Encyclopaedia of Agrophysics. pp. 231-232. Dordrecht, Germany, Springer Science + Business Media 2011.
7. JHA, S. N., NARSAIAH, K., BASEDIYA, A. L., SHARMA, R., JAISWAL, P., KUMAR, R., BHARDWAJ, R.: Measurement Techniques and Application of Electrical Properties for Non-destructive Quality Evaluation of Foods - a Review. J FOOD SCI TECH MYS, 48, 2011: 387-411.
8. KERTÉSZ, A., HLAVÁČOVÁ, Z., VOZÁRY, E., STAROŇOVÁ, L.: Relationship between moisture content and electrical impedance of carrot slices during drying. Int. Agrophys., 29, 2015: 61-66.
9. KILIC, A.: Mathematical modelling of low temperature high velocity (LTHV) drying in foods. J FOOD PROCESS ENG, 00, 2016: 1-17.
10. KUBÍK, Ľ., ZEMAN, S.: Determination of oxygen permeability and mechanical properties of the aluminium paper foils. Res. Agr. Eng., 60, 2014: 172-179.
11. MISHA, S., MAT, S., RUSLAN, M. H., SALLEH, E., SOPIAN, K.: Performance of solar assisted solid desiccant dryer for oil palm fronds drying. SOL ENERGY, 132, 2016: 415-429.
12. RAGHAVAN, V. G. S., SOSLE, V.: GRAIN DRYING. IN: MUJUMDAR, A. S. (ED.): Handbook of Industrial Drying, pp. 563-573. Boca Raton, USA, CRC Press 2007.
13. RODRÍGUEZ, Ó., SANTACATALINA, J. V., SIMAL, S., GARCIA-PEREZ, J. V., FEMENIA, A., ROSSELLÓ, C.: Influence of power ultrasound application on drying kinetics of apple and its antioxidant and microstructural properties. J FOOD ENG, 129, 2014: 21–29.
14. VENKATESH, M. S., RAGHAVAN, G. S. V.: An overview of microwave processing and dielectric properties of agri-food materials. BIOSYST ENG, 88, 2004: 1–18.
15. VERMA, S. S., TOMER, R. P. S., VERMA, U., SAINI, S. L.: Electrical conductivity and accelerated aging techniques for evaluating deterioration in Brassica species. CROP RES Hisar, 21, 2001: 148-152.
16. ŽITŇÁK, M., KOLLÁROVÁ, K., MACÁK, M., PRÍSTAVKOVÁ, M., BOŠANSKÝ, M.: Assessment of risks in the field of safety, quality and environment in post-harvest line. Res. Agr. Eng. 61, 2015: 26-36.

Corresponding author:

Zuzana Hlaváčová, Department of Physics, Slovak University of Agriculture in Nitra, Slovakia

MECHANICAL BEHAVIOUR OF OIL RAPE SEEDS DURING RELAXATION AND CREEP

P. Hrabě, A. Sedláček

Czech University of Life Sciences Prague, Czech Republic

Abstract
This article is focused on determination of the relaxation and creep behaviours of bulk rapeseeds under compressive loading. First part of the measurement examines the relaxation of seeds. In this case, the pressing vessel was filled with a certain amount of seeds and they were loaded compressively. Upon reaching a selected amount of force the decrease of the function of interest in time was observed and recorded. The second part of the measurement was focused on creep. During creep measurements a certain amount of rape seeds was loaded compressively; after attainment, the test load was maintained for a predetermined time. Recorded characteristics during both measurements and their mathematical descriptions are included in this article.

Key words: mathematical model; compression; force; deformation; oil.

INTRODUCTION

Rapeseed (*Brassica napus* L.) is grown on a number of Czech fields and is the oldest and most widespread economic crop in the country. It is widely used in the production of oils for food and cosmetic products. Rapeseed oil is used for the production of lubricating and hydraulic oils, varnishes, soaps, detergents and massage oils. The cakes from the seeds can be used as feed for livestock or as a fuel in the form of densified biomass pellets or briquettes (IZLI ET AL., 2009; SIRISOMBOON ET AL., 2007).

Mechanical behaviour of rapeseeds has been described by several authors (IZLI ET AL., 2009; RUSINEK ET AL., 2007; UNAL ET AL., 2009), but the course of creep and relaxation of rapes is seldom reported in literature. HERAK ET AL., (2011b) established the tangent curve function to describe the deformation characteristics of bulk rapeseeds under compression loading and few studies have been focused on rupture force and deformation characteristics (FOMIN ET AL., 1978; HERAK ET AL., 2011a; KABUTEY ET AL., 2011; HERAK ET AL., 2015; MREMA AND MC NLUTY, 1985) as well as on the mathematical description of the deformation characteristics, limit deformation ratio, maximal deformation ratio, energy ratio and oil point deformation ratio.

The optimal design and control of many primary production and postharvest operations requires an understanding to the dynamic behaviour of agricultural particulates. Agricultural and food materials tend to behave as viscoelastic materials when they are subjected to various conditions of stress and strain (RONG ET AL., 1995; RAJI AND FAVIER, 2003). Furthermore, most agricultural materials exhibit elastic behaviour during initial loading and viscoelastic behaviour with increased loading (ZOERB, 1967). It is clear that mechanical properties are time-dependent and the effect of deformation rate becomes more noticeable over time. Design of pressing devices with minimum energy requirements with respect to maximum oil output requires detailed understanding of the mechanical behaviour of pressed seeds as well as to their relaxation and creep responses under load (BLAHOVEC AND REZNICEK, 1980; FOMIN, 1978). Thus the aim of this study was to describe relaxation and creep behaviour of bulk rapeseeds under compression loading.

MATERIALS AND METHODS

For this experiment the purified rapeseeds from Czech Republic were used. Initial moisture content of seeds was 8.6 ± 0.3% DB. Pressing container with a diameter of 60 mm was filled with rape seeds to a height of 100 mm (Fig. 1). For measurement of relaxation the bulk seeds were compressed about Δl = 10mm, Δl = 20mm, Δl = 30 mm. The dependency between compressive force and time was recorded for 6 minutes on the device (Labortech, MPTest 5.050, Czech Republic).

For measurement of creep the bulk seeds were loaded by constant compressive force F = 4000 N, F = 10000 N and F =19000 N. The dependency between deformation and time was recorded for 6 minutes on the device (Labortech, MPTest 5.050, Czech Republic).

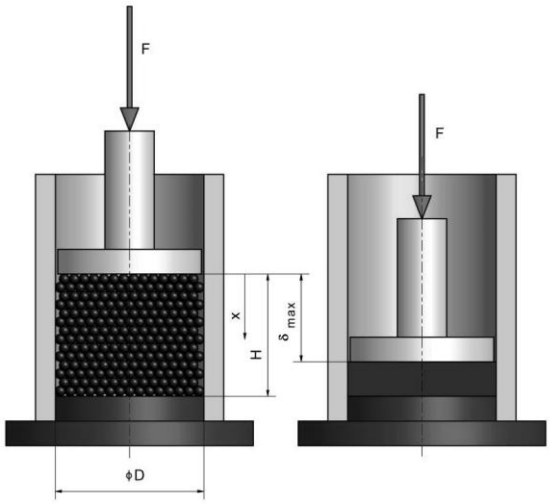

Fig. 1. – Scheme of pressing equipment (HERAK, 2015)

The measured values were evaluated in Mathcad 14. Schematic models of relaxation and creep according to which the functions of the mechanical behavior of viscoelastic materials were determined are shown in Fig. 2. The equations for relaxation and creep are described by following formulas:

Equation for relaxation:

$$R = a + b \cdot e^{c \cdot t} + d \cdot e^{f \cdot t} \tag{1}$$

Equation for creep:

$$C = a + b \cdot (1 - e^{c \cdot t}) + d \cdot (1 - e^{f \cdot t}) \tag{2}$$

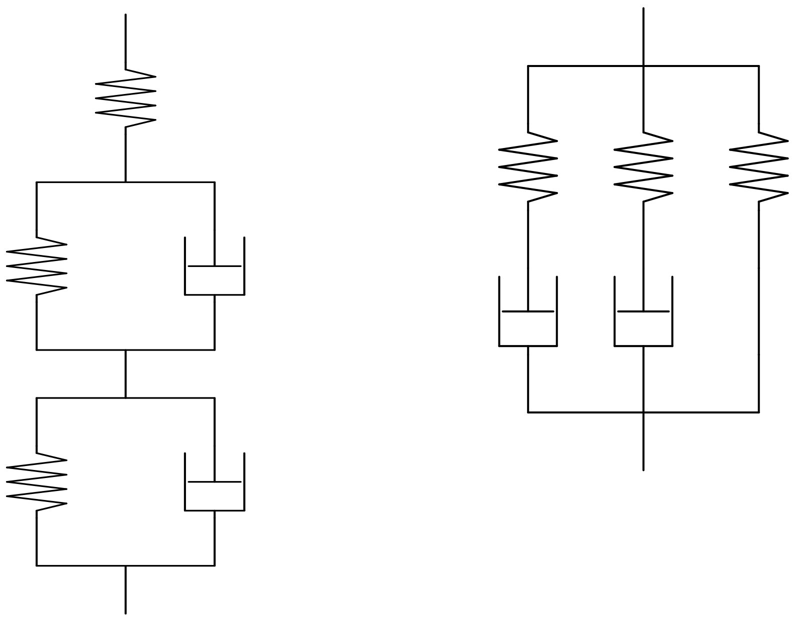

Fig. 2. – Schematic model of relaxation and creep

RESULTS AND DISCUSSION

The measured data of the individual curves of creep and relaxation are shown in Fig. 3 and 4.

The coefficients of the equations for description of relaxation and creep were determined using measured data as shown in Tab. 1 and Tab. 2.

Tab. 1. – Coefficients of relaxation

	Deformation [mm]		
	10	20	30
a [N]	2.187*10^3	4.444*10^3	5.891*10^3
b [N]	955.027	2.976*10^3	8.743*10^3
c [s^{-1}]	-0.148	-0.135	-0.104
d [N]	843.247	2.375*10^3	4.298*10^3
f [s^{-1}]	-0.013	-0.013	-0.0098

Tab. 2. – Coefficients of creep

	Force [N]		
	4000	10000	19000
a [mm]	11.33	23.458	29.891
b [mm]	1.548	3.875	4.549
c [s^{-1}]	-0.004754	-0.005435	-0.005271
d [mm]	0.285	2.628	1.713
f [s^{-1}]	-0.029	-0.057	-0.046

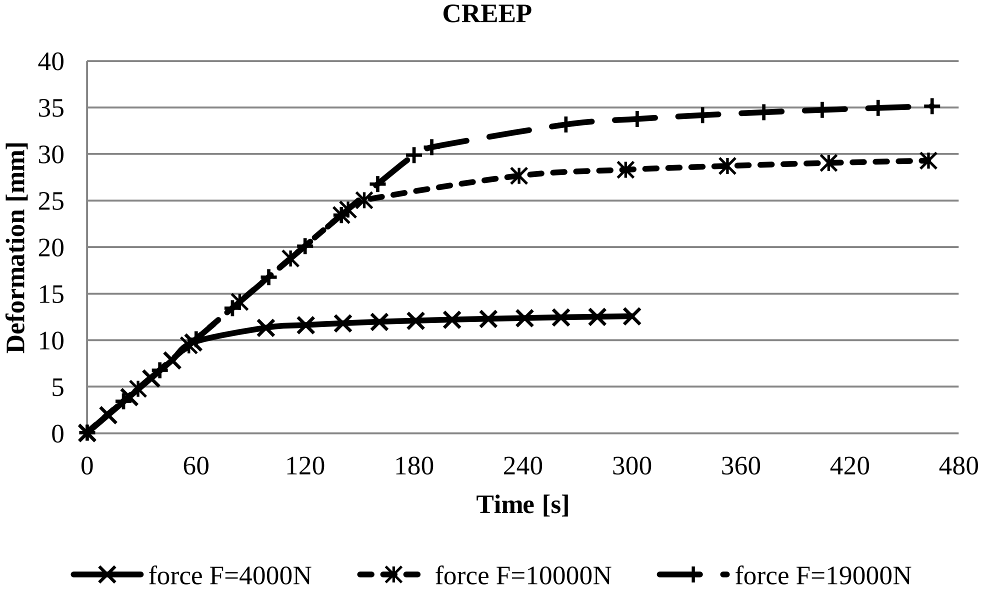

Fig. 3. – Measured values of creep

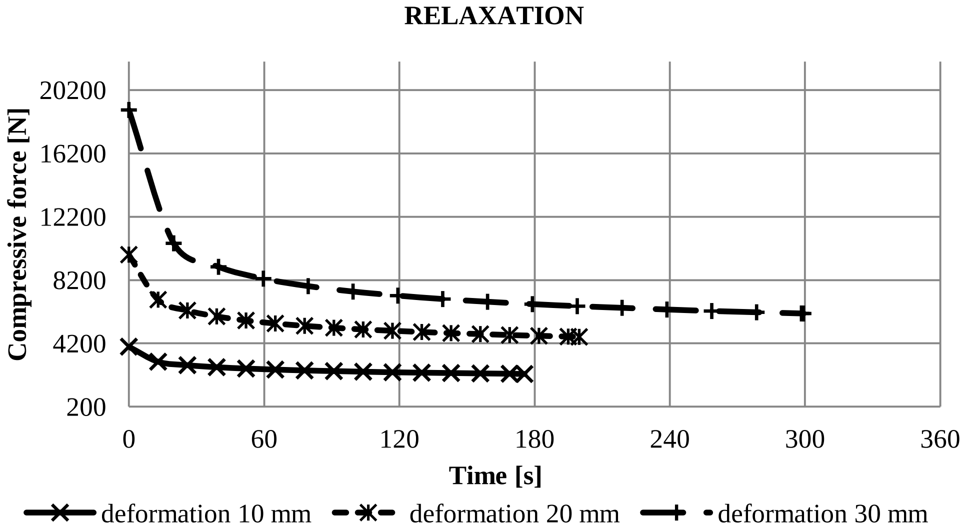

Fig. 4. – Measured values of relaxation

Individual coefficients for relaxation and creep are presented in Tab. 1 and 2.

The coefficient of variation for compressive force and deformation was determined from measured amounts as CV = (7.3 ± 1) % and is in agreement with earlier findings (HERÁK ET AL., 2011; IZLI ET AL., 2009). The largest decrease in compressive force was elicitted by the maximum applied load of 19000 N (Fig. 4). This was significantly larger than those resulting at the smaller imposed loads. Minimal decrease in compressive load with time at 4000 and 10000 N is as a result of the re-arrangement of bulk seeds within the pressing vessel, with minimal resultant deformations (BLAHOVEC ET AL., 1980).

Mathematical models which are based on experimental measurements aid the determination of optimal parameters in the design of processing technologies. However, knowledge of various material parameters such as water content, composition of oilseeds, pretreatment and mechanical pressure is requisite for optimisation.

Earlier studies have focused mainly on on response of bulk rapeseeds under compressive loads (HERÁK ET AL., 2011). However, the response of unloading bulk rape columns subjected to known compressive preloads were observed to be decreasing functions of time (relaxation), the rate of which was amplified by the magnitude of the deformation rate; the rate of deformation with time (creep) varied, and considerable with different loads being less severe at the lower loads.

The loss of energy is caused by internal changes in the seeds, which causes the release of oil; part of the energy is however converted into heat (PETRŮ ET AL., 2012).

Obtained mathematical equations would be useful in modeling extruder systems based on maximum oil yield and optimum energy requirements.

CONCLUSIONS

This study was focused on the determination of relaxation and creep behaviours of bulk rape seeds under compressive loads. Relaxation behaviour was studied at three deformations of 10, 20 and 30 mm. Creep in the bulk seed sections was studied at three compressive loads of 4000, 10000 and 19000 N.

1. The equations of creep and relaxation were determined.
2. The largest decline of relaxation force was observed under loading of 19000N.
3. The results obtained in this study may be used in the further research related to the modeling of extruding systems.

REFERENCES

1. BLAHOVEC, J., REZNICEK, R.: Frakcionace pice (Fractionation of the forage). Prague, VSZ v Praze, 1980: 370 p.
2. FOMIN, V., I.: Wet fractionation of green forage. Rostov on Don, Izdatelstvo Rostovskovo universiteta, 1978: 160 p.
3. HERAK, D., KABUTEY, A., SEDLACEK, A., GURDIL, G.: Tangent curve utilization for description of mechanical behaviour of pressed mixture. Res in Agric Eng 57, 2011b: 13-18.
4. HERAK, D., KABUTEY, A., SEDLACEK, A.: Mathematical description of rape seeds' (Brassica napus L.) mixture mechanical behavior under compression loading. Sci Agr Bohemica 42, 2011a: 31-36.
5. HERAK, D., KABUTEY, A., SEDLACEK, A.: 2011 Mathematical description of rape seeds` (Brassica napus L.) mixture mechanical behavior under compression loading. Scientia Agriculturae Bohemica, 42, 2011: 31-36.
6. HERAK, D., SLEGER, V., MIZERA, C., SEDLACEK, A.: Mechanical behaviour of bulk rapeseeds under quasi dynamic compression loading. Engineering for rural development, Jelgava, 2015: 28–32.
7. IZLI, N., UNAL, H., SINCIK, M.: Physical and mechanical properties of rapeseed at different moisture content. Int Agrophys 23, 2009: 137-145.
8. KABUTEY, A., HERAK, D., SEDLACEK, A.: Behaviour of different moisture contents of Jatropha curcas L. seeds under compression loading. Res in Agric Eng 57, 2011: 72-77.
9. MREMA, G., C., MC NULTY, P., B.: Mathematical model of mechanical oil expression from oilseeds. J Agric Eng Res 31, 1985: 361-370.
10. PETRŮ, M., NOVÁK, O., HERÁK, D., SIMANJUNTAK, S.: Finite element method model of the mechanical behaviour of Jatropha curcas L. seed under compression loading. Biosystems Engineering, 111, 2012: 412–421.
11. RAJI, A., O., FAVIER, J., F.: Discrete element modelling of the impact parameters of a selected fruit: application. Journal of Applied Science and Technology, 21, 2002: 7–12.
12. RONG, G., NEGI, S., C., JOFRIET, J., C.: Simulation of the flow behaviour of bulk solids in bins. Part 2: Shear bands, flow, corrective inserts and velocity profile. Journal of Agricultural Engineering Research, 62, 1995: 257–269.
13. RUSINEK, R., MOLENDA, M., SYKUT, J., PITS, N., TYS, J.: Uniaxial compression of rapeseed using apparatus with cuboid chamber. Acta Agrophysica 10, 2007: 677-685.
14. SIRISOMBOON, P., KITCHAIYA, P., PHOLPHO, T., MAHUTTANYAVANITCH, W.: Physical and mechanical properties of Jatropha curcas L. fruits, nuts and kernels. Biosyst Eng 97, 2007: 201-207.
15. UNAL, H., SINCIK, M., IZLI, N.: Comparison of some engineering properties of rapeseed cultivars. Ind Crop Prod 30, 2009: 131-136.
16. ZOERB, G., C.: Instrumentation and measurement techniques for determining physical properties of farm products. Transactions of the ASAE, 10, 1967: 100–113.

Corresponding author:
Ing. Petr Hrabě. Ph.D., Department of Material Science and Manufacturing Technology, Faculty of Engineering, Czech University of Life Sciences Prague, Kamýcká 129, Praha 6, Prague, 16521, Czech Republic, phone: +420 22438 3274, e-mail: hrabe@tf.czu.cz

SURFACE WATER RUNOFF AND SOIL LOSS IN MAIZE CULTIVATION

J. Hůla[1,2], P. Kovaříček[1*], P. Novák[2], M. Vlášková[1]

[1]*Research Institute of Agricultural Engineering, p.r.i., Prague 6 – Ruzyně, Czech Republic*
[2]*Department of Agricultural Machines, Faculty of Engineering, Czech University of Life Sciences Prague, Czech Republic*

Abstract
In a field trial with four variants of cultural practices in maize for silage cumulative surface runoff and soil loss were measured under artificial rainfall generated by a rainfall simulator. Measurements in June 2015 showed that water infiltration into the soil in a maize stand on ploughed land was markedly lower than in variants with soil tillage for maize without ploughing. The highest soil loss at surface water runoff in June was found out in variants of maize cultivation with ploughing. The results of measurement of water intake by the soil and soil loss due to the flow of water in the period of the events of intensive rainfall in storms indicated that maize cultivation with ploughing is a risky practice compared to soil tillage without ploughing.

Key words: rainfall simulation, soil tillage, soil moisture, water infiltration speed into soil.

INTRODUCTION

In the Czech Republic soil protection against water erosion is a particularly crucial issue – almost 50% of the arable land area is threatened by this type of erosion (JANEČEK ET AL., 2008). In farming practice permanent damage to the soil by excessive surface water runoff and soil washing away occurs also in those fields that meet the defined requirements for good farming practices with regard to the cultivation of maize and other broad-row crops. As the areas under maize have been increasing, especially because maize is used as an energy source and raw material for biogas plants, maize is planted on less sloping lands but in conditions with low soil resistance to water erosion where severe and irreversible deterioration of soil fertility by water erosion occurs. Many times, washing away of soil, mainly by torrential rains, may cause damage to the property of municipalities and inhabitants.

The commonly used maize planting on vast lands with long fall lines is risky when no crops with a higher protective effect against water erosion are included on these lands. The importance of soil conservation technologies for the planting of broad-row crops was accentuated by TRUMAN, SHAW AND REEVERS (2005).

To increase the efficiency of the soil erosion control it is necessary to decrease surface water runoff during intensive rains and to transfer the greatest possible amount of water from rainfall into the soil profile. An increase in the infiltration capacity of soil is assumed, as stated by SHIPITALO ET AL. (2000). If the surface water runoff cannot be prevented, it is necessary to decrease at least the velocity of flowing water so that the soil amount carried away by water would be reduced. BAUMHARD & JONES (2002) mentioned inappropriate soil tillage that can contribute to the creation of compacted layers in the soil profile. TITI ET AL. (2002) emphasized a decrease in soil permeability for water as a result of the creation of a homogeneous soil layer under the long-term use of conventional soil tillage. An increase in soil suction for water is another contribution to soil moisture management with respect to cultivated crops.

This paper presents the results of measuring the characteristics that indicate the risk of water erosion in the soil where maize (*Zea mays* L.) is planted and conventional tillage with ploughing and soil tillage practices without ploughing are used.

MATERIALS AND METHODS

Measurements of water intake by the soil were conducted in June 2015 after variants of soil tillage and planting for maize were used for several years. A field trial in the Nesperská Lhota locality has been conducted in this site since 2010. The locality is situated on the border of the Benešovská pahorkatina and Vlašimská pahorkatina hills. The trial was established on light loamy-sandy Cambisol at an altitude of 420 m a.s.l. and on a land of average slope of 5.4°. Surface water runoff and soil loss were measured in the variants of the field trial shown in Tab. 1.

To measure surface water runoff and soil loss a rainfall simulator was used (KOVAŘÍČEK ET AL., 2008). During artificially generated rainfall the soil was exposed to the effects of falling water drops at a rate of 87 mm/h. The flow of water washing away the soil was taken into a vessel located on an automated balance and the values of weight were continually recorded by a portable computer (Fig. 1). For determination of soil moisture and physical properties of soil standard methods of soil sampling and laboratory analyses were used (VALLA ET AL., 2008). The Vantage Vue meteorological station was used for rainfall registration during the field trial.

Tab. 1. – Variants of soil tillage practices and establishment of maize stand

Variants of maize cultivation		Description of maize cultivation
1	Conventional practice of maize cultivation with ploughing	Autumn ploughing, rough furrow left over winter, in spring seedbed preparation, maize sowing with Kinze 3600 planter.
2	Maize planted into cover undersown crop (with ploughing)	Autumn ploughing, rough furrow left overwinter, in spring seedbed preparation, sowing of spring cereal (common oat) with Flora 601 sowing machine with disk coulters (row spacing 0.125 m, 2 rows sown, 4 rows left out), maize planted into unsown strips of emerged spring cereal with Kinze 3 600 planter, visual navigation.
3	Minimization for maize with spring loosening	Skimming with disk harrow after forecrop harvest; in spring soil tillage with Kromexim 300 tine cultivator to a depth of 0.10 m, maize sowing with Kinze 3600 planter.
4	Maize sowing into winter killed catch crop	Skimming with disk harrow in autumn after forecrop harvest, sowing of winter kill catch crop, in spring maize sowing with Kinze 3600 planter (without seedbed preparation).

Fig. 1. – Rainfall simulator

RESULTS AND DISCUSSION

In the period from February to June 2015, when measurements were done with a rainfall simulator, precipitation was low – the precipitation amount from the beginning of February was only 48 mm on an experimental plot. It was reflected in low soil moisture at the time of measurements. In the surface layer of soil on 24th June 2015 there was a moderate increase in soil moisture as a result of rainfall events on 13th – 15th June with the precipitation amount of 17 mm (Figs. 2 and 3).

Figure 4 shows surface water runoff during artificial rainfall generated by a simulator. The graph illustrates that during artificial rainfall there was an increase in differences in cumulative surface runoff between the variants of maize cultivation with ploughing and without it. Differences between these variants further increased at subsequent measurements with a rainfall simulator after two weeks in the same space (Fig. 5). Figure 5 documents that lower values of cumulative surface runoff were recorded in the maize cultivation without ploughing (with spring seedbed preparation as well as without seedbed preparation) compared to maize cultivation by ploughing technology of soil tillage. High values of cumulative runoff were found out not only for the conventional practice of maize cultivation with ploughing but also for the cultivation technology using a cover crop (after ploughing).

Soil loss by the flow of water is an indicator with the still higher measure of relevance. Tab. 2 shows the values of soil loss at the second measurement (24^{th} June 2015). Low values of soil loss were determined in variants of maize cultivation without ploughing (12.4 and/or 12.6 g per hour/square meter). The soil loss in the variant of conventional maize cultivation with ploughing was higher by an order – 142.2 g/(h.m^2), which is 1.42 tons per hectare per hour of artificial rainfall. In the variant of maize cultivation with ploughing and use of a cover crop (oat) the higher soil loss of 54.2 g/(h.m^2) was measured than in the variants of maize cultivation with minimization of soil tillage with spring seedbed preparation and without spring seedbed preparation (maize sowing into a winter killed catch crop). It does not confirm the expected effect of cover undersown crop in the maize cultivation that should contribute to soil conservation. Technologies of maize cultivation with ploughing appeared to be risky in conditions with lower natural resistance of soil to erosion. It is consistent with the results of the authors who reported a significant reduction in soil loss by erosion when soil tillage without ploughing is used – RASMUSSEN (1999) reported a reduction in soil loss by half or even by two thirds depending on the soil type. Truman, Shaw et Reeves (2005) found out twice lower surface runoff and five times lower soil loss for tillage without ploughing compared to the conventional soil tillage during rainfall simulation for 60 minutes.

Measurements of surface runoff and soil loss during artificial rainfall generated by a simulator confirmed previous findings: water infiltration into the soil after ploughing is usually high only for some time, and it markedly decreases with time. When the conventional practice of soil tillage with ploughing was used for maize cultivation, in the course of measurements in the maize stand in June water infiltration into the soil on ploughed land was markedly lower than in variants with soil tillage for maize without ploughing (HŮLA & KOVAŘÍČEK, 2010). An assumed reason is the creation of the surface layer of topsoil with a decreased proportion of macropores and hence reduced permeability for water on ploughed land. In variants with soil tillage for maize without ploughing no such a tendency of pronounced decrease in soil permeability for water in spring and summer was recorded. A relation between the creation of the surface non-structural layer of soil on conventionally tilled land with ploughing and the reduced permeability of soil for water was described by TEBRÜGGE & DÜRING (1999).

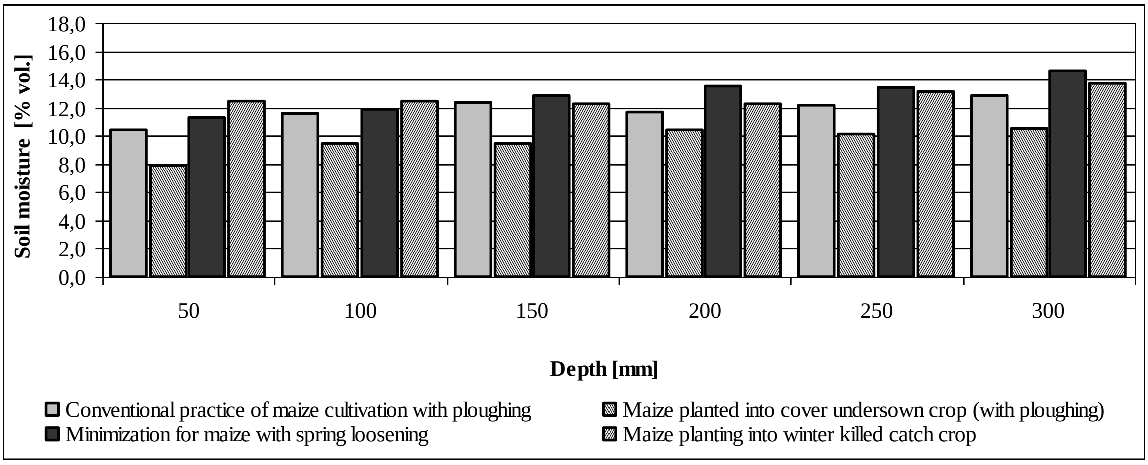

Fig. 2. – Soil moisture before measurement with rainfall simulator on 11^{th} June 2015

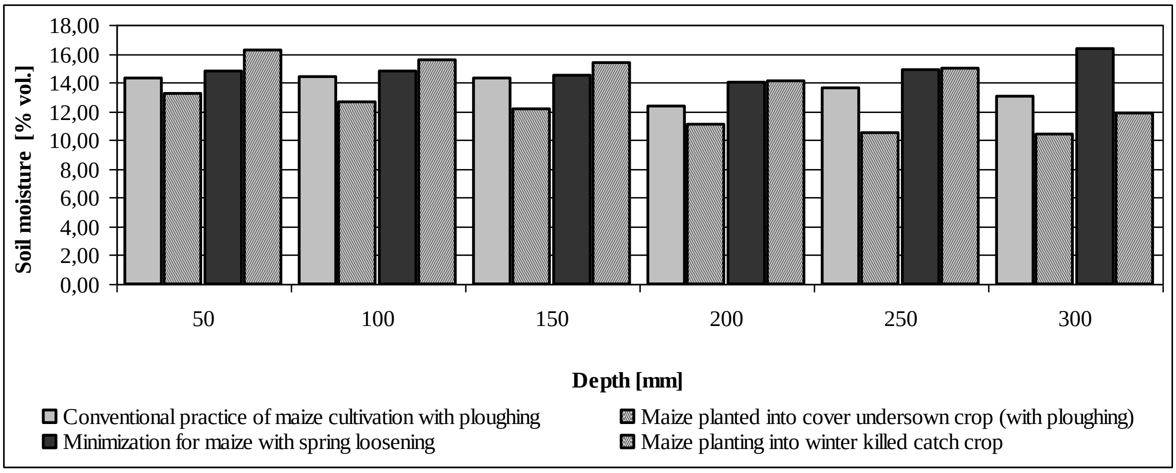

Fig. 3. – Soil moisture before measurement with rainfall simulator on 24th June 2015

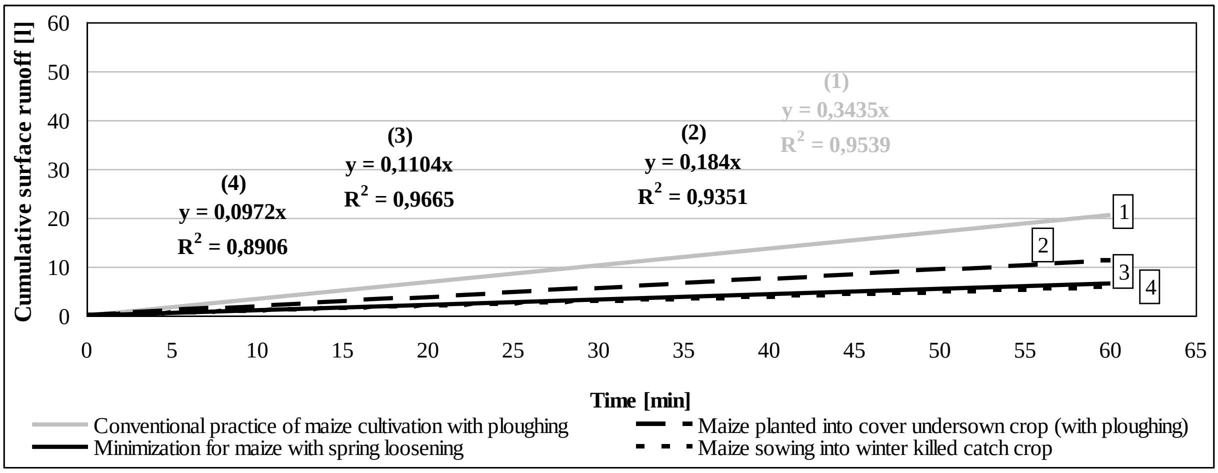

Fig. 4. – Surface water runoff during rainfall simulation on 11th June 2015

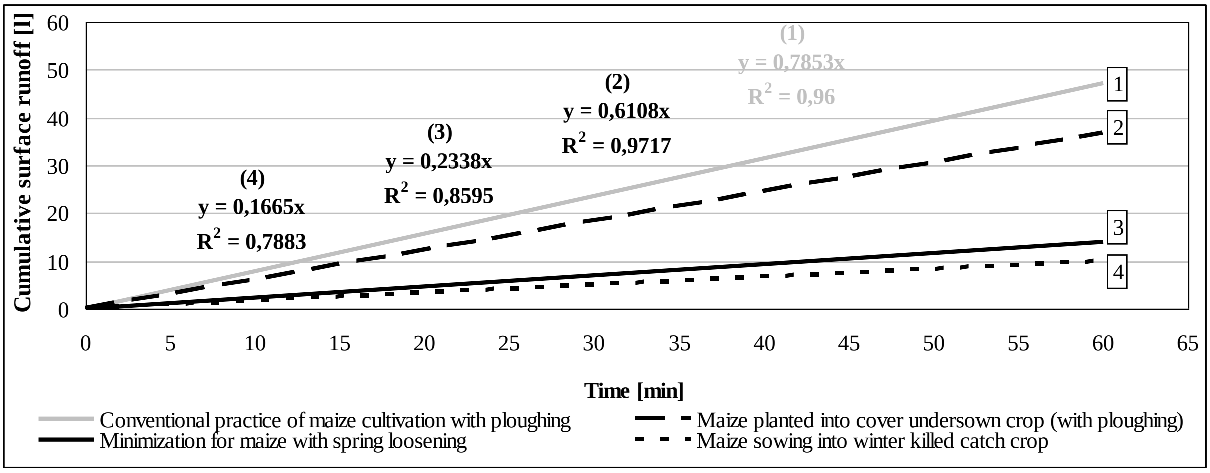

Fig. 5. – Surface water runoff during repeated rainfall simulation on 24th June 2015

Note: the order of variants from the lowest surface runoff – maize planting into a winter killed catch crop, minimization for maize with spring loosening, maize planted into a cover undersown crop (with ploughing), conventional practice of maize cultivation with ploughing.

Tab. 2. – Soil loss during a simulated rainfall event of 87 mm/h

Variant	Soil loss g/(h.m^2)
Conventional practice of maize cultivation with ploughing	142.2
Maize planted into cover undersown crop (with ploughing)	54.2
Minimization for maize with spring loosening	12.4
Maize planting into winter killed catch crop	12.6

CONCLUSIONS

The variant of maize cultivation by conventional soil tillage with ploughing was the most risky from the aspect of surface water runoff during rainfall and soil vulnerability to water erosion. Obviously, for maize cultivation it is necessary to use practices that will ensure sufficient permeability of soil for water in combination with the utilization of dead plant biomass on the soil surface. Promising from this aspect is the practice of strip tillage when deeper loosening of soil is used in a space under future maize rows, while in strips between maize rows there may remain untilled soil with crushed cereal straw on the soil surface.

ACKNOWLEDGEMENTS

Supported by the Ministry of Agriculture of the Czech Republic – Project No. QJ1210263 and RO0614.

REFERENCES

1. BAUMHARD, R.L., JONES O.R.: Residue management and paratillage effects on some soil properties and rain infiltration. Soil & Tillage Research, 65, 2002: 19-27.
2. HANGEN, E., BUCZKO, U., BENS, O., BRUNOTTE, J., HÜTTL, R.F.: Infiltration patterns into two soils under conventional and conservation tillage. Soil & Tillage Research, 63, 2002: 181-186.
3. HŮLA, J., KOVAŘÍČEK, P.: Water infiltration into soil and surface water runoff in maize growing by three cultivation technologies. In: 4th International Conference TAE 2010. Trends in Agricultural Engineering 2010, Czech University of Life Sciences Prague, 2010, p. 232-235.
4. JANEČEK, M. ET AL.: Basics erodologie. Prague, ČZU in Prague, first ed., 2008, 172 p. (in Czech).
5. KOVAŘÍČEK, P., ŠINDELÁŘ, R., HŮLA, J., HONZÍK, I.: Measurement of water infiltration in soil using the rain simulation method. Research in Agricultural Engineering, 54, 2008: 3 123-129.
6. RASMUSSEN, K.J.: Impact of ploughless soil tillage on yield and soil quality: A Scandinavian review. Soil & Tillage Research 53, 1999: 3-14.
7. SHIPITALO, M.J., DICK, W.A., EDWARDS, W.M.: Conservation tillage and macropore factors that affect water movement and the fate of chemicals. Soil & Tillage Research, 53 (3-4), 2000: 167-183.
8. TITI, E.A.: Soil tillage in agroecosystems. CRC Press, the U.S.A. 2002, 367 p.
9. TRUMAN, C.C., SHAW, J.N., REEVES, D.W.: Tillage efects on rainfall partitioning and sediment yield from an ultisol in central Alabama. In: Journal of Soil and Water conservation. 60 (2), 2005: 89-98.
10. VALLA, M. ET AL.: Pedological practicum. Prague, ČZU in Prague, 2008, 151 p. (in Czech).
11. TEBRÜGGE, F., DÜRING, R.A.: Reducing tillage intensity – a review of results from a long-term study in Germany. Soil & Tillage Research, 53, 1999: 15-28.

Corresponding author:

Ing. Pavel Kovaříček, CSc., Research Institute of Agricultural Engineering, p.r.i., Drnovská 507, 161 01 Prague 6 – Ruzyně, Czech, e-mail: pavel.kovaricek@vuzt.cz.

DIFFERENT WAYS OF FERTILIZER APPLICATION TOGETHER WITHBIO-EFFECTORS FOR MAIZE BIOTOPE

L. Chládek[1], Z. Holečková[2], P. Vaculík[1]

[1]Department of Technological Equipment of Buildings, Faculty of Engineering, Czech University of Life Sciences Prague, Czech Republic
[2]Department of Agro-Environmental Chemistry and Plant Nutrition, Faculty of Agrobiology, Food and Natural Resources, Czech University of Life Sciences Prague, Czech Republic

Abstract
This project is focused on different effect of applications of so-called bio-effectors on hectare yield and dry matter in maize plants. The difference between local and broad applications was monitored in field conditions on two sites. Local application was performed using machine GFI 3A and broad application was performed manually by tap. The results show that difference between local and broad application of bio-effectors does not have a statistically significant effect on yield per hectare or on a percentage of dry matter.

Key words: fertilizer, application, bio-effector, maize.

INTRODUCTION

The aim of this study was to evaluate the influence of different fertilizer application together with so-called bio-effectors in field conditions on percentage of dry matter and yield of maize. Today's society is dependent on inorganic compounds of nutrients (fertilizers, feed or food additives) and largely exploits limited world natural resources of minerals this way, which are important for fertilizer production. For these reasons, there is a common need for development of more sustainable mechanisms that would maintain availability of nutrients for crops and livestock, with a smaller amount of supplied mineral fertilizer which will also lead to improvement of soil functions. Creation of new strategy requires better public awareness about consequences of farming approaches on the environment, better understanding of the dynamics of nutrients in the soil-plant relationship, the creation of new innovative technologies in order to reduce dependance of world population on mined minerals and increase efficiency of fertilization. Development of new strategies is expected to have significant economical and environmental impact WITHERS (2014). Due to growing world population it is expected that demand for food and feed will be continuously increasing and limited availability of productive agricultural land and increasing dependance on mineral fertilizers will be among main issues for society to cope with. It is necessary to develop alternative strategies for plant nutrition NEUMANN (2012) and HOGENHOUT (2009). This project deals with different effects of applications so-called bio-effectors on hectare yield and dry matter in maize plants. These compounds containing microorganisms (bacteria, fungi) and active natural substances, such as extracts from soil or compost, microbial residues, plant extracts or products of biological processes. These products are developed for a wide variety of crops (e.g. maize, wheat, tomatoes, rape, spinach, grass, ornamentals). Their efficiency causes mobilization of nutrients from less accessible forms in soil NEUMANN (2012) and SMALLA (2012), they further support root growth GALLETTI (2015) and FERRIGO (2014) and mycorrhiza development YUSRAN (2009). Examined the difference between local applications, which was performed using machine GFI 3A (Maschinen und Antriebstechnik GmbH Güstrow, Germany) and broad application, which was performed manually by tap.

Principle of local application

Mineral fertilizers are the most expensive and most important annual volume input into agriculture ŠANTRŮČEK (2007). For this reason was especially in Germany, intensively studied and gradually applied in agricultural practice a new system of plant nutrition using local applications, which should increase the use of nutrients from applied fertilizer or other substances applied BALÍK (2007). Local application is based on earlier discoveries of Mr. Prof. Karl Sommer from Bonn University and current research in small plot trials in the Czech Republic. One of the new liquid fertilizer application technologies, pesticides or different nutrient solutions is so-called injectable dosage. MAŠEK (2005) and JUREN (2006) report that so-called injection dosage of liquid fertilizer or other nutritive substances is agro technical act "in reserve", where plant can uptake amount of nutrients, which it needs from the depot in soil. The machine consists of tank, pumps and application frame, which can reach up to 18 meters width (picture 1 and 2A/B). On the frame there are small spaced wheels, which are circumferentially positioned apexes, which deliver nutrient solution to the soil. The wheels roll over the soil surface and apex which just enters soil and applies nutrient solution. In the application site there is high concentration of nutrients, which are toxic for roots and organisms, but around this stock is formed so-called diffusion zone. From this zone a plant can uptake nutrients via roots depending on the growth stage. The solution is injected under pressure of 150-600 kPa.

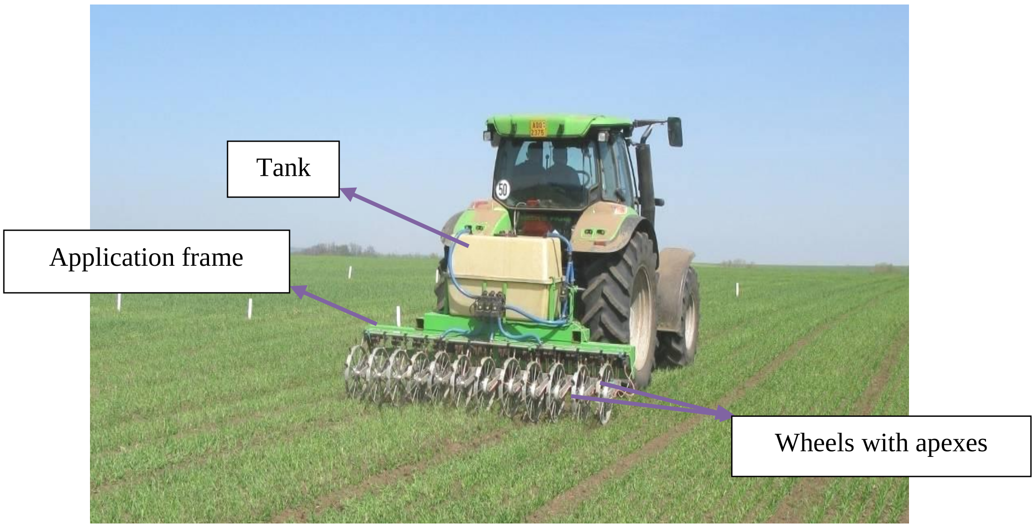

Fig. 1. – Injecting applicator

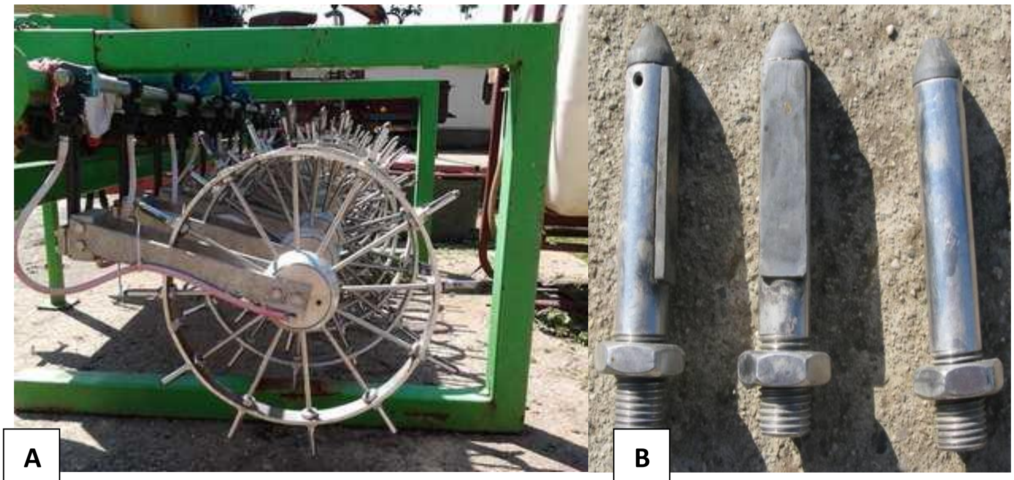

Fig. 2. – Wheels with apexes GFI 3A (A) and application apexes (B) (A – SEDLÁŘ (2013) and B – KOZLOVSKÝ (2011))

MATERIALS AND METHODS

Field experiments

Field experiments were established on 23rd April 2014 at Humpolec site and on 25rd April 2014 at Lukavec site. Test plants was maize (variety Colisee) and machine, seeding rate was 90,000 seeds per hectare. During the field experiment in plots with an area of 31.5 square meters two bio-effectors (Proradix and RhizoVital) were applied in combination with rock phosphate (RP) and triple superphosphate (TSP), which were applied at the same dose of P (2 kg P/ha). Experiments were uniformly fertilized with nitrogen, which was delivered in the form of calcium ammonium nitrate with limestone (CAN) and potassium (Patentkali), which were applied at the same dose of N (120 kg N/ha) and K (50 kg/ha). Each treatment was carried out in ten repetitions. Bio-effectors used in the field experiment were following, with active substance (in parentheses):

i) BE0: Control (water only)
ii) BE1: Proradix (*Pseudomonas sp.*)
iii) BE2: RhizoVital (*Bacillus amyloliquefaciens*, strain FZB42).

Bio-effectors (22.7 kg/ha of Proradix and 2 l/ha of RhizoVital) for the broad application were applied in the form of solution diluted with tap water to the final volume 9 litters per plot (l/plot). For the local application, injection application to the depot was conducted using the machine GFI 3A (Maschinen und Antriebstechnik GmbH Güstrow, Germany). The dose of the Proradix was 10 times lower compared to broad application and the dose of RhizoVital was 1.5 l/ha. Both bio-effectors were applied diluted with tap water (solution dose of 2 l/plot). The same dose of water was also applied (9 l/plot) in control treatment. Experiment was harvested on 18th September 2014 at Humpolec site and on 24th September 2014 at Lukavec site.

Tab. 1. – Design of field experiment (Humpolec and Lukavec site)

No.	Treatment	Fertilizer	BE application
1	0	0	0
2	BE0 (water)	0	broad
3	BE0 (water)	RP	broad
4	BE0 (water)	TSP	broad
5	BE1	0	broad
6	BE2	0	broad
7	BE1	RP	broad
8	BE1	TSP	broad
9	BE2	RP	broad
10	BE2	TSP	broad
11	BE1	RP	local
12	BE1	TSP	local
13	BE2	RP	local
14	BE2	TSP	local

RESULTS AND DISCUSSION

Results of measuremets are described in Tab. 1, 2 and 3. Results were processed in the software Statistica, concretely one-way ANOVA. The introduced results in the Tab. 2 are an average arithmetic values from 14 measurements.

Tab. 2. – Characteristics of experimental fields

Site	Humpolec	Lukavec
Latitude	49°33'15" N	49°33'36" N
Longitude	15°21'02" E	15°58'22" E
Altitude (m above sea level)	525	610
Mean yearly temperature (°C)	7.0	8.2
Mean yearly rainfall (mm)	665	573
Soil type	cambisol	cambisol
Soil sort	sandy loam	sandy loam
pH[1)]	5.1	5.4
P (mg/kg)[2)]	77 (±10) B[3)]	120 (±10) B[3)]

1) Estimated in air dried soil, 0.01 mol/l $CaCl_2$, 1:10 w/v
2) Average basic data estimated using Mehlich 3 method
3) Cathegory B – low content

Tab. 3. – Percentage of dry matter (%) and yield per hectare (t/ha) field experiments in 2014 at Humpolec and Lukavec sites

	Humpolec		Lukavec	
No.	dry matter (%)	yield (t/ha)	dry matter (%)	yield (t/ha)
1	19.4[a]	34.4[a]	25.2[a]	30.2[a]
2	20.6[a]	35.4[a]	25.5[a]	32.3[a]
3	21.1[a]	38.1[a]	24.1[a]	34.9[a]
4	21.4[a]	34.7[a]	24.6[a]	32.8[a]
5	20.3[a]	33.0[a]	24.5[a]	26.9[a]
6	18.8[a]	35.8[a]	24.7[a]	31.4[a]
7	19.2[a]	36.3[a]	24.3[a]	30.6[a]
8	18.4[a]	31.4[a]	25.1[a]	30.1[a]
9	18.9[a]	33.9[a]	23.9[a]	32.5[a]
10	18.7[a]	31.6[a]	26.8[a]	30.4[a]
11	21.4[a]	35.4[a]	23.9[a]	33.1[a]
12	22.4[a]	33.6[a]	23.9[a]	32.8[a]
13	20.5[a]	34.6[a]	24.1[a]	30.3[a]
14	21.2[a]	34.2[a]	28[a]	32[a]
F-test	1.03	1.21	1.00	0.68
p≤*	n.s.**	n.s.**	n.s.**	n.s.**

* p – significance level
** n.s. – no significant

Tab. 3 presents average percentage of dry matter and yield for conducted field experiments. In 2014 had the lowest dry matter percentage variants 8 and 10. On the contrary, the highest percentage of dry matter had treatments 11 and 12, which were treatments of local bio-effector application. The highest average yield per hectare had treatment 3, which was conducted within broad application without bio-effector, only the same volume of water and 7, which was treatment of broad bio-effector application. The lowest yield showed treatment 8 and 10 both at Humpolec site. At Lukavec site had the lowest dry matter percentage treatments 9, 11 and 12. The highest percentage of dry matter had treatment 10, where was conducted broad application of bio-effectors and 14, where was conducted local application. The highest average yield per hectare had treatment 3 where was conducted broad application without bio-effector, only the same volume of water and 11 with local application. On the contrary, the lowest hectare yield had treatments 5 and 8, where broad applications were conducted.

The results show that difference between local and broad application of bio-effectors did not have statistically significant positive effect on yield per hectare or on percentage of dry matter at either of experiment sites in 2014.

Several experiments were realized with bio-effectors in field conditions with various test plants, and there were evaluated the effect of application bio-effectors on plant growth and a many different parameters. And so we cannot confirm results, which were reported by FRÖHLICH ET AL. (2012). They reported positive effects of this preparate in barley cultivation in field conditions. When Proradix was used in field conditions, it increased grain yield (up to 20%) and also increased weight and mass of straw. In our field conditions there was not statistically positive effect of bio-effector application on dry matter or yield.

CONCLUSIONS

Due to growing world population it is expected that demand for food and feed will be increasing and limited availability of productive agricultural land and increasing dependance on mineral fertilizers will ever more come into a question. It is therefore necessary to develop alternative strategies for plant nutrition. This project was focused on different effects of applications so-called bio-effectors on hectare yield and dry matter volume in maize plants. The difference between local applications, which was performed using machine GFI 3A and broad application, which was performed manually by tap was observed. Test plants was maize (variety Colisee) and field experiments were realized at Humpolec and Lukavec site. The results show, that different way of bio-effectors application did not have statistically significant effect on yield per hectare or on a percentage of dry matter at either of experiment sites in 2014. Due to limited number of experiments in the year 2014 only is necessary to continue in this research to obtain the objective results under impact of different climatic condition in following periods.

ACKNOWLEDGEMENTS

This research was financially supported by the Resource Preservation by Application of bio-effectors in European Crop Production nr. 7. RP 312117.

REFERENCES

1. BALÍK, J., LIPAVSKÝ, J., HLUŠEK, J., PAVLÍKOVÁ, D., ČERNÝ, J.: Streamlining of plant nutrition by ammonium nitrogen (system CULTAN). Proceedings of the conference "Rational use of fertilizers are focused on phosphorus in crop production". CULS in Prague, 2007: pp. 39–45.
2. FERRIGO, D., RAIOLA, A., RASERA, R.., CAUSIN, R.: Trichoderma harzianum seed treatment controls Fusarium verticillioides colonization and fumonisin contamination in maize under field conditions. Crop Protection. 65, 2014: pp. 51-56. ISSN: 0261-2194.
3. GALLETTI, S., FORNASIER, F., CIANCHETTA, S., LAZZERI, L.: Soil incorporation of brassica materials and seed treatment with Trichoderma harzianum: Effects on melon growth and soil microbial aktivity. Industrial Crops and Products. 75 Part A., 2015: pp. 73-78. ISSN: 0926-6690.
4. HOGENHOUT, S. A., VAN DER HOORN, R. A. L., TERAUCHI, R., KAMOUN, S.: Emerging Concepts in Effector Biology of Plant-Associated Organisms. MOL PLANT MICROBE INTERACTION. United Kingdom. 22 (2), 2009: pp. 115-122. ISSN: 0894-0282.
5. JUREN, J.: Application technology. Agricultural weekly. 46, 2006 pp. 13-14.
6. KOZLOVSKÝ, O.: Evaluation of the new system of plant nutrition cultan nitrogen in winter wheat. Doctor dissertation thesis. CULS in Prague. 2011: 104 p.
7. MAŠEK, J.: Development trends in application of fertilizers and pesticides. The Farmer. 12, 2005: pp. 59-64.
8. NEUMANN, G.: EU-funded research collaboration on use of bio-effectors in agriculture launched. Press Release. University of Hohenheim. Germany. [cit. 2011-11-04]. Available at: <http://www.biofector.info/about-biofector.html>. Accessed 2012.
9. SMALLA, K., ET AL.: EU-funded research collaboration on use of bio-effectors in agriculture launched. First kick-off meeting at University of Hohenheim. Julius Kühn-Institut (JKI). Germany. [cit. 2011-10-24]. Available from <http://www.jki.bund.de/en/startseite/presse/english-press/eu-funded-research-collaboration-on-use-of-bio-effectors-in-agriculture-launched.html>. Accessed 2012.
10. SEDLÁŘ, O.: Ověření systému výživy jarního ječmene dusíkem metodou CULTAN = Verification of the spring barley nitrogen nutrition by CULTAN method. Doctor dissertation thesis. CULS in Prague, 2013: 113 p.
11. ŠANTRŮČEK, J. ET AL.: Encyclopedia of Grasslands. CULS in Prague. The Department of Forage Crops and Grasslands. Prague, 2007: 120 p.
12. WITHERS, P. J., SYLVESTER-BRADLEY, R., JONES, D. L., HEALEY, J. R., TALBOYS, P. J.: Feed the crop not the soil: rethinking phosphorus management in the food chain. Environmental Science and technology. 48 (12), 2014: pp. 6523-6530.
13. YUSRAN, Y., WEINMANN, M., NEUMANN, G., RÖMHELD, V., MÜLLER, T.: Effects of Pseudomonas sp. ”Proradix” and Bacillus amyloliquefaciens FZB42 on the Establishment of AMF Infection, Nutrient Acquisition and Growth of Tomato Affected by Fusarium oxysporum Schlechtf.sp. radicis-lycopersici Jarvis and Shoemaker. The Proceedings of the International Plant Nutrition Colloquium XVI. University of California, 2009: pp. 13-20.

Corresponding author:

doc. Ing. Ladislav Chládek, CSc., Department of Technological Equipment of Buildings,Faculty of Engineering, Czech University of Life Sciences Prague, Kamýcká 129, Praha 6, Prague, 16521, Czech Republic, phone: +420 22438 3250, e-mail: chladekl@tf.czu.cz

DETECTION OF AUSTENITE TRANSFORMATION OF ADI CAST IRON USING ELECTROMAGNETIC SENSOR

R. Chotěborský[1], M. Linda[2], A. Kabutey[3]

[1]*Department of Material Science and Manufacturing Technology, Faculty of Engineering, Czech University of Life Sciences in Prague, Czech Republic*
[2]*Department of Electrical Engineering and Automation, Faculty of Engineering, Czech University of Life Sciences in Prague, Czech Republic*
[3]*Department of Mechanical Engineering, Faculty of Engineering, Czech University of Life Sciences in Prague, Czech Republic*

Abstract
An electromagnetic sensor was used to evaluate the microstructure in austempered ductile cast iron for austempering at varying temperature. Microstructural changes in cast iron as a result of changes in the permeability were observed. The electromagnetic sensor could be used for detection of bainite and martensite at isothermal treatment within specific temperature range. Light optical metallography revealed that samples microstructure contains bainite, martensite and austenite. Based on theoretical assumption, the value of the inductance difference should be directly proportional to volume of austenite phase in microstructure. The device could be used for the investigation of multiphase iron alloys of different ratio microstructure phases.

Key words: bainite, austempered, ductile, iron.

INTRODUCTION

Commercial iron products are produced using heat treatment procedure in which the austenite transformation is cooled continuously at varying temperature resulting into a mixture of different microstructure transformation products namely ferritic or martensite (ZHANG ET AL., 2012; YIN ET AL., 2002; PIETRZYK AND KUZIAK, 2011). However, the different transformation products of the microstructure are based on different mechanism and mechanical properties of the products (GAO ET AL., 2011; CHEN ET AL., 2012). To obtain a particular microstructure, the transformation product of austenite is transformed without rapid cooling at constant temperature or within a temperature limit according to isothermal transformation of austenite cooling kinetics. The monitoring of isothermal transformation of austenite especially in real steel/cast iron is difficult therefore the knowledge of isothermal heat treatment from time temperature transformation diagram is applied (LEE ET AL., 2010). The process of austenite transformation depends on the chemical composition and austenitizing temperature and time respectively.

Electromagnetic sensor (EMS) has been reported to be suitable for the detection of phase transformation in carbon steel cooling below the Curie temperature (T_c) (YIN ET AL., 2007; WANG ET AL., 2014B, 2014A; REISSMAN ET AL., 2012; PACURAR ET AL., 2012; LIU ET AL., 2013; GHANEI ET AL., 2013). The electromagnetic field created by the EMS is sensitive to any variations in the electrical resistivity and magnetic permeability of the sample resulting in changes in the complex trans-impedance value recorded. This is particularly useful because resistivity and permeability are known to be directly influenced by the microstructure and carbon content. Austenite is paramagnetic (μ_r = 1) whereas ferrite, pearlite, bainite and martensite are ferromagnetic below T_c (μ_r = 200+). Hence EMS is able to detect the ferromagnetic phase change below T_c. But microstructure phases in iron products (steels, cast iron) contain ferrite with $T_c \approx 770$°C, cementite Fe_3C with $T_c \approx 210$°C or M_7C_3 carbide with $T_c \approx 250$°C. Magnetic permeability of martensite and cementite phase is less than ferrite phase therefore an increase in the martensite percentage decreases the magnetic permeability of the material leading to a reduction in the impedance. The isothermal heat treatment of austempered ductile iron (ADI) is from 270°C up to 400°C, therefore only ferrite as ferromagnetic material can be detected by electromagnetic sensor during isothermal heat treatment whereas cementite and graphite are paramagnetic at temperature limit.

The mechanical properties such as strength, toughness and wear resistance depend on ratio of microstructure phases (KOLAŘÍKOVÁ ET AL., 2013; CHALA ET AL., 2005; CHOTĚBORSKÝ AND HRABĚ, 2013;

CHOTĚBORSKÝ ET AL., 2009; ZHANG ET AL., 2012). The use of an isothermal heat treatment can determine the mechanical properties of austenite transformation products (HUNG ET AL., 2002; ERFANIAN-NAZIFTOOSI ET AL., 2011; ZHANG ET AL., 2012). The actual ratio of austenite transformation products is usually controlled off-line by metallography after heat treatment. The present study investigates the relationship between electromagnetic sensor (EMS) and signal of a micro-structure austempered ductile iron (ADI cast iron).

MATERIALS AND METHODS

ADI cast iron samples with dimension of 8 mm x 25 mm x 50 mm were used for the isothermal heat treatment. EMS (40 threads and 4 layers of 1 mm Cu wire) was used. The chemical composition of ADI cast iron was Fe-3.7C-0.9Mn-2.3Si-0.7Ni-0.014S (wt. pct.). ADI cast iron samples were austenitized at 920 °C for 30 min. After austenitizing the samples were cooled in sodium/potassium nitrate salt bath. The experimental conditions are presented in Tab. 1. The maximal cooling time in salt bath was 60 seconds and thereafter the samples were moved into EMS sensor which was placed in a furnace. Temperature in the furnace was controlled by a PID regulator. Temperature of the sample was measured by K-type thermocouples which were embedded with the samples where it was connected to a Nanodac data logger (co. Eurotherm). Inductivity of the samples was measured by Agilent U1731C LCR meter (accuracy 0.2%, 1 kHz frequency) and data were saved on the PC (Fig. 1). Further analyses were developed by an algorithm of synchronizing time from temperature data logger and Agilent LCR meter in SciLab 5.4.1 (Scilab Enterprises 2014).

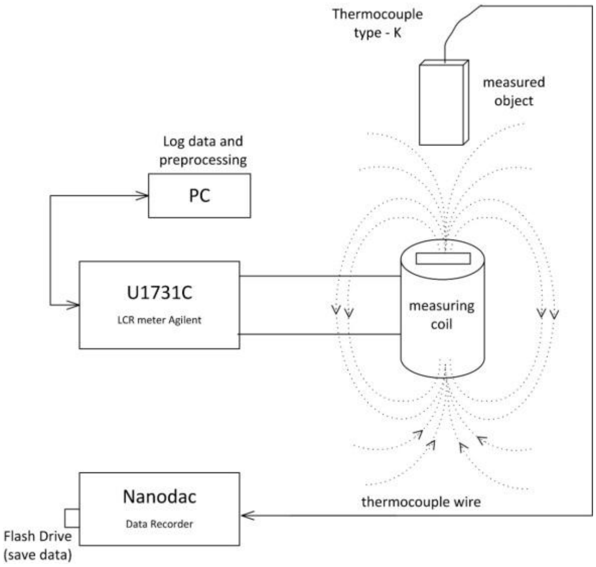

Fig. 1. – Schematic illustration of experimental set-up

Tab. 1. – Measured sample parameters from the experiment

Sample no.	Temperature (°C) PID/sample	Austempered time (min.)	Secondary cooling in	Inductance of the sample at temperature before austenizing (ΔH)
1	200			415
2	250			417
3	300			420
4	350	240	Air	425
5	400			433
6	450			438
7	500			442

Metallographic samples were cut and polished from heat treated samples and etched in a solution obtained by dissolving nitric acid (2 ml) in ethanol (100 ml) Nital. The nital etchant was used for the determination of bainite volume. Austenite phase was determined by using Klemm etchant (2g $K_2S_2O_5$ + 100 ml supersaturated $K_2S_2O_3$ in water) where austenite phase was not attached and bainite or martensite showed dark blue colour. Phase percentage in each sample was measured using SciLab Image and Video Processing toolbox, where threshold was obtained by a binary matrix algorithm. The algorithm was written for a proportion phase's evaluation.

Equation (1) expresses the change of inductance ΔH which is proportional to the change of ferrite volume ΔV_{FB}.

$$\Delta H = \Delta V_{FB} \times F(H)^{-1} \quad (1)$$

Where $F(H)$ is the relationship between inductance (-) and ferrite volume percentage. The study conducted by (YIN ET AL. 2007) shows that $F(H)$ depends on frequency. The relationship between inductance and ferrite can be described by equation (2) which has been previously determined in published study involving fine ferromagnetic pure iron powder.

$F(H) =$

$0.48 \times \frac{H_{act}-H_{ec}}{H_A-H_{ec}} + 0.19 \times \left(\frac{H_{act}-H_{ec}}{H_A-H_{ec}}\right)^2 \; if \; \frac{H_{act}-H_{ec}}{H_A-H_{ec}} \in \langle 0, 0.921)$

$F(H) = 5 \times \frac{H_{act}-H_{ec}}{H_A-H_{ec}} - 4 \; if \; \frac{H_{act}-H_{ec}}{H_A-H_{ec}} \in \langle 0.921, 1\rangle$ (2)

Where $H_{act} \in [H_{ec}, H_A]$ is the actual inductance, H_{ec} is the empty coil inductance, H_A is the inductance of the sample at temperature before austenizing.

Two austempering stages have been identified due to different transformation products. The products of the first stage are small bainite ferrite plates with high carbon austenite. High concentration of carbon is produced from the rejection process as the bainitic ferrite grows towards the untransformed high carbon austenite. The second stage of transformation produces the transformation of metastable high carbon austenite to ferrite and ε-carbide, or cementite during long austempering times. The paramagnetic high carbon austenite causes the inductance not to be equal to H_A. This drawback was taken into account in the Avrami equation (3) as the coefficient of $1 - A_{ret}$.

$V_{FB} = (1 - A_{ret}) \times \left(1 - e^{-k \times t^n}\right)$ (3)

Where A_{ret} is volume of retained austenite, k is coefficient for an initial nucleation time, t is time and n is coefficient for the saturation process of the transformation austenite. The measured data was fitted by Marquard-Lavenberg method, where coefficients k and n were obtained. Value A_{ret} was determined by an optical metallography of the sample which was austempered, and can also be determined by coefficient $1 - A_{ret}$ from Marquard-Lavenberg measured data. Martensite transformation can be detected by electromagnetic sensor as well as martensite temperature.

RESULTS AND DISCUSSION

In Tab. 2 is presented the experimental results. Inductance difference was calculated from the values of empty coil inductance, inductance with heat treated sample at austempered temperature and inductance of the sample at austempered temperature. The results indicate that austempered temperature influenced the maximal value of sample inductance and value of the inductance difference due to untransformed paramagnetic austenite phase. Light optical metallography revealed that samples microstructure contains bainite, martensite and austenite (Fig. 2). Based on theoretical assumption, the value of the inductance difference should be directly proportional to volume of austenite phase in microstructure. The experimental procedure assumed that austempered time (350 min.) should be less than the total transformation time of the austenite phase. The austempered time was set for the first stage where bainitic ferrite and high carbon austenite coexisted at limited time. Cooling of the specimen in air after austempering permitted the transformation of the austenite to martensite. Hence, volume of the austenite phase at austempered temperature before cooling was given as sum of the martensite and austenite phase microstructures.

Tab. 2. – Samples measured parameters

Sample no.	Inductance H_A of the sample at temperature after austenizing (ΔH)	Inductance difference (%)	Volume of austenite (%) in the matrix (Klemm)	Volume of bainite (%) in the matrix (Nital)	Volume of martensite (%) in the matrix – balance
1	392	15	15 ± 2.6	62 ± 4.8	23
2	391	17	16 ± 3	63 ± 4.9	21
3	387	21	15 ± 2.8	59 ± 3.4	26
4	393	20	13 ± 2.9	61 ± 3.6	26
5	385	28	21 ± 3.5	62 ± 4.1	17
6	413	30	25 ± 2.1	57 ± 4.5	18
7	429	7	12 ± 1.8	78 ± 5	10

The relationship between inductance difference and volume of the austenite shows that austenite volume is not directly proportional to the inductance difference. This confirms the metallographic method where austenite phase is partially etched by Klemm etchant.

The use of an electromagnetic sensor in isothermal treatment for detection of austenite transformation was monitored by applying Eq. 3. Four samples were respectively austempered at 250°C, 300°C, 350°C and 400°C and samples quenched in water. Austempered time was equal to $H(\%) = 55 - 60$. At specific temperature of 350°C the same samples were austempered and quenched in water. Austempered time was equal to $H(\%) = 10;\ 25;\ 35$ and 55. Microstructure of the samples contains bainite, martensite and retained austenite. The relationship between volume of bainite and inductance H (%) is shown in Fig. 3.

Since the evaluation process of microstructure was similar to sample no. 1-7, the threshold errors and standard deviation of mean values of bainite phase was relatively high. The results show that the inductance corresponded with volume of bainite but limit of saturation (62 vol. % of bainitic ferrite) showed high errors. Lower volume of the bainite phase corresponded with inductance with high correlation efficiency (R^2 = 0.97). The correlation between inductance and ferromagnetic ferrite greater than 62 vol. % was not possible due to high deviation by the metallographic method for evaluation of austenite transformation phase products.

Actually volume of bainite phase at austempered temperature was used for determination of time temperature diagram for ADI cast iron. TTT diagram was developed by fitted measured values using Eq. 3. Determination of the martensite temperature was by electromagnetic sensor where the sample was cooled at 200°C in salt bath and further cooled by air in electromagnetic sensor at room temperature. Martensite transformation of the austenite was independent on time but volume of martensite phase was dependent on temperature. The relation dH/dT showed a peak of the actual temperature during the austenite to martensite transformation.

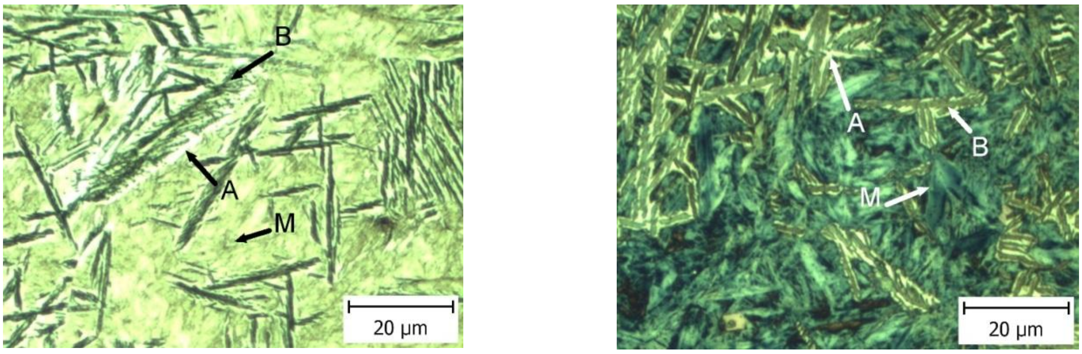

a) b)

Fig. 2. – Microstructure of the ADI cast iron at H (%) = 35; a) etched by Nital, B-bainite, A-austenite, M-martensite b) etched by Klemm

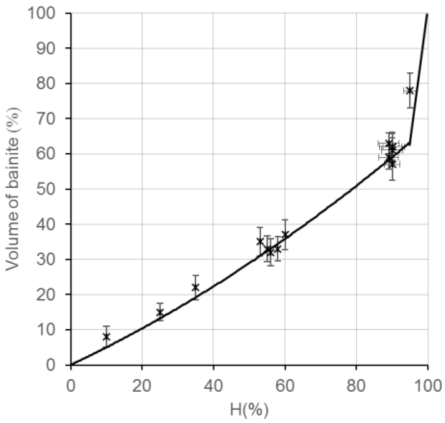

Fig. 3. – Relationship between volume of bainite and inductance (%); line represent Eq. 2

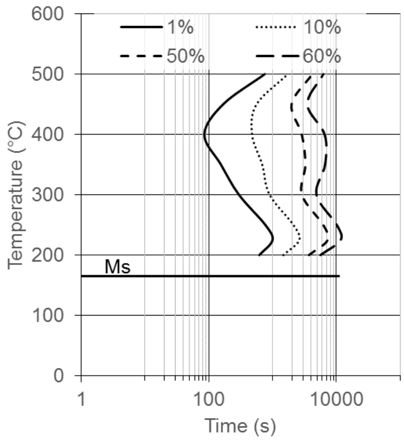

Fig. 4. – TTT diagram developed by results from EMS sensor

CONCLUSIONS

Electromagnetic sensor was suitable for detection of ferromagnetic phase in iron alloys due its sensitivity and good relationship with ferrite phase percentage in austempered cast iron. The correlation efficiency was found to be 97%. Ferrite percentage greater than 62 vol. % decreased the sensitivity of the electromagnetic method. In addition, electromagnetic sensor detection of the austenite phase transformation at constant temperature could also be used for the description of kinetic austenitic transformation. The device could be used for the investigation of multi-phase iron alloys of different ratio microstructure phases.

ACKNOWLEDGEMENT

The study was supported by project Technology Agency of the Czech Republic no. TA01010192.

REFERENCES

1. ERFANIAN-NAZIFTOOSI, H. R., N. HAGHDADI AND A. R. KIANI-RASHID, 2011. The Effect of Isothermal Heat Treatment Time on the Microstructure and Properties of 2.11% Al Austempered Ductile Iron. Journal of Materials Engineering and Performance [online]. 30.11., vol. 21, no. 8, pp. 1785–1792 [accessed. 8. April 2014]. ISSN 1059-9495.
2. GAO, GUHUİ, HAN ZHANG AND BİNGZHE BAI, 2011. Effect of tempering temperature on low temperature impact toughness of a low carbon Mn-series bainitic steel. Jinshu Xuebao/Acta Metallurgica Sinica [online]. vol. 47, no. 5, pp. 513–519. ISSN 04121961.
3. GHANEI, SADEGH, MEHRDAD KASHEFI AND MOHAMMAD MAZINANI, 2013. Eddy current nondestructive evaluation of dual phase steel. Materials & Design [online]. 9., vol. 50, pp. 491–496 [accessed. 15. April 2014]. ISSN 02613069.
4. HUNG, F.Y, L.H CHEN AND T.S LUI, 2002. A study on the particle erosion of upper bainitic austempered ductile iron. Wear [online]. 7., vol. 252, no. 11-12, pp. 985–991 [accessed. 10. April 2014]. ISSN 00431648.
5. CHALA, A., L. CHEKOUR, C. NOUVEAU, C. SAIED, M.S. AIDA AND M.A. DJOUADI, 2005. Study of the duplex treatment on 32CrMoV13 low alloy steel: Application in wood machining. Surface and Coatings Technology [online]. 10., vol. 200, no. 1-4, pp. 512–516 [accessed. 9. May 2012]. ISSN 02578972.
6. CHEN, JUNDAN, WENLİN MO, PEİ WANG AND SHANPİNG LU, 2012. Effects of tempering temperature on the impact toughness of steel 42CrMo. Jinshu Xuebao/Acta Metallurgica Sinica [online]. vol. 48, no. 10, pp. 1186–1193. ISSN 04121961.
7. CHOTĚBORSKÝ, R. AND P. HRABĚ, 2013. Effect of destabilization treatment on microstructure, hardness and abrasive wear of high chromium hardfacing. Research in Agricultural Engineering [online]. vol. 59, no. 4, pp. 128–135. ISSN 12129151.
8. CHOTĚBORSKÝ, R., P. HRABĚ, M. MÜLLER, R. VÁLEK, J. SAVKOVÁ AND M. JIRKA, 2009. Effect of carbide size in hardfacing on abrasive wear. Research in Agricultural Engineering [online]. vol. 55, no. 4, pp. 149–158. ISSN 12129151.
9. KOLAŘÍKOVÁ, MARİE, ROSTİSLAV CHOTĚBORSKÝ, JARMİLA SAVKOVÁ AND BARBORA BRYKSÍ STUNOVÁ, 2013. Local Mechanical Properties of Borides in Fe-B Steels. Key Engineering Materials [online]. 9., vol. 586, pp. 170–173 [accessed. 14. March 2014]. ISSN 1662-9795.
10. LEE, SEOK-JAE, ERİK J. PAVLINA AND CHESTER J. VAN TYNE, 2010. Kinetics modeling of austenite decomposition for an end-quenched 1045 steel. Materials Science and Engineering: A [online]. 5., vol. 527, no. 13-14, pp. 3186–3194 [accessed. 11. February 2014]. ISSN 09215093.
11. LIU, JUN, MARTİN STRANGWOOD, CLAİRE L. DAVIS AND ANTHONY J. PEYTON, 2013. Magnetic Evaluation of Microstructure Changes in 9Cr-1Mo and 2.25Cr-1Mo Steels Using Electromagnetic Sensors. Metallurgical and Materials Transactions A [online]. 13.8., vol. 44, no. 13, pp. 5897–5909 [accessed. 15. April 2014]. ISSN 1073-5623.
12. PACURAR, CLAUDİA, VASİLE TOPA, ADİNA RACASAN AND CALİN MUNTEANU, 2012. Inductance calculation and layout optimization for planar spiral inductors. In: 2012 13th International Conference on Optimization of Electrical and Electronic Equipment (OPTIM) [online]. B.m.: IEEE, p. 225–232 [accessed. 17. March 2014]. ISBN 978-1-4673-1653-8.
13. PIETRZYK, M. AND R. KUZIAK, 2011. Computer aided interpretation of results of the Jominy test. Archives of Civil and Mechanical Engineering [online]. vol. 11, no. 3, pp. 707–722. ISSN 16449665.
14. REISSMAN, TİMOTHY, JOON-SİK PARK AND EPHRAHİM GARCIA, 2012. Multilayer, Stacked Spiral Copper Inductors on Silicon with Micro-Henry Inductance Using Single-Level Lithography. Active and Passive Electronic Components [online]. vol. 2012, pp. 1–8 [accessed. 17. March 2014]. ISSN 0882-7516.
15. SCILAB ENTERPRISES, 2014. Scilab [online]. 2014.
16. WANG, BOWEN, YAN LV, GUOLU LI, WENMEİ HUANG, YİNG SUN AND BAOZHİ CUI, 2014a. The magnetostriction and its ratio to hysteresis for Tb-Dy-Ho-Fe alloys. Journal of Applied Physics [online]. 7.5., vol. 115, no. 17, p. 17A902 [accessed. 17. March 2014]. ISSN 0021-8979.
17. WANG, X.L., K.M. WU, F. HU, L. YU AND X.L. WAN, 2014b. Multi-step isothermal bainitic transformation in medium-carbon steel. Scripta Materialia [online]. 3., vol. 74, pp. 56–59 [accessed. 10. April 2014]. ISSN 13596462.
18. YIN, W., A. J. PEYTON, M. STRANGWOOD AND C. L. DAVIS, 2007. Exploring the relationship between ferrite fraction and morphology and the electromagnetic properties of steel. Journal of Materials Science [online]. 26.4., vol. 42, no. 16, pp. 6854–6861 [accessed. 15. April 2014]. ISSN 0022-2461.
19. YIN, ZHİXİN, WEİCHENG YU, GE YAO, ZHENGUO YANG, SHOUXİN LI, CHANGXİANG MA, MAOQİU WANG, WEİJUN HUI, HAN DONG AND YUQİNG WENG, 2002. Effect of cycle quenching on structure and fatigue property of 42CrMo steel. Kang T'ieh/Iron and Steel (Peking) [online]. vol. 37, no. 10, pp. 52–56. ISSN 0449749X.
20. ZHANG, CHUANYOU, QİNGFENG WANG, JUANXİA REN, RUİXİN LI, MİNGZHİ WANG, FUCHENG ZHANG AND ZESHENG YAN, 2012. Effect of microstructure on the strength of 25CrMo48V martensitic steel tempered at different temperature and time. Materials & Design [online]. 4., vol. 36, pp. 220–226 [accessed. 18. March 2014]. ISSN 02613069.

Corresponding author:

Ing. Miloslav Linda, Ph.D., Department of Material Science and Manufacturing Technology, Faculty of Engineering, Czech University of Life Sciences in Prague, Kamýcká 129, Praha 6, Prague, 16521, Czech Republic, phone: +420 22438 3315, e-mail: linda@tf.czu.cz

INFLUENCE OF WEATHER CONDITIONS ON WASTE BIOMASS PRODUCTION IN THE VYSOČINA REGION OF THE CZECH REPUBLIC

O. Chotovinský[1], V. Altmann[2], M. Přikryl[1]

[1]Department of Technological Equipment of Buildings, Faculty of Engineering, Czech University of Life Sciences Prague, Czech Republic
[2]Department of Machinery Utilization, Faculty of Agrobiology, Food and Natural Resources, Czech University of Life Sciences Prague, Czech Republic

Abstract
The significant effect of change climatic and weather conditions on crop biomass yields is often observed in various regional production areas during the last decade. Starting with the Vysočina Region within the period of 2007–2011, the present article studies the relation between weather conditions and the volume of municipal residue biomass. A statistically significant impact of rainfall level on municipal residue biomass production has been demonstrated by simple regression. Available data for individual years confirm the regression compensation straight line of average monthly precipitation $\boldsymbol{p}$ and the average biodegradable municipal solid waste production per one collection $\boldsymbol{T}$ in the researched municipality of the Vysočina Region: $T = 0.542 + 0.659.p$. The development of biodegradable municipal solid waste collection in the researched municipality has also been described and evaluated.

Key words: biodegradable municipal solid waste, biodegradable municipal solid waste collection, municipal residue biomass, weather conditions.

INTRODUCTION

Residual Waste biomass (MRB), the source of which is biodegradable municipal solid waste (BMSW) or the biodegradable part of rest municipal solid waste (RMSW) is considered a potential source of perennial bioenergy (GREG, 2010). Most of the biomass of this kind is collected and aggregated in population centers with high energy demands. The availability of this energy source increases together with the population growth rate and energy consumption per capita (BOGNER ET AL., 2003). Implementation of equipment utilizing this potential requires significant investments (EIA, 2009). Nevertheless, technologies using this type of biomass are improving and gradually displacing fossil energy. As a consequence, the formation of methane during storage of biological biodegradable components of MSW at dump areas can be reduced (CONSONNI ET AL., 2005).

Biodegradable municipal waste means biodegradable waste from households, as well as other biodegradable waste, which because of its nature and composition is similar to biodegradable waste from households (EEA, 2002). Tab. 1 shows an overview of BMSW types according to legislation in the Czech Republic (MŽP, 2001).

Tab. 1. – Summary of biodegradable municipal solid waste

Code No.*	Name of the Type of Waste
20 01 01	Paper and cardboard with the exception of highly glossing paper and the wallpaper waste
20 01 08	Cafeteria biodegradable waste
20 01 10	Clothing
20 01 11	Textiles
20 01 38	Wood not included in 20 01 37
20 02 01	Biodegradable waste
20 03 01	Rest municipal solid waste
20 03 02	Marketplace waste
20 03 07	Bulky waste

The service of waste collection is defined as a combination of a certain technology and a human labor (BILITEWSKY ET AL., 1997). The term 'waste collection' includes not only the collection itself, but also the transfer of waste to places where collecting vehicles are unloaded and loaded (TCHOBANOGLOUS ET AL., 1993). Typically, BMSW separated at the source are separated for reuse (recycled). The three principial methods now used for the collection of BMSW from residential sources include (TCHOBANOGLOUS ET AL., 2002):

1. Curbside collection using conventional and specially designed collection vehicles
2. Incidental curbside collection by charitable organizations
3. Delivery by residents to drop-off centers

The potential for the use of BMSW in the Czech Republic is based on an analysis of MSW potential. The potential of the remaining municipal waste (RMSW) and garden waste (including public green) in 2020 are forecasted to amount to 3.8 and 0.6 million tons respectively (MZE, 2012).

A number of recent studies have analyzed the role of climate effects and weather conditions on biomass production from the perspective of varying crop yields. The climate-biomass production relationships are documented and several examples of extremely/very low yields in the selected region and periods improve our understanding of the most important climatic factors and weather conditions. Understanding these causes and role of these events is critical for improving our ability to analyze chances both under present and, more importantly, expected conditions (E.G. LOBELL ET AL., 2011; OLSEN ET AL., 2012; LAVALLE ET AL., 2009; PELTONEN–SAINIO ET AL., 2010; KOLAŘ ET AL., 2013). However, the possible response of weather conditions on waste biomass production is not extensively observed today.

The basic objective of the study is an evaluation of BMSW separate collection data in the urban municipality of Náměšť nad Oslavou, covering the period of 2007–2011. Weather conditions of the same period and region are also analyzed and compared to their actual impact on waste biomass production. Description of the influence on waste biomass production including the impact of weather change as a possible limiting factor for continues reuse of biomass.

MATERIALS AND METHODS

Náměšť nad Oslavou – Biodegradable municipal solid waste production data

The urban municipality of Náměšť nad Oslavou (49.217°N, 16.150°E) is situated on the foot of the Czech-Moravian Highlands at an altitude of 365 metres. The urban municipality belongs to the Vysočina Region (Třebíč district); 20 km east of Trebic on the River Oslava. Its territory mostly constitutes agricultural and forest land (795 and 796 hectares respectively). The built-up area spans 48 hectares with 53 hectares of gardens. 4955 permanent residents live in 862 family houses and 52 blocks of flats in 2011 year. Gas is the most common heating medium. Separate collection of BMSW can be considered fully developed, with good access throughout the territory of municipality. Both drop-off and curbside collections are applied. 0.77 m^3 containers and 0.24 m^3 containers (previously used), as well as large volume containers (18 m^3) are placed in the municipality.

Tab. 2 and 3 specify, on a month-by-month basis, the BMSW production in Náměšť nad Oslavou in 2007 and 2011 (peripheral input data). These tables summarize also the real number of containers/month, available per collection drive.

Tab. 2. – Biodegradable municipal solid waste (20 02 01) in Náměšť nad Oslavou in 2007

Month	Production [t]		Collected containers per month [pcs.month^{-1}]		Collections per month [drives.month^{-1}]	
	C_{BMSW} 0.24 m^3	LSC 18 m^3	C_{BMSW} 0.24 m^3	LSC 18 m^3	C_{BMSW} 0.24 m^3	LSC 18 m^3
April	2.06	-	80	-	1	-
May	8.69	-	80	-	4	-
June	7.99	14.24	80	1	4	3
July	10.77	9.53	80	1	5	2
August	10.93	4.03	80	1	4	1
September	8.25	8.02	80	1	4	2
October	12.66	4.07	80	1	5	1
November	4.91	21.20	80	-	2	-

C_{BMSW} – adjusted BMSW containers; LSC – large-sized containers; Source: RESEARCH ESKO-T S.R.O.

Tab. 3. – Biodegradable municipal solid waste (20 02 01) in Náměšť nad Oslavou in 2011

Month	Production [t]		Collected containers per month [pcs.month^{-1}]		Collections per month [drives.month^{-1}]	
	C_{BMSW} 0.77 m^3	LSC 18 m^3	C_{BMSW} 0.77 m^3	LSC 18 m^3	C_{BMSW} 0.77 m^3	LSC 18 m^3
April	7.96	3.57	34	1	3	3
May	16.07	3.84	34	1	5	3
June	13.84	3.59	34	1	4	2
July	12.44	-	34	-	4	-
August	16.20	-	34	-	4	-
September	19.16	-	34	-	5	-
October	11.62	-	34	-	3	-
November	3.93	-	34	-	1	-

C_{BMSW} – adjusted BMSW containers; LSC – large-sized containers; adjusted BMSW containers (volumes of 0.24 m^3) were changed for adjusted BMSW containers with volumes of 0.77 m^3 in 2009
Source: research ESKO-T s.r.o.

Náměšť nad Oslavou - Long-term climate data

The region is moderate warm. Favourable water regime ensures stable soil water content. The period annual average air temperature is 14–18°C in June and -3°C in January. The annual precipitation totals reach 350–400 mm in the vegetation period and 200–250 mm in winter.

The Czech Hydrometeorological Institute (CHMI) conducts regular meteorological observations at more stations within the concerned region. Manually measured data used for this study cover long term monthly average air temperatures [°C], measured at the Sedlec station, and long term monthly total precipitation [mm] at Náměšť nad Oslavou, both for the period of 2007 to 2011 (see input, Tab. 4 and 5).

Tab. 4. – Monthly average air temperatures [°C]

Year	Month											
	I	**II**	**III**	**IV**	**V**	**VI**	**VII**	**VIII**	**IX**	**X**	**XI**	**XII**
2010	3.0	2.6	5.7	11.5	15.0	19.2	19.4	19.0	12.2	7.7	1.3	-1.5
2011	0.7	2.3	3.4	8.9	14.7	18.8	19.1	18.9	13.0	8.9	5.2	0.8
2012	-3.3	-0.8	3.5	13.2	13.9	15.6	18.9	19.4	15.9	7.9	5.2	-0.8
2013	-4.2	-1.5	3.5	8.8	12.2	17.0	20.4	17.6	12.2	6.3	5.1	-4.8
2014	-1.2	-1.4	4.8	11.1	14.1	17.6	17.3	19.4	16.0	8.4	2.2	1.3

Source: CHMI

Tab. 5. – Monthly total precipitation [mm]

Year	Month											
	I	**II**	**III**	**IV**	**V**	**VI**	**VII**	**VIII**	**IX**	**X**	**XI**	**XII**
2010	1.9	2.2	6.3	2.6	2.5	4.2	4.8	3.9	3.6	1.2	3.3	0.9
2011	1.0	1.5	2.3	2.8	2.4	4.2	2.9	3.1	2.5	1.0	1.8	1.6
2012	1.7	2.3	3.3	2.1	3.4	5.4	7.0	2.4	2.0	1.8	2.4	2.2
2013	2.6	1.4	1.0	5.0	5.7	10.7	8.0	6.7	5.6	1.3	1.9	1.9
2014	1.4	0.7	4.8	2.7	7.4	6.2	4.5	3.8	6.3	2.9	0.3	1.0

Partial correlation and regression model – Methodology

When working simultaneously with several variables, we need to assess the mutual dependence of their pairs without the influence of the others. The first option is to calculate correlation coefficients for all pairs of variables and establish the so-called correlation matrix. Calculation of correlation coefficients for the pairs, however, cannot capture higher-level interactions. To obtain these, we can use partial correlation coefficients. These express an interdependence of two variables, provided that other variable does not change. For example $r_{ij.k}$ expresses the interdependence of variables *Xi* and *Xj*, provided that *Xk* does not change (LEPŠ & ŠMILAUER, 2014).

The simplest regression method is the linear model of regression, i.e. a straight line, where the relation between two quantitatively measured characteristics (*Y* and *X*) is represented the equation the $Y = a + b * X + \varepsilon$. The parameters (regression coefficients) *a* and *b* have specific numerical values that we try to estimate based on the collected data (sample data); the symbol ε represents the stochastic (non-deterministic) part of the model (ŠMILAUER, 2007).

Analysis of variance is a part of regression analysis. Through this analysis, we determine the suitability of the selected regression model by using the *F*-test (ANOVA in regression). In this decomposition, we describe how a large part of the total variability in the values of the given variable can be explained by the chosen model and how significant is the remaining (unexplained) part. This analysis is based on the relation. A suitable regression model must contain a sum of explained squares which is greater than the residual sum of squares. When testing this assumption, we verify the null hypothesis H_0: The selected functional relation between the dependent and independent variable does not exist (LITSCHMANNOVÁ, 2011).

The program STATISTICA 8 was used to analyze the data and obtain the necessary characteristics of above-mentioned statistical methods.

Standard transformation for the regression model – Methodology

In order to obtain a more precise interpretation of the described data, a standardized transformation has been applied. This eliminates possible interruptions in the continuous measurement conducted by CHMI (unmeasured precipitation). This model, which is also more suitable for handling winter months without BMSW (20 02 01) collection in the municipality, is depicted in Tab. 6.

Tab. 6. – Standard transformation

Quater of Years	Average BMSW production per one drive of collection [t]	Average Monthly temperature [°C]	Average Monthly precipitation [mm]
1Q	$\frac{1}{3}(\frac{1}{n}\sum_{i=1}^{n} x_i + \frac{1}{n}\sum_{i=1}^{n} x_i + \frac{1}{n}\sum_{i=1}^{n} x_i)$	$\frac{t_1 + t_2 + t_3}{3}$	$\frac{p_1 + p_2 + p_3}{3}$
2Q	- „ -	- „ -	- „ -
3Q	- „ -	- „ -	- „ -
4Q	- „ -	- „ -	- „ -

$x_{i(0.12;\,0.23)}$ – amount of biodegradable municipal solid waste in C_{BMSW} – adjusted BMSW containers in C_{BMSW} containers (0.12 and 0.24 m^3)/drive of collection; n – number of collection (drive of collection); t_1, t_2, t_3 – monthly average air temperatures of the relevant quarter; p_1, p_2, p_3 – monthly total precipitation of the relevant quarter

RESULTS

The Municipality placed three types of BMSW containers in the built-up area already in recently time. Their usage is as follows:

- C_{BMSW} containers 0.24 m^3 and 0.77 m^3 – BMSW from residences,
- LSC containers 18 m^3 – BMSW from public green areas.

The year-by-year development of the number of BMSW containers and their collection is presented in Tab. 7 below.

The number of C_{bmsw} 0.24 m^3 containers and the number of C_{bmsw} 0.77 m^3 containers (and the associated change of the number of participating residences) influenced the total volume of collected BMSW between 2007 and 2011. This trend, recalculated to

BMSW production per one collection drive, is presented in Tab. 8 below. This table also represents the standard data transformation for the regression model.

Tab. 7. – Number of biodegradable municipal solid waste containers and number of collected containers per month in the municipality of Náměšť nad Oslavou

Year	C_{BMSW} 0.24 m^3 (total containers/ collected containers per month)	C_{BMSW} 0.77 m^3 (total containers/ collected containers per month)	LSC 18 m^3 (total containers/ collected containers per month)
2007	88/330	-	1/2.7
2008	88/310	-	1/3.8
2009	-	33/137	1/1.5
2010	-	34/123	1/2.3
2011	-	34/123	1/2.6

C_{BMSW} – adjusted BMSW containers; LSC – large-sized containers

Tab. 8. – Average values from data obtained for individual quarters of the years 2007 – 2011 (Standard transformation)

Quarter and year	Average BMSW production per one collection drive [t]*	Average Monthly temperature [°C]	Average Monthly precipitation [mm]
1Q 2007	0	0	0
1Q 2008	0	0	0
1Q 2009	0	0	0
1Q 2010	0	0	0
1Q 2011	0	0	0
2Q 2007	2.07	13.82	2.56
2Q 2008	2.98	14.12	3.13
2Q 2009	2.48	14.21	3.64
2Q 2010	3.78	12.65	7.15**
2Q 2011	3.11	14.29	5.42
3Q 2007	2.31	16.85	4.12
3Q 2008	4.03	17.00	2.80
3Q 2009	4.59	18.08	3.78
3Q 2010	4.32	16.76	6.76
3Q 2011	3.66	17.56	4.87
4Q 2007	1.66	3.85	2.24
4Q 2008	1.96	4.97	1.44
4Q 2009	2.58	4.11	2.13
4Q 2010	2.74	2.18	1.68
4Q 2011	2.06	3.94	1.38

* - collection of C_{BMSW} containers (0.24 and 0.77 m^3)
** - high leverage point, extreme precipitation in June

The results of the analysis, presented in the Tab. 8, first focused on determining the correlation coefficient (the Correlations matrices function) between the average BMSW production per one collection drive in the given quarter [t] and other variables, namely the average monthly temperature [°C] and the average monthly precipitation [mm]. The results, presented in Tab. 9, confirm an individual linear dependence. The partial coefficient 0.5707 demonstrated a correlation between the average daily temperatures and average daily precipitation (Tab. 10). Therefore only the more significant variable (average monthly precipitation) has been used for the next calculation.

'*F* statistics', resulting from the analysis of the variance regression model, was carried out as an intermediate step of the selected regression function (Tab. 11).

Tab. 9. – Result of correlation values

	Correlations (Tab. 8) Marked correlations are significant at $p < 0.05000$ N=20 (Case deletion of missing data)	
Variable	[°C]	[mm]
[t]	0.8475	0.8518
	p=0.000	p=0.000

Tab. 10. – Result of partial correlations

	Partial correlations (Tab. 8) Marked correlations are significant at $p < 0.05000$ N=20 (Case deletion of missing data)	
Variable	[°C]	[mm]
[°C]	1.0000	0.5707
	p= ---	p=0.011
[mm]	0.5707	1.0000
	p=0.011	p= ---

Tab. 11. – ANOVA results

	Analysis of Variance; *DV*: [t] (Tab. 8)				
N=20	Sums of Squares	*df*	Mean Squares	*F*	*p*-level
Regress	34.02646	1	34.02646	47.57438	0.000002
Residual	12.87408	18	0.71523		
Total	46.90053				

Values of the Mean Squares in Tab. 12 were used for testing the significance of the regression model, whereas the key value used was the ratio of the model mean square and the residual mean square. In the case of the null hypothesis, the value of this ratio should be relatively close to 1 (i.e., the explained and unexplained variability should be of a similar size). More precisely (for this particular model), it should originate from the F disturbance with a parameter value of 1.18 (for the presented model). Nevertheless, the probability that the true value of this ratio, i.e. the *F* statistic (with a value of 47.57438), originates from this F disturbance is less than 0.000001 or equal to 0^6, as confirmed by the values in the '*p*-level' column. Hence H_0 can be rejected with this probability of a Type I error (at the concerned level of significance).

We present below a graphical representation of the regression line, (Fig. 1).

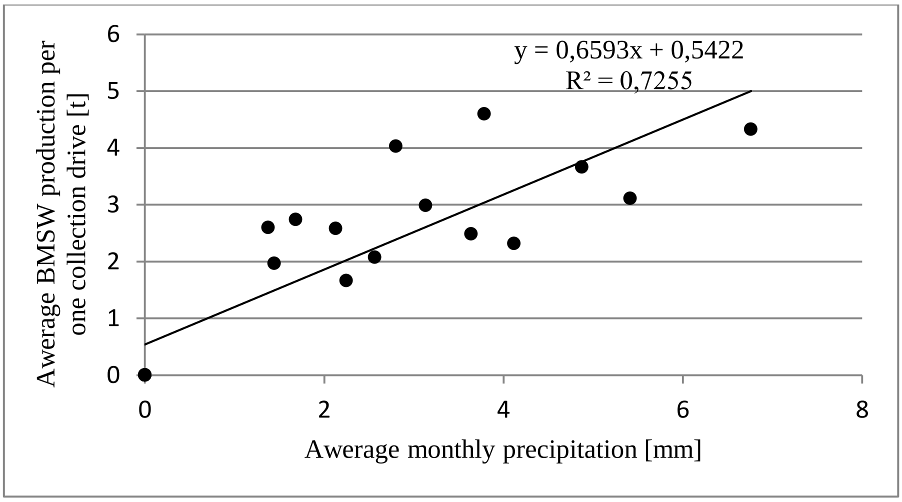

Fig. 1. – Graphical representation of regression

DISCUSSION

An assessment of the mean values of weather conditions proves a statistically significant relation between the average BMSW production per collection and the average monthly precipitation (r = 0.8518, α = 0.05, n = 20), as well as between the BMSW production and the average monthly temperature (r = 0.8475, α = 0.05, n = 20). SIDLAUSKAS (2003) has shown a very similar that seed yield of spring oilseed rape correlated well with the duration of vegetative growth period, precipitation rate and mean daily temperature. In other words, the biomass waste production in the municipality of Náměšť nad Oslavou could depend on weather conditions of the growing season. The positive relationship was furthermore enriched by regression analysis; however this does not necessarily reflect a causal relation (in fact, only non-manipulated areas have been observed). Together with some other factors, the yield of biomass is considerably dependent on the weather condition. For instance, these factors generaly include the onset of the spring, moisture and temperature conditions for emergence and tillering and the content of the available soil nitrogen (PETR & MIČÁK, 2009). Furthermore, as the distribution of regression residuals around the x-axis shows, there exist some differences between real (observed) and predicted (fitted by the regression model) values of the variables in the regression equation. Thus, BMSW production could have been influenced by others non-measured factors.

The change of technological parameters, respectively the associated change of volumes of C_{BMSW} 0.24 m^3 containers for C_{BMSW} 0.77 m^3 containers may influence unexplained points of analyzed components; additionally, fluctuations of both analyzed climate data could also played a role.

MUŽÍKOVÁ ET AL. (2013) describe similar statistically conclusive results concerning the influence of weather conditions; they proved a close relation between the values of available water capacity and biomass production of selected crops in the Czech Republic (in 1976–2007). STŘEDOVÁ ET AL. (2011) published an analysis of several temperature and precipitation indexes and their changes, with an emphasis on the increase of above-normal temperature months and the loss of normal rainfall months. MUŽÍKOVÁ ET AL. (2011) have also documented the future increase of extremities in the weather conditions across the Czech Republic.

CONCLUSIONS

The principal objective of the present study was an evaluation of BMSW collection in the municipality of Náměšť nad Oslavou in the period of 2007–2011. The authors also studied the influence of selected climatic factors on BMSW production of an urban municipality.

The study proves that weather conditions influence BMSW production and mathematically defines this dependence. Available data for individual quarters of 2007–2014 confirm the following regression compensation straight line of average monthly precipitation $\boldsymbol{p}$ and the average BMSW production per one collection $\boldsymbol{T}$ in the municipality of Náměšť nad Oslavou: $T = 0.542 + 0.659.p$.

A perspective BMSW separete collection that includes full cost accounting of separete collection of waste, handling, and processing must incorporate marketing, distributing, and recycling in a life cycle analysis that reflects external costs and societal benefits. In this view of systems perspective, the influence of weather conditions may become a new, complementary, approach to flowing the costs of separate collection of BMSW, including the limiting impact on the balance of input converting matter for reuse. This should be taken into consideration when developing BMSW collection processes. The well-chosen technological parameters of BMSW separate collection play an important role too.

ACKNOWLEDGEMENTS

The work has been supported by the Internal Grant Agency of Czech University of Life Sciences Prague, Project No. 2014: 31180/1312/3132.

REFERENCES

1. BILITEWSKY, B., HARDTLE, G., MAREK, K.: Waste Manegement . 1st ed. Verlag Berlin Heidelberg, DEA, Springer 1997.
2. BOGNER, J., MATTHEWS. E.: Global methane emissions from landfills: new methodology and annual estimates 1980–1996. Global Biogeochemical Cycles, 17, 2003: 1–18.
3. CONSONNI, S., GIUGLIANO, M., GROSSO, M.: Alternative strategies for energy recovery from municipal solid waste, Part B, emission and cost estimates. Waste Management, 25, 2005: 137–148.
4. GREG, J. S.: National and regional generation of municipal residue biomass and the future potential for waste-to-energy implementation. Biomass & Bioenergy, 34, 2010: 379–388.
5. KOLÁŘ, P., TRNKA, M., BRÁZDIL, R. HLAVINKA, P.: Influence of climatic factors on the low yields of spring barley and winter wheat in Southern Moravia (Czech Republic) during the 1961–2007 period. Theoretical and applied Climatology, 117, 2014: 707–721.
6. LAVALLE, C., MICALE, F., HOUSTON, TD., CAMIA, A., HIEDERER, R., LAZAR, C., CONTE, C., AMATULLI, G.,

GENOVESE, G.: Climate change in Europe. 3. Impact on agriculture and forestry. A review. Agronomy for Sustainable Development, 29, 2009: 433–446.
7. LEPŠ, J., ŠMILAUER, P.: Biostatistika. České Budějovice, the Czech Republic, Univerzity of South Bohemia in České Budějovice 2014.
8. LITSCHMANNOVÁ, M.: Úvod do statistiky. Ostrava, the Czech Republic, VŠB – Technical University of Ostrava 2011.
9. LOBEL, D. B., SCHLENKER, W. , COSTA-ROBERTS, J.: Climate trends and global crop production since 1980. Science, 29, 2011: 616–620.
10. EEA: Biodegradable municipal waste management in Europe. European Environment Agency, Copenhagen, DKA. Available at: www.eea.europa.eu. Accessed 21 March 2002.
11. EIA: Methodology for allocating municipal solid waste to biogenic and non-biogenic energy. US. Energy Information Administration, Washington DC, USA. Available at: www.eia.gov. Accessed 1 May 2007.
12. MŽP: Katalog odpadů. Ministry of the Environment of the Czech Republic, Prague, CZA. Available at: www..mzp.cz. Accessed 17 October 2001.
13. MZE: Akční plan pro biomasu v ČR na období (2012–2020). The Ministry of Agriculture of the Czech Republic, Prague, CZA, 2012. Available at: www.eagri.cz. Accessed 12 September 2012.
14. MUŽÍKOVÁ, B., VLČEK, V., STŘEDA, T.: Tendencies of climatic extremes occurrence in different Moravian regions and landscape types. Acta Universitatis Agriculturae et Silviculturae Mendelianae Brunensis, 5, 2011: 169–178.
15. MUŽÍKOVÁ, B., STŘEDA, T., KRMELOVÁ P.: Výnosy ječmene setého v klimatických podmínkách České republiky. Kvasný průmysl, 59, 2013: 352–357.
16. OLESEN, JE., BORGENSEN, CD., ELSGAARD, L., PALOSUO, T., ROTTER, R., SKJELVAG, AO., PELTONEN-SAINIO, P., BORJESSON, T., TRNKA, M., EWERT, F., SIEBERT, S., BRISSON, N., EITZINGER, J., VAN DERFELS-KLERX, HJ., VAN ASSELT, E.: Changes in time of sowing, flowering and maturity of cereals in Europe under climate change. Food Additives & Contaminants, 29, 2012: 1527–1542.
17. PELTONEN-SAINIO, P., JAUHIAINEN, L., TRNKA, M., OLESEN, JE., CALANC, PL., ECKERSTEN, H., EITZINGER, J., GOBIN, A., KERSEBAUN, KC., KOZYRA, J., KUMAR, S., MART, AD., MICALE, F., SCHAAP, B., SEGUIN, B., SKJELVAG, AO., ORLANDINI, S.: Coincidence of variation in yield and climate in Europe. Agriculture, Ecosystems Environment, 139, 2010: 483–489.
18. PETR, J., MIČÁK, L.: Yield formation in the spring barley in organic farming. Scientia Agriculturae Bohemica, 10, 2009: 110–114.
19. SIDLAUSKAS, G., BERNOTAS, S.: Some factors affecting seed yield of spring oilseed rape (Brassica napus L.). Agronomy Researched, 1, 2003: 229-243.
20. STŘEDOVÁ, H., STŘEDA, T., MUŽIKOVÁ, B.: Trend teplotních a srážkových podmínek v zemědělsky intenzivních oblastech. Úroda, vědecká příloha, 10, 2011: 590–596.
21. ŠMILAUER, P.: Moderní regresní metody. České Budějovice, the Czech Republic, Univerzity of South Bohemia in České Budějovice 2007.
22. TCHOBANOGLOUS, G., THEISEN, H., VIGIL AS.: Integrated Solid Waste Management.1st ed. New York, USA, McGraw-Hill 1993.
23. TCHOBANOGLOUS, G., KREITH, F.: Handbook of solid waste management. 2nd ed. New York, USA, McGraw-Hill 2002.

Corresponding author:
Ing. Ondřej Chotovinský, Department of Technological Equipment of Buildings, Faculty of Engineering, Czech University of Life Sciences Prague, Kamýcká 129, Praha 6, Prague, 16521, Czech Republic, e-mail: chotovinsky@tf.czu.cz

MAPPING AND DIFFERENCES OF SOIL PHYSICAL PROPERTIES

J. Chyba, F. Kumhála, P. Novák

Department of Agricultural Machines, Faculty of Engineering, Czech University of Life Sciences Prague, Czech Republic

Abstract
Soil physical properties are of great importance for the evaluation of soil compaction or for soil conditions characterization. The latter option is important for the purpose of soil tillage machines. Field measurements were arranged in order to characterize the variation of soil physical properties within the plot. Two methods of soil physical characteristics evaluation were used: soil cone index and undisturbed soil sampling. Undisturbed soil samples were taken from 102 points in almost regular grid 6 x 6 m. Cone index was measured thrice in the each point. The maps of mentioned measurements were created and compared by using statistical methods. Penetration resistance generally copied soil bulk density but otherwise than expected. Nevertheless, the most important finding was that relatively very small changes of soil moisture content can influence penetration resistance regardless, or with minimal impact, of soil bulk density results.

Key words: soil bulk density, cone index, moisture content, soil properties.

INTRODUCTION

Soil compaction is a major problem of modern agriculture management and grows with size and weight of agricultural machines. For monitoring of soil compaction e.g. soil physical properties is useful to monitor bulk density and cone index values. These values are interrelated and influence each other. The main indicator of soil compaction is value of bulk density; it is a parameter that is often used to describe the level of soil compaction (JOHNSON & BAILEY, 2002). Relationship between soil compaction and physical properties of the soil at various depths were monitored by DEFOSSEZ & RICHARD (2002). In their work was created a model of the relationship between the density and depth of soil. Model of soil compaction was developed and then compared with measurements under real conditions. The main result was that the rides of agricultural technology are reflected in the depth of 0.35 m. Compacted soil has a higher density than non-compacted soil about 0.2 $t \cdot m^{-3}$ to a depth of 0.2 m. The influence of soil compaction has decreased to a depth of 0.45 m, where has achieved similar values as non-compressed soil.

Another very good method for monitoring physical properties of soil is a cone index measurement. Cone index measurement has advantages over measurements of soil bulk density in a simple acquisition of data from all over the soil horizon (this value is limited by penetrometer depth range), the process of penetration measurement can also be automated (RAPER, 2005). Values of cone index can be largely influenced by soil tillage as point's measurement of ALAKUKKU (1996). In the case of this measurement was performed plowing to a depth of 0.25 m. The increasing trend of cone index with depth indicates that there was no significant statistical difference between compacted and non-compacted areas to a depth where the plowing was conducted. Significant differences occurred only at depths where plowing was not performed (higher values for the compacted and lower values for non-compacted areas). The largest differences were observed at depths of 0.3–0.5 m, these differences were amounted to 22%. Nevertheless, the cone index values are to some extent influenced by soil bulk density but also by soil moisture content. AYERS & PERUMPRAL (1982) created a graph of the cone index, dry density and moisture content and their relationship for a soil with a share of 50% clay and 50% sand. Fig. 1 shows the significant influence of moisture content on cone index, while at higher moisture content the cone index is affected by the dry density only slightly. Similar measurement to the mentioned model was performed by VAZ ET.AL. (2011) who estimated correction which significantly lower the influence of soil water content on cone index measurements. Nevertheless, from their work is also obvious high influence of water content on cone index values.

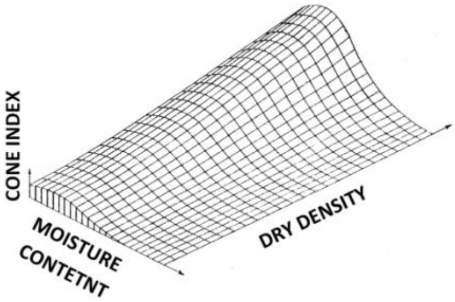

Fig. 1. – The relationship between cone index, dry density and moisture content (AYERS & PERUMPRAL, 1982)

This was confirmed by the experiment in which the penetrometer was combined with a TDR probe. The experiment was carried out on four parcels 1.2 x 1.2 m^2, wherein one plot was a reference and on the others was applied the water of the volume 100, 150 and 300 l. Results pointed to the fact that the increase in soil moisture by 0.05 cm^3·cm^{-3} can lead to reduction of penetration resistance up to 40% (VAZ ET AL., 2001). BUSSCHER ET AL. (1997) stated that the cone index values can be interpreted for known values of moisture content or with a suitable correction of cone index values using the equation related to the soil initial moisture content. However, using multiple-equation correction cannot guarantee that the resulting values and the differences are not just a result of these corrections. The result of this research was that the correction of cone index, for known water content, led to increased significance of differences. In the case of one-equation correction the difference had been influenced by differences in water content before correction. In the case of multiple-correction equation the difference may be real or a result of different corrections. Influence of soil moisture content on soil mechanical resistance was also mentioned in other works (VARGA ET AL., 2014; DA SILVA & KAY, 1997).

From literature it is obvious that great care must be taken when measuring the cone index with regard to, not only, bulk density but especially also to the soil moisture content. For that reason, this article focuses on interdependencies of soil moisture content, bulk density and cone index values within one plot and time horizon to provide authoritative results.

MATERIALS AND METHODS

Field measurements took place in the field near to Městec Králové in Central Bohemia, N 50°10.88725', E 15°17.78900'. The measurements were taken in 30th of October 2014. The soil type was classified as clayey-sandy *rendzina* according to FAO (Food and Agriculture Organization of the United Nations, 1974) and taxonomic soil classification system (TKSP in Czech Republic). Sugar beet was grown on the field before measurements.

Field test area was 46 x 100 m and two methods of soil physical characteristics evaluation were used: soil cone index measurement by horizontal penetrometer and undisturbed soil samples measurement. Undisturbed samples were taken into Kopecky's rings (stainless steel cylinders Fig. 2) and have standardized dimensions: 4.9 cm of diameter, 5.3 cm of height and volume of 100 cm^3. Undisturbed soil samples were taken from 102 points in almost regular grid 6 x 6 m from the depth of 0.1-0.15 m. Subsequently the data were evaluated according to VALLA ET AL. (2011). The content of the samples was weighed (weight of natural moist soil was obtained G_A (g)) and then put into the oven, which was set to a temperature 105°C, and the samples were dried for minimum period of 24 hours. After 24 hours drying the samples were re-weighted and weight of dry soil was obtained G_H (g). From the results it is possible to calculate the actual moisture content θ_m (%) of the soil,

$$\Theta_m = G_A - G_H \tag{1}$$

And soil bulk density ρ_d (g.cm^{-3}) was evaluated according to volume of sampling cylinders V (cm^3).

$$\rho_d = \frac{G_H}{V} \tag{2}$$

Fig. 2. – Kopecky's stainless steel ring during evaluation

Cone index was measured thrice in the each place of soil samples taking. In total, 306 cone index measurements were done. Cone index measurement was carried out to a minimum depth of 0.32 m and measurement results were saved for every 0.04 m of the depth. For the cone index measurement was used penetrometer Pn-10 with 30° cone angle and area of 1 cm^2. For future details see ASABE standard S313.3 (ASAE STANDARDS, 2004).

The number of points allowed to compare the results and to create maps resulted from both types of measurement.

Based on preliminary results from MS Excel and ArcGIS maps the data were divided into two groups with regards to soil bulk density map (according to Fig. 3). In the first group were included the first 51 measurement points, where the values were found higher in bulk density. The remaining 51 points were included in the second group. This kind of distribution on the basis of soil bulk density is the core for comparison of results and the influence of soil moisture content and soil bulk density on the cone index. Subsequently, these two groups were compared statistically, by STATISTICA 12 software (see below), with respect to a sufficient number of measurements.

For the evaluation of the results was used program for map creation ArcGIS 10.1. Basic evaluation has been done via MS Excel 2010 and for statistical evaluation was used program STATISTICA 12 (*U-test, Kolmogorov-Smirnov test, t-test*).

RESULTS AND DISCUSSION

The maps were created from the measured values of soil moisture content, soil bulk density and cone index (Fig. 2–4). From map of soil bulk density (see Fig. 3) is a clear division of the plot into two similar parts. According to literature (JOHNSON & BAILEY, 2002; DEFOSSEZ & RICHARD, 2002) is obvious that the division of field is caused by different soil physical properties within the field (soil compaction). For this reason, the data set was divided into two similar groups, which were then statistically compared.

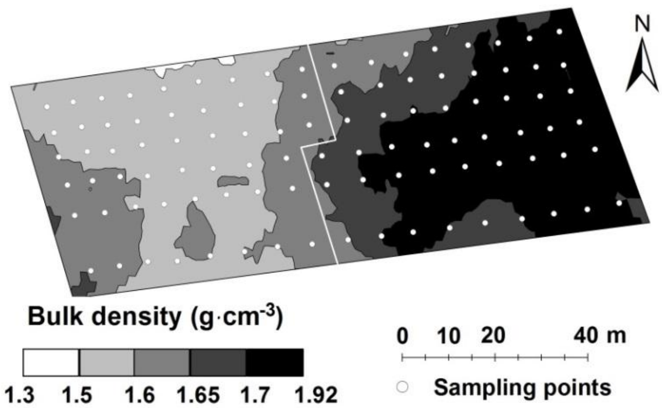

Fig. 3. – Map of soil bulk density (white line shows the division of land: left – lower bulk density 2st group, right – higher bulk density 1st group)

Upon closer observation of soil bulk density and cone index map (Fig. 4), was found an interesting finding namely at lower values of bulk density were the cone index values higher, whereas the opposite effect was expected. This finding contradicts the assertion (ALAKUKKU, 1996) that the cone index copies the soil bulk density as consequences of soil compaction. However, after taking into account soil moisture content values is all clear, because ALAKUKKU'S (1996) research was done under similar moisture content conditions.

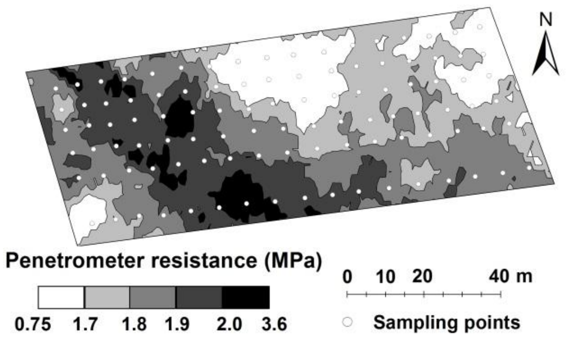

Fig. 4. – Map of cone index

By comparing maps of initial soil moisture (Fig. 5) content and cone index have been found areas where higher values of initial soil moisture content pointed out lower values of cone index and conversely. This finding was very surprising, since the soil moisture content affecting the cone index values more than soil bulk density in some areas. With regard to the hitherto mentioned results it is more than obvious that the cone index is to a certain degree affected by soil moisture content as was stated by AYERS & PERUMPRAL (1982), VAZ ET.AL. (2001; 2011) *etc*.

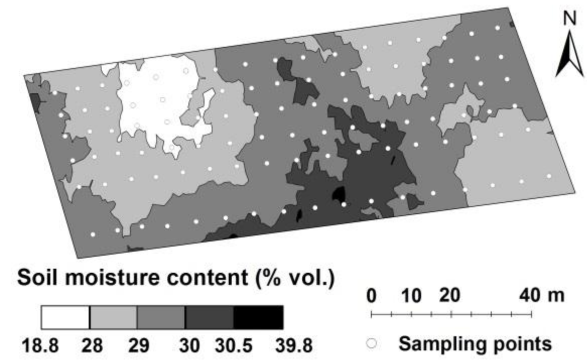

Fig. 5. – Map of soil moisture contetnt

Soil moisture content did not show a normal distribution, for this reason was primarily performed non-parametric test; however, a parametric test was also conducted. The result of initial moisture content is shown in Fig. 5. From the non-parametric test, it is clear that the groups differ in the distribution. The parametric test showed that the groups match each other in variability of soil moisture content, but there was a significant difference in average values. However, the parametric test is not inconclusive according the data distribution that's why the graph is not shown. From Fig. 6 is seen that group 1 has slightly higher average values in initial soil moisture content.

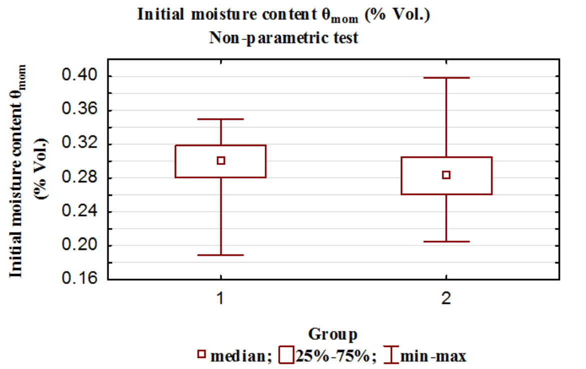

Fig. 6. – The values of initial moisture content by non-parametric

Soil bulk density values were classified as normal distribution, for this reason, has been used only a parametric test. The Fig. 7 indicates a statistically significant difference between groups of data measured for a soil bulk density. The figure also shows lower values of the second group. The difference between the average values is 0.13 g·cm^{-3} with very small confidence intervals. From a small confidence interval, we can assume a very homogeneous soil bulk density conditions in both groups. For this reason the soil bulk density was set as a core for comparison of measured values.

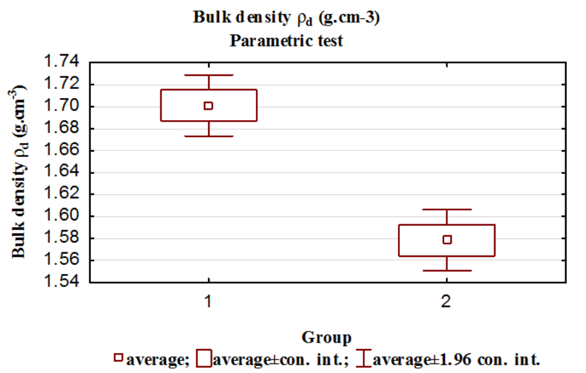

Fig. 7. – The results of bulk density

The cone index values, as in the case of soil moisture content, have not been determined as a normal distribution. As in the case of initial soil moisture content was performed as non-parametric as well as parametric test. Non-parametric test (Fig. 8) showed that there is no statistically significant difference, but the figure also points out slight increased values of the second group. If taking into account the parametric test, it is possible to detect statistically significant differences not only in average values but also in variability. Unfortunately as in the case of initial soil moisture content the parametric test cannot be taken in to account due to its inconclusiveness.

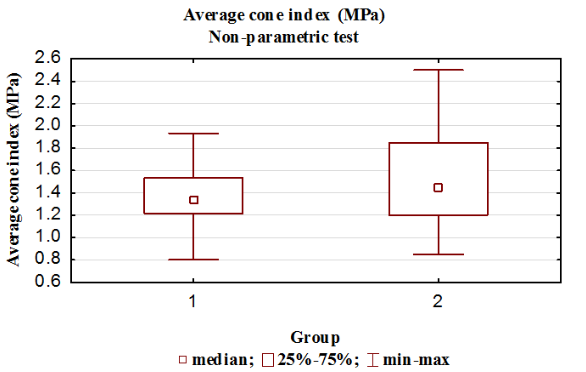

Fig. 8. – The cone index values by non-parametric (left) and parametric test (right)

From the measured values it is clear that the measurement area can be separated, on the basis of soil bulk density, into two groups, as was done. Based on the above figure of the soil bulk density could be assumed that the cone index values will be higher in the first group and lower in the second group. Results of cone index, however, showed statistically insignificant increase in the values in the second group (non-parametric test) and a statistically significant increase in the second group (parametric test - inconclusive). From the perspective of statistical evaluation could be said that the change of soil bulk density has no significant effect on the cone index value. But after taking into account the literature and soil moisture content we assume that the cone index copies the values of soil bulk and thus can indicate soil compaction for the same moisture content conditions within one field. Within this measurement and despite inconclusive statistical tests, we can assume that the cone index is largely influenced by the soil moisture content more likely than by soil bulk density, under these conditions.

On these foundations, we can assume a greater effect of initial moisture content on cone index, than effect of soil bulk density, under given conditions. Above results can also be affected by various factors such as a grain size composition of the soil, which, unfortunately, has not been included into this measurement.

CONCLUSIONS

Based on the results it was found surprising fact that at significantly lower soil bulk density were measured higher insignificant cone index values and conversely. This fact can be explained by soil moisture content. According to the literature can be said that the results of cone index are affected by soil moisture content despite the fact that there was not found statistically significant effect of soil moisture content on cone index measurement.

From the measured values is clear that the determination of soil compaction by cone index measurement without knowledge of soil moisture conditions can be very misleading. Therefore it can be only recommend to investigate soil moisture content for each measured point by penetrometer irrespective of the size of the field or take soil samples (soil bulk density values) and based on these values determine if the parts of field are or not compacted.

These results will be included in future evaluation of work of agricultural machinery, with regard to tensile ratios and the quality of work.

REFERENCES

1. ALAKUKKU, L.: Persistence of soil compaction due to high axle load traffic. II. Long-term effects on the properties of fine-textured and organic soils. Soil and Tillage Research, 37, 1996: 223–238.
2. ASAE STANDARDS: Soil cone penetrometer. St. Joseph, Mich.: ASAE. 49th Ed. 2004: S313.3.
3. AYERS, P., PERUMPRAL, J.: Moisture and density effect on cone index. Transactions of the ASAE, 25, 1982: 1169–1172.
4. BUSSCHER, W., BAUER, P., CAMP, C., SOJKA, R.: Correction of cone index for soil water content differences in a coastal plain soil. Soil & Tillage Research, 43, 1997: 205–217.
5. DA SILVA, A.P., KAY, B.D.: Estimating the least limiting water range of soils from properties and management. Soil Science Society of America Journal, 61, 1997: 877–883.
6. DEFOSSEZ, P., RICHARD, G.: Models of soil compaction due to traffic and their evaluation. Soil & Tillage Research, 67, 2002: 41–64.
7. JOHNSON, C., BAILEY, A.: Soil Compaction. Advances in Soil Dynamics, 2, 2002: 155–183.
8. RAPER, R.: Agricultural traffic impacts on soil. Journal of Terramechanics, 42, 2005: 259–280.
9. VALLA, M., KOZÁK, J., NĚMEČEK, J., MATULA, S., BORŮVKA, L., DRÁBEK, O.: Analysis of undisturbed soil sample. In: VALLA. M. et. al.: Pedologické praktikum (Pe-

dologic practice). pp. 29–34. Czech University of Life Sciences Prague, Prague, 2011. (in Czech).
10. VARGA, F., TKÁČ, Z., ŠIMA, T., HUJO, Ľ., KOSIBA, J., UHRINOVÁ, D.: Measurement of soil resistance by using a horizontal penetrometer working with the two-argument comparative method. Agronomy Research, 12, 2014: 187–196.
11. VAZ, C., BASSOI, L., HOPMANS, J.: Contribution of water content and bulk density to field soil penetration resistance as measured by a combined cone penetrometer–TDR probe. Soil & Tillage Research, 60, 2001: 35–42.
12. VAZ, C., MANIERI, J., DE MARIA, I., TULLER, M.: Modeling and correction of soil penetration resistance for varying soil water content. Geoderma, 166, 2011: 92-101.

Corresponding author:
Ing. Jan Chyba, Ph.D., Department of agricultural machines, Faculty of Engineering, Czech University of Life Sciences Prague, Kamýcká 129, Praha 6, Prague, 16521, Czech Republic, phone: +420 22438 3160, e-mail: chyba@tf.czu.cz

THE MACHINE LEARNING CONCEPT FOR AN INCLINATION SENSOR

G. İrsel

Department of Mechanical Engineering, Trakya University, Edirne, Turkey

Abstract

In this study, it is aimed to create a sensor which may be able to learn with artificial intelligence. The sensor constituted is an industrial inclination sensor. Due to centrifugal force and/or shocking impacts, inclination sensors may have incorrect measurements. Decree of action that causes this error however has been measured by an acceleration sensor. It has been intended to remedy and correct the error of inclination and obtain a usable inclination data. Acceleration sensor, inclination sensor, data logger card have been installed on a platform. Inclination and acceleration values have been simultaneously observed and recorded. Data have been analyzed with WEKA Machine Learning Program. Rules obtained have been used as code in "Arduino". Thus, using the machine learning technique, and with the support of arduino programming card, a system which transforms measurements of inclination and acceleration sensor to utilizable inclination measurement value has been achieved.

Key words: machine learning, inclination sensor, acceleration sensor, arduino, weka, inclination balancing system.

INTRODUCTION

Inclination sensors perform inclination measurement according to a specified reference position angle. As from the position which was accepted as a reference the inclination sensor gives an analog output pro rata the amount of angle made. This analog output is generally 4-20 mA or 0-10 V for industrial sensors, according to the type of the sensor chosen. Inclination sensors are vital for systems which are specifically mobile and requiring self-balancing. Inclination sensors are used for providing information to the operators working at fixed positioned construction machines, concrete pumps, drilling platforms (rigs), military platforms, etc. which are prone to tipping risk due to gradient. In the more widespread manner, however, they are used at industrial automation systems in such sectors as space, aviation, agriculture, production and construction machines, etc. (BAYRAKÇEKEN AND YEŞILIRMAK, 2009). Inclination balancing systems however are very important for military vehicles, construction machines. Inclination sensors beside protection of tipping inclination limits of military vehicles and construction machines have been used for operation at construction machines (KÖSE ET AL., 2012). Preference of inclination balancing/stabilization systems in agricultural equipment and machinery, in combined harvester (Fig. 1) with over 4,20 m work width, in agricultural pesticide machines and specifically in sensitive ground leveling machines is popular and common.


Fig. 1. – Combined harvester

Likewise, in ground leveling machines, in controlling the scraper blade, it is also common to use the inclination sensors (Fig. 2).

Fig. 2. – Ground leveling with grader

In such kind of machines which do not make circular movements inclination sensors have been usually supported with oil and spring reinforced dampers. Response times are adequate for longer and general utilization purposes. Nevertheless inclination sensor's behaviors in much sensitive works robot control or for

a sensitive ground leveling must be within a specified tolerances. Success of automation systems has a direct relation with the achievement of sensors. For an item which can be measured incorrectly in an automation system the decision given by the automation system will not be correct in this respect.
In this study, it is aimed to create a sensor system which may be able to learn with artificial intelligence. The sensor system will be used to measure the precise inclination in an automation system. In order to correct the errors of inclination sensor, an acceleration sensor is added into the system. The variables of acceleration and inclination sensors are obtained by ARDUINO sd module and then analized by WEKA. The rules used to correct inclination errors are obtained by WEKA and these rules are used as a software in the system.

MATERIALS AND METHODS

In this study it is intended to correct an erroneous measurement which was performed by an inclination sensor under the effect of centrifugal force. The inclination sensor is a system made up of pendulum, potentiometer and damping components. The damping components cause small vibrations to lead measurement error and help prevent shocking impacts. However if at the axis (Z) where inclination is measured the sensor is moved laterally at axis X (Fig. 3), pendulum of the sensor cannot preserve its inertia against this movement. The sensor gives an erroneous output value under the impact of centrifugal force (KUBAT AND KIRAZ, 2012). Moreover, if the pendulum preserves its inertia, then it cannot measure the inclination under the normal conditions.

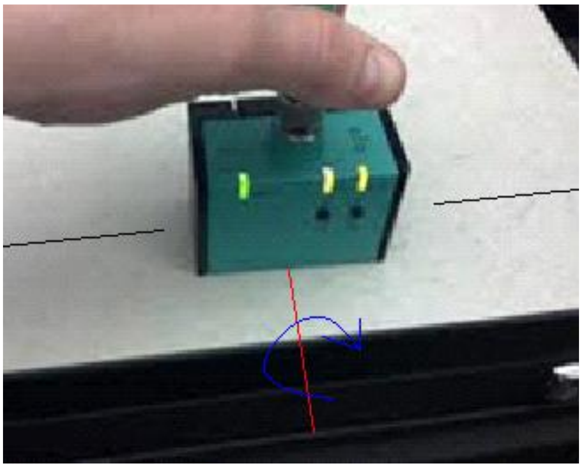

Fig. 3. – Centrifugal force impact to which the inclination sensor was exposed

Centrifugal Force Effect causes measurement error in the inclination sensor and the automation system gives a response by considering such erroneous measurement as a real inclination value (ÇALIŞKAN, 2007). Consequently, the incorrect gradient causes to access to a response of another automation system which is different from the desired one.
A lot of studies have been carried out for filtering measurement values for general sensor errors. However the most known is Kalman filter. In a dynamic system shown with state space model, it is such a filter that conditions of the system can be forecasted from input and output information together with the previous data and information of the model. It was found by Rudolf Kalman who was Hungarian origin, American mathematical system theorist.
Observation theory, based on a decided point of view, is a path to be followed for the system's condition forecast. If the system's stochastic or random noisy aspect is taken into account, minimum variance estimate or Kalman filter is convenient. Kalman Filter, as is the same for the conventional estimators, despite its filtering feature, is very powerful and talented in order to estimate non-measurable conditions of the system. It is an algorithm which has been used especially in car navigation (despite the aviation typical, other fields of application are also available) since 1960s, providing an estimation optimized on the system's state. Algorithm, operating as recursive real time on noisy, input observation data flows (typically sensor measurements) filters errors by least square curve fitting method and optimize according to the mathematical estimate of the future state generated by modeling of the system's physical characteristics.
Model estimation is compared with the observation and this difference is scaled with a multiplier known as Kalman's gain, which later on is feedback to the mode as an input in order to improve the next coming estimates. The gain can be "adjustable" for improved performance. With a high gain the filter follows the observations more closely. With a lower gain, it follows the filter model estimates more closely. The method converges to produce closer estimates than the estimates that may be obtained on the basis of the real unknown values, a single measurement or solely model estimates. At each time step, Kalman filter produces the estimates of real unknown values together with their uncertainties. When the result of the next measurement is observed, these estimates are

updated with weighted mean, by giving much more weight onto the estimates whose uncertainty is low.

From a theoretical point of view, the main hypothesis of Kalman filter is that the underlying system was a linear dynamic system and all errors and measurements have got Gaussian distribution (often multivariable Gaussian distribution). In this system however what effects behavior of the sensor is the impact of a centrifugal force whose time is not known. This system is not a linear dynamic system. A centrifugal force whose time is uncertain and its size is uncertain affects this system as an external force. To make a long story short, Kalman filter is not also a solution for this system.

Such size which affects inclination sensor with acceleration sensor. Data of inclination sensor and data of acceleration sensor have been recorded simultaneously. However, thousands of data must be assessed in order to examine this relationship. Manually processing of huge amount of data and making their analysis are impossible. For the purpose of finding solution machine learning methods have been developed.

Artificial intelligence technology has been developing more every passing day. New products have been produced and they have appeared mostly in daily life. Automation systems however have been equipped with artificial intelligence and eventually users have been benefiting from computer's decision making power. Brand new commercial systems have been emerging every passing day and functional features of systems have been increased. The present technology has been making contribution to people for producing useful products in daily life of people. Artificial neural networks ensure computer's learning (ÖZTEMEL, 2012).

Machine learning is a method paradigm making inferences from existing data by using mathematical and statistical methods, making estimations on the unknown through these inferences and it is also defined as the improvement of behaviors in time. The purpose of machine learning is to create systems that think like human beings, behaves like human beings, conduct logic/reason and act rational/wisely (PIRIM, 2006).

Machine learning, specifically in case of absence of human experience, when space duties, imitation of our inexplicable skills, facial recognition, speech recognition, solutions depending on situation (time) become necessary, in a computer network orientation operation, special applications, biometry, diagnosis in the field of health, in the fields of automatic problem solving can be used.

Machine learning methods try to find the best suitable model to the data by using the previous data. They analyze new data also in accordance with this model and get result. Different applications have had expectations different from analyses. Thus, a problem can be solved by making inference from previous existing examples. Machine learning methods may be classified as classification, clustering, regression and curve fitting.

RESULTS AND DISCUSSION

Empirical study method includes that in addition to the inclination sensor, at the direction of axis X of the inclination sensor an acceleration sensor is to be involved in the system. At the same direction data of sensor is observed on Arduino LCD screen and is recorded with Arduino sd card module. Choice of sensor is as follows: PEPERL FUCHS make acceleration sensor and inclination sensor were chosen for the empirical study. Code of the inclination sensor is INY360D-F99-2I2E2-V17, complete with double axes measuring feature. In this study it was used at one-way measurement (Fig. 4).

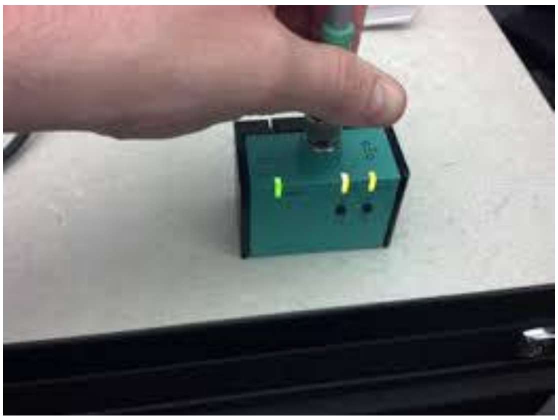

Fig. 4. – Inclination sensor reference position

Fig. 5. – Single axis acceleration sensor

Inclination Sensor Technical Data

General specifications

- Type Inclination sensor, 2-axis
- Measurement range 0 ... 360°
- Absolute accuracy ≤ ± 0,5 °
- Response delay ≤ 25 ms
- Resolution ≤ 0,1 °
- Repeat accuracy ≤ ± 0,1 °
- Temperature influence ≤ 0,027 °/K

Electrical specifications

- Operating voltage UB 10 ... 30 V DC
- No-load supply current I0 ≤ 25 mA
- Time delay before availability tv ≤ 200 ms

Analog output

- Output type 2 current outputs 4 ... 20 mA
- (one output for each axis)
- Load resistor 0 ... 200 Ω at UB = 10 ... 18 V
- 0 ... 500 Ω at UB = 18 ... 30 V
- Mass 240 g

While inclination sensors' being two or single axis do not affect measurement of individual inclinations at axes, axes interact on the acceleration sensors. This is a great problem. Therefore, a single axis acceleration sensor with Code No: ACX04-F99-I-V15 was chosen (Fig. 5).

Acceleration Sensor Technical Data

General specifications

- Type 1 axis
- Measurement range -2 ... 2 *g*
- Resolution ≤ 5 m*g*
- Repeat accuracy ≤ ± 5 m*g*
- Frequency range 0 ... 100 Hz

Electrical specifications

- Operating voltage UB 10 ... 30 V DC
- No-load supply current I0 ≤ 25 mA
- Time delay before availability tv ≤ 100 ms

Analog output

- Output type 1 current output 4 ... 20 mA
- Zero signal 12 mA
- Slope of output characteristic 4 mA / *g*
- Linearity error ± 1,2 %
- Load resistor 0 ... 200 Ω at UB = 10 ... 18 V
- 0 ... 500 Ω at UB = 18 ... 30 V
- Mass 240 g

The two sensors were fixed together on a metal plate (Fig. 6). This plate can rotate around axis 1° +/-45°. It can be fixed at a specified position with a bolt.

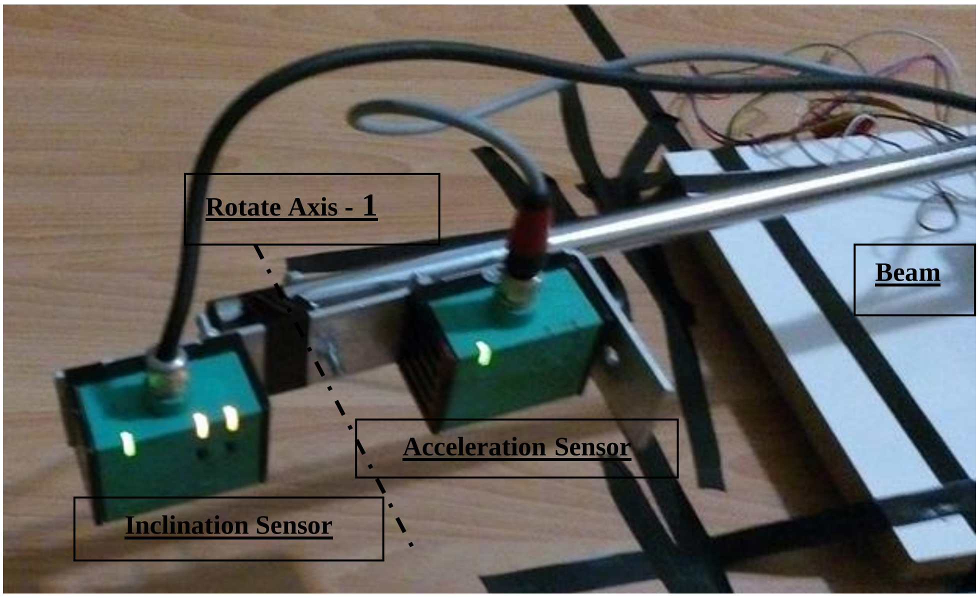

Fig. 6. – Positioning of inclination and acceleration sensors on a metal plate

The two sensors have been mounted to the tip of a 1,2 m long rod with this metal plate. The long carrier bar can be moved by a step motor at different speeds. Several tests were conducted consecutively at different rotational speeds of step motor. While the fixed inclination sensor's measurement value should not change, a change was observed on the inclination and acceleration with the rotational movement of the long bar (Fig. 7).

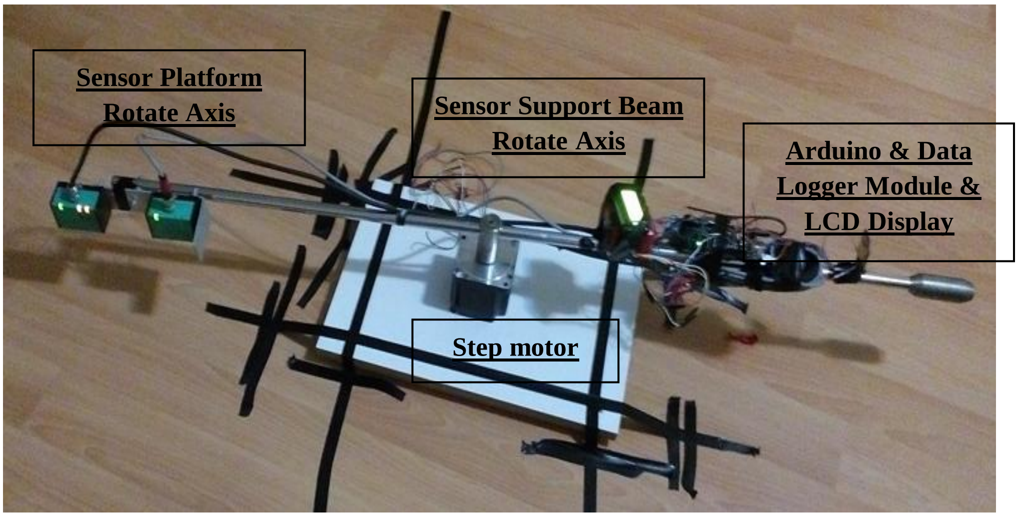

Fig. 7. – Test system

Plate, while the long bar was not rotating, was moved at (-45°/+45°) angles and values were recorded. Additionally, for 17 different random angle values (-45°/+45°) at which the plate was fixed, instantaneous acceleration and inclination values were also recorded with the rotation of the long carrier bar at different speeds (Tab. 1).

Tab. 2 – Simultaneous data values recorded with Arduino sd Card module

Instantaneous Inclination	Instantaneous Acceleration	Inclination Required to be Measured	Inclination Error	Acceleration Difference to the Reference (544-544)
534	544	534	0	0
544	552	534	-10	-8
551	549	534	-17	-5
545	540	534	-11	4
511	529	534	23	15
465	518	534	69	26
415	506	534	119	38
363	504	534	171	40
341	504	534	193	40
544	552	534	-10	-8
551	549	534	-17	-5
545	540	534	-11	4
511	529	534	23	15
465	518	534	69	26
415	506	534	119	38
434	523	534	100	21
386	524	534	148	20
392	513	534	142	31
313	500	534	221	44
316	497	534	218	47
318	499	534	216	45
322	504	534	212	40
392	513	534	142	31
395	521	534	139	23

Upon analyzing the table, in the relation between acceleration difference and inclination difference, Equation 1 may be obtained. However, whenever the acceleration difference gets higher, then it is seen that the coefficient of 2.24 rises up to 4.68.

Inclination Error = (Acceleration Difference) x 2.24 (2.24.....4.68) (1)

Inasmuch as the fact that our purpose is to protect and preserve the measured inclination value against centrifugal force and to obtain a useable inclination value, it is not necessary that we should reveal and indicate the relationship between the inclination and the acceleration by means of a formulation. We will use the relationship in Arduino as code. Therefore the relationship may be expressed in all manners as multi-formulation, classification and clustering, etc. Data can be analyzed with WEKA which is a data mining program. WEKA which has got a completely modular design and with its specifications is capable of doing such operations as visualization, data analysis, business intelligence applications, data mining, etc. on datasets. WEKA software, as sui generis, has come with the support of ARFF extension. However WEKA software contains tools that may be used for converting CSV files to ARFF format. Basically the following 3 Data Mining transaction may be performed by WEKA:

- Classification
- Clustering
- Association

WEKA is one of the most used 10 software in the field of business intelligence, likewise ranks among the top three in the most used free software ranking on the issue of business intelligence. With WEKA you can use artificial neural networks algorithms, classification and clustering algorithms, regression algorithms and association algorithms, even if you do not know their content. It covers almost all known data mining algorithms. Moreover, graphical presentation of the consisting outputs is rather satisfactory.

In this study data for WEKA was prepared in Excel file and saved as WEKA file. While performing examination, for the choice of filter, unsupervised - attribute -Numeric to Nominal was preferred (Fig. 8).

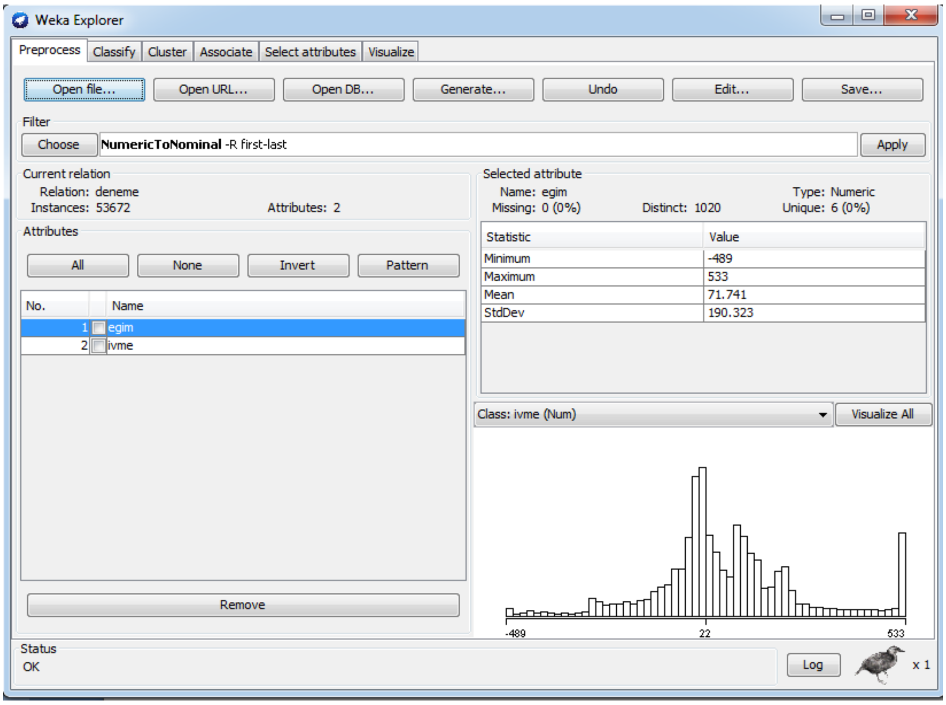

Fig. 8 – Example of selected static positions of pressure distribution in tyre tread pattern of bias ply tyres under dynamic measuring regime; (passage speed 10 cm.s^{-1})

Classify - OneR is chosen. Inclination difference values related with the acceleration difference were thus obtained. A certain part of data obtained, are shown in Tab. 3.

All of Data shown in Tab. 3 were converted to Arduino codes. Arduino codes calculate the correction inclination value related to the acceleration difference size with the instantaneous inclination value. Thus inclination error based on the centrifugal force has been eliminated.

Tab. 3 – Inclination correction values due to the acceleration difference

Acceleration Difference	Inclination Difference
-205 <	=AccDiff * 2.5
-205	-448
-204	-444
-203	-442
...	
-3	-11
-2	-11
-1	-5
0	0
1	0
2	14
3	15
...	
141	526
142	529
143	529
144	530
AccDiff >= 145	(AccDiff * 4)

CONCLUSIONS

Machine learning is crucial and most important issue for humanoid machines and it has been developing and improving day by day. Sensor system arranged with the machine learning application can be improved further by means of new data. The probability of risking the automation system at taught sensors is rather low in reference to a non-processed sensor with direct connection. Acceleration sensor has been reflected to this system as an additional cost. However, net and reliable inclination measurement has been ensured. Sensor - Arduino system yields 0-5V analog output. It can be connected to an automation system as inclination sensor. Machine Learning is efficient and reliable method in order to be able to evaluate and assess a lot of effects simultaneously in systems consisting of inclination sensor or combination of several sensors.

WEKA which is machine learning software, is included in the top ten machine learning program which has been preferred because of its process success and being satisfactory. Supporting of sensors with the machine learning protects automation systems and operators against bad and unexpected surprises and a more stable automation system is obtained.

Measurement success of the sensor affects directly the success of automation system. Inclination sensors have been used widespread at such sectors as agriculture, industry, space, robot, aviation, etc. It is impossible for a person to examine and analyze thousands of data and to establish a relationship among data. The system that obtained in this study can be successfully used specifically in precision ground leveling machines, robots, agricultural pesticide machines and agricultural machines such as combine harvester, etc. which are in need of balancing system. Total cost of the system is USD 320.

Arduino, with its best economic cost and ergonomic usage, is one of the most preferred programming cards. In the system so created sensor reading speed, Arduino data output speed can be adjustable. The system is able to give 0-5v analog output and 0-5v digital output.

In this study a sensor which can make successfully an inclination measurement at the moment of linear progressing in a circular orbit, the sensor which made incorrect measurement due to the effect of centrifugal force in addition to affect of centrifugal force along with the gravity force to the sensor pendulum was examined. It has been aimed that affect of the centrifugal force has been specified with the acceleration sensor, and eventually that the sensor should make measurement as if sensor was making measurement only under the affect of gravity.

REFERENCES

1. BAYRAKÇEKEN, H., YEŞİLIRMAK, M.: The effect of accelerations on vehicles and acceleration measurements. In: Proceedings of the 5th International Advanced Technologies Symposium (IATS'09), May 13-15, 2009, Karabük, TURKEY.
2. ÇALISKAN, Ö.: Vehicle Yaw Rate Estimation Using Virtual Sensor and Vehicle Lateral Dynamics Control (in Turkish), Institute of Science, İstanbul Technical University, İstanbul, TURKEY, 2007: p. 89.
3. KOSE, E., KORKMAZ, H., BULUT, A., OZER, M., UZUNOĞLU, M., TUMLUKOLCU, S.: Automaticly positioned conveyor system, Electronic Journal of Machine Technologies, 9 (1), 2012: p. 15-24.
4. KUBAT, C., KİRAZ, A.: The modeling of tensile test in virtual laboratory design using artificial intelligence, Journal of the Faculty of Engineering and Architecture of Gazi University, 27 (1), 2012: p. 205-209.
5. ÖZTEMEL, E.: Yapay sinir ağları, Papatya Yayıncılık, 3rd Edition, İstanbul, TURKEY, 2012.
6. PİRİM, H.: Artificial intelligence, Journal of Yasar University, 1(1), 2006: p. 81-93.

Corresponding author:
Gürkan İrsel, Department of Mechanical Engineering, Trakya University, Edirne, Turkey

INFLUENCE OF DEPIGMENTATION ON MECHANICAL PARAMETERS OF HORSEHAIR OF OLD KLADRUBER HORSE

M. Janošíková[1], B. Chalupa[2]

[1]Department of Animal Husbandry, Faculty of Agrobiology, Food and Natural Resources, Czech University of Life Sciences Prague, Czech Republic
[2]Department of Physics, Faculty of Engineering, Czech University of Life Sciences Prague, Czech Republic

Abstract
For groups of black and white hairs of Old Kladruber grey horse stress-strain curves have been measured and subjected to a multi-parameter analysis. A total of 15 material and mechanical parameters have been taken for each hair analysed. Both groups have been compared statistically, with an unexpected result. Discoloured hairs gain higher values in three parameters than hairs of still un-discoloured foals. They also have lower variance than the hairs from the group of young, still pigmented horses.

Key words: stress, strain, deformation, curve, mechanical properties, elasticity.

INTRODUCTION

Most dark polymers have considerably different and mostly better mechanical parameters than light ones due to higher carbon content. Biopolymers make no exception, as shows a whole number of prior works. Elasticity module, extensibility, ultimate stress and yield strength increase significantly with colour deep-ness. This fact holds both for human hair and porcu-pine spines as well as guinea pig or ferret hair, and holds for horsehair also. Up to now, these mechanical parameters have been measured for non-discolouring individuals only – see e.g. ŠIMKOVÁ ET AL. (2013). Most species have their colour fixed from the moment of reaching adult age.

For these reasons, we have decided to find whether aforesaid characteristics manifest in the discolouring species also. We have opted for horsehair of the grey form of Old Kladruber horse.

Old Kladruber horse, belonging to the group of west-ern horses, whose predecessor was Equus robustus, developed together with the Spanish breed under the influence of Arab-Berber blood. It's a typical carriage horse; its history in the Czech lands extends to the year 1579 when Holy Roman Emperor Rudolf II pro-moted the imperial park to a horse-breeding farm. It is ranked among 4 breeds registered in genic resources of the Czech Republic. It is our only live national cultural monument. Leading Czech hippologist Prof. František Bílek was responsible for the regeneration of Old Kladruber black horse. Genetic relationship between grey and black Kladruber horses is low, as each colour has been bred autonomously in the history – see PŘIBYL ET AL. (1997). The black and grey varie-ties differ slightly in some traits;the conformation of the grey variety corresponds more to the breeding goal (JAKUBEC ET AL., 2007).

Old Kladruber grey horse is black colour both coat and horsehair up to the age of 1–5 years (according to the lineage); after reaching this age they change their colour completely to a white one over the whole body surface relatively quickly, generally through two moultings. Question therefore arises, whether and how do mechanical parameters of these discoloured hairs change compared to the original ones.

Following mechanical and material parameters of the hairs have been determined for testing:

Hair diameter, engineering module of elasticity, true module of elasticity, nominal linearity limit, yield strength, ultimate stress, true ultimate stress, length at rupture, fracture strain, true relative elongation to rupture, total mechanical work necessary to break the hair, toughness and resilience.

All these parameters have been compared between the black and the white hairs of Kladruber horses.

Fig. 1. – A grey („white“) mare with a black foal.
Photo: Dalibor Gregor

A load curve is divided into three parts (see Fig. 2):

- First part – elastic (1) – the part where the deformation is small enough for the sample to return to its original shape and dimension if external forces cease to affect it. In the case of hair it contains Hook area (1a) where tension is directly proportional to deformation. By a constant of this proportionality and therefore the slope of the line Young's modulus is determined. The rest of this part is non-linear (1b) and ends by yield strength (A), by which the maximum elastic deformation is defined. Deformations beyond this point of the curve are already plastic; after application of such external force the sample remains permanently deformed. At that point the stress-strain curve passes into the plastic deformation area.

Starting moment of the deformation is determined from the equation of the line interpolating the stress-strain curve in the Hook area. The constant in this equation determines the intersection of the line with the axis of deformation. We move all the deformation data observed on the deformation curve backwards by this value.

- The second part (2) where irreversible changes already take place in the sample and where even application of a constant force may lead to increasing deformation, simply put the area beyond yield strength, is characterized by viscoplastic deformation. The shape of the curve in this area is greatly influenced by the deformation speed and at higher speeds (from 10 %/min up for hair), the start of that second phase may be characterized by a negative slope.

- Third part (3) is the area of reinforcement before rupture where the slope of the breaking curve increases again (B). Steady increase in tension leads to rupture of the sample (BENZARTI ET AL., 2011).

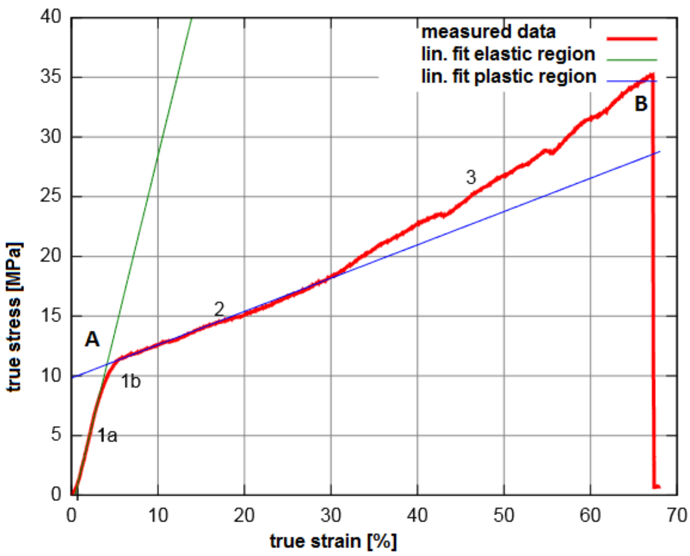

Fig. 2. – Load curve obtained from the tensile test of a hair

MATERIALS AND METHODS

Two groups of Old Kladruber horses have been chosen for the study. First group consisted of the hairs of still non-discoloured horses born in 2015, the second group comprised the hairs of horses over 5 years of age. Horsehairs of 10 horses have been processed in all, namely 3 hairs from the mane of each horse. Hairs had been extracted at their roots; all hairs had been taken within one day. From this part, a 5 cm long sample had been separated, that had been recorded with an optical microscope with a digital camera for determining its diameter. From each snap, partial diameters have been measured in 5 locations, and overall diameter has then been established for each particular hair from them. After the imaging, hair sample had been fixed in the jaws of the mechanical testing machine Deform type 2 (see e.g. JELEN ET AL., 2014), and there it has been tested with a constant machine speed of 1 mm/min up to its breakage. All measurements on the testing machine have been carried out in constant relative humidity of 43–47 % and a constant temperature of 24–27 °C. From these measurements stress-strain curve data have been obtained that have then been processed with computational software. It can evaluate mechanical parameters like initial cross-section area, nominal and true Young's moduli, nominal linearity limit, elastic limit, ultimate stress, true ultimate stress, elongation to fracture, true relative elongation to fracture, total mechanical work necessary to break the matter, tensile toughness (the amount of energy necessary to break the matter per unit of the initial tensile volume), resilience (the amount of energy in a volume unit of the material loaded with $\sigma_{0.05}$ stress). Measuring procedure is an extension of the procedure that is described in more detail e.g. in SKŘONTOVÁ ET AL. (2011), SKŘONTOVÁ ET AL. (2014).

Young's modulus (E) is found from the Hook (linear) area of a load curve approximated by a linear function. Yield strength is determined by coordinates of the intersection of linear approximation of the load curve in a Hook area and the beginning of plastic zone. Ultimate strength is the maximum tension before a rupture of a hair, which was determined together with the fracture strain as the coordinates of the end point of the load curve, when the coordinate on the axis of independent variables is the fracture strain [%] and the coordinate on the axis of the dependent variables gives ultimate strength [MPa].

RESULTS

Tab. 1 Mechanical and material properties of the horsehair. Y – young, A – adult, D – hair diameter, E – nominal elastic modulus, E' – true elastic modulus, σ – ultimate stress, σ' – true ultimate stress, ε – fracture strain, ε' – true relative elongation to rupture, W – total mechanical work necessary to break the hair, W_A – toughness, W_e – resilience.

For comparison, in previous literature, e.g. ŠIMKOVÁ ET AL. (2013), only E and E' are listed from the above mentioned quantities; their values agree with the current ones within the limits of the variance. Determination of all the other quantities is a new contribution of this work.

At 5% significance level, assuming normality, only diameter, cross-sectional area, volume, elongation to fracture and energy necessary to breakage do differ (f-test, t-test). The first three quantities are dependent though, thus cross-section and volume are omitted from further analysis for this reason and only diameter is followed hereafter.

For the remaining three quantities that differ provably statistically for the groups of discoloured and non-discoloured Kladruber horses, detailed comparison of distribution histograms is presented, each quantity for both groups of horses in one figure.

Tab. 1. – Contains measured mechanical and material properties of horsehair from discoloured and non-discoloured Kladruber horses.

	D(μm)	*E*(GPa)	E'(MPa)	σ(MPa)	σ'(MPa)	ε()	ε'()	W(mJ)	W_A(MJ/m^3)	W_e(MJ/m^3)
Y	136±19	2.3±0.8	2.3±0.8	76±32	95±46	0.2±0.1	0.2±0.1	9±6	15±19	0.25±0.26
A	149±13	2.2±0.4	2.2±0.3	79±24	106±41	0.3±0.2	0.3±0.1	14±10	11±12	0.15±0.22

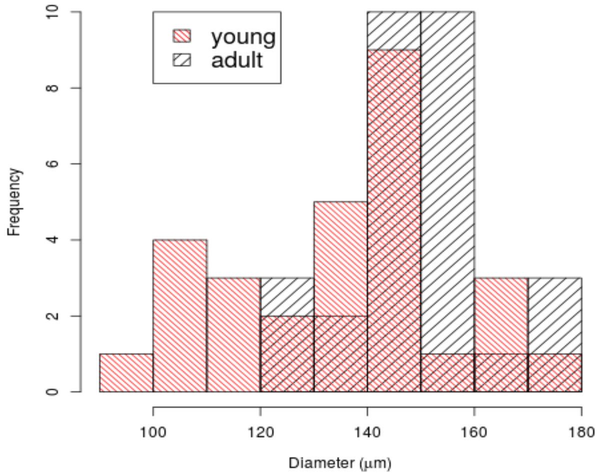

Fig. 1. – Distribution of horsehair diameter of adult (discoloured) and young Kladruber horses

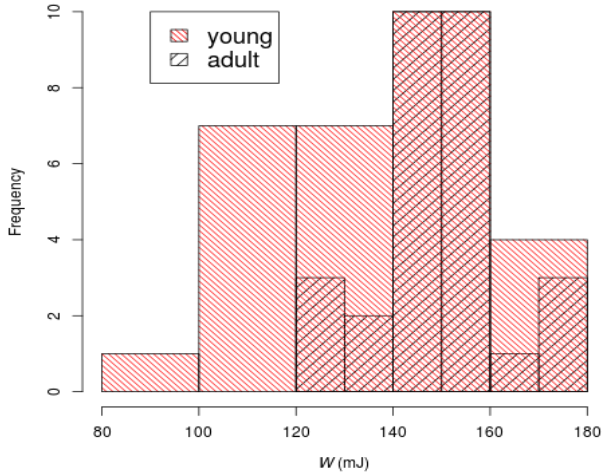

Fig. 2. – Distribution of total work necessary to break the hair of adult and young Kladruber horses

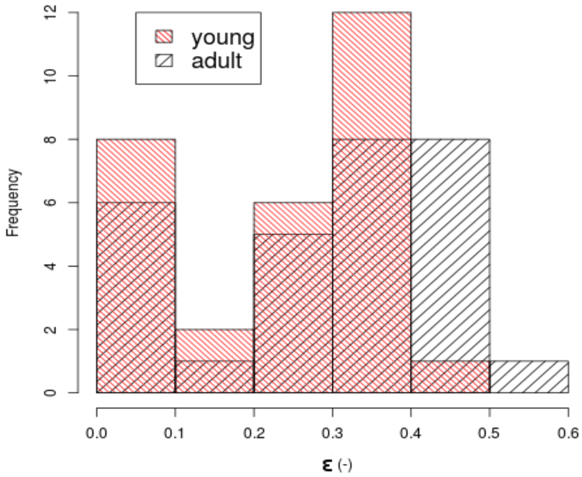

Fig. 3. – Distribution of horsehair fracture strain of adult and young Kladruber horses

DISCUSSION

Present experience shows that dark hairs are stronger than the light ones – e.g. BENZARTI ET AL., (2011), ŠIMKOVÁ ET AL. (2013), and similar behaviour could have been expected in this case also. The expectation that elasticity modulus of black horsehairs would be severalfold higher than the one of discoloured hairs did not prove true. Differences are only verifiable at three quantities, always in favour of discoloured horses over 5 years of age. Their values are always higher in mean value and besides more equal, i.e. with lower variance.

This is probably the reason why there are horsehairs of older horses used for technological use, e.g. for bow production. What is the advantage of black hair for the young horses is therefore in no way clear. The reason might be ethological, e.g. in the approach from the side of discoloured stallions or mares. No mechanical advantage of the black horsehairs in young horses has been found.

Authors are not aware of any previous measurements results on discolouring horsehairs in comparison to the black ones and they consider the results quite new, and in this sense no comparison to other works could be found.

CONCLUSIONS

Although provable difference has been found in three mechanical and material parameters between discoloured and dark horsehairs of Old Kladruber horse, these differences are always in favour of whitened hairs, i.e. the ones of older horses. We consider this fact surprising, since in non-discolouring species' the advantages are always on the black biopolymers side.

REFERENCES

1. BENZARTI, M., TKAYA, M. B., MATTEI, C. P., ZAHOUANI, H.: Hair Mechanical Properties Depending on Age and Origin. World Academy of Science, Engineering and Technology, 74, 2011: 471–477.
2. JAKUBEC, V., REJFKOVÁ, M., VOLENEC, J., MAJZLÍK, I., VOSTRÝ, L.: Analysis of linear description of type traits in the varieties and studs of the Old Kladrub horse. Czech J. Anim. Sci., 52, 2007 (9): 299–307.
3. JELEN, K., SKŘONTOVÁ, M., ŠIMKOVÁ, L., ZEMAN, J., TLAPÁKOVÁ, E., FANTA, O.: Changes in the mechanical parameters of hair in a group of women in reproductive age. Neuroendocrinology Letters, 35 (6), 2014: 101–109. ISSN 0172–780X.
4. PŘIBYL, J., JAKUBEC, V., JELÍNEK, J., VOLENEC, J., KRYS, J.: Clustering of Kladrub horses on the basis of kinship. Živočišná výroba, Inst Sci Tech Inform Agr, Prague, Czech Republic, 42 (5), 1997: 199–205. ISSN 0044-4847.
5. SKŘONTOVÁ, M., ŠIMKOVÁ, L., JELEN, K.: Hair Quality in Gravid Versus Non-gravid Women. Acta Universitatis Carolinae Kinanthropologica, Charles University in Prague, 47 (2), 2011: 117–125. ISSN 1212-1428.
6. SKŘONTOVÁ, M., ŠIMKOVÁ, L., ZEMAN, J., JELEN, K.: The dependence of viscoelastic parameters of hair on its structure. In: Human Biomechanics 2014, Pilsen, Book of Abstracts, p. 22. Published by University of West Bohemia, Plzeň, Czech Republic VAT No. 49777513.
7. ŠIMKOVÁ, L., SKŘONTOVÁ, M., JELEN, K., CHALUPA, B.: Determination of different animal species hair viscoelastic properties. In: 5th International Conference Trends in Agricultural Engineering 2013, Published by Czech University of Life Sciences Prague, 3 – 6 September 2013, Prague, Czech Republic, p. 590 – 594.

Corresponding author:

Mgr. Bohumil Chalupa, Department of physics, Faculty of Engineering, Czech University of Life Sciences Prague, Kamýcká 129, Praha 6, Prague, 16521, Czech Republic, phone: +420 22438 3291, e-mail: chalupab@tf.czu.cz

RESEARCH OF WILLOW PREPARATION AND UTILIZATION FOR ENERGY PURPOSES

A. Jasinskas[1], I. Kibirkštienė[1], R. Domeika[1], J. Čėsna[1], K. Romaneckas[1], J. Mašek[2]

[1]*Aleksandras Stulginskis University, Kaunas – Akademija, Lithuania*
[2]*Faculty of Engineering, Czech University of Life Sciences Prague, Czech Republic*

Abstract
For the middle and short rotation energy plants chopping, the conical screw chopper is the most appropriate to use, because this chopper cut plant stems by conical screw with a sharpened outer edge, therefore can cut the longer chips. There were investigated the biometric characteristics of willow stems and physical-mechanical properties of chaff, such as humidity, bulk density, fall and natural crumble angles, chaff fractional composition, ash content as well as the calorific value. Determined bulk density of osier willow chaff decreased from 136.4 to 123.9 kg m^{-3} DM, and the natural crumble angle changed from 39 to 47 degrees, whereas the fall angle – from 66 to 78 degrees. After evaluation of willow chaff fractional composition it was estimated that the largest part of fraction was received on the sieves with the diameter of 8 and 16 mm holes – from 62.1 to 75.8%, and very small amount of the dust was formed – from 0.02 to 0.08%. Research results of willow chaff ash content and calorific value shows that the estimated ash content was relatively low and reached only 1.44%, it shows that the chaff of such energy plants as willows burns relatively well and in comparison with other energy plants, determined the lower calorific value of willow chaff dry mass was relatively big – 18.5 MJ/kg. Presented research results show that the usage of osier willows for bio-fuel is justified very well. Chopped by conical screw chopper plants can be used in the boiler rooms of average or big power (more than 0.5 MW), which have special burning devices suitable for burning the wet and partially dried bio-fuel.

Key words: energy plants, willows, conical screw chopper, chaff properties, fractional composition, ash content, calorific value.

INTRODUCTION

Recently, when the environmental crisis-induced excessive people hands in exploiting natural resources including massive fossil fuel use become the big driving force for the use of renewable energy then so biomass energy again received fresh momentum and become a focus for some circles (BIOMASS PROJECTS, 2016).

The European Union (EU) is being approached in 2020 for the realization of the 20-20-20 targets but on the other hand they began to prepare the draft for the new policy climate and energy issues from years 2020-2030. EU has proposed a new target in 2030 including a 40% decrease in greenhouse gas emissions, a 30% decrease in energy consumption and 27% for the use of renewable energy (BIOMASS PROJECTS, 2015). History shows how biomass policies is the main driver for the development of various sorts of biofuel market in Europe. It is also widely used as a model of a particular region or country to implement renewable energy policies, especially biomass sector (BIOMASS PROJECTS, 2016).

The plant biomass for energy purposes is a major source of renewable energy. Currently, biomass accounts for about half of the renewable energy used in the European Union (BLUMBERGA, 2008; ŠATEIKIS, 2006; MATIAS AND DEVEZAS, 2007; SCHAUMANN, 2007). European Union countries, estimated the volume of biomass energy by 2020 increase to 3-3.5 times, and by 2030 – 3.5-4.5 times (GREEN PAPER, 2000). Predicted that the EU renewable energy consumption in 2020 year reach 20% of total domestic consumption, and biomass energy will deposit about 13% of total domestic consumption (65% of the total renewable energy). The target for share of energy from renewable sources in the final consumption of energy in 2020 for Lithuania is equal to 23% according to proposed Directive on renewable energy sources (RES) (ANENERGYPOLICY, 2007; JASINSKAS AND LIUBARSKIS, 2005). People in many countries of the World are growing and using for biofuel many different sorts of short rotation trees – willows, poplar, short rotation aspen, etc. (SCHAUMANN, 2007; ANENERGYPOLICY, 2007; JASINSKAS AND LIUBARSKIS, 2005). The Government of Saskatchewan is evaluating whether biomass crops can be successfully used as an affordable, reliable, and environmentally sustainable bioenergy source. The objective of this study was to determine the first 3-year-rotation biomass yields of 30 willow cultivars planted in central Saskatchewan. Annual willow morphological data were collected throughout the first rotation, and stem biomass equations were developed. A willow yield map was produced for these willow cultivars across climates and soils of Saskatchewan (AMICHEV ET AL., 2015). The use of willow as a bioenergy source appears promising, but further research is needed.

Green biomass energy stock – quick-growing trees and bushes, willow, a tall perennial grass. There are more than 500 ha of cultivated willow (Salix Viminalis) plantations in Lithuania, which has become to use as a hard bio-fuel. Therefore, with increasing uptake of renewable energy sources are necessary new technologies research and development work.

Energy plants cultivation and their usage for fuel contribute to solve a number of environmental problems (PIENKOWSKI, 2010; FILHO AND BADR, 2004; LUKASZEWICZ ET AL., 2009; KRYŽEVIČIENĖ, 2003; JONIEC AND FURCZAK, 2010; JASINSKAS ET AL., 2008; STAJNKO ET AL., 2009; JASINSKAS AND SCHOLZ, 2008; VARES ET AL., 2007):

- vegetate plants improves the environmental climate;
- improves soil structure and allows for a smaller demand for chemical fertilizer;
- burning of plant biomass reduces environmental pollution by harmful substances.

Energy plants and their plantations are useful to grow around the residential facilities, farmhouses, because plants may improve the ambient air microclimate. As a result, the energy plant plantations is best to plant the prevailing wind side to separate of the population and household residential premises from polluting facilities: the factories and plants, water treatment plants, landfills, roads. For projection of environmentally sound farm, it is appropriate to distinguish energy plant plantations between the residential sector of the livestock farms and sheds, silage trench, manure pits, manure storage, etc. (VARES ET AL., 2007; FABER ET AL., 2007).

Harvesting technologies of short rotation energy plants depends on many factors: the biological properties of plant maturity, humidity, and weather conditions. For plant harvesting can be used two technologies: direct – plant harvesting by self-propelled harvester or indirect – removal of plant stems and pressing or loose stems harvesting, storage and chopping (JASINSKAS AND SCHOLZ, 2008; FABER ET AL., 2007). Naturally, the direct stem harvesting technology prevails, in which the plant stalks are cut, chopped and removed from the field. Indirect harvesting technology is used less frequently.

For plant chopping in the energy plant chopping mechanisms three types of choppers are usually used: drum, disc, and conical screw. They differ in the construction of the chopping mechanism, whereas their supply mechanisms are similar. The results of the experiments have shown that a larger chaff is received by chopping with the drum and disc choppers. However, by chopping the stems with the disc chopper, the amount of the dust in the chaff is very huge (by 8-10%). For the middle and short rotation energy plants chopping the conical screw chopper is the most appropriate to use. The chaff in this chopper is being cut by conical screw with a sharpened outer edge. Therefore, this chopper can cut the longer chips (JASINSKAS AND SCHOLZ, 2008).

Therefore, it is appropriate to determine the technological-technical parameters of willow stems chopping and to evaluate the most important chaff properties.

The aim of this work – to investigate the technical means of willow stems preparation for biofuel by using the conical screw chopper and to determine the biometrical characteristics of willow stems and physical-mechanical properties of chaff, such as humidity, bulk density, flow angles, chaff fractional composition, ash content and calorific value.

MATERIALS AND METHODS

The experimental analysis of the wet (approximately 50% of humidity) willows was carried out in 2014-2015 in the base of the Institute of Agricultural Engineering and Safety, Aleksandras Stulginskis University (ASU) and in the plantations of osier willows (*Salix viminalis*L.) belonging to Lithuanian Research Centre for Agriculture and Forestry (LRCAF).

The stems of osier willows of various diameters and 3 years of growth were cut down on the early spring (on February 2015). There were measured the diameters of the stems in 1 m of the height from the soil surface: Gl.1 (28 mm); Gl.2 (20 mm); Gl.3 (15 mm); Gl.4 (13 mm).

The stems of plants were chopped with the mounted to the tractor stationary conical screw chopper *Laimet-21*. There were investigated the biometric characteristics of energy plants' stems and physical-mechanical properties of chaff, such as humidity, bulk density, fall and natural crumble angles, the chaff thinness (fractional composition), ash content as well as the calorific value.

Estimation of biometric characteristics of the energy plants` stems.

Measurements of stems: the length and diameter of stems. Five stems from the plantation were selected and measured. The length of the stem was determined by the measuring tape (1 mm proximity). The diameter of the stem was determined by the calliper (0.1 mm proximity) in 1 m of the height.

The *mass* of the stem was determined by weighting the stems with the weight (by 0.1 g proximity). The average weight of 5 stems was estimated and written down with a measurement deviation.

*The moisture content of stems*was determined in the chemical laboratory according to the standard methodology CEN/TC 14774-1:2005). To determine the moisture content, 3 stems were chopped and 3 samples were taken for 200 g each. The moisture of the stem was the ratio between the water amount in the sample and the mass of the sample. The average mass of three stems was estimated and written down with a measurement deviation.

*The density of stems***.** When the diameter of the stems had already been found, the volume V_{st} of 1 m length of the stem and the plot m^2 of the stem`s cross-section was estimated. Since the mass $m_{st}$ of 1 m length of the stem was known (the proximity of the weight 0.1 g), the density $\rho_{st}$ of the stem`s mass was estimated. When the moisture content of the stems was estimated, the density of each stem and the average density of the dry matter (DM) with the confidence interval of the data dispersion were estimated.

Equipment and measuring devices used during the experiment were as follows:

- weight SB 16001, weight limit 0-16 kg, measuring range 0.1 g;
- ruler, measurement range 1 mm;
- callipers, measurement range 0.05 mm.;
- cylinder to determine the chaff`s density:
  - diameter d_i = 0.18 m;
  - heighth_i = 0.23 m;
  - volumeV_i= 0.00585 m^3.

Characteristics of the chaff chopped with a conical chopper.

Three types of choppers are usually used in the energy plant chopping mechanisms: drum, disc, and conical screw. These choppers have different construction of the chopping mechanism, but their supply mechanisms are similar. For willow stems chopping was used the conical screw chopper, because this chopper can cut the longer and high quality chips (Fig. 1).

The individual stems are being chopped. The chopped mass is supplied in the bags from which the samples of the chaff are taken to determine their physical-mechanical properties.

Fig. 1. – Conical screw blade and example of chaff

The density of the chaff's mass. At first, empty 5 dm^3 cylinder is weighted and the chaff is poured by the top edge. Then the cylinder with the chaff is weighted. Finally, the mass and the density of the chaff were estimated. The experiment is repeated 5 times.

*The moisture of the chaff*is determined in the same way as biometric characteristics of the plant.

*Determination of thechaff`s fall and natural crumble angles.*These angles of the chaff are necessary for projection of the chaff`s storages and mechanisms for the chaff`s transportation to the boiler-rooms and storages. They are determined by the stands, whereas fall and natural crumble angles are determined with the help of the special device (JASINSKAS AND SCHOLZ, 2008).

Fractional composition of the chaff.

To determine the chopping quality of the plant`s stems (fractional structure), the same research methodology is used as in Germany and other EU countries (EU DD CENT/TS15149 – 1: 2006; CEN/TS 14961: 2005). The chaff fractional composition is determined using a set of sieves of 400 mm diameter. The sieves are placed on top of one another with the round holes (in the sequence from the top sieve): 63 mm, 45 mm, 16 mm, 8 mm, 3.15 mm, and 1 mm of diameter. The sample (3 kg of mass) is being sifted with a special shaker *Haver EML Digital plus*. The set of sieves in the horizontal surface is being vibrated for 2 minutes (Fig. 2).

The mass left on the sieves is weighted and the portion of every fraction is estimated by percent's. Each experiment repeated 5 times.


Fig. 2. – Laboratory sieve shaker *Haver EML Digital plus*

Determination of willow quality indicators, ash content and calorific value.

The research of the produced energy plant chips` quality indicators – ash content and heat parameters (calorific value) is performed in the Laboratory of Heat Equipment Research and Testing, Lithuanian Energy Institute (LEI) according to the standard methodology used in Lithuania and in other European countries:

- in the experimental mechanism of moisture No. 8B/1 according to LST EN 14774-1:2010 standard requirements;
- in the experimental mechanism of ash content No. 8B/5 according to LST EN 14775:2010 standard requirements;
- in the experimental mechanism of heating No. 8B/2 according to LST EN 14918:2010 standard requirements.

One of the most important quality indicators of the chips is their calorific value. To determine this index, the succinct `IKA C5000` was used. To make the experiment more accurate, the chip samples of unconventional energy plants were dried. The experiment was repeated 5 times with each type of the chips. The measurement deviation was 0.02%. The experiment deviation was evaluated by estimating the arithmetic averageof the data of every repeated experiment.

RESULTS AND DISCUSSION

The results of experimental research have shown: biometric characteristics of energy plants` stems, the analysis of the chaff chopping quality, chaff`s density, and flow angles. Moreover, fractional composition and moisture content of the energy plants were determined, and the ash content and calorific value of willow chaff were evaluated.

4 types of osier willow stems were investigated which were classified according to the thickness (diameter) of their stem.

Biometrical properties of energy plants.

The individual growth rate and development, as well as reaction to biotic and abiotic factors are common to biometric characteristics of the plant development for different plant species. The research results of biometrical characteristics of osier willows are presented in Tab. 1.

The results of biometric characteristics of energy plants` stems show that willow stems of three-year-old growth grew from 2.5 m to 4.4 m of height. The diameter of every willow stem depended on the height of the willow. The taller the willow, the thicker was its stem. When the diameter of stems was Gl.1 (28 mm), its length reached 4.5 m, and when the diameter of willow stems was twice smaller Gl.4 (13 mm), the height was 2.5 m.

Analysing the stems` mass of the osier willow, the same tendency as with their lengths could be seen, i.e., when was the bigger diameter of the osier willow stems, the bigger was the mass of full length stem. The mass of full length willow stem Gl.4 was 73% smaller than Gl.1.

While estimating the moisture content of osier willow, it was determined that when was the bigger diameter of the osier willow Gl.1 (28 mm), the smaller was its moisture content – 52.49 ± 0.55%. The largest moisture content was of Gl.4 (13 mm) –54.56 ± 0.39%. Stems of such moisture content can be used for the fuel in the boiler-rooms with the fire-places which are suitable to burn the wet wood.

When the moisture content of the stems is determined, the density of the stem`s dry matter can be estimated. The smallest density of the stem was estimated in Gl.1 (28 mm) – 694.47 ± 74.50 kg m^{-3}, whereas the largest of Gl.3 (15 mm) – 893.76 ± 60.50 kg m^{-3}.

Tab. 1. – The biometrical properties of osier willow stems (*Salix viminalis*L.)

Indicators and measurement units	Plant stems			
	Gl.1 (28 mm)	Gl.2 (20 mm)	Gl.3 (15 mm)	Gl.4 (13 mm)
Lengthof stem, mm	4445.33 ±80.04	4150.33 ± 95.74	2754.33 ± 92.24	2546.33 ± 68.01
Diameter of stem, at 1.0 m distance from the soil surface, mm	28.0 ± 1.26	19.92 ± 0.96	15.18 ± 0.86	13.25 ± 0.80
Mass of full stem length, g	1019.0± 48.93	758.47 ± 45.11	383.87 ± 40.92	250.50 ± 38.95
Moisture content of stem, %	52.49 ± 0.55	53.46 ±0.46	53.74 ± 0.42	54.56 ± 0.39
Density of stem dry mass, kg m^{-3} DM	695.47 ± 74.50	870.06 ± 66.18	893.76 ± 60.50	815.34±24.79

Physical-mechanical properties of willow stems.
Physical-mechanical properties of individual osier willow stems after 3 months of cutting and chopping with conical screw chopper were determined (moisture content, bulk density, fall α_{gr} and natural crumble α_n angles), and the test results of willows stems chaff are presented in Tab. 2.

Tab. 2. - Physical-mechanical properties of osier willows *(Salix viminalis*L.*)*stems chaff (chopped with the conical screw chopper)

Plant species	Chaff moisture content, %	Chaff parameters			Flow angles	
		Mass, g	Volume, m^3	Density, kg m^{-3}	$\alpha_{n,}{}^{0}$	$\alpha_{gr,}{}^{0}$
Gl.1 (28 mm)	32.54 ±0.34	2287.5±0.87	0.003	206.57±0.72 (136.43±0.84 DM)	47±6.6	78±7.5
Gl.2 (20 mm)	26.34±0.24	633.53±0.22	0.003	204.52±0.52 (128.01±0.13 DM)	42±5.5	70±7.4
Gl.3 (15 mm)	25.73± 0.19	830.66±0.12	0.004	177.67±0.53 (124.24±0.05 DM)	40±3.5	68±4.2
Gl.4 (13 mm)	22.88± 0.18	521.03±0.09	0.003	173.67±0.43 (123.94±0.06 DM)	39±3.2	66±3.6

From the data presented in Tab. 2 we can to see that bulk density of the willow chaff decreased from 136.43 ± 0.84 kg m^{-3} DM to 123.94 ± 0.06 kg m^{-3} DM. It is possible to state that with the increase of the stem diameter, the produced chaff bulk density also increases.

It was determined that the natural crumble angle of the osier willow stems` chaff changed from 39 to 47 degrees, whereas the fall angle – from 66 to 78 degrees. Received results of physical-mechanical properties of the chaff can be used to estimate the size of the willow chaff`s storages and sites (on the basis of the natural crumble angle, it is possible to determine how the chaff which is being poured from the transport will change). Moreover, on the basis of chaff`s crumble angle, the constructive parameters of storages and walls of the supply to the fire-places mechanisms (the crumble angles of the walls should be larger than the determined limitary) can be determined.

Fractional compositionof willow plant stems chaff.
The chaff of osier willow was used for experimental research. To perform the analysis of fractional composition, a set of sieves of 400 mm diameter with round holes of 1 mm, 3.15 mm, 8 mm 16 mm, 45 mm were used. Fractional composition of the plant`s chaff is provided in Fig. 3 – Fig. 6.

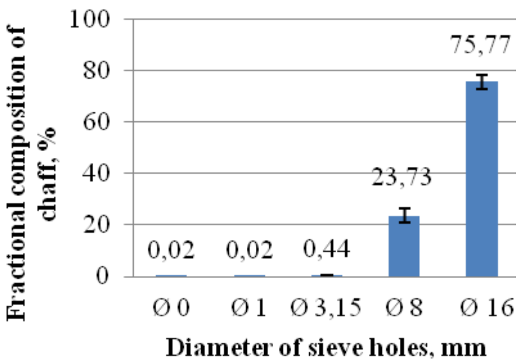

Fig. 3. – Gl.1(28 mm) fractional composition

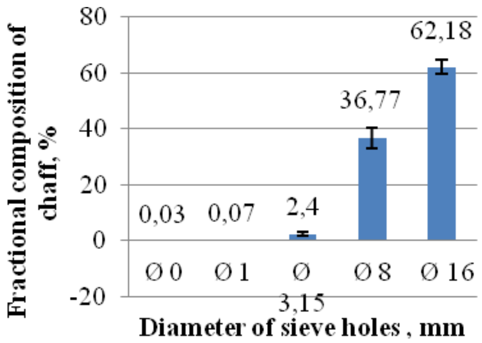

Fig. 4. – Gl.2 (20 mm) fractional composition

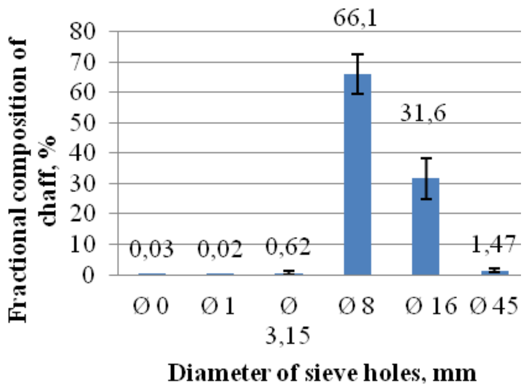

Fig. 5. – Gl.3 (15 mm) fractional composition

When the fractional composition of the plant`s chaff was determined according to the methodology used in the EU countries, it was estimated that the largest fractional composition was received when the diameter of the sieves holes was 8 mm and 16 mm. Moreover, it was determined that the willows which had a thicker stem (Gl.1 and Gl.2), the largest portion of the chaff`s fraction concentrated on the sieves with the holes of 16 mm diameter (accordingly 75.77% and 62.18%), whereas the willows which had the thinness stems (GL.3 and GL.4), the largest portion of the chaff`s fraction concentrated on the sieves with the holes of 8 mm diameter (accordingly 66.1% and 62.1%). It was determined, that very small amount of the dust was formed (from 0.02 to 0.08 %).

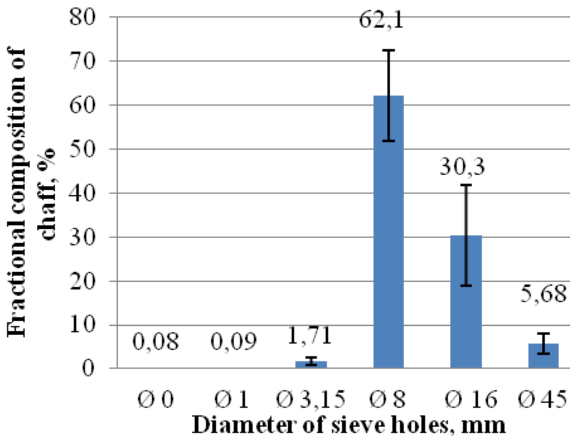

Fig. 6. – Gl.4 (13 mm) fractional composition

Determination of willow stem`s chaff`s ash content and calorific value.

The analysis of willow chaff`s ash content and calorific value shows that the estimated ash content of is relatively low and reached only 1.44%. The small amount of ashes shows that the chaff of such energy plants as willows burns relatively well and in comparison with other energy plants with the small calorific value, determined the lower calorific value of willow chaff dry mass is relatively big – 18.5 MJ/kg).

The results of these experiments show that the usage of osier willows for bio-fuel is justified very well. Cut and chopped stems can be used in the boiler rooms of average or big power (more than 0.5 MW), which have special burning devices suitable to burn the wet and partially dried bio-fuel.

CONCLUSIONS

Presented research results of willow stems biometrical properties and physical-mechanical properties of chaff, such as moisture content, bulk density, flow angles, chaff fractional composition, ash content and the calorific value. Investigated bulk density of willow chaff decreased from 136.43 ± 0.84 to 123.94± 0.06 kg m^{-3} DM, and the natural crumble angle changed from 39 to 47 degrees, the fall angle varied from 66 to 78 degrees. Research results of willow chaff fractional composition show, that the largest part of fraction was received on the sieves with the diameter of 8 and 16 mm holes – from 62.1 to 75.77%, dust amount was very small (0.02-0.08%). After burning of willow chaff determined ash content was relatively low and reached only 1.44%, estimated the lower calorific value of willow chaff dry mass was relatively big – 18.5 MJ/kg. After analysis of presented research results should be concluded, that chopped by conical screw chopper osier willows can be used in the boiler rooms of average or big power.

REFERENCES

1. AMICHEV, B. Y., HANGS, R.D., BÉLANGER, N., VOLK, T. A., VUJANOVIC, V., SCHOENAU, J.J., REES V.: First-Rotation Yieldsof 30 Short-Rotation Willow Cultivars in Central Saskatchewan, Canada. BioEnergy Research. 8 (1), March 2015: 292-306.
2. AN ENERGY POLICY FOR EUROPE: Communication from the Commission to the European Council and the European Parliament. Brussels, 1 final, COM. 2007: 27 p.
3. BIOMASS INDUSTRIAL INNOVATIVE PROJECTS: Kamis, 07 Januari 2016. History Repeated Back In The Field of Biomass. Acessed: 15.04.2016: http://biomassproject.blogspot.lt/2016/01/history-back-repeated-in-field-of.html.
4. BIOMASS INDUSTRIAL INNOVATIVE PROJECTS: Rabu, 13 Januari 2016. Acessed: 20.09.2015: http://biomassproject.blogspot.lt/2015/09/racing-for-lowering-temperature-of.html
5. BLUMBERGA, D., OZOLINA, L., ROSA, M., VRUBLIAUSKAS, S., PEREDNIS, E.: BIOMASS CO-FIRING IN LATVIA AND LITHUANIA. Biosystems Engineering and Processes in Agriculture: Proceedings, 2008: 25-31.
6. CEN/TC 14774-1:2005. Solid biofuels – Methods for the determinativ of monture content – Oven dry method – Part 1: Total moisture – Reference method. 2005.
7. CEN/TS 14961: Solid Biofuels – Fuel Specification and Classes. 40 p., April, 2005.
8. DD CEN/TS 15149-1:2006. Solid biofuels – Methods for the determination of particle size distribution. Part 1: Oscillating screen method using sieve apertures of 3.15 mm and above. 2006.
9. FABER, A., STASIAK, M., KUŚ, J.: Preliminary assessment of the productivity of selected energy plants. Progress in Plant Protection. 47(4), 2007: 339–346 (in Polish).
10. FILHO, P. A., BADR, O.: Biomass resources for energy in North-Eastern Brazil. Applied Energy. 77 (1), 2004: 51-67.
11. GREEN PAPER: Towards a a European strategy for the security of energy supply. Brussels, COM (2000) 769. 2000, 115 p.
12. JASINSKAS, A., LIUBARSKIS, V.: Technologies of energy plants growing and usage forf uel: study. Raudondvaris, 2005: 90 p. (in Lithuanian).
13. JASINSKAS, A., SCHOLZ, V.: Plant biomass harvesting and preparation for fuel technologies and thein evaluation: study. Raudondvaris, 2008: 74 p. (in Lithuanian).
14. JASINSKAS, A., ŽALTAUSKAS, A., KRYŽEVIČIENĖ, A.: The investigation of growing and using of tall perennial grasses as energy crops. Biomass and Bioenergy. 32 (11), 2008: 981-987.
15. JONIEC, J., FURCZAK, J.: Studies on Stability and Changes in Microbiological and Biochemical Activity of Podzolic Soil under Plantation of Basket Willow after Introduction of Sewage Sludge. Polish Journal of Environmental Studies. 19 (5), 2010: 921-930.
16. KRYŽEVIČIENĖ, A: Potential of Perennial Grasses and their possible local and renewable resources as a biofuel. Rural Development in 2003: set of reports. 274 p., 2003 (in Lithuanian).
17. ŁUKASZEWICZ, J.P., WESOLOWSKI, R.P., CYGANIUK, A.: Enrichment of Salix viminalis Wood in Metal Ions by Phytoextraction. Polish Journal of Environmental Studies. 18 (3), 2009: 507-511.
18. MATIAS, J.C., DEVEZAS, T.C.: Consumption dynamics of primary-energy sources: The century of alternative energies. Applied Energy. 84 (7-8), 2007: 763-770.
19. PIENKOWSKI, C.A.: The Possibilities of Using Renewable Sources of Energy in Podlaskie Province. Polish Journal of Environmental Studies. 19 (3), 2010: 537-544.
20. SCHAUMANN, G.: The efficiency of the rational use of energy. Applied Energy. 84 (7-8), 2007: 719-726.
21. STAJNKO, D., LAKOTA, M., VUČAJNK, F., BERNIK, R.: .: Effects of Different Tillage Systems on Fuel Savings and Reduction of CO2 Emissions in Production of Silage Corn in Eastern Slovenia. Polish Journal of Environmental Studies. 18 (4), 2009: 711-716.
22. ŠATEIKIS, I.: Potential of plant biomass cultivation and use for solid fuels and priority of research the present problems. Agricultural engineering: IAE LUA and LUA research papers. Raudondvaris. 38 (3), 2006: 5-21 (in Lithuanian).
23. VARES, V., KASK, U., MUISTE, P., PIHUT, T., SOOSAAR, S.: Biofuel user manual. Vilnius, 2007: 168 p. (in Lithuanian).

Corresponding author:
assoc. prof., chief researcher, doctor of technological sciences Algirdas Jasinskas, Institute of Agricultural Engineering and Safety, Faculty of Agricultural Engineering, Aleksandras Stulginskis University,Studentu str. 15, Akademija, LT-53362 Kaunas reg., Lithuania, phone: +37061204002, e-mail: algirdas.jasinskas@asu.lt

THE INFLUENCE OF INJECTION TIME'S DYNAMIC CHANGES ON PARTICULATE MATTERS PRODUCTION

P. Jindra, M. Kotek, T. Kotek, M. Hruška

Faculty of Engineering, Czech University of Life Sciences Prague, Czech Republic

Abstract
In last years the European Union has exhibited a significant interest in the reduction of crude oil usage. Biofuels can be used in conventional engines and they should reduce the emissions production. This article deals with analysis of particulate matters (PM) production in spark ignition combustion engine Skoda 1.2 HTP operating on E85 fuel.
The experiment searched optimum fuel injection time with respect to the capabilities of the original engine control unit (ECU) using special auxiliary control unit (ACU), which allowed the expansion of the adaptive range of the engine.
The conventional emission analysers are capable to detect gaseous emission components but they are not able to classify PM. Analysis of PM was performed with a TSI Engine Exhaust Particle Sizer 3090 (EEPS) which is able to classify particles from 5.6 nm to 560 nm.
The given size of PM can be taken as an impact on human organism's cells consequently human health. PM create an ideal medium for polyaromatic hydrocarbons (PAH), due to their composition and structure. Analysis of PM should become a standard component of every emission parameter assessment.

Key words: E85, bioethanol, emission, control unit.

INTRODUCTION

Currently has been issue of biofuels becoming more and more actual topic. All over the world we can see raising the usage of fossils fuels and growth of greenhouse gases (GHG) production. According to the assumptions 80 % of primary energy from fossil fuels is acquired and 60 % this energy is used for transport ESCOBAR ET AL. (2009). In the various parts of the world are introduced different legislative actions to reduce production of GHG.

One possible solution is using bio-ethanol as a high-percentage mixed biofuel in the E85 form. Potential problem is the lower energy density of ethanol compared to gasoline. To maintain similar performance parameters is needed to burn a higher amount of ethanol. This leads to increased fuel consumption. Advantage of ethanol is its higher octane number (ethanol 104, gasoline 95) and also quicker combustion ČEDÍK ET AL. (2014), ROBERTS (2007), PARK ET AL. (2010). Among its disadvantages are less able to start the engine at low temperatures and property through which binds water. This leads to corrosion ROVAI (2005).

For the operation of engines on a high-percentage alcohol fuel mixture is required small engine modifications. The stoichiometric ratio for a specific mixture of alcohol and gasoline must be respected. Mix ratio between air and fuel must be observed. Ethanol has mixing ration 9:1 and gasoline has 14.7:1. It is clear that compared to gasoline, it is necessary to create a richer mixture. Several different modifications are possible for solve this problem IRIMESCU (2012).

As the particulate matter (or solid particle) according to the laws of the USA is referred to any substance which is normally contained in the exhaust gas as solid particle (ash, soot) or as a liquid. They consist of elemental carbon forming particles and organic compounds (condensed water, sulphur compounds and nitrogen compounds). Solid particle itself is not toxic, but on the solid particles are adsorbed substances with high health hazards. LWEBUGA–MUKASA ET AL. (2004) found correlation between asthma and truck traffic volumes. Most of the emitted particles have a size from one to hundreds of nanometers (nano–particles) CHIEN (2009), VOJTISEK–LOM (2015).

This article deals with the issue of blended biofuels in terms of particulate matters production depending on the settings of the injection time. The measurement was aimed not only on the total production of solid particles but on their size distribution.

MATERIALS AND METHODS

The whole experiment was conducted on the test bed at the Department of Vehicles and Ground transport, CULS Prague.

The measurement was carried out with a four-stroke inline three-cylinder engine Skoda Fabia 1.2 HTP (see Tab. 1 for detailed parameters) with multipoint injection system with close-loop control mode at part engine loads to keep the engine operating near stoichiometric air–fuel ratio (AFR) and open-loop control mode at full engine loads to produce maximum power.

The tested engine was loaded using whirl dynamometer V125, the torque and engine speed were captured during measuring. Dynamometer reactions were captured with tensometric sensor with nominal load of 2 kN and with accuracy of 0.5 % of the nominal load. Diagnostic system VAG-COM was used for communication with ECU. This system was primary used to read values from engine control unit as engine speed, engine load and to check errors.

The EEPS analyser was used for the measuring of particulate matters production. Detailed specifications of EEPS are shown in Tab. 2.

Tab. 1. – Technical parameters of tested engine

Engine code	AWY
Construction	3-cylinders, row, 6 valves
Volume	1198 cm^3
Compression ratio	10,3 : 1
Power	40 kW at 4750 rpm
Torque	106 Nm at 3000 rpm
ECU	Simos 3PD (multipoint injection)
Fuel	unleaded N95
Emission standard	EU4

Tab. 2. – Technical parameters of the TSI EEPS 3090

TSI EEPS 3090	
Particle size range	5.6 – 560 nm
Particle size resolution	16 channels per decade (32 total)
Electrometer channels	20
Time resolution	10 size distribution per second
Sample flow	10 l min^{-1}
Dilution accessories	Rotation Disk thermodilution
Charger mode of operation	Unipolar diffusion charger
Inlet cyclone 50% cutpoint	1 µm
Maximal time Resolution	10 size distributions/sec

The special dynamic driving cycle (Fig. 1) was used for engine testing under conditions close to real engine load in real traffic conditions.

The additional control unit (ACU) (Kotek et al, 2015) was used for the operative change of injection time extension. Two strategies were chosen: constant extension of 10 % and degressive extension when the basic 10 % extensions was set at the engine idle and with growing engine load the injection time was decreased to basic injection time (i.e. zero extension). Degressive calculation of injection time was realized by equation (1).

$$t_{inj} = t_{ECU} \cdot 0.87 \cdot (5 - p_{in}) \qquad (1)$$

t_{inj} - calculated injection time (ms)
t_{ECU} - original injection time from ECU (ms)
p_{in} - intake air pressure (measured voltage analog value from MAF sensor - V)

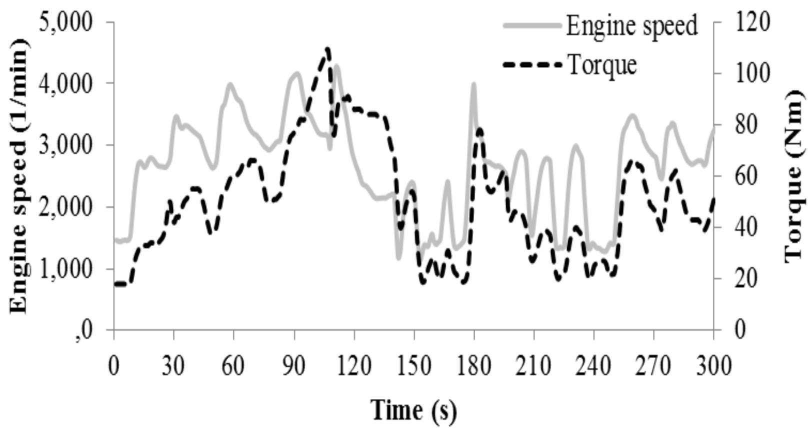

Fig. 1. – Dynamic driving cycle

RESULTS AND DISCUSSION

The production of PM in different size spectra for all researched fuels is shown in following figures. Analyzer EEPS has 32 channels for dimension of particulate matters. To simplify the graphs are showed only for particle sizes of 10, 60, 200, 400 nm.

The Fig. 2 shows the numbers of particles about 10 nm during driving cycle. In high engine load between 50 and 100 second is visible higher particles production for gasoline. Both setting for ethanol produce less volume of particles. These dimensions are considered to high dangerous.

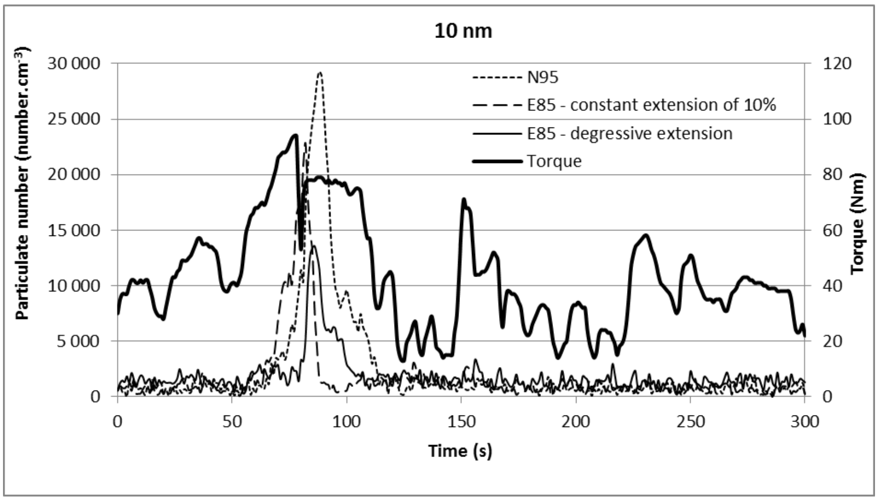

Fig. 2. – Numbers of particles of size up to 10 nm

Particles about 60 nm are shown in Fig. 3. There is visible bigger difference in settings of ACU. Higher production is in setting with constant extension. Degressive settings produce less volume of particles than constant extension.

Gasoline is situated in the middle between two settings of ethanol.

Course of the 200 nm particles production is shonw in Fig. 4. First time is visible higher production of PM when is used degressive setting. Most of time in driving cycle was produced more PM than others two measuring. Except when there was an increased demand at the engine load in time around 150 s and 255 s.

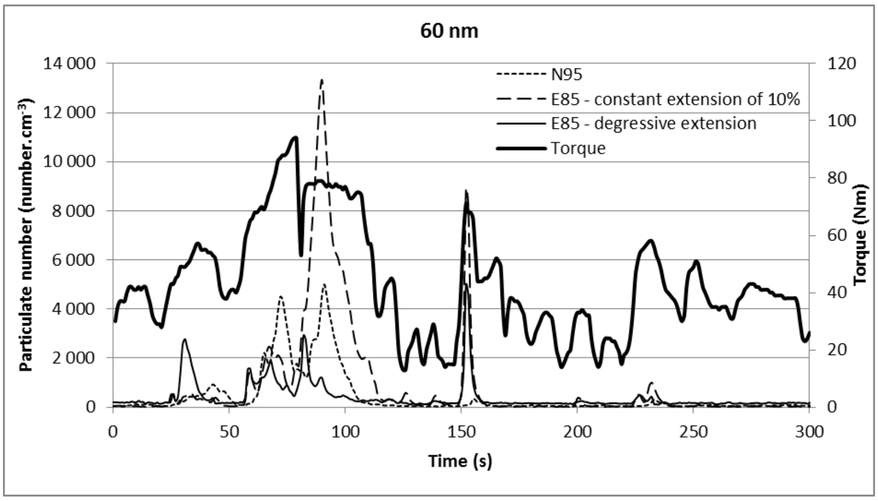

Fig. 3. – Numbers of particles of size up to 60 nm

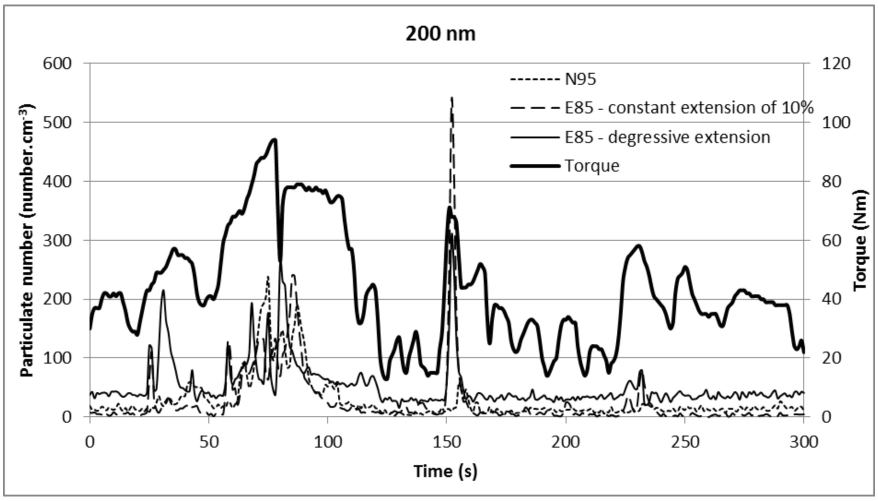

Fig. 4. – Numbers of particles of size up to 200 nm

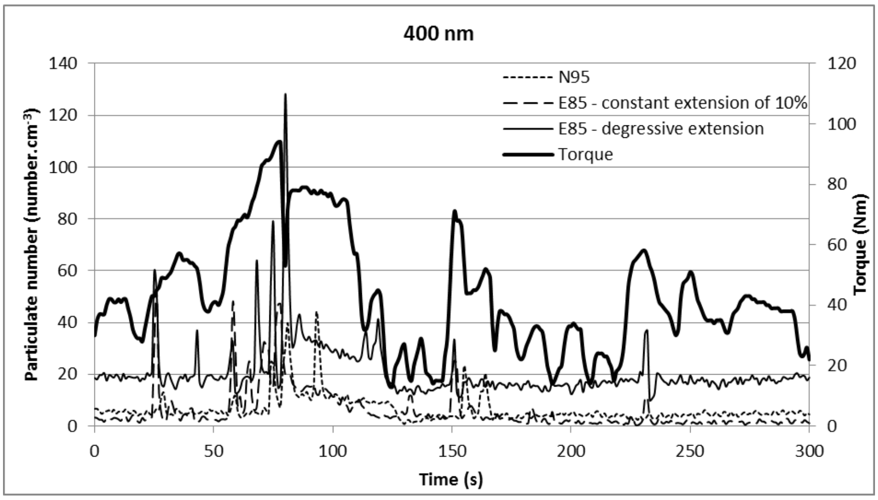

Fig. 5. – Numbers of particles of size up to 400 nm

In Fig. 5 is showed clear impact of degressive setting. In this settings is higher particles production about 400 nm. Standard settings for gasoline and setting for constant extension are very similar.

The following Fig. 6 shows the total quantity of particles produced for the entire duration of the measurement. The positive impact of degressive setting on the total production of particles is obvious.

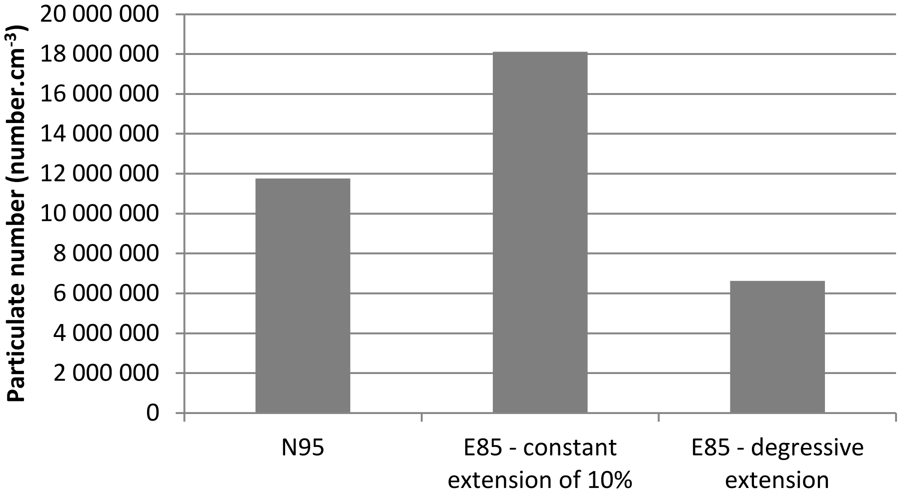

Fig. 6. – Total production of PM

Measuring confirmed that using ACU allows E85 in conventional engine. ACU expands adaptive ability of the original control unit.

Measuring spectra production particulate matters showed that the use of bioethanol causes changes in the distribution of particulate matters. For comparison are results compared with gasoline.

In settings with constant extension is distinct decrease produce very small particles and high increase production in all others situation. Very important is increase in the production of particles during high and fast engine load. Generally this situation occurs very rarely under real traffic condition.

In degressive settings is significantly higher production of particles larger than 100 nm. Compared with standart settings and settings with constant extension is increase 2 – 3 times higher. Total production of particulate matters is lowest at degressive settings.

CONCLUSIONS

Following the article Determination of the optimal injection time for adaptation SI engine on E85 fuel using self-designed auxiliary control unit KOTEK (2015) the depends of particullate matters production on settings of engine control units were determined. Generally engine operating on bioethanol reduces the production of small particles (less than 100 nm) and increases the production of large particles. In the case of high engine load is the production of large particles more pronounced.

Possible solutions to this problem is the assembly of the diesel particulate filter (DPF), which are capable very effectively removed particles larger than 100 nm. In the case of the use of bioethanol and DPF is possible reducing the particulate production in all size spectra.

ACKNOWLEDGEMENTS

This work has been realized with the contribution of Czech University of Life Sciences in Prague Internal Grant Agency, project 2016:31150/1312/3111 „Analysis of impact using biofuels on operating parameters of combustion engines.“.

REFERENCES

1. CHIEN, S. M., HUANG, Y. J., CHUANG, S. C., YANG, H. H.: Effects of biodiesel blending on particulate and polycyclic aromatic hydrocarbon emissions in nano/ultrafine/fine/coarse ranges from diesel engine. Aerosol and Air Quality Research 9, 2009: 18–31.
2. ČEDÍK, J., PEXA, M., KOTEK, M., HROMÁDKO, J.: Effect of E85 fuel on performance parameters, fuel consumption and engine efficiency – Škoda Fabia 1.2 HTP. Agronomy Research 12(2), 2014: 307–314.
3. ESCOBAR, J.C., LORA, E.S., VENTURINI, O.J., YANEZ, E.E., CASTILLO, E.F., ALMAZAN, O.: Biofuels: environment, technology and food security, Renew. Sustain. Energy Rev. 13, 2009: 1275–1287.

4. IRIMESCU, A.: Fuel conversion efficiency of a port injection engine fueled with gasoline-isobutanol blends, Energy 36, 2011: 3030-3035.
5. KOTEK, T., KOTEK, M., JINDRA, P., PEXA, M.: Determination of the optimal injection time for adaptation SI engine on E85 fuel using self-designed auxiliary control unit. Agronomy Research 13(2), 2025: 577–584.
6. LWEBUGA–MUKASA, J.S., OYANA, T., THENAPPAN, A., AYIROOKUZHI, S.J.: Association Between Traffic Volume and Health Care Use for Asthma Among Residents at a U.S.–Canadian Border Crossing Point. Journal of Asthma 41, 2004: 289–304.
7. PARK, C., CHOI, Y., KIM, CH., OH, S., LIM, G., MORIYOSHI, Y.: Performance and exhaust emission characteristics of a spark ignition engine using ethanol and ethanol-reformed gas, Fuel 89, 2010: 2118–2125.
8. ROBERTS, M. C.: E85 and fuel efficiency: An empirical analysis of 2007 EPA test data, Energy Policy 36, 2008: 1233–1235.
9. ROVAI, F., TANAKA D., SINATORA, A: Wear and corrosion evaluation of electric fuel pumps with ethanol/gasoline blends. SAE Technical Paper 2005-01-2196, 2005.
10. VOJTISEK–LOM, M., PECHOUT, M., DITTRICH, L., BERANEK, V., KOTEK, M., SCHWARZ, J., VODICKA, P., MILCOVA, A., ROSSNERVOA, A., AMBROZ, A., TOPINKA, J.: Polycyclic aromatic hydrocarbons (PAH) and their genotoxicity in exhaust emissions from a diesel engine during extended low–load operation on diesel and biodiesel fuels. Atmospheric Environment 109, 2015: 9–18.

Corresponding author:

Ing. Petr Jindra, Department of Vehicles and Ground Transport, Faculty of Engineering, Czech University of Life Sciences Prague, Kamýcká 129, Praha 6, Prague, 16521, Czech Republic, phone: +420 22438 3153, e-mail: jindra.petr@gmail.com

EFFECTS OF DIFFERENT CONVERSATION TILLAGE SYSTEMS ON SOIL PHYSICAL PROPERTIES IN WEST MEDITERRANEAN IN TURKEY

O. Kabas, İ. Ünal

Akdeniz University, Vocational School of Technical Science, Antalya, Turkey

Abstract
The study was conducted during two summer seasons (2012 and 2013) under Mediterranean area conditions (South of Turkey) to determine the effect of four tillage system (conventional tillage (T_1) "Plough + disc harrowing + float + pneumatic seeding machine", reduced tillage I (T_2) "rotovator + float + pneumatic seeding machine", reduced tillage II (T_3) "rotary tiller combination + pneumatic seeding machine" and no tillage (T_4) "seeding by direct seeding machine") on the soil physical properties in the area. The soil of the experimental parcel was classified as silty. There was no significant different statistically among soil porosities of tillage systems in all depths at after tillage and harvesting operation. For variation though conversation tillage methods, tillage methods X measuring time, tillage methods X depth and tillage methods X measuring time X depth interactions were significant statistically for four tillage systems ($p<0.001$).

Key words: conversation tillage, maize, soil properties, penetration resistance.

INTRODUCTION

Farming systems today have more obvious and detectable social, ecological, economic, and environmental implications than ever before because of the growing concerns about agricultural sustainability and the environment (SHRESTHA AND CLEMENTS, 2003). "Agricultural sustainability implies an increasing trend in per capita productivity to meet the present needs without jeopardizing the future potential. This demands appropriate methods of land stewardship for the development of sustainable agricultural systems".

An important aspect of land stewardship is tillage that important to provide the correct conditions for crop establishment and growth, and in general, requires mechanical manipulation of the soil by equipment that either cuts, shatters, inverts or mixes the soil (CANNELL, 1985; GAJRI ET AL., 2002). Tillage is performed in order to optimize productivity by alleviating physical, chemical and biological constraints of soil (GAJRI ET AL., 2002). Current tillage systems can be divided into two broad categories; inversion tillage, known as conventional plough tillage, and non-inversion tillage, known as conservation tillage including minimal tillage and direct drilling (DAVIES AND FINNEY, 2002).

The tilth or soil condition resulting from the use of different tillage tools depends on both the type of implement used and the soil condition. At present, it is not possible to adequately predict the resulting soil conditions from a tillage practice (TAPELA AND COLVIN, 2002). Studies have shown that tillage practices alter soil physical properties (BARZEGAR ET AL., 2003), influencing the water storage and hydraulic conductivity of soil and consequently the hydrological behavior of agricultural watersheds (XU & MERMUD, 2001). Tillage treatments affect the soil physical properties, especially when a similar tillage system has been practiced for a long period (JORDHAL & KARLEN, 1993; MIELKE & WILHELM, 1998). BUSCHIAZZO ET AL. (1998) reported that tillage systems had greater influence on the soil physical properties in a humid climate and in loamy soils compared to that in an arid climate and sandy soils. Soil physical properties mediate several physical chemical, and biological processes in soil that should be kept optimal (LAL, 1991). Therefore, it is important to apply a proper tillage system that results in the soil sustaining physical properties suitable for the successful growth of agricultural crops.

Although a lot of literature on tillage is available, still the degree in which various tillage operations alter soil physical properties is poorly understood and cannot be adequately predicted (CRUSE AND LINDEN, 1980).

"The soil physical properties are important in determining plant growth and yield. It has been realized for many years that low productivity of soil may be associated with unfavorable physical conditions for growth such as infiltration rate, soil bulk density, soil mechanical resistance to penetration, and water percolation and distribution".

Soil physical properties such as dry bulk density, moisture storage capacities, porosity and resistance to penetration were commonly assessed and evaluated to detect the influence of different tillage practices on soil and crop growth and yield. Therefore, an experiment was conducted at Antalya, Turkiye to examine the prospective effects of tillage practices on physical properties of soil in the area to cultivate second crop maize (*Zea mays* L.) after tillage and harvesting operation.

MATERIALS AND METHODS

Work area and soil

This experiment was conducted at the Bati Akdeniz Agricultural Research Institute, Antalya, Turkiye, during two summer seasons (2012 and 2013). The soil in the experiment field was a clay silty with pH of 7.5 and organic matter matter content of 1.8%. The results of soil analyses are given Tab. 1. The average weather conditions during growing seasons such as annual temperatures and rainfall etc. are showed in Tab. 2.

Tab. 1. – The result of soil analyses

pH (1:2.5)	7.5
Lime (%)	19.6
EC micromhos/cm (25°C)	195
Sand (%)	21
Clay (%)	33
Silty (%)	46
Organic matter (%)	1.8
P ppm	16
K ppm	250
Ca ppm	4585
Mg ppm	409

Tab. 2. – Average climate dates of a long-term at the site of experimentation

	May	June	July	August	September	October
Temperature (°C)	20.4	25.4	28.4	28.1	24.7	19.8
The highest Temperature (°C)	25.9	31.3	34.4	34.3	31.3	26.7
The lowest Temperature (°C)	14.8	19.4	22.5	22.4	19.1	14.9
Sunshine duration (hour)	9.5	11.4	11.5	11.3	9.5	8.0
Number of rainy days	5.0	2.4	0.7	0.5	1.7	5.4
Rainfall (kg/m^2)	29.3	7.1	3.3	1.6	11.0	74.8

The experiment, which was begun in June 2012 and finished 2014 compared four tillage systems for maize (*Zea mays* L.) production following a wheat-maize rotation. Seeds of maize (Zea mays saccharata Sturt.) were used in this study. The standard cultural practices recommended by Batı Akdeniz Agricultural Research Institute; other than treatments, were followed throughout the growing seasons.

The experiment was established as a randomized block design with four replications. Plots were 5 m wide (four rows) and 25 m long with an inter row spacing of 0.7 m distance. After the field had been selected and before the application of the treatments, the land was freed from weeds and crop residues except the no-tilled plots. The experimental procedures were the same for the both seasons.

Tab. 3. – Soil tillage methods utilized in experiments

Tillage systems	**Tillage operations**
T_1 (conventional tillage)	plough + disc harrowing + float + pneumatic seeding machine
T_2 (reduced tillage I)	rotovator + float + pneumatic seeding machine
T_3 (reduced tillage II)	rotary tiller combination + pneumatic seeding machine
T_4 (no tillage)	Seeding by direct seeding machine

Conservation Tillage Systems

Tillage systems are shown in Tab. 3 and the specifications of the tools used in the experiment are given Tab. 4.

For the conventional tillage method, the soil was first ploughed with five bottom moldboard plough. After plowing, the field was harrowed with disc harrow and leveled with float. In the reduced tillage method I, soil was prepared for seeding with only one pass of soil tillage, float and pneumatic seeding machine. In the reduced tillage method II, soil was prepared for seeding with only one pass of soil tillage with rotary tiller combination and then pneumatic seeding machine. For the direct seeding application, seeding was made without tillage. Massey Ferguson 5400 (Engine Power 105 HP) tractor was used in the experiments.

Tab. 4. - The specifications of the tools used in experiments

Tools	Avarage speed (km h^{-1})	Working depth (mm)	Working width (mm)
Plough	5.5	300	1500
Disc harrowing	6.5	150	2200
Rotovator	6	220	2000
Rotary tiller combination	2.8	200	2500
Float	7	-	3000
Seeding machine	6.3	40-50	2800
Direct seeding machine	5.6	40-50	2800

Investigations and data collection

Soil samples were collected from the field with three replications on each plot after tillage and harvesting operation at 0–30 cm for bulk density, porosity, moisture content and penetration resistance at 0-60 cm

The determination of water content of soil (% d.b.) was carried out twice during the season. The first one was done before tillage operations and the second one was done before harvesting. Samples were transported to the laboratory and then oven dried at 105°C for 24 hours to determine dry-basis gravimetric soil water content.

Dry bulk density of the soil was determined after tillage and harvesting operations both seasons using the clod method (BLACK ET AL., 1965). Soil samples were randomly taken from each strip-plot from 0-30 cm soil depths.

Total porosity (φ) was obtained through the following equation:

$$\varphi = \left(1 - \frac{\delta b}{\delta r}\right) x100 \tag{1}$$

Where δr was the soil particle density assumed to be 2.65 Mgm^{-3} and δb was the soil bulk density

Soil resistance to penetration was measured after tillage and harvesting operations both seasons using a manually operated cone penetrometer. Three samples were randomly taken from each strip-plot using a cone with a 2.0 cm^2 area from soil depths of 0-10, 10-20, 20-30, and 30-40, 40-50, 50-60 cm, then converted to MPa.

RESULTS AND DISCUSSION

Soil moisture

Data pertaining to soil moisture content at 0-30 cm depth before the tillage operation and after harvesting during 2012-2103 growing season the second growing period of maize are presented in the Tab. 5.

Maximum soil moisture contents were observed in soil tilled with T4 at 20-30 cm soil depths followed by that in soil tilled with T3 at 20-30 soil depths after tillage and harvesting operation, maximum soil moisture content were determined in soil tilled with T4 at 20-30 cm soil depths followed by that in soil tilled with T3 at 20-30 cm soil depths during both years. These results are in agreement with those reported by BOYDAS AND TURGUT (2007), RASHİDİ AND KESHAVARZPOUR (2008).

Soil bulk density

The results found to soil bulk density at 0-30 cm depth after the tillage and harvesting operation during 2012-2103 the second growing period of maize are shown in the Tab. 6.

Tab. 5. - Effect of Conversation Tillage Systems on Soil Moisture content (2012-2013 growing season)

		T1	T2	T3	T4	CV	LSD	Sign.
After tillage	0-10	18.42	20.36	19.35	21.26	1.622	0.011	***
	10-20	20.40	21.37	22.32	21.16			N.S
	20-30	21.90	22.01	22.24	22.40			N.S
After harvest	0-10	22.21	20.07	18.61	21.35	0.841	0.022	***
	10-20	23.01	22.93	23.41	23.90			N.S
	20-30	23.24	22.93	23.93	24.64			N.S

Tab. 6. – Effect of Conversation Tillage Systems on Soil bulk density (2012-2013 growing season)

		T1	T2	T3	T4	CV	LSD	Sign.
After tillage	0-10	1.305	1.304	1.306	1.287			N.S
	10-20	1.296	1.288	1.303	1.309	1.214	1.021	**
	20-30	1.309	1.299	1.308	1.311			N.S
After harvest	0-10	1.307	1.298	1.294	1.305			N.S
	10-20	1.295	1.308	1.300	1.305			N.S
	20-30	1.295	1.309	1.284	1.311	1.678	0.265	***

For After tillage operation, the lowest soil bulk density (1.28 g.cm^{-3}) was recorded in soil tilled with T2 at 10-20 cm soil depths and for after harvesting operation, the lowest soil bulk density (1.284 g.cm^{-3}) was recorded in soil tilled with T3 at 20-30 cm soil depths. BARZEGAR ET AL. (2003) also observed significant differences in soil bulk density among tillage practices and these results are in agreement with RASHİDİ AND KESHAVARZPOUR (2008), KARAYEL AND OZMERZİ (2003).

Soil bulk porosity

Soil porosity as a function of depth (0-30 cm) and conversation tillage systems are shown in Tab. 7, after the tillage and harvesting operation during 2012-2103 the second growing period of maize.

Tab. 7. – Effect of Conversation Tillage Systems on Soil porosity (2012-2013 growing season)

		T1	T2	T3	T4	CV	LSD	Sign.
After tillage	0-10	0.420	0.420	0.423	0.423	-	-	N.S
	10-20	0.427	0.450	0.443	0.417	-	-	N.S
	20-30	0.417	0.420	0.417	0.427	-	-	N.S
After harvest	0-10	0.433	0.430	0.430	0.431	-	-	N.S
	10-20	0.413	0.440	0.423	0.430	-	-	N.S
	20-30	0.427	0.430	0.417	0.420	-	-	N.S

The result of the soil samples analyses in terms of soil porosity after tillage operation and harvest operation are shown for four different conversation tillage system in Tab. 3. As you see, the porosity of samples at 0-30 cm soil dept was over 40% for all tillage systems. There was no significant different statistically among soil porosities of tillage systems in all depths at after tillage operation and harvesting operation. After tillage operation, the lowest soil porosity (41.7 %) was recorded in soil tilled with T1 and T3 at 20-30 cm soil depths. After harvest operation, the lowest soil porosity (41.3 %) was found in soil tilled with T1 at 10-20 cm soil depths. The similar results were determined by BARUT AND AKBOLAT (2005) and OZPİNAR AND CAY (2005).

Soil penetration resistance

The result of penetration different point in the field in terms of soil penetration resistance After tillage operation and harvesting operation are explained for different conversation tillahe system in 2012-2013 growing season in Fig. 1 ve Fig. 2.

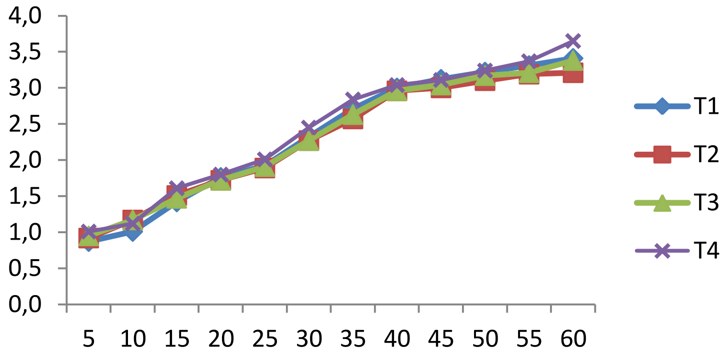

Fig. 1. – Soil penetration resistance (0-60 cm) before tillage harvesting operation

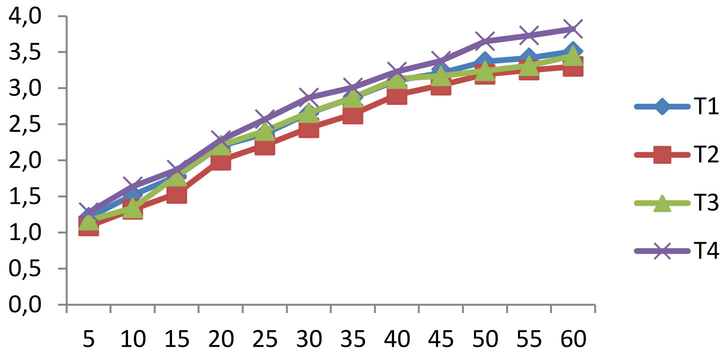

Fig. 2. – Soil penetration resistance (0-60 cm) after harvesting operation

As you see in Tab. 4, soil penetration resistance for all tillage system increase with soil depth (0-60 cm). After tillage operation, the highest soil penetration resistance (3.65 and 3.41 MPa) was recorded in soil tilled with T4 and then T1 at 0-60 cm soil depths, respectively. After harvesting operation, the highest soil penetration resistance (3.82 and 3.51 MPa) was found in soil tilled with T4 and then T1 at 0-60 cm soil depths, respectively. OSUNBİTAN ET AL. (2004) reported that soil penetration resistance for different tillage methods increased with soil dept. For variation though conversation tillage methods, tillage methods X measuring time, tillage methods X depth and tillage methods X measuring time X depth interactions were significant statistically for four tillage systems ($p<0.001$).

CONCLUSIONS

As a result of study, conversation tillage system significantly affected soil penetration resistance, dry bulk density, moisture content in all depths at after tillage and harvesting operation. There was no significant different statistically among soil porosities of tillage systems in all depths at after tillage and harvest operation. For variation though conversation tillage methods, tillage methods X measuring time, tillage methods X depth and tillage methods X measuring time X depth interactions were significant statistically for four tillage systems ($p<0.001$). The no tillage system produced the highest soil penetration resistance both after tillage and harvesting operation in 0-60 cm soil depth.

REFERENCES

1. BARUT, Z. B., AKBOLAT, D.: Evaluation of conventional and conversation tillage systems for maize. J. Agron., 4, 2005:122-126.
2. BARZEGAR, A. R., ASOODAR, M. A., KHADISH, A., HASHEMI, A. M., HERBERT, S. J.: Soil physical characteristics and chickpea yield responses to tillage treatments. Soil and Tillage Research, 71, 2003: 49-57.
3. BLACK, C. A., EVANS, D. D., WHITE, J. L., ENSMINAGER, L. E., CLARK, F. E.: Method of soil analysis, Part 1, Physical and mineralogical properties, including statistics of measurement and sampling. American Society of Agronomy Inc. Publisher, Madison, U.S.A 1965.
4. BOYDAS, M. G., TURGUT, N.: Effect of tillage implements and operating speeds on soil physical properties and wheat

emergence. Turkish Journal of Agriculture and Forestry, 31, 2007: 399–412.
5. BUSCHIAZZO, D. E., PANIGATTI, J. L., UNGER, P. W.: Tillage effect on soil properties and crop production in subhumid and semiarid Argentinean Pampas. Soil and Tillage Research, 49, 1998: 105-116.
6. CANNELL, R. Q.: Reduced tillage in north-west Europe - A review. Soil & Tillage Research, 5, 1985: 129-177
7. CRUSE, R. M., LINDEN, D. R.: A model to predict tillage effects on soil temperature. Soil Science Society of America Journal, 44, 1980: 378-383.
8. DAVIES, B., FINNEY, B.: Reduced cultivations for cereals: Research, development and advisory needs under changing economic circumstances. Home Grown Cereals Authority, London 2002.
9. GAJRI, P. R., ARORA, V. K., PRIHAR, S. S.: Tillage for sustainable cropping. Food Products Press, New York 2002.
10. JORDAHL, J. L., KARLEN, D. L.: Comparison of alternative farming system. III. Soil aggregate stability. American Journal of Alternative Agriculture, 8, 1993: 27-33.
11. KARAYEL, D., OZMERZİ, A.: Effect of different seedbed preparation methods on physical properties of soil. Agricultural Mechanization in Asia, 34, 2003: 9–11.
12. LAL, R.: Tillage and agricultural sustainability. Soil and Tillage Research, 20, 1991: 133-146.
13. MIELKE, L. N., WILHELM, W. W.: Comparisons of soil physical characteristics in long-term tillage, winter wheat-fallow tillage experiments. Soil and Tillage Research, 49, 1998: 29-35.
14. OSUNBITAN, J. A., OYEDELE, D. J., ADEKALU, K. O.: Tillage effects on bulk density, hydraulica conductivity and strength of a loamy sand soil in Southwestern Nigeria. Soil Tillage Res., 2004:57-64
15. OZPINAR, S., CAY, A.: Effect of minimum and conventional tillage system on soil properties and yield of winter wheat in clay-loam in the Canakkale region. Turk J. Agric. Forest., 29, 2005: 9-18.
16. RASHIDI, M., KESHAVARZPOUR, F.: Effect of different tillage methods on soil physical properties and crop yield of mellon (*Cucumis melo*). Journal of Agricultural and Biological Sciences, 3(1), 2008: 41–46.
17. SHRESTHA, A., CLEMENTS, D. R.: Emerging trends in cropping systems research. J.Crop Prod., 8, 2003: 1-32.
18. TAPELA, M., COLVIN, T. S.: Quantifying seedbed condition using soil physical properties. Soil and Tillage Research, 64, 2002: 203-210.
19. XU, D., MERMOUD, A.: Topsoil properties as affected by tillage practices in north China. Soil and Tillage Research, 60, 2001: 11-19.

Corresponding author:
Onder KABAS, Akdeniz University, Vocational School of Technical Science, Antalya, Turkey, e-mail: onderkabas@hotmail.com

PREDICTION OF PRESSURE AND ENERGY REQUIREMENT OF *JATROPHA CURCAS* L BULK SEEDS UNDER NON-LINEAR PRESSING

A. Kabutey[1], D. Herák[1], J. Hanuš[2], R. Chotěborský[3], O. Dajbych[1], R. Sigalingging[4], O. L. Akangbe[1]

[1]*Department of Mechanical Engineering, Faculty of Engineering, Czech University of Life Sciences Prague, Czech Republic*
[2]*Department of Material Sciences and Manufacturing Technology Faculty of Engineering, , Czech University of Life Sciences Prague, Czech Republic*
[3]*Farmet Company, Česká Skalice, Czech Republic*
[4]*Department of Agricultural Engineering, Faculty of Agriculture, University of Sumatera Utara, Medan, Indonesia*

Abstract
This article presents the theoretical evaluation of pressure and energy requirement of screw press FL 200 (Farmet Model, Czech Republic) for oil processing of *Jatropha curcas* L. bulk oilseeds. Both the linear and non-linear compression information were analysed. The tangent curve mathematical model was applied which is appropriate for fitting of linear experimental data as the dependency between compressive force and deformation in relation to bulk seeds pressing height and vessel diameter. The integral of the tangent model represents energy. The non-linear pressing involving a mechanical screw press FL 200 geometric parameters namely screw shaft diameter (mm), inner and outer diameters (mm), screw thickness (mm) and screw pitch diameter (mm) were incorporated into the tangent curve mathematical model. The press designed with 44 lamellas at the oil outlet were divided into seven pressing sections or chambers. The determined amounts of pressure and energy substantially increased along the pressing sections. The results require validation to confirm the suitability of the tangent curve mathematical model for optimising the performance of screw press FL 200.

Key words: compression, screw press configuration, mathematical model, optimization.

INTRODUCTION

Despite the considerable studies on the optimization of mechanical screw presses for oil extraction of oilseed crops such as jatropha, further research is still necessary to improve the mechanical process regarding pressure and energy demand for oil recovery efficiency as stated by DELI ET AL. (2011), HARMANTO ET AL. (2009) and SINGH AND BARGALE (2000). The general hypothesis is that higher pressure produces higher temperature and oil percentage as described in the studies of KARAJ AND MULLER (2011) and WILLEMS ET AL. (2008, 2009). BEERENS (2007), however, indicated that increasing temperature thus affects the quality of the oil by increasing the amount of phospholipids contained in the oil. Determining the specific pressure and energy along the screw pressing sections could reduce temperature increment during oil extraction. To achieve this objective, it is important to understand the linear compression of bulk oilseeds, where considerable studies have been described by the authors DIVISOVA ET AL. (2014), STUART AND MUNSON-MCGEE (2014), HERAK ET AL. (2013, 2014, 2015) and KABUTEY ET AL. (2012, 2013).

HERAK ET AL. (2012, 2013A) and SIGALINGGING ET AL. (2014A) have drawn the attention to the applicability of the tangent curve mathematical model for describing the mechanical behaviour and deformation curve characteristics of jatropha, rape, sunflower and other bulk oilseeds under compression loading. The Mathcad 14 software with Levenberg-Marquardt algorithm for data fitting is optimal for the tangent curve approximation according to PRITCHARD (1998). The advantage of the Mathcad software is that it does not require high memory computer for more rigorous algorithm compared to other simulation programmes like finite element method as reported by PETRU ET AL. (2012). Furthermore, as stated by HERAK ET AL. (2013) and SIGALINGGING ET AL. (2014) the use of the tangent curve mathematical model takes into account the boundary conditions of the linear compression test which are: when the compressive force is approaching infinity the deformation reaches a maximum limit, zero compressive force relates to zero deformation and the integral of the tangent curve function describes the energy.

HERAK ET AL. (2013A) and SIGALINGGING ET AL. (2014, 2015) described the tangent model as given by equation (Eq. 1):

$$F(x,D,H) = C \cdot D^2 \cdot \left[\tan\left(G \cdot \frac{x}{H} \right) \right]^2 \quad (1)$$

Where: $F(x,D,H)$ is the compressive force (N) as a function of deformation, x (mm),the vessel diameter, D (mm) and pressing height, H (mm), C is the stress coefficient of mechanical behaviour (N·mm^{-2}), G is the compression coefficient (-), $\frac{x}{H}$ is the strain or compression ratio (-). The stress and compression coefficients have been in detail discussed in the study published by HERAK ET AL. (2013A). The objective of the study was to determine theoretically the amounts of pressure and energy in each of the screw pressing chambers for oil extraction of *Jatropha curcas* L. bulk oilseeds by combining both the tangent curve mathematical model and screw press FL 200 geometric characteristics.

MATERIALS AND METHODS

Sample and compression test

The results of jatropha bulk seeds of moisture content 10 % (w. b.) published by HERAK ET AL. (2013A) and KABUTEY ET AL. (2013) were further processed. In those studies, varying pressing heights of 30, 40 50, 60, 70 and 80 mm and vessel diameters of 60, 80 and 100 mm (Fig. 2) at maximum force 100 kN and speed 1 mm·s^{-1} were investigated. In linear pressing, the bulk material is compressed in a pressing vessel by applying a specific compressive force and speed using a Universal Testing Machine. The pressing vessel contains holes beneath which allow the oil leakage whiles the pressed solids are retained as indicated by HERAK ET AL. (2013), KABUTEY ET AL. (2013) and MUNSON-MCGEE (2014). The increasing force results in the deformation of the bulk material which can be described as the dependency between the pressing force and deformation (Fig. 1) where the area under the curve is denoted as the deformation energy as defined by DIVIŠOVÁ ET AL. (2014), HERAK ET AL. (2013A) AND KABUTEY (2014).

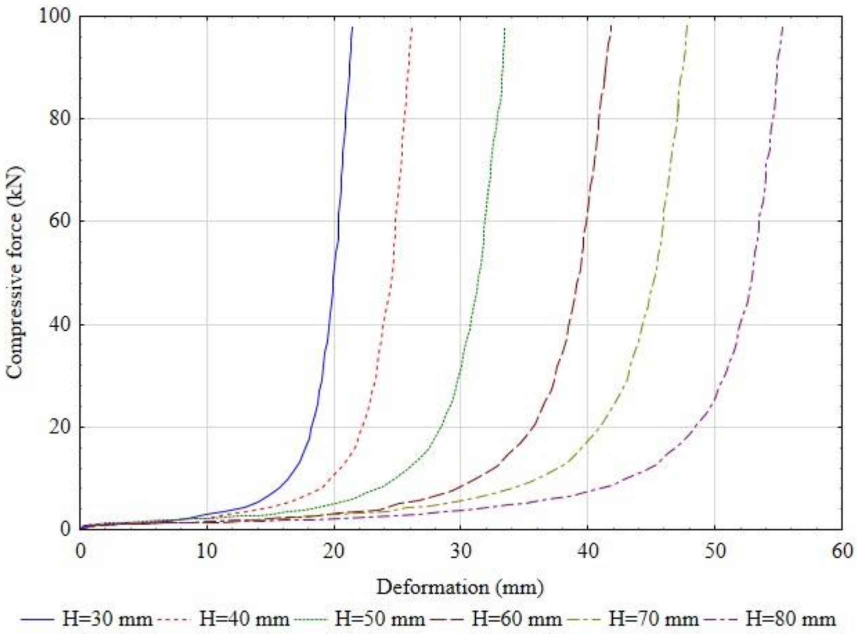

Fig. 1. – Dependency between compressive force and deformation curves for different pressing heights of jatropha bulk seeds for vessel diameter 60 mm similar to diameters 80 and 100 mm given by HERAK ET AL. (2013A) AND KABUTEY ET AL. (2013)

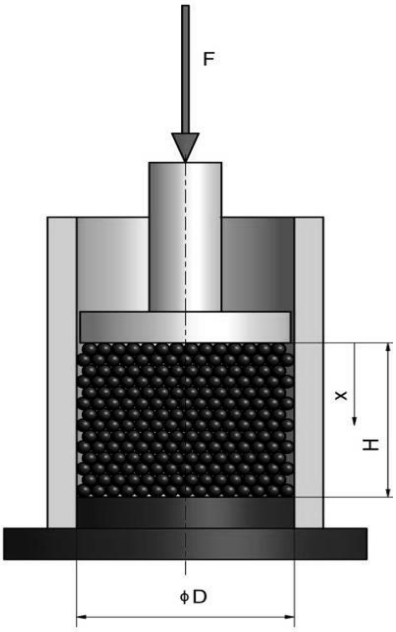

Fig. 2. – Schematic of pressing vessel diameter

Screw press FL 200 and principles of operation

The mechanical screw press FL 200 (Farmet model, Czech Republic) was examined. The press designed with 44 lamellas at the oil outlet were divided into seven pressing sections as shown in Fig. 3. The press parameters include throughput 180 kg·hr^{-1}, input power 16 kW, length 2120 mm, width 640 mm, height 840 mm and weight 930 kg. The press speed can be controlled between 25 and 40 min^{-1}. Specific parameters of press FL 200 namely the screw pitch diameter P_T (mm), screw thickness T_K (mm) and screw shaft inner and outer diameters (mm) were used for the theoretical calculations of pressure. The screw pitch diameters are represented here as screw pressing sections as 0, 1, 2, 3, 4, 5, 6 and 7 respectively. Screw pitch is the distance from a point of one thread to the corresponding point of the next measured parallel to the axis as described by the authors HERAK ET AL. (2010) AND KHURMI AND GUPTA (2005). Mathematically, the screw pitch for the screw shaft (Fig 4) is given by equation (Eq. 2).

$$P = \pi \cdot D \cdot tg\alpha \tag{2}$$

where P is the screw pitch (mm), D is the diameter of the screw pitch (mm) and α is the pitch angle (◦).

Accurate dimensions of the screw press during the design phase are relevant for optimal performance according to KHURMI AND GUPTA (2005), DELI ET AL. (2011) AND BARYEH (2001). Operationally, the screw rotates around a nut with corresponding helical grooves on the internal surface. When the nut remains stationary the screw rotates and translates axially; and vice versa. The contact surfaces will eventually produce friction which requires power to be overcome. However, the power demand of the the screw and nut connection will be lower than the actual power utilization. The screw thread and nut groove contact surfaces are perpendicular to the outside and inside cylindrical surfaces which keep coefficient of friction at a lower rate. SINGH AND BARGALE (2000) AND KARAJ AND MULLER (2011) indicated that during the mechanical oil extraction, bulk oilseeds are fed through the hopper continuously into the screw press where they are compressed under high pressure, for instance, at 35 MPa which ruptures the cell walls causing the oil globules to escape allowing the oil through the slits provided along the screw. The compressed solids are continuously discharged through a choke given at the end of the press.

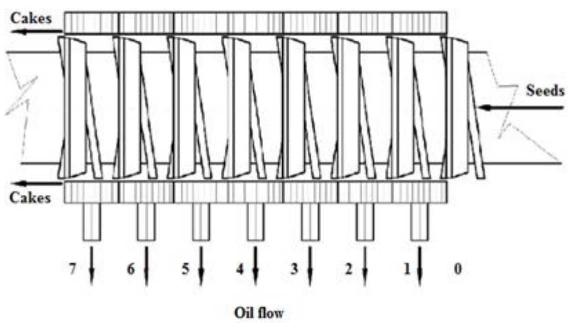

Fig. 3. – Schematic of screw press FL 200 (KABUTEY ET AL., 2010)

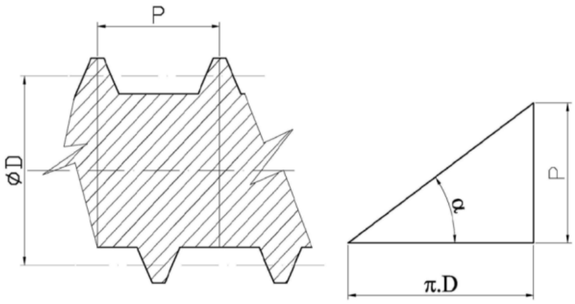

Fig. 4. – Schematic of screw shaft (HERAK ET AL., 2010)

Theoretical calculations

Screw press volume of material

The volume expression of bulk jatropha seeds in the screw press was calculated using (Eq. 3):

$$V_T = \left[\frac{\pi}{4} \cdot D_O^2 - \left[\left(\frac{D_1 + D_2}{2}\right)^2\right] - \left(P_T - T_K\right)\right] \tag{3}$$

Where V_T is the theoretical volume of bulk seeds (m^3), P_T is the screw pitch diameter (mm), T_K is the screw thickness (mm), D_O is the screw shaft diameter (mm), D_1 is the screw inner diameter (mm), D_2 is the screw outer diameter (mm).

Initial bulk seeds height

Using (Eq. 4) the initial height of bulk seeds was determined.

$$H_{BK_i} = \left[\frac{V_T \cdot 4}{\pi \cdot D^2}\right] \tag{4}$$

Where H_{BK} is the bulk seeds height (mm), D is the pressing vessel diameter (mm) (Fig. 2).

Bulk seeds deformation

This was determined as the difference between bulk seeds initial and final pressing height(Eq. 5).

$$D_T = \left[H_{BK_i} - H_{BK_f}\right] \tag{5}$$

Where D_T is the theoretical deformation (mm), H_{BK_i} is the initial height of bulk seeds (mm) and H_{BK_f} is the final height of bulk seeds (mm).

Compression ratio

This was determined as the ratio of deformation (Eq. 5) to initial bulk seeds height (Eq. 4).

$$C_R = \left[\frac{D_T}{H_{BK_i}}\right] \tag{6}$$

Where C_R is the compression ratio (-).

Compressive force

The compressive force was determined using the modified form of (Eq. 1) as described in (Eq. 7).

$$F(x, D, H) = C \cdot D^2 \cdot \left[\tan\left(G \cdot \frac{C_R}{f}\right)\right]^2 \tag{7}$$

Where f expresses the coefficient of pressing factors and/or screw press configuration (-).

Pressure

The pressure (Eq. 8) was determined combining Eq. 7 and 9 respectively.

$$P_T = \left[\frac{F}{A_S}\right] \tag{8}$$

$$A_S = \left[\frac{\pi}{4} \cdot D_O^2 - \left[\left(\frac{D_1 + D_2}{2}\right)\right]^2\right] \tag{9}$$

Where P_T is the theoretical pressure, F is the compressive force (N) (Eq. 1 or Eq. 7) and A_S is the cross-sectional area of the screw press (m^2).

Energy

The integral of the tangent curve model (Eq. 1 or Eq. 7) represents energy (Eq. 10)

$$E_T = \int C \cdot D^2 \cdot \tan\left(G \cdot \frac{x}{H}\right)^2 dx \rightarrow \frac{C \cdot D^2 \cdot H \cdot \left(\tan\left(\frac{G \cdot C_R}{f}\right) - \frac{G \cdot C_R}{f}\right)}{G} \tag{10}$$

Where E_T is the theoretical energy (J).

RESULTS AND DISCUSSION

The initial height (mm), deformation (mm), compression ratio (-) and volume (mm^3) of bulk jatropha seeds are given in Tab. 1, 2 and 3 respectively. These parameters were considered for the theoretical analysis of pressure and energy requirements using the tangent curve mathematical models (Eqs. 1, 7 and 10). The ratio of deformation to initial bulk seeds pressing height describing the strain is related to the compression ratio. The compression ratio influences the performance of the screw press as reported by SINGH AND BARGALE (2000). It is defined as the ratio of volume of material displaced per revolution of the shaft at the feed section to the volume displaced at the choke section. SINGH AND BARGALE (2000) again stated that compression ratios higher than the theoretical values of high oil content seeds are used to compensate for slip and rotation of meal with respect to the screw shaft. The volume of material that is processed through the pressing sections or screw length is related to the throughput within a given time which should be largest at the beginning of the pressing and smallest at the end.

Tab. 1. – Determined amounts of Jatropha bulk seeds using vessel diameter 60 mm

*Pressingsections (-)	Initalheight (mm)	Deformation (mm)	Compression ratio (-)	Volume ($\cdot 10^3$ mm^3)
0	144.18	144.18	0.00	408
1	85.75	58.43	0.41	242
2	44.39	99.79	0.69	126
3	41.96	102.22	0.71	119
4	37.02	107.16	0.74	105
5	34.52	109.66	0.76	98
6	28.17	116.01	0.80	80
7	19.06	125.12	0.87	54

Tab. 2. – Determined amounts of Jatropha bulk seeds using vessel diameter 80 mm

Pressing-sections (-)	Initalheight (mm)	Deformation (mm)	Compression ratio (-)	Volume ($\cdot 10^3$ mm^3)
0	81.10	81.10	0.00	408
1	48.23	32.87	0.41	242
2	24.97	56.13	0.69	126
3	23.60	57.50	0.71	119
4	20.82	60.28	0.74	105
5	19.42	61.68	0.76	98
6	15.85	65.25	0.80	80
7	10.72	70.38	0.87	54

Tab. 3. – Determined amounts of Jatropha bulk seeds using vessel diameter

Pressing-sections (-)	Initalheight (mm)	Deformation (mm)	Compression ratio (-)	Volume ($\cdot 10^3$ mm^3)
0	51.91	51.91	0.00	408
1	30.87	21.04	0.41	242
2	15.98	35.93	0.69	126
3	15.10	36.80	0.71	119
4	13.33	38.58	0.74	105
5	12.43	39.48	0.76	98
6	10.14	41.75	0.80	80
7	6.86	45.05	0.87	54

* Each screw pressing section has a specific pitch diameter (mm)

The theoretical amounts of pressure and energy are shown in Tab. 4 and illustrated in Fig. 5 and 6.Clearly, the pressing vessel diameter has great influence on the tangent curve model, that is, the change of the vessel diameter directly affects the other coefficients of the model. However, this change does not influence the compression ratio or strain. Therefore, using the tangent curve model for each pressing vessel diameter of 60, 80 and 100; pressure increased from 0.34 to 51.74 MPa, 0.42 to 50.71 MPa and 0.58 to 48.53 MPa along the pressing chambers.Similarly, energy increased from 12.22 to 330.47 J, 7.76 to 191.68 J and 6.32 to 132.55 J. Since oil yield in screw press is directly related to higher pressure and higher energy then the vessel diameter 60 mm becomes a constant variable of the tangent curve model for the evaluation of pressure and energy in a screw press. The lowest amount of energy obtained by the vessel diameter 100 mm suggests lower oil recovery efficiency, higher oil residue in press cake and higher material throughput as published by KARAJ AND MULLER (2011).

In the screw press, DELI, ET AL. (2011), HARMANTO ET AL. (2009) and KARAJ AND MULLER (2011) observed that the increasing pressure thus produces the output oil. However, higher pressure thus increase the friction and temperature between the bulk material and the press which adversely affects the cake and quality of the oil as noticed by BEERENS (2007) and SINGH AND BARGALE (2000). The screw press FL 200 design or configuration characteristics might have also contributed to the pressure or energy increment along the pressing chambers. This can be related to the results of DELI ET AL. (2011) who compared both the smaller and bigger screw shaft diameters in terms of pressure, rotational speed and percentage oil yield. They observed that the smaller screw shaft provided much smaller space for the compression of the seeds resulting in higher pressure compared to the bigger screw shaft diameter which required bigger space for the seeds to be filled hence lower pressure towards the bulk seeds which subsequently affected speed and oil yield.

Tab. 4. – Theorectical amounts of *Jatropha curcas* L. bulk seeds of screw press FL 200

Screw-sections (-)	**Force (kN)**	**Pressure (MPa)**	**Energy (J)**	***Cumulative amounts***		
				Force (kN)	***Pressure (MPa)***	***Energy (J)***
Vessel diameter 60 mm (*f* =1.42)						
0	0.00	0.00	0.00	0.00	0.00	0.00
1	1.65	0.34	12.22	1.65	0.34	12.22
2	8.97	2.86	45.10	10.62	3.20	57.32
3	9.99	3.37	47.38	20.61	6.57	104.70
4	12.51	4.78	51.81	33.12	11.35	156.51
5	14.11	5.78	53.95	47.23	17.13	210.46
6	19.50	9.79	58.58	66.73	26.92	269.04
7	33.43	24.82	61.44	**100.16**	**51.74**	**330.48**
Vessel diameter 80 mm (*f* =1.55)						
0	0.00	0.00	0.00	0.00	0.00	0.00
1	2.01	0.42	7.76	2.01	0.42	7.76
2	9.91	3.16	27.08	11.92	3.58	34.84
3	10.91	3.68	28.27	22.83	7.26	63.12
4	13.32	5.09	30.49	36.15	12.35	93.60
5	14.79	6.06	31.50	50.94	18.41	125.01
6	19.50	9.79	33.36	70.44	28.20	158.46
7	30.32	22.51	33.22	**100.76**	**50.71**	**191.68**
Vessel diameter 100 mm (*f* =1.74)						
0	0.00	0.00	0.00	0.00	0.00	0.00
1	2.79	0.58	6.32	2.79	0.58	6.32
2	11.33	3.61	19.76	14.12	4.19	26.08
3	12.23	4.12	20.39	26.35	8.31	46.47
4	14.27	5.46	21.47	40.62	13.77	67.94
5	15.45	6.33	21.87	56.07	20.10	89.81
6	18.91	9.49	22.23	74.98	29.59	112.03
7	25.51	18.94	20.52	**100.49**	**48.53**	**132.55**

f is the coefficient of pressing factors (determined by considering the maximum force applied in Eq. 1)

The pressing factors function described in equations (Eq. 7 and Eq. 10) also explain but not limited to the following; the friction between the pressing vessel and bulk seeds, applied compressive force, speed, temperature, biological status of the bulk material in terms of quality of bulk seeds and moisture content and screw press design or configuration. These parameters could also influence the tangent curve mathematical model coefficients for accurate evaluation of pressure or compressive force and energy needs in both linear and non-linear pressing. For example, KARAJ AND MULLER (2011) mentioned that higher screw speed requires higher material throughput and higher oil content residue in press cake since less time is available for the oil to drain from the solids. In addition, the viscosity at higher speed reamins lower resulting in lower pressure build-up hence more oil content in press cake as established by BEERENS (2007), KARAJ AND MULLER (2011) and WILLEMS ET AL. (2008, 2009). FABORADE AND FAVIER (1996) as well as DELI ET AL. (2011) referred that the increase of temperature might reduce the moisture content of the seeds causing reduction of oil yield. On the other hand, BARYEH (2001) stated that the quality of bulk seeds, moisture content and screw press configuration could contribute to lower oil yield.

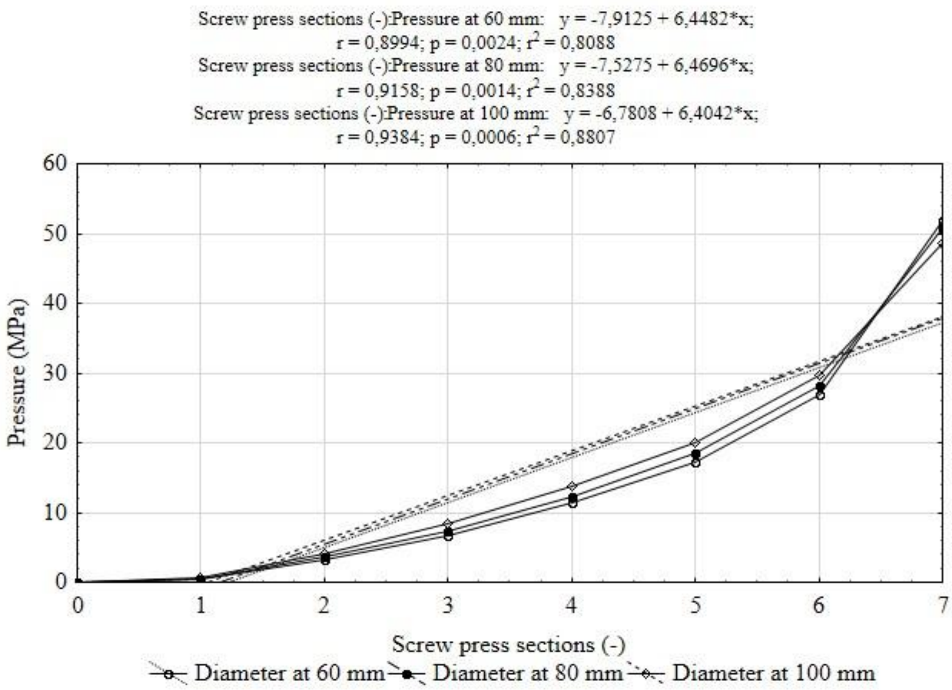

Fig. 5. – Pressure requirement at screw pressing sections of varying vessel diameters applying the tangent model (Eq. 8 and 9)

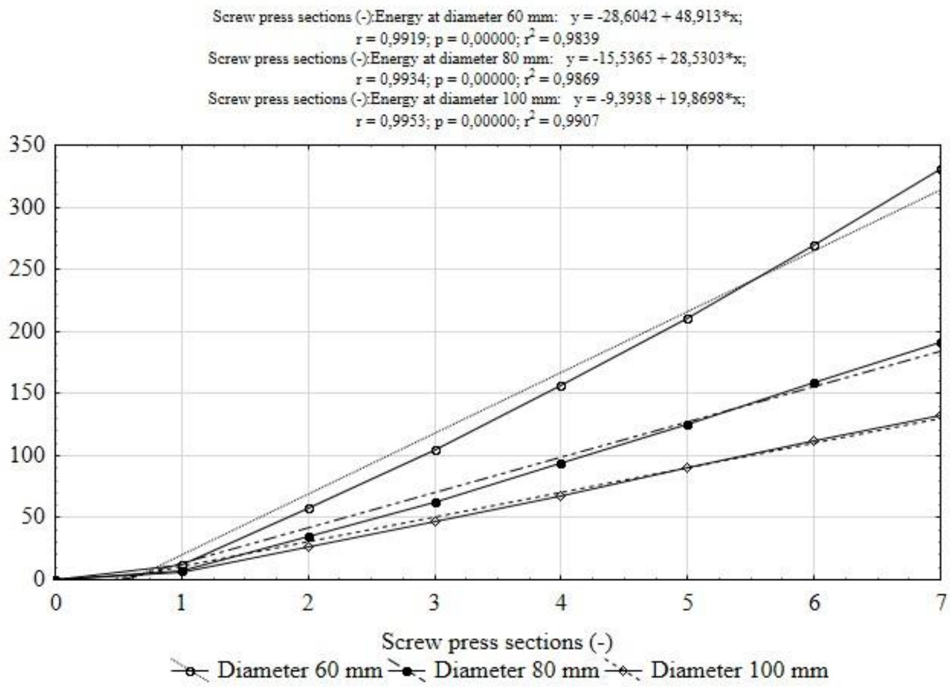

Fig. 6. – Energy requirement at screw pressing sections of varying vessel diameters applying the tangent model (Eq. 10)

CONCLUSIONS

Determining the specific pressure and energy would improve the press performance in terms of oil recovery efficiency. The findings provided herein can be useful for engineers and scientists in design and development of mechanical oil presses. However, the results require validation to establish the suitability of the tangent curve mathematical model for optimising pressure and energy utilization. The pressing factors should be incorporated into further mathematical models.

Acknowledgement

The authors would like to thank the support of Ing. Jiří Hanuš, Ph.D., Head of Research and Development, Farmet Company, Česká Skalice, Czech Republic.

REFERENCES

1. BARYEH, E. A.: Effect of palm oil processing parameters on yield. J. Food Eng., 48, 2001: 1–6.
2. BEERENS, P.: Screw-pressing of Jatropha seeds for fuelling purposes in less developed countries [MSc. Thesis.] Department of Sustainable Energy Technology, Eindhoven University of Technology, 2007, 87 p.
3. DELI, S., FARAH MASTURAH, M., TAJUL ARIS, Y., WAN NADIAH, W. A.: The effects of physical parameters of the screw press oil expeller on oil yield from Nigella sativa L. seeds. Int. Food. Res. J., 18, 2011: 1367–1373.
4. DIVIŠOVÁ, M., HERÁK, D., KABUTEY, A., ŠLEGER, V., SIGALINGGIN, R., SVATOŇOVÁ, T.: Deformation curve characteristics of rapeseeds and sunflower seeds under compression loading. Sci. Agric. Bohemica., 45, 2014: 180–186.
5. HARMANTO, A., HENDRIADI, E., RAHMARESTIA, M., WIYONO., J.: Performance test of a screw-press machine for extracting Jatropha curcas seed into crude oil as an alternative energy source. Ind. J. Agric, 2, 2009: 35–40.
6. HERÁK, D., GURDIL, G., SEDLACEK, A., DAJBYCH, O., SIMANJUNTAK, S.: Energy demands for pressing Jatropha curcas L. seeds. Biosyst. Eng., 106, 2010: 527–534.
7. HERAK, D., SEDLACEK, A., KABUTEY, A.: Determination of the complete geometry of the worm extruder screwline for compressive pressing of the oil bearings crops. In: Trends in Agricultural Engineering, 7th September 2010, pp. 207–210, Prague, Czech Republic.
8. HERÁK, D., KABUTEY, A., DIVISOVA, M., SIMANJUNTAK, S.: Mathematical model of mechanical behaviour of Jatropha curcas L. seeds under compression loading. Biosyst. Eng., 114, 2013a: 279–288.
9. HERAK, D., KABUTEY, A., PETRU, M., HRABE, P., LEPSIK, P., SIMANJUNTAK, S.: Relaxation behaviour of Jatropha curcas L. seeds under compression loading, Biosyst. Eng., 125, 2014: 17–23.
10. HERAK, D., KABUTEY, A., CHOTEBORSKY, R., PETRU, M., SIGALINGGING, R.: Mathematical models describing the relaxation behaviour of Jatropha curcas L. bulk seeds under axial compression, Biosyst. Eng., 131, 2015: 77–83.
11. KABUTEY, A., HERAK, D., HANUS, J.: Screw press performance for oil extraction from Jatropha curcas L. seeds of different moisture content. Sci. Agric. Bohemica., 41, 2010: 225–230.
12. KABUTEY, A., HERAK, D., CHOTĚBORSKÝ, R., DAJBYCH, O., DIVIŠOVA, M., BOATRI, W. E.: Linear pressing analysis of Jatropha curcas L. seeds using different pressing vessel diameters and seed pressing heights. Biosyst. Eng., 115, 2013: 43–49.
13. KABUTEY, A.: Optimizing the use of screw presses for processing oilseed crops [Ph.D. Dissertation] Department of Mechanical Engineering, Czech University of Life Sciences Prague, Czech Republic, 2014, 1–155pp.
14. KARAJ, S., MULLER, J.: Optimizing mechanical oil extraction of Jatropha curcas L. seeds with respect to press capacity, oil recovery and energy efficiency. Ind. Crops Prod., 34, 2011: 1010–1016.
15. KHURMI, R. S., GUPTA J. K..: A textbook of machine design, 1st Multicolour Edition, Eurasia publishing house (PVT.) Ltd. Ram Nagar, New Delhi 2005.
16. MUNSON-MCGEE, S. H.: D-optimal experimental designs for uniaxial expression, J. Food Process Eng., 37, 2014: 248–256.
17. PETRŮ, M., NOVÁK, O., HERÁK, D., SIMANJUNTAK, S.: Finite element method model of the mechanical behaviour of Jatropha curcas L. seed under compression loading. Biosyst. Eng., 111, 2012: 412–421.
18. PRITCHARD, P. J.: Mathcad: A tool for engineering problem solving. McGraw-Hill Science Engineering, New York 1998.
19. SIGALINGGING, R., HERAK, D., KABUTEY, A., CESMIR, M., DIVISOVA, M.: Tangent curve function description of mechanical behaviour of bulk oilseeds: A review; Sci. Agric. Bohemica., 45, 2014: 259–264.
20. SINGH, J., BARGALE, P. C.: Development of a small capacity double stage compression screw press for oil expression. J. Food Eng., 43, 2000: 75-82.
21. STUART, H., MUNSON-MCGEE.: D-optimal experimental designs for uniaxial expression. J. Food Process Eng., 37, 2014: 248–256.
22. WILLEMS, P., KUIPERS, N. J. M., HAAH DE, A. B.: Hydraulic pressing of oilseeds: Experimental determination and modeling of yield and pressing rates, J. Food Eng., 89, 2008: 8 –16.
23. WILLEMS, P., KUIPERS, N. J. M., HAAH DE, A. B.: A consolidation based extruder model to explore GAME process configurations, J. Food Eng., 90, 2009: 238–245.

Corresponding author:

Ing. Abraham Kabutey, Ph.D, Department of Mechanical Engineering, Faculty of Engineering, Czech University of Life Sciences Prague, Kamýcká 129, Praha 6, Prague, 16521, Czech Republic, phone: +420 22438 3180, e-mail: kabutey@tf.czu.cz

REDUCING FIELD PERMEABILITY AND WATER INPUT WITH SURFACE COMPACTION IN DRY SEEDED RICE FIELD

H. Kammuri, R. Otani

National Agriculture and Food Research Organization, Tohoku Agricultural Research Center, Akahira 4, Shimo-Kuriyagawa, Morioka, Iwatae, JAPAN

Abstract

For development of a water-saving dry seeded rice production method (DSR), observations of water consumption of a DSR with and without compaction of the dry paddy field were conducted to clarify the water use reduction effects of soil compaction. Saturated hydraulic conductivity decreased to 4.9×10^{-5} cm s^{-1} by soil compaction with a Cambridge-roller in the field with compaction (CO). Water requirements decreased to 7 mm d^{-1}, which is lower than the value of 21 mm d^{-1} obtained for a Non-compacted field (NC). Amounts of irrigation water used for the growing season in CO were 1255 mm, which was 62% of water used for NC. Results show that preparation of a low-permeability layer near the field surface is effective to conserve irrigation water, thereby increasing water productivity. This DSR method with compaction is useful for coping with irrigation water supply variation that might occur with climate change.

Key words: dry seeded rice with compaction, hydraulic conductivity, water requirement, water productivity.

INTRODUCTION

Dry seeded rice production (DSR) systems are necessary for Japanese agriculture to reduce labor and production costs related to rice cultivation. Recently, reduction of rice production costs is necessary for Japanese rice farmers to compete with imported low-cost rice. The traditional puddled and transplanted rice production system (TPR) accounts for over 95% of Japanese rice production. The method requires puddling, raising of young rice plants, and their transplantation, which entail much labor and higher costs. TPR has generally higher production costs. Therefore, changing cultivating methods from TPR to DSR is expected to be necessary at some point.

The former DSR methods could not be conducted in highly permeable paddy rice fields because the former DSR methods could not prevent water seepage or deep percolation. In these paddy rice fields, farmers had to use TPR with puddling to cope with water seepage. Mainly for that reason, farmers in Japan have been reluctant or unable to adopt DSR in such paddy rice fields.

Recently, we developed a new DSR method that includes compaction of dry paddy fields to prevent water seepage and deep percolation. This new method is expected to replace traditional planting methods with DSR (OTANI ET AL., 2013).

Reportedly, DSR can conserve more irrigation water used for rice cultivation than TPR can (KUMAR AND LADHA, 2011). Some parts of Japan need efficient water usage to accommodate temporary water shortages that occur during the rice transplanting season. In addition, the possibility of water shortages deriving from climate change has been increasing, thereby threatening rice production sustainability. As in other countries, water shortages pose serious risks to food security. Therefore, enhancing the water productivity of rice is crucially important.

From these perspectives, new methods that use little irrigation water and less labor input for rice production must be sought. Observations of water consumption at DSR with and without compaction of dry paddy fields were conducted to clarify the effects of water use reduction through soil compaction.

MATERIALS AND METHODS

1) Site description

Experiments were conducted during the growing season in 2015 at rice paddy fields (38°09', 141°54') in Miyagi prefecture, Japan. Two test plots were set (Fig. 1): a 2.2 ha rice paddy field cultivated using DSR with compaction (CO), and a 0.3 ha rice paddy field cultivated using DSR with no compaction (NC). The soil properties and the values of saturated hydraulic conductivity in the subsoil are presented in Fig. 2. The topsoil of the experiment site was light clay. The plastic limit value and liquid limit value of topsoil were, respectively, 35.9% and 63.8%.

The subsoil, which affects deep percolation, was mostly in an aerobic condition, with saturated hydraulic conductivity of 1.7×10^{-3} cm s^{-1}, 1.4×10^{-3} cm s^{-1}, 5.9×10^{-4} cm s^{-1}, respectively, at 40 cm below in CO, 60 cm below in CO, and 60 cm below in NC.

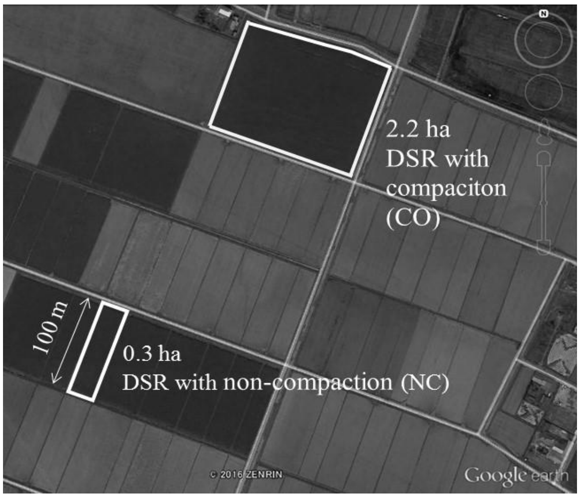

Fig. 1. – Locations of test plots (Added to Google Earth)

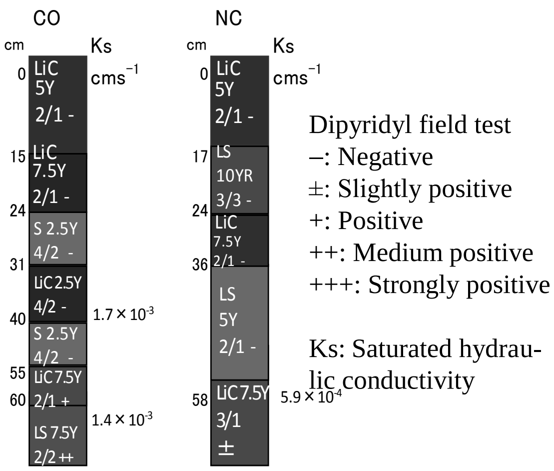

Fig. 2. – Profile description of CO and NC

2) Field management

Field management conducted in both CO and NC is presented Tab. 1 and Fig. 3. CO was tilled with a chisel plow and was compacted using a Cambridge-roller before seeding. Weight of the Cambridge-roller was 3700 kg with 5.3 m working width. Rice was seeded using a grain drill seeder. After seeding, the field surface was compacted again with the Cambridge-roller. Each compaction practice was counted one time for the entire field, compacted with one direction of working. CO was compacted once before seeding and twice after seeding: it was compacted three times, in all.

Actually, NC was tilled with a rotary cultivator before seeding. Seeds were sown by a seeder with an attached reverse rotary cultivator used simultaneously to break soil clods. In this seeding method, the NC field was not compacted in the entire field as with CO: only a part of the soil near seeds was compacted with a small and light roller attached with each seeder individually. Both plots were flooded after standing of rice seedlings. Thereafter, herbicides were applied in both plots. Flooding continued to mid-September in CO. In contrast, NC remained flooded except for about two weeks from July 2 through July 14.

3) Data collection

a) Soil hardness in the field

Using a digital cone penetrometer (DIK-5531; Daiki Rika Kogyo Co. Ltd.), soil hardness of the field profile was measured vertically from the field surface after compaction in CO or after seeding in NC. A top angle of the cone was 30°with 2 cm^2 section area.

b) Soil moisture content

Soil samples from CO were collected at depths of 0–5 cm and of 5–10 cm with a 100 ml stainless steel sampling tube to confirm soil moisture conditions under soil compaction working. Six soil samples were collected from each depth in CO. Soil moisture contents were measured from these samples drying at 105°C over 24 h.

c) Saturated hydraulic conductivity

The Cambridge-roller breaks up clods of soil by a protuberance at the outer circumference of the roller. It compacts the seedbed by the weight of the roller. As a result of compaction, about 0–5 cm in the seedbed becomes soft. The underlying 5 cm of soil texture turns to hard pan with reduced permeability to water. Therefore, undisturbed soils were sampled from 5–10 cm in seedbed with 100 ml stainless steel sampling tube for saturated water permeability tests to confirm the reduction of permeability by compaction. Samples were collected from 10 points in CO and 3 points in NC.

d) Water requirement

Water levels of both plots were measured using the water level meter (S&DL mini; OYO Corp.) to record the water requirement: consumption of water in the plot in a day. The water requirement consists of vertical or deep percolation to subsoil, lateral percolation or seepage through a levee, evaporation, and transpiration. Water level meters were set at two points in CO and at one point in NC. The data were recorded to a data logger at intervals of one hour.

e) Irrigation water applied

The amount of irrigation water supplied to NC was measured using a water flow meter (SA065GMS; Aichi Tokei Denki Corp.) set at the water inlet in NC. The water level meter (UIZ-WLR; Uizin) was set to measure the irrigation water input to CO at an open irrigation channel connected to CO. The amount of irrigation water for CO was calculated using the Manning Formula with water level data at the irrigation channel and the average gradient of the channel. The irrigation water was expressed in depth of millimeters to be divided observed water volumes by the area of each plot. The supplied irrigation water was measured during the pre-establishment period and during the rice growing season in both plots. The irrigation water was needed during the pre-establishment period to promote germination under dry climate conditions and to prevent formation of a soil crust that hinders seedling emergence.

f) Grain yield

The yield of brown rice in the whole plot with over 1.9 mm thickness was measured in both plots. The grain yield with rice-husks was calculated conveniently by dividing the brown rice yield with a 0.8 ripening rate and a 0.8 rice-husk rate.

g) Weather data

Rainfall data were collected from AMeDAS, operated by Japan Meteorological Agency, observed at the nearest point to our study site, where was about 1.8km far from it.

a) Compaction in CO b) Seeding in CO c) Seeding in NC

Fig. 3. – Working practice in CO and NC

Tab. 1. – Working practice in CO and NC

a) CO

Date	Working practice	Equipment
16-Mar	Tillage	Chisel plow Kongskilde HSF250 Tractor FENDT 415 vario(103 kW)
9-Apr	Compaction	Cambridge-roller DALBO MAXROLL530* Tractor Kubota M135A (99 kW)
	Seeding	Grain-drill AMAZONE D9-30 Tractor FENDT 415 vario (103 kW)
28-May	Flooding	
		*Weight: 3700 kg, Working width: 5.3 m

b) NC

Date	Working practice	Equipment
28-Mar	Tillage	Rotary cultivator Kubota RM220Z Tractor Kubota MZ65 (48 kW)
11-May	Seeding	Reverse rotary cultivator Nipro BUR2010U Seeder Agritecno Yazaki TDR-2CE Tractor Kubota MZ65 (48 kW)
26-May	Flooding	

RESULTS

1) Soil water contents under compaction work

Soil water contents after compaction work are portrayed in Fig. 4. Soil water contents of 0–5 cm in CO were 37.5%. Soil water contents in 5–10 cm were higher than those of 0–5 cm. Compaction working was conducted without soil adhering to the surface of the Cambridge-roller under such soil water conditions.

2) Soil hardness

Fig. 5 shows soil hardness in both plots. The hardest layer was observed at 5 cm below the field surface in CO. NC did not have such a hard layer in 0–15 cm.

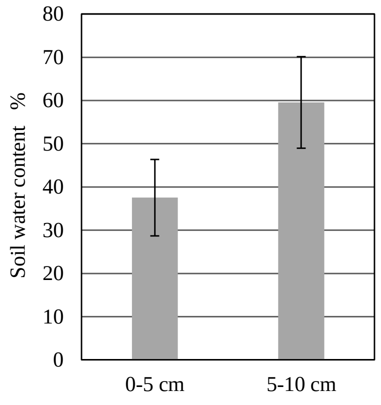

Fig. 4. – Soil water content at compaction working

3) Saturated hydraulic conductivity

Fig. 6 shows the saturated hydraulic conductivity in a logarithmic value of 5–10 cm of both plots. The average values of saturated hydraulic conductivity in CO and NC were -4.31 and -1.76, which were respectively equal to 4.9×10^{-5} cm s^{-1} and 1.7×10^{-2} cm s^{-1} in real value. The value of saturated hydraulic conductivity that is equivalent to our target value of water requirement 20 mm d^{-1} was 2.3×10^{-5} cm s^{-1}. The value of saturated hydraulic conductivity in NC was significantly higher (1.7×10^{-2} cm s^{-1}) than that value in CO of 4.9×10^{-5} cm s^{-1} and our target value.

4) Water requirement and irrigation water applied

The water requirements in CO and NC were 7 mm d^{-1} and 22 mm d^{-1}; that of NC was three times greater than that of CO (Fig. 7). The amounts of irrigation water inputted to both plots to promote an emergence of rice seedling are shown in Fig. 8. Before emergence, 209 mm of irrigation water was applied to CO to prevent soil crust formation on the field surface. In NC, 96 mm irrigation water was used before emergence. Cumulative irrigation water in the whole rice growing season before maturity is shown in Fig. 8. In CO with lower saturated hydraulic conductivity at the field surface than NC (Fig. 6), the amount of irrigation water during the whole season was 1225 mm, which was about 60% of 2019 mm in NC.

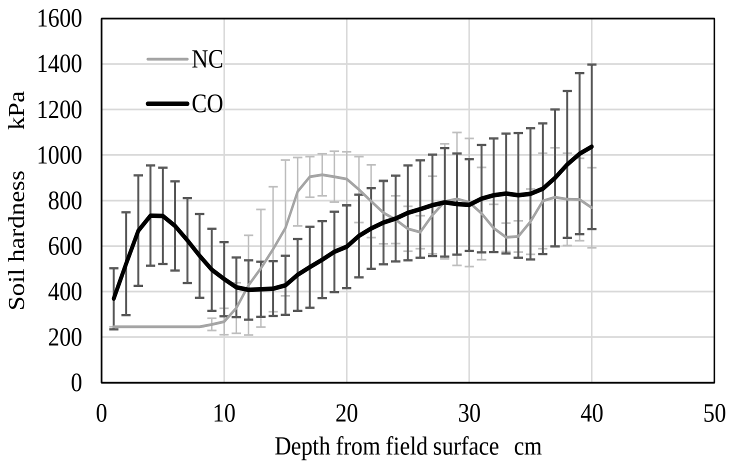

Fig. 5. – Soil hardness of field profile

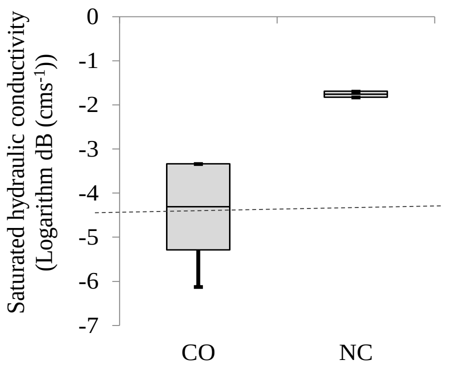

Fig. 6. – Saturated hydraulic conductivity
*Broken line signifies our target value of -4.6: water requirement 20 mm d^{-1}: 2.3×10^{-5} cm s^{-1}

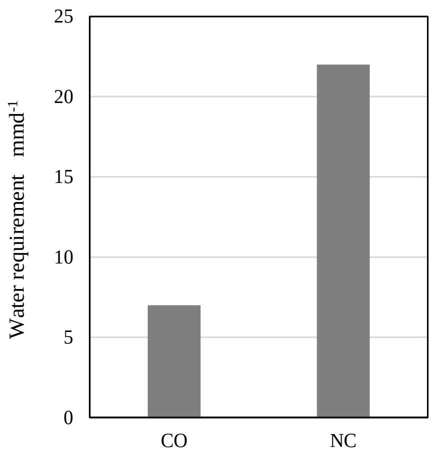

Fig. 7. – Water requirement

DISCUSSION

1) Reduction of permeability with soil compaction.

Regarding soil water condition under soil compaction, KANMURI ET AL. (2015) reported that soil permeability tends to decrease concomitantly with increased soil moisture at compaction working. For compaction with a Cambridge-roller, compaction will be impossible in high soil moisture conditions on field surfaces because of adherence of high-water-content soil to the roller. In this study, water contents of surface soil (0–5 cm) in the CO were 37.5% (Fig. 4), which is nearly equal to the soil plastic limit value of 35.9%, allowing compaction with a roller. Soil moisture under 5 cm from the field surface was 59.6%, which was slightly lower than the value of the soil liquid limit of 63.8%. That was a sufficient soil water condition to reduce soil permeability. Conducting compaction work under high soil water conditions is important to reduce the DSR field permeability.

2) Saturated hydraulic conductivity

When the value of the saturated hydraulic conductivity was calculated from the value of water consumption in both plots investigated in this study, CO and NC were 8.1×10^{-6} cm s^{-1} and 2.5×10^{-5} cm s^{-1}, respectively. The value of CO was similar to the observed value of 4.9×10^{-5} cm s^{-1} (Fig. 6), which was apparently derived from the low permeability layer formed by compaction. The corn index of the layer measured the saturated hydraulic conductivity was the highest of the field profile according to Fig. 5. At that layer, soil density of the layer was enhanced by compaction with increasing of cone index. As the result, the saturated hydraulic conductivity seemed to decrease enough to reduce the water consumption.

The value of NC was lower than the observed value of 1.7×10^{-2} cm s^{-1}. In this case, because no layer existed to reduce deep percolation at the field surface, it was regarded as affected directly by in-situ permeability in subsoil.

3) Saving irrigation water and increasing water productivity

The amount of water use during the growing season in CO was 1046 mm. That for NC was 1923 mm. The total value including flushing water used for emergence of rice plants in CO was estimated as 1225 mm, which was 62% of the NC value of 2019 mm. Compaction working in DSR can conserve about 40% of irrigation water. In the field conditions of high-permeability at the subsoil layer such as our test fields, making a low-permeability layer near the field surface is expected to be quite effective for irrigation water conservation.

From the viewpoint of demand for irrigation water, puddling practices for transplanting of rice are not conducted in DSR. Therefore irrigation water for puddling can be eliminated from DSR calculations. LIU ET AL. (2015) reported that DSR used 15.3% less water than transplanted flooded rice. Based on these results, DSR can decentralize the peak period of irrigation water use by farmers at the beginning of the rice growing and transplanting season.

The grain yield of CO was 7.9 t ha^{-1}, which is higher than that of NC 6.2 t ha^{-1} (Tab. 2). The prevailing aerobic conditions during the period without irrigation water might lose nitrogen from the field in NC, which is regarded as one factor contributing to lower grain yield than that of CO.

Water productivity in CO was 0.5 kg m^{-3}, which is 190% higher than NC of 0.26 kg m^{-3}, which resulted from the greater amount of water used in NC than in CO. KATO ET AL. (2009) reported water productivity measured in Japan as a value from 0.45 to 0.58 by some varieties with DSR cultivation under flooded conditions after seedling establishment. Our value of water productivity is similar to that value. However, the water productivity decreases concomitantly with the increase of the water input in NC. Therefore, reduction of deep percolation and seepage is needed. In addition to enhanced water productivity, irrigation water should be saved without decreasing the grain yield. CABANGON ET AL. (2002) pointed out that although DSR was able to conserve irrigation water, the lower yield of DSR than TPR presents an important consideration for farmers conducting DSR. The control of permeability in DSR fields with field surface compaction is expected to be useful to avoid low yields caused by failure of weed control and by runoff of nitrogen.

Saving irrigation water can provide increased water production in areas where irrigation water is short or limited. In other areas, it is considered that the DSR method with conservation of irrigation water enhances the rice cultivation area.

Tab. 2. – Yield and water productivity.

	brown rice yield	grain yield	irrigation	total water	IWP	WP
	t ha^{-1}	t ha^{-1}	mm	mm	kg m^{-3}	kg m^{-3}
CO	5.1	7.9	1255	1590	0.63	0.50
NC	4.0	6.2	2019	2354	0.31	0.26

*IWP: Water productivity for irrigation water
*WP: Water productivity for total water

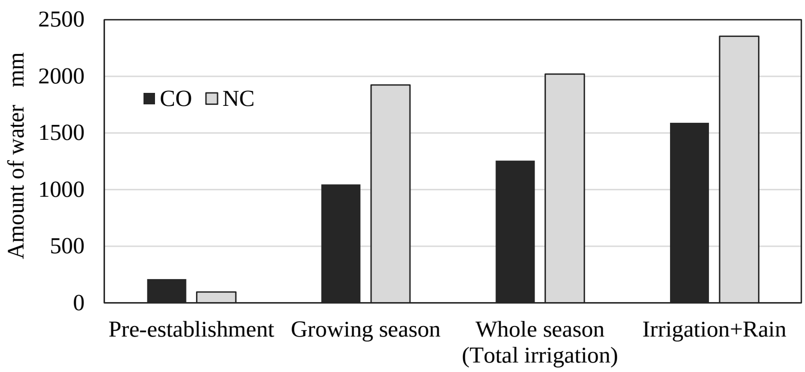

Fig. 8. – Amount of water used in each season

CONCLUSIONS

Effects of water saving on DSR with compaction were revealed by investigating the characteristics of paddy rice fields and amounts of irrigation water in fields with or without compaction working in DSR fields. Saturated hydraulic conductivity decreased to 4.9×10^{-5} cm s^{-1} by compacting soil with a Cambridge-roller in the CO plot. Water requirements decreased to 7 mm d^{-1}, which is lower than the Non-compacted plot value of 21 mm d^{-1}. The amount of irrigation water used for the growing season in CO was about 1255 mm, which was 62% of that in NC. The water productivity in CO increased in 67% compared with NC. Results show that field surface compaction reduces the amount of irrigation water, which increases water productivity. This DSR cultivation method is useful for coping with the variation of supply in irrigation water during an era of climate change.

ACKNOWLEDGEMENT

This research was conducted as a research project of "Advanced technology development for reproduce of food production area" with financial assistance by Japan Reconstruction Agency and Ministry of Agriculture, Forestry and Fisheries.

REFERENCES

1. CABANGON, R. J., TUONG, T. P., ABDULLAH, N. B.: Comparing water input and water productivity of transplanted and direct-seeded rice production systems. Agric. Water Manage., 57, 2002: 11–31.
2. KANMURI, H., OTANI, R., SEKIYA, H., NAKAYAMA, S., SAITO, H.: Permeability Reduction Caused by Surface Compaction in Large Dry Paddy Fields under Direct-seeding Rice Cultivation. Jpn. J. Farm Work Res., 165, 2015: 103–114 (in Japanese, Abstract in English).
3. KATO, Y.; OKAMI, M.; KATSURA, K.: Yield potential and water use efficiency of aerobic rice (Oryza sativa L.) in Japan. Field Crops Research, 113 (3), 2009: 328–334.
4. KUMAR, V., LADHA, J. K.: Direct Seeding of Rice: Recent Developments and Future Research Needs. Advances in Agronomy, 111, 2011: 297–413.
5. LIU, H., HUSSAIN, S., ZHENG, M., PENG, S., HUANG, J., CUI, K., NIE, L.: Dry direct-seeded rice as an alternative to transplanted-flooded rice in Central China. Agronomy for Sustainable Development, 35(1), 2015: 285–294.
6. OTANI, R., SEKIYA, H., KANMURI, H., NAKAYAMA, S., SAITO, H.: Crop Rotation System of Three-Crop per Two-Year utilizing Dry Direct-Seeding of Rice with Plowing in Large Scale Paddy Field. J. Jap. Agricultural Machinery, 75(4), 2013: 220–224 (in Japanese).

Corresponding author:

Hideaki Kammuri, National Agriculture and Food Research Organization, Tohoku Agricultural Research Center, Akahira 4, Shimo-Kuriyagawa, Morioka, Iwatae, JAPAN

GENETIC OPERATORS EFFECT ON STACKING SEQUENCE OPTIMIZATION

F. Karaçam

Department of Mechanical Engineering, Trakya University, Edirne, Turkey

Abstract

In the study, stacking sequence optimization of a composite beam is carried out for various boundary conditions. Genetic algorithm (GA) is used as an optimization technique and genetic operators such as crossover and mutation ratio are changed throughout the optimization process. In the minimization of deflection parameters due to the corresponding stacking sequences, the effect of genetic operators are investigated for various boundary conditions, number of layers and fiber angle increments. A unified shear deformation theory is used in analytical solution. Minimum deflection parameters and corresponding stacking sequences are compared with the analytical solution. The variation of deflection parameters with respect to the number of generation are presented for different crossover and mutation ratios.

Key words: composite beam, deflection, genetic algorithm, optimization.

INTRODUCTION

Composite materials have gained popularity in modern structures that need to be light-weight and yet strong enough to carry various loading types for different boundary conditions. Because of high elasticity modulus and strength, composite materials are popular than any conventional materials, besides, by changing the design parameters such as stacking sequence, geometrical properties, matrix and fiber materials, structures can be designed variously in order to satisfy the desired mechanical properties. Too many design parameters in optimization problem will bring about too many solutions with it. Instead of dealing with the whole possible solutions and obtain the optimum, using an evolutionary optimization technique would be inevitable. Genetic algorithm is widely used in the design of laminated composite structures with too many variables and different fitness functions. LOPEZ ET AL. (2009) developed a GA to pursue the optimization of hybrid laminated composite structures. They considered the fiber orientation, material and total number of plies as design variables and investigated the maximum stresses. SCIUVA ET AL. (2003), optimized the stacking sequences by genetic algorithm in order to obtain the minimum buckling load and minimum weight. LEE ET AL. (2012), used a parallel evolutionary algorithm in multi-objective optimization of the stacking sequences in composite plates by choosing fiber type, thickness and orientation angles as design parameters for each layer. ALMEIDA AND AWRUCH (2009), used GA in the optimization of composite structures by using genetic operators effectively in the design process and compared the results with the ones obtained by a finite element method. BRIGHENTI (2005), investigated the optimum fiber orientation of fiber reinforced composite materials in order to optimize a certain fitness function by use of GA.

In this study, on the basis of a unified shear deformation beam theory, the minimum deflection parameters and corresponding stacking sequences are obtained for various boundary conditions and compared with the ones obtained by GA. The variation of deflection parameters with respect to the number of generations are illustrated for different crossover and mutation ratios.

MATERIALS AND METHODS

During the optimization process, a beam with rectangular cross-section, unit width, length of "L", thickness of "h" is considered (Fig. 1). The coordinate system is placed in the mid-plane where $0 \leq x \leq L$ and $-h/2 \leq z \leq h/2$. The beam is assumed to be constructed of linearly elastic layers and under of a uniform distributed transverse load "$q(x)$" on its top plane.

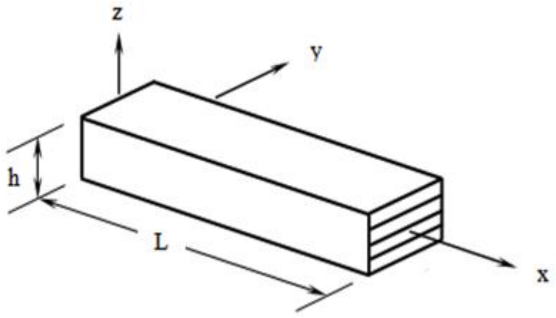

Fig. 1. – Beam geometry and coordinate axis

A uniform shear deformation beam theory is used at which classical and shear deformation theories can be obtained as a special case by use of a shape function. The displacement fields used are in parallel with general shear deformation theory (SOLDATOS AND TIMARCI, 1993) and given as follows:

$$U(x,z) = u(x) - z\, w_{,x} + \emptyset(z)\, u_1(x) \qquad W(x,z) = w(x) \tag{1}$$

The terms of "U" and "W" represent the displacement fields with respect to x and z axis where "u", "u_1" and "w" represent the displacement fields of the mid-plane. ",x" denotes the differentiation with respect to x. "$\emptyset(z)$" is the shape function and chosen as a cubic function of layer thickness (KARAÇAM, 2005). The displacement fields to the following kinematic relations:

$$\varepsilon_x = u_{,x} - z w_{,xx} + z\left(1 - \frac{4z^2}{3h^2}\right) u_{1,x} \qquad \gamma_{xz} = \left(1 - \frac{4z^2}{h^2}\right) u_1 \tag{2}$$

Hooke's Law for the stresses of each k[th] layer is given as follows:

$$\begin{bmatrix} \sigma_x^{(k)} \\ \tau_{xz}^{(k)} \end{bmatrix} = \begin{bmatrix} Q_{11}^{(k)} & 0 \\ 0 & Q_{55}^{(k)} \end{bmatrix} \begin{bmatrix} \varepsilon_x \\ \gamma_{xz} \end{bmatrix} \tag{3}$$

The terms of "$Q_{ij}^{(k)}$" are the transformed reduced stiffnesses depending on material properties such as elasticity modulus (E_{ij}), shear modulus (G_{ij}) and Poisson ratio (υ_{ij}) (JONES, 1975). Using stress-strain relations into force and moment definitions (TIMARCI AND SOLDATOS, 1995), the constitutive equations are obtained as follows:

$$\begin{bmatrix} N_x \\ M_x \\ M_x^a \end{bmatrix} = \begin{bmatrix} A_{11} & B_{11} & B_{111} \\ B_{11} & D_{11} & D_{111} \\ B_{111} & D_{111} & D_{1111} \end{bmatrix} \begin{bmatrix} u_{,x} \\ -w_{,xx} \\ u_{1,x} \end{bmatrix}, \qquad Q_x^a = A_{55}\, u_1 \tag{4}$$

The superscript "a" stands for the shear deformation effects. "A_{ij}", "B_{ij}" and "D_{ij}" are the material rigidities that correspond to extensional, coupling and bending rigidities respectively. Rigidities with more than two indices correspond to shear deformation beam theories where the ones with two indices correspond to classical beam theories. "Q_x^a" is the resultant force. The governing equations used in the analysis of a laminated composite beam under a uniform distributed load are given as follows:

$$N_{x,x} = 0 \qquad M_{x,xx} = q(x) \qquad M_{x,x}^a - Q_x^a = 0 \tag{5}$$

By use of constitutive equations into the governing equations, a set of differential equations and their derivatives depending on material rigidities and displacement functions are obtained as follows:

$$\begin{aligned} &A_{11}u_{,xx} - B_{11}w_{,xxx} + B_{111}u_{1,xx} = 0 \\ &B_{11}u_{,xxx} - D_{11}w_{,xxxx} + D_{111}u_{1,xxx} = q(x) \\ &B_{111}u_{,xx} - D_{111}w_{,xxx} + D_{1111}u_{1,xx} - A_{55}u_1 = 0 \end{aligned} \tag{6}$$

Boundary conditions at both edges of the beam when x=0 and x=L are given respectively for simply supported, cantilever and free cases (SOLDATOS AND TIMARCI, 1993):

$$\begin{aligned} &N_x = w = M_x = M_x^a = 0 \\ &u = w = w_{,x} = u_1 = 0 \\ &N_x = M_x = M_{x,x} = M_x^a = 0 \end{aligned} \tag{7}$$

By integrating and solving equations simultaneously and using the boundary conditions at both edges, three unknown displacement functions are obtained with eight integration constants (C_k). The displacement functions are given as below:

$$\begin{aligned} u_1(x) &= C_1 e^{-px} + C_2 e^{px} - (qx + C_3)\frac{D_{111}}{A_{55}D_{11}} = 0 \\ u(x) &= -\frac{B_{111}}{A_{11}} u_1(x) + C_7 x + C_8 = 0 \\ w(x) &= \frac{D_{111}}{pD_{11}}\left[-C_1 e^{-px} + C_2 e^{px} - \frac{p}{A_{55}}\left(\frac{qx^2}{2} + C_3 x\right)\right] + \frac{1}{D_{11}}\left(\frac{qx^4}{24} + C_3\frac{x^3}{6}\right) + C_4\frac{x^2}{2} + C_5 x + C_6 = 0 \end{aligned} \tag{8}$$

$$p = \sqrt{\frac{-A_{55}A_{11}D_{11}}{D_{111}^2 A_{11} - D_{1111}A_{11}D_{11}}}$$

In the study, genetic algorithm is used as an optimization technique. Genetic algorithm is an evolutionary optimization technique using Darwin's principal of "survival of the fittest". It's a guided random search technique that works on a population of designs. The principals of GA are firstly proposed by HOLLAND

(1995) in optimization problems. Early applications of GA to structural optimization are due to GOLDBERG (1989) and HAJELA (1990). GA starts with a random initial population of possible design alternatives. If the population is suitably large enough, GA is not at the risk of being stuck in a local optimum (GHIASI ET AL., 2009). They are also derivative-free optimization methods as they don't need functional derivative information. By using such algorithms in the optimization, robustness and flexibility can easily be obtained (GOLDBERG, 1989). A major limitation of traditional GA's, especially in larger populations, is the time waste to distinguish the convenient fitness function. In order to prevent this, genetic operators such as reproduction, crossover and mutation are applied to the algorithm. In the optimization process, stacking sequences are used as the design parameters. Initially, fiber orientation angles of each layer are coded in order to build up the stacking sequences of composite beam which also correspond to the chromosomes of each generation in GA. After the coding operation, a random population of stacking sequences which is also called as the initial population is generated. Reproduction is the first genetic operator used in genetic algorithm at which the population is generated and ranked depending on the design parameters. Besides, by use of elitism in reproduction, the quality of the population can be increased by copying the best individuals of each generation into the next generation. Then crossover is applied to generate new individuals by swapping one or more genes which correspond to the fiber orientation angle of a chromosome. Mutation is another genetic operator used in GA. It's generally used to maintain the genetic diversity from one generation to another. It basically depends on altering one or more genes of a chromosome among the population. The mutation ratio is generally chosen between 0.01 and 0.001 in order to prevent the negative influence (GOLDBERG, 1989). The genetic operators are applied until the stopping criteria or the targeted value is obtained. A simple genetic algorithm flowchart is given in Fig. 2.

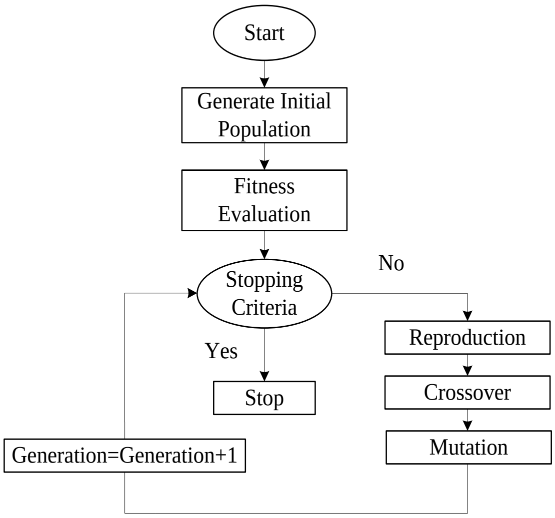

Fig. 2. – A simple genetic algorithm flowchart

RESULTS AND DISCUSSION

In the study, in order to ensure the reliability of the theory used, the deflection parameters are compared with KHDEIR AND REDDY (1997) for classical and parabolic shear deformation beam theories initially. In Tab. 1, non-dimensional deflection parameters are presented for classical and parabolic shear deformation beam theories and various boundary conditions. For parabolic shear deformation beam theory, the results are very close to reference values for clamped-clamped (C-C) and simply supported (S-S) boundary conditions and the same for clamped-free (C-F) boundary condition. As for the classical beam theory, all of the non-dimensional deflection parameters are the same with reference values.

Tab. 1. – Non-dimensional deflection parameters for various boundary conditions

L/h	Theory	C-C		C-F		S-S	
		Model	Ref.	Model	Ref.	Model	Ref.
10	PSDT	0.5316	0.5320	3.4550	3.4550	1.0663	1.0960
	CBT	0.1290	0.1290	2.1980	2.1980	0.6460	0.6460
50	PSDT	0.1469	0.1470	2.2510	2.2510	0.6645	0.6650
	CBT	0.1290	0.1290	2.1980	2.1980	0.6460	0.6460

In the study presented, the composite beam is assumed to be constructed of graphite/epoxy and under of a uniform distributed load where $q(x)$=1000 N/m. Mechanical properties of graphite/epoxy are given as follows (KARAMA ET AL., 2003):

$$E_{11}=241.5 \text{ GPa}, E_{22}=E_{33}=18.89 \text{ GPa}$$
$$G_{23}=3.45 \text{ GPa}, G_{12}=G_{13}=5.18 \text{ GPa} \quad (9)$$
$$\upsilon_{23}=0.25, \upsilon_{12}=\upsilon_{13}=0.24$$

The population is considered to be consisted of 100 individuals and fiber orientation angles (θ) are assumed to be changing with an increment of 10° and 30° where 0° ≤ θ ≤ 90°. The minimization of the deflection parameter is carried out at certain points of the beam for various boundary conditions where the maximum deflections may occur. For C-C and S-S boundary conditions, the deflection parameters are calculated in the middle of beam where $x=L/2$ and for (C-F) boundary condition at the free edge of the beam where $x=L$.

Tab. 2. – The minimum deflection parameters and corresponding stacking sequences for various boundary conditions and number of layers

Boundary Conditions	Number of Layers	Exact Solution		GA Solution	
		w (×10^{-5}) [m]	Stacking Sequence	w (×10^{-5}) [m]	Stacking Sequence
C-C	3	1.7523	0°/0°/0°	1.7523	0°/0°/0°
C-F		49.5405	0°/90°/90°	49.5405	0°/90°/90°
S-S		10.2264	0°/0°/30°	10.2264	0°/0°/30°
C-C	4	1.7523	0°/0°/0°/0°	1.7523	0°/0°/0°/0°
C-F		47.8485	0°/60°/60°/30°	47.8485	0°/60°/60°/30°
S-S		8.4360	0°/0°/30°/0°	8.4360	0°/0°/30°/0°
C-C	5	1.6772	0°/30°/90°/30°/30°	1.6772	0°/30°/90°/30°/30°
C-F		35.7074	0°/0°/90°/90°/30°	35.7074	0°/0°/90°/90°/30°
S-S		8.5742	0°/0°/0°/30°/0°	8.5742	0°/0°/0°/30°/0°

Tab. 3. – The minimum deflection parameters and corresponding stacking sequences for various boundary conditions and number of layers

Boundary Conditions	Number of Layers	Exact Solution		GA Solution	
		w (×10^{-5}) [m]	Stacking Sequence	w (×10^{-5}) [m]	Stacking Sequence
C-C	3	1.7523	0°/0°/0°	1.7523	0°/0°/0°
C-F		42.8886	0°/70°/40°	42.8886	0°/70°/40°
S-S		8.4238	0°/0°/10°	8.4238	0°/0°/10°
C-C	4	0.9943	0°/10°/70°/30°	0.9943	0°/10°/70°/30°
C-F		35.9179	0°/0°/70°/20°	35.9179	0°/0°/70°/20°
S-S		8.2277	0°/0°/10°/0°	8.2277	0°/0°/10°/0°
C-C	5	0.0110	40°/0°/30°/60°/90°	0.0365	0°/70°/40°/50°/70°
C-F		31.9941	0°/0°/70°/90°/20°	31.9941	0°/0°/70°/90°/20°
S-S		8.2456	0°/0°/0°/10°/0°	8.2456	0°/0°/0°/10°/0°

After a random initial population being generated, the deflection parameters with corresponding stacking sequences are ranked from minimum to maximum along 50 generation. After 50th generation, the minimum deflection parameters and corresponding stacking sequences are obtained for various boundary conditions. In Tab. 2 and Tab. 3, minimum deflection parameters (w) and corresponding stacking sequences are given for various boundary conditions and number of layers respectively. In Tab. 2, the fiber orientation

angles are changed with an increment of 30° and the deflection parameters obtained by genetic algorithm are compared with the exact solution. For all boundary conditions and number of layers, the identical deflection parameters are obtained for both exact and GA solution.
In Tab. 3, the fiber orientation angles are changed with an increment of 10°. Although the results are identical for 3 and 4 number of layers for both solution, there is a minor difference in deflection parameters for 5 number of layers due to the excessive number of possible stacking sequences. The convergence to minimum can be increased by an efficient use of genetic operators or a convenient number of population and generation.

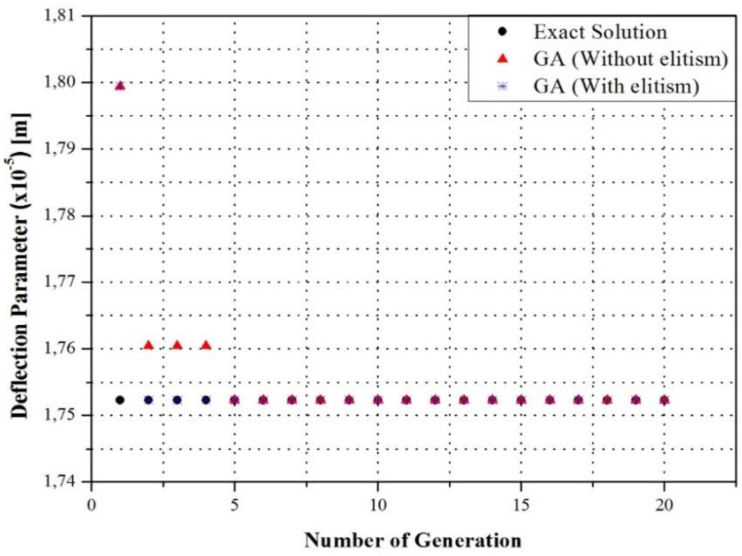

Fig. 3. – The variation of deflection parameters with respect to the generation for C-C

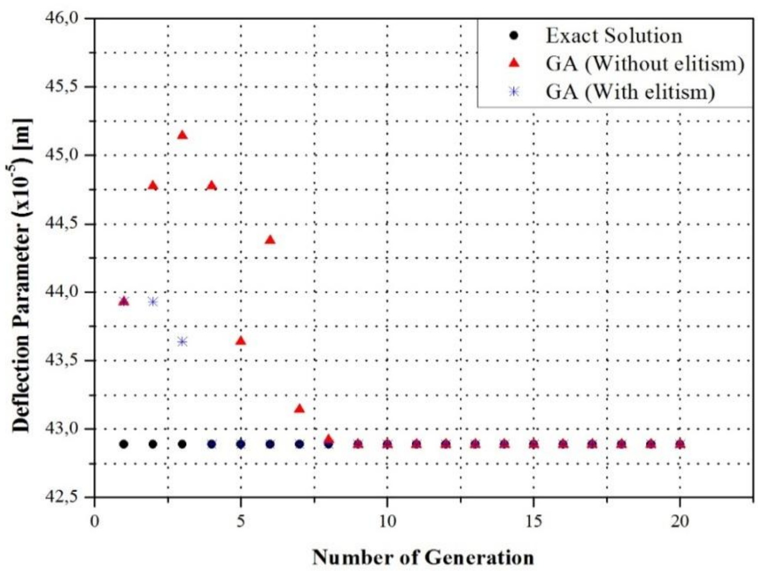

Fig. 4. – The variation of deflection parameters with respect to the generation for C-F

During the optimization process, initially the exact solution which gives the minimum deflection is performed. Stacking sequence optimization is carried out for two cases. In the first case, deflection parameters are obtained without using elitism, then elitism is included into the algorithm. In both cases, the crossover ratio (CR) and mutation ratio (MR) are chosen as 0.2 and 0.1 respectively. In Fig. 3, Fig. 4 and Fig. 5, the variation of deflection parameters with respect to the number of generation are illustrated for various boundary conditions. The beam is assumed to be constructed of three layers with a fiber orientation angle increment of 10°. Although the minimum values are obtained for both cases, they are obtained in earlier generations by use of elitism in 2nd, 4th and 3rd generation for C-C, C-F and S-S boundary condition respectively.

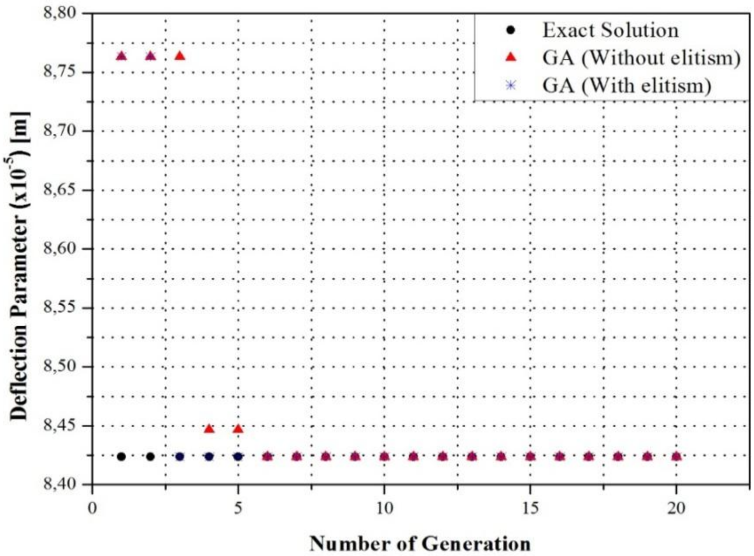

Fig. 5. – The variation of deflection parameters with respect to the generation for S-S

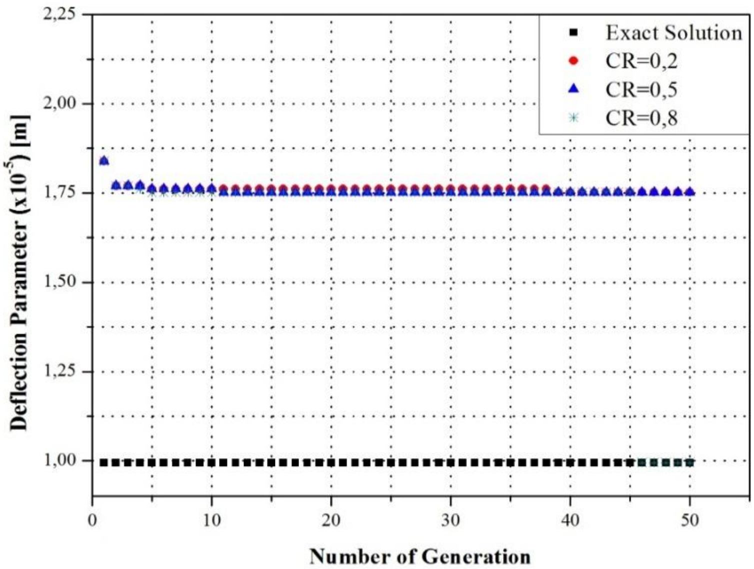

Fig. 6. – The variation of deflection parameters with respect to the generation for C-C

In Fig. 6, Fig. 7 and Fig. 8, the variation of deflection parameters with respect to the number of generation are illustrated for various crossover ratios and boundary conditions. The beam is assumed to be constructed of four layers with a fiber orientation angle increment of 10°. Firstly, exact solution of the problem is performed for each boundary condition. In the optimization stage, mutation ratio is chosen as 0.01 and different crossover ratios are considered such as 0.2, 0.5 and 0.8. These crossover ratios correspond to various number of swapping layers. For instance, a beam with four layers corresponds to an individual of four genes. Only one and the first gene of an individual is changed with the consecutive one for a crossover ratio of 0.2. The first two and three genes of the consecutive individuals are changed respectively for crossover ratio of 0.5 and 0.8. Due to a number of possible stacking sequences, elitism is included into the algorithm in order to increase the convergence and prevent local minimum. Therefore, the minimum deflection parameters are generally obtained in recent generations. Although the minimum value is obtained at CR=0.8 in C-C boundary condition, they are obtained at CR=0.5 for C-F and S-S boundary conditions respectively. The stacking sequences with a crossover ratio of 0.5 have better results and they converge faster than the others for given conditions.

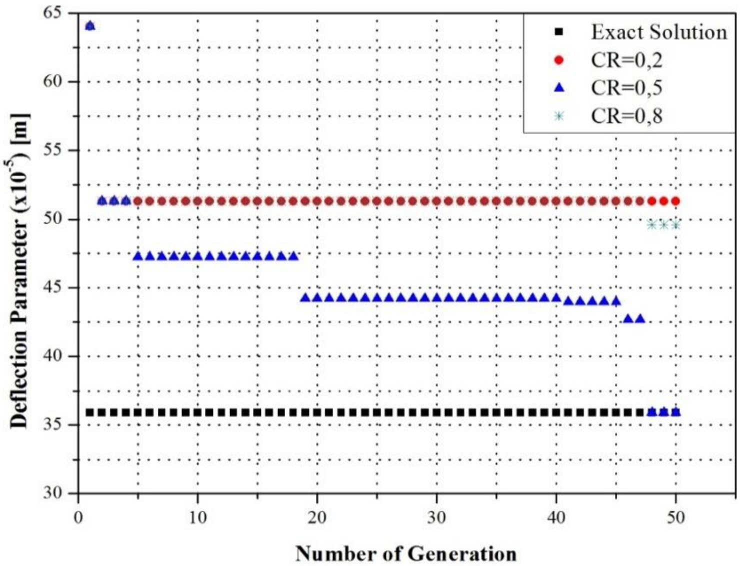

Fig. 7. – The variation of deflection parameters with respect to the generation for C-F

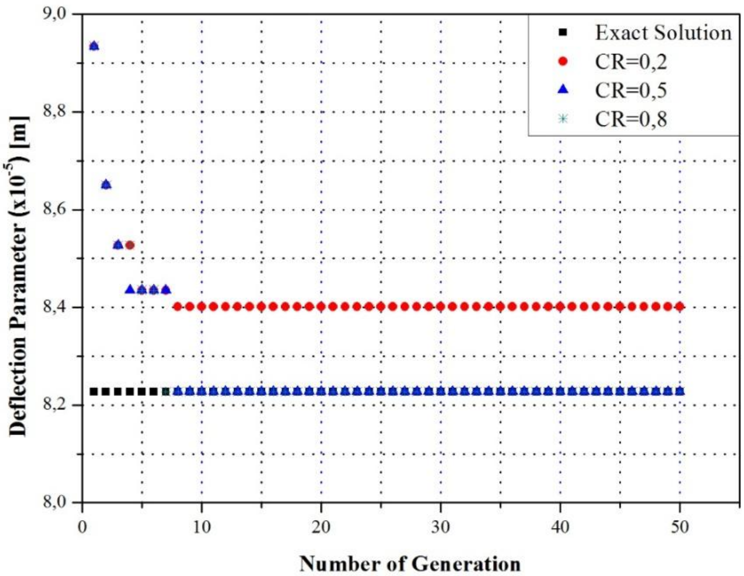

Fig. 8. – The variation of deflection parameters with respect to the generation for S-S

The reliability of the algorithm can be expressed as a percentage of minimum deflection parameters equal to the optimum values. The values in Tab. 2 and 3 are obtained among a large number of possible solutions depending on number of layers and fiber angle increment. Although there are 64, 256 and 1024 possible stacking sequences for an increment of 30° for 3, 4 and 5 layers respectively, there are 1000, 10000 and 100000 values for an increment of 10°. Since all the deflection parameters are the same with exact solutions in Tab. 2, % 100 reliability is satisfied in all boundary conditions. 89% reliability is obtained in Tab. 3 due to the excessive number of possible stacking sequences.

CONCLUSIONS

In the study, in order to minimize the deflection parameters, stacking sequence optimization of laminated composite beam is carried out for various boundary conditions and genetic operators by use of genetic algorithm. The fiber angles are assumed to be changing between 0° and 90° with an increment of 10°, 30°. Since it is very difficult to produce and analyze a composite beam consisting of specific stacking sequences, material and geometrical properties in real life, the algorithm developed in this study will be helpful in the development and analysis of a prototype without any cost. On the other hand, too many design parameters which correspond to a number of possible solutions will increase the processing time in the optimization of composite structures. Owing to evolving individuals in each generation, the algorithm developed will decrease the processing time. Since the composite beams are quite thin, the same results are obtained both for exact and GA solution. Depending on the applicability of technique to various type of optimization problems and regardless of the number of design parameters, it is concluded that using an evolutionary optimization technique in the design of composite beams will be inevitable.

REFERENCES

1. ALMEIDA, F. S., AWRUCH, A. M.: Design optimization of composite laminated structures using genetic algorithms and finite element analysis, Composite Structures, 88, 2009: 443-454.
2. BRIGHENTI, R.: Fibre distribution optimisation in fibre-reinforced composites by a genetic algorithm, Composite Structures, 71, 2005: 1-15.
3. GHIASI, H., PASINI, D., LESSARD, L.: Optimum stacking sequence design of composite materials, Part I: Constant stiffness design, Composite Structures, 90, 2009: 1-11.
4. GOLDBERG, D. E.: Genetic algorithm in search, optimization and machine learning Addison-Wesley Publishing, Inc., Reading, Massachusetts, USA, 1989.
5. HAJELA, P.: Genetic search an approach to the nonconvex optimization problem, AIAA Journal, 26 (7), 1990: 1205-1210.
6. HOLLAND, J. H.: Adaptation in natural and artificial systems: An introductory analysis with applications to biology, control and artificial intelligence, MIT Press, Cambridge, MA, USA, 1995.
7. JONES, R. M.: Mechanics of composite materials, McGraw-Hill, New York, USA, 1975.
8. KARAÇAM, F.: Bending Analysis of Laminated Composite Beams (in Turkish) [M.Sc. Thesis], Institute of Science, Department of Mechanical Engineering, Trakya University, Edirne, TURKEY, 2005, 47 p.
9. KARAMA, M., AFAQ, K. S., MISTOU, S.: Mechanical behaviour of laminated composite beam by the new multi-layered laminated composite structures model with transverse shear stress continuity, International Journal of Solids and Structures, 40, 2003: 1525-1546.
10. KHDEIR, A. A., REDDY, J. N.: An exact solution for the bending of thin and thick cross-ply laminated beams, Composite Structures, 37, 1997: 195-203.
11. LEE, D. S., MORILLO, C., BUGEDA, G., OLLER, S., ONATE, E.: Multilayered composite structure design optimisation using distributed/parallel multi-objective evolutionary algorithms, Composite Structures, 94, 2012: 1087-1096.
12. LOPEZ, R. H., LUERSEN, M. A., CURSI, J. E. S.: Optimization of hybrid laminated composites using a genetic algorithm, Journal of the Brazilian Society of Mechanical Sciences and Engineering, 31 (3), 2009: 269-278.
13. SCIUVA, D. M., GHERLONE, M., LOMARIO, D.: Multiconstrained optimization of laminated and sandwich plates using evolutionary algorithms and higher-order plate theories, Composite Structures, 50, 2003: 149-154.
14. SOLDATOS, K. P., TIMARCI, T.: A unified formulation of laminated composite, shear deformable, five-degrees-of-freedom cylindrical shell theories, Composite Structures, 25, 1993: 165-171.
15. TIMARCI, T., SOLDATOS, K. P.: Comparative dynamic studies for symmetric cross-ply circular cylindrical shells on the basis of a unified shear deformable shell theory, Journal of Sound and Vibration, 187 (4), 1995: 609-624.

Corresponding author:
Fatih Karaçam, Department of Mechanical Engineering, Trakya University, Edirne, Turkey

IMPACT OF ALCOHOL ADDITION TO FUEL ON THE NOISE LEVEL OF SMALL COMBUSTION ENGINES

J. Kaszkowiak[1], E. Kaszkowiak[2], M. Markiewicz-Patalon[1]

[1]Institute of Machine Operation and Transport, Faculty of Mechanical Engineering, UTP University of Science and Technology in Bydgoszcz, Poland
[2]Faculty of Agriculture and Biotechnology, UTP University of Science and Technology in Bydgoszcz, Poland

Abstract
Nuisance of small combustion engines' operation with special consideration of engines driving machines designed for work at green areas is discussed in the article. Main hazards connected with noise occurring during their operation have been discussed. The basic problems of bioethanol generation as well as the course and results of the surveys on the impact of ethanol addition to fuel on the noise level at the time of engine's operation depending on the rotational speed is presented in the paper. Occurrence of essential differences between the noise level and the content of ethanol in the operating motor's fuel has been found.

Key words: combustion engines, ethanol, biofuel, noise.

INTRODUCTION

Sound emission accompanies operation of all the machines. Its impact on the comfort of an operator's operation and on the environment (outsiders, wild or farm animals) has been the subject matter of numerous surveys and legal provisions. Even the sources of energy considered to be ecological ones and environment friendly may constitute a threat. It concerns for example wind power plants the impact of which, as mentioned by KARWOWSKA ET AL. (2015), KARWOWSKA ET AL. (2014), MIKOŁAJCZAK ET AL. (2013), has an intensive impact within a sphere of up to 500 m, and extremely unfavourably within the distance of up to 50 m. In case of machines for cutting and shredding, a considerable part of energy generated by the motor is converted into a working element motion resistances not connected with the performed work accompanied by noise emission BOCHAT ET AL. (2013).

Sounds connected with a combustion engine's operation may be used for its technical condition's diagnosing. As mentioned by KOMOROWSKA AND GÓRNICKA (2010), sound intensity within the scope of selected frequencies may determine the technical condition of an engine's elements. Lowering of environmental nuisance for combustion engines is reached at different levels. There may be included design changes reducing both fuel consumption as well as betterment of combustion gases' composition or the use of engine oils on the organic basis what, as mentioned by TULIK ET AL. (2013), may contribute to the decrease of combustion engines' for the environmental nuisance.

Application of bio additives to fuels aims at lowering of fossil fuels' consumption. The surveys of EVANGELOS ET AL. (2013) confirm their beneficial impact most of all on combustion gases' composition, and in case of engines with self-ignition, additional reduction of the volume of solid particles MULEROVA ET AL (2013). However, effective acquiring of both ethanol as well as vegetable oil used as fuel additives has become a problem.

Instability of crude oil's prices together with the necessity to guarantee permanent and safe energy supplies, in the last few decades contributes to the quite rapid increase of biofuels generation. It is anticipated, that the area of farm lands designed for cultivation of plants for energy purposes shall significantly increase only by 2025, and biofuels may then provide about 10% of supply of the world demand for transport fuel KERCKOW (2007).

However, there are more and more negative opinions in the world on production of bioethanol. Oponents of biofuels say, that the increase of bio components' production may pose a threat both for the food prices as well as to contribute to the escalation of competition for farm land designed for cultivation of plants for consumption purposes Production of first generation fuels attributes to many environmental, economic and ethical problems, and its increase leads to the increasing competition of fuels with food and natural factors the resources of which are limited. Insufficient number of surveys assessing the impact of biofuels production on environment causes, that the development of that industry on a big scale becomes risky.

However, the manners of new methods of energy resources' management acquisition are still one of the most important problems influencing the world's economy development.

Biofuels originating from biological raw materials provide, as compared to fossil fuels, many economic and habitat benefits. Bioethanol driving to reduction of greenhouse gases for 31% (through substitution of petrol and diesel oil) has become the most often used fuel in the world. In the union countries, where it is mainly produced from grain crops and sugar beets, the interest in corn being one of the most energetic distiller raw material has been growing.

The researches of GUMIENNA ET AL. (2016), concerning many corn's hybrids have confirmed, that not only the content of starch in corn's grain determines ethanol productivity. Variations of corn of higher starch content have lower saccharification's efficiency, while variations of the highest level of reducing sugar in grains are characterized by higher ethanol productivity. Very high yielding prospects of that species and possibility of corn's cultivation on weaker soils cause, that in the European conditions it becomes, apart from beet, one of the most important raw material for bioethanol production GUMIENNA ET AL. (2014).

The purpose of the conducted surveys was to establish, if in the engines with magneto ignition the addition of ethanol influences the level of noise at different engine speeds.

MATERIALS AND METHODS

The experiment has been planned as a two-factor experiment of 4 levels of the prime factor (content of alcohol in fuel) and 2 levels of the second factor (rotational speed). The experiment factors and their values are presented in Tab. 1.

The researches were conducted for a four-stroke combustion engine, (which can operate in each position 0-360 degrees), overhead valve OHC, air cooled of engine cubic capacity 35,8 cm^3 and power 1,0 kW (1,3 kM). Such an engine is used to drive combustion lawn mowers, aerators and small electric power generators. At the time of measurements, the engine did not drive any machines, before measurements' starting it operated for 30 minutes with maximum rotational speed 733 rad s^{-1} (7000 rpm), at feeding with fuel of octane number 95, without ethanol admixture. In the distance of 0,5 m from the motor's edge, in the axis of crankshaft, the sound level was measured with the use of an integrating sound meter HD 2010 UC. The time of the experiment's conducting was 5 minutes for the rotational speed of the idle running 83 rad s^{-1} (800 rpm) and 5 min for maximum speed 733 rad s^{-1} (7000 rpm). The reading was repeated 5 times after each 45 seconds of operation. The rotational speed was measured with a laser revolution counter Voltcraft DT-10L with measurement precision ±0,5%, according to the manufacturer's data.

Having performed the measurements, the remaining part of the fuel was removed from the tank and a new portion of fuel with ethanol additive (10%) was spilled. The started engine was left on idle running for about 10 minutes, for possible use of the fuel residues in fuel pipes after the previous measurement. The fuel sample no 2 was once again removed from the tank and a new portion of fuel of identical composition was spilled to exclude the impact of the previous type of fuel's impact in the tank and fuel pipes. After 5 minutes of operation and possible correction of the mixtures' composition by changing of the volume of air supplied to the engine,, the next measurement cycle for maximum rotations and then for idle running's rotations was started. There was analogical procedure with the remaining types of fuels.

The composition of the mixture applied in the measurements is presented in Fig. 1.

Tab. 1. – Factors of the experiment and their values

Fuel's composition (factor A)	Rotational speed (factor B)	
	83 rad s^{-1} (800 rpm)	733 rad s^{-1} (7000 rpm)
	100 petrol /0% ethanol	100 petrol /0% ethanol
	90% petrol /10% ethanol	90% petrol /10% ethanol
	75% petrol /25% ethanol	75% petrol /25% ethanol
	60% petrol /40% ethanol	60% petrol /40% ethanol

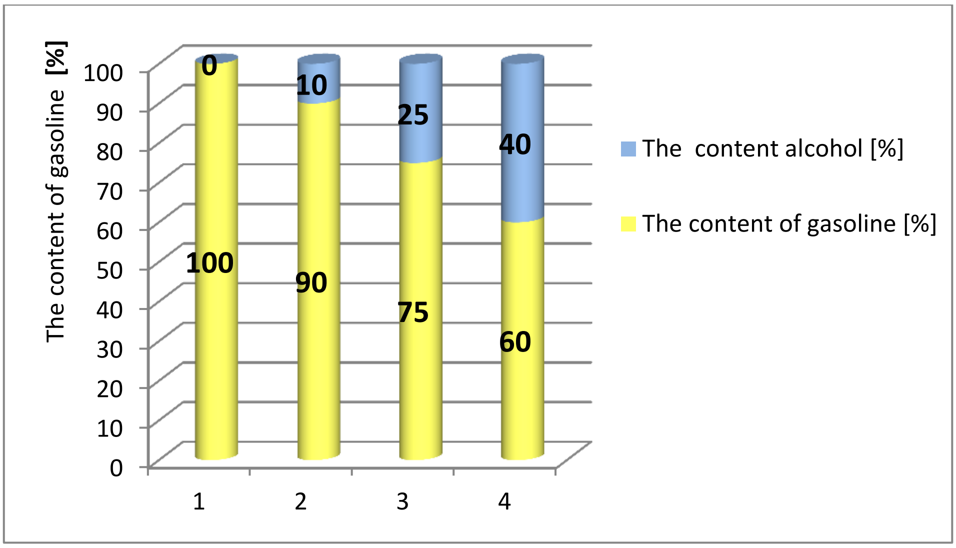

Fig. 1. – Content of alcohol and petrol in the next fuel samples

RESULTS AND DISCUSSION

The results obtained in the experiment are presented in the Tab. 2, then they were subject to statistical analysis for a two-factor experiment with testing of differences' significance applying the Tukey test on the level 0,05. The software FR-ANALWAR on the basis of Excel was used for the analysis.

As a result of the conducted analysis, significance of the value of the sound level for the level of 0,05 for the factor B (rotational speed) and the factor A (content of alcohol in fuel) and A x B interaction was found.

Tab. 2. – Results of volume measurement

Content of petroleum in fuel	Sound level for 83 rad s^{-1} (800 rpm)					Sound level for 733 rad s^{-1} (7000 rpm)				
%	dB(A)					dB(A)				
100	75.4	75.5	75.3	75.8	75.4	93.2	92.7	92.4	91.9	93.2
90	74.1	74.3	74.2	74.3	73.9	89.4	90.1	90.4	90.5	89.4
75	75.1	74.8	73.6	75	73.3	91.5	88.2	88.7	87.8	88.7
60	74.9	74.5	75.6	74.8	74.5	88.9	89.1	88.5	88.3	88.4

For the increasing content of ethanol in fuel already at 10% alcohol additive, the drop of the sound level was found both for the speed 83 rad s^{-1} (800 rpm) as well as for 733 rad s^{-1} (7000 pm). For 83 rad s^{-1} (800 rpm) the highest sound level was found for fuel of 100% petroleum content. An essential difference (drop in sound level) has occurred already at 10% of alcohol addition of fuel, the further increase of alcohol content in fuel did not result in any significant drop in sound level.

The sound level at rotational speed 733 rad s^{-1} (7000 rpm) decreased together with the content of ethanol in fuel. The biggest drop in sound level was noticed in addition of 10% of ethanol, it amounted to 2,72 dB(A). It was only when the content of ethanol in fuel exceeded 25% when no drop of sound level was noticed.

The influence of the factor B (rotational speed) on the sound level is confirmed by many authors. Such a phenomenon is described by EVANGELOS (2016), it concerns both the engines with self-ignition as well as with spark ignition. Similar results were obtained by YASAR (2010), who in spite of application of butyl and methyl alcohol as additives, for both these additives received reduction of the sound level.

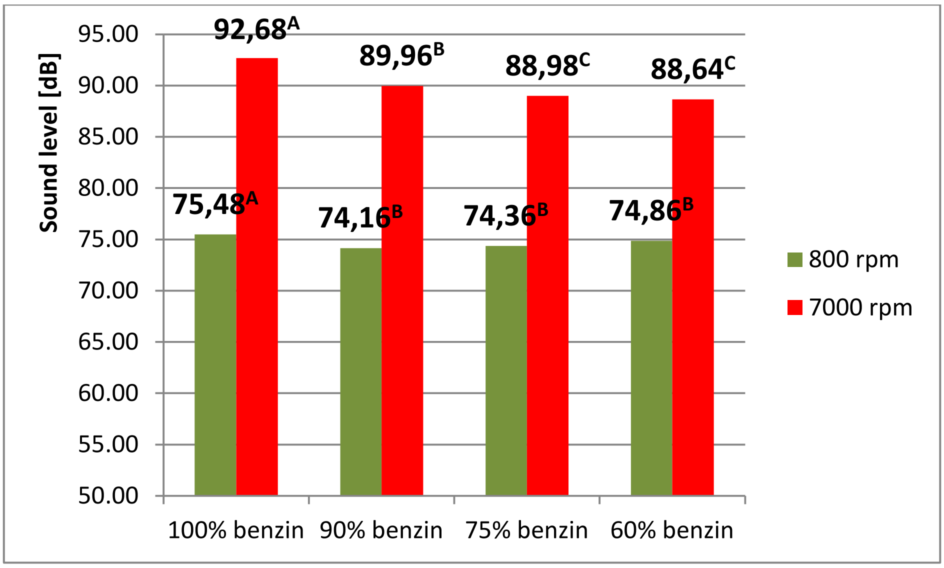

Fig. 2. – Dependency of the sound level on the content of alcohol (factor A) and rotational speed (factor B)

KESKIN (2010) in his surveys also confirmed the statistically significant drop in the noise's level for 1500 and 2500 rpm already for the addition of ethanol 5%. However KESKIN AND GURU (2011) in other surveys found the increase of the noise level for the addition of ethanol 25%, but they conducted these surveys for the variable engine loadings.
This effect may be connected with application of ethanol of octane number 108, much higher than petrol (95). It decreases propensity of detonation's occurring in an engine, in particular in engines without adjustment ignition advance angle. It has been confirmed by JAROMIRO AND DAVID (2013). Kumar AND AGARWAL (2011) draw attention to the fact, that addition of alcohol results in the decrease of pressure in the combustion chamber during the engine's operation. However, Turner at al. suggest, that addition of alcohol to petroleum results in raising of the heat of evaporation what decreases the speed of combustion. During the subsequent surveys, it shall be necessary to assess within which considerable degree, for lowering of the sound level there attributes demand for air for fuel combustion connected with the share of alcohol resulting both in smaller suction murmurs as well as with lower combustion gases volume, and as a consequence – lower noise from exhaust system.

CONCLUSIONS

As a result of the connected experiment it was found, that the additive of ethylene alcohol to petrol influenced lowering of the engine's sound level. The highest drop (for about 2,7 dB(A) of sound level was found at 10% of ethanol addition and engine's rotations 733 rad s^{-1} (7000 rpm). In the realized experiment, addition of alcohol to fuel above 25%, for the rotational speed 733 rad s^{-1} (7000 rpm), it did not result in statistically significant drop in noise's level.
For the engine rotational speed amounting to 83 rad s^{-1} (800 rpm) addition of ethanol above 10% did not result in statistically significant drop in noise's level.
Usage of alcohol as fuel additive may be, apart from betterment of exhaust gases' composition, an additional factor decreasing the noise level for the environment of the combustion engines' operation.

REFERENCES

1. BOCHAT, A., ZASTEMPOWSKI, M.: Modeling the Dynamics of the Vegetable Material Detachment Process from Undisturbed Areas to Improve the Design of Selected Agricultural Machines. Transactions of the ASABE. Vol. 56(4), 2013: 1309-1314.
2. EVANGELOS, G., GIAKOUMIS, N., CONSTANTINE, D., RAKOPOULOS, S., ATHANASIOS, M., DIMITRIOS C.: Exhaust emission swith ethanolor n-butanol diesel fuel blendsduring transient operation, Renewable and Sustainable Energy Reviews (17), 2013: 170–190.
3. EVANGELOS, G., GIAKOUMIS, N., DIMITRIOS, C., RAKOPOULOS, S., CONSTANTINE, D.: Combustion noise radiation during dynamic diesel engine operation including effects of various biofuel blends: A review Renewable and Sustainable Energy Reviews 54, 2016: 1099–1113.
4. GUMIENNA, M., SZWINGIEL, A., LASIK, M., SZAMBELAN, K., MAJCHRZYCKI, D., ADAMCZYK, J., NOWAK, J., CZARNECKI, Z.: Effect of corn grain variety on the bioethanol production efficiency, Fuel 164, 2016: 386–392.

5. GUMIENNA, M., SZAMBELAN, K., JELEŃ, H., CZARNECKI, Z.: Evaluation of ethanol fermentation parameters for bioethanol production from sugar beet pulp and juice, Journal of the Institute of Brewing, 2014.
6. JAROMIRO, T., DAVID, J.: Theoretical research - experimental performance of a HCCI engine operated with Anhydrous Ethanol (Investigación teórico - experimental del desempeño de un motor HCCI operado con Etanol Anhidro), 2013, http://www.bdigital.unal.edu.co/45997/#sthash.3co1YdK6.dpuf (22.02.2012).
7. KARWOWSKA, M., MIKOŁAJCZAK, J., BOROWSKI, S., DOLATOWSKI, Z J., MARC-PIENKOWSKA, J., BUDZIŃSKI, W.: Effect of noise generated by the wind turbineon the qualityof goose muscles and abdominal fat Annals of animal science 14, 2014: 441-451.
8. KARWOWSKA, M., MIKOŁAJCZAK, J., DOLATOWSKI, Z. J., BOROWSKI, S.: The effect of varying distances from the wind turbine on meat quality of growing-finishing pigs, Annals of animal science 15, 2015: 1043-1054.
9. KESKIN, A.: The Influence of Ethanol–Gasoline Blends on Spark Ignition Engine Vibration Characteristics and Noise Emissions, Energy Sources, Part A: Recovery, Utilization, and Environmental Effects. 20(30), 2010: 1851-1862.
10. KESKIN, A., GÜRÜ, M.: The Effects of Ethanol and Propanol Additions Into Unleaded Gasoline on Exhaust and Noise Emissions of a Spark Ignition Engine, Energy Sources, Part A: Recovery, Utilization, and Environmental Effects. 23(33), 2011: 2194-2205.
11. KUMAR, R., AGARWAL, A.: Experimental study of combustion and emission characteristics of ethanol fuelled port injected homogeneous charge compression ignition (HCCI) combustion engine, Applied Energy 88(4), 2011: 1169-1180.
12. KERCKOW, B.: Competition between agricultural and renewable energy production. Quartely Jurnal of International Agricilture, 46, 2007: 333-347.
13. KOMORSKA, I., GÓRNICKA, D.: Adaptation of engine vibration characteristics for diagnostics of mechanical defects, Combustion Engines (pol) Silniki Spalinowe 50(3), 2011.
14. MIKOŁAJCZAK, J., BOROWSKI, S., MARC-PIENKOWSKA, J., ODROWĄŻ-SYPNIEWSKA, G., BERNACKI, Z., SIODMIAK, J., SZTERK, P.: Preliminary studies on the reaction of growing geese (Anser anser f. domestica) to the proximity of wind turbines, Polish Journal of veterinary sciences 16, 2013: 679-686.
15. MULLEROVA, D., JABLONICKY, J., HUJO, L., KOSIBA, J., TKAC, Z., KRALIK, M., CHRASTINA, J.: Research of limited and unlimited emission effect on the environment during the burning of alternative fuels in agricultural tractors, Journal of Central European Agriculture, 14(4), 2013: 1402-1414.
16. TULIK, J., HUJO, L., STANCIK, B., SEVCIK, P.: Research of new ecological synthetic oil-based fluid, Journal of Central European Agriculture, 14(4), 2013: 1384-1393.
17. TURNER, D., XU, H., CRACKNELL, R. F., NATARAJAN, V., CHEN, X.: Combustion performance of bio-ethanol at various blend ratios in a gasoline direct injection engine. Fuel, 90(5), 2011: 1999-2006.
18. YASAR, A.: Effects of alcohol-gasoline blends on exhaust and noise emissions in small scaled generators Metalurgija (4)49, 2010: 335-338.

Corresponding author:
Jerzy Kaszkowiak, Institute of Machine Operation and Transport, Faculty of Mechanical Engineering, UTP University of Science and Technology in Bydgoszcz, ul. Prof. S. Kaliskiego 7, 85-789 Bydgoszcz, Poland, phone: +48523408208, e-mail: kaszk@utp.edu.pl

A NEW APPROACH TO FAULT DIAGNOSIS IN AGRICULTURAL TRACTOR MECHANICAL GEARBOX

D. Kateris[1], I. Gravalos[2], Th. Gialamas[2], P. Xyradakis[1], D. Moshou[1]

[1]Aristotle University of Thessaloniki, School of Agriculture, Agricultural Engineering Laboratory, 54124, Thessaloniki, Greece
[2]Department of Biosystems Engineering, Technological Educational Institute of Thessaly, School of Agricultural Technology, 41110, Larissa, Greece

Abstract
This paper proposes a new expert system tool in order to diagnose with a great accuracy and speed the existence of faults – failures in an agricultural tractor mechanical gearbox. In addition, the system is able to diagnose which of the bearings is not operational so that the repair becomes selective and the maintenance cost-effective. The research showed that such problems could be dealt with using Neural Networks. The Bayesian Multilayer Perceptron Neural Network with Automatic Relevance Determination (MLP-ARD) makes a good approach. Time and frequency-domain vibration signals of normal and faulty bearings are processed for feature extraction. These features from all the signals are used as input to the MLP-ARD. The experimental results show that the proposed approach is highly accurate regarding different bearing fault detection. This approach will be extended with regards to real-time fault detection of rotating parts in agricultural vehicles where the anticipation of detection of incipient failure can lead to reduced downtime.

Key words: condition monitoring, expert system, bearings, reliability, MLP-ARD neural network.

INTRODUCTION

In our days, agricultural tractors are the most important part of agricultural machinery. Without them agricultural operations such as plowing, planting and harvesting would not be feasible. Hence, agricultural tractors should be maintained correctly in order to ensure that they work effectively for a long period without any serious breakdown. A tractor that breaks down and must be prematurely maintained incurs large expenses.

The gearbox is one of the most important components of an agricultural tractors mechanical transmission system. Its function is to transfer power of revolution from one shaft to another. Therefore, the gearbox fault diagnosis is crucial to prevent the mechanical system from malfunctioning that could cause serious damages or the entire system to halt, even personnel casualties (LOUTRIDIS, 2008). So, it is very important to detect and diagnose early faults that may arise in such gearboxes.

The gearbox has a significant number of moving components (axles, gears and bearings). These components give rise to vibration. Every component has a unique – specific vibration signature related to the construction and the operating condition of it. If the operating condition of the component changes, the vibration signature will also change. This change in combination with acoustic emission can be used to detect faults before they become critical.

Bearing as one of the basic gearbox components, plays an important role in many transmission systems. Early fault diagnosis of bearing may prevent unnecessary failures of most of the rotating machinery system and thereby increase operational reliability and availability of the machine. It is well known that when a fault appears at a single gearbox bearing, all bearings are replaced even though most of them are still operational. This happens because it is impossible for the technician to diagnose exactly which bearing is faulty. As a result, every bearing of the gearbox is replaced, increasing the total repair costs.

In the last decades, many researchers have developed different fault diagnosis methods. One of the principal tools for diagnosing bearing faults is the vibration-based analysis (HENG AND NOR, 1998; RANDALL ET AL., 2001; STACK ET AL., 2006; DU AND YANG, 2006). Using signal processing techniques in vibration signals, it is possible to obtain vital diagnostic information (LEI ET AL., 2008). Fault signal detection and recognition are often accomplished by pattern recognition using a neural network (BROTHERTON AND POLLARD, 1992; YANG ET AL., 2002), RBF network (LEONARD AND KRAMER, 1991), Gaussian mixture model network (CHOW ET AL., 1993; HECK AND CHOU, 1994), fuzzy logic network (CHOW ET AL., 1993), Bayesian classifier (MEYER AND TUTHILL, 1995), vector correlation or vector distance measure (BAUGH, 1993). Commonly used feature generation methods including the short-time Fourier transform (STFT) (BROTHERTON AND POLLARD, 1992), wavelet time-scale decomposition (BROTHERTON AND POLLARD, 1992; CHOE ET AL., 1995; PENG ET AL., 2001), cumulant spectrum (BAUGH, 1993), etc.

The aim of this paper is to present an expert system tool which gives a solution to the above problem. The system can diagnose with great accuracy and speed the existence of faults – failures. In addition, the system is able to diagnose which of the bearings is not operational so the repair becomes selective and the maintenance cost-effective. The originality of the developed system focuses on the accurate determination of the faulty bearing that needs to be replaced. The absence of large scale data to be used for training and verification of the system's effectiveness, led to the design and the construction of an experimental device in order to take the measurements required.

Research showed that such problems could be dealt with effectively using Neural Networks. The Bayesian Multilayer Perceptron Neural Network with Automatic Relevance Determination (MLP-ARD) is a very good approach. The developing system is based on the performance of two Bayesian multilayer neural networks with automatic relevance determination (Multilayer Perceptron Neural Network with Automatic Relevance Determination, MLP-ARD) that combine data from mono-axial and tri-axial accelerometers positioned at selected locations on the gearbox.

MATERIALS AND METHODS

Work area and soil

In order to develop and validate the expert system an experimental test rig was used. This test rig was designed and constructed entirely at the Department of Biosystems Engineering, Technological Educational Institute of Thessaly, Greece (Fig. 1).

The test rig consists of a 6-speed manual transmission gearbox (5 forward and 1 reverse) with 4 bearings (Fig. 4), a three phase AC motor (5,5 Hp), a hydraulic dynamometer for gearbox loading and a complete vibration recording system of Brüel & Kjær company (Fig. 2). In order to collect the vibration data, which is used as input to the expert system, two types of accelerometers (2 tri-axial and 4 mono-axial) were placed at selected locations on the gearbox. Specifically, as shown in Fig. 3, 5 and 6 of the tri-axial accelerometers were placed on the gearbox at the front and at the rear vertical axis and the mono-axial accelerometers were placed on the gearbox at the front and the rear horizontal axis.

Fig. 1. – (a) Gearbox test rig, (b) Data acquisition system, (c) Bearing fault (inner race)

Fig. 2. – Vibration recording system

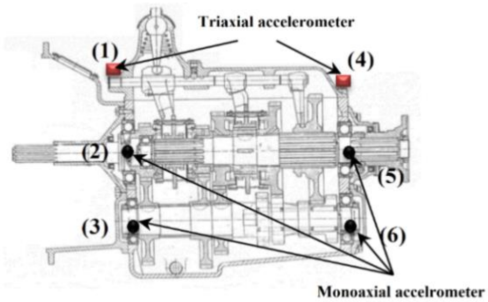

Fig. 3. – Locations where the accelerometers were placed on the gearbox**.**

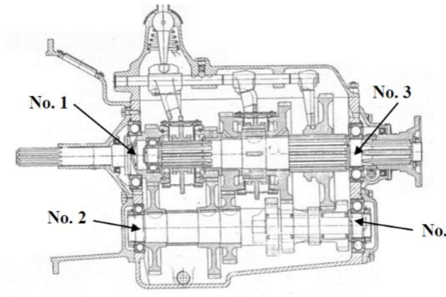

Fig. 4. – Gearbox cut section - four bearings locations (No 1 to 4).

Fig. 5. – Locations where the mono-axial accelerometers were placed on the gearbox

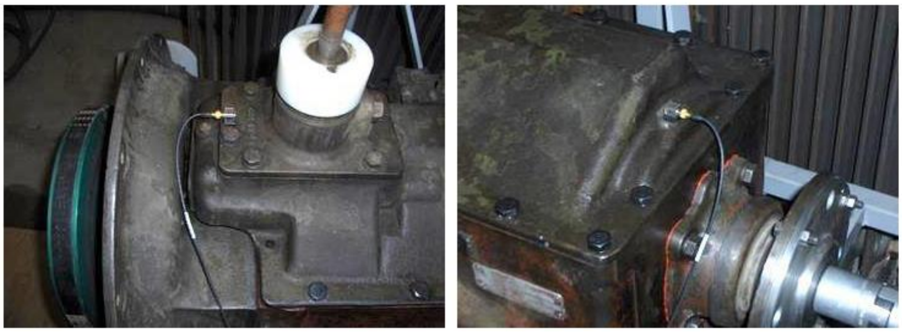

Fig. 6. – Locations where the tri-axial accelerometers were placed on the gearbox

Feature extraction

The first and maybe the most important step in any fault diagnosis problem, is the feature extraction from the raw signal. The aim of this is to reflect the general changes of the machine operation conditions. However, though some features are closely related to the fault, others are not. In this paper, twenty-four (24) features parameters, twelve (12) time-domain (T_1-T_{12}) and twelve (12) frequency-domain (F_1-F_{12}) were selected.

Time-domain features

The first eleven features were introduced by LEI ET. AL (2008). These were Mean value (T_1), Standard deviation (T_2), (T_3), Root mean square (T_4), Peak (T_5), Skewness (T_6), Kurtosis (T_7), Crest factor (T_8), Clearance factor (T_9), Shape indicator (T_{10}) and Impulse Indicator (T_{11}). The twelfth one was introduced by MOSHOU ET AL. (2010) and regards the linear integral of the acceleration signal (Line integral, T_{12}). All the used features provide statistical information about the nature of data, and were found to be reasonably good features for bearing fault detection. These features are presented in Tab. 1.

The new feature (Line Integral) is based on the observation that the higher frequencies are presented in a signal, the higher density of the signal is. The signal path due to its direct correlation to the signal variation affected by this. This parameter is sufficient to give an accurate indication of changing frequency content reflecting the total length of the signal. For high sampling rates the approximation can be simplified.

Tab. 1. – Time-domain feature parameters

Time-domain feature parameters			
$T_1 = \frac{\sum_{n=1}^{N} x(n)}{N}$	(1)	$T_7 = \frac{\sum_{n=1}^{N}\left(x(n)-T_1\right)^4}{(N-1)T_2^4}$	(7)
$T_2 = \sqrt{\frac{\sum_{n=1}^{N}(x(n)-T_1)^2}{N-1}}$	(2)	$T_8 = \frac{T_5}{T_4}$	(8)
$T_3 = \left(\frac{\sum_{n=1}^{N}\sqrt{\lvert x(n)\rvert}}{N}\right)^2$	(3)	$T_9 = \frac{T_5}{T_3}$	(9)
$T_4 = \sqrt{\frac{\sum_{n=1}^{N}(x(n))^2}{N}}$	(4)	$T_{10} = \frac{T_4}{\frac{1}{N}\sum_{n=1}^{N}\lvert x(n)\rvert}$	(10)
$T_5 = max\lvert x(n)\rvert$	(5)	$T_{11} = \frac{T_5}{\frac{1}{N}\sum_{n=1}^{N}\lvert x(n)\rvert}$	(11)
$T_6 = \frac{\sum_{n=1}^{N}\left(x(n)-T_1\right)^3}{(N-1)T_2^3}$	(6)		
$T_{12} = \int_a^b ds \approx \sum_{i=1}^{N} \vec{r}(t_i+T_s)-\vec{r}(t_i) = \sum_{i=1}^{N}\sqrt{\left(x(t_i+T_s)-x(t_i)\right)^2+T_s^2} \approx \sum_{i=1}^{N}\lvert x(t_i+T_s)-x(t_i)\rvert$			(12)

Where: x(n) for the time-domain feature is a signal series for n=1,2,….,N, N is the number of data points. Especially for the line integral *N* is the number of sample points (equal to 500) in the non-overlapping windows used to calculate Kurtosis (T_7), the other features and the line integral feature, T_s is the sampling period.

Tab. 2. – Frequency-domain feature parameters

Frequency -domain feature parameters			
$F_1 = \frac{\sum_{k=1}^{K} s(k)}{K}$	(13)	$F_7 = \sqrt{\frac{\sum_{k=1}^{K} f_k{}^2 s(k)}{\sum_{k=1}^{K} s(k)}}$	(19)
$F_2 = \frac{\sum_{k=1}^{K}\left(s(k)-F_1\right)^2}{K-1}$	(14)	$F_8 = \sqrt{\frac{\sum_{k=1}^{K} f_k{}^4 s(k)}{\sum_{k=1}^{K} f_k{}^2 s(k)}}$	(20)
$F_3 = \frac{\sum_{k=1}^{K}\left(s(k)-F_1\right)^3}{K\left(\sqrt{F_2}\right)^2}$	(15)	$F_9 = \frac{\sum_{k=1}^{K} f_k^2 s(k)}{\sqrt{\sum_{k=1}^{K}\sum_{k=1}^{K} f_k^4 s(k)}}$	(21)
$F_4 = \frac{\sum_{k=1}^{K}\left(s(k)-F_1\right)^4}{KF_2^2}$	(16)	$F_{10} = \frac{F_6}{F_5}$	(22)
$F_5 = \frac{\sum_{k=1}^{K} f_k s(k)}{\sum_{k=1}^{K} s(k)}$	(17)	$F_{11} = \frac{\sum_{k=1}^{K}\left(f_k-F_5\right)^3 s(k)}{KF_6^3}$	(23)
$F_6 = \sqrt{\frac{\sum_{k=1}^{K}\left(f_k-F_5\right)^2 s(k)}{K}}$	(18)	$F_{12} = \frac{\sum_{k=1}^{K}\left(f_k-F_5\right)^4 s(k)}{KF_6^4}$	(24)

Where: (k) is a spectrum for k=1,2,…,K, K is the number of spectrum lines, f_k is the frequency value of the kth spectrum line.

Frequency-domain features

Frequency-domain is another description of a signal. This type of description includes some information that cannot be found in time-domain. In this study another twelve features (LEI ET AL., 2008) were used in order to feed the MLP-ARD with additional information with respect to the time domain features. These twelve features were based on the Fourier transform of the vibration signals. Feature F_1 may indicate the vibration energy in the frequency-domain. Features F_2-F_4, F_6 and F_{10}-F_{12} may describe the convergence of the spectrum power. Finally, F_5 and F_7-F_9 give information about the position change of main frequencies. These features are presented in Tab. 2.

Structure of the system

In this paragraph the structure of the system is analyzed. The diagnosis system was based on three Multilayer Perceptron with Bayesian Automatic Relevance (MLP-ARD) with a 10 neurons hidden layer each. The number of neurons at the input level was equal to the number of selected features.

The first stage includes the data acquisition. At the second stage, from the recording signal the system export two new time signals 1s and 10s. Then, these signals segregate to smaller sections containing 500 values each. For each subdivision (500 values) of the 1s or 10s signal exported 12 features in the time domain and the 12 features in the frequency domain. These 24 features feed the first MLP-ARD (1st level) which have three outputs (healthy condition (no fault) – fault at the front side of the gearbox (No.1 or No.2) – fault at the rear side of the gearbox (No. 3 or No. 4). After this the system was trained in all situations (healthy condition and bearing faults) and for 5Nm load at the output gearbox shaft, in two different gearbox speeds (1st and 5th speed) and in three different rpm (730-1370-2700rpm) at the input gearbox shaft. After, follows the 2nd level. This level consists of two MLP-ARD which have two outputs each. (1st MLP-ARD – Fault to bearing No. 1 or No.2 and 2nd MLP-ARD – Fault to bearing No. 3 or No.4).

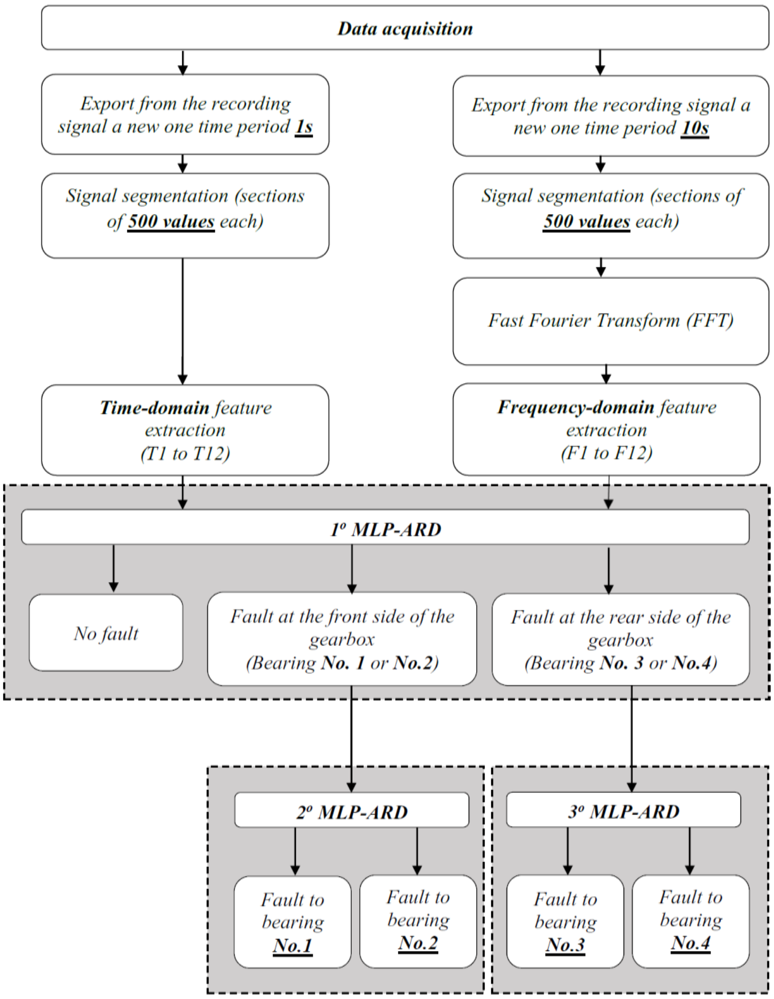

Fig. 7. – Expert system flow chart

After fault bearing assembly at the gearbox, a new vibration signature was carried out in two different gearbox speeds (1st and 5th speed), three different loads (0, 5, 10Nm) at the output gearbox shaft and three different rpm (730-1370-2700rpm) at the input gearbox shaft. The recorded vibration signals were used for feature extraction. These features are descriptive or high-order statistical data, which were extracted from the vibration signals in time and frequency domain.

The combination of results from both levels gives the exact defective bearing. The code of the expert system was written in Matlab. In the next Fig. (Fig. 7) the expert system flow chart is presented.

RESULTS AND DISCUSSION

In order to confirm the systems efficiency, it was trained under the following operation conditions, load 5 Nm at the outlet gearbox shaft, 1st and 5th gearbox speed and 1370rpm at the inlet gearbox shaft. After the training the system tested under different operation conditions - case scenarios (three different loads 0, 5 and 10 Nm at the outlet gearbox shaft, two gearbox speeds (1st and 5th) and three different rpm (730 – 1370 – 2700rpm) at the inlet gearbox shaft). The aim of these case scenarios is to investigate system efficiency in different operational conditions.

Specifically, as shown in Tab. 3, in the case scenario with a small rpm (760rpm) at the gearbox input shaft the system has very good efficiency with little to no fault in the gearbox (98.7-100%) and a fault at the rear part of it (83.2-100%). But when there was a fault at the front part of the gearbox, the system efficiency was significantly reduced (3.1-46.6%). In the second level, in order to diagnose if the fault is at the upper or at the lower bearing the 2nd and the 3rd MLP-ARD were executed. In this situation the diagnostic levels are particularly high (91.8-100%).

Tab. 3. – Evaluation of the efficiency of diagnostic system with training in 5 Nm load at the output gearbox shaft, 1st gearbox speed and 730rpm at the input gearbox shaft

	(Training) 1st speed at the gearbox 1370rpm input shaft - 187rpm output shaft **(Time period 1sec- 131 values)**			(Training) 1st speed at the gearbox 1370rpm input shaft - 187rpm output shaft **(Time period 10sec- 1310 values)**		
	(Scenario) 1st speed at the gearbox 730rpm input shaft - 99rpm outputshaft					
	1st MLP-ARD execution			**1st MLP-ARD execution**		
(Nm)	Bearing without fault (%)	Damage at the front side of the gearbox (%)	Damage at the rear side of the gearbox (%)	Bearing without fault (%)	Damage at the front side of the gearbox (%)	Damage at the rear side of the gearbox (%)
0	100	3.1	83.2	98.7	20.6	100
5	100	17.6	100	100	46.6	100
10	100	17.6	100	99.9	42.7	99.7

	2nd MLP-ARD execution		**3rdMLP-ARD execution**		**2nd MLP-ARD execution**		**3rd MLP-ARD execution**	
	Fault to bearing No.1	Fault to bearing No.2	Fault to bearing No.3	Fault to bearing No.4	Fault to bearing No.1	Fault to bearing No.2	Fault to bearing No.3	Fault to bear-ing No.4
	100	98.5	100	100	100	91.8	100	100
	100	100	100	100	100	100	100	100
	100	100	100	100	100	100	100	100

In the case study of 1370rpm at the gearbox input shaft the results are very high (>85.6%) for all the cases. This happens, because the system has been trained in these operation conditions. But in the case study of 2700rpm the efficiency is low only when there is a fault at the at the rear part of the gearbox and for 1s signal (38.9-52.7%). This confirms previous suspicions about lack of reliability using small signals (1s) as input to the expert system.

Tab. 4. – Evaluation of theefficiency of diagnostic system with training in load 5Nm at the output gearbox shaft, 1st gearbox speed and 1370rpm at the input gearbox shaft

	(Training) 1st speed at the gearbox 1370rpm input shaft - 187rpm output shaft **(Time period 1sec- 131 values)**			(Training) 1st speed at the gearbox 1370rpm input shaft - 187rpm output shaft **(Time period 10sec- 1310 values)**		
(Scenario) 1st speed at the gearbox 1370rpm input shaft - 187rpm output shaft						
	1st MLP-ARD execution			**1st MLP-ARD execution**		
(Nm)	Bearing without fault (%)	Damage at the front side of the gearbox (%)	Damage at the rear side of the gearbox (%)	Bearing without fault (%)	Damage at the front side of the gearbox (%)	Damage at the rear side of the gearbox (%)
0	100	90.8	100	100	85.6	100
5	100	100	100	100	100	100
10	100	100	100	100	100	100

2nd MLP-ARD execution		**3rd MLP-ARD execution**		**2nd MLP-ARD execution**		**3rd MLP-ARD execution**	
Fault to bearing No.1	Fault to bearing No.2	Fault to bearing No.3	Fault to bearing No.4	Fault to bearing No.1	Fault to bearing No.2	Fault to bearing No.3	Fault to bearing No.4
100	100	100	100	100	100	100	100
100	100	100	100	100	100	100	100
100	100	100	100	100	100	100	100

Tab. 5. – Evaluation of theefficiency of diagnostic system after training with a 5 Nm load at the output gearbox shaft, 1st gearbox speed and 2700rpm at the input gearbox shaft

	(Training) 1st speed at the gearbox 1370rpm input shaft - 187rpm output shaft **(Time period 1sec- 131 values)**			(Training) 1st speed at the gearbox 1370rpm input shaft - 187rpm output shaft **(Time period 10sec- 1310 values)**		
(Scenario) 1st speed at the gearbox 2700rpm input shaft - 380rpm output shaft						
	1st MLP-ARD execution			**1st MLP-ARD execution**		
(Nm)	Bearing without fault (%)	Damage at the front side of the gearbox (%)	Damage at the rear side of the gearbox (%)	Bearing without fault (%)	Damage at the front side of the gearbox (%)	Damage at the rear side of the gearbox (%)
0	100	100	38.9	97.4	94.1	93.1
5	100	100	48.1	60.2	99.8	83.3
10	100	100	52.7	45.9	95.3	94.1

2nd MLP-ARD execution		**3rd MLP-ARD execution**		**2nd MLP-ARD execution**		**3rd MLP-ARD execution**	
Fault to bearing No.1	Fault to bearing No.2	Fault to bearing No.3	Fault to bearing No.4	Fault to bearing No.1	Fault to bearing No.2	Fault to bearing No.3	Fault to bearing No.4
100	100	100	80.9	100	100	100	100
94.7	100	100	6.1	91.7	100	100	100
97.7	100	100	3.8	97.7	100	100	100

In the case where the 5th gearbox speed was selected the problem that occurs at low speed at the input shaft continues for diagnosis at the front side of the gearbox which means that the systems weakness is not affected by the selected gearbox speed. This hypothesis is confirmed by the recorded results after the other gearbox speeds selection where the phenomenon continues. As shown in Tab. 6, in the scenario with a small rpm (760rpm) at the gearbox input shaft the system has excellent efficiency in all cases, there is no fault in the gearbox (100%) and a fault at the rear part of the gearbox (100%). But when there is a fault at the front part of the gearbox, the system efficiency was significantly reduced (3.8-84.7%). In the second level, in order to diagnose whether the damage is at the upper or at the lower bearing the 2nd and the 3rd MLP-ARD were executed. In this case the diagnostic efficiency is extremely high close to 100%.

Tab. 6. – Evaluation of the efficiency of diagnostic system after training with a 5 Nm load at the output gearbox shaft, 5th gearbox speed and 730rpm at the input gearbox shaft

	(Training) 5th speed at the gearbox 1370rpm input shaft - 1370rpm output shaft **(Time period 1sec- 131 values)**					(Training) 5th speed at the gearbox 1370rpm input shaft - 1370rpm output shaft **(Time period 10sec- 1310 values)**				
(Scenario) 5th speed at the gearbox 730rpm input shaft - 730rpm output shaft										
	1st MLP-ARD execution					**1st MLP-ARD execution**				
(Nm)	Bearing without fault (%)	Damage at the front side of the gearbox (%)		Damage at the rear side of the gearbox (%)		Bearing without fault (%)	Damage at the front side of the gearbox (%)		Damage at the rear side of the gearbox (%)	
0	100	3.8		100		100	84.7		100	
5	100	32.1		100		100	48.9		100	
10	100	36.7		100		100	52.7		100	
		2nd MLP-ARD execution		**3rd MLP-ARD execution**			**2nd MLP-ARD execution**		**3rd MLP-ARD execution**	
		Fault to bearing No.1	Fault to bearing No.2	Fault to bearing No.3	Fault to bearing No.4		Fault to bearing No.1	Fault to bearing No.2	Fault to bearing No.3	Fault to bearing No.4
		100	100	100	100		100	100	100	100
		100	100	100	100		100	100	100	100
		100	100	100	100		100	100	100	100

In the case study of 1370rpm at the gearbox input shaft the results are very high for all the cases (99.2-100%). This occurs, because the system has been trained in these operation conditions. But in the case study of 2700rpm the efficiency is low only when there is a fault at the at the rear part of the gearbox and for 1s signal (60.3-100%). This confirms previous suspicions concerning the low reliability of the use of such a small signal as input to the expert system. In the second level, in order to diagnose whether the damage is at the upper or at the lower bearing the 2th and the 3rd MLP-ARD were executed. In this case the diagnostic efficiency is good (64.1-100%).

Tab. 7. – Evaluation of theefficiency of diagnostic system after training with a 5 Nm load at the output gearbox shaft, 5th gearbox speed and 1370rpm at the input gearbox shaft

	(Training) 5th speed at the gearbox 1370rpm input shaft - 1370rpm output shaft **(Time period 1sec- 131 values)**						(Training) 5th speed at the gearbox 1370rpm input shaft - 1370rpm output shaft **(Time period 10sec- 1310 values)**				
(Scenario) 5th speed at the gearbox 1370rpm input shaft -1370rpm output shaft										
	1st MLP-ARD execution					**1st MLP-ARD execution**				
(Nm)	Bearing without fault (%)	Damage at the front side of the gearbox (%)		Damage at the rear side of the gearbox (%)		Bearing without fault (%)	Damage at the front side of the gearbox (%)		Damage at the rear side of the gearbox (%)	
0	100	100		100		100	100		100	
5	100	100		100		100	100		100	
10	100	100		100		100	100		100	
		2nd MLP-ARD execution		**3rdMLP-ARD execution**			**2nd MLP-ARD execution**		**3rd MLP-ARD execution**	
		Fault to bearing No.1	Fault to bearing No.2	Fault to bearing No.3	Fault to bearing No.4		Fault to bearing No.1	Fault to bearing No.2	Fault to bearing No.3	Fault to bearing No.4
		99.2	100	100	100		100	100	100	100
		100	100	100	100		100	100	100	100
		100	100	100	100		100	100	100	100

Tab. 8. – Evaluation of theefficiency of diagnostic system after training with a 5 Nm load at the output gearbox shaft, 5th gearbox speed and 2700rpm at the input gearbox shaft

	(Training) 5th speed at the gearbox 1370rpm input shaft - 1370rpm output shaft **(Time period 1sec- 131 values)**						(Training) 5th speed at the gearbox 1370rpm input shaft - 1370rpm output shaft **(Time period 10sec- 1310 values)**				
(Scenario) 5th speed at the gearbox 2700rpm input shaft -2700rpm output shaft										
	1st MLP-ARD execution					**1st MLP-ARD execution**				
(Nm)	Bearing without fault (%)	Damage at the front side of the gearbox (%)		Damage at the rear side of the gearbox (%)		Bearing without fault (%)	Damage at the front side of the gearbox (%)		Damage at the rear side of the gearbox (%)	
0	100	100		60.3		100	100		100	
5	100	100		74.8		100	100		100	
10	100	100		60.3		100	100		100	
		2nd MLP-ARD execution		**3rdMLP-ARD execution**			**2nd MLP-ARD execution**		**3rd MLP-ARD execution**	
		Fault to bearing No.1	Fault to bearing No.2	Fault to bearing No.3	Fault to bearing No.4		Fault to bearing No.1	Fault to bearing No.2	Fault to bearing No.3	Fault to bearing No.4
		94.7	99.7	99.2	100		100	100	100	100
		64.1	100	100	100		100	100	100	100
		72.5	100	100	100		100	100	100	100

CONCLUSIONS

It is evident that the neural network MLP-ARD can provide reliable results using as inputs features in time domain and in frequency domain. These features were extracted from vibration signals with different time lengths (1s and 10s). These features (according to their nature) can be used with success for fault diagnosis of rolling and roller bearings. The combination of the futures with the appropriate neural network gives us a powerful tool for bearing condition monitoring and early fault diagnosis in mechanical gearboxes. Furthermore, the features can identify with sufficient precision the point in which the fault occurs. It has been observed that a small signal (1s) provides a smaller diagnostic efficiency compared to a larger one (10s). Also, when the system is verified in training operational conditions then it gives better results relative to all other combinations training - verification. The system has a strong ability to be trained in a specific load at the output gearbox shaft. In future work the expert system effectiveness will be investigated using more data from different types of faults in rolling bearings of the gearbox in order to confirm further the system reliability.

REFERENCES

1. BAUGH, K. W.: On Parametrically Phase-Coupled Random Harmonic Processes, In: Proceedings of the IEEE Signal Processing Workshop on Higher-Order Statics, 1993: pp. 346–350.
2. BROTHERTON, T. B., POLLARD, T: Applications of time-frequency and time-scale representations to fault detection and classification. In: Proceedings of the IEEE Signal Processing International Symposium on Time-Frequency and Time- Scale Analysis, Orlando, FL, Vol. 2242, 1992: pp. 95–98.
3. CHOE, H. C., POOLE, C. E., YU, A. M., SZU, H. H.: Novel Identification of Intercepted Signals from Unknown Radio Transmitters, In: Proceedings of the SPIE Wavelet Applications, 2419, 17 April 1995: pp. 504–517.
4. CHOW, M., SHARPE, R. N., HUNG, J.: On the application and design of artificial neural network for motor fault detection—II, IEEE Transactions on Industrial Electronics, 40 (2), 1993: 189–196.
5. DU, Q., YANG, S.: Improvement of the EMD method and applications in defect diagnosis of ball bearings, Measurement Science and Technology, 17, 2006: 2355-2361.
6. HECK, L. P., CHOU, K. C.: Gaussian mixture model classifier for machine monitoring, In: Proceedings of the IEEE world Congress on Computational Neural Network and International Conference on Intelligence, Vol. 7, 1994: pp. 4493–4496.
7. HENG, R., NOR, M.: Statistical analysis of sound and vibration signals for monitoring rolling element bearing condition, Applied Acoustics, 53, 1998: 211-226.
8. LEONARD, J. A., KRAMER, M. A.: Radial basis function networks for classifying process faults, IEEE Control Systems Magazine, 1991: 31–38.
9. LOUTRIDIS, S.: Gear failure prediction using multiscale local statistics, Engineering Structures, 30, 2008: 1214-1223.
10. LEI, Y., HE, Z., ZI, Y.: A new approach to intelligent fault diagnosis of rotating machinery, Expert Systems and Applications, 36, 2008: 1593-1600.
11. MEYER, E., TUTHILL, T.: Bayesian classification of ultrasound signals using wavelet coefficients, In: Proceedings of the IEEE National Aerospace and Electronics Conference (NAECON), Vol. 1, 1995: pp. 240–243.
12. MOSHOU, D., KATERIS, D., GRAVALOS, I., LOUTRIDIS, S., SAWALHI, N., GIALAMAS, TH., XYRADAKIS, P., TSIROPOULOS, Z.: Determination of fault topology in mechanical subsystems of agricultural machinery based on feature fusion and neural networks. In Proceedings of the 4th International Conference TAE 2010, 7-10 September 2010: pp. 448-453, Prague, Czech Republic.
13. PENG, T., GUI, W., WU, M., XIE, H.: A fusion diagnosis approach to bearing faults, In: Proceedings of the International Conference on Modeling and Simulation in Distributed Applications, 2001: pp. 759–766.
14. RANDALL, R. B., ANTONI, J. AND CHOBSAARD, S.: The relationship between spectral correlation and envelope analysis in the diagnostics of bearing faults and other cyclostationary machine signals. Mechanical Systems and Signal Processing, 15(5), 2001: 945-962.
15. STACK, J. R., HABETLER, T. G., HARLEY, R. G.: Fault Classification and Fault Signature Production for Rolling Element Bearing in Electric Machines. In: Proceedings of the 4th IEEE Symp. on Diagnostics for Electric Machines, Power Electronics and Drives, 2004, 172-176.
16. YANG, D. M., STRONACH, A. F., MACCONNEL, P.: Third-order spectral techniques for the diagnosis of motor bearing condition using artificial neural network, Mechanical Systems and Signal Processing, 16 (2-3), 2002: 391–411.

Corresponding author:

Dimitrios Kateris Aristotle University of Thessaloniki, School of Agriculture, Agricultural Engineering Laboratory, 54124, Thessaloniki, Greece, email: dkateris@agro.auth.gr

A NUMERICAL SIMULATION OF STEEL QUENCHING

A. Kešner, R. Chotěborský, M. Linda

Department of Material Science and Manufacturing Technology,Faculty of Engineering, Czech University of Life Sciences Prague, Czech Republic

Abstract
This article deals with the appropriate setting of marginal conditions for the creation of mathematical model. For description of transformation kinetics of diffusion Johnson-Mehl-Avrami-Kolmogorov equation was utilized and for the construction of FEM model the pattern Ø25mm x 50 mm was used. Determined FEM model was verified experimentally and results showed that there is good agreement between the mathematical model and the experimental method. From conducted study it follows that FEM models can be utilized for the design and optimization of thermal processing and that these models are important tools for heat treatment prediction.

Key words: FEM model, microstructure, steels.

INTRODUCTION

Mathematical models are important for the design and optimization of heat treatment. Their application in the production enables prediction of microstructure. Mathematical models require low time consumption and finances sources than practical tests. Compilation of mathematical models requires knowledge of several important parameters such as: physical parameters of the material, the chemical composition of the material, boundary conditions of the material (heat capacity, thermal conductivity, density, temperature of phase transformation) (SERAJZADEH, 2004; ŞIMŞIR A GÜR, 2008). Another important condition is the knowledge of heat flux during cooling. Heat flux is usually calculated based on experimental measurements (PRABHU A PRASAD 2003; BARDELCIK ET AL., 2014) however it can be also modelled, but this solution requires a very demanding model on discretization and complicated and time-consuming calculation (DU ET AL., 2016; CARON ET AL., 2013).

Quenching parameters such as heating temperature, the type of cooling medium influencing the phase transformation from austenite to bainite, pearlite, ferrite and martensite in dependence on the chemical composition of the material (YU ET AL., 2010; YANG A BHADESHIA, 2009). Obviously it is very well known that these quenching parameters can be optimized using mathematical models. Isothermal cooling models are formed with Johnson-Mehl-Avrami-Kolgomov equations for diffusion transformation. These equations are a function of nucleation and growth of a new phase from austenite in dependence on time (KIANEZHAD A SAJJADI, 2013; NEUMANN A BÖHLKE, 2016). For a non-diffusion transformation are used Koistinen-Marburger equations where transformation from austenite to martensite is a function of temperature (NEUMANN A BÖHLKE, 2016; CASEIRO ET AL., 2011). Time of the beginning and time of the end of phase transformations are other important boundary conditions which should also be considered in development of mathematical model. These data are determined from the CCT diagrams for the steel (BABU A PRASANNA KUMAR, 2014; KIM ET AL., 2007; YUAN ET AL., 2003).

The aim of this article is to propose a system for calculating and to determine algorithms which will calculate and predict the microstructure of carbon steels during their heat treatment in various cooling environments.

MATERIALS AND METHODS

The Neumann's boundary conditions together with Lagrange algorithm were chosen to complete the FEM model (DOMAŃSKI A BOKOTA, 2011; PIEKARSKA ET AL., 2011).

In this model the heat flux was used as one of the Neumann's boundary conditions. Practical experiment to determine heat flux was measured on the cylinder ø25-50 mm made of steel 25CrMo4. Heat treatment was carried out at temperatures of heating of 800°C, 900°C and 1000°C. Water was chosen as the cooling medium for the quenching. Temperatures were recorded during the heat treatment in the axis and on the surface of the cylinder. Measured data (temperatures depending on time) was processed in the program Scilab 5.5.1. (SCILAB ENTERPRISES, 2014) in which the algorithms were solute. Heat flux was calculated from the data for hardening (LI A WELLS, 2005; FERNANDES A PRABHU, 2007).

Specific heat capacity *cp* and coefficient of thermal conductivity λ were other boundary conditions which were taken from published data (HUO ET AL., 2015).

Next step for the assembly FEM model was to create mesh. The density of the mesh was chosen based on the sample size (ø25-50 mm). Mesh had the highest density on the surface; toward to the middle of the cylinder the mesh was less dense. Condition that the calculation must not diverge was met. The calculation was terminated using an algorithm and mesh density was not changed by the algorithm. A model describing the temperature field counting on nontransient heat conduction was described by equation 1:

$$\frac{\partial}{\partial x}\left(k\frac{\partial T}{\partial x}\right)+\frac{\partial}{\partial y}\left(k\frac{\partial T}{\partial y}\right)+\frac{\partial}{\partial z}\left(k\frac{\partial T}{\partial z}\right)+Q=\rho\times c\times\frac{\partial T}{\partial t} \qquad (1)$$

Where: k – thermal conductivity ($W\times m^{-1}\times K^{-1}$), Q – inner heat – generation rate per unit volume ($J\times m^{-3}$), T – temperature (K), q – heat transfer coefficient ($W\times m^{-2}\times K^{-1}$), ρ – density ($kg\times m^{-3}$), c – heat capacity ($J\times kg^{-1}\times K^{-1}$), t – time (s).

Heat capacity and heat thermal coefficient were determined by iteration algorithm from measured data.

Phase transformation from austenite to martensite is nondiffusion process. Koistinen-Hamburger Displacive law describes the process as a function of temperature - Equation 2, 3.

$$V_m = 1 - e^{-\alpha\times(M_S - T)} \qquad (2)$$

$$V_{P,B} = 1 - e^{-k\times t^n} \qquad (3)$$

Where: α, Ms – constants based on material type (-), k – constant dependent on temperature (-), n – Avrami's exponent (-)

Phase transformations from austenite to ferrite, perlite or bainite are diffusion processes that are time dependent. The kinetics of diffusion transformation was described by Johnson-Mehl-Avrami-Kolmogorov equation. Approximate solution of development phases of the individual transformations was predicted on the basis of data from TTT diagram (CHOTĚBORSKÝ AND LINDA, 2015; SINHA ET AL., 2007). The algorithm for the calculation was written in Basic (MICROSOFT, 2010) because processed data were filed faster by visual basic than by already mentioned Scilab(SCILAB ENTERPRISES, 2014).

Derivation of equations 2 and 3 were performed to determine the amount of emerging new phase. Speed generated phase per unit of time was thereby obtained. So obtained equations were modified for the numerical solution (4-6).

$$Vf = \sum_{i=1}^{n} -Kf\times Nf\times t^{Nf-1}\times e^{-Kf\times t^{Nf}}\times(1-Vf_{\max}) \qquad (4)$$

$$Vp = \sum_{i=1}^{n} -Kp\times Np\times t^{Np-1}\times e^{-Kp\times t^{Np}}\times(1-Vf) \qquad (5)$$

$$Vb = \sum_{i=1}^{n} -Kb\times Nb\times t^{Nb-1}\times e^{-Kb\times t^{Nb}}\times(1-Vf-Vp) \qquad (6)$$

Where: Vf – volume of ferite phase (-), Vp – volume of pearlite phase (-), Vb – volume of bainite phase (-), Kf, Kp, Kb – overall rate constant of feritic, pearlitic and bainitic transformation that generally depends on temperature (-), Nf, Np, Nb – Avrami's exponent for feritic, pearlitic and bainitic transformation that depends on temperature (-).

Metallographic samples of tested steel were cut and polished from heat treated samples and etched in a solution obtained by dissolving nitric acid (2 ml) in ethanol (100 ml) Nital. The nital etchant was used for the determination of bainite volume. Austenite phase was determined by using Klemm etchant (2 g K2S2O5 + 100 ml supersaturated K2S2O3 in water) where austenite phase was not attached and bainite or martensite showed dark blue colour. Phase percentage in each sample was measured using SciLab Image and Video Processing toolbox, where threshold was obtained by a binary matrix algorithm. The algorithm was written for a proportion phase's evaluation.

Correlations and index of determination were calculated between measured data and computed data.

RESULTS AND DISCUSSION

Examples of coefficients c_o, c_1 and c_2 of heat flux are shown in Equations 7-10. These coefficients determine the character of the heat flux curve depending on the relative surface temperature. The coefficients are valid for the range of heating temperatures from 800°C to 1000°C and for the temperature of cooling in the water. General equation was obtained from the individual results of experimental measurement of steel.

$$q(T) = C_0 \times T^{C_1} \times (1-T)^{C_2} \qquad (7)$$

$$C_0 = 1{,}545x10-7 \cdot \log(T) + 1{,}273 \cdot 108 \qquad (8)$$

$$C_1 = -0.357 \cdot \log(T) + 3.566 \qquad (9)$$

$$C_2 = -0.902 \cdot \log(T) + 7.299 \qquad (10)$$

Where: q – heat flux ($W\times m^{-2}$), T – relative temperature (0 to 1) calculated from Tp a Ts(-), c_o – constant of reinforcement (-), c_1, c_2 – constant slope from the peak, may characterize curve slope (-), Tp – furnace temperature (K)

Maximum volume fraction V are already known from preliminary isothermal investigations, temperature-dependend parameters K(T) and n(T) can be determined from the measured isothermal transformation diagrams. Generally, times t_s and t_f characterizing the start and finish of isothermal austenite transformation as a function of temperature are plotted in a form C-curves in IT diagrams. According to the traditional definition of C-curves, times t_s and t_f denote 1% and 99% of relative transformed fractions, respectively. Based on the use of Eq. 3, the following relationships can be derived:

$$ln\frac{1}{1-0.01} = K \times t_s^n \qquad (11)$$

and

$$ln\frac{1}{1-0.99} = K \times t_f^n \qquad (12)$$

The parameters K and n can be obtained directly from Eq. 11 and 12:

$$n(T) = \frac{6.1273}{ln\frac{t_f}{t_s}} \qquad (13)$$

and

$$K(T) = \frac{0.01005}{t_s^{n(T)}} \qquad (14)$$

For every constant temperature it follows from consideration above, that the multi-phase model can be applied to the prediction of isothermal as well as to the anisothermal transformation processes. The pseudo-autonomous differential equation can be solved only by numerical methods, provided that model parameters V, K and n are previously estimated, and given as a function of temperature.

Data for model of phase transformation were:

Steel 51CrV4

A1=732 °C, A3=775 °C, Ms=286 °C, M50=250 °C, Bs=500 °C and limits for austenite phase transformation were:

Ferite:

Temperature range from 550 to 732 °C

$$n(T) = 39{,}714 + 0{,}13596 \times T - 0{,}000\,1098 \times T^2$$

$$K(T) = -1{,}3873 \times 10^{-3} + 1{,}19388 \times 10^{-5} \times T - 4{,}0959 \times 10^{-8} \times T^2 + 7{,}0035 \times 10^{-11} \times T^3 - 5{,}9687 \times 10^{-14} \times T^4 + 2{,}028 \times 10^{-17} \times T^5$$

Pearlite:

Temperature range from 500 to 700 °C

$$n(T) = 91{,}6391 + 0{,}512 \times T + 0{,}000\,9503 \times T^2 - 0{,}000\,000\,57653 \times T^3$$

$$K(T) = -4{,}6049 \times 10^{-4} + 4{,}124 \times 10^{-6} \times T - 1{,}47412 \times 10^{-8} \times T^2 + 2{,}62946 \times 10^{-11} \times T^3 - 2{,}34169 \times 10^{-14} \times T^4 + 8{,}3313 \times 10^{-18} \times T^5$$

Bainite:

Temperature range from 286 °C to 500 °C

$$n(T) = -0{,}4241 - 0{,}011\,852 \times T + 0{,}000\,0179\,4 \times T^2$$

$$K(T) = -1{,}004 \times 10^{-4} + 1{,}1117 \times 10^{-6} \times T - 3{,}90286 \times 10^{-9} \times T^2 + 4{,}49955 \times 10^{-12} \times T^3$$

Martensite:

Temperature range from under 286 °C

$$M(T) = 1 - e^{-0{,}01964 \times (Ms - T)}$$

Specific heat capacity and thermal conductivity are not constant during the cooling of the material such as evident from Fig. 1. It is clear that the right graph presents the dependency between thermal conductivity and a relative temperature and left graph presents dependency between the heat capacity and relative temperatures for material C60. These characteristics were determined using iteration algorithm with aid of obtained data from measurement of temperature during cooling. Each of iteration found minimal deviation between measured cooling curve and modelled temperature by FEM where dependency of thermal conductivity and thermal heat specific were fitted by Newton polygons. In the case where the deviation between measured data and predicted were minimal the algorithm began to calculate new FEM model using obtained data and boundary conditions.

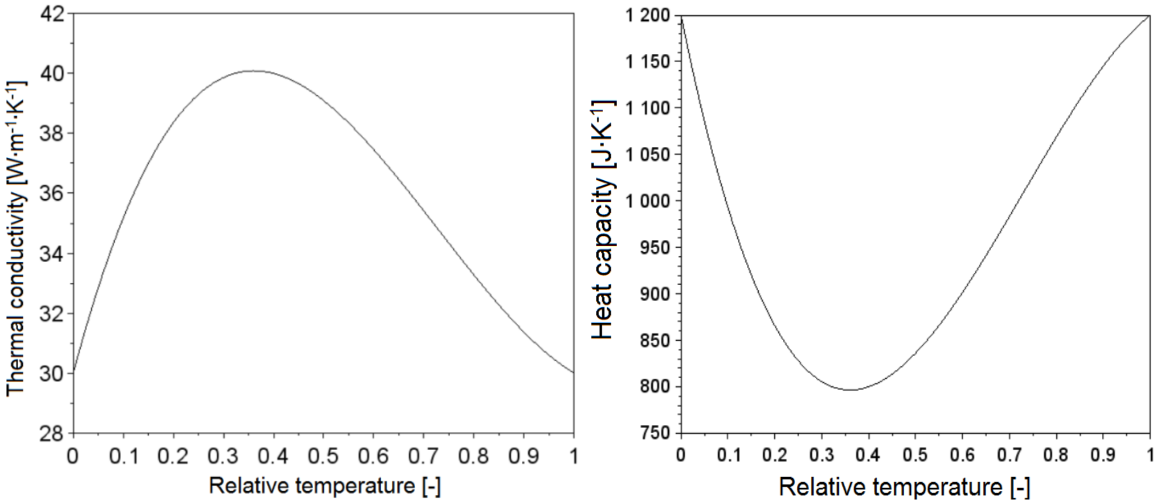

Fig. 1. – On the left side it is relationship between thermal conductivity and relative temperature and right side is relationship between heat capacity and relative temperature for material C60 – heating temperature 800°C and cooling in calm water

Content of phases depending on the distance from the surface are compared to material C60 and they are shown in Fig. 2. The sample was heated at a heating temperature of 900 °C and quenched in a calm water of 20 °C. Result shown a good correlation between predicted and measured microstructure of tested steel which was quenched in water. Correlation analysis and F-test are shown a significant dependency between computed and measured martensite volume phase (R=0.899 and F=0.9265, F_{krit}=0.4285), also for pearlite (R=0.8975 and F=1.0840, F_{krit}=2.3335), but correlation between computed and measured ferritic volume phase was not significant (R=0.6646 and F=1.6939, F_{krit}=0.4285). The computed volume phase of ferrite depend on strict boundary condition of the numerical model and each of deviance of the temperature-time kinetics dependency influence a coefficients n and k for JMAK equation. Also kinetic of austenite phase transformation of tested steel and other materials properties such as austenite grain size directly influence start and finish of transformation phase (BHADESHIA, 2004; PRABHU A FERNANDES, 2007).

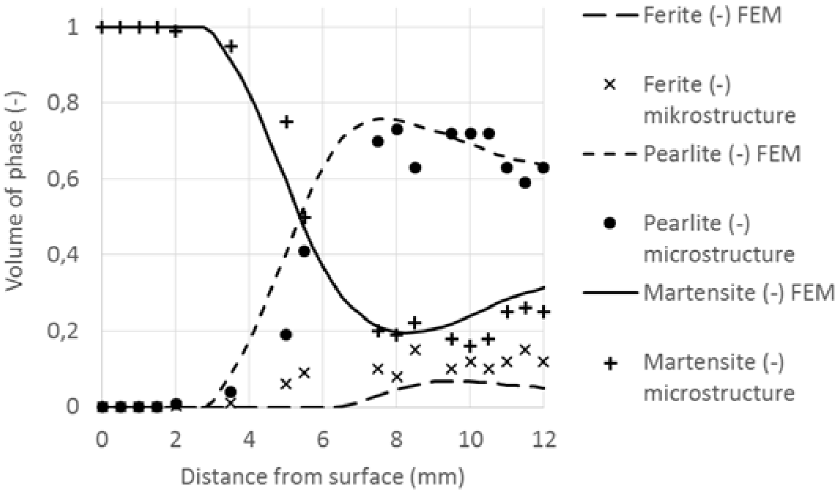

Fig. 2. – Volume of phase content depends on distance from surface

In already published study (PRASANNA KUMAR, 2013) the heat flux of different types of steel was described. It was discovered that the chemical composition of the steel significantly affects the heat flow that is one of the important boundary conditions. The differences between the estimated phase of the model (FEM) and the experimentally determined structure were detected. These differences are caused by negligence of phase transformations, different chemical composition of the material and the grain size. These differences can incorporate into the model. MI ET AL. (2014) also included these differences in their models of phase transformation. Differences between the model and the practical measurements have diminished, but not completely eliminated. SERAJZADEH (2004) in his work explored the transformation of austenite phase and his results also show good agreement of FEM model and experimentally obtained data, however, they are still noticeable differences.

CONCLUSIONS

FEM model was developed to simulate thermal processing. FEM model was validated by an experimental method. The obtained results and the literature cited include the following conclusions:

- Between the model and calculations are differences. Their size may be regarded as unacceptable. Measured and calculated phase in the steel shown a good correlation
- Using the FEM model it can be predicted other properties for heat treatment such as the microstructure of the treated material.
- Described procedure can be used for an optimization of heat treatment plain carbon and low alloying steels for agriculture tools and assemblies.

This procedure can also be used to optimize the design steps of heat treatment in workshops, to set up heat treatment and their next qualitative controls.

ACKNOWLEDGEMENTS

This study was supported by Internal grant 31140/1312/3108 agency of Faculty of Engineering, Czech University of Life Sciences Prague.

REFERENCES

1. BABU, K. A T. S. PRASANNA KUMAR, 2014: Comparison of Austenite Decomposition Models During Finite Element Simulation of Water Quenching and Air Cooling of AISI 4140 Steel. *Metallurgical and Materials Transactions B* [online]. 19.4., roč. 45, č. 4, s. 1530–1544 [vid. 14. září 2015]. ISSN 1073-5615.
2. BARDELCIK, ALEXANDER, MICHAEL J. WORSWICK A MARY A. WELLS, 2014: The influence of martensite, bainite and ferrite on the as-quenched constitutive response of simultaneously quenched and deformed boron steel – Experiments and model. *Materials & Design* [online]. 3., roč. 55, s. 509–525 [vid. 4. leden 2015]. ISSN 02613069.
3. BHADESHIA, H.K.D.H., 2004:Developments in martensitic and bainitic steels: role of the shape deformation. *Materials Science and Engineering: A* [online]. roč. 378, č. 1-2, s. 34–39 [vid. 11. listopad 2014]. ISSN 09215093.
4. CARON, ETIENNE, KYLE J. DAUN A MARY A. WELLS, 2013: Experimental Characterization of Heat Transfer Coefficients During Hot Forming Die Quenching of Boron Steel. *Metallurgical and Materials Transactions B* [online]. 1.4., roč. 44, č. 2, s. 332–343. ISSN 1073-5615.
5. CASEIRO, J. F., J. A. OLIVEIRA A A. ANDRADE-CAMPOS, 2011: On the thermomechanical modelling of multiphase materials during heat treatments and subsequent forming. In: [online]. s. 1568–1573. Dostupné z: doi:10.1063/1.3589740
6. DOMAŃSKI, T. A A. BOKOTA, 2011: Numerical Models of Hardening Phenomena of Tools Steel Base on the TTT and CCT Diagrams. *Archives of Metallurgy and Materials* [online]. 1.1., roč. 56, č. 2 [vid. 11. listopad 2014]. ISSN 1733-3490.
7. DU, FENG-MING, XU-DONG WANG, YU LIU, TIAN-YI LI A MAN YAO, 2016: Analysis of Non-uniform Mechanical Behavior for a Continuous Casting Mold Based on Heat Flux from Inverse Problem. *Journal of Iron and Steel Research, International* [online]. 2., roč. 23, č. 2, s. 83–91. ISSN 1006706X.
8. FERNANDES, PETER A K. NARAYAN PRABHU, 2007: Effect of section size and agitation on heat transfer during quenching of AISI 1040 steel. *Journal of Materials Processing Technology* [online]. 3., roč. 183, č. 1, s. 1–5 [vid. 9. září 2015]. ISSN 09240136.
9. HUO, YUANMING, QIAN BAI, BAOYU WANG, JIANGUO LIN A JING ZHOU, 2015: A new application of unified constitutive equations for cross wedge rolling of a high-speed railway axle steel. *Journal of Materials Processing Technology* [online]. 9., roč. 223, s. 274–283. ISSN 09240136.
10. CHOTĚBORSKÝ, R. A M. LINDA, 2015: FEM based numerical simulation for heat treatment of the agricultural tools. *Agronomy Research* [online]. B.m.: Eesti Pollumajandusulikool, roč. 13, č. 3, s. 629–638. ISSN 1406894X.
11. KIANEZHAD, M. A S. A. SAJJADI, 2013:Improvement of Quench Factor Analysis in Phase and Hardness Prediction of a Quenched Steel. *Metallurgical and Materials Transactions A* [online]. 19.5., roč. 44, č. 5, s. 2053–2059. ISSN 1073-5623.
12. KIM, YOON-JUN, L. SCOTT CHUMBLEY A BRIAN GLEESON, 2007: Continuous Cooling Transformation in Cast Duplex Stainless Steels CD3MN and CD3MWCuN. *Journal of Materials Engineering and Performance* [online]. 22.6., roč. 17, č. 2, s. 234–239 [vid. 11. listopad 2014]. ISSN 1059-9495.
13. LI, D. I. A M. A. WELLS, 2005: Effect of subsurface thermocouple installation on the discrepancy of the measured thermal history and predicted surface heat flux during a quench operation. *Metallurgical and Materials Transactions B* [online]. 6., roč. 36, č. 3, s. 343–354 [vid. 6. červenec 2015]. ISSN 1073-5615.
14. MI, GAOYANG, YANHONG WEI, XIAOHONG ZHAN, CHENG GU A FENGYI YU, 2014: A coupled thermal and metallurgical model for welding simulation of Ti–6Al–4V alloy. *Journal of Materials Processing Technology* [online]. 11., roč. 214, č. 11, s. 2434–2443 [vid. 11. listopad 2014]. ISSN 09240136.
15. MICROSOFT, 2010.*Visual Basic . NET*. 2010.
16. NEUMANN, RUDOLF A THOMAS BÖHLKE, 2016: Hashin–Shtrikman type mean field model for the two-scale simulation of the thermomechanical processing of steel. *International Journal of Plasticity* [online]. 2., roč. 77, s. 1–29. ISSN 07496419.

17. PIEKARSKA, W., M. KUBIAK A A. BOKOTA, 2011: Numerical Simulation of Thermal Phenomena and Phase Transformations in Laser-Arc Hybrid Welded Joints. *Archives of Metallurgy and Materials* [online]. 1.1., roč. 56, č. 2 [vid. 11. listopad 2014]. ISSN 1733-3490.
18. PRABHU, K. NARAYAN A PETER FERNANDES, 2007: Effect of surface roughness on metal/quenchant interfacial heat transfer and evolution of microstructure. *Materials & Design* [online]. 1., roč. 28, č. 2, s. 544–550 [vid. 11. listopad 2014]. ISSN 02613069.
19. PRABHU, K. NARAYAN A AMLAN PRASAD, 2003: Metal/Quenchant Interfacial Heat Flux Transients During Quenching in Conventional Quench Media and Vegetable Oils. *Journal of Materials Engineering and Performance* [online]. 1.2., roč. 12, č. 1, s. 48–55 [vid. 14. září 2015]. ISSN 00000000.
20. PRASANNA KUMAR, T. S., 2013: Influence of Steel Grade on Surface Cooling Rates and Heat Flux during Quenching. *Journal of Materials Engineering and Performance* [online]. 18.4., roč. 22, č. 7, s. 1848–1854 [vid. 11. listopad 2014]. ISSN 1059-9495.
21. SCILAB ENTERPRISES, 2014:*Scilab-5.5.1* [online]. 2014. Dostupné z: http://www.scilab.org/
22. SERAJZADEH, SIAMAK, 2004: A mathematical model for prediction of austenite phase transformation. *Materials Letters* [online]. 4., roč. 58, č. 10, s. 1597–1601 [vid. 11. listopad 2014]. ISSN 0167577X.
23. ŞIMŞIR, CANER A CEMIL HAKAN GÜR, 2008: A FEM based framework for simulation of thermal treatments: Application to steel quenching. *Computational Materials Science* [online]. 12., roč. 44, č. 2, s. 588–600 [vid. 11. listopad 2014]. ISSN 09270256.
24. SINHA, V.K., R.S. PRASAD, A. MANDAL A J. MAITY, 2007:A Mathematical Model to Predict Microstructure of Heat-Treated Steel. *Journal of Materials Engineering and Performance* [online]. 17.4., roč. 16, č. 4, s. 461–469 [vid. 11. listopad 2014]. ISSN 1059-9495.
25. YANG, H A H BHADESHIA, 2009: Austenite grain size and the martensite-start temperature. *Scripta Materialia* [online]. 4., roč. 60, č. 7, s. 493–495 [vid. 28. říjen 2014]. ISSN 13596462.
26. YU,WAN-HUA, LÜ-TING XU, GUANG-HONG FENG, CHUN-JING WU, CHENG ZHOU A HUI-FENG WANG, 2010: Modeling the austenite-ferrite transformation in microalloyed steel P510L. *International Journal of Minerals, Metallurgy, and Materials* [online]. 9.10., roč. 17, č. 5, s. 558–566 [vid. 11. listopad 2014]. ISSN 1674-4799.
27. YUAN, J., J. KANG, Y. RONG A R. D. SISSON JR, 2003: FEM Modeling of Induction Hardening Processes in Steel. *Journal of Materials Engineering and Performance* [online]. 1.10., roč. 12, č. 5, s. 589–596 [vid. 11. listopad 2014]. ISSN 00000000.

Corresponding author:
Ing. Adam Kešner, Department of Material Science and Manufacturing Technology, Faculty of Engineering, Czech University of Life Sciences Prague, Kamýcká 129, Praha 6, Prague, 16521, Czech Republic, phone: +420 22438 3271, e-mail: kesner@tf.czu.cz

DUST POLLUTION IN BUILDINGS FOR CHICKEN FATTENING

P. Kic

Department of Technological Equipment of Buildings, Faculty of Engineering, Czech University of Life Sciences Prague, Czech Republic

Abstract

The aim of this paper is to present the results of dust measurement in two poultry houses. Total dust concentrations measured by Dust-Track aerosol monitor were 1,425.4 ± 270.8 and 1,476.4 ± 219.4 μg·m^{-3}. Using impactors PM_1, $PM_{2.5}$, PM_4, PM_{10} size fractions were measured. The majority of dust particles inside poultry houses created the particles bigger than 4 μm (83 % hall A, 82 % hall B). The biggest percentage (50 % hall A, 43 % hall B) of dust were the particles bigger than 10 μm. The parallel arrangement of halls and cross ventilation increased by 31 % dust pollution of air inlet of second hall B than in air supplied into the first hall A. Removal efficiency of total dust by ventilation was 0.13 in hall A and 0.19 in hall B, in the case of smaller particles PM_1, $PM_{2.5}$, PM_4 was from 0.44 to 0.76.

Key words: air, dust fractions, efficiency of dust removal, measurement.

INTRODUCTION

Poultry housing technology, external climatic conditions and weather influence the indoor microclimate during different periods of the year. Creation of internal environment in the halls for poultry housing is complicated mainly because of the high biological load of indoor environment, resulting from the large number of chickens per 1 m^2 of the floor area. Problems occur particularly towards the end of fattening. Chickens have a large mass; they produce large quantities of pollutants (AARNINK ET AL., 2009; KIC ET AL., 2012). Usually this problem is solved by intensive ventilation (KIC ET AL., 2007A; ŠOTTNÍK, 2007; ZAJÍČEK AND KIC, 2013A), but it has a rather negative influence also on the technical equipment (KIC ET AL., 2007B).

Dust particles which are smaller than 10 μm occur in the air in small amounts, but they have a great biological importance. They are inhaled, but for the most part they are already captured in the upper respiratory airways. Here, they are deposited a film of mucus, which is moved by cilia toward the nasopharynx. Smaller particles with an aerodynamic diameter of about 0.003 to 5 μm are deposited in the tracheobronchial and alveolar regions. Particle size of about 1 μm permeate bronchioles until the alveoli, where they are captured sometimes more than 90 %. These particles are therefore in the terms of retention of aerosol in the lungs the most dangerous. One of the best known diseases caused by organic dust is so called Farmer's lung (SETHI ET AL., 2013; VIEGAS ET AL., 2013).

To improve internal conditions inside the buildings can help different methods for reduction of noxious gases concentration or bad odor pollution (LIŠKA AND KIC, 2010; LIŠKA AND KIC, 2011), but the dust pollution can be by these methods hardly reduced. The source of dust is the poultry feather, particles of feed and bedding on the floor. Dust pollution can be reduced either by reduced production of dust at the source, which is in this case rather difficult, or by intensive ventilation. Some of publications present the methods of calculation of main parameters of ventilation system (GŰRDIL ET AL., 2001) and simulation of indoors conditions (MISTRIOTIS ET AL., 1997; MUTAI ET AL., 2011; ZAJÍČEK AND KIC, 2012; ZAJÍČEK AND KIC, 2013B; ZAJÍČEK AND KIC, 2013C).

The aim of this paper is to characterize particulate matter (PM) contamination and to show the measurement results of dust pollution in poultry houses and to study the influences of the indoor dust pollution by the hall construction and the farm design, particularly the possibility of influencing the dust pollution inside by surroundings and appropriate solution of the ventilation system.

MATERIALS AND METHODS

This research work and measurements were carried out in two buildings for fattening of meat chickens. Both poultry houses are located parallel to each other in one farm, and they are situated on the small slope, the 1st building is on the top, the 2nd hall is in the down part of the farm. Both halls have the same dimensions:

length 76 m, width 11.5 m, height 2.7 m, and inside each hall is housing of 16,800 chickens on the floor. The measurements were carried out on the 24th day of fattening when the chickens have average weight about 1.1 kg. The floor in the halls is covered by the bedding material Absorfyt made from chopped wheat straw.

The cross ventilation of halls is transverse, with under-pressure created by the axial fans in the side wall in outlets, with a total maximum air flow of 93,250 $m^3 \cdot h^{-1}$. The fresh air is sucked in the 1st hall from its opposite wall into the inlets from the open area. Into the 2nd hall the air is sucked from the space between these halls. The distance between the halls is about 16 m. Because of this arrangement of buildings the attention in this research is paid to the relations between the outlet from the hall and the suction into the inlet of the next hall.

The total concentration of air dust was measured by special exact instrument Dust-Track™ II Aerosol Monitor 8530 produced by TSI in USA, 500 Cardigan Road Shoreview, MN 55126, with operating range 0.001 to 150 $mg \cdot m^{-3}$ with resolution ± 0.1 % of reading of 0.001 $mg \cdot m^{-3}$, whichever is greater. Total dust concentration and after the installation of different impactors PM_{10}, PM_4, $PM_{2.5}$, PM_1 size segregated mass fractions of dust were also measured.

According to the type of material, dust has specific characteristics to which respond the properties. According to the Act Government Regulation No. 361/2007 Coll., this type of dust has irritating effects (poultry feather, particles of feed, straw and sawdust from the wood). For this type of dust the prescribed Occupational Exposure Limits (OEL) are permissible exposure limits of total concentration. There are Exposure Limits of some noxious gases in the animal houses from the animals' point of view, but there are not the limit values for the dust concentrations. Occupational Exposure Limits are listed in Tab. 1.

Tab. 1. – Types of dust and occupational exposure limits (OEL)

Dust	OEL ($\mu g \cdot m^{-3}$)
Feather	4,000
Feed	6,000
Straw	6,000
Sawdust	5,000

Measured dust inside this type of buildings is not aggressive, therefore, as a criterion for comparative evaluation of the measured values can be also used the limit level of outdoor dust. According to the Air Protection Act No. 201/2012 PM_{10} limit value in 24 hours is 50 $\mu g \cdot m^{-3}$, 1 year limit value is 40 $\mu g \cdot m^{-3}$ and 1 year limit value $PM_{2.5}$ is 25 $\mu g \cdot m^{-3}$.

Measuring devices and equipment technology environment continues to improve and provide a larger volume and more accurate results. New studies are constantly providing fresh information, but there are still many uncertainties. Maybe, new and more precise ideas about the influence on the human health or on the animals can be discovered.

Very helpful and also important is to know the details about the composition and size of dust particles from the point of view of technical equipment and technology of indoor environment. This is important among other things for the selection of appropriate filters, scheduling maintenance and cleaning, and overall management options how to reduce the dust inside the buildings.

One of the possibilities how to use the measurement results of dust concentrations is an assessment of the effectiveness of ventilation. Air moves inside a ventilated hall due to the pressure gradient between the air inlets and outlets. Location of air inlets and outlets together with the other factors inside the ventilated space affects the final effect of ventilation and manifests purity of the air. The final effect can be assessed as a dust removal efficiency, calculated according to equation (1). The maximum of dust removal efficiency could be theoretically $e_v = 1$, if the concentration of dust in the outgoing air is the same like the concentration inside the building. The same evaluation principle can be used not only for the total dust, but also for the calculation of a removal efficiency of dust particles, probably influenced also by air velocity, properties of particles and other factors. These results could be useful for improvement of ventilation system designs.

$$e_V = \frac{(k_o - k_e)}{(k_i - k_e)} \qquad (1)$$

Where: e_V – dust removal efficiency of ventilation, -;
k_o – concentration of dust in the outgoing air, $\mu g \cdot m^{-3}$;

k_e – concentration of dust in the incoming air, μg·m^{-3};

k_i – concentration of dust inside the poultry house, μg·m^{-3}.

Therefore the dust measurements have been provided not only according to the prescribed normal national or international standards (e.g. PM_{10} and $PM_{2.5}$), but it was also measured the total dust concentration and particulate matter by all available impactors PM. Larger amounts of information allow to obtain more detailed information on the composition and percentage of size fractions of dust.

The 90 data of dust concentration for total dust as well as of each fraction size in air inlets, inside the hall and in the outlet from the halls were collected. The obtained results of dust measurements were processed by Excel software and verified by statistical software STATISTICA 12 (*ANOVA and TUKEY HSD Test*).

Different superscript letters (a, b) mean values in common are significantly different from each other in the rows of the tables (*ANOVA; Tukey HSD Test;* $P \leq 0.05$), e.g. if there are the same superscript letters in all the rows it means the differences between the values are not statistically significant at the significance level of 0.05.

RESULTS AND DISCUSSION

Principal results of dust measurement in the halls A and B are summarized and presented in Tables 2-5 and Figures 1-3.

Tab. 2. – Dust concentrations total and fractions in air inlets, data in the table are means ± SD. Different letters (a, b) in the superscript are the sign of high significant difference (*ANOVA; Tukey HSD Test;* $P \leq 0.05$)

Hall	**A**	**B**
Dust	**(μg·m^{-3})**	**(μg·m^{-3})**
Total	127.3 ± 3.2^a	166.2 ± 2.9^b
PM_{10}	108.0 ± 1.1^a	164.7 ± 1.4^b
PM_4	116.9 ± 0.7^a	147.7 ± 1.9^b
$PM_{2.5}$	13.1 ± 1.7^a	14.5 ± 1.3^b
PM_1	9.2 ± 2.7^a	13.1 ± 1.3^b

The comparison of dust concentrations in the inlets of both halls (Tab. 2) shows that fresh air sucked into the inlet of hall A is less polluted than the air in inlet of the hall B. The concentration of dust in the air inlet of the hall B is higher by approximately 31 %, than the concentration of dust in the air supplied to the hall A.

This pollution of inlet air of hall B can be caused by discharged air from the outlet of the hall A. The side distance between the halls is probably not sufficient. The distribution of dust size fractions in air inlets into the poultry houses is presented in Fig. 1. The biggest percentage (73 % hall A, 79 % hall B) of dust are the particles smaller than 1 μm.

Comparison of dust concentration inside both halls is in Tab. 3. Total dust concentrations are not significantly different in both halls; also the difference of PM_4 is not statistically significant. OEL limits are not over crossed, but the concentrations of all dust particles are very high, which is obvious in comparison with the limit level of outdoor dust (PM_{10} limit value in 24 hours is 50 μg·m^{-3}, 1 year limit value is 40 μg·m^{-3} and 1 year limit value $PM_{2.5}$ is 25 μg·m^{-3}). These limit values are over crossed in all cases.

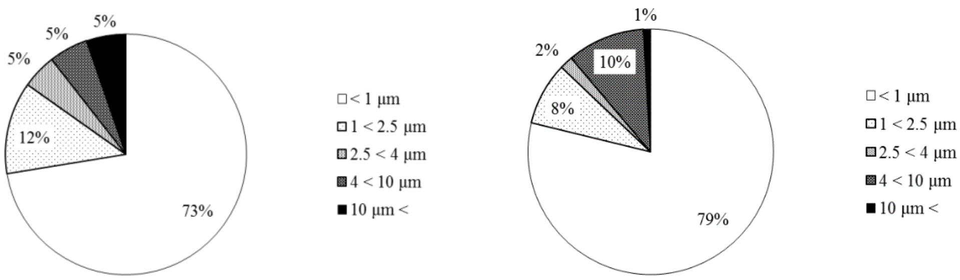

Fig. 1. – The distribution of dust size fractions in air inlet of the halls A (left) and B (right)

Tab. 3. – Dust concentration total and dust fractions inside, data in the table are means ± SD. Different letters (a, b) in the superscript are the sign of high significant difference (*ANOVA; Tukey HSD Test; P ≤ 0.05*)

Hall	**A**	**B**
Dust	**($\mu g \cdot m^{-3}$)**	**($\mu g \cdot m^{-3}$)**
Total	$1,425.4 \pm 270.8^{a}$	$1,476.4 \pm 219.4^{a}$
PM_{10}	716.4 ± 97.5^{a}	839.5 ± 113.5^{b}
PM_4	252.9 ± 45.6^{a}	256.7 ± 19.8^{a}
$PM_{2.5}$	118.8 ± 16.5^{a}	172.3 ± 17.0^{b}
PM_1	63.9 ± 17.6^{a}	75.8 ± 15.8^{b}

The distribution of dust size fractions inside the poultry houses is presented in Fig. 2. The biggest percentage (50 % hall A, 43 % hall B) of dust are the particles bigger than 10 µm. Rather big portion of dust (33 % hall A, 39 % hall B) create the dust particles smaller than 10 µm and bigger than 4 µm, which means that the majority of dust inside these poultry houses create the particles bigger than 4 µm (83 % hall A, 82 % hall B).

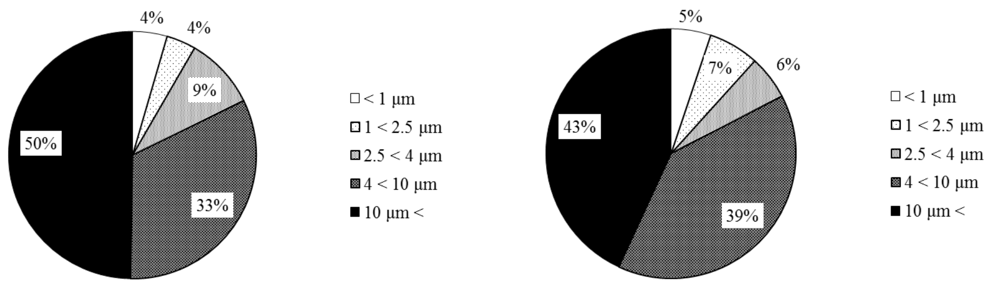

Fig. 2. – The distribution of dust size fractions in air inside the halls A (left) and B (right)

Tab. 4 – Dust concentration total and fractions in the air outlet, data in the table are means ± SD. Different letters (a, b) in the superscript are the sign of high significant difference (*ANOVA; Tukey HSD Test; P ≤ 0.05*)

Hall	**A**	**B**
Dust	**($\mu g \cdot m^{-3}$)**	**($\mu g \cdot m^{-3}$)**
Total	198.8 ± 56.6^{a}	295.6 ± 97.1^{b}
PM_{10}	176.3 ± 44.4^{a}	254.3 ± 44.9^{b}
PM_4	140.7 ± 42.5^{a}	197.5 ± 29.4^{b}
$PM_{2.5}$	76.6 ± 21.4^{a}	96.9 ± 16.4^{b}
PM_1	46.4 ± 11.1^{a}	40.6 ± 14.3^{b}

The comparison of dust concentrations in the outlets from both halls (Tab. 4) shows that air discharged from the outlet of hall A is less polluted than the air in outlet from the hall B. The total concentration of dust in the air outlet from the hall B is higher by approximately 49 %, than the concentration of dust in the air discharged from the hall A. This pollution of outlet air from hall B can be caused by higher concentration of dust inside the hall A.

The distribution of dust size fractions in air outlets from the poultry houses is presented in Fig. 3. The majority of dust inside these poultry houses is created by the particles smaller than 4 µm (70 % hall A, 67 % hall B). The biggest percentage (32 % hall A, 34 % hall B) of dust create particles bigger than 2.5 µm and smaller than 4 µm. Rather big portion (23 % hall A, 14 % hall B) of dust are the particles smaller than 1 µm.

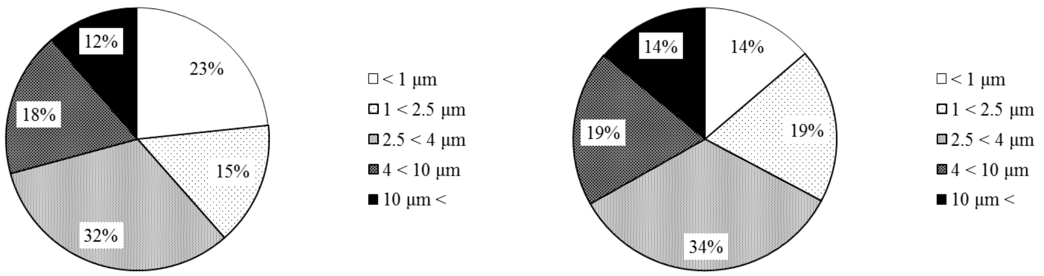

Fig. 3. – The distribution of dust size fractions in air outlet of the halls A (left) and B (right)

The measured values of dust concentrations of air in the inlet, inside the halls and in the outlet enable to calculate the dust removal efficiency of ventilation according to the equation (1).

Tab. 5. – Dust removal efficiency of ventilation in the halls A and B

	e_v (-)	
Hall	**A**	**B**
Total	0.13	0.19
PM_{10}	0.23	0.29
PM_4	0.54	0.76
$PM_{2.5}$	0.61	0.52
PM_1	0.68	0.44

The results of these measurements and calculations presented in Tab. 5 show that the dust removal efficiency of ventilation is rather dependent on the size of dust particles. If it is calculated for the case of total dust removal, the efficiency e_v is 0.13 in the hall A; e_v is 0.19 in the hall B. More efficient is dust removal of smaller particles PM_1, $PM_{2.5}$ and PM_4.

CONCLUSIONS

Total dust concentrations in poultry houses were 1,425.4 ± 270.8 and 1,476.4 ± 219.4 $\mu g \cdot m^{-3}$. The biggest percentage (50 % hall A, 43 % hall B) of dust are the particles bigger than 10 µm.

The comparison of dust concentrations in the inlets of both halls (Tab. 2) shows that the concentration of dust in the air inlet of the hall B is by approximately 31 % higher than the concentration of dust in the air supplied to the hall A. This pollution of inlet air of hall B can be caused by discharged air from the outlet of the hall A. The parallel arrangement of both buildings and cross transverse ventilation would need bigger side distance between the halls or another positioning and construction of inlets and outlets of air.

The suitable location of air outlets should prevent undesired recirculation of exhaust air back inside the hall or pollution of air sucked into another building. The poultry houses are characterized by huge ventilation rates, therefore it is necessary to strictly separate the areas of air inlets (suction of fresh air) and outlets (discharge of polluted air). More suitable dissipation zone of polluted air seems to be outlets in the same area between two halls or above the buildings.

The dust removal efficiency by ventilation calculated according to the equation (1) show that it is more efficient in the case of smaller particles. It can be the reason why the majority of dust particles inside these poultry houses create the particles bigger than 4 µm (83 % hall A, 82 % hall B).

REFERENCES

1. AARNINK, A.J.A., VAN HARN, J., WINKEL, A., DE BUISONJE, F.E., VAN HATTUM, T.G., OGINK, N.W.M.: Spraying rapeseed oil reduces dust in poultry houses. Proceedings of International conference Precision Livestock Farming 2009, 4th European Conference on Precision Livestock Farming, ECPLF, 2009, Elsevier, Wageningen, pp. 73-79.
2. Act Government Regulation No. 361/2007 Coll. Laying down the conditions for the protection of health at work. Changes: 9/2013 Coll. (in Czech).
3. Act No. 201/2012 Coll. Air Protection Act. (in Czech).
4. GŰRDIL, G.A.K., KIC, P., DAĞTEKIN, M., YILDIZ, Y.: The determination of ventilation rates in poultry houses. Journal of Agricultural Faculty, vol. 16 (3), 2001, pp. 61-68. (In Turkish).
5. KIC, P., HUBENÝ, M., LEDVINKA, Z., TŮMOVÁ, E., CAMPOS, C.G., MARTÍNEZ, C.T.: Control of indoor environment in housing of laying hens. Proceedings of International conference Trends in Agricultural Engineering, 2007a, CULS, Prague, pp. 212-214.
6. KIC, P., KALVODA, M., ZAVADIL, V.: Energy savings by heat recovery in ventilation. Proceedings of International conference Trends in Agricultural Engineering, 2007b, CULS, Prague, pp. 215-218.
7. KIC, P., RŮŽEK, L., LEDVINKA, Z., ZITA, L., GARDIÁNOVÁ, I.: Pollution of indoor environment in poultry housing. Proceedings of International conference 11th International Scientific Conference Engineering for Rural Development. Latvia University of Agriculture, 2012, Jelgava, pp. 480- 483.
8. LIŠKA, R., KIC, P.: Drying process of poultry manure at various temperatures. Proceedings of International conference Trends in Agricultural Engineering, 2010, CULS, Prague, pp. 398-400.
9. LIŠKA, R., KIC, P.: Characteristics of drying process of poultry manure at various temperatures. Scientia Agriculturae Bohemica, vol. 42 (2), 2011, pp. 79-86.
10. MISTRIOTIS, A., DE JONG, T., WAGEMANS, M.J.M., BOT, G.P.A.: Computational Fluid Dynamics (CFD) as a tool for the analysis of ventilation and indoor microclimate in agricultural buildings. Netherlands Journal of Agricultural Science, vol. 45 (1), 1997, pp. 81-96.
11. MUTAI, E.B.K., OTIENO, P.O., GITAU, A.N., MBUGE, D.O., MUTULI, D.A.: Simulation of the microclimate in poultry structures in Kenya. Research Journal of Applied Sciences, Engineering and Technology, vol. 3 (7), 2011, pp. 579-588.
12. SETHI, R.S., SCHNEBERGER, D., SINGH, B.: Characterization of the lung epithelium of wild-type and TLR9-/- mice after single and repeated exposures to chicken barn air. Experimental and Toxicologic Pathology, vol. 65 (4), 2013, pp. 357-364.
13. ŠOTTNÍK, J.: Principles and experience of heat stress reduction in buildings for housing of animals. Proceedings of International conference Trends in Agricultural Engineering, 2007, CULS, Prague, pp. 441-446.
14. VIEGAS, S., MATEUS, V., ALMEIDA-SILVA, M., CAROLINO, E., VIEGAS, C.: Occupational exposure to particulate matter and respiratory symptoms in Portuguese swine barn workers. Journal of Toxicology and Environmental Health, vol. 76 (17), 2013, pp. 1007-1014.
15. ZAJÍČEK, M., KIC, P.: Improvement of the broiler house ventilation using the CFD simulation. Agronomy Research, vol. 10 (1), 2012, pp. 235-242.
16. ZAJÍČEK, M., KIC, P.: Longitudinal ventilation of broiler house - simulation of variants. Proceedings of International conference 12th International Scientific Conference Engineering for Rural Development, 2013a, Latvia University of Agriculture, Jelgava, pp. 198-202.
17. ZAJÍČEK, M., KIC, P.: CFD Analysis of Broiler House Ventilation Patterns with Respect to the Poultry Welfare. Proceedings of International conference The sixth international scientific conference Rural Development, 2013b, Aleksandras Stulginskis University Akademia, Kaunas, pp. 151-156.
18. ZAJÍČEK, M., KIC, P.: Simulation of Broiler House Ventilation. Scientia Agriculturae Bohemica, vol. 44 (1), 2013c, pp. 32-37.

Corresponding author:

prof. Ing. Pavel Kic, DrSc., Department of technological equipment of buildings, Faculty of Engineering, Czech University of Life Sciences Prague, Kamýcká 129, Praha 6, Prague, 16521, Czech Republic, phone: +420 22438 3141, email: kic@tf.czu.cz

FUEL CONSUMPTION OF AGRICULTURAL MACHINES ON PADDY FIELDS

S. Konno[1], H. Shindo[2], M. Katahira[1], M. Natasuga[1]

[1]*Yamagata University, 1-23, Wakabamachi, Tsuruoka, Yamagata, 998-8555, Japan*
[2]*Akita Agricultural Experiment Station, Yuwa, Akita, 010-0864, Japan*

Abstract
Recently, Japanese rice-growing farmers have confronted difficult conditions and decreasing market prices of rice. The Shonai area of Yamagata prefecture, which has many medium scale cultivated fields, is one of Japan's largest rice cultivation areas. We discussed factors affecting fuel consumption through investigation of the working properties of tillage, puddling, and harvesting of paddy fields to decrease power farming system fuel consumption. Tillage increased fuel consumption as the working speed increased. Puddling increased fuel consumption as the turning time and distance increased. Harvest of paddy rice was related with fuel consumption and field conditions.

Key words: paddy field, tillage, puddling, harvest, fuel consumption.

INTRODUCTION

In recent years, weather modification has been remarkable because of increasing amounts of greenhouse gas discharge. Among all industrial fields, agriculture accounts for a small amount of greenhouse gas discharge. Nevertheless, one must consider greenhouse gas reduction methods as long as it accounts for even some amount of discharge. Actually, carbon dioxide causes 95% of greenhouse gas problems. To decrease greenhouse gas emissions, one must decrease carbon dioxide emitted by cars and tractors. Oil prices have been unstable in recent years. Because Japan holds miniscule mineral resources and is strongly affected by oil prices, high oil prices engender increasing costs of fossil fuels used for agriculture, thereby increasing agricultural product costs. Rice farmers in Japan are in a difficult predicament of agriculture management because of the downward trend of rice prices. Japanese farmers must decrease amounts of gas oil usage to control production costs. This study of the Shonai area of Yamagata prefecture, one of Japan's most productive rice cultivation areas, was conducted of medium scale cultivated fields in Yamagata prefecture, Japan. However, few reports have described studies of fuel consumption of agricultural machines in medium scale paddy fields. The objectives of this study are to decrease fuel consumption, to improve working efficiency, and to increase farmer income by reducing the variable costs of rice production to use power farming system. So, we discussed factors affecting fuel consumption to change shift gear and engine revolution of tractor, working system of tractor and combine harvester through an investigation of working properties of tillage, puddling, and harvesting of paddy fields.

MATERIALS AND METHODS

(1) Test location

We conducted tests in paddy fields of the Yamagata Field Science Center in Faculty of Agriculture, Yamagata University in Takasaka, Yamagata, Japan during April–November in 2015. Additionally, we used the rice cultivar "Haenuki."

(2) Machine components

We used any farm machines to investigate fuel consumption and work rate of power farming system on paddy field. We used a wheel type tractor (GL467, 33.8 kW; Kubota Corp.), a rotary tiller (ML197R: Kobashi Kogyo Co., Ltd.), a semi-crawler tractor (T1164C, 30.9 kW; Iseki Co. Ltd.), and rotary tiller (WXY205 L-S; Iseki Co. Ltd.) for tillage. Puddling was done by a wheel type tractor (GL467, 33.8 kW; Kubota Corp.) and a paddy harrow (PS248; Kobashi Kogyo Co., Ltd.). Then, we harvested rice by head-feeding combine (H064G, 44.9 kW; Iseki Co. Ltd.).

(3) Investigation contents

Working information for each was obtained using a GPS logger (Trip Recorder 747 Pro; TranSystems Corp.) attached to a tractor. That GPS logger can record the work speed and coordinates. Therefore, we analyzed the work speed, work distance, total work time and work rate using the data logger system. The tractor fuel consumption was measured using a top fill method for each work test (TEST METHODS OF FARM WORK, 1987).

(4) Test and investigation contents

1)Tractor setting

Tab. 1 shows the setting of tractors for tillage and puddling We set engine revolutions at 2000 rpm or 2500 rpm, and changed the main shift gear by two steps for every machine for tillage. PTO gear had one step. For puddling, we set the engine revolutions at 2000 rpm or 2500 rpm, and changed the main shift gear by three steps.

Tab. 1. – The setting of tractors for tillage and puddling

Test blocks	n	Engine revolution(rpm)	The main shift gear	PTO gear	PTO Rev.(rpm)	Operater	Type[1)]
T1	1	2000	High2	1	425	A	Ⅰ
T2	1	2000	High3	1	425	A	Ⅰ
T3	1	2500	High2	1	500	A	Ⅰ
T4	3	2500	High2	1	500	B	Ⅰ
T5	1	2500	medium-speed6	1	586	A	Ⅱ
T6	1	2500	medium-speed7	1	586	A	Ⅱ
S1	1	2500	High3	2	750	C	-
S2	2	2500	High3	2	750	A	-
S3	1	2000	High4	2	610	A	-
S4	1	2000	High3	3	940	A	-
S5	1	2000	High4	3	940	A	-
S6	1	2000	High3	2	610	A	-

1) No. Ⅰ was wheel type tractor (GL467, Kubota Co. Ltd.) and rotary tiller (ML197R, Kobashi Kogyo Co.Ltd). No. Ⅱ was semi-crawler tractor (T1164C, Iseki Co. Ltd.) and rotary tiller (WXY205 L-S, Iseki Co. Ltd.).

2)Working system of tractor and combine harvester

We set the headland in a paddy field. We performed tillage using return tilling at first. Then, we tilled using return and round tilling of about two rounds in the paddy field. Operator A started tillage near the paddy field entrance. Operator B started tillage from the distant entrance place on the paddy field. Puddling was done using return and round tilling at first. Then, we performed puddling using return tilling. We harvested using both return and round harvesting in about four rounds in the paddy field; then we used a method of return harvesting (method 1). Furthermore, we harvested using methods of both return and round harvesting with about seven rounds in the paddy field. Then we used return harvesting (method 2). Each method harvested from outside to inside on the paddy fields.

RESULTS AND DISCUSSION

(1) Tillage

Tab. 2 presents tillage results. Pulverizing rates were 29.6–49.2%, with standard deviations of 4.0–20.4%. The pulverizing rates differed greatly among test blocks. The dry basis moisture content was 0.47 for test block T-1, and 0.65–0.69 in other test blocks. The pulverizing rate of test block T-2, which was set on the transmission high-gear was higher than test block T-1. In addition, the pulverizing rate of test block T-6 was lower than that of test block T-5. Because of low dry basis moisture content, test blocks T-1 had a low pulverizing rate. The average working speed of advance work was 0.43–0.67 $m \cdot s^{-1}$. The working speeds of test blocks T-2 and T-6, which were set on transmission high gear, were higher than the other test blocks. Fuel consumption of test blocks T-1 to T-4 were 1.98–2.90 $L \cdot 10\ a^{-1}$, test blocks T-5 and T-6 were 1.84 and 2.13 $L \cdot 10\ a^{-1}$. The fuel consumption of test blocks T-2 and T-6, which were set on high gear, was lower than that of the other test blocks. These results correspond with the results from the past experiments (GOTO ET AL, 2009; C.M.KICHER. ET AL., 2010). The total work rates of test blocks T-1 to T-4 were 0.35–0.50 $h \cdot 10\ a^{-1}$, test blocks T-5 and T-6 were 0.32 and 0.36 $L \cdot 10\ a^{-1}$. The total work rates of test blocks T-2 and T-6 which were set on high-gear were lower than those of the other test blocks. Furthermore, these work rate were similar to standard data of Japan (FARM WORK SCIENCE, 1999). Fig. 1 shows the relation of fuel consumption and working speed. Although the correlation coefficient of those data was 0.31, the fuel consumption increased as the working speed increased.

Tab. 2 – The result of tillage

		T-1	T-2	T-3	T-4	T-5	T-6
Pulverizing rates(%)	Average	40.5	48.4	45.9	33.9	49.2	29.6
	S.D.	11.0	20.4	11.5	6.9	9.2	4.0
Dry basis moisture content(%)	Average	0.47	0.68	0.69	0.67	0.65	0.66
	S.D.	0.04	0.12	0.08	0.04	0.08	0.02
Tillage depth(cm)	Average	12.8	10.9	13.8	12.5	14.7	11.3
	S.D.	1.8	1.6	1.6	0.2	0.6	1.7
Working speeds($m \cdot s^{-1}$)	Average	0.43	0.63	0.50	0.51	0.54	0.67
	S.D.	0.01	0.03	0.02	0.01	0.01	0.01
Total work rates($h \cdot 10a^{-1}$)		0.50	0.35	0.44	0.35	0.36	0.32
Fuel consumption($L \cdot 10a^{-1}$)		2.22	1.57	2.90	1.98	2.13	1.84

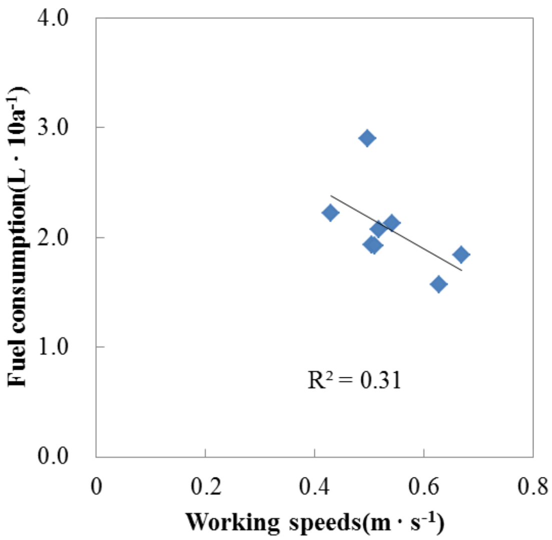

Fig. 1. – The relation of fuel consumption and working speed

(2) Puddling

Tab. 3 presents the puddling results. Working times were 2214–3603 s for advance work, and 498–783 s for turning. Working distances were 1655–1971 m for advance work, and 216–244 m for turning. Working speeds were 0.55–0.85 $m \cdot s^{-1}$, and 0.008-0.032 for standard deviations. When we set high engine revolutions and high gear, puddling tended to achieve short working times to have high working speed. The working distance showed much difference by test blocks. The fuel consumption was 0.85–1.51 $L \cdot 10\ a^{-1}$. Total work rates were 0.27–0.45 $h \cdot 10\ a^{-1}$. These work rate were similar to standard data of Japan (FARM WORK SCIENCE, 1999). And, these results correspond with the results from the past experiments (GOTO ET AL, 2009). Fig. 2 portrays the relation of PTO revolution and fuel consumption. Fig. 3 depicts the relation of turning time and fuel consumption. The relation of turn distance and fuel consumption is exhibited in Fig. 4. Actually, PTO revolution and fuel consumption showed a positive correlation for which the coefficient of determination was 0.58. The turn time and fuel consumption also showed a positive correlation for which the coefficient of determination was 0.77. Turn distance and fuel consumption showed a positive correlation for which the coefficient of determination was 0.47. Puddling had much fuel consumption as the turn time and distance increased.

Tab. 3 – The result of puddling

		S-1	S-2	S-3	S-4	S-5	S-6
Working times(s)	advance work	2568	2408	2214	3603	2610	3372
	turning	624	606	498	783	537	555
Working distances(m)	advance work	1709	1655	1764	1896	1882	1971
	turning	224	244	217	233	228	216
Working speeds($m \cdot s^{-1}$)	Average	0.68	0.73	0.83	0.55	0.85	0.56
	S.D.	0.024	0.026	0.019	0.008	0.019	0.032
Total work rates($h \cdot 10a^{-1}$)		0.34	0.30	0.27	0.42	0.31	0.45
Fuel consumption($L \cdot 10a^{-1}$)		1.33	1.30	0.85	1.51	1.19	0.99

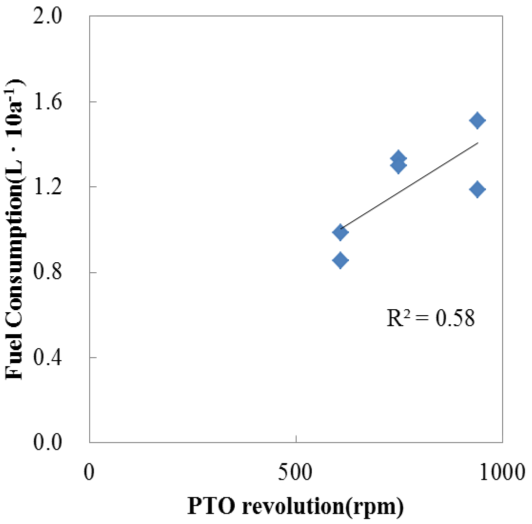

Fig. 2. – The relation of PTO revolution and fuel consumption

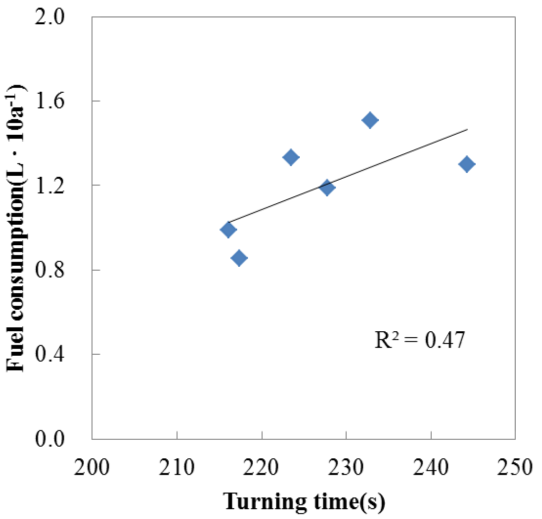

Fig. 3. – The relation of turning time and fuel consumption

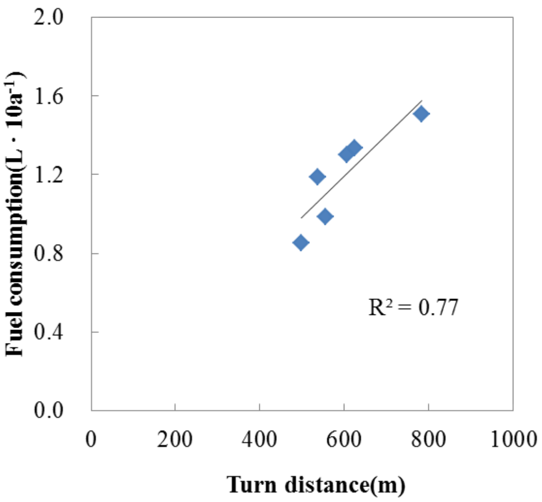

Fig. 4. – The relation of turn distance and fuel consumption

(3) Harvest

Tab. 4 shows data related to the paddy rice harvest. Dry basis moisture contents were 0.62 (S.D. 0.199) for test 1 and 0.55 (S.D. 0.108) for test 2. Soil hardness was 51.5 MPa (S.D. 25.58) for test 1 and 55.8 mm (S.D. 63.56) for test 2. Soil hardness increased as the dry basis moisture contents decreased. Working speeds were 1.26 $m \cdot s^{-1}$ (S.D. 0.085) for test 1, and 1.38 $m \cdot s^{-1}$ (S.D. 0.032) for test 2. Rice harvests were done with high working speed to improve traffic ability with high soil hardness. Advance times were 2198 s (S.D. 184) for test 1, and 1916 s (S.D. 117) for test 2. Turn times were 919 s (S.D. 93) for test 1, and 776 s (S.D. 143) for test 2. Advance distances were 2398 m (S.D. 54) for test 1 and 2343 m (S.D. 64) for test 2. Advance distances showed no difference among tests. Working distances of turning were 656 m (S.D. 39) for test 1, and 627 m (S.D. 69) for test 2. Test 2 showed a shorter turning distance than test 1 did. Total distances were 3111 m (S.D. 58) for test 1, and 3064 m (S.D. 96) for test 2. Fuel consumption was 3.05 $L \cdot 10\ a^{-1}$ (S.D. 0.369) for test 1, and 2.68 $L \cdot 10\ a^{-1}$ (S.D. 0.420) for test 2. Total work rates were 0.42 $h \cdot 10\ a^{-1}$ (S.D. 0.074) for test 1, and 0.48 $h \cdot 10\ a^{-1}$ (S.D. 0.222) for test 2. These work rate were similar to standard data of Japan (FARM WORK SCIENCE, 1999), too. Tab. 5 describes the coefficient of determination of fuel consumption and each investigation item. Dry basis moisture contents and fuel consumption showed a positive correlation, although soil hardness and fuel consumption showed a negative correlation. Coefficients of determination were, respectively, 0.57 and 0.67. Consequently, the fuel consumption of the combined rice harvest showed some relation to field conditions. Given high moisture contents in the field, decreased trafficability occurred because of softened soil. Therefore, the combine consumed fuel because of increased turn distance. Fuel consumption increased as the moisture contents of rough rice and foliage increased. Coefficients of determination were, respectively, 0.41 and 0.61. When it had high moisture contents of rough rice and foliage, the combine consumed much fuel to increase threshing power. Working speed and fuel consumption showed a negative correlation. The fuel consumption decreased as the working speed increased. Furthermore, the fuel consumption increased as the motion and turning time increased. Coefficients of determination between fuel consumption and advance and turn distances, and total distance were, respectively, 0.37, 0.40, and 0.42. These data showed only slight positive correlation. Fuel consumption increased as the distance increased.

Tab. 4. – The result of paddy rice harvest

	working method 1		working method2	
	Average	S.D.	Average	S.D.
Dry basis moisture contents	0.62	0.199	0.55	0.108
Soil hardness(MPa)	51.5	25.58	55.8	63.56
Moisture contents of rough rice(%)	23.6	2.31	23.6	2.77
Moisture contents of foliage(%)	67.4	3.35	66.0	2.56
Working speeds($m \cdot s^{-1}$)	1.26	0.085	1.38	0.032
Advance times(s)	2198	184	1916	118
Turn times(s)	919	94	776	143
Advance distances(m)	2398	54	2343	64
Working distances of turning(m)	656	39	627	69
Total distances(m)	3113	58	3064	96
Total work rates($h \cdot 10a^{-1}$)	0.42	0.074	0.48	0.222
Fuel consumption($L \cdot 10a^{-1}$)	3.05	0.369	2.68	0.420

Tab. 5. – The coefficient of determination of fuel consumption and each investigation item

	Coefficients of determination
Dry basis moisture contents	0.57
Soil hardness(mm)	0.77
Moisture contents of rough rice(%)	0.41
Moisture contents of foliage(%)	0.61
Working speeds($m \cdot s^{-1}$)	0.52
Advance times(s)	0.58
Turn times(s)	0.52
Advance distances(m)	0.37
Working distances of turn(m)	0.38
Total distances(m)	0.42

CONCLUSIONS

We examined factors that affect fuel consumption to change setting and work system through investigation of working properties of tillage, puddling, and harvesting of the paddy field to decrease fuel consumption using a power farming system. Tillage showed increased fuel consumption as the working speed increased. Puddling increased fuel consumption as the turning time and distance increased. Paddy rice harvesting showed a strong relation with fuel consumption and field conditions.

REFERENCES

1. EDITORIAL COMMITTEE OF TEST METHODS OF FARM WORK: Test methods of farm work., Japan forest technology association, Japan, 1987.
2. GOTOH, T., TESHIMA, T.: Effect of Operating Conditions of an Agricultural Tractor on Fuel Consumption (Part 2), Journal of the Japanese Society of Agricultural Machinery, 71(5), 2009: 73-90,
3. GOTOH, T., TESHIMA, T.: Effect of Operating Conditions of an Agricultural Tractor on Fuel Consumption (Part 3), Journal of the Japanese Society of Agricultural Machinery, 72(1), 2010: 63-71.
4. JAPANESE SOCIETY OF FARM WORK RESEARCH: Farm work science., Association of agriculture and forestry statistics, Japan, 1999.
5. KICHLER, C. M., FULTON, J. P., RAPER, R. L., MCDONALD, T. P., ZECH, W. C.: Effects of transmission gear selection on tractor performance and fuel costs during deep tillage operations, Soil & Tillage Research, 113, 2011: 105-111.

Corresponding author:
Shinsuke Konno, Yamagata University, 1-23, Wakabamachi, Tsuruoka, Yamagata, 998-8555, Japan

EFFECT OF ECOLOGICAL HYDRAULIC FLUID ON OPERATION OF TRACTOR HYDRAULIC CIRCUIT

J. Kosiba[1], J. Jablonický[1], R. Bernát[2], P. Kuchar[1]

[1]Department of Transport and Handling, Faculty of Engineering, Slovak University of Agriculture in Nitra, Slovak Republic
[2]Department of Quality and Engineering Technologies, Faculty of Engineering, Slovak University of Agriculture in Nitra, Slovak Republic

Abstract
This paper deals with the effect of biodegradable synthetic fluid on operation of tractor hydraulic circuit. Biodegradable synthetic fluid was applied in the hydraulic circuits of the tractor Zetor Proxima 6321. Operation test of this fluid was set at 500 engine hours. The flow efficiency of hydraulic pump was determined with the start of the test and after completing 500 engine hours and fluid samples were taken from the tractor hydraulic circuit. In terms of a decrease in hydraulic pump flow efficiency, operation tests of this fluid did not show negative effects of its application. These samples were subject to a measuring of kinematic viscosity at 40 °C and total acid number.

Key words: flow efficiency, kinematic viscosity at 40 °C, total acid number, density at 15 °C.

INTRODUCTION

Hydraulic equipment is widely used in powerful mechanisms of agricultural and forest machines as well as in many other areas. The development of modern hydraulic components is aimed at increasing the transmitted power, reducing the energy intensity, minimizing the environmental pollution and increasing the technical life and machine reliability (TKÁČ ET AL., 2008; HOFFMANN ET AL., 2013). Universal tractor transmission oils (UTTO) are designed for hydraulic and transmission systems of agricultural tractors. These fluids provide lubrication functions in the gear box and transmission of energy in the hydraulic system of the tractor (HUJO ET AL., 2013; KUČERA ET AL., 2013).

Environmental protection is an actual topic already for several years, and it becomes a preferred problem in the established trend of economic development (TÓTH ET AL., 2014). Agricultural technology has a negative impact on all elements of the environment (KUČERA ET AL., 2008). It was reported that over 60% of all lubricants end up in soil and water. Hydraulic line breaks are extremely common. If not attended to, these releases can cause contamination of the soil, ground and surface water (MAJDAN ET AL., 2014). The ecological fluids market is expanding, and ecological oils which can be used in hydraulic and transmission systems are one of the provided products (KUČERA ET AL., 2014A; KOSIBA ET AL., 2013). This paper presents the results of a long-term operational test of the biodegradable synthetic fluid. The operational test was performed on the tractor Zetor Proxima 6321 (ZETOR TRACTORS A. S., BRNO, CZECH REPUBLIC).

The aim of this work is application biodegradable synthetic fluid in tractor gear and hydraulic circuit. A biodegradable fluid was used in the gear and hydraulic circuit of a tractor Zetor Proxima 6321. The fluid was assessed in terms of the lubrication properties and their effect on the wear of a tractor hydraulic pump during application. The basic indicator of hydraulic pump lifetime is flow characteristics. During operating of a tractor were evaluated the major characteristics of the biodegradable fluids; kinematic viscosity at 40 ºC, total acid number (TAN) and density at 15 ºC. Experimental results bring important information from the point of view of oil degradation. The majority of tractors are subjected to the conditions which can cause undesirable phase transition of oil in hydraulic systems. It is necessary to develop the flow of oil due to correct operation of hydraulic equipment. The rate of oil flow is important to the life of the hydraulic system.

MATERIALS AND METHODS

Operational test of biodegradable synthetic fluid type universal tractor transmission oil (UTTO) was set at 500 engine hours (EH). Tab. 1 shows the basic technical parameters of biodegradable synthetic fluid type UTTO. Fluid samples were taken from the tractor hydraulic circuit at the start of the test and after completing 500 EH. Subsequently, fluid samples were collected for laboratory analysis. The following parameters were evaluated:

- kinematic viscosity at 40 °C,
- total acid number (TAN),
- density at 15 °C.

Tab. 1. – Technical parameters of biodegradable synthetic fluid

Properties	Unit	Amount
Kinematic viscosity at 40°C	mm*s^{-2}	67.52
Density at 15°C	kg*m^{-3}	931
Flash point	°C	212
Pour point	°C	- 48

To establish a methodology for the flow of hydraulic characteristics of hydraulic pumps measuring, it is needed to set up the components that would be used to achieve the intended results. The most important components include a flow sensor, pressure sensor, temperature sensor, recording unit, load member and joint flange. By the draft of the measurement chain, it is required to follow the certain measurement conditions. The most important condition by measuring of the flow characteristics of hydraulic pumps is the oil temperature. The temperature must be maintained at constant value, because the viscosity of the oil depends on it. At the same time, by measuring of the flow characteristics, the oil temperature must be on operating value. Another extremely important parameter is speed of hydraulic pump. The speed of hydraulic pump will be monitored based on the combustion engine speed among which is transference (TKÁČET, 2014). The speed of the hydraulic pump will be monitored based on speed of the combustion engine, whereas the internal combustion engine and the hydraulic pump axle ratio i = 1.467 reducing. Tab. 1 shows the speed of hydraulic pump type UD 20 (Jihostroj Aero Technology and Hydraulics, Velesin, Czech Republic) during measuring of flow rate. Fig. 1 shows of kinematic scheme of hydraulic pump flow rate measuring.

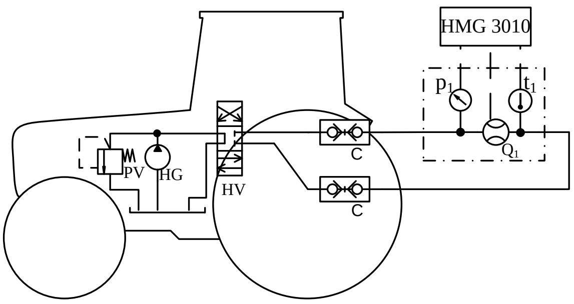

Fig. 1. – Scheme of hydraulic pump flow rate measuring
(PV – pressure relief valve, HG – hydraulic pump, HV – hydraulic valve, C – quick couplings, p1 – pressure sensor HDA 3774-A-600-000, Q1 – flow rate sensor EVS 3100, temperature sensor ETS 4144-A-000, HMG 3010 – portable data recorder).

Tab. 2. – Speed of combustion engine and hydraulic pump

Combustion engine speed (rpm)	Hydraulic pump speed (rpm)
1600	1090
2200	1500
2300	1570

The flow, temperature and pressure sensors were placed on the joint flange Hydac (Fig. 2). On the both ends of the joint flange Hydac, there were placed glad-hands. On the inlet side of the joint flange Hydac (oil inflow from the tractor distributor), there was placed plug-in "male" glad-hand and on the output side (oil run-off from the joint flange), there was placed plug "female" glad-hand. The measuring device was placed between the exit glad-hand from the tractor and loading equipment Owattona.

The measurement of the flow characteristics is used to determine the impact of the biodegradable synthetic oil on the hydraulic pump life. The flow hydraulic pump efficiency was calculated from the measured flow characteristics:

$$\eta_{pr} = \frac{Q}{VG \cdot n} \cdot 100 \tag{1}$$

where:

Q – output flow rate (dm^3.rpm),

V_G – geometrical volume of hydraulic pump (dm^3),

n – nominal rotation speed of hydraulic pump (rpm).

Fig. 2. – Placing of the flow, temperature and pressure sensor on the joint flange HYDAC (Hydac GmbH, Sulzbach/Saar, Germany)

Statistical analysis

Standard deviation σ is defined as a positive square root of variance. Standard deviation is calculated if we have a complete set of possible states of the process (system). In probability theory and in statistics, standard deviation or mean square deviation is a measure of statistical dispersion. Simply said, it refers to how widely are the values distributed in a set (HILL AND LEWICKY, 2006).

$$\sigma = \sqrt{\frac{1}{n}\sum_{i=1}^{n}(x_i - \bar{x})^2} \tag{2}$$

where:

n – population size,

x_i – individual values of population,

$\bar{x}$ – arithmetic average of population.

We say that a continuous random variable x has normal (Gaussian) distribution with parameters $\bar{x}$, σ^2 if density is:

$$f(x) = \frac{1}{\sigma\sqrt{2\pi}}.e^{-\frac{(\bar{x}-\alpha)^2}{2\sigma^2}} \text{ for } x \in R_1, \alpha \in (-\infty, \infty), \sigma > 0 \tag{3}$$

where:

e – base of natural logarithm,

σ – standard deviation,

$\bar{x}$ – arithmetic average of population.

If a variable x has normal distribution with parameters $\bar{x}$, σ^2, then, after transformation:

$$Z_i = \frac{x_i - \bar{x}}{\sigma} \tag{4}$$

where:

σ – standard deviation,

x_i – individual values of population,

$\bar{x}$ – arithmetic average of population,

z_i – variable with normal distribution,

the variable has normal distribution with mean value 0 and variation 1 (then standard deviation is also 1). This distribution is called as standardized normal distribution (HILL AND LEWICKY, 2006).

- When selecting a value from the range –1σ, +1σ, the probability of standard normal distribution is 68.27 %;
- When selecting a value from the range –2σ, +2σ, the probability of standard normal distribution is 95.46 %;
- When selecting a value from the range –3 σ, +3σ, the probability of standard normal distribution is 99.73 %.

We have chosen to evaluate the data of -1σ and +1 σ so that we obtain the values as close as possible to the nominal pressure of the hydraulic pump (p = 16 MPa). When choosing the range of -1σ and +1 σ, the credibility of results is 68.27 %. The flow efficiency of the hydraulic pump was calculated from this sample of values.

RESULTS AND DISCUSSION

The flow characteristics were measurement at 0 EH and after completing 500 EH. The measurement of the flow characteristics was performed at speeds of hydraulic pump n = 1,090 rpm, n = 1,500 rpm and n = 1,570 rpm. Fig. 3 a, b and c shows the flow characteristics of the hydraulic pump UD 20 at different speeds.

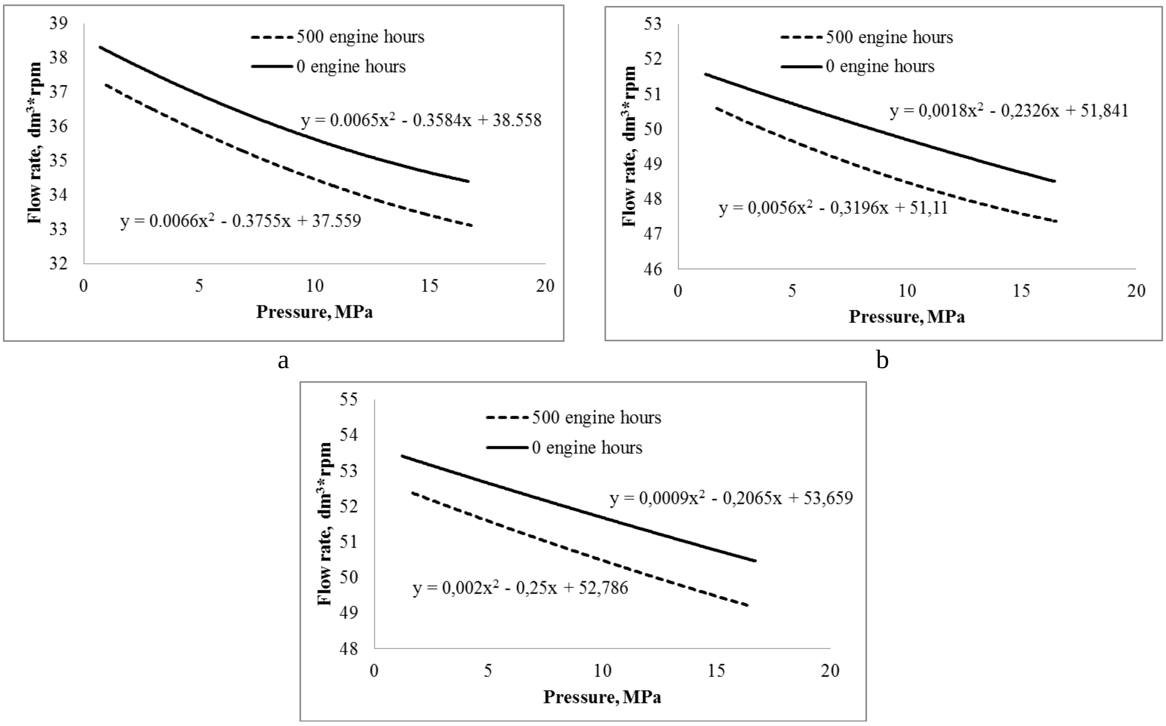

Fig. 3. – Flow characteristics of hydraulic pump (a - flow characteristics at n = 1,090 rpm, b - flow characteristics at n = 1,500 rpm, c - flow characteristics at n = 1.570 rpm)

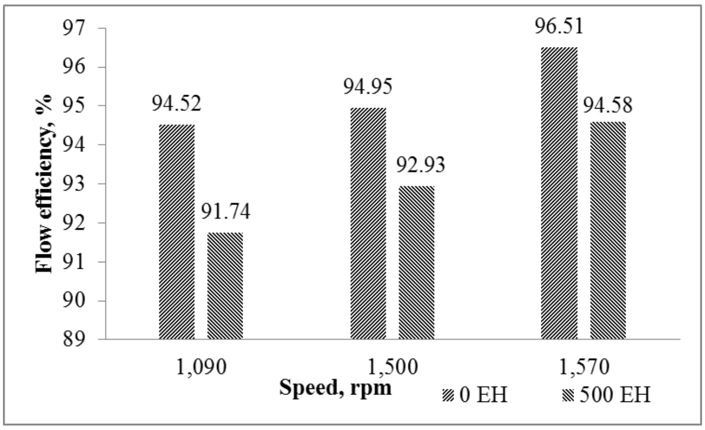

Fig. 4. – Flow efficiency of the hydraulic pump

Fig. 4 shows the hydraulic pump flow efficiency at particular speeds and engine hours.

The greatest decrease in the hydraulic pump flow efficiency was detected at a speed n = 1,090 rpm. The flow efficiency of the hydraulic pump dropped from η_0 = 94.52% to η_{500} = 91.74%. Under the nominal speed of the hydraulic pump n = 1,500 rpm, the flow efficiency of the hydraulic pump declined from η_0 = 96.51% to η_{500} = 94.58%.

When applying the oil EKOUNIVERZÁL, the tractor type ZTS 8011 with the hydraulic pump PZ 2 – 18 KS was used in operation from 0 EH to 2,242 EH. For p = 16 Mpa pressure at hydraulic pump output and n = 2,200 rpm nominal speed, flow rate measured at

0 Eh was Q = 22.80 dm^3*rpm. After 2,242 EH, the measured flow rate was Q = 19.05 dm3*rpm. The lifetime of hydraulic pump type PZ 2 – 18 KS is 2,000 EH. The measurement revealed a necessity to replace the hydraulic pump because the minimally allowed flow rate of the hydraulic pump at nominal speed is Q = 19 dm^3*rpm (TKÁČ ET AL., 2002, 2003). In case of the hydraulic pump type PZ 2 – 19 KS with the oil EKOUNIVERZÁL, ŠKULEC ET AL. (2001) found at speeds n = 1,500 rpm and pressure p = 16 MPa a decrease in flow rate by Δη = 1.25 % after 300 EH. Škulec used a new hydraulic pump type PZ 2 – 19 KS in test. For this reason, there was two times higher decrease in flow rate with the hydraulic pump UD 20 than with the hydraulic pump PZ 2 – 19 KS.

Tab. 3 shows the following parameters of biodegradable synthetic fluid (kinematic viscosity at 40 °C, total acid number and density at 15 °C).

Tab. 3. – Following parameters of biodegradable hydraulic fluid

Count of engine hours	Kinematic viscosity at 40 °C, mm*s^{-2}	Total acid number, mgKOH*g^{-1}	Density at 15 °C, kg*m^{-3}
0 engine hours	68.41	0.75	910.40
500 engine hours	71.08	0.80	909.20

The increase of kinematic viscosity at 40 °C was V = 2.67 mm*s^{-2} (ΔV = 3.9%), based on the value of new oil v_0 = 68.41 mm^2*s^{-1} and value of used oil v_{500} = 71.08 mm^2*s^{-1}. ALIAS ET AL, (2009) evaluated the kinematic viscosity at 40 °C of palm oil-based TMP ester (TMPE) and found the increase of kinematic viscosity after completing 400 hours ΔV = 1.72%. The increase of total acid number was TAN = 0.05 mgKOH*g^{-1} (ΔTAN = 6.6%). The decrease of density at 15 °C was D = 1.20 kg*m^{-3} (ΔD = 0.13%), based on the value of new oil D_0 = 910.40 mm^2*s^{-1} and value of used oil D_{500} = 909.20 mm^2*s^{-1}. According to ASSAF ET AL. (2014), the total acid number (TAN) is of interest because it indicates the degree of fluid oxidation. ASSAF ET AL. (2014) evaluated the total acid number (TAN) of biodegradable hydraulic fluid of TAN = 0.95 mgKOH*g^{-1}. Concerning the acid content, this value is acceptable in the vegetable-based formulations in comparison with the reference oil. Concentration of the acid content of the biodegradable synthetic fluid druring the test is acceptable and in accord by authors ASSAF ET AL. (2014) and KUČERA ET AL. (2013B).

CONCLUSIONS

Agricultural technology has a negative impact on all elements of the environment. This paper presents the results of a long-term operational test of the biodegradable synthetic fluid. The operational test was performed on one of the most used tractors, the tractor Zetor Proxima 6321 in the conditions of Slovak farms. Based on the results obtained, it is possible to state that the biodegradable synthetic fluid is a full-value hydraulic oil for the tractor Zetor Proxima 6321. Operational test of this fluid was set at 500 engine hours. During the performance test, there were measured changes in the most important qualitative indicator (flow efficiency) corresponding to engine hours for the ecological oil. The measured values of flow efficiency correspond to standard and they do not influence the technical and exploitation properties of the tractor hydraulic circuit. The decrease in the flow efficiency of the UD 20 hydraulic pump at nominal speed (n = 1,500 rpm) during the test was Δηpr = 2.127 %. This decrease showed a negative impact of the biodegradable synthetic fluid on hydraulic pump flow efficiency.

Kinematic viscosity is one of the most important properties for the characterization of lubricants and their transport properties, and it is a measure of internal friction in a fluid (ALIAS ET AL, 2009). The increase of kinematic viscosity at 40 °C during operating test was V = 2.67 mm*s^{-2}. For this reason we need remember the difference of kinematic viscosity during of the operating test. The evaluation of fluid's TAN (Total acid number) is important because of an increasing amount of acids in the fluid, which is characteristic for the ageing process and directly determines the degree of fluid degradation (MIHALČOVÁ, 2016). The measured values of TAN had a slightly increasing trend up to 500 engine hours. Testing of biodegradable synthetic fluid were researched by authors KUSAK ET AL., (2012), RIDDERIKHOFF ET AL., (2005) and MICHAEL ET AL., (2009).

ACKNOWLEDGEMENT

Supported by the Ministry of Education of the Slovak Republic, Project VEGA 1/0337/15 "Research aimed at influence of agricultural, forest and transport machinery on environment and its elimination on the basis of ecological measures application".

The research leading to these results has received funding from the European Community under project no 26220220180: Building Research Centre „AgroBioTech".

REFERENCES

1. ALIAS, N.H., YUNUS, R., IDRIS, A., OMAR. R.: Effect of additives on oxidation characteristics of palm oil-based trimethylolpropane ester in hydraulic applications. European Journal of Lipid Science and Technology 111, 4, 2009: 368–375.
2. ASAFF, Y., NEGRI, V. J., THEISSEN, H., MURRENHOFF, H.: Analysis of the influence of contaminats on the biodegradability characteristics and ageing of biodegradable hydraulic fluids. Journal of Mechanical Engineering 60, 6, 2014: 417–424.
3. HILL, P., LEWICKY.: Statistics: Methods and applications. Statsoft Inc., Tulsa USA, 2006.
4. HOFFMANN, D., HEŘMÁNEK, P., RYBKA, A., HONZÍK, I.: Design a drive for interaxle mechanical cutter used in low trellises. Agronomy Research 11, 2013: 39–46.
5. HUJO, Ľ., TKÁČ, Z., TULÍK, J., HAJDÁK, V.: Design of laboratory test device for evaluating the lifetime of hydraulic components of tractor three-point hitch. Advanced Materials Research 801, 2013: 137–142.
6. KOSIBA, J., TKÁČ, Z., HUJO, Ľ., TULÍK, J., ŠEVČÍK, P., ŠINSKÝ, V., RAŠO, M.: Effect of ecological energy carriers on flow characteristics of tractor hydraulic pump. Journal of Central European Agriculture 14, 4, 2013: 1415–1425.
7. KUČERA, M., RÉDL J.: Vplyv podmienok experimentu na tribologické vlastnosti vybraných materiálov (Effects of experimental conditions on tribologic properties of selected materials). Acta technologica agriculturae, 1, 2008: 98–104.
8. KUČERA, M., BUJNA, M., KORENKOVÁ, M., HAAS, P.: Possibilities of using ecological fluid in agriculture. Advanced Materials Research 1059, 2014: 61–66.
9. KUČERA, M., CHOTĚBORSKÝ, R.: Analysis of the process of abrasive wear under experimental conditions. Scientia agriculturae bohemica 44, 2, 2013a: 102–106.
10. KUČERA, M., ALEŠ, Z., IVANDIĆ, Z., HUJO, Ľ.: Possibility of hydraulic fluids with a low environmental impact application in agriculture and transport machinery. Journal of Central European Agriculture 14, 4, 2013b: 1575–1584.
11. KUSAK, B., WRIGHT, G., KROL, R., BAILEY, M.: Characteristics of base fluid environmentally acceptable lubricants. Symposium on Testing and Use of environmentally Acceptable Lubricants, 2010, pp. 47–57, Jacksonville, FL, USA.
12. MICHAEL, P., JELINSKI, C., SCHICK, D., WHITTAKER, K.: Compatibility and filterability of hydraulic fluids. SAE Commercial Vehicle Engineering Congress and Exhibition, 2009, Rosemont, Il USA.
13. MIHALČOVÁ, J.: Verification and comparison of two tribodiagnostic methods for analyzing of the worn out oils in service. Key engineering Materials 669, 2016: 426–433.
14. ŠKULEC, R., POKORNÝ, K., TKÁČ, Z.: The Laboratory Test of Tractor Hydrostatic Pump. Proceedings of the Agrotech Nitra 2001. pp. 390 -395, Nitra, Slovakia.
15. TKÁČ, Z., DRABANT, Š., MAJDAN, R., CVÍČELA, P.: Testing stands for laboratory tests of hydrostatic pump of agricultural machinery. Research in Agricultural Engineering 54, 1, 2008: 183–191.
16. TKÁČ, Z., HUJO, Ľ., TULÍK, J., KOSIBA, J, UHRINOVÁ, D., ŠINSKÝ, V.: Greening of agricultural and forestry tractors. Acta Universitatis Agriculturae et Silviculturae Mendelianae Brunensis 62, 5, 2014: 1135–1139.
17. TKÁČ, Z., ŠKULEC, R.: Aplikácia bioodbúrateľného oleja v prevodovom a hydraulickom systéme traktora. (Application of bio-degradable oil in the gear and hydraulic system of the tractor). Acta Mechanika, 2002: 297–270.
18. TKÁČ, Z., PETRANSKÝ, I., VARGA, D., HUJO, Ľ., BOLLA, M.: Hydraulický a prevodový systém traktora ZTS 8011 pri práci s bioolejom. (Hydraulic and transmission system of tractor ZTS 8011 at work with bio oil). Hydraulika a pneumatika 2003: 32–35.
19. TÓTH, F., RUSNÁK, J., KADNÁR, M., VÁLIKOVÁ, V.: Study of tribological properties of chosen types of environmentally friendly oils in combined friction conditions. Journal of Central European Agriculture 15, 1, 2014: 185–192.
20. RIDDERIKHOFF, H., OOSTERMAN, J.: Biodegradable hydraulic fluids: Rheological behaviour at low temperatures of several oleochemically derived synthetic esters. Journal of Synthetic Lubrication 21, 4, 2005: 299–313.

Corresponding author:

Ján Kosiba, Department of Transport and Handling, Faculty of Engineering, Slovak University of Agriculture in Nitra, Slovak Republic,e-mail: jan.kosiba@gmail.com

THE INFLUENCE OF EXHAUST CATALYST WITH REDUCED EFFICIENCY ON REAL EXHAUST EMISSIONS

M. Kotek, P. Jindra, J. Mařík, F. Lachnit

Faculty of Engineering, Czech University of Life Sciences Prague

Abstract
The aim of the paper is to assess the real emission production of passenger car with high mileage. The car was suspected of a reduction of catalyst's efficiency (stored fault in OBD system). Experiments were carried out with a usage of the idle emission test and methodology similar to homologation process under homologation cycle NEDC. The results prove that the idle test is not able to detect lower catalyst's efficiency while the NEDC cycle results show even 5-times increase of emission production.

Key words: idle test, homologation cycle, NEDC, chassis dynamometer.

INTRODUCTION

The introduction of the widely known three-way catalytic (TWC) converter in the early 80's, which effectively removes CO, unburned HCs and NOx emissions, in stoichiometrically operated gasoline vehicles has proven to be an efficient technique to meet the ever more stringent emission limits BIRGERSSON (2006). The catalyst uses a ceramic or metallic substrate with an active coating incorporating alumina, ceria and other oxides and combinations of the precious metals - platinum, palladium and rhodium. By the highly porous structure and resulting large surface area for the noble metal phase is ensured the high catalyst efficiency. The catalyst requires the operating temperature around 400 – 800 °C, that might be a problem especially during cold starts. Therefore, the close-coupled catalyst (CCC) placed very near to engine is mainly used for reducing the cold start emissions JIA (2008). According to *EU DIRECTIVE 70/220/EEC* the catalyst durability must be minimally by 160 000 km.

The aim of planned experiments was to compare results of 2 different emission tests conducted on original CCC with high mileage and on the new one and confirm or disprove the fault stored in the OBD system.

MATERIALS AND METHODS

The vehicle Skoda Fabia combi first generation with 1.2 litre spark engine was used for this experiment. Detailed technical specification is summarized in Tab. 1. The fault in a form: "low catalyst efficiency" was saved in on-board diagnostic system (OBD).

The catalyst's efficiency will be tested using two different methodologies. At the first the vehicle will be tested by the methodology of regular emission test in the Czech Republic. There are the idle emission tests, when the vehicles engine is tested at idle and raised idling speed. The Tab. 2 show the maximum limits for this vehicle.

At the second the car will be tested with usage of methodology similar to homologation process. The vehicle will be driven according to the homologation cycle NEDC (New European Driving Cycle) and total emission production will be evaluated. The vehicle should fulfil the EURO-4 limits which are showed in the Tab. 3.

After completing the above tests the replacement of the catalyst for a new will be conducted and then the testing methodology will be repeated with using a new catalyst.

VMK emission analyser was used for emission measurement on the chassis dynamometer. Standard analyser ATAL AT505 was used for the regular inspection of emission measurement. Both analysers use non-dispersive infrared (NDIR) method to detect CO, CO_2, and HC emissions and electrochemical cell to O_2 and NO_X emissions. Data was recorded with 1 Hz frequency on memory card (VMK) and on hard disk in case of the Atal analyser. The technical data of analysers are summarized in Tab. 4 and 5.

Tab. 1. – Vehicle technical specification

Vehicle	Skoda Fabia 1.2 HTP
Manufacture year	2004
Mileage	202, 000 km
COMBUSTION ENGINE	
Design	spark ignition, atmospheric
Number of cylinders and valves	3 in row, 12 valves
Fuel	gasoline
Volume of cylinders	1198 ccm
Power	47 kW at 5400 rpm
Torque	112 Nm at 3000 rpm
CO_2 emission	140 $g \cdot km^{-1}$
EU limit	EU4
CAR BODY	
Service weight	1250 kg
Total weight	1750 kg
DRIVE PERFORMANCE	
Max. speed	162 $km \cdot h^{-1}$
Acceleration (0-100 $km \cdot h^{-1}$)	16.3 s
Fuel consumption	7.7 / 5.1 / 6 litre/100 km

Tab. 2. – Maximal emission limits for tested vehicle at the idle tests

regime	engine speed min^{-1}	CO %	CO_2 %	HC ppm	NO_X ppm	Lambda -
idle	600-800	0.5	-	300	-	-
raised idling	2400-2600	0.3	-	300	-	0.97-1.03

Tab. 3. – Maximal emission limits for tested vehicle at the homologation tests

Stage	Date	CO	HC	NOx
		$g \cdot km^{-1}$		
Euro 4	2005.01	1.0	0.1	0.08

Tab. 4. – Technical parameters of VMK emission analyser

Measured values	Measurement range	Resolution	Accuracy
CO	0 ... 10 % Vol.	0.001 % Vol.	0 … 0.67%: 0.02% absolute, 0.67% … 10%: 3% of measured value
CO_2	0 ... 16 % Vol.	0.01 % Vol.	0 … 10%: 0.3% absolute, 10 … 16%: 3% m.v.
HC	0 ... 20 000 ppm	1 ppm	10 ppm or 5% m.v.
NO_X	0 ...5 000 ppm	1 ppm	0 … 1000 ppm: 25 ppm, 1000 … 4000 ppm: 4% m.v.
O_2	0 ... 22 % Vol.	0.1 % Vol.	0 … 3%: 0.1%, 3 … 21%: 3%

Tab. 5. – Technical parameters of Atal emission analyser

Measured values	Measurement range	Resolution	Accuracy
CO	0 ... 10 % Vol.	0.01 % Vol.	0.03 % Vol or 5 % of measured value
CO_2	0 ... 20 % Vol.	0.1 % Vol.	0 … 10%: 0.3% absolute, 10 … 16%: 3% m.v.
HC	0 ... 2 000 ppm Vol.	0.01 % Vol.	0.1 % Vol. or 5 % m.v.
	2001 … 9000 ppm Vol.	10 ppm Vol.	5 % of m.v.
NO_X	0 ...5 000 ppm	1 ppm Vol.	1 ppm Vol.
O_2	0 ... 4 % Vol.	0.01 % Vol.	0.01 % Vol.
	4 ... 21 % Vol.	0.1 % Vol.	5 % of m.v.

The car diagnostic system VAG-COM was used for communication with ECU for obtaining immediate values of the engine operational parameters (revolutions, engine load, MAF, IAT, etc.). These values were used for calculating weight emission production in ($g \cdot s^{-1}$) using method described by SAINI ET AL. (2013) as shown in Eq. (1):

$$E_{(g \cdot s^{-1})} = \frac{\left(\left(M_{af} + F_f\right) \cdot M_Q \cdot Q\right)}{M_{exh}} \qquad (1)$$

where $E_{(g \cdot s^{-1})}$ is the emission rate in ($g \cdot s^{-1}$), F_f is the instantaneous fuel flow rate in ($g \cdot s^{-1}$), M_Q is the molecular weight of the exhaust gases ($g \cdot mol^{-1}$), Q the fraction of exhaust gases (%), M_{af} is the mass air flow ($g \cdot s^{-1}$) and M_{exh} is the exhaust molar mass ($g \cdot mol^{-1}$).

Fig. 1. – The experiment setup

RESULTS AND DISCUSSION

At first the idle emission measuring was performed. In the Tab. 6 are results of idle test for both catalysts. There is evident that original catalyst fulfils all required limits but the new one reaches significantly better values (especially in case of CO emissions). These simple tests led to suspect for the lower efficiency of original catalyst.

Tab. 6. – The results of idle tests for both catalysts.

	Speed	CO	CO_2	HC	NO_X	Lambda
	min^{-1}	%	%	ppm	ppm	-
original	740	0.22	14.7	3	6	0.999
catalyst	2560	0.1	15.1	2	5	0.998
new	730	0.01	15	5	0	0.999
catalyst	2520	0.02	14.9	6	4	0.999

Secondly tests on the chassis dynamometer were conducted with the aim to engine's operating under higher load in comparison with idle tests. On the fig. 2 are shown the immediate values of CO emissions production for both catalysts in the EUDC (Extra Urban Driving Cycle), which is the second part of NEDC cycle. The engine is more loaded at the moment and the effect of worse catalyst efficiency is more evident. As can be seen from fig. 2, in this case original catalyst during intensified acceleration was followed by an increased production of CO. The suspect of lower catalyst efficiency has been confirmed by summary results for whole NEDC cycle.

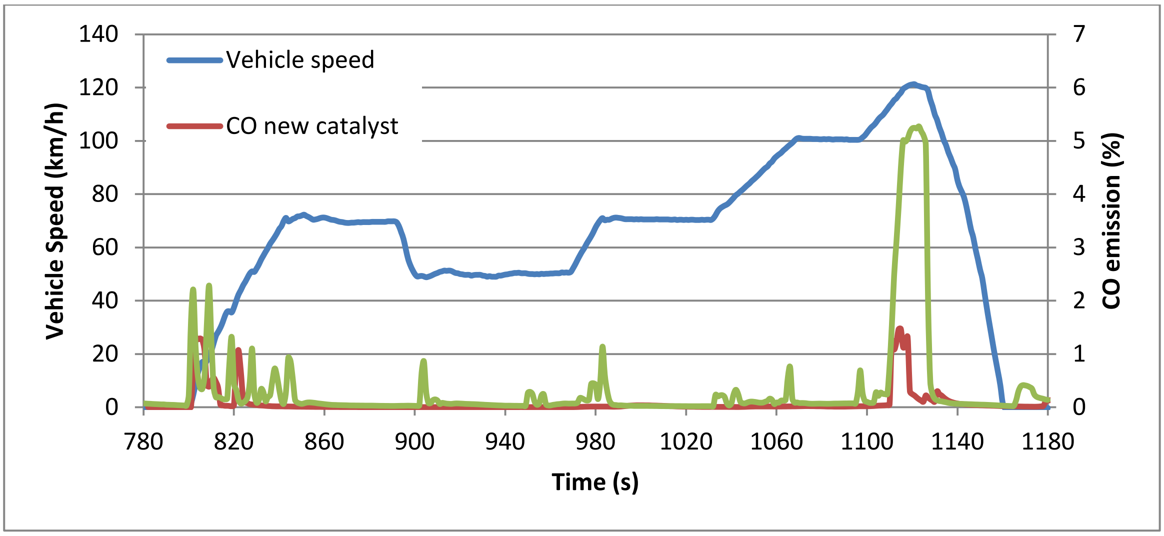

Fig. 2. – Immediate values of CO emissions for both catalysts in the EUDC cycle.

Tab. 7. – The results of NEDC tests for both catalysts

	Distance	CO	CO_2	NO	HC
	km	$g \cdot km^{-1}$	$g \cdot km^{-1}$	$g \cdot km^{-1}$	$g \cdot km^{-1}$
original catalyst	10.92	3.82	171	0.28	0.01
new catalyst	10.95	0.71	178	0.07	0.005
directive EU4 and manufacturer data	10.93	1.00	140	0.08	0.1

In the Tab. 7 are summarized results of all emission production in the NEDC cycle.
From the Tab. 7 is evident that the CO and NO emissions of original catalyst exceeded many times the limits for EU4 standard, while the HC emissions are reduced sufficiently. Slightly increased CO_2 emissions may be caused by using winter tyres. The original catalyst's poor results were probably caused by its ending durability due to high mileage of tested car. As was mentioned above, according to EU directive 70/220/EEC the catalyst durability must be minimally 160 000 km. On the other hand, the reason for these results could be caused by the aging phenomena of catalyst. There are many distinct types of catalyst deactivation. As is reported by BARTHOLOMEW (2001) they can be classified into six distinct types: (i) poisoning, (ii) fouling, (iii) thermal degradation, (iv) vapour compound formation accompanied by transport, (v) vapour-solid and/or solid-solid reactions, and (vi) attrition/crushing. Especially on the tested car is well known problem with the catalyst overheating due to the placement of the catalyst direct behind the exhaust pipe and very close to the engine block. WINKLER ET AL. (2001) concluded that the thermal degradation has a major impact to the reduction of catalyst efficiency.

CONCLUSIONS

The aim of the paper was to compare results of 2 different emission tests conducted on original CCC with high mileage and on the new one and confirm or disprove the fault stored in the OBD system. Although the tested car passed the standard idle emission test for regular checks, by testing under real engine loading test (similar to the homologation process) it is evident significant increase in emission production. Especially in items as CO and NO, production was achieved 4 times higher than permitted by the EU4 directive. According to the results the fault stored in the OBD system was confirmed. Regardless to very often criticism linked with homologation cycles that they are not representative for real-world vehicles' usage. On the hand the use of idle test as a methodology for regular emission checks proves to be insufficient. As is seen from Tab. 7, after replacing the catalyst all emission limits has been fulfilled.

ACKNOWLEDGEMENTS

Paper was created with the grant support of Czech University of Life Sciences Prague – project no. CZU 2016:31150/1312/3111 - Analysis of impact using biofuels on operating parameters of combustion engines.

REFERENCES

1. BARTHOLOMEW, C., H.: Mechanisms of catalyst deactivation, Applied Catalysis A: General, 212, 2001, 17–60.
2. BIRGERSSON, H., BOUTONNET, M., KLINGSTEDT, F., MURZIN Y. D., STEFANOV, P., NAYDENOV, A.: An investigation of a new regeneration method of commercial aged three-way catalysts, Applied Catalysis B: Environmental 65, 2006, 93–100.
3. EUROPEAN DIRECTIVE 70/220/EC.
4. JIA L., SHEN, M., WANG, J., WANG, J., CHU, X., GU, W.: Durability of three-way and close-coupled catalysts for Euro IV regulation, JOURNAL OF RARE EARTHS, Vol. 26, No. 6, 2008, p. 827.
5. SAINI, B., VERMA, R., HIMANSHU, S., GUPTA, S.: Analysis of exhaust emissions from gasoline powered vehicles in a suburban Indian town, International Research Journal of Environment Sciences, 2 (1), 2013, 37–42.
6. WINKLER, A., FERRI, D., HAUERT, R.: Influence of aging effects on the conversion efficiency of automotive exhaust gas catalysts, Catalysis Today 155, 2010, 140–146.

Corresponding author:

Ing. Martin Kotek, Ph.D., Department of Vehicles and Ground Transport, Faculty of Engineering, Czech University of Life Sciences Prague, Kamýcká 129, Praha 6, Prague, 16521, Czech Republic, phone: +420 22438 3115, e-mail: kotekm@oikt.czu.cz

THE INFLUENCE OF NOZZLE TYPE AND PRESSURE ON THE DOSAGE UNIFORMITY OF RAINFALL SIMULATOR

S. Kovář

Department of Agricultural Machines, Faculty of Engineering, Czech University of Life Sciences Prague, Czech Republic

Abstract
Water erosion and its symptoms represent worldwide problem. In the Czech Republic conditions is at risk by water erosion more than half of the agricultural land. A rainfall simulator is a promising method of measuring of erosion values such as infiltration rate, surface runoff and amount of washed off soil. At the department of agricultural machines (Czech University of Life Sciences Prague) has been developed the rainfall simulator for mentioned measurements. For the operation of rainfall simulator is necessary to know the progress of surface dose of rainfall simulator for individual nozzles. The aim of this measurement was to compare the dependence of fluid pressure to the uniformity of dispersion nozzles during the simulated rainfall. Three types of nozzles were selected. The two of nozzles have circular spray pattern and the third has a square spray pattern. Firstly the flow through the nozzles was measured for different operating pressures. Secondly the surface dose of water per unit area was measured. The measurements showed the lack of for nozzle with square spray pattern. The correlation between precision in surface dose and operating pressure was also observed. The measurements took place in laboratory conditions. The nozzle Lechler 460.788.30.CE with circular spray pattern showed the smallest scatter of measured values of all measured nozzles. It is therefore the most suitable nozzle for use of simulator rain.

Key words: dosage, nozzles, rainfall simulator.

INTRODUCTION

Water erosion is a problem of global significance. Water erosion causes destruction or damage to enormous areas of agricultural land every year (MORGAN, 2005). Agricultural land in the Czech Republic is largely exposed to the risk of water erosion on grounds of habitat, but as well agro technology. More than half of agricultural land is endangered by water erosion in the Czech Republic (JANEČEK, 2005).

Due to water erosion the soil is depleted of its most fertile part – topsoil. The physical and chemical properties of the Earth's surface are deteriorating, the content of nutrients and humus in the soil reduce, and the thickness of the soil profile decreases. Losses of soil most threaten the agriculture and the forestry because this loss is permanent. The affected soil is only in very exceptional cases returned to the original site. For example, the loss in 5-15 mm of topsoil layer can reduce crop yields by up to 15 - 30% (TRUMAN ET AL., 2005).

Intensity and process of water erosion can be most accurately determine at exactly defined drainage areas that have a certain slope and are able to capture surface water run-off and washed off soil particles. The advantage of this mentioned method is relatively quick and easy data collection (NOVÁK, 2011). For these surfaces it is possible to use for measurement the natural rainfall, which is time consuming. The second option is to use the rainfall simulator. Rainfall simulators have common characteristics in portability, mobile sources of water, bounded test area, spraying mechanism of various types, which allows control of the applied water. In addition, as the device that concentrate rainfall and measuring surface water runoff. The rainfall simulator should be cheap in production and in operating, it must be able to authentically imitate the natural rainfalls and it should be portable and ready to use in any conditions. Despite all the problems, the practice shows that the rainfall simulator is very necessary tools to research the process of erosion, infiltration and rainfall-runoff relationships. The most commonly used rainfall simulator in the world is portable rainfall simulator with scattering up to 1.5 m^2 (SCHINDEWOLF, SCHMIDT, 2012).

To identify the characteristics of rainfall simulator is vital to know the process of the scatter for different types of nozzles. For this reason, experimental measurements were performed to determine the surface dose for each individual nozzle (total of 3 selected models) at different working pressure. Simulated rainfall intensity and kinetic energy of raindrops is regulated by changing the spraying pressure (KOVAŘÍČEK ET AL., 2008).

NOVÁK ET AL., (2014) also measured the uniformity of the dose surface of nozzles for different shapes of the deflector. He concluded that nozzles with circular spray pattern have the smallest uniformity of dose of dispersion. Thus the aim of this measurement was to compare the dependence of fluid pressure to the uniformity of dispersion nozzles during the simulated rainfall.

Fig. 1. – The nozzles with circular spray pattern

MATERIALS AND METHODS

Between years 2012 and 2013 was constructed the entirely new rainfall simulator at the department of agricultural machines (Czech University of Life Sciences Prague - CULS). Concept of the simulator is partially different from the above-described design. The simulator has a modular design, being accepted that most of the technological parts is placed on the chassis of the car trailer. The rainfall simulator is designed as a universal. It is used to measure erosion values such as surface water or soil runoff, or for monitoring of the infiltration processes.

Fig. 2. – Rainfall simulator

The pump can draw water from the tank or, after turning the valve, from an external source. The pump draws water into switchboard. Switchboard has a control valve which serves for setting the pressure. The water is then guided into hoses with a diameter of ½ inch. The hoses are wound up on the drum. The length of these hoses is always 30 m. The hoses are provided with couplings at the ends for connection to the nozzle frame (with total number of four nozzle frames). Each nozzle frame is equipped with a selected pair of nozzles (always only one nozzle operates) and also a pressure gauge to check the set pressure. Measuring nozzle frame allows continuous adjustment of the nozzle height above the soil surface (eventually vegetation). It is possible to measure very high vegetation (eg. grown maize).

The measurement is related to three types of nozzles with surface scattering. The first part of the measurements was to determine the flow of water through the nozzle. All water from the nozzle was collected in a container for a set period of time (one minute) and then weighed by Kern scales. Water flow through the nozzles was designed for working pressures in the range of 0.04 – 0.12 MPa. The second part of the measurement was the measurement of surface doses in different locations of the spray pattern. From the irrigated area was chosen the area of square shaped 1 x 1 m. The water was collected into square bowls with a side 14.2 cm, which were marked with numbers 1-7 in the horizontal section and the letters A to G in the vertical section. Bowls were placed side by side in a grid of 7x7 pieces.

The height of the nozzle above the edge of the bowls was exactly one meter. The measurement was carried out again at a pressure of from 0.04 to 0.12 MPa. After pump starts was followed by measurements for a given period of time (depending on the type of nozzle 1-3 minutes). After that was done weighing of all the bowls on the laboratory scale Kern with accuracy of 0.01. After resetting the settings of bowls a new measurement began. The same pressure was measured total of 3 times to be able to statistically process the output data. Subsequently, the values were converted to the intensity of rainfall in mm·h^{-1}.

RESULTS AND DISCUSSION

A graph showing the dependence of the flow through the nozzle on the working pressure is shown in Fig. 3. For all selected nozzle was found a very strong linear relationship in the measured section 0.04 – 0.12 MPa. However, the progress of linearity in terms of changes in water flow is not the same for all nozzles. The greatest dependence was detected for the nozzle Lechler 460.888.30.CG with a circular scattering in the case of pressure. The R^2shows the size dependency of pressure on the resulting water flow. The flow increases with the increasing pressure.

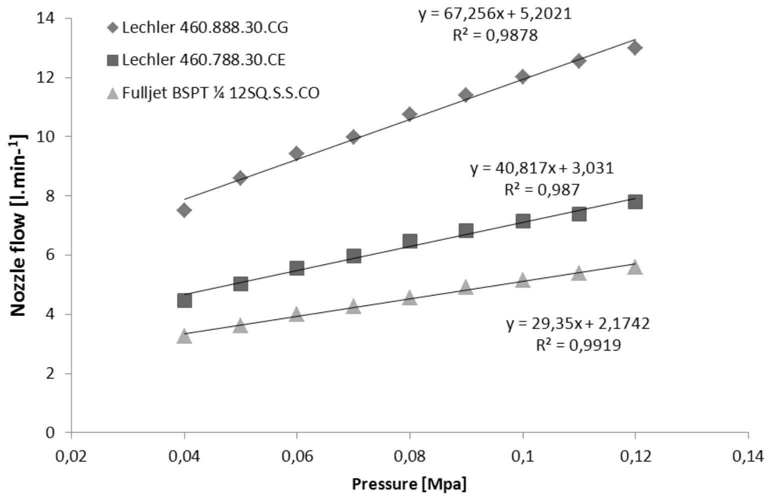

Fig. 3. – Measurement of water nozzle flow

Fig. 4 shows the progression of the surface dose for the nozzle Lechler 460.788.30.CE. It shows the progression of the working pressures of 0.05 and 0.11 MPa. This nozzle showed the smallest variance of measured values in both cases working pressures from all of measured nozzles. Also, this nozzle is most suitable for rainfall simulator in terms of uniformity of the scattering dose. However, there is a obvious dependence of scattering dose on the position towards to its centre. The nozzle in areas under its center has a higher value than towards the edge of its scattering pattern.

Fig. 5 shows the progression of the surface dose for a second nozzle with a circular shape 460.888.30.CG. This nozzle also showed similar non-uniformity values as previous nozzle for square grid measurement. However the surface dose is due to flow through the nozzle incomparably greater than previous nozzle. The values of non-uniformity are similar to the second nozzle with a circular pattern. Even for this nozzle is increased tendency surface dose toward the centre of the scattering pattern as in the first case. Also in this case it was demonstrated that increased the operating pressure positively affects the uniformity of dosage. For this measurement has not been clearly shown whether improved accuracy of the dose is connected with increasing pressure.

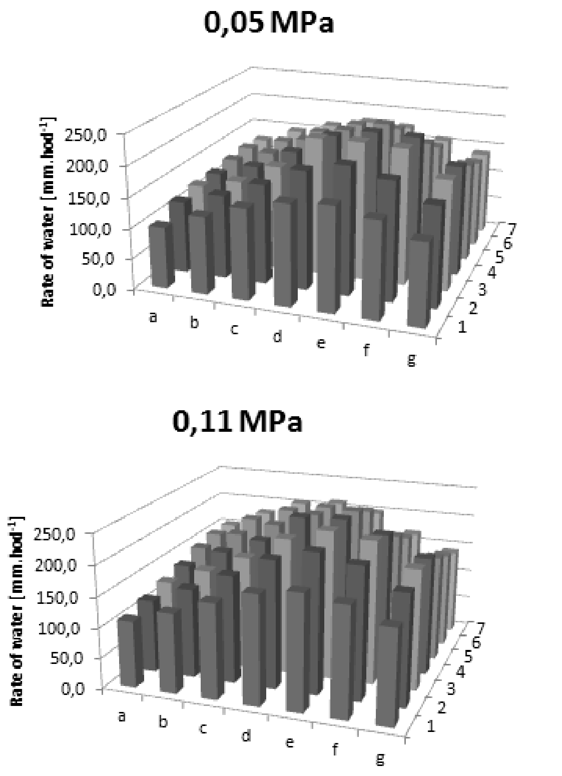

Fig. 4. – The progression of surface unevenness of the nozzle Lechler 460.788.30.CE

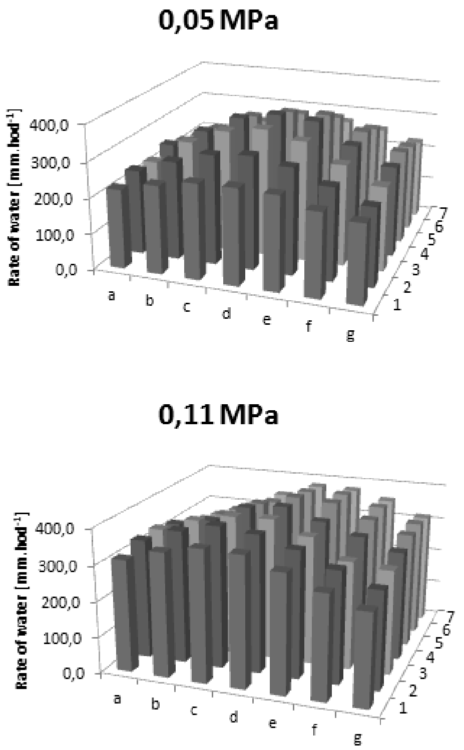

Fig. 5. – The progression of surface unevenness of the nozzle Lechler 460.888.30.CG

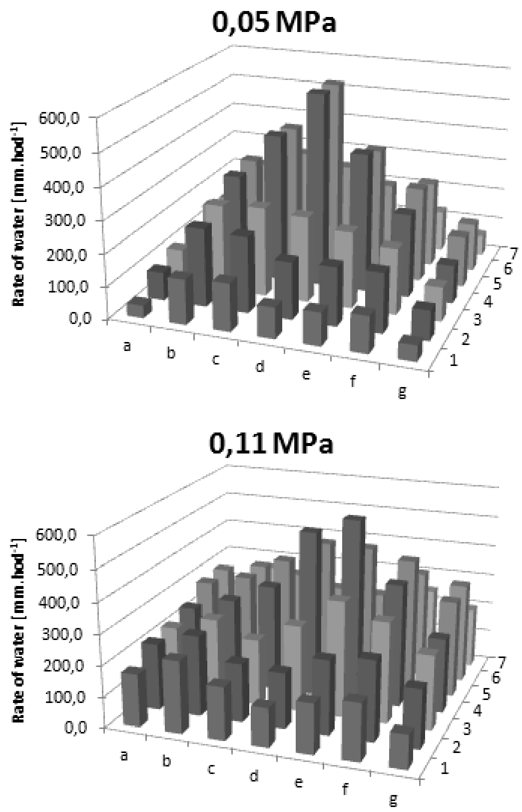

Fig. 6. – The progression of surface unevenness of the nozzle FullJet BSPT ¼ 12SQ.ssco

Fig. 6 shows the measurement progression for FullJet BSPT ¼ 12SQ.ssco. This nozzle has according to the manufacturer's a square shape of the spray pattern. Many rainfall simulators utilize this type of nozzle to create a rectangular shape measurement using a serial arrangement of these nozzles. However, from our measurement was detected large non-uniformity area of the dose for this nozzle. The non-uniformity of dose far exceeded both the measured nozzle with a circular pattern. Variations in this case are much higher for all measured pressures. Nevertheless, with increasing pressure the non-uniformity of dosage decreases slightly.

It is obvious from the graphs above that the nozzles with circular spray pattern of deflector have a more uniform splashing than the nozzles with a square shape. NOVAK ET AL. (2014) also points out that the circular nozzles have better uniformity than square nozzles.

CONCLUSIONS

From the measured values, which were converted into the graphs above, show great difficulty in simulating rain. 100% uniform spray cannot be reached at the given dimension. It has been proven that the nozzles have a linear dependence of water flow on the working pressure regardless of the shape of the deflector. It was also proven that the accuracy of dose per unit area is influenced by the shape of a nozzle deflector. Nozzles with circular pattern showed more precise uniformity of dosage, for the selected measurement conditions.

ACKNOWLEDGMENTS

Project is supported by the CULS Prague, Project No CIGA 20123006.

REFERENCES

1. MORGAN, R. P. C.: Soil erosion and conservation. 3rd Edition. Blackwell Publishing Company, Malden, USA, 2005: 304 p.
2. JANEČEK, M. ET AL.: Soil erosion protection. Prague: ISV publishing, 2005: 195 p.
3. TRUMANN, C.C., SHAW, J.N., REEVES, D.W.: Tillage efects on rainfall partitioning and sediment yield from an ultisol in central Alabama. Journal of Soil and Water conservation, vol. 60, 2005: pp. 89-98.
4. NOVÁK, P.: Evaluation of surface water runoff and soil loses in the cultivation maize crops. In The Fifth International Scientific Conference Rural Development in Global Changes 2011, Vol 5, Book 1 24.11.2011, Akademija, Kaunas District, Lithuania. Akademija, Kaunas District, Lithuania: Aleksandras Stulginskis University, 2011, pp. 405-411.
5. NOVÁK, P., CHYBA, J., KROULÍK, M., MAŠEK, K.: Dosage uniformity of rainfall simulator depending on nozzle type and pressure, Conference on Engineering for Rural Development 2014; Jelgava; pp. 69-73
6. SCHINDEWOLF, M., SCHMIDT, J.: Parameterization of the EROSION 2D/3D soil erosion model using a small-scale rainfall simulator and upstream runoff simulation, Catena, vol. 91, 2012, pp. 47-55.
7. KOVAŘÍČEK P., ŠINDELÁŘ R., HŮLA J., HONZÍK I.: Measurement of water infiltration in soil using the rain simulation method. Research in Agricultural Engineering, 54, 3: 2008: pp. 123-129.

Corresponding author:

Ing. Stanislav Kovář, Department of Agricultural Machines, Faculty of Engineering, Czech University of Life Sciences Prague, Kamýcká 129, Praha 6, Prague, 16521, Czech Republic, phone: +420 22438 3133, e-mail: kovars@tf.czu.cz

INFLUENCE OF DESTINATION AT ADHESIVE BOND PRODUCTION ON ITS STRENGTH

A. Krofová, M. Müller

Department of Material Science and Manufacturing, Faculty of Engineering, Czech University of Life Sciences Prague, Czech Republic,

Abstract

The manufacturing process running at various countries at present, these differ from each other in particular climatic condition influencing the production technology. This paper is focused on the analysis of steel adhesive bonds produced in Central Europe (Czech Republic) and in the province of North Sumatra (Indonesia). The aim of the research was to evaluate the strength of adhesive bonds produced in Central Europe and Indonesia (North Sumatra). The second aim was evaluate the effect of adhesive bonded surface treatment.

The results of the experiment confirmed a clear positive or negative trend between places of creation the bond for two-component epoxy. The positive effect was reflected in Central Europe (Czech Republic) on the creation of cyanoacrylates adhesive bond. There were no effects of the adhesive bond creation to change the failure area.

Key words: adhesive bonding technology, Central Europe, North Sumatra, AlCu4Mg, adhesive bond strength.

INTRODUCTION

The adhesive bonding technology is a prospective method of bonding of diverse materials, when bonds between adhesively bonded material and adhesive itself arise (MÜLLER, 2016; MÜLLER & HERÁK, 2013).

The adhesive bonding technology is cheap and quick method of bonding, which is utilized in almost all fields (PEREIRA ET AL., 2010; MÜLLER 2015B). Bonding of aluminium and its alloys was introduced in England in the 1940's.

The adhesive bonding technology depends on the adhesion of the adhesive to the adhesive bonded surface, on wettability of adhesive bonded surface and on the cohesion that means on own strength of the adhesive (MÜLLER, 2016).

The adhesive bond is the complex of three layers – adhesive bonded material (called adherent), adhesive layer and cohesive layer.

All three layers are significantly influenced for example by the surface treatment, environment etc.

GERALD, PETHRICK (2009) AND SARGENT (2005) ascertained the influence of the environment on a change of physical properties of adhesives. Namely, it was the adhesive bond strength.

A large part of industrial production is currently being transferred to the development countries and areas. These countries have quite different geographical, climatic, and technological conditions than are those found in the countries in which such production import is the aim. In the equatorial countries the usage of bonded joints is increasing, mainly in the automobile and naval industries as well as in the agricultural machines and tools production and, last but not least, in the production of daily use devices (HERÁK ET AL., 2009).

Polymeric materials in its practical use are almost never exposed to only one factor. It is usually a combination according to the climatic conditions. Influence of atmosphere on the adhesive used is given mainly by the simultaneous action of four basic factors. These factors include temperature, water and its vapors, oxygen and ultraviolet radiation (HU ET AL., 2013; COMYN, 1983; OUDAD, 2012).

LOH A CROCOMBE (2002) given as the most common factor causing failure of the adhesive bond at the interface of the adhesive / adherend exposure of such a joint combination of increased humidity and temperature.

The atmosphere has an effect the adhesive bonds cyclical character. We define daily, seasonal cycles, cycles associated with changes in weather etc. This action of the atmosphere generated thermal and moisture stress cyclical character of the adhesive bonded joints. The faster turns, the faster fatigue occurs connections, which limits its life.

Acting of changeable moisten, which often happens under atmospherics conditions, can be even more dangerous. Tensions mentioned above gain the cyclic features, which significantly increases destruction process. Methods of accelerated aging are based on this effect (COMYN, 1983; MÜLLER, 2016).

Environmental influences applied to adhesive not only in the formation of the bond, as well as during

transport and storage, for example du to direct solar radiation, solar radiation (MÜLLER & VALÁŠEK, 2014A).
Considerable part of the research on single-lap adhesive bonds is focused on geometrical design of adhesive bonds, thickness of adhesive layer and on mechanical properties of adherents (MÜLLER ET. AL., 2010; MÜLLER & VALÁŠEK, 2013).
The aim of the research was to evaluate the strength of adhesive bonds produced in Central Europe and Indonesia (North Sumatra). The second aim was evaluate the effect of adhesive bonded surface treatment.

MATERIALS AND METHODS

Adhesive bonds and process of testing the adhesive bonds was in accordance with standard ČSN EN 1465. The basis of adhesive bonds laboratory testing was the determination of the tensile lap-shear strength of rigid-to-rigid bonded assemblies according to the standard ČSN EN 1465. Laboratory tests of the adhesive bonds were performed using the standard test specimens made according to the standard CSN EN 1465 (dimensions $100 \pm 0.25 \times 25 \pm 0.25 \times 1.5 \pm 0.1$ mm and lapped length of 12.5 ± 0.25 mm) from duralumin AlCu4Mg. Treatment surface is showed in the Tab. 1.
Three kinds of structural epoxy adhesives were used for this experiment. In Tab. 1 are showed the used adhesives, surface treatment and sign type of experiment.

Tab. 1. – Characteristics used adhesives and surface treatment

Adhesive	Type	Sign	Treatment surface
loctite super bond	cyanoacrylates	LSB-WT	Without mechanical and chemical treatment AlCu4Mg
3-ton quick	two-component epoxy	3TQ-WT	
3-ton epoxy	two-component epoxy	3TE-WT	
loctite super bond	cyanoacrylates	LSB-GU	Mechanical treatment by abrasive cloth of grit P220 (at right angles to the loading force in the destruction of the adhesive bond) and without chemical treatment AlCu4Mg
3-ton quick	two-component epoxy	3TQ-GU	
3-ton epoxy	two-component epoxy	3TE-GU	
loctite super bond	cyanoacrylates	LSB-GP	Mechanical treatment by abrasive cloth of grit P220 (parallel to the loading force in the destruction of the adhesive bond) and without chemical treatment AlCu4Mg
3-ton quick	two-component epoxy	3TQ-GP	
3-ton epoxy	two-component epoxy	3TE-GP	

Chemical composition of test alloy AlCu4Mg detected by spectral analysis is given in Tab. 2. This is a construction material suitable for components and construction elements of aircraft, railway carriages, agricultural machines, automobiles and other vehicles.

Tab. 2. – Chemical composition (mass %)

Element	Al	Cu	Mg	Mn	Fe	Ti	Si	Zn
AlCu4Mg - ČSN 42 4201	93.2	5.01	0.57	0.51	0.31	0.01	0.35	0.02

On the surface of bonded adherents roughness parameters Ra and Rz were measured. Roughness parameters were measured with a portable profilometer Mitutoyo Surftest 301. Limit wavelength cut-off was set as 0.8 mm.
An even thickness of the adhesive layer was reached by a constant pressure 0.5 MPa. The lapping was according to the standard 12.5 ± 0.25 mm.
Specification of the environment where adhesive bonds was created:

In the experimental part the environment of Central Europe is marked with "CE-CZ", Indonesia, North Sumatra is marked with "NS-I".

- **Prague, CZ, Central Europe** is situated in the mild climatic zone of the northern hemisphere. It is the transition zone. Warm summer with rainfalls alternates with winter with lasting snow cover. Europe is especially characteristic by industrial production, which is exported all around the world. But at the present time this influence goes missing (MÜLLER ET. AL., 2013). Adhesive bonds were create in the laboratory characterized the constant temperature of 22 ± 2 °C and relative humidity 50 ± 5%.
- **Indonesia, North Sumatra, region Balige** is of tropical climate, which is during the whole year without fluctuations. The division into classic times of the year does not exist here. The division is related to the dryness and rainy seasons (MÜLLER ET. AL., 2013; HERÁK ET. AL., 2009). The average air humidity ranges from 70 to 100%. Region Balige - elevation 900 m, average daily temperature of 25 °C, relative humidity 80%. Adhesive bonds were create in the laboratory characterized the constant temperature of 26 ± 2 °C and relative humidity 95 ± 5%.

Adhesive bonds and bended materials (adherent) were packed in Indonesia and airlifted to CZ. There were destructively tested.

It can be assumed that the impurities on the surface of the bonded material greatly reduce the overall strength of the adhesive bond. A similar incidence of dust contaminants can be expected after mechanical surface treatment. The volume of impurities was determined by weighing (Scales Kern). The test specimens were weighed before and after chemical cleaning in a bath of acetone.

Laboratory tests were performed using the universal tensile strength testing machine LABTest 5.50ST (a sensing unit AST type KAF 50 kN, an evaluating software Test&Motion). The failure type according to ISO 10365 was determined at the adhesive bonds. The loading speed at the static test of the adhesive bond strength was always set as 10 $mm.min^{-1}$.

The results of measuring were statistically analysed. Statistical hypotheses were also tested at measured sets of data by means of the program STATISTICA. A validity of the zero hypothesis (H_0) shows that there is no statistically significant difference ($p > 0.05$) among tested sets of data. On the contrary, the hypothesis H_1 denies the zero hypothesis and it says that there is a statistically significant difference among tested sets of data or a dependence among variables ($p < 0.05$).

RESULTS AND DISCUSSION

Significance of bonding surface modification has been demonstrated in many studies. Development of adhesives, however, aims to minimize the factors affecting the preparation of bonding surface. This trend is particularly pronounced in establishments, where the automatic production is introduced (MÜLLER & VALÁŠEK, 2013; MÜLLER, 2013, 2014).

Determination of volume of pollution on specimens intended for adhesive bonding was v CE-CZ cca 2.13 mg a v NS-I 1.01 mg.

The results show that the test specimens without chemical modification of bonding surface contained a considerable amount of impurities on their surface.

The surface roughness of the adhesive bonded material AlCu4Mg after mechanical treatment by abrasive cloth of grit P220 was Ra 1.08 ± 0.15 μm, Rz 7.38 ± 0.99 μm and without mechanical treatment was Ra 0.38 ± 0.07 μm, Rz 2.48 ± 0.43 μm.

Results of the adhesive bond strength are visible from Fig. 1.

Results of ANOVA F-test are following:

- In terms of statistical test (T-test, $\alpha = 0.05$) influence of different modification on bonded surface of AlCu4Mg is possible to state that the different surface treatments are statistically inhomogeneous groups. Hypothesis H_0 was not confirmed, i.e. there is a difference in the strength of the adhesive bond between the different types of experiments, i.e. various adhesives and place of bond creation NS-I and CE-E.in the significance level of 0.05. Statistical parameter $p = 0.0000$ was on all tested groups. A statistical comparison of the values shows that treatment bonded surface has an influence on adhesive bond strength.
- In terms of statistical test (T-test, $\alpha = 0.05$) influence the type of adhesive LSB, 3TE and 3TQ is possible to state that each adhesive are statistically inhomogeneous groups. Hypothesis H_0 was not confirmed, i.e. there is a difference between the each types of experiments, i.e. various place of bond creation NS-I and CE-E in the significance level of 0.05. Statistical parameter $p = 0.0000$ was

on all tested groups. A statistical comparison of the values shows that type of adhesive has an influence on adhesive bond strength.

- In terms of statistical test (T-test, $\alpha = 0.05$) influence the place of bond creation NS-I a CE-CZ is possible to state that the regions of bond creation are statistically inhomogeneous groups. Hypothesis H_0 was not confirmed, i.e. there is a difference between the each types of experiments, i.e. treatment surfaces and various place of bond creation i.e. NS-I and CE-E in the significance level of 0.05. Statistical parameter p = 0.0000 was on all tested groups. A statistical comparison of the values shows that type of adhesive has an influence on adhesive bond strength.
- Statistical comparison (T-test $\alpha = 0.05$) influence the place of bonding, i.e. the NS-I and CE-E on the adhesive bond strength is showed in Tab. 3. From a statistical comparison of the values shows that place of bonding has an influence on adhesive bond strength.

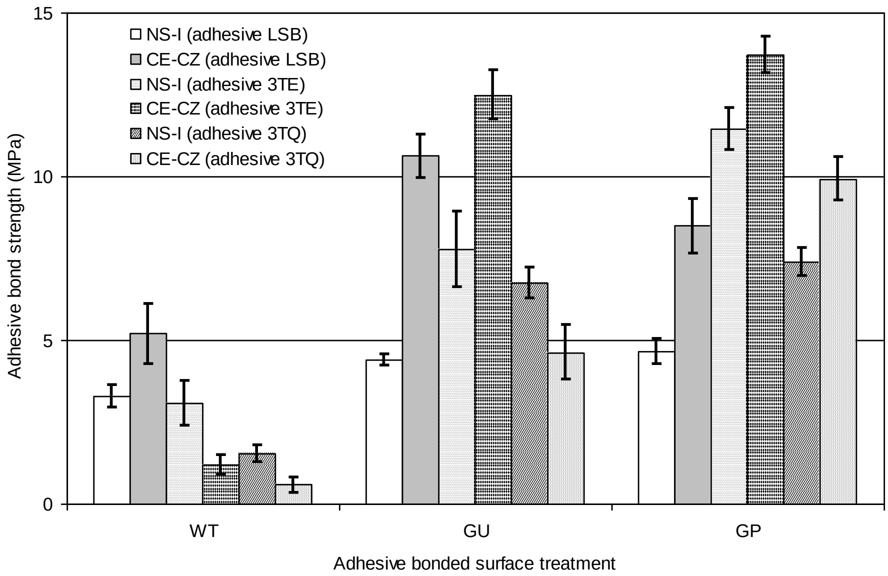

Fig. 1. – Results of the adhesive bond strength

Tab. 3. – Statistical comparison of place where adhesive bond was created NS-I and CE-CZ on adhesive bond strength (T-test)

Sign	H_0: (p>0.05)
LSB-WT	0.0005
SSB-GU	0.0000
LSB-GP	0.0000
3TE-WT	0.0005
3TE-GU	0.0000
3TE-GP	0.0003
3TQ-WT	0.0002
3TQ-GU	0.0001
3TQ-GP	0.0000

The experimental results confirmed the importance of mechanical surface treatment. Adhesive bonds for each of the series increased strength from 34 to 1612%. A significant increase in the strength of the adhesive bond occurred in two-component epoxy adhesives labeled 3TE and 3TQ. Cyanoacrylate adhesive LSB indicate relatively high strength without treatment surface (sign WT).

The results of the experiment confirmed a clear positive or negative trend between the place of creation the adhesive bond for two-component epoxy, i.e. NS-I (Indonesia, North Sumatra, region Balige) and

CE-CZ (Prague, CZ, Central Europe). Positively was reflected environments CE-EN for creating of cyanoacrylates bonds (LSB). It was determined increase the adhesive strength from 37 to 59% depending on the surface treatment. This is mainly due to the fact that cyanoacrylate adhesives are during the hardening process sensitive to humidity change. Optimum strength of adhesive bonds by using cyanoacrylate adhesives is achieved at humidity from 40 to 60%. Lower humidity leads to slower hardening. Higher humidity accelerates the hardening process, but simultaneously worsens the final strength of adhesive bond. (LOCTITE, 1998; MÜLLER & VALÁŠEK, 2014B, 2014C).

A principle of the adhesive bond rise is based on a polymeration of put adhesive which is activated by air humidity of the environment and of the adherent. The humidity is neutralized by a stabilizer which is involved in the adhesive and which activates the polymeration process. It comes to a creation of polymerating links in a few “seconds”, so the strong bond arises (MÜLLER & VALÁŠEK, 2014B, 2014C).

The adhesive bonds are of adhesive-cohesive failure area. There were no effects to adhesive bond where the adhesive bonds was created Type failure area was dependent on the surface treatment. Especially for adhesive bonds without surface treatment (sign WT) were adhesive failure area.

We concur with the DUCHÁČEK (2006) AND FAIRES (1955) that due to geography and the associated climatic conditions the strength of cyanoacrylate adhesives is changing.

TAMAI AND ARATANIC (1972) observed that within certain limits the roughening of the samples causes decrease of wettability. The simple explanation is that protrusions of elongated ridges create barriers that prevent expansion of drops. Similar conclusions on the aluminium alloy were reached by PEREIRA (2010). He notes that the mechanical properties of unmodified aluminium were higher than for mechanically treated aluminium. These conclusions were not confirmed by experiments.

CONCLUSIONS

Following conclusions can be deduced from performed experiments:

- The results of experiments confirmed the importance of the mechanical surface treatment AlCu4Mg. The strength adhesive bond with mechanical surface treatment by abrasive cloth of grit P220 increased up to more than 1600%. Two-component epoxy has a higher dependence on mechanical surface treatment AlCu4Mg.
- The results of the experiment confirmed a clear positive or negative trend between the place of creation the adhesive bond for two-component epoxy, i.e. NS-I (Indonesia, North Sumatra, region Balige) and CE-CZ (Prague, CZ, Central Europe). Positively was reflected environments CE-EN for creating of cyanoacrylates bonds (LSB). It was determined increase the adhesive strength up to 59% depending on the surface treatment.
- The adhesive bonds are of adhesive-cohesive failure area. There were no effects to adhesive bond where the adhesive bonds was created Type failure area was dependent on the surface treatment.

ACKNOWLEDGEMENT

Supported by Internal grant agency of Faculty of Engineering, Czech University of Life Sciences Prague (No. 2016:31140/1312/3109 and No. 2015:31140/1312/3106).

Special thanks to the organizers of the Summer School on North Sumatra in Indonesia for that they make it possible to carry out this research.

REFERENCES

1. COMYN, J.: Kinetics and Mechanism of Environmental Attack. Durability of structural adhesives. Reprinted. Ed. Kinloch A. J. London: Applied Science, 1983, pp. 85-131.
2. DUCHÁČEK, V.: Polymery výroba, vlastnosti, zpracování, použití. Praha: VŠCHT Kanag, 2006, pp. 278.
3. FAIRES, V. M.: Design of machine elements. New York: The Macmillan Company, 1955, pp. 624.
4. GERALD D., PETHRICK R. A.: Environmental effects on the ageing of epoxy adhesive joinst. In: International Journal of Adhesion & Adhesives, 2009, pp. 77–90.
5. HERÁK, D., MÜLLER, M., DAJBYCH, O., SIMANJUNTAK, S.: Bearing capacity and corrosion weight losses of the bonded metal joints in the conditions of Indonesia, North Sumatra province. In: Research in Agricultural Engineering (Zemědělská technika), 2009, pp. 94-100.
6. HU, P., X. HAN, W.D. LI, L. LI A Q. SHAO.: Research on the static strength performance of adhesive single lap joints subjected to extreme temperature environment for automotive industry. In: International Journal of Adhesion and Adhesives. 2013, pp. 119-126.
7. LOCTITE: Worldwide design handbook, Erasmusdruck GmbH, Mainz, 1998.
8. LOH, W.K., CROCOMBE A.D., ABDEL WAHAB M.M., ASHCROFT, I.A.: Environmental degradation of the interfacial fracture energy in an adhesively bonded joint. In: Engineering Fracture Mechanics. 2002, pp. 2113-2128.

9. MÜLLER, M., VALÁŠEK, P.: The logistics aspects influencing the resultant strength of adhesives at practical application. In: Agronomy Research. 2014a, pp. 285-290.
10. MÜLLER, M., HERÁK, D., VALÁŠEK, P.: Degradation limits of bonding technology depending on destinations Europe, Indonesia. In: Tehnicki Vjesnik-Technical Gazette, 2013, pp. 571-575.
11. MÜLLER, M., HERÁK, D.: Application possibilities of adhesive bonds – Europe, Indonesia. In: Scientia Agriculturae Bohemica, 2013, pp. 167-171.
12. MÜLLER, M., HERÁK, D.: Dimensioning of the bonded lap joint. In: Research in Agricultural Engineering (Zemědělská technika), 2010, pp. 59-68.
13. MÜLLER, M., VALÁŠEK, P.: Comparison of variables influence on adhesive bonds strength calculations. In: Manufacturing Technology, 2013, pp. 205-210.
14. MÜLLER, M., VALÁŠEK, P.: Influence of environment temperature on strength of quick-setting adhesives based on cyanoacrylates. In 2nd International Conference on Materials, Transportation and Environmental Engineering, Kunming; China. Kunming; China: Trans Tech Publications Ltd, 2014b, pp. 1030-1032.
15. MÜLLER, M., VALÁŠEK, P.: Optimization of surface treatment of carbon steel in area of adhesive bonding technology with application of quik-setting adhesives. In: Manufacturing Technology, 2014c, pp. 579-584.
16. MÜLLER, M.: Influence of cyclic degradation in saline solution on mechanical properties of adhesive bonds. In: Manufacturing technology. 2016, pp. 204-209.
17. MÜLLER, M.: Influence of loading speed on a change of parameters of adhesive bonds based on cyanoacrylates. In: Res. Agr. Eng., 2015a, pp. 177-182
18. MÜLLER, M.: Research of liquid contaminants influence on adhesive bond strength applied in agricultural machine construction. In: Agronomy Research, 2013, pp. 147-154.
19. MÜLLER, M.: Research on surface treatment of alloy AlCu4Mg adhesive bonded with structural single-component epoxy adhesives. In: Manufacturing Technology, 2015b, pp. 629-633.
20. MÜLLER, M.: Setting of causes of adhesive bonds destruction by means of optical analysis. In: Manufacturing Technology, 2014, pp. 371-375.
21. OUDAD, W., ET AL.: Effect of humidity absorption by the adhesive on the performances of bonded composite repairs in aircraft structures. Composites Part B: Engineering. 2012, pp. 3419-3424.
22. PEREIRA, J.M., FERREIRA, F.V., ANTUNES, P.J., BÁRTOLO A.M.: Analysis of manufacturing parameters on the shear strength of aluminium adhesive single-lap joints. In: Journal of Materials Processing Technology, 2010, pp. 610-617.
23. SARGENT, J. P.: Durability studies for aerospace applications using peel and wedge tests. International Journal of Adhesion & Adhesives, 2005, pp. 247-256.
24. TAMAI, Y., ARATANIC, K..: Experimental study of the relation between contact angle and surface roughness. In: The Journal of Physical Chemistry, 1972, pp. 3267–3271.

Corresponding author:
Ing. Alena Krofová, Department of Material Science and Manufacturing Technology, Faculty of Engineering, Czech University of Life Sciences Prague, Kamýcká 129, Praha 6, Prague, 16521, Czech Republic, email: krofovaa@tf.czu.cz

MEASUREMENT OF ELECTRICAL CONDUCTIVITY OF FERTILIZER LAD 27

J. Krupička[1], P. Šařec[2]

[1]*Department of Agricultural Machines, Faculty of Engineering, Czech University of Life Sciences Prague, Czech Republic*
[2]*Department of Machinery Utilization, Faculty of Engineering, Czech University of Life Sciences Prague Czech Republic*

Abstract
Paper deals with the measurement of electrical conductivity of significant size groups of mineral fertilizer LAD 27 divided in the air stream. Samples of these groups were dissolved in distilled water and the values of electrical conductivity recorded. Measurements will be used to monitor the electrical conductivity of other mineral fertilizers and to create a standard for qualitative assessment of fertilizer solutions.

Key words: electrical conductivity, air flow, fertilizer solution, concentration, LAD 27.

INTRODUCTION

Fertilisation is an important factor that affects crop yields (LOŽEK ET AL., 1997; KAJANOVIČOVÁ ET AL., 2011). Correct application of fertilisers has both positive economic and environmental effects (NOZDROVICKÝ ET AL., 2009; ŠIMA ET AL., 2012; ALARU ET AL., 2003; ŠIMA & DUBEŇOVÁ, 2013). One of the most important factors is the fertiliser particle-size distribution which depends upon the size of the fertiliser particles (MACÁK ET AL., 2011). The differences and variability in physical properties of fertilisers causes problems during the field application by the commonest spinning disc fertiliser spreaders. This process depends upon the particle's dimension, so that the dimension of particles is one of the main parameters that influence fertiliser effectiveness (KRUPIČKA & HANOUSEK, 2006). Therefore, granulometric studies of various fertilizers were carried out (KRUPIČKA & HANOUSEK, 2006; ŠIMA ET AL., 2013). In order to enable more accurate fertilizer application also in its liquid form, it is important to measure concentration of solution (KRUPIČKA&ŠAŘEC, 2013; KRUPIČKA ET AL., 2015). The concentration of fertilizers can be determined on the basis of the electrical conductivity (increasing the electrical conductivity). The value of the electrical conductivity can be used for precise application of fertilizers in liquid form. Monitoring the conductivity and knowing its value for target fertilizer concentrations enables to start the field application of fertilizers at an optimum moment. This would significantly increase the precision compared to the commonly used "mass percentage method" where the concentration accuracy attains only ±10 % according to fertilizer manufacturers. According to the electrical conductivity, the quality of the measured fluid can be assess accurately along with other data such as the level of pollution, the concentration of the various components of the solution, etc. (KABEŠ, 1999). In that way, electrical conductivity is the reciprocal of electrical resistance, is indicated with the letter G and its basic unit is the Siemens (S).

The effectiveness of mineral fertilizers in crop cultivation depends on the particle stability and speed of their transformation to solution state to be acceptable by plants. This process depends on the particles dimensions, so that the dimension of particles is one of the main parameters that influence the fertilizer effectiveness.

Application of solid commercial fertilizers play important role in precision farming technologies. The application quality is dependent on chemical composition and physical properties of fertilizer. Important from physical properties point of view is the grading of aggregate evaluation that is still performed by standard ČSN 01 50 30. The dimension of fertilizer particles only is characterized by this way.

In this paper, we continue in the previous research program, in which the granulometric examinations of mineral fertilizers were studied. In contrary to the similar study of other authors, sieve and airflow sorting were combined.

Experiments with particles can be designed differently. An elutriator was designed and constructed in which an airflow is supplied by a centrifugal fan (CSIZMAZIA, 2000). Methods for measuring the coefficient of friction, the coefficient of restitution, the aerodynamic resistance coefficient, and the breaking force (particle strength) of fertilizers (HOFSTEE, 1992) were taken into account. The breaking force feature was skipped. The problem of particle destruction was overcome by fertilizer selection. The control of fertilizer discharge was studied for different designs of distributors and an experimental accurate fertilizer distributor with a rotary vessel type feeder was developed (KUDOH, 1989) what shows that dissolution of fertilizer also makes some problems. Consequent logistical problems are difficult the same way both for pumping liquids, and for transportation of particles by the air.

The size of particles makes the fertilizer's shelf life and stability of particulars behavior in the airflow more stable in storage and better acceptable by the plant. Therefore, experiments studying motion of particles through the air were accompanied by grading of particles.

This paper contains results obtained for LAD 27 using the method developed previously.

MATERIALS AND METHODS

Electrical conductivity was measured using the device inoLab model WTW Cond 720. Instruments for the measurement of electrolytic conductivity, specifically electrical conductivity of liquids, consist of a measuring probe or conductivity sensor, transducer and evaluation unit. According to the manufacturer, accuracy of the device is 0.5% of value when measuring conductivity. Most of the apparatus is adapted for measuring the resistivity and weight concentrations of some components of the solution, which can be derived from the electrical conductivity. They are very sensitive and allow you to measure the content of various substances from small to very high concentrations and is often used to control a wide range of industrial processes (KABEŠ, 1999). Measurement was carried out for mineral fertilizer LAD 27 (alternative trade name LOVOFERT LAD 27; manufacturer LOVOCHEMIE, a.s. – the Czech Republic). The composition of LAD 27 is the following: nitrogen fertilizer containing 27 % of nitrogen and 4 % of MgO. It is a mixture of ammonium nitrate with finely ground dolomite in the form of whitish to light brown granules sized 2 mm to 5 mm. Fertilizer is an all-purpose fertilizer suitable for basic fertilization as well as fertilization during vegetation of winter crops and spring crops. Distribution of the air stream was carried out in the laboratory of the Department of Agricultural Machinery using the laboratory air sorting machine K - 293 (see Fig. 1).

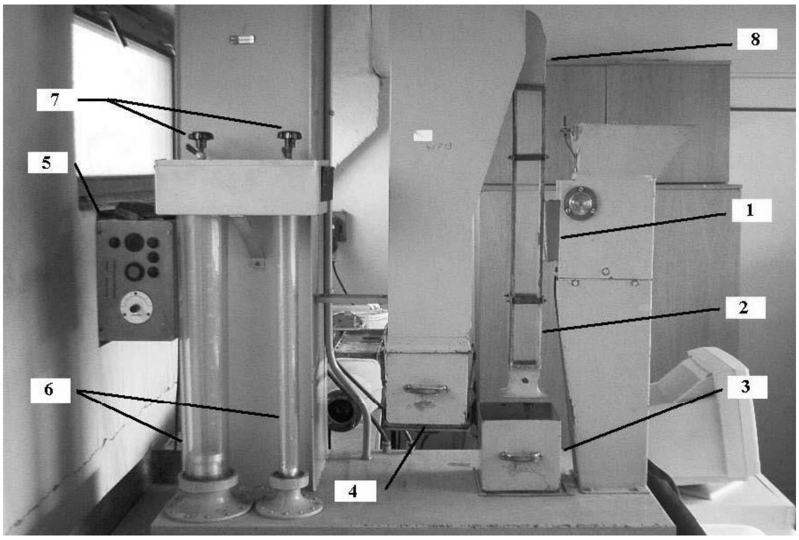

Fig. 1. – Laboratory Air sorter K - 293

Labels: 1 - adjustable damper hoppers, 2 - vertical (aspiration) channel, 3.4 - tanks, 5 - control panel with buttons, 6 - small and large graduated cylinder, 7 - cylinder adjusting screws, 8 – fan

The measurement procedure was as follows. First the laboratory sorting machine K-293 determined ranges of required amount of air, i.e. the minimum amount of air in which the particles are carried, and in the opposite a maximum amount of air in which the sample is completely sorted. With the help of graduated cylinders, interval of gradually increasing speed of the air flow is selected so that the number of classes was 7 to 10. It is necessary to ensure the right plane for the weights to ensure accuracy. Scales are calibrated and set to zero. Fertilizer is mixed because of the measurement accuracy and a sample of fertilizer weighing 500 g removed. An appropriate, predetermined, air speed is set for the laboratory device using graduated cylinders and adjusting screws. A sample of fertilizer is poured into the tank (1) with pre-set for the damper. With the help of a vibrator, fertilizer gets into the air flow in a vertical channel (see Fig. 2). Here comes the separation. Granules with larger than the critical speed set fall through the channel into the container (3). Granules with lower critical speeds are vertically entrained in air stream and in the extended portion of the channel are falling into the tray (4). The amount of fertilizer separated using air flow into the tank (4) is then placed in a pre-labeled bowl for later use. Emptied tank (4) is placed back into the machine and the speed of the air flow is checked. Then the fertilizer from the tank (3) is filled back to the tank (1) and the graduated cylinder is set to the next value of air stream speed. In this way, the experiment continues until the entire sample of fertilizer gradually falls into the tank (4).

The whole process is repeated with eight different samples of fertilizers to maintain the accuracy and reliability of statistical data measurements. Measurement in an air stream was carried out at a temperature of 22 °C and humidity of 22 %.

Subsequently, the material sorted by the air stream was further divided by laboratory sieves Haver EML 200. Three samples weighing 5 grams were taken from the portions with significant share.

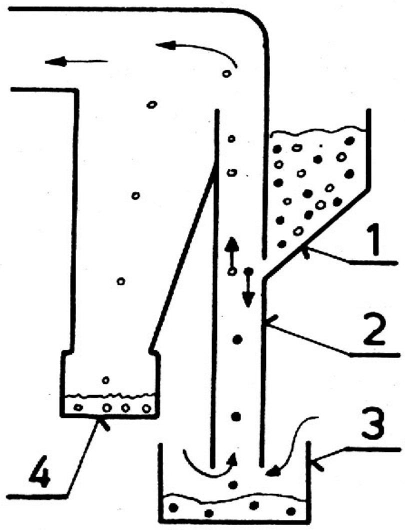

Fig. 2. – Thevertical channel (detailed view)
Labels: 1 - tray, 2 - vertical (aspiration) channel, 3 - stack, 4 - tray (particles of lower critical speed are carried into this tank)

Their electrical conductivity was measured on the machine Conductivity meter WTW inoLab model Cond 720. The measurements were carried out over nine hours in one-hour intervals. Before each conductivity measurement took place, the sample had been mixed to ensure its homogeneity.

RESULTS AND DISCUSSION

From the material divided by the air stream and the sieves, three samples weighing 5 grams were taken of each of significant proportions that were gained by the air stream of 105, 115, 125 $m^3.h^{-1}$ and by the sieves of size 1, 2, 3.15 and 4 mm (Tab. 1). The fertiliser meets the requirements of the national standards and is in conformity with the demanded range given by the manufacturer. ŠIMA ET AL. (2013) came with the same conclusion in the case of DASA 26/13 and ENSIN fertilizers.

Subsequently, the samples were collected and mixed and then dissolved in distilled water of the volume of 50 ml and of the room temperature of 17 °C.

Tab. 1. – Relative representation of groups of LAD 27 after sorting by air stream and sieves (significant proportions highlighted by italics)

Air stream	**Sieves [mm]**				**Total**
[$m^3.h^{-1}$]	**1.00**	**2.00**	**3.15**	**4.00**	
105	0.01 %	***8.09 %***	***11.79 %***	0.40 %	**20.31 %**
115	0.01 %	***3.13 %***	***38.84 %***	2.82 %	**44.80 %**
125	0.00 %	0.76 %	***24.38 %***	***9.76 %***	**34.90 %**

Tab. 2 to 4 show the measured values of electrical conductivity. Conductivity measurements were performed in one-hour steps and started half an hour after solution had begun.

Tab.2. – Measured values of electrical conductivity of LAD 27 fertilizer for the air stream of 105 $m^3.h^{-1}$

Time [h]	Electrical conductivity[$m^{-2}.kg^{-1}s^3.A^2$] Sieve 2.00 mm			Sieve 3.15 mm			Average
0.5	55.40	53.00	51.20	51.20	45.60	46.70	50.52
1.5	81.60	78.90	79.80	73.50	68.20	71.50	75.58
2.5	92.40	86.20	84.50	81.50	79.70	82.40	84.45
3.5	97.40	94.50	95.50	92.10	89.80	85.40	92.45
4.5	99.80	96.30	98.10	98.60	96.40	97.10	97.72
5.5	102.20	97.40	99.50	99.40	97.50	98.60	99.10
6.5	103.10	98.10	99.70	100.20	98.90	99.80	99.97
7.5	103.80	98.60	100.40	101.30	100.40	101.50	101.00
8.5	104.30	99.40	101.70	102.40	101.10	102.60	101.92
9.5	105.10	100.90	102.10	103.00	101.90	103.10	102.68

Tab. 3. – Measured values of electrical conductivity of LAD 27 fertilizer for the air stream of 115 $m^3.h^{-1}$

Time [h]	Electrical conductivity[$m^{-2}.kg^{-1}s^3.A^2$] Sieve 2.00 mm			Sieve 3.15 mm			Average
0.5	46.80	47.80	45.40	46.80	47.80	45.40	46.67
1.5	74.10	76.20	78.70	74.10	76.20	78.70	76.33
2.5	85.70	84.50	86.40	85.70	84.50	86.40	85.53
3.5	88.60	89.80	91.50	88.60	89.80	91.50	89.97
4.5	94.40	95.00	95.70	94.40	95.00	95.70	95.03
5.5	95.70	95.30	96.70	95.70	95.30	96.70	95.90
6.5	96.40	96.10	97.80	96.40	96.10	97.80	96.77
7.5	99.40	99.70	99.80	99.40	99.70	99.80	99.63
8.5	99.80	100.50	100.20	99.80	100.50	100.20	100.17
9.5	101.30	102.20	102.10	101.30	102.20	102.10	101.87

Tab. 4. – Measured values of electrical conductivity of LAD 27 fertilizer for the air stream of 125 $m^3.h^{-1}$

Time [h]	Electrical conductivity[$m^{-2}.kg^{-1}s^3.A^2$] Sieve 3.15 mm			Sieve 4.00 mm			Average
0.5	51.20	49.30	52.40	56.70	55.90	58.90	54.07
1.5	78.60	72.50	81.20	79.70	84.80	86.90	80.62
2.5	86.50	81.20	92.40	85.20	92.30	97.80	89.23
3.5	94.50	88.70	97.80	97.30	96.10	103.60	96.33
4.5	98.70	94.60	101.20	99.10	95.70	107.00	99.38
5.5	101.60	95.80	104.30	101.70	96.80	107.80	101.33
6.5	103.70	96.80	105.20	102.90	97.80	108.50	102.48
7.5	104.50	98.20	106.10	104.50	99.80	109.90	103.83
8.5	105.90	99.10	106.80	105.60	101.20	111.60	105.03
9.5	106.50	100.40	108.50	107.70	103.20	113.60	106.65

Fig. 3 demonstrates the logarithmical increase of electrical conductivity of air flow classes 105, 115, and 125 $m^3.h^{-1}$. The differences among classes were minor only. KRUPIČKA & ŠAŘEC (2013) and KRUPIČKA ET AL. (2015) concluded the same for Lovogreen, resp. DAP fertilizers. After five hours, electrical conductivity values of LAD 27 got stabilised and showed only slight increase. Similar study concerning DAP fertilizer showed on the other hand linear increase of the conductivity even after ten hours (KRUPIČKA ET AL., 2015). Concerning Lovogreen fertilizer (KRUPIČKA & ŠAŘEC, 2013), the conductivity decreased with time, but still did not get stabilised after ten hours. Hence, the results could not be generalized for different fertilizers.

Undissolved residues were detected by using filter paper - the solution was filtered and the solids were weighed and dried in a dryer at a constant temperature of 105 ° C to constant weight. These weights are not given here, because the amount of undissolved fertilizer cannot be determined, i.e. it would require nutrient analysis to decide whether undiluted sample contains nutrients, or it is carrier roughage only.

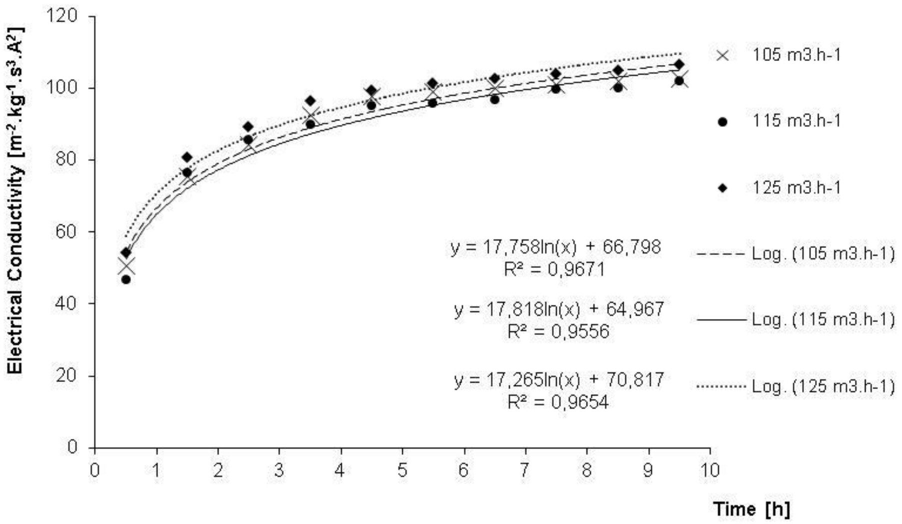

Fig. 3. – Graph of time dependence of electrical conductivity on the air stream of 105, 115 and 125 $m^3.h^{-1}$ respectively

CONCLUSIONS

On the basis of the electrical conductivity, the concentration of dissolved mineral fertilizer can be determined. Fig. 3 indicates that the values for the significant proportions are analogous. These values are crucial for the production of concentrated solutions of mineral fertilizers that LAD 27 fertilizer is well soluble, and thus five hours are a sufficient time period for dissolving it. Electrical conductivity values are noticeably high which means that the ions can be absorbed easily by plant roots. The LAD 27 is therefore suitable for application into soil.

Measurements are taken as the guidance for the methodology verification that will be used to measure other samples of similar fertilizers. These results will be used for the precise application of fertilizers and can be used as a reference for qualitative assessment fertilizer solutions. The research is about to continue with simultaneous measurement of concentrations in order to determine the relationship between concentration and electrical conductivity. Unfortunately, current measurement devices available to authors do not allow such approach.

ACKNOWLEDGEMENTS

This work was supported by Research Project of the Ministry of Education of the CR no. MSM 6046070905.

REFERENCES

1. ALARU, M., LAUR, Ü., JAAMA, E.: Influence of nitrogen and weather conditions on the grain quality of winter triticale. Agronomy Research, 1, 2003: 3–10.
2. CSIZMAZIA, Z.: Some physical properties of fertiliser particles. In: Aspects-of-Applied-Biology, Department of Agricultural Engineering, Faculty of Agricultural Sciences, Debrecen University, Hungary. 2000: 219-226.
3. HOFSTEE, J.W.: Handling and spreading of fertilizers: part 2, physical properties of fertilizer, measuring methods and data. Journal of Agricultural Engineering Research, 53, 1992: 141-162.
4. KABEŠ, K.: Instruments for conductivity measuring. Automatization, 42(11), 1999: 826–832. (in Czech).
5. KADLEC, K.: Sensors for electrolytic conductivity of liquids. Automatization, 42 (3), 1999: 823–825. (in Czech).
6. KAJANOVIČOVÁ, I., LOŽEK, O., SLAMKA, P., VÁRADY, T. 2011: Bilancia dusíka v integrovanom a ekologickom systéme hospodárenia na pôde. Agrochémia, 51, 2011:7–11 (in Slovak).
7. KRUPIČKA, J., HANOUSEK, B.: Granulometric study of Synferta N-22 and Synferta N-17. Res. Agr. Eng., 52, 2006: 152–155.
8. KRUPIČKA, J., ŠAŘEC, P.: Measurement of electrical conductivity of lovogreen fertilizer. In 5th International Conference Trends in Agricultural Engineering 2013, Prague: Czech University of Life Sciences Prague, 2013: 368-371.
9. KRUPIČKA, J., ŠAŘEC, P., NOVÁK, P.: Measurement of electrical conductivity of DAP fertilizer. Agronomy Research, 13(1), 2015: 109-114.
10. KUDOH, M.: Flowability of fertilizers and development of an accurate fertilizer DISTRIBUTOR. JOURNAL OF HOKKAIDO COLLEGE, 22, 1989: 1-87.
11. LOŽEK, O., BIZÍK, J., FECENKO, J., KOVÁČIK, P., VNUK, Ľ.: Výživa a hnojenie rastlín: Trvale udržateľné systémy v poľnohospodárstve. Nitra: SUA in Nitra, 1997: 104 pp. (in Slovak).
12. MACÁK, M., NOZDROVICKÝ, L., ŽITŇÁK, M.: Vplyv granulometrického zloženia priemyselných hnojív na kvalitu práce rozhadzovača. Agrochémia, 51, 2011: 11–15, (in Slovak).
13. NOZDROVICKÝ, L., MACÁK, M., FINDURA, P.: Effect of the fertilizer particle size distribution on the transversal uniformity distribution. In New Trends in Design and Utilisation of Machines in Agriculture, Landscape Maintenance and Environ-

ment Protection: Proceedings of the International Scientific Conference. CULS Prague, Prague, 2009: 210–218.
14. ŠIMA, T., NOZDROVICKÝ, L., KRIŠTOF, K., DUBEŇOVÁ, M., KRUPIČKA, J., KRÁLIK, S.: Method for measuring of N2O emissions from fertilized soil after the using of fertilizer. Poljoprivrednatehnika. 38, 2012: 51–60.
15. ŠIMA, T., KRUPIČKA, J., NOZDROVICKÝ, V.: Effect of nitrification inhibitors on fertiliser particle size distribution of the DASA 26/13 and ENSIN fertilisers. Agronomy Research, 11(1), 2013: 111-116.
16. ŠIMA, T., DUBEŇOVÁ, M.: Effect of crop residues on CO2 flux in the CTF system during soil tillage by a disc harrow Lemken Rubin 9. Res. Agr. Eng., 59, 2013: S15-S21

Corresponding author:
Ing. Josef Krupička, CSc.,Department of Agricultural Machines,Faculty of Engineering, Czech University of Life Sciences Prague, Kamýcká 129, Praha 6, Prague, 16521, Czech Republic, phone: +420 22438 3127,e-mail: krup@tf.czu.cz

ANALYSIS OF HOP MATTER SEPARATION WITH INCREASED ROLLER CONVEYOR THROUGHPUT

M. Krupička, A. Rybka, P. Heřmánek, I. Honzík

Department of Agricultural Machines, Faculty of Engineering, Czech University of Life Sciences Prague, Czech Republic

Abstract

This paper focuses on a roller conveyor, which forms a part of separating machine line and is located after the secondary picker. The roller conveyor serves here as a roller sieve.

Before the 2015 harvest season started, rollers with new structure had been designed and manufactured. These rollers were to enhance the share of admixtures that had been separated out. In the season of 2015, several laboratory measurements were carried out in order to verify the function of these rollers.

This paper presents results of the measurement verifying the function of rollers at enhanced throughput of the roller conveyor. The throughput was enhanced from the standard 450 $kg.h^{-1}$ to 900 $kg.h^{-1}$in order to simulate a situation when the material entering the roller conveyor is not evenly layered. The aim was to determine the dependency of hop matter falling through on the gap size between rollers and on the roller rotation frequency.

Key words: separation line, hop matter, roller conveyor, curve of falling through.

INTRODUCTION

Hops are nowadays used principally as one of the basic ingredients in hop brewing. Ninety-eight percent of the world hop production is grown for exactly this purpose (CARTER ET AL., 2000). Their use for other purposes is not mentioned in the world statistics. However, their importance in pharmaceutics is well-known, as besides the basic substances adding the basic sensory characteristics to produced beer (bitterness, aroma and full flavour), hops also contain a number of other substances of medical importance (JURKOVÁ ET AL., 2011; VRZALOVÁ&FRIC, 1994). For instance, flavonoids contained in hop cones appear promising as antioxidants and antivirals, particularly against the HIV virus (WANG ET AL., 2004).

This paper deals with separating the hop matter which is harvested from low trellises. In this growing system, hop bines climb (twine) spontaneously up a special plastic network that is a substantial part of the low trellis system. This way eliminates a complicated hiring of labour for the most difficult operations, such as hanging and sticking of hop strings and hop-bine training (ŠTRANC ET AL., 2012; ŠTRANC ET AL., 2010).

Majority of the traditional hop varieties cannot be grown on low trellises, for then they reach only 40 to 60% of the yield they would achieve on classic trellises (SEIGNER ET AL., 2008). The new “dwarf” varieties bred for low trellises should, according to breeders and economists, reach at least 80% of the yield reached by the varieties grown on classic trellises (DARBY, 1999).

In the Czech Republic, hop growing on low trellises is now in the experimental stage and the current acreage of low-trellis hop-fields counts for only less than 50 ha (EAGRI, 2014).

For this growing technology different machinery is needed. The hops from low trellis are harvested by means of a mobile harvester, pulled by tractor. The hop matter brought from the mobile harvester is then submitted to separation on a mechanical line which is adjusted in a way compared to the classic mechanical picking line. The process of separation shall ensure that hop cones are separated from stems and leaves (JECH ET AL., 2011).

This paper is focused on the part of separating machine which is located after the secondary picker, namely the roller conveyor with infinitely adjustable pitch of each roller. Its importance lies in separating hop cones from stems and leaves. The main function of the roller conveyor is to separate the hop matter into small-sized fraction formed by hop cones, leaves and fragments of size smaller than the size of the gap between individual rollers, and into large-sized fraction such as stems, clumps, big leaves which cannot fall through the rollers (NEUBAUER ET AL., 1989).

The right operation of the roller conveyor depends on several parameters. They are the rotation frequency of the rollers, roller profile, and the gap between individual rollers. To be able to determine the precise significance of these parameters, a model of such a roller conveyor was made in 2014, which is a scale copy of the real roller conveyor used in the separation line employed for separation of hops grown on low trellis (KRUPIČKA & RYBKA, 2014).

Previous measurements from the 2015 harvest season showed the advantages of rollers with tooth profile which had been designed and manufactured in the same year. The measurements confirmed our assumption that more leaves and small-sized admixtures are separated out into the waste with a shrinking gap.

A frequent problem that has not been sufficiently solved yet with the separation line prototype is uneven feeding of hop matter from the line feeder. For that reason larger clusters of hop matter sometimes get onto the roller conveyor.

The aim of this measurement was to determine the quantity of admixtures and cones separated out using these new rollers with tooth profile at double material throughput on the roller conveyor. Double throughput means double amount of material, thus simulating the already mentioned hop matter clusters.

MATERIALS AND METHODS

Roller conveyor model

The model (Fig. 1) has 9 rollers in total and they are 600 mm long. The first roller is rigidly attached to the frame, the remaining 8 rollers have adjustable pitch allowing to change the between them. The space underneath the rollers had been divided by means of KAPA boards to be able to determine the amount of hop matter fallen through the gaps. The hop supply was provided by a belt conveyor 600 mm wide and 1000 mm long.

Fig. 1. – Model of roller conveyor

For the purpose of the measurement new rollers were used, with a diameter of 89 mm and tooth profile of their metal welded collars (Fig. 2). On a tube there are 14 welded collars 39 mm apart. A welded collar has 30 teeth and an outer diameter of 125 mm. Owing to an enlarged tube diameter and a welded collar height of 17.5 mm the gap between rollers can be set to 20 mm. This profile of metal welded collars is more efficient in catching leaves and small twigs and moving them further upon the rollers.

Fig. 2. – Laboratory roller conveyor with rollers fitted with tooth profile welded collars

Methodology of the measurement

The 2015 harvest season measurements used again the hop variety Sládek, harvested from low trellises. To prevent the hops from changing their characteristics during their separation, fresh hop matter was brought from the hop grower every single measurement day. The hop matter sample was selected so that the percentage representation of individual components (hop cones, leaves) remained unchanged.

The sample corresponding to the standard throughput of the model roller conveyor, which is 450 kg.h^{-1}, weighs 450 g. For the purpose of this measurement the sample weight was doubled to a value of 900 g (Fig. 3). This way simulated the doubled amount of material conveyed by the roller conveyor. The other parameters remained unchanged – the peripheral speed of the conveyor belt 0.27 m.s^{-1} and the basic rotation frequency of the rollers 0.67 s^{-1}. These values correspond to the real ones and had been set by means of frequency converters.

Fig. 3. – A hop matter sample evenly spread over the conveyor belt

The sample contained 336 g of cones and 564 g of leaves. The average hop cone size was determined out of a sample comprising of 100 pieces. The average value of the hop cone length was 28.3 mm and the average value of the cone diameter was 16.6 mm.

The measurement was conducted in such a way that the hop matter sample was mixed and evenly spread over the conveyor belt. Then the roller drive was switched on, followed by the belt conveyor drive. The hop matter was being continuously separated on the roller conveyor and thanks to KAPA boards, installed underneath each roller, was falling through into 7 containers. The individual components of the hop matter that fell in between rollers were weighed accurate to 1 g.

The dependency of hop matter falling through on the gap size between rollers at doubled throughput was determined for these three gaps – 20, 24 and 28 mm. Also the dependency of hop matter falling through on the roller rotation frequency was examined with all the gap sizes between rollers.

RESULTS AND DISCUSSION

Comparison of three different gaps between rollers and the basic rotation frequency

Based on the measured data a curve of hop matter falling through was established for three gap sizes between rollers (20, 24 and 28 mm) and is depicted in the graph of Fig. 4. The graph clearly shows that at the smallest gap setting of 20 mm the hop matter falls through more evenly. This is noticeable particularly with the first two gaps between rollers. It is favourable in terms of separation, since the amount of neither the hop matter nor admixtures fallen through the first gap was so great.

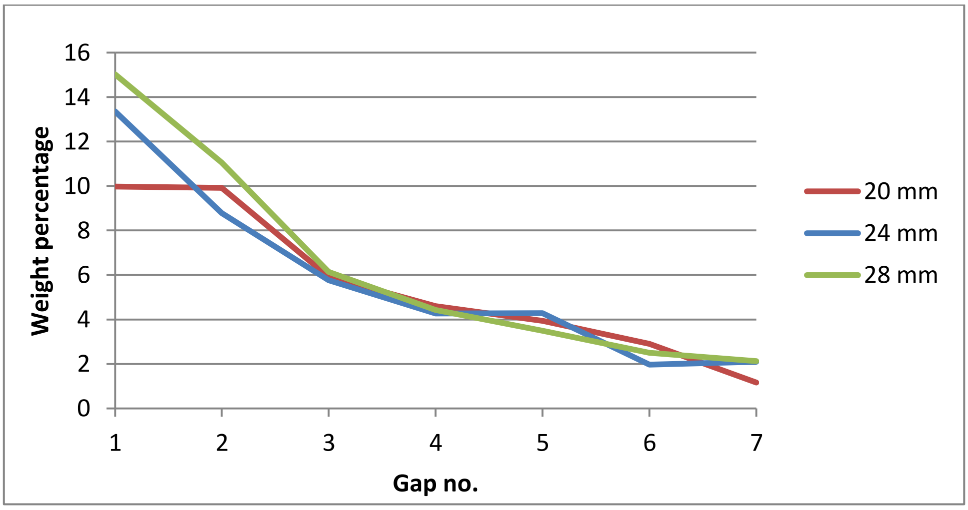

Fig. 4. – Weight percentage of the hop matter fallen through the separate gaps with rollers of 89 mm in diameter and rotation frequency of 0.67 s^{-1}

As regards the leaves and cones in the waste, the best results in terms of separation were measured with the gap setting of 20 and 24 mm (Fig. 5). The values measured for these two gaps were almost identical. Approximately 91% of all leaves were conveyed into the waste. With the gap set to 28 mm they were 86%. The following graph in Fig. 6 illustrates a comparison with the standard throughput of 450 $kg.h^{-1}$ measured in the previous measurements. It can be seen that at doubled throughput by approx. 20% more admixtures are conveyed into the waste. With the gap of 20 mm it is by about 10% more admixtures. These results are logical because the hop matter sample is not quite ideally separated between nine rollers.

The measured values correspond to theoretical assumptions of the relationship for the calculating the quantity of small-sized fraction coming to *Qs*, which fall through on the length of the roller track *l* per unit of time (NEUBAUER AT AL., 1989).

$$Q_p = \left(\frac{1}{Q_2} + \frac{G_o}{{Q_2}^2} * \frac{1}{\beta * l}\right)^{-1} \quad (1)$$

Where:

Q_2 - the quantity of small-sized fraction coming to the track per unit time [kg.h^{-1}]

G_o - the quantity of large-sized fraction coming to the track per unit time [kg.h^{-1}]

β - coefficient of intensity of sieving which depends on the height of the layer of the incoming material and it is in the range $0 < \beta \leq 1$

The relationship shows that an increase in weight of small-sized and large-sized fraction, but maintaining the same length of tracks, fall through less the quantity of small-sized fraction *Qp*. For this reason is in the waste found relatively large percentage of hop cones (NEUBAUER AT AL., 1989).

Theory of grain separation is the similar when it is separated straw from grain. With the increased flow of material through the walker is not sufficiently material separated and arises losses, when the grain goes to waste (SRIVASTAVA ET AL., 2006).

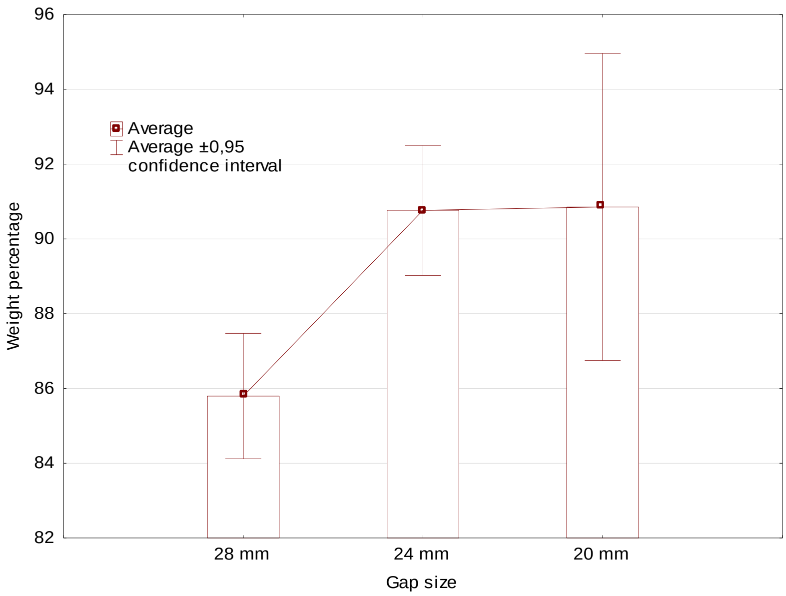

Fig. 5. – Weight percentage of leaves and small-sized admixtures in the waste with rollers of 89 mm in diameter and rotation frequency of 0.67 s^{-1}

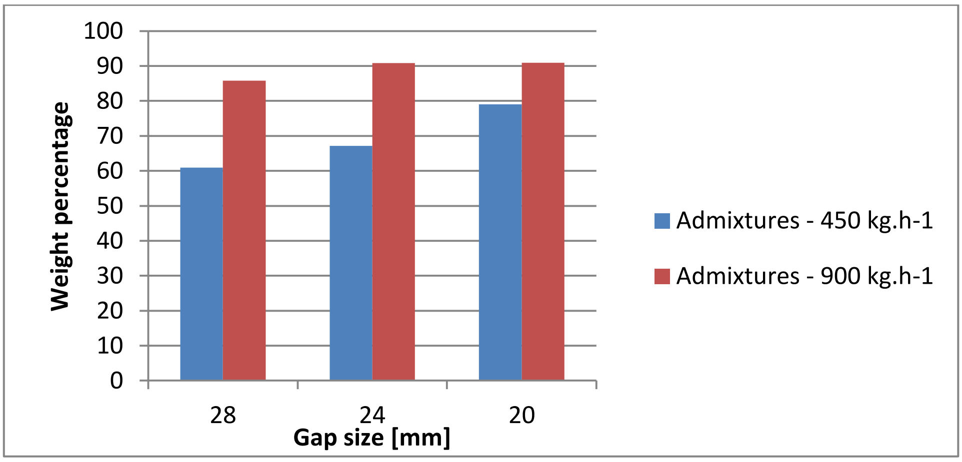

Fig. 6. – Weight percentage of leaves and small-sized admixtures in the waste with rollers of 89 mm in diameter, rotation frequency of 0.67 s^{-1} and two versions of throughput

Insufficient separation was reflected in the quantity of cones that were found in the waste. The graph of the following figure (Fig. 7) illustrates how many hop cones were conveyed into the waste. It shows that with decreasing gap between rollers more cones get into the waste. With the gap setting of 28 mm it is 3.7%, and with the smallest gap sized 20 mm it is even 12.8%. In terms of losses these values are absolutely unacceptable.

The following graph in Fig. 8 again compares the standard throughput of 450 kg.h^{-1}. Here it can be seen that at the standard throughput of 450 kg.h^{-1}cone losses are minimal. With the gap of 28 mm they are zero. With the gap set to 24 mm only 0.2% of cones were found in the waste. With the smallest gap of 20 mm the results were a little worse, on average 1.6% of cones get into the waste.

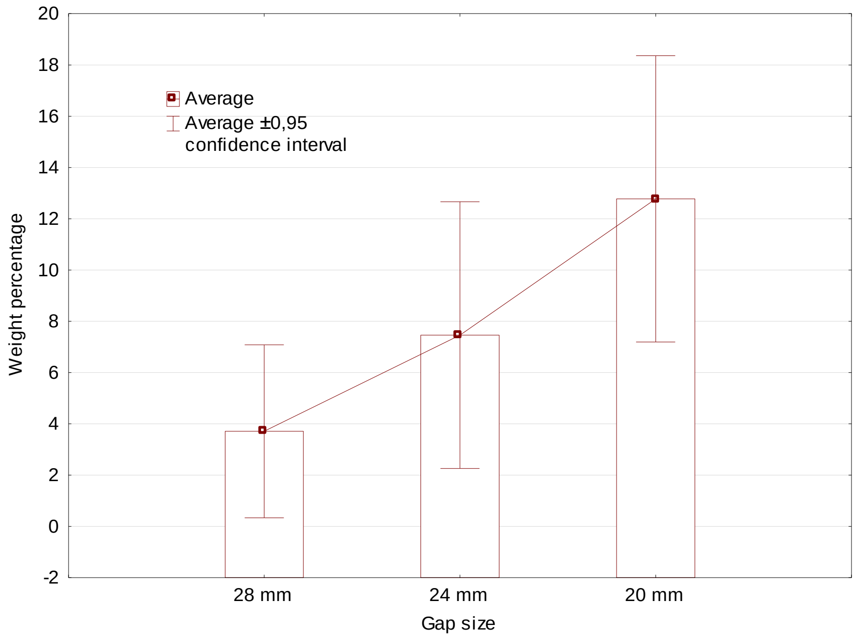

Fig. 7. – Weight percentage of hop cones in the waste with rollers of 89 mm in diameter and rotation frequency of 0.67 s^{-1}

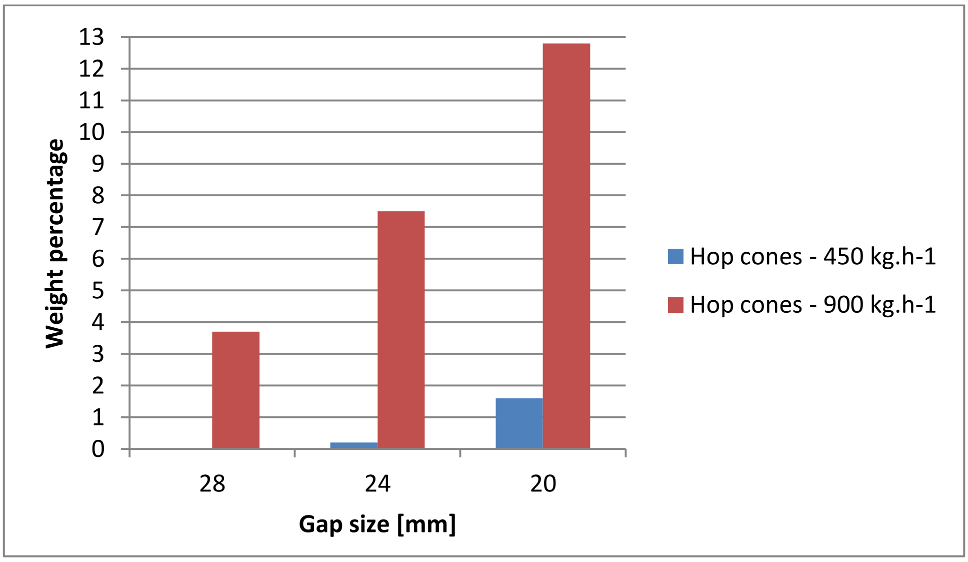

Fig. 8. – Weight percentage of hop cones in the waste with rollers of 89 mm in diameter, rotation frequency of 0.67 s^{-1} and two versions of throughput

Dependency of hop matter falling through on the gap size and rotation frequency of rollers

The processed measured data revealed that the rotation frequency of rollers have no significant effect on separation of leaves or cones. Our assumption that an increased rotation frequency of rollers would cause a higher percentage of leaves and small-sized admixtures to leave for the waste, was not confirmed. The following graph in Fig. 9 illustrates the weight percentage of leaves and small-sized admixtures in the waste for the gap of 24 mm and three rotation frequencies of rollers. With an increased rotation frequency of rollers a slight decline in the amount of leaves separated out in the waste can be observed, although from a statistical point of view no dependency can be derived from the measured data.

The graph in Fig. 10 presents the weight percentage of hop cones in the waste for the gap of 24 mm and three rotation frequencies of rollers. Here the difference is really minimal and again no dependency can be derived.

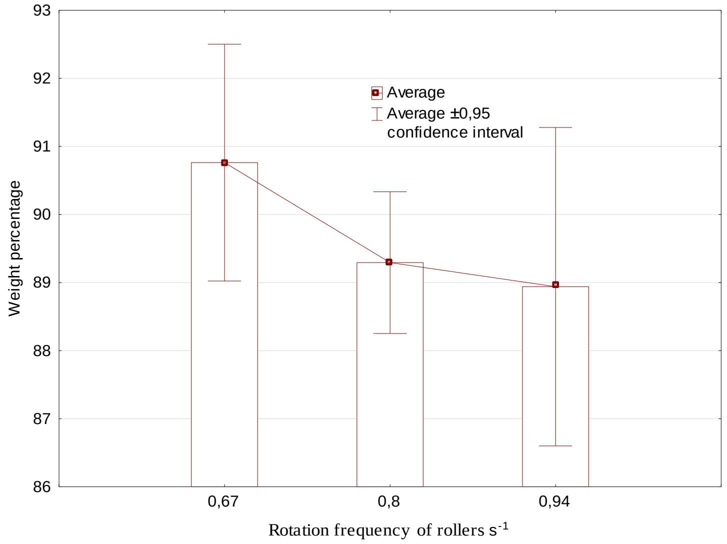

Fig. 9. – Weight percentage of leaves and small-sized admixtures in the waste with rollers of 89 mm in diameter, gap of 24 mm and three rotation frequencies

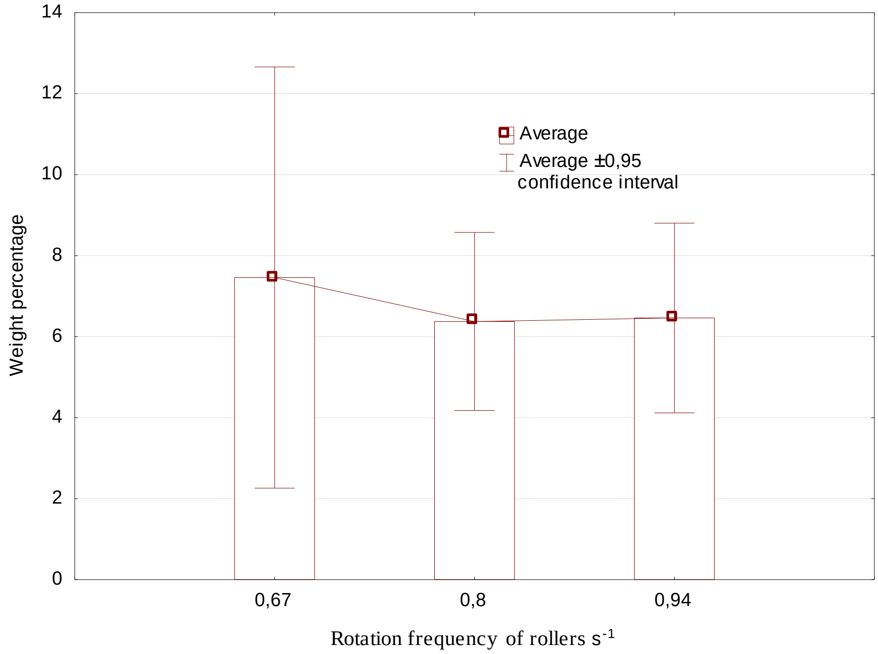

Fig. 10. – Weight percentage of hop cones in the waste with rollers of 89 mm in diameter, gap of 24 mm and three rotation frequencies

CONCLUSIONS

These measurements, the same way as the previous ones in 2015, were carried out with a hop matter sample that contained only hop cones and leaves. The amount of these two components had been precisely defined. The measurements simulated an increased material throughput on the roller conveyor. They confirmed the assumption that decreasing gap between rollers results in a larger amount of admixtures that are conveyed to the waste. Compared to the common throughput, by approx. 10 to 20% of leaves more were separated out into the waste. Hop cone losses of 3.7 to 12.8% according to the gap setting are unacceptable. It can be seen that hop matter is not sufficiently separated on a conveyor consisting of nine rollers with the gap size of 20 to 28 mm between them. To achieve a real inclusion of these rollers into the separating line, the number of rollers would need to be increased.

No statistically significant differences were found when comparing different rotation frequencies of the rollers.

ACKNOWLEDGEMENTS

Processed with the support of TA CR within the TA03021046 project solution.

REFERENCES

1. CARTER, P., OELKE, E., KAMINSKI, A., HANSON, C., COMBS, S., DOLL, J., WORF, G., OPLINGER. E.: 2007: Alternative field crops manual—hop. [online] Last revision 1.8.2011). [cit. 12.3.2016]. Available from <http://corn.agronomy.wisc.edu/Crops/Hop.aspx>.
2. DARBY, P.: Economic yield potential of dwarf hop varieties. In: New Procedures in Hop Growing, Proceedings of International Symposium, Hull, Bavaria, Federal Ministry of Food, Agriculture and Forestry, Germany, 1999.
3. EAGRI: Situační a výhledová zpráva Chmel[online]. Last revision December 2015 [cit. 12.3.2016]. Available from: <http://eagri.cz/public/web/file/433497/SVZ_Chmel_2014.PDF >.
4. JECH, J., ARTIM, J., ANGELOVIČOVÁ, M., ANGELOVIČ, M., BERNÁŠEK, K., HONZÍK, I., KVÍZ, Z., MAREČEK, J., KRČÁLOVÁ, E., POLÁK, P., PONIČAN, J., RYBKA, A., RUŽBARSKÝ, J., SLOBODA, A., SOSNOWSKI, S., SYPULA, M., ŽITŇÁK, M.: Stroje pre rastlinnú výrobu 3: stroje a zariadenia na pozberovú úpravu rastlinných materiálov.Praha, Profi Press s.r.o., 2011: 368 s. ISBN 978-80-86726-41-0.
5. KRUPIČKA, M., RYBKA, A.:Parametry ovlivňující oddělení drobné frakce na válečkové trati separační linky chmele, XVI. Mezinárodní konference mladých 2014, 9.- 10.9 2014, Česká zemědělská univerzita v Praze, Technická fakulta, 2014: p. 91 - 96. ISBN 978-80-213-2476-3
6. KRUPIČKA, M., RYBKA, A.: Dependency of hop material fall through on the size of gaps between rollers of the roller conveyor in separating machine. Agronomy Research, 2015, yr 13, č. 1, 2015: p. 101-108. ISSN: 1406-894X
7. NEUBAUER, K., FRIEDMAN, M., JECH, J., PÁLTIK, J., PTÁČEK, F.:Stroje pro rostlinnou výrobu. SZN Praha, 1989: 716 s. ISBN 80-209-0075-6.
8. SEIGNER, E., LUTZ, A., OBERHOLLENZER, K., SEIDENBERGER, R., SEEFELDER, S., FELSENSTEIN, F.: Breeding of hop varieties for the future. Second International Humulus Symposium, Ghent, Belgium. ISHS Acta Horticulturae 848, 2008: p. 49–58.
9. SRIVASTAVA, A. K., GOERING, C. E., ROHRBACH, R. P., BUCKMASTER, D. R.:Engineering Principles of Agricultural Machines 2nd Edition. American Society of Agricultural Engineers, Michigan, USA, 2006: p. 604. ISBN 978-1892769503.
10. ŠTRANC, P., ŠTRANC, J., ŠTRANC, D., HOLOPÍREK, F., PODSEDNÍK, J., ZÍDEK, J., ALT, A., VENT, L.: Přínos technologie nízkých konstrukcí[online]. Last revision 19.3.2010 [cit. 10.3.2015]. Available from: < http://zemedelec.cz/prinos-technologie-nizkych-konstrukci/ >.
11. ŠTRANC, P., ŠTRANC, J., HOLÝ, K., ŠTRANC, D., SKLENIČKA, P.: Pěstování vzrůstných odrůd chmele v nízké konstrukci. Praha:FAPPZ, ČZU v Praze a Zemědělská společnost při ČZU v Praze, 2012. ISBN 978-80-87111-33-8.
12. VRZALOVÁ, J., FRIC, V.: Rostlinná výroba – IV.Praha:ČZU v Praze, FAPPZ, 1994: 80 s. ISBN 80-213-0155-4.
13. WANG, Q., DING, Z.,H., LIU, J.,K., ZHENG., Y.,T.: Xanthohumol, a novel anti-HIV-1 agent purified from hops Humulus lupulus. Antiviral Res. 64., 2004: p. 189–194.
14. JURKOVÁ, M., KELLNER, V., HAŠKOVÁ, D., ČULÍK, J., ČEJKA, P., HORÁK, T., DVOŘÁK, J.: Hops–an Abundant Source of Antioxidants. Methods to Assessment of Antioxidant Activity of Hop Matrix. Journal for brewing, malting & beverage industry, 2011: p. 366.

Corresponding author:

Ing. Martin Krupička, Department ofAgricultural Machines, Faculty of Engineering, Czech University of Life Sciences Prague, Kamýcká 129, Praha 6, Prague, 16521, Czech Republic, e-mail: krupicka@tf.czu.cz

MECHANICAL PROPERTIES OF BIOMASS PELLETS

Ľ. Kubík[1], F. Adamovský[2]

[1]Department of Physics, Faculty of Engineering, Slovak University of Agriculture in Nitra, Slovak Republic
[2]Department of Electrical Engineering, Automation and Informatics, Faculty of Engineering, Slovak University of Agriculture in Nitra, Slovak Republic

Abstract
The paper dealt with the determination of mechanical properties of the cylinder pellet samples. Wheat straw, rapeseed straw and 50/50% mixed wheat and rapeseed straw were used for study of compress loading. The pellets were made by the granulating machine MGL 200 (Kovonovak). The compressive loading curves of dependencies of stress on strain were realised by the equipment Andilog Stentor 1000 (Andilog Technologies, Vitrolles, France). Initial force, initial stress, strain in maximum of loading curve, stress in maximum of loading curve and modulus of elasticity were determined. Significant correlations of the mechanical parameters pellet samples were observed among initial force and initial stress and modulus of elasticity. Significant correlations of force in maximum with stress and strain in the maximum were observed.

Key words: biomass pellets, compression, mechanical parameters.

INTRODUCTION

Straw has a different chemical composition depending on the species of plant, location and growing technology, so straw should be properly processed in order to improve its energy efficiency. Hence, efforts are being made to compact these plant resources by briquetting or pelleting, which leads to a higher concentration of mass and energy per unit of volume and the distribution and utilization of this type of biofuel is significantly facilitated (NIEDZIOŁKA ET AL., 2015). Mechanical properties of wheat straw, barley straw, corn stover and switchgrass at different compressive forces, particle sizes, and moisture contents are very interesting to determination of mechanical quality of pellets. Barley straw had the highest asymptotic modulus among all biomasses (SUDHAGARET ET AL., 2006). BOŽIKOVÁ ET AL. (2015) studied physical parameters as density, heat of combustion, calorific value and basic thermophysical parameters (thermal conductivity, thermal diffusivity and volume specific heat) of rape straw pellets, straw pellets, softwood pellets and hardwood pellets. The highest volume specific heat 0.6562×107 $J.m^{-3}.K^{-1}$ had straw pellets and then rape straw pellets 0.5122×107 $J.m^{-3}.K^{-1}$. The second series of measurement was focused on combustion heat and calorific value determination. Obtained values of combustion heat were from range 14.3 – 20.2 $MJ.kg^{-1}$ and calorific values were from range 12.2 – 19.0 $MJ.kg^{-1}$. MIŠLJENOVIĆ ET AL. (2016) interested in the determination of the strength of pellets through a three-point bending test. The three-point bending test was selected in lieu of the typically used diametric compression test because of the inability to precisely determine the length of pellets. The three-point bending test was used to asses pellet strength. A pellet was placed on a specially designed holder attached to the Lloyd LR 5K texture analyzer. The pellet was loaded at a speed of 1 $mm.min^{-1}$ until breakage, and the force was recorded. SHAW ET AL. (2009) reported higher mechanical resistance when using smaller particle sizes to produce wheat straw and poplar wood pellets. By contrast, SERRANO ET AL. (2011) found no significant differences in the mechanical durability of barley straw pellets when milling the raw materials at 4 and 7 mm. BERTHET ET AL. (2015) evaluated nominal stress at break, nominal strain at break and Young's modulus from stress strain curves of the wheat straw fibres. The energy for the rupture was calculated from the total area under the curve of the force as a function of the elongation. Initial grip distance and cross-head speed were 45 mm and 10 $mm.min^{-1}$. MANI ET AL. (2006) studied mechanical properties of wheat straw, barley straw, corn stover and switchgrass at different compressive forces, particle sizes and moisture contents. Ground biomass samples were compressed with five levels of compressive forces (1000, 2000, 3000, 4000 and 4400 N) and three levels of particle sizes (3.2, 1.6 and 0.8 mm) at two levels of moisture contents (12% and 15% (wet basis)) to establish compression and relaxation data. Compressive force, particle size and moisture content significantly affected the pellet density of barley straw, corn stover and switchgrass. However, different particle sizes of wheat straw did not produce any significant difference on pellet density. NEDOMOVÁ ET AL. (2013) investigated the effect of the compression orientation on the mechanical properties of Ostrich eggs. The mechanical properties examined were rupture force, specific deformation, rupture energy and firmness. STRNKOVÁ ET AL. (2016) have been studied the mechanical behaviour of eggshell membranes under tensile loading. Samples were cut out of the membrane in latitudinal direction. TIRA test 27025 tensile testing machine equipped with a 200 N load-cell was used. Tensile deformation exhibits both non-linear as well as linear region. The experiments were performed at five loading velocities 1, 10, 100, 400 and 800 mm.min^{-1}. The main parameters describing the eggshell strength increase with the loading rate. VALACH ET AL. (2015) interested in the pressure and measurements of the biomass. The viscosity of the material increases at the pressure 7 MPa by 20 – 25% and at pressure 40 MPa increases by 120 – 160%. In gears and bearing with high pressures, it is necessary to consider the increase of viscosity. HLAVÁČOVÁ (2005) studied electrical properties of the granular materials. She found out that the conductivity increases and the resistivity decreases with temperature exponentially for all samples at all moisture contents. The permittivity of all samples increases with temperature linearly in frequency range from 2 to 50 MHz. The electrical properties dependence on temperature of treated material is necessary in the case of its thermal treatment.

The objective of this study was the investigation of the effects of the compression load on the pellets and determination of the mechanical parameters at the loading.

MATERIALS AND METHODS

The pellets were made from wheat straw (*Triticumaestivum*), rapeseed straw (*Brassicanapus*) and mixed straw, 50% wheat straw and 50% rapeseed straw, by the granulating machine MGL 200 (Kovonovak). Granulator is equipment in which the transformation of the crushed biomass on the pellets is realized. Basic components of the granulator are scrolls (driving drums) extruding biomass trough matrix and the matrix (metal plate with the holes of the specific size the biomass is extruded through. In the production of the wheat, rapeseed straw and 50/50% mixed straw pellets no binding agent was used except for water. The moisture of the wheat pellets was 13.6%, the moisture of the rapeseed straw pellets was 16% and the moisture of 50/50% mixed straw pellets was 13.5%. The bulk density of the wheat pellets was 335.880 kg.m^{-3}, the bulk density of rapeseed pellets was 531.556 kg.m^{-3} and 50/50% mixed straw was 431.990 kg.m^{-3}. Heat of combustion value of the wheat straw pellets was 17.013 MJ.kg^{-1}, heat of combustion of the rapeseed straw pellets was 16.241 MJ.kg^{-1} and heat of combustion of the 50/50% mixed straw pellets was 16.511 MJ.kg^{-1} (ADAMOVSKÝ AND OPÁTH, 2013).

The pellets were submitted to the compressive loading. The strength of the pellets was evaluated via the quasi static compression test, which was used to study the compaction behavior of tomatoes by BLAHOVEC ET AL. (1988). The result of the single test were the loading curves, which represent dependence between compressive stresses σ (MPa) and compressive strains ε (mm.mm^{-1}) of the pellets. The initial firmness of the pellets was determined as the initial force F_{10} (N) at the 10 % of the compressive strain on the loading curve and as the initial stress σ_{10} (MPa) at the 10% of the compressive strain. The next parameters of the firmness were force F_p (N), the stress σ_p (MPa) and compressive strain ε_p (mm.mm^{-1}) in the maximum of the loading curve. The last important parameter was Young's modulus of elasticity E (MPa). Young's modulus of elasticity E (MPa) was evaluated as the slope of the linear part of dependences of stress σ (MPa) on the strain ε (mm.mm^{-1}). The regression equations were determined as:

$$\sigma = E\,\varepsilon + b \tag{1}$$

where:

σ – compressive stress (MPa)

ε – compressive strain (mm.mm^{-1})

E – regression coefficient –Young's modulus of elasticity (MPa)

b – regression coefficient (MPa)

The cylindrical pellets were compressed between a lower steel plate and an upper steel circular plate in the longitudinal direction. The upper plate, attached to the Andilog Stentor 1000 test stand (Andilog Technologies, Vitrolles, France), compressed the cylinder of sample at a speed of 10 mm.min^{-1} until failure was observed.

RESULTS AND DISCUSSION

Eight regular samples were selected for wheat straw pellets, nine regular samples for rapeseed pellets and eight samples for mixed straw pellets. The loading curves were created in the software Microsoft Excel 2010. Results of mechanical parameters are presented in the Tab. 1, 2, and 3. Selected compression curves of the cylinder pellet samples (sample WS4, RS1, and WS50RS50_10 according to Tab. 1, 2, and 3) as dependence of stress σ (MPa) on strain ε ($mm.mm^{-1}$) are presented in Fig. 1. Loading curves showed similar shape with the characteristic maximum.The loading curves of different pellets had similar development and the line shapes. Determination of the Young's modulus of elasticity is presented in the Fig. 2 for the selected materials. Dependencies were fitted by the linear regression equations (1). The slopes of the equations represent the moduli of elasticity. Mean value of the initial force (force at 10% of compress strain) was maximal for mixed straw pellet samples (52.49 N, according to Tab. 3). Mean values of the initial force of the wheat straw samples and the rapeseed straw samples were smaller and almost identical (43.58 N and 43.12 N, according to Tab. 1 and 2). The variation of the mean value of the initial force was from 12 to 16 %.

Fig. 1. – Compression curves of the selected cylinder pellet samples as a dependence of stress (MPa) on strain ($mm.mm^{-1}$). 50% WS and 50% RS means 50% wheat straw and 50% rapeseed straw, 100% WS means 100% wheat straw and 100% RS means 100% rapeseed straw, (sample WS4, RS1, and WS50RS50_10 according to Tab. 1, 2, and 3).

Mean values of the initial stress of loading curve, of the wheat straw samples reached 1.46 MPa, according to Tab. 1, the rapeseed straw samples reached value 1.40 MPa, according to Tab. 2 and the mixed straw samples reached value 1.63 MPa according to Tab. 3. The variation of the mean value of the force in maximum of loading curve was from 13 to 17 %.

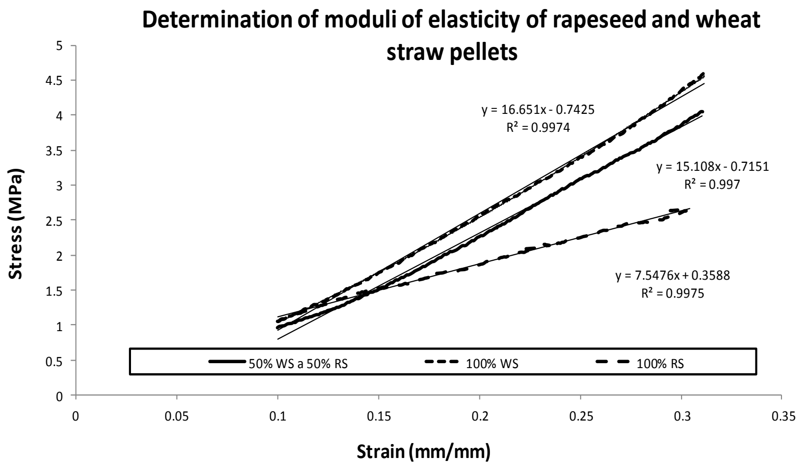

Fig. 2. – Determination of moduli of elasticity of wheat, rapeseed and mixed straw pellets. 50% WS and 50% RS means 50% wheat straw and 50% rapeseed straw, 100% WS means 100% wheat straw and 100% RS means 100% rapeseed straw, (sample WS9, RS7, and WS50RS50_10 according to Tab. 1, 2, and 3). The slopes of equation represent the moduli of elasticity.

Tab. 1. – Tab. of wheat straw pellet samples initial length (l), diameter of sample (d), initial force (F_{10}), force in maximum (F_m), strain in maximum (ε_m), initial stress (σ_{10}), stress in maximum (σ_m) and modulus of elasticity (E)

Wheatstraw 100 %			Moisture	13.6%				
			Compression	August,11th 2011				
			Measurement	March,16th 2015				
Sample	**l (mm)**	**d (mm)**	**F_{10} (N)**	**F_m(N)**	**ε_m (%)**	**σ_{10} (MPa)**	**σ_m (MPa)**	**E (MPa)**
WS3	12.20	6.10	49.74	110.14	32.62	1.70	3.77	18.70
WS4	12.35	6.10	30.61	238.77	45.58	1.05	8.17	20.57
WS5	11.80	6.10	82.49	186.29	24.48	2.82	6.38	24.97
WS7	10.80	6.30	18.36	167.44	53.51	0.59	5.35	12.64
WS8	12.05	6.20	32.70	231.21	55.26	1.08	7.66	14.62
WS9	12.05	6.20	28.88	186.20	34.18	0.96	6.17	16.65
WS10	11.95	6.20	62.27	156.92	25.85	2.06	5.20	20.09
WS13	10.20	6.30	43.64	147.90	30.97	1.40	4.75	17.13
Mean	11.68	6.19	43.58	178.11	37.81	1.46	5.93	18.27
Standard deviation	0.27	0.03	7.37	15.08	4.27	0.25	0.52	1.34
Coefficientofvariation	2.30	0.48	16.90	8.46	11.28	17.41	8.79	7.34

Mean value of the force in maximum of loading curve was also maximal for mixed straw pellet samples (213.26 N, according to Tab. 3). Mean values of the force in maximum of loading curve of the wheat straw samples reached 178.11 N, according to Tab. 1. The rapeseed straw samples reached value 95.95 N according to Tab. 2 and the mixed straw samples reached value 213.26 N according to Tab. 3. The variation of the mean value of the force in maximum of loading curve was from 8 to 19 %. Mean values of the strain in maximum of loading curve, of the wheat straw samples reached 37.81 %, according to Tab. 1, the rapeseed straw samples reached value 26.81%, according to Tab. 2 and the mixed straw samples reached value 47.01% according to Tab. 3. The variation of the mean value of the force in maximum of loading curve was from 4 to 11%.

Tab. 2. – Tab. of rapeseed straw pellet samples initial length (l), diameter of sample (d), initial force (F_{10}), force in maximum (F_m), strain in maximum (ε_m), initial stress (σ_{10}), stress in maximum (σ_m) and modulus of elasticity (E)

Rapeseedstraw 100 %			Moisture	16%				
			Compression	August,11th 2011				
			Measurement	March,16th 2015				
Sample	**l (mm)**	**d (mm)**	**F_{10} (N)**	**F_m(N)**	**ε_m (%)**	**σ_{10} (MPa)**	**σ_m (MPa)**	**E (MPa)**
RS1	11.20	6.30	32.70	180.10	58.12	1.05	5.78	8.51
RS2	13.70	6.10	57.12	108.36	13.80	1.96	3.71	19.98
RS4	12.40	6.60	48.56	91.28	20.08	1.42	2.67	13.40
RS5	13.60	6.50	36.85	60.72	20.58	1.11	1.83	8.82
RS7	11.50	6.45	22.82	54.07	24.60	0.70	1.66	7.54
RS10	13.95	6.10	16.99	49.10	21.29	0.58	1.70	10.32
RS11	10.40	6.10	58.76	90.69	22.68	2.01	3.10	15.42
RS12	12.60	6.20	57.07	115.28	32.84	1.89	3.82	14.47
RS13	14.30	6.20	57.21	113.97	27.26	1.90	3.75	19.59
Mean	12.63	6.28	43.12	95.95	26.81	1.40	3.11	13.08
Standard deviation	0.46	0.06	5.41	13.53	4.29	0.19	0.45	1.58
Coefficientofvariation	3.61	1.01	12.54	14.10	15.99	13.39	14.33	12.05

Mean values of the stress in maximum of loading curve, of the wheat straw samples reached 5.93 MPa according to Tab. 1, the rapeseed straw samples reached value 3.11 MPa according to Tab. 2 and the mixed straw samples reached value 7.10 MPa according to Tab. 3. The variation of the mean value of the force in maximum of loading curve was from 9 to 16%.

Mean values of the modulus of elasticity, of the wheat straw samples reached 18.27 MPa according to Tab. 1, the rapeseed straw samples reached value 13.08 MPa according to Tab. 2 and the mixed straw samples reached value 14.97 MPa according to Tab. 3. The variation of the mean value of the force in maximum of loading curve was from 7 to 9%.The maximal firmness at compression in the initial state and in the maximal compress loading showed the mixed straw pellet samples. The quantities determined in the compression test of the pellets were correlated. These are confirmed mathematically by the matrix of the correlation coefficients in Tab. 4. The initial force of the wheat straw pellet samples significantly influenced on the initial stress and modulus of elasticity of the wheat straw pellet samples and significantly negative proportionally influenced on the strain in maximum.

Tab. 3. – Tab. of mixed straw pellet samples initial length (l), diameter of sample (d), initial force (F_{10}), force in maximum (F_m), strain in maximum (ε_m), initial stress (σ_{10}), stress in maximum (σ_m) and modulus of elasticity (E)

Wheatstraw 50 %	Moisture	13.5%
Rapeseedstraw 50 %	Compression	August,11th 2011
	Measurement	March,16th 2015

Sample	l (mm)	d (mm)	F_{10} (N)	F_m(N)	ε_m (%)	σ_{10} (MPa)	σ_m (MPa)	E (MPa)
WS50RS50_01	11.20	6.30	29.88	283.18	59.28	0.96	8.79	17.88
WS50RS50_02	13.70	6.10	49.97	117.52	49.70	1.71	8.15	12.06
WS50RS50_04	12.40	6.60	80.03	179.00	37.00	2.34	5.12	11.85
WS50RS50_05	13.60	6.50	58.03	238.04	52.49	1.75	7.21	19.81
WS50RS50_07	11.50	6.45	56.66	98.02	24.95	1.74	3.00	12.43
WS50RS50_09	11.50	6.45	91.37	421.33	46.43	2.80	12.90	19.93
WS50RS50_10	11.50	6.45	26.69	246.01	56.43	0.82	7.53	15.10
WS50RS50_11	10.40	6.20	27.28	123.03	49.80	0.90	4.08	10.85
Mean	11.98	6.38	52.49	213.26	47.01	1.63	7.10	14.97
Standard deviation	0.41	0.06	8.59	38.18	3.94	0.25	1.10	1.32
Coefficientofvariation	3.45	0.92	16.37	17.90	8.39	15.45	15.49	8.84

Force in maximum of the wheat straw pellet samples significantly influenced on the strain in maximum and stress in maximum of wheat straw samples and correlates proportionally with the initial stress of mixed straw samples and non-proportionally with strain in maximum, force in maximum and stress in maximum of rapeseed straw samples and strain in maximum of mixed straw pellets. Strain in maximum of wheat straw pellet samples correlated non-proportionally with initial stress and modulus of elasticity of wheat straw pellet samples. Initial stress of wheat straw pellets samples correlated with modulus of elasticity of wheat straw pellet samples. Stress in maximum of wheat pellet samples correlated proportionally with initial stress of mixes straw samples and correlated non-proportionally with force in maximum, strain in maximum and stress in maximum of rapeseed straw pellet samples and with the strain in maximum of mixed straw pellet samples. Modulus of elasticity of wheat pellet samples correlated proportionally with the modulus of elasticity of the rapeseed pellet samples. Initial force of rapeseed pellet samples correlated significantly proportionally with the initial stress and modulus elasticity of the rapeseed samples and correlated non-proportionally with the initial force, force in maximum, initial stress and modulus of elasticity of mixed pellet samples. Force in maximum of rapeseed pellet samples correlated proportionally significantly with strain in maximum and stress in maximum of rapeseed samples and correlated with strain in maximum of mixed straw samples. Force in maximum of rapeseed pellet samples correlates non-proportionally with initial force and initial stress of the mixed straw samples. Strain in maximum of rapeseed pellet samples correlated proportionally with stress in maximum of the rapeseed pellet samples and correlated non-proportionally with the initial force and initial stress of mixed straw pellet samples. Initial stress of rapeseed pellet samples correlated with the modulus of elasticity of the rapeseed pellet samples and correlated non-proportionally with initial force, initial stress and modulus of elasticity of mixed straw pellet samples.

Tab. 4. – Tab. of correlation coefficients of initial force (F_{10}), force in maximum (F_m), strain in maximum (ε_m), initial stress (σ_{10}), stress in maximum (σ_m) and modulus of elasticity (E)for wheat, rapeseed and mixed pellets samples

	Wheatstraw						**Rapeseedstraw**						**Mixedstraw**					
	F_{10}	F_m	ε_m	σ_{10}	σ_m	E	F_{10}	F_m	ε_m	σ_{10}	σ_m	E	F_{10}	F_m	ε_m	σ_{10}	σ_m	E
Wheatstraw																		
F_{10}	1																	
F_m		1																
ε_m	-0.80	0.53	1															
σ_{10}	1.00		-0.79	1														
σ_m		0.99			1													
E	0.83		-0.74	0.85		1												
Rapeseed-straw																		
F_{10}							1											
F_m		-0.60			-0.54			1										
ε_m		-0.77			-0.74			0.77	1									
σ_{10}							0.99			1								
σ_m		-0.58			-0.52			0.99	0.74		1							
E						0.58	0.83			0.86		1						
Mixedstraw																		
F_{10}							-0.55	-0.63	-0.50	-0.59			1					
F_m							-0.50							1				
ε_m		-0.68			-0.67			0.56			0.61		-0.50		1			
σ_{10}		0.51			0.52		-0.54	-0.62	-0.52	-0.57	-0.65		0.99			1		
σ_m														0.87	0.52		1	
E							-0.59			-0.57		-0.53		0.85			0.74	1

Stress in maximum of rapeseed pellet samples correlated proportionally with the strain in maximum of the mixed pellet samples and correlated non-proportionally with the initial stress of the mixed straw pellet samples. Modulus of elasticity of rapeseed pellet samples correlated non-proportionally with modulus of elasticity of the mixed straw pellet samples. Initial force of the mixed straw pellet samples correlated proportionally significantly with the initial stress of the mixed straw pellet samples and correlated non-proportionally with strain in maximum of the mixed straw pellet samples. Force in maximum of the mixed straw pellet samples correlated proportionally significantly with the stress in maximum and modulus of elasticity of the mixed straw pellet samples. Strain in maximum of the mixed straw pellet samples correlated proportionally with stress in maximum of the mixed straw pellet samples. Stress in maximum correlated proportionally with modulus of elasticity of the mixed straw pellet samples. According to Tab. 4, the initial firmnessof the wheat straw pellets samples depends mainly on the coordinates: strain in maximum, initial stress and modulus of elasticity. The maximal firmness of the wheat straw pellets samples depends mainly on the stress in maximum and strain in maximum. The initial firmness of the rapeseed straw samples depends mainly on the initial stress and modulus of elasticity. The maximal firmness of the rapeseed straw samples depends mainly on the force in maximum, strain in maximum and stress in maximum. The initial firmness of the mixed straw samples depends mainly on the initial stress. The maximal firmness of the mixed straw samples depends mainly on the stress in maximum and modulus of elasticity.

LIU ET AL. (2014) present the values of the tensile strength of the pellets in the range from 1.51 MPa to 7.10 MPa. MANI ET AL. (2006) present the values of modulus of elasticity of the pellets in the range from

0.92 MPa to 1.33 MPa. KALIYAN AND MOREY (2009) introduce the minimum pellet hardness for 6.0 – 8.0 mm diameter pellets of 63.7 N and for 4.0 – 5.0 mm diameter pellets of 39.2 N. CARONE ET AL, (2011) present the dependence of compression strength of the biomass pellets on the density of pellets, when the diameter of pellets ranged between 6.03 and 6.31 mm, from 2 MPa to 16 MPa. Dependence of the modulus elasticity of the biomass pellets on the density ranged from 0.1 GPa to 6 GPa. Strong correlation between density and modulus of elasticity and between compression strength and modulus of elasticity was found. STELTE ET AL. (2011) studied straw pellets 16 mm in length and between 7.9 and 8.2 mm in diameter which were manufactured in a single pellet press. The average calculated force at break of straw pellets was 240 ± 60 N.

CONCLUSIONS

The initial firmness of the wheat straw pellets samples depends mainly on the coordinates: strain in maximum, initial stress and modulus of elasticity. The maximal firmness of the wheat straw pellets samples depends mainly on the stress in maximum and strain in maximum. The initial firmness of the rapeseed straw samples depends mainly on the initial stress and modulus of elasticity. The maximal firmness of the rapeseed straw samples depends mainly on the force in maximum, strain in maximum and stress in maximum. The initial firmness of the mixed straw samples depends mainly on the initial stress. The maximal firmness of the mixed straw samples depends mainly on the stress in maximum and modulus of elasticity. Significant correlations of the mechanical parameters pellet samples were observed among initial force and initial stress and modulus of elasticity. Significant correlations of force in maximum with stress and strain in the maximum were observed. The maximal firmness at compression in the initial state and in the maximal compress loading showed the mixed straw pellet samples.

ACKNOWLEDGEMENT

The research leading to these results has received funding from the European Community under project no 26220220180: Building Research Centre „AgroBioTech“.

Author express the appreciations of the Scientific Grant Agency of the Ministry of Education of Slovak Republic and the Slovak Academy of Sciences within the framework of the research were realized in the project Physical properties of biomaterials and the application of physical methods at the evaluation of the specific quality indicators of agricultural materials, No. 1/085400/14.

REFERENCES

1. ADAMOVSKÝ, F., OPÁTH, R.: Výroba tepla spaľovaním biomasy. Nitra: SUA in Nitra, 2013.
2. BLAHOVEC, J., HOUŠKA, M., POKORNÝ, D., PATOČKA, K., KUBEŠOVÁ, A., BAREŠ J.: Mechanical properties of tomato fruits and their determination. Research in Agriculture Engineering, 34(12), 1988: 739 – 751.
3. BERTHET, M. A., GONTARD, N., ANGELLIER, COUSSY, H.: Impact of fibre moisture content on the structure/mechanical properties relationships of PHBV/wheat straw fibres biocomposites. Composites Science and Technology, 117, 2015: 386 – 391.
4. BOŽIKOVÁ, M., HLAVÁČ, P., VOZÁROVÁ, V., VALACH, M.: Selected thermo-energetic parameters of pellets. Journal on processing and energy in agriculture, 19(2), 2015: 83 – 86.
5. CARONE, M. T., PANTALEO, A., PELLERANO, A.: Influence of process parameter and biomass characteristics on the durability of pellets from the pruning residues of Olea europaea L. Biomass and Bioenergy, 35, 2011: 402 – 410.
6. HLAVÁČOVÁ, Z.: Utilization of Electrical Properties of Granular and Powdery Materials. International Agrophysics, 19(3), 2005: 209 – 213.
7. KALIYAN, N. R., MOREY, R. V.: Factors affecting strength and durability of densified biomass products. Biomass and Bioenergy, 33, 2009: 337 – 359.
8. LIU, Z., QUEK, A., BALASUBRAMANIAN, R.: Preparation and characterization of fuel pellets from woody biomass, agro-residues and their corresponding hydrochars. Applied Energy, 113, 2014: 1315–1322.
9. MANI, S., TABILB, G. L., SOKHANSANJ, S.: Effects of compressive force, particle size and moisture content on mechanical properties of biomass pellets from grasses. Biomass and Bioenergy, 30, 2006: 648–654.
10. MIŠLJENOVIĆ, N., ČOLOVIĆ, R., VUKMIROVIĆ, D., BRLEK, T., BRINGAS, C. S.: The effects of sugar beet molasses on heat straw pelleting and pellet quality. A comparative study of pelleting by using a single pellet press and a pilot-scale pellet press. Fuel Processing Technology, 144, 2016: 220 – 229.
11. NEDOMOVÁ, Š., BUCHAR, J., STRNKOVÁ, J.: Mechanical behaviour of ostrich's eggshell at compression. Actauniversitatisagriculturaeetsilviculturaemendelianaebrunensis, (61)3, 2013: 729 – 734.
12. NIEDZIOŁKA, I., SZPRYNGIEL, M., KACHEL, JAKUBOWSKA, M., KRASZKIEWICZ, A., ZAWISLAK, K., SOBCZAK, P., NADULSKI, R.: Assessment of the energetic and mechanical properties of pellets produced from agricultural biomass. Renewable Energy, 76, 2015: 312 – 317.
13. SHAW, M. D., KARUNAKARAN, C., TABIL, L. G.: Physicochemical characteristics of densified untreated and steam ex-

ploded poplar wood and wheat straw grinds. Biosystem Engineering, 103, 2009: 198–207.
14. SERRANO, C., MONEDERO, E., LAPUERTA, M., PORTERO, H.: Effect of moisture content, particle size and pine addition on quality parameters of barley straw pellets. Fuel Process Technology, 92, 2011: 699–706.
15. STELTE, W., HOLM, J. K., SANADI, A. R., BARSBERG, S., AHRENFELDT, J., HENRIKSEN, U. B.: A study of bonding and failure mechanisms in fuel pellets from different biomass resources. Biomass and Bioenergy, 35, 2011: 910 – 918.
16. STRNKOVÁ, J., NEDOMOVÁ, Š., KUMBÁR, V., TRNKA, J.: Tensile strength of the eggshell membranes. Actauniversitatisagriculturaeetsilviculturaemendelianaebrunensis, (64)1, 2016: 159 – 164.
17. SUDHAGAR, M., TABILB, L. G., SOKHANSANJ S.: Effects of compressive force, particle size and moisture content on mechanical properties of biomass pellets from grasses. Biomass and Bioenergy, 30, 2006: 648 – 654.
18. VALACH, M., HÍREŠ, Ľ., KANGALOV, P.: Biofuels and biolubricants in agricultural machinery. Ruse: University of Ruse "Angel Kanchev", 2015.

Corresponding author:
RNDr. ĽubomírKubík, Ph.D., Department of Physics, Faculty of Engineering, Slovak University of Agriculture in Nitra, Tr. A. Hlinku 2, 949 76 Nitra, Slovak Republic, e-mail: Lubomir.Kubik@uniag.sk

PRECISE AUTOMATIC DETECTION OF PLANT SEED GERMINATION

J. Lev, M. Lahodová, J. Blahovec

Department of Physics, Faculty of Engineering, Czech University of Life Sciences Prague, Czech Republic

Abstract
The paper deals with an automatic system for precise detection and evaluation of the most important stages in laboratory germination tests using photographic camera and special illumination procedure. The system makes possible to detect the main pre-plant stages of the germination process via image analysis including the detailed description of the shape changes. The relation between seed's area increase and the shape changes is shown in some special cases. More detailed evaluation of the obtained data is in progress and will be published later.

Key words: wheat, seeds, germination, imbibition, area, shape, evaluation.

INTRODUCTION

Movement of water into ripe and dry grains is on one side a critical step of germination and on the other side the important step of wetting, the undesirable process leading to the losses of both quality and quantity of the stored cereals. For seed germination, the wetting of seeds in moist conditions plays the crucial role (McGuinness et al., 2000). The initial part of this process is known with the complex term "imbibition" (Schopfer, 2006; Weitbrecht et al., 2011). During imbibition the dimensions of the seeds change following wetting. Variation in the rate or the pathway of water movement may be affected by the plant species including the dormancy phenotype (Finch-Savage and Leubner-Metzger, 2006; Rathjen et al., 2009) studied by Mares (Mares, 1983, 1999; Mares et al., 2005). Most of the biochemical and molecular changes are intensified during the first hours of imbibition (Harb, 2012; Mares et al., 2005) and also later during the proper germination (Shopfer and Plachy, 1984).

In germination, the imbibition process is followed by two more phases (Rathjen et al., 2009; Weitbrecht et al., 2011). Whereas in the imbibition the seed moisture content steeply increases up to a value representing about few tens percent increase of the imbibed seed mass, in germination (Blahovec and Lahodová, 2015a), there is a second phase where the process of wetting stops and then in a third phase, the process of wetting continues again (Weitbrecht et al., 2011). The prolongation of the first phase for wheat is about 5 hours and does not strongly depend on the seed state dormancy (Rathjen et al., 2009). In this phase, the grain wetting is limited to the seed coleoptile and to the surface of the seed (Rathjen et al., 2009). The second phase represents a set of metabolic processes (Weitbrecht et al., 2011; Manz et al., 2005; Shopfer and Plachy, 1984) necessary for the seed germination in the third phase. The second and the third phases are very variable depending on the different species and different conditions.

Seeds have different shapes, so that shape differences can be used for sorting them according to type, cultivar, quality etc. (Mebatsion et al., 2012; Dornez et al., 2011). The seed shape was studied with computer vision (Shouche et al., 2001) as a basis for automatic sorting. The volume of the seeds during their germination increases and also their shape changes even in cases of very symmetric shapes close to the spherical one (Robert et al., 2008). The process of wetting is an inhomogeneous process (Rathjen et al., 2009), so that the changes in shape during the seed wetting should be nontrivial (Waszkiewicz, 1988; Blahovec and Lahodová, 2015b,). There are several methods that can be used for a quantitative shape description. Among others, a method based on elliptic Fourier descriptors (Kuhl and Giardina, 1982) is the most commonly used. This method describes an overall shape mathematically by transforming coordinate information concerning its contours into Fourier coefficients (Yoshioka et al., 2004).

Previous paper (Blahovec and Lahodová, 2015b) brought information on mass and dimensions of cereal seeds (barley, wheat rye and oat) after 10 and 24 hours of wetting. It was found that variability of all tested parameters can be described by Gaussian distribution and the distribution differences can be expressed via CP (crossing point of the distributions) and RSD (ratio of standard deviations). The grain mass increase due to wetting under the same conditions was different for different crops and/or varieties but generally is in relation with changes of dimensions and shape that could be detected automatically using some forms of vision systems (DELL' AQUILLA, 2009). The relative change of dimension was irregular, the higher for length and lower for width and thickness of grains. The dimensional changes during wetting sensitively depended on the initial dimensions. The seed changes during its wetting are usually described by changes of its mass, more difficult studies of its volume, density and porosity are rather rare even for the seed characteristics in the base dry state (CHANG, 1988).

The aim of this paper consists in development of an automatic method for observation and detection the image processes connected with the seed germination. The potential of the detection of the seed area and the shape is studied in this paper.

MATERIALS AND METHODS

A simple laboratory setup was developed for the purpose of precise automatic detection of a seed area and a shape in laboratory germination tests. The setup consists of photographic camera (Canon 450D with lens Canon EFS 18-55 mm), tripod, illumination LED panel and glass vessel for germination test (see Fig. 1). The camera was controlled via a computer using software DSLR Remote Pro for windows ver. 2.7.2 (Breeze Systems, United Kingdom). Images from camera were stored in a hard disk of the computer in RAW format. A focal length was set to the top surface of the seeds. The LED panel was controlled via a computer and it illuminates the specimens only during taking pictures. The illumination period was 3 seconds. Whole setup is placed in a dark box thus the germination process is under dark conditions.

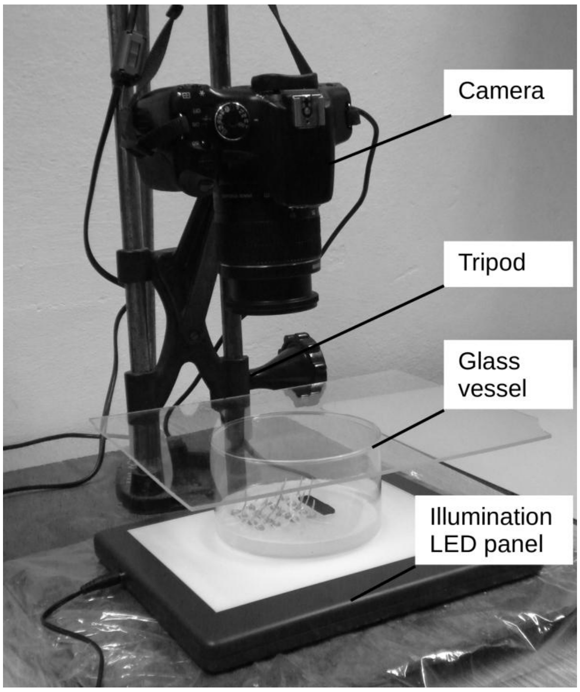

Fig. 1. – The laboratory setup for precise automatic detection in laboratory germination tests.

The area of seeds and their shape parameters were determined by a special program (programmed in language Python 2.7). The supporting libraries for image processing and data analysis were OpenCV 2.4.8, NumPy 1.8.2 and Matplotlib 1.3.1. The shape of seeds was characterized by elliptic Fourier descriptors (EFD; KUHL AND GIARDINA, 1982). In this work a modified python-implementation available at Github repository (https://github.com/alessandroferrari/ elliptic-fourier-descriptors) was used. This method describes an overall shape mathematically by transforming coordinate information concerning its contours into Fourier coefficients (YOSHIOKA ET AL., 2004). Each harmonic contains four coefficients a_n, b_n, c_n and d_n, where n is number of harmonic. In this work the shapes were approximated by the first 20 harmonics and others were omitted. It means that 80 coefficients were obtained for each seed.

The program procedure can be described in the following steps.

1. Loading of images.
2. Conversion to grey scale (it is possible to use red, green or blue channel).
3. Conversion to binary image. A threshold value used in this step is user defined.
4. Application of the erosion-dilation filter for noise reduction.
5. Outline definition and determination of seeds areas. The seed area in pixels is determined.
6. An object with known area (scale) is identified and the seed areas in square millimetres are determined.
7. Calculation of EFDs from outlines.

The laboratory setup and program were tested during germination test of winter wheat (variety Tosca, supplier: Selgen a.s.) harvested in 2014. Moisture content (wet basic) of the seeds was 8.7%. The germination test was performed on agar 0.8 % in a glass vessel. 20 seeds were evenly placed on the agar and next to them a scale with area 318.5 mm^2 was added. The vessel was covered by a thin acrylic glass plate. The experiment was started on the 7th March and terminated on the 11th March. Total length of the experiment was 90 hours and 25 minutes. Temperature in the laboratory during experiment was 20.1 ± 1.0 °C.

Pictures were taken in 5 minutes intervals during germination test.

The seed area development was evaluated using seed area rate (SAR). SAR is time derivative of the seed area and it can be defined by the following formula:

$$SAR = \frac{dSA}{dt}, \ (\mathrm{mm^2\ h^{-1}}) \quad (1)$$

where *SA* is the seed area (mm^2) and *t* is time (h). The time derivative of the seed area was calculated numerically. Experimental data were sequentially fitted by straight lines in order to estimate the course of the first derivative. The straight lines parameters were determined by application of a least squares method always in an interval containing twelve measured values. The interval was moving after measured value and the estimate of the derivative in the middle of the interval expressed the slope of the straight line found.

RESULTS AND DISCUSSION

First visible signs of the third phase of germination (embryo evolution) were observed already 30 hours after the experiment started and 19 seeds successfully germinated during the whole germination test. Total 1,083 pictures were obtained during the experiment but only the first 446 pictures were used for the precise analysis. These pictures represent approximately the first 37 hours.

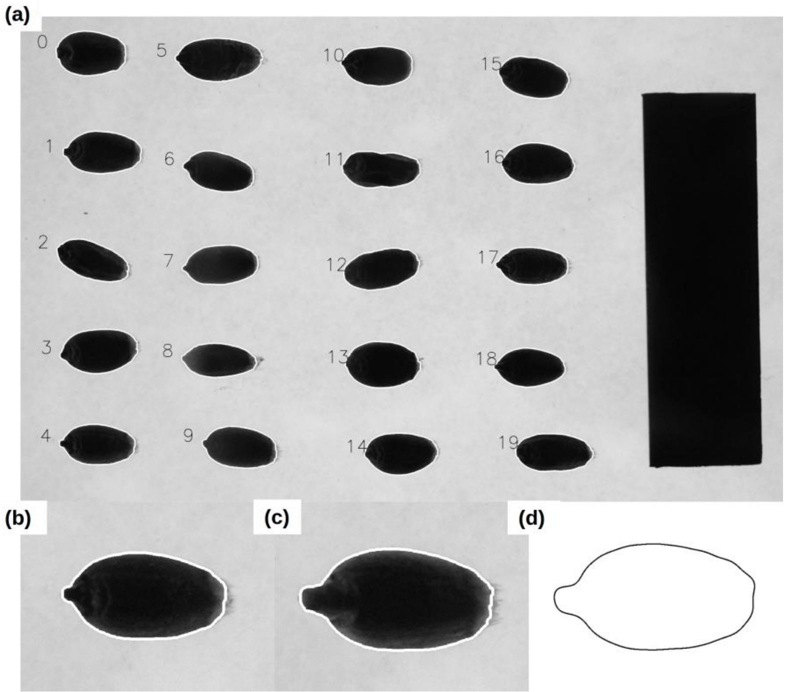

Fig. 2. – (a) The initial frame after conversion to grey scale (blue channel); (b) Detail of the seed 4 in the beginning of the experiment; (c) detail of the seed 4 after 37 hours; (d) the approximated shape of the seed 4 (after 37 hours) by the first 20 harmonics

The Fig. 2 (a) shows the initial frame. In the figure there are located 20 seeds and the seeds are labelled by identification number (numbers 0 – 19). The detected outlines of all seeds are highlighted by white colour. The scale is located on the right side of the picture. It is apparent that seed outlines were successfully recognized in all cases.

Fig. (b) and (c) represent details of the seed 4. The part (b) shows seed 4 in the beginning of the experiment and the part (c) shows the same seed after 37 hours. It is possible to observe the significant seed area change. The area increase is approximately 35 %. In the Fig. 2 (c) the beginning of the radicle penetration is visible as well. Fig. 2 (d) shows approximated shape of the seed 4 (after 37 hours) by the first 20 harmonics. It is possible to state that approximated shape is very close to original outline.

One example (seed 4) of the time courses of the SA and the SAR depicted in Fig. 3 (a). The time course of the SA can be divided into three stage. The first stage terminates at the moment when the SAR has maximum magnitude and the curve (SA) is convex in this stage. In this short stage (approximately 40 minutes), probably, the moisture transports through the dry seed coat. The second stage is characteristic with a decreasing SAR and thus the time course of the SA is concave. The end of the second stage comes approximately after 25 hours when the SAR has minimum magnitude. Then the time course continues in the third stage. In this stage the SA is increasing more quickly. The increase is caused by embryo evolution. The seed behaviour in the second and third stage is in agreement with observations of DELL' AQUILLA (2004).

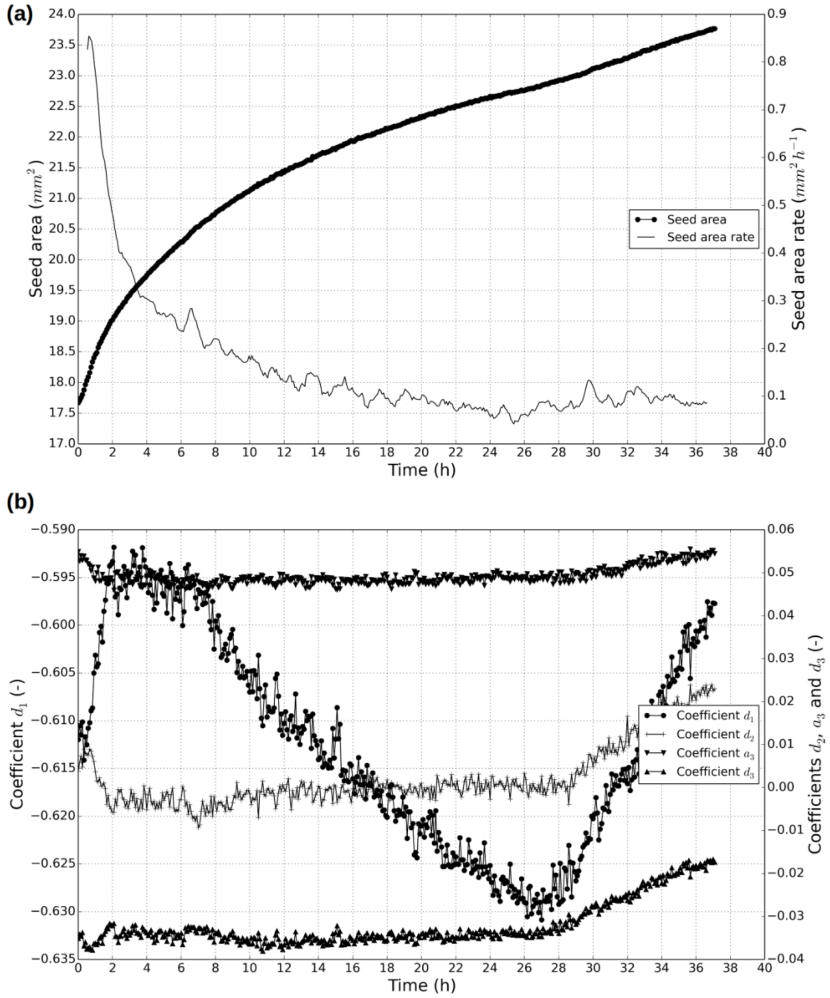

Fig. 3. – (a) the time courses of the seed area (SA) and the seed area rate (SAR); (b) the time courses of four elliptic Fourier coefficients (d_1, d_2, a_3 and d_3)

The time courses of four elliptic Fourier coefficients (d_1, d_2, a_3 and d_3) are depicted in Fig. 3 (b). These coefficients were chosen because they significantly influences the shape approximation. The coefficient d_1 plays the key role of the process. If the shape is approximated by the first harmonic only, the result is simple ellipse and d_1 represents a negative ration of the minor axis to the major axis. Thus it is possible to assume that d_1 corresponds approximately or with the negative ratio of the seed width to the length.

The situation in the Fig. 3 (b) can be divided into three time stages again. The first stage is terminated approximately after 2 hours. All monitored coefficients are significantly changing in this period. The end of this stage is very close to the time where the time course of the SAR should has an inflexion point. The second stage is relatively long and it is terminated at around 27 hours. The coefficients d_2, a_3 and d_3 are more or less constant but the absolute value of the coefficient d_1 is significantly increasing. This behaviour can be caused by an internal processes in the seed and its structure (DONG ET AL., 2015). In the last third stage all coefficients responds to the embryo evolution and the final germination phase because the shape is significantly changing.

The behaviour of only one seed is presented in this paper. However, very similar behaviour was observed for all the tested seeds. The detailed analysis of the whole seed set will be subject of the future paper.

CONCLUSIONS

Setup for precise automatic detection of seed germination in laboratory conditions was developed including the methods of testing and evaluation of the obtained data. It is possible to precisely detect seed area and shape parameters during the germination test. Preliminary results shows that there is nontrivial relations between the area and shape data. It is evident that there is a big challenge for future research. More precise evaluation of the data will be given later.

ACKNOWLEDGEMENTS

This work was supported by the Internal Grant Agency of the Czech University of Life Sciences Prague (Project No. 20163001).

REFERENCES

1. BLAHOVEC, J., LAHODOVÁ, M.: Moisture induced changes of volume and density of some cereal seeds. Plant Soil Environ., 61, 2015a: 43–48.
2. BLAHOVEC, J., LAHODOVÁ, M.: Moisture-induced changes of mass and dimension characteristics in some cereal grains. Int. Agrophys., 29, 2015b: 1–12.
3. CHANG, C.S.: Measuring density and porosity of grain kernels using a gas pycnometer. Cereal Chemistry 65, 1988: 13–15.
4. DELL'AQUILA, A.: Application of a Computer–Aided Image Analysis System to Evaluate Seed.
5. DELL'AQUILLA, A.: Digital imaging information technology applied to seed germination.
6. DONG, K., ZHEN, S., CHENG, Z., CAO, H., GE, P., YAN, Y.: Proteomic Analysis Reveals Key Proteins and Phosphoproteins upon Seed Germination of Wheat (Triticum aestivum L.). Front Plant Sci. 6, 2015: Article 1017.
7. DORNEZ, E., HOLOPAINEN, U., CUYVERS, S., POUTANEN, K., DELCOUR, J.A., COURTIN C.M., NORDLUND, E.: Study of grain cell wall structures by microscopic analysis with four different staining techniques. J. Cereal Science 54, 2011: 363–373.
8. FINCH-SAVAGE W.E., LEUBNER-METZGER G.: Seed dormancy and the control of germination. New Phytologist 171, 2006: 501–523.
9. Germination under Different Environmental Conditions. Ital. J. Agron., 8, 1, 2004: 51-62.
10. HARB, A.M.: Reserve Mobilization, Total sugars and proteins in germinating seeds of durum wheat (*Triticum durum* DESF.) Under water deficit after short period of imbibition. American-Eurasian J. Agric. & Environ. Sci., 12, 2012: 1469-1474.
11. KUHL, F. P., GIARDINA, C. R.: Elliptic Fourier features of a closed contour. Computer Graphics and Image Processing 18, 1982: 236–258.
12. MANZ, B., MÜLLER, K., KUCERA, B., VOLKE, F., LEUBNER-METZGER, G.: Water uptake and distribution in germinating tobacco seeds investigated in vivo by nuclear magnetic resonance imaging. Plant Physiology 138, 2005: 1538–1551.
13. MARES, D.J., MRVA, K., CHEONG, J., WILLIAMS, K., WATSON, B., STORLIE, E., SUTHERLAND, M., ZOU, Y. A.: QTL located on chromosome 4A associated with dormancy in white- and red-grained wheats of diverse origin. Theoretical and Applied Genetics 111, 2005: 1357–1364.
14. MARES, D.J.: Preservation of dormancy in freshly harvested wheat grain. Australian Journal of Agricultural Research 34, 1983: 33–38.
15. MARES, D.J.: The seed coat and dormancy in wheat grains. In: Weipert D. (ed.) Eighth international symposium on preharvest sprouting in cereals. Germany: Detmold: 77–81. 1999.
16. MCGUINNESS, M.J., PLEASE, C.P., FOWKES, N., MCGOWAN, P., RYDER, L., FORTE, D.: Modelling the wetting and cooking of a single cereal grain. IMA J. Management Math. 11, 2000: 49-70.
17. MEBATSION, H.K., PALIWAL, J., JAYAS, D.S.: Evaluation of variations in the shape of grain types using principal components analysis of the elliptic Fourier descriptors. Computers and Electronics in Agriculture 80, 2012: 63–70.
18. RATHJEN, J.R., STROUNINA, E.V., MARES, D.J.: Water movement into dormant and non-dormant wheat (*Triticum aestivum L.*) grains. Journal of Experimental Botany, 60, 2009: 1619–1631.
19. ROBERT, C., NORIEGA, A., TOCINO, A., CERVANTES, E.: Morphological analysis of seed shape in *Arabidopsis thaliana* reveals altered polarity in mutants of the ethylene signalling pathway. Journal of Plant Physiology 165, 2008: 911—919.
20. SCHOPFER P., PLACHY C.: Control of seed germination by abscisic acid. II. Effect on embryo water uptake in Brassica napus L. Plant Physiology 76, 1984: 155–160.
21. SCHOPFER P.: Biomechanics of plant growth. American Journal of Botany 93, 2015: 1415–1425.
22. SHOUCHE, S.P., RASTOGI, R., BHAGWAT, S.G., SAINIS, J.K.: Shape analysis of grains of Indian wheat varieties. Computers and Electronics in Agriculture 33, 2001: 55–76.
23. WASZKIEWICZ, C.: Effect of the water content on physical properties of the cereal grain. Part III Grain dimensions (in Polish). Roczniki Nauk Rolniczych T. 78-C-3, 1988: 57-62.
24. WEITBRECHT, K., MÜLLER, K., LEUBNER-METZGER, G.: First off the mark: early seed germination. Journal of Experimental Botany 62, 2011: 3289–3309.
25. YOSHIOKA, Y., IWATA, H., OHSAWA, R., NINOMIYA, S.: Analysis of Petal Shape Variation of Primula sieboldii by Elliptic Fourier Descriptors and Principal Component Analysis. Annals of Botany 94, 2004: 657–664.

Corresponding author:

Ing. Jakub Lev, Ph.D., Department of Physics, Faculty of Engineering, Czech University of Life Sciences Prague, Kamýcká 129, Praha 6, Prague, 16521, Czech Republic, phone: +420 2 2438 3281, e-mail: jlev@tf.czu.cz

ANALYSIS OF RAPID TEMPERATURE CHANGES OF THE OBJECT WITH HIGHER THERMAL CONSTANT

M. Linda, M. Hromasová

Department of Electrical Engineering and Automation, Faculty of Engineering, Czech University of Life Sciences Prague, Czech Republic

Abstract
The paper describes a dependence of change of the power load-factor when analysing an object with a higher time constant. The inertia of the protective layers and the temperature field distribution of the surface layers are shown. Analysis of the temperature change is carried out in three methods. Measurement of surface warming was carried out independently by two thermocouples, the first one with a leading wire diameter of 0.12 mm and the second one of 0.012 mm. The time constant difference of the sensors is influencing the measured temperature pattern, so the accuracy of measurement. Measured object is metallised resistor with maximum load of 1 W.

Key words: measurement, thermocouple, temperature field, dynamic change of temperature, sensor.

INTRODUCTION

The pulse load mode is one of the most common operational modes in switching circuits. Another correlation that is shown, is a link comparison of the temperature measurement using broadly different time constants of the sensor (HROMASOVÁ AND LINDA, 2016).

In operation of the object is particularly important to know the operating characteristics of the device. A power increase over maximal load capacity can lead to a damage of the resistive layer which subsequently shows different characteristics, therefore it is important to know the operational temperature characteristics for different cooling modes. Thereafter it is possible to select appropriate operational parameters for a maximum load of the object during pulse load mode. For analysis of the object are applied 3 methods of measurement (LINDA AND HROMASOVÁ, 2016). Since the spot measurement is aggravated by inaccuracies of information inconsistency, the analysis is complemented with images of infrared spectroscopy.

Kalita and Wegrlarski analysed a solution of an impact of dynamic changes in temperature on degradation processes and procedures in resistive layers in the article „Dynamic states of temperature in pulse loaded thick film resistors" (KALITA AND WEGLARSKI, 2001). In the model is taken into consideration substrate, protective layer and mechanism of heat exchange with the environment (SAKASHITA, 2016; SESSLER AND MOAYERI, 1990). The output is determined by the influence of heat accumulation in the resistor layer under dynamic load. The analysis was carried out as a pulsed one with a high load factor. (JIAO ET AL., 2015)

The contact temperature measurement is defined as a direct contact of the sensor with the measured object. We can therefore distinguish between permanently located sensors on the object, and those that are in contact with the object only at the time of measurement. During the contact measurements must take into account a number of parameters such as the surface flatness (curved), surface quality (polished, oxidized, rough) and a surface treatment (varnishing, laminating), thermal conductivity at the contact, the heat dissipation of sensor, etc. Basic requirements for the sensors are light weight, small size, and suitable construction modifications. Light weight of the sensor provides a rapid warming, and therefore a small time constant and the associated dynamic in correlation with the measured object. Small size ensures more accurate measurements, for example on a semiconductor object, SMD resistors and other. The thermocouples suit the most for these requirements, where only the cross section of the used wire matters. It can also be used for measuring high temperatures above 1000 °C (HROMASOVÁ AND LINDA, 2016). This paper aims to conduct an analysis of the temperature course distribution during a dynamic load of the resistance component.

MATERIALS AND METHODS

In practice, in most cases, we do not encounter only one thermal energy conversion (sharing). As a general rule we encounter two, or all types of thermal energy sharing. Fig. 1 shows heat sharing through SMD resistor wiring. The figure shows the heat transfer from the lead wires to the pads. Another type of heat transfer is radiation, i. e. a heat exchange with the surrounding environment. These effect subsequently influence the actual measurement on the objects. (FARRÉ ET AL., 1998).

Under the assumptions is evident that the measurements on such element will be most suitable in the middle on small area, where the temperature gradient is not distorted. A heat dissipation occurs in location of heat transfer and near "feet", and therefore we would measure lower temperature. This element of dynamic distortion will be examined in the actual analysis alongside with conclusions.

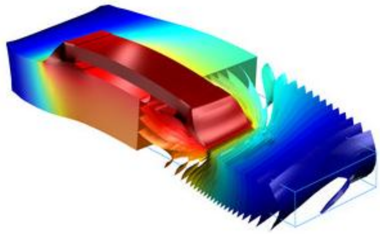

Fig. 1. – Model of heat sharing of SMD resistor with surroundings. (COMSOL, 2009)

Fig. 2a) shows the dynamic temperature pattern in the resistive layer with a power pulse of 100 W with a duration of 1 μs, i. e. the temperature response to a very short pulse. The pulse response is linear. Fig. 2 b) shows another case of power pulse response of 1 W with a duration of 10 ms. The response represents a non-linear pattern with stabilization and a linear pattern of temperature change (KALITA AND WEGLARSKI, 2001).

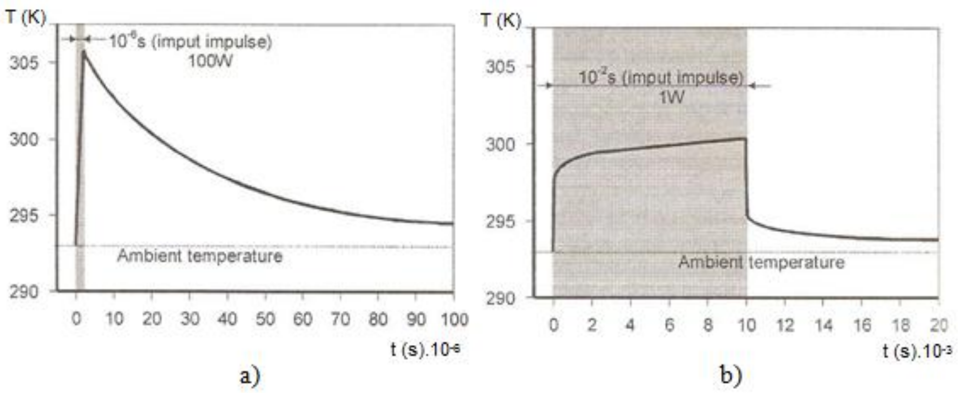

Fig. 2. – Dynamic temperature pattern in the resistive layer: a) 100 W, 1 μs, b) 1 W, 10 ms (KALITA AND WEGLARSKI, 2001)

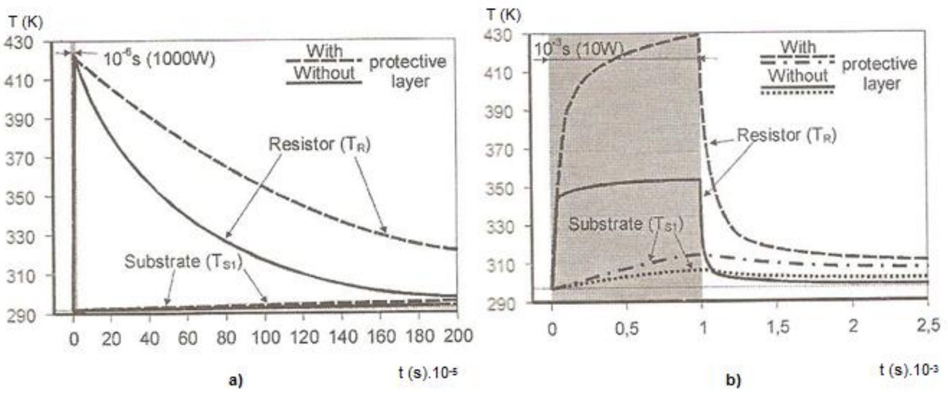

Fig. 3. – Dynamic temperature pattern in the resistive layer with/without protective layer: a) 1000 W, 1 μs, b) 10 W, 10 ms (KALITA AND WEGLARSKI, 2001)

Fig. 3a) shows the temperature pattern when the power load is 1000 W with a duration of 1 μs. An increase of the maximum achieved temperature, and influence of heat accumulation through individual layers of the model are evident from the pattern. The most evident is the effect on Fig. 3b) at a load of 10 W with a duration of 10 ms (KALITA AND WEGLARSKI, 2001).

It follows from the above that we could draw up requirements or principles for a correct positioning of the measuring section on the object, i. e. ensure a minimum thermal resistance between the measuring section and the measured object surface, ensure maximum heat transfer coefficient from the object to the measuring device, ensure minimal heat flow from the measuring device to the environment and finally one important requirement, but to a certain extent hardly feasible, not to distort a thermal field in measured location, this condition can be met by a proportion between the sensor surface and the measured object (KREIDL, 2005).

In simple terms, the objective is to maintain thermal conditions on the object surface in the same configuration as if there was no sensor. Fig. 4a) shows the deformation of the isotherms after stabilization of conditions when sensor is applied, whereas without the sensor, the isotherms take place on the object surface (CHEN ET AL., 2015).

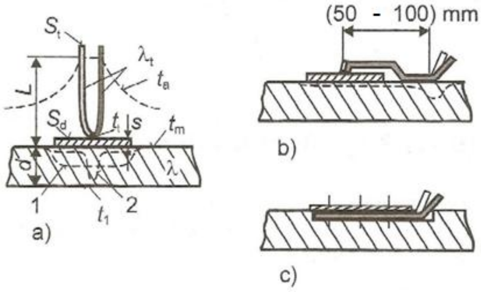

Fig. 4. – Measurement of surface temperature using a thermocouple: a) incorrect configuration, b) correct configuration, c) configuration with a cover plate (KREIDL, 2005).

When conducting a surface measurement of the object temperature, the contact of the measuring device causes a change of heat transfer between the object and the environment in the measurement location, that distorts the temperature field inside of the object (Fig. 4). In this way, the measured temperature will be different from the actual one that would be on the object without the measuring device (LINDA ET AL., 2012). The sensor attached to the object warms itself up, and therefore removes heat from the measured object. Furthermore, the sensor may cause a) permanent heat dissipation (the measured temperature is lower) or b) preventing heat dissipation (the measured temperature is higher).

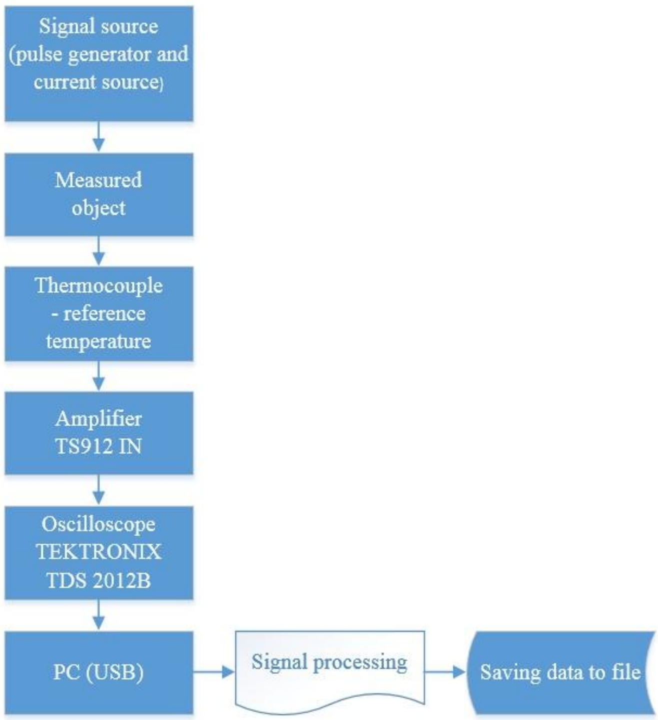

Fig. 5. – The diagram of the measuringc hain

Use of sensors is necessary for the above measurements, whose conductors must have the cross-section S_t as small as possible and low coefficient of thermal conductivity λ_t.(KREIDL, 2005)

The established laboratory environment (Fig. 5) for measurement of pulsed temperatures waveforms on selected power loaded objects, is comprised of pulse generator, loaded/measured object and measuring devices.

Used measuring methods can be divided into three groups. The first method "The measurement of a steady-state" is based on measuring surface temperature of the electric component up until its stabilization. This method is favorable for the possibility to observe the component's behavior at a permanent load, or up to the critical load, and subsequently concludes how many of such cycles the component is capable to endure without an evident damage, or without changing parameters (HUESGEN ET AL., 2008; CHEN ET AL., 2015; KALITA AND WEGLARSKI, 2001). This method is showing an apparent oscillation when measured with a micro thermocouple, which is only a reaction to the measurement of the power pulses, and this change is detailed in another type of test. This phenomenon is not as evident in the second type of thermocouple, where there is furthermore a heat dissipation through conductors that have 10 times larger diameter (YA ET AL., 2016; ZHAO ET AL., 2015).

The second method "The Pulse Test" is based on examination of the surface temperature waveform as a response to one or more pulses at the input of the system, as in our case. The result of such analysis is not only about the exact dynamics of the response, but also about the maximum transferable power of the component (HROMASOVÁ AND LINDA, 2016).

The complementary method, which is primarily used to analyze temperature distribution on the electronic component's surface, is called "The method of measuring local temperature ". In our case, we chose it with regard to selected resistors, where because of dimensions, is convenient to know waveforms of the thermal gradient on the component's surface (SONG ET AL., 2016).

RESULTS AND DISCUSSION

Metallic resistor 1 W, method "The measurement of a steady-state"

Fig. 6, Fig. 7 and Fig. 8 show the patterns for metallic resistor 1 W with load factor of 0.0385, 0.056 and 0.0741. For measurement we used thermocouples 5TC-TT 0.12 mm and CHAL0005 0.012 mm. The influence of the object's thermal capacity is evident from the patterns, which reduce system dynamics. Comparison of the thermocouple's measured patterns gives us a clear indication of the slow change in surface temperature under power load pulses (HROMASOVÁ AND LINDA, 2016). Among the measured patterns are large deflections because the changes of surface temperature are slow. It can therefore be established that the measurements can be conducted on this type of resistor even with a lower time constant systems. However, it is difficult to mention the time constant of the sensor, because the manufacturer does not exactly specify the time constant, it is defined only as "very low time constant" (LINDA AND HROMASOVÁ, 2016).

Fig. 6 shows a load factor of $z = 0.0385$ for the case number of cycles $n_p = 60$, pulse duration $t_1 = 20$ m sand no pulse period $t_2 = 500$ ms, the measured temperature is 62 °C. The time when the temperature decrease occurs via equalizing of the thermal gradient is 7.5 s.

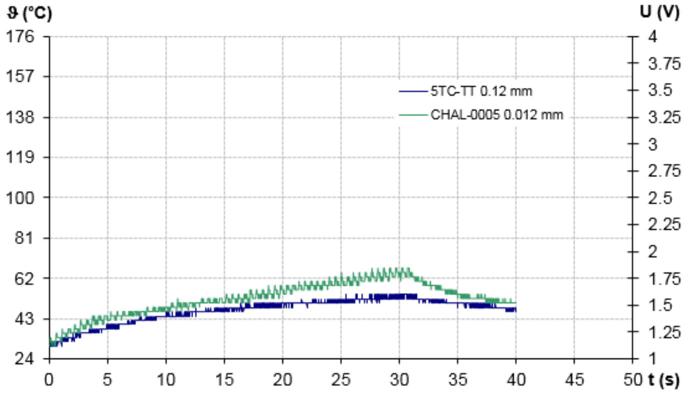

Fig. 6. – The measured waveform – case a) $z = 0.0385$

Fig. 7 shows a case with load factor of $z = 0.0566$ for the case $n_p = 60$, $t_1 = 30$ ms and $t_2 = 500$ ms, the achieved temperature is 89 °C, the pattern shows apparent flicks measured by the thermocouple. The difference compared to the previous case is 27 °C, when load factor increased by 0.0181.

Fig. 8 shows a case with load factor of $z = 0.0741$ for the case $n_p = 60$, $t_1 = 40$ ms and $t_2 = 500$ ms, the achieved temperature is 100 °C. The difference compared to the previous case is 11 °C, when load factor increased by 0.0175. The time when the temperature decrease occurs via equalizing of the thermal gradient is 7.5 s.

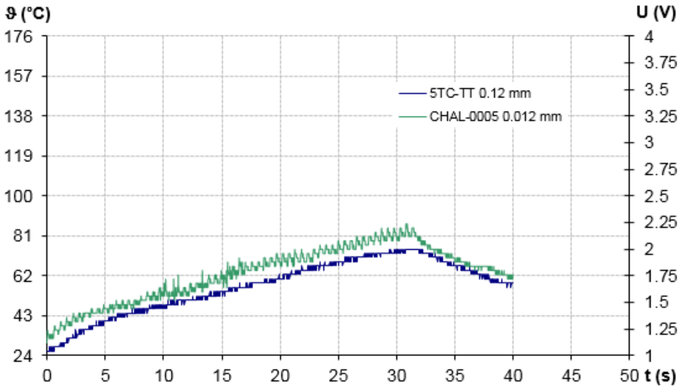

Fig. 7. – The measured waveform – case b) $z = 0.0566$

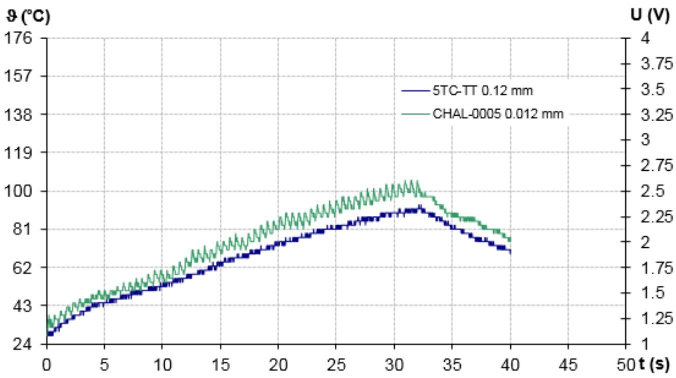

Fig. 8. – The measured waveform – case c) $z = 0.0741$

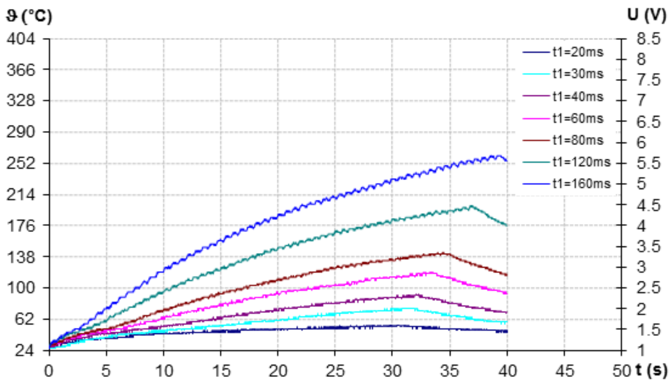

Fig. 9. – Measurement with change load factor, $n_p = 60$, $t_2 = 500$ ms

Fig. 9 shows an analysis of load factor change when a shift of decrease interval and a steepness of temperature onset occur. The time interval t_1 is in range from 20 ms to 160 ms in the nonlinear scale. For measurement we used thermocouple 5TC-TT 0.12 mm. The measured temperature reaches a maximum of 260 °C for $t_1 = 160$ ms. The temperature decrease interval shifted from 7.5 s to 2.5 s due to the temperature increase to the critical limit which is determined by the temperature gradient when 45 °C. Nonlinear scale of the load factor was chosen as a result of low temperature increase through change by t_1 = 10 ms, and then by 20 ms. Load factor z_i is 0.0385; 0.0566; 0.074; 0.1071; 0.1379; 0.1935; 0.2424.

Fig. 10 and Fig. 11 show images from thermal camera for the case of n_p = 60, t_1 = 40 ms and t_2 = 500 ms Three images are given in chronological order, so that the delineation of the examined areas is visible. A dependence of heat dissipation through wiring of the resistor and an increased temperature of the resistor's core is obvious from the carried out images. Fig. 10 shows a warming up of the resistor, and Fig. 11 shows a cooling of the resistor.

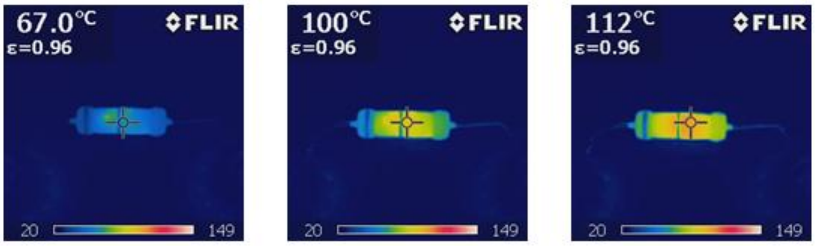

Fig. 10. – Images from thermal camera - warming up of the resistor

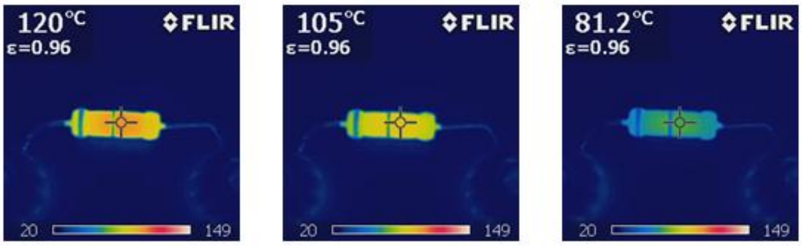

Fig. 11. – Images from thermal camera - cooling of the resistor

A strip that is presented by a cold colour is the labelling by a gold strip on the resistor. The strip disrupts the heat dissipation by its conductivity, and therefore it is not suitable to conduct a contact measurement in this location, it would lead to a lower temperature measurements. It is therefore necessary to analysis the component's surface before conducting the actual contact measurement. For the purpose of infrared measuring, the surface was not modified. The surface was abraded for the contact measurement so that the measuring would not affect the lacquering of the surface.

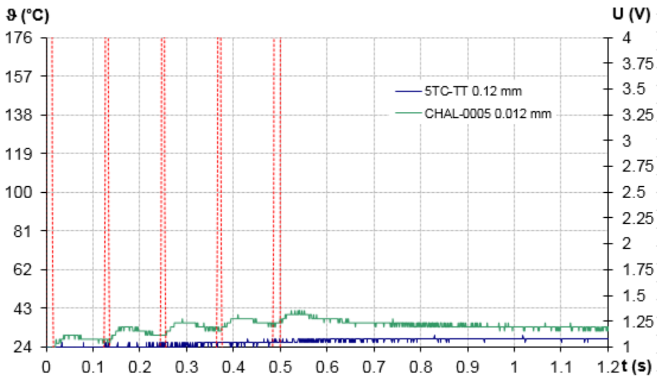

Fig. 12. – The measured waveform – case a) z = 0.167

Metallic resistor 1 W, method "The Pulse Test"

Fig. 12 shows a pulse test for a resistor with a load capacity of 1 W with load factor of 0.167 for the case number of cycles n_p = 5, pulse duration t_1 = 20 ms and no pulse periodt_2 = 100 ms. Fig. 12 shows an apparent dynamic change of the surface temperature, which, however, does not copy the pulse dependency, the expression is phase-shifted, and in this dependence is the effect of heat transfer through inlets, and a heat

radiation to the surroundings, much more evident. The maximum temperature reached is 45 °C.
Fig. 13 shows a pulse test for a resistor with load factor of 0.286 for the case $n_p = 5$, $t_1 = 20$ ms. The time change $t_2 = 50$ ms is more evident than in, previous cases and affects the final temperature pattern and therefore leads to a disruption of a heating period. This phenomenon is more noticeable with components of higher mass and is proportional to the changed time t_2.

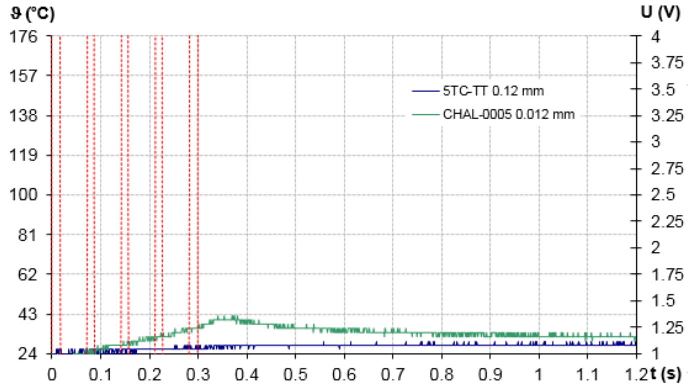

Fig. 13. – The measured waveform – case b) $z = 0.286$

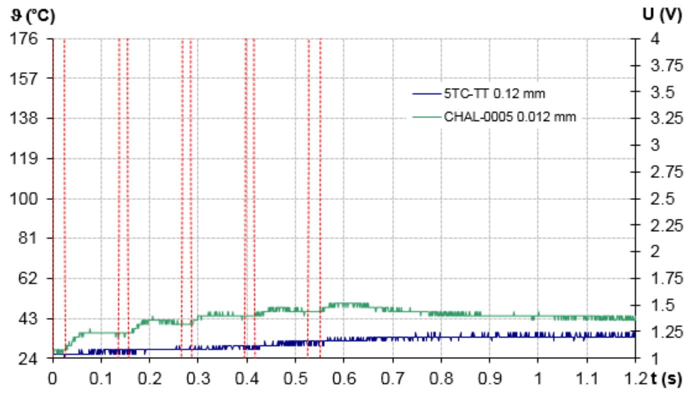

Fig. 14. – The measured waveform – case a) $z = 0.231$

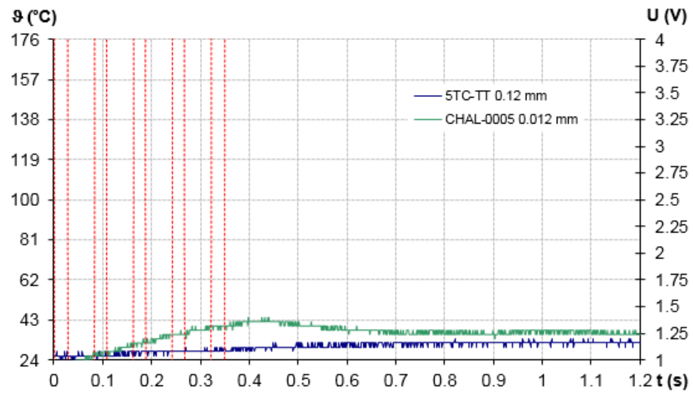

Fig. 15. – The measured waveform – case b) $z = 0.375$

Fig. 14 shows a pulse test with load factor of 0.231 for the case $n_p = 5$, $t_1 = 30$ ms and $t_2 = 100$ ms. Fig. 15 shows a pulse test with load factor of 0.375 for the case $n_p = 5$, $t_1 = 30$ ms and $t_2 = 50$ ms.

Fig. 16 shows a pulse test with load factor of 0.286 for the case $n_p = 5$, $t_1 = 40$ ms and $t_2 = 100$ ms. Fig. 17 shows a pulse test with load factor of 0.444 for the case $n_p = 5$, $t_1 = 40$ ms and $t_2 = 50$ ms.

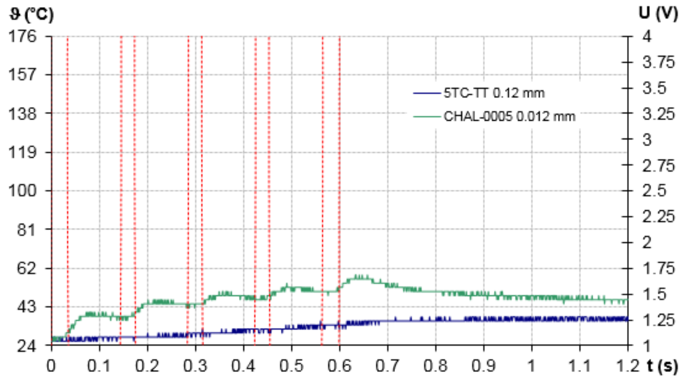

Fig. 16. – The measured waveform – case a) $z = 0.286$

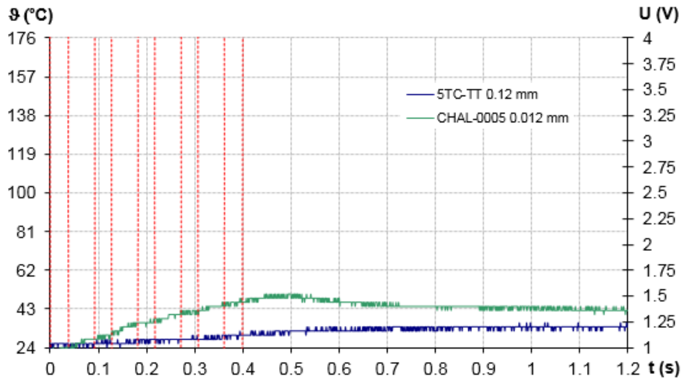

Fig. 17. – The measured waveform – case b) $z = 0.444$

Fig. 18 shows dependence and comparison of temperature vs. load factor in time sphere. See picture for evident dependencies of used thermocouples. There is an evident flattening on the other set of images, that is caused by this factor.

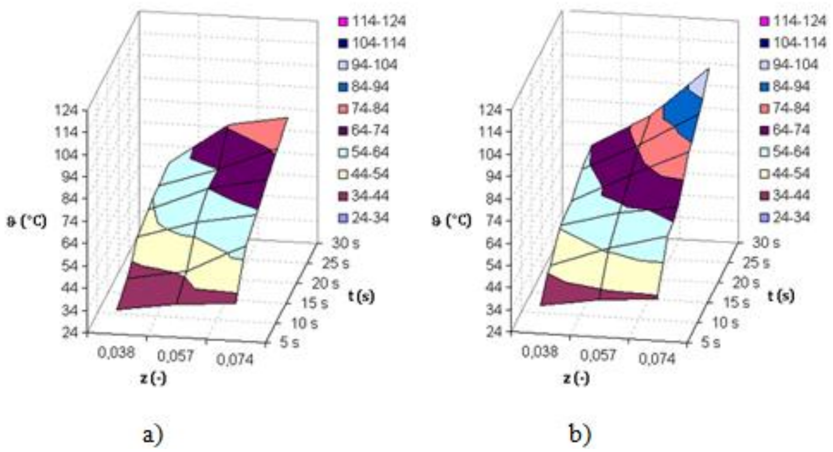

Fig. 18. – 3D dependency graph of surface temperature vs. load factor, resistor 1 W measured with thermocouple a) 0.12 mm and b) 0.012 mm

During the pulse test, only in some load factor combinations (Fig. 12 and Fig. 14) a phase shift of the measured signal is apparent, compared to the power pulses at the input, similarly as described in the measurement on the object with half load (FARRÉ, ET AL., 1998). During a temperature dependence analysis using the method to a steady state, no significant deviation is apparent when using sensors with different time constants, this is caused by the thermal inertia of the object compared to the dependencies mentioned in the paper (HROMASOVÁ AND LINDA, 2016).

CONCLUSIONS

This paper describes the dependence of the temperature pattern under dynamic load of the object with a higher time constant. Due to the high time constant, negligible power pulses of the temperature are apparent during measurement. A permanent damage takes place on the resistive layer of the resistor, which leads to a change of its parameter, esp. the resistance and the maximum power load. The resistor case is unable to transfer the created thermal energy quickly, which leads to a local overheating of the resistive layer section. The measurement is supplemented by shots from infrared spectrometry which shows thermal changes of the volume. For a cost and data evaluation reasons, this method is not applicable for continuous measurements in electronic applications. If it was necessary to use non-contact temperature measurement, it would possible to use pyrometers with a thermocouple output. They can be incorporated into existing electrotechnical measuring systems because their output characteristics are the same as a conventional thermocouple.

REFERENCES

1. COMSOL: Thermo-Mechanical Analysis of a Surface Mounted Resistor [online]. COMSOL Model Gall, 2009. Available at: http://www.comsol.com/showroom/gallery/481/ (accessed 6.9.09).
2. FARRÉ, R., MONTSERRAT, J.M., ROTGER, M., BALLESTER, E., NAVAJAS, D.: Accuracy of thermistors and thermocouples as flow-measuring devices for detecting hypopnoeas. Eur. Respir. J. 11, 1998, pp. 179–182.
3. HROMASOVÁ, M., LINDA, M.: Analysis of rapid temperature changes. Agron. Res. 14, 2016: pp. 768–778.
4. HUESGEN, T., WOIAS, P., KOCKMANN, N.: Design and fabrication of MEMS thermoelectric generators with high temperature efficiency. Sensors Actuators A Phys, 2008: pp. 145-146, 423–429.
5. CHEN, S., LI, H., LU, S., NI, R., DONG, J.: Temperature measurement and control of bobbin tool friction stir welding. Int. J. Adv. Manuf. Technol, 2015: pp. 1–10.
6. JIAO, L., WANG, X., QIAN, Y., LIANG, Z., LIU, Z.: Modelling and analysis for the temperature field of the machined surface in the face milling of aluminium alloy. Int. J. Adv. Manuf. Technol. 81, 2015: pp. 1797–1808.
7. KALITA, W., WEGLARSKI, M.: Dynamic states of temperature in pulse loaded thick-film resitors. Electron. Horiz. 58, 2001: pp. 21–24.
8. KREIDL, M.: Měřeníteploty, senzoryaměřicíobvody, Praha: BEN. ed. 2005.
9. LINDA, M., HROMASOVÁ, M.: MODEL ANALYSIS OF TEMPERATURE SENSORS, in: Engineering for Rural Development. Latvia University of Agriculture, Jelgava, 2016: pp. 566–573.
10. LINDA, M., KUNZEL, G., HROMASOVA, M.: Temperature measurement in technical applications, in: Engineering for Rural Development, 2012: pp. 145–150.
11. SAKASHITA, H: Temperature measurements near the heating surface at high heat fluxes in pool boiling of 2-propanol/water mixtures. Int. J. Heat Mass Transf. 93, 2016: pp. 1000–1007.
12. SESSLER, D.I., MOAYERI, A.: Skin-surface warming: heat flux and central temperature. Anesthesiology 73, 1990: pp, 218–224.
13. SONG, H., ZHAN, X., LI, D., ZHOU, Y., YANG, B., ZENG, K., ZHONG, J., MIAO, X., TANG, J.: Rapid thermal evaporation of Bi2S3 layer for thin film photovoltaics. Sol. Energy Mater. Sol. Cells 146, 2016: pp. 1–7.
14. YA, W., PATHIRAJ, B., LIU, S.: 2D modelling of clad geometry and resulting thermal cycles during laser cladding. J. Mater. Process. Technol. 230, 2016: pp. 217–232.
15. ZHAO, X., YANG, K., WANG, Y., CHEN, Y., JIANG, H.: Stability and thermoelectric properties of ITON:Pt thin film thermocouples. J. Mater. Sci. Mater. Electron, 2015.

Corresponding author:

Ing. Monika Hromasová, Ph.D., Department of Electrical Engineering and Automation, Faculty of Engineering, Czech University of Life Sciences Prague, Kamýcká 129, Praha 6, Prague, 16521, Czech Republic, phone: +420 22438 3206, e-mail: hromasova@tf.czu.cz

POWER REQUIREMENT FOR PROCESSING OF MAIZE PLANT BY FORAGE HARVESTER

A. Lisowski[1], J. Klonowski[1], A. Świętochowski[1], Z. Gut[2]

[1]Department of Agricultural and Forest Engineering, Faculty of Production Engineering, Warsaw University of Life Sciences, Poland
[2]Institute of Heat Engineering, Faculty of Power and Aeronautical Engineering, Warsaw University of Technology, Poland

Abstract
The aim of this study was to investigate the influence of the chosen technical parameters on the effective power needed to the process of cutting, feeding and picking-up of the material from maize plants by the forage harvester. The studies were conducted in the stationary conditions, using pulled forager equipped with a chopping flywheel unit with 5 or 10 knives, sensors to the measurement of the rotational speed and the torque of the PTO and pick-up shaft, and pressure and oil flow intensity transducers in the hydraulic actuator. The moisture content of the plants were 68 and 57%, the samples mass were 5, 10 and 15 kg (the material feeding of 1.13, 2.25 and 3.38 $kg \cdot s^{-1}$, respectively). It was found that the requirement for effective power for cutting was inverse than for the power to feeding. The maximum and minimum values, respectively were obtained under optimal material moisture content (65%), at which the rigidity of the plants is the lowest. The doubled cutting frequency do not generates the same increase of requirement for power for cutting unit work, because the smaller particles require lower kinetic energy to overcome their lower inertia.

Key words: forage harvester, biomass, cut, compression, feeding.

INTRODUCTION

The preparation process of plant material for ensilage with the use of forage harvesters requires considerable energetic expenditures. Since the most energy-consuming process, using up even 85% of total energy, is chopping the plant material (O'DOUGHERTY, 1982; SAVOIE ET AL., 1989), therefore a detailed analysis of the chopping process is very important. The power requirement for cutting of plant material depends not only on its properties and technical parameters of the cutting unit, but also on the initial compression of the material by the feed rolls or picking-up of swath by header (ROBERGE ET AL., 1998). The work of these units also requires energetic expenditures, which should be considered together.

Hitherto existing investigations focused on the influence of basic constructional and exploitation parameters of the cutting unit on its energetic loads. The load sources related to cutting, accelerating and material friction of the unit housing were determined. The optimum design parameters of individual unit elements – the micro-, the macro-geometry of knives and anti-cutting edge were established. The influence of kinematic parameters – the speed of particles movement and direction of cut and exploitation parameters – the theoretical length of cut were studied. Impact of plant physical properties and moisture content on energy consumption of the chopping process were also analysed (REZNIK, 1967; SHINNERS ET AL., 1994; CHATTOPADHYAY AND PANDEY, 2001).

One of the development trends in agricultural engineering is precision farming, based on the knowledge of yield variability, physico-chemical soil properties, weed content, pests, etc., within a given field (AUERNHAMMER, 2001).

The mass flow intensity is often measured with the use of indirect mechanical methods, based on measurements of dynamical pressure in the forage harvester discharge spot or the torque or power needed for driving the knife disk of machine chopping unit.

The analysed references point out that investigations on monitoring of mass flow intensity for the plants harvested with forage harvesters, based on power or torque measurements (VANSICHEN AND DE BAERDEMAEKER, 1993; KROMER ET AL., 1999; SCHMITTMANN ET AL., 2000) did not considered the effect of plant material parameters or machine parameters on physical quantities being measured.

Authors (KLONOWSKI ET AL., 2005) presented the effect of material mass flow rate, knife disc rotational speed, and number of cutting knives on dynamic pressure force of mass in the discharge spot and power requirements for driving forage harvester units during grass chopping. It was found that power values were statistically different for all the analyzed factors, while the varied dynamic pressure force has depended on the mass stream and knife disc rotational speed.

It was also found (KLONOWSKI AND LISOWSKI, 2007) that application of knife disk power measurement to determination of harvested grass yield calls for consideration of number of knives, knife disk rotational speed and the constant measurements on plant material moisture content and tractor outfit ground speed, as a component of the mass flow.

At another paper of authors (LISOWSKI ET AL., 2007) were presented the research results of the operational effect of additional elements used in the chopping unit of forage harvester on breaking-up of maize grain harvested for silage. It was found that application of bottom beater plate and plain thrower paddles, working at working clearance between them set to 8 mm at the inlet and 2 mm at the outlet, allowed for effective increase in grain breaking-up. Application of other additional elements in the form of bottom plate with beater and bar notches, the thrower paddles of notched and plain surfaces, and the radial notched and plain bars resulted in lower effectiveness of maize grain breaking-up.

Because of permanent improvement of the investigations methods, the undertaken investigations aimed at determination of significance of the effect of selected plant material parameters and machine parameters on effective power requirements for driving the knife disk, feed rolls and pick-up unit during maize chopping with the pulled forage harvester.

MATERIALS AND METHODS

Plant material

All experimental measurements were performed for maize, variety Inagua FAO 240, cut by a manual brush cutter. For the purpose of the research, the plant material was described by establishing the chopped material moisture content and geometric mean value of particle size.

The average moisture contents (wet basis) of two groups of plant material 68 ± 2% (higher moisture) and 57 ± 2% (lower moisture) were determined by the dried-weight method according to standard S358.2 ASABE for silage (ASABE STANDARDS, 2011B). Five samples of 20 g each were collected daily from the cut material. The samples were weighed on the electronic scales with an accuracy of 0.01 g and dried at 103 ± 2 °C for 24 h.

A sieve separator (LISOWSKI ET AL., 2014) meeting the requirements of ASABE Standard S424.1 (ASABE STANDARDS, 2011A) was used to evaluate the particle size distribution of cut plant material. Five averaged, uncompressed samples of 10 dm^3 were used for measurements. Screening time of 120 s was controlled with a stopwatch and individual particle fractions were weighed on the electronic scales with an accuracy of 0.01 g. For moisture content of 68% and cutterhead rotational speed of 1000 rpm and 10 knives and 5 knives the geometric mean value of size particles were 12.04 mm and 8.54 mm, respectively and for moisture content of 57% with the same working parameters were a little higher and amounted to 13.34 mm and 10.25 mm, respectively. The geometric mean value of particle size was not depended on material mass flow rate in the range of 1.13 kg s^{-1}–3.38 kg·s^{-1} and the geometric mean value had a narrow range of 10.95 mm–11.20 mm.

2.2. Power measurements

The principal study was carried out on a test stand designed around a Z 374 pulled forager (SIPMA, Lublin, Poland) with a chopping flywheel unit (Fig. 1). Conveyor belt was used for the transport of whole corn shoots. Forage harvester was equipped with a pick-up. Rotational speed of the PTO shaft of a tractor 1234 Ursus was recorded with a tachometer (accuracy ± 0.1 rpm) integrated with an MIR 1000 induction torque meter (accuracy ± 0.5 N·m) (Laboratory of Electronics, Poznań, Poland).

The PC-28 pressure (accuracy ± 0.05 MPa) and the FT12 oil flow (accuracy ± 1 dm^3·min^{-1}) intensity transducers (APEK, Marki, Poland) were installed in the duct bleeding oil to sump to measure power requirements of feed rolls. The power requirement of a pick-up unit was measured by a tachometer (accuracy ± 0.1 rpm) integrated with a torque meter (accuracy ± 0.1 N·m) (APEK, Marki, Poland).

The chaff measurements were carried out with the use of the CLP 500/LC510 electronic scales (Radwag, Radom, Poland) with the analog output of the measuring signals, on which the bearing structure of tarpaulin container was mounted; the cut plant material from harvester's discharge spot was collected in this container.

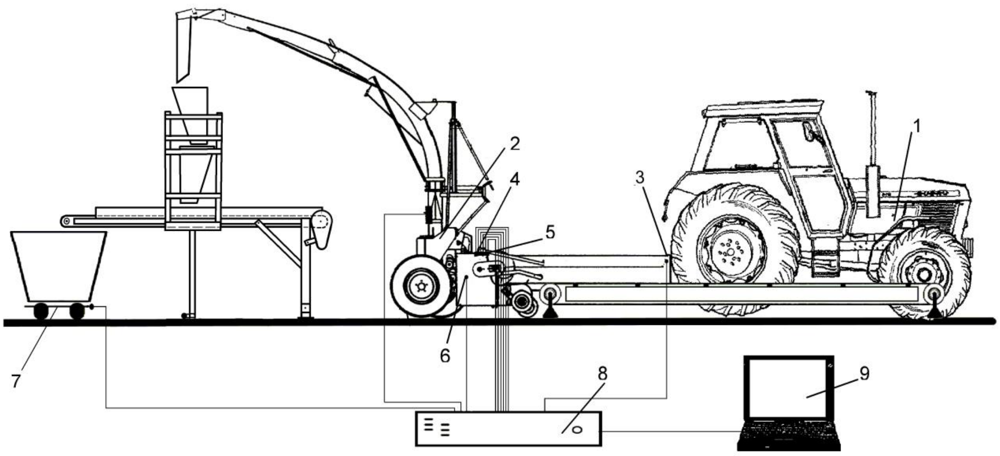

Fig. 1. – The measurement stand: 1 – tractor, 2 – cutter tachometer, 3 – PTO tachometer and torque meter, 4 – pressure and oil flow transducers of hydraulic drive to feed rolls and pick-up, 5 – tachometers on the feed rolls shafts (for control only), 6 – tachometer and torque meter on the pick-up shaft, 7 – electronic scales, 8 – amplifier, 9 – computer

The transducers worked with a Hottinger DMCplus amplifier (HBM, Darmstadt, Germany) and a computer equipped with special software.

On a four-meter section of the conveyor belt the samples of maize shoots of 5 kg, 10 kg and 15 kg were placed (weighing accuracy of ± 0.2 kg). At a constant speed of the conveyor belt of 0.9 m s^{-1} the material mass flow rate of 1.13 kg s^{-1}, 2.25 kg s^{-1} and 3.38 kg s^{-1}, respectively, were obtained. Cutterhead rotation speed was 1000 rpm and the number of knives were 2 and 10. For each measuring system three tests were carried out.

In order to determine the effective power to cutting and feeding and picking-up of the material were taken into account the kinematics of the forage harvester drive.

The power requirement of the flywheel cutter unit was calculated as the difference of the tractor PTO power and the power consumed by the feed rolls and pick-up.

$$P_t = 10^{-3} M_p \frac{\pi n_p}{30}\left(1-\frac{n_p-n_t}{n_p}\right)-\left(\frac{Q_{shg}(p_{shg}-p_o)+Q_{shd}(p_{shd}-p_o)}{60}\right)\frac{1}{\eta_p \eta_c} \tag{1}$$

The power requirement of the feed rolls was calculated as the difference of power absorbed by the hydraulic drive both units and the power require by the pick-up.

$$P_w = \left(\frac{Q_{shg}(p_{shg}-p_o)+Q_{shd}(p_{shd}-p_o)}{60}\right)\eta_s \eta_{cg} \eta_{cd} - 10^{-3} M_a \frac{\pi n_a}{30}\eta_{c1}\eta_{c2} \tag{2}$$

The power requirement of the pick-up was calculated from the formula.

$$P_a = 10^{-3} M_a \frac{\pi n_a}{30}\eta_{c1}\eta_{c2} \tag{3}$$

where: P_t, P_w, P_a – power of cutting, feeding, picking-up, respectively, kW; M_p, M_a – PTO and pick-up shaft torque, respectively, N·m; n_p, n_t, n_a – PTO and cutter and pick-up shafts rotational speed, respectively, rpm; Q_{shg}, Q_{shd} – oil flow to upper and lower hydraulic motors, respectively, dm^3·min^{-1}; p_{shg}, p_{shd} – pressure of oil flowing to upper and lower hydraulic motors, respectively, MPa; p_o – oil pressure at the outlet of the hydraulic motors, MPa; η_p, η_s – overall hydraulic pump and motor efficiency, respectively, $\eta_p = \eta_s = 0.8$; η_s, η_{s1}, η_{s2}, η_{sg}, η_{sd}, effciency of different transmission chains, $\eta_s = \eta_{s1} = \eta_{s2} = \eta_{sg} = \eta_{sd} = 0.98$.

Calculations were made for the two conditions: under load and idling of the forage harvester and on the basis of the difference the effective power for cutting and feeding and picking-up were designated.

The investigation results were analysed statistically with the use of computer statistical package STATGRAPHICS V.12.5.

From each test sample, recorded with a frequency of 50 Hz were obtained about 150 records. After its transformation by the coefficients of the transducer calibration and determination of the power, the assumptions of variance analysis were verified, i.e. normality (Kolmogorov-Smirnov and Lilliefors and Shapiro-Wilk tests and skewness and kurtosis coefficients) and the equality of variance tests (Levene and Brown-Forsythe).

For the power values the analysis of variance relative to the studied factors (moisture content, sample mass, number of knives) was done and then a detailed analysis of the Duncan test was done.

Based on the results of variance analysis and correlation matrix the non-linear regression models of power were evaluated, and its characteristics relative to the main parameters were presented graphically.

RESULTS AND DISCUSSION

On the basis of the carried out tests (Tab. 1) it was stated that the distributions of the values of power for cutting the material can be include to the normal distributions, because in the all cases the p-values at least for one of the Kołmogorow-Smirnow test were not lower than 0.01. More differentiated results were received for tests by Lilliefors and the most powerful by Shapiro-Wilk.

Tab. 1. – The results of the normality test of power cutting (P_t) by Kołmogorow-Smirnow (K-S, D) and Lilliefors (p-Lillifors) and Shapiro-Wilk (WS, W) tests and the skewness and kurtosis coefficients for the power distributions (*w* – moisture content, %; *z* – number of knives; *m* – sample mass, kg; N – number)

Power	*w*	*z*	*m*	N	max D	K-S	p-Lillief.	WS	p-value	Skewness	Kurtosis
P_t	68	5	5	483	0.047872	p > 0.20	p < 0.01	0.9886	0.0008	0.37	0.09
P_t	68	5	10	483	0.048529	p > 0.20	p < 0.01	0.9798	<0.0001	0.53	0.21
P_t	68	5	15	483	0.034326	p > 0.20	p < 0.20	0.9913	0.0062	0.18	–0.45
P_t	68	10	5	644	0.028172	p > 0.20	p > 0.20	0.9946	0.0230	0.27	0.07
P_t	68	10	10	483	0.045982	p > 0.20	p < 0.05	0.9830	<0.0001	0.49	0.17
P_t	68	10	15	483	0.049372	p < 0.20	p < 0.01	0.9866	0.0002	0.15	–0.64
P_t	57	5	5	322	0.073975	p < 0.10	p < 0.01	0.9804	0.0002	0.47	–0.15
P_t	57	5	10	483	0.025433	p > 0.20	p > 0.20	0.9972	0.5903	0.10	–0.20
P_t	57	5	15	483	0.030517	p > 0.20	p > 0.20	0.9930	0.0248	0.23	–0.18
P_t	57	10	5	483	0.045728	p > 0.20	p < 0.05	0.9879	0.0005	0.41	0.10
Pt	57	10	10	483	0.033617	p > 0.20	p < 0.20	0.9899	0.0021	0.36	0.25
Pt	57	10	15	483	0.024129	p > 0.20	p > 0.20	0.9895	0.0015	0.28	0.64

In relation to the values of power feeding and picking-up of the material a slightly weaker test results were obtained (Tab. 2). However it should be emphasized that for all groups of the values of power cutting, feeding and picking-up, the values of skewness and kurtosis coefficients do not exceed the values from the range of <–3,3>. On the basis of the guidelines in the literature (STANISZ, 2007) results that distributions of that skewness and kurtosis indicators can be consider as normal distributions. In the power distributions dominate these with a slight right-skewed, because the values of skewness coefficient *A* are positive (except of one case for P_w, $w = 67\%$, $z = 5$, where the skewness coefficient $A = –0.04$ – it is a very small left-hand skewness, Tab. 2). The power distributions are generally more slender, so they are leptokurtic and for these cases the kurtosis coefficients have positive values. Six from the 24 power distributions are less slender (the values of kurtosis coefficients *K* are negative, Tables 1 and 2), that means they are flattened in relation to the normal distribution – they are platykurtic.

Tab. 2. – The results of the normality test of power feeding (P_w) and picking-up (P_a) by Kołmogorow-Smirnow (K-S, D) and Lilliefors (p-Lillifors) and Shapiro-Wilk (WS, W) tests and the skewness and kurtosis coefficients for these power distributions (w – moisture content, %; z – number of knives; m – sample mass, kg; N – number)

Power	w	m	N	max D	K-S	p-Lillief.	WS	p-value	Skewness A	Kurtosis K
P_w	68	5	1127	0.022783	p > 0.20	p < 0.20	0.9976	0.0961	0.10	0.21
P_w	68	10	966	0.061425	p < 0.01	p < 0.01	0.9758	<0.0001	0.58	1.58
P_w	68	15	966	0.040728	p < 0.10	p < 0.01	0.9956	0.0072	0.15	–0.23
P_w	57	5	805	0.017938	p > 0.20	p > 0.20	0.9983	0.6236	–0.04	0.00
P_w	57	10	966	0.038118	p < 0.15	p < 0.01	0.9943	0.0010	0.21	0.19
P_w	57	15	966	0.047819	p < 0.05	p < 0.01	0.9846	<0.0001	0.47	0.54
P_a	68	5	1127	0.127746	p < 0.01	p < 0.01	0.8850	<0.0001	1.48	2.86
P_a	68	10	966	0.083538	p < 0.01	p < 0.01	0.9273	<0.0001	1.04	1.08
P_a	68	15	966	0.076961	p < 0.01	p < 0.01	0.9462	<0.0001	0.88	0.78
P_a	57	5	805	0.110716	p < 0.01	p < 0.01	0.8834	<0.0001	1.47	2.79
P_a	57	10	966	0.095900	p < 0.01	p < 0.01	0.9182	<0.0001	1.16	1.66
P_a	57	15	966	0.072785	p < 0.01	p < 0.01	0.9446	<0.0001	0.84	0.37

The test results of the analysis of equality of variance (Tab. 3) allow to inference that all of the parameters meet this assumption, because the values of the critical level of significance are not lower than 0.01.

Tab. 3. – The results of the variance equality analysis by Levene and Browna-Forsythe and Welch tests for the power cutting (P_t), feeding (P_w) and picking-up (P_a) of plant material (w – moisture content, %; z – number of knives; m – sample mass, kg).

Parameter	w	z	m	Levene'a test	p-value	Brown-Forsythe test	p-value
P_a	68	5	5	2.92	0.0886	1.55	0.2138
P_a	68	5	10	2.72	0.1002	1.64	0.2013
P_a	68	5	15	6.87	0.0106	6.45	0.0110
P_a	68	10	5	1.60	0.2070	1.08	0.3002
P_a	68	10	10	1.26	0.2712	1.11	0.2776
P_a	68	10	15	0.93	0.3354	1.14	0.2855
P_a	57	5	5	3.20	0.0747	2.09	0.1495
P_a	57	5	10	5.96	0.0152	4.46	0.0355
P_a	57	5	15	5.20	0.0232	4.41	0.0365
P_a	57	10	5	1.87	0.1726	0.67	0.4125
P_a	57	10	10	1.07	0.3019	0.43	0.5105
P_a	57	10	15	0.36	0.5517	0.11	0.7459
P_t	68	5	5	2.59	0.1082	2.29	0.1309
P_t	68	5	10	0.01	0.9234	0.01	0.9267
P_t	68	5	15	0.49	0.4842	0.49	0.4839
P_t	68	10	5	1.32	0.2523	1.24	0.2671
P_t	68	10	10	2.37	0.1588	2.24	0.1696
P_t	68	10	15	3.42	0.0654	3.25	0.0722
P_t	57	5	5	0.29	0.5903	0.32	0.5718
P_t	57	5	10	6.96	0.0101	6.70	0.0102
P_t	57	5	15	3.82	0.0516	3.60	0.0588
P_t	57	10	5	3.10	0.0792	3.11	0.0787
P_t	57	10	10	6.64	0.0101	6.61	0.0101

Parameter	w	z	m	Levene'a test	p-value	Brown-Forsythe test	p-value
P_t	57	10	15	0.06	0.8002	0.12	0.7241
P_w	68	5	5	1.97	0.1616	1.82	0.1779
P_w	68	5	10	0.23	0.6317	0.10	0.7471
P_w	68	5	15	6.19	0.0105	6.77	0.0107
P_w	68	10	5	0.27	0.6057	0.67	0.4128
P_w	68	10	10	5.23	0.3036	3.94	0.2102
P_w	68	10	15	5.89	0.0116	5.21	0.0176
P_w	57	5	5	0.48	0.4878	0.50	0.4785
P_w	57	5	10	6.73	0.0102	6.80	0.0102
P_w	57	5	15	6.79	0.0101	6.68	0.0101
P_w	57	10	5	0.28	0.5981	0.23	0.6292
P_w	57	10	10	6.45	0.0114	6.17	0.0116
P_w	57	10	15	0.95	0.3298	0.92	0.3393

After the verification of assumptions, that the values of power have distributions close to the normal and the equality of variances and considering the large number of observations in the trial ($n_i > 30$), the multivariate analysis of variance was carried out (Tab. 4). On the basis of the test results it can be concluded, that all of the main factors (moisture content, number of knives and sample mass for the power of cutting, or moisture content and sample mass for the power of feeding and picking-up) and the most of double interactions and the triple interaction had statistically significant influence on the power values differentiation ($p < 0.05$). Only for power cutting, the double interaction of the number of knives and sample mass was statistically insignificant ($p = 0.3788$).

Tab. 4. – The results of the variance analysis for the power cutting (P_t), feeding (P_w) and picking-up (P_a) relative to the moisture content (w) and number of knives (z) and sample mass (m)

Power	P_t		P_w		P_a	
	F	p-value	F	p-value	F	p-value
w	134.34	<0.0001[a]	136.24	<0.0001	19.41	<0.0001
z	120.35	<0.0001[a]				
m	3156.97	<0.0001[a]	2057.49	<0.0001	478.40	<0.0001
$w \times z$	37.71	<0.0001[a]				
$w \times m$	5.60	0.0037[a]	28.17	<0.0001	12.06	<0.0001
$z \times m$	0.97	0.3788				
$w \times z \times m$	3.92	0.0200[a]				

[a] – statistically significant difference at $p < 0.05$.

For the identified significance of the Fisher-Snedecor statistic ($p<0.05$), the further detailed analysis of the differences between the values of independent means was conducted. For this purpose the Duncan test was used (Tab. 5). In the Tab. 5 the results for moisture content and number of knives were summarized, although the inference about differentiation for the two levels of factor is possible directly from the analysis of variance (Tab. 4). The results of the Duncan test allow to inference that the differences between the power values are statistically significant differentiated between all of the factors levels.

The developed matrix of the correlation indicators for the variable input parameters of power (Tab. 6) allows to inference, that all of the values combinations are characterized by cohesion between themselves. Although in some cases the values of correlation coefficients are low, they are statistically significant, because the critical value of the correlation coefficient is 0.0021. The values of the correlation coefficients between the power and the moisture content are negative. It is logical, because the plant material of higher moisture content (68%) was characterized by lower rigidity than the material of less moisture content

(57%). The higher moisture content (68%) was near the value identified as an optimal value (65%), when the rigidity of the plant, calculated as a product of the modulus of elasticity and the moment of inertia, is the lowest one. At this moisture content, the plant deformation consisting in the compaction, compressing or bending, requires the lowest energy expenditures (KANAFOJSKI, 1980).

Tab. 5. – The results of a detailed analysis of the average values made by Duncan test

Parameter	Level	P_t, kW	P_w, kW	P_a, kW
Moisture w, %	68	9.39^a	0.70^a	0.13^a
	57	11.28^b	0.80^b	0.16^b
Sample mass m, kg	5	4.91^a	0.41^a	0.05^a
	10	10.39^b	0.74^b	0.13^b
	15	15.56^c	1.10^c	0.24^c
Knive z	5	9.98^a		
	10	10.56^b		

Tab. 6. – Correlation matrix of variables and power parameters

Parameter	w	z	m	P_t	P_w	P_a
w	1.0000					
z	0.0399	1.0000				
m	–0.0492	–0.0681	1.0000			
P_t	–0.1555	0.0474	0.7174	1.0000		
P_w	–0.1688	0.0340	0.6419	0.6105	1.0000	
P_a	–0.0731	–0.0311	0.3763	0.3249	–0.0691	1.0000

The critical values for the number of 5796 at the significance level of α=0.05 are 0.0021.

The very high (rating by STANISZ, 2007) positive (0.7174) correlation was also obtained between the power cutting and the sample mass and between the power feeding and the sample mass (0.6419). Noteworthy is also a very high cohesion (0.6105) between the power cutting and the power feeding. The power picking-up rather weakly correlates with the input parameters, and with the rest of power cutting and feeding values.

On the basis of the previous conclusion, the nonlinear models of regression for power cutting, feeding and picking-up were developed (Tab. 7). Only formulas for which statistically significant regression coefficients were obtained, were summarized in that table. The best evaluation (R = 0.735) has the model of power cutting and afterward the model of power feeding (R = 0.667). Although the model of power picking-up has statistically significant regression coefficients, the general evaluation of this model is weak (R = 0.383) and it should be taken and interpreted with caution.

Tab. 7. – Analysis of regression for power cutting, feeding and picking-up

Parameter	P_t				P_w				P_a			
	estimate	error	t-value	p-value	estimate	error	t-value	p-value	estimate	error	t-value	p-value
b_0	–2.280	0.226	–10.10	<0.001	5.7044	0.742	7.68	<0.001	–0.1817	0.0741	–2.45	0.014
$b_1(w^2)$					0.0015	<0.001	8.08	<0.001				
$b_2(m^2)$					0.0008	<0.001	2.11	0.035				
$b_3(w)$	–0.006	0.002	–2.42	0.016	–0.1856	0.024	–7.82	<0.001	0.0021	0.0012	1.79	0.073
$b_4(m)$	1.576	0.125	12.61	<0.001	0.1566	0.014	11.36	<0.001	0.0444	0.0068	6.55	<0.001
$b_5(wm)$	–0.008	0.002	–4.09	<0.001	–0.0017	<0.001	–9.14	<0.001	–0.0004	0.0001	–3.76	<0.001
$b_6(z)$	0.598	0.147	4.06	<0.001								
Equation	$P_t = b_0 + b_3 w + b_4 m + b_5 wm + b_6 z$				$P_w = b_0 + b_1 w^2 + b_2 m^2 + b_3 w + b_4 m + b_5 wm$				$P_a = b_0 + b_3 w + b_4 m + b_5 wm$			
R	0.735				0.667				0.383			

The graphic interpretation of these models were presented on the Fig. 2 and 3. The waveforms of the power cutting graphs are different from the power feeding ones. In the optimal range of the material moisture content of 65%, the power cutting has reached the highest value. It results from the plants rigidity. In the cutting process occur phenomena involved with a convertible compression of the material and its cutting, namely the fragmentation under influence of the knife-edge pressure and exceeding of the acceptable material stresses. At this moisture content, the material has compacted easier but it was harder to divide it. From the cutting theory results (REZNIK, 1967; KANAFOJSKI, 1980), that in that process dominates fragmentation of the material under influence of the knife-edge pressure and it is easier to compact and cut thinner layers of the material. With a smaller number of knives ($z = 5$), the frequency of cutting is lower and because of that the power request for cutting was lower than with a higher number of knives ($z = 10$) and it was 9.98 kW and 10.56 kW, respectively (for average values of the moisture content and sample mass). The doubling of knives number did not increase directly proportional the request for power, because the smaller particles require lower kinetics energy for their ejection to overcome their lower inertia. LISOWSKI ET AL. (2005) found that during cutting the material for longer sections there is required a lower torque, but the ratio of the top request for the torque to average value is higher. That indicates that in this conditions the tractor of lower power can be used, but the higher engine power reserve is necessary.

The mathematical model of the effective power requirement for work of the chopping unit reflecting the phenomena occurring during the cuts, friction, ripping, compression and the dynamic influence of the working elements on corn plant.

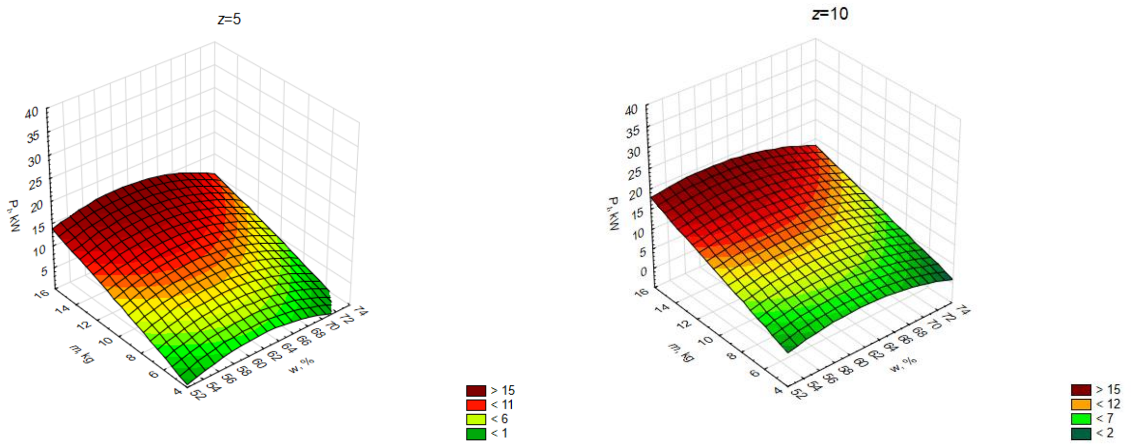

Fig. 2. – Power cutting (P_t) regarding to the moisture content (w) and the mass of the material (*m*) during work by unit with 5 and 10 knives

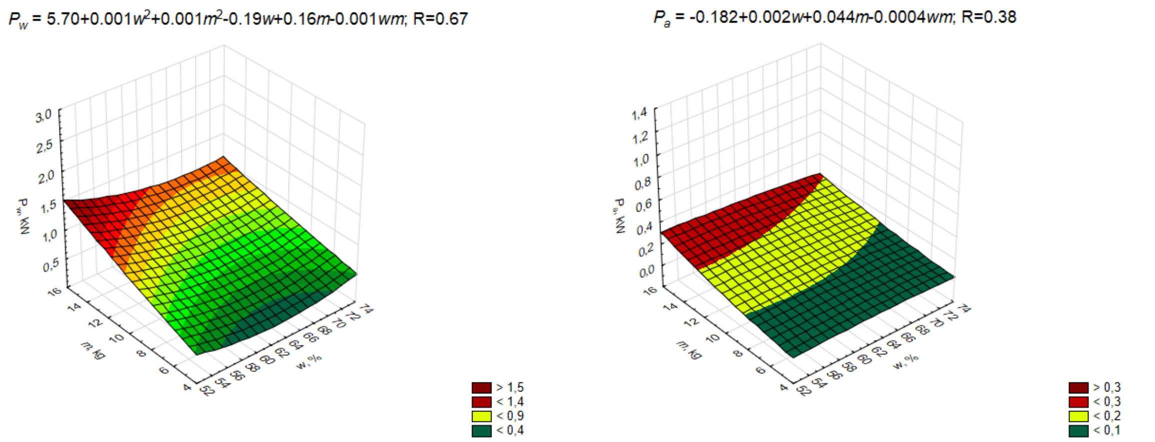

Fig. 3. – Power feeding (P_w) and picking-up (P_a) regarding to the moisture content (w) and the mass of the material (m)

The wide review of research works relating to chopping, conducted by O'DOGHERTY (1982), contained also similar information on an energetic model structure of work of the chopping unit.

All those works also considered components of idle running power which is related to the friction resistances at kinematic pairs of working elements and movement resistances of the driving gear and air resistances. O'DOGHERTY (1982) clearly pointed out that both components of power were related to the work resistances on idle running of the unit.

Because the material is compacted, compressed and bent between the feed rolls, under optimal moisture content of the material (65%), when it has the lowest rigidity, the request for the power feeding was the lowest (Fig. 3). The plant material of the lowest moisture content has generated higher resistances and it was harder to compact it and in the consequence this has translated into increase of the request for the feeding power by feed rolls.

The share of the effective power for the cutting unit was 92%, for the feed rolls 7%, and for the pick-up unit 1% only.

GARBERS AND FRERICHS (2001) indicate that the power needed to rolling the machine is 9% of the total power, and the cutting units of maize consume 7% of that power, the feed and bent rolls – 4%, the chopping trammel – 54%, and the additional chopping devices – 26%, including 8% for the power used to the actuator of the chopped material discharge spout.

KLONOWSKI ET AL. (2005) proved that the total power measured on the PTO during picking-up the grass from the shaft, under the full load of the machine, was 40.8 kW, whereof 3.6 kW was on the units feeding the plant material to the cutting unit and 4.2 kW on the rolling the machine. Because in the forage harvester the additional devices or elements that support chopping were not used, it can be accept that the power taken on the chopping process is the difference of the total power and the power of feeding units and the power involved with the rolling. This difference is 35.4 kW, which is 86% of the power request for the entire machine. The total idle running power was approximately 8 kW, where was 50% for the flywheel chopping unit.

The obtained results from the conducted tests indicate that the share of the power cutting is significantly higher than it results from previous tests, but these investigations were conducted in the stationary conditions and therefore the share of the power needed to feeding the material was significantly lower than in the natural conditions.

At increasing load of the forage harvester by pant material, under constant feeding speed, the relative request on the process of cutting and picking-up has increased and for the sample mass of 5, 10 and 15 kg was 0.982, 1.039 and 1.037 $kW\cdot kg^{-1}$, and 0.010, 0.013 and 1016 $kW\cdot kg^{-1}$, respectively, and for feeding – it has decreased and was 0.082, 0.074 and 0.073 $kW\cdot kg^{-1}$, respectively. These results confirm the theoretical considerations that the thicker layers of the material are more difficult to cut.

CONCLUSIONS

1. The characteristics of the request for the effective power for cutting and feeding processes of the maize plant material in the units of the forage harvester were inverse in relations to each other and had the maximum and minimum values, respectively, under optimal material moisture content (65%), at which the rigidity of the plants is the lowest.
2. The doubled cutting frequency doesn't generate the same increase of requirement for power for cutting unit work, because the smaller particles require lower kinetic energy to overcome their lower inertia.

ACKNOWLEDGEMENTS

This work was funded by the National Centre for Research and Development by a grant PBS2/A8/18/2013, which is gratefully acknowledged.

REFERENCES

1. ASABE STANDARDS: Method of determining and expressing particle size of chopped forage materials by screening ANSI/ASABE S424.1 (R2007). In: ASABE Standards 2011, ASABE, St. Joseph, MI, USA, 2011a: 792–794.
2. ASABE STANDARDS: Moisture measurement – forages ASABE S358.2 (R2008). In: ASABE Standards 2011, ASABE, St. Joseph, MI, USA, 2011b: 781.
3. AUERNHAMMER, H.: Precision farming – the environmental challenge. Comput. Electron. Agr., 30(1–3), 2001: 31–43.
4. CHATTOPADHYAY, P.S. – PANDEY, K.P.: Influence of

knife configuration and tip speed on conveyance in flail forage harvesting. J. Agr. Eng. Res., 78(3), 2001: 245–252.
5. GARBERS, H. – FRERICHS, L.: Leistungs- und Technologieentwicklung von selbstfahrenden Feldhäckslern. Landtechnik, 56(6), 2001: 394–395.
6. KANAFOJSKI, C.: Agricultural machines, theory and construction. 2(1), PWRiL, Warsaw, 1980.
7. KLONOWSKI J., LISOWSKI A., SYPUŁA M.: Investigation on mass dynamic pressure force in discharge channel and power requirement for driving the forage harvester during grasses chopping. Ann. Warsaw Agr. U. SGGW – AR, Agr., 47, 2005: 19–26.
8. KLONOWSKI J., LISOWSKI A.: Investigation on power requirement for driving the forage harvester knife disk with respect to yield monitoring. Ann. Warsaw Agr. U. SGGW – AR, Agr., 50, 2007: 27–31.
9. KROMER, K.-H., SCHMITTMANN, O., OSMAN, A.M.: Crop yield monitoring on forage harvesters. ASAE Paper No. 99–1051. St Joseph, MI, 1999.
10. LISOWSKI, A., FIGURSKI, R., KOSTYRA, K., SYPUŁA, M., KLONOWSKI, J., ŚWIĘTOCHOWSKI, A., SOBOTKA, T.: Effect of maize variety and harvesting conditions on the maize chopping process, compacting susceptibility and quality of silage designed for biogas production. Ann. Warsaw U. Life Sci. – SGGW, Agr. (Agr. Forest Eng.), 2014, 64: 25–38.
11. LISOWSKI, A., KLONOWSKI J., NIEWĘGŁOWSKI K.: Effect of additional elements on breaking-up of maize grain harvested with forage harvester with the chopping unit. Ann. Warsaw Agr. U. SGGW – AR, Agr., 50, 2007: 21–26.
12. LISOWSKI, A., KLONOWSKI, J., BULIŃSKI, J., GACH, S., WARDECKI, P.: Loading on tractor PTO during shredding of maize with the forage harvester under conditions of stationary investigations. Ann. Warsaw Agr. U. SGGW – AR, Agr., 48, 2005: 35–40.
13. LISOWSKI, A., ŚWIĄTEK, K., KLONOWSKI, J., SYPUŁA M., CHLEBOWSKI, J., NOWAKOWSKI, T., KOSTYRA, K., STRUŻYK, A.: Movement of chopped material in the discharge spout of forage harvester with a flywheel chopping unit: measurements using maize and simulation. Biosyst. Eng., 111, 2012: 381–391.
14. O'DOGHERTY, M.J.: A review of research on forage chopping. J. Agr. Eng. Res., 27, 1982: 267–289.
15. OSOBOV, W.I., BARANOV, A.A., KUZNECOV, N.W.: Analysis of broken up mass in the forage harvester. Trakt. Sel'khoz., 2, 2002: 29–30 (in Russian).
16. REZNIK, N.E.: Development direction of the resistance and durability of the agriculture machine elements. Tract. Sel'khoz., 2, 1967: 29–31 (in Russian).
17. ROBERGE, M., SAVOIE, P., NORRIS, E.R.: Evaluation of crop processor in pull-type forage harvester. Trans. ASAE, 41(4), 1998: 967–972.
18. SAVOIE, P., TREMBLAY, D., THÉRIAULT, R., WAUTHY, J.-M., VIGNEAULT, C.: Forage chopping energy vs. length of cut. Trans. ASAE, 32(2), 1989: 437–442.
19. SCHMITTMANN, O., OSMAN, A.M., KROMER, K.H.: Durchsatzmessung bei Feldhäckslern. Landtechnik, Jg., 55(4), 2000: 286–287.
20. SHINNERS, K.J., STELZLE, M., KOEGEL, R.G.: Improving the throwing effectiveness of an upward-cutting forage harvester. Trans. ASAE, 37(4), 1994: 1059–1067.
21. STANISZ A.: Accessible statistics course using the Statistica.pl on examples from medicine. 1, 2, 3, StatSoft Polska, Cracow, 2007 (in Polish).
22. VANSICHEN, R., DE BAERDEMAEKER J.: A measurement technique for yield mapping of corn silage. J. Agr. Eng. Res., 55, 1993: 1–10.

Corresponding author:
Aleksander Lisowski, Department of Agricultural and Forest Engineering, Faculty of Production Engineering, Warsaw University of Life Sciences, Nowoursynowska Street 166, 02-787 Warsaw, Poland

ENERGY UTILIZATION OF BY-PRODUCTS FROM MECHANICAL RECYCLING PROCESS OF ELECTRONIC WASTE

J. Malaťák[1], J. Bradna[1], P. Hrabě[1], M. Kučera[2]

[1]*Department of Technological Equipment of Buildings, Faculty of Engineering, Czech University of Life Sciences Prague, Czech Republic*
[2]*Faculty of Environmental and Manufacturing Technology, Technical University in Zvolen, Slovakia*

Abstract
The article deals with energy utilization of by-products from the mechanical recycling of electrical and electronic equipment. This is essentially crushed mixed plastic and dust from dust removal and filtration process. Final products of this technology are primarily metal parts, other by-products are landfilled. Individual samples are analysed for fuel properties and are determined element analyses and defined stoichiometric models of combustion.
The values of elemental composition show a high proportion of non-combustible particles that reach up to 77%. Mixed plastic is only material which can be used without major modifications (under 0.7 mm) and has 34% of ash with calorific value of 22.39 MJ.kg^{-1}. The values of stoichiometric calculations indicate different parameters of supplied combustion air amount, amount of flue gas and combustion temperatures. These differences are based primarily on total amount of carbon and hydrogen in the elemental composition of the original samples and the differences are also recorded in the graphic dependency of CO_2 on oxygen content in exhaust gas.

Key words: calorific value, combustion temperature, carbon dioxide, excess air coefficient, ash.

INTRODUCTION

Production of electrical and electronic equipment is the fastest growing sector of industrial development. Handling and processing of electronic waste (e-waste) will continue to be a topic of interest in the future (WIDMER ET AL., 2005; CUI, FORSSBERG, 2009). High diversity in the composition of e-waste is the result of fast technological progress in the electronics industry, which introduces difficulties for the development of universal, sustainable recycling processes (HILTY, 2005; BAZARGAN ET AL., 2012). The effects of various organic and metal components of electronic waste on human health and the environment are summarized based on the available knowledge in (WONG ET AL., 2007; DIMITRAKAKIS ET AL., 2009). A negative effect on the environment and health caused by electronic waste is increasingly important. E-wastes are made up of different organic substances and metals in a polymer matrix. Organic substances, particularly fire retardants and other additives are potential carcinogens (NNOROM&OSIBANJO, 2009). Toxic heavy metals such as cadmium, chromium, mercury and lead are released into the environment, mainly through electronic waste leaching and incineration. These metals are highly toxic and represent a high risk to human health and are a major negative influence on the environment (WONG ET AL., 2007; DIMITRAKAKIS ET AL., 2009).

Among methods for recycling of electronic waste there are chemical processes: pyrolysis, gasification, depolymerization and hydrogenolytic degradation to obtain chemical raw materials or fuels or currently perspective mechanical processing (GUO ET AL., 2009). Some experience in the pyrolysis and combustion processing of printed circuit boards in a horizontal combustion unit to determine the level of pollutant gaseous substances are described by MOLTÓ ET AL. (2009) at temperature 500°°C and MOLTÓ ET AL. (2011) at temperatures around 850°°C. Kinetic study of mobile phone thermal decomposition was carried out under variousthermogravimetric measurements at temperature 500°°C in study FONT ET AL. (2011). More than 50 compounds, including carbon oxides, light hydrocarbons and polycyclic aromatic hydrocarbons (PAHs) were identified and quantified.
The aim of the article is not research of the main products of recycling technology. The article deals with by-products from recycling line for e-waste, for which there is no further use and therefore are landfilled. New legislative requirements for waste treatment strictly recommend energy utilization before landfilling. Therefore this article deals with the energy use of by-products for combustion with regard to their combustion characteristics and emission production. The contribution of the article is the analysis of by-

products from mechanical processing of electronic waste which are intended for energy use. The materials are plastics sized up to 1.5 mm, dust captured from the cyclone and dust from the filter.

MATERIALS AND METHODS

Sampling is carried out on a line for processing e-waste by physical methods. Incoming material is mainly from offices and collective collection of e-waste. Hazardous substances are first sorted out from the e-waste at the input to the line. Subsequently twin-shaft shredder coarsely crushes and a single shaft grinder finely grinds this material. Crushed and ground material is led by air into cyclone separators where a dust fraction is separated and the finest particles end in a dust filter. Material for separation proceeds to a buffer container and from there by vibratory conveyor is led to a fluidized bed sluice. On the separation area of the fluidized bed sluice separation occurs due to vibrations and material suspension by air stream. Input material into several product groups according to their specific weight, e.g. pertinax (PCB?) and metals separation. By-products from fluidized bed sluice are collected into separate containers.

The following material fractions were captured: I. mixed plastic from fluidized bed sluice (1.5 to 0.7 mm), II. mixed plastic from fluidized bed sluice (below 0.7 mm), III. dust from cyclone and IV. dust from filter. The proportion of these individual fractions in the line consists of: about 6.2% wt. for I. mixed plastic, about 2.3% wt. for II. mixed plastic, about 2.5% wt. for dust from cyclone and about 3% wt. for dust from filter.

Determination of water and ash contents is done according to CSN Solid recovered fuels - Determination of ash content using a thermogravimetric analyzer (EN 15403). Determination of sulfur (S), hydrogen (H), carbon (C) is measured by infrared spectroscopy (analyzer CHN+S) and the emission factor by calculation. Determination of nitrogen (N) by thermal conductivity detection in a CHN analyzer. Determination of chloride concentration after combustion is determined spectrophotometrically according to CSN Stationary sources of emissions - Determination of mass concentration of gaseous chlorides expressed as HCl - Standard reference method (CSN EN 1911). Determination of gross calorific value is determined by the calorimetric method in an isoperibolic calorimeter and heating value by calculation using standard Solid recovered fuels - Determination of gross calorific value and heating value (CSN EN 15400).

Individual samples were analysed by stoichiometric calculations. During this analysis real molar volumes of gas were used values to calculate the theoretical dependence of the emission concentration amounts of CO_2 on the excess air coefficient n.

The theoretical amount of emission concentrations of CO_2 (m^3.kg^{-1}) is based on the equation:

$$CO_2 = \frac{\frac{22{,}27}{12{,}01} \cdot C}{v^s_{sp_{\min}}} \cdot 100 \tag{1}$$

The theoretical amount of dry flue gases (m^3.kg^{-1}) is based on the equation:

$$v^s_{sp_{\min}} = \frac{22{,}27}{12{,}01} \cdot C + \frac{21{,}89}{32{,}06} \cdot S + \frac{22{,}40}{28{,}013} \cdot N + 0{,}7805 \cdot L \tag{2}$$

Where the theoretical amount of dry air L (m^3.kg^{-1}) is determined from the equation:

$$L = O_{\min} \cdot \frac{100}{21} \tag{3}$$

The theoretical amount of oxygen O_{min} (m^3.kg^{-1}) is based on the equation:

$$O_{\min} = \frac{22.39}{12.01} \cdot C + \frac{22.39}{4.032} \cdot H + \frac{22.39}{32.06} \cdot S - \frac{22.39}{31.99} \cdot O \tag{4}$$

Where C, H, S and O are contents of carbon, hydrogen, sulfur and oxygen in the fuel sample (% wt.).

Adiabatic combustion temperature t_a (°C) is determined for further evaluation of the samples. This temperature characterizes a fuel's adiabatic combustion conditions and determines the conditions of complete combustion when $n = 1$. The adiabatic temperature of combustion is expressed by the equation:

$$t_a = \frac{Q_n}{v^s_{sp_{\min}} \cdot c_{sp}} \tag{5}$$

Where $v^s_{sp,\ min}$ is the volume of flue gas when n = 1 (m^3.kg^{-1}) and c_{sp} is the specific heat capacity of flue gas (kJ.m^{-3}.K^{-1}).

The theoretical combustion temperature t_t (°C)is used as a reference for different fuels at different or the same conditions of the combustion process. This temperature allows to change the values of combustion air consumption ($n \geq 1$), fuel enthalpy value ($Q_p \geq 0$) and air specific enthalpy ($Q_{vz} \geq 0$) and is determined from the equation:

$$t_t = \frac{Q_n + Q_p + Q_{vz}}{v^s_{sp_{\min}} \cdot c_{sp}} \tag{6}$$

RESULTS AND DISCUSSION

The average values of elemental composition most important for fuel utilization are shown in Tab. 1. The limiting factor for direct combustion is the concentration of combustible and non-combustible components in the samples. Most limiting for chosen samples is the measured high concentration of ash. Especially in samples of mixed plastic in size of 1.5 to 0.7 mm, samples from the cyclone and the dust filter determined ash content has gone above the limit amount. The amount of ash significantly affects the fuel properties of assessed solid samples and consequently affects both the selection and the setting of combustion device as indicated by MALAŤÁK ET AL. (2015). Similar results of mineral composition of raw input material have been achieved by MOLTÓ ET AL. (2009).

Tab. 1. – The final values of elemental analysis

Sample / Average values	Water Content (% wt.)	Ash (% wt.)	Gross Calorific Value (MJ/kg)	Net Calorific Value (MJ/kg)	Carbon C (% wt.)	Hydrogen H (% wt.)	Nitrogen N (% wt.)	Sulphur S (% wt.)	Oxygen O (% wt.)	Chlorine (% wt.)
	W	*A*	Q_s	Q_i	*C*	*H*	*N*	*S*	*O*	*Cl*
I. original sample	0.84	**33.74**	22.39	21.76	41.56	5.27	0.01	0.17	18.2	1.89
I. dry sample	-	**34.02**	23.12	21.96	41.92	5.31	0.01	0.17	18.34	-
II. original sample	0.49	11.85	**31.49**	**29.86**	63.23	**7.42**	0.01	0.11	15.90	**2.84**
II. dry sample	-	11.91	**31.65**	**30.02**	63.54	**7.46**	0.01	0.11	15.97	-
III. original sample	0.99	**76.70**	**6.26**	**5.89**	**13.70**	1.58	> 0.01	0.15	5.90	0.391
III. dry sample	-	**77.46**	**6.32**	**5.97**	**13.87**	1.60	> 0.01	0.15	5.96	-
IV. original sample	0.78	**75.04**	**6.98**	**6.58**	**15.91**	1.73	>0.01	0.09	5.40	0.337
IV. dry sample	-	**75.63**	**7.03**	**6.65**	**16.03**	1.74	> 0.01	0.09	5.44	-

Large amounts of ash influenced mainly the calorific value of samples and thus percentage of combustible elements. Highest calorific value was achieved in the sample of mixed plastic in the size under 0.7 mm as shown in Tab. 1 while the sample also reached the highest hydrogen concentration.

Significant quantities of chlorine have been found mainly in samples of mixed plastic. The negative influence of chlorine is based on two effects of HCl emissions. First, it may affect the formation of polychlorinated dibenzo / dioxins and furans (PCDD / F) and there are also the corrosive effects of HCl and its derived compounds (LAUNHARDT ET AL., 1998).

The values of stoichiometric calculations (Tab. 2) show various flue gas parameters of examined samples converted to normal conditions, dry flue gas and to n = 1. Stoichiometry shows how parameters of calorific value, ash content and energy density affect selection or design of the combustion device and setting for optimum combustion. Concentration particularly of ash, hydrogen, oxygen and chlorine in the assessed samples are varying relatively widely. This fact is confirmed also by performed flue gas analyses.

Tab. 2. – Theoretical flue gas values from stoichiometric calculations

Sample / Average values	Theoretical amount of air		Theoretical amount of dry flue gases		Theoretical concentration of carbon dioxide in dry flue gases	
	$kg.kg^{-1}$	$m^3.kg^{-1}$	$kg.kg^{-1}$	$m^3.kg^{-1}$	% wt.	% vol.
I. original sample	5.82	4.48	7.92	4.27	19.24	18.04
II. original sample	9.15	7.05	11.23	6.68	20.64	17.54
III. original sample	1.87	1.44	3.93	3.03	12.79	18.29
IV. original sample	2.20	1.69	4.25	1.62	13.72	18.16

I. original sample

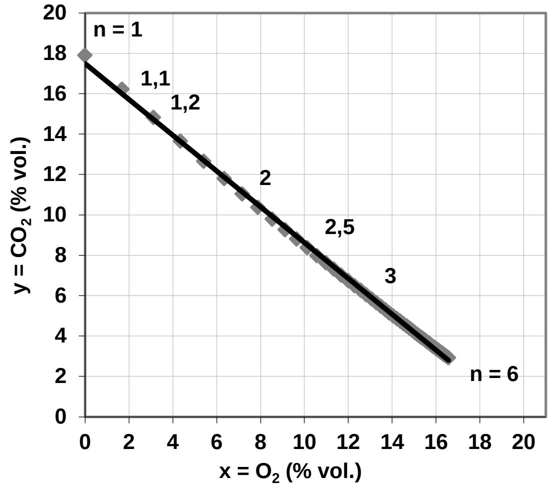

y = -0.8861x + 17.482

II. original sample

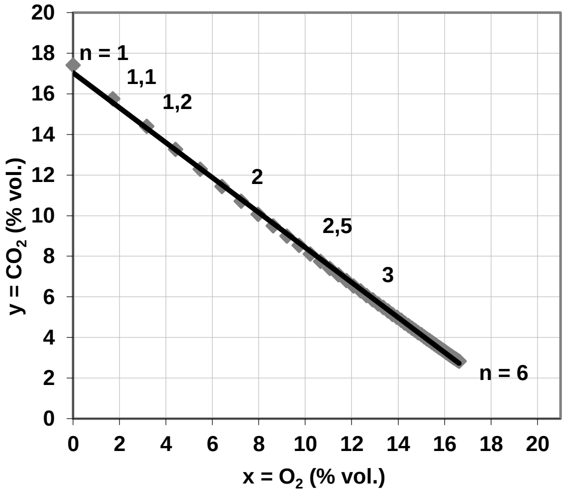

y = -0.8614x + 17.041

III. original sample

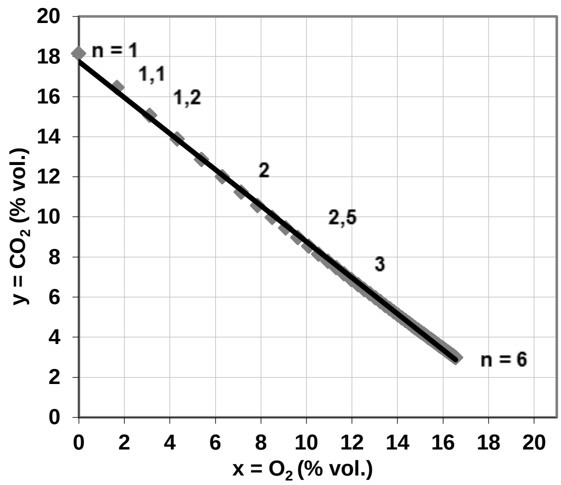

y = -0.8987x + 17.742

IV. original sample

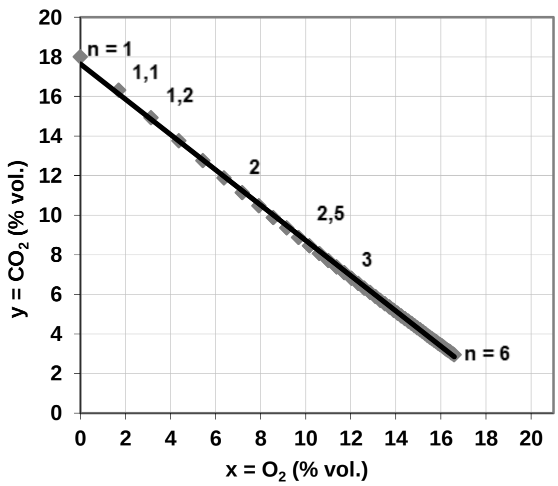

y = -0.8918x + 17.64

Fig. 1. – Dependence of CO_2 emission concentration on the oxygen content O_2 in the flue gas with the expression of the excess air coefficient n

For each sample a graph of dependence of the carbon combustion to carbon dioxide on the oxygen content in the flue gas (Fig. 1) is shown. For these dependencies a linear regression equation was fitted. The trends are influenced by the amount of carbon and the share of other elements in the fuel and thus by the maximum concentration of carbon dioxide in the flue gas (see Tab. 2). Similar results were achieved by MALAŤÁK ET AL. (2008); WEI ET AL. (2012); MALAŤÁK & BRADNA (2014).

No less important parameter for comparison of samples is the adiabatic combustion temperature t_a (°C). This is determined for I. sample of mixed plastic (1.5 to 0.7 mm) t_a =*2808 °C*, for II. sample of mixed plastic (under 0.7 mm) t_a =*2560 °C*, for III. sample of dust from the cyclone t_a =*2446 °C*and for IV. sample of dust from the filter t_a =*2350 °C*. The theoretical combustion temperature t_t (°C) is used for comparison of samples at the same conditions of the combustion process in dependence on excess air coefficient *n*. LIU ET AL. (2013); LOU ET AL. (2016) confirm that the concentration of nitrogen oxides depends both on combustion temperatures above 1000 °C, but also on the amount of supplied air, which is expressed by excess air coefficient, which is mentioned in the literature by value about 2–3 (CHAIKLANGMUANG ET AL., 2002; MALAŤÁK ET AL., 2008; HOUSHFAR ET AL., 2011).

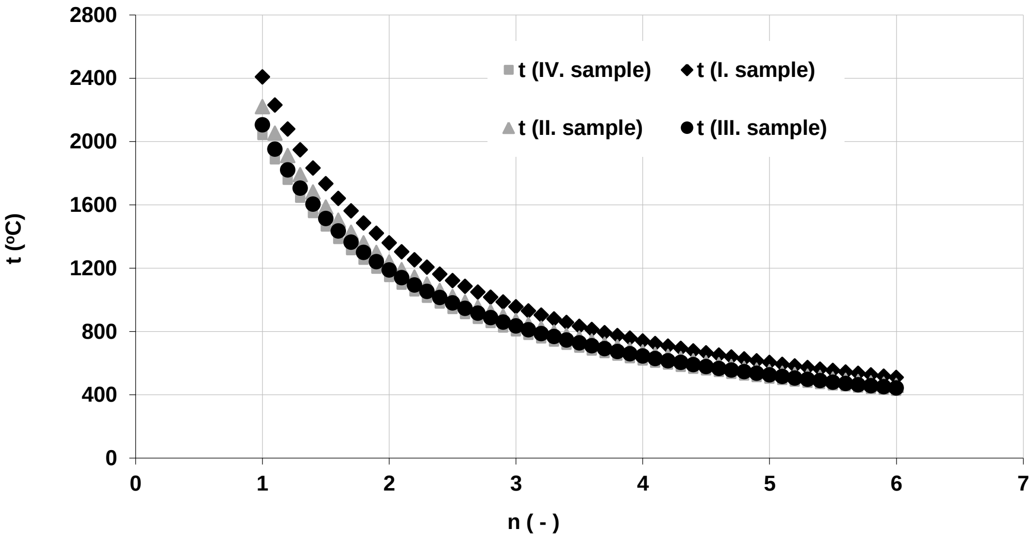

Fig. 2. – Theoretical combustion temperature t_t of individual original samples depending on the excess air coefficient *n*

CONCLUSIONS

Samples of mixed plastic I. (under 0.7 mm) have a high calorific value and a reasonable amount of non-combustible matter. These samples may serve as an alternative fuel that is equal to the quality of coal. Unfortunately the size of these samples under 0.7 does not allow direct combustion in conventional boilers, but is possible for example in a fluidised combustion device. Another possibility is pyrolysis processing.

High portion of non-combustible matter of 34% wt. in samples of mixed plastic (1.5 to 0.7 mm) rather restricts its other direct energy utilization. Therefore it is necessary to modify this material by reduction of the ash concentration to the allowable amount by mixing with other energetic material (e.g. biomass). Such modified fuel can be used in combustion devices where the intended fuel has similar properties. There is also the possibility of co-combustion with other energetic material or new design of specific combustion device.

The other, very problematic, samples from the process of e-waste recycling are those from the cyclone and the dust filter with a high percentage of non-combustible matter above 75%. This material is finally evaluated as energetically negative and cannot be used without substantial modification for energy purposes. Another issue is the actual elemental composition of ash, which contains some risky elements such as lead, mercury and PAHs coming from the e-waste. These risk characteristics are also monitored, but not discussed in this article.

ACKNOWLEDGEMENTS.

The article was financially supported by the Internal Grant Agency of the Czech University of Life Sciences Prague TF (IGA) no. 2016:31170/1312/3114.

REFERENCES

1. FONT, R., MOLTÓ, J., EGEA, S., CONESA, J.A.: Thermogravimetric kinetic analysis and pollutant evolution during the pyrolysis and combustion of mobile phone case. Chemosphere, 85 (3), 2011: 516-524.
2. GUO, J., GUO, J., XU, Z.: Recycling of non-metallic fractions from waste printed circuit boards: A review. Journal of Hazardous Materials 168 (2-3), 2009: 567-590.
3. HILTY, L.M.: Electronic waste - An emerging risk? (Editorial). Environmental Impact Assessment Review, 25 (5), 2005: 431-435.
4. HOUSHFAR, E., SKREIBERG, Ø., LØVÅS, T., TODOROVIĆ, D., SØRUM, L.: Effect of excess air ratio and temperature on NOx emission from grate combustion of biomass in the staged air combustion scenario. Energy and Fuels, 25, 2011: 4643– 4654.
5. CHAIKLANGMUANG, S., JONES, J.M., POURKASHANIAN, M., WILLIAMS, A.: Conversion of volatile-nitrogen and char-nitrogen to NO during combustion. Fuel, 81 (18), 2002: 2363-2369.
6. LAUNHARDT, T., STREHLER, A., DUMLER-GRADL, R., THOMA, H., VIERLE, O.: PCDD/F- and PAH-emission from house heating systems. Chemosphere, 37 (9-12), 1998: 2013–2020.
7. LIU, H., CHANEY, J., LI, J., SUN, C.: Control of NOx emissions of a domestic/small-scale biomass pellet boiler by air staging. Fuel, 103, 2013: 792–798.
8. LOU, B., XIONG, Y., LI, M., WANG, X., MA, K.: NOx emission model for the grate firing of biomass fuel. BioResources, 11 (1), 2016: 634-650.
9. MALAŤÁK, J., BRADNA, J.: Use of waste material mixtures for energy purposes in small combustion devices. Research in Agricultural Engineering, 60 (2), 2014:50-59.
10. MALAŤÁK, J., JEVIČ, P., GÜRDIL, G.A.K., SELVI, K.C.: Biomass heat-emission characteristics of energy plants. AMA, Agricultural Mechanization in Asia, Africa and Latin America, 39 (4), 2008: 9-13.
11. MALAŤÁK, J., KIC, P., SKANDEROVÁ, K.: Energetic use of solid products of pyrolysis technology. Agricultural Engineering International: CIGR Journal 2015, 2015: 208-217.
12. MOLTÓ, J., EGEA, S., CONESA, J.A., FONT, R.: Thermal decomposition of electronic wastes: Mobile phone case and other parts. Waste Management, 31 (12), 2011: 2546-2552.
13. MOLTÓ, J., FONT, R., GÁLVEZ, A., CONESA, J.A.: Pyrolysis and combustion of electronic wastes. Journal of Analytical and Applied Pyrolysis, 84 (1), 2009: 68-78.
14. NNOROM, I.C., OSIBANJO, O.: Toxicity characterization of waste mobile phone plastics. Journal of Hazardous Materials, 161 (1), 2009: 183-188.
15. WEI, W., ZHANG, W., HU, D., OU, L., TONG, Y., SHEN, G., SHEN, H., WANG, X.: Emissions of carbon monoxide and carbon dioxide from uncompressed and pelletized biomass fuel burning in typical household stoves in China, Atmospheric Environment, 56, 2012: 136 – 142.
16. WIDMER, R., OSWALD-KRAPF, H., SINHA-KHETRIWAL, D., SCHNELLMANN, M., BÖNI, H.: Global perspectives on e-waste (Review). Environmental Impact Assessment, 25 (5), 2005: 436-458.
17. WONG, M.H., WU, S.C., DENG, W.J., YU, X.Z., LUO, Q., LEUNG, A.O.W., WONG, C.S.C., LUKSEMBURG, W.J., WONG, A.S.: Export of toxic chemicals - A review of the case of uncontrolled electronic-waste recycling. Environmental Pollution, 149 (2), 2007: 131-140.

Corresponding author:

doc. Ing. Jan Malaťák, Ph.D., Department of Technological Equipment of Buildings, Faculty of Engineering, Czech University of Life Sciences Prague, Kamýcká 129, Praha 6, Prague, 16521, Czech Republic, phone: +420 22438 3205, e-mail: malatak@tf.czu.cz

EFFECT OF SOIL TILLAGE TECHNOLOGIES ON SOIL PROPERTIES IN LONG TERM EVALUATION

J. Mašek[1], J. Chyba[1], J. Kumhálová[1], P. Novák[1], A. Jasinskas[2]

[1]*Czech University of Life Sciences Prague, Czech Republic*
[2]*Aleksandras Stulginskis University, Lithuania*

Abstract
Soil compaction is a major problem of modern agriculture. Soil compaction increases due to growth of the weight of agricultural machines and the number of passes over land. Soil compaction may be significantly reduced by using suitable soil tillage. One indicator of compaction can be cone index. It was established field trial with six variants of tillage. On 3 variants were used ploughing systems and other 3 used reduced systems of tillage. Experiment was conceived as a multi-annual and was run from 2010 to 2014. The soil on the land was shallow sandy loam cambisol. Registration penetrometer was used for measurement. Cone index was measured at the depth of 0.04 m to 0.32. Each plot had size 6 x 50 m. The results were evaluated after 5 years of the experiment. The results showed a difference of the cone index values between variants. The variants with ploughing are apparent initial favourable effect of loosening with a strong transition of not processed layers. There are no visible transitions in variants with reduced tillage. But the values of cone index in the surface layers have higher values than the variants with ploughing.

Key words: cone index; soil compaction; soil compaction; tillage systems.

INTRODUCTION

Agricultural machinery is an integral part of modern agriculture; however, it brings adverse effect on soil compaction. The soil compaction affects soil physical properties; for example increases soil bulk density leads to a reduction of soil water infiltration rate. Combination of these adverse effects that leads to soil erosion and may affect overall crop yields (CHYBA ET AL., 2014). Besides the influence of the wheels, soil compaction may occur during some operations, such as mouldboard plough tillage (especially during the subsequent ploughing processes to the same depth every year) when there is a compaction layer under the bottom of furrows. Soil compaction leads to yield losses, because it prevents crop root systems penetrating through the compacted soil and reaching the water and nutrition, compaction also has adverse impacts on ecology (HŮLA ET AL., 2009). There is a decrease in the ability of soil to absorb water and during intense rainfall can lead to surface water runoff. For lighter soils there is an increased risk of soil erosion due to surface runoff and erosive wash (BALL ET AL., 1999). Another consequence of soil compaction is an increase in energy demands of soil tillage, which adversely affects the germination of cultivated crops (GELDER ET AL., 2006).

Soil compaction affects mainly the physical properties of soil either in the short term or the long term. For example, at higher soil moisture, agricultural traffic may lead to excessive soil compaction (NOVÁK ET AL., 2015). The negative effect of soil compaction is manifested for example by increasing cone index, bulk density, etc. which results in reduced porosity, soil infiltration, stability index, etc. (CASTELLANO AND VALONE, 2007). All these parameters are interconnected and together affect crop yields negatively. Another factor that affects the named values is soil structure and its aeration. In the event that soil is loosened the soil has greater water capacity than non-loosened soil (KROULÍK ET AL., 2007). Each soil structure has its own typical values of bulk density, porosity, hydraulic properties etc. For example, sandy loam soil has higher cumulative infiltration than clay loam soil. While the lowest values can be found for clay soils (EKWUE AND HARRILAL., 2010).

MATERIALS AND METHODS

The field trial was established on the light cambisol with an average slope of 5.4 °. The plot is located in the area Nesperká Lhota in central Bohemia Region at an altitude of 420 m. The field trial consists of six variants. Plot of land for each variant was 6 m x 50 m in length side is facing the fall line.

After the harvest of triticale (crush straw) the site was in the second half of August 2009 followed by shallow tillage with disc tiller. In variants 4, 5, 6 the post-harvest residues were remained on the ground in autumn, without further processing Three followed options in October 2009 the unilaterally plow tillage to a depth of 0.2 m (driving in the direction of contour sets, tilting the hunk the slope). Then tillage and seeding in the spring as indicated in each experiment variants below. The field trial is repeated for several years since 2009. Tillage and seeding was repeated for each variant every year.

Variants of experiment:

1. Conventional tillage technology for corn - ploughing in the fall, winter left rough wake, spring sowing soil preparation with harrow, corn sowing.
2. Variant of tillage, spring cereals - ploughing in the fall, winter left rough wake, spring sowing soil preparation with harrow, oats sowing.
3. Variant of tillage, corn with inter row crop (winter cereal crop sown in spring- triticale) - ploughing in the fall, winter left rough wake, spring sowing soil preparation with harrow, triticale sowing, corn sowing.
4. Variant of reduced tillage- in the fall without tillage, spring tillage by tine cultivator to a depth of 0.10 m, corn sowing.
5. Variant no tillage, spring cereals - only spring oats sowing.

Variant conservation tillage- corn without spring sowing soil preparation – loosening into depth of 0.2 m, sowing intercrop in autumn (white mustard), corn sowing in the spring.

Cone index has been another measured value provided by the registration penetrometer. For measuerement was used PN-10 penetrometer with cone angle of 30 ° (area of 100 mm^2). Soil physical properties have been evaluated by Kopecky's cylinders with volume of 100 cm^3. Samples were taken and then subsequently analyzed in the laboratories of the CULS Prague. Each measurement was repeated 10 times. Measuring point was always out of the track of the tractor. Data were processed by the programmes MS EXCEL (MICROSOFT CORP., USA) and STATISTICA 12 (STATSOFT INC.,USA).

RESULTS AND DISCUSSION

Table 1 shows the values of density of the soil for all variants. It is possible to conclude a gradual change in the physical properties of soil especially in variants with reduced soil tillage. It consists in reducing the bulk density. For bulk density, the values of 2013 were generally highest in all seasons of measurement. This was probably due to persistent rain, which caused the leaching of fine soil particles. The lowest values of bulk density were recorded for variant 6. This is probably due to the influence of freezable intercrop and its root system. Conversely, a positive effect was not observed during autumn ploughing. The soil was exposed to settlement of soil particles through the winter. Tab. 2 shows the porosity of the soil in all variants. Tab. 1 and Tab. 2 shows average values of ten repetitions. The measured values confirmed the trend which was inferred from the values of bulk density. The measured values showed a gradual increase porosity values for variants with reduced soil tillage. Influence of freezable crops has been again recorded in the sixth variant.

Tab. 1. – Bulk density [g.cm^{-3}] of individual variants

Variant	Depth [m]	2010	2011	2012	2013	2014
1	0.05-0.1	1.53	1.54	1.57	1.62	1.57
	0.1-0.15	1.48	1.52	1.47	1.57	1.55
	0.15-0.2	1.44	1.48	1.61	1.53	1.53
2	0.05-0.1	1.54	1.51	1.59	1.63	1.57
	0.1-0.15	1.48	1.56	1.58	1.57	1.55
	0.15-0.2	1.46	1.51	1.51	1.61	1.52
3	0.05-0.1	1.33	1.45	1.54	1.49	1.48
	0.1-0.15	1.45	1.55	1.48	1.53	1.52
	0.15-0.2	1.47	1.49	1.52	1.56	1.51
4	0.05-0.1	1.57	1.48	1.44	1.52	1.50
	0.1-0.15	1.47	1.42	1.47	1.50	1.46
	0.15-0.2	1.61	1.40	1.42	1.54	1.49
5	0.05-0.1	1.59	1.47	1.46	1.49	1.50
	0.1-0.15	1.58	1.41	1.48	1.48	1.49
	0.15-0.2	1.51	1.47	1.56	1.54	1.52
6	0.05-0.1	1.53	1.51	1.44	1.48	1.49
	0.1-0.15	1.44	1.47	1.48	1.47	1.46
	0.15-0.2	1.48	1.44	1.44	1.51	1.47

Tab. 2. – Porosity [%] of individual variants

Variant	Depth [m]	2010	2011	2012	2013	2014
1	0.05-0.1	39.90	37.56	37.04	37.50	38.50
	0.1-0.15	41.99	39.47	38.51	39.48	40.62
	0.15-0.2	43.44	40.18	42.41	40.84	41.92
2	0.05-0.1	38.63	39.12	40.99	36.31	38.47
	0.1-0.15	41.23	36.64	37.90	38.76	37.88
	0.15-0.2	40.97	42.9	40.86	38.51	40.91
3	0.05-0.1	47.78	38.33	38.63	40.21	37.65
	0.1-0.15	43.22	37.24	41.23	40.62	39.16
	0.15-0.2	42.32	36.14	40.97	39.78	40.44
4	0.05-0.1	37.04	40.27	42.98	40.01	39.85
	0.1-0.15	38.51	42.79	44.24	41.59	40.85
	0.15-0.2	42.41	43.06	41.64	45.80	39.74
5	0.05-0.1	40.99	43.92	44.87	41.81	39.86
	0.1-0.15	37.90	42.44	41.10	41.20	41.20
	0.15-0.2	40.86	41.62	39.40	41.67	40.08
6	0.05-0.1	39.58	44.12	43.45	40.37	38.85
	0.1-0.15	43.45	40.76	42.05	44.32	41.23
	0.15-0.2	42.05	42.25	42.25	42.90	40.61

Root system of the white mustard plants influenced porosity values especially in the topsoil layer. For variants 1-3, the loosening effect subsided after ploughing during winter when the soil was left dormant. It was quite surprising that the porosity values for variant 4 had not been much influenced by loosening during spring season.

Fig. 1 is a graph of cone index values for individual variations in 2010. Measurements by penetrometer was performed on 1. 6. 2010. Due to the shallow soil profile the measurement was made into a relatively small depth. Among the variants was lower trend of penetration resistance for plowed variants (1,2,3) versus reduced (4,5,6). This applies especially to the depth of tillage. In greater depth the differences were minimal. Cone index values in 2010 were influenced by the previous method of soil tillage before establishment of experiment.

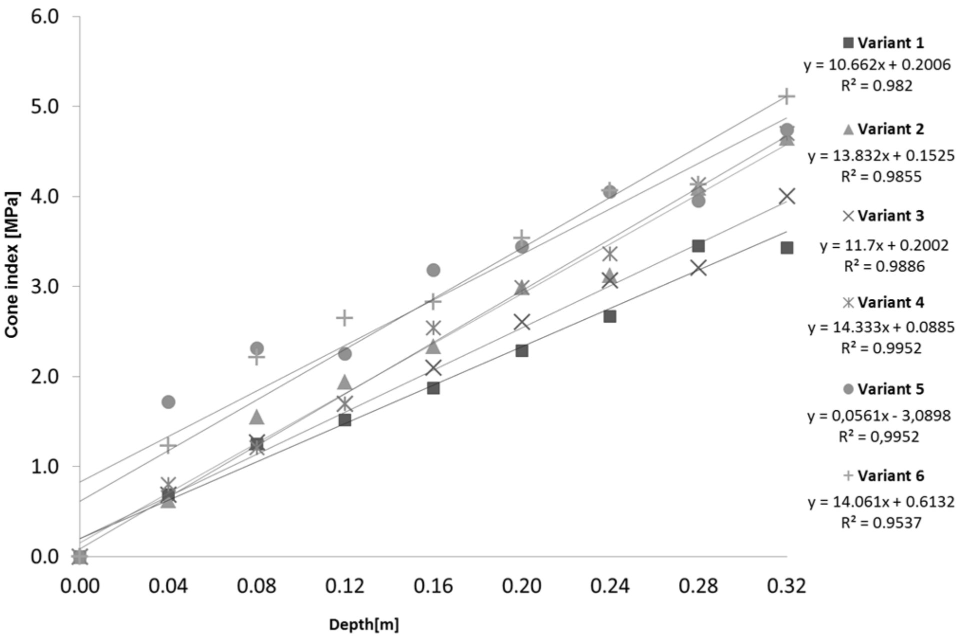

Fig. 1. – Cone index of all variants in 2010

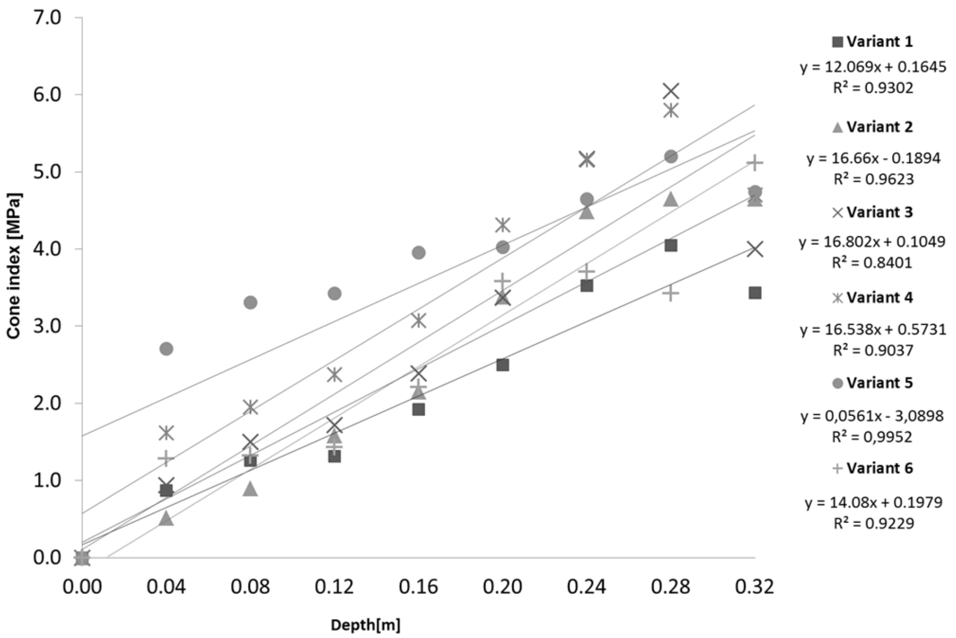

Fig. 2. – Cone index of all variants in 2011

The graph in Fig. 2 shows values of cone index in 2011. Measurements by registration penetrometer was held on 24. 5. 2011. The results confirmed the conclusions from the measurements of undisturbed soil samples (Tab. 1 and 2). It shows partial reduction of cone index values for variants with reduced soil tillage. Most of this applies to variant 6, where there was a noticeable positive effect of freezable crop. Lower values again showed variants using ploughing (1,2,3). This is especially applicable for the depth less than 0.2 m. Conversely, variant 5 (no till- oats) showed high values even at low depths.

The graph in Fig. 3 shows the values of cone index in 2012. Measurements by registration penetrometer were carried out 1. 6. 2012. It marked reduction of cone index values, especially in variants 6. Positive effect of freezable crop is again noticeable. Lower values showed variations with ploughing especially to a depth of 0.24 m. Conversely, variant 5 (oats – no till) again showed high values even at low depths. Cone index values are generally lower than in previous years. This could be caused by long lasting black frosts in March, 2012.

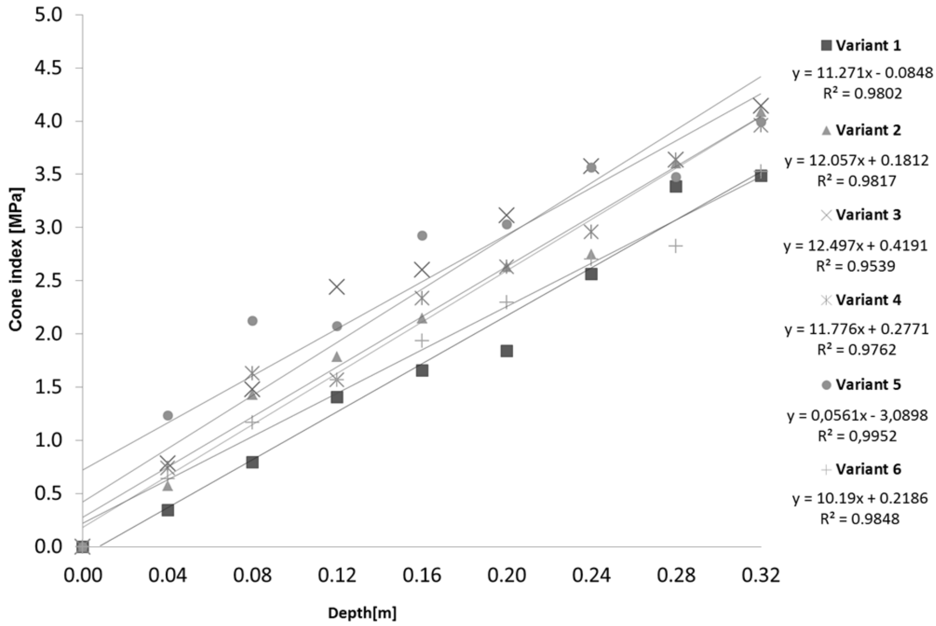

Fig. 3. – Cone index of all variants in 2012

The graph in Fig. 4 shows the values of cone index in 2013. The cone index measurement was carried out 11. 6. 2013. The results of measured cone index values mirrored the trend of previous measurements. Sharp increase in cone index was seen at a depth of 0.24 m for variants with ploughing, it was obviously compaction under depth of processing. In contrast, positive effect of the intercrops could be seen for variant 6, again also at greater depths. The highest values in the surface layer were recorded for variant 5. Measured values could be affected by the heavy rains during late May. Moisture conditions of individual variants were different. The graph in Fig. 5 shows the values of cone index in 2014. Cone index measurements were carried out 3. 6. 2014. This trend was also confirmed during last year. Variants using ploughing, again, exhibited lower values than the variants with reduced tillage technology.

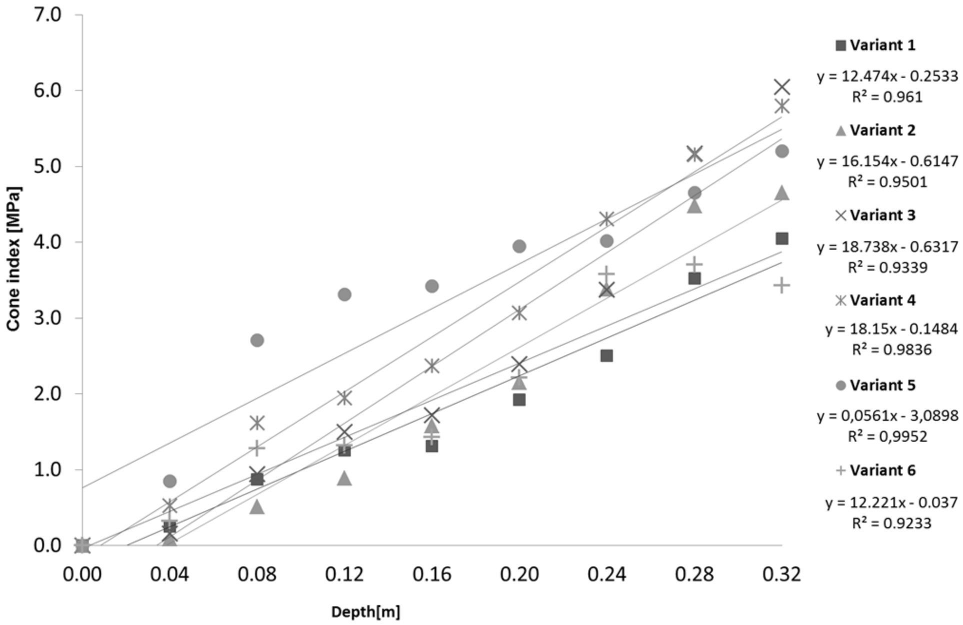

Fig. 4. – Cone index of all variants in 2013

Increase of cone index can be successfully described by linear regression. This is evident from Fig. 1 to 5, despite the changes in the values it can be observed particularly in depths of tillage and just below. This is mainly due to the effect of various working tools of machines for tillage. There was no observed decrease in cone index values when using reduced tillage technologies. Conversely KOUWENHOVEN ET AL. (2002) found positive effect of reduced technology on this parameter. This pertained to lands with clay soil. HŮLA ET AL. (2009) also did not find beneficial effect of reduced technologies on cone index. EKWUEME & HARRIL ET AL. (2010) highlights the possibility of different behavior of individual soil types. This probably explains the difference in the studies. Measurements were also affected the moisture conditions and date of measurement.

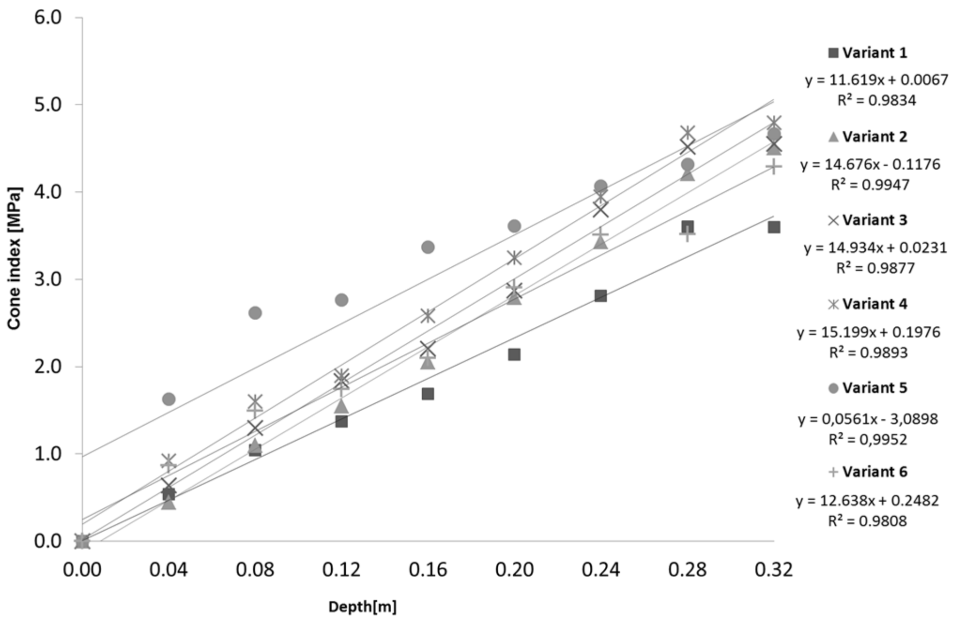

Fig. 5. – Cone index of all variants in 2014

Decrease in bulk density and increase in porosity has been observed for variants using reduced technology during the five year trial. The presented results are consistent with the conclusions of MOTAVALLI ET AL. (2003). There was a gradual change in soil structure, accompanied by changing of the soil physical properties. It also confirms the conclusions drawn by RADFORD ET AL. (2007).

CONCLUSIONS

During the measurement of soil physical properties can be observed favorable effect of reduced technology on the soil bulk density. However this was not confirmed by cone index measurements. So far, the work has been unable to clearly demonstrate the beneficial effect of reduced soil tillage technology on cone index. This is probably due to the variance of the measured values. Another possibility is the influence of soil parameters. The third possibility is the influence of organic matter.

Firm conclusions cannot be drawn by these measurements. It was measured in only one location with one soil type. Research needs to be validated in more locations in order to eliminate the influence of the local environment.

ACKNOWLEDGEMENTS

Supported by the Ministry of Agriculture of the Czech Republic - Project no. QJ1520028.

REFERENCES

1. BALL, B. C., PARKER, J. P., SCOTT, A.: Soil and residue management effects on cropping conditions and nitrous oxide fluxes under controlled traffic in Scotland. Soil & Tillage Research 52, 1999: 191-201.
2. CASTELLANO, M. J., VALONE, T. J.: Livestock, soil compaction and water infiltration rate: Evaluating a potential desertification recovery mechanism. Journal of Arid Environments, 71, 2007: 97–108.
3. CHYBA, J., KROULÍK, M., KRIŠTOF, K., MISIEWICZ, P., CHANEY, K.: Influence of soil compaction by farm machinery and livestock on water infiltration rate on grassland. Agronomy Research 12, 2014: 59-64.
4. EKWUE, E. I., HARRILAL, A.: Effect of soil type, peat, slope, compaction effort and their interactions on infiltration, runoff and raindrop erosion of some Trinidadian soils. Biosystems Engineering, 105(1), 2010: 112–118.
5. GELDER, B. K., CRUSE, R. M., ZHANG, X. Y.: Comparison of Track and Tire Effects of Planter Tractors on Corn Yield and Soil Properties. The Power & Machinery Division of ASABE, 50, 2006: 365-370.
6. HŮLA, J., KROULÍK, M., KOVAŘIČEK, P.: Effect of repeated passes over the soil on degree of soil compaction, pp., Prague: ČZU, In GPS autopiloty v zemědělstvi. CULS Prague, 2009: 39-44 (in Czech).
7. KOUWENHOVEN J.K., PERDOK U.D., BOER J., OOMEN G.J.M.: Soil management by shallow mouldboard ploughing in The Netherlands. Soil & Tillage Research 65, 2002: 125–139.
8. KROULÍK, M., HŮLA, J., ŠINDELÁŘ, R., ILLEK, F.: Water Infiltration into soil related to the soil tillage intensity. Soil & Water Research, 1, 2007: 15-24.
9. NOVAK, P., MAŠEK, J., BENEŠ, L., KUMHALOVA, J.: Evaluation of qualitative parameters of selected soil tillage machines for loosening soil without turning, Engineering for Rural Development 2015, 2015: 16-21.
10. MOTAVALLI P.P., STEVENS W.E., HARTWIG G.: Remediation of subsoil compaction and compaction effects on corn N availability by deep tillage and application of poultry manure in a sandy-textured soil. Soil & Tillage Research 71, 2003: 121–131.
11. RADFORD B.J., YULE D.F., MCGARRY D., PLAYFORD C.: Amelioration of soil compaction can take 5 years on a Vertisol under no till in the semi-arid subtropics. Soil & Tillage Research 97, 2007: 249-255.

Corresponding author:

assoc. prof. Ing. Jiří Mašek. Ph.D., Department of agricultural machines, Faculty of Engineering, Czech University of Life Sciences Prague, Kamýcká 129, Praha 6, Prague, 16521, Czech Republic, phone: +420 22438 3213, e-mail: masekj@tf.czu.cz

DYNAMIC CHARACTERISTICS OF THE KARAKURI TRANSPORT TROLLEY

I. Mašín[1], T. Riegr[2]

[1]Institute for Nanomaterials, Advanced Technology and Innovation, Technical University in Liberec, Czech Republic
[2]Department of the Design of Machine Elements and Mechanism, Technical University in Liberec, Czech Republic

Abstract
Karakuri is a mechanical device that utilizes natural physical phenomena (most frequently gravity force and electromagnetism) and elemental mechanisms (cams, springs, levers, rollers etc.) to perform handling operations in a less-energy or low-energy mode. Karakuri mechanisms may be utilized for handling of individual objects (e.g. product or component) or substances in packaging (e.g. animal fodder in bags). The paper deals with the dynamic behaviour of the karakuri transport trolley that uses accumulation of potential energy in compression springs. The presented research was focused on the basic speed-time and distance-time characteristics of the specific karakuri trolley that has significant potential for use in agriculture.

Key words: karakuri, trolley, transport, mechanism, distance, speed.

INTRODUCTION
The Japanese word „karakuri“ means a mechanical device to trick, or take a person by surprise. Central to the karakuri philosophy is concealment of technology, to evoke feelings and emotions, and a sense of hidden inner magic (MURATA and KATAYAMA, 2010, KATAYAMA et al. 2014). Traditional application of karakuri mechanisms are unique Japanese karakuri dolls (see Fig. 1). The karakuri tradition continues to influence the Japanese view of robots, robotics, low cost automation or lean manufacturing (OLSON, 2000). Karakuri devices are now used to make production or handling operations easier and more ergonomic and to increase productivity or decrease operational costs. A significant characteristic of karakuri devices is their minimal impact on the environment because they consume little or no energy. During last two decades karakuri-based devices were designed and realized mainly in the automotive industry to save energy, to decrease work-load or to reduce time of production or handling operations. These (kaizen) activities are carried out mainly in progressive companies such as Toyota, Daikin, Aisin Seiki, Honda and other.

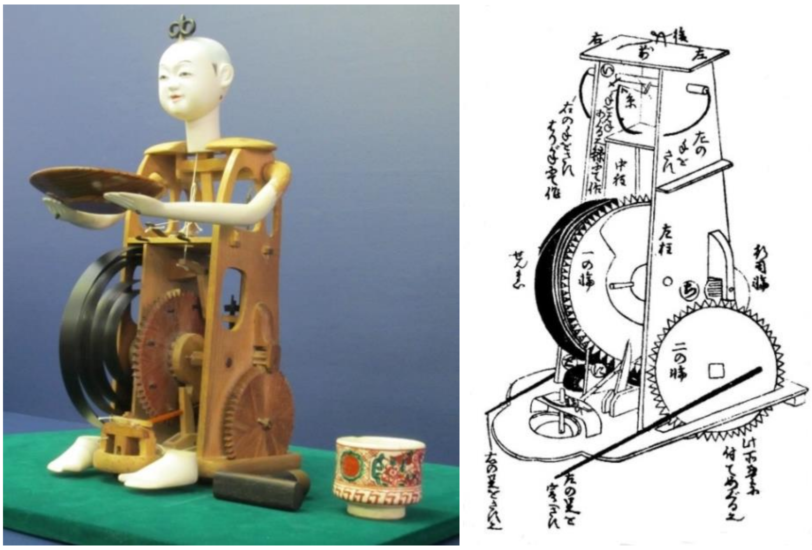

Fig. 1. – Mechanical moving doll (JAPAN TODAY,2015; KYOTO UNIVERSITY MUSEUM,2007)

These and other industrial enterprises use karakuri devices for the following purposes:

- Development, design and installation of low CO2 production technologies based on simplification, process streamlining or energy saving of moving parts.
- Improvement of energy use efficiency by recovery of wasted energy or storing of energy,
- Elimination of unnecessary or irrational (human) efforts.
- Utilization of unpowered technologies or technologies based on low-thrust operation energy.

From the point of view of unpowered technologies or technologies based on low-thrust operation energy we can use following elementary phenomena, mechanisms or components:

- Gravitation force (weight) - see Fig. 2
- Magnetic force
- Lever mechanism (seesaw mechanism)
- Cam mechanism
- Link mechanism
- Lock-up or release mechanism
- Spring
- Gear etc.

Fig. 2. – Simple karakuri structure for handling operation using gravitation force to provide efficient storage and easy unloading process (AMS, 2014)

In the field of agriculture, various (manual) handling operations must be performed through the year. Farmers have to move objects off the ground on a conveyor or move objects manually or by conveyor from point A to point B (e.g. handling of containers with vegetables or bags with compost or animal fodder). Most of these operations are trivial, repetitive, and require quite a lot of energy and power delivered by workers or technology (Fig. 3).

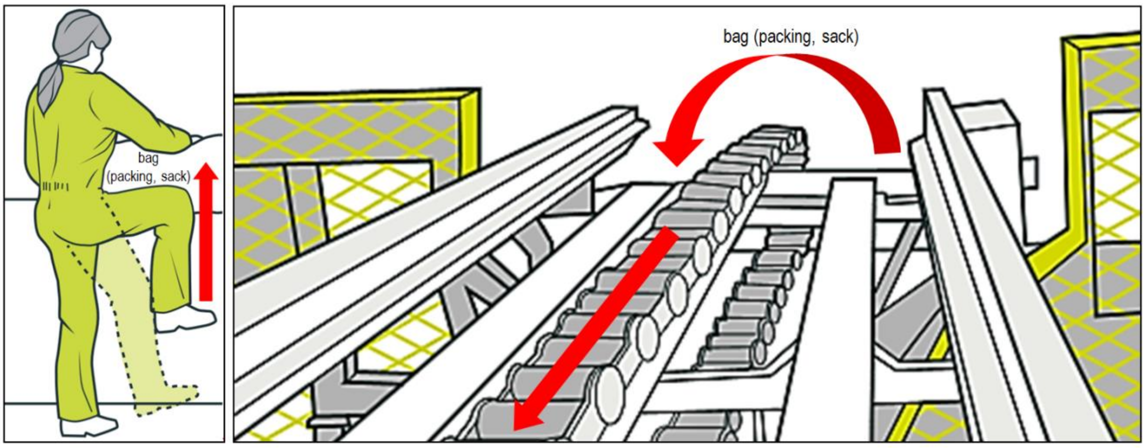

Fig. 3. – Examples of manual handling operation and chain conveyor used in agriculture(WORK SAFE NZ, 2014)

From the above it is clear the use of karakuri idea in agriculture and agricultural engineering is meaningful. Therefore the paper discusses one aspect of agricultural karakuri based device - the dynamic behavior of karakuri transport trolley. The goal of presented initial research was determination of time dependence for passed distance and trolley movement speed by defined transported weight (10 kg and 20 kg).

MATERIALS AND METHODS

The experimental trolley was designed for internal transport of objects between two places away 3.0 m (defined by kinematic design of gearbox). After insertion of transferred object to the box located on top of trolley the movement trolley is started (potential energy of transferred object is changed to kinematic energy). When the trolley drives off the distance it stops and after removal of the transported object from the box the trolley starts to move back to the starting position using the energy accumulated into the press springs during the forward movement.

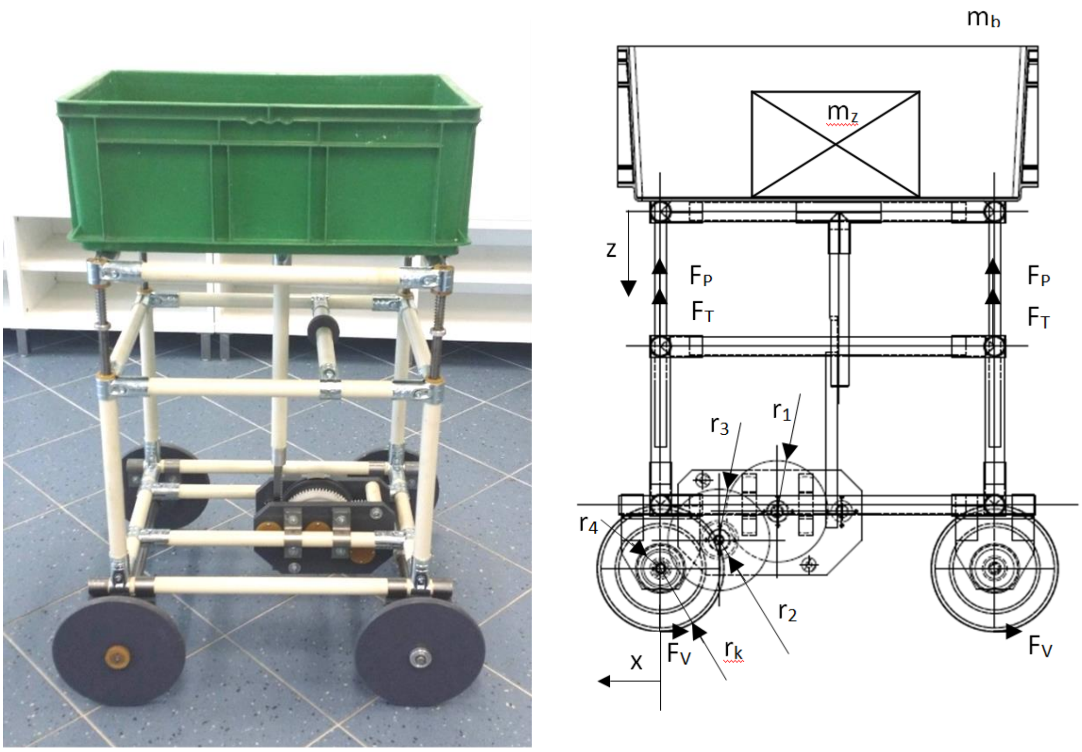

Fig. 4. – Design of the experimental karakuri trolley

Tab. 1. – Characteristics of trolley parts

Quantity	Name of part	Weight	MOI	Velocity		
				Shift X	Shift Z	Rotation
1	box + upper frame + cogged rack	m_b	-	$\dot{x}$	$\dot{z}$	0
1	transferred object	m_z	-	$\dot{x}$	$\dot{z}$	0
1	frame of trolley	m_p	-	$\dot{x}$	0	0
1	gear wheel Nr.1	m_1	J_1	$\dot{x}$	0	$\dot{\phi}_1$
1	gear wheel Nr.2	m_2	J_2	$\dot{x}$	0	$\dot{\phi}_2$
1	driven gear incl. pinion	ms_1	J_{s1}	$\dot{x}$	0	$\dot{\phi}_s$
1	not driven gear	ms_2	Js_2	$\dot{x}$	0	$\dot{\phi}s$

Total trolley weight:

$$m_{total} = m_b + m_z + m_p + m_1 + m_2 + m_{s1} + m_{s2} \qquad (1)$$

Dynamic characteristics were solved by defining a second order differential movement equations using the method of reduction of mass and force magnitudes on his frame. For solving mathematical equations software Maple were then used. Used method for reduction of mass and force magnitudes on frame is based on theory of kinetic energy change:

$$\frac{dK}{dt} = P \qquad (2)$$

$$\overset{*}{K} = \frac{1}{2} m_r \dot{x}^2 \ , \quad m_r = \text{konst.} \qquad (3)$$

$$\frac{\overset{*}{d}K}{dt} = m_r \ \dot{x} \ \ddot{x} \qquad (4)$$

Kinetic energy of karakuri trolley during his movement:

$$K = \frac{1}{2}(m_b+m_z)(\dot{x}^2+\dot{z}^2) + \frac{1}{2} m_p \dot{x}^2 + \frac{1}{2}(m_1+m_2+m_{s1}+m_{s2}) \dot{x}^2 + \frac{1}{2} J_1 \dot{\phi}_1^2 + \frac{1}{2} J_2 \dot{\phi}_2^2 + \frac{1}{2} J_{s1} \dot{\phi}_s^2 + \frac{1}{2} J_{s2} \dot{\phi}_s^2 \qquad (5)$$

Kinematic linkages:

$$\dot{x} = r_k \dot{\phi}_s \ ; \quad \dot{\phi}_s = \frac{1}{r_k} \dot{x} \qquad (6)$$

$$r_4 \dot{\phi}_s = - r_3 \dot{\phi}_2 \ ; \quad \dot{\phi}_2 = - \frac{r_4}{r_3} \dot{\phi}s \ ; \quad \dot{\phi}_2 = - \frac{r_4}{r_3 r_k} \dot{x} \qquad (7)$$

$$r_2 \dot{\phi}_2 = - r_1 \dot{\phi}_1 \ ; \quad \dot{\phi}_1 = - \frac{r_2}{r_1} \dot{\phi}_2 \ ; \quad \dot{\phi}_1 = - \frac{r_2 r_4}{r_1 r_3 r_k} \dot{x} \qquad (8)$$

$$r_1 \dot{\phi}_1 = \dot{z} \ ; \quad \dot{z} = - r_2 \dot{\phi}_2 \ ; \quad \dot{z} = \frac{r_2 r_4}{r_3 r_k} \dot{x} \qquad (9)$$

Afterwards:

$$K = \frac{1}{2}(m_b+m_z+m_p+m_1+m_2+m_{s1}+m_{s2}) \dot{x}^2 + \frac{1}{2}(m_b+m_z)\left(\frac{r_2}{r_3}\frac{r_4}{r_k}\right)^2 \dot{x}^2 + \frac{1}{2} J_1 \left(\frac{r_2 r_4}{r_1 r_3 r_k}\right)^2 \dot{x}^2 + \frac{1}{2} J_2 \left(-\frac{r_4}{r_3 r_k}\right)^2 \dot{x}^2 + \frac{1}{2} J_{s1} \left(\frac{1}{r_k}\right)^2 \dot{x}^2 + \frac{1}{2} J_{s2} \left(\frac{1}{r_k}\right)^2 \dot{x}^2 = \frac{1}{2} m_p \overset{*}{\dot{x}}{}^2 \qquad (10)$$

$$m_p = (m_b+m_z)\left[1+\left(\frac{r_2 r_4}{r_3 r_k}\right)^2\right] + m_p+m_1+m_2+m_{s1}+m_{s2} + \frac{J_1}{r_k^2}\left(\frac{r_2 r_4}{r_1 r_3}\right)^2 + \frac{J_2}{r_k^2}\left(\frac{r_4}{r_3}\right)^2 + \frac{J_{s1}+J_{s2}}{r_k^2} \qquad (11)$$

Tab. 2. – Force and power effects on trolley

Force effect	Power effect
Gravity	$(m_b+m_z)\ g\ \dot{z}$
Spring forces	$-4\ k\ z\ \dot{z}$
Friction	$-4\ F_T\ \dot{z}$
Rolling resistance	$-4\ \frac{m_{celk}}{4}\ g\ \xi\ \dot{\phi}_s$

Total power:

$$P = [(m_b+m_z)\, g - 4\, k\, z - 4\, F_T]\, \dot{z} - m_{celk}\, g\, \xi \phi_s \quad (12)$$

Transferred to $\dot{x}$:

$$P = \left\{[(m_b+m_z)\, g - 4\, k\, z - 4\, F_T]\, \frac{r_2 r_4}{r_3 r_k} - m_{celk}\, g\, \frac{\xi}{r_k}\right\} \dot{x} \quad (13)$$

The equation of motion:

$$\overset{*}{m}_r\ \dot{x}\ \ddot{x} = \left\{[(m_b+m_z)\, g - 4\, k\, z - 4\, F_T]\, \frac{r_2 r_4}{r_3 r_k} - m_{celk}\, g\, \frac{\xi}{r_k}\right\} \dot{x} \quad (14)$$

$$\overset{*}{m}_r\, \ddot{x} = [(m_b+m_z)\, g - 4\, F_T]\, \frac{r_2 r_4}{r_3 r_k} - m_{celk}\, g\, \frac{\xi}{r_k} - 4\, k\, \frac{r_2 r_4}{r_3 r_k}\, z \quad (15)$$

In which

$$z - z0 = \frac{r_2 r_4}{r_3 r_k}\, (x - x0) \quad (16)$$

Achieved:

$$\overset{*}{m}_r\, \ddot{x} + 4\, k\, \frac{r_2 r_4}{r_3 r_k}\left[z_0 + \frac{r_2 r_4}{r_3 r_k}(x - x_0)\right] = [(m_b+m_z)\, g - 4\, F_T]\, \frac{r_2 r_4}{r_3 r_k} - m_{celk}\, g\, \frac{\xi}{r_k}\ \ m_r\, \ddot{x} + 4\, k \left(\frac{r_2 r_4}{r_3 r_k}\right)^2 x = [(m_b+m_z)\, g - 4\, F_T]\, \frac{r_2 r_4}{r_3 r_k} - m_{celk}\, g\, \frac{\xi}{r_k} - 4\, k\, \frac{r_2 r_4}{r_3 r_k}\left(z_0 - \frac{r_2 r_4}{r_3 r_k} x_0\right) \quad (17)$$

$$\text{difrov: } = m_R\left(\frac{d^2}{d_x^2}\, y(x)\right) + K\, y(x) = F_R \quad (18)$$

This motion equation (17) was solved using the specialized software MAPLE with graphic output for two different weights of transported object (10 kg and 20 kg) by inserting parameters obtained from created CATIA V5 (Dassault Systèmes') model of karakuri transport trolley:

m_p	- 29 kg
m_b	- 5 kg
m_z	- 10 kg
m_1	- 0.315 kg
m_2	- 0.345kg
m_{s1}	- 2.29kg
m_{s2}	- 2.26kg
r_1	- 0.07 m
r_2	- 0.02 m
r_3	- 0.07 m
r_4	- 0.02 m
r_k	- 0.11 m
J_1	- 0.00096 kgm^2
J_2	- 0.00098 kgm^2
J_{s1}	- 0.00445kgm^2
J_{s2}	- 0.00444kgm^2
F_t	- 5 N
ξ	- 0.0008 m
g	- 9.81m/s^2
k	- 2.5 N/mm
x_0	- 0.02 m
z_0	- 0.02 m

RESULTS AND DISCUSSION

The results obtained by experiments and by calculation of the motion equation (17) showed the following:

- Karakuri-based transport trolley was functional for object movement along a linear trajectory.
- Experimental karakuri transport trolley transported (moved) an object with 10 kg (20 kg) weight at a distance of 2 (3) m and returned back to starting position without additional energy supply.
- Both travelled distance and velocity of karakuri trolley depend on weight of transported object – see Fig. 5 and Fig. 6.
- Moving of trolley is uniformly accelerated for both variants of transported object weight (10 kg and 20 kg) – see Fig. 5 and Fig. 6.
- Velocity and acceleration of karakuri transport trolley was linear and depends on transported weight.

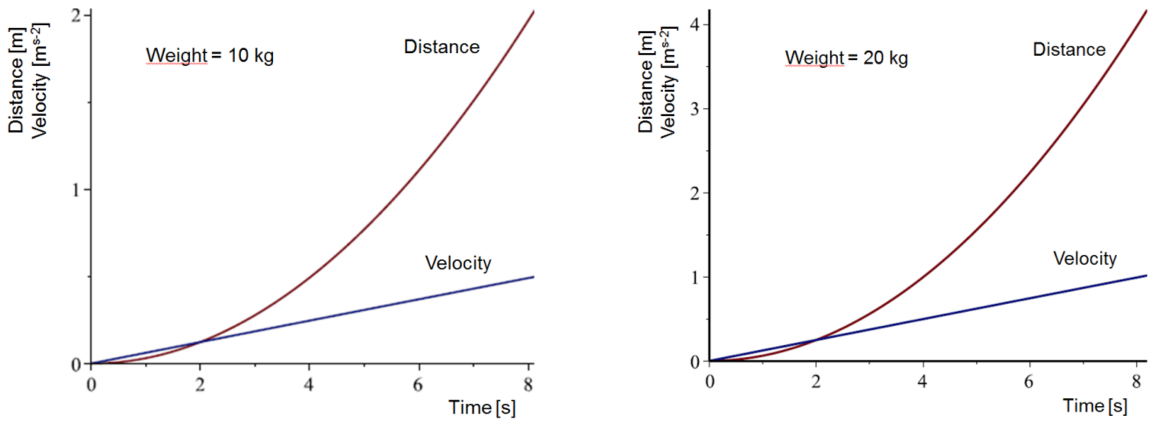

Fig. 5. – Diagram showing dependence of velocity and travelled distance on time (weight of transported object = 10 kg (left) and 20 kg (right)

The dynamic behaviour of the karakuri transport trolley has been tested through repeated physical measuring of time and distance by standard measuring instruments, calibrated scale and by video-records analysis. When comparing the calculated results with the measured values across distance 0 – 2 (3) m we can conclude that results obtained by calculation and by solving of motion equation well correspond to the real behaviour of the experimental karakuri trolley tested under practical conditions.

CONCLUSIONS

Karakuri transport trolley transported (moved) an object with common weight and dimensions at a distance of 2 (3) m and returned back to starting position without additional energy supply. The calculations confirmed the validity of the following differential equation for the proposed karakuri transport trolley:

Obtained results indicate there is potential for karakuri-based technical means in agriculture to save energy and human effort. For future development is necessary to deeply study the issues connected to karakuri mechanisms and present obtained results to agricultural engineers.

ACKNOWLEDGEMENT

The results of this project No. LO1201 were obtained through the financial support of the Ministry of Education, Youth and Sports in the framework of the targeted support of the “National Programme for Sustainability I”.

REFERENCES

1. AMS, INC.: Available at: https://www.youtube.com/watch?v=hcDQ6BPWj90. Published 25 February 2014. Accessed 22 April 2016.
2. JAPAN TODAY: Japan Pavilion reopens in London with new exhibits, demonstrations. Available at:http://www.japantoday.com/category/national/view/japan-pavilion-reopens-in-london-with-new-exhibits-demonstrations. Published 26 October 2015. Accessed 22 April 2016.
3. KYOTO UNIVERSITY MUSEUM: Mechanisms of a tea serving doll. Available at: http://www.museum.kyoto-u.ac.jp/english/materials/chakumiDolleng.html. Published 1 November 2007. Accessed 22 April 2016.
4. WORK SAFE NZ: Preventing manual handling injuries on farms. Good Practice Guidelines. 1st ed., New Zealand, WorkSafe NZ 2014.
5. KATAYAMA, H., SAWA, K., HWANG, R., ISHIWATARI, N., & HAYASHI, N.: Analysis and classification of Karakuri technologies for reinforcement of their visibility, improvement and transferability: An attempt for enhancing lean management. In PICMET 2014 - Portland International Center for Management of Engineering and Technology, Proceedings: Infrastructure and Service Integration, 2014: 1895-1906.
6. OLSON, C. F.: Probabilistic self-localization for mobile robots. IEEE Transactions on Robotics and Automation 16(1), 2000: 55–66.
7. MURATA, K., KATAYAMA H.: Development of Kaizen case-base for effective technology transfer-A case of visual management technology, International Journal of Production Research (IJPR), Vol. 48, Issue 16, 2000: 4901-4917.

Corresponding author:

doc. Dr. Ing. Ivan Mašín, Department of the Design of Machine Elements and Mechanism,Technical University in Liberec, Czech Republic, Studentská 1402/2, 461 17 Liberec I, Czech Republic, phone: 48 535 3383, e-mail: ivan.masin@tul.cz

RISK ANALYSIS OF DESIRED MINIMUM ANNUAL UTILIZATION

M. Mimra, M. Kavka

Department of Machinery Utilization, Faculty of Engineering, Czech University of Life Sciences Prague, Czech Republic

Abstract
The paper presents the results of the risk analysis to achieve a minimum annual utilisation for the group of combine harvesters operated in services. For modelling, an appropriate economic model was created. The results of sensitivity analyses were used to determine the key factors within the risk analysis to achieve a minimum annual utilisation. The key factors were lilting within the range of ± 10%. The risk analysis was carried out using a stochastic simulation methods using a triangular distribution of these values. The risk to achieve minimum annual usage was evaluated for each harvester. The result of the analysis showed that the most frequent values of the minimum annual utilisation, i.e. 697 ha / year, will be achieved with a probability of 50.48%. The sub-profit of the enterprise arising from the operation of the combine harvesters is directly influenced by their accomplished annual utilisation.

Key words: harvester, economic model, key parameters, profit, business risk, machinery utilization.

INTRODUCTION

According to KAVKA (1997) the minimum annual usage is the turning point in the search for the purposefulness of purchasing your own machine in comparison with the use of mechanised services. This is one of the results of the so-called economic considerations relating to the development of strategies in the use of mechanical equipment. When searching for an appropriate strategy it is necessary to combine the operational parameters influencing the formation of profit, i.e. in particular: income from the operation of the machine; operation costs of the selected machine type (in relation to the purchase price, in the form of financing, the usage time and changing operating parameters in dependence on time).

From these variables the combination of the service prices of mechanised works in the market with duration of use, cost and annual utilisation of the machine can be emphasised. This combination of the operating parameters can determine operating spaces according to RATAJ (2005). The minimum annual usage is then the interface between the operating space of profit and a loss.

The annual performance of combine harvesters in agricultural enterprise must meet the security requirements of the harvest in agro-technical deadlines, to avoid generating losses by reducing crop yields. KAVKA ET AL. (1997) and KOLEK ET AL. (1997) dealt with the timeliness factor and its impact on the losses amount. ZACHARDA AND PEICH (2002) discovered in their research that the performance of combine harvesters operated in the services is up to 99% higher (834.8 hectares, while in agricultural enterprises it is only 419.4 hectares per year). SZUK AND BERBEKA (2014) reported on the basis of the analyses that for a business that doesn't reach the required minimum usage, it is more economical to buy a used combine harvester.

The unit costs of combine harvesters are directly affected by the achieved annual usage, when its growth means a decline in the proportion of fixed costs. KAVKA ET AL. (2010) states that the size of the fixed costs is also influenced by a machines usage time, when there is a decrease in fixed costs at the same annual performance with the extension of the machinery usage period.

MONTASER AND MOSELHI (2014) state that most forecasts concerning use of machines use deterministic or stochastic approaches, which are based on historical data. The disadvantage of this approach they see in the inaccuracy of the resulting simulations, since they don't take into account the unique characteristics of the machine operation. Therefore, they recommend the use data obtained through online monitoring of machines operation for modelling. From the data obtained it is possible to analyse the factors that increase the uncertainty of achieving the desired machine performance, such as e.g. the type of work carried out or the weather.

As the above review of the literature shows, the achieved annual performance of combine harvesters has a major impact on the economy of their operation.

Therefore, the main objective of this paper is to perform a risk analysis using stochastic simulation methods and to assess the impact of key parameters to achieve a minimum annual utilisation of combine harvesters.

MATERIALS AND METHODS

The key parameters are determined based on the results of the cost analysis. To determine the break-even point the analysis of the operational area is used. The results of these analyses carried out showed that the greatest impact on both the average annual partial gain from the combine harvesters operation as well as unit costs of combine harvesters, is a change in the price of services provided by threshing machine, the annual performance of threshing machine, purchase price of threshing machine and the fuel costs. For these key parameters there was a risk analysis carried out on the achievement of a minimum annual utilisation of combine harvesters. The equations 1–3 were used to calculate the minimum annual utilisation of combine harvesters according to KAVKA (1997) and RATAJ (2005).

$$aW\min = \frac{aCf}{Ph - uCv} \quad \text{[ha/year]} \qquad (1)$$

where:

$$aCf = aCd + aCioc + aCibl + aCai + aCci + aCg \quad \text{[Kč/year]} \qquad (2)$$

$$uCv = uCm + uCfl + uCp \quad \text{[Kč/year]} \qquad (3)$$

aWmin – minim annual performance [ha/year]
aCioc – annual costs on interest of own capital [CZK/year]
aCd – annual depreciation costs [CZK/year]
aCibl – annual costs on interest of bank loan [CZK/year]
aCci – annual cost of compulsory insurance [CZK/year]
aCai – annual cost of accident insurance [CZK/year]
uCfl – unit cost of fuel and lubricants[CZK/ha]
aCf – annual fixed costs [CZK/year]
uCv – unit variable costs [CZK/ha]
Ph – price of harvest [CZK/ha]
uCm – unit maintenance costs [CZK/ha]
aCg – annual cost of garaging [CZK/year]
uCp – unit personal costs [CZK/ha]

GLEISSNER AND BERGE (2004) have defined an algorithm of random numbers generation based on in advance determined conditions and statistical distribution in order to model the risky situation. Efficiency of the minimal annual utilisation of harvesters is effected by a large number of potential risk situations (key factors) and therefore KOENKER ET AL. (1996) have used the method of quantilles allowing to resolve the distribution type. There were selected parameters by which can be expected the changes in order to provide modelling.

The paper is based on the principle of the neoclassical economic theory. It considers maximisation of the company's annual profit as the main criterion for enterprise decision making, which can be determined by the procedure set out in KAVKA (1997). This criterion is extended to take account of the risks to the business. The parameter of annual utilisation of combine harvesters has the greatest impact on achieving annual profits and it shows how effectively the combine harvesters are used.

The risk analysis uses the stochastic Monte Carlo simulation method for generating random variables with the probability distribution of criterion variable using a triangular distribution at a significance level of 0.05. Random variables of the operating parameters are generated for one million high-risk situations. The key parameters are the lilting of ± 10% of the most common value. This defines the boundaries of the pessimistic and optimistic value of variables (annual usage, cost of mechanised labour, variable unit costs and fixed annual costs). Modelling is carried out in MS Excel.

Performance and operating parameters were monitored during the period 2009 to 2012 with a group of three combine harvesters, the John Deere model 9880i STS combine harvester (hereinafter referred to as 'JD 9880i STS'), John Deere model S 9660 WTS (hereinafter referred to as 'JD S 9660 WTS') and John Deere model S 690i (hereinafter referred to as; JD S 690i'). Data obtained from this monitoring is used in the analysis.

RESULTS AND DISCUSSION

Overlay chart in Fig. 1 shows the frequency distribution of a minimum annual utilisation for individual combine harvesters and generated random variables together with the probability of achieving them. The probability distribution of the output variable is interspersed with the most appropriate type of theoretical distributions – the best for all was binomial (the curve in the graph). As is apparent from the graph, the maximum value of the probability of achieving a minimum annual utilisation of 7.9% is performed by JD S 9660 WTS combine harvesters, which also has the lowest value of the minimum annual utilisation. The lowest value of the probability of achieving a minimum annual utilisation of combine harvesters, i.e. 5.2%, is achieved by the JD S 690i combine harvester, but it achieves the highest value of the minimum annual utilisation. The analysis of the sensitivity of the individual combine harvesters showed that the greatest impact on achieving minimum annual utilisation at the desired economical profit belongs to the cost of mechanised work (its influence ranged from 63.8 to 65.8%, followed by the unit variable costs (their influence ranged from 27.3 to 31.7%) and annual fixed costs (their effect ranged from 4.5 to 6.9%).

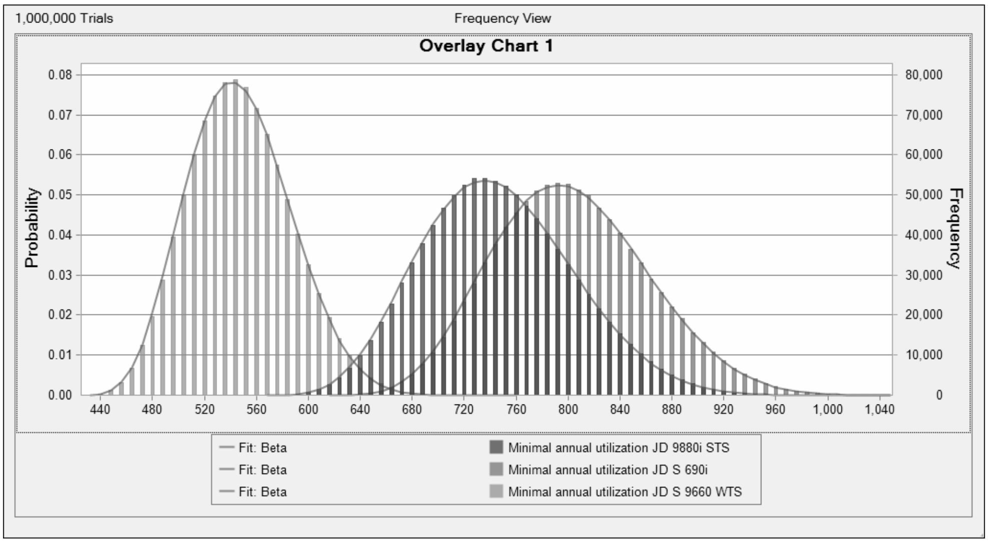

Fig. 1. – Distribution curve of probability minimum annual utilization of each combine harvesters, John Deere [ha/year]

As is evident from the values in Tab. 1, regarding the JD S 690i combine harvester the minimum annual utilisation is 799 ha/year, the maximum value of the minimum annual utilisation reaches 1,046 ha/year, the arithmetic average of 802 ha/year, the median, i.e. the value that after ranking the values from the smallest to the largest is found in the middle, is 799 ha/year and modus, i.e. the most frequently occurring reference value of 797 ha/year, which also indicates the most likely scenario. The value of the minimum annual utilisation of 799 ha/year will be achieved with a probability of 50.33%. Variance, i.e. the average of squared deviations of individual values from their arithmetic criteria averaging 3,454 ha/year. Standard deviation, i.e. the likelihood of diversion the resulting value of criteria from its expected value is 59 ha/year, coefficient of variation, i.e. variation of the criterion value in relation to the risk is 0.0733, skewness, i.e. value indicating whether the values selected around the mean value are symmetrical or are more focused on one side, is 0.22503. In this case, the average is greater than the median, which is larger than a mode, therefore it's a positive skewness of the distribution to the right. Kurtosis, that expresses how the values of the criteria are laid out around the middle, is 2.80. Kurtosis exceeds 1, so the probability is distributed around mean values in a thicker and steeper way, than it is outside the normal distribution. Graf is deflected slightly to the right, when the average value is higher than the median. The combine harvester should probably achieve a basic minimum annual utilisation even with negative development in risk factors within a defined range.

Regarding the JD 9880i STS combine harvester within the simulation the minimum annual utilisation is 570 ha/year, maximum annual usage is 988 ha/year, the arithmetic average of 746 ha/year, median of 743 ha/year and modus 729 ha/year. The value of the basic minimum annual utilization of 743 ha/year will be achieved with a probability of 50.07%. Scattering is 3329 ha/year, standard deviation of 58 ha/year, the variation coefficient of 0.0774, 0.2781 skewness and kurtosis 2.83. Kurtosis again exceeds 1, so the probability is distributed around mean values thicker and steeper than it is outside the normal distribution. The chart is again deflected slightly to the right, when the average value is higher than the median. The combine harvester should probably achieve a basic minimum annual utilisation even with negative development in risk factors within a defined range.

Regarding the JD S 9660 WTS combine harvester within the simulation the minimum annual utilisation of 428 ha/year, maximum of minimum annual utilisation of 716 ha/year, the arithmetic average of 547 ha/year, median of 545 ha/year and modus 535 ha/year. The combine harvester achieves about 46.62% lower average annual utilisation compared to the JD S 690i combine harvester. The value of the minimum annual utilisation of 545 ha/year will be achieved with a probability of 49.58%. Scattering is 1,550 ha/year and it is 122.84% lower than in the JD S 690i combine harvester. The standard deviation is 39 ha/year, the variation coefficient of 0.0719, 0.2427 skewness, kurtosis 2.80. Kurtosis here exceeds the value 1, so the probability is distributed around the mean values densely and steeply than it is in the normal distribution. Even this graph is deflected slightly to the right, although there is an average value higher than the median. The combine harvester should probably achieve a basic minimum annual utilisation even with negative development in risk factors within a defined range.

The combine harvesters can also be compared on the basis of the rules of mean value and variance. The highest mean value and smallest variance belongs to the JD S 9660 WTS combine harvester. Regarding the JD S 690i and JD 9880i STS combine harvesters it is not possible to clearly state that one dominates over the other on the basis of the rules of mean value and variance. The JD S 690i combine harvester, which has a higher average value, also has higher variance.

Tab. 1. – Statistical processing of high-risk situations a minimum annual utilization combines harvesters

Statistic	JD S 690i	JD 9880i STS	JD S 9660 WTS
Trials	1,000,000	1,000,000	1,000,000
Base Case	799	743	545
Mean	802	746	547
Median	799	743	545
Mode	797	729	535
Standard Deviation	59	58	39
Variance	3,454	3,329	1,550
Skewness	0.2503	0.2781	0.2427
Kurtosis	2.80	2.83	2.80
Coefficient of Variation	0.0733	0.0774	0.0719
Minimum	618	570	428
Maximum	1,046	988	716
Mean Std. Error	0	0	0

For the assessment of the combine harvesters we can therefore use the stochastic dominance rules, which evaluates the entire probability distribution of selected criteria, not just some of its features. According to the first rule of stochastic dominance, such a variant is preferred, in which the value of the distribution function at each point reaches higher values than the value of function for non-preferred option. Fig. 2 shows graphs of cumulative distribution function values and their mutual overlap. The graph shows that the distribution functions of the JD S 690i combine harvester is on the right of the cumulative frequency graph for distribution functions of the JD 9880i STS combine harvester, which lies to the right of the cumulative frequencies graph for the JD S 9660 WTS combine harvester. From this we can deduce that the distribution value of JD S 690i combine harvester is smaller for any value of the minimum annual utilisation, or equal, corresponding to the value of the distribution function of the JD 9880i STS combine harvester. The JD S 690i combine harvester stochastically dominates the JD 9880i STS combine harvester, regardless of risk. The 9880i STS combine harvester stochastically dominates the JD S 9660 WTS combine harvester JD S 9660 WTS. Therefore, for the above reasons, it is no longer necessary to access the application of the second rule of stochastic dominance. In terms of risk of reaching the required minimum annual utilisation, the best is the JD 690i combine harvester, followed by the JD 9880i STS combine harvester and in last place is the JD S 9660 WTS combine harvester, but which has the highest probability of achieving the average value of the minimum annual utilisation. However, it is necessary to closely monitor the development of individual risk factors, particularly the cost of mechanised labour and unit variable costs. In the event that their development would significantly deviate from the values used for this analysis, it will be necessary to re-analyse the risks based on changed conditions.

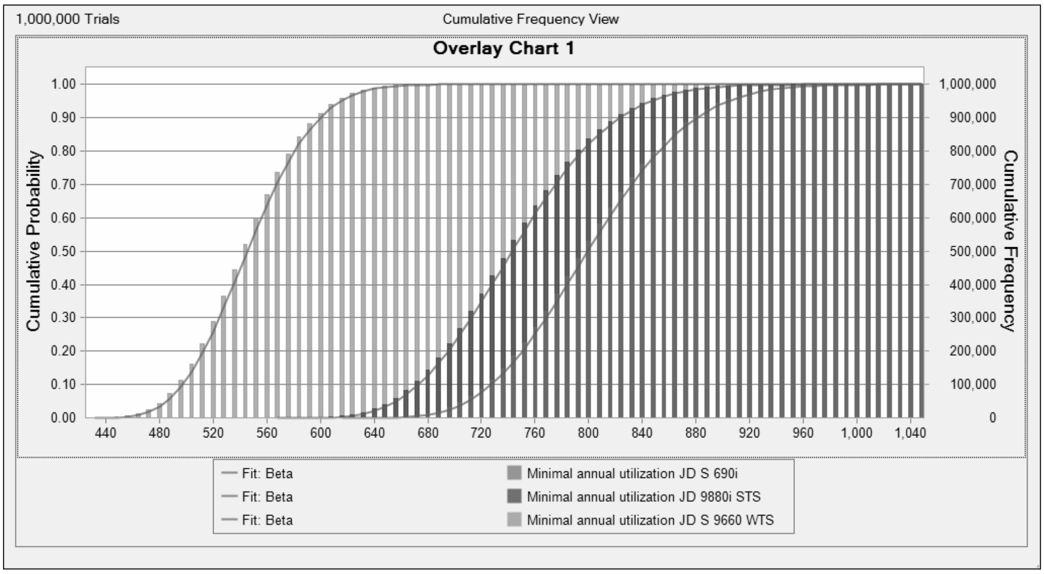

Fig. 2. – Graph the cumulative frequency distribution of the probability distribution function

Tab. 2 lists predicted values of achievement of a minimum annual utilisation for each combine harvester for different values of the probability in increments of 10%. From this table it can be determined on a specific degree of probability, which values of the minimum annual utilisation will be achieved in individual combine harvesters.

Tab.2. – The probability of achieving a specified range of a minimum annual utilization combines harvesters

Percentile	JD S 690i	JD 9880i STS	JD S 9660 WTS
100%	618	570	428
90%	728	673	497
80%	751	695	513
70%	768	713	525
60%	784	728	535
50%	799	743	545
40%	815	758	556
30%	832	775	567
20%	852	795	581
10%	881	823	600
0%	1,046	988	716

CONCLUSIONS

The risk is the probability of achieving or failing to achieve common values of annual performance. The minimum annual utilisation has essential impact on the achievement of positive economic results. Therefore, with the acquisition of combine harvester it is necessary to pay attention to those parameters that may affect it. The sensitivity analysis showed that the minimum annual utilisation at the desired economic result is mostly affected by price of mechanised labour, unit costs, variable and fixed costs. These parameters affecting revenues and costs, which stipulate the tipping point. Due to the seasonality of the deployment of combine harvesters it is necessary for an enterprise to try to maximize the annual utilisation. When creating a business strategy, it is important to decide how much risk is acceptable for the company, and how much risk is not acceptable. Agribusiness due to the biological nature and quantity of the factors influencing it, belongs to riskier sector. Based on the experience we can state that for a company it is acceptable to have the risk in the range of 0–60%.

Price of mechanised work is influenced by many factors, such as competition from other service providers in a given place and time, supplier-customer relationships, model of harvester, whether straw is crushed, the size and slope of the land, humidity and vegetation state, the type of crop being harvested etc. Major effect on the variable component of the cost is fuel consumption that is the reason why often the price is indicated without the diesel used, which is paid according to the actual consumption. The average market prices of mechanised labour in the years 2006–2015 found on a sample survey are given in Tab. 3. As Tab. 3 shows the average price of mechanised labour in the market is growing annually by about 0.8%. At the JD S 690i combine harvester there was an increase in price of the mechanised work in 2015 compared to 2008 by 5.76%. Regarding the JD W650 combine harvester the price increase of mechanised work in 2015 compared to 2007 amounted to 6.64%. This increase, however, due to high competition in the market, however, does not fully cover changes in inputs. Therefore, it is necessary to look for possible savings in cost items and increase the annual use of combine harvesters, to avoid generating negative partial profit.

Tab. 3. – Average market prices of mechanized work in the years 2006–2015

Year	Price of mechanized work in the services of JD 9880i STS / JD S690 [CZK/ha]	Annual change in the price of services [%]	Changing the price of services compared with 2006 [%]	Price of mechanized work in the services of JD WTS 9660/ JD W650 [CZK/ha]	Annual change in the price of services [CZK/ha]	Changing the price of services compared with 2006 [%]
2006	1,861			1,674*		
2007	1,876	0.81	0.81	1,688	0.84	0.84
2008	1,891	0.80	1.61	1,702	0.83	1.67
2009	1,906	0.79	2.42	1,715	0.76	2.45
2010	1,921	0.79	3.22	1,729	0.82	3.29
2011	1,937	0.83	4.08	1,743	0.81	4.12
2012	1,952	0.77	4.89	1,757	0.80	4.96
2013	1,968	0.82	5.75	1,771	0.80	5.79
2014	1,984	0.81	6.61	1,786	0.85	6.69
2015	2,000	0.81	7.47	1,800	0.78	7.53

The unit costs consist of variable and fixed components. Each component is influenced by many other factors, whose influence must be assessed individually. For example, fuel costs are influenced by development in oil prices on world markets, and it is almost impossible to influence the development of its price.

Costs for repairs and maintenance are very individual for each produced piece of machinery. CALCANTE ET AL. (2013) reports that the calculated costs for repairs and maintenance, adapted to the conditions in Italy for the combine harvester with a planned utilisation of 3,000 engine hours, amounted to 23.1% compared to 40.2% calculated according to the latest U.S. model. Usually, the cost of maintaining and repairing are for the first two years paid by the vendor of the technology within the warranty period. In the following years the costs then go to the operator. Based on the sample survey repair costs were monitored. The following Tab. 4 and Fig. 3 shows the average annual maintenance costs. As the table shows, the average cost of repairs and maintenance grow with the use of combine harvesters. Therefore, it is necessary to monitor their development and at the appropriate moment to carry out recovery of the techniques.

Tab. 4. – Average annual maintenance and repair costs for combine harvesters in the years 2006–2015

Year	Maintenance and repair costs for JD 9880i STS [CZK/year]	Annual change in maintenance and repair costs [%]	Changing the maintenance and repair costs compared with 2006 [%]	Maintenance and repair costs for JD 9660 WTS [CZK/year]	Annual change in maintenance and repair [%]	Changing the maintenance and repair costs compared with 2006 [%]
2006	162,583			77,864		
2007	160,973	-0.99	-0.99	79,453	2.04	2.04
2008	162,599	1.01	0.01	85,433	7.53	9.72
2009	189,069	16.28	16.29	90,887	6.38	16.72
2010	212,437	12.36	30.66	97,728	7.53	25.51
2011	241,406	13.64	48.48	107,393	9.89	37.92
2012	277,478	14.94	70.67	115,476	7.53	48.31
2013	311,773	12.36	91.76	124,168	7.53	59.47
2014	342,950	10.00	110.94	147,760	19.00	89.77
2015	390,963	14.00	140.47	189,133	28.00	142.90

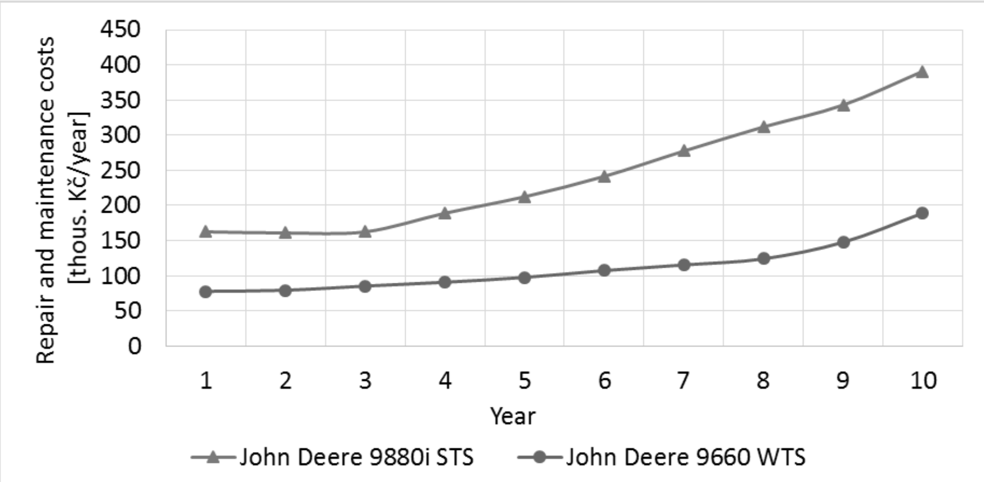

Fig. 3. – Course of costs for repairs and maintenance in time

ACKNOWLEDGEMENT

This paper was carried out as a part of the project no. MSM6046070905 supported by the Czech Ministry of Education, Youth and Sports.

REFERENCES

1. GLEISSNER, W., BERGER, T.: Auf nach Monte Carlo: Simulation sverfahrenzur Risiko-Aggregation (According to Monte Carlo method: Simulation methods for risk-aggregation). Risknews 1(1), 2004: p. 30-37.
2. KAVKA, M.: Využití zemědělské techniky v podmínkách tržního hospodářství.. (Utilization of agricultural machinery in a market economy.) Praha: ÚZPI, 1997: p. 39. ISSN 1222-9199l.
3. KAVKA, M., KOLEK, L., VAŠÁK, J., FÁMĚRA, O., POŠAR, B.: Optimalizace počtu a využití sklízecích mlátiček s ohledem na faktor včasnosti sklizně.. (Optimisation of the number and utilisation of combines according to the term of harvest.) Zemědělská technika, 43, 1997: p. 59–73.
4. KAVKA, M., NOZDROVICKÝ, L., KADLEC, F., MIMRA, M.: Analysis of the Effects of the Machine Life-Time on the Direct Unit Cost and Minimal Annual Use of the Field Machines in Tractor-Machine Sets. In: Trends in Agricultural Engineering, 2010, p. 18–24.
5. KOENKER, R., HALLOCK, K.: Quantile Regression: An Introduction, Journal of Economic Perspectives, 15, 2001: p. 143–156.

6. KOLEK, L., VAŠÁK, J., FÁMĚRA, O., KAVKA, M.: Vliv termínu sklizně na ztráty a kvalitu produkce řepky, pšenice a ječmene. (The effect of time of harvest on losses and quality of production of rape, wheat and barley.) Rostlinná výroba, 43, 1997: p. 257–282.
7. MONTASER, A., MOSELHI, O.: Truck for earthmoving operations. Journal of Information Technology in Construction, Vol. 19, 2014: p. 412–433
8. RATAJ, V.: Projektovanie výrobných systémov: výpočty a analýzy (Design of Production Systems: Calculations and Analysis). 1st ed. Nitra: SPU, 121 s, 2005. ISBN 80-8069-609-8.
9. SZUK, T., BERBEKA, T.: Annual Use as a Criterion for Selection of a Combine Harvester Utilisation Form. Agricultural Engineering, Scientific quarterly journal, 1 (149), p. 221–227, 2014. ISNN 1429-7264.
10. ZACHARDA, F., PEPICH, S.: Economy of the grain harvesters utilisation in agricultural enterprises. Agroinštitút Nitra, Center for Information Services and Technologies, Poľnohospodárstvo. Vol. 48, Is. 4, 2002: p. 187–191.

Corresponding author:
Ing. Miroslav Mimra, MBA, Ph.D., Department of Machinery Utilization, Faculty of Engineering, Czech University of Life Sciences Prague, Kamýcká 129, Praha 6, Prague, 16521, Czech Republic, phone: +420 22438 3145, e-mail: mimra@tf.czu.cz

INFLUENCE OF FILLER CONTENT ON MECHANICAL PROPERTIES OF ALUMINIUM AL99.5 SINGLE-LAP BONDS BONDED WITH ALUMINIUM AND POLYMER POWDER FILLED EPOXY ADHESIVE

M. Müller[1], P. Valášek[1], A. Rudawska[2]

[1]*Department of Material Science and Manufacturing Technology. Faculty of Engineering, Czech University of Life Sciences Prague. Czech Republic*
[2]*Department of Production Engineering, Politechnika Lubelska, Lublin, Poland*

Abstract
An adhesive bonding technology is a promising method of a bonding. Aluminium ranks among significant technical materials, which are suitable for the adhesive bonding. The paper deals with the testing of composite materials based on aluminium and polymer microparticles. The aim of the research was to determine an influence of a content of a microparticle filler on mechanical properties of the polymer particle composite and adhesive bonds of the adhesive bonded material Al99.5. A tensile strength as well as a strength of the adhesive bond did not change when adding the filler. The highest increase of the tensile strength of 23 % (42.18 ± 1.92 MPa) was at the composite created from 2.5 g of the filler: 100 g of the matrix. The adhesive bond strength was increased when adding the filler except for the concentration 25 g of the filler: 100 g of the matrix (a decrease of 22 %). The adhesive bond strength increase was the highest at the adhesive bond with the adhesive in the form of the composite (2.5 g of the filler: 100 g of the matrix).The adhesive bond strength increase was 25.7 %. Adhesive bonds evinced an adhesive type of a fracture surface. By adding the filler in a form of microparticles there was not a change of the failure type. Using the electron microscopy within the experimental research the presence of cracks in the boundary adherent / adhesive (the matrix – two-component epoxy adhesive and the composite adhesive) at the adhesive bonds was proved.

Key words: adhesive bond strength, SEM, microparticles filler, tensile strength.

INTRODUCTION

A requirement for a mass decreasing of the construction is put when designing constructions of cars or agricultural machines etc. (BORSELLINO ET AL., 2009; MÜLLER, 2013). This requirement is secured namely by a use of aluminium materials in the constructions of machines. The aluminium constructions are lighter than traditional steel ones. However, the aluminium is of worse mechanical properties than the steel. The adhesive bonding technology is an effective method for the connecting of the aluminium and its alloys. The adhesive bonding technology advantage is a possibility to introduce an automation in the production process (SADEK, 1987). The use of the adhesive bonding technology in the construction of transport means and agricultural machines secures a stiffness comparable with mechanical fasteners or spot-welds. Further, the adhesive bonding technology increases an energy absorption reducing a noise and vibrations (BORSELLINO ET AL., 2009; MÜLLER, 2013).

However, the adhesive bonding technology has also its disadvantages, e.g. the strength of the bond depends on a choice of the adhesive, an overlapping geometry, a service life of the bond is limited etc. These properties can significantly influenced the final bond (BORSELLINO ET AL., 2009).

In the area of the bonding of sheets of metals, e.g. in the construction of agricultural machines, single-lap adhesive bonds are used. Technologies such as an adhesive bonding, a riveting and a welding are particularly used in manufacturing corporations focused on bonding of the metal sheets. These methods are frequently combined (MÜLLER, 2013).

Epoxies are widely used as high-performance structural adhesives. Epoxy resins are attractive for metal-bonding adhesive systems. Epoxies are able to bond well a variety of treated or untreated metal surfaces (RAMAZAN ET AL., 2008). Epoxy adhesives have a good affinity for aluminium alloy surfaces and the oxide layers produced during a surface preparation (CHASSER ET AL., 1993). A substantial change in mechanical properties can be achieved by adding an optimum volume of a filler i.e. a reinforcement. A composite material is created by this way. Composite materials are promising structural components (MÜLLER ET AL., 2015; RUGGIERO ET AL., 2015A; MÜLLER, 2011). They comprise one or more discrete phases stored in the continuous phase (VALÁŠEK AND MÜLLER, 2015; VALÁŠEK ET AL., 2015). They can be used as the adhesive or a cement.

Polymers are important matrix materials for forming of advanced composites. The reinforcing materials in advanced composites take many forms. In addition to continuous fibres, many types of short reinforcing elements are used in composites. One popular form of short ‘‘fibres’’ is a spherical particle. A number of studies in particle composites have been undertaken with microparticles (CHO ET AL., 2006).

The filler of composite materials is different: Al_2O_3, SiC, glass beads, minerals, various metals, rubber particles. Mechanical properties of polymer composites strongly depend on the particle size (SHAO YUN FU ET AL., 2008; MÜLLER 2011). The type and the size of the filler depend on an application of the composite. A mild increase of the adhesive bond strength can occur by adding the filler (MÜLLER ET AL., 2015).

It was ascertained that an interfacial fracture toughness does not depend on the particle size but it increases substantially when the sliding fracture mode prevails (RAMAZAN ET AL., 2008; CHO ET AL.,. 2006).

The tensile strength of particle composites can be improved with decreasing particle size. However, composites with 3 vol% of nanoparticles resulted in lower tensile strength due to the likely poor dispersion of nanoparticles at higher particle loading than that ones with microparticles (CHO ET AL., 2006).

The finite element analysis results on stresses show that the aluminium content in the adhesive adversely affects the mechanical strength of the bond. However, a promising result was obtained through an experimental investigation that the epoxy adhesive retains its adhesion strength even with as much as 50 wt% addition of the aluminium filler. Even though the finite element analysis shows higher stresses at the adhesive–metal substrate interface, the actual failure occurs within the adhesive indicating that the strength of the adhesion to the metal substrate surface is stronger than the strength of the adhesive itself (RAMAZAN ET AL., 2008).

The aim of the research was to determine the influence of the content of the microparticle filler on the mechanical properties of the polymer particle composite and the adhesive bond of the bonded material Al99.5.

MATERIALS AND METHODS

In order to understand the size effect of all scales in particle composites, the failure mechanism and mechanical properties in these composites have to be understood. This study presents the laboratory experiment results performed on aluminium Al99.5 with the polymer composites reinforced with the aluminium microparticles (a multi-plate shape) and the plastics (a spherical shape). Mechanical properties of the composites were measured through tensile tests.

The objective of this study was to develop an influence of the aluminium and plastic filler content on the mechanical properties of the adhesive bonds bonded by the two-component epoxy ChS Epoxy 1200 (hardener P11 – Diethylentriamin).

The concentration of the filler in the matrix is indicated by the wt. fraction of the filler. The determination of the concentration of the sub-components was expressed using a weight relative to 100 g of the matrix (the two-component adhesive).

The filler was added into the matrix ChS Epoxy 1200 (two-component reactoplastics resin) in the ratio of 0.5, 1, 2.5, 10, 15, 20, 25 wt% to 100 wt% of the matrix. Weight percentages were chosen with a respect to a practical application when the filler is mixed mainly on the basis of weight ratios.

The adhesive bond strength was determined using the single-lap shear test according to CSN EN 1465. Laboratory experiments were performed on normalized testing samples of the aluminium Al99.5 prepared under the standard CSN EN 1465 by cutting the metallurgical semi-finished product in a form of the metal sheet.

The testing samples without a mechanical and a chemical treatment of the surface were used for the adhesive bonding. The untreated samples were used due to minimizing the factors effecting the preparation of the bonded surface. This trend is significant particularly in operations where the automation is implemented (NOVÁK, 2012; HRICOVA 2014; RUGGIERO ET AL., 2016; RUGGIERO ET AL., 2015B; VESELÁ ET AL., 2013; ALEŠ ET AL., 2012).

The roughness parameters Ra and Rz were measured on the adherent surface designated for the adhesive bonding. Roughness parameters were measured with the portable profilometer Mitutoyo Surftest 301. A boundary wave length of cut-off was placed to 0.8 mm.

The test specimens of the matrix and the composite materials for the tensile properties determination according to the standard CSN EN ISO 527-1 (Plastics – Determination of tensile properties – Part 1: General principles) were prepared according to the standard CSN EN ISO 3167 (Plastics – Multipurpose test specimens, Czech Standard Institution). By mixing of the specified matrix – filler phases ratio the composite was made, which was used for the preparation of test specimens according to the specified standards. The moulds for casting were made from the material Lukapren N using models. The form and the size of moulds meet the corresponding standards.

The testing sample of the matrix and the composite materials was kept under the laboratory temperature 22 ± 2 °C for 48 hours after the fixation of the adhesive bond. A constant thickness of the adhesive layer was secured by the weight of 750 g. Afer that the destructive testing followed. The adhesive layer thickness was determined by the optical analysis of the adhesive bond cut.

The tensile strength and the adhesive bond strength were performed using the universal tensile strength testing machine LABTest 5.50ST (a sensing unit AST type KAF 50 kN, an evaluating software Test&Motion). A speed of the deformation corresponded to 10 mm.min^{-1}. The optical analysis of fracture surfaces and the adhesive bond cut was examined with SEM (scanning electron microscopy) using a microscope MIRA 3 TESCAN. The fracture surfaces were dusted with gold.

The effect of the microparticle dispersion on the composite failure was studied with SEM (scanning electron microscopy) images. The effect of the particle size, the wettability and the porosity on the interfacial crack was investigated with SEM.

An evaluation of the shape and the dimension was performed using the program GWIDDION. The results of measuring were statistically analysed. Statistical hypotheses were also tested at measured sets of data by means of the program STATISTICA. A validity of the zero hypothesis (H_0) shows that there is no statistically significant difference ($p > 0.05$) among tested sets of data. On the contrary, the hypothesis H_1 denies the zero hypothesis and it says that there is a statistically significant difference among tested sets of data or a dependence among variables ($p < 0.05$).

RESULTS AND DISCUSSION

The surface roughness of the tested specimens made by casting from the matrix was Ra 0.24 ± 0.06 μm, Rz 1.44 ± 0.47 μm. The surface roughness of the tested specimens made by casting from the matrix and the filler, i.e. the composite was Ra 0.23 ± 0.05 μm, Rz 1.40 ± 0.41 μm.

The matrix, i.e. the two-component structural adhesive showed the tensile strength 34.21 ± 3.01 MPa. It is obvious from the results of the strength of the matrix and the composite materials of various filler concentrations that adding the filler changes the tensile strength (Fig. 1). The highest increase of the tensile strength of 23 % (42.18 ± 1.92 MPa) was at the composite from 2.5 g of the filler: 100 g of the matrix.

It is possible to say in terms of the statistical testing of the influence of various filler concentrations on the tensile strength that they are statistically non-homogeneous groups. The hypothesis H_0 was not certified, i.e. there is a difference in the tensile strength in 0.05 significance level among single tested materials, i.e. the matrix and various concentrations of the filler ($p = 0.0000$).

The presence of diversely large filler particles was proved using the electron microscopy within the experimental research (Fig. 2). The aluminium microparticles were of the multi-plate shape. The plastics microparticles were of the spherical shape.

The considered particle sizes reached 14.71 ± 7.81 μm (aluminium length), 2.12 ± 1.03 μm (aluminium width) and 23.86 ± 18.62 μm (polymer – spherical particles).

The non-homogeneity of the adhesive is also evident from the fracture surface (Fig. 3). This is caused by air bubbles arisen during both the mixing process of the two-component epoxy adhesive and the hardening without using vacuum.

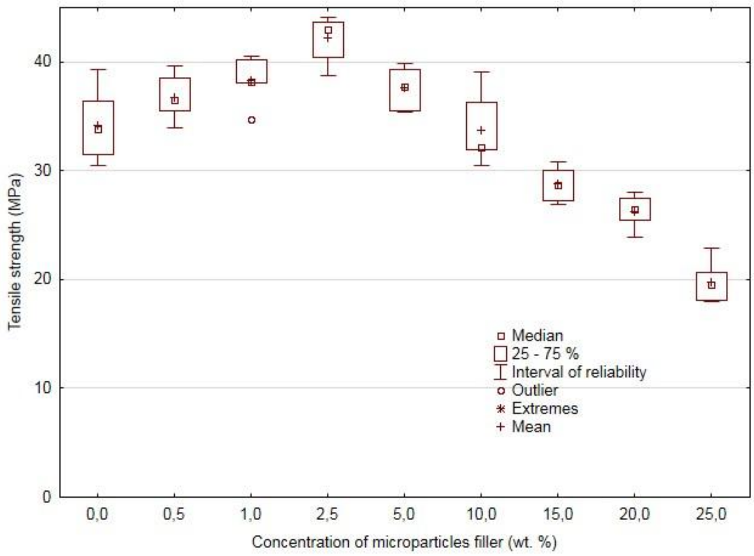

Fig. 1. – Influence of filler concentration on tensile strength

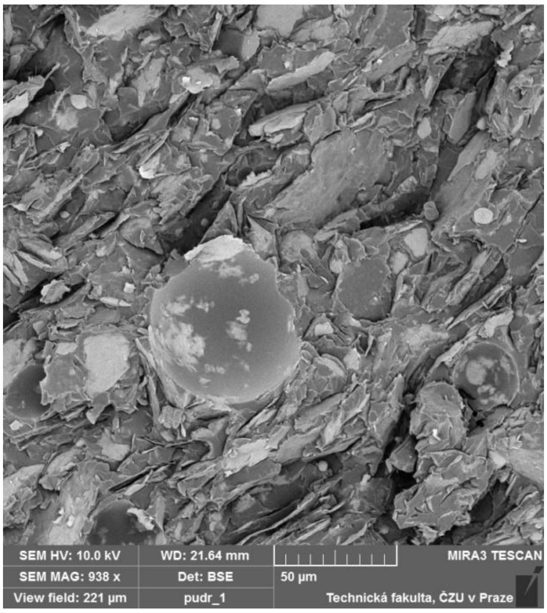

Fig. 2. – SEM images of composite material - microparticles of aluminium (multi-plate shape) and polymer particles (spherical shape)

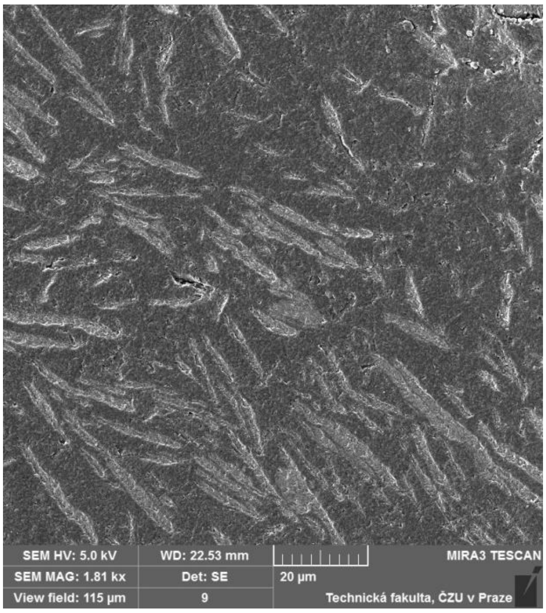

Fig. 3. – SEM images of cut through composite layer containing aluminium microparticles (multi-plate shape) and porosity

Fig. 4 and 5 show a histogram of a frequency of aluminium microparticles. It is obvious from the results that the highest portion was at the aluminium microparticles among 5 to 15 μm (a length) and 1 to 3 μm (a width).

The surface roughness of the adhesive bonded material Al99.5 was in the direction parallel to the loading force at the destructive testing of the adhesive bonds Ra 0.17 ± 0.02 μm, Rz 1.00 ± 0.28 μm and in the direction perpendicular to the loading force at the destructive testing of the adhesive bonds Ra 0.26 ± 0.02 μm, Rz 1.50 ± 0.20 μm.

The adhesive layer thickness was measured as 171.22 ± 21.97 μm. The optimum shear strength was reached at the two-component structural epoxy adhesives in the interval of the adhesive layer thickness 0.1 to 0.25 mm (MÜLLER AND VALÁŠEK, 2013).

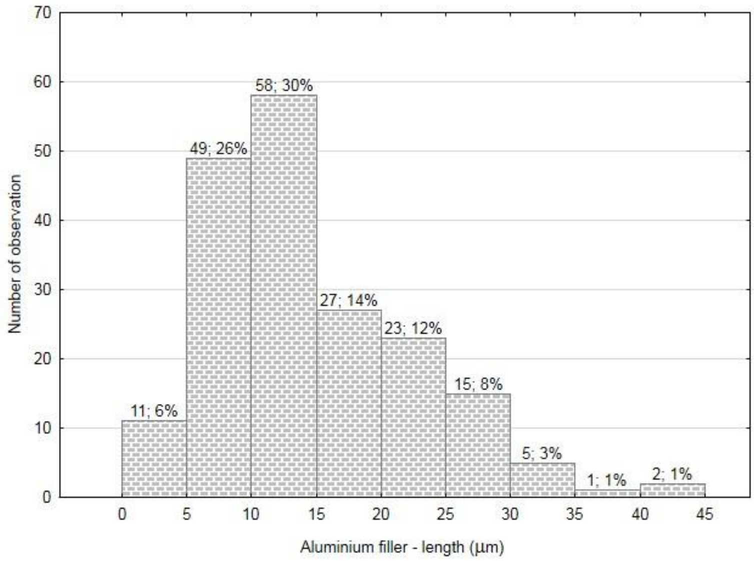

Fig. 4. – Histogram of length of filler in form of aluminium microparticles

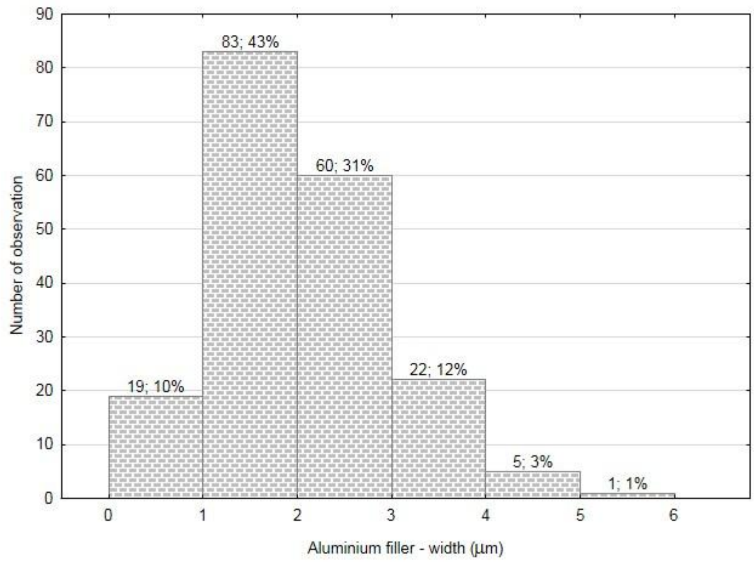

Fig. 5. – Histogram of width of filler in form of aluminium microparticles

It is obvious from the adhesive bond strength results that adding the filler changes the adhesive bond strength (Fig. 6). The highest adhesive bond strength increase was at the adhesive bond with the adhesive in the form of the composite (2.5 g of the filler: 100 g of the matrix). The adhesive bond strength increase was 25.7 %.

It is possible to say in terms of the statistical testing of the influence of various filler concentrations on the adhesive bond strength that concentrations are statistically non-homogeneous groups. The hypothesis H_0 was not certified, i.e. there is a difference in the adhesive bond strength in 0.05 significance level among single tested materials, i.e. the matrix and various concentrations of the filler (p = 0.0001).

Adhesive bonds evinced an adhesive type of the fracture surface. There was no difference between the adhesive bonds without the filler (the matrix) and with the filler.

It came to the increase of the adhesive bond strength but the adhesion of the adhesive was not increased owing to adding the aluminium microparticles.

A presence of cracks in the boundary adherent / adhesive was proved using the electron microscopy within the experimental research (Fig. 7). The adhesive failure of the adhesive bonds originated also in these cracks. It came to decreasing of the adhesive strength of the adhesive bond.

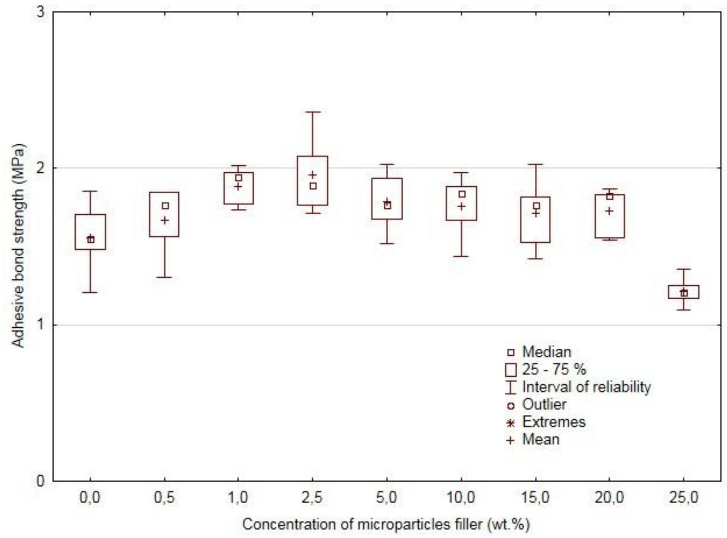

Fig. 6. – Influence of filler concentration on adhesive bond strength (adherent Al99)

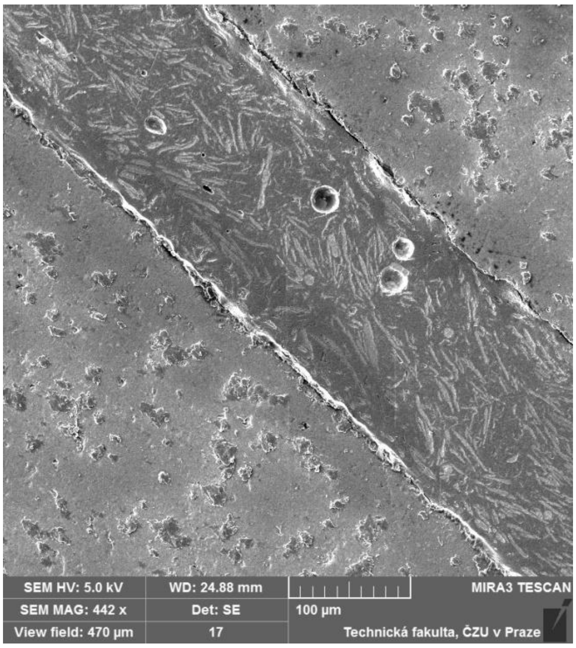

Fig. 7. – SEM images of microcracks in boundary adherent Al99.5 / adhesive (polymeric particle composite 1 g filler: 100 g matrix, without surface treatment of adherent)

The experiment results proved a bad wettability between the adhesive layer and the adherent. A weak interfacial bond was measured as 2.13 ± 1.56 µm. The research results proved a good wettability between the adhesive and the filler.

From the results of the experiment it is possible to agree with the statement that epoxy adhesives preserve their adhesive bond strength also at high concentrations of the filler (RAMAZAN ET AL., 2008).

A strong interaction between adhesive and particles is evident. When applying the filler into the resin, the wetting of the filler with the matrix is very important (JACKEL AND SCHEIBNER, 1991). Results of the experiment also show the irregular stratification of filler microparticles in the matrix (Fig. 3). CHANG ET AL. (2001) proved in their experiments that the irregular shape of the particles ensured good interaction between the matrix and the filler. The assumption about a negative influence of the filler on the tensile strength was not confirmed. CHO ET AL. (2006) state that there is a decrease in the strength of the composite with increasing volume of filler particles.

Results of the experiments confirmed conclusions of RAMAZAN ET AL. (2008), where they state that there was a slight increase of the adhesive bond strength of testing samples from the aluminium alloy with adding the aluminium microparticles. Microparticles of Al_2O_3, SiC affect the tensile strength in a negative way (CHO ET AL., 2006).

By adding the filler in the form of aluminium microparticles there was not a change in a failure type. Therefore it is not possible to agree with the statement of RAMAZAN ET AL. (2008) that filled epoxy resin improved the adhesion to the bonded surface, i.e. there was not a cohesive failure of the adhesive bond (RAMAZAN ET AL., 2008).

CONCLUSIONS

Following conclusions can be deduced from the results of the experiment focused on the research on the influence of the filler concentrations in the form of the aluminium microparticles and polymer on the mechanical properties of the polymeric particle composite and adhesive bonds of the material Al99.5:

- The tensile strength of the composite material changed when adding the filler. The highest increase of the tensile strength of 23 % (42.18 ± 1.92 MPa) was at the composite from 2.5 g of the filler: 100 g of the matrix. The tensile strength got worse compared to the matrix in the form of the two-component epoxy adhesive at the composite from 10 g of the filler: 100 g of the matrix when adding the filler.
- The adhesive bond strength changed when adding the filler. The adhesive bond strength increased (except for the concentration 25 g of the filler: 100 g of the matrix - a fall of 22 %) when adding the filler. The highest increase of the adhesive bond strength was at the adhesive bond with the adhesive in the form of the composite (2.5 g of the filler: 100 g of the matrix). The increase of the adhesive bond strength was 25.7 %.
- The adhesive bonds evinced an adhesive type of the fracture surface. The failure type did not change when adding the filler in the form of the microparticles.

The presence of cracks was proved at the adhesive bonds in the boundary adherent / adhesive (the matrix – the two-component epoxy adhesive and the composite adhesive) using the electron microscopy within the experimental research.

REFERENCES

1. BORSELLINO, C., BELL, G., DI, RUISI V. F.: Adhesive joining of aluminium AA6082: The effects of resin and surface treatment. International Journal of Adhesion and Adhesives, 29, 2009: 36–44.
2. HRICOVA, J.: Environmentally conscious manufacturing: the effect of metalworking fluid in high speed machining. Key engineering materials, 581, 2014: 89–94.
3. CHASSER, A.M., MAKHLOUF, J.M., SCHNEIDER, J.R.: Rubber-based structural adhesive is a new option for metal bonding. Adhes., 1993: 36–39.
4. CHO, J., JOSHI, M.S., SUN, C.T.: Effect of inclusion size on mechanical properties of polymeric composites with micro and nano particles. Composites Science and Technology, 66, 2006: 1941–1952.
5. JÄCKEL, M., SCHEIBNER, W.: Boundary layer induced modification of thermal and mechanical properties of epoxy resin composites Boundary layer induced modification of thermal and mechanical properties of epoxy resin composites, Cryogenics, 31(4), 1991: 269–272.
6. CHANG, J.J., YEIH. W.CH: The effect of particle shape on bond strength improvement of epoxy particle coating composites. Journal of Marine Science and Technology, 9, 2001: 153–160.
7. MÜLLER, M., CIDLINA, J., DĚDIČOVÁ, K., KROFOVÁ, A.: Mechanical properties of polymer composite based on aluminium microparticles. Manufacturing Technology,15(4), 2015: 624–628.
8. MÜLLER, M.: Research of liquid contaminants influence on adhesive bond strength applied in agricultural machine construction. Agronomy Research, 11(1), 2013: 147–154.
9. MÜLLER, M., VALÁŠEK, P.: Comparison of variables influence on adhesive bonds strength calculations. Manufacturing Technology, 13(2), 2013: 205–210.
10. MÜLLER, M.: Polymer composites based on AL2O3 reinforcing particles. Engineering for Rural Development 26.05.2011, Jelgava. Jelgava: Latvia University of Agriculture, 2011: 423-427.
11. NOVÁK, M.: Surfaces with high precision of roughness after grinding. Manufacturing technology, 12, 2012: 66–70.
12. RAMAZAN, K., MEHMET, S., BEKIR, Y.: Influence of adhesive thickness and filler content on the mechanical performance of aluminium single-lap joints bonded with aluminium powder filled epoxy adhesive. Journal of materials processing technology, 205, 2008: 183–189.
13. RUGGIERO, A., D'AMATO, R., GÓMEZ, E., MEROLA, M.: Experimental comparison on tribological pairs UHMWPE/TIAL6V4 alloy, UHMWPE/AISI316L austenitic stainless and UHMWPE/AL2O3 ceramic, under dry and lubricated conditions. Tribology International, 96, 2016: 349–360.
14. RUGGIERO, A., VALÁŠEK, P., MEROLA, M: Friction and wear behaviors of Al/Epoxy composites during reciprocating sliding tests. Manufacturing Technology, 15(4), 2015a: 684–689.
15. RUGGIERO, A., MEROLA, M., CARLONE, P., ARCHODOULAKI, V.: Tribo-mechanical characterization of reinforced epoxy resin under dry and lubricated contact conditions. Compos Part B: Eng., 79, 2015b: 595–603.
16. SADEK, M.M.: Industrial application of adhesive bonding. London, Elsevier Applied Sciency, London, 1987.
17. SHAO-YUN, F., XI-QIAO, F., BEMD, L., YIU-WING, M.: Effects of particle size, particle/matrix interface adhesion and particle loading on mechanical properties of particulate-polymer composites. Composites: Part B, 39, 2008: 933–961.
18. VALÁŠEK, P., MÜLLER, M.: Abrasive wear in three-phase waste-based polymeric particle composites. Teh Vjesn., 22(2), 2015: 257–262.
19. VALÁŠEK, P., MÜLLER, M., SERGEJ, H.: Recycling of corundum particles – two-body abrasive wear of polymeric composites based on waste. Teh Vjesn., 22(3), 2015: 567–572.
20. VESELÁ, K., PEXA, M., MAŘIK, J.: Analysis of particle abrasive wear of engine oil when using lasernet fines analyzer. In: 5th International Conference on Trends in Agricultural Engineering. Prague, CULSP 2013. 637-641.
21. ALEŠ, Z., PEXA, M., PAVLU, J.: Tribotechnical diagnostics of agricultural machies. In: 11th International Scientific Conference on Engineering for Rural Development. Jelgava Latvia, LUA 2012. 88-92.

Corresponding author:

doc. Ing. Miroslav Müller, Ph.D., Department of Material Science and Manufacturing Technology, Faculty of Engineering, Czech University of Life Sciences Prague, Kamýcká 129, Praha 6, Prague, 16521, Czech Republic, phone: +420 22438 3261, e-mail: muller@tf.czu.cz

SIMPLE SOLAR COOKING BOX DESIGN FOR BOILING WATER

R. A. Napitupulu[1], S. Ginting[1], W. Naibaho[1], T. Silaban[1], F. Gultom[1], H. Ambarita[2]

[1]*Mechanical Engineering Department, Nommensen HKBP University, Medan, Indonesia*
[2]*Mechanical Engineering Department, University of North Sumatera, Medan, Indonesia*

Abstract
A simple solar cooker box was designed and constructed in this paper. The main objective is to make solar heating that can be used to boil water, as an alternative fuel for housewives in cooking. The main dimension of solar cooker design is 117 cm x 117 cm nd 30 cm height. Cooking experiment was conducted with different load (3, 4, 5 and 6 liters of water) in the field with the coordinates of 3°35' north latitude and 98°40' east longitude, starting at 09.00 am to 15.00 pm. The results show that the solar cooker box was able to boil 3 liters of water which can be increased up to 5 liters under better weather conditions.

Key words: solar, cooking, design, water.

INTRODUCTION

During this time the housewives in Indonesia always used kerosene or LPG as a fuel source in the cooking of food, especially rice and water. This is due to the lack of alternative fuel that can be used in cooking as well as equipment energy conversion technology is still limited. MEANWHILE, LUBIS (2007) and KHOLIQ (2015) described that the potential of renewable energy such as biomass, solar energy, wind energy, geothermal and so has not been widely used, although the potential of renewable energy is quite a lot in Indonesia. Renewable energy resources will be offered a choice of fuel that is cleaner than the kerosene and LPG. The resources are less or even not pollute or produce gas pollution, and these resources will remain available. According to SEPTIADI AND NANLOHY (2009), one source of renewable energy that can be exploited in Indonesia is solar energy. Solar energy can be converted into other energy forms in accordance with the needs, for example electrical energy, mechanical energy or thermal energy which can be used directly through an intermediary medium. Indonesia as an archipelagic country located in equator line has a bigger potential of solar energy. Estimated solar energy in Indonesia has been investigated by several agencies and research institutions. Based on a white paper published by the MINISTRY OF RESEARCH AND TECHNOLOGY OF INDONESIA (2006) states that regions in Indonesia have the potential of solar energy is 4.8 $kWh \cdot m^{-2} \cdot day^{-1}$ or a total of 17.28 $MJ \cdot m^{-2} \cdot day^{-1}$. AMBARITA (2012) has conducted radiation measurements in the city of Medan and the result is daily radiation varies from 0.53 $kWh \cdot m^{-2} \cdot day^{-1}$ until to 5.64 $kWh \cdot m^{-2} \cdot day^{-1}$ with an average value of 3.54 $kWh \cdot m^{-2} \cdot day^{-1}$ and radiation is on average 11.9 hours per day.

The considerable potential is still largely wasted. YANDRI (2012) had described that only a small fraction has been utilized, either to produce electricity with photovoltaic systems as well as to generate heat for heating the thermal system as reported by FAUZI ET AL. (2012). Therefore, the authors saw an opportunity to use solar energy to reduce dependence housewives in Indonesia to kerosene and LPG, where the cooking stove with a solar thermal system can be one alternative. For cooking water to boil it takes a minimum temperature of 100 °C. Therefore, solar cooker box must be able to exceed this temperature. PANWAR ET AL. (2012) made some reviews about solar cooking as renewable and sustainable energy, and AKOY AND AHMED (2015) had designed, constructed and evaluated the solar cookers performance. KRISHNAN ET AL. (2012) designed and constructed the residential solar cooker used of the thermal storage media and using reflector by BUDHI ET AL. (2015). MUTHUSIVAGAMI ET AL. (2010) and MAHAVAR ET AL. (2011) constructed and evaluated solar cooker without thermal of heat storage media. Based on the evaluation results of previous studies, as well as view factor to the overall economy and ease to use, the aim study of this research is to make solar heating that can be used to boil water, as an alternative fuel for housewives in cooking.

MATERIALS AND METHODS

In designing the solar cookers box need to be understood first heat transfer mechanism, the capacity of water to be cooked as well as the assumptions used in the calculation. The heat obtained from the calculation is then converted into the design of the heater box in the shape, dimensions and type of material to be used. According to AMBARITA (2013) the working principle of solar cookers box is as follows. Solar energy that comes from solar radiation will be absorbed by the absorber. At this energy absorber will be turned into heat because the temperature of the plate will go up. High temperature absorber plate which will be used for cooking or raise the temperature of the water is cooked. In other words, the solar energy will go into the water cooked as useful energy. Because the temperature rises, they absorb part of the energy will be emitted again out by radiation. While some of them to the environment in combination convection and conduction through the walls, the floor, and the glass layer.

The assumptions of heat transfer used in the design of solar cooker box are as follows:

- Air temperature and items cooked T_a in the solar box is considered uniform.
- Outside air temperature changes according to the daily temperature of air measured by the data logger
- The intensity of sunlight changes according to data logger measured
- The intensity of the incoming radiation to the absorber was partially obstructed by two layers of glass is turned into heat by 90%. Usually the glass transmissivity was 95%.
- Temperatures are distinguished on the current temperature calculation T' and the previous temperature T.

The radiant energy into the heating box is:

$$Q\text{rad} = IxAx\ \Delta tx\ 90\% \quad (1)$$

Δt is the time interval of observation and A is the area of the absorber plate. The energy required to heat the air inside the solar heater is:

$$Q\text{a} = m\text{a}\ x\ c\text{a}\ x\ (T'\text{a} - T\text{a}) \quad (2)$$

m_a is the mass of air, c_a is the specific heat of air in the heater box and *T'*a is the current air temperature calculation in the heater box. Due to differences in temperature difference that occurs very small time interval Δt measurement is small, then the nature of the temperature difference can be evaluated using the initial temperature T_a. The energy used to boil the water or rice is:

$$Q\text{c} = m\text{c}\ x\ c\text{c}\ x\ (T'\text{a} - T\text{a}) \quad (3)$$

m_c is the mass of water that is cooked and c_c is the specific heat of water is cooked. The energy required to heat the solar wall material is:

$$Q\text{m} = \sum m\text{m} x c\text{pm}\ x\ (T'\text{am} - T\text{am}) \quad (4)$$

$\Sigma m_m x c_{pm}$ is the sum of the product of the respective weight of the material with a specific heat of solar box wall materials. Planned wall layer consists of aluminum, rock-wool, stereo-foam and wood. While T_{am} is the average temperature of the material, calculated by the equation:

$$T\text{am} = \frac{1}{2}(T\text{a} + T\text{ao}) \text{ and } T'\text{am} = \frac{1}{2}(T'\text{a} + T'\text{ao}) \quad (5)$$

This happens because the wall temperature is not the same as the air temperature in the solar box but varies between T_a and T_{ao}. The energy required to heat the absorber plate is:

$$Q\text{b} = m\text{b}\ x\ c\text{b}\ x\ (T'\text{b} - T\text{b}) \quad (6)$$

m_b and c_b are the mass and heat absorber plate type of material used. While the heat is lost from the double glass roof is calculated by the equation:

$$Q\text{r} = U\ x\ A\ x\ (T'\text{a} - T\text{a} \quad (7)$$

$$\frac{1}{U} = \frac{1}{h\text{i}} + \frac{d}{k} + \frac{1}{h\text{c}} + \frac{d}{k} + \frac{1}{h\text{o}} \quad (8)$$

U is the total heat transfer resistance coefficient, h_i is the coefficient of convection in the inner surface (natural convection bottom horizontal plate), *k* is the material coefficient of conductivity, h_c is air convection coefficient between the first glass and the second glass (natural convection in a confined space), h_o is the coefficient of convection in the outer surface (natural convection upper horizontal plate). All these equations are calculated using the formula Nusselt numbers and that the settlement was not a trial and error, we recommend physical properties are analyzed at the temperature T_a. The heat loss from the walls of solar cookers is calculated using the equation:

$$Q\text{w} = U\ x\ A\ (T'\text{a} - T\text{a}) \quad (9)$$

$$\frac{1}{U} = \frac{1}{h\text{i}} + \frac{d}{k\text{Al}} + \frac{d}{k\text{rockwool}} + \frac{d}{k\text{stereoform}} + \frac{d}{k\text{wood}} + \frac{1}{h\text{o}} \quad (10)$$

h_i is the coefficient of convection in the inner surface (convection natural on the plate vertical) and is calculated on the nature of the air temperature T_a, h_o is the coefficient of convection in the outer surface (convection natural on the plate vertical) and is calculated on the nature of the air in the outdoor air temperature T_{ao}, A is the total area of the four side walls. All of these equations are calculated using the formula Nusselt numbers.

Heat lost from the base of the box cookers is:

$$Q\text{f} = U\ x\ A\ (T'\text{a} - T\text{a}) \quad (11)$$

$$\frac{1}{U} = \frac{1}{hi} + \frac{d}{k\mathrm{Al}} + \frac{d}{k\mathrm{rockwool}} + \frac{d}{k\mathrm{stereoform}} + \frac{d}{k\mathrm{wood}} + \frac{1}{ho} \quad (12)$$

So that the energy balance in the box of this solar heater can be written as:

$$\sum Q\mathrm{in} = \sum m.c.\Delta t + \sum Q\mathrm{losses} \quad (13)$$

which if translated would be the equation:

$$Q\mathrm{rad} = [Q\mathrm{a} + Q\mathrm{c} + Q\mathrm{m} + Q\mathrm{b}] + [Q\mathrm{r} + Q\mathrm{w} + Q\mathrm{f}] \quad (14)$$

These equations were solved every minute to obtain the temperature of the heater box.

This research was conducted in the field with the coordinates of 3°35' north latitude and 98°40' east longitude. In the process of designing the solar intensity measurement results on location will be used as a reference. At the beginning of the measurement of the intensity of radiation and daily temperature for five days, starting at 09.00 am to 15.00 pm and found that the intensity of the radiation can reach 800 W/m^2 for at least 30 minutes in a day. The observation of this intensity is used as a basic assumption in the calculation and design.

Solar cooker box designed to be able to cook up to five liters of boiling temperature. The energy balance of the heating box was calculated using equations (13) and (14). A form of solar cooking design results is shown in Fig. 1 in which the basic form is a simple box. In order to keep the temperature inside the box (T_a) reaches more than 100°C, the material composition and solar heating components must be designed and manufactured appropriately. On the floors and walls was used plate Aluminum painted black. This serves to be able to absorb all the energy radiation that comes to the surface. This will be called the absorber plate. At the top is made of two layers of glass separated. The aim is to ensure the solar radiation energy can get into the box, but the incoming summer detained to not get out too much. In other words, the function of the layer of air between the two glass plates is a heat resistant material. The wall is made of four layers, namely inside the aluminum layer, insulating layer consisting of rock-wool and stereo-foam, as well as a layer of wood on the outside. The function of the aluminum layer in the black paint is in addition to the energy-absorbing radiation coming from sunlight and heat radiation reflected by the floor. The function of the insulation layer is to inhibit heat transfer by conduction from the inner wall to the outer wall. Likewise, the wooden walls in addition to inhibiting the conduction transfer from the inside; it also serves as a holder construction of this cooker box.

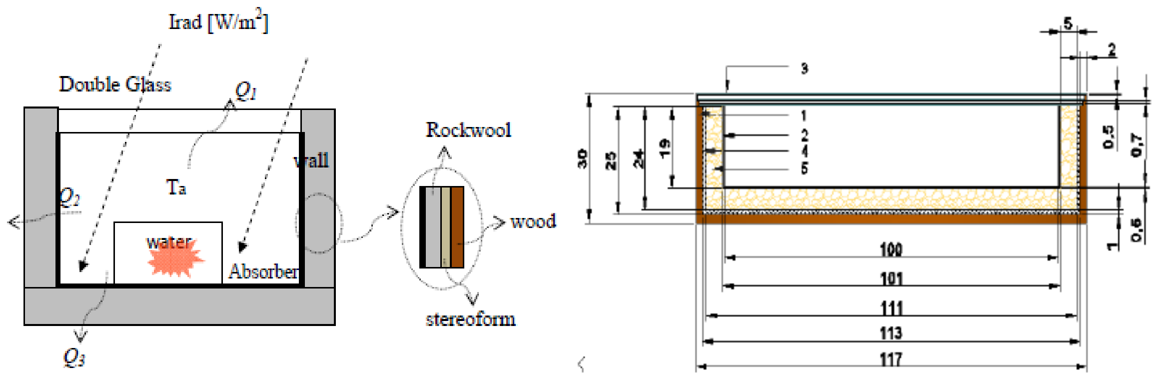

Fig. 1. – Thermal flow equilibrium and solar cooking box dimensions

By using the material and arrangement mentioned above, as well as dimensional calculation results as shown in Fig. 1, the solar heater box is made manually at the Laboratory Department of Mechanical Engineering University of HKBP Nommensen Medan. Solar cooker box that has been created is then used to boil water as shown in Fig. 2 below.

Fig. 2. – Solar heater box for boiling water

To be able to do analysis of the equation (1) until (14), it is necessary to test and record all data changes in temperature and radiation. Data acquisition system was used for recording. Experimental set-up for the heating process with this simple solar box can be seen in Fig. 3.

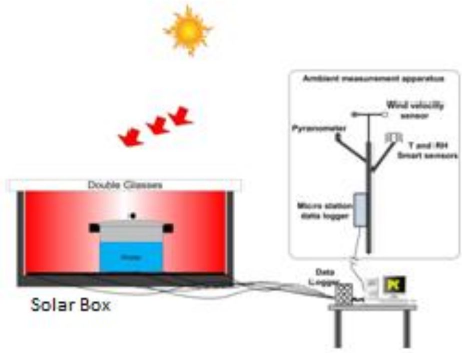

Fig. 3. – Experimental set-up of boiling water

RESULTS AND DISCUSSION

Testing was done with the cooking water as much as three, four, five and six liters for four consecutive days and the data of the temperature of the floor, walls and glass box constantly observed solar heating as well as pots and water temperature. The amount of radiation that comes to the surface of the solar cooker box and the ambient temperature were also observed, as shown in Fig. 4, 5, 6 and 7.

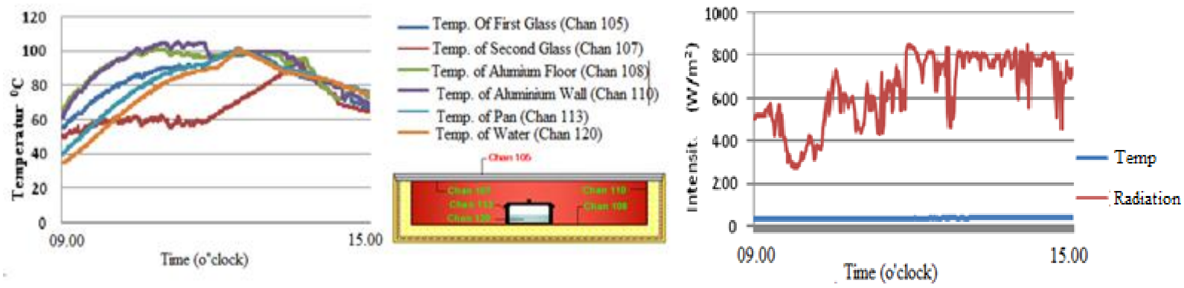

Fig. 4. – Temperature and radiation data for boiling three liters of water

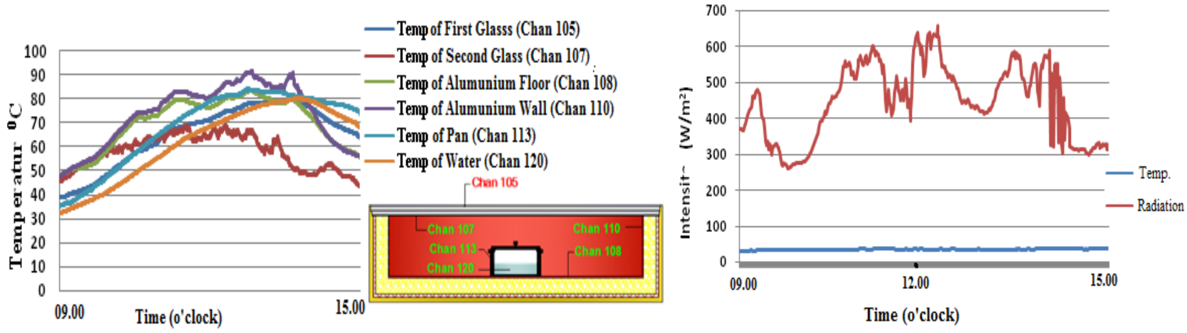

Fig. 5. – Temperature and radiation data for boiling four liters of water

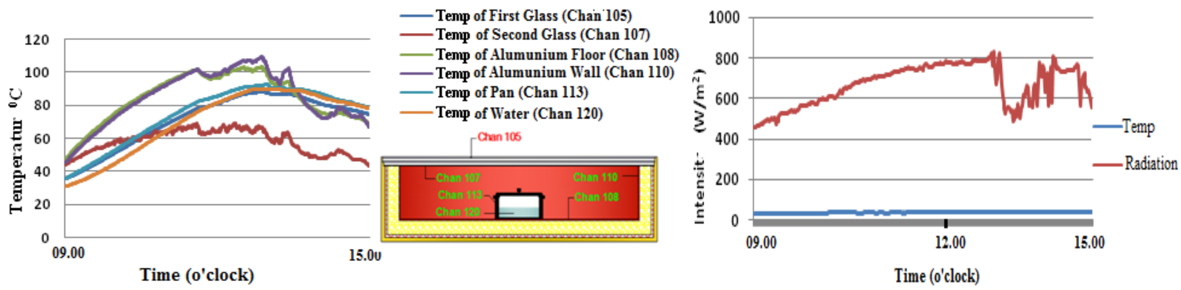

Fig. 6. – Temperature and radiation data for boiling five liters of water

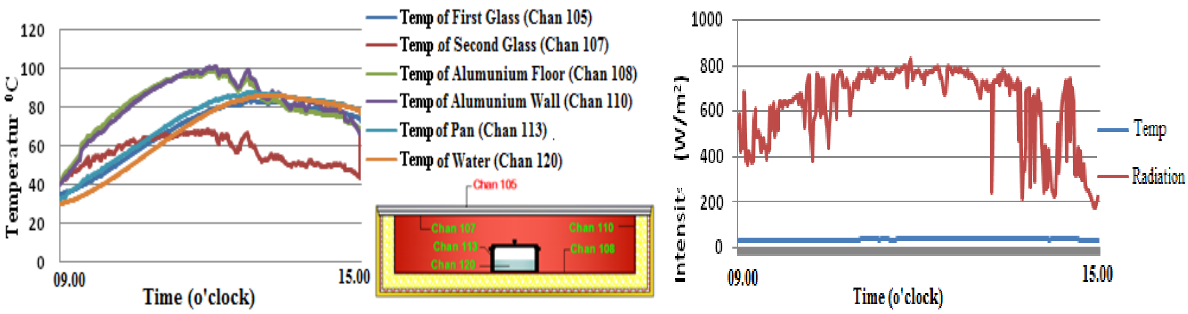

Fig. 7. – Temperature and radiation data for boiling six liters of water

Fig. 4, 5, 6 and 7 above shows that the boiling water reaches 100.97°C when the heat three liters of water. Meanwhile, when heat four liters of water, the maximum temperature that can be achieved is 79.84°C, the maximum temperature of heat five liters of water is 89.93°C and maximum temperature when heating six liters of water is 85.98°C, as shown in Fig. 8a.

This is understandable because in accordance with the equilibrium energy at the solar cooker box as shown by equation (14) that the energy required to heat the box cooker, the pot, and the water is proportional to energy radiation into the box cooker is reduced by energy lost in box heating. The value of energy radiation that comes also depends on the intensity of solar radiation, as stated in equation (1).

If we look at the magnitude of the average intensity of solar radiation received when heating the three, four, five and six liters of water from 09:00 am to 15:00 pm, it can be seen that the average intensity of solar radiation is highest during cook five liters of water that is equal 640 W·m^{-2}, whereas the three liters of water when cooking in the amount of 601.33 W·m^{-2}, and six liters of water when cooking in the amount of 611.5 W/m^2. Comparison of the amount of radiation that occurs for all four testing can be seen in Fig. 8b.

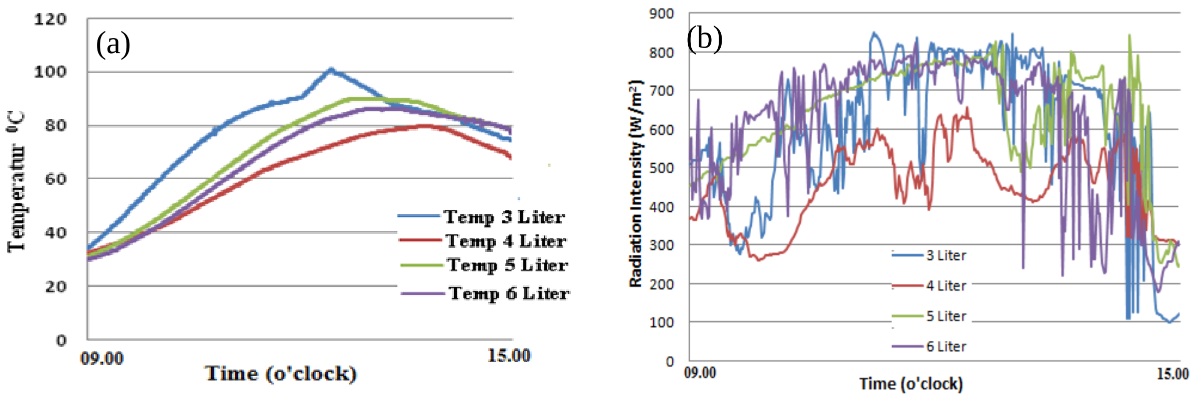

Fig. 8. – (a) Temperature and (b) radiation data for boiling all the liters of water

It is understood that three liters of water can reach a temperature of 100°C despite boiling average radiation intensity is lower than the heating five and six liters of water. This can happen because the energy generated from the radiation is able to satisfy the equation (14) above where the radiant energy received minus the energy lost from the cooker box is still able to heat the cooking box and pot to meet the energy needs for heating three liters of water.

As for testing the load five and six liters of water, although the intensity of the radiation received is greater than the test with a load of three liters of water, but the energy generated by the intensity of the radiation after subtracted by the heat lost from the box is not enough to heat up the box heater and pot to boil water to a temperature of 100°C. If we observe Fig. 6b, initially occurring radiation intensity has increased from 09.00 am to 13.00 pm approached the intensity value of 800 W·m^{-2}. But when it was approaching the intensity, the weather began overcast so not reached an intensity of 800 W/m^2 as the initial planning heater box, where the assumptions used to the intensity of solar radiation at a minimum of 800 W/m^2 for at least 30 minutes. This is likely to cause the solar cooker box can't boiling five liters of water. It is necessary for further testing on the weather conditions. As for heating six liters of water, although Fig. 7 shows the intensity of the radiation that reaches $800 \cdot m^{-2}$ for a while, but because this box is designed for load testing five liters of water, then this box cannot afford to boil six liters of water.

AKOY AND AHMED (2010) research by using the solar box cooker uses a reflector system with dimensions of 0.25 by the design volume of this study can heat water up to temperature 52.36°C. A similar study conducted by UHUEQBU AND CHIDI (2011) using a solar heater box with black painted aluminum absorber plate and the dimensions of 0.3 by volume this study design can produce heat absorber plate at 72°C indicating not be able to boil the water. MAHAVAR ET AL. (2011) did a similar study using dimensions of 0.14 times of the design volume of this study, using a plate of aluminum painted black as an absorber and using a reflector, can heat the water of 1.2 kg until the temperature 94.5°C. If we see the test results of this solar cooker box, this indicates that the design of this solar heater box is in conformity with that required to be used by housewives to boil water.

CONCLUSIONS

The design of the box simple solar heater can already be used to boil water to boiling as much as three liters. The use of two layers of glass to forward incoming solar radiation and heat blocking out has been quite good. Plate wear aluminum painted black apart as the floor as well as wall heating box further enhance the ability to absorb heat. The use of two layers of insulation of rock-wool and stereo-foam also reduce the heat dissipated into the outside wall, and the use of wood in addition to as thermal insulation but also as construction makes the cooker box is quite sturdy.

REFERENCES

1. AKOY, E. E. M., AHMED, A. I. A.: Design construction and performance evaluation of solar cookers, Journal of Agricultural Science and Engineering, Vol. 1 No. 2, 2015: 75-82.
2. AMBARITA, H.: Characteristics of solar energy Medan as energy source refrigeration cycle for air conditioning (in Indonesian), In: Proceeding of the National Seminar on Science and Technology Supports MP3EI, Faculty of Engineering University of North Sumatera, Medan, 23 November 2012.
3. AMBARITA, H.: Design and testing of solar heaters are suitable for Indonesia conditions a case study city field (in Indonesian), Journal Dynamic, Vol. 1 No. 13, 2013: 1 – 8.
4. BUDDHI, D., SHARMA, S.D., SHARMA, A.: Thermal performance evaluation of a latent heat storage unit for late evening cooking in a solar cooking having three reflector, Energy Conversation and Management, Vol. 44 No. 6, 2003: 809 – 817.
5. FAUZI – SITORUS, T. B., AMBARITA, H.: Design build solar water heater box type simple phase change materials that comes with a capacity of 100 liters of water (in Indonesian), Journal Dynamic, Vol. 1 No. 11, 2012: 44 – 50.
6. KHOLIQ, I.: Utilization of alternative energy as renewable energy to support oil fuel substitution (in Indonesian), Journal IPTEK, Vol. 19 No. 2, 2015: 76 – 91.
7. KRISHNAN, S. M., SIVAGNANAM, V., MATHEW, S. A.: Residential solar cooker, International Journal of Scientific and Research Publication, Vol. 2 No. 1, 2012: 1 – 3.
8. LUBIS, A.: Renewable energy in sustainable development (in Indonesian), J. Tek. Ling, 2007, Vol. 8 No. 2, 2007: 155 – 162.
9. MAHAVAR, S., SENGAR, N., VERMA, M., DASHORA, P.: Extensive experimental studies of a single family solar cooker, International Journal of Energy, Information and Communications, Vol. 2 No. 4, 2011: 169 – 179.
10. MINISTRY OF RESEARCH AND TECHNOLOGY OF THE REPUBLIC OF INDONESIA: White paper on research, development and application of science and technology field of new and renewable energy sources to support the availability of energy security 2025 (in Indonesian), Jakarta, 2006.
11. MUTHUSIVAGAMI, R. M., VELRAJ, M., SETHUMADAVAN, R.: Solar cookers with and without thermal storage – A Review, Renewable and Sustainable Energy Reviews 14, 2010: 691 – 701.
12. PANWAR, N. L., KAUSHIK, S. C., KOTHARI, S.: State of the art of solar cooking: An Overview, Renewable and Sustainable Energy Reviews, 16, 2012: 3776 – 3785.
13. SEPTIADI, D., NANLOHY, P.: Projection of Solar Energy Potential For Renewable Energy (in Indonesian), Journal Meteorology and Geophysics, Vol. 10 No. 1, 2009: 22 – 28.
14. UHUEGBU – CHIDI, C.: Design and construction of a wooden solar box cooker with performance and efficiency test, Journal of Basic and Applied Scientific Research, Vol. 1 No. 7, 2011: 533 – 538.
15. YANDRI, R.: Prospects for development of solar energy for electricity needs in Indonesia (in Indonesian), Journal of Physics, Vol. 4. No. 1, 2012: 14 – 19.

Corresponding author:

Richard Alfonso Napitupulu, Mechanical Engineering Department, Nommensen HKBP University, Medan, Indonesia

CHANGES IN TEMPERATURE AND ENERGY IN THE GROUND MASS WITH LINEAR HORIZONTAL HEAT EXCHANGER

P. Neuberger[1], D. Adamovský[2], R. Adamovský[1]

[1]*Department of Mechanical Engineering, Faculty of Engineering, Czech University of Life Sciences Prague, Czech Republic*
[2]*University Centre for Energy Efficient Buildings,Czech Technical University in Prague, Czech republic*

Abstract
The aim of the verifications was to analyze the temperature changes of the ground mass with linear HGHE in the heating period, determine the values of the heat flows and energies extracted from the ground mass via linear HGHE and evaluate the temperature regeneration of the ground mass during the HGHE stagnation. The linear HGHE is made from polyethylene piping PE 100RC 40×3.7 mm. HGHE with a total length of 330 m was installed at a depth of 1.8 m in three loops with a spacing of 1 m. Monitoring and analysing the linear HGHE showed that the average daily ground mass temperatures with linear HGHE were above zero in the heating season and energy extraction from the ground mass reached 16.98 $kWh \cdot m^{-2}$. Temperature difference of the ground mass within the linear HGHE area at the beginning of the heating seasons 2013/2014 and 2012/2013 was quite insignificant.

Key words: heat pump, ground mass, horizontal ground heat exchanger, temperature, heat flow, thermal energy, thermal characteristics of the ground mass.

INTRODUCTION

The energy potential of the ground mass is used via horizontal ground heat exchangers (HGHE) or vertical ground heat exchangers (VGHE), where a heat-transfer fluid is wormed up by the heat contained in the ground or rock mass, and supplied to the evaporator of the heat pump; thereby it performs a function of its low-potential source. According to BRANDL (2006), HGHE are made linear, helical or spiral; they require larger land area than VGHE but demand smaller investment costs. They present a compromise between high efficiency and investment costs. Mainly linear HGHE are widespread in the Czech Republic. In terms of usable energy potential, HGHE durability and good performance of the whole energy system, the knowledge of thermal characteristics of the ground mass, temperatures, extracted heat and heat flows at a given HGHE configuration are important. Especially knowledge of mutual interconnections is of essential importance, allowing optimizing HGHE design and operation and the operation of the entire system. Also the knowledge of the regeneration capabilities of the energy potential in the stagnation period or during its partial use in summer period is important.

One of the most important variables influencing the effect of the heat pump is the temperature of the medium of the low-potential energy source supplied to the evaporator of the heat pump. This results from the reversed cooling Carnot cycle. Its effect, which is expressed by the heating factor for a heat pump, is the higher, the smaller the temperature difference at which we supply and drain the heat of the cycle. Results of our verifications NEUBERGER ET AL. (2014), ADAMOVSKÝ ET AL. (2015) as well as verifications and modelling of foreign authors INALLI AND ESEN (2004), KUPIEC ET AL. (2015) showed that for most of the heating period the temperatures of the ground mass are higher than the ambient air temperatures. In the summer period, the ground mass temperatures are on the contrary lower than the ambient air temperatures. This fact makes more favourable ground mass, in comparison to the ambient air, as stable low-potential source for the heat pumps for heating of the buildings in the winter period and for their cooling in the summer period.

The aim of the verifications was to:

- Analyze the temperature changes of the ground mass with linear HGHE in the heating period;
- Determine the values of the heat flows and energies extracted from the ground mass via linear HGHE in the heating period;
- Evaluate the temperature regeneration of the ground mass during the HGHE stagnation.

The following hypotheses were verified:

a) The ground mass temperatures in the heating period will be mostly above zero. The ground mass temperatures in the HGHE area will be below zero only in exceptional cases;

b) The ground mass temperatures in the heating period in the HGHE area will be lower by maximum 4 K than the reference temperature of the ground mass;

c) The ground mass temperatures in the heating period will comply with the VDI STANDARDS (2001);

d) The energies extracted from the ground mass will comply with the VDI STANDARDS (2001);

e) The temperature difference of the ground mass at the beginning of the heating period will not be significant.

HEPBURN ET AL. (2016) devoted to sustainability of HGHE as a low-potential energy source for heat pumps, depending on temperatures and thermal characteristics of the ground mass. Extensive measurements brought new knowledge of the influence of heat extraction by HGHE and ambient climatic conditions on the ground mass. The interaction between the ground mass and HGHE was addressed by GARCIA ET AL. (2012) and POPIEL (2001). The values and distribution of the temperatures in the ground mass with HGHE used as a low-potential energy source for a conventional heat pump with a compressor and absorption heat pump is addressed by WEI (2013). PHILLIPPE ET AL. (2010) monitored responses of the ground mass temperatures to horizontal GSHP system within four different surfaces of the ground mass. BANKS (2012) evaluated the influence of the heat-transfer fluid flow type on specific heat output of the HGHE and indicated limit values of the energy extraction from the ground mass in the heating period.

MATERIALS AND METHODS

2.1 Determination of the course of the average daily temperatures

Based on the equation of free, undamped oscillation of a mass point, NEUBERGER ET AL. (2014) formulated the dependence of the average daily ground mass temperatures in the heating period:

$$t_{GR} = \bar{t}_G + \Delta t_{am.} \cdot \sin\left(\Omega.\tau + \varphi\right) (°C) \qquad (1)$$

Where:

t_{GR} - ground mass temperature (°C); $\bar{t}_G$ - mean ground mass temperature (°C);

$\Delta t_{am.}$ - oscillation amplitude around the temperature $\bar{t}$ (K); τ - number of days from the start of measurement (day);

φ - initial phase of oscillation (rad); Ω - angular velocity ($2 \cdot \pi/365$ rad $\cdot$ day^{-1}).

According to BOWERMAN ET AL. (1997), a determination index I^2_{yx} (-) was used to determine the degree of tightness in the relation between both random quantities.

2.2 Measurement methods

The linear HGHE is made from polyethylene piping PE 100RC 40×3.7 mm (LUNA PLAST Inc., Hořín, Czech Republic) resistant to point loads and cracking. HGHE with a total length of 330 m with heat transfer surface 41.473 m^2 was installed at a depth of 1.8 m in three loops with a spacing of 1 m. The length of each loop is 54.62 m. The land area with HGHE is 273 m^2.

The layout identifying the location of temperature sensors and HGHE is presented in Fig. 1 and 2.

The heat-transfer fluid flowing through the heat exchanger was a mixture of 33% ethanol and 67% water. The tested HGHE was one of the energy sources for heat pumps IVT PremiumLine EQ E17 (Industriell Värme Teknik, Tnanas, Sweden) with a nominal heat output of 17 kW (0/35 °C). The heat pumps were used only for heating, not for cooling the administration building and manufacturing halls of the company VESKOM Ltd. based in Prague, Dolní Měcholupy.

The ground mass profile, where the HGHE is deposited, consists of two layers; an arable land layer (approximately 0.25 m) and a layer of detritus (approximately 2 m), consisting of dark-brown sandy loam soil, coarse gravel, crushed rock and bricks debris.

The ambient air temperatures t_e were measured at a height of 2 m above the soil surface and at a distance of 20 m from the horizontal ground heat exchangers by sensor ALMEMO FHA646AG (AHLBORN Mess- und Regulungstechnik, Holzkirchen, Germany). The ground mass temperatures were measured by sensors GKF 125 and GKF 200 (GREISINGER electronic GmbH, Regenstauf Germany). All temperatures were recorded at half-hour intervals by measuring operators ALMEMO 5990 and ALMEMO 2890-9 (AHLBORN Mess-und Regulungstechnik, Holzkirchen, Germany). Global radiation sensor FLA613GS (AHLBORN Mess-und Regulungstechnik, Holzkirchen, Germany) was used to measure the intensity of the incident solar radiation.

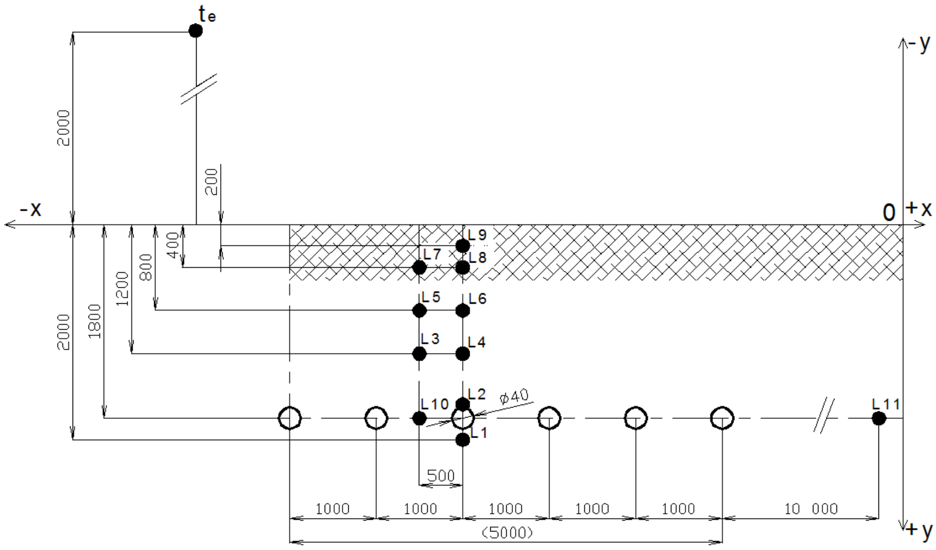

Fig. 1. – Layout identifying the location of temperature sensors in the ground mass

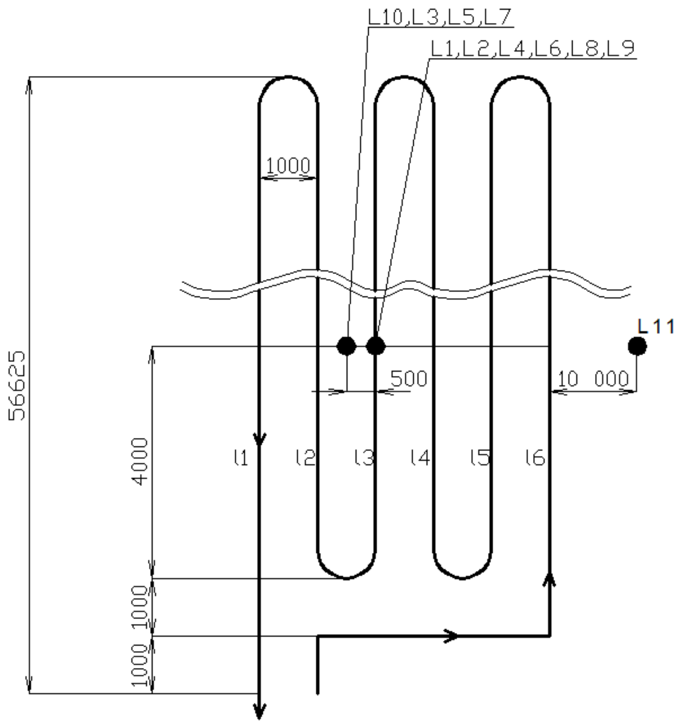

Fig. 2. – Site layout of the linear HGHE and location of the temperature sensors

Tab. 1. – Parameters of equation (1) for calculating the average daily temperatures of the ground mass with linear HGHE in the heating and stagnation period

	Δt_A	φ	$\bar{t}$	I^2_{yx}
t_{L1}	6.938	1.892	10.217	0.976
t_{L2}	7.797	2.039	9.984	0.982
t_{L3}	8.131	2.105	10.495	0.975
t_{L5}	7.961	2.24	10.066	0.953
t_{L7}	8.752	2.369	10.264	0.945
t_{L8}	9.038	2.389	10.338	0.941
t_{L9}	8.958	2.438	10.205	0.926
t_{L11}	5.525	1.826	10.806	0.988
t_e	9.542	2.563	10.137	0.776

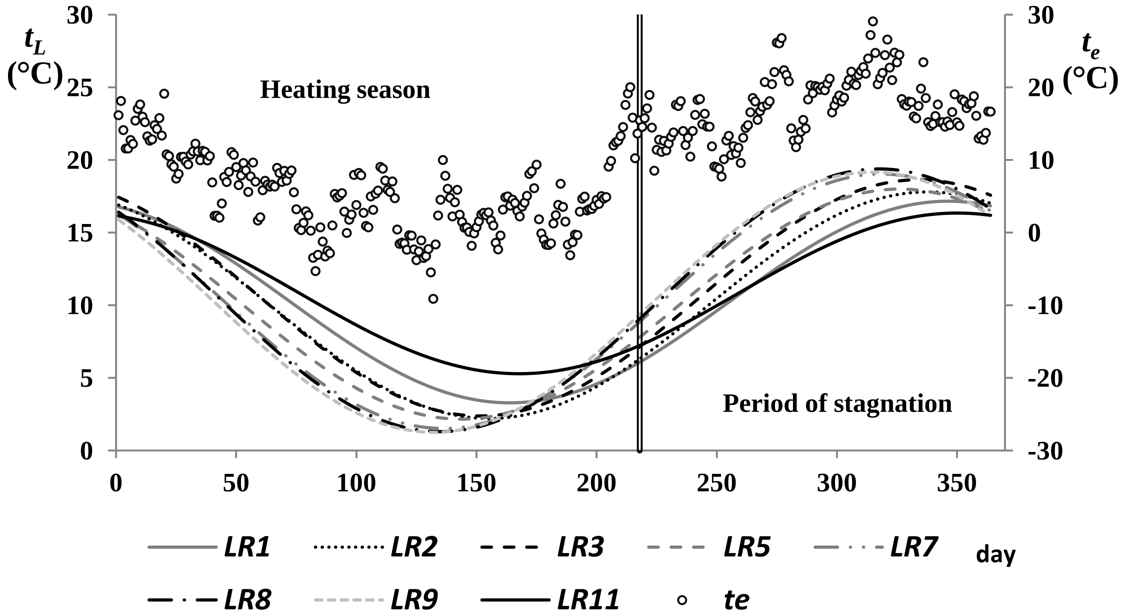

Fig. 3. – Average daily ground mass temperatures calculated from equation (1)

RESULTS AND DISCUSSION

3.1 Ground mass temperatures with HGHE

Parameters of equation (1) presented in Tab. 1 can be used to calculate average daily temperatures of the ground mass in the heating period and the period of stagnation. Fig. 3 shows the average daily temperature trends of the ground mass with HGHE in monitored depths calculated from equation (1).

The line parallel to the vertical axis in Fig. 3 separates the heating period (218 days) from the period of HGHE stagnation (146 days). The plot in this figure demonstrates that the average daily temperature of the ground mass with the linear HGHE decreased towards the ground mass surface in the heating season. The lowest temperatures were not attained in the area of HGHE but near the mass surface. Also the oscillation amplitudes Δt_A around the mean ground mass temperature $\bar{t}_G$ increased towards the ground mass surface. These trends confirmed the influence of the ambient air temperatures t_e. The relevant temperatures of the ground mass in the area of HGHE (t_{L1},t_{L2}) decreased evenly from 17.11 °C, by approximately 1 K per 13 days, up to a day 192 of the heating period when it was 2.42 °C. Subsequently, the ground mass temperatures increased and at the end of the heating period reached 5.54 °C. From the beginning of the stagnation period, the ground mass temperatures in the area of HGHE increased by approximately 1 K per

9.8 days. It reached the value of the temperatures before the heating period already on day 105 of the stagnation period. The ground mass temperatures with HGHE decreased slightly at the end of the stagnation period due to ambient air temperature decrease. The temperature difference of the ground mass in the area of linear HGHE at the beginning of the heating periods 2013/2014 and 2012/2013 were quite insignificant, it was 0.05 K. The ground mass temperatures in the area of linear HGHE were higher than the ambient air temperatures t_e during 68.8% of the heating period.

3.2 Heat flows and energies transferred from the ground mass

Tab. 2 shows the average and extreme values of the ambient temperatures t_e, ground mass temperatures t_{L2} in the HGHE area and reference temperatures t_{L11} measured away from HGHE area in the heating period. Furthermore, specific heat outputs $q_{pL,s}$ and energies $q_{dL,s}$ calculated per 1 m^2 of the land area with HGHE and a day, intensity $I_{p,s.r.}$ and total energy of incident solar radiation $I_{d,s.r.}$ per a day are presented in this table. Trends of temperatures of ground mass and ambient air, heat flows and specific energies transferred from the ground mass via linear HGHE in the heating season is displayed in Fig. 3.

The plot in Fig. 3 and the data in Tab. 2 show that the temperatures in the HGHE area were above zero. Temperatures above zero are important in terms of the heat pump factor value as well as in terms of ice formation in the vicinity of HGHE pipes. According to BANKS (2012), ice formation can lead to connection of ice cylinders around the HGHE pipes, or their connection with naturally frozen ground mass. If this occurs, there is a serious risk that such an extensive frozen ground mass exposed to the solar radiation in the summer period will not thaw.

Tab. 2. – Average and extreme values of the temperatures, specific heat outputs and energies in the heating period.

	Heating period		
	Min.	Average	Max.
t_e (°C)	-9.15	5.44 ± 5.57	19.99
t_{L2} (°C)	2.00	7.08 ± 4.76	17.14
t_{L11} (°C)	5.23	9.30 ± 3.74	16.74
$q_{pL,s}$ (W/m^2)	0.21	5.93 ± 3.04	12.96
$q_{dL,s}$ (Wh/m^2·day)	0.34	77.88 ± 50.63	255.22
$I_{p,s.r.}$ (W/m^2)	3.52	66.27 ± 55.35	270.29
$I_{d,s.r.}$ (kWh/m^2·day)	0.085	1.61 ± 1.35	6.49

The observed difference between the reference ground mass temperature t_{L11} and the mass temperature in the area of the exchanger t_{L2} was not significant; on average 2.22 ± 1.23, maximum 4.25 K. The temperature to which the ground mass is cooled has practical meaning, especially in terms of the heat-transfer fluid temperature, the size of a land area, where HGHE is deposited and also the sustainability of the low-potential source. The average temperature of the heat-transfer fluid flowing through the linear HGHE to the evaporator of the heat pump in the heating period was 8.13 ± 4.51 °C, minimum 1.67 °C. The minimum temperature from the heat pump evaporator to HGHE was -2.09 °C, the average 5.80 ± 5.12 °C.

According to the German VDI STANDARD (2001), the temperature of the heat-transfer fluid flowing from the heat pump to the ground loop must not deviate by more than ±12 °C from the ground mass temperature at rated load conditions of HGHE or more than ±18 °C from peak load. In case of the tested linear HGHE, the average difference between the ground mass temperature away from HGHE area and the heat-fluid temperature at the heat pump evaporator was 3.48 ± 2.71 K, maximum 9.49 K. Operation of linear HGHE is in accordance with the VDI STANDARD (2001).

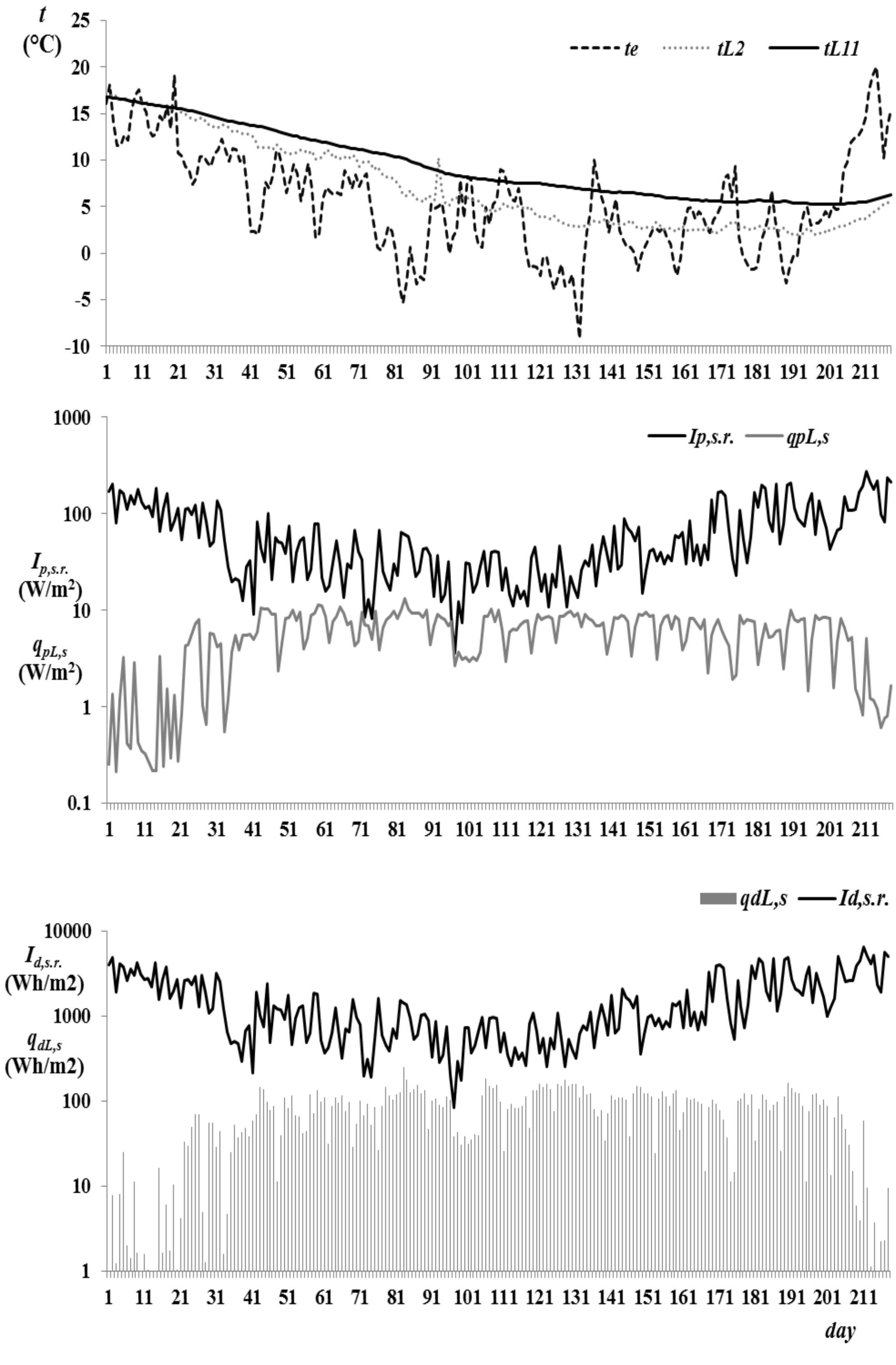

Fig. 4. – Temperatures of the ground mass and the ambient air temperatures, heat flows and specific energies transferred from the ground mass via linear HGHE

In respect of sustainability of the low-potential source, the VDI STANDARD (2001) also recommended not to exceed the total annual energy extraction from the ground mass 50-70 kWh per 1 m^2 of land area with HGHE. In the case analysed in this paper, the energy extraction from the ground mass reached only 16.98 kWh/m^2. The lower value of the energy extraction was caused by high concentration of ethanol in the heat-transfer fluid and its low flow rate.

According to The Engineering ToolBox, the freezing point of the used heat-transfer fluid is -17.4 °C. The measurement results showed that the minimum temperature of the heat-transfer fluid at the outlet of the heat pump was -2.09 °C. More suitable for HGHE would thus be lower concentration, e.g. 20% ethanol, when the freezing temperature of the mixture is -9.0 °C. Lowering the ethanol concentration would reduce the kinematic viscosity of the heat-transfer fluid by 47.3% (at 0 °C), increase the value of the Reynolds criterion by 44.28% and increase the coefficient of heat transfer between the HGHE inner pipe wall and the heat-transfer fluid by 13.96%. Mentioned heat transfer coefficient can be a limiting variable of heat transfer between the ground mass and the heat-transfer fluid in HGHE.

BANKS (2012) indicated that to obtain temporary turbulent flow ($Re > 2500$) in a hydraulically smooth pipe of an outer diameter 40 mm at a volume concentration of ethanol 22.5% (freezing point -10 °C), it is necessary to achieve a volume flow of the heat-transfer fluid 19.7 l/min. The heat-transfer fluid flow in the tested HGHE reached value 5.0 l/min in the first stage of the circulation pump operation and 10.32 l/min in the second stage.

CONCLUSIONS

Monitoring and analysing the linear HGHE operation during the heating and stagnation periods showed the following:

- The average daily ground mass temperatures above the linear HGHE decreased in the heating period towards the ground mass surface. Minimum temperatures were not reached in the HGHE area but near the mass surface. Major effect of ambient air temperatures $t_e$on the ground mass temperatures in the heating period was confirmed by HEPBURN ET AL. (2016) and POPIEL ET AL. (2001);
- The ground mass temperatures in the area of linear HGHE were higher than the ambient air temperatures t_e.during 68.8%. Ground mass temperatures were lower than the ambient air temperatures particularly at the end of the heating season. The importance of temperatures of the low-potential energy source for heat pumps was confirmed by DE SWARDT, MEYER (2001);
- The average daily ground mass temperatures with linear HGHE were above zero in the heating season. Temperatures below zero did not occur in HGHE area during the heating period. Hypothesis *a)* formulated at the beginning of this paper was thereby confirmed;
- The observed difference of reference ground mass temperature t_{L11} and ground mass temperature in the area of the heat exchanger t_{L2} was not significant, on average 2.22 ± 1.23 K; maximum difference reached the value of 4.25 K. A temperature difference of more than 4 K occurred in 5 days of the heating season. Hypothesis *b)* was not confirmed;
- The average daily ground mass temperatures with the linear HGHE during the heating and stagnation period can be expressed by equation (1) and parameters presented in Tab. 1;
- The temperature difference of the ground mass within the linear HGHE area at the beginning of the heating seasons 2013/2014 and 2012/2013 was quite insignificant, amounted to 0.05 K. Hypothesis *e)* was confirmed;
- The average daily temperature difference of the ground mass away from the HGHE area and the heat-transfer fluid temperatures from the heat pump evaporator was 3.48 ± 2.71 K, maximum 9.49 K. The HGHE operation is in accordance with the VDI recommendations (2001). Hypothesis *c)* was confirmed;
- Energy extraction from the ground mass during the heating period was significantly lower than the VDI limiting values (2001), it reached 16.98 kWh/m^2. The cause of lower energy extraction was high concentration of ethanol in the heat-transfer fluid and its low flow rate. Hypothesis *d)* was confirmed.

The results of the linear HGHE verification pointed out to deficiencies, inspired further research in this area and brought new knowledge usable in construction and design practice. Further studies will be aimed at increasing the specific heat output of the linear HGHE, on the base of monitoring and analysing obtained results, and at reducing the size of a land area required for ground mass energy extraction.

REFERENCES

1. ADAMOVSKÝ, D., NEUBERGER, P., ADAMOVSKÝ, R.: Changes in energy and temperature in the grand mass with horizontal heat exchangers – The energy source for heat pumps. Energy and Buildings, 92, 2015: 107-115.
2. BANKS, D.: AnIntroduction to Thermogeology: Ground Source Heating and Cooling. 2 nded., Oxford, UK, John Wiley&Sons, Ltd. 2012.
3. BRANDL, H.: Energy foundations and other thermo-active grand structures. Géotechnique, 56, 2006: 81-122.
4. DE SWARDT, C. A., MEYER, J. P.: A performance comparison between an air-coupled and a ground-coupled reversible heat pump. Inter. Jour. ofEnerg. Res, 25, 2001: 810-899.
5. GARCIA, G., R., VERHOEF, A., VIDALE, P. L., MAIN, B. G. G., WU, Y.: Interactions between the physical soil environment and a horizontal groundcoupled heat pump, for a domesticsite in the UK. Renew. Energy, 44, 2012: 141-153.
6. HEPBURN, D. P. B., SEDIGHIA, M., MANJU, H. R. T.: Field-scale monitoring of a horizontal ground source heat system. Geothermics, 61, 2016: 86-103.
7. INALLI, M., ESEN, H.: Experimental thermal performance evaluation of a horizontal ground-source heat pump systém. Applied Thermal Engineering 24, 2004: 2219-2232.
8. KUPIEC, K., LARWA, B., GWADERA, M.: Heat transfer in horizontal grand heat exchangers. Applied Thermal Engineering ,75, 2015: 270-276.
9. NEUBERGER, P., ADAMOVSKÝ, R., ŠEĎOVÁ, M.: Temperatures and Heat Flows in a Soil Enclosing a Slinky Horizontal Heat Exchanger. Energies, 7, 2014: 972-978.
10. PHILLIPPE, M., MARCHIO, D. L. H., VRAIN, A.: An Evolution of Ground Thermal Properties Measurement Accuracy by Thermal Response Test ofHorizontal Ground Source Heat Exchangers. In: World Geothermal Congress, 25-30 April 2010, Bali, Indonesia.
11. POPIEL, C., WOJTKOWIAK, J., BIERNACKA, B.: Measurements of temperature distribution in ground. Experimental Thermal and Fluid Science, 25, 2001: 301-309.
12. THE ENGINEERING TOOLBOX: Ethanol Freeze Protected Water-Solutions, Available online http://www.engineeringtoolbox.com/ethanol-water-d_989.html. (accessed 2 July 2015).
13. VDI 4640- PART 2, Thermal use of the underground – Ground source heat pump systems. Verein Deutscher Ingenieure, Düsseldorf, (2001).
14. WU, W., WANG, B., YOU, T., SHI, W., LI, X.: A potential solution for thermal imbalance of ground source heat pump systems in coldregions: Ground source absorptionheat pump. Renew. Energy, 59, 2013: 39-48.

Corresponding author:

doc. Ing. Pavel Neuberger, Ph.D., Department of Mechanical Engineering, Faculty of Engineering, Czech University of Life Sciences Prague, Kamýcká 129, Praha 6, Prague, 16521, Czech Republic, phone: +420 22438 3179, e-mail: neuberger@tf.czu.cz

TRANSLOCATION OF SOIL PARTICLES AT DIFFERENT SPEED OF TILLERS

P. Novák[1], J. Hůla[1], J. Kumhálová[2]

[1]Department of Agricultural Machines, Faculty of Engineering, Czech University of Life Sciences Prague, Czech Republic
[2]Department of Applied Geoinformatics and Spatial Planning, Faculty of Environmental Sciences, Czech University of Life Sciences Prague, Czech Republic

Abstract
Soil tillage may contribute to the undesirable translocation of soil particles towards lower-lying parts of fields on slopes. The effect of tillage implements on soil particle translocation has not been sufficiently explained yet. The object of research was to assess the influence of different operating speed of disc tiller and tine tiller on soil particle translocation during shallow primary tillage. In both tillers a significant translocation of soil particles in the direction of the implement movement was observed while the most distant particles after tillage with a tine tiller were found more than 3 m from their original location in the topsoil layer. The disc tiller translocated soil particles to a shorter distance than the tine tiller. Statistical significance of differences in the distance of translocated particles was evaluated for different operating speeds of tillers from 4.5 to 14 km.h^{-1}.

Key words: soil tillage; tillage erosion; operating speed.

INTRODUCTION

In the study of soil erosion processes attention is rightfully paid particularly to water erosion of soil. Naturally, besides water and/or wind erosion soil properties are negatively influenced by tillage erosion. Tillage erosion and translocation of soil particles by implements during soil tillage are relatively little examined areas of research on soil erosion (GOVERS ET AL., 1999). Soil tillage significantly contributes to the topsoil profile diminishment on tops of sloping lands and to gradual translocation of soil particles in the fall line direction (LOBB ET AL., 1995). TIESSEN ET AL. (2007) emphasized that the majority of the implements for primary and secondary tillage have potential erosive effects on the soil. VAN MUYSEN ET AL. (2002) and DA SILVA ET AL. (2004) considered operating speed and working depth during soil tillage as the main factors participating in the translocation of soil particles. The lack of experimental results is evident mainly in the effect of the operating speed of implements on the soil particle translocation.

The methodology of measuring the movement of soil particles is currently being defined in greater detail. An overview of the use of tracers incorporated into the soil for indication of the soil particle movement was presented by LOGSDON (2013). Besides metal tracers (Al cubes, steel nuts) limestone grit can be used. An advantage of limestone is that its colour is distinctly different from the soil.

The objective of a field experiment was to evaluate the effect of two tillers used for primary tillage on the translocation of soil particles at different operating speed. Three operating speeds were chosen to be compared that represent the potential operating use of tillers.

MATERIALS AND METHODS

Measurements of the effect of different operating speed on the movement of soil particles during primary tillage were carried out on sandy loam Cambisol after harvest of common oat for green forage. Basic data on a field where measurements were done: the locality Nesperska Lhota near Vlasim (GPS 49.690435, 14.815578), altitude of 420 m a.s.l. Before measurements soil samples were taken for determination of the basic physical properties of soil at a tillage depth, soil moisture was determined and the field slope was measured (average 2.7°).

To measure the translocation of soil particles by tillage two implements were chosen:

- Lemken Karat 9 tine tiller with working width 2.6 m
- Akpil 3 OX disc tiller with working width 3 m.

Lemken Karat 9 was equipped with chisel tines with side wings for soil loosening and three disc pairs for soil crumbling and mixing. Working tools of cultivator Akpil 3 OX are discs 500 mm in diameter. Zetor-12045 (90 kW) tractor was used as a power-supplying vehicle. Soil particle translocation was measured after shallow primary tillage to a depth of 0.11 m (tine tiller) and 0.08 m (disc tiller). Operating speeds of 4.5 km.h^{-1}, 9 km.h^{-1} and 14 km.h^{-1} were chosen for both tillers. For measurement of the machine sets speed was used the tractor-board equipment. Soil moisture at a depth of its tillage was 12.2% by volume (before loosening), bulk density was 1.51 g.cm^{-3}, total porosity 43.6% by volume.

To evaluate the movement of soil particles white limestone grit (particle size 10-16 mm) was used. Before soil tillage grits were incorporated into grooves of 0.20 m in width and 1 m in length. The longer side of the grooves was oriented perpendicularly to the direction of subsequent passes of tillage implements. The groove depth was chosen to match the working depth of tiller tools.

After the set of a tractor with the respective implement (2 tillers, 3 operating speeds) passed across the field, the tracers were picked by hand from the soil in segments of 0.30 m in the direction of the machine movement- segments were marked by metal plates pressed into the topsoil. After the machines passed across the field, the segments were divided into three segments of 0.33 m also in a crosswise direction. When the tracers were picked from the soil, their weight was determined in each segment as an indicator of the soil particle translocation by soil tillage. For data processing MS Excel (Microsoft, USA) and Statistica 12 (Statsoft, USA) were used with the analytical tool ANOVA for statistical evaluation of results, specifically by Tukey's HSD test.

RESULTS AND DISCUSSION

Fig. 1 shows the translocation of soil particles during tillage with a disc tiller. Tab. 1 documents average values of the weight of translocated particles and statistically significant differences are shown by means of indices. The graph illustrates decreasing weight of translocated particles with increasing lengthwise distance at all measured operating speeds. This graph also indicates the effect of operating speed on particle translocation. The translocation pattern can be described by the logarithmic regression method when very strong relationship is reached in all studied cases in the given range of measurements. At a higher operating speed the disc tiller translocates a larger amount of particles, and to a longer distance. Some differences were found out, but mostly below the statistical significance level (see Tab. 1). Statistically significant differences were recorded at distances of 0.3-0.6 m, 0.9-1.2 m, 1.5 m and more. Particles at a distance more than 1.5 m were observed only at the speed of 14 km.h^{-1} (the most distant particle was at 1.6 m). At the speed of 9 km.h^{-1} the most distant particle was found 1.22 m from the original location and at the speed of 4.5 km.h^{-1} it was at 1.23 m. The disc tiller generally translocates particles mainly in the surface layer of the tilled soil when the topsoil layer is cut off. High kinetic energy of discs causes the soil particles to fly away from the discs. At a higher speed the effect of discs is also higher, resulting in a more intensive mixing effect. The discs translocate particles also in a crosswise direction. It depends on the design and construction of the tiller.

Tab. 1. – Average translocation of particles with a disc tiller (g) in a lengthwise direction and marked out homogeneous groups (Tukey's HSD test)

Distance (m)	**14 km.ha^{-1}**	**9 km.ha^{-1}**	**4.5 km.ha^{-1}**
0-0.3	1267^{a}	823^{a}	1045^{a}
0.3-0.6	488^{a}	437^{a}	463^{b}
0.6-0.9	265^{a}	154^{a}	209^{a}
0.9-1.2	137^{a}	29^{b}	83^{b}
1.2-1.5	110^{a}	5^{a}	57^{a}
1.5 and more	4^{a}	0^{b}	0^{b}

Homogeneous groups are marked by letters a, b.

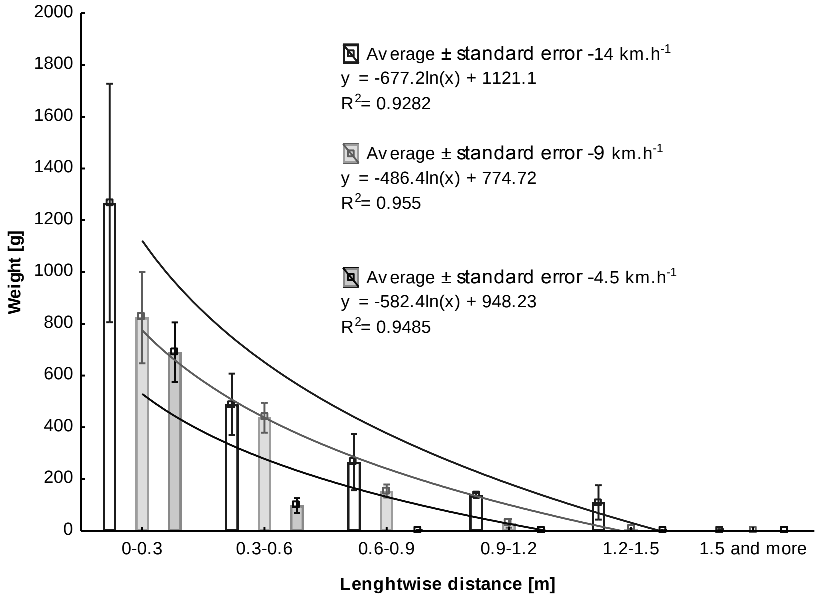

Fig. 1. – Translocation of soil particles during tillage with a disc tiller

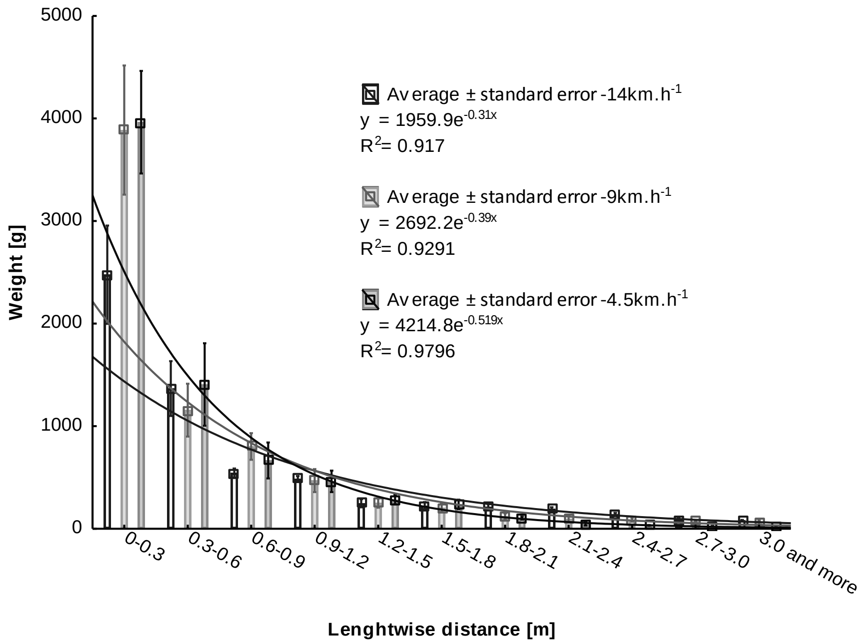

Fig. 2. – Translocation of soil particles during tillage with a tine tiller

Fig. 2 illustrates the translocation of soil particles during tillage with a tine tiller. Tab. 2 shows average values of the weight of translocated particles and statistically significant differences are shown by means of indices. The translocation pattern and the effect of speed are completely different from measurements when a disc tiller is used. At a shorter distance from the original location surprisingly fewer particles were translocated at the highest operating speed. However, these differences were below the statistical significance level without exception. But this trend was opposite at a distance more than 1.5 m and the highest amount of particles was translocated at a speed of 14 km.h^{-1}. In the intervals from 1.5 to 3 m statistically significant differences were found out between the particular speeds (see Tab. 2). At a speed of 14 km.h^{-1} the most distant particle was 5.75 m from the original location. At a speed of 9 km.h^{-1} the most distant particle was at 5.1 m and at a speed of 4.5 km.h^{-1} it was only 3.7 m. The pattern of particle translocation is different from the former machine. The majority of the soil particles are translocated to a short distance, then the translocation intensity decreases very rapidly. It is caused mainly by the effect of tines when the soil is carried away with tines along the whole tilled depth of the soil profile. The translocation effect will surely be influenced by an organic matter amount on the soil surface and in the subsurface layer of soil. The translocation pattern can be described by exponential regression with a very strong relationship for all cases of observation.

Tab. 2. – Average translocation of particles (g) with a tine tiller in a lengthwise direction and marked out homogeneous groups (Tukey's HSD test)

Distance (m)	**14 km.ha-1**	**9 km.ha-1**	**4.5 km.ha-1**
0-0.3	2477[a]	3887[a]	3963[a]
0.3-0.6	1367[a]	1157[a]	1407[a]
0.6-0.9	543[a]	803[a]	667[a]
0.9-122	487[a]	470[a]	463[a]
1.2-1.5	249[a]	251[a]	284[a]
1.5-1.8	225[a]	206[a]	237[a]
1.8-2.1	216[a]	120[ab]	104[b]
2.1-2.4	192[a]	98[ab]	49[b]
2.4-2.7	139[a]	89[ab]	34[b]
2.7-3.0	90[a]	71[a]	25[b]
3.0 and more	80[a]	56[a]	20[a]

Homogeneous groups are marked by letters a, b.

Van Muysen et al. (2006) reported that the average movement of soil particles caused by tillage implements was in the range of 0 to 0.9 m, scarcely were the soil particles found at a distance above 10 m. This was confirmed by our measurements only partly. The conclusions drawn by Tiessen et al. (2007) were confirmed that any treatment during soil tillage puts a large amount of soil into movement and is potentially erosive. The performed measurements also confirmed a good usability of tracers, which is consistent with the results of Logsdon (2013). This author also used calcium carbonate (limestone), careful hand picking of tracers from the soil and weighing. Li et al. (2007) emphasized the need of measuring the soil particle translocation to a greater extent in soil tillage systems. The results presented in this paper are a part of gradual evaluation of the effect of main implement groups on soil particle translocation and of the share of implements in the erosion risk on arable land. The results of implement effects on soil tillage can be appropriately used for the modelling of erosion processes (Takken et al., 2001).

CONCLUSIONS

Disc cultivator and tine cultivators are implements that are used on a large scale for soil tillage. The operating speed is an important factor influencing the quality of their work and area performance. For disc and tine cultivators is a typical working speed between 10-15 km.h^{-1}. Therefore it is important to clarify the influence of the different working speeds on displacement of soil particles. This was confirmed in the aforementioned measurements. The results of evaluation of soil particle translocation at different operating speed of cultivators can contribute to better knowledge of the share of tillage treatments in soil erosion processes. It was confirmed that the choice of machines for soil tillage can substantially influence the intensity of undesirable soil translocation especially in sloping fields.

ACKNOWLEDGEMENTS.

Supported by the Ministry of Agriculture of the Czech Republic - Project no. QJ1520028.

REFERENCES

1. DA SILVA, J. R. M., SOARES, J. M. C. N., KARLEN, D. L.: Implement and soil condition effect on tillage-induced erosion. Soil & Tillage Research, 78, 2004: 207-216.
2. GOVERS, G., LOBB, D. A., QUINE, T. A.: Tillage erosion and translocation: emergence of new paradigm in soil erosion research. Soil & Tillage Research, 51, 1999: 167-174.
3. LI, S., LOBB, D. A., LINDSTROM, M. J.: Tillage translocation and tillage erosion in cereal-based production in Manitoba, Canada. Soil & Tillage Research, 94, 2007: 164-182.
4. LOBB, D. A., KACHANOSKI, R. G., MILLER, M. H.: Tillage translocation and tillage erosion on shoulder slope landscape positions measured using ^{137}Cs as a tracer. Canadian Journal of Soil Science, 75, 1995: 211-218.
5. LOGSDON, S. D.: Depth dependence of chisel plow tillage erosion. Soil & Tillage Research, 128, 2013: 119-124.
6. TAKKEN, I., GOVERS, G., JETTEN, V., NACHTERGAELE, J., STEEGEN, A., POESEN, J.: Effects of tillage on runoff and erosion patterns. Soil & Tillage Research, 61, 2001: 55-60.
7. TIESSEN, K. H. D., LOBB, D. A., MEHUYS, G. R., REES, H. W.: Tillage erosion within potato production in Atlantic Canada: II. Erosivity of primary and secondary tillage operations. Soil & Tillage Research, 95, 2007: 320-331.
8. VAN MUYSEN, W., GOVERS, G., VAN OOST, K.: Identification of important factors in the process of tillage erosion: the case of mouldboard tillage. Soil & Tillage Research, 65, 2002: 77-93.

Corresponding author:

Ing. Petr Novák, Ph.D., Department of agricultural machines, Faculty of Engineering, Czech University of Life Sciences Prague, Kamýcká 129, Praha 6, Prague, 16521, Czech Republic, phone: +420 22438 3133, e-mail: novakpetr@tf.czu.cz

MEASUREMENT OF PRESSURE CONVERTER WITH CONDUCTIVE INK

V. Novák[1], J. Volf[1], D. Novák[2], V. Ryzhenko[1]

[1]*Faculty of Engineering, Czech University of Life Sciences Prague, Czech Republic*
[2]*Facultyof Natural Sciences, Matej Bel University Banská Bystrica, Slovakia*

Abstract
The paper presents characteristics and measurement process of conductive ink of type DZT-3K, acting as a converter of pressure into electrical signal. It mentions basic properties of the ink, including the explanation of the principle of function. Further it describes the measurement process with tactile sensors with circular electrodes of type PD. It studies the dependency of electrical resistance of the ink on the applied pressure. Various setups with different ink layer thicknesses are compared and their suitability to act as pressure converter is finally discussed.

Key words: conductive ink, tactile sensors, electrodes, pressure converter.

INTRODUCTION

For a planar converter of pressure into electric signal in a tactile sensor, there are generally two suitable materials: conductive rubber and conductive ink. The principle of converting pressure into electric signal is similar as in a microphone: as the pressure is applied, microscopic conductive particles in the transducer get closer, which causes the decrease of the measured resistivity of the material and increased current flow due the Ohm's law.

While before we used to employ conductive rubber, whose specification is closer described by SOUZA ET AL. (2005), VOLF ET AL. (1997, 2006, 2007, 2009, 2012). Now we decided to try and measure electrical properties of conductive inks. Among the reasons to try a new material is a relatively large hysteresis of conductive rubber, which prevents the measuring of the absolute pressure acting on the electrodes' field.

Conductive inks consist of ink filled with small pieces of conductive particles; we tested inks containing graphite and silver particles. For testing, we obtained four types of conductive inks: KH WS SWCNT (KH Chemicals, Korea) Luxor (Luxor, Taiwan), NGAP FI Ag-4101 (NANOGAP, Spain) and DZT-3K (DZP Technologies, United Kingdom). After preliminary evaluations, the ink DZT-3K has been chosen and used in the measurements since owing to its composition; it could form a relatively high-quality conductive layer. The other inks did not meet the requirements, either they were too thin and they did not form a continuous layer, or they did not adhere to the substrate (first two, both water-based inks) or they were excessively conductive – as the third ink with silver particles as a filler – the resistance of the ink was only in units of Ω. The selected ink uses carbon particles as filler. A possible disadvantage of the conductive ink might be the difficulty by creating a compact and stable layer, compared to the conductive rubber, according to TRINKL (2011) and VOLF (2016).

The aim of the study is to evaluate electrical and mechanical properties of selected conductive ink, which is used as transducer between pressure and electrical quantities in a planar sensor.

MATERIALS AND METHODS

The ink cannot be applied to the electrodes in the same way as the rubber layer, because it is unable to create a coherent conductive layer while applied to the electrodes directly, i.e. to sustain its integrity. Any negligible mechanical load caused the separation of the ink from the electrodes' surface. The measuring method – pushing with a force sensor tip on the ink layer – would not be applicable in this case. Additionally, a certain deformation of the ink layer between the inner and outer electrode was observed. As this setup proved not to be utilizable, we proceeded to an alternative layout: the selected ink was deposited on the surface of a PET foil and it was applied to the electrodes similarly as rubber.

The layout of a small section of the electrodes field is depicted in Fig. 1. The arrow at the picture indicates the direction of the current between two circular electrodes of the sensor. It means that the current flows from the inner electrode through the conductive ink to the outer electrode. The common electrode, supplied by a voltage of 1.8 V, is used to mutual separation of individual sensors, which prevents – by hardware – the mutual interaction of the sensors.

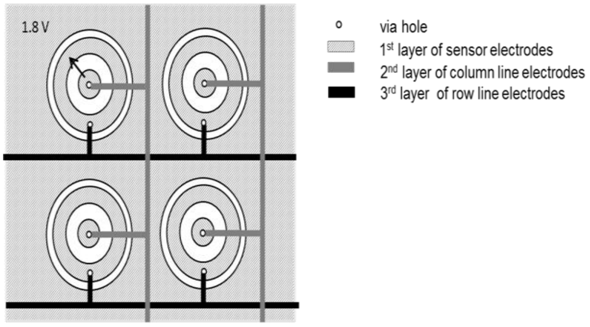

Fig.1. – Layout of the electrodes

The thickness of the selected PET foil was 0,3 mm. The ink was deposited on the foil by a TG-130 spray gun which can spray very low amounts of ink and enables fine control of spraying. A unique 12V Škoda 8P0012615A compressor originally used for inflating tyres was used as a compressor. Three thicknesses were selected of the deposited ink layer: 7 µm, 15 µm and 23 µm. The thicknesses were obtained by 6-fold, 12-fold and 18-fold repeated application. The spray applications were performed through a template made of the same foil with 3 mm holes in view of the 2,5 mm outer diameter of the circular electrodes. The thickness of the deposited ink layer was measured with a Mitutoyo SR44x1 digital micrometer with a measuring range of 0-25 mm and accuracy of 0,001 mm.

The measurements were performed on a scanning matrix comprising circular electrodes with a 2,5 mm diameter. The electrodes were placed on a Cuflex printed circuit board. Conductors were soldered to the outlets of lines and columns which enabled easy choice of a particular electrode. The dimensions of the PD marked electrode are described as follows, see Fig. 2:

$\varnothing E$ = 2,5 mm, $\varnothing d$ = 0,1 mm, M = 0,25 mm.

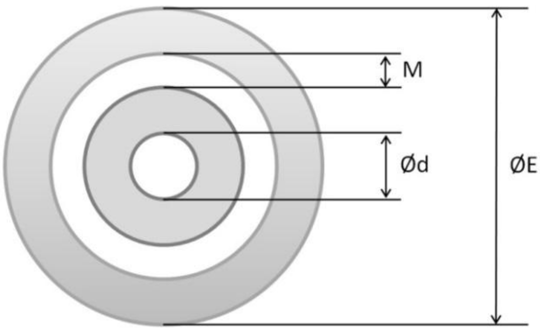

Fig. 2. – Dimensions of the measured PD electrodes

Measurements of the properties of conductive ink were performed at a robotized workplace equipped with a Turbo Scara SR60 robot. Pressure was imposed by means of the vertical motion of the robot´s arm. A Hottinger DF2S-3 tensometer force sensor with a measuring tip was fixed to the end of the robot´s arm. The foil with the deposited inks was placed on the electrode field. The measuring tip with its circular Ø 3 mm surface, which is larger than the diameter of the electrodes, touched down on the surface of one tactile point and pressed on the conductive ink deposited on the foil against the circular electrodes via which the electric resistance of the conductive ink was measured. The basic step of vertical motion of the robot's arm is 0,025 mm with a 0,01 mm resolution. The pressure was imposed by means of the vertical motion of the robot's arm by the measuring tip with mm in diameter. The load force was selected in the range from 1 N to 16 N. The pressure imposed on the electrodes was calculated from the known area of the surface of the measuring tip and the exerted force. This resulted in the measured range of pressure values ca. from 100 kPa up to 2 200 kPa for the particular measuring tip. The output voltage of the type DF2S-3 tensometer force sensor was measured by an Almemo 2890-9 Data Logger. Frequency response of the system is according to PAVLOVKIN ET AL. (2012) measured by system rc2000 eventually. The measuring workspace is depicted in Fig. 3, where (1) marks the foil with deposited conductive ink, (2) is for the measuring tip, (3) is the force sensor DF2S-3 and (4) indicates the robot's head.

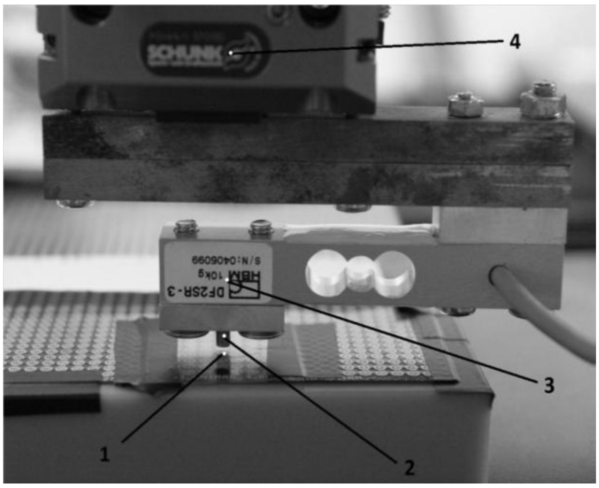

Fig. 3. – Robotized measuring workspace

RESULTS AND DISCUSSION

The measurements were carried out ten times for each ink layer, i.e. the 7 µm, 15 µm and 23 µm ink layer with the PD electrode type. The graphs bellow this paragraph show the dependency of the measured electrical resistance on the applied pressure. Based on the principle explained at the beginning of the paper, the electrical resistance should decrease with increasing pressure. Now it is to study the course of the dependency for selected ink layer and to evaluate its eligibility to act as a pressure converter. Fig. 4 bellow this paragraph give first an overall comparison of all measured ink layers and the following Fig. 5 describes a selected setup in more detail.

Fig. 4 compares the dependency of electrical resistance on the applied pressure for all three ink layers; each curve represents the respective ink layer thickness. As we can see from the figure, the resistivity of the 23 µm ink layer changes only insignificantly from the pressure above ca. 200 kPa. This is evoked by the high conductivity of ink layer. It causes such a low resolution (distinct change in pressure brings only negligible change in resistance), that we consider this useless for measuring in this pressure range. However, thicker layers may give acceptable resolution in lower pressure range, but this was not the subject of our measurements.

The 15 µm ink layer gave acceptable resolution for the pressure range 100 – 800 kPa, but above this value the resolution decreases as well. Other issue is the apparent nonlinearity of the dependency in the 200 – 400 kPa range, which has a very negative effect on the accuracy of the measurement in this range. The cause of the mentioned nonlinearity in this range is not exactly known, it might be a specific combination of ink layer thickness and used PD electrode, as this does not appear by other electrode types.

Last curve denote the dependency of the electrical resistivity for the 7 µm ink layer. It exhibits a quasi-linear shape of the dependency in the range from 200 kPa to 1 200 kPa, with sufficient resolution. This setup gave the best result, which is, however, not optimal; the dependency is still not perfectly linear, with significant changes in 300 kPa and 900 kPa pressure value, and we consider the maximum pressure limitation 1 200 kPa rather low for use in a planar transducer.

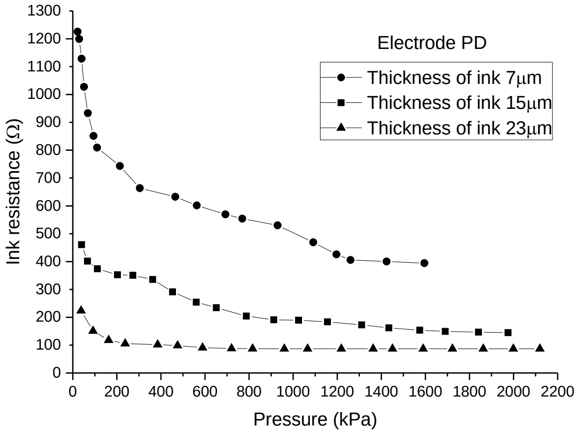

Fig. 4. – Overall comparison of three ink layer thicknesses

In the following Fig. 5 the circle marked curve represents the loading cycle and the triangle marked curve the unloading cycle. It also captures the uncertainty interval for individual measured values of the PD-type electrode in the loading cycle. The short dash style curve represents the approximation of the dependence of the electrical resistance on the pressure in the loading cycle.

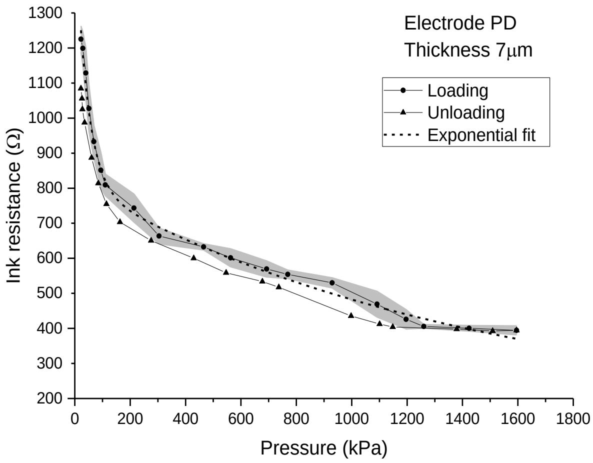

Fig. 5. – Loading and unloading cycle of 7 µm ink layer

We proved that conductive ink may act as a converter between pressure and electrical quantities in a planar pressure transducer. We measured the dependency of the electrical resistance of the ink on the applied pressure. We obtained satisfactory results for the 7 µm ink layer, with some limitations, e.g. limited pressure range, certain nonlinearity of the dependency and some hysteresis of the measured material. We also concluded that higher ink layer thicknesses of the

selected ink DZT-3K decrease the resolution of the transducer significantly, which is caused by high conductivity of ink. Due to lower hysteresis and better resolution, conductive ink may be a good alternative for previously used conductive rubber; the problem poses its limited adherence to the electrodes. This may be solved by using polymer-based inks instead water-based, which we are expected to do in the future.

CONCLUSIONS

We proved that conductive ink may act as a converter between pressure and electrical quantities in a planar pressure transducer. We measured the dependency of the electrical resistance of the ink on the applied pressure. We obtained satisfactory results for the 7 μm ink layer, with some limitations, e.g. limited pressure range, certain nonlinearity of the dependency and some hysteresis of the measured material. We also concluded that higher ink layer thicknesses of the selected ink DZT-3K decrease the resolution of the transducer significantly, which is caused by high conductivity of ink. Due to lower hysteresis and better resolution, conductive ink may be a good alternative for previously used conductive rubber; the problem poses its limited adherence to the electrodes. This may be solved by using polymer-based inks instead water-based, which we are expected to do in the future.

ACKNOWLEDGEMENT

The measurements were carried out within the IGA project No. 31200/1312/3118 of the Faculty of Engineering, Czech University of Life Sciences in Prague.

REFERENCES

1. PAVLOVKIN, J., NOVÁK, D.: Measuring of Frequency Characteristics of Passive Filters by System rc2000. In: EDUKACJA–TECHNIKA–INFORMATYKA, vol. 3 (2), 2012: pp. 257-264 (in German).
2. SOARES, B. G., AMORIM, G.S. ET AL.: The in situ polymerization of aniline in nitrile rubber. In: SYNTHETIC METALS, 156 (2-4),2006: pp. 91-98.
3. SOUZA, F.G., MICHEL, R.C., SOARES, B.G.: A methodology for studying the dependence of electrical resistivity with pressure in conducting composites. In: Polymer testing, vol. 24 (8), 2005: pp. 998-1004.
4. TRINKL, A.: Optimization of Design of Flat Tactile Transducers. [Ph.D. thesis], Czech University of Life Sciences Prague, Prague, 2014 (in Czech).
5. VOLF, J., HOLÝ, S., VLČEK, J.: Using of Tactile Transducer for Pressure Distribution Measurement on Sole. In: Sensor and Actuators A62. Physical, ELSEVIER SEQUOIA S.A., 1997: pp. 556-561, Lousanne, Switzerland.
6. VOLF, J., NOVÁK, V., RYZHENKO, V.: Effect of conductive ink on transfer characteristics of pressure into electric signal for tactile sensors. In: Agronomy Research, Vol. 14, Special Issue I, 2016: pp. 1123-1129. ISSN 1406-894X.
7. VOLF, J., PAPEŽOVÁ, S. ET AL.: Gait Locomotion Analysing System for Relevant Measurement Pressure Cognition. In: Proceedings ISHF, Lisbon, Faculdade de Motricidade Humana, 2007: pp. 155-160. ISBN 978-972-735-145-9.
8. VOLF, J., VLČEK, J. ET AL.: Orthopaedic Investigation System For Medical Non-Invasive Diagnostics. In: IMEKO - XVIII World Congress and IV. Brazilian Congress of Metrology Rio de Janeiro, IMEKO, 2006.
9. VOLF, J., TRINKL, A. ET AL.: Optimal Size Determination of Tactile Sensor Plantograf V08 and its Electrodes. In: 26th Symposium on Advances in Experimental Mechanics, Leoben, Austria 2009. ISBN: 978-3-902544-025.
10. VOLF, J., TRINKL, A. ET AL.: Plantograf V12 with Optimal Size Determination Sensor Electrodes and its Using for Pressure Distribution Between Tire and Road. In: XX World Congress IMEKO, Busan, 2012, 1-4, ISBN 978-89-950000-5-2 95400.

Corresponding author:

Ing. Viktor Novák, Department of Electrical Engineering and Automation, Faculty of Engineering, Czech University of Life Sciences Prague, Kamýcká 129, Praha 6, Prague, 16521, Czech Republic,e-mail: novakviktor@tf.czu.cz

PROPERTIES OF FUEL BRIQUETTES AFTER THREE YEARS STORAGE

A. Nováková, M. Brožek

Department of Material Science and Manufacturing Technology, Faculty of Engineering, Czech University of Life Sciences Prague, Czech Republic

Abstract
The paper presents the results of laboratory tests intent on the study of storage place, placing manner and storage time on mechanical properties of briquettes made from spruce sawdust. The briquettes properties were evaluated by their density and rupture force determination. Moreover the mechanical durability, the gross calorific value, the total moisture and the ash content were determined. By the carried out tests it was univocally proved that the mode of storage influences briquettes durability at their long-term storage most of all. On the basis of the carried out tests it is possible to state that for the parameter of briquettes quality evaluation the rupture force can be recommended.

Key words: spruce sawdust, gross calorific value, density, rupture force, moisture content, mechanical durability.

INTRODUCTION

Briquetting is a relatively old technology. The first mentions of their use have been published in the first half of the 18th Century. The Otto's Encyclopedic Dictionary (OTTO, 1891) describes relatively lengthily the basis and the use of briquetting and of briquettes in practice. The mention of briquetting technology and of briquettes can be found practically in all older as well in newly domestic (STEHLÍK ET AL., 1966; VŠEOBECNÁ ENCYKLOPEDIE, 1999) as well as in foreign encyclopedias (ENCYCLOPEDIA BRITANNICA, 1991).
In the twenty last years in the Czech Republic the briquetting technology asserted oneself in the field of metallic and non-metallic processing, too. The basis of this method is the high pressure effect on a fine-grained material. Briquettes, most often of cylindrical form and various diameter and length, are the final product. But briquettes can be of various shape, e.g. of cuboid with rounded corners, of hexagonal cuboid etc., according to the design of the press chamber of the used briquetting press.
The use of briquetting technology can bring substantial savings. Waste pressed from flammable materials, e.g. from wood waste (chips, sawdust), straw, coal, paper, cellulose, tobacco etc. is mostly utilized energetically (by combustion) (BASORE, 1929; PLÍŠTIL ET AL., 2004; BROŽEK, 2011; BROŽEK ET AL., 2012; BROŽEK AND NOVÁKOVÁ, 2013). After its compression the waste from combustible materials, e.g. dust collected on air filters, abrasion dust or chips from cutting of metals and their alloys (ČSN 42 0030, 1994; ČSN 42 1331, 1991) is better usable. After compression the waste volume strongly decreases. This makes easy its handling and decreases costs in transport or storage on a waste disposal site. The aim of carried out experiments has been to assess the properties of the newly made briquettes and of briquettes stored during three years under suitable and less suitable conditions.

MATERIALS AND METHODS

On briquettes from wood waste determined for combustion a row of demands are laid, which are specified in relevant national directives. In the Czech Republic the demands on briquettes properties are prescribed by the Directive of Ministry of the Environment Nr. 14-2009. It demands the briquettes minimum density of 900 $kg \cdot m^{-3}$. The briquettes strength demands are not prescribed. Nevertheless for operational reasons the adequate compactness is very important in order that at a common handling neither crumbling nor disintegration occur. The briquettes minimum gross calorific value must be 17 $MJ \cdot kg^{-1}$, the total moisture content max. 10 % by weight and the ash content max 1.5 %. Moreover the briquettes must guarantee 9 months of the minimum storability. During this time the changes of briquettes size, density and moisture content must not exceed the limit of 10 %. The tested briquettes were made from spruce sawdust. For the briquettes production the briquetting press of the firm Briklis (Malšice, Czech Republic), type BrikStar 30-12, pressure chamber diameter of 50 mm, was used. All briquettes were made at the briquetting parameters constant adjustment.

Briquettes were divided into four groups and deposited in following storage spaces:

- Storage space I – in closed heated room, in plastic net bag and in plastic bag,
- Storage space II – in closed unheated room, in plastic net bag and in plastic bag.

Plastic net bags (so called raschel bags) are universal packaging material. They are lightweight, strong and breathable. They are used e.g. for storage of vegetables (potatoes, onions, carrots), fruit (apples, oranges), lump wood, wood chips etc.

Plastic bags have universal use. Bags were made from LDPE (low density polyethylene) with a thickness of 150 microns. They have high strength, stored material protects from moisture and dust.

The properties changes of briquettes for energy purpose have been studied by BROŽEK (2013A, 2014) and NOVÁKOVÁ AND BROŽEK (2016). They proved that during the briquettes storage their properties changed already after several months. At the briquettes storage in the closed heated room the changes are smaller than at their storage in the closed, but unheated room. But the radical influence occurs at storage in the closed plastic bag and in the plastic net bag.

After sampling the briquettes were numbered, weighted and their length and diameter measured. Then single briquettes were loaded by pressure using the universal tensile strength testing machine (Fig. 1). The test is finished at the briquette rupture, which is accompanied with the rapid load decrease. From the load indicator the maximum load is taken down (BROŽEK, 2013B).

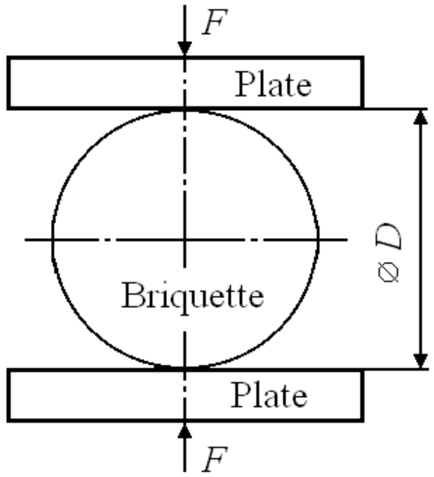

Fig. 1. – Principle of the plate-loading test

From the measured values the briquettes density was calculated. With regard to the production technology the briquettes are of different length. Therefore their rupture force was recalculated and it is presented as the force per unit.

The determination of the mechanical durability according to ČSN EN 14961-1 (2010) and ČSN EN 15210-2 (2011) was the part of carried out test. This test simulates the effect of transportation to change the properties of briquettes. Moreover the gross calorific value according to ČSN EN 14918 (2010), the ash content according to ČSN EN 14775 (2010) and the total moisture content according to ČSN EN 14774-2 (2010) were determined.

RESULTS AND DISCUSSION

The gross calorific value (19.3 $MJ \cdot kg^{-1}$) of spruce sawdust, used for briquettes production, was determined according to ČSN EN 14918 (2010). The ash content (0.40 %) was determined according to ČSN EN 14775 (2010).

The test results are presented in Fig. 2, Fig. 3 and Tab. 1. Fig. 2 presents the relationship between rupture force and density (for new briquettes). Fig. 3 presents the relationship between rupture force and density (for all tested briquettes; the average values from all measurements are plotted). In Fig. 2 and Fig. 3 the standard deviation is demonstrated by the line segments. All measured values were evaluated statistically (see Tab. 1).

From Fig. 3 and Tab. 1 it is evident that the briquettes density decreased after three years storage that is regardless of the storage space and manner. The insignificant density decrease (of 0.6 %) was determined at briquettes (sample B) stored in the plastic bag in the closed heated room (space I). Higher density decrease (of 8.1 %) was determined at briquettes (sample C) stored in the net plastic bag in the closed heated room (space I) and at briquettes (sample D) (of 8.6 %) stored in the plastic net bag in the unheated room (space II). On the contrary at briquettes (sample E) storage in the plastic net bag in the closed unheated room (space II) the significant density decrease occurred (of 22.7 %).

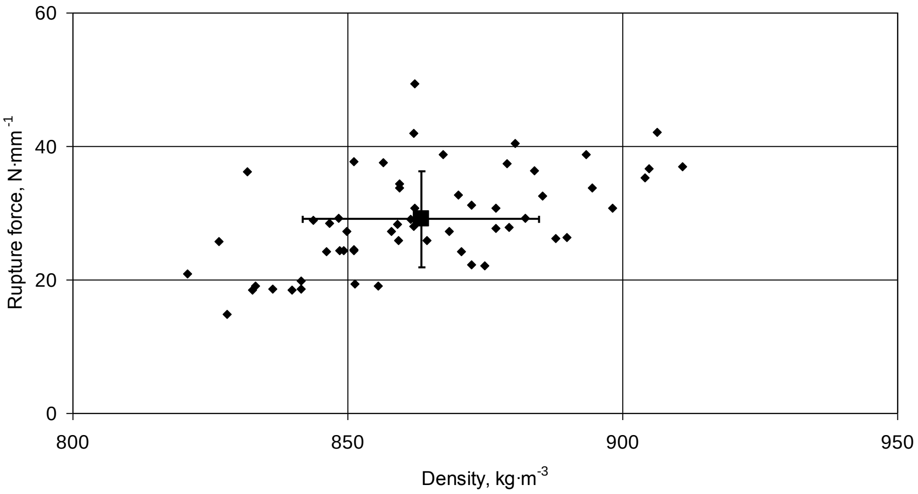

Fig. 2. – Relation between rupture force and density for briquettes stored in closed heated room in plastic net bag (sample C in Fig. 3; standard deviation is demonstrated by the line segments**)**

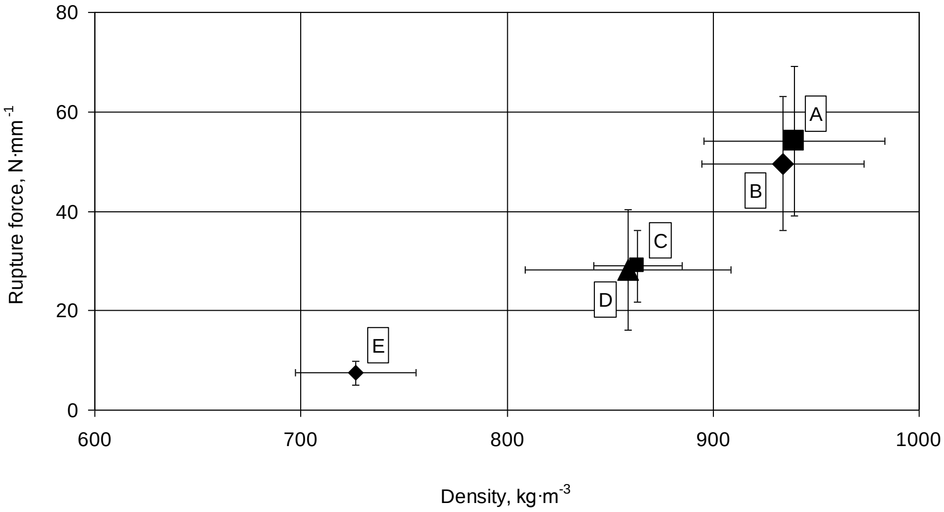

Fig. 3. – Relation between rupture force and density for all tested briquettes (standard deviation is demonstrated by the line segments): sample A – without exposure; sample B – storage space I, plastic bag; sample C – storage space I, plastic net bag; sample D – storage space II, plastic bag; sample E – storage space II, plastic net bag

Tab. 1. – Test results

Sample	Density ($kg \cdot m^{-3}$)	Rupture force per unit ($N \cdot mm^{-1}$)	Mechanical durability (%)	Moisture content (%)
A: Without exposure	939.5 ± 43.7	54.1 ± 15.1	84.0 ± 3.1	7.3
B: Storage space I, plastic bag	934.0 ± 39.3	49.6 ± 13.5	83.8 ± 1.4	7.4
C: Storage space I, plastic net bag	863.5 ± 21.5	29.0 ± 7.2	75.5 ± 1.9	7.4
D: Storage space II, plastic bag	858.7 ± 49.8	28.2 ± 12.1	77.0 ± 6.3	8.0
E: Storage space II, plastic net bag	726.5 ± 29.2	7.5 ± 2.4	43.9 ± 4.2	11.4

Tab. 1. – Test results (continued)

Sample	Diameter (mm)	Length (mm)	Weight (g)
A: Without exposure	51.21 ± 0.21	57.01 ± 8.09	109.9 ± 13.0
B: Storage space I, plastic bag	51.72 ± 0.26	61.46 ± 7.05	120.3 ± 12.5
C: Storage space I, plastic net bag	52.27 ± 0.30	58.28 ± 5.61	107.9 ± 10.0
D: Storage space II, plastic bag	52.29 ± 0.44	60.39 ± 8.86	110.8 ± 14.3
E: Storage space II, plastic net bag	53.98 ± 0.68	69.86 ± 5.79	116.1 ± 9.9

Such results were determined at the rupture force. Although the Directive of the Ministry of the Environment of the Czech Republic No 14-2009 does not prescribe the watching of this parameter, the results are interesting.

After the briquettes storage in the plastic bag in the closed heated room (sample B) and at the plate-loading testing (Fig. 1) only the rupture force mild decrease (of 8.3 %) occurred, so that in this way stored briquettes meet the requirements also after three years storage. After storage in the plastic bag in the closed unheated room (sample D) the rupture force decrease (of 47.9 %) occurred. After storage in the net bag the rupture force decrease occurred, namely at their storage in the closed heated room (sample C, of 46.4 %) as well in the closed unheated room (sample E, of 86.1 %).

At the briquettes is different decrease in mechanical durability occur (Tab. 1). At the briquettes stored in space I in the plastic bag (sample B) of 0.2 %, in the plastic net bag (sample C) of 10.1 %. At the briquettes stored in space II in the plastic bag (sample D) of 8.3 %, in the plastic net bag (sample E) even of 47.7 %.

After the long-term storage the briquettes moisture changed, but relatively little. At three from four samples it was after three years lower than 8 %. Only at storage in the plastic net bag in the closed unheated room (sample E) it increased considerably, namely up to 11.4 %.

From the mentioned tests evaluation it follows that in the course of the long-term storage the briquettes loosening occurs. Their size (diameter, length) become larger, their density as well as the rupture force decrease (Tab. 1). Contemporarily their mechanical durability decreases. The change of the moisture content depends first of all on the storage location and conditions. In conclusion it is possible to state that briquettes degrade, at that practically all watched parameters get worse.

From the test results it follows that on the briquettes durability the storage time is of no substantial influence, but primarily they are their storage space and manner. According to the producer recommendation the dry and heated rooms can be considered as the suitable spaces. On the contrary unheated spaces are less suitable. Briquettes should be always stored in leak proof closed plastic containers.

The results published in this paper confirm the results published by Brožek (2013a; 2014) and by Nováková and Brožek (2016) for briquettes made from spruce shavings or birch chips.

CONCLUSIONS

In the paper the study results of three factors influencing the briquettes mechanical properties at the long-time storage are presented. The influence of the briquettes storage space (closed heated room, closed unheated room) was the first studied factor, the second the storage manner (plastic bag, plastic net bag) and the third the storage time (new briquettes, briquettes after three years storage). Density and rupture force were criterions for the briquettes evaluation. Contemporarily next parameters were also watched, namely mechanical durability, moisture content, diameter, length and weight of briquettes.

By the carried out tests it was unambiguously proved that the manner of briquettes long-term storage is of the highest influence on their durability.

Briquettes, stored in the well closed plastic bag in the closed heated room (space I, sample B), changed their properties after three years only little. The density decreases of 0.6 %, the mechanical durability of 0.2 % and the rupture force of 8.3 %. Briquettes, stored in the same place, but in the plastic net bag (sample C), changed their properties substantially more. Clearly it was evident from the value of rupture force which decreased of 46.4 %. The density decreased of 8.1 %, the mechanical durability of 10.1 %.

Briquettes, stored in the closed, but unheated room (space II), changed their properties after three years very considerably. At their storage in the plastic bag (sample D) the decrease in density of 8.6 %, mechanical durability of 8.3 % and rupture force of 47.9 % occurred. At their storage in the plastic net bag (sample E) the decrease in density of 22.7 %, mechanical durability of 47.7 % and rupture force of 86.1 % occurred. These briquettes were practically unusable.

On the basis of the carried out tests it follows that for the briquettes quality evaluation it is possible to recommend the parameter rupture force.

From the above mentioned conclusions it follows that briquettes should be always stored in leak proof well closed plastic containers. If briquettes are by their producers supplied in different containers or even in bulk it is without delay necessary to transfer them into suitable containers. Only in this way it is possible to guarantee their demanded properties also after three years storage, too.

ACKNOWLEDGEMENTS

Supported by the Internal Grant Agency of the Faculty of Engineering, CULS Prague, Prague, Czech Republic IGA 2016: 31140/1312/3107 "Influence of feedstock specific mechanical parameters and type of storage conditions on final quality of briquettes from waste biomass".

REFERENCES

1. BASORE, C. A.: Fuel Briquettes from Southern Pine Sawdust. Auburn, Alabama Polytechnic Institute 1929.
2. BROŽEK, M.: Quality evaluation of briquettes made from biomass. The Fifth International Scientific Conference Rural Development 2011. 24-25 November 2011. Akademija, Aleksandras Stulginskis University, pp. 308-313.
3. BROŽEK, M., NOVÁKOVÁ, A., KOLÁŘOVÁ, M.: Quality evaluation of briquettes made from wood waste. Res. Agr. Eng., 58, 2012: 30-35.
4. BROŽEK, M.: Study of briquettes properties at their long-time storage. Journal of Forest Science, 59, 2013a: 101-106.
5. BROŽEK, M.: Properties of briquettes from paper waste. Manufacturing Technology, 13, 2013b: 138-142.
6. BROŽEK, M., NOVÁKOVÁ, A.: Briquettes from recovered paper and board. 12th International Scientific Conference Engineering for Rural Development. 24-25 May 2013. Jelgava, Latvia University of Agriculture, pp. 488-493.
7. BROŽEK, M.: Influence of storage on briquettes mechanical properties. Scientia Agriculturae Bohemica, 45, 2014: 175-179.
8. NOVÁKOVÁ, A., BROŽEK, M.: Briquettes properties after three years storage. 15th International Scientific Conference Engineering for Rural Development. 25-27 May 2016. Jelgava, Latvia University of Agriculture, pp. 80-85.
9. OTTO, J.: Ottův slovník naučný (Otto's encyclopaedia). Vol IV. Prague, J. Otto, 1891.
10. PLÍŠTIL, D., BROŽEK, M., MALAŤÁK, J., HENEMAN, P.: Heating briquettes from energy crops. Res. Agr. Eng., 50, 2004: 136-139.
11. STEHLÍK, V. ET AL.: Naučný slovník zemědělský (Encyclopaedia agricultural). Vol I. Prague, ÚVTI 1966.
12. TEAM OF AUTHORS: Všeobecná encyklopedie (General encyclopaedia). Vol I. Prague, Diderot 1999.
13. TEAM OF AUTHORS: The New Encyclopaedia Britannica. Index A-K. 15th Ed. Chicago, Encyclopaedia Britannica 1991.
14. DIRECTIVE OF MINISTRY OF ENVIRONMENT: No. 14–2009. Brikety z dřevního odpadu (Briquettes from Wood Waste). Prague, Ministry of Environment of the Czech Republic. 2009.
15. ČSN 42 0030: Ocelový a litinový odpad (Steel and cast iron scrap). 1994.
16. ČSN 42 1331: Odpady neželezných kovů a jejich slitin (Scraps from nonferrous metals and their alloys). 1991.
17. ČSN EN 14774-2: Tuhá biopaliva – Stanovení obsahu vody – Metoda sušení v sušárně – Část 2: Celková voda – Zjednodušená metoda (Solid biofuels – Determination of moisture content – Oven dry method – Part 2: Total moisture – Simplified method). 2010.
18. ČSN EN 14775: Tuhá biopaliva – Stanovení obsahu popela (Solid biofuels – Determination of ash content). 2010.
19. ČSN EN 14918: Tuhá biopaliva – Stanovení spalného tepla a výhřevnosti (Solid biofuels – Determination of calorific value). 2010.
20. ČSN EN 14961-1: Tuhá biopaliva – Specifikace a třídy paliv – Část 1: Obecné požadavky (Solid biofuels – Fuel specifications and classes – Part 1: General requirements). 2010.
21. ČSN EN 15210-2: Tuhá biopaliva – Stanovení mechanické odolnosti pelet a briket – Část 2: Brikety (Solid biofuels – Determination of mechanical durability of pellets and briquettes – Part 2: Briquettes). 2011.

Corresponding author:

Alexandra Nováková, Department of Material Science and Manufacturing Technology, Faculty of Engineering, Czech University of Life Sciences Prague, Kamýcká 129, Praha 6, Prague, 16521, Czech Republic, phone: +420 22438 3308, e-mail: novakovaa@tf.czu.cz

POWER FARMING SYSTEMS FOR WELSH ONION CULTIVATION

T. Otake[1], M. Sato[2], H. Shindo[3], M. Honjo[3], M. Saito[3], M. Katahira[2], S. Koide[4], M. Natsuga[2]

[1]*Fukushima Agricultural Technology Center, 116, Hiwada, Koriyama, Fukushima, Japan*
[2]*Yamagata University, 1-23, Wakabamachi, Tsuruoka, Yamagata, Japan*
[3] *Akita Agricultural Experiment Station, Yuwa, Akita, Japan*
[4]*Iwate University, 18-8, Ueda, Morioka, Iwate, Japan*

Abstract
Welsh onion cultivation places many demands on labor-saving technologies, which include low-cost cultivation by fertilizer reduction. We developed a chisel and two fertilizing openers for a fertilizer-applicator ditcher to improve the work rate and nitrogen absorption. This study investigated the influence of a softened ditch bottom and drill fertilizing positions on Welsh onion root growth when using drill fertilizing cultivation systems with a prototype fertilizer-applicator ditcher. Results show that prototype fertilizer-applicator ditcher increased root length and root length density and decreased soil hardness on the ditch bottom of the soil because of its chisel action. The drill-fertilized block showed a lower rate of root distribution to reach the fertilizer position quickly. Each test block processed with a chisel showed a higher rate of root distribution in deep locations in the ditch. However, in non-fertilized areas left by a fertilizer-opener, gas phase was present in large quantities in soil buried by a fertilizer-applicator ditcher.

Key words: welsh onion, fertilizer-applicator ditcher, root, drill fertilizing.

INTRODUCTION

Welsh onion cultivation places many demands on the labor-saving technologies of Japanese farmers, which include low-cost cultivation by fertilizer reduction. A fertilizer-applicator ditcher that can achieve low-cost cultivation is reported to have coverage that is 3.8–5.3 times greater than normal cultivation, achieving yields equal to those of normal cultivation by drill fertilizing. We developed a chisel and two fertilizing openers in a fertilizer-applicator ditcher to improve the work rate and nitrogen absorption. Fertilizing positions were 5 cm from the center horizontally of the seedling and 7 cm from the bottom of the ditch vertically. The total root length in 35% decreased fertilizing was longer than that of normal fertilizing in the germination experiment using no root seedlings. Nitrogen content in the territorial part for the drill fertilizing had lower reduction rate after transplanting and maintained higher until the middle growth stage than usual fertilizing. The plant height, branch height, stem diameter and dry matter mass were greater for the drill fertilizing than for the normal fertilizing through the middle growth stage. The drill fertilizing produced greater total mass and thicker stem diameter (before processing) than normal fertilizing. After processing, the drill fertilizing with 17–20% decreased fertilizing by had thicker stem diameter and higher total yields by 7–13% than the normal fertilizing (Shindo et al., 2015; Honjo et al., 2015). However, a new type of Welsh onion cultivation system that uses a prototype fertilizer-applicator ditcher did not take into account the influence of chisel and drill fertilizing positions by fertilizing openers on Welsh onion growth and yields. To improve Welsh onion root growth, this study therefore investigated the influence of a softened ditch bottom and drill fertilizing positions for producing Welsh onion drill fertilizing cultivation systems with a prototype fertilizer-applicator ditcher.

MATERIALS AND METHODS

1) Test location

We conducted tests in horticulture fields of the Akita Agricultural Experiment Station in Akita, Japan, and the Yamagata Field Science Center in Faculty of Agriculture, Yamagata University in Takasaka, Yamagata, Japan during 2014–2015. At the Akita field, we cultivated summer harvesting type one time and autumn–winter cultivation type two times. At the Takasaka fields, summer harvesting type was cultivated one time.

2) Machine components

This study examined open ditching and fertilizing using a tractor (Akita field: 25 kW, KL3450; Kubota Corp. / Takasaka field: 25 kW, KL34R; Kubota Corp.)

and a rotary machine with two fertilizer-applicator ditchers (prototype, R-47) set to 100 cm for the ditch space. The fertilizer-applicator ditcher included a chisel and two fertilizer openers in the body (Fig. 1).

We transplanted Welsh onion seedlings to open ditches using a paper pot transplanter (HP-6; Nippon Beet Sugar Mfg. Co. Ltd.)(OTAKE ET AL., 2015).

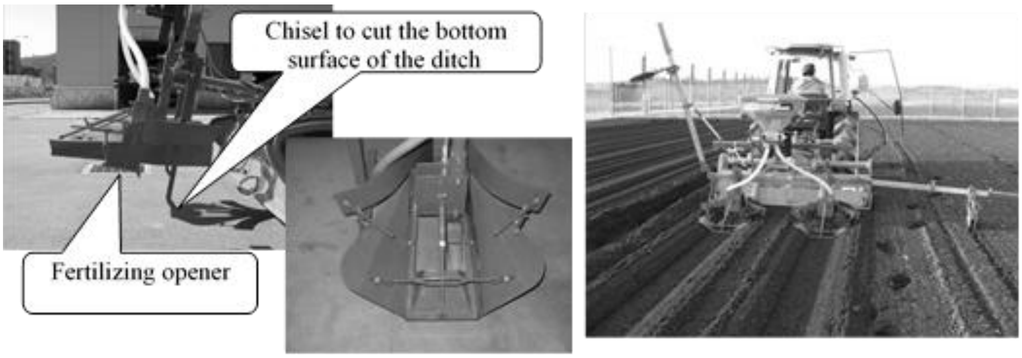

Fig. 1. – Outline of fertilizer-applicator ditcher

3) Cultivation outline

We used the Welsh onion cultivar "Natsu-Ougi Power" (Sakata Seed Co., Japan). The drill fertilizing of the summer harvest type was 75 kg/ 10 a, set 9.0 kg-N/ 10 a for nitrogen content, for the amount of basal fertilizer. Furthermore, topdressing was done four times with 125 kg / 10 a. Total amounts of fertilizer of these types were 200 kg / 10 a. Broadcast fertilizing of the summer harvesting type was 125 kg/10 a, set 15.0 kg-N/ 10 a for nitrogen content, for the amount of basal fertilizer. Topdressing was done four times with 125 kg / 10 a. The total amount of fertilizer of type was 250 kg /10 a. All fertilizing for autumn–winter harvesting types were 92 kg/10 a, set 23 kg-N/10 a for nitrogen content used controlled-release fertilizer, for the amount of basal fertilizer. Fertilizing positions were 5 cm from the seedling center horizontally and 3 cm from the ditch bottom vertically. The chisel was 15 cm from the ditch bottom vertically and seedling center. Test blocks of "Ar block were the following: One fertilizer opener, chisel, drill-fertilized type," "Br block: One fertilizer opener, no chisel, drill-fertilized type," "Cr block: Two fertilizer openers, chisel, drill-fertilized type," "Normally fertilized block: Two fertilizer openers, chisel, broadcast fertilized type" and "Non-fertilized block: Two fertilizer openers, chisel, non-fertilized type."

4) Test contents

Sampling times of Welsh onion roots were 21 days after transplanting for the 2014 summer harvest type, 17 days after transplanting for the 2014 autumn–winter harvest type, 30 days after transplanting at 2015 summer harvest type and 21 days after transplanting at 2015 autumn–winter harvest. We obtained Welsh onion roots and soil from each sampling block. The sampling areas that contained six seedlings were 21 cm wide, 15 cm long, and 14 cm deep. Therefore, we divided the sampling area to six sampling blocks that were 7 cm wide, 15 cm long, and 7 cm deep. They were three divisions for sampling area width and two divisions for the sampling area depth. We investigated the root length using a root scanner (Root Length Scanner; Comair). We calculated the root length density (mm/cm^3) and the rate of root length distribution (%) from those data. The following formulas were used to calculate the rate of root length distribution.

Rate of root length distribution (%) = (Total root length (mm) for a sampling block / Total root length (mm) for sampling area) × 100.

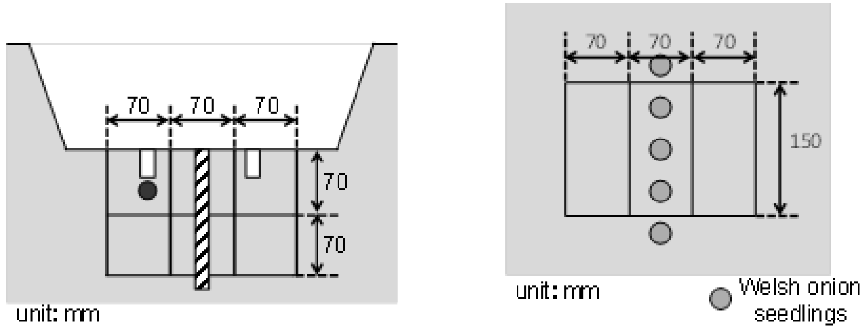

Fig. 2. – Sampling positions of Welsh onion root (left: sectional view; right, bird's-eye view)

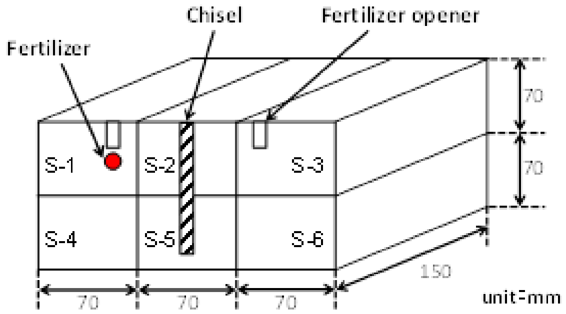

Fig. 3. – Sampling blocks

RESULTS AND DISCUSSION

(1) Root length and root length density.

The influence of total root length and root length density to be composed by cultivation and fertilizing types are shown in Fig. 4 and Fig. 5.

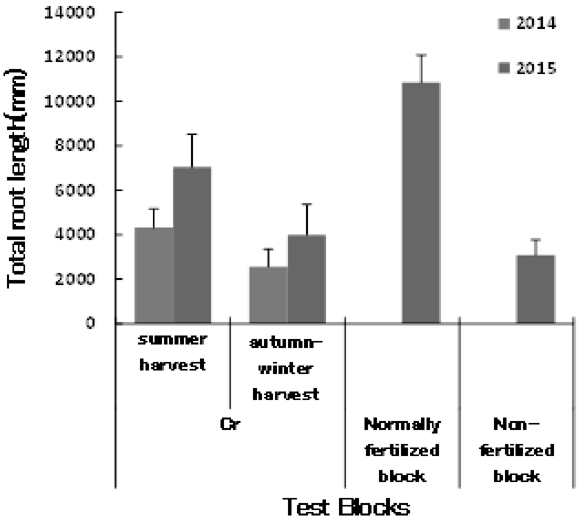

Fig. 4. – Influence of total root length by fertilizing and cultivation type

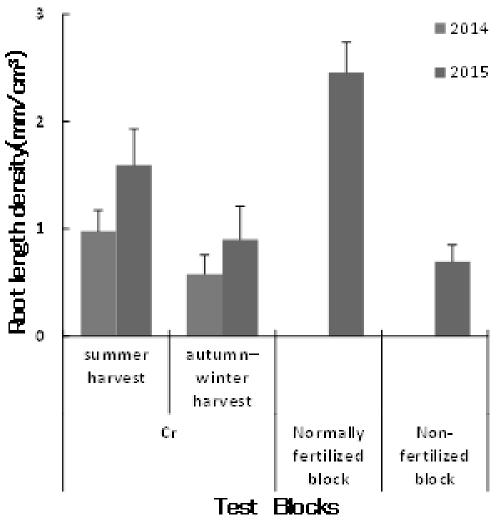

Fig. 5. – Influence of root length density by fertilization and cultivation type

Normally fertilized blocks exhibited the longest root length compared to Cr and non-fertilized blocks. Normally fertilized blocks displayed about 10,800 mm root length. That value was about twice that of other test blocks. Normally fertilized blocks exhibited the highest root length density compared to Cr and non-fertilized blocks. Test blocks that had greater distributions of fertilizer showed longer root length and higher root length density.

The influence of total root length and root length density to be composed by fertilizer openers and chisel is shown in Fig. 6 and Fig. 7.

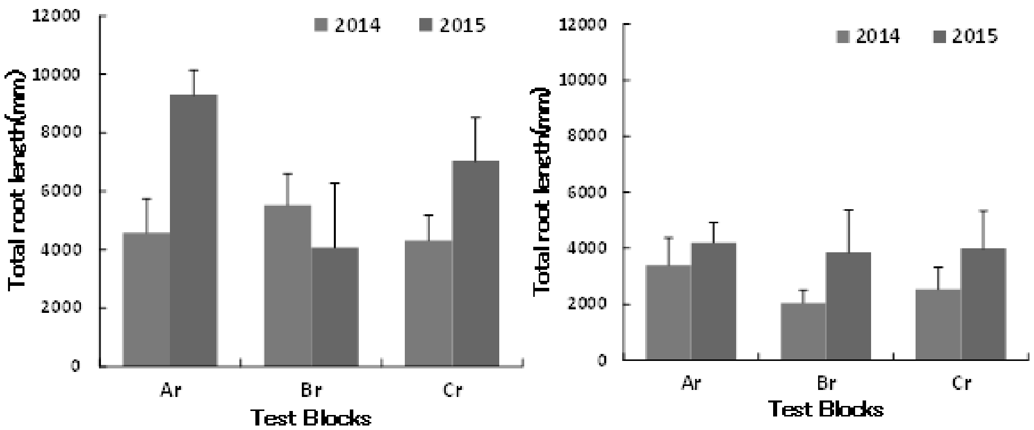

Fig. 6. – Fertilizer openers and chisel influence on total root length (left, summer harvest; right, autumn–winter harvest)

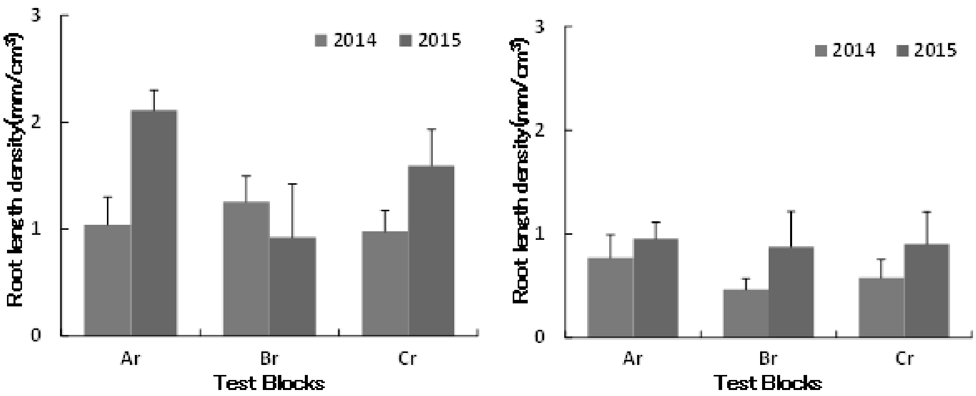

Fig. 7. – Fertilizer openers and chisel influence on root length density (left, summer harvest; right, autumn–winter harvest)

The Ar block showed greater total root length and root length density values than the Cr block did. The Br block showed the shortest total root length compared to the other blocks. The Br block exhibited the longest total root length compared to the other blocks for the summer harvest in 2014.

(2) Rate of root length distribution.

The cultivation and fertilization influence on the rate of root length distribution is shown in Fig. 8.

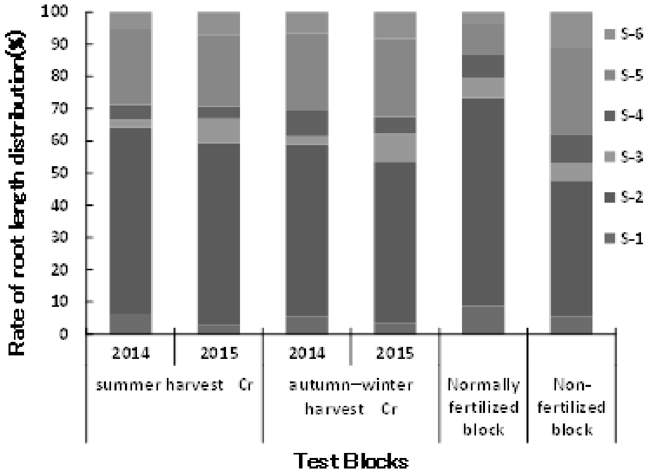

Fig. 8. – Influence of rate of root length distribution by cultivation and fertilization type

Sampling block S-2 of the transplant position exhibited the highest rate of root length distribution among all sampling blocks. The Cr block, which was drill-fertilized, had much higher rates of root distribution in sampling blocks S-5 and S-2, for which a chisel was used. Furthermore, other sampling blocks had high rates of root distribution in S-1 at 2014 and S-3 at 2015. In addition, drill-fertilized types had a two times higher rate of root distribution in sampling block S-5 than normally fertilized type. The normally fertilized type showed differences of root distribution for drill-fertilized and non-fertilized types to distribute in sampling blocks equally, except S-2. The non-fertilized type showed lower rates of root distribution in sampling blocks S-1 to S-3, which were shallow places of ditches, than those of other fertilizing types. That type showed higher rates of root distribution in sampling blocks S-4 to S-6, which were deep places of ditches, than those of other fertilizing types. However, that type showed a similar root distribution tendency for drill-fertilized type because the drill-fertilized type which had fertilizer in sampling block S-1 had short roots that quickly reached the fertilizer position. However, the drill-fertilized type grew roots into a non-fertilized area. Sampling block S-5 of drill-fertilized type had numerous growing roots in the chisel-softened soil. Normally fertilized types showed few if any roots for deep places of ditches to have fertilizer for a shallow place of the ditch.

Results showed the influence of the rate of root distribution to be composed by fertilizing openers and chisels, as presented in Fig. 9 and Fig. 10.

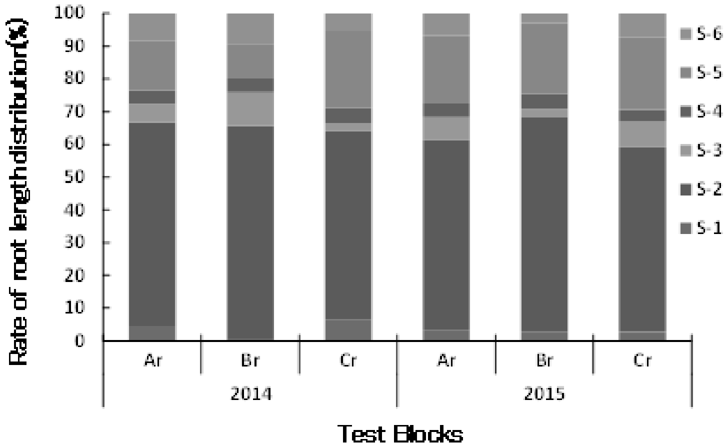

Fig. 9. – Fertilizer opener and chisel effects on the rate of root length distribution (summer harvest type)

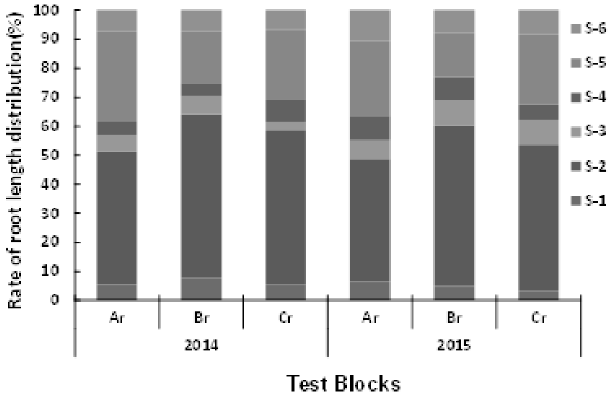

Fig. 10. – Fertilizer opener and chisel effects on the rate of root length distribution (autumn–winter harvest type)

Sampling block S-2 exhibited the highest rate of root distribution at all test blocks. Sampling block S-5 was the next highest. Sampling block S-5 of Ar and Cr blocks showed a higher rate of root distribution than Br block, except for the summer harvesting type in 2015. That difference was greater for the autumn–winter harvesting type. Sampling blocks S-1, S-2, and S-5 of shallow places in ditches made by fertilizer openers and chisels were higher rates of root distributions. Especially, block S-1, to which a fertilizer was applied, had many short roots; S-3 of the non-fertilized block showed many long roots. Using a chisel in the ditch encouraged many long roots penetrating to deep places in ditches to soften soil in the ditch. Sampling block S-3 of the Cr block, in which a fertilizing opener was used, showed greater differences in the amounts of roots than sampling block S-1 because S-3 had great differences of gas phase in the soil to have no fertilizer area.

CONCLUSIONS

The fertilizer-applicator ditcher developed for this research increased root length and root length density and decreased soil hardness because of a chisel used in the soil. The drill-fertilized block of Welsh onion plants showed a lower rate of root distribution because roots reached the fertilizer quickly. Each test block that had been prepared using a chisel in the ditch exhibited an increased rate of root distribution in deep parts of the ditch. However, non-fertilized areas prepared using a fertilizer-opener showed great differences in the root amounts because those areas showed large differences of gas phase in the buried soil as a result of the plate arrangement in the fertilizer-applicator ditcher.

REFERENCES

1. HONJO, M., SHINDO, H., OTAKE, T., SAITO, M., KATAHIRA, M., NATSUGA, M., YOSHIDA, Y., KANETA, Y.: Studies of Power Farming Systems of Welsh Onion Cultivation (Part 2) —Field test of new cropping type of Welsh onion using chain paper pots—ASABE, Paper Number: 152188880, 2015.
2. OTAKE, T., SHINDO, H., HONJO, M., SAITO, M., KATAHIRA, M., NATSUGA, M.: Studies of Power Farming Systems of Welsh Onion Cultivation (Part 1) —Optimization of chain pot connection—.ASABE, Paper Number: 152180882, 2015.
3. SHINDO, H., OTAKE, T., HONJO, M., SAITO, M., KATAHIRA, M., NATSUGA, M.: Studies of Power Farming Systems of Welsh Onion Cultivation (Part 3) —Growth promotion effects and fertilizer amount reduction with drill fertilizing—ASABE, Paper Number: 152188876, 2015.

Corresponding author:
Mitsuhiko Katahira, *Yamagata University, 1-23, Wakabamachi, Tsuruoka, Yamagata, Japan*

RESPONSE OF PADDY RICE UNDER SYSTEM OF RICE INTENSIFICATION

S. Pandiangan, P. Lumbanraja, E. T. S. Saragih

Agriculture Faculty of Nommensen HKBP University, Jl.Sutomo No. 4 Medan, Indonesia, 20234

Abstract

Field experiment was conducted in October 2014 until January 2015, at Pasar Melintang Village, Deli Serdang regency, North Sumatra, Indonesia, with elevation of 26 m above sea level, wet tropical climate, on sandy loam, pH 5.6. The purpose of this study was to investigate the response of paddy rice on plant spacing and seedling age under System of Rice Intensification. The experimental design was Randomized Completely Block Design Factorial with two factors. The first factor was two different ages of seedlings [8 days old (U1) and 12 days old (U2)]. Second factor was four different of plant spacings [25 cm x 25 cm (J1), 30 cm x 30 cm (J2), 35 cm x 35 cm (J3), and 40 cm x 40 cm (J4)]. The results showed that there was no effect of seedling age on paddy rice growth and yield. However, plant spacing significantly affected the growth and yield, except the height and stem diameter.

Key words: System of Rice Intensification, seedling age, plant spacing, days after planting, rice Ciherang.

INTRODUCTION

Indonesia ranks third in rice production in the world after China and India. Rice (*Oryza sativa* L.) is the staple cereal food grain in Indonesia for more than 90% Indonesian population consumes rice, provides more than 70% national caloric needs. Rice is cultivated by more than 90% of small subsistence farmers, rice is a main source income of more than 60% Indonesian population, so that rice is considered as a strategic commodity (GANI AND WIDARTA, 2009). Therefore, Indonesian government has put much efforts to develop a technology that can improve the productivity of rice in oder to meet the population need on rice. The Green Revolution was the fundamental changes in the cultivation technology of rice that began in the 1950s and 1980s in many developing countries in Asia, included, Indonesia. The Green Revolution based on four important pillars namely the provision of water through irrigation systems (soil saturated), optimal use of chemical fertilizers, pesticides application in accordance with the level of pest attacks, and the use of high yielding varieties (SISWORO, 2007). Cultivation practices with Green revolution, the paddy fields continously saturated, planted 3 to 5 seedlings per planting hole, with the age of seedlings of 21 days old, plant spacing 20 cm x 20 cm and applied high external input, such as chemical ferlizers and chemical pesticides. Through this system, increased rice yields and enable cultivation doubled, even three times a year for rice in certain places, something that previously was not possible. The positive impact of the green revolution in Indonesia was production of rice increased. For example: Indonesia from a rice importer is able to self-sufficiency and to export rice to India from 1984 – 1989. However, The Green Revolution has received criticism in line with the increasing awareness of environmental sustainability because it caused severe environmental damage. Some problems and negative impacts of green revolution: the decline of biodiversity, continues use of fertilizers cause dependence of plant on fertilizer, and the excessive use of pesticides led to the emergence of new strains of resistant pests (ANDERSON AND HAZEL, 1985).

The possible way to increase the productivity is through formulating better production technologies with improved cultivars and efficient nutrient management practices. The System of Rice Intensification (SRI) was was originally developed in Madagascar between 1983-1984 (RANJITHA ET AL., 2013). SRI practices mainly based on six components: (1) transplanting of young seedlings, (2) transplanting of single seedling, (3) wide plant spacing, (4) aerobic soil moisture, (5) only compost application, and (6) weeding (STOOP ET AL., 2002). In Indonesia SRI concept was also tested and practiced at some districts in Java, Sumatera, Bali, West Nusa Tenggara, Kalimantan, Sulawesi and Papua. (ANUGRAH ET AL., 2008). However, since the concept of SRI is a pure organic farming, farmers in the area of research is very difficult to implement SRI 100%, due to the availability of organic materials, including organic fertilizers and organic pesticides to meet the need of rice are very unlikely to be implemented. Economically, if the SRI implemented 100% accordingly it would cost much higher than conventional system that the farmer implemented. Some researches that applied some concepts of SRI such as Kumar et al. (invited paper) applied SRI method at 25 locations for four years across India found clearly indicated that SRI resulted 7 – 20 percent higher grain yield over the traditional irrigated transplanted rice, reduced the seed rate by 80%, water requirement by 29% and growth duration by 8 – 12 days. JONHARNAS ET AL. (2003) found that the number of seedlings per planting hole did not affect the productivity of four paddy varieties. Research conducted by SEMBIRING ET AL. (2003) showed that the seedlings number and seedling age did not affect the productivity of rice. According to SALAHUDDIN ET AL. (2009) that plant spacing affected panicle length, number of grain per panicle and yield. PANDIANGAN ET AL. (2014) recorded that plant spacing with 35 cm x 35 cm of rice cultivar IR-64 resulted the highest yield compared with plant spacings of 25 cm x 25 cm, 30 cm x 30 cm and 40 cm x 40 cm. NAIDU ET AL. (2013) found that transplanting of 12 days old seedlings resulted in the highest grain yield, grain protein and N P K uptake compared with 8, 16, 20 days old seedlings and planting pattern of 25 cm x 25 cm recorded higher grain yield, grain protein and N P K uptake compared with 20 cm x 20 cm, 30 cm x 30 cm and 35 cm x 35 cm. while these parameters were lowest with planting pattern of 35 cm x 35 cm.

This research was to investigate the response of rice on some principle concepts of SRI, those are age of seedlings and plant spacing which may be applied by farmers.

MATERIALS AND METHODS

Site and time: The experiment was conducted in October 2014 until January 2015, at Pasar Melintang Village, Deli Serdang regency, North Sumatra, Indonesia, with elevation of 26 m above sea level, wet tropical climate, soil texture sandy loam with pH 5.6.

Experimental design: Experiments were conducted in a randomized block design with factorial with three replications. The treatments consisted of combination of four different plant spacings [J1 (25 cm x 25 cm), J2 (30 cm x 30 cm), J3 (35 cm x 35 cm) and J4 (40 cm x 40 cm)] and two ages of seedlings [A1(8 days old), A2 (12 days old).

Materials: paddy rice (*Oryza sativa* L.) Variety Ciherang, compost, Urea, N P K Mutiara, SP-36 and KCL. Pesticides: insecticides (Bestox 50 EC and Hamasid 25 EC), Fungicide (Sorento and Dennis 75 WP), molluscicide (Besnoit).

Tools: meter, hoe, harrow, hand sprinkler, ruler, bucket, analytical scale Ohaus (0.001 g), pencil, pen, and logbook.

***Land preparation*:** Compost was spread over the land as much as 1,250 kg·ha^{-1} before plowing. The soil was plowed as deep as 30 cm and buried residual plants on the land, then the soil was crumbed with harrow, then was leveled. The trenches were made around the whole land and around each plot, to maintain aerob condition wherever possible.

Nursery preparation: The nursery was prepared on seedbed with 1.5 m x 2.0 m, in the main research land. Soil was plowed as deep as 30 cm and buried residual plants on the land, then the soil was crumbed, with harrow, then was leveled. The trenches were made around the seedbed, to avoid over irrigated. Before the seeds were sown, beds firstly was sown with compost as much as 30 kg. Seedbed then was sprayed with molluscicide, Besnoit.

Seed preparation: The seeds were soaked in a bucket filled with water until all the seeds were submerged. The seeds that float were discarded, and the seeds that sink were soaked for 12 h and incubated in moist gunny suck for 24 h to accelerate germination. Germinated seeds then were sown on the surface of the seedbeds, then covered with a thin layer of soil.

Transplanting: Before transplanting, firstly plant spacings were drawn for each plot as treatment accordingly. One seedling per hole was planted with 1-1.5 cm depth, and aerob condition.

Fertilization: Broadcasting of fertilization was applied twice, firstly, when the plant age 10 DAP with urea 60 kg·ha^{-1}, N P K Mutiara 30 kg·ha^{-1} and SP-36 30 kg·ha^{-1}. Secondly, when plant age 25 DAP with 30 kg Urea·ha^{-1}, KCl 60 kg·ha^{-1}, SP-36 90 kg·ha^{-1} and NPK Mutiara 30 kg·ha^{-1}. Irrigation, was maintained moist.

Pest and disease control: Pest and disease was controlled by spraying insecticides and fungicides. Insecticide used was BESTOX, Hamasid 50 EC and 25 EC. Fungicides used were Sorento and Dennis 75 WP.

Measurement of parameters: Before conducting measurements of parameters, firstly it was determined 1m^2 the most homogeneous growth from each treatment plot as samples from each treatment plot. Of 1 m^2 was determined three clumps for measurements of parameters. Plant height was measured from ground level to the highest leaves by using meter rolls. Measurements were made per 10 DAP (Day After Planting) for 60 days. Number tillers was conducted at harvest. Stem diameter was measured at the end of the observation by using vernier calipers. Stem diameter of three plants from each clumb was measured. Measurements were taken at the third segment of each stem. Panicle length was measured from 3 stalks of each sample clump. Number of grain per panicle was derived from 3 stalks of each three clumbs. Number of filled grains per panicle was derived from 3 plants from each 3 clumbs. Yield was measured by harvesting the three sample plots, then it wasaveraged then converted into ton·ha^{-1}. Dry weight of 1000 grains was measured by picking up 1000 filled grains from the yield by hand, then dried under the sun light until water content 16%, then weight by using analytical scale.

RESULTS AND DISCUSSION

Results of the study regarding the influence of age of seedling and plant spacing and their interactions on growth and yield of rice variety Ciherang presented in Tab. 1, 2 and 3 as well as Fig. 1,2, 3, 4 and 5.

Effect of Age of Seedlings.

This research result showed there was no significantly different of growth and yield of rice between transplanted seedling age of 8 days old and 12 days old. (Tab. 1 and 2), These results correspond with the results of the research of SEMBIRING ET AL. (2003). However, this result was different from research conducted by NAIDU1 ET AL. (2013) where they found that planting of 12 days old seedlings resulted in the highest grain yield compared with 8 days old seedlings. This difference result might due to different environment and cultivars used.

Effect of plant spacing:

Number of tillers: As the plant spacing increased the larger the number of tillers. The highest number tillers was resulted upon plant spacing 40 cm x 40 cm and was very significantly diferrent from three other plant spacings (Tab. 3). The correlation between plant spacings and number of tillers was linearly positive, and was very significant, with co-efficient of determination (R^2=0.978) (Fig. 1) indicating that 97.8% of the total variation of number of tiller could be attributed to the plant spacing treatment alone and 2.2% by other factors were not investigated.

Tab. 1. – The effect of plant spacing and seedling age on height at 60 DAP

Seedling age (day)	Height of paddy rice at 60 DAP (cm)				
	Plant spacing (cm)				
	J1 (25x25)	J2(30x30)	J3 (35x35)	J4 (40x40)	Average
U1 (8 days)	112.0	110.6	109.2	110.4	110.5
U2 (12 days)	108.3	110.9	112.6	110.9	110.67
Average	110.15	110.75	110.9	110.65	n.s

DAP : Day after planting. n.s: non significant

Tab. 2. – The effect of seedling age on growth and yield of paddy rice at 100 DAP

Seedling age (day)	Number of tillers	Stem diameter (cm)	Panicle length (cm)	Number of grain per panicle	Number of filled grain per panicle	weight of 1000 dry grain (g)	Yield (ton·ha^{-1})
U1 (8)	21.93	0.59	27.18	205.18	189.39	43.18	5.26
U2 (12)	21.21	0.55	26.59	204.75	188.68	43.57	5.07
	n.s	n.s	n.s	n.s	n.s	n.s	n.s

DAP : Day after planting

Tab. 3. – The effect of plant spacing on growth and yield of rice at 100 DAP

Plant spacing (cm)	Number of tillers	Stem diameter (cm)	Panicle length (cm)	Number of grain per panicle	Number of filled grain per panicle	weight of 1000 dry grain (g)	Yield (ton·ha^{-1})
J1(25 x 25)	15.27aA	0.58	26.64aAB	195.03aA	180.78aA	43.05	5.995cB
J2(30 x30)	18.77 bAB	0.57	27.05abAB	204.91aAB	188.46aAB	43.32	5.01bB
J3(35 x 35)	22.88 cB	0.55	26.14aA	199.33aA	185.95aAB	43.43	6.095cB
J4(40 x 40)	29.38dC	0.57	29.38dC	220.41bB	200.96bB	43.71	3.465aA
		n.s				n.s	

Figures followed by the same letter on the same column showed no significant effect on the level of α = 0.05(lowercase) and α = 0.01 (uppercase) by Duncan. DAP : Day after planting

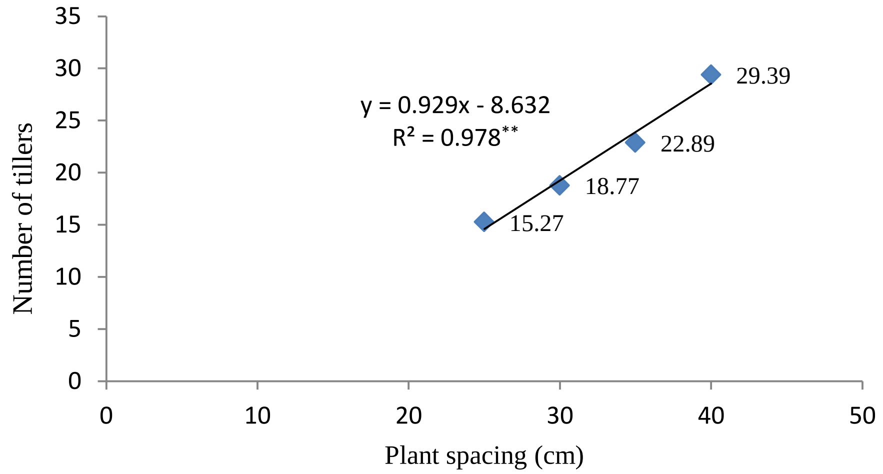

Fig. 1. – Correlation between plant spacing and number of tiller

Stem diameter: Final measurement of stem diameter was 60 DAP, for the generative growth was started at 60 DAP. The results showed that there was no significantly different of stem diameter among plant spacing tested (Tab. 1). This due to that the closet plant spacing J1 (25 cm x 25 cm) had might had reached the maximum of stem diameter of rice namely 0.55 cm this result supported BY PASARIBU ET AL., (2013) that recorded that stem diameter of rice Ciherang was less than 0.5 cm.

Panicle length: Plant spacing of 40 cm x 40 cm resulted the longest panicle and was very significantly different from three other plant spacings (p<0.01). While the other three plant spacings were not significantly different (p>0.05) (Tab. 3). This results agreed with the research result conducted by SALAHUDDIN ET AL. (2009) where they found that plant spacing did affect panicle length of aman rice. There was a quadratic correlation between plant spacing and panicle length with co-efficient of determination (R^2=0.455) and was significant. indicating that 45,5 % of the total variation of panicle length could be attributed to the plant spacing treatment alone and 54.5% by other factors were not investigated.

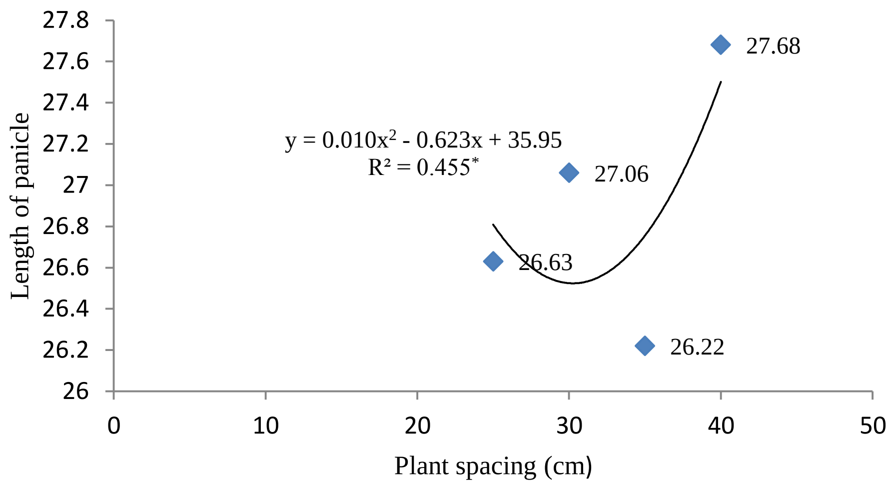

Fig. 2. – Correlation between panicle length and plant spacing

Number of grain per panicle: Plant spacing of 40 cm x 40 cm resulted the highest number of grain per panicle, and it was very significantly different from plant spacing of 25 cm x 25 cm and 30 cm x 30 cm ($p<0.01$) and significantly different from plant spacing of 30 cm x 30 cm ($p<0.05$) (Tab. 3). This results agreed with the research result conducted by Salahuddin, et al.(2009) where they found that plant spacing did affect number of grain per panicle of aman rice. The correlation between plant spacing and number of grain per panicle was very significant linear positive with co-efficient of determination (R^2=0.671) (Fig. 3). This indicated that plant spacing alone could be attributed 67% upon the total variation of number of grain per panicle and about 37% was due to other factors were not observed.

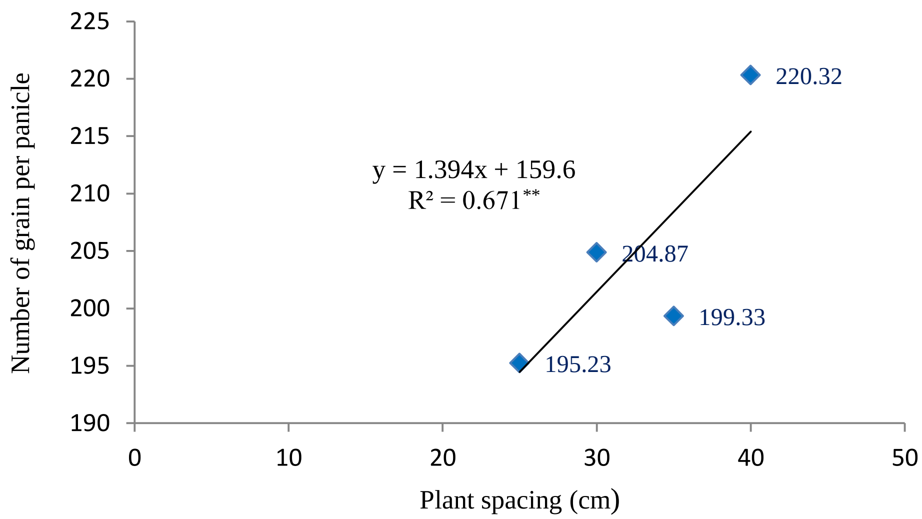

Fig. 3. – Correlation between number of grain per panicle and plant spacing

Number of filled grain per panicle: Plant spacing of 40 cm x 40 cm resulted the highest number of filled grain per panicle, and it was significantly different from three other plant spacings ($p<0.05$) and was very significantly different from plant spacing of 25 cm x 25 cm ($p<0.01$) (Tab. 3). The correlation between plant spacing and number of filled grain was very significantly linear positive ($p<0.01$) with co-efficient of determination (R^2=0.764) (Fig. 4). This indicated that plant spacing alone could be attributed 76.4% on total variation of filled grain was contributed due to plant spacing.

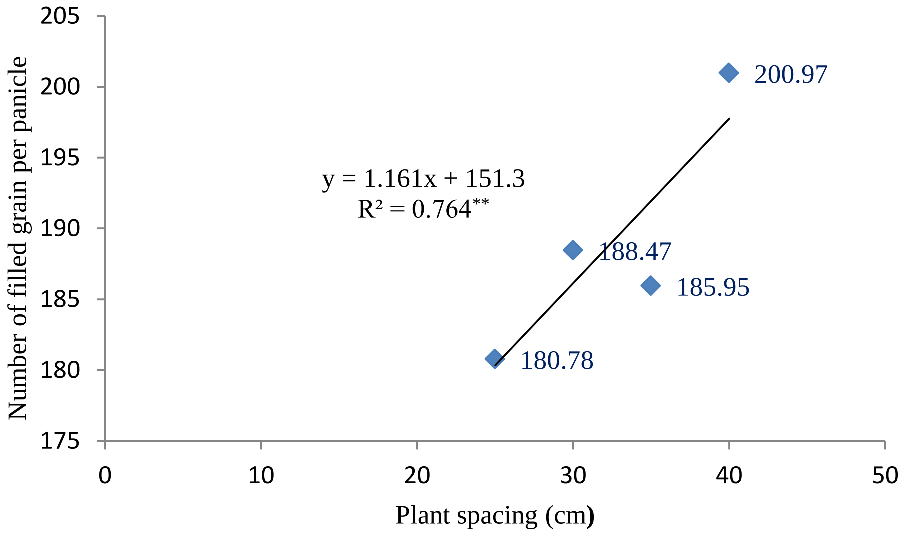

Fig. 4. – Correlation between plant spacing and number of filled grain per panicle

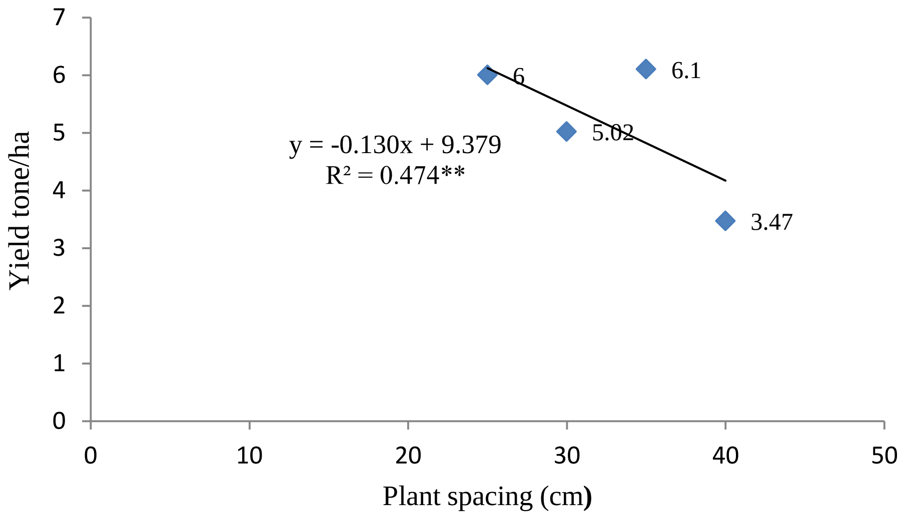

Fig. 5. – Correlation between plant spacing and yield (ton·ha^{-1})

Weight of 1000 dry grain: There was no effect of plant spacing on weight of 1000 dried grain. This might be for the closet plant spacing had reached the maximum weight of 1000 dry grain, this suggestion was supported by the description of rice Ciherang that the weight of 1000 grain of rice Ciherang was 27 – 28 g (Balai Besar Penelitian Tanaman Padi, 2016).

Yield: plant spacing did affect significantly yield, this result was supported by SALAHUDDIN, ET AL. (2009) and Naidu1 et al.(2013). The highest grain yield was produced with plant spacing of 35 x 35 cm (J3), and was significant different from plant spacing fo 30 cm x 30 cm (J2) and 40 cm x 40 cm (J4) ($p<0.05$), but was not significantly different from plant spacing of 25cm x 25 cm (J1) ($p<0.05$). The correlation between plant spacing and yield was very significantly linear negative ($p<0.01$) with co-efficient of determination (R^2=0.474) (Fig. 5). This indicated that plant spacing alone could be attributed 47.4% on total variation of yield and 52.6% was due to other factors were not observed. This results was similar to the results of research conducted BY PANDIANGAN, ET AL. (2014) where plant spacing of 35 cm x 35 cm resulted the highest yield compared with 25 cm x 25 cm, 30 cm x 30 cm and 40 cm x 40 cm on rice cultivar IR 64. The lowest yield was recorded with the plant spacing of 40 cm x 40 cm (J4) (Tab. 3). This results was different from result found by NAIDU1 ET AL. (2013) where plant spacing of 25 cm x 25 cm resulted the highest yield compared with plant spacings of 20 cm x

20 cm, 30 cm x 30 cm and 35 cm x 35 cm. They found that plant spacing of 35cm x 35 cm resulted the lowest yield. This might be due to different variety used. Plant spacing of 40 cm x 40 cm resulted the lowest yield, whereas, it resulted the highest on other growth parameters, that logically would resulted the highest yield as well. The lowest yield resulted from plant spacing of 40 cm x 40 cm might be due to the number of population per ha much lower than population of other plant spacings. The number of clumps per hectar of plant spacing 40 cm x 40 cm was 62,522 clumps compared with the number of clumps per hectar of plant spacing 35 cm x 35 cm was 81,632 clumps.

CONCLUSIONS

The result of the study realized that age of seedlings between 8 and 12 days old did not affect growth and yield, plant spacing did affect yield, number of tillers, length of panicle, number of grain per panicle, but did not affect plant height, stem diameter and weight of 1000 dry grain, plant spacing of 35 cm x 35 cm resulted the highest yield, there was no interaction between plant spacing and age of seedlings on growth and yield.

REFERENCES

1. ANUGRAH, I. S., SUMEDI WARDANA, P.: Concept and Implementation of System of Rice Intensification (SRI) in Rice Cultivation of Ecological Event. Agricultural Policy Analysis. 4(1), 2008:75- 79. (in Indonesian).
2. ANDERSEN, P. P., HAZEL, P. B.: The Impact of Green Revolution and Prospect for Future. International Food Policy Research Institute Washington,D.C. Food Reviews International, 1(1), 1-25 (1985). Available at:http://pdf.usaid.gov/pdf_docs/. Accessed 19 May 2016 (online).
3. GANI, A., WIDARTA, N.: Opportunities for rice self sufficiency in Indonesia with the system of rice intensification. SRI-Rice, International Programs, CALS, Cornell University. 2009. Available at: http://www.slideshare.net/SRI.CORNELL.Accessed 19 May 2016. (online).
4. JONHARNAS, S., BAHRI MARBUN, T.: Effect of Number of Seedling on Growth and Productivity Some Rice Varieties. In: National Seminar Location Specific Technology Support Food Security and Agribusiness to Increase Farmers' Income in the Era of Globalization. 2003. (in Indonesian)
5. KUMAR, R. M., SUREKHA, K., PADMAVATHI, CH., RAO, L. V. S., LATHA, P. C., PRASAD, M. S., BABU, V. R., RAMPRASAD, A. S., RUPELA, O. P., GOUD, V., RAMAN, P. M., SOMASHEKAR, N., RAVICHANDRAN, S., SINGH, S. P., VIRAKTAMATH, B. C.: Research Experiences on System of Rice Intensification and Future Directions. J. Rice Research., vol 2, 2, invited paper : 61-71.
6. NAIDU, G. J., RAO, K. T., RAO, A. U, REDDY, D. S.: Age of Seedlings and Planting Pattern on Grain yield, Protein Content, NPK Uptake and Post-harvest Nutrient Status of Rice under SRI. Journal of Academia and Industrial Research (JAIR).,2, 2013: 334-337.
7. PANDIANGAN,S., LUMBANTORUAN, M., PANJAITAN, P. J.: Rice Cultivation (*Oryza sativa* L.) Based of System of Rice Intensification. In: Proceedings National Seminar on Biology, Optimization of Biological Research in Agriculture, Livestock, Fisheries, Marine, Pharmacy and Medicine. NINGSIH, H.W. Department of Biology, Faculty of Mathematics and Natural Sciences, University of North Sumatra, Medan, Indonesia. 2014, pp 196 -203. (CD-ROM). (in Indonesian).
8. PASARIBU, A., KARDHINATA, E. H., BANGUN, M. K.: Test of Several varieties of Irrigated Rice (*Oryza sativa* L.) and Potassium Fertilizer Application (KCl) to Increase Production and Resilience on fall down. Journal Online Agroekoteknologi, Vol.1(2), 2013:45-57. (in Indonesian).
9. PLANT RESEARCH CENTER FOR RICE. Ciherang. Available at:
10. http://bbpadi.litbang.pertanian.go.id. Accessed 24 May 2016.(Online). (in Indonesian).
11. RANJITHA, P. S., KUMAR, R. M., JAYASREE, G.: Evaluation of rice (*Oryza sativa* L.) varieties and hybrids in relation to different nutrient management practices for yield, nutrient uptake and economics in SRI. Annals of Biological Research, 4 (10), 2013:25-28
12. SALAHUDDIN, K. M., CHOWHDURY, S. H., MUNIRA, S., ISLAM, M.M., PARVIN, S.: Response of nitrogen and plant spacing of transplanted Aman Rice. Bangladesh J. Agril. Res. 34(2) : 2009:279-285.
13. SEMBIRING, H., HIPPI, A., WIRAJASWADI, L.: Influence of Age and Number of Seedling on Yield of Irrigated Rice on Entisol and inceptisol Soil in West Nusa Tenggara. In: National Seminar Location Specific Technology Support Food Security and Agribusiness to Increase Farmers' Income in the Era of Globalization, 2003. (in Indonesian).
14. SISWORO, W. H.: Rebuilding Self Sufficiency of Rice. Available at:
15. https://id.wikipedia.org/wiki/Revolusi_Hijau, 2007: Accessed 15 May 2016. (online). (in Indonesian)
16. STOOP, W. A., UPHOFF, N., KASSAM, A.: A review of agricultural research issues raised by the system of rice intensification (SRI) from Madagascar; opportunities for improving farming systems for resource poor farmers. *Agric. System*. 71, 2002:249-274.

Corresponding author:
Samse Pandiangan, Agriculture Faculty of Nommensen HKBP University, Jl.Sutomo No. 4 Medan, Indonesia, 20234, phone: +62 08126426302, e-mail: samsepandiangan@yahoo.com.

STANDARDS AND REAL PARAMETERS OF DAIRY FARM TECHNOLOGY IN CZECH REPUBLIC

J. Papež, P. Kic

Department of Technological Equipment of Buildings, Faculty of Engineering, Czech University of Life Sciences Prague, Czech Republic

Abstract
The aim of this study is to evaluate the current conditions of buildings for dairy farming and show promising methods important for the further development in this area of agricultural production in the Czech Republic. The paper contains an analysis of the current technical state of cowsheds including milking parlours and waiting rooms. Attention is paid to the types of barns and construction materials and to the technical implementation of technological equipment with regard to animal welfare. The required parameters are evaluated according to scientific literature. For the purposes of this study there were examined several new and modernized objects for dairy farming of different design concepts and age. Technological equipment for housing, dimensions and location of feeding and watering troughs, manipulation with manure and other equipment to enhance animal welfare were examined. The types of milking parlour, movement of cows on the farm and methods of heating and ventilation were studied.

Key words: cowshed, milking parlour, waiting room, welfare.

INTRODUCTION

Livestock production in countries with intensive agriculture is currently undergoing big and rapid changes. These changes are also taking place in many dairy farms. If farmers want to be competitive, they must achieve bigger milk yields and higher quality of milk, partly thanks to the better milking system on the farm. Capacity of the farms is expanding and increasing is also the average annual milk production per cow. The number of dairy cows was reduced significantly in the last twenty years in the Czech Republic. Vice versa, average milk yield was significantly improved during this period. There were 1,989,000 cows with average milk yield of 4,117.2 $l.cow^{-1}$ in the Czech Republic in 1995. In 2013, there are 552,000 cows with average milk yield of 7,443.4 $l.cow^{-1}$ in the Czech Republic (ČSÚ, 2014). Development of the dairy farms needs also new constructions of barn and modernization of older buildings. Similar problems on dairy farms are solved not only in the Czech Republic but also abroad (GAWORSKI & LEOLA, 2014; GAWORSKI & PRIEKULIS, 2014).

The cattle were kept on pasturelands or small family farms in previous times (VEGRICHT ET AL., 2008). The period of collectivization and large scale farming began in the fifties of the 20th century. Big cowsheds were mostly masonry or wooden constructions. Tie-stall housing was preferred during that period. However, nowadays almost everywhere is preferred loose housing of dairy cows which is spread to Europe from the US in the second half of the 20th century (SÝKORA, 2014; RIST, 1994). After 1989, began the transition to breeding cows with high milk production in the Czech Republic. This resulted in the formation of new breeding technologies, reconstruction of old barns and building of completely new cowsheds (DOLEŽAL ET AL. 2002).

The aim of this study is to evaluate the current conditions of the buildings for dairy farming and to show promising methods important for further development in this area of agricultural production in the Czech Republic. The paper contains an analysis of the current technical state of the cowsheds including milking parlours and waiting rooms.

MATERIALS AND METHODS

For the purposes of this study there were examined 7 farms (A – G) for dairy farming of different design concepts and age. There were examined 2 different cowsheds at farm B (B1 and B2). We examined also parameters of milking parlours and waiting rooms belonging to the cowsheds. The research is based on the investigation of required parameters personally in the real conditions in the farms, by discussions with designers, managers and farm workers and by evaluation of technical documentation and designs representing the most common types of dairy farms and cowsheds.

In particular, the following parameters were investigated and collected in cowsheds: housing capacity; type of construction and building materials; dimensions; housing technology; internal corridors; dividing barriers and feeding and watering equipment; type of beds; type of slurry and manure removal; ventilation and cooling systems; using of the cow brushes, or other facilities for animal welfare improvement.

Following parameters were investigated in the milking parlours and waiting rooms: the length of the transition into the milking parlour; type of milking equipment; methods of heating and ventilation; number of workers; capacity and dimensions of waiting rooms. To compare different cowsheds, many evaluated parameters were recalculated to specific values per one dairy cow.

RESULTS AND DISCUSSION

The results of our investigation in cowsheds are shown in the Tab. 1 (farm A – C) and Tab. 2 (farm D – G). The results of our investigation in milking parlours and waiting rooms belonging to the cowsheds are presented in the Tab. 3.

The barns are often constructed as a frame construction. The common materials used for supporting structures are: steel, timber, concrete, and masonry (MÁLEK, 2002).

- The most common type of cowshed barn is a steel structure. It is used for construction of cowsheds B1, E and G. The width can be to 36 m without internal support columns (BELADA, 2005).
- Wood is a traditional material suitable for agricultural buildings. There different types of timber constructions (used at farms C and D), however the supporting columns are required in this cowsheds (BELADA, 2005).
- The newest type is a lattice structure in combination with cloth envelope (farm F) (SÝKORA, 2014).
- The bricked constructions are used only in the case of old reconstructed cowsheds (A and B1).

The module of the old renovated cowsheds is 4.5 m (farm A and B1); the newly built cowsheds use mostly the module of 4.8 m or 6 m (farm D).

Indoor air quality is affected by the volume of the barn. Recommended value of specific cowshed volume is 42 $m^3.cow^{-1}$. This value ensures relatively good transfer of excess body heat into the environment. It is also the space which captures excess water vapour, CO_2 and other pollutants (DOLEŽAL ET AL., 2002; BOUŠKA ET AL., 2006). This requirement is not fulfilled just in case of reconstruction cowsheds. The newly built barns have more than sufficient volume per cow. The trend is to build cowshed with higher volume per cow. The requirement on minimum specific area 7.5 $m^2.cow^{-1}$ according to (DOLEŽAL ET AL., 2002; BOUŠKA ET AL., 2006) is fulfilled in all cowsheds.

There is used the roll tarpaulin for inlet of fresh air on the side walls to ensure sufficient ventilation in the barn. The dimensions of the roll tarpaulin should correspond to the requirement of 0.23 $m^2.cow^{-1}$ (DOLEŽAL ET AL., 2002). This requirement is fulfilled in all cowsheds except the cowshed at farm A (there is not used the roll tarpaulin). The trend is to ensure a higher area of roll tarpaulin per cow in the modern cowsheds. Outlet of the warm and humid air ensures the ridge slit whose specific width should be 0.025 m per 1 m of stale width (DOLEŽAL ET AL., 2004). Also this requirement is fulfilled in all cowsheds except the cowshed at farm A. The roof slope is also important for sufficient ventilation. The requirement of minimum roof slope 15° (optimally 20°) according to (DOLEŽAL ET AL., 2002) is fulfilled at all newly built cowshed.

The dimensions of internal corridors are designed with respect to passing of cows. Comfortable width of manure corridor should not be less than 2.5 m, preferably 2.7 m and more. Also applies that the wider the corridor, the lower layer of excrement. The minimum size of the feeding corridor is 3.3 m (DOLEŽAL ET AL., 2002). The width of the feeding table should be at least 3.8 m (DOLEŽAL ET AL., 2004). The results of our research show that the dimensions of these corridors correspond with the recommendation in all cowsheds.

Specific length of feeding trough should be at least 0.52 $m.cow^{-1}$ (cow to trough ratio 1.5 : 1) or 0.72 $m.cow^{-1}$ (cow to trough ratio 1 : 1) (DOLEŽAL ET AL., 2004). However the results of our research show that in many cowsheds (B1, B2, D, E and G) the specific length of trough is shorter. Only in cowsheds at farm A, C and F is this parameter of welfare sufficient.

Watering troughs are usually located in passageways to the feeding area. The optimum length of watering edge is 0.1 $m.cow^{-1}$, but it should not be shorter than 0.05 $m.cow^{-1}$ (DOLEŽAL ET AL., 2002; DOLEŽAL ET AL., 2004). The results of our research show that this optimum length is fulfilled mainly in the newly built cowsheds.

Loose housing can be solved as a cubicle or in group pens (BOUŠKA ET AL., 2006). According to the Czech standard the minimum width of the cubicle is 1.1 m, the minimum length of single cubicle is 2.3 m and the minimum length of double cubicle is 4.1 m (208/2004 SB). However in practice are recommended these dimensions: single cubicle 1.2 x 2.5 m and double cubicle 1.2 x 4.6 m (DOLEŽAL ET AL., 2002; BOUŠKA ET AL., 2006). This is confirmed also by our research. Another option of loose housing is in group pens, which is used at farm F. For the housing in group pens it is necessary to ensure the specific area of 5 m^2 per cow (208/2004 SB). The specific area of the group pen is 5.4 $m^2.cow^{-1}$ at farm F.

Tab. 1. – Parameters of cowsheds at farm A – C

Parameter	**A**	**B1**	**B2**	**C**
Type of building	old barn	old barn	new barn	new barn
Year of construction	1996	2001	2001	2003
Type of construction	bricked	bricked	steel	wooden
Structure of side wall	masonry	masonry	wood and roll tarpaulin	wood and roll tarpaulin
Structure of front wall	masonry	masonry	masonry and metal sheet	wood
Number of cows	120	237	360	200
Height of cowshed, m	3	5	7.4	9.6
Width of cowshed, m	19.4	30.7	31.7	31.5
Length of cowshed, m	81.8	68.9	94.2	57.8
Module, m	4.5	4.5	4.8	4.8
Roof slope	0°	11.5°	16°	20°
Area, $m^2.cow^{-1}$	13.22	8.93	8.29	9.10
Volume, $m^3.cow^{-1}$	39.67	35.70	42.31	61.00
Area of roll tarpaulin, $m^2.cow^{-1}$	0.00	0.70	0.63	1.04
Width of ridge ventilation slot per 1 m of barn width, $m.m^{-1}$	0.000	0.036	0.025	0.038
Width of feeding table, m	3.75	4.30	4.50	5.00
Width of feeding corridor, m	3.00	3.40	3.55	3.40
Width of manure corridor, m	3.50	2.50	2.60	2.60
Length of feeding trough, $m.cow^{-1}$	0.67	0.50	0.46	0.52
Number of watering troughs	4	8	12	8
Watering trough, $m.cow^{-1}$	0.05	0.06	0.06	0.09
Housing technology	straw-bedding	bedding-free	bedding-free	straw-bedding
Beds	straw	rubber	rubber	straw
Slurry or manure removal	mobile scrapers	scrapers	scrapers	mobile scrapers
width of cubicles, m	1.125	1.125	1.2	1.2
Length of single cubicles, m	2.4	2.4	2.5	2.5
Length of double cubicles, m	not used	4.6	4.8	4.7
Cow brushes	no	no	no	no
Cooling systems	no	no	no	no
Ventilators	no	no	no	no

Tab. 2. – Parameters of cowsheds at farm D – G

Parameter	**D**	**E**	**F**	**G**
Type of building	new barn	new barn	new barn	new barn
Year of construction	2007	2008	2012	2014
Type of construction	wooden	steel	lattice steel	steel
Structure of side wall	wood and roll tarpaulin	concrete, roll tarpaulin	concrete and roll tarpaulin	concrete and roll tarpaulin
Structure of front wall	wood	concrete and metal sheet	cloth	concrete and metal sheet
Number of cows	254	352	160	368
Height of cowshed, m	10.4	11.3	14.6	11.4
Width of cowshed, m	32.6	33.6	36	34
Length of cowshed, m	66.5	101.2	62.4	91.2
Module, m	6	4.8	4.8	4.8
Roof slope	22°	23°	30°	22°
Area, $m^2.cow^{-1}$	8.54	9.04	14.04	8.43
Volume, $m^3.cow^{-1}$	60.59	73.89	127.81	66.98
Area of roll tarpaulin, $m^2.cow^{-1}$	0.97	1.24	2.03	1.69
Width of ridge ventilation slot per 1 m of barn width, $m.m^{-1}$	0.037	0.027	0.028	0.032
Width of feeding table, m	4.90	5.00	4.90	5.20
Width of feeding corridor, m	3.20	3.60	3.30	3.80
Width of manure corridor, m	2.70	2.50	0.00	3.00
Length of feeding trough, $m.cow^{-1}$	0.50	0.49	0.72	0.45
Number of watering troughs	8	9	8	9
Watering trough, $m.cow^{-1}$	0.09	0.10	0.15	0.14
Housing technology	bedding-free	bedding-free	straw-bedding	bedding-free
Beds	mattresses	mattresses	straw	water mattres-ses
Slurry or manure removal	slates	slates	mobile scrapers	slates
Width of cubicles, m	1.2	1.2	pens (9x24 m) for 40 cows	1.2
Length of single cubicles, m	2.5	2.7		2.7
Length of double cubicles, m	5	4.8		4.8
Cow brushes	no	no	yes	yes
Cooling systems	no	no	no	yes
Ventilators	no	no	no	yes

The surface of the beds can be made by various materials depending of housing type (straw-beddings or bedding-free). Most common type of these materials is straw, rubber mattresses (DOLEŽAL ET AL., 2004; BOUŠKA ET AL., 2006). In the case of straw-bedding system the slurry and manure are removed mechanically. In the case of bedding-free system the slurry and manure are removed by scrapers or channels covered by slatted floor (DOLEŽAL ET AL., 2002).

The welfare in the cowshed could be improved by cow brushes, cooling system and ventilators. The cow brushes are located near to the watering troughs (DOLEŽAL ET AL., 2002). The cooling system consists of a metallic arm and the supply hose with nozzles. The period of application with minimal water consumption is about 20 – 30 seconds. Satisfactory is 1 sprinkler for 40 cows (DOLEŽAL ET AL., 2004).

Tab. 3. – Parameters of waiting rooms and milking parlours at farm A – G

Parameter	**A**	**B1**	**B2**	**C**
Walking distance to milking parlour, m	90	135	65	130
Capacity of waiting room	30	90		60
Area of waiting room, $m^2.cow^{-1}$	1.47	1.50		1.50
Type of milking parlour	auto-tandem	rotary		rotary
Capacity of milking parlour	2 x 4	32		24
Number of workers	2	2		2
Ventilation of milking parlour	natural (windows and chimneys)	natural (windows and skylights)		natural (windows and chimneys)
Heating of milking parlour	ceramic emitters and floor heating	heat recovery from milk cooling room		radiant heating panels
	D	**E**	**F**	**G**
Walking distance to milking parlour, m	80	86	70	75
Capacity of waiting room	70	100	40	70
Area of waiting room, $m^2.cow^{-1}$	1.56	1.62	1.70	1.70
Type of milking parlour	side-by-side	rotary	side-by-side	side-by-side
Capacity of milking parlour	2x12	24	2x8	2x12
Number of workers	2	2	2	2
Ventilation of milking parlour	natural (windows and skylights)	forced (over pressure) and skylights	natural (windows and skylights)	natural (windows and skylights)
Heating of milking parlour	heat recovery from milk cooling room	heater of external air	heat recovery from milk cooling room	heat recovery from milk cooling room

Capacity of the waiting room should correspond with number of cows in the biggest production department of the cowshed. In the waiting room is a necessary to ensure area of 1.4 – 1.5 $m^2.cow^{-1}$ (KAVKA, 2003). The results of our research show that this parameter is fulfilled at all farms. Moreover, the trend is to ensure higher specific area for one cow. The length of the transition into the milking parlour should not be longer than 100 m (DOLEŽAL ET AL., 2002). The results of our research show that this distance is sometimes exceeded (B2 and C).

For ventilation of milking parlours is used mostly natural system: windows in combination with skylights or ventilation chimneys. Utilization of heat recovery from milk cooling room is the most common way of heating of the milking parlours. Other options of heating are radiant heating panels, ceramic emitters, floor heating and the heater of external air.

CONCLUSIONS

1. The only used type of housing in the Czech Republic is loose housing with straw-bedding or bedding-free housing technology.
2. The specific volume of cowsheds $m^3.cow^{-1}$ is constantly increasing in recent years.
3. The specific surface of openings for natural ventilation of cowsheds increases.
4. The specific length of the watering troughs increases.
5. More attention is paid to the capacity and dimensions of waiting rooms.
6. There are used mostly side-by-side or rotary milking parlours with 16 or more milking stalls.
7. The equipment for enhance of animal welfare is more common in new cowsheds.

ACKNOWLEDGEMENT

Supported by Internal grant agency of Faculty of Engineering, Czech University of Life Sciences in Prague no: 2015:31170/1312/3114.

REFERENCES

1. BELADA, B.: Designing a stalls for cows. In: Modern livestock production, vol. 1, 2005, pp. 14 – 16 (in Czech).
2. BOUŠKA, J., DOLEŽAL, O., JÍLEK, F. ET AL.: Breeding of dairy cattle. 1st ed., Praha, Czech Republic, PROFI PRESS 2006 (in Czech).
3. ČSÚ. Statistical Yearbook of the Czech Republic. 1st ed., Praha, Czech Republic, ČSÚ 2014 (in Czech).
4. DOLEŽAL, O., BÍLEK, M., ČERNÁ, D. ET AL.: Comfortable housing of high-yield dairy cows. 1st ed., Praha, Czech Republic, VÚŽV 2002. (in Czech)
5. DOLEŽAL, O., BÍLEK, M., DOLEJŠ, J.: The principles of welfare and new EU standards in cattle breeding. 1st ed., Praha, Czech Republic, VÚŽV 2004. (in Czech)
6. GAWORSKI, M., LEOLA, A.: Effect of technical and biological potential on dairy production development. J. Agronomy Research, 12, 2014: 215–222.
7. GAWORSKI, M., PRIEKULIS, J.: Analysis of milking system development on example of two baltic countries. J. Engineering for Rural Development, 13, 2014: 79–84.
8. KAVKA, M., ANDRT, M., BEDNÁR, I. ET AL.: Normatives for agricultural and food production. 6th ed., Praha, Czech Republic, ÚZPI 2003. (in Czech)
9. MÁLEK, P.: Building materials and construction. 1st ed., České Budějovice, Czech Republic, ZF JČU 2002 (in Czech).
10. RIST, M.: Natural ways of livestock farming. 1st ed., Olomouc, Czech Republic, RUBICO 1994 (in Czech).
11. SÝKORA, J.: Agricultural Buildings. 1st ed., Praha, Czech Republic, Grada Publishing 2014 (in Czech).
12. VEGRICHT, J., MACHÁLEK, A., FABIÁNOVÁ, M. ET AL.: Model solutions of cowsheds and farms for dairy farming. 1st ed., Praha, Czech Republic, VÚZT 2008 (in Czech).
13. 208/2004 SB. Edict “about minimum standards for the protection of farm animals” (in Czech).

Corresponding author:

Ing. et Ing. Jan Papež, Department of Technological Equipment of Buildings, Faculty of Engineering, Czech University of Life Sciences Prague, Kamýcká 129, Praha 6, Prague, 16521, Czech Republic, e-mail: papez@tf.czu.cz

METHODS USED TO MEASURING FUEL CONSUMPTION DURING OPERATION OF TRACTORS BY TELEMATICS SYSTEMS

J. Pavlů, Z. Aleš, V. Jurča

Department of Quality and Dependability of Machines, Faculty of Engineering, Czech University of Life Sciences Prague, Czech Republic

Abstract
Nowadays agricultural companies routinely use mainly two ways of measuring fuel consumption through telematics systems namely fuel consumption data from CAN–BUS and capacitance probe in the fuel tank. After turning on the ignition system, control unit starts up from sleep mode, it will start to measure and store data into memory and connects to the server. Experiment involved brand of tractor manufacturers John Deere. This brand was represented by 11 tractors.
The aim of this paper is to compare the methods of fuel consumption measuring through the CAN–BUS and utilization of capacitive fuel probe. The purpose of this paper is to prove or disprove the hypothesis that measured fuel consumption is statistically significant between measuring through CAN–BUS compared to capacitance probe during operation of tractors.

Key words: telematics system, fuel consumption, capacitance probe, CAN-BUS.

INTRODUCTION
Tractors are the basic machines for agricultural company and the task for company is to carry out all planned activities with the lowest operating costs, which affects the overall efficiency of operations (PEXA ET AL., 2014). Fuel consumption is a significant part of operating costs that companies constantly observe (KOTEK ET AL., 2015).There are various methods for measuring fuel consumption, which are based on detection of the fuel level in fuel tank. These methods for example include measurements using mechanical floats, ultrasonic sensors, digital rulers with mechanical float, pressure sensors, relay floats. Mentioned methods of measuring fuel level have a number of disadvantages. Mechanical floats are often unreliable due to the use of mechanical components. Ultrasonic sensors may have difficulty with obtaining a proper signal at wavy surface of fuel level and are also more expensive. Pressure sensors have problems with the accuracy of measurement when overpressure occurs in the fuel tank due to temperature changes. Measuring accuracy of relay floats is relatively low (PARTNER MB, 2010).

Nowadays agricultural companies routinely use mainly two ways of measuring fuel consumption through telematics systems with respect to the acquisition price, reliability, accuracy of measuring and control of unfair methods of treating fuels.
By default, the fuel consumption data are transmitted from CAN–BUS which does not always coincide with the value of the real fuel consumption. Another possible way of fuel consumption monitoring is realized via installation of capacitance probe mounted directly into the fuel tank (LI X. & FAN Y, 2007). The principle of measurement of these two methods is different, and each method has its own specifics. For instance, a capacitive probe enables detection of non-standard decreases of fuel level in the fuel tank.
The data from both of these methods are transferred telematics systems and via web interface are available in real time (DANIEL ET AL., 2011).
The purpose of this paper is to prove or disprove the hypothesis that measured fuel consumption is statistically significant between measuring through CAN–BUS compared to capacitance probe during operation of tractors.

MATERIALS AND METHODS
Principle of telematics system of machinery is widely known (CAI ET AL., 2011; GESKE, 2007), therefore there are only briefly described issues related to this paper. Telematics system is an technology which merges telecommunications and informatics. This blending of wireless telecommunication technologies along with computers is done ostensibly with the goal of conveying information over vast networks to handle tractor information. The entire system consists of TeCU (Telematics Control Unit) which is called

Gcom, server and webpage application to monitor and to sense ample information's received from tractor. Telematics Control Unit (TeCU) has to be designed and developed, which could be used in real time and off time monitoring, tracking and reporting system (DHIVYASRI ET AL., 2015).

After turning on the ignition system, control unit starts up from sleep mode, it will start to measure and store data into memory and connects to the server. After connecting the control unit sends quickly the recorded data, clears the memory and subsequent data sends at specified intervals. Data about fuel level in the tank were transmitted each 120 s from capacitance probe CAP04. From the CAN–BUS were transmitted data with the same period, but fuel rate was recorded by Gcom each 1 s.

Observed tractors for experiment were chosen from a agricultural company, which has a 25 tractors. From the total number of tractor were selected tractors with operating time of more than 1,000 hrs over a period of six months.

Records of re-fueling are continuously downloaded from the fuel dispenser and also were compared with records from tractor re–fueling measured by capacitance probe. The differences were up to ± 1.5% which is not statistically significant.

Principle of measuring fuel consumption via CAN-BUS

It seems as a convenient solution is obtaining information about fuel consumption via CAN–BUS. This information is contained in the messages of engine diagnostic interface or in the messages of on–board bus of tractor.

Currently, some of tractor manufacturers voluntarily comply the standardization in field CAN–BUS according to the standard SAE J1939. These standards contain information about the instantaneous fuel rate to the engine (SAE INTERNATIONAL, 2015).

Instantaneous fuel rate depends on the designers of engine control system. Usually instantaneous fuel rate is measured by length of the injection and it is conversion to fuel rate.

CAN is a serial communication protocol that allows distributed management of systems in real-time with transmission speed up to 1 Mbit/s and with a high degree of security of transmission against errors. CAN protocol ensures that a message of higher priority is preferentially delivered in case a collision of two messages. For the realization of the physical transmission medium is usually used a differential bus that is defined according to ISO 11898. CAN-BUS comprises two wires, which are called CAN_H and CAN_L, where dominant or recessive level on the bus is defined by the differential voltage of the two conductors.

CAN protocol specification defines four types of messages: Data Frame, Remote Frame, Error Frame, Overload Frame.

CAN protocol uses two types of data messages. The first type is defined by specifications 2.0A (Standard Frame), while 2.0B specification defines Extended Frame (J1939). The only significant difference between the two these formats is the length of the message identifier which is 11 bits for a Standard Frame and 29 bits for the Extended Frame.

The data link layer describes the general characteristics of the CAN–BUS as a structure of data frame identification, transport protocol for transmitting messages that contain more than 8 bytes and encoding parameter groups.

Standard SAE J1939–71 (Vehicle Application Layer) defines groups of parameters and contained therein signals, for example engine coolant temperature, engine oil temperature, fuel rate etc. Groups of current parameters are transmitted in the data message. Each group of parameters is defined by a unique PGN (Parameter Group Numbers) (Fig.1). This number consists of two parts in the message identifier. The first part is the PDU format and the second is a specific PDU.

For transmitted values are defined attributes: length of data, variables type (default or specific), range of incoming data, distribution of physical quantities, diagnostic data.

0x00FEF2					PGN Hex
65 266					PGN
100 ms					Rep. Rate
Data Byte 1	**Data Byte 2**	**Data Byte 3**	**Data Byte 4**	**Data Byte 5-8**	Byte No.
8 7 6 5 4 3 2 1	8 7 6 5 4 3 2 1	8 7 6 5 4 3 2 1	8 7 6 5 4 3 2 1		Bit No.
Fuel Rate	Fuel Rate	Instantaneous Fuel Economy	Instantaneous Fuel Economy	Not used for (BUS) FMS standard	Name Name
0.05 l/h per bit	0.05 l/h per bit	1/512 km/l per bit	1/512 km/l per bit		Values
0 offset	0 offset	0 offset	0 offset		Values
0 to 3,212.75 l/h	0 to 3,212.75 l/h	0 to 125.5 km/l	0 to 125.5 km/l		Values
SPN 183	SPN 183	SPN 184	SPN 184		SPN

Fig. 1. – Parameters CAN-BUS according SAE J1939 (SAE INTERNATIONAL, 2015)

Principle of measuring of fuel level in the tank by the capacitance probe CAP04

The principle of measuring of fuel level by the capacitance fuel level sensor is based on the fact that diesel is electrically non–conductive liquid. Capacitive probe CAP04 consists of two tubes of different diameter, which are the electrodes of capacitor. The dielectric is composed of electrically non-conductive material, specifically with a fuel and air. The relative permittivity of air is $\varepsilon_r = 1$, during refuelling the air is replaced with diesel which has relative permittivity $\varepsilon_r = 2$ and due to this fact the capacity of the capacitor increases. The capacitive sensor measures the position of the boundary between air and diesel fuel (Fig.2) (PARTNER MB, 2010).

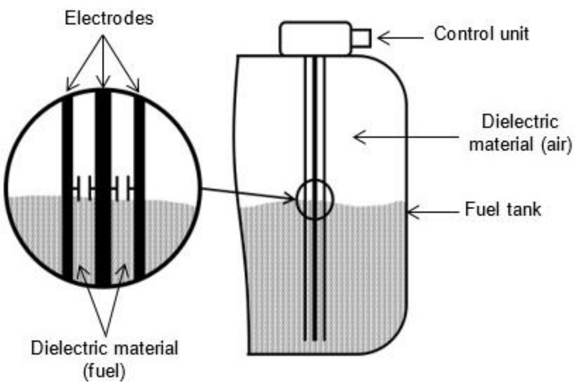

Fig. 2. – Principle of measuring of fuel level in the tank by the capacitance probe

The probe is also equipped with thermometers to sense temperature of fuel and the surface temperature of the fuel tank. The processor evaluates data according to the actual capacity of the probe to match the measured volume of diesel at a reference temperature 15°C. This method ensures that the reported amounts of fuel are not distorted by thermal expansion of diesel. Furthermore, the probe measures the tilt of the tank in two axes. While driving terrain when the level of diesel fluctuates rapidly and strongly, the probe indicates stable signal. This is achieved through suitable filters of the signal e.g. adaptive moving average depending on the tilt of fuel tank (PAVLU ET AL., 2013; ALES ET AL., 2015).

Experiment involved brand of tractor manufacturers (John Deere). This brand was represented by 11 tractors. Tractors were operated in agricultural companies focused on crop and livestock production (tillage, seedbed preparation, forage harvesting, forage wagons). The observation period of operation of tractors was determined for the second half of year 2015. Average operational time of one tractor was around 1,240 hours.

RESULTS AND DISCUSSION

Collected data from the telematics system must always be properly processed. Data on fuel consumption measured via CAN–BUS are in incremental format and do not include information about refuelling. Calculation of cumulative trend of consumption is simple (dotted line in Fig. 3). In terms of capacitance probe each user has continuous information about consumption and refuelling (referenced to the distance travelled). This data represents a saw–tooth pattern in Fig. 3. Such data must be converted into cumulative form. For this purpose, a complex code in Visual Basic for Applications was created. Program code can reliably distinguish between consumption and refuelling or other factors as may be fuel tank tilting or fuel theft. The linear trend of cumulative consumption with linear equation (Fig. 3). Slope of linear equation represents consumption of a tractor for 1 operational hours.

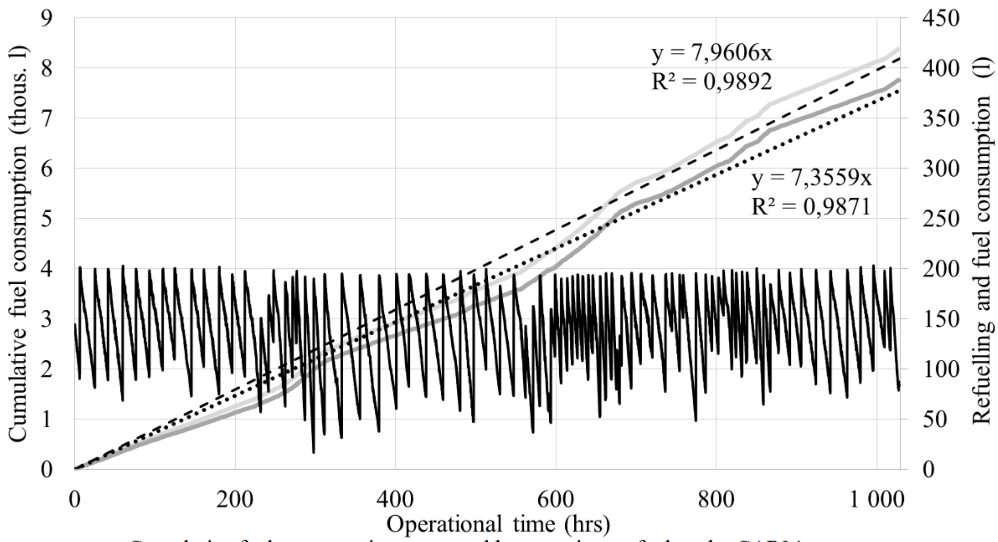

Fig. 3. – Measured and calculated data of fuel consumption –John Deere 6630

Results calculated from obtained data are for John Deere of tractors (Tab. 1). Results show the average values of specific values of fuel consumption, both from the CAN-BUS and capacitance probe. The last column shows the difference between the fuel consumption compared methods in the tables.

Tab. 1. – Results of calculated data from telematics systems – John Deere

Number of tractors	Type of tractors	Operational hours (hrs)	Average values of fuel consumption CAN-BUS (l/hrs)	Average values of fuel consumption capacitance probe (l/hrs)	Difference of fuel consumption (l/hrs)
1	**John Deere 6630**	**1,028**	**7.3559**	**7.9606**	**0.6047**
2	John Deere 6630	1,158	11.594	12.377	0.783
3	John Deere 6630	1,257	8.807	9.986	1.179
4	John Deere 6630	1,023	7.247	7.776	0.529
5	John Deere 6630	1,268	10.58	11.392	0.812
6	John Deere 6530	1,087	11.698	12.61	0.912
7	John Deere 6530	1,587	8.837	9.903	1.066
8	John Deere 6530	1,698	8.356	8.929	0.573
9	John Deere 6430	1,147	12.546	13.259	0.713
10	John Deere 6430	1,158	10.458	11.431	0.973
11	John Deere 6430	1,236	7.549	8.623	1.074

* - measured and calculated data of fuel consumption (Fig. 2)

From the calculated data can be determined null hypothesis H_0: there is no statistically significant difference between consumption measured via CAN-BUS and capacitance probe. Wilcoxon Signed-Rank non-parametric test (Equation 1–2) was used to verify this hypothesis (MOSNA, 2015). Significance level was set at α=0.05 and two-tailed hypothesis was chosen.

$$Z = \frac{\min\left(W^{+};W^{-}\right)-\frac{1}{4}n\cdot(n+1)}{\sqrt{\frac{1}{24}n\cdot(n+1)\cdot(2n+1)}} \tag{1}$$

$$Z = \frac{\min(66;0)-\frac{1}{4}11\cdot(11+1)}{\sqrt{\frac{1}{24}11\cdot(11+1)\cdot(2\cdot 11+1)}} = -2.934058 \tag{2}$$

where: W – sum of the signed ranks ($^{+}$positive, $^{-}$ negative); n – sample size

The Z-value is -2.934058. The p-value is 0. The result is significant at p≤ 0.05. That can be concluded that nullhypothesis$H_0$is rejected. Therefore, there is statistically significant difference between consumption measured via CAN-BUS and capacitance probe.

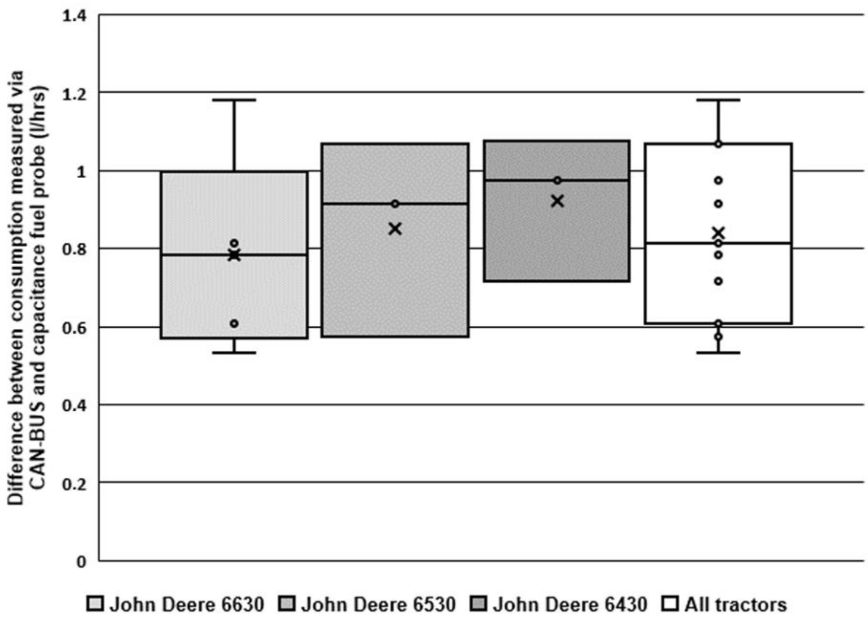

Fig. 4. – Box plot representing measured difference between consumption measured by capacitance probe and CAN–BUS

All results of difference between fuel consumption measured via CAN-BUS and capacitance probe are shown in box plot in Fig. 4. The average difference between compared methods for all tractors under consideration was 0.86 l/hrs of fuel consumption.

Besides, similar results were reported in a pilot study that there was a difference (up to a 6.22% error) between data collected using the machine controller area network (CAN) bus Society of Automotive Engineers (SAE) J1939 standard fuel rate and data collected from a physical measurement system utilized by the Nebraska Tractor Test Laboratory (NTTL) (MARX ET AL., 2015).

CONCLUSIONS

Fuel consumption of tractors is an important part of the economy of operation of entire company. Tractors are equipped with various systems for measuring fuel consumption. The aim of the paper was to prove or disprove the hypothesis, if there is statistically significant difference between described methods of measuring fuel consumption.

Designed experiment involved 11 tractors. Tractors were operated in agricultural companies focused on crop and livestock production (tillage, seedbed preparation, forage harvesting, forage wagons). The observation period of operation of tractors was determined for 6 months. Average operational hours of one tractors was around 1,240 hrs. Fuel consumption was monitored for each tractors using two methods via CAN-BUS and capacitance probe. Collected data was transmitted through telematics systems and then processed based on an algorithm created in Visual Basic for Applications. Results were statistically processed in order to accept or reject the hypothesis. Null hypothesis H0 was rejected, it means, there is statistically significant difference between consumption measured via CAN-BUS and capacitance probe. Created box plot shows that average difference between compared methods for all tractors under consideration was 0.86 l/hrs of fuel consumption. The results confirm the general opinion that the fuel consumption measured via CAN-BUS shows lower values compared to real fuel consumption. In practice, this means that data from the capacitance probe correspond to the real fuel consumption and addition through capacitance probe may control of unfair methods of treating fuels.

ACKNOWLEDGEMENTS

Paper was created with the grant support – CZU CIGA 2015 - 20153001 - Use of butanol in internal combustion engines.

REFERENCES

1. ALES, Z., PAVLU, J., JURCA, V.: Maintenance interval optimization based on fuel consumption data via GPS monitoring. Agronomy Research 13, 2015: pp. 17–24.
2. CAI, S., BECHERIF, M., HENNI, A., WACK, M., ABOUBOU, A.: Processing of information gathered from hybrid or electrical vehicle for reduction of fuel consumption and gas emission. Mediterranean Journal of Measurement and Control, 7(2), 2011: pp. 236-242.
3. DANIEL O.G., DAYO O., ANNE O.O.: Monitoring and controlling fuel level of remote tanks using aplicom 12 GSM module. ARPN Journal of Engineering and Applied Sciences 6, 2011: pp. 56-60.
4. DHIVYASRI, G., MARIAPPAN, R., SATHYA, R.: Telematic unit for advanced fuel level monitoring system. In: Proceedings of 2015 IEEE 9th International Conference on Intelligent Systems and Control, ISCO 2015, DOI: 10.1109/ISCO.2015.7282260
5. GESKE, D. M.: Mapping a cleaner route. Diesel Progress North American Edition, 73(6), 2011: pp. 108-109.
6. KOTEK, T., KOTEK, M., JINDRA, P., PEXA, M.: Determination of the optimal injection time for adaptation SI engine on E85 fuel using self-designed auxiliary control unit. Agronomy Research, 13, 2015: pp. 577-584.
7. LI, X., FAN, Y.: Study on high precision capacitance sensor of the fuel level. Yi Qi Yi Biao XueBao/Chinese Journal of Scientific Instrument 28, 2007: pp. 32-35
8. MARX, S. E., LUCK, J. D., HOY, R. M., PITLA, S. K., BLANKENSHIP, E. E., DARR, M.J.: Validation of machine CAN bus J1939 fuel rate accuracy using Nebraska Tractor Test Laboratory fuel rate data. Computers and Electronics in Agriculture, 118, 2015: pp. 179-185.
9. MOSNA, F.: Riemann integral-possibilities of definition. In: Proceedings of APLIMAT 2015 - 14th Conference on Applied Mathematics, 2015: pp. 602-607.
10. PARTNER MB, S.R.O.: Device for measuring the level of liquid in the reservoir, e.g. in Czech 2009-21834, Prague, 2010. Available at: http://spisy.upv.cz/UtilityModels/FullDocuments/FDUM0020/uv020522.pdf. Accessed 2. 1. 2016.
11. PAVLU, J., ALES, Z., JURCA, V.: Utilization of satellite monitoring for determination of optimal maintenance interval. Scientia AgriculturaeBohemica, 2013(3): pp. 159-166.
12. PEXA, M., MARÍK, J.: The impact of biofuels and technical engine condition to its smoke - Zetor 8641 Forterra. Agronomy Research12, 2014: pp. 367–372.
13. SAE INTERNATIONAL: SAE J1939 –71Vehicle Application Layer. Truck Bus Control And Communications Network Committee, Revised 2015: 30 p.

Corresponding author:

Ing. Jindřich Pavlů, Department of Quality and Dependability of Machines, Faculty of Engineering, Czech University of Life Sciences Prague, Kamýcká 129, Praha 6, Prague, 16521, Czech Republic, e-mail: jindrichpavlu@seznam.cz

MECHANICAL PROPERTIES OF JUTE FIBRES REINFORCED PLASTICS

M. Petrů, O. Novák, M. Syrovátková

Institut of Nanomaterials, Advanced Technologies and Innovation, Technical University of Liberec, Czech Republic

Abstract

The article describing the preparation of composites with reinforcement of jute fabrics of different basis weights in combination with an epoxy and a polyester matrix. Samples were tested for mechanical properties as tensile strength in warp and weft direction. The experiment showed that a better combination of mechanical properties achieved jute/polyester. Strength of the composite is greater in the weft (about 30%) than in the warp direction whatever the combination fiber / matrix. Research of composite materials is a broad area that provides in aerospace, automotive and other technical areas materials with excellent properties such as low weight and improved mechanical properties.

Key words: natural fibres, jute fabric, composite, tensile stress.

INTRODUCTION

Basic mechanical properties of technical materials are low weight, stiffness, strength and etc. A basic requirement in terms of internal structure is homogeneity. Most of the industrial materials are considered as homogeneous and isotropic from macroscopic view. The composite material consists of two or more components which vary in shape and composition. Each component is physically identifiable and among them an interface is located. Ingredient connection produces a synergistic effect. The composite is a multi-phase material that is composed of continuous phases and dispersion. A matrix is continuous phase of the composite that can be metal, ceramic or polymers. The dispersion is composite reinforcement that is in the form of fibres or particles. Fibre dispersion is continuous or discontinuous. Carbon, glass and aramid fibres have excellent mechanical, chemical and thermal properties and represent most commonly used fibre reinforcements. The resulting composites, which are a combination of fibres with plastic matrices, have excellent mechanical properties and they are used in the aerospace, energetic, automotive, engineering industry and many others, not only in technically oriented industries (GAY, SUONG 2007; LIU ET AL. 2004). Biopolymers are alternative of composites that are not based on fossil fuels (oil, coal and gas). They can be divided into three groups according to their origin.

Natural fibres are a large group of traditional fibres, which are further subdivided on animal and plant fibres. Plant fibres consist of fibres from seeds, stems and leaves. Fibres from stems - bast fibres consist of filaments, having a similar composition, properties and similar microscopic appearance. To this group flax, hemp, jute, kenaf, bamboo and nettle fibres belong. The fibres are obtained by the help of mechanical and physical processes from the woody stems (MILITKÝ 2005). Generally a composite production is very inefficient from an economic point of view. A production of hybrid bio composites (NFPC - Natural Fibre Polymer Composite) can replace expensive reinforcements, especially carbon fibres and represent an acceptable compromise. It may be applied when very high strength is not required. Additional benefit can be seen in the reducing of the oil and energy consumption and lower environmental footprint. Natural fibres have lower or comparable density especially in comparison with glass fibres. They are non-toxic, environmentally degradable and they do not cause a damage of machine parts during the production. Also their production requires less energy compared to glass and carbon fibre production (HOLBERY, HOUSTON 2006, LAYTH ET AL. 2015). The disadvantage of natural fibres consists in poor water resistance that causes water absorption or swelling, the possibility of damage by pests and fungi and also impairment of the mechanical properties in comparison with carbon and glass fibres. Tab. 1 shows comparison of different fibre reinforcement properties, Fig. 1 show jute fibres (FIDELIS 2013) and carbon and E-glass fibres (PETRŮ ET AL. 2015). Tensile properties of resulting composite are mostly influenced by a volume fraction of fibres (FOWLER ET AL 2006). For this is important to select an appropriate matrix. The polymeric matrixes are typically divided on thermoplastics and thermosets. Thermoplastics melt when heated and harden after cooling. Most commonly used

thermoplastics are following: polyethylene, polypropylene and polyvinyl chloride. Thermosets are highly cross linked due to covalent bonds among chains. To thermoset group belongs for example polyester and epoxy resins. The used matrix has an influence on the resulting properties of the composite (LAYTH ET AL. 2015; LIU ET AL 2004). A composition of natural fibres and polymeric matrix is not chemically compatible. It leads to insufficient properties of the interface and its low capability of a stress distribution. Incompatibility of natural fibres with polymer matrix can be influenced by a fibre modification. Very suitable is the addiction of the reactive functional groups that are responsible for the reduction of moisture absorption and also improve final affinity of fibres to the matrix. Especially chemical treatment of natural fibres leads to an increase in strength and improvement of a dimensional stability of bio composites with polymeric matrix (LAYTH ET AL. 2015).
The aim of this study is to describe the preparation of composites with reinforcement of jute fabrics of different basis weights in combination with an epoxy and a polyester matrix.

Tab. 1. – Compared mechanical properties of selected fibres (LAYTH ET AL. 2015)

Fibre	Density [g/cm^3]	Elongation [%]	Tensile Strength [MPa]	Young's Modules [GPa]
Flax	1.5	2.7-3.2	345-1035	27.6
Jute	1.3	1.5-1.8	393-773	26.5
Carbon (HT)	1.4	1.4-1.8	4000	230-240
Glass-E	2.5	2.5	2000-3500	70

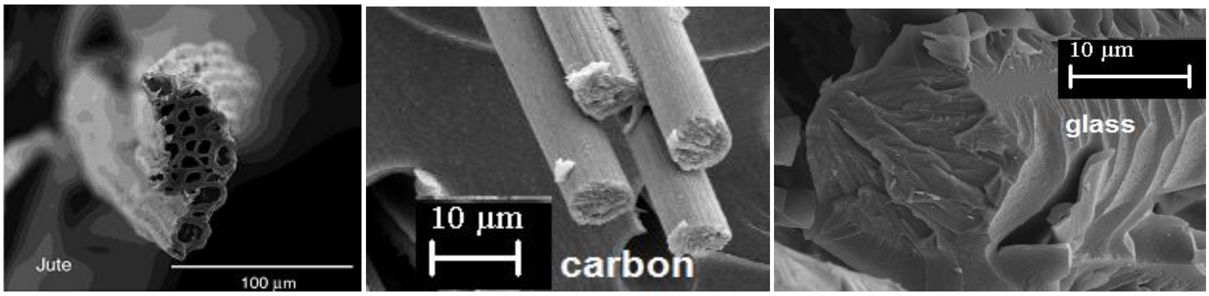

Fig. 1. – Natural fibres; jute, technical fibres: carbon and glass fibre

MATERIALS AND METHODS

Bio composites with jute reinforcement were obtained for basic knowledge about the NFPC properties. Jute fabrics having different weight were chosen because of commercial availability, and lower cost in comparison with flax fibres. For the production two matrices were applied - epoxy and polyester thermosetting resins. The composite single-layer samples were made by hand lay-up. Basic parameters of the samples are given in Tab. 2.

Tab. 2. – NFPC parameters

<table>
<tr><th>Samples</th><th>Reinforcement type and orientation</th><th>m_j^c [g/m^2]</th><th>Resin</th><th>M^f [%]</th></tr>
<tr><td>E1WA</td><td>jute/warp direction (J1WA)</td><td rowspan="2">170</td><td rowspan="4">EPOXY</td><td rowspan="2">15.53</td></tr>
<tr><td>E1WE</td><td>jute/weft direction (J1WE)</td></tr>
<tr><td>E2WA</td><td>jute/warp direction (J2WA)</td><td rowspan="2">400</td><td rowspan="2">31.85</td></tr>
<tr><td>E2WE</td><td>jute/weft direction (J2WE)</td></tr>
<tr><td>P1WA</td><td>jute/warp direction (J1WA)</td><td rowspan="2">170</td><td rowspan="4">POLYESTER</td><td rowspan="2">15.21</td></tr>
<tr><td>P1WE</td><td>jute/weft direction (J1WE)</td></tr>
<tr><td>P2WA</td><td>jute/warp direction (J2WA)</td><td rowspan="2">400</td><td rowspan="2">29.89</td></tr>
<tr><td>P2WE</td><td>jute/weft direction (J2WE)</td></tr>
</table>

Samples of jute fabric and a complete composite plate you can see in the Fig. 2. Samples for tensile stress test were prepared from fabrics and composites; test was conducted in the warp and weft direction according to EN ISO 13934-1 (textiles) and EN ISO 527-4 (composites). The tests were performed at room temperature on the unit Labortech 2.050. Jute fabric samples for testing are seen in Fig. 3 and dynamometer for tensile testing is in Fig. 4. Samples after test show in the Fig. 5.

Fig. 2. – On left side - jute fabric; on right side sample P1 (jute fabric 170 g.m^{-2}, polyester resin) and sample E2 (jute fabric 400 g.m^{-2}, epoxy resin)

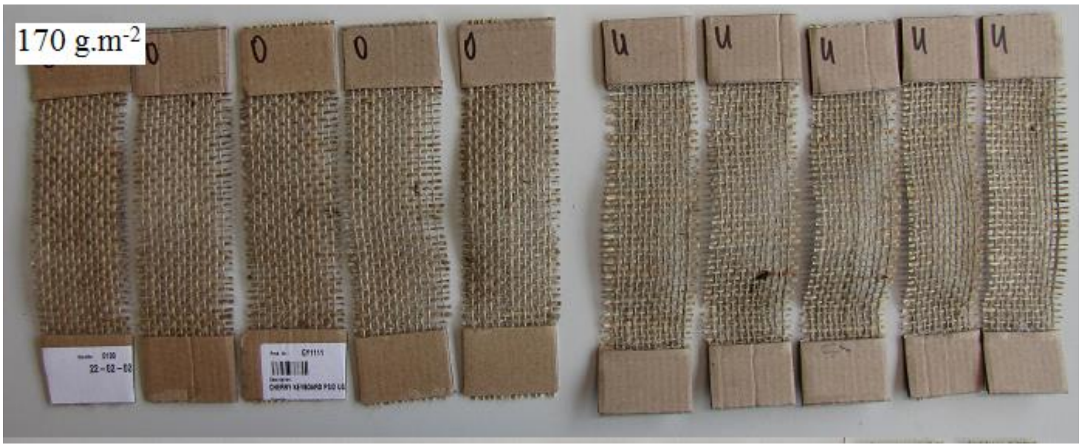

Fig. 3. – Jute fabric samples for tensile strength test (warp and weft direction)

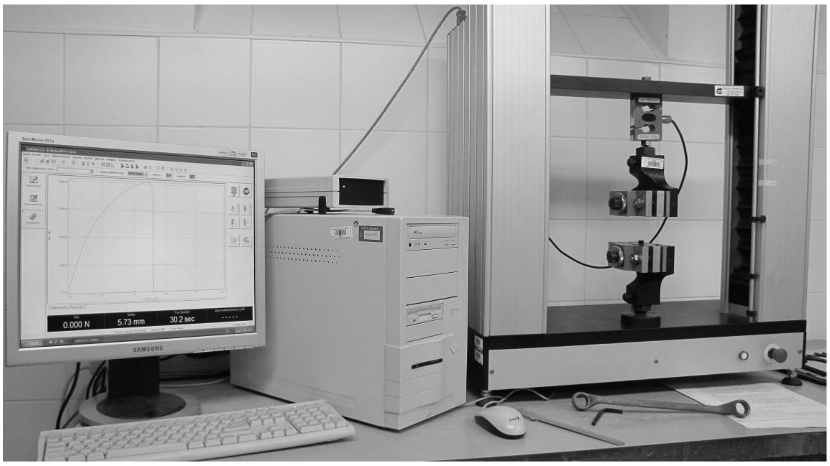

Fig. 4. – Dynamometer Labortech for tensile testing

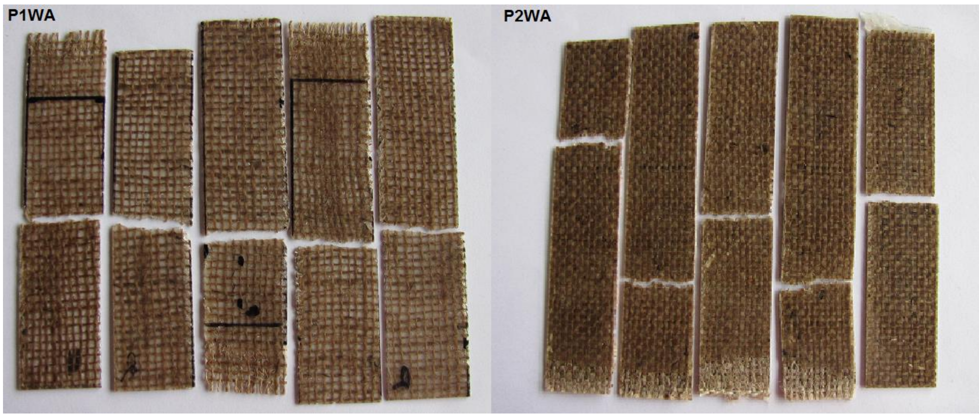

Fig. 5. – The samples after tensile strength test (P1WA - jute fabric 176 g.m^{-2}/ polyester resin, warp direction; P2WA - jute fabric 400 g.m^{-2}/ polyester resin, warp direction)

RESULTS AND DISCUSSION

From results it is seen that composite properties are significantly different depending on applied matrix even though they have similar mechanical properties. These differences could be obtained with different viscosity of the matrix during the application. Epoxy resin is more viscous and its ability to penetrate into the yarn structure is significantly lower. The viscosity of the resin can be decreased by a warming, but it also accelerates a cross linking process of the matrix. It leads to a shortening of application time that is relatively long in the case of hand lay-up process. Results of initial modulus calculated for the jute fabric 400 gm^{-2} reinforced with epoxy and polyester matrix in weft direction are shown in Tab. 3. The results show increased initial modulus of composites compared with raw jute fabric. Module has grown to ten times. Comparison the strength of jute fabric and jute composite with polyester matrix shows the graph in Fig. 6. Comparison the strength of warp and weft direction for all samples you can see in Fig. 7. Strength in weft direction is about 30% higher than strength in warp direction. Difference of strength between P2 samples (in warp and weft direction) is up to 50%. Strength of jute/polyester composite was measured about 100% higher than strength of jute/epoxy composite. The results obtained during the experiment were compared with the results of other authors. Tab. 4 presents own measured results, and this results were comparison of the results from Ajith et al 2014. Parameters of composites were similar for type of fibers, matrix and fibers nominal content. The resulting values are in agreement. Differences are for examples in a different type of reinforcement (fiber – woven fabric) and on the use of chemical addition.

Comparison the modules of single layer composite and ten layers composites from jute fabric (SABEEL AHMED, VIJAYARANGAN, 2008) show the possibility of significant growth of module. Similar composite input parameters are required. The comparative results are shown in Tab. 5. Table shows the resulting modulus measured in the warp direction and weft direction.

Tab. 3. – NFPC parameters

	Jute fabric (J2WE)	**Epoxy resin (E2WE)**	**Polyester resin (P2WE)**
Initial modulus [MPa]	18.77	1336.93	1848.86

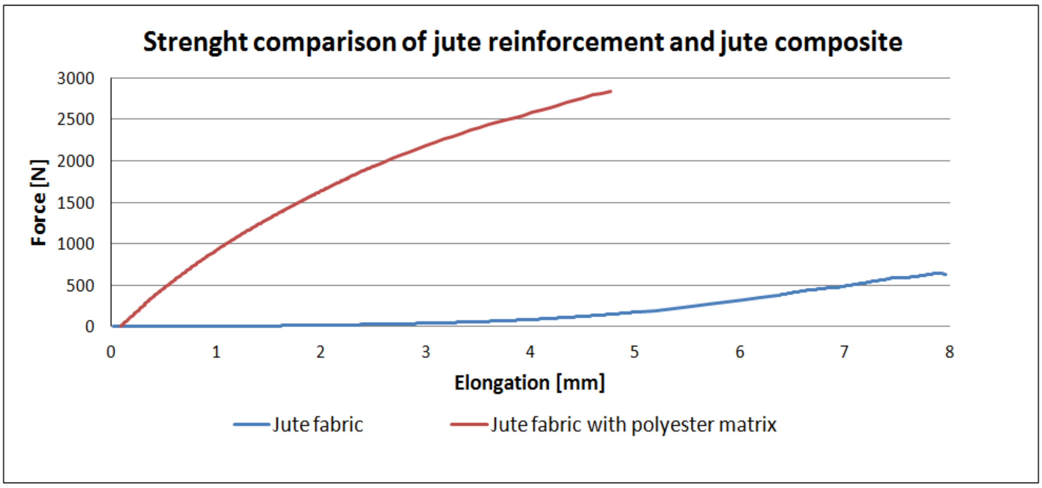

Fig. 6. – Graphs of tensile strength a) J2WE sample (jute fabric, m_j^c 400 g.m^{-2}, weft direction), b) P2WE sample (jute/polyester composite, m_j^c 400 g.m^{-2}, weft direction)

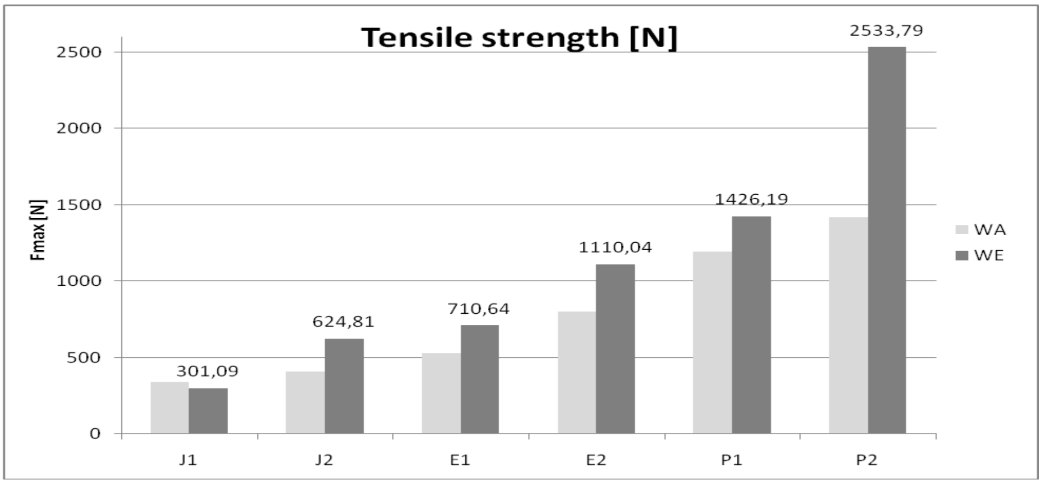

Fig. 7. – Graph of result; average tensile strength from jute fabrics and jute reinforced composites

Tab. 4. – Results comparison

composite parameters		results of measurement	*references result*
jute/epoxy	nominal fibres content	15.53 [%]	*18 [%]*
	force	512 [N]	*748 [N]*
	tensile modulus	1.14 [GPa]	*1.06 [GPa]*
jute/polyester	nominal fibres content	15.21 [%]	*18 [%]*
	force	1283 [N]	*554 [N]*
	tensile modulus	0.93 [GPa]	*0.81 [GPa]*

Tab. 5. – Results comparison

composite parameters		results of measurement	*references result*
jute/polyester	nominal fibres content	30 [%]	*43 [%]*
	tensile modulus	1.3 (wa); 1.8 (we) [GPa]	*9.5 [GPa]*

CONCLUSIONS

From the results it is evident that bio composite production is easy and has good mechanical properties. The low price of the reinforcing material compared to glass or carbon fibres to be noted. Also the environmental footprint is very low compared with technical man-made fibres not only from point of view of easy recycling.

ACKNOWLEDGEMENTS

The results of this project No. LO1201 were obtained through the financial support of the Ministry of Education, Youth and Sports in the framework of the targeted support of the "National Programme for Sustainability I".

REFERENCES

1. AJITH, G., SENTHIL, K. M., ELAYAPERUMAL, A.: Experimental Investigations on Mechanical Properties Of Jute Fiber Reinforced Composites with Polyester and Epoxy Resin Matrix. Procedia Engineering 97, 2014, pp.2052-63. Available: www.sciencedirect.com
2. FIDELIS, M.: The effect of fibre morphology on the tensile strength of natural fibres. Journal of Materials Research and Technology, Volume 2, Issue 2, Pages 149–157, 2013. Available: http://www.sciencedirect.com
3. FOWLER, P., HUGHES, M., ELIAS R.: Biocomposites: technology, environmental credentials and market forces. Journal of the Science of Food and Agriculture 86, 2006, pp. 1781 – 89.
4. GAY, D., SUONG V. HOA: Composite materials (second edition). CRC Press Taylor & Francis Group, 2007, ISBN 978-1-4200-4519-2
5. HOLBERY, J., HOUSTON, D.: Natural-Fibre-Reinforced Polymer Composites in Automotive Applications. JOM, Volume 58, Issue 11, 2006, pp. 80-86.
6. LAYTH, M., ANSARI, M., PUA, G., JAWAID, M., ISLAM, M.: A Review on Natural Fibre Reinforced Polymer Composite and Its Applications. Hindawi Publishing Corporation, International Journal of Polymer Science, Volume 2015, Article ID 243947, 15 pages. Available: http://dx.doi.org/10.1155/2015/243947
7. LIU, D., FLECK, N. A., SUTCLIFFE, M. P. F.: C. Journal of the Mechanics and Physics of Solids, 52 (7), 2004, pp. 1481-1505.
8. MILITKÝ, J.: Textile fibres, classic and special. Technical University of Liberec, 2012, ISBN 978-80-7372-844-1; original language – Czech
9. PETRŮ, M., SYROVÁTKOVÁ, M., MARTINEC, T., LEPŠÍK P.: Analysis of changes in the surface quality of a UD prepregs composite due to mechanical loading, Mat.Sci.Forum, 818, 2015, pp.109-112.
10. SABEEL AHMED, K., VIJAYARANGAN, S.: Tensile, flexural and interlaminar shear properties of woven jute and jute-glass fabric reinforced polyester composites. Journal of Materials Processing Technology, Volume 207, Issues 1–3, 16 October 2008, pp. 330–335.
11. SHAIKH, CHANNIWALA, S. A.: To Study the Characteristics of Jute Polyester Composite for Randomly Distributed Fiber Reinforcement. Proceedings of the World Congress on Engineering 2010, Vol II WCE 2010, London, (2010).

Corresponding author:

Martina Syrovátková, Institut of Nanomaterials, Advanced Technologies and Innovation, Technical University of Liberec, Studentská 2, 461 17 Liberec 1, Czech Republic

ANALYSIS OF THE NRSC TEST DURING THE USE OF BIOFUELS FOR THE ZETOR FORTERRA TRACTOR

M. Pexa[1], J. Čedík[1], R. Pražan[2]

[1]*Department for Quality and Dependability of Machines, Faculty of Engineering, Czech University of Life Sciences, Czech Republic*
[2]*Research Institute of Agricultural Engineering, p.r.i, Czech Republic*

Abstract
Production of solid particles increases significantly the degree of danger of combustion engines. Currently there are many design solutions which aim to reduce smoke of combustion engines. One of the most significant solutions suggests the increase of injection pressures up to the limit of 250 MPa and filtering the exhaust gases. The paper compares different fuels and biofuels and their effect on emissions of supercharged engine. The comparison uses the 8-point NRSC test during which the following fuels were used: diesel, rapeseed methyl ester, and hydrogenated oil.

Key words: engine, biofuels, emissions, smoke.

INTRODUCTION

Environmental protection makes the polluters reduce production of harmful substances. This restriction significantly affects automotive industry as well, i.e. cars, trucks and agricultural machinery. Agricultural machines are driven mainly by diesel combustion engines. The most harmful products of diesel combustion engines are particles, smoke and nitrogen oxides.

The literature describes several basic possibilities how to reduce smoke of diesel combustion engines in order to meet increasingly strict limits set by the international regulations:

- Increasing the injection pressure – injection pressure is continuously increased from several MPa to several hundred MPa. Injection of the fuel under higher pressure causes finer atomization of fuel which is better burnt in the combustion chamber of the engine. (Woo et al., 2016; Liu et al., 2015; Hwang et al., 2014)
- Filter of solid particles – combustion products such as solid particles are collected by filters at the outlet of the combustion chamber. When the filter is full, the particles collected by filters are additionally burnt at a higher temperature. (Armas et al., 2013; Sun et al., 2013)
- Selective catalytic reduction (SCR) – gradual reduction of nitrogen oxide limits brought the system of injecting urea into the exhaust pipe. This system helps to reduce the amount of nitrogen oxide and smoke. The smoke is reduced by up to 30%. However, inappropriate doses of ammonia may cause increased number of particles in exhaust gases. (Cao et al., 2016; Kang & Choi, 2016; Athappan et al., 2015; Amanatidis et al., 2014)
- Use of more appropriate fuel – many kinds of biofuels are tested within the research and practice, especially biofuels from renewable resources. Fuels which are preferred have a positive impact on emissions and smoke and the influence on performance parameters are not too negative. (Hönig et al., 2015a,b; Müller, Šleger et al., 2015; Martínez et al., 2014; Moghaddam & Moghaddam, 2014; Vallinayagam et al., 2014; Müller, Chotěborský et al., 2015; Müller et al., 2013; Kučera & Rousek, 2008)

The aim of this paper is to verify the possibility of reducing the smoke by using different kinds of biofuels. The verification is done by means of the 8-point NRSC test applied on a turbocharged engine Zetor Forterra 8641.

MATERIALS AND METHODS

The measurement was done using the tractor engine Zetor 1204 prefilled by means of turbocharger and placed in the tractor Zetor Forterra 8641. It is in-line 4 cylinder engine, its volume is 4.156 and rated power 60 kW (it is 53.4 kW on PTO according to the measurement made by Deutsche Landwirtschafts-Gesellschaft), the maximum torque is 351 Nm, the nominal specific fuel consumption is 253 $g.kWh^{-1}$ and the rated speed is 2200 min^{-1}. The fuel is delivered to the engine by means of mechanical in-line injection pump. It is one injection with pressure 22 MPa, 12° before top dead center. The operation time of the mentioned engine does not exceed 100 operation hours.

The engine was loaded by the dynamometer AW NEB 400 connected to PTO, torque was recorded by the torque sensor MANNER Mfi 2500 Nm_2000U/min with accuracy 0.25%. The torque values recorded by the sensor placed on PTO are converted to the engine torque by means of appropriate gear ratio (3.543). The losses in the gearbox have no effect on the comparative measuring of the influence of fuel on the external speed characteristics of the engine and therefore they are not taken into consideration. The fuel consumption was recorded by means of the flowmeter AIC VERITAS 4004 with measurement error 1%. Data were saved on the hard disk of the measuring computer (netbook), with the use of A/D converter LabJack U6 with frequency 2 Hz, in the form of text file. The programmes MS Excel and Mathcad were used for data evaluation.

The fuels used for testing are diesel which meets the regulation EN 14 214 (RME) and hydrotreated vegetable oil (HVO). The table presents parameters for these basic fuels such as: density, viscosity, cetane number and calorific value.

Tab. 1. – Basic parameters of the fuels (ATMANLI ET AL., 2015; QI ET AL., 2014; MURALI KRISHNA ET AL., 2014; AATOLA ET AL., 2008; TZIOURTZIOUMIS, 2012; KIBUGE ET AL., 2015)

Fuel	Density at 15°C (kg m^{-3})	Calorific value (MJ kg^{-1})	Viscosity at 40°C (mm^2 s^{-1})	Cetane number
HVO	780	44	2.5–3.5	80–99
RME	880	37.5	4.5	51
diesel – EN 590	825	43.3	2.5	50

The external speed characteristics of the engine were measured for all tested fuels. Then the measuring points of the eight-point NRSC (Non-Road Steady Cycle) test were determined according to ISO 8178-4 (type C1) (Fig. 1). The points of the test are defined by rotation speed (idle, at max. torque and rated) and load in percentage (0, 10, 50, 75 and 100%). The test was used for measuring the specific fuel consumption. Specific fuel consumption for the whole NRSC test was calculated according to the equation (1). In every predetermined measurement point the measured parameters were stabilized.

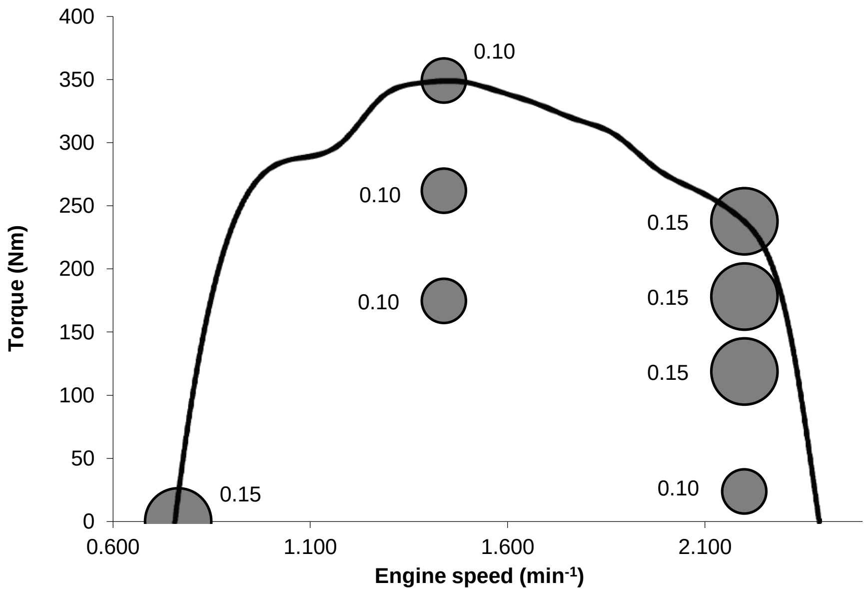

Fig. 1. – Measurements points for the NRSC test for HVO with weight factors

$$m_{NRSC} = \frac{\sum_{i=1}^{8}\left(M_{Pi} \cdot WF_i\right)}{\sum_{i=1}^{8}\left(P_{PTO,i} \cdot WF_i\right)} \qquad (1)$$

where: m_{NRSC} – Specific fuel consumption for the whole NRSC test (g kWh^{-1}); $M_{P,i}$ – hourly fuel consumption (g h^{-1}); WF_i – weight factor (–); $P_{PTO,i}$ – power on the PTO (kW)

RESULTS AND DISCUSSION

The results are resumed in the Tab. 2 (diesel – EN 590), No. 3 (RME) and No. 4 (HVO). The values marked by light grey colour show the best value from tested fuels. The values marked by dark grey colour show the worst value from tested fuels.

Tab. 2. – NRSC cycle – Zetor Forterra 8641 – diesel (EN 590)

Speed	Torque	Power - PTO	Fuel consumption	CO	CO_2	HC	NO_x	Smoke
(rpm)	(Nm)	(kW)	(kg h^{-1})	(g h^{-1})	(g h^{-1})	(g h^{-1})	(g h^{-1})	(g h^{-1})
2,199	770.1	50.05	15.12	105.30	57.077	2.12	578.49	16.44
2,199	590.6	38.39	11.95	52.13	49.967	1.54	478.80	5.00
2,202	402.9	26.22	10.17	66.75	41.954	1.44	314.36	5.70
2,195	69.4	4.50	5.84	80.23	25.213	1.26	103.95	5.69
1,440	1,038.5	44.21	11.75	347.26	49.925	1.18	591.84	36.19
1,440	822.6	35.02	9.23	129.11	40.572	0.89	525.12	14.23
1,439	536.0	22.81	6.53	23.58	28.527	0.70	375.49	4.47
725	0.0	0.00	0.99	36.88	4.636	0.61	69.96	0.21
Weighted value		**27.85**	**9.07**	**97.18**	**37.469**	**1.26**	**375.88**	**10,16**
NRSC (g.kWh^{-1})			**325.61**	**3.49**	**1.345**	**0.045**	**13.50**	**0.365**

Tab. 3. – NRSC cycle – Zetor Forterra 8641 – RME

Speed	Torque	Power - PTO	Fuel consumption	CO	CO_2	HC	NO_x	Smoke
(rpm)	(Nm)	(kW)	(kg h^{-1})	(g h^{-1})	(g h^{-1})	(g h^{-1})	(g h^{-1})	(g h^{-1})
2,202	758.2	49.36	16.51	53.98	58.519	1.65	719.70	2.38
2,201	596.9	38.84	13.85	49.85	48.564	1.43	560.05	1.92
2,196	383.1	24.87	11.01	45.21	39.067	1.34	317.33	1.27
2,197	85.6	5.56	6.95	78.16	24.562	1.16	119.22	0.85
1,496	1,020.7	45.14	12.90	113.64	47.763	0.70	690.05	2.04
1,496	803.9	35.55	10.58	52.35	38.658	0.67	602.68	1.16
1,495	520.3	22.99	7.65	24.02	27.247	0.67	419.90	0.63
730	0.0	0.00	1.40	23.16	4.731	0.24	10.41	0.25
Weighted value		**27.89**	**10.22**	**52.65**	**36.455**	**1.02**	**424.31**	**1,34**
NRSC (g.kWh^{-1})			**366.61**	**1.89**	**1.307**	**0.037**	**15.22**	**0.048**

Number of evaluated points is 48 (8 point NRSC cycle and 6 evaluated components). From the 48 points the diesel fuel – EN 590 achieved the best values in 10.4 % of points and the worst results in 58.3 % of points.

From 48 points the RME fuel achieved the best values in 39.6 % of points and the worst results in 39.6 % of points.

From the 48 points the HVO fuel achieved the best values in 50.0 % of points and the worst results in 2.1 % of points.

Tab. 4. – NRSC cycle – Zetor Forterra 8641 –HVO

Speed	Torque	Power - PTO	Fuel consumption	CO	CO_2	HC	NO_x	Smoke
(rpm)	(Nm)	(kW)	(kg h^{-1})	(g h^{-1})	(g h^{-1})	(g h^{-1})	(g h^{-1})	(g h^{-1})
2,196	721.0	46.80	14.75	104.29	57.078	2.02	468.37	4.67
2,200	543.0	35.32	12.16	50.52	46.041	1.24	343.03	2.04
2,198	358.0	23.26	10.01	46.66	37.392	1.48	205.86	1.31
2,196	79.6	5.17	6.51	39.64	24.289	0.21	86.46	1.11
1,506	1,021.6	45.49	11.61	117.40	45.192	0.75	496.26	5.11
1,506	778.3	34.64	9.24	52.84	36.114	0.81	412.05	2.02
1,506	521.9	23.23	6.93	23.40	25.741	0.24	282.50	0.86
715	0.0	0.00	0.99	31.50	3.630	0.52	35.99	0.18
Weighted value		**26.66**	**9.11**	**58.27**	**34.755**	**0.99**	**285.71**	**2.14**
NRSC (g.kWh^{-1})			**341.85**	**2.19**	**1.304**	**0.037**	**10.72**	**0.080**

Generally, in relation to the NRSC test, the HVO fuel achieved the best results for production of HC, CO_2 and above all NO_x. The RME fuel achieved the best results in case of CO and mainly smoke emissions. The diesel fuel achieved the best results only in fuel consumption.

Similar results with slightly higher fuel consumption were obtained by BEATRICE ET AL. (2010). Authors AATOLA ET AL. (2008) and RANTANEN ET AL. (2005) reached the reduction of fuel consumption. The fuel consumption is affected by the design of the engine and properties of the fuel. The engines with mechanically controlled injection pump and injectors reaches higher fuel consumption while running on HVO since it has lower density. RANTANEN ET AL. (2005) and BEATRICE ET AL. (2010) reached reduce of the emissions of CO while using HVO fuel. On the contrary, KRAHL ET AL. (2009) stated the slight increase of the emissions of CO. AATOLA ET AL. (2008), RANTANEN ET AL. (2005) and Beatrice et al. (2010) reached positive results of the emissions of HC with HVO fuel. The reduction was up to 50 % in comparison with diesel. AATOLA ET AL. (2008), RANTANEN ET AL. (2005), KRAHL ET AL. (2009) and BEATRICE ET AL. (2010) confirms the positive impact of the HVO fuel on the emissions of NO_X. Because of the better ratio of carbon and hydrogen the HVO fuel also slightly reduces the production of CO_2 according to RANTANEN ET AL. (2005) and BEATRICE ET AL. (2010). In the case of smoke or production of particulate matter the other authors (AATOLA ET AL., 2008; KRAHL ET AL., 2009; NYLUND & KOPONEN, 2012; RANTANEN ET AL., 2005; BEATRICE ET AL., 2010) also confirms the reduction of smoke in connection with the HVO fuel. The similar results were also obtained by other authors (MAGNO ET AL., 2016; MAGNO ET AL., 2015; MANCARUSO & VAGLIECO, 2012; LEBEDEVAS ET AL., 2010) with RME fuel. The RME fuel causes mainly the increase of the fuel consumption and NO_X production and the reduction of smoke, hydrocarbon and carbon monoxide production.

CONCLUSIONS

Comparison by means of the NRSC test when using three kinds of fuels (diesel fuel - EN 590, RME, HVO) at a supercharged engine of Zetor Forterra 8641 resulted in the following conclusions:

- in production of HC, CO_2 and NO_x the best results have been achieved in case of HVO fuel,
- in production of CO and smoke emissions the best results were recorded in case of RME fuel
- in fuel consumption the best results were achieved in case of diesel fuel - EN 590,
- from 48 measured points the HVO fuel achieved the best results at 50 % of points, RME at 39.6 % of points and diesel fuel – EN 590 at 10.4 % of points,
- from 48 measured points the HVO fuel achieved the worst results at 2.1 % of points, RME fuel at 39.6 % of points and diesel fuel – EN 590 at 59.3 % of points,

From the measured results obtained during the NRSC test it is obvious, that the biofuels can have a considerable share in reduction of production of harmful emissions from combustion engines. It is entirely clear, that it was achieved considerable reduction of smoke emissions even by more than 80 %, CO production till by 40 % and NO_x production by use of HVO fuel by 20 %. It seems, that the HVO fuel could be the biofuel of the future for compression ignition engines.

ACKNOWLEDGEMENTS

This work was carried out within the project of long-term development of IGA CULS Prague 2016: 31190/1312/3117 Effect of mixture of biofuels on production of nitrogen oxide and smoke emissions of combustion engine during the NRSC test and the project of the Research Institute of Agricultural Engineering p.r.i. No. RO0614.

REFERENCES

1. AATOLA, H., LARMI, M., SARJOVAARA, T., MIKKONEN, S. 2008: Hydrotreated vegetable oil (HVO) as a renewable diesel fuel: trade-off between NOx, particulate emission, and fuel consumption of a heavy duty engine. *SAE paper*, 2008–01–2500.
2. AMANATIDIS, S., NTZIACHRISTOS, L., GIECHASKIEL B., BERGMANN, A., SAMARAS, Z.: Impact of selective catalytic reduction on exhaust particle formation over excess ammonia events, Environmental Science and Technology 48(19), 2014: 11527–11534.
3. ARMAS, O., GÓMEZ, A., RAMOS, Á.: Comparative study of pollutant emissions from engine starting with animal fat biodiesel and GTL fuels. *Fuel* 113, 2013: 560–570.
4. ATHAPPAN, A., SATTLER, M.L., SETHUPATHI, S.: Selective catalytic reduction of nitric oxide over cerium-doped activated carbons. *Journal of Environmental Chemical Engineering* 3(4) Part A, 2015: 2502–2513.
5. ATMANLI, A., İLERI, E., YÜKSEL, B.: Effects of higher ratios of n-butanol addition to diesel–vegetable oil blends on performance and exhaust emissions of a diesel engine, *Journal of the Energy Institute* 3, 2015: 209–220.
6. BEATRICE, C., GUIDO, C., IORIO, S.: Experimental analysis of alternative fuel impact on a new ‘‘torque-controlled” light-duty diesel engine for passenger cars. *Fuel* 89, 2010: 3278–3286.
7. CAO, Y., FENG, X., XU, H., LAN, L., GONG, M., CHEN, Y. 2016: Novel promotional effect of yttrium on Cu–SAPO-34 monolith catalyst for selective catalytic reduction of NOx by NH3 (NH3-SCR). *Catalysis Communications* 76, 2016: 33–36.
8. EN 14214: Liquid petroleum products. Fatty acid methyl esters (FAME) for use in diesel engines and heating applications. Requirements and test methods. 2014.
9. EN 590: Automotive fuels. Diesel. Requirements and test methods. 2013.
10. HÖNIG, V., ORSÁK, M., PEXA, M., LINHART, Z.: The distillation characteristics of automotive gasoline containing biobutanol, bioethanol and the influence of the oxygenates. *Agronomy Research* 13(2), 2015b: 558–567.
11. HÖNIG, V., SMRČKA, L., ILVES, R., KÜÜT, A.: Adding biobutanol to diesel fuel and impact on fuel blend parametres. *Agronomy Research* 13(5), 2015a: 1227–1233.
12. HWANG, J., QI, D., JUNG, Y., BAE, CH.: Effect of injection parameters on the combustion and emission characteristics in a common-rail direct injection diesel engine fueled with waste cooking oil biodiesel. *Renewable Energy* 63, 2014: 9–17.
13. ISO 8178-4: Reciprocating internal combustion engines-Exhaust emission measurement-Part 4: Steady-state test cycles for different engine applications. 2007.
14. KANG, W., CHOI, B.: Effect of copper precursor on simultaneous removal of PM and NOx of a 2-way SCR/CDPF. *Chemical Engineering Science*. 141, 2016: 175–183.
15. KIBUGE, R. M., KARIUKI, S.T., NJUE, M. R.: Influence of fuel properties on the burning characteristics of sour plum (Ximenia americana L.) seed oil compared with Jatropha curcas L. seed oil. *Renewable Energy* 78, 2015: 128–131.
16. KRAHL, J., KNOTHE, G., MUNACK, A., RUSCHEL, Y., SCHRÖDER, O., HALLIER, E., WESPHAL, G., BÜNGER, J.: Comparison of exhaust emissions and their mutagenicity from the combustion of biodiesel, vegetable oil, gas-to-liquid and petrodiesel fuels. *Fuel* 88, 2009: 1064–1069.
17. KUČERA, M., ROUSEK, M.: Evaluation of thermooxidation stability of biodegradable recycled rapeseed-based oil NAPRO-HO 2003. *Research in Agricultural Engineering* 54(4), 2008: 163–169.
18. LEBEDEVAS, S., LEBEDEVA, G., SENDZIKIENE, E., MAKAREVICIENE, V.: Investigation of the performance and emission characteristics of biodiesel fuel containing butanol under the conditions of diesel engine operation. *Energy and Fuels*, 24 (8), 2010: 4503-4509.
19. LIU, J., YAO, A., YAO, CH.: Effects of diesel injection pressure on the performance and emissions of a HD common-rail diesel engine fueled with diesel/methanol dual fuel. *Fuel* 140, 2015: 192–200.
20. MAGNO, A., MANCARUSO, E., VAGLIECO, B. M.: Effects of both blended and pure biodiesel on waste heat recovery potentiality and exhaust emissions of a small CI (compression ignition) engine. *Energy*, 86, 2015: 661-671.
21. MAGNO, A., MANCARUSO, E., VAGLIECO, B. M.: Analysis of combustion phenomena and pollutant formation in a small compression ignition engine fuelled with blended and pure rapeseed methyl ester. *Energy*, 106, 2016: 618-630.
22. MANCARUSO, E., VAGLIECO, B. M.: Premixed combustion of GTL and RME fuels in a single cylinder research engine. *Applied Energy*, 91 (1), 2012: 385-394.
23. MARTÍNEZ, J.D., RODRÍGUEZ-FERNÁNDEZ, J., SÁNCHEZ-VALDEPEÑAS, J., MURILLO, R., GARCÍA, T.: Performance and emissions of an automotive diesel engine using a tire pyrolysis liquid blend. *Fuel* 115, 2014: 490–499.
24. MOGHADDAM, M. S., MOGHADDAM, A. Z.: Performance and exhaust emission characteristics of a CI engine fueled with diesel-nitrogenated additives, *Chemical Engineering Research and Design* 92(4), 2014: 720–726.
25. MÜLLER, M., CHOTĚBORSKÝ, R., HRABĚ, P.: Application of Overlay Material on Soil Processing Tools for Purpose of Increasing their Abrasive Wear Resistance. Listy cukrovarnické a řepařské, 2015, roč. 131, č. 9-10, s. 279-283. ISSN: 1210-3306.
26. MÜLLER, M., HERÁK, D., VALÁŠEK, P.: DEGRADATION LIMITS OF BONDING TECHNOLOGY DEPENDING ON DESTINATIONS EUROPE, INDONESIA. Tehnicki Vjesnik-Technical Gazette, 2013, roč. 20, č. 4, s. 571-575. ISSN: 1330-3651.
27. MÜLLER, M., ŠLEGER, V., PEXA, M., MAŘÍK, J., MIZERA, Č.: Evaluation of stability of elastomer packing exposed to influ-

ence of various biofuels. *Agronomy Research* 13(2), 2015: 604–612.
28. MURALI KRISHNA, M. V. S., SESHAGIRI RAO, V. V. R., REDDY, K. K. T., MURTHY, P. V. K.: Performance evaluation of medium grade low heat rejection diesel engine with carbureted methanol and crude jatropha oil. *Renewable and Sustainable Energy Reviews* 34, 2014: 122–135.
29. NYLUND, N.O., KOPONEN, K.: Fuel and technology alternatives for buses. VTT Technical Research Centre, VTT Technology 48. Espoo 2012. 294 p + appendixes. [online]. Available at: <http://www.vtt.fi/inf/pdf/technology/2012/T46.pdf>. Accessed 30 May 2016.
30. QI, D. H., LEE, C. F., JIA, C. C., WANG, P. P., WU, S. T.: Experimental investigations of combustion and emission characteristics of rapeseed oil–diesel blends in a two cylinder agricultural diesel engine. *Energy Conversion and Management* 77, 2014: 227–232.
31. RANTANEN, L., LINNAILA, R., AAKKO, P., HARJU, T. 2005: NExBTL – Biodiesel fuel of the second generation, SAE paper 2005-01-3771.
32. SUN, Z., SUN, P., WU, Q.M., HU, J., ZHANG, M.: Study of diesel particulate filter filtration efficiency and the effects on performance of diesel engine. *Advanced Materials Research* 726–731, 2013: 2280–2283.
33. TZIOURTZIOUMIS, D., STAMATELOS, A.: Effects of a 70% biodiesel blend on the fuel injection system operation during steady-state and transient performance of a common rail diesel engine. *Energy Conversion and Management* 60, 2012: 56–67.
34. VALLINAYAGAM, R., VEDHARAJ, S., YANG, W. M., LEE, P. S.: Operation of neat pine oil biofuel in a diesel engine by providing ignition assistance. *Energy Conversion and Management* 88, 2014: 1032–1040.
35. WOO, CH., KOOK, S., HAWKES, E. R., ROGERS, P. L., MARQUIS, CH.: Dependency of engine combustion on blending ratio variations of lipase-catalysed coconut oil biodiesel and petroleum diesel. *Fuel* 169, 2016: 146–157.

Corresponding author:
doc. Ing. Martin Pexa, Ph.D., Department for Quality and Dependability of Machines, Faculty of Engineering, Czech University of Life Sciences Prague, Kamýcká 129, Praha 6, Prague, 16521, Czech Republic, phone: +420 22438 3278, e-mail: pexa@tf.czu.cz

RELATIONSHIP BETWEEN SATELLITE-DERIVED NDVI AND SOIL ELECTRICAL RESISTIVITY: A CASE STUDY

A. Pezzuolo, D. Cillis, F. Marinello, L. Sartori

TeSAF Department, University of Padova, Legnaro, PD, Italy

Abstract

Efficient and reliable methods for measuring spatial variations in soil properties are fundamental in precision agriculture.

In the present work a survey on soil variability and within-farm plant is reported, coupling a multi-depth automatic resistivity profiler (ARP©, Geocarta, France) and the NDVI index derived from Sentinel-2 imagery data. Based on the relationship between resistivity and NDVI index, the objective of the analysis was to test the possibility to monitor the evolution of vegetation index and modulate the agricultural operations depending on soil features and soil tillage techniques management on soft wheat (Triticum Aestivum L.).

A comparison of the same homogeneous zones managed with different soil tillage techniques shows an increase of NDVI index from conventional tillage (CT) to minimum tillage (MT) and no-tillage (NT). This is caused by conservation tillage techniques which allow a mitigation of cooling phenomena, higher availability of nutrients and lower number of passages across the field preventing soil compaction.

Key words: geophysical mapping, normalized difference vegetation index, durum wheat, soil spatial variability, remote sensing, precision agriculture.

INTRODUCTION

Efficient and reliable methods for measuring spatial variations in soil properties are fundamental in precision agriculture (PEZZUOLO ET AL., 2014; BASSO ET AL., 2016). Over the last decade geophysical sensors based on the non-destructive measurement of soil electrical conductivity (or its inverse resistivity) have been extensively used in precision agriculture (PERALTA AND COSTA, 2013; ROSSI ET AL., 2015). These advantages may include lower cost, increased capacity and efficiency, and more timely results (MARINELLO ET AL., 2015). In addition, the ability of a sensor to collect data at many more points, as compared to sampling and removal methods, provides an overall increase of spatial estimation accuracy even if the accuracy of individual measurements is lower (SUDDUTH ET AL., 2013).

At the same time, satellite and airborne sensors offer an increasing amount of information about soil properties and ground cover (NOUVELLON ET AL., 2001). In particular, vegetation indices, based on remotely-sensed spectral reflectance in the near-infrared and visible bands, have been widely used for monitoring vegetation cover and health condition, plant phenology, and ecosystem changes (GONG ET AL., 2012). Among many vegetation indices such as Normalized Difference Vegetation Index (NDVI), Soil Adjusted Vegetation Index (SAVI) and Enhanced Vegetation Index (EVI), NDVI has been most commonly used for vegetation-related monitoring in numerous studies (KE ET AL., 2015). However, the increasing number of satellite sensors provides great opportunities for NDVI derivation at various spatial and temporal scales, and enables the synergistic use of observations from other sensors to better understand land processes (TUCKER ET AL., 2005) such as spatial variations or delineate the homogeneous zones at farm scale.

In the present work a survey on soil variability and within-farm plant is reported, coupling a multi-depth automatic resistivity profiler (ARP©, Geocarta, France) and the NDVI index derived from Sentinel-2 imagery data.

Based on the relationship between resistivity and NDVI index, the objective of the analysis was to test the possibility to monitor the evolution of vegetation index and modulate the agricultural operations depending on soil features and soil tillage techniques management on soft wheat (Triticum Aestivum L.).

MATERIALS AND METHODS

Site description and experimental management

The study was carried out in the 2015-2016 season in a farm located in Caorle (VE) – Veneto, Italy (45.63°N 12.95°E). From a climate point of view, the average annual rainfall in 20 years recorded by an agro-meteorological station located in nearby Lugugnana (VE) were equal to 935 mm·year^{-1}.

The study considered wheat (Triticum Aestivum L.) crop cultivation, managed with three soil tillage techniques (Tab. 1), characterized by the different impact to the soil, and by decreasing order are: conventional tillage (CT), minimum tillage (MT) and no tillage (NT). Each plot was characterized by an average 1.5 ha area.

Tab. 1. – Agricultural practices for each tillage systems adopted by the farm

Tillage System	Agricultural practices	Date	Product	Rate
CT	Pre-sowing fertilization	27/10/2015	NPK fertilizer (8-24-24)	400 kg·ha^{-1}
	Sowing	27/10/2015	Wheat – var. Solehio	450 seeds·m^{2}
	Tillering fertilization	28/01/2016	Ammonium nitrate (26 %)	200 kg·ha^{-1}
	Stem elongation fertilization	15/03/2016	Urea (46 %)	200 kg·ha^{-1}
MT	Pre-sowing fertilization	27/10/2015	NPK fertilizer (8-24-24)	400 kg·ha^{-1}
	Sowing	27/10/2015	Wheat – var. Solehio	450 seeds·m^{2}
	Tillering fertilization	28/01/2016	Ammonium nitrate (26 %)	200 kg·ha^{-1}
	Stem elongation fertilization	15/03/2016	Urea (46 %)	200 kg·ha^{-1}
NT	Pre-sowing fertilization	27/10/2015	NPK fertilizer (8-24-24)	400 kg·ha^{-1}
	Sowing	27/10/2015	Wheat – var. Solehio	500 seeds·m^{2}
	Tillering fertilization	28/01/2016	Ammonium nitrate (26 %)	200 kg·ha^{-1}
	Stem elongation fertilization	15/03/2016	Urea (46 %)	200 kg·ha^{-1}

Automatic resistivity profiling

On-the-go multi-depth resistivity measurements (ARP©, Geocarta) were carried out on the whole 4.5 ha area. The ARP instrument consists of a console that collect electrical data derived from a succession of electrodes represented by four toothed metal wheels; the electrodes are inserted into the soil through the movement of rotation of the same wheels along the ground surface. The first dipole enters a stabilized current to the subsoil, the following three wheels measure the potential that derives from the injected current. The distance between the three dipoles increases with the current introduction distance (equatorial dipole). The distance is respectively 0.5 m, 1 m and 2 m. Data were real-time referenced by differential global positioning system (DGPS). Data were collected along parallel transects at 5 m apart.

Remote sensing data collection

Data needed to assess NDVI vegetation index during crop cycle were derived from Sentinel-2 mission's satellites. Sentinel-2 mission provides continuity to services relying on multi-spectral high resolution optical observations over global terrestrial surfaces. The mission is characterized by a high quality multi-spectral Earth observation system implementing the Multi Spectral Instrument (MSI) with 13 spectral bands spanning from the visible to the short wave infrared. The spatial resolution ranges between10 m and 60 m (depending on the spectral band) with a 290 km field of view (DRUSCH ET AL., 2012). The present work took into consideration 5 satellite spectral bands, from 20 January 2016 to 30 March 2016, selecting only high signal to noise rate clear maps and excluding those presenting a marginal interference caused by clouds or fog.

Data elaboration and statistical analysis

Data derived from Sentinel-2 images are relative to different dates. In this way, it was possible to collect multispectral-data during crop development. These data were useful to assess NDVI index of the wheat. In order to evaluate such vegetation-index, red and infrared multispectral bands are needed: in this study the so called B4 and B8 spectral bands were specifically considered, featuring respectively 665 and 842 nm central wavelength with 30 and 115 nm band width.

Firstly, ARP data were divided in classes representing step values of resistivity of 5 Ohm·m in order to evaluate the correlation between ARP and NDVI. Then, ARP data derived from all 3 depth levels were processed using the statistical software MZA-Management Zone Analyst - University of Missouri-Columbia (FRIDGEN ET AL., 2004). MZA uses a fuzzy c-means unsupervised clustering algorithm that assigns field information into like classes, or potential management zones (Fig. 1).

In order to performs the analysis, NDVI and ARP data were standardized building a 10 x 10 m reference grid with a total of 488 control points ("pixels"). Each pixel of the grid has an average value of NDVI and ARP defined as the mean of the values included into the same pixel area.

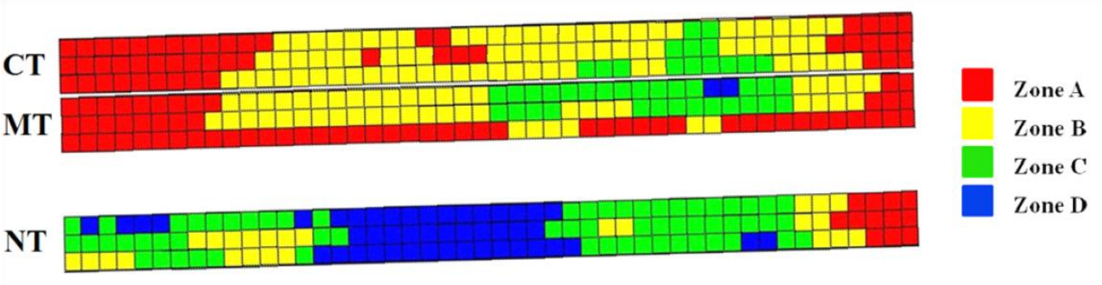

Fig. 1. – Homogeneous zones derived from MZA analysis

RESULTS AND DISCUSSION

Data analysis relationship

Soil resistivity data showed that the study area is characterized by high variability in terms of soil features. In fact, a wide range of resistivity was observed. Soil resistivity is mostly influenced by texture, water content and salinity. Therefore, high resistivity levels characterize sandy soil with high water drainage, while low resistivity levels distinguish clay soil with high salinity that can occurs in stagnant situation if affected by soil compaction. To this end, the result of classes division based on the ARP depth level 0-50 cm was 18, each one ranged in 5 Ohm·m. In order to avoid interference related to unexpected data the average of the 5 dates NDVI data was taken into consideration. As shown in Fig. 2, a clear correlation can be detected between soil features and vegetation vigour. Increases in ARP value correspond to high vegetation vigour expressed as NDVI.

On the other hand, high values of standard deviation of several classes shows high variability within data. This can be ascribed to the presence of other factors affecting the relation between NDVI and ARP. Different soil tillage techniques adopted in the study area are certainly one of the first factors causing such variability, as discussed in the following.

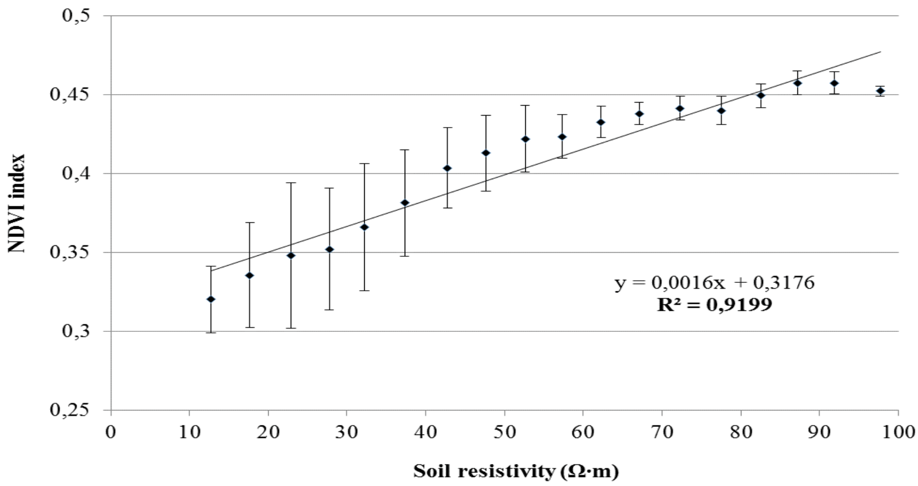

Fig. 2. – Correlation between soil features and vegetation vigour. Increases in soil resistivity value correspond to high vegetation vigour expressed as NDVI index.

Relationship under MZA's homogeneous zone characterization

In this second step, a characterization of homogeneous zones of the study area based on ARP data has been made. In this way it is possible to compare NDVI index belonging to the same homogeneous zones managed with different soil tillage techniques. From the MZA analysis, 4 homogeneous zones have been characterized: 3 of them cover all the tillage conditions, while the forth zone affects only the side of the field managed with MT and NT. These homogenous zones (namely A, B C and D) are characterized by increasing ARP values. Again a high correlation between NDVI and ARP was found (Fig. 3).

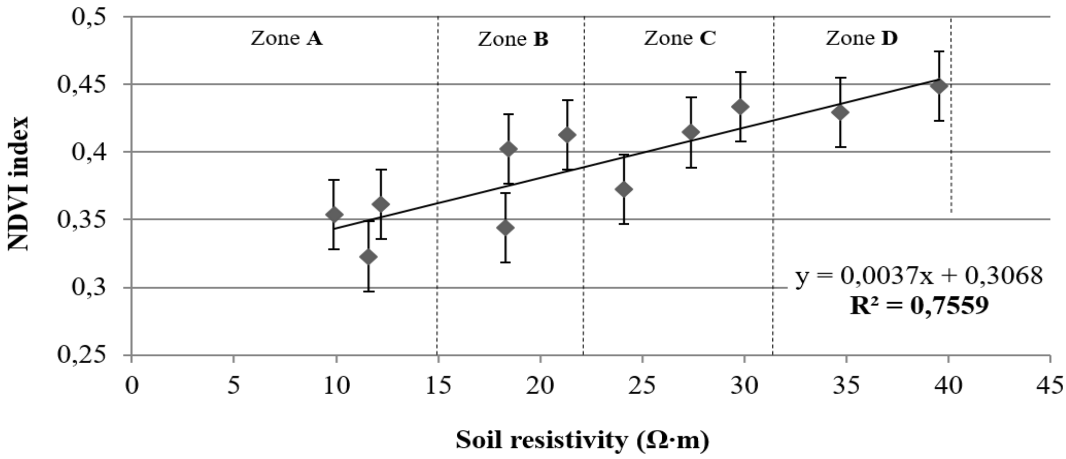

Fig. 3. – Homogenous zones are characterized by increasing soil resistivity values and NDVI index

Besides, standard deviation was approximately the same for each point meaning that the homogeneous zones characterization made by MZA software is more representative of the relation between NDVI and ARP than the first classification approach made by the authors. This is due to the fact that MZA use the ARP data derived from all the 3 depth level to classify homogeneous zones. Homogeneous zone A, having lower level of resistivity, has lesser NDVI value than other zones. This trend is repeated for B, C and D zones. This evolution of the vegetation vigour in wheat could be ascribable to the higher soil temperature, a higher drainage efficiency and a more suitable seedbed characterizing homogeneous zones with increasing resistivity level.

Soil tillage system effect

Finally, it is possible to observe the NDVI temporal trend of the single homogeneous zones under different soil tillage techniques management. Correspondingly the contribution of the soil tillage technique on NDVI index and the influence on soil features can be investigated (Fig. 4).

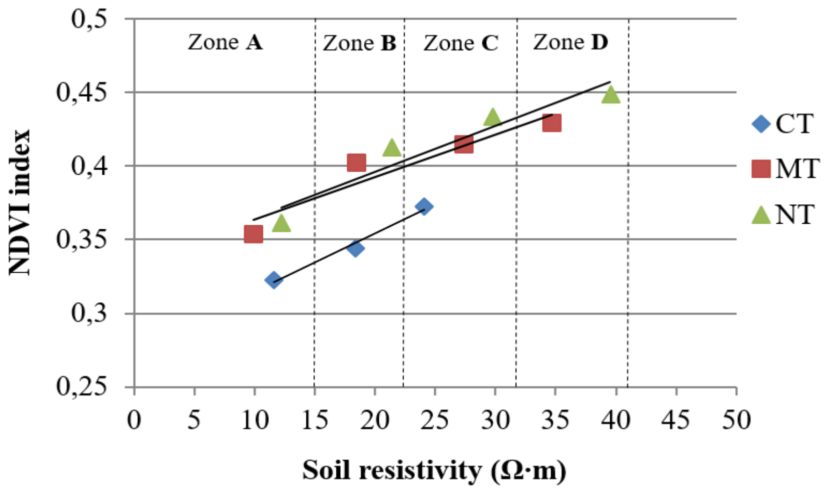

Fig. 4. – NDVI trend of the single homogeneous zones under different soil tillage techniques management

Considering approximately similar the sowing dates and the soil features characterizing the study area, CT shows lower NDVI than MT and NT for all homogeneous zones. This is caused by its features: indeed, CT tends to cool soil faster than MT and NT. In addition, continually inversion of soil layer leads to a decrease in soil fertility and nutrients availability. Finally, the higher number of passages distinguishing CT for the seedbed preparation could affect soil compaction leading to a stress condition for plants growing in the field defined by clay soil. Conversely, MT and NT do not include inversion of soil layer and they need a lower number of passages across the field. Besides, their features lead to a mitigation of soil cooling phenomena allowing fast seeds germination.

NDVI trend during crop development

All of these information can be seen under two complementary points of view. The first one considers the possibility to assess the vegetation vigour starting by soil features, and its evolution under different soil tillage techniques management. The second one is to monitor crop during its cycle and to take decision about agricultural operations taking advantage of vegetation indexes, soil features and soil tillage techniques management. Fig. 5 shows the NDVI trend during the time from the first monitoring date (day 0, on 20 January 2016) to the fifth one (day 69) and the dates of the two nitrogen fertilizer applications.

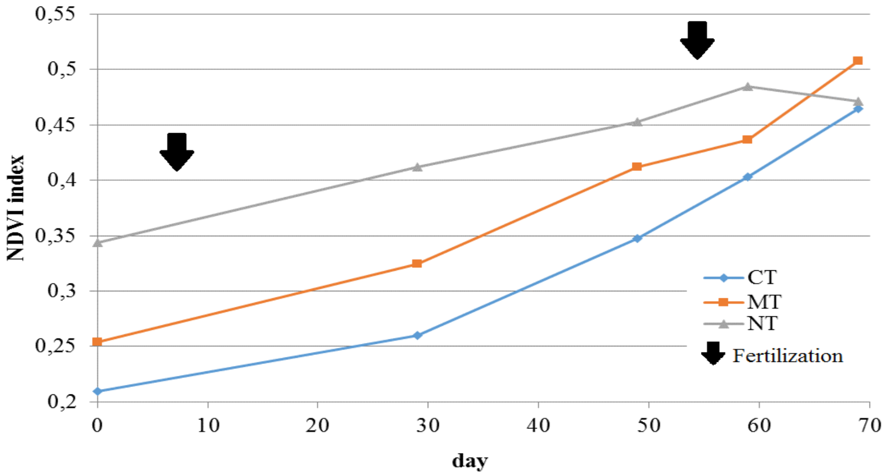

Fig. 5. – NDVI trend during the time from the first monitoring date (day 0, on 20 January 2016) to the fifth one (day 69) and the dates of the two nitrogen fertilizer applications

It is interesting to note that the CT's curve slope is more accentuate than other theses, suggesting in a later increase of the NDVI index during the crop cycle. In fact, the NDVI values related to the last monitoring date are close for all the theses, even observing a decrease in NT. This condition could be due to the CT soil warming faster than other theses and to a better response to nitrogen fertilization.

CONCLUSIONS

Monitoring vegetation vigour during crop cycle and relating its evolution to soil features is useful to identify the optimal agricultural operation to carry out under different soil tillage techniques management. Besides, collecting information derived from other sources such as climate data and historical crop yield data it is possible to modulate those operations which provide fertilizer application. Regarding wheat, a correlation was verified between vegetation index expressed as NDVI and soil feature represented by ARP analysis. In addition, the implementation of MZA allows to obtain steady homogeneous zones derived from the interpolation of different data highly correlated with NDVI. A comparison of the same homogeneous zones managed with different soil tillage techniques shows an increase of NDVI index from CT to MT and NT. This is caused by conservation tillage techniques which allow a mitigation of cooling phenomena, higher availability of nutrients and lower number of passages across the field preventing soil compaction. Repeating and validating the results of this work in the next years in order to model the correlation between NDVI and ARP data for the different soil tillage techniques management could be useful in the future to predict crop yield in wheat.

REFERENCES

1. BASSO, B., DUMONT, B., CAMMARANO, D., PEZZUOLO, A., MARINELLO, F., SARTORI, L.: Environmental and economic benefits of variable rate nitrogen fertilization in a nitrate vulnerable zone. Science of Total Environment, 545-546, 2016: 227-235.
2. DRUSCH, M., DEL BELLO, U., CARLIER, S., COLIN, S., FERNANDEZ, V., GASCON, F., HOERSCH, B., ISOLA, C., LABERINTI, P., MARTIMORT, P., MEYGRET, A., SPOTO, F., SY, O., MARCHESE, F., BARGELLINI, P.: Sentinel-2: ESA's Optical High-Resolution Mission for GMES Operational Services. Remote Sensing of Environment, 120, 2012:25-36.
3. FRIDGEN J. J., KITCHEN N. R., SUDDUTH K. A., DRUMMOND S. T., WIEBOLD W. J., FRAISSE C. W.: Management Zone Analyst (MZA): Software for Subfield Management Zone Delineation. Agron. J., 96, 2004: 100–108.
4. GONG, P., WANG, J., YU, L., ZHAO, Y. C., ZHAO, Y. Y., LIANG, L.: Finer resolution observation and monitoring of global land cover: First mapping results with Landsat TM and ETM+ data. International Journal of Remote Sensing, 34, 2013: 2607–2654.
5. KE, Y., IM, J., LEE, J., GONG, H., RYU, Y.: Characteristics of Landsat 8 OLI-derived NDVI by comparison with multiple satellite sensors and in situ observations. Remote Sens. Environ, 164, 2015: 298–313.
6. MARINELLO, F., PEZZUOLO, A., GASPARINI, F., ARVIDSSON, J., SARTORI, L.: Application of the Kinect sensor for dynamic soil surface characterization. Precision Agriculture, 5, 2015: 1-12.
7. NOUVELLON, Y., MORAN, M. S., LO SEEN, D., BRYANT, R., RAMBAL, S., NI, W., BEGUE, A., CHEHBOUNI, A., EMMERICH, W. E., HEILMAN, P., QI, J.: Coupling a grassland ecosystem model with Landsat imagery for a 10-year simulation of carbon and water budgets. Remote Sens. Environ., 78, 2001:131–149.
8. PERALTA, N. R., COSTA J. L.: Delineation of management zones with soil apparent electrical conductivity to improve nutrient management. Comput. Electron. Agric., 99, 2013:218-26.
9. PEZZUOLO, A., BASSO, B., MARINELLO, F., SARTORI, L.: Using SALUS model for medium and long term simulations of energy efficiency in different tillage systems. Applied Mathematical Sciences, 8, 2014: 129–132.
10. ROSSI, R., POLLICE, A., BITELLA, G., BOCHICCHIO, R., D'ANTONIO, A., ALROMEED, A. A., STELLACCI, AM., LABELLA, R., AMATO, M.: Soil bulk electrical resistivity and forage ground cover: nonlinear models in an alfalfa (Medicago sativa L.) case study. Italian Journal of Agronomy, 10, 2015: 215-219.
11. SUDDUTH, K. A., MYERS, D. B., KITCHEN, N. R., DRUMMOND S. T.: Modeling soil electrical conductivity-depth relationships with data from proximal and penetrating ECa sensors. Geoderma, 199, 2013: 12–21.
12. TUCKER, C. J., PINZON, J. E., BROWN, M. E., SLAYBACK, D. A., PAK, E. W., MAHONEY, R.: An extended AVHRR 8-km NDVI dataset compatible with MODIS and SPOT vegetation NDVI data. International Journal of Remote Sensing, 26, 2005: 4485–449.

Corresponding author:
Andrea Pezzuolo TeSAF Department, University of Padova, Legnaro, PD, Italy, e-mail: andrea.pezzuolo@unipd.it

VERIFICATION OF MODEL CALCULATIONS FOR THE KAPLAN TURBINE DESIGN

M. Polák[1], V. Polák[2], M. Hudousková[3]

[1]*Faculty of Engineering, Czech University of Life Sciences in Prague, Czech Republic*
[2]*Institute of Geophysics of the Czech Academy of Sciences, Prague, Czech Republic*
[3]*Faculty of Economics and Management, Czech University of Life Sciences in Prague, Czech Republic*

Abstract
In order to design a water turbine, the Theory of the Physical Similarity of Hydraulic Machines is used in technical practice. This principle has been known and used by manufacturers of turbines and pumps, but is not available to general public. This paper describes author´s calculation program for turbine design that is well accessible to the widest possible range of users of mainly small hydropower sources. Based on the given hydraulic potential (water head and flowrate), the program determines the most suitable turbine type and calculates its main geometric parameters. In addition to numerical results, the program is also endowed with graphic output which renders in true scale hydraulic profiles of rotor blades and guide blades as well as the hydraulic profile of a spiral casing. The process of the Kaplan turbine design is used as an example in this paper. The comparisons of the calculated results with the verified standard 4-K-69 Kaplan turbine confirm the compliance of numerical results with reality.

Key words: blade geometry, calculation program, hydropower, theory of physical similarity, turbine design.

INTRODUCTION

On a global scale, there is a great unused renewable hydropower, especially in small water resources. In this area, besides a wide variety of simple water engines like a bladeless turbine, POLÁK (2013A), split reaction turbine DATE (2010), etc., the conventional blade turbines are used the most, KHAN (2009). The design principles of water turbines have been known and used for a long time by the manufacturers of turbines and pumps, but they use their know-how exclusively for their own needs, keeping it away from the public. The authors present here an original calculation program for turbine design, which has been simplified in order to address as wide an audience as possible. However, the simplification does not mean that the quality of the achieved results would suffer. Moreover, the authors extended the program by adding its own graphic output to it, which immediately renders the calculated key turbine components in true scale. In this way, the end users of small hydropower sources are able to find out detailed information on the device for the most effective use of renewable water energy in their specific local conditions.

For the purpose of the turbine design, the technical practice uses the theory of physical similarity of hydraulic machines. Its principle is based on the geometric similarity of velocity triangles (Fig. 1) of so called model (etalon) and real turbines or in other words on the Euler turbine equation:

$$Y_T = u_1 \cdot c_{u1} - u_2 \cdot c_{u2} \tag{1}$$

Where Y_T [J.kg^{-1}] is specific energy of turbine and u [m.s^{-1}] is circumferential and c_u [m.s^{-1}] absolute velocity according to MUNSON (2006) and ANAGNOSTOPOULOS (2009).

The main turbine design parameters are determined by the recalculations of model (etalon) turbines which are processed and described in detail using nomograms and tabulated values. Other design parameters are determined using fluid mechanics relations.

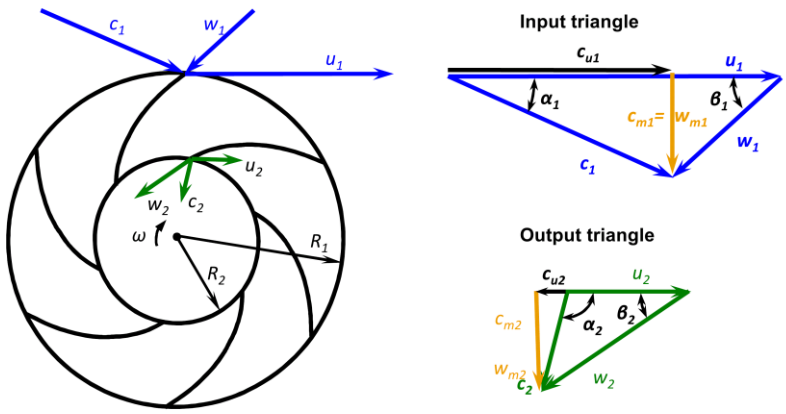

Fig. 1. – Velocity triangles of the radial turbine runner

The hydraulic design of the turbine itself can be converted into a calculation program. However, the tables and nomograms are pitfalls from which it is necessary to "manually" subtract values for other calculations. The authors of the paper converted all necessary tabulated values into mathematical functions. These functions and other fluid mechanics relations were used in order to create a calculation program. This has significantly simplified the whole process of turbine design. In addition to numerical results, the program also offers a graphic extension which displays real scale hydraulic profiles of individual components of the turbine. These are especially blade grid cross sections in stretched stream surfaces which are necessary for the designing and construction of runner blades and guide blades. Moreover, the program allows you to change the angle setting of blades (opening) in the rendered cross-sections and thus display different operating states. Other graphic output draws input and output velocity triangles, another depicts a hydraulic profile of a spiral casing in a cross-section. All the mathematical functions that are the principal of graphic extensions were created by the authors of this paper. The program for the turbine design is possible to edit in any program that can work with mathematical functions (for example MathCAD, Matlab, MS Excel, etc.).

MATERIALS AND METHODS

The calculation program for the turbine design

The following text schematically describes a Kaplan turbine hydraulic design as it is elaborated in the calculation program. Using this program, it is possible to design also Pelton, Francis or Banki turbine. Minding the extent of this paper, these variations are not further discussed and the attention is focused only on the Kaplan turbine. Numerical results of the calculation are subsequently compared with the geometry of the standard 4-K-69 Kaplan turbine (Fig. 6), which is used to verify the model recalculation.

The calculation program has been developed on the basis of the cited literature: MUNSON ET AL. (2006); BRADA ET AL. (1995); SUTIKNO (2011); MELICHAR ET AL. (1998); MELICHAR ET AL. (2002); NECHLEBA (1962); ULRYCH (2007); HUTAREW (1973) and its simplified algorithm is illustrated in Fig. 2.

The values of hydraulic potential, which is water head H [m], flowrate Q [m^3.s^{-1}] and desired turbine shaft speed n [min^{-1}], are entered into program as input variables (green fields in Fig. 5). Subsequently these are used to calculate the specific speed n_q [min^{-1}] by the flow which determines an appropriate turbine type according to DRTINA ET AL. (1999) and TRIVEDI ET AL. (2016):

$$n_q = n \cdot \frac{Q^{\frac{1}{2}}}{H^{\frac{3}{4}}} \tag{2}$$

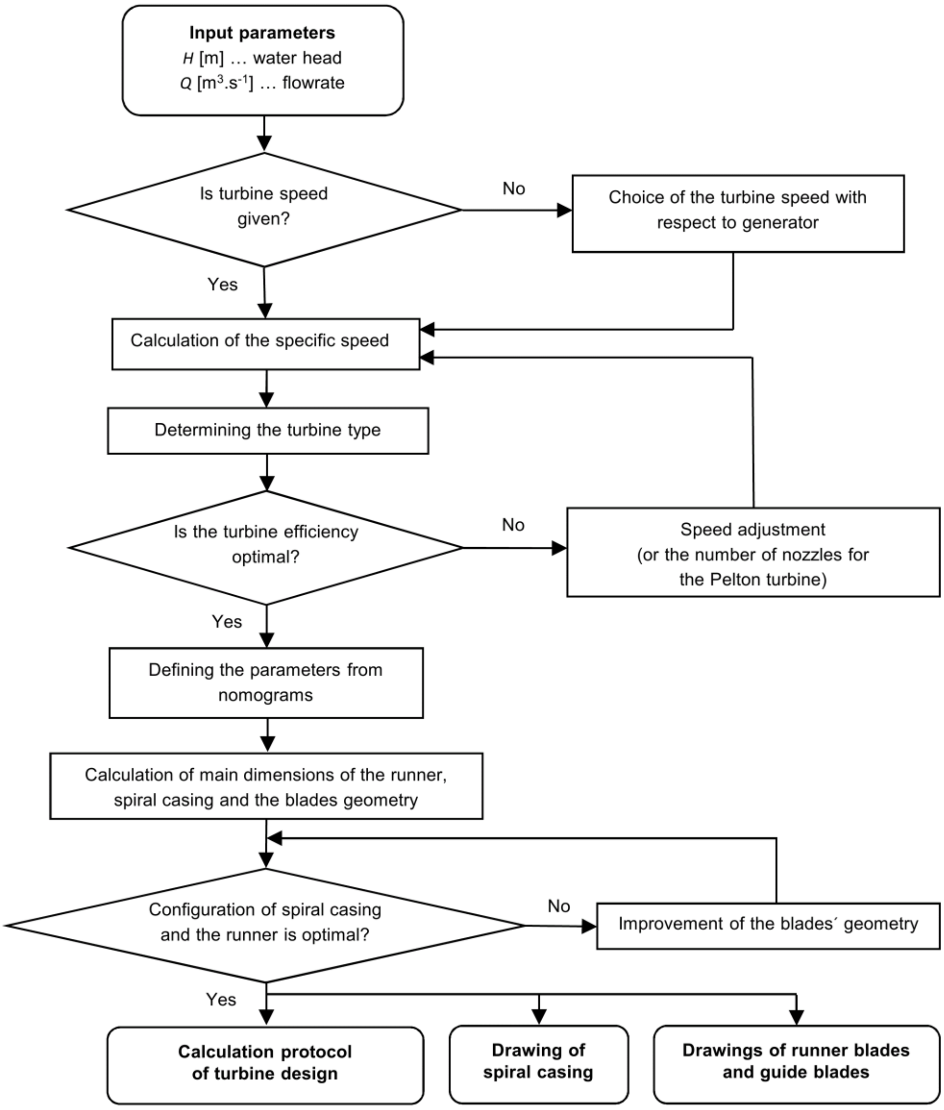

Fig. 2. – Simplified block diagram of the turbine design in the calculation program

Then main dimensions of the turbine runner are recalculated using geometric characteristics of a model turbine. For example the outside runner diameter D_1 [m] is calculated by:

$$D_1 = \left(\frac{Q}{Q'}\right)^{\frac{1}{2}} \cdot \left(\frac{1}{H}\right)^{\frac{1}{4}} \tag{3}$$

The value Q' [m^3.s^{-1}] (flowrate in a model/etalon turbine) is a tabulated value dependent on the specific speed n_q by the flow. Using the correlation analysis, this value and other tabulated values were converted into mathematical equations as polynomial functions of second-, third- or even fourth-degree. The program then calculates the equation which in terms of correlation analysis R^2 proved to be the most suitable. These equations form the basis of the calculation program on which the entire hydraulic design of individual components of the turbine depends. Fig. 3 shows an example of conversion of maximum efficiency values of Kaplan turbine depending on the specific speed n_q. The black line represents a curve of the tabulated values, the red one corresponds to values calculated from determined polynomial function used in the program:

$$\eta_T = -0.0000055 \cdot n_q^{\;2} + 0.0014 \cdot n_q + 0.84 \tag{4}$$

Other design parameters of the turbine are determined using the formulas of fluid mechanics and geometry of the velocity triangles (Fig. 1). The following text, due to the extent of the paper, focuses only on the design of runner blades geometry. When designing the blades, it is possible to use similar principles like those used in the construction of wind power plants propellers. However, it is necessary to take into consideration a number of fundamental differences arising from different operating states, especially the possibility of cavitation BAHAJ ET AL. (2007).

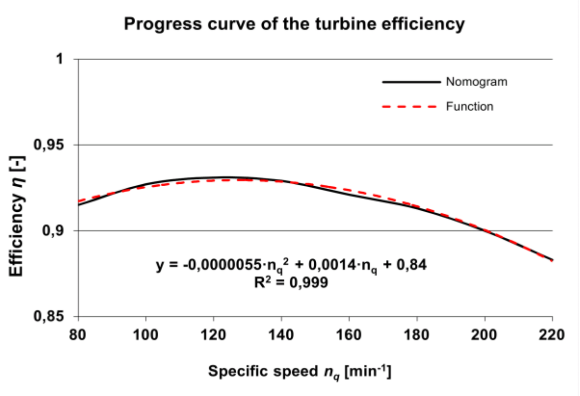

Fig. 3. – Sample of conversion into a mathematical function (PETIT ET AL., 2010)

For the construction of the blade, which is formed by generally curved surface, it is necessary to determine the velocity triangles in several cross-sections along the blade. This is based on the theorem of constant meridian velocity in the flow profile, which in case of the Kaplan turbine has axial direction. Meridian velocity c_m [m.s^{-1}] is determined:

$$c_m = w_m = \frac{Q}{S} \tag{5}$$

Meridian velocity c_m [m.s^{-1}] and w_m [m.s^{-1}] (Fig. 1) and the angular speed ω remain constant throughout the profile. Only the circumferential blade velocity u and the absolute velocity c resulting from it will change. On the basis of the turbine specific energy $Y_T = g{\cdot}H$, the projection of absolute velocity c_1 to direction of the circumferential velocity is determined from the Euler turbine equation (prerequisite being the vortex-free water output $c_{u2} = 0$):

$$c_{u\,i} = \frac{Y_T}{u_1} = \frac{g \cdot H}{u_1} \tag{6}$$

Then the input angle of absolute velocity α_1 [deg] is calculated:

$$tg\ \alpha_1 = \frac{c_m}{c_{u\,1}} \tag{7}$$

This determines the velocity triangle on the outside diameter D_1. From thus defined triangle the geometry of the runner blade is calculated (β_1 correspond to the blade angle on the leading edge and, β_2 the blade angle on the trailing edge), NECHLEBA (1962) and DRTINA ET AL. (1999).

The blade angle β_1 [deg] at the inlet:

$$tg\ \beta_1 = \frac{c_m}{u_1 - c_{u1}} \tag{8}$$

The blade angle β_2 [deg] of the output will be, provided the same circumferential velocity ($u_1 = u_2$) and vortex-free output of water from the turbine:

$$tg\ \beta_2 = \frac{c_m}{u_1} \tag{9}$$

This determines the blade geometry on the outside diameter D_1. By analogy, the input and output blade angles (β_1 and β_2) on the diameters D_1 to D_N are determined – see Fig. 4a).

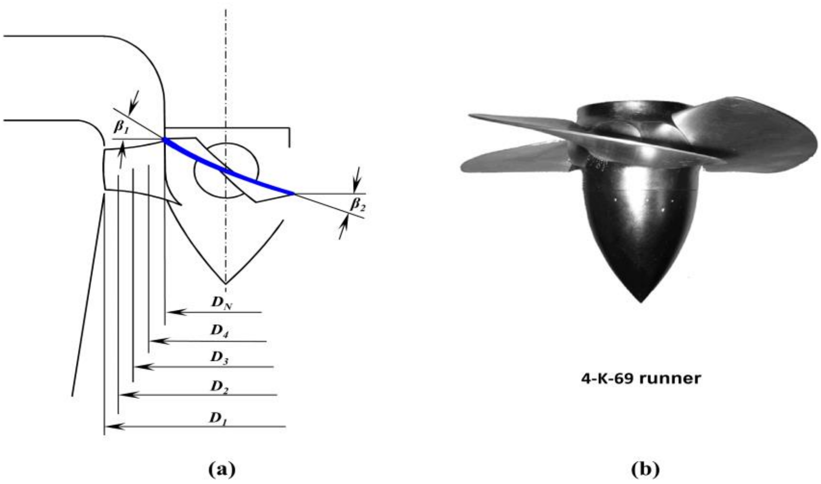

Fig. 4. – a) Specification of cylindrical cross-sections for calculation of the blade geometry according POLÁK, (2013B), b) turbine runner 4-K-69

All numerical results of blade runner hydraulic design, including the velocity triangles rendered in real scale, are summarized in a calculation protocol. Fig. 5 shows an example of such a protocol developed for the standard 4-K-69 Kaplan turbine which is used to verify calculated values. Fig. 4b) shows a blade runner and Fig. 6 shows a plan of the entire 4-K-69 turbine.

Kaplan turbine

Input parameters

Water head	h=	3,7	m
Flowrate	Q=	0,073	$m^3.s^{-1}$
Gear ratio*	p=	2,17	-

* with respect to the generator speed N_G = 3 000 min^{-1}

Runner design

Turbine speed	N=	1381	min^{-1}
Specific speed	Nq=	139,8	min^{-1}
Etalon flowrate	Q´=	1,234	$m^3.s^{-1}$
Outside runner diameter	D_1=	0,195	m
Channel width ratio	B_o/D_1=	0,37	-
Channel width	B_o=	0,080	m
Hub diameter ratio	D_N/D_1=	0,46	-
Hub diameter	D_N=	0,078	m
Angle of suction pipe	δ=	8,7	°
Computed number of blades	z´=	3,3	ks
Number of blades	z =	4	ks
Blade spacing	T =	0,153	m
Relative spacing	T/L =	0,87	0,62 - 0,87
Blade lenght	L=	0,176	m
Clear opening	S=	0,025	m^2
Meridian velocity	c_m=	2,9	$m.s^{-1}$
Wheel angular speed	ω =	144,6	s^{-1}
Blade speed on D_1	u_1=	14,1	$m.s^{-1}$
Specific head energy	Y_t =	36,3	$J.kg^{-1}$
Projection of c_1 to u_1	C_{u1}=	2,6	$m.s^{-1}$
Inlet angle of streamline	α_1=	48,50	°
Outlet angle of streamline	α_2=	90	°
Inlet blade angle	β_1=	14,18	°
Outlet blade angle	β_2=	11,67	°
Middle diameter of runner	D_s=	0,137	m
Blade-hub clearance	r_N=	0	mm
Inside runner diameter	D_N=	0,078	m
Turbine efficiency	η =	0,93	-
Real power output	P =	2,46	kW

Cavitation check

Barometric presure	p_a=	100	kPa
Pressure of saturated water	p_d=	4	kPa
Thoma cavitation coefficient	σ =	0,51	-
Max. suction height	h_s=	7,91	m

Max. turbine efficiency

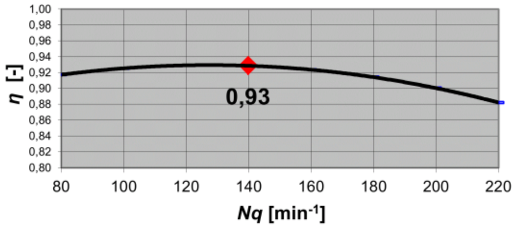

View of computed data - blade geometry

cut	D [m]	u_1 [$m.s^{-1}$]	c_{u1} [$m.s^{-1}$]	α_1°	α_2°	β_1°	β_2°
D_1	0,195	14,1	2,6	48,5	90	14,2	11,7
D_2	0,166	12,0	3,0	43,8	90	18,0	13,7
D_3	0,137	9,9	3,7	38,3	90	25,2	16,4
D_4	0,107	7,8	4,7	31,9	90	43,5	20,6
D_N	0,078	5,6	6,4	24,3	90	74,6	27,3

Sketch of turbine runner

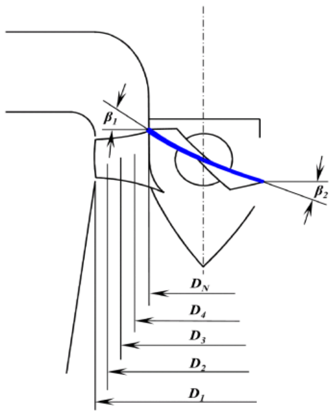

Velocity triangle (D_1) - input

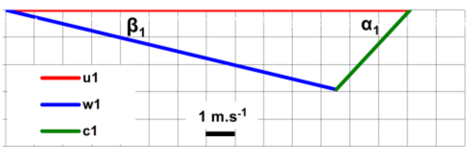

Velocity triangle (D_1) - output

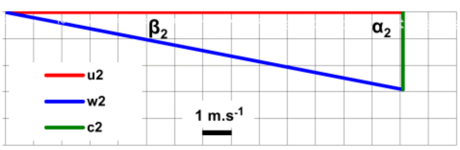

Fig. 5. – Calculation protocol in MS Excel for the standard 4-K-69 Kaplan turbine runner design

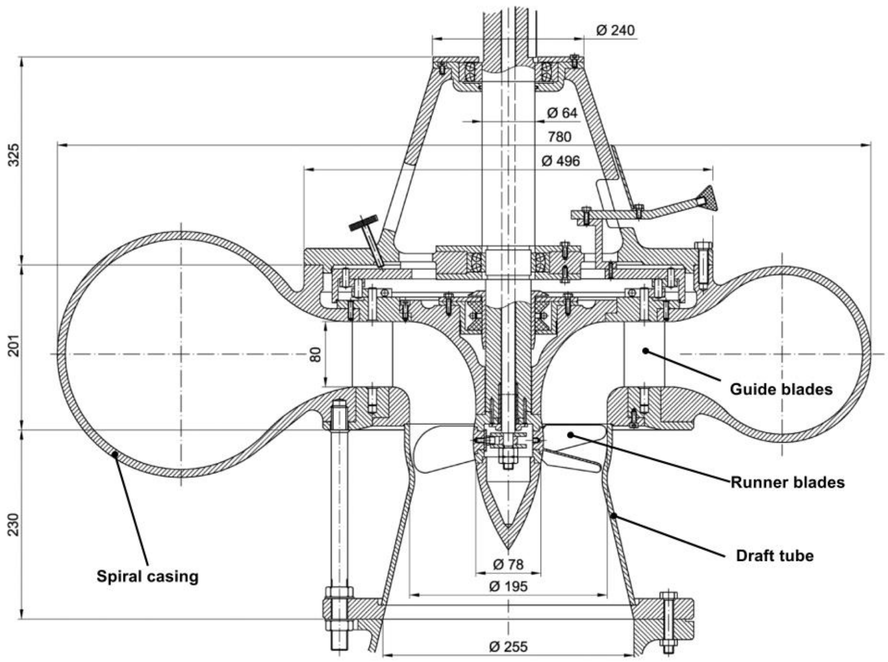

Fig. 6. – The standard 4-K-69 Kaplan turbine

Graphic extension of the program - rotor blades and guide blades

Graphic extension of the program builds on previous calculated angles β_1 and β_2 and renders in real scale longitudinal profiles of runner blades in several cross-sections. The assumption is that in case of structured flow, fluid streamlines in axial runner are distributed along cylindrical stream surfaces. The common axis of these surfaces is the axis of the turbine runner. The stream surfaces intersect runner blades in individual longitudinal profiles according MELICHAR ET AL. (1998). By stretching the particular cylindrical stream surface the flat grid of blade profiles appear, run by the flat flow field as seen in Fig. 7.

The program divides the turbine clear opening by five coaxial cylindrical cross-sections. Their diameters are shown in Fig. 4a. On the stretched cylinder surfaces thus formed are then deposited centerline profiles of the blades. The centerlines are not straight, but curved – due to different angles on the leading and trailing edge β_1 and β_2. The program calculates together with the length of the blade profile the mathematical function of the smooth transition curve between the leading and trailing edge in response to both tangents. The result of this is a centerline which is then „wrapped" by streamline airfoil that is again converted into a mathematical function. The program works with a NACA 0015 streamline airfoil from BRITO ET AL. (2002) which is, in case of need, possible to change. In the above-mentioned procedure the cross-sections of blade grids are constructed in all five cylindrical stream surfaces.

In addition to displaying the basic position of the blades, the graphic extension allows to „tilt" them to any angle. It shows the opening/closing of the turbine blades at different operating conditions. The essence of tilt consists again in mathematical description of blades profiles which the program operates with. Fig. 7 shows an example of the standard 4-K-69 turbine graphic output of a hydraulic design of runner blades in two cylindrical cross-sections – on the diameters D_4 and D_3 (see Fig. 4a). Cross-sections are displayed in a grid division of 10 mm. Based on the above-mentioned principles, the blade grid of guide blades are modelled.

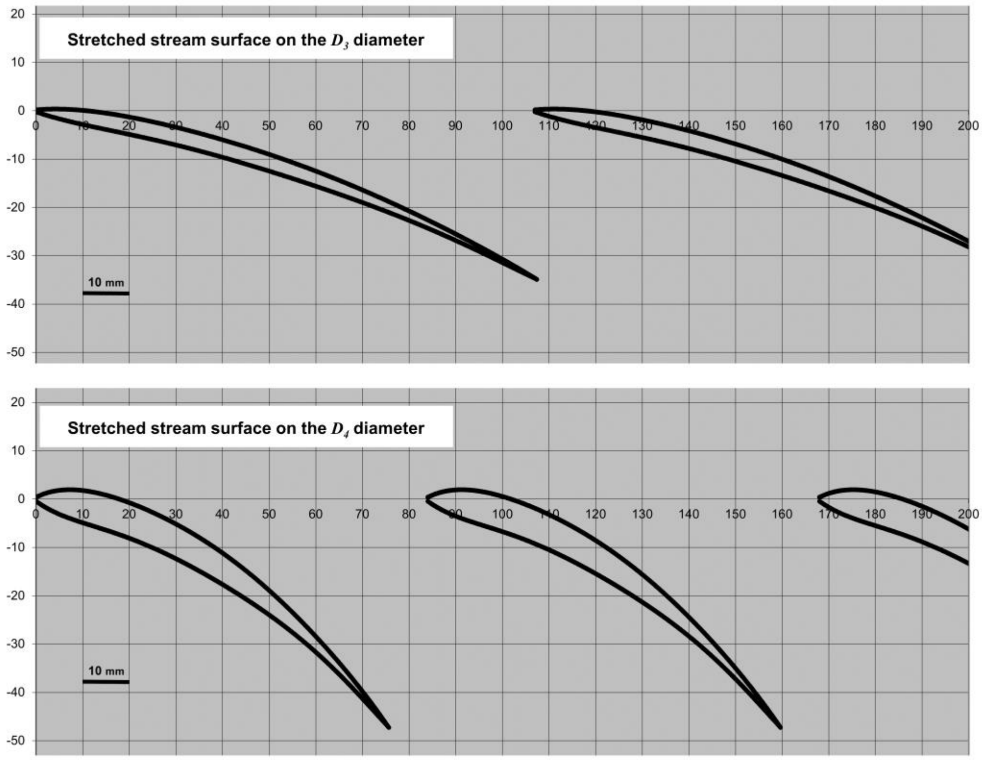

Fig. 7. – Graphic output of the program for the rotor blades design (POLÁK ET AL., 2013)

Graphic extension of the program – spiral casing

Another calculation program extension allows to solve a hydraulic profile of the spiral casing. The calculation program uses one- and two-dimensional stream theory by prof. Kaplan. Nowadays, when the use of CFD models, thanks to its flexibility, has been increasingly popular, such a procedure, based on the classical theory, seems to be a step backwards, PETIT ET AL. 2010). Nevertheless, CFD models require a specialized program and considerable demands on its operation NILSSON ET AL. (2003). These circumstances make the use of CFD model complicated and it hinders its wider usage. Therefore, the calculation program uses more available one- and two-dimensional theory. This is based on the law of constant circulation according to MUNSON ET AL. (2006), NECHLEBA (1962):

$$R_i \cdot c_{u\,i} = K \tag{10}$$

The constant K [m^2.s^{-1}] is determined by the circumferential velocity component c_{u1} on the inlet radius R_1 on the runner (see Fig. 1). On the assumption of a circular profile of a spiral, which is in practice the most common, the inner radius of the circular flow profile is given by:

$$r_i = \frac{\varphi \cdot Q}{720 \cdot \pi \cdot K} + \sqrt{2R_0 \frac{\varphi \cdot Q}{720 \cdot \pi \cdot K}} \tag{11}$$

The calculation program thus calculates total of 72 internal flow profiles over the entire circumference of the spiral casing (where φ [deg] is angular distance from inlet cross section – see Fig. 6a). In addition to numerical results, the graphic output as a radial cross-section (Fig. 8a) and transverse cross sections I - VI (Fig. 8b) is again available. This figure shows a calculated hydraulic profile of a spiral casing for the standard 4-K-69 Kaplan turbine. The indicated network shows the radial dimensions in meters and divides the spiral circumferentially of 5° to the individual calculated sections. This spiral casing is a result of using a one-dimensional stream theory which is more suitable for this case. The graphic output can be compared with the standard 4-K-69 turbine spiral casing in Fig. 8c.

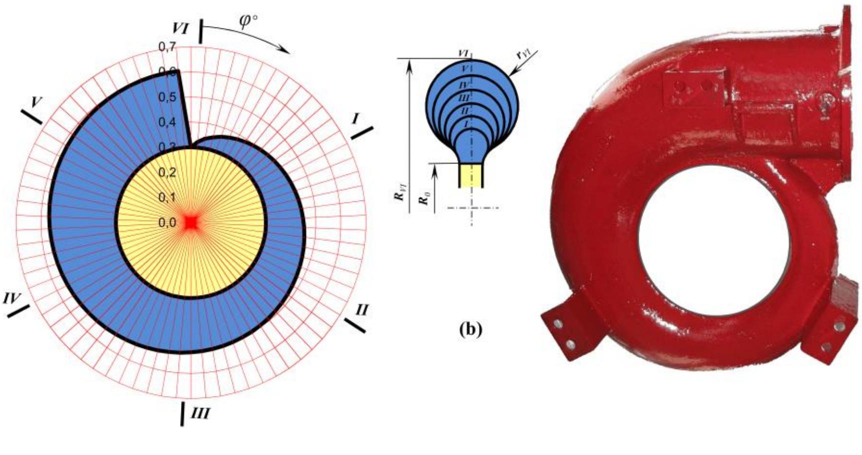

(a) (c)

Fig. 8. – Graphic output of calculation program (a, b) and real 4-K-69 turbine spiral casing (c) (POLÁK ET AL., 2013)

RESULTS AND DISCUSSION

The comparison of the runner blade geometry was chosen for a more detailed verification of calculation program results. Numerical results of the calculation program are together with the standard 4-K-69 turbine runner blade (Fig. 4b) summarized in Tab. 1.

In the left part of the table there are the angles for the blade leading and trailing edge of the β_1 and β_2 calculated by the program. In the middle part of the table there are angles of the standard 4-K-69 turbine blade β^*_1 a β^*_2. On the right there are the differences of corresponding values.

Tab. 1. – Comparison of calculated results and geometry of the standard 4-K-69 Kaplan turbine blades

Cross section D [m]	Calculated		Standard		Difference of Values	
	Leading Edge β^*_1	Trailing Edge β^*_2	Leading Edge β_1	Trailing Edge β_2	Leading Edge $\beta^*_1 - \beta_1$	Trailing Edge $\beta^*_2 - \beta_2$
D_1 = 0.195	14.2°	11.7°	14°	11°	0.2°	0.7°
D_2 = 0.166	18°	13.7°	19°	13°	-1°	0.7°
D_3 = 0.137	25.2°	16.4°	28°	17°	-2.8°	-0.6°
D_4 = 0.107	43.5°	20.6°	44°	18°	-0.5°	2.6°
D_N = 0.078	74.6°	27.3°	72°	32°	2.6°	-4.7°

Fig. 9 shows the dependence of the average angle of the blade setting $(\beta_1 + \beta_2)/2$ on the diameter of the runner, i.e. the position of each cut. The red dashed curve indicates the calculated course of middle-angle setting, the blue line is the course of real values.

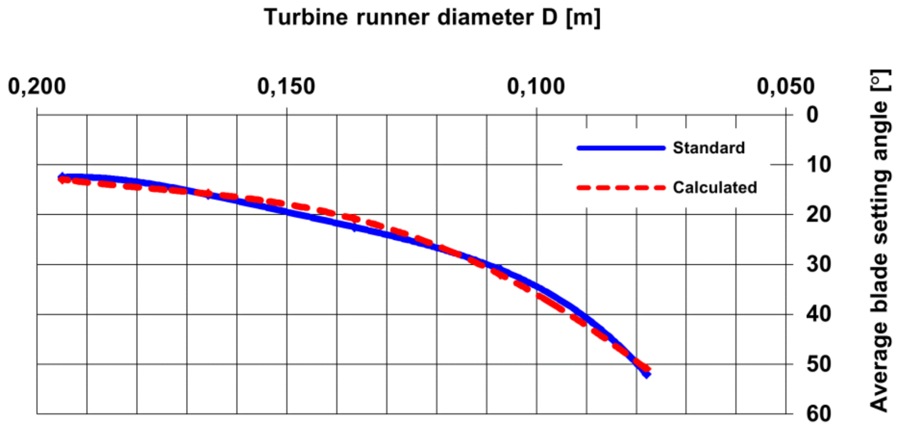

Fig. 9. – The course of the blade average setting angle across cutting surfaces

CONCLUSIONS

Tab. 1 and Fig. 9 show the comparison of calculated values and the reality of runner blade geometry. There is only one case where, in the absolute value, the difference between the calculated and actual angle is greater than 3°, i. e. 10% of the true value (the angle of the trailing edge to the diameter D_N). The difference is probably caused by other operating conditions (cavitation characteristics of runner, etc.) resulting from specific laboratory tests, which calculation program does not include.

In the case of the spiral casing, the difference between the inner diameter at the inlet into a spiral and the calculation (D_0 = 306 mm) is only 2%. As for other dimensions, the differences are not greater than 4%.

In case of other calculated parameters (main dimensions of the runner, guide blades, draft tube, suction height, width of guide blades, etc.), the differences between the calculated values and the real parameters of the standard 4-K-69 Kaplan turbine are always reliably smaller than 10% (compare the calculation protocol Fig. 5 and the turbine drawing Fig. 6).

From the point of view of used methods, the above mentioned results can be considered satisfactory. The essential advantage of the calculation program is a significant simplification of the whole process of turbine design along with graphic outputs of key parts.

Thanks to its user accessibility it is a suitable tool for designing the basic parameters of conventional blade water turbine types, especially for the low-potential hydropower resources.

ACKNOWLEDGEMENT

Supported by Internal grant agency of Faculty of Engineering, Czech University of Life Sciences in Prague no: 2015:31170/1312/3114.

REFERENCES

1. ANAGNOSTOPOULOS, JOHN S.: A fast numerical method for flow analysis and blade design in centrifugal pump impellers. In: Computers & Fluids 38, 2009: pp. 284–289, ISSN 0045-7930.
2. BAHAJ, A. S., BATTEN, W.M.J., MCCANN G.: Experimental verifications of numerical predictions for the hydrodynamic performance of horizontal axis marine current turbines. In: Renewable Energy 32, 2007: 2479–2490, ISSN 0960-1481.
3. BRADA, K., BLÁHA, J.: Method of experiments and modelling. Prague 1995, Czech Technical University in Prague, 103 pages, ISBN 80-01-01236-0 (in Czech).
4. BRITO-MELO, A., GATO, L. M. C., SARMENTO, A.J.N.A.: Analysis of Wells turbine design parameters by numerical simulation of the OWC performance. In: Ocean Engineering 29, 2002: 1463–1477, ISSN 0029-8018.
5. DATE, A., AKBARZADEH, A.: Design and analysis of a split reaction water turbine. In: Renewable Energy 35, 2010: pp. 1947–1955, ISSN 0960-1481.
6. DERAKHSHAN, S., NOURBAKHSH, A.: Theoretical, numerical and experimental investigation of centrifugal pumps in reverse operation. In: Experimental Thermal and Fluid Science 32, 2008: pp. 1620–1627, ISSN 0894-1777.
7. DRTINA, P., SALLABERGER, M.: Hydraulic turbines—basic principles and state-of-threat computational fluid dynamics applications. In: Proceedings of the Institution of Mechanical Engineers, Part C: Journal of Mechanical Engineering Science 213, 1999: pp. 85–102, ISSN 0954-4062.
8. HUTAREW, G.: Einführung in die Technische Hydraulik. Berlin, Springer-Verlag, 1973, ISBN 3-540-05979-2
9. KHAN, M. J., BHUYAN, G., IQBAL M. T., QUAICOE; J. E.: Hydrokinetic energy conversion systems and assessment of horizontal and vertical axis turbines for river and tidal applica-

tions: A technology status review. In: Applied Energy 86, 2009: pp. 1823–1835, ISSN 0306-2619.
10. MELICHAR, J., VOJTEK, J., BLÁHA, J.: Small water turbines, construction and operation. Czech Technical University in Prague, 1998, 296 p., ISBN 80-01-01808-0. (in Czech)
11. MELICHAR, J., BLÁHA, J., BRADA, K.: Hydraulic machinery – construction and operation. Prague 2002, Czech Technical University in Prague, 378 pages, ISBN 80-01-02657-4 (in Czech).
12. MUNSON, B. R., ZOUNY, D. F., OKIISHI, T., H.: Fundamentals of fluid mechanics – fifth edition, 2006, John Wiley & Sons, Inc., USA, 770 p.
13. NECHLEBA, M.: Water turbines, construction and accessories. Prague 1962, SNTL, 673 pages, (in Czech).
14. NILSSON, H., DAVIDSON, L.: Validations of CFD against detailed velocity and pressure measurements in water turbine runner fow. In: International Journal for Numerical Methods in Fluids 41, 2003: pp. 863–879, ISSN 0271-2091. DOI: 10.1002/_d.472.
15. PETIT, O., MULU, B., NILSSON, H., CERVANTES, M.: Comparison of numerical and experimental results of the flow in the U9 Kaplan turbine model. In: 25th IAHR Symposium on Hydraulic Machinery and Systems, IOP Conf. Series: Earth and Environmental Science 12, 2010: DOI: 10.1088/1755-1315/12/1/012024.
16. POLÁK, M.: The issue of the use of low-potential energy of water resources. Habilitation thesis. Czech University of Life Sciences Prague, Prague 2013a (in Czech).
17. POLÁK, M. ET AL.: Bladeless miniturbine – the path to energy recovery of the smallest water resources. Czech Technical University Publishing House, Prague 2013b: 168 p. ISBN 978-80-01-05233-4 (in Czech).
18. POLÁK, M., POLÁK, V.: Introducing a practical model for turbines´ designing in small hydropower plants, In: Trends in Agricultural Engineering 2010 – book of abstracts. CULS Prague, 2010: p. 482 - 487. ISBN 978-80-213-2088-8
19. SUTIKNO, P., ADAM, I. K.: Design, Simulation and Experimental of the Very Low Head Turbine with Minimum Pressure and Free Vortex Criterions. In: International Journal of Mechanical & Mechatronics Engineering, Vol: 11, No: 01 9 113701-2828 IJMME-IJENS, February 2011.
20. TRIVEDI, C., CERVANTES, M., J., DAHLHAUG, O. G.: Experimental and Numerical Studies of a High-Head Francis Turbine: A Review of the Francis-99 Test Case. In: Energies 2016, 9, 74. ISSN 1996-1073.
21. ULRYCH, E.: Applied hydromechanics I (basics of hydropower). Praha 2007, Faculty of Engineering of the CULS in Prague, 126 pages, ISBN 978-80-213-1609-6. (in Czech).

Corresponding author:
doc. Ing. Martin Polák, Ph.D., Department of Mechanical Engineering, Faculty of Engineering, Czech University of Life Sciences Prague, Kamýcká 129, Praha 6, Prague, 16521, Czech Republic, phone: +420 22438 3183, e-mail: karel@tf.czu.cz

CENTRIFUGAL PUMP IN TURBINE MODE FOR SMALL HYDROPOWER

Z. Poláková, M. Polák

Department of Mechanical Engineering, Faculty of Engineering, Czech University of Life Sciences, Czech Republic

Abstract
In order to minimize investment costs when setting up small hydropower plants, pumps in reverse turbine mode are used in some cases. However, small pump units in turbine mode show decrease of overall efficiency compared to pump efficiency. The article describes innovative design changes, which reduce this negative effect. The proposed changes were verified in a hydraulic testing circuit with the following results: modifications of the existing pump design showed an increase in the efficiency by several percent, significantly increased power output and shaft torque. The best results were achieved with a new turbine runner geometry: efficiency increased by 12,5%, torque by 48% and power output by nearly 29%.

Key words: efficiency, hydraulic profile, modification, pump as turbine, runner blade.

INTRODUCTION

Many localities with low potential of hydropower resources remain unexploited. Frequent reasons include high initial costs with long payback period for investors. In terms of investment in small hydropower plants the most expensive part is water engine (turbine). Thus, there is a need for such technical solutions that would be acceptable to investors. One possibility is the use of hydrodynamic pumps as turbines (PAT). The free flow space between the blades of runner of hydrodynamic engines enables reversibility of energy transformation. In pumps, input mechanical energy changes into hydraulic energy, whereas in turbines incoming hydraulic energy changes into mechanical energy. BLÁHA, ET AL. (2012) given the offer on the pumps market, these relatively inexpensive and reliable devices, that are even in terms of maintenance and service often more advantageous than conventional turbine supplied "on demand", should be taken into consideration. Some practical experiences with PAT are known and have been described in reference literature SIGH ET AL. (2012); ALATORE (1994); DERAKHSHAN ET AL. (2008); NAUTIYAL ET AL. (2011); RAMAN ET AL. (2013); POCHYLÝ ET AL. (2013).

In some cases, when the pump is operated in PAT mode, efficiency is an issue. In case of large machines, the efficiency of both pump and turbine mode is the same or comparable and therefore could be predicted from the known pump efficiency. However, small pumps have lower efficiency in turbine mode. Moreover, the rate of decrease in efficiency can be different for different engines. The question therefore is how to determine efficiency, or rather, how to eliminate its decrease. Some simple improvements of pumps for turbine mode have already been tested and are described in SIGH (2005) and SIGH ET AL. (2012), however more detailed information on this issue in the research literature is still missing.

MATERIALS AND METHODS

For the research of pumps operating in turbine mode, a single-stage centrifugal pump with spiral casing was selected in order to verify its specific design modifications. The pump outline including its characteristics is shown in Fig. 1. This is a specific low-speed pump with specific speed $n_{qp} = 24$ min^{-1}, runner outer diameter $D_1 = 132$ mm. The optimum in pump mode for pump speed $n_p = 1450$ min^{-1} corresponds to: flowrate $Q_p = 3.54$ l.s^{-1}; water head $H_p = 5.85$ m; power input $P_p = 0.33$ kW; overall efficiency $\eta_p = 62.5$ % (see Fig. 1).

The essence of individual improvements made on the pump consists mainly in reducing hydraulic losses. These modifications include improvement of the runner geometry and of immediately connected zones, i.e. the zones of input, flow and output of fluid from the runner. For example, for a pump with similar specific speed the flow analysis in both pump and turbine mode is provided in SEDLÁŘ ET AL. (2009).

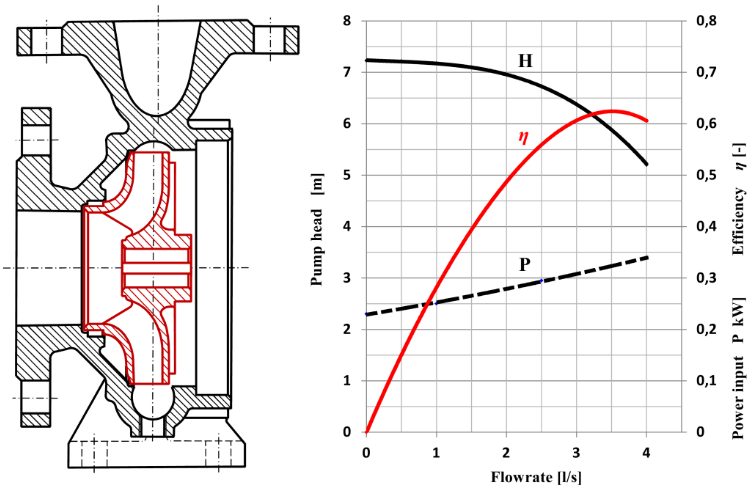

Fig. 1. – Centrifugal pump for testing in turbine mode

The idea for individual construction improvements, mainly the modification of the geometry of runner blades, results from the theory of radial Francis turbine design according to MUNSON ET AL. (2006); NECH LEBA (1962); NECHLEBA ET AL. (1966); ULRYCH (2007); HÝBL (1928); MELICHAR ET AL. (1998); POLÁK ET AL. (2010). The results served as basis for improvements, respectively for manufacturing a prototype, mainly the runners. Additional improvements relating to the reduction of hydraulic losses during reverse flow through the pump resulted from the technical documentation and experience described in SIGH (2005) and POLÁK (2013). All proposed design improvements were subsequently tested experimentally on the hydraulic circuit in the Laboratory of Fluid Mechanics at the Faculty of Engineering (Czech University of Life Sciences Prague). Fig. 2 shows the hydraulic circuit outline for pump testing in turbine mode.

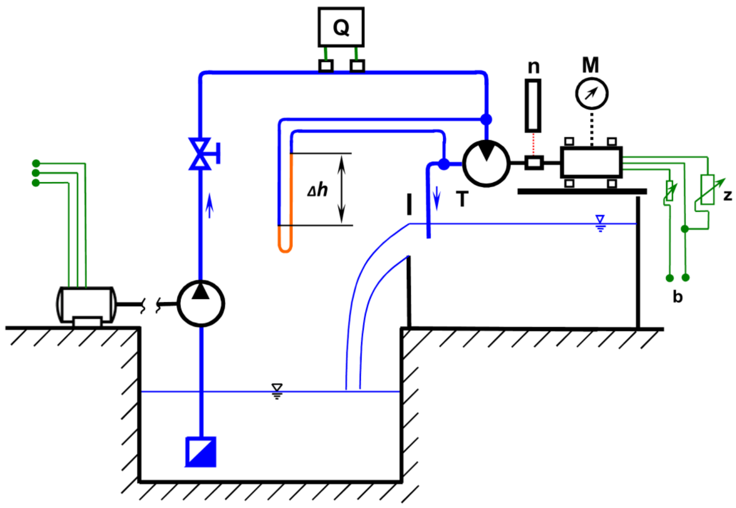

Fig. 2. – Hydraulic circuit for testing of pumps in turbine mode

Q – flowmeter, T – pump in turbine mode, M – dynamometer (shaft torque measuring), n – revolution counter, b – excitation of dynamometer, z – resistance load of dynamometer.

The testing circuit consists of a water reservoir with a pump that generates hydraulic potential for the tested turbine (T), or more precisely pump in turbine mode. The turbine is connected to the dynamometer with a stator placed on a bed allowing a slight rotation, which enables a measurement of the reaction torque (M) at load. Dynamometer is a DC engine connected to continuous resistance load control unit (z). The flow of water through the turbine is measured by the ultrasonic flowmeter Siemens SITRANS

FUP1010 (Q), which was calibrated by using the volumetric tank method, before measurement. The specific energy of the turbine is determined on the basis of the flowrate Q_T and the differential pressure of the U-tube mercury manometer (Δh), connected to the pipe by collecting probes. The scheme for pressure collection for gauging in the 1st precision class is in accordance with the ČSN EN ISO 9906 (2013) and HODÁK (1982). The revolutions of the turbine shaft were measured by a contactless infrared sensor.

Fig. 3. – Connection of the turbine in testing circuit

The following parameters were monitored during the turbine tests: differential pressure determined by level difference Δh [m], flowrate Q_T [m^3.s^{-1}], turbine shaft speed n_T [min^{-1}] and the shaft torque on the dynamometer M_T [N.m]. From these parameters, additional values necessary for the graphical characteristics of the turbine were then calculated.

Based on the measured values, the specific energy gained by the turbine Y_T [J.kg^{-1}] is given by the equation:

$$Y_T = \frac{\rho_{Hg}}{\rho_w} \cdot \Delta h \cdot g + \frac{v_i^2 - v_o^2}{g} + g \cdot y \qquad (1)$$

Where ρ_{Hg} [kg.m^{-3}] is mercury density, ρ_w [kg.m^{-3}] is water density, v_i, v_o [m.s^{-1}] is water velocity in inlet and outlet pipe, respectively and y [m] is vertical distance of zones generating pressure. The power of the fluid gained by the turbine (the power input) P_w [W]is given by:

$$P_W = \rho_W \cdot Q_T \cdot Y_T \qquad (2)$$

The power output of the turbine is determined from the shaft revolutions n_T [min^{-1}] and the shaft torque M_T:

$$P_T = M_T \frac{\pi \cdot n_T}{30} \qquad (3)$$

The overall efficiency of the turbine is:

$$\eta_T = \frac{P_T}{P_W} \qquad (4)$$

RESULTS

The characteristics of the original non-modified pump were first tested in turbine mode in the hydraulic circuit. On the same testing circuit and under the same conditions, different types of modifications of the pump were then tested, their mutual combinations and also new geometries of runner blades. From all tested options the following four modifications were selected for evaluation:

- **I.** Non-modified original pump – illustrated by blue double-line curves in the characteristics on Fig. 4 and Fig. 5.
- **II.** Original pump with modified runner. The modification consisted of changes reducing local and friction losses – yellow curves.
- **III.** Original pump with modified runner (see modification II.), and modified spiral casing. The purpose of the modification was to reduce hydraulic losses – brown curves.
- **IV.** Original pump with original runner, but with modified blades length and modified spiral casing (modification of the spiral casing is the same as in modification III.) – black dashed curves.
- **V.** Pump with new geometry of runner blades and modified spiral casing (modification of the spiral casing is identical to III. and IV.) – green double-line dashed curves.

Measurements were carried out in the way that, by constant opening of the throttle valve, the turbine was gradually loaded from idle speed up to 900 or 800 rpm. In this way, uniform conditions were set up for all tested options so that the results are mutually comparable.

The diagrams in Fig. 3 and 4 provide a summary of the measured characteristics for the above described modifications I – V, i.e. efficiency, power output, shaft torque and flowrate, depending on unit speed:

$$n_{11} = \frac{n_T \cdot D_1}{\sqrt{Y_T}} \qquad (5)$$

Given the possibilities of the testing circuit, where the hydraulic potential for the turbine is created by a centrifugal pump, measurements did not take place under constant water gradient. Therefore the course of the net water gradient depending on unit speed revolutions is in addition also specified here.

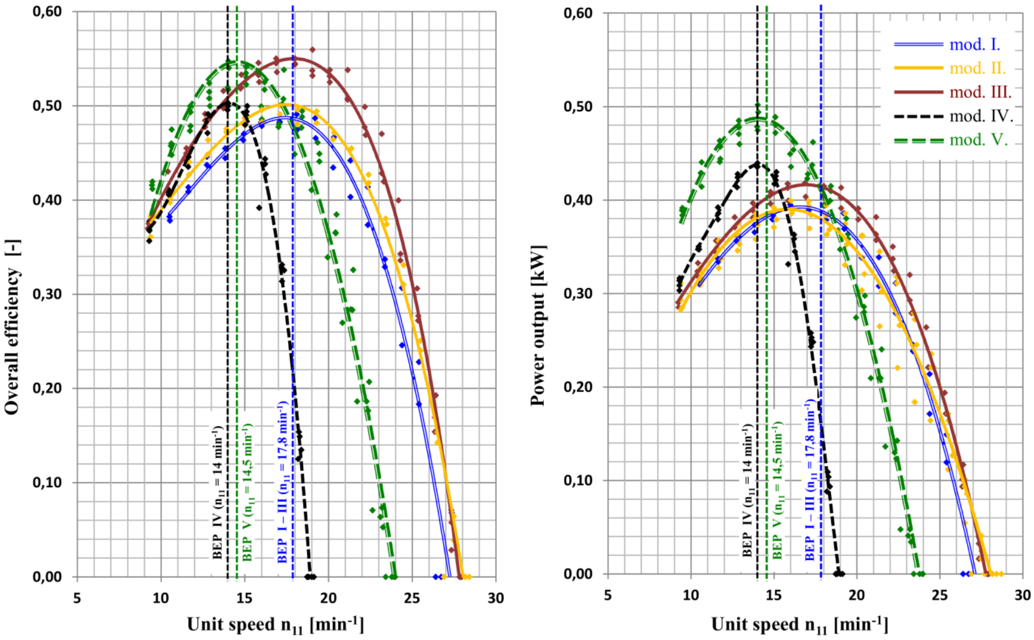

Fig. 4. – Efficiency and power output depending on unit speed

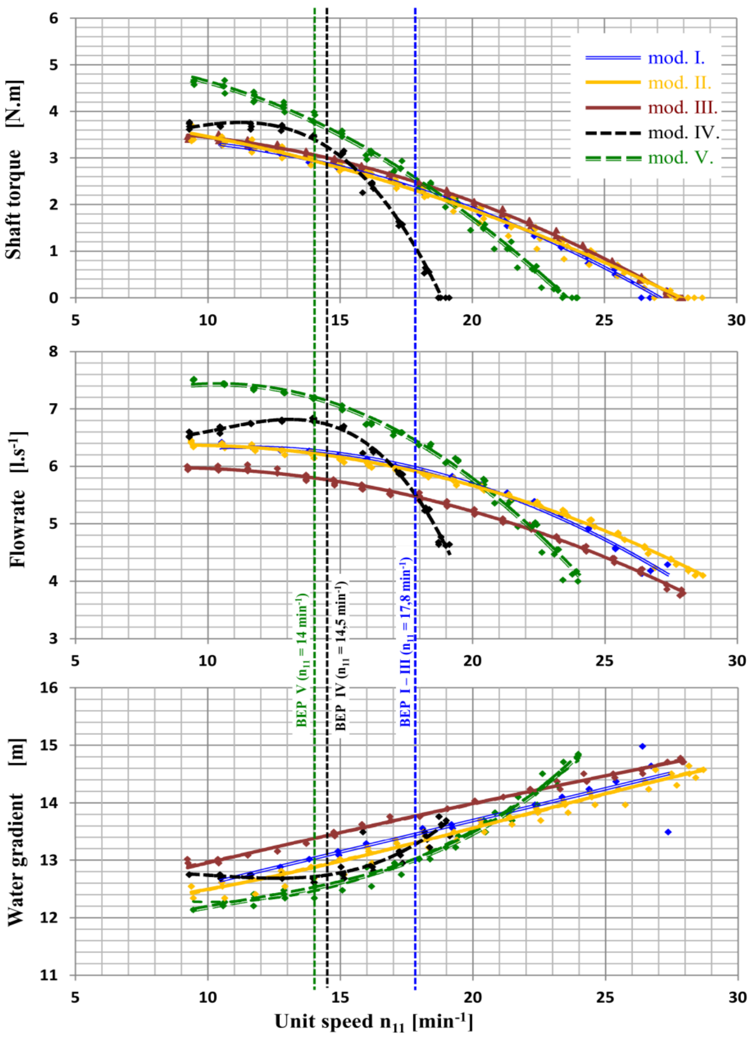

Fig. 5. – Water gradient, flowrate and shaft torque depending on unit speed

On the basis of the above mentioned characteristics, the following table (Tab. 1) explicitly summarizes the results obtained for each modification. These are the parameters of the turbine reached at the highest efficiency – in the characteristics indicated as BEP (Best Efficiency Point).

Tab. 1. – Absolute values of the parameters in turbine mode (BEP)

Modification	η_T [%]	P_T [W]	M_T [N.m]	Q_T [l.s^{-1}]	H_T [m]
I.	48	380	2.5	6.0	13.5
II.	50	390	2.4	6.0	13.4
III.	55	400	2.6	5.5	13.8
IV.	50	440	3.5	6.8	12.7
V.	54	490	3.7	7.2	12.6

The following table (Tab. 2) shows clearly the results achieved by each modification and quantifies the increase of the observed parameters. The proportional increase of each parameter is always related to the modification I, i.e. non-modified original pump. The increase is calculated as follows:

$$\Delta x_n = \frac{x_n - x_I}{x_I} \cdot 100 \qquad (6)$$

Where x_n is absolute values (η, P, M_T, Q a H) for options II. up to V and x_I is absolute values (η, P, M_T, Q a H) for modification I.

Tab. 2 - Proportional increase of parameters in turbine mode (BEP).

Modification	$\Delta\eta_T$ [%]	ΔP_T [%]	ΔM_T [%]	ΔQ_T [%]	ΔH_T [%]
II.	4.2	2.6	-4.0	0.0	-0.7
III.	14.6	5.3	4.0	-8.3	2.2
IV.	4.2	15.8	40.0	13.3	-5.9
V.	12.5	28.9	48.0	20.0	-6.7

DISCUSSION AND CONCLUSIONS

The pump used in the tests has in pump mode a maximum efficiency of $\eta_č$ = 62.5% (manufacturer's data). However, the same engine operated in reverse turbine mode shows the highest efficiency only η_T = 48%. That means a relative fall of 23.2% related to the pump efficiency. If the pump is modified in order to reduce hydraulic losses during reverse liquid flow, it is possible to achieve a proportional increase in efficiency by $\Delta\eta_T$ = 14.6% (see modification III), the shaft torque increasing by 4% and the turbine output by 5.3%.

For comparison – in a research on this issue in Germany at the University of Karlsruhe [8], comparable modifications with similar type of engine (n_q = 36.4 min^{-1}, D_1 = 174 mm) led to an increase of efficiency by a maximum of $\Delta\eta$ = 4.7% and power output by approx. ΔP = 3.4%. For the remaining seven pumps of similar size and specific speed (n_q = 24.5 ÷ 79.1 min^{-1}) mentioned in [8], the achieved efficiency increase was only about $\Delta\eta$ = 1.3%. It therefore highly depends on the engine individual constructional design, and mainly, on the precision of the performed modifications.

The modifications of the runner blades also give various results. Even though the modification of their length shows efficiency increase by only 4.2% (modification IV), the shaft torque increases by 40% and the power output of the engine by 15.8%. In this respect, the best results are achieved by a runner with completely new blades geometry (modification V). In this case efficiency increases by 12.5%, shaft torque by 48% and the performance by nearly 29%. Moreover, the engine shows an additional plus – it reaches these parameters at lower water gradient in comparison with the other modifications. The reason for this is a greater throughput of the runner which is manifested by an increased flowrate ΔQ_T = 13.3% or 20%.

When deciding about possible modifications of the pump for turbine mode, it is therefore necessary to take into consideration the purpose of the modifications – whether it is primarily to increase efficiency, or if the aim is to maximize energy production. An optimal solution is a combination of both, i.e. partial improvements to reduce hydraulic losses along with a new runner blades design. This option contains the greatest potential – both for the user and in terms of further research.

REFERENCES

1. ALATORRE-FRENK, C.: Cost minimization in microhydro systems using pumps-as-turbines, [Ph.D. Thesis], University of Warwick, 1994.
2. BLÁHA, J.; MELICHAR, J.; MOSLER, P.: Contribution to the use of hydrodynamic pumps as turbines. In: Energetika 5/2012. ISSN 0375-8842 (in Czech).
3. ČSN EN ISO 9906: Hydrodynamic pumps - Acceptance tests of hydraulic performance parameters - Degrees accuracy of 1, 2 and 3, ČSNI 2013 (in Czech).
4. DERAKHSHAN, S.; NOURBAKHSH, A.: Theoretical, numerical and experimental investigation of centrifugal pumps in reverse operation. In: Experimental Thermal and Fluid Science 32 (2008) 1620–1627, Elsevier. ISSN 0894-1777.
5. HODÁK, T. A KOL.: Utilization of hydropower (Instructions for exercise) SVŠT, Bratislava, 1982 (in Slovak).
6. HÝBL, J.: Water engines I, II, III, Czech Technical Institute in Prague (in Czech).
7. MELICHAR, J., VOJTEK, J., BLÁHA, J.: Small hydro turbines, construction and operation. ČVUT Praha 1998, 296 s., ISBN 80-01-01808-0 (in Czech).
8. MUNSON, B. R, ZOUNY, D. F., OKIISHI, T., H.: Fundamentals of Fluid Mechanics – Fifth edition, 2006, John Wiley & Sons, Inc., USA, 770 s.
9. NAUTIYAL, H., VARUN, KUMAR, A., YADAV, S.: Experimental investigation of centrifugal pump working as turbine for small hydropower systeme. In: Energy Science and Technology, Vol. 1, No. 1, 2011: 79-86. ISSN 1923-8479.
10. NECHLEBA, M.: Water turbines - their design and accessories, 2nd Edition, SNTL Praha 1962, 673 s. (in Czech).
11. NECHLEBA, M.; HUŠEK, J.: Hydraulic machines, SNTL Prague, Prague 1966, 388 s. (in Czech).
12. POCHYLÝ, F., HALUZA, M., RUDOLF, P., HABÁN, V., KLAS, R., HUDEC, M., HIMR, D., STEJSKAL, J.: Mutual cooperation SIGMA GROUP, Inc. Lutin, SIGMA RDI, Ltd. Lutin and the Department of Fluid Engineering of V. Kaplan FSI in Brno in research pumps. In: Current trends pumping equipment - Proceedings of the scientific-technical conference, Sigma Group a. s. Lutín, 2013. ISBN 978-80-905478-0-3. (in Czech)
13. POLÁK, M.; POLÁK, V.: Application of the theory of physical similarity in calculation program for the design of hydraulic turbines. In: Jemná mechanika a optika 10/2010. Přerov 2010. str. 281-284, ISSN 0447-6441. (in Czech)
14. POLÁK, M.: The issue of energy utilization of low-potential water sources. CULS Prague, Prague 2013. [hab. thesis] (in Czech).
15. RAMAN, N., HUSSEIN, I., PALANISAMY, K., FOO, B.: An experimental investigation of pump as turbine for micro hydro application. In: Proceedings of 4th International Conference on Energy and Environment 2013 (ICEE 2013), IOP Conf. Series: Earth and Environmental Science 16 (2013) 012064.
16. SEDLÁŘ, M., ŠOUKAL, J., KOMÁREK, M.: CFD analysis of middle stage of multistage pump opereting in turbine regime. In: Engineering MECHANICS, Vol. 16, No. 6, 2009: p. 413–421
17. SINGH, P.: Optimization of internal hydraulics system design for pumps as turbinek with Field Implementation and Evaluation, [PhD thesis], Universität Fridericiana, Karlsruhe 2005.
18. ULRYCH, E.: Applied hydromechanic I - Basic of hydropower, Powerprint s.r.o. Prague, 2007: 126 s. ISBN 978-80-213-1609-6. (in Czech).
19. SINGH, P.; NESTMANN, F.: Internal hydraulic analysis of impeller rounding in centrifugal pumps as turbines. In: Experimental Thermal and Fluid Science 35, 2011: 121–134, ISSN: 0894-1777.

Corresponding author:

Mgr. Zuzana Poláková, Department of Mechanical Engineering, Faculty of Engineering, Czech University of Life Sciences Prague, Kamýcká 129, Praha 6, Prague, 16521, Czech Republic, phone: +420 22438 3177, e-mail: polakovaz@tf.czu.cz

APPROXIMATE TEST OF THE THERMAL DEGRADATION OF ENGINE OIL

J. Pošta, B. Peterka

Department for Quality and Dependability of Machines, Faculty of Engineering, Czech University of Life Sciences Prague, Czech Republic

Abstract
Engine oils are one of the most stressed operating fluids of combustion engines. European manufacturers of combustion engines are creating degradation models of engine oils taking into account the operational conditions of each of vehicle. The engine oil is checked and changed on the base of these models. For stationary working gas engines of cogeneration units, these models are not fully suitable. This kind of combustion engines has very high requirements on the quality of engine oils, especially on the thermo-oxidative stability. Modern oils with high portion of additives are commonly used. In this case, tribodiagnostic does not serve as predictive utility, but serves as confirmation of properly chosen service period of engine oil.
Experiment was set to prove the possibility of evaluation of thermo-oxidative degradation of synthetic, hydrocracked and mineral oils. The change of colour, caused due to high temperature and presence of air, was chosen as evaluation criteria. The aim of article was to set time course of colour changes. This paper presents results for synthetic, hydrocracked and mineral oils.

Key words: engine oil, thermo-oxidation, colour changes, image analysis.

INTRODUCTION

Engine oils are one of the most stressed operating fluids of combustion engines. Operating conditions are more difficult and requirements for engine oils are ever growing. European manufactures of engine oils are involved in searching of optimal service period of engine oils replacement. Manufacturers are creating degradation models of engine oils taking into account the operational conditions of each of car type. The engine oil is checked and replaced on the base of these models.
Combustion engines are also used in very different applications. Then, the operation condition of combustion engine is very different than in a vehicle. In those cases, the engine oils degradation models used for cars are not fully suitable, so it is necessary to seek for more suitable models. Such as gas combustion engines of cogeneration units of biogas plants are continuously working 24 hours per day while high load and constant speed. This operating conditions result in thermal stress of engine oil, which is also exposed to acid products mainly created from sulphurous parts of biogas combustion process. This operational mode has extremely high requirements on engine oils, especially on their thermo-oxidative stability. Therefore, high quality and high additive containing oils belonging to Group II and Group III are most used. The need to replace oil filling is relatively soon in case of those oils. According to engine type, the service period is in range of 500 to 2000 operating hours. The engine has to be stopped due to oil change. Engine oil and oil filters are changed and the centrifugal cleaner must be cleaned.
In most of bio-gas stations, the change of engine oil is controlled such that small sample of used oil is taken and subjected to tribological analysis. This analysis is commonly done in independent and accredited laboratory. Based on analysis results and taking into account the content of sulphur in biogas obtained during simplified operation monitoring, the service period is appropriately changed. Thus applied tribotechnical diagnostic is not predictive in nature and only serves as feedback of the accuracy of estimated time of oil change.
MACHALIKOVA ET. AL. (2013) states, that detonation level of engine oil can be determined using comparative differential spectroscopy of original oil and degraded oil. Therefore, it is possible to relatively compare the content of oxidative, nitrating and sulphating products, water content, fuel content, coolant content and decrease of content of anti-oxidation additives. Due to both temperature stress and water in oil leakage, the exhaustion of base anti-wear and anti-oxidative additives occurs. The oil change is recommended in case of decrease of the content below 20% compared to content of additives in new oil.
Spectroscopy analysis uses complex equipment. Result of analysis is available in relatively long time and operation itself is relatively expensive. Therefore, it

would be useful to have at least approximate method for easy, fast and inexpensive evaluation of change of operating conditions of given oil. This would enable correction of real operational time in particular operating conditions.

It is known that the degradation process of engine oil, which will require its change, pass in different ways in case of various types of engine oils. As an example CERNY (2005) states that exploited oil keeps lubricating and load-carrying capacity can be even higher as effect of polar oxidation products formed while machine operation. Waste oil has to be changed for other reasons than lubricity loss. Waste oils contain, in most cases, mechanical wear particles and lot of soot particles in case of diesel engines. Petrol engines oils can be excessively oxidative deteriorated and they may effect significantly corrosion, etc. SVOBODA (2015) states that lubrication of oil is crucial in term of boundary friction. But CERNY (2015) also states that while oil oxidation there are created numerous oxidation products, i.e. while nitrification organic nitrates are formed. These substances have polar character and affect positively on carrying-load capacity of lubricating film and lubricity of oil in general. On the other side during operation there is loss of synthetic antiwear and friction modifiers additives which act also as antioxidants. The final effect is that intensity of oil lubricity degradation after decrease of additives concentration is faster.

NOVACEK (2013) states that transition of actual oils from Group I to Group II and III was accompanied with general changes in oil composition. New generation of oils mentioned above deteriorate another way as traditional oils. Nonlinear degradation of most of modern lubricants is determined by antioxidants additive selection and oxidation stability of base oils belonging to Group II and III. This base oils show lower oxidation stability than Group II and III. This kinds of oils deteriorate rapidly when they lose antioxidant additives. As consequence, most of standard oil analyses gives none of alert when the oil begins deteriorate or exhibit oil deposits.

It is obvious, that thermo-oxidation of engine oil in initial stages does not mean a significant risk of lubricity loss. As the thermo-oxidation process continues, the oxidation products are polymerising and creating strongly adhesive deposits that could affect function of combustion engine. Increasing content of polymerised oxidation products in engine oil is accompanied by a change of colour of engine oil – oil darkening.

VUTAN HIEN (2016) states that change in colour can be evaluated by image analysis of spot that engine oil will leave on the filtration membrane. The coloured spot can be obtained either by filtering of specified amount of oil or by dropping the oil onto filtration paper.

Partial influence of permanent thermal stress on the process of darkening of engine oil was experimentally proved. Results of this experiment are described in this article.

MATERIALS AND METHODS

Materials

Experiment was performed using mineral oil Group I, hydrocracked oil Group II and synthetic oil Group III. Base technical parameters of tested engine oils are shown in Tab. 1.

Mineral oil under test is declared as oil with low content of sulphated ash intended for use in stationary gas engines and for use in engines without turbocharger.

Hydrocracked oil under test is declared as oil with mid-range content of sulphated ash, without content of Zn, intended for use in all types of stationary gas engines.

Synthetic oil under test is declared as oil without content of Zn, containing very low sulphur and phosphor content, intended for use in diesel engine equipped with a turbocharger, engines of commercial vehicles and engines equipped with exhaust gas treatment.

Methods

Engine oil samples of volume 80 ml were kept at temperature 132°C (±3°C) for 382 hours. At 24 hour interval the drop of oil from each of particular sample was dropped in the centre of Macherey-Nagel MN 1640w filtration paper. After next 12 hours was the resultant colour spot digitized by scanner to TIF file with 24 bit of colour depth and 1200 dpi resolution.

Evaluation of images was performed in Zoner Photo Studio software. The evaluated area was taken as centred circle of 500 pixels in diameter. Using the Advanced histogram function, the evaluation in RGB colour space was performed for each of additive primary colours. Intensity and colour distribution for each of luminosity (intensity), red (R), green (G) and blue (B) components was obtained.

Tab. 1. – Base technical parameters of tested engine oils

Properties	Units	Mineral oil	Hydrocracked oil	Synthetic oil	Standard
SAE classification	-	40	---	5W-30	SAE J300
Density at 15°C	$kg.m^{-3}$	893	866	861	DIN 51 757
Flash point	°C	240	260	238	DIN ISO 2592
Pour point	°C	-15	- 35	- 45	DIN ISO 3016
TBN	$mgKOH.g^{-1}$	5.5	8.9	---	DIN ISO 3771
Sulphate ash	% hm.	0.45	0.7	0.99	DIN 51 575
Kinematic viscosity at 40°C	$mm^2.s^{-1}$	149	105.00	71.8	DIN 51 562-1
Kinematic viscosity at 100°C	$mm^2.s^{-1}$	14.5	13.40	12.16	DIN 51 562-1

In RGB colour space model each pixel can be represented as combination of three colours (RGB), while intensity of each component ranges from 0 to 255. With this system, 16,777,216 (256^3) discrete combinations of R, G and B values are specified.

For the RGB model, this is represented by a cube using non-negative values within a 0–255 range, assigning black to the origin at the vertex (0, 0, 0), and with increasing intensity values running along the three axes up to white at the vertex (255, 255, 255), diagonally opposite black.

A colour histogram of an image represents the distribution of the composition of colours in the image. It shows different types of colours appeared and the number of pixels in each type of the colours appeared.

Fig. 2 show examples of luminance histogram and colour histograms of all RGB colour components for one particular colour spot of oil under test.

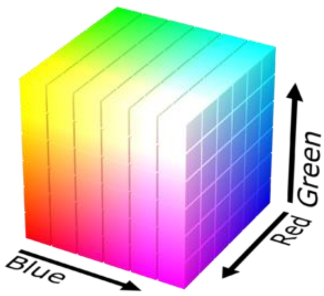

Fig. 1. – RGB colour model

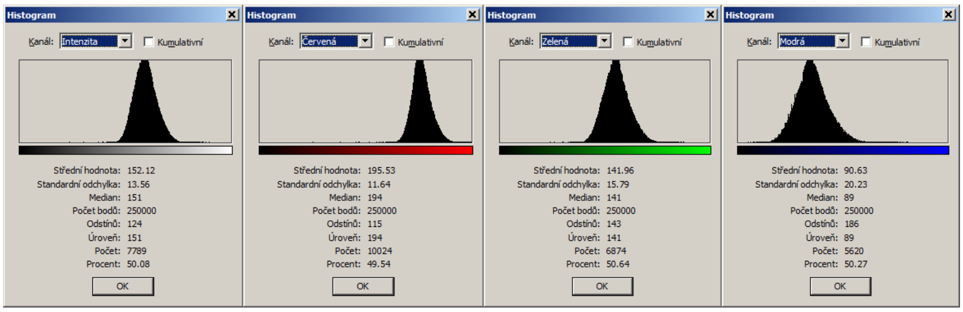

Fig. 2. – Example of histograms

RESULTS

Results of image analysis of synthetic oil Group III, hydrocracked oil Group II and mineral oil Group I are shown in Fig. 4, Fig. 5 and Fig. 6 respectively.

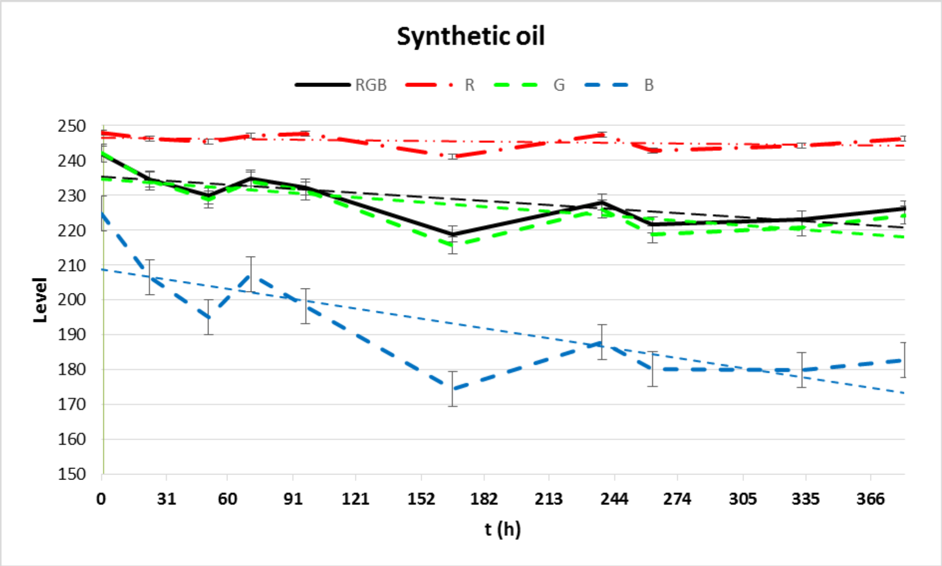

Fig. 3. – Intensity of RGB components of spot picture of synthetic oil Group III, error bars shown for each graph

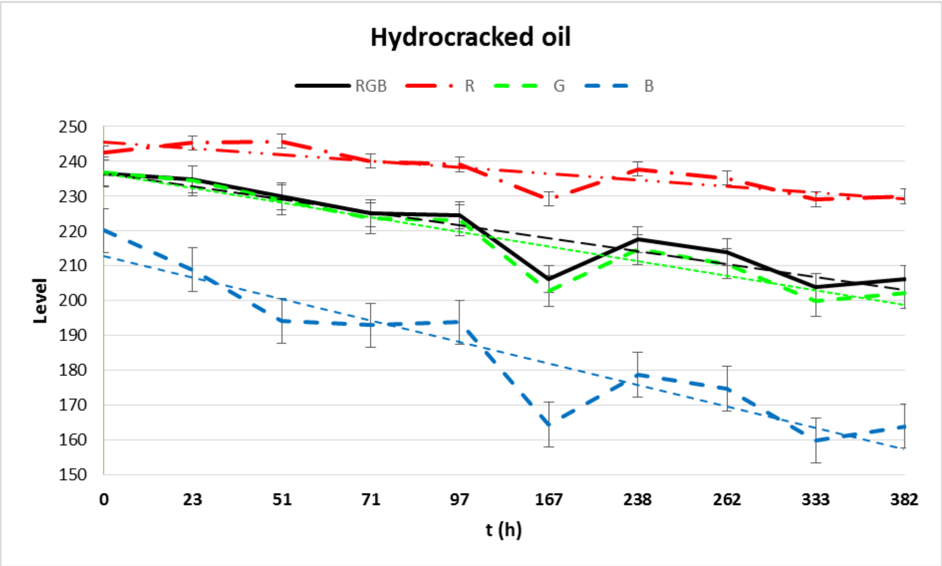

Fig. 4. – Intensity of RGB components of spot picture of hydrocracked oil Group II, error bars shown for each graph

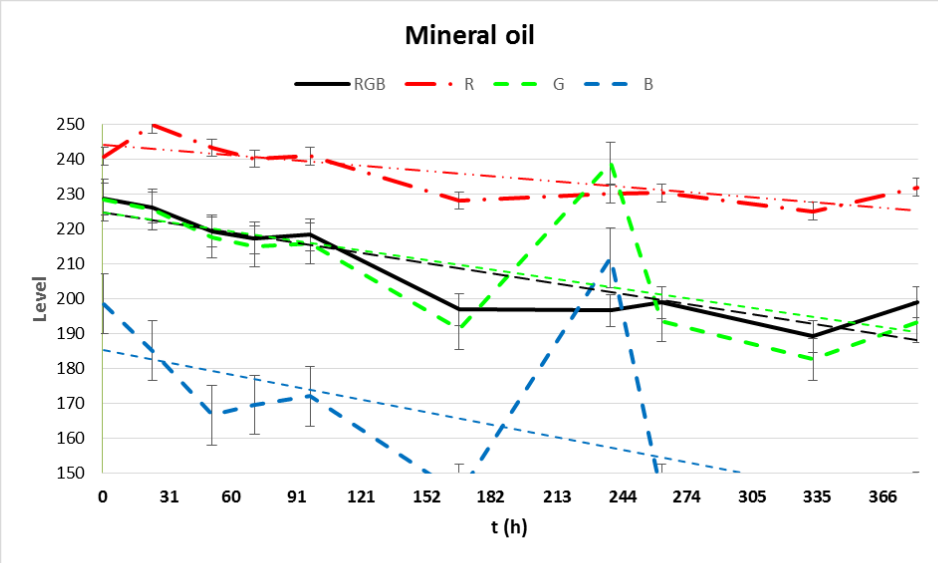

Fig. 5. – Intensity of RGB components of spot picture of mineral oil Group I, error bars shown for each graph

DISCUSSION

As NOVACEK (2013) states, degradation of almost all of modern lubricants depends on additives selection and on oxidation stability of base oil as well. Oxidation stability of base oils of Group II and Group III is naturally worse than Group I so, when this oils lose antioxidant additives, they deteriorate rapidly. As consequence, most of standard oil analyses gives none of alert when the oil begins degraded or exhibit oil deposits.

In case of synthetic oil Group III with high anti-oxidation additive content, it can be expected that degradation will rise very slowly at the beginning and will rise very progressively when all of additives are exhausted. In case of hydrocracked oil Group II which is also highly doped with anti-oxidation additives, similar behavior can be expected. In case of mineral oil Group I with naturally better anti-oxidation properties and lower content of additives, linear progression of degradation can be expected from the beginning of operating time.

Experimental results correspond with these assumptions. Progress of thermo-oxidation process characterized by colour changes of oil when other influences are omitted, corresponds with statements of NOVACEK (2013), CERNY (2015) and MACHALIKOVA ET AL. (2013)

Progression of degradation of synthetic oil, Fig. 3, corresponds to expected slow degradation rate at the beginning of operating time. Therefore, we can assume that in this particular case, the content of anti-oxidation additives was not exhausted. Progression of degradation of hydrocracked oil, Fig. 4, is from the beginning of operating time relatively faster as is in case of hydrocracked oil Group III with high content of additives, but degradation rate is slight. Progression of degradation of mineral oil, Fig. 5, is faster from the beginning of operating time than in case of hydrocracked and synthetic oil.

CONCLUSIONS

It is obvious, that initial stages of thermo-oxidation process of engine oils do not pose significant risk of loss of lubricity. In case of modern engine oils which are massively highly doped with anti-oxidation additives, the degradation is determined by content of this additives. Degradation rate of this kind of oils is slow at the beginning of operating time, but it can be indirectly monitored as colour change of oil compared to his initial colour.

Experimentally obtained rate of thermo-oxidation which is expressed as change of colour (darkening) during experiment was 4.1% in case of Group I, 8% in case of hydrocracked oil Group II and 10.3% in case of mineral oil. These findings can serve for development of degradation models of engine oils of biogas combustion engines.

ACKNOWLEDGEMENT

This proceeding originated within the project of long time development of IGA CULS Prague 2016: 31190/1312/3117 Effect of mixtures of biofuels on production of nitrogen oxide and smoke of combustion engine during NRSC.

REFERENCES

1. ČERNÝ, J.: Mazací schopnost motorového oleje. In: Autoexpert, Vol. 10, 6/2005, p. 36, ISSN1211-2380, Available from <https://www.oleje.cz/imgs/articles/524-2_AutoEXPERT_Mytus_8.pdf>, (in Czech)
2. ČERNÝ, J. 2015: The properties of motor oils - Oxidation stability, nitration oil. Oleje-cz, [21.03.2016]. Available from <http://www.oleje.cz/clanek/Vlastnosti-motorovych-oleju---Oxidacni-stabilita—nitrace-oleje>, (in Czech)
3. MACHALÍKOVÁ, J., SEJKOROVÁ, M., LIVOROVÁ, M.: Aplikace instrumentálních metod v analýze provozních hmot pro dopravní prostředky. In: Scientific papers of the University of Pardubice. Series B, The Jan Perner Transport Faculty. 18 (2012), ISSN: 1211-6610, dostupné na http://hdl.handle.net/10195/54099, 2013 (citováno dne 25.4.2016), (d:\Downloads\MachalikovaJ_AplikaceInstrumentalnich_2013.pdf)
4. NOVÁČEK, V., NOVÁK, J. 2013: A new approach to monitoring oil condition. In: Tribotechnika, Vol. VI., No. 6/2013, pp. 26 - 28, ISSN 1338-0524, Available from <http://www.tribotechnika.sk/rocnik-2013.html>, (in Czech)
5. SVOBODA, P., ET AL.: Lubrication film formation at start-up of smooth surfaces [online]. DOI: 10.17973/MMSJ.2015_12_201529 [07.03.2016]. Available from <http://www.mmscience.eu/december-2015.html>
6. VUTAN HIEN: The selected properties mineral and synthetic oils. Diplomová práce. ČZU v Praze, Technická fakulta, Praha, 2016, 90 s., (in Czech).

Corresponding author:

prof. Ing. Josef Pošta, CSc., Department for Quality and Dependability of Machines, Faculty of Engineering, Czech University of Life Sciences Prague, Kamýcká 129, Praha 6, Prague, 16521, Czech Republic, phone: +420 22438 3266, e-mail: posta@tf.czu.cz

ADVANCED CONSTRUCTIONS OF RADIATION CONCENTRATORS FOR PHOTOVOLTAIC SYSTEMS (REVIEW)

V. Poulek[1], M. Libra[1], A. Khudysh[2]

[1]Department of Physics, Czech University of Life Sciences Prague, Faculty of Engineering, Prague, Czech Republic,
[2]SOLEX-R. Ltd., Ryazan, Russia

Abstract
Different constructions of low concentration photovoltaic (LCPV) systems were designed and tested in our laboratory. The bifacial PV panels were used. Results are presented in the article. The electric energy production was increased by up to +167% in the case of pseudo parabolic concentration system in comparison with standard fixed PV panels. In summer, the operating temperature of PV panels was round about +95°C. The polysiloxane gel lamination technology was used to prevent degradation of the PV cells encapsulation and reliability troubles.

Key words: radiation concentrator, PV cell, bifacial PV panel, polysiloxane gel.

INTRODUCTION

Although the price of PV panels was reduced many times within last decade, the price of photovoltaic energy remains still high. Advanced PV systems with radiation concentrators are constructed. This is the way how the price could be reduced. So we have decided to design LCPV systems with bifacial PV panels. Bifacial PV cells were manufactured by the Solar Wind Company in Krasnodar, Russia. All systems use polar axis tracking system (POULEK AND LIBRA, 1998). Flat plate glass/glass bifacial PV panels for pseudo parabolic concentrator systems were laminated by the polysiloxane gel technology (POULEK ET AL., 2012). Three Low Concentration PV (LCPV) systems using bifacial flat plate PV panels based on monocrystalline silicon were developed in cooperation of the Czech university of Life Sciences Prague and SOLEX-R, Ltd., (Ryazan, Russia). Basic parameters of the LCPV systems are summarized in the Tab. 1.

Tab. 1. – Parameters of LCPV systems with bifacial PV panels

Concentrator	Number & power of PV panels	Bifacial cells size and layout	Operation temperature of PV panels	GCR	Bifacial ratio of PV cells front/back (%)	Energy gain	Lamination
Ridge (TRAXLE)	14 x170 W	125x125 mm^2 6 x 12	55°C	1.5	100/50	+72%	Glass/EVA/TPT
Pseudo parabolic I (TRAXLE)	4 x170 W	125x125 mm^2 6 x 12	95°C	4.1	100/60	+167%	Glass/silicone gel/Glass
Pseudo parabolic II (SOLEX-R)	2x175 W	125x62,5 mm^2 10 x 14	96 °C	3.6	100/65	+114%	Glass/silicone gel/Glass

Ridge concentrators with bifacial PV panels

The ridge concentrator with Geometrical Concentration Ratio GCR=1.5 (POULEK AND LIBRA, 2000) was developed to avoid troubles with V-trough concentrators (GCR=2). Fig. 1 shows scheme of the ridge concentrator. There is high wind induced torque by V-trough concentrators, which can destroy gearbox of the tracker. But there is low wind induced torque by ridge concentrators, because external mirrors were eliminated. Additionally the overheating of PV panels is substantially reduced by ridge concentrators, in comparison to V-trough concentrators (NANN, 1991; ANDERSON, 2013; TANG AND LIU, 2011). While summer operating temperatures of PV panels at ridge concentrators are below 70°C the temperature of panels at V-trough concentrators are above 95°C. The operating temperature +85°C is strict limit for all EVA laminated PV panels. There is no warranty above the operation temperature +85°C and lifetime of PV panels is substantially reduced.

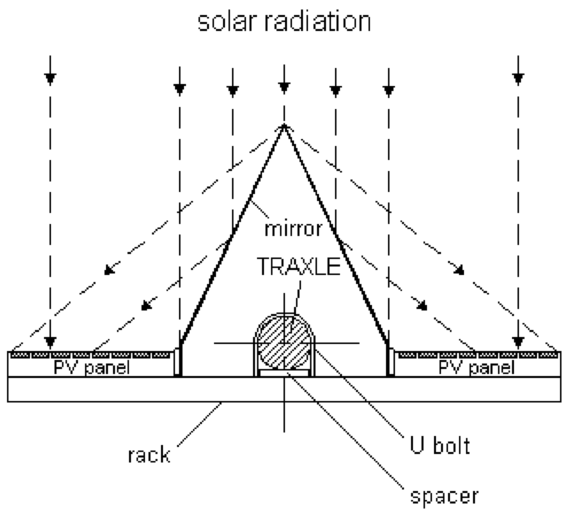

Fig. 1. – Scheme of the tracking ridge concentrator

The ridge concentrator was further improved using bifacial PV panels. The bifacial PV panels yield about +7% higher energy harvest because of additional albedo energy collected at the rear surface and because of reduced temperature of the panels. The bifacial panels are transparent for the infrared radiation above the wavelength 1100 nm so the operating temperature of bifacial panels is reduced by about 3÷7°C in comparison with standard monofacial PV panels.

Several ridge concentrator systems with bifacial PV panels were installed in the Czech Republic and Russia including the 0.5 MW_p PV plant. The energy harvest of the ridge concentrator systems with bifacial PV panels is enhanced by about +72% in comparison with standard fixed PV systems.

Fig. 2 shows energy production of the tracking ridge concentrator with bifacial PV panels in comparison with energy production of standard fixed panels during a sunny day. Fig. 3 shows our ridge concentrators with bifacial PV panels (0.5 MW_p PV power plant).

Pseudo parabolic PV concentrators with bifacial PV panels

The energy gain of ridge concentrator +72% or V-trough concentrator about +90% is not very high. So we have developed pseudo parabolic PV concentrators with bifacial PV panels with geometrical concentration ratio GCR= 3.6 and GCR= 4.1 respectively.

The first variant of pseudo parabolic concentrator with bifacial PV panels was developed in cooperation of the Czech University of Life Sciences Prague (CULS) and TRAXLE Solar Company.

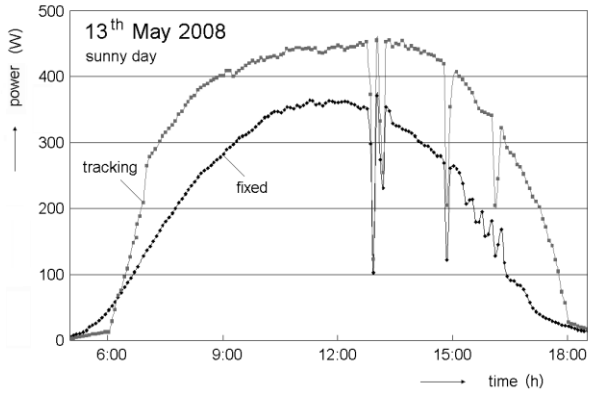

Fig. 2. – Time dependence of the power output of the tracking ridge concentrator with bifacial PV panels in comparison with standard fixed PV panels. The areas below the respective curves represent energy gain of the PV systems.

Fig. 3. – The tracking ridge concentrators with bifacial PV panels (0.5 MW_p PV power plant)

The bifacial PV panels were arranged parallel to the tracking axle and perpendicular to the solar radiation. Fig. 4 shows the scheme and Figs. 5÷6 show the photograph of the tracking concentrator. Although the bifacial PV panels transparent for infrared radiation have been used the temperature of the PV panels have been above +90°C during summer months at noon. The design of PV panels was similar to standard flat plate ones using 6x12 bifacial mono-Si PV cells sized 125x125 mm^2. But glass/glass design of the panel with silicone gel lamination was used instead of glass/EVA/TPT design. The silicone gel encapsulant will last many years at temperature +250°C. The energy gain +167% (in comparison with fixed standard PV panels) was measured. No degradation like yellowing/browning or delamination of the polysiloxane gel encapsulant was observed.

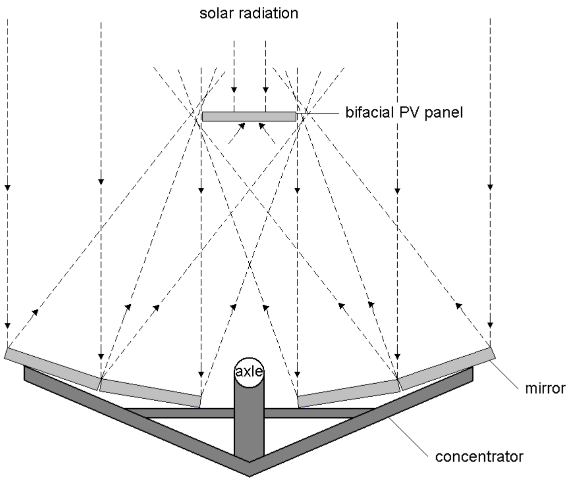

Fig. 4. – Scheme of the 1st variant of the pseudo parabolic concentrator with bifacial PV panels

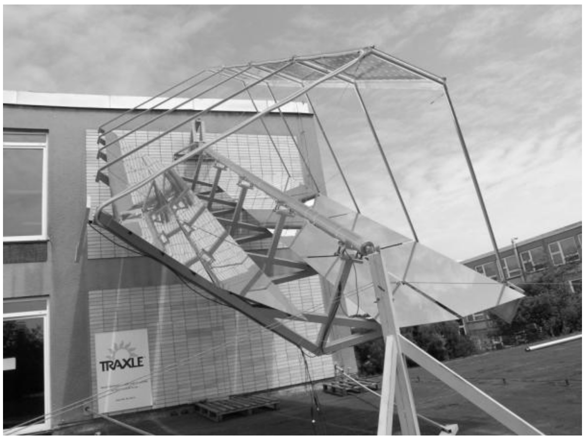

Fig. 5. – Pseudo parabolic concentrator TRAXLE with bifacial PV panels fixed to the building of CULS in Prague

Fig. 6. – Detail of the concentrated solar radiation

The second variant of pseudo parabolic concentrator design with bifacial PV panels was developed at the SOLEX-R Company in Ryazan, Russia (POULEK ET AL., 2015). The bifacial PV panels were arranged parallel to the tracking axle and parallel to the solar radiation. The design of PV panels was similar to standard flat plate ones using 10x14 bifacial mono-Si PV cells sized 125x62.5 mm^2. Fig. 7 shows the scheme and Fig. 8 shows the photograph of the concentrator. The temperature of bifacial PV panels was above +95°C in summer. So this design have to use silicone gel lamination of glass/glass PV panels otherwise the high temperature could cause reliability troubles. The energy gain +114% (compared to fixed standard PV panel) was measured.

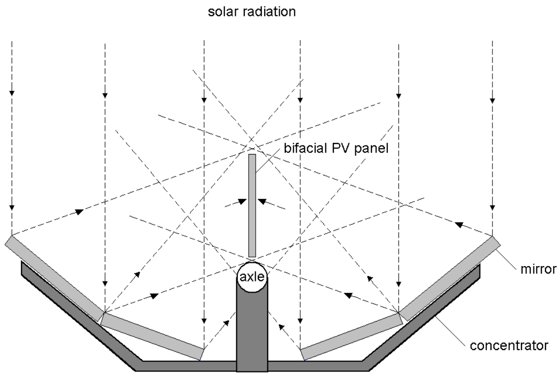

Fig. 7. – Scheme of the 2nd variant of the tracking pseudo parabolic concentrator with bifacial PV panels

Fig. 8. – Photograph of the 2nd variant of the tracking pseudo parabolic concentrator with bifacial PV panels in Ryazan

CONCLUSIONS

Three variants of tracking PV concentrators have been developed using bifacial solar panels. Silicone gel laminated bifacial panels were successfully tested in pseudo parabolic concentrator systems. Energy gain up to +167% was measured. Further improvements of the pseudo parabolic LCPV design are under development. Active cooling system will be introduced as well as advanced bifacial solar cells with front/back efficiency ratio 100/90. The energy gain can reach more than +200% in comparison to standard fixed PV panels.

REFERENCES

1. POULEK, V., LIBRA, M.: New solar tracker. Solar Energy Materials and Solar Cells, 51, 2, 1998: 113-120.
2. POULEK, V., LIBRA, M.: A New Low Cost Tracking Ridge Concentrator. Solar Energy Materials and Solar Cells, 61, 2, 2000: 199-202.
3. POULEK, V., STREBKOV, D.S., PERSIC, I.S., LIBRA, M.: Towards 50 years lifetime of PV panels laminated with silicone gel technology. Solar Energy, 86, 10, 2012: 3103–3108.
4. POULEK, V., KHUDYSH, A., LIBRA, M.: Innovative low concentration PV systems with bifacial solar panels. Solar Energy, 120, 2015: 113-116.
5. NANN, S.: Potentials for tracking photovoltaic systems and V-troughs in moderate climates. Solar Energy, 45, 1991: 385-393.
6. ANDERSON, T.N.: Natural convection heat transfer in V-trough solar concentrators. Solar Energy, 95, 2013: 224-228.
7. TANG, R., LIU, X.: Optical performance and design optimization of V-trough concentrators for photovoltaic applications. Solar Energy, 85, 2011: 2154-2166.

Corresponding author:

Ing. Vladislav Poulek, CSc., Department of physics, Faculty of Engineering, Czech University of Life Sciences Prague, Kamýcká 129, Praha 6, Prague, 16521, Czech Republic, tel: +420 22438 3288, email: poulek@tf.czu.cz

COMPARISON OF THREE SETS OF DRIVE TRACTOR TYRES WITH RESPECT TO TRACTION PROPERTIES

R. Pražan[1], J. Čedík[1], I. Gerndtová [1], J. Neřold[1], M. Pexa[2]

[1]*Research institute of Agriculture Engineering, Drnovská 507, 161 01, Prague 6, Czech Republic;*
[2]*Czech University of Life Sciences, Faculty of Engineering, Department for Quality and Dependability of Machines, Czech Republic*

Abstract
The paper deals with comparison of three types of tractor tyres with same proportions 600/65 R38 from the producer Mitas (IF and VF tyres and PneuTrac prototypes). The tyres are made from different blends and have different structure which allows operation at lower inflation pressure. The comparison is based on tyre footprints, specific pressure and traction properties of the tyres. The inflation pressure was determined according to values recommended by the producer for a given load (3650 kg). The inflation pressure was 160 kPa for IF tyres, 100 kPa for VF tyres and 60 kPa for prototype tyres PneuTrac. The dependence of the slip on the tractive force was measured in order to compare the traction properties. Results show that the prototype tyres PneuTrac with the inflation pressure 60 kPa made the largest footprints and had the most favourable traction properties.

Key words: tyres, traction properties, Very High Flexion tyre, tyre footprint.

INTRODUCTION

Tyres with higher demands on operation are used increasingly in agriculture. Main features of the tyres include higher load at lower inflation pressure which reduces negative impact on soil and positively affects the traction properties.

The traction properties of tyres, especially dependence of the tractive force or the traction coefficient on wheel slip, influence the tractive efficiency and the fuel consumption. Increasing slipping of the wheel causes increase of the fuel consumption and decrease of the traction efficiency. The traction properties depend on the load and soil conditions such as humidity, type of soil or hardness of the surface (ABRAHÁM ET AL., 2014; AHOKAS & JOKINIEMI, 2014). The traction properties also depend on parameters of the tyres (SCHREIBER & KUTZBACH, 2008; DABROWSKI ET AL., 2006) especially on the inflation pressure (NORÉUS & TRIGELL, 2008). In case of frictional soil the traction force primarily depends on normal load while in case of cohesive soil the traction force primarily depends on the overall size of the contact area (WONG & HUANG, 2006). Šmerda & Čupera (2010) claim that reduction of the inflation pressure from 180 to 65 kPa causes increase of the traction coefficient from 0.66 to 0.74.

The main negative impact of tyres moving on the agricultural land is its compaction. The compaction causes changes in bulk density, porosity, air and water capacity. Therefore it limits water infiltration, reduces retention capacity of the soil, accelerates its erosion and increases soil resistance (GŁĄB, 2014; CHYBA ET AL., 2014; CHYBA ET AL., 2013; SYROVÝ ET AL., 2013; HŮLA ET AL., 2011). High degree of soil compaction negatively affects crop yields depending on the type of crop (ARVIDSSON & HÅKANSSON, 2014; KUTH ET AL., 2012; BRAUNACK ET. AL., 2006).

The structure of tyres for agriculture focuses mainly on reducing inflation pressure and increasing the contact area of the tyre and the surface while maintaining the load and maximum speed limit (ČEDÍK & PRAŽAN, 2015).

The inflation pressure is one of the main parameters affecting work of the tyres, especially the traction properties (LYASKO, 2010). The increasing inflation pressure causes that the area of footprint reduces and the pressure on soil increases especially in the centre of the tyre (MOHSENIMANESH & WARD, 2010). On the contrary, the decreasing pressure under 80 kPa causes that the pressure at the tyre edges increases and it is concentrated in a smaller area (SYROVÝ ET AL., 2013). Maximum pressure applied on the soil may be more than two times greater than the specific pressure calculated from the footprint area and the load (LAMANDÉ AND SCHJØNNING, 2011A, B, C). Therefore it is desirable to achieve evenly distributed pressure at low inflation of the tyres. The contact pressure in the area of contact of the tyre and the surface affects mainly topsoil and upper subsoil layers (0.3 m), stress at deeper layers reflects the tyre overall load (LAMANDÉ & SCHJØNNING, 2011B).

The contact area of the tyre and the surface may be calculated by means of mathematical models based on commonly observable parameters such as the diameter and the width of tyres, the inflation pressure etc. and also by means of different empirically determined coefficients (PALANCAR ET AL., 2001; MCKYES, 1985).

The aim of the paper is to compare the traction properties and the footprint areas of three sets of tyres made by the manufacturer Mitas, with proportions 600/65 R38, which differ in used material blend and structural design of the tyre. The manufacturer determined significantly different inflation pressure at the same load for each set of tyres.

MATERIALS AND METHODS

Three types of tyres with proportions 600/65 R38 were selected for the measurement. The tyres differ in structure and used material blend. The following types of tyres were selected: IF – Improved Flexion, these tyres were used as reference tyres; VF – Very High Flexion, these tyres have more flexible structure mainly due to used material blend and different structure; PneuTrac – tyre prototypes. Regarding current tyres and mainly the VF tyres, the most exposed part during the operation is the sidewall which bends considerably due to currently used low inflation pressures in the area of contact of the tyre and the surface. This entails higher demands on the structure, manufacturing accuracy and used materials. At the same time it can be said that this structure of the sidewall and materials is limiting because the current trend in the agriculture continues to use tyres with lower inflation pressure. Change of the sidewall structure may enable reduction of pressure and achievement of larger tyre footprints.

This footprint is extended mainly in the length, in the track direction. The above mentioned change of the sidewall structure is applied to the measured prototype tyres PneuTrac and its shape is depicted in Fig. 1. Sidewalls of this tyre have a V shape in the cross-section of the tyre. This special structure of the sidewalls is deformed inwards and enables operation of tyres at even lower inflation pressure in comparison with currently best commercial tyres, i.e. VF tyres. It can be said that the tread of the tyre partially behaves like a belt.

Measurement of the tyre footprints was carried out in laboratory conditions at a constant load of 3650 kg and at the pressure which was recommended by the manufacturer for each tyre. The inflation pressure for the IF tyres was 160 kPa, 100 kPa for the VF tyres and 60 kPa for the prototype tyres PneuTrac.

Measurement of traction properties of the tyres was carried out on the property of the agricultural cooperative Rosovice ((latitude 49.7410817°N, longitude 14.1392356°E) with the average altitude 411 m.a.s.l., the land slope was within 2°. The surface consisted of a barley stubble field ploughed by a disc harrow to a depth of 120 mm. The measurement was carried out by means of a tractor John Deere 6150 R with the rated power 125 kW, with IPM 97/68EC, with the front axle ballasted with a weight 900 kg and with a weight 1800 kg placed at the rear three-point hitch. The overall weight of the braked tractor was 8910 kg.

Fig. 1. – Prototype tyres PneuTrac mounted on tractor John Deere 6150 R

New Holland 8770 tractor with the rated power 141.7 kW and with IPM 97/68EC was used as the braking tractor; its front axle was loaded with a weight 880 kg. The overall weight of the braking tractor was 8930 kg. Portable scales Haenni WL 103 (accuracy ±20 kg) were used for weighing the tractors. The wheel slip was measured by the incremental rotary encoder SICK DKS 40 with 360 pulse/rev and the radar RDS K/TGSS/MK (accuracy - $< \pm$ 3% for 0.5-3 km.hr^{-1} $< \pm$ 1% for 3-70 km.hr^{-1}. The traction force was measured by HBM U10M force transducer with a nominal load 120 kN and the position of the set was determined by the GPS receiver Qstarz BT-Q1000X. All data were stored on the hard disk of the measuring computer HP mini 5103 with a frequency of 5 Hz by means of the analog-to-digital converter LabJack U6 and the I/O module for pulse sensors Papouch Quido 10/1. Rolling circumference of each set of tyres was measured by means of the measuring tape. Before the actual measurement was carried out, the real driving speed of both tractors was measured at each individual gear and at the rated engine speed.

The ground speed of 10 km/h was set for the measurement. Such speed corresponds to the common work operations in the field. Measuring of each set of tyres was carried out for seven different traction forces made by the braking tractor. The wheel slip of the tractor was measured during driving on the stubble. Altogether 8 sections were set for the test drives, each section was 25 m long with a gap of 10 m between the sections. One section provided data necessary for calculation of one measurement point at a given setting of the braking tractor. This setting was identical for all variants of measured tyres. Between the individual sections, in so called "gap", there was a change of the traction force and stabilization of conditions (breaking force) for the next measured section. The traction force was changed due to downshift of the braked tractor. The rear axle drive with a differential lock turned on was used during the measurement.

Samples were taken in order to determine the measurement conditions, i.e. the type of soil and soil moisture. The evaluation of granularity of the soil samples proved presence of particles with diameter smaller than 0.01 mm in the range from 23.31% to 28.58%. According to the granular analysis (ČSN 46 5302) there was medium, sandy loam soil (according to the Novak granular scale), in lower layers 150 – 300 mm there was sandy loam soil to loamy soil. Content of sandy fractions prevailed over fine dust particles to the depth of 150 mm. The soil was loose, well friable, with coherent clods. The soil moisture was determined by the actual content of water in the soil. The soil moisture depending on the depth of taken sample is presented in the Fig. 2. The soil is marked as parched on the surface (0-50 mm) and as dry in other layers. The soil moisture was determined by means of gravimetric analysis.

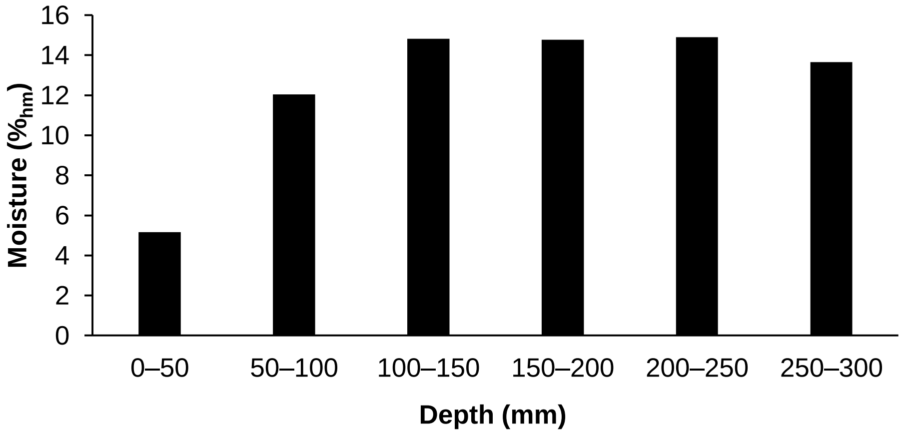

Fig. 2. – Soil moisture

RESULTS AND DISCUSSION

Fig. 3 depicts areas of tyre footprints at load 3650 kg and at manufacturer´s recommended inflation pressure for this load. It can be seen that the tyre Mitas VF600/65 R38 has a 28 % larger footprint area and the tyre Mitas 600/65 R38 PneuTrac has a 49 % larger footprint area than the referential tyre Mitas IF 600/65 R38.

Tab. 1 shows results of the tyre footprints measurement. It is evident that the specific pressure is 32.3% lower in case of Mitas VF tyre and 37.33% lower in case of Mitas PneuTrac tyre than in case of the standard tyre Mitas 600/65 R38. Deflection is higher for Mitas VF and Mitas PneuTrac than for standard Mitas 600/65 R38 which proves usage of more flexible blend. Lateral stiffness is significantly higher in case of Mitas PneuTrac tyre than in case of standard Mitas 600/65 R38 and Mitas VF.

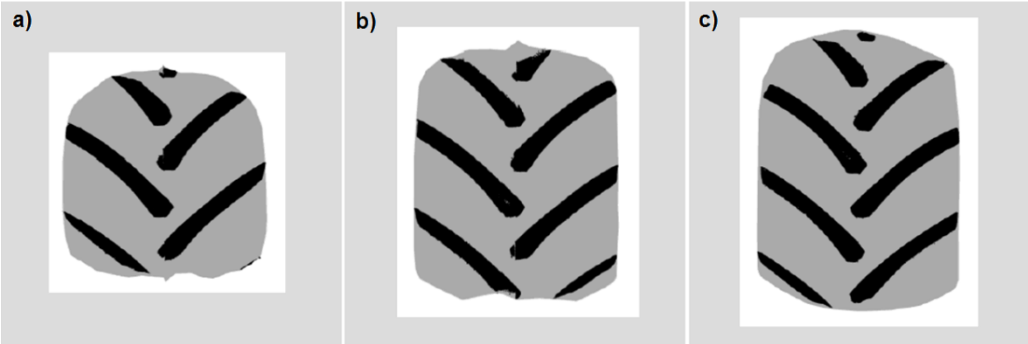

Fig. 3. – Tyre footprints (a – Standard Mitas IF tyre 600/65 R38, b – Mitas VF tyre 600/65 R38, c – Mitas PneuTrac tyre 600/65 R38)

Tab. 1. – Results of the tyre footprints

		Mitas IF 600/65 R38	Mitas VF600/65 R38	Mitas 600/65 R38 PneuTrac
Inflation pressure	kPa	160	100	60
	(%)	100	62.50	37.50
Deflection	(mm)	102	140	152
	(%)	100	137.25	149.02
Footprint	(cm^2)	2584	3299	3557
	(%)	100	127.67	137.65
Ground pressure	(kPa)	139	108	101
	(%)	100	77.70	72.66
Lateral stiffness	(daN/mm)	19	31	65
	(%)	100	163.16	342.11

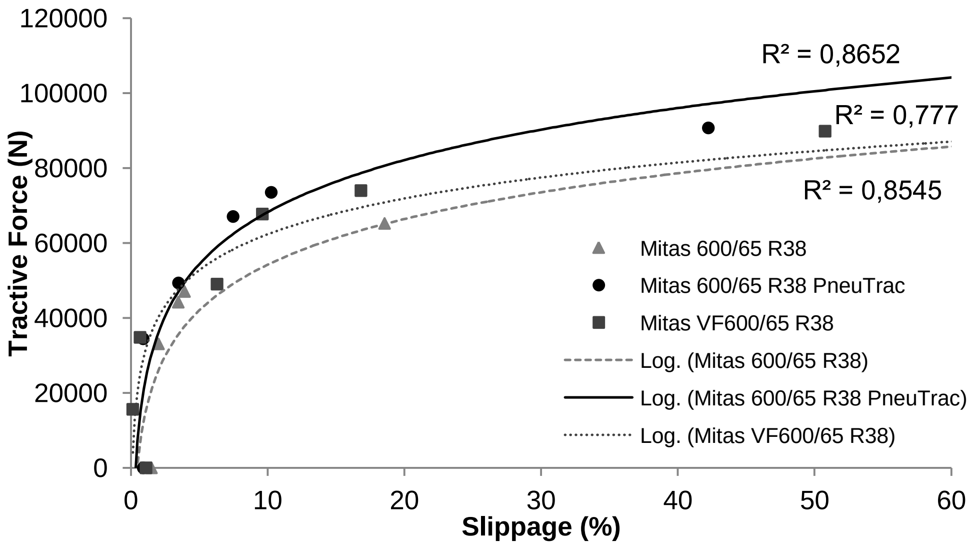

Fig. 4. – Dependence of tractive force on rear tyre slip

Fig. 4 shows dependency of the tractive force on the rare tyre slip. It can be seen that lower slip at lower tractive force was reached by tyres Mitas VF (approximately up to 40-50 kN), and the lowest slip at higher tractive force was reached by tyres Mitas PneuTrac that managed to maintain the highest tractive force 90.7 kN within the measurement. This is most likely due to larger area of the footprint and more favourable distribution of pressure in the footprint since the tread is not deformed to such extent as in case of common tyres at a given inflation pressure. This is caused by the structure of sidewalls because common underinflated tyres tend to push the edges of the tread inward the footprint and thus adversely affect distribution of the pressure. The structure of PneuTrac tyres pushes the edges of the tread away from the longitudinal axis of the footprint at all circumstances and thus ensures contact of the whole tyre footprint with the surface.

CONCLUSIONS

Results make it evident that Mitas PneuTrac tyres proved most flexible blend and structure in radial direction while maintaining lateral stiffness which helped to maintain the maneuverability of the tractor. It is also possible to significantly reduce the inflation pressure by up to 62.5 % compared to standard tyres of the same size and the same load. These tyres reduce negative impact on soil and plants because of lower pressure and larger area of tyre footprint.

From the point of view of traction properties Mitas VF tyres reached the lowest slip at lower tractive force. With increasing tractive force the slip of Mitas VF tyres significantly increased when compared to Mitas PneuTrac tyres. When compared to standard Mitas tyres, Mitas VF tyres maintained c. 12% higher tractive force and Mitas PneuTrac tyres maintained ' c. 26% higher tractive force at the slip of15 %. Mitas PneuTrac tyres maintained the highest tractive force from all compared tyres and thus increased tractive efficiency of the tractor. Better traction properties also contribute to lower fuel consumption and more economic operation.

ACKNOWLEDGEMENT

The paper was created with institutional support for long-term conceptual development VÚZT, v.v.i. RO0614 and with the grant support CLUS – 2016: 31190/1312/3116 "Effect of cutting tool shape on air flow in working area of mulcher with vertical axis of rotation."

REFERENCES

1. ABRAHÁM, R., MAJDAN, R., ŠIMA, T., CHRASTINA, J. & TULÍK, J. 2014: Increase in tractor drawbar pull using special wheels. *Agronomy Research* 12(1), pp. 7–16
2. AHOKAS, J. & JOKINIEMI, T. 2014: Light tractor simulator. *Agronomy Research* **12**(1), pp. 17–24
3. ARVIDSSON, J. & HÅKANSSON, I. 2014: Response of different crops to soil compaction—Short-term effects in Swedish field experiments. *Soil and Tillage Research* 138, pp. 56–63.
4. BRAUNACK, M.V., ARVIDSSON, J. & HÅKANSSON, I. 2006: Effect of harvest traffic position on soil conditions and sugarcane (Saccharum officinarum) response to environmental conditions in Queensland, Australia. *Soil and Tillage Research* 89(1), pp. 103–121
5. ČEDÍK, J. & PRAŽAN, R. 2015: Comparison of tyres for self-propelled sprayers. *Agronomy Research*, 13(1), pp. 53–62
6. DABROWSKI, J., PYTKA, J., TARKOWSKI, P. & ZAJAC, M. 2006: Advantages of all-season versus snow tyres for off-road traction and soil stresses. *Journal of Terramechanics* 43(2), pp. 163–175.
7. GŁĄB, T. 2014: Effect of soil compaction and N fertilization on soil pore characteristics and physical quality of sandy loam soil under red clover/grass sward. *Soil and Tillage Research* 144, pp. 8–19
8. HŮLA, J., GUTU, D., KOVAŘÍČEK, P., STANĚK, L. & KROULÍK, M. 2011: Odolnost půdy vůči zhutňování při řízených přejezdech strojů. (Soil Resistance Against Compaction During the Machines Controlled Traffic). *Agritech Science* 5(1), [online] http://www.agritech.cz/clanky/2011-1-3.pdf. Accessed 11.1.2016 (in Czech)
9. CHYBA, J., KROULÍK, M., KRIŠTOF, K., MISIEWICZ, P.A., CHANEY, K. 2014: Influence of soil compaction by farm machinery and livestock on water infiltration rate on grassland. *Agronomy Research* 12(1), pp. 59-64
10. CHYBA, J., KROULÍK, M., LEV, J., KUMHÁLA, F. 2013: Influence of soil cultivation and farm machinery passes on water preferential flow using brilliant blue dye tracer. *Agronomy Research* 11(1), pp. 25-30
11. KUHT, J., REINTAM, E., EDESI, L. & NUGIS, E. 2012: Influence of subsoil compaction on soil physical properties and on growing conditions of barley. *Agronomy Research* 10(1-2), pp. 329–334
12. LAMANDÉ, M. & SCHJØNNING, P. 2011A: Transmission of vertical stress in a real soil profile. Part I: Site description, evaluation of the Söhne model, and the effect of topsoil tillage. *Soil and Tillage Research* 114(2), pp. 57–70
13. LAMANDÉ, M. & SCHJØNNING, P. 2011B: Transmission of vertical stress in a real soil profile. Part II: Effect of tyre size, inflation pressure and wheel load. *Soil and Tillage* Research 114(2), pp. 71–77
14. LAMANDÉ, M. & SCHJØNNING, P. 2011C: Transmission of vertical stress in a real soil profile. Part III: Effect of soil water content. *Soil and Tillage Research* 114(2), pp. 78–85
15. LYASKO, M. 2010: Slip sinkage effect in soil–vehicle mechanics. *Journal of Terramechanics*, 47(1), pp. 21–31
16. MCKYES E. 1985: *Soil cutting and tillage*. Elsevier Science Publishers, Amsterdam. 217 pp.
17. MOHSENIMANESH, A., & WARD, S. M. 2010: Estimation of a three-dimensional tyre footprint using dynamic soil–tyre contact pressures. *Journal of Terramechanics*, 47(6), pp. 415–421

18. NORÉUS, O. & TRIGELL, A. 2008: Measurement of terrain values and drawbar pull for six wheeled vehicle on sand. In: *16th International Conference of the International Society for Terrain Vehicle Systems*. ISTVS, Turin, pp. 250–257 (in Italy)
19. PALANCAR, T.C., & TERMINIELLO, A.M., 2001: *Jorajuría D. Determinación Expeditiva del Área de Contacto Rueda-Suelo en Máquinas Agrícolas*. Universidad Nacional de La Plata
20. SCHREIBER, M. & KUTZBACH, H. 2008: Influence of soil and tire parameters on traction. *Research in Agricultural Engineering* 54(2), pp. 43-49
21. SYROVÝ, O., SVĚTLÍK, M., PRAŽAN, R., PASTOREK, Z., KUBÍN, K. & GERNDTOVÁ I. 2013: *Mobilní energetické prostředky a orientační hodnoty jednotkových spotřeb paliv a energií (Mobile energy devices and the approximate values of unit fuel and energy consumption)*. Research Institute of Agricultural Engineering, p.r.i., Prague, pp. 56 (in Czech)
22. ŠMERDA, T., & ČUPERA, J. 2010: Tire inflation and its influence on drawbar characteristics and performance – Energetic indicators of a tractor set. *Journal of Terramechanics,* 47(6), 395–400
23. WONG, J. Y., & HUANG, W. 2006: “Wheels vs. tracks” – A fundamental evaluation from the traction perspective. *Journal of Terramechanics*, 43(1), 27–42.

Corresponding author:

Ing. Radek Pražan, Ph.D., Research institute of Agriculture Engineering, Drnovská 507, 161 01, Prague 6, Czech Republic, phone: +420 233 022 536, e-mail: prazan@vuzt.cz

CONTACT PRESSURE DISTRIBUTION IN TYRE TREAD PATTERN

P. Prikner[1], J. Volf[2]

[1]*Department of Vehicles and Ground Transport, Faculty of Engineering, Czech University of Life Sciences in Prague, Czech Republic*
[2]*Electrical Engineering and Automation, Faculty of Engineering, Czech University of Life Sciences in Prague, Czech Republic*

Abstract
The paper described a testing procedure for detection of tread pattern contact area and contact pressure under the loading simulations. The tyre contact pressure - contact area interaction includes tyre deformation that can be formulated as a function of load with respect to the specific tyre parameters under continuous load including the detection of pressure distribution within tyre lugs' contact area. The usage of tactile pressure sensors detects the uniform tyre footprint detection and contact pressure distribution that includes the determination of a contact area loaded off-road tyres for contact pressure extreme values up to 400 kPa. The construction of mechanical spin model enables to test the different types of displacements, squares and structures as well. The tested pressure sensor allows apply nominal load 34 kN for large agriculture tyres, it may correspond with 145 kN tractor total weight.

Key words: tyre, load, pressure evaluation, tactile pressure sensor.

INTRODUCTION

The general trend in soil protection is to reduce detrimental soil compaction by loaded wheels of power and transport equipment (HÅKANSSON, 1990; GREČENKO & PRIKNER, 2014). These approaches enhance evaluation of soil damage under standardized conditions that guarantee the repeatability of the testing and produce comparable results for other research.

The fact that the contact pressure of tyre contact area produces soil stress, size of tyre contact area strictly depends on tyre dimensions, inflation pressure, load dependence on external factors as vehicle speed, soil type, soil moisture content, depth of rut, etc., is generally known, (SOANE, 1983). In dynamic contact pressure measuring can be use the sensing contact surfaces strain transducer placed in tyre tread pattern (RAPER ET AL., 1995), and further e.g. (WAY ET AL., 2004; MOHSENIMANESH AND WARD, 2007). Contact pressure in loaded tyre area can produce soil stress soil up to depths 50–60 cm (SÖHNE, 1958; VAN AKKER ET AL., 2004; KELLER ET AL., 2007; O´SULLIVAN ET AL., 1999). All conclusions closely depend on individual soil-tyre interaction, therefore these outputs cannot be taken as a final. The size empirical estimation of contact area on a soft ground was published by SWANGHART (1990). The approaches based on predetermined contact area dimensions were published e.g. (HALLONBORG 1996; KELLER 2005 ETC.). Especially engineering branch used measured data in relation to catalogues tyre dimensions for empirical calculation of tyre contact area e.g. GREČENKO (1995). Laboratory scanning of tyre footprint area and contact pressure evaluation used the tactile pressure sensors (VOLF ET. AL., 1997, 2010) and it can produce more precise results then field experiments. In–situ experiments are carried out with various transducer types implemented on tyre tread pattern or commercial pressure mapping sensors with low screening resolution and application of individual soil sensors into predefined soil profile depth positions (WAY ET AL. 1995; MOHNESIMANEHS & WARD, 2007; BAROSSA ET AL., 2015; KELLER ET AL., 2007).

This paper presents results obtained at the initial development stage of implementation of pressure scanning system for heavy loaded agriculture traction tyres. The objectives of this study were: (a) to analyse relative load calibration function of selected contact areas for an adequate contact pressure value; (b) to analyse dependence between a wheel load and a contact pressures distribution on tyre tread pattern contact area.

MATERIALS AND METHODS

Laboratory testing were carried out on a part of the laboratory soil compactor and its operation were described earlier (GREČENKO & PRIKNER, 2014). A tyre footprint attachment with hydraulic actuation and electronic scales in the platform 1 m^2 allows maximum tyre load up to 69 kN. This attachment enables direct contact area measurement and screening pressure distribution in tyre tread pattern with improved precision. The system of measuring of the contact pressure between tyre and the matrix was proposed to arrange miniature tactile pressure sensors and it was designed as a compact portable device (VOLF, 1997). This equipment enables static and dynamic loading sensing regimes. The sensors are controlled by electronic circuits which control function and transmit acquired data to PC for further evaluation (Fig. 1). The pressure scanning system (Plantograf – trademark; VOLF, 2010) guarantees minimization of mutual influence of matrix sensing points and maximise the matrix point sensitivity. The matrix construction is described in a patent application (VOLF, 2010). The tested pressure area is fitted with 7500 pcs sensors an active area of 40 x 30 cm (approx. 6.25 pcs.cm^{-2}). The inner matrix is precisely covered with the conductive elastomer and non-conductive flexible material to prevent an outer damage and it includes a top resilient geotextile coating. The measured data were saved on internal hard disk drive (HDD) or flash drive in the system for later transfer to PC (Fig. 2). Scanning speed ranges up to 300 frames per seconds. The output from the device is a colourful raster and matrix of pressure values on tyre detected by each miniature sensors. Basic technical data of the measuring devices are described in Tab. 1.

Fig. 1. – Laboratory device for tyre testing up to 69 kN with pressure evaluation equipment; (Mitas tyre 650/65R38 RD-03, inflation pressure 100 kPa, load 9.8 kN)

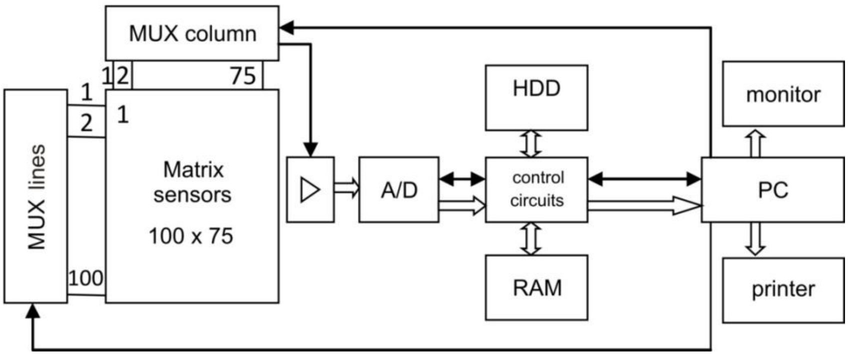

Fig. 2. – Block diagram of multiplex control circuits

In the first part of testing procedure, establishment of calibration function was provided using high load loading tests. Specific contact areas 3.8 cm^2 (25 pcs.cm^{-2}), 27 cm^2 (175 pcs.cm^{-2}) and 125 cm^2 (781 pcs.cm^{-2}) were loaded in require pressure range from 10 to 400 kPa in tolerance interval ± 2 kPa. The area sizes were selected with respect to overloading effect elimination and precise description of pressure behaviour that depends on score of sensing points per centimetre square. Adequate combinations of contact pressure q (kPa) and specific loading W (kN) were statistically evaluated. Equation for fundamental relation of relative loading RL (%) and contact pressure was obtained with the use of an exponential function. Plantoraf stiffness tests estimatimating pressure distribution in tyre tread pattern contact area were provided in two static and dynamic load regimes. Static load tests were carried out with radial tyre Mitas 650/65R38 RD-03 in load range from 1.9 to 6.9 kN per one tread pattern lug.

Fig. 3. – Dynamic contact pressure sensing with a Plantograf equipment

Fullness of tyre contact area depends on ratio of total contact area of tread pattern footprint to total contact area of tyre. The range 21-25% is obviously taken as a standard for driving agriculture tyres; however, it depends strictly on tyre dimensions. The dynamic testing allows scanning pressure behaviour directly and reducing extreme deviations in pressure distribution on sensing plate due to minimization of tyre tread pattern deformation. Tests were carried out with use of tyres Barum 14.9-24 (front) inflated on 140 kPa and 16.9-38 (rear) inflated on 160 kPa mounted on tractor Zetor Forterra 8641 (Fig. 3). Both inflation pressure levels were setup as a manufacture´s recommended standard. Front tyre load 11.5 kN and rear tyre load 13.5 kN were calculated according to standard total weight distribution on both axles as 48/52%; the total tractor weight of 50 kN produces 26 kN on rear and 23 kN front axle load. Testing pass speed was set up for 10 cm.sec^{-1}.

Tab. 1. – Technical parameters of the Plantograf

Load capacity	up to 34 kN
Range of pressures	0–400 kPa
Permanent overload	1.4 MPa
Active array sensor	40 x 30 cm
Overall dimensions of the sensor	75 x 65 cm
Number of sensors	7500 pieces
Digital output	256 levels
Number of frames per sec.	60
Sampling frequency	2.5 MHz

RESULTS AND DISCUSSION

A calibration function precisely describes relation between contact pressure and relative loading *RL* (%) in term of standardized value for the specific range of pressure distribution in a given range 0–100% under 256 bit sensing level (Fig. 4). A change of optimal range for pressure limit reading regulates a parameter *Gain* (1–5). The general trend of contact pressure and *RL* behaviour describes Eq. 1:

$$RL = 35.4615 \cdot \ln(q) - 111.511 \quad (1)$$

(R^2 = 95.59; *F-ratio* = 238.25, P<0.0001)

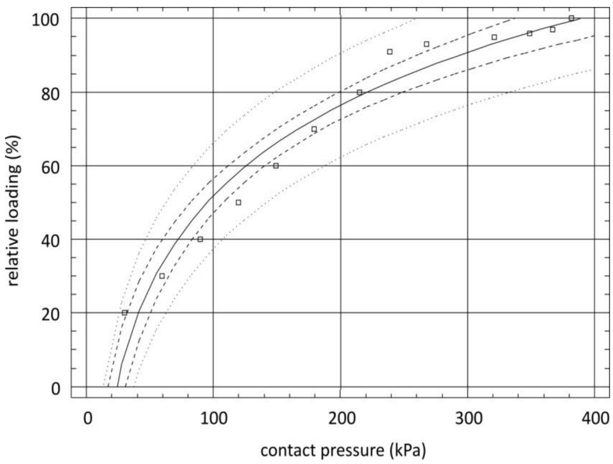

Fig. 4. – Calibration function for contact pressure range from 20 to 395 kPa

Size of tyre contact area and contact pressure values depend on actual vertical load. In this calibration step, tyre load was function of contact pressure and contact area S_x (Eq.2) as well:

$$F = \int_{q_0}^{q_{max}} S_x(dq) \qquad (2)$$

First tests (static tyre load) were performed with the use a large tyre 650/65R38 mounted in laboratory stand (Fig. 1). Primarily, tests were performed in order to establish maximal load capacity of the Plantograf. Tyre total load 35 kN confirmed required load capacity for further heavy load tests. Tyre inflation pressure was set up on 100 kPa due to better lug footprint spreading on sensing plate and also recommended inflation pressure level for field operation.

A maximal contact pressure in tread pattern was verified. Tyre tread pattern was loaded 29 kN (as standard operation load when tyre is used for total tractor weight 92 kN). When tyre tread pattern fullness is 24 %, a number of lugs 4 ± 0.25 can be placed in contact area (approximately 700 ± 10 cm^2) under 29 kN load. Thus contact pressure in specific lug areas can be increase up to 400 kPa indisputably. The combination confirmed optimal load 6.9 kN per 175 cm^2 as a maximum for standard operation conditions. Documentation of acceptable load capacity, one lug footprint (175 cm^2) for total tyre load 29 kN and inflation pressure 100 kPa shows Fig. 5.

The contact pressure size corresponds with estimation of total tyre contact area according GREČENKO & PRIKNER (2014); e.g. when tyre 650/60R38 was inflated on 100 kPa and loaded 29 kN, size of total tyre contact area achieved 2900 cm^2 approximately, thus a mean contact pressure 93 kPa corresponds with results described previously. Very similar results were published by JUN ET AL. (2004), KELLER ET AL. (2007) and MOHNESIMANEHS & WARD (2007). The advantages of presented approach are evident. Fig. 6 presents dependence between tyre load and contact pressure.

A linear trend can be achieved if contact area of lugs is unchangeable (in the praxis can be consider in specific combination $W - p_i$); however these results describe real behaviour for selected lug contact areas reliably. Fig. 7 presents the confirming effect of tyre lug number on relative loading scale that can be obtained from calibration function behaviour. The value of relative loading 100 % occurs in the event and corresponds with a nominal contact pressure 395 kPa.

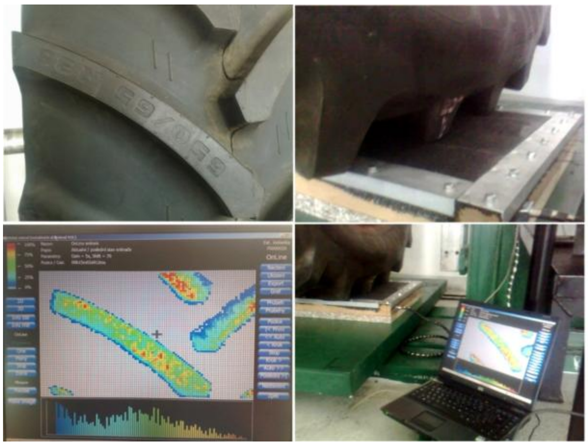

Fig. 5. – Accuracy at pressure screening of the lug text (tyre 650/65R38, total tyre load 29 kN, average lug loading 6.9 kN, p_i = 100 kPa)

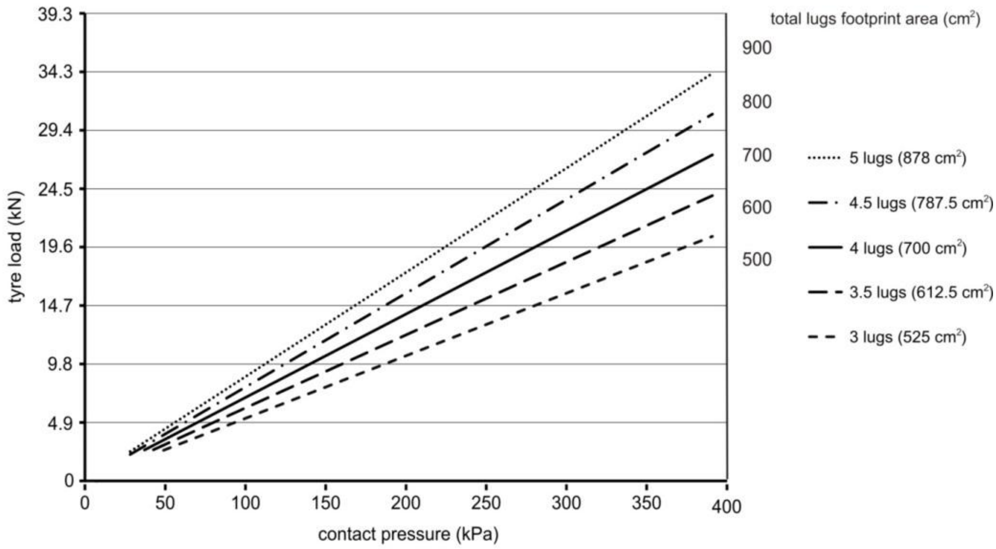

Fig. 6. – Linear dependence $W = f(q)$ for lugs contact area (lug area 175 cm^2)

The obtained outputs of dynamic tests declare previous idea of better lug footprint spreading on sensing plate when tyre is underinflated or contact pressure is sensing under dynamic conditions. Generally, distribution of maximal pressure range in the relative loading scale 75–85% for bias-ply tyres shows effect of high toughness. A maximum of contact pressure can be found for 20-25 % of lugs contact area approximately (see Fig. 8), but it is necessary to remark that some extremal shapes can cause a rubber friction on used a geotextile cover.

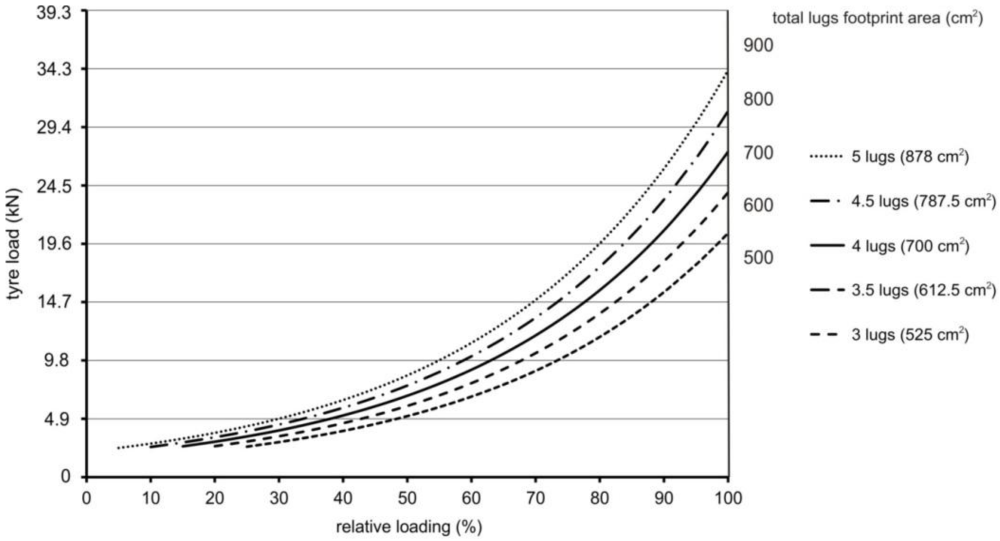

Fig. 7. – Exponential behaviour $W = f(RL)$ of pressure distribution trend in the tyre tread pattern for selected lugs contact area (lug area 175 cm^2)

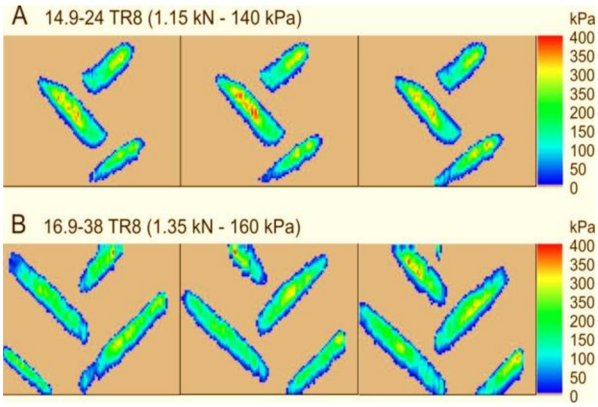

Fig. 8. – Example of selected static positions of pressure distribution in tyre tread pattern of bias ply tyres under dynamic measuring regime; (passage speed 10 cm.s^{-1})

The comparison of all results prove that tyre thread pattern of radial types can dispose more flexibility and higher contact area depending on contact area of lugs including fullness of tread pattern. Total area of lugs and contact area of tyre has a strictly dependence on lug design and tread pattern spreading on elastic surface. The elaboration doesn´t close inflation pressure of tyre as main parameter; however, this significantly affects tyre mechanical properties. Notice; both tyre size types were used for testing of usability of the Plantograf device primary in the first step of research.

CONCLUSIONS

The paper demonstrates a progress achieved in mapping and screening of contact pressure distribution of agricultural driving tyres contact area. The calibration function of relative loading depends on a lug contact area size and on fullness of tyre tread pattern. The evaluation accuracy is reliable when different contact areas are compared for specific contact pressures and number of sensing points is specified. A static load can cause some differences in pressure distribution on the contact area due to friction rubber – plate cover when tyre tread pattern spread out on the sensing plate. It is possible to conclude that the dynamic pressure sensing produces acceptable outputs; however tyre tread pattern contact area is not precisely described due to short contact time.

It is evident that sensing matrix withstands high load up to 35 kN. Planned experiments will use a large sensing matrix 50 x 50 cm (16800 pcs sensors, approx. 6.72 sensing point.cm^{-2}) in the future. The sensing matrix with 7500 pcs sensors (approx. 6.25 sensing point.cm^{-2}) corresponds with similar commercial product (Tekscan, XSensor etc.); thus tested high load capacity and dynamic testing confirmed using in experiments under terrain conditions; e.g. direct measurement of actual contact pressure in contact area of moving wheel with tyre with different depth rut etc.

REFERENCES

1. BARBOSA, L. A. P., MAGALHÃES, P. S. G.: Tyre tread pattern design trigger on the stress distribution over rigid surfaces and soil compaction. Journal of Terramechanics, 58, 2015: 27–38.
2. GREČENKO, A.: Tyre footprint area on hard ground computed from catalogue values. Journal of Terramechanics, 32, 1996: 326–333.
3. GREČENKO, A., PRIKNER, P.: Progress in tyre rating based on soil compaction potential. Journal of Terramechanics, 46, 2009: 211–216.
4. GREČENKO, A., PRIKNER, P.: Tyre rating based on soil compaction capacity. Journal of Terramechanics, 52, 2014: 77–92.
5. HALLONBORG, U.: Super ellipse as tyre - ground contact area. Journal of Terramechanics, 33, 1996: 125–132.
6. HÅKANSSON, I.: A method for characterizing the state of compactness of the plough layer. Soil and Tillage Research,. 16, 1990: 105–120.
7. JUN, H., WAY, T. R., LÖFGREN, B., LANDSTRÖM, M., BAILEY, A. C., BUR, E. C., MCDONALD, T. P.: Dynamic load and inflation pressure effects on contact pressures of a forestry forwarder tyre. Journal of Terramechanics, 41, 2004: 209–222.
8. KELLER, T.: A model for the prediction of the contact area and the distribution of vertical stress below agricultural tyres from readily available tyre parameters. Biosystems Engineering, 92, 2005: 85–96.
9. KELLER, T., DÉFFOZES, P., WEISSKOPF, P., ARVIDSSON, J. – RICHARD, G.: SoilFlex: A model for prediction of soil stresses and soil compaction due to agricultural field traffic including a synthesis of analytical approaches. Soil and Tillage Research, 93, 2007: 391–411.
10. MOHSENIMANESH, A., WARD, S. M.: On-the-move monitoring of soil-tyre interaction on soft soil using wireless data acquisition. Transaction of the ASABE, 50, 2007: 1919–1925.
11. MOHSENIMANESH, A., WARD, S. M.: Estimation of a three-dimensional tyre footprint using dynamic soil–tyre contact pressures. Journal of Terramechanics, 47, 2010: 415–421.
12. O'SULLIVAN, M. F., HENSHALL, J. K., DICKSON. J. W.: A simplified method for estimating soil compaction. Soil and Tillage Research, 49, 1999: 325–335.
13. RAPER, R. L., BAILEY, A. C., BURT, E. C., WAY, T. R., LIBERATI, P.: Inflation pressure and dynamic load effects on soil deformation and soil-tyre interface stresses. Transactions of the ASAE 38, 1995: 685–689.
14. SCHWANGHART, H.: Measurement of contact area, contact pressure and compaction under tyres on soft ground. Journal of Terramechanics, 28, 1990: 309–318.
15. VOLF, J., HOLÝ, S., VLČEK, J.: Using of tactile transducer for pressure-distribution measurement on the sole of the foot. Sensors and Actuators A, 62, 1997: 556–561.
16. VOLF, J., NOVÁK, M., VLČEK, J., TRINKL, A.: Device for tactile information sensing. Czech Republic Patent. No.: 301717, 2010, Prague.
17. SOANE, B. D. (editor and co-author): Compaction by agricultural vehicles: a review. Scottish Institute of Agricultural Engineering. Penicuik: reprint of 4 papers from Soil and Tillage Research, 1983: vols. 1 and 2.
18. SŐHNE, W.: Fundamentals of pressure distribution and soil compaction under tractor tyres. Agriculture Engineering, 39, 1958: 276–281, 290.
19. VAN DEN AKKER, J. J. H.: SOCOMO: a soil compaction model to calculate soil stresses and the subsoil carrying capacity. Soil and Tillage Research, 79, 2004: 113–127.
20. WAY, T. R., BAILEY, A. C., RAPER, R. L., BURT, E. C.: Tyre lug height effect on soil stress and bulk density. Transactions of the ASAE, 38, 1995: 669–674.
21. WAY, T. R., KISHIMOTO, T.: Interface pressures of a tractor drive tyre on structured and loose soils. Biosystems Engineering, 87, 2004: 109–120.

Corresponding author:
Ing. Patrik Prikner, Ph.D., Department of Vehicles and Ground Transport, Faculty of Engineering, Czech University of Life Sciences in Prague, Kamýcká 129, Praha 6, Prague, 16521, Czech Republic, phone: +420 22438 3316, e-mail:prikner@tf.czu.cz

SOIL COMPACTION AND SOIL MOISTURE CONTENT IN EXTREME CLIMATE CONDITIONS

V. Rataj, M. Macák, M. Barát, J. Galambošová

Department of Machines and Production, Faculty of Engineering, Slovak University of Agriculture in Nitra

Abstract

The work deals with the impact of soil compaction on moisture content during extremely hot and dry season of 2015 with heavy storm rainfall. The period (July and August) is divided on three parts – period of drought, heavy rainfall, and drought after heavy rainfall. Soil moisture was measured at a depth of 20 cm at two blocks on a slope with a gradient of 2.5 °, yield of pumpkin seed (Cucurbita pepo L, var. olerifera) was monitored as well. The results show, that soil moisture is higher in compacted soil what resulted in better yield of pumpkin. Similar trend was confirmed also by control measurement in CTF experiment.

Key words: soil, humidity, compaction, dry, rainfall.

INTRODUCTION

Climate change and increased production of greenhouse gases are predicting more frequent occurrence of temperature extremes - droughts and heat waves, and intensive rainfall (BRESTIČ, 2010). In the context of sustainable farming and for maximizing crop yields it is necessary to know all the factors that have an influence on crop yield (KUMHÁLOVÁ, 2011). Terrain elevation (BAKHSH ET AL., 2000; KRAVCHENKO ET AL. 2000), slope (KRAVCHENKO AND BULLOCK 2002), location (KRAVCHENKO AND BULLOCK 2002B), flow indey, flow direction, flow length and flow accumulation (JENSON AND DOMINGUE 1988) are considered the most important topographical and hydrological attributes in crop production in conventional tillage systems.

Technological development in agriculture heads to increasing the working width of the machines along with the increasing power of tractors. Strong and heavy machinery has a negative impact on soil and its properties (RATAJ, 2014). Since 1966, the mean weight and power of agricultural machinery has increased three times (KUMHÁLA, 2013).

Publishes research results on the soil physical properties showed that the compaction of soil results in increasing the bulk density of soil, reducing the porosity (especially lowering the volume of non-capillary pores), and in higher level causes destruction of soil aggregates. These facts lead to further deterioration of the physical soil properties, such as a reduction in the water infiltration, changing the water content in the soil horizon and its relative movement in the soil (JAVŮREK, VACH, 2008). The inability to hold water also increases the probability of floods, drought, and other soil degradation as well. Lack of organic matter causes serious risk of erosion, reducing infiltration abilities**,** but also soil compaction and other degradation processes (HERMANOVSKÁ, 2013). Soil erosion robs the most fertile agricultural part of soil - topsoil. It also deteriorates the physical-chemical properties of the soil, it reduces the size of the soil profile, increases rockiness, it reduces the content of nutrients and organic matter, and also damages the arable crops. JANECEK (2012) refers, that in the Czech Republic, there is about 50% of arable land endangered by water erosion (JANEČEK, 2012).

Soil erosion is caused by poorly water infiltration in the soil. Infiltration indicates the volume of water, which soaks to the soil over time and additional water rolls off the surface - for example due to the heavy rainfall. Infiltration can be used as one of the important soil properties, which has a major impact on soil fertility and also on soil erosion (DIBAL, 2013). The amount of water that can soak the soil depends on the soil type as well. Sandy soils can retain more water than heavier clayish soils (SCHWANKL, 2007).

Excessive soil compaction causes creation of anaerobic environment, that reduces the air exchange and microbial activity, and increases the denitrification and also rate of the pores filled with water (Torbert - Wood, 1992). Soil compaction reduces pore size and this has a big impact on volume of water that can be absorbed into the soil. This reduces mainly the number of large pores (WOLKOWSKI - LOWERY, 2008).

Layed soil (slightly compacted) is important for optimal water regime. For better seed germination, the soil should be softened in the top layer, and slightly compacted in the bottom of seed bed. The optimal porosity in the seedbed is 48-52% for cereals on loamy soils. Also, the optimal bulk density for spring barley on loamy soils should be 1.30 – 1.40 t.m^{-3} (POSPÍŠIL, CANDRÁKOVÁ, 2015). Soil compaction has a direct impact on crop yield, but in conditions of extreme drought the yield could be positively affected (DEJONG-HUGHES, J. ET AL, 2001).

The aim of this work was to determine the level of soil moisture at differently compacted soil in conditions of extreme drought and heat. This effect is documented on yield of pumpkin seed (Cucurbita pepo L, var. olerifera).

MATERIALS AND METHODS

Experiments took place in Kolíňany in the area of University farm of the Slovak University of Agriculture in Nitra.

The experimental field was deep tilled up to 30 cm, followed by soil preparation technology with disc harrow and secondary tillage equipment (combinator). On this field two experimental zones were designed (55x55 m) with the chernozem soil types, middle-heavy soils, classified after BPEJ to 0139102 (VÚPU, 2015, LINKEŠ V. ET AL., 1996). These zones were 55 m apart on a slope with a gradient of 2.5 degrees (area TOP, area BOTTOM).

Each zone was divided into two blocks. One block was purposely compacted with tractor (track to track), the second block was not compacted and served as a control point (Fig. 1). Both blocks were located so two monitoring areas were assessed, location TOP and location BOTTOM. Locations were located 55 m apart along the slope.

Fig. 1. – Lokalisation of experimental blocks, left site of block – compacted wheel by wheel, right site – not compacted soil

Crop grown on this field was pumpkin for seed (Cucurbita pepo L, var. olerifera). Two sets of measuring systems Eas**y**Log (DECAGONDEVICES, 2015) were used to measure soil moisture content. Each set consists of volumetric soil moisture sensors and a datalogger, which ensures continuous monitoring of soil‘s volumetric water content (in units % VWC). The sensors were placed at the centre of each block, at a depth of 20 cm below the surface.

Fig. 2. – Installing the soil sensors

The level of soil moisture at different compacted soil in conditions of extreme drought and heat was studied in July and August of 2015. This period could be divided into 3 parts:

- A – long drought with minimal rainfall,
- B – period of heavy storm rainfall,
- C – dry period after heavy rainfall.

Climate characteristics of 2015 in Slovak Republic by LAPIN (2015) and resources SHMÚ (2015) states, that summer of 2015 was extremely abnormal, regarding the temperatures overall. The experimental area had an average summer temperature of 22.9 °C, with relatively low humidity, drought, and frequently high night temperatures above 20 °C. Summer of 2015 was very dry, with rainfall of only 82 % of long-term observations (1901-1990).

Weather development was monitored with the weather station located in the area of University farm in Kolíňany, in a distance of 500 m from the experimental field. In this monitored period of time the values of air temperature, relative humidity, and rainfall volume were recorded. Data sampling frequency was 10 minutes.

The period of extreme drought is well documented on rainfall, in April – 25 mm precipitation with a maximum value of 1.2 mm, in May – 43.4 mm with maximum of 35.6 mm (29.05.2015) and in June – 25.6 mm – maximum of 18.6 mm (09.06.2015). The overview of monitored values during the experiment is shown in Tab. 1.

To complete the information on climate conditions, which affected the soil moisture predominantly, air temperature and moisture content of the second decade of August is provided. Here, in the period of 3 days (17th to 19th August 2015), precipitation of 98.2 mm was observed, what is equal to 96.5% of the total month precipitation. Looking at the all assessed period (July – August), this is equal to 81% (Fig. 3).

Tab. 1. – Overview of climate parameters at University farm in summer 2015

Average value	1. - 10. 07. 2015	11. - 20. 07. 2015	21. - 31. 07. 2015
Air temperature, °C	23.06	23.04	24.58
Air humidity, %	63.10	63.41	72.54
Rainfall, mm	6.80	2.30	11.50
Average value	1. - 10. 08. 2015	11. - 20. 08. 2015	21. - 31. 08. 2015
Air temperature, °C	24.31	23.69	23.09
Air humidity, %	63.89	68.87	81.02
Rainfall, mm	0.30	98.90	2.53
Rainfall totally, mm		147.93	

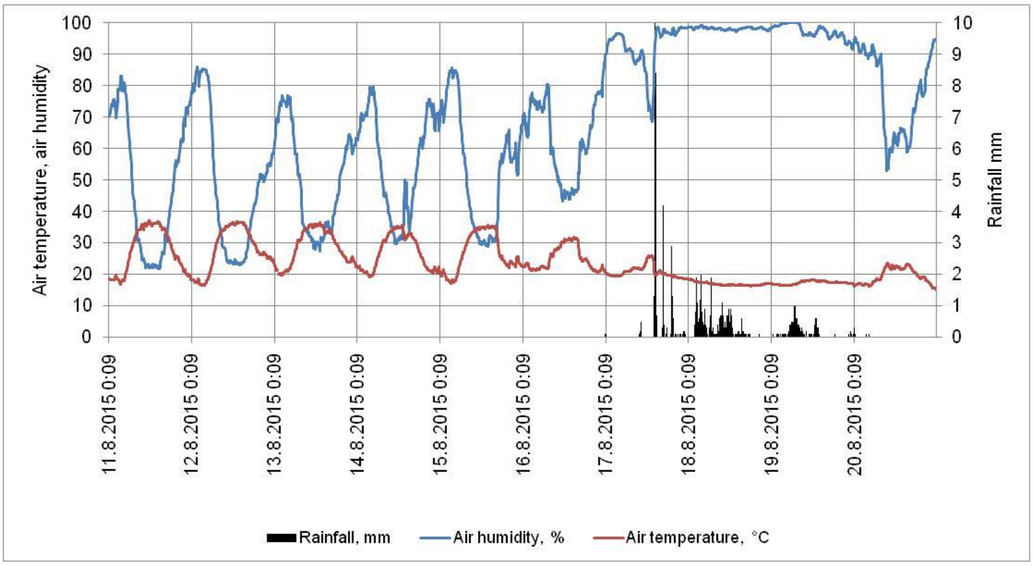

Fig. 3. – Climate parameters during the assessed period of the august 2015

Fig. 4. – Soil moisture sensor used in the experiment

Soil sensors were placed into non-disturbed soil. In order to do this, installing pit was excavated and the sensor´s fork was plugged into the pit-site (Fig. 4). The pit was filled with soil afterwards.Soil moisture data measured with the sensor were downloaded from the web server of company Physicus (PHYSICUS, 2015). To analyse the data these were downloaded and statistically processed. As a result of dry weather, the crop suffered from drought stress and the soil cracks were present as showed in Fig. 5.

Fig. 5. – Pumpkin crop during the heat stress

The soil moisture was assessed during 2 months (July to August 2015). Effect of soil compaction on soil moisture content was determined according to formula 1.

$$\Delta W = Wc - Wu \qquad (1)$$

where: ΔW difference of soil moisture content, %

Wc soil moisture content of compacted soil, %

Wu soil moisture content of non-compacted soil, %

Following parameters were evaluated for each set of sensors:

- Changes on soil moisture during the 62 days period
- Basic statistics parameters of soil moisture on hourly base
- Extend of variation of hourly monitored soil moisture
- Difference of soil moisture values ΔW

RESULTS AND DISCUSSION

Based on obtained data, following results were achieved. Fig. 6 shows the soil moisture data of compacted and non compacted soil at the experimental area TOP. Results show, that the soil moisture of compacted soil reached higher values during all experiment.

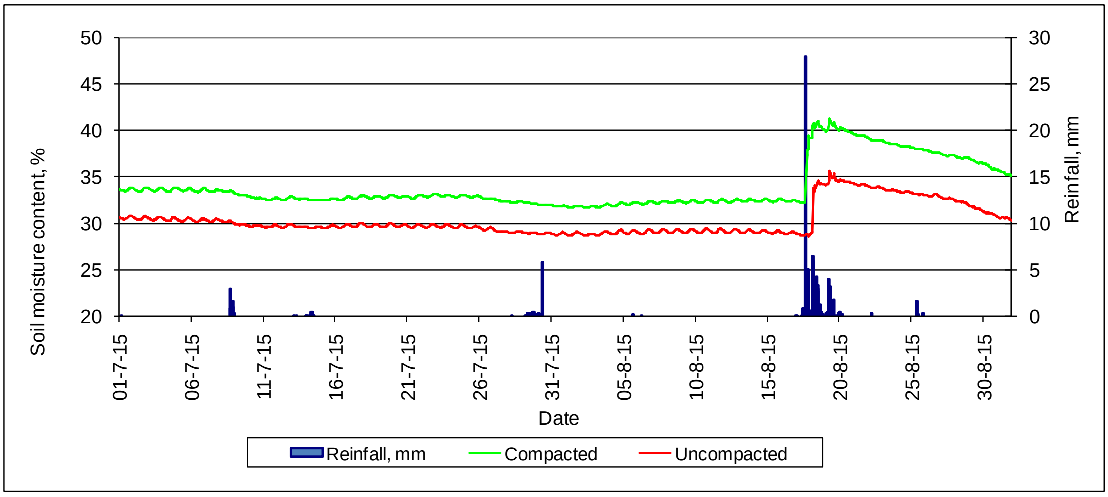

Fig 6. – Soil moisture content in the area TOP

Drought time period (A)

Drought time period lasted 48 days (1st July 2015 to 17th August 2015) with precipitation of 22 mm only. Soil moisture content decreased due to the dry weather. The ΔW reached values in the range of 2.8 to 3.6% (Fig. 7, Tab. 2).

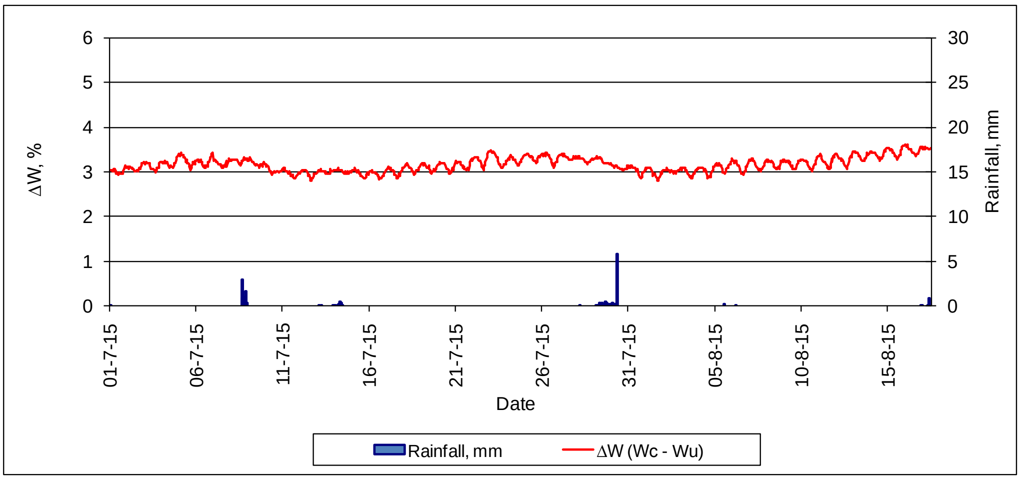

Fig.7. – Soil moisture difference ΔW at the experimental are TOP during the drought time period

Heavy rain period (B)

The time period of heavy rainfall lasted 2 days (17th to 18th August 2015). During the time of 27 hours, precipitation reached 79.1 mm. The soil moisture data during this time period are presented in Fig. 8.

Naturally, the rainfall increased the soil moisture content. In the depth of 20 cm, where the soil sensors were installed, soil moisture increased immediately at compacted area and after 13 hours at non-compacted area. The parameter ΔW increased to the range of 3.5 – 11.4% (Tab. 2).

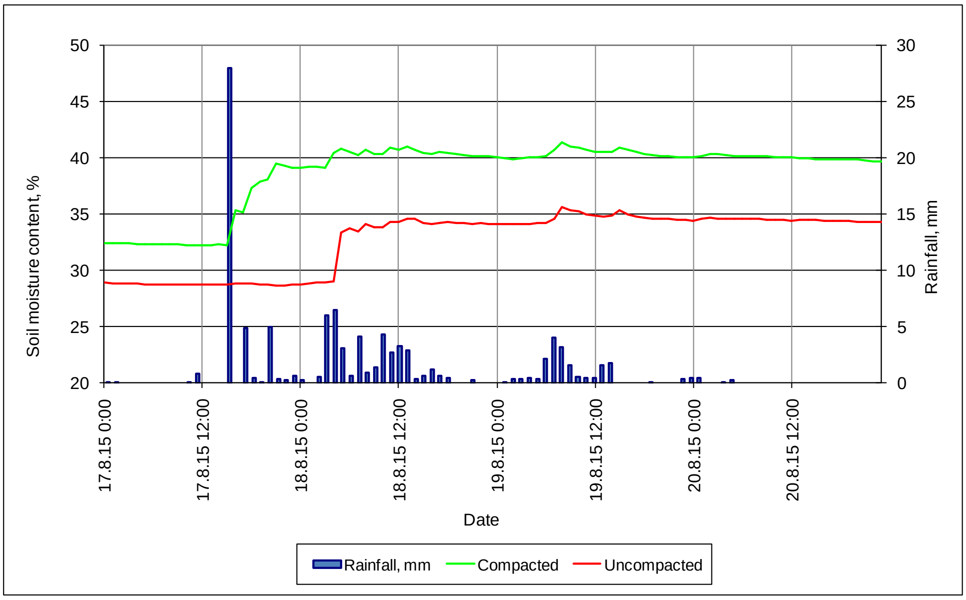

Fig.8. – Soil moisture data at the are TOP during the heavy rainfall time period

Dry period after heavy rain (C)

This period lasted 13 days (19. 08. – 31. 08. 2015). Precipitation was 21.2mm, out of which 13.6mm was considered as decay of the heavy rainfall from previous period. Soil moisture increased by 27% at the compacted area and by 18% at the non-compacted area. Same trend was present during next time period and the decrease of soil moisture was even more significant. The difference in soil moisture content expressed by parameter ΔW increased and ranged between values of 3.5 – 11.4 % (Fig. 9; Tab.2).

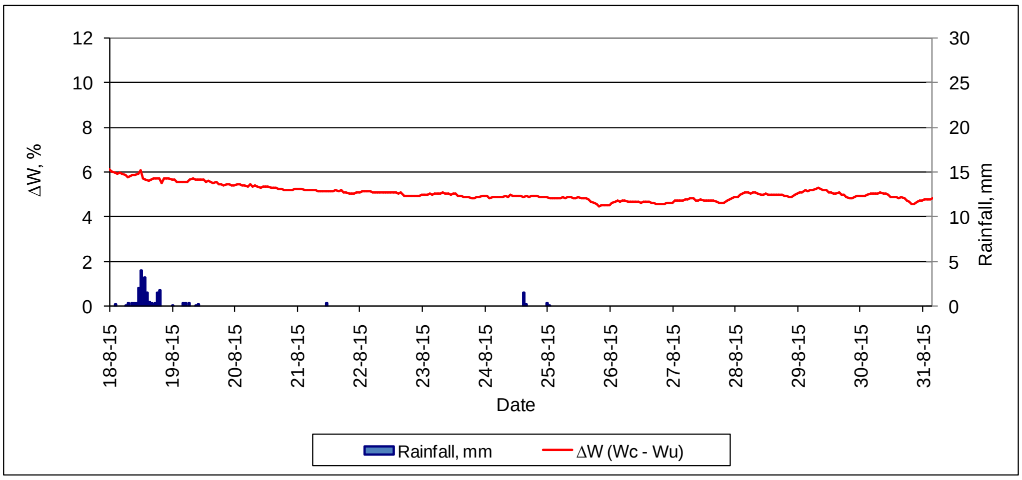

Fig. 9. – Difference in soil moisture content at the experimental area TOP during dry period after heavy rainfall

Tab. 2. – Basic parameters of the soil moisture difference at the areal TOP during monitored periods

?W -difference of soil moisture content	Monitoring period		
	A	B	C
Average, %	3.16	7.83	5.07
Standard deviation, %	0.16	2.06	0.34
Minimum, %	2.80	3.49	4.47
Maximum, %	3.62	11.39	6.14
Number of observations	1142	28	317

End of the monitored period was typical with high air temperature, the soil moisture reached values similar to the time of experiment start.

At the experimental area BOTTOM, same situation was observed, where the compacted soil showed higher soil moisture content (Fig. 10).

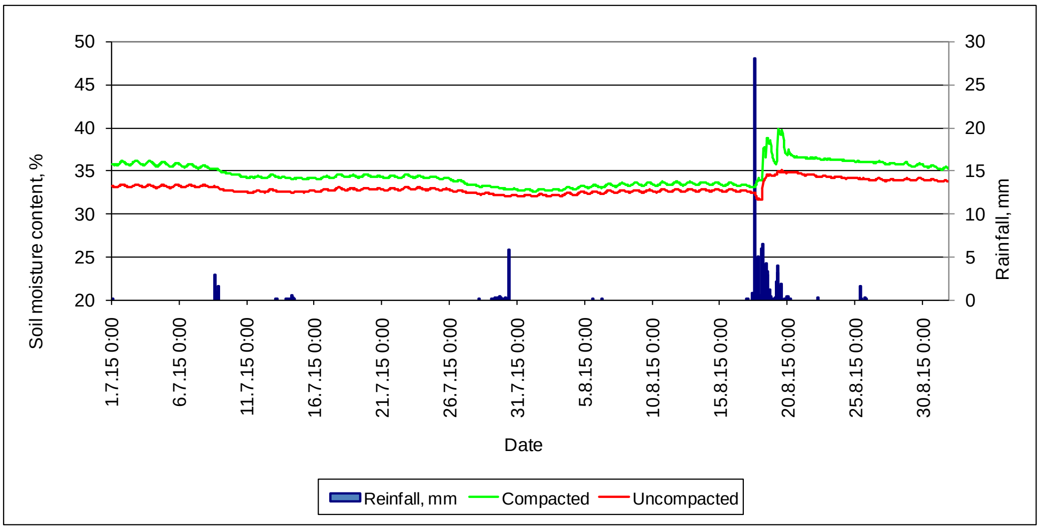

Fig. 10. – Soil moisture content at the area BOTTOM

Values of the parameter ΔW were, however, significantly lower. Experimental measurements of soil moisture using this principle are conducted at experimental field with controlled traffic farming at the moment. This project has been since 2009. Permanent traffic lines are considered to be compacted block and areas with zero traffic as non-compacted block. Data from the period 1st May 2016 to 27th May 2016 are provided in Fig. 11. Soil moisture content at the permanent traffic lines (compacted soil) was significantly higher compared to the non compacted soil.

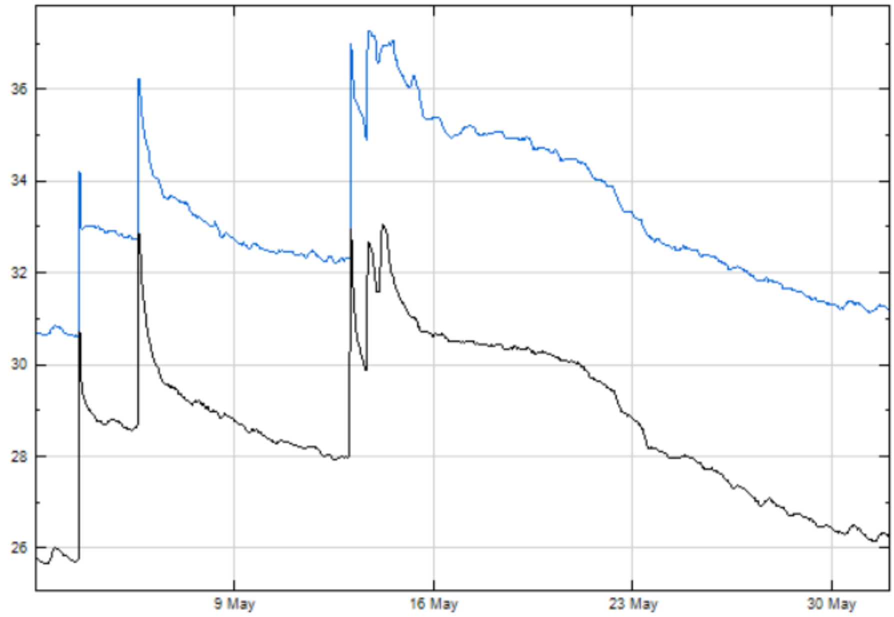

Fig. 11. – Soil moisture content at the experimental field with CTF, top line – permanent traffic line, bottom line – uncompacted soil (PHYSICUS, 2015)

Effect of soil compaction on soil physical parameters is well known. Among all, the infiltration is affected. Results showed, that in conditions of extreme drought, soil moisture is higher in compacted soil. Crops, grown in 2015 were exposed to extreme temperature stress and deficit of available moisture in soil. Yield of the pumpkin seed was low and effect of different soil moisture was reflected on yield (Fig.12).

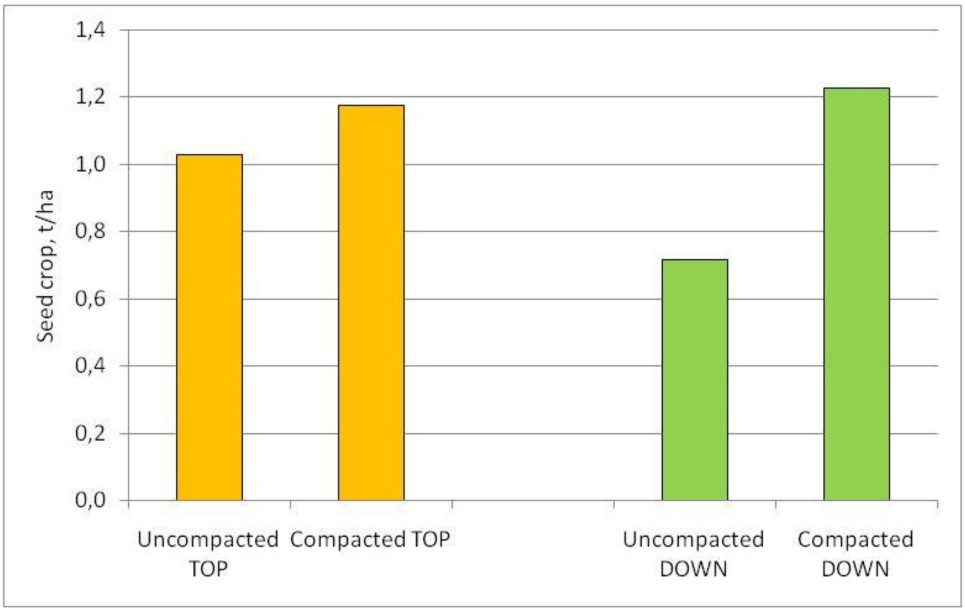

Fig. 12. – Yield of the pumpkin seed reached at the experimental blocks at the two locations

Generally, soil compaction is one of the factors reducing yield, lowering water infiltration to the soil, and factors that cause environmental risks of water erosion (BRANT, V. ET AT. , 2016 and others) However, in extreme drought an opposite effect can be found. At example of pumpkin, results of DEJONG-HUGHES, J. ET AL, 2016 were confirmed saying that during the extreme dry weather conditions, soil compaction may increase yield. AL KAISI AND LICHT (2016) states that there are relations that sets the maximum soil compaction according to the soil moisture content.

CONCLUSIONS

The work was aimed at effect of soil compaction on soil moisture content in the extreme drought conditions in the 2015. Experiments were conducted at University farm in Kolinany in the time period of extreme drought as well as heavy rainfall. Soil moisture content of the compacted soil was higher compared to the non compacted soil. Negative effect was evident in the time period of heavy rainfall. Soil moisture content of the compacted soil increased immediately what indicates the risk of water erosion. Soil moisture content of non compacted soil started to increase after 13 hours. In this time period, the threefold increased of the difference of soil moisture content of the compacted and non compacted soil was present. The year 2015 was extremely dry and hot, what effected the yield of grown crops.

ACKNOWLEDGEMENTS

This article was prepared in the framework of a research project funded by the European Union entitled: "ITEPAg: Application of information technologies to increase the environmental and economic efficiency of production agro-system" (ITMS no. 26220220014) and „Building the Research Centre AgroBioTech" (ITMS no. 26220220180). The authors are grateful to staff at the University Farm in Kolinany (Slovakia) for technical and operational support to conduct this research.

REFERENCES

1. Al-KAISI, M., LICHT, M. 2005. Soil moisture conditions — consideration for soil compaction. Iowa State University Extension. IC-494(9). [online] [cit:2016-05-20] Dostupné na: http://www.ipm.iastate.edu
2. BAKHSH, A., COLVIN, T. S., JAYNES, D. B., KANWAR, R. S., &TIM, U. S. 2000. Using soil attributes and GIS for interpretation of spatial variability in yield. Transactions of the ASAE, 43, 819–828.
3. BRANT, V. et. al. 2016. Strip tillage. In Czech: Pásové zpracování půdy. Praha: ProfiPress, 136 s. ISBN 978-80-86726-76-2
4. BRESTIČ, M., 2010. Climate change and crop production in 21st century. Agricultural advice system. In Slovak: Klimatická zmena a rastlinná produkcia v 21. storočí. Poľnohospodársky poradenský systém. [online] [cit:2016-05-25] Dostupnéna:<http://old.agroporadenstvo.sk/rv/klimzmena_21st.htm>.
5. DeJong-Hughes, J. - Moncrief, J. F. - Voorhees, W. B. – Swan, J. B. 2001. Soil compaction: causes, effects and control. University of Minesota. [2015.03.10] [online] [cit. 2016.03.10] Dostupné na:<http://www.extension.umn.edu/agriculture/tillage/soil-compaction/>.
6. DIBAL, J.M. et al. 2013. Water Intake Characteristics of Different Soil Types in Southern Borno Nigeria. In International Journal of Science Inventions Today, 2, 502-509. ISSN 2319-5436. [online] [cit:2016-05-24] Dostupné na:<http://ijsit.com/admin/ijsit_files/WATER%20INTAKE%20CHARACTERISTICS%20OF%20DIFFERENT%20SOIL%20TYPES%20IN%20SOUTHERN%20BORNO%20NIGERIA_IJSIT_2.6.4.pdf>.
7. HEŘMANOVSKÁ, D. a kol., 2013.Manual compiled from an analysis that deals with actions to maintain the water regime in monitored area. Method for complex solution for erosion processes in the country. In Czech: Manuál sestavený z analýzy zabývající se opatřeními k zachování vodního režimu ve sledovaném území. Metodický postup pro komplexnířešeníerozníchprocesů v krajině. 38s. [online] [cit:2016-05-23] Dostupné na:<http://eagri.cz/public/web/file/279060/Manual_sestaveny_z_anylyzy_zabyvajici_se_opatrenimi_k_zachovani_vodniho_rezimu_ve_sledovanem_uzemi.pdf>.
8. ISO STN 11465. 1993. Soil quality. Determination of dry matter content and water content. Gravimetric method. In Slovak: Kvalita pôdy. Stanovenie obsahu sušiny a hmotnostného obsahu vody. Gravimetrická metóda.
9. JANEČEK, M. a kol., 2012.Protection of agricultural soil from erosion. Method. In Czech: Ochrana zemědělské půdy před erozí. Metodika. Česká zemědelská univerzita Praha. 2012. 113s. [online] [cit:2016-05-24] Dostupné na:<http://fzp.czu.cz/vyzkum/metodiky/Metodika_Ochrana_zemedelske_pudy_pred_erozi.pdf>.
10. JAVŮREK, M., VACH, M. 2008. Negative effects of soil compactions and actions for their elimination. Method for praxis. In Czech: Negativní vlivy zhutnění půd a soustava opatření k jejich odstranění.Metodika pro praxi. Výskumný ústav rostlinné výroby. 2008. 26s., ISBN: 978-80-87011-57-7. [online] [cit:2016-05-23] Dostupné na:<http://www.vurv.cz/files/Publications/ISBN978-80-87011-57-7.pdf>.
11. JENSON, S. K., &DOMINGUE, J. O. (1988). Extracting topographic structure from digital elevation data for geographic information system analysis. Photogrammetric Engineering and Remote Sensing, 54, 1593–1600.
12. KRAVCHENKO, A. N., BULLOCK, D. G., &BOAST, C. W. 2000. Joint multifractal analysis of cropyield and terrain slope. Agronomy Journal, 92, 1279–1290.
13. KRAVCHENKO, A. N., &BULLOCK, D. G. 2002a. Spatial variability of soybean quality data as a function of fieldtopography: I, spatial dataanalysis. Crop Science, 42, 804–815.
14. KRAVCHENKO, A. N., &BULLOCK, D. G. 2002B. Spatial variability of soybean quality data as a function of field topography: II. A proposed technique for calculating thesize of the area for differential soybean harvest. Crop Science, 42, 816–821.
15. KUMHÁLA, F. ET AL., 2013. Controlled traffic farming technology. In Czech: Technologie řízených přejezdů po pozemcích. Praha: ČZU, 2013. 40 s. ISBN 978-80-213-2425-1.
16. KUHMÁLOVÁ, J. ET AL., 2011. The impact of topography on soil properties and yield and the effect of weather conditions. In PrecisionAgric. 2011. 12. 813-830.
17. LAPIN, M. 2015. Current temperature changes in Slovakia. In Slovak: Aktuálne zmeny teploty na Slovensku.[2015.10.12] [online] [cit. 2015.10.12] Dostupné na:<http://www.milanlapin.estranky.sk/clanky/aktualne-zmeny-teploty-na-Slovensku/>.

18. LINKEŠ, V. ET AL. 1998.Guide for the use of map op valued soil-ecological units. In Slovak: Príručka pre používaniemáp-bonitovanýchpôdno-ekologickýchjednotiek.Tretievydanie. Bratislava: Výskumný ústav pôdnej úrodnosti. 104 s. ISBN 80-85361-19-1
19. PHYSICUS, 2015. [2015.05.01] [online] [cit. 2015.05.01] Dostupné na:<:http://test.physicus.eu/>.
20. POSPIŠIL, R., CANDRÁKOVÁ, E. 2015.General crop production. In Slovak:Všeobecná rastlinná výroba. 1. vyd. Nitra: Garmond, 2015. 206s. ISBN 978-80-552-1353-8.
21. RATAJ, V., GALAMBOŠOVÁ, J., MACÁK, M., NOZDROVICKÝ, L. 2014.Precision Agriculture: system – machines – experience. In Slovak: Presné poľnohospodárstvo: systém – stroje – skúsenosti. 1. vyd. Praha: Profi Press, 2014. 157s. ISBN 978-80-86726-64-9.
22. TORBERT, H. A., WOOD, C. W., 1992. Effects of soilcompactipon and water-filledporespace on soil microbial activity and N losses. In Commun. SoilSci. PlantAnal., 23, 1321-1331. [online] [cit:2016-05-25] Dostupné na:<http://citeseerx.ist.psu.edu/viewdoc/download?doi=10.1.1.470.3317&rep=rep1&type=pdf>.
23. SCHWANKL, L. J. ET AL. 2007. Soil Intake Rates and Application Rates in Sprinkler-Irrigated Orchards. University of California – Agriculture and NaturalResources. 2007. ISBN: 978-1-60107-435-5. [online] [cit:2016-05-24] Dostupnéna:<http://anrcatalog.ucanr.edu/pdf/8216.pdf>.
24. VÚPU, 2015. Land maps. In Slovak: Pôdne mapy. J. B. Dostupné na:<http://www.podnemapy.sk/bpej/viewer.htm?activelayer=2&layers=001>.
25. Development of air temperature. In Slovak: Vývoj teploty vzduchu. 2015. [2015.10.12] [online] [cit. 2015.10.12] Dostupnéna:<http://www.shmu.sk/sk/?page=1&id=klimat_operativneudaje1>.
26. WOLKOWSKI, R., LOWERY, B., 2008. Soilcompaction: Causes, concerns, and cures. University of Wisconsin-Extension. [online] [cit:2016-05-23] Dostupnéna:<http://www.soils.wisc.edu/extension/pubs/A3367.pdf>.

Corresponding author:
Vladimir Rataj, Department of Machines and Production Biosystems, Faculty of Engineering, Slovak University of Agriculture in Nitra, Slovak

BIOGAS AS A PROMISING ENERGY SOURCE FOR SUMATRA (REVIEW)

H. Roubík[1], J. Mazancová[1], T. Heller[1], A. Brunerová[2], D. Herák[3]

[1]*Department of Sustainable Technologies, Faculty of Tropical AgriSciences, Czech University of Life Sciences Prague, Czech Republic*
[2]*Department of Material Science and Manufacturing Technology, Faculty of Engineering, Czech University of Life Sciences Prague, Czech Republic*
[3]*Depatment of Mechanical Engineering, Faculty of Engineering, Czech University of Life Sciences Prague, Czech Republic*

Abstract
As modern energy is seen as a key element to reduce poverty and enable human development, various international programmes currently focus on the distribution and implementation of appropriate ways of energy worldwide. Such technology may provide small-scale biogas plants; as they offer production of biogas via the anaerobic digestion of organic waste materials solving the waste management problems and simultaneously and digestate as a by-product. Interest of use of small-scale biogas technology in rural areas is increasing with numerous organisations promoting their use for both socio-economic and environmental reasons. Currently, biogas technology is not habitual in Sumatra; however this technology for rural areas of Sumatra has not only the potential to tackle the negative impact of livestock and increasing waste generation, but also to alleviate poverty by supporting agriculture (including the livestock sector), providing clean energy and fertilizer.

Key words: small-scale biogas technology, Indonesia, waste utilization, anaerobic digestion.

INTRODUCTION

Due to the factors as population growth, industrialization, urbanization and economic growth the rapid increase of waste generation is caused, especially in developing countries (DHOKHIKAH AND TRIHADINGRUM, 2012) such as Indonesia. The energy consumption is likely to grow faster than the population. In Indonesia (the fourth most populated nation) ranks as the 13th in the primary energy use which is about 893 Mboe (HASAN ET AL., 2013). Currently the final energy supply is dominated by non-renewable energy sources such as oil, gas and coal (contributing for 75 % of the final energy consumption) (MUJIYANTO AND TIESS, 2013; HASAN ET AL., 2013). Therefore, this situation makes the government and the energy society worry as the fossil energy resources and supply might be diminished in the near future (HASAN ET AL., 2013). Currently, is modern energy seen as a key element to reduce poverty and enable human development, various international programmes currently focus on the distribution (as well as implementation) of appropriate ways of energy worldwide (MARTÍ-HERRERO ET AL., 2015). One of such technologies and options are small-scale biogas plants; as they offer production of biogas via the anaerobic digestion of organic waste materials solving the waste management problems and simultaneously produces digestate as a by-product, which may serve as an organic fertiliser (ROUBÍK ET AL., 2016). Small-scale biogas plants have also great potential to contribute sustainable development by providing wide variety of socioeconomic benefits (MSHANDETE AND PARAWIRA, 2009) such as energy supply diversification, rural development opportunities enhancement and creation of employment opportunities.
The potential of biogas technology in rural areas of Indonesia is encouraging, as biogas produced from various types of excrements (mainly buffaloes, pigs and cow, but also human) can be found in all Indonesian provinces, though the quantities are different (IEO, 2006; HASAN ET AL., 2012; ANDRIANI ET AL., 2015). But the use of organic waste to produce biogas is not only limited to the excrements transformation (ANDRIANI ET AL., 2015) but Indonesia also offers possibility to produce biogas from oil palm waste and other agricultural wastes (CHAIKITKAEW ET AL., 2015). Biomass from residues of palm is; however, only scratching the surface of Indonesia's biomass capacities. It is estimated that Indonesia produces over 146.7 million tons of biomass per year (equivalent to about 470 $GJ \cdot y^{-1}$) comprising of agricultural residues, estate crops and forestry wastes.

Biomass has been used traditionally for household energy needs for cooking and water heating in Indonesia. Mainly two major biomass sources, wood and agricultural residues (wastes) were and still are used in rural areas (SINGH AND SETIAWAN, 2013). However, such a usage cannot be considered as sustainable. Furthermore, collecting of these fuels is not only physically challenging, but also time consuming and through its burning mainly women and children are exposed to the harmful indoor air pollution which may cause respiratory diseases and eye inflammation (HUBOYO ET AL., 2014). Therefore it is essential to realize that successful implementation of biogas projects which reduce greenhouse gas (GHG) emissions and substitute fossil fuels and mineral fertilizers can also attract funding under the Kyoto Protocol's Clean Development Mechanism and related funds (JURGENS ET AL., 2006). Furthermore, most of Indonesian people lives in rural areas and depends on the agricultural sector, however, on the other side, they still do not concern about the side products becoming often wastes from agricultural production (PURWONO ET AL., 2013). Nevertheless, these agricultural wastes (mainly livestock waste) may also become valuable energy sources.

The Indonesian Domestic Biogas Programme (BIRU) in Indonesia is not only focused on the technology of small-scale biogas plants (BGPs), but also on its community potential (one biogas plant, depending on its capacity, can supply energy for multiple households or community purposes). However, according to the SINGH AND SETIVAN (2013) majority of households is not adequately interested in using and implementing the biogas technology due to the relatively low prices of kerosene and subsidised LPG bottles.

Interest in use of small-scale biogas technology in rural areas with aim to solve waste management problems and simultaneously produce biogas and digestate is increasing, especially with numerous organizations promoting their use (both for socioeconomic and environmental reasons). Therefore, biogas potential from agricultural waste of small-scale biogas plants in case of Sumatra, especially in connection with livestock waste should be considered. This paper is composed mainly from secondary sources and will serve as a pilot for terrain research design.

Review of small-scale biogas technology in Indonesia and Sumatra

For the production of biogas, various organic material can be used, as it is placed along with water into an anaerobic (oxygen free) conditions. This can be executed by usage of a digester in form of a tank or a plastic membrane.

Biogas is mainly composed of methane, a combustible gas, and carbon dioxide (Tab. 1). Due to containing incombustible components (like CO_2) the calorific value of biogas (produced from manure) is lower (4800-6700 kcal·m^{-3}) than that of pure methane (8900 kcal·m^{-3}). In addition, there might be present other substances (not involved in Tab. 1 as they are not always part of biogas) as chlorine and fluorine (combustion of these compounds produces aggressive products such as: SO_2, SO_3, HCl or HF and consequentially it can have negative effects on the equipment and fittings, such as biogas cookers). The energy content of biogas is higher than energy content of traditional biomass (such as fuelwood, charcoal and cow dung) (LAM AND HEEGDE, 2012). The energy content of biogas is lower in comparison to fossil fuels, however it is cleaner and sustainable (WAHYUDI ET AL., 2015). Due to its characteristics it is an adequate substitute to fossil fuels and biomass usually used for cooking, heating and electricity generation (MAITHEL, 2009; WAHYUDI ET AL., 2015).

Tab. 1. – Composition of biogas in small-scale biogas plants

Compound	**Symbol**	**Content (%)**
Methane	CH_4	50-75
Carbon dioxide	CO_2	25-45
Water vapour	H_2O	2 (20 °C)
Oxygen	O_2	<2
Nitrogen	N_2	<2
Ammonia	NH_3	<1
Hydrogen	H_2	<1
Hydrogen sulphide	H_2S	<1

MAITHEL, 2009; BOND AND TEMPLETON, 2011; WAHYUDI ET AL., 2015

In general, all organic materials can be digested, however, only homogenous and liquid substrates can be considered for simple biogas plants (OLUGASA ET AL., 2014; ROUBÍK ET AL., 2016). Therefore, it is also necessary to dilute the organic material (waste) with adequate quantity of liquid (OLUGASA ET AL., 2014). In case of manure the water/manure ratio should be around 3-6:1 as was described for case of central Vietnam (ROUBÍK ET AL., 2016). The maximum of gas production from a given amount of raw material depends on the type of a substrate. For example, pig liquid manure produces 300 m^3 of methane per a ton of ODM (Organic Dry Matter) and 30 m^3 biogas/m^{-3} liquid, cattle manure produces 200 m^3 methane/t ODM and 20 m^3 biogas/m^{-3} liquid (OLUGASA ET AL., 2014). About the heat retention time it varies in case of different wastes and in the temperature in the digester. As in the case of Indonesia, mesophilic temperature range (20-40 °C) is considered. Therefore the following approximate hydraulic retention time (HRT) can be applied (WERNER ET AL., 1999; OLUGASA ET AL., 2014):

- Liquid pig manure (15 – 25 days);
- Liquid cow manure (20 – 30 days);
- Animal manure mixture with plant material (50 – 80 days).

It is essential to keep HRT because when HRT is too short, the bacteria in the digester are "washed out" faster than they can reproduce, so the fermentation can comes out to a standstill (OLUGASA ET AL., 2014). Furthermore, HRT is important for proper pathogens removal or preventing pathogen spread, therefore is recommended to keep HRT at least 45 days (HUONG ET AL., 2014). These days, in Indonesia all from the main four types can be found (WAHYUDI ET AL., 2015):

- Plastic tubular biogas plant;
- Floating drum;
- Fibreglass;
- Fixed dome.

2. Integration of biogas technology into the farm unit

Lack of access to the basic energy call for the need to integrate the biogas technology into the farm unit to meet energy challenges of rural households and farm units. The raw material for BGPs must be conveniently available on a daily basis. Tab. 2 shows quantity of organic material needed for BGPs. If the daily access is not assured, the technology will not be viable. The integration of biogas technology into the farm unit may reduce the use of fuelwood for cooking and reduce the involvement of farmers in charcoal production. It is therefore imperative for the government and other relevant stakeholders to support and encourage the integration of biogas technology into the farm units in Sumatra.

The design of the BGP should have suitable inlets and outlets to allow the introduction of organic waste and the use of digestate without a large input of labour. The digester should be positioned to minimise transport labour; the biogas pipe line is easily to be extended, whereas the transport of feedstock can be labour exigent. The digesters should be positioned close to a ready flow of wastewater (which should be used in a preference against fresh potable water).

Tab. 2. – Quantity of organic material needed according to the volume of the biogas digester

	Volume of biogas plant (m^3)*				
	4	6	8	10	12
Required heads of animals / quantity of excrements (kg/day)					
Buffaloes	3/25-30	4-5/30-45	6/45-60	7-8/60-75	9/75-90
Pigs	7/15-20	10/20-30	13/30-40	17/40-50	20/50-60
Poultry	600/56	900/84	1200/112	1500/140	1800/168
Biogas production (m^3day)	1-2	1.5-3	2-4	2.5-5	3-6
Equivalent biogas production (hours of cooking)	4	6	8	10	12

Based on: SA PPLPP, 2009; BIRU, 2014

*Volumes are taken according to the most commonly installed volumes by National Biogas Programme BIRU

When considering the feedstock for BGP feeding, the C: N ration and pH of the matter must be followed. Both (C: N ration and pH) can be adjusted by selecting an appropriate mixture of feedstocks. Different feedstocks have different gas yield potentials (Tab. 3). In general, materials with high C: N ratios (such as waste wheat and bread), typically have a higher biogas yields than materials with a low C: N ratio (such as cattle and pig manure). Therefore, co-digestion can be used to selectively improve the biological and nutrient environment in the digester, while increasing available biogas and nutrients and improving waste management.

Tab. 3. – Calculation of typical biogas yields of different feedstocks

Substrate	Daily production (kg/animal)	Content of dry matter (%)	Biogas yield (m^3/kg dry matter)	Biogas yields (m^3/animal/day)	References
Pig manure	2	17	0.25-0.50 0.66 0.47	1.43	Steffen et al., 1998 An and Preston, 1999 Maithel, 2009
Cow manure	8	16	0.2-0.3 0.3	0.32	Bond and Templeton, 2011 Steffen et al., 1998 Maithel, 2009
Chicken excrements	0.08	25	0.35-0.8 0.35-0.6 0.5	0.01	Templeton, 2011 Steffen et al., 1998 Maithel, 2009
Human faeces	0.5	20	0.35-0.5 0.49	0.04	Templeton, 2011 SEAI, 2015
Straw, grass	-	80	0.35-0.4 0.35-0.55	-	Templeton, 2011 Steffen et al., 1998
Water hyacinth (EcengGondok, *Eichhorniacrassipes*)	-	7	0.17-0.25	-	Bond and Templeton, 2011
Corn	-	20	0.25-0.40 0.20	-	Bond and Templeton, 2011 KWS, 2015
Barley	-	25	0.62-0.86	-	Bond and Templeton, 2011
Hemp	-	28	0.25-0.27	-	Bond and Templeton, 2011
Rice straw	-	87	0.18	-	Bond and Templeton, 2011
Rice husk	-	86	0.014-0.018	-	Bond and Templeton, 2011
Waste green biomass (leaves)	-	80	0.06 0.1-0.3	-	Bond and Templeton, 2011 Steffen et al., 1998
Food remains	-	10	0.5-0.6		Steffen et al., 1998

Based on Steffen et al., 1998; An and Preston, 1999; Maithel, 2009; Bond and Templeton 2011; KWS, 2015; SEAI, 2015

There is an adequate and popular on-farm use of biogas as fuel for engine-generator to produce electricity for farm site use (OLUGASA ET AL., 2014) or as fuel for irrigation pumps, engine driven refrigeration compressors etc. Biogas treatment to prevent corrosion from H_2S is usually not necessary if proper maintenance procedures are followed, however H_2S filter for device (biogas cooker) life extension is recommended.

Issues associated with use of small-scale biogas plants in Sumatra

Despite the obvious benefits of the small-scale biogas technology, possible negative impacts shall be also mentioned. Majority of them can be found in next chapters (Technical and Policy issues, Socio-Economic issues and Environmental issues). It is essential to identify factors influencing the demand for biogas technology. It is presented by the following section Biogas technology potential in Indonesia (3.1.-3.4.).

Biogas technology potential in Indonesia – Policy issues

Energy policy development in Indonesia has been generally slow and the role of renewable energy has been overshadowed by other energy sources. However, today, the issue of energy situation in Indonesia is still more and more discussed topic. According to the Indonesian Presidential Regulation No. 5/2006 (dated January 25th), Indonesia established to diversify the use of energy sources by 2025 in the following proportion: coal 33 %, natural gas 30 %, crude oil 20 %, and renewable energy 17 % (MUJIYANTO AND TIESS, 2013).

In the study of ROSYIDI ET AL. (2014) was concluded that two proposed energy programs should be implemented for better dissemination of biogas technology in Indonesia: i) Biogas Energy Package (BGEP) for cooking purposes (because cooking represents a high portion of energy used in rural areas) and ii) Biogas Energy Package (BGEP) for local entrepreneurs (meaning the complete low-cost biogas installation with capacity of 5-10 cows for local farm units).

Currently Indonesian Domestic Biogas Programme – known as Biogas Rumah (BIRU) is running. BIRU is programme implemented by the Dutch NGO Hivos in cooperation with construction partner organizations. It started in May 2009 and by the 2012 it disseminated over 8,000 BGPs (BIRU, 2014) and by the 2015 over 16,000 BGPs. Programme is currently working in ten provinces: Lampung, West Java, Banten, Central Java, DI Yogyakarta, East Java, South Sulawesi, Bali, West Nusa Tenggara and East Nusa Tenggara. HHs benefiting from BIRU programme has above average income and level of education (compared to the average for their region in Indonesia). Biogas users receive subsidy of 2 000 000 IDR (194 USD) per plant. In the case of the most common volume (6 m^3) it is around ¼ of the total price.

Biogas technology potential in Indonesia – Technical issues

It is essential to realize, that with spreading of small-scale biogas plants is bringing also various technical problems, which may harm the further technology dissemination potential. Therefore it is essential to identify the problems and minimize them. Strictly technical issues can be various in nature as obvious in study ROUBÍK ET AL. (2016) where failure criteria were descripted in 5 main technical subsystems where problem can occur: structural components (*i.e.* problems with inlet and outlet system), piping system (*i.e.* leakages and blockages in the piping system), biogas utilization equipment (*i.e.* malfunction of biogas cookers and biogas lamps), digestate disposal system (*i.e.* lack of OM in digestate), anaerobic digestion process and biogas production (*i.e.* leakages in reactor, poor quality biogas and its smell, breakdown of the AD process). Furthermore, feedstock for the BGP needs to be conveniently available on the daily basis.

Biogas technology potential in Indonesia - Socio-Economic issues

As described in MWIRIGI ET AL. (2014) there are some key socio-economic characteristics, which impact the decision of a household to adopt biogas technology. Therefore we tried to set up the costs and benefits associated with biogas technology at the household level (summarized in Tab. 4).

Tab. 4. – Financial costs and benefits associated with biogas technology

Costs	Benefits
Costs of a biogas technology	Cooking and lightening fuel savings
Repair and maintenance costs	Time saving due to the biogas technology
Costs of extra time consumed due to the BGP installation	Saving in households health related expenditures
	Income effects of improved health

However, there are many socio-economic constraints for adoption as well. While implementing the biogas technology in larger scope, challenges of adoption mentioned studies from Asian and African countries shall be taken into consideration also in Indonesia. The most influential socio-economic factors are demonstrated in Tab. 5 which are affecting the adoption process in other regions, however there are applicable for Indonesia. Therefore there is a need to address country specifics for widespread adoption of biogas technology. Costs and subsidies are also an important factor that can positively influence adoption process within the region. As for renewable energy projects (including biogas technology) their economic competitiveness is much lower without subsidies when compared with their alternatives (*i.e.* fossil fuels) (WANG ET AL., 2016). Also awareness about the technology needs to be addressed, using various methods of dissemination, for end users to realize value of the technology.

Tab. 5. – Social and economic factors affecting biogas purchasing and adoption

Category	Factors	References
Social		
	Education	Mwirigi et al., 2009;, Alonbami et al., 2001; Mwakaje, 2008; Omer and Fadalla, 2003; Roubík and Mazancová, 2014
	Awareness about technology	Mwirigi et al., 2009; Alonbami et al., 2001; Mwakaje, 2008; Omer and Fadalla, 2003; Roubík et al., 2016
	Age and sex of households head	Mwirigi et al., 2009; Roubík et al., 2014
Economic		
	Costs and ability to pay	Mwirigi et al., 2009
	Family income	Mwirigi et al., 2009
	Size of farm	Mwirigi et al., 2009; Walekhwa et al., 2009
	Construction costs	Akinbami et al., 2001; Mwakaje, 2008; Omer and Fadalla, 2003; Roubík et al., 2016
	Costs of traditional fuels	Walekhwa et al., 2009; Omer and Fadalla, 2003
	Availability of feedstock	Mwirigi et al., 2009; Mwakaje et al., 2009; Roubík et al., 2016
	Number of dairy cattle	Mwirigi et al., 2009; Akinbami et al., 2001; Walekhwa et al., 2009
	Average costs of a dairy cow	Mwirigi et al., 2009

Biogas technology potential in Indonesia – Environmental issues

Anaerobic digestion utilization is an appropriate solution to environmental problems and can play a fundamental role in conditions improvement. The extensive use of fuelwood for energy purposes in developing countries has fundamental effect on local forests (SURENDRA ET AL., 2014). Deforestation is responsible for up to 25 % of all anthropogenic GHG emissions (STRASSBURG ET AL., 2009) and has also impact on soil erosion and land degradation (GAUTAM ET AL., 2009). In study done by KATUWAL AND BOHARA (2009) it was estimated that annually a small-scale biogas plant spares the direct burning of around 3 metric tons of firewood and 576 kg of dung, subsequently eliminating around 4.5 metric tons of CO_2 emissions to the atmosphere. Furthermore, biogas technology installations reduce pathogenic content of substrate materials (HUONG ET AL., 2014) and also improve health of users. Especially through reduction of indoor smoke coming from solid fuels (traditional biomass), which is widely used by the farmers in developing countries, as well as in Indonesia. Majority of victims of exposure to the indoor air pollution are women and children, mainly from low-income homes in rural areas (LOHANI, 2011; SURENDRA ET AL., 2014). Furthermore, the biogas production does not come with the environmental pollution of degradation; instead it comes with clean energy as a main product and fertilizer as a by-product.

However, biogas plants also produce a significant number of problems and complications regarding their operation (ROUBÍK ET AL., 2016), thereby reducing the benefits of this technology. Afterwards, environmental benefits of biogas technology may not be as great as it initially appears, because the digesters may release methane (CH_4) through leaks as well as from the inlets and outlets (BRUUN ET AL., 2014; ROUBÍK ET AL., 2016). In study done by BRUUN ET AL. (2014) calculations showed that CH_4 emissions from the biogas plants (from leaks and intentional releases), are likely to be substantial because of poor maintenance and poor biogas handling. Furthermore, inappropriate handling with digestate or its uncontrolled disposal may cause environmental contamination.

Small-scale biogas plants can be a very useful tool for energy creation and for waste management, if managed properly. Otherwise benefits of this technology may be compromised.

Recommendations

The following recommendations are drawn for consideration for optimal integration of biogas technology as an energy source in Sumatra:

- There is need for creation of adequate loan system, improving possibility of farmers to increase their livestock capacity and improve stables and pig-pens;
- Exemptions of tax on material made purposely for biogas plants (biogas cookers, generators running on biogas) should be considered;
- Subsidies for farmers who wants to integrate a biogas technology into the farm unit;
- Identification of the suitable institution serving as disseminator;
- Facilitators (extension agents) should be trained to improve integration of biogas technology into the farm units and its adoption;

and

- Systematic empirical studies in case of Indonesia are a high priority for further research

CONCLUSIONS

With the increasing demand for the farm animal products it is coming a growing trend of livestock population resulting in the production of plenty of the organic waste. Such a waste can be used within the biogas technology in Sumatra. Whereas abundant potential for widespread of the biogas technology as it offers significant advantages, especially in regard to energy, the environmental and economic development. However, this development might be compromised and slowed by the lack of technical and policy implications, socio-economical obstacles and by the lack of institutional support. Therefore, these challenges have to be adequately addressed. Biogas technology has not only the potential to tackle the negative impact of livestock and increasing waste generation, but also to alleviate poverty by supporting agriculture (including the livestock sector), it can provide clean energy in form of biogas and fertilizer as a by-product.

ACKNOWLEDGEMENT

This research was conducted with the financial support of Internal Grant Agency of the Czech University of Life Sciences Prague project No. (20165003) and Internal Grant Agency of the Faculty of Tropical AgriSciences, Czech University of Life Sciences Prague No. (20165006).

REFERENCES

1. AKINBAMI, J.F.K., ILORI, M.O., OYEBISI, T.O., AKINWUMI, I.O., ADEOTI, O. (2001): Biogas energy use in Nigeria: current status, future prospects and policy implications. Renewable and Sustainable Energy Reviews 5, 97-112.
2. ANDRIANI, D., WRESTA, A., SAEPUDIN, A., PRAWAEA, B. (2015): A review of recycling of human excreta to energy through biogas generation: Indonesian case. Energy Procedia 68, 219-225.
3. AN, B.X., PRESTON, T.R. (1999): Gas production from pig manure fed at different loading rates to polyethylene tubular digesters. Livestock Research for Rural Development. Volume 11.
4. SEAE.2015. Gas Yields Table. Available at: http://www.seai.ie/Renewables/Bioenergy/Bioenergy_Technologies/Anaerobic_Digestion/The_Process_and_Techniques_of_Anaerobic_Digestion/Gas_Yields_Table.pdf .
5. BIRU. 2014. Get Biru Digester. Available at http://www.biru.or.id/en/index.php/get-biru-digester/.
6. BOND, T., TEMPLETON, M.R. (2011): History and future of domestic biogas plants in developing world. Energy for Sustainable Development 15, 347-354.
7. BRUUN, S., JENSEN, L.S., VU, V.T., SOMMER, S. (2014): Small-scale household biogas digesters: An option for global warming mitigation of a potential climate bomb? Renewable and Sustainable Energy Reviews 33, 736-741.
8. DHOKHIKAH, Y., TRIHADININGRUM, Y. (2012): Solid waste management in Asian developing countries: challenges and opportunities. Journal of Applied Biological Sciences 2, 329-335.
9. GAUTAM, R., BARAL, S., HERAT, S. (2009): Biogas as sustainable energy source in Nepal: present status and future challenges. Renewable and Sustainable Energy Reviews 13, 248-252.
10. HASAN, M.H., MAHLIA, T.M.I., NUR, H. (2012): A review on energy scenario and sustainable energy in Indonesia. Renewable and Sustainable Energy Reviews 16, 2316-2328.

11. HUBOYO, H.S., TOHNO, S., LESTARI, P., MIZOHATA, A., OKUMARA, M. (2014): Characteristics of indoor air pollution in rural mountainous and rural coastal communities in Indonesia. Atmospheric Environment 82, 343-350.
12. HUONG, L.Q., MADSEN, H., ANH, L.X., NGOC, P.T., DALSGAARD, A. (2014): Hygienic aspects of livestock manure management and biogas systems operated by small-scale pig farmers in Vietnam. Science of the Total Environment 470-471, 53-57. doi:10.1016/j.scitotenv.2013.09.023
13. CHAIKITKAEW, S., KONGJAN, P., O-THONG, S. (2015): Biogas Production from Biomass Residues of Palm Oil Mill by Solid State Anaerobic Digestion. Energy Procedia 79, 838-844.
14. IEOS, 2006. Indonesia energy outlook and statistics 2006. Available at: https://kunaifien.files.wordpress.com/2008/12/2006-indonesia-energy-outlook-statistic1.pdf
15. JURGENS, I., SCHLAMADINGER, B., GOMEZ, P. (2006): Bioenergy and the CDM in the emerging market for carbon credits. Mitigation and Adaptation Strategies for Global Change 11, 1051-1081.
16. KATUWAL, H., BOHARA, A.K. (2009): Biogas: a promising renewable technology and its impact on rural households in Nepal. Renewable and Sustainable Energy Reviews 13, 2668-2674.
17. KWS UK LTD. 2015. Biogas in Practice. Available at: http://adbioresources.org/wp-content/uploads/2012/08/Biogas-in-Practice_Guide.pdf.
18. LAM, J., HEEGDE, F. (2012): Domestic Biogas, Technology and Mass Dissemination, Version:March 2012, SNV. 64 pp.
19. LOHANI, S.P. (2011): Biomass as a source of household energy and indoor air pollution in Nepal. Iranica Journal of Energy and Environment 2, 74-78.
20. MAITHEL, S. (2009): Biomass Energy. Resources Assessment Handbook. Solution Centre for Renewable Energy Cooperation Network for the Asia Pacific Asian and Pacific. Centre for Transfer of Technology (2009). http://recap.apctt.org/Docs/Biomass.pdf.
21. MARTÍ-HERRERO, J., CERON, M., GARCIA, R., PRACEJUS, L., ALVAREZ, R., CIPRIANO, X. (2015): The influence of users´ behaviour on biogas production from low cost tubular digesters: A technical and socio-cultural field analysis. Energy for Sustainable Development 27, 73-83.
22. MSHANDETE, A.M., PARAWIRA, W. (2009): Biogas technology research in selected Sub-Saharan African countries – A review. African Journal of Biotechnology 8, 116-125.
23. MUJIYANTO, S., TIESS, G. (2013): Secure energy supply in 2025: Indonesia´s need for an energy policy strategy. Energy Policy 61, 31-41.
24. MWAKAJE, A.G. (2008): Dairy farming and biogas use in Rungwe district, South-west Tanzania: a study of opportunities and constraints. Renewable and Sustainable Energy Reviews 12, 2240-2252.
25. MWIRIGI, J.W., MAKENZI, P.M., OCHOLA, W.O. (2009): Socio-Economic constraints to adoption and sustainability of biogas technology by farmers in Nakuru districts, Kenya. Energy for Sustainable Development 13, 106-115.
26. OLUGASA, T.T., ODESOLA, I.F., OYEWOLA, M.O. (2014): Energy production from biogas: A conceptual review for use in Nigeria. Renewable and Sustainable Energy Reviews 32, 770-776.
27. OMER, A.M., DAFALLY, Y. (2003): Biogas energy technology in Sudan. Renewable Energy 28, 499-507.
28. PURWONO, B.S.A., SUYANTA, RAHBINI, (2013): Biogas digester as an alternative energy strategy in the marginal villages in Indonesia. Energy Procedia 32, 136-144.
29. ROSYIDI, S.A.P., BOLE-RENTEL, T., LESMANA, S.B., IKHSAN, J. (2014): Lessons Learnt from the Energy Needs Assessment carried out for the Biogas Program for Rural Development in Yogyakarta, Indonesia. Procedia Environmental Sciences 20, 20-29.
30. ROUBÍK, H., MAZANCOVÁ, J. (2014): Identification of Context Specific Knowledge as Tool for Facilitators and their Quality Involvement. 2014, Proceedings of the 11th International Conference of Efficiency and Responsibility in Education (ERIE 2014), Prague, pp. 664-670. ISBN 978-80- 213-2468-8. WoS: 000351960900088
31. ROUBÍK, H., MAZANCOVÁ, J., BANOUT, J., VERNER, V. (2016): Addressing problems at small-scale biogas plants: a case study from central Vietnam. Journal of Cleaner Production 112, 2784-2792.
32. ROUBÍK, H., VALEŠOVÁ, L., VERNER, V., MAZANCOVÁ, J. (2014): Gender Inequality in Rural Areas of Central Vietnam * Case Study in ThuaThien Hue Biogas Plant Owners. 2014, SGEM2014 Conference Proceedings, ISBN 978-619-7105-23-0/ ISSN 2367-5659, September 1-9, 2014, Vol. 2, pp. 319-326. WoS:000357835100042
33. SA PPLPP.2009: "Lighting up Lives - Biogas from Poultry Litter as a Sustainable Energy Resource". Potential Good Practice Note. Delhi. India. BDGP04
34. SINGH, R., SETIAWAN, A.D. (2013): Biomass energy policies and strategies: Harvesting potential in India and Indonesia. Renewable and Sustainable Energy Reviews 22, 332-345.
35. STEFFEN R, SZOLAR, O., BRAUN R. (1998): Feedstocks for anaerobic digestion. Available at: http://www.agrienvarchive.ca/bioenergy/download/feedstocks_AD.pdf .
36. STRASSBURG, B., TURNER, B.K., FISHER, B., SCHAEFFER, R., LOVETT, A. (2009): Reducing emissions from deforestation – the combined incentives mechanism and empirical simulations. Global Environmental Change 19, 265-278.
37. SURENDRA, K.C., TAKARA, D., HASHIMOTO, A.G., KHANAL, S.K. (2014): Biogas as a sustainable energy source for developing countries: Opportunities and challenges. Renewable and Sustainable Energy Reviews, 31. 846-869.
38. WANG, CH., ZHANG, Y., ZHANG, L., PANG, M. (2016): Alternative policies to subsidize rural household biogas digesters. Energy Policy 93, 187-195.
39. WAHYUDI, J., KURNANI, T.B.A., CLANCY, J. (2015): Biogas Production in Dairy Farming in Indonesia: A Challenge for Sustainability. International Journal of Renewable Energy Development 4, 219-226.
40. WALEKHWA, P.N., MUGISHA, J., DRAKE, L. (2009): Biogas energy from family-sized digesters in Uganda: Critical factors and policy implications. Energy Policy 37, 2754-2762.
41. WERNER, K., PONITZ, U., HABERMEHL, S., HOERZ, T., KRAMER, P., KLINGER, B., ET AL.: Biogas basics. Biogas digest volume. 145 pp. Information and Advisory Service on Appropriate Technology; 1999. www.gate-isat.gtz.de.

Corresponding author:

Ing. Hynek Roubík, Department of Sustainable Technologies, Faculty of Tropical AgriSciences, Czech University of Life Sciences Prague, Kamýcká 129, Praha 6, Prague, 16521, Czech Republic, tel: +420 22438 2508, e-mail: roubik@tf.czu.cz

YIELD COMPARISON OF NORTH- AND SOUTH-FACING PHOTOVOLTAIC PANELS

V. Roubík, B. Chalupa, P. Kouřím

Department of Physics, Faculty of Engineering, Czech University of Life Sciences Prague, Czech Republic

Abstract

The paper summarizes the results of a several-month experiment carried out on the roof of one of the objects of the Faculty of Engineering. The aim of the experiment was to ascertain how many percent of energy is a north-oriented panel capable to deliver to an off-grid solar system in comparison to a south-oriented one. The point is to determine the effectiveness of deployment of a northern panel in case that it is not possible to install another panel to the south from space, aesthetical, or other reasons. During a three-month observation it has been reckoned up that with the north-oriented panel added, only 26 % more energy can be generated totally, but in the poorest days the benefit can make up to 99.8 %.

Key words: energy, solar, renewable, power, performance, sun, earth.

INTRODUCTION

Energy shortage appears in off-grid solar systems, especially in winter. Many such facilities need to assure at least a certain minimum energy to fulfil its objective, e.g. data acquisition and transmission. For these systems it is desirable to produce at least this minimum daily duty, so as to the number of missed days be minimised – MAREŠ (2013), GORDON (1987). For space and financial reasons it may not be possible to provide an accumulator for such device that would supply the system by surplus summer energy during winter months. One is also often met with instances where it's not possible to add another photovoltaic panel to the south side. For this reason, we consider interesting to find how many percent of energy a northern panel can produce during winter season. Winter period in Czech basin is generally characterized, besides the low sun path, by frequent inversions and low clouds that prevent direct sun visibility; various reflections and scattering can, on the other hand, occur from these atmospheric layers. It isn't easy to assess theoretically how intense any of the effects would be and what percentage of the winter period it would take– e.g. GOH, TAN (1977). For this reason, we have proceeded to do an experiment that compares the outputs of north- and south-facing photovoltaic panels in the conditions of central-Bohemia region.

MATERIALS AND METHODS

Two photovoltaic panels by SHANDONG LINUO PHOTOVOLTAIC HI-TECH CO., LTD., with 72 “125*125-C”mono-crystalline cells each have been used for the measurements, their peak power being 170 W and open-circuit voltage 42.7 V. The panels were mounted to a steel frame. The whole construction was placed on the roof of a faculty object at geographical coordinates 50.1287331 N, 14.3741250 E. A 0.7 Ω resistor was connected to the output of each panel. Voltage over the resistors has been sensed by a two-channel data logger Comet S5021. Data had been acquired with 14-bit resolution at the frequency of 1 sample per 10 seconds, from January to April 2016. Only values higher than 7 mV had been recorded. That would correspond to a minimum logged output power of 13 mW at optimal load – i.e. still a negligible value. Contingent snow had been removed regularly from the panels. Overall situation after the installation can be seen in Fig. 1.

Fig. 1. – Frame with panels installed on the roof – situation

RESULTS AND DISCUSSION

From the experiment, 92 winter days have been recorded and evaluated in all. In the following chart (Fig. 2) we can see daily amounts of energy supplied by the north-facing panel in comparison to the south-oriented one. Histogram is added in the chart that indicates how often particular daily solar radiation amounts occurred in the watched period. Solar irradiation data from a nearby meteostation METEO (2016) are available online. For typical yearly waveforms of solar irradiation and possible panel tilt adjustment see e.g. LIBRA (2010).

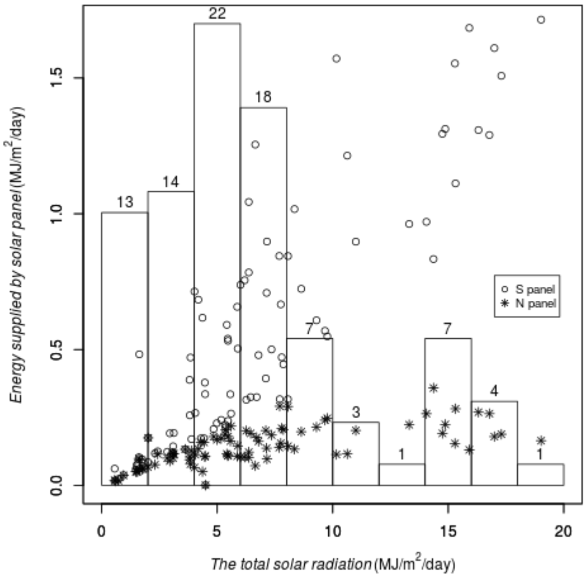

Fig. 2. – Daily energy output totals for both panels and distribution of daily solar radiation

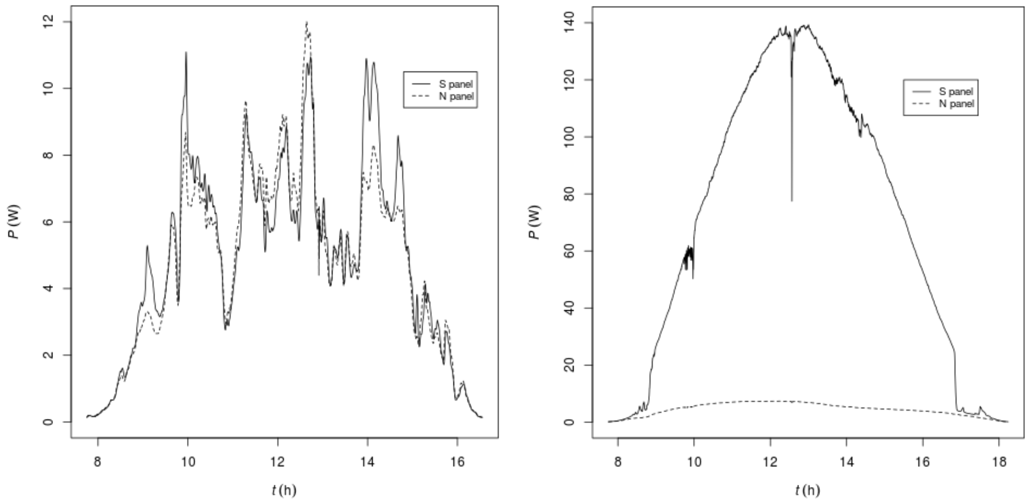

Fig. 3. and 4. – Typical daily runs of generated power in the north- and south-facing panels on an overcast (left) and a sunny (right) days (note the different vertical scales)

It is clearly visible in these charts that in cloudy days, energy supplied by the north-facing panel is equal and in some moments even higher than the energy supplied by the south-facing one, while in clear days the energy of the north panel stays between 8–15 % of the south one. The effectiveness of deployment of a north-oriented panel is thus indirectly proportional to the actual yield of the south panel, as shows the next chart.

Histogram of the daily share of the north panel on the total (both panels) energy production distribution can be seen in Fig. 5.

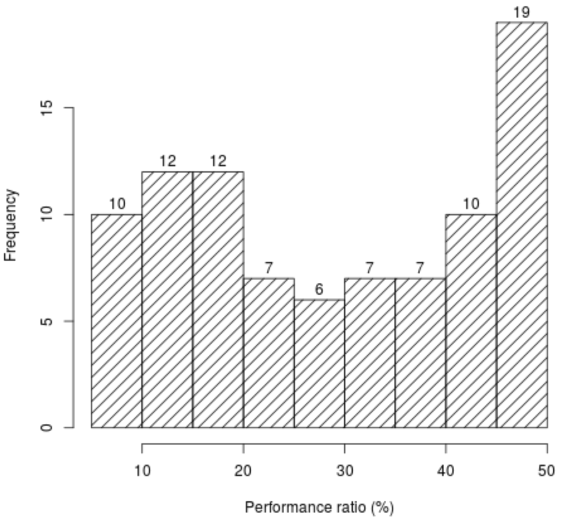

Fig. 5. – Daily shares of the north panel on the total performance

Basic descriptive statistics for the whole measured period are as follows: Total energy produced by the north-facing panel amounts 17440 kJ. Likewise, electric energy supplied by the south panel during researched period totals 66410 kJ. It works out thus that it is possible to supply 26.3 % in all, i.e. roughly one quarter, of electric power from north panel, compared to the south one. Minimum daily ratio of energy supplied by the north panel over the south one amounts 5.74 %, maximum daily ratio amounts 99.8 % by contrast. Mean amount of energy generated by the north panel over the south one makes 47±31 %.

This result is worth a little commentary. According to a strongly non-Gaussian distribution of the ratios visible in Fig. 5, there's a considerable difference between the mean value of the ratios at particular days on one side, the median (which amounts 41±29 %) and all the more so the total ratio of energies produced in the course of the whole period. It actually follows from the chart in Fig. 5 that the majority of the winter season consists of days that are favourable for the deployment of a north-facing photovoltaic panel, as the fraction of clear days, when the effect of its deployment lies below 20 %, is only 20 %.

CONCLUSIONS

The study has demonstrated appropriateness of north-facing panel deployment for the cases where there isn't possible to use a second south-facing panel. During winter season, that is the critical one for off-grid systems, there has been generated 26 % more energy than there would be without the use of north panel, in the case of past winter. In this sense, deployment of a north-facing panel is five times less effective than using a second south-oriented one; though especially during long runs of days without direct sun visibility, that are the most critical moments of the operation– see e.g. KOUŘÍM (2015), the effectiveness of the north panel deployment is identical to the south one. It turned out for the past winter that the sum of the time when the sun could not be seen directly during the days is equal to 82 % of the total time, so one can say that in 82 % of the time the effectiveness of north-facing panel deployment equals the effectiveness of the south orientation.

REFERENCES

1. GOH, T. N., TAN, K. J.: Stochastic modeling and forecasting of solar radiation data. Solar Energy,19 (6), 1977: 755–757.
2. GORDON, J. M.: Optimalsizing of standalone photovoltaic solar power systems. Solar Cells, 20 (4), 1987: 295–313.
3. KOUŘÍM, P., LIBRA, M., POULEK, V.: Off-grid photovoltaic system forillumination. Res. Agr. Eng., 61, 2015: 106–110.
4. LIBRA, M., POULEK, V.: Fotovoltaika- Teorie I praxe využití solární energie (Photovoltaics – theory and practice of solar energy utilisation) 2. vydání, Praha: ILSA, 2010. ISBN 978-80-904311-5-7.
5. MAREŠ, J., LIBRA, M., POULEK, V.: Off-grid photovoltaic system with LED. Proc. 5th International Conference Trends in Agricultural Engineering, Prague, 3rd-6th September 2013: 409–412. ISBN 978-80-213-2388-9.
6. METEO: Meteostation of the Czech University of Agriculture Prague Czech University of Life Sciences Prague, Faculty of Agrobiology, Food and Natural Resources, Department of Agroecology and Biometeorology. Available online at: http://meteostanice.agrobiologie.cz/grafy.php?graf=graf5. Accessed 18 April 2016.

Corresponding author:
RNDr. Vladimír Roubík, CSc., Department of Physics,, Faculty of Engineering, Czech University of Life Sciences Prague, Kamýcká 129, Praha 6, Prague, 16521, Czech Republic, phone: +420 22438 3288,e-mail: roubikv@tf.czu.cz

THE PARKING GENERATION AT SUPERMARKETS AND ITS INFLUENCE ON PLANNING

M. Růžička, D. Marčev, D. Topol

Department of Vehicles and Ground Transport, Faculty of Engineering, Czech University of Life Sciences Prague, Czech Republic

Abstract
The paper is focused on a parking generation in “full-assortment shops” usually called supermarkets. It tries to address an issue taken as dogma in retail i.e. „no parking, no business“. The paper presents results of traffic and questionnaire surveys carried out at 31 supermarkets with the identical assortment and similar gross building square (GBS). All traffic surveys were organised on Fridays at peak hours. The aim of the concurrent questionnaire survey was to find out data about customers’ origin-destination distances, used traffic mode and other information. The results obtained show low strength linear correlation R^2 for dependence of parking lots’ size and capacity on GBS. Dependence with higher strength was established among the number of parking spaces and parking lots’ square (R^2=0.6822); i.e. parking lots are rationally explored, but differences can be seen in area types. Intensities of in/out coming cars ranged from 175 to 575 per three hours (I_{3H}); maximal one hour intensity (I_H) ranged from 66 to 215 in all supermarkets. Dependence of both the intensities on population density or intensity of the nearest important road was determined and was assessed by R^2 with a low strength. Supermarkets’ parking generation rates and their dependence on 100m^2 of GBS with the R^2 = 0.0039 presenting low strength. There were determined parking turnovers and parking turnover’s dependence on number of parking spaces for different area types. The final results did not prove dependence of financial annual turnover on the offer of parking capacity. In conclusion, parking generation is influenced by many other factors – the question remains if the spatial planning process is able to take into account all these factors with appropriate measures in time.

Key words: parking generation, parking turnover, supermarkets’ financial turnover.

INTRODUCTION

Spatial planning of parking lots surrounding retail facilities encounters two main issues. These issues are: what parking capacity (e.g. lot’s square and number of parking spaces) would sufficiently supply a supermarket’s need (or retail area, shopping mall etc.) and what type of parking policy should take place there (i.e. paid parking or time restriction and some others). It is possible to say that especially among shop owners, retail managers and branch organisations, there is a widespread belief that parking plays a fundamental role in the performance of shopping. Local authorities are under the pressure to increase parking capacity or reduce parking fees around shopping areas and even in the downtown. It is evident that to determine parking capacity is the ultimate goal.

The procedure to determine area parking demand (not only retail areas but with every various functions) is generally carried out in these three basic ways. The first one is the usage of standards (e.g. ČSN EN 73 6056, ČSN 73 6110), the second one is through zoning regulations (e.g. PSP, 2014, Building codes etc.) and the third one is modelling (BOSSERHOFF, 2009; CHENG TIEXINA ET AL., 2012; MARTALOS, 2013 ETC.). The principle of all these accesses is based on squares called e.g. gross building square (GBS), gross floor area (GFA) or sale floor surface etc. Consequently different square quantities (square units) are taken as the generator of the number of customers, of students, of clerks, of transit frequency, of passenger cars per time (trip generation rate), parking generation rate and other information according to experience supported by traffic surveys. The results are often further modified and particularised by different influences (coefficients) e.g. areas type (urban, suburban, rural) of shopping, density of population, transit accessibility, offer of different goods, discount actions, the growth factor of motor vehicles etc. SHOUP (1999) has discussed these procedures and has pointed out several discrepancies in e.g. number, place and duration of the traffic surveys carried out, the relation validity between generation rates and GFA and accepting conclusions based on these presumptions. He proposed to plan spatial development with the support of pricing of parking lots (“pricing of curb parking rather than requiring off-street parking will improve urban design”, but “cities should establish Parking Benefit Districts” as well).

MINGARDO (2012) reviewed the literature on the relationship between parking and retail and divided the topic into two groups: those suggesting that parking is important for retail activities and those arguing the opposite. The first group's authors perceive the topic thus: "'the consumer choice of supermarkets is influenced by store characteristics and by parking characteristics" (WAERDEN VAN DER ET AL., 1998), "retailers' perception that the provision of parking facilities for shoppers is positively related to the vitality of retail centres" (STILL - SIMMONDS, 2000) or 40% drivers find parking "too expensive and too difficult to find" (RAC FOUNDATION, 2006). The second group's authors object that retailers have the wrong perception of the modal split of their customers, they overestimate the percentage of their customers using the car to reach the shop, which in reality is much lower (SUSTRANS, 2006). Further, authors are interested in the use of other transport modes – frequency of shopping by cyclists, pedestrians in comparison with drivers (VERHOEK, 2000; MINGARDO, 2009). TELLER (2008) found that retail tenant mix and atmosphere has the highest relative importance. He concludes also that parking does not seem ''to provide potential to change the attractiveness of the investigated agglomeration factors". MINGARDO (2012) concluded: "The main driver of the retail sector is the dogma that parking plays a crucial role in the success of shopping areas, often referred to with the motto 'no parking, no business'. This study shows that this dogma is mostly incorrect." and accordingly four implications for policy were recommended.

The second issue linked with the parking policy can also have significant spill-over effects on urban areas. For example, under-priced on-street parking (during peak periods) can exacerbate urban traffic congestion by inducing drivers to cruise for an inexpensive parking space. These phenomena have been modelled by ROWSE (1999), ARNOTT AND INCI (2006) AND SHOUP (2006). The topic is bound with curb-side parking within shopping areas' surroundings even when the private sector provides parking lots or garage parking (ARNOTT ET AL., 2015). HYMEL (2014) found that in both saturated and non-saturated parking environments, the evidence does not suggest that parking meters (fees) help increase retail sales, which hinge importantly on customer flow. But in comments on the study's validity he remarks that specific findings are somewhat limited: the results are based on observations from one location, and the discontinuity in enforcement occurs at only two points in time. Hence, the estimates can only be interpreted as local effects specific to two times of day at Belmont Shore. The complete literature overview of the economics of parking was published by INCI (2015).

The aims of this paper is to assess and evaluate under different area conditions (urban, suburban, rural) mainly these hypotheses: the dependence of number supermarket's parking places on GBS per 100 m^2, the dependence of parking generation rate characterised by passenger car intensities (I_{3H}, I_H) on a density of surrounding population, the dependence of these intensities (I_{3H}, I_H) on the intensity of the nearest important road, the dependence of higher number of parking places on a higher parking turnover and the dependence of the supermarket's financial turnover on the number of offered parking places per 100 m^2 GBS. Other obtained information is discussed there to specify their influence on the conclusion.

MATERIALS AND METHODS

31 supermarkets with free (not priced) parking lots were chosen, located throughout the Czech Republic. Every supermarket's offer i.e. food, drugstore and other basic consumer goods and management is identical in time therefore all shops belong to one retail chain. The supermarkets were located in Prague- city with app. 1.3 million inhabitants (10) and Prague's suburb (8). Other supermarkets (13) were located in municipalities and smaller cities with the number of inhabitants from 3,000 to 170,000. The mean number of inhabitants was 23,207. The density of population in Prague was taken from ČSÚ (2015) data. For the purpose of this study the density of city population was determined within a radius of 5 km from the supermarket's location i.e. a territory with a square 78.5 km^2 was taken into account. Population data about villages in this circle were derived from ČSU (2015), as well.

The traffic surveys were carried out on Friday from 3 to 6 p.m., in October 2014 and April 2015. They were carried out three times at every supermarket. The decision about the limited number of surveys is linked with the fact that half of the reported parking data by ITE are based on four or fewer surveys (SHOUP, 1999) – assuming that this number of surveys should provide similar results. The number of all incoming and outgoing vehicles was recorded at quarter of an hour intervals, together with vehicles' occupancy and vehicle types arriving at parking lots. The time of Friday's afternoon peak hours was chosen with regard to preliminary surveillance that proved the highest attendance of customers at this time and in this type of supermarkets.

Parking turnover is the rate of use of a facility. It is determined by dividing the number of available parking spaces into the number of vehicles parked in those spaces in a stated time period (SHOUP, 1999; KUMAR, 2016). Data processing of parking turnover per maximal hour intensity or per three hours intensity of passenger vehicles was determined i.e.

$$\tau = \frac{I_H}{P} \quad (1)$$

where: τ *- parking turnover (1)*

I_H – max. intensity of vehicles per 1 hour [I_{3H} per 3 hours] (number of cars)

P – parking capacity or total number of parking lots (number of lots)

The maximal hour intensity of passenger vehicles was determined by cumulative means when the following four quarters of the hour during the survey were taken into account (sum up) and the maximal value selected. The presented three hour intensity is the arithmetical average of three traffic surveys.

Concurrent with the traffic survey, the questionnaire survey was carried out in the supermarkets. The customers were asked questions aimed to specify in more detail the surveyed topic e.g. the type of used transport (walk, cycling, public transit, passenger car), the distance of their journey to supermarkets i.e. origin-destination (OD), the main motivation for using alternative transport mode and others. The total number of incoming customers to the supermarket was recorded as well for the whole duration of the traffic survey.

It was necessary to determine the gross squares of buildings and the square of the whole parking. These squares were determined with the support of application ÚZK (2015). The capacity of the parking infrastructure (max. number of parking vehicles or total number of parking lots) was established on the spot.

The traffic surveys and further necessary data consist of further information such as the 24 hour intensity of passenger cars on the nearest important road (NIR) (source CSD, 2010), the accessibility and quality of public transit, the opportunities for parking in near surroundings (curb-side parking), competing nearby supermarkets etc. The owner of this retail chain provided information about yearly turnover of several supermarkets in relative values for the purpose of this study.

It is necessary to remark that coefficients of determination are used in other parts of this paper to point out none existing dependence. Their value is nearing to zero and it has not any practical meaning. It is supposed that the usage of other statistical methods would not bring any different conclusion under these specific and real conditions.

RESULTS AND DISCUSSION

The results of the questionnaire survey confirmed some expected presumptions but it is necessary to remark that the supermarkets' surrounding conditions differed significantly (e.g. one supermarket was accessible by passenger car only, the other one had good transit nearby etc.). That is why it is questionable to accept these results without objections as a generalisation of customers' behaviour. The total number of customers addressed was 263; 87% of them used passenger cars; transit was used by 4%; 8% used bicycles or walked. Customers came from OD distance: 35% up to 5 km; 67% up to 10 km (includes 5 km OD as well). The main reasons for using transit, bicycles or walk were as follows: I do not have a car (driving licence) 23%; good accessibility 32%; shortest way (in time) to get there 13%; I do not want to use a car 19% and walking is good for health 13%. Customers were asked to guess their time spent by shopping: 25% up to 10 minutes; 40% 10-20 minutes; 28% 20-30 minutes. It means that 93% of customers perceive half an hour as sufficient for their shopping in this type of shop. This shopping time corresponds with parking turnover (Fig. 6) where the majority of parking places were occupied app. twice.

The gross building squares (GBS) and parking squares (PS) were determined in all surveyed supermarkets i.e. GBS ranged from 1195 to 2488 m^2 (average GBS 1745 m^2), PS ranged from 1246 to 5802 m^2 (mean PS 3443 m^2). The smallest PS is the one exceptional case when the supermarket had a limited surrounding space and its parking lot was built on its building's roof. The PS's dependence on GBS was assessed; the coefficient of determination R^2 for linear correlation is equal to 0.3355.

The expected dependence with higher strength was established among the parking capacity (number of parking spaces) and PS that is proved by linear correlation R^2=0.6822; this value shows that parking lots are rationally explored. The total square of parking spaces covers on average 40% of PS (lowest 24%); it means that the layout of parking spaces is designed very similarly. The layout is done by standards (the space's dimensions), by shape of plot and by the designer's efforts to maximize number of parking spaces. Fig.1 shows dependence of PS on GBS according to their location. It is evident that the highest deviation occurs in the suburban area (standard deviation = 1243.2). Coefficient of determination R^2 = 0.5074 would be even higher (0.6793) without „roof parking" in Prague.

The number of parking spaces per 100 m^2 of GBS was determined to be from 1.93 to 8.29. The dependence of number parking places per 100 m^2 of GBS on total GBS is presented in Fig. 2 - where R^2 of 0.0022 shows low strength i.e. supermarkets with larger buildings do not have more parking places per 100 m^2 of GBS.

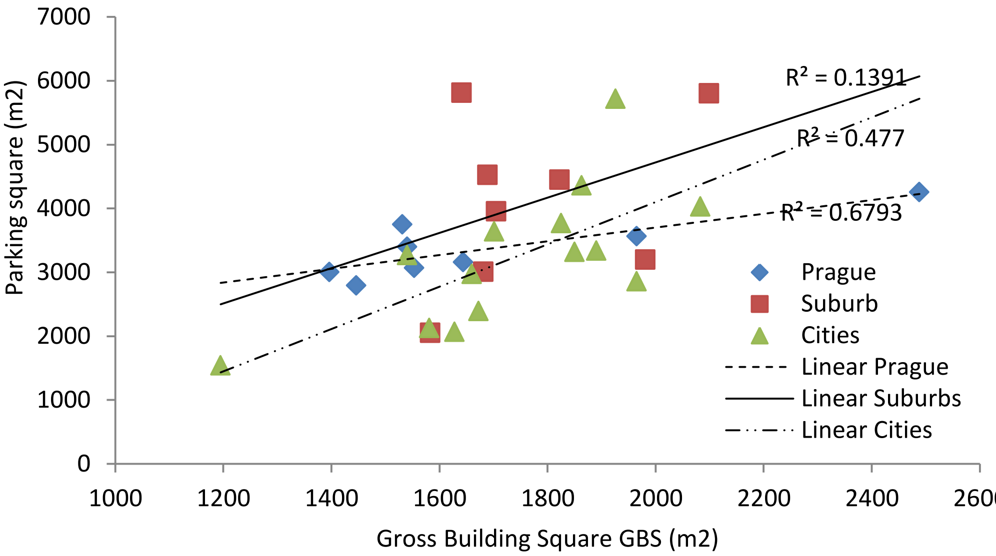

Fig. 1. – Parking squares' dependence on GBS and area

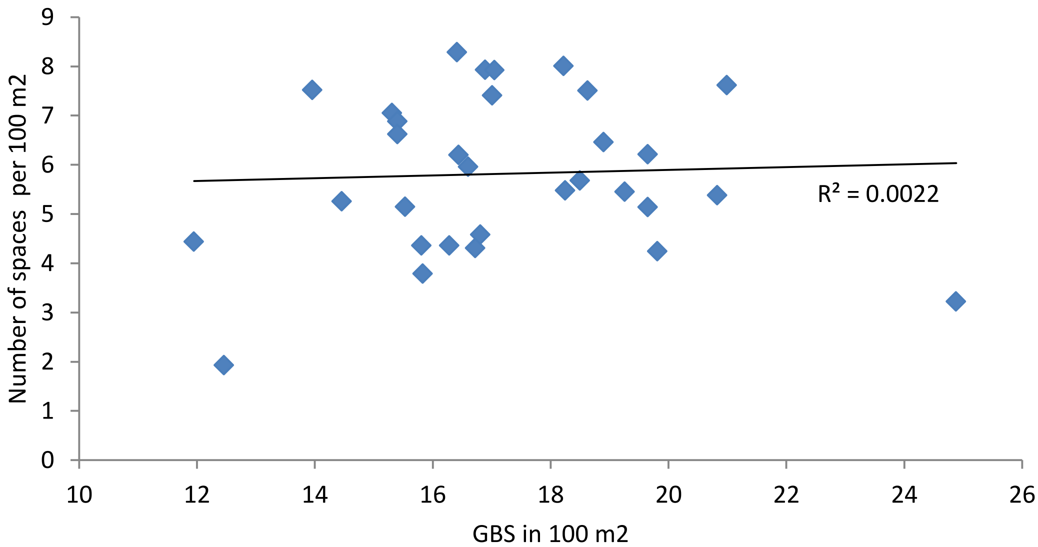

Fig. 2. – Number of parking spaces' dependence on 100 m^2 of GBS

The three traffic surveys carried out recorded the number of passenger cars (out/incoming parking lot) and their occupancy. The mean number of incoming passenger cars (I_{3H}) ranged from 175 to 575 during three hours (the exception was only 46 cars on the "roof parking lot") for all supermarkets. Maximal one hour intensity (I_H) was determined by 15 minute intervals and ranged from 66 to 215 for all supermarkets. 62% of supermarkets had I_H during time interval from 4 p.m. to 5:30 p.m. – this confirms an assumption for

Friday's peak hours. Only 10% of supermarkets had I_H in the last hour of survey. The average occupancy of passenger cars was determined as 1.5 persons per car (range from 1.29 to 2).

The dependence of intensities (I_{3H}, I_H) on density of population was determined. Both dependencies on population density was assessed with low strength, I_{3H} had R^2 = 0.0005 and I_H R^2=0.0021 for all supermarkets. Dependence of intensity I_{3H} on density of population and different areas proves low strength by R^2 (Fig. 3).

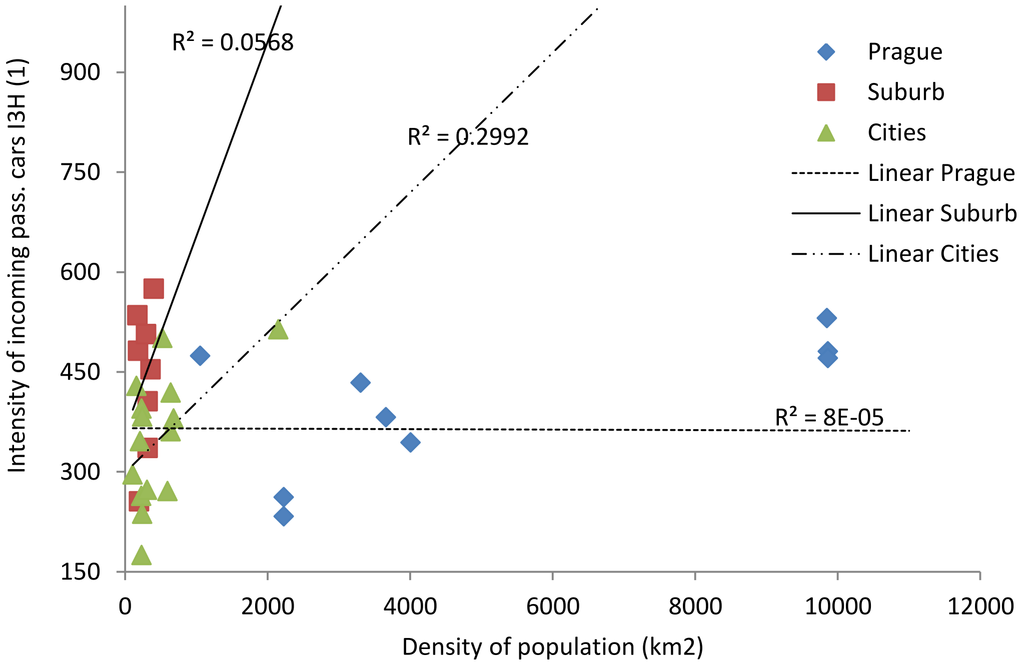

Fig. 3. – Dependence of I_{3H} on density of population

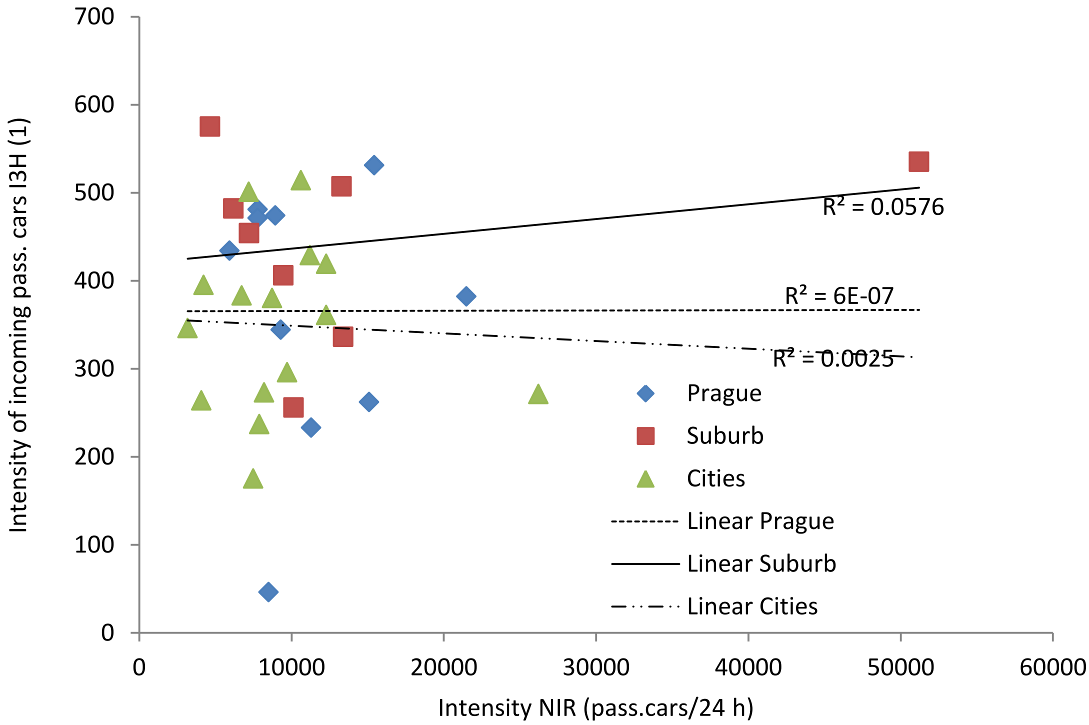

Fig. 4. – Dependence of I_{3H} on intensity of NIR

Dependence of intensities (I_{3H}, I_H) on intensity of passenger cars on the nearest important road (NIR) was determined. Both dependencies on NIR was assessed as low strength, I_{3H} had R^2 = 0.0218 and I_H R^2=0.019 for all supermarkets. Dependence of intensity I_{3H} on density of population and different areas proves low strength by R^2 (Fig. 4).

The parking generation rate defined as the peak parking occupancy (THE INSTITUTE OF TRANSPORTATION ENGINEERS, 1987,a) was determined for I_{3H} or I_H. The peak of occupancy was presumed for maximal one hour intensity (or three hours intensity was taken into account as well). The parking generation rate was stated in relation to the number of parking spaces per 100 m^2 of GBS. In other words, it states how many cars replaced themselves on one parking place during one hour or three hours i.e. how many parking spaces were theoretically needed for 100 m2 of GBS. Supermarkets' parking generation rates and their dependence on 100 m^2 GBS are shown on Fig. **1**. – the R^2 = 0.0039 presents low strength. Similar research was done with I_{3H} with the result of R^2 = 0.0174. The values of parking generation rates for I_H are in the range from 0.65 to 2.79 (I_{3H} from 1.72 to 7.47).

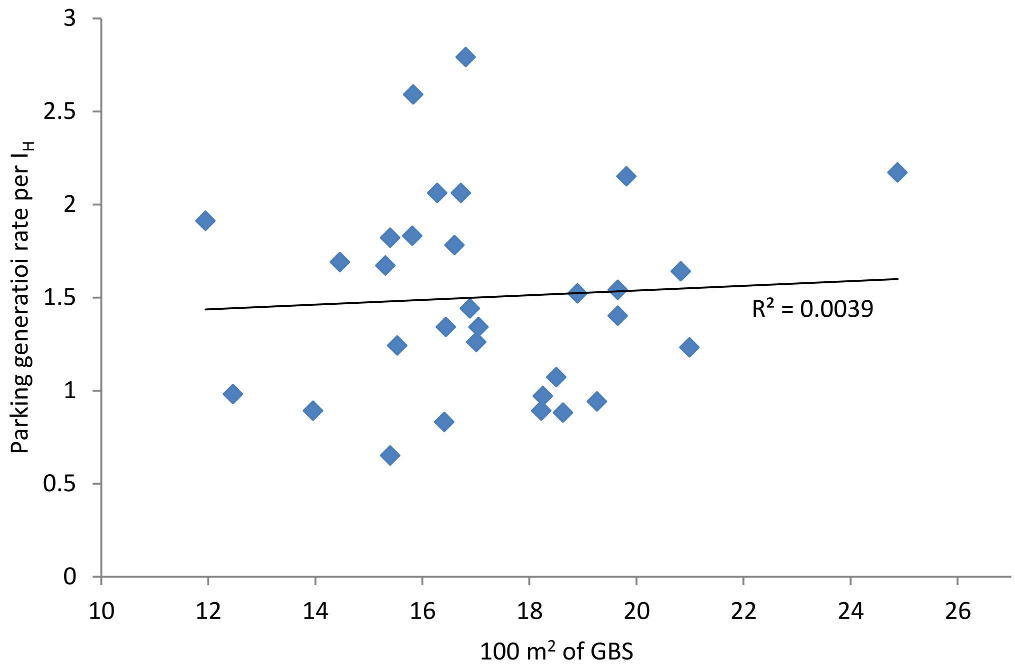

Fig. 1. – Parking generation per I_H and 100 m^2 of GBS

Parking turnover τ was determined at every supermarket for I_{3H} and I_H for the whole parking square. The τ for I_{3H} ranged from 1.7 to 7.5 (average 3.9); for I_H ranged from 0.6 to 2.8 (average 1.5). Linear correlation of parking places and parking turnover rate was determined for I_{3H} as R^2 = 0.2009, for I_H it was R^2 = 0.2747. Fig.6 presents parking turnover τ dependence on the number of parking spaces that are offered in different areas. The highest strength can be seen at Suburb's area R^2 = 0.8497, Cities' area had R= 0.4685 and Prague's area had the lowest strength R^2 = 0.0115.

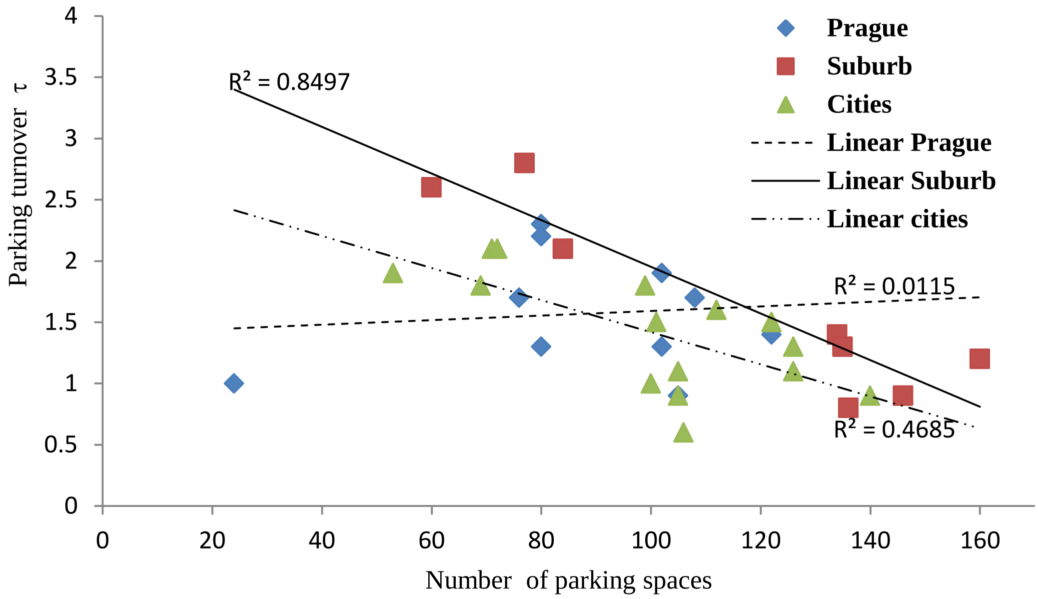

Fig. 6. – Dependence of parking turnover τ (I_H) on number of parking spaces and area

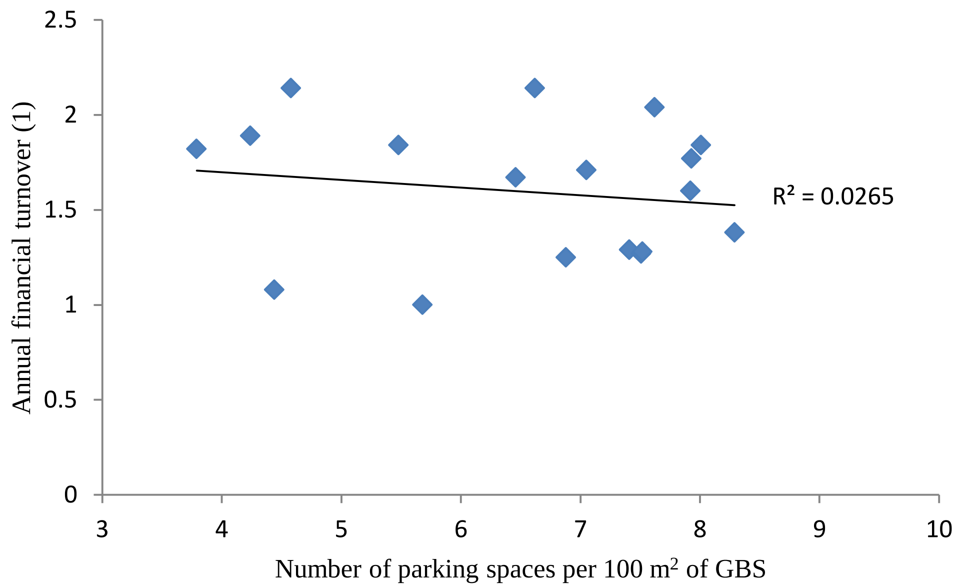

Fig. 7. – Dependence of shop's financial turnover on number of parking spaces

The annual financial turnover was provided by the owner of supermarket chain for 18 shops in relative values. Fig. 7 presents the dependence of the financial turnover on the number of parking places per 100 m^2 GBS. The presumption of a correlation between increased number parking places and a supermarket's turnover was not confirmed. The coefficient of determination $R^2 = 0.0265$ has a low strength. It would be possible to say that only 3% of supermarkets will have a higher turnover through the provision of more parking places per 100 m^2 of GBS.

CONCLUSIONS

In total, 31 supermarkets were surveyed during the year. They differed slightly in gross building square but they had an identical assortment and management. The strength of the coefficient R^2 between gross building square (GBS) and parking square (PS) was rather low in all supermarkets. It is possible to say that only 33% of the surveyed cases can be explained by the relation between GBS and PS. On the one hand, the dependence from the point of location had the higher strength (R^2=0.6793) in Prague (metropolis). This fact can be explained by the higher price of land (plots) in comparison with the other areas, or by limited space in higher density of buildings etc. But on the other hand, R^2 of Prague's suburban areas provide the evidence that PS was designed according to local possibilities regardless of any spatial planning rules or directives. The planners, designers and investors used their chance to obtain non-restricted land-take.

The number of parking places per 100 m^2 of GBS is in range from 1.93 to 8.29 (average 5.8). These values show that a parking lot's capacity or the number of parking spaces do not take into account the total GBS and even R^2 of 0.0022 shows the low strength i.e. supermarkets with larger GBS do not have more parking places per 100 m^2. It is evident that standards, regulations and models were not kept or even taken into account.

The determined intensities of incoming and outgoing passenger cars to parking places and the influence of population density or intensity of NIR on them was not proved. It can be explained by many different factors. One of the very important factors can be competition of nearby other supermarkets, retail areas or malls. The lowest R^2 strength was found out in Prague where the shopping conditions are the most accessible in comparison with other areas.

THE INSTITUTE OF TRANSPORTATION ENGINEERS, 1987A in SHOUP (1999) declares the parking generation rate equal to 2.9 per supermarket i.e. parking spaces per 1000 square feet of gross floor area (it is app. 93 m^2 , the difference of square is negligible, it means a difference of app.1 parking place). If these conditions are met, it is expected that 22 passenger cars will be on one parking place per day. The results of parking generation rates obtained exhibit a wide range, these values differ nearly 4 times. If the expected three hours' parking generation rate characterises one quarter of a supermarket's open hours (not supposed non-stop time) then the result can be from 7 to 30 passenger cars per place per day. It means high deviations from the declared standard. It supports the conclusion that parking generation is essentially unrelated to GBS in the surveyed cases and this confirms SHOUP'S (1999) conclusions with GFA (backed up by a traffic survey carried out at 18 fast-food restaurants). The generally accepted expectation that the higher is number of parking spaces the lower is parking turnover τ was confirmed in low strength. It is possible to say that only 23% (average of I_{3H} a I_H) of surveyed cases confirmed this dependence. During I_H seven supermarkets had the parking turnover $\tau \leq 1$. It means that these supermarkets provide overestimated the capacity of parking places; therefore, a majority of customers spend there then less 30 minutes (according to their own estimation obtained from questionnaire survey 93%). The R^2 in suburban areas proves that a higher supply of parking places really reduced parking turnover τ. The wide range of parking turnover proves that customers would like to accept a shorter shopping time in this type of supermarkets. It all depends on shopping management and customers' clearance. Even more, this access enables the supermarket to increase financial turnover more than higher parking capacity. Shop owners, retail managers and branch organisations often believe that parking plays a fundamental role in the performance of shopping. They try to persuade local authorities to increase parking capacity or reduce parking fees around retail areas and even in the downtown. Results of the research carried out did not confirm this dependence of shopping performance on parking capacity. The presumption that a higher number of parking places should lead to a higher turnover was not confirmed by this study. The coefficient of determination $R^2 = 0.0265$ has low strength. It would be possible to say that only 3% of supermarkets will have a higher turnover with a higher number of parking places offered per 100 m^2 of GBS. This fact confirms results of MINGARDO ET AL. (2012).

In conclusion, the research carried out proved in the case of 31 supermarkets that parking generation is influenced by many factors. It is very complicated to forecast future parking demands. The question remains if the spatial planning process is able to take into account all these factors with appropriate measures in time. The current access, i.e. minimum parking requirements and free parking, imposes hidden costs on spatial development and parking lots' construction which impede our progress toward important social, economic and environmental goals. Spatial planning and parking design deserves a new paradigm (SHOUP, 1999).

ACKNOWLEDGEMENTS

I would like to acknowledge financial support from the Czech university of Life Sciences in Prague, internal grant agency (IGA 2015:31150/1312/3109). At the same time I want to thank owner of retail chain for traffic survey permission and providing data.

REFERENCES

1. ARNOTT, R., INCI, E., ROWSE, J.: Downtown curbside parking capacity, Journal of Urban Economics, Volume 86, pp. 83–97, 2015: http://dx.doi.org/10.1016/j.jue.2014.12.005.
2. ARNOTT, R., INCI, E.: An integrated model of downtown parking and traffic Congestion, Journal of Urban Economics, Volume 60, 2006, pp.418–442.
3. BOSSERHOFF, D.: Programm Ver_Bau: Abschatzung des Verkehrsaufkommens durch Vorhaben der Bauleitplanung mit Excel-Tabellen am PC. Gustavsburg, 2001 (every year update, 2009), in Doprava generovaná komerčními zónami, ISBN 978-80-902527-9-0, pp. 23-39.
4. CSD 2010 (statewide traffic survey), The Road and Motorway Directorate of the Czech Republic (RSD CR) http://scitani2010.rsd.cz/pages/shop/default.aspx (available 23.7.2015).
5. ČSN 73 6110: Projektování místních komunikací (Design of urban roads), ICS 93.080.10, Český normalizační institut, 2006.
6. ČSN EN 73 6056: Odstavné a parkovací plochy silničních vozidel (Parking areas for road vehicles), ICS 93.080, Úřad pro technickou normalizaci, metrologii a státní zkušebnictví, 2011.
7. ČESKÝ STATISTICKÝ ÚŘAD (Czech statistical authority) http://vdb.czso.cz/vdbvo/tabparam.jsp?voa=tabulka&cislotab=DEM9020PC_MC&vo=null&kapitola_id=370 (available 23.7.2015).
8. ČESKÝ STATISTICKÝ ÚŘAD (Czech statistical authority) Published: 30.04.2015 https://www.czso.cz/csu/czso/population-of-municipalities-1-january-2015 (available 23.7.2015).
9. CHENG, T., TAI MIAOMIAOA, M. Z.: The Model of Parking Demand Forecast for the Urban CCD, Energy Procedia 16 (2012) 1393 – 1400, doi:10.1016/j.egypro.2012.01.221 Elsevier www.sciencedirect.com (available 2015).
10. HYMEL K.: Do parking fees affect retail sales? Evidence from Starbucks, Economics of Transportation 3 (2014), http://dx.doi.org/10.1016/j.ecotra.2014.08.001 , 2212-0122/ pp.221–233 (8.2.2015).
11. KUMAR, E. N.: Parking Patterns In Order To Menace Traffic Chaos Department of civil engineering university, Gwalior, Civil engineering portal, http://www.engineeringcivil.com/parking-patterns-in-order-to-menace-traffic-chaos.html (30.6.2016).
12. INSTITUTE OF TRANSPORTATION ENGINEERS (ITE), 1987a, Parking generation, Institute of Transportation engineers, 2nd. ed., Washington DC.
13. INSTITUTE OF TRANSPORTATION ENGINEERS (ITE), 1987b, Trip generation, Institute of Transportation engineers, 4nd. ed., Washington DC.
14. MARTOLOS, J. A KOL.: Metody prognózy intenzit generované dopravy, certifikovaná metodika MD ČR ze dne 4. října 2012, ISBN 8087394089, 9788087394083, vydal EDIP s.r.o., Plzeň, 2013.
15. MINGARDO, G., VAN MEERKERK, J.: Is parking supply related to turnover of shopping areas? The case of the Netherlands. Journal of Retailing and Consumer Services19 (2012), doi:10.1016/j.jretconser. 2011.12.001, pp 195–201.
16. MINGARDO, G.,MOUTER., N.,TALENS,H.: No parking, still business, vol.4. Verkeerskunde, June 2009.
17. PSP - Pražské stavební předpisy, (Prague's construction regulations), IPR Praha, Institut plánování a rozvoje hlavního města Prahy, 2014, http://www.iprpraha.cz/uploads/assets/dokumenty/otpp/psp/final/01_psp_uplne-zneni_text_priloha1-a-2.pdf (8.2.2015).
18. RAC FOUNDATION, 2006.Motoring Toward 2050, Shopping and Transport Policy, London.
19. SHOUP, D.C.: The trouble with minimum parking requirements, Transportation research Part A 33, Issues 7–8, 1999: pp. 547-574.
20. SHOUP, D.C.: Cruising for parking. Transport Policy, Volume 13, Issue 6, November 2006, Pages 479-486,
21. Still, B., Simmonds,D.: Parking restraint policy and urban vitality. Transport Reviews 20(3), 2000, pp. 291–316.
22. SUSTRANS, 2006. Real and perceived travel behaviour in neighbourhood shopping areas in Bristol. Final report prepared by Sustrans on behalf of Bristol City Council, January 2006.
23. SUSTRANS, Traffic Restraint and Retail Vitality, available via / http://www.sustrans.org.uk/resources/publications S. 2003.
24. TELLER, C.: Shopping streets versus shopping malls - determinants of agglomeration format attractiveness from the consumers' point of view. The International Review of Retail, Distribution and Consumer Research 18(4), 2008: pp.381–403.
25. ÚZK, 2015 "Nahlížení do katastru nemovitostí" (Surveillance of land registry) http://nahlizenidokn.cuzk.cz/VyberKatastrMapa.aspx (2015).
26. VERHOEK, B.,: Bestedingen fietsers en automobilisten.Studie verricht ten behoeve van het I-ce project Kosten en Baten van Fietsverkeer. Grontmij, 2000 Eindhoven.
27. WAERDEN VAN DER, P., BORGERS, A., TIMMERMANS, H,: The impact of the parking situation in shopping centres on store choice behaviour. GeoJournal45, 1998, pp. 309–315
28. INCI, E.: A review of the economics of parking, Economics of Transportation,, Volume 4, Issues 1–2, 2015: pp 50–63 doi:10.1016/j.ecotra.2014.11.001 (23.7.2015).

Corresponding author:

doc. Ing. Miroslav Růžička, CSc., Department of Vehicles and Ground Transport, Faculty of Engineering, Czech University of Life Sciences Prague, Kamýcká 129, Praha 6, Prague, 16521, Czech Republic, phone: +420 22438 3106, e-mail: ruzicka@tf.czu.cz

ANALYSIS OF THE TECHNOLOGICAL PROCESS OF HOP DRYING IN BELT DRYERS

A. Rybka[1], P. Heřmánek[1], I. Honzík[1], D. Hoffmann[1], K. Krofta[2]

[1]*Department of Agricultural Machines, Faculty of Engineering, Czech University of Life Sciences Prague, Czech Republic*
[2]*Hop Research Institute Co., Ltd., Žatec, Czech Republic*

Abstract
Current problems of the present technology of hop growing include complex innovation in the drying process in existing belt dryers. An emphasis is put on increasing the drying efficiency and innovating the current conditioning. The presented output needs to be preceded by an analysis of the existing drying state. The operating measurement was carried out in three belt dryers and included a measurement of the temperature and moisture content parameters of the drying medium as well as the qualitative parameters of the hops being dried. The drying parameters were monitored by means of continuously recording data- loggers and a laboratory analysis of the samples (hop moisture, alpha bitter acids, hop storage index). The drying process revealed that the hops are virtually dry (10 ± 2.0 % of moisture content) already at the end of the second belt, or possibly at the beginning of the third belt (Stekník). The hop drying in Velká Bystřice proved that hops are considerably over-dried (moisture content of 4 to 8 %) and are subsequently adjusted through conditioning to the final moisture content of 8-10 %. Over-drying leads to a substantial shattering of hop cones, a factor which renders the manipulation with hops for further processing more difficult, leading to larger losses in the lupulin content.

Key words: hops, belt dryer, temperature, moisture content.

INTRODUCTION

The most common method of hop preservation is drying, during which the water content in hop cones reduces from former approx.75 % of moisture content to 8 or up to 10%. Drying is carried out immediately after the hop harvest mostly in belt dryers that are operated continuously (3 belts). Hot air is the drying medium here which is heated by burning natural gas or light heating oil. The maximum drying temperature ranges between 55°C to 60°C and is practically stable for the entire duration of drying. Hops are exposed to this temperature for 6 to 8 hours (HENDERSON, MILLER, 1972; HENDERSON, 1973).

The stability of alpha bitter acids as a key substance in hops from the point of view of brewing technology is sufficient at drying temperatures not exceeding 60°C (DOE, MENARY, 1979). However, for some heat-labile substances the drying temperatures ranging from 50 to 60°C in the final stage of drying are too high. At such temperatures irreversible transformation and losses occur. An example of these substances is hop essential oils that are contained in hops in the amount of 0.5 – 3.5 % depending on variety (HOFMANN ET AL., 2013). The pilot studies proved that 15 to 25 % of the total content of essential oils present in hops before drying decrease under the current drying conditions (KIENINGER, FORSTER, 1973). Besides the loss in amount, also the sensory profile alters as a consequence of decrease in more volatile components. Regarding special aroma hop varieties, so-called "flavour hops", in which the content and composition of essential oils are key quality parameters, such losses lead to a decline in the product quality.

The currently used belt dryers are out-dated, implemented in the 70s and 80s of the last century. The overall capacity of drying technologies is now 9500 tons of dry hops, which represents a capacity that is higher by 38 %, the total production being approx. 6000 tons of dry hops. It follows that there is no need to build new dryers for hops but to focus on modernisation and automation of the drying process as a whole in the existing drying technologies.

One of the tasks referring to the currently solved NAZV research project of the Czech Ministry of Agriculture is therefore the complex innovation in the drying process in existing belt dryers. The expected economic benefit should be brought by saving the heating medium as well as electricity, deriving from shortening of the drying time, increasing of the facility capacity and shortening of the harvesting time (RYBÁČEK, 1991). The object of the given research is to pass on to hop-processing plants inter alia a drying process that had gone through a complex innovation, with particular emphasis on increasing the efficiency of drying and on innovating the conditioning system

(HANOUSEK ET AL., 2008). Related to that is a design and implementation of belt dryer adjustments, including automation of the operations and continuous measuring of stability and control of the drying process. The object of this paper is an analysis of the current state of hop drying, conditioning and stabilization, which precedes in terms of content the innovation in the entire process of hop drying.

MATERIALS AND METHODS

The operating measurement was carried out in belt dryers being parts of the plants of the co-researchers:

- The Research Farm in Stekník, Hop Research Institute Co., Ltd., Žatec - PSCH 325 belt dryer,
- Agrospol Velká Bystřice Ltd. - PSCH 750 belt dryer and PSCH 900 belt dryer.

The measured parameters were the temperature and moisture parameters of the drying medium, and the qualitative parameters of the hops being dried – temperature, moisture content, drying time (JECH ET AL., 2011). Given the large extent of the measured values, only selected results constitute the content of this paper. Further results are available at the authors.

The monitored parameters were being determined in two ways:

- through measuring by means of inserted data-loggers,
- through a laboratory analysis of the samples.

To measure continuously the air temperature and relative humidity inside a layer of the hops being dried, VOLTCRAFT DL-121-TH data-loggers were employed which allow for setting the frequency of data storage (SRIVASTAVA ET AL., 2006). In our case this frequency was set to 5 minutes. The data-logger internal memory is able to store 32000 of measured data, which is absolutely sufficient. The data-logger was integrated together with the sensor in a plastic case and powered via an inserted battery. The plastic case was fitted with a USB connector at one of its ends, via which the stored data were imported into the computer.

To protect them against mechanical damage in the course of passing through the dryer and against being soiled by lupulin, we fixed the data-loggers into polyurethane material and inserted them into two stainless half-spherical sieves. This guaranteed their sufficient protection, the sieves did not impede the air permeation and there were no mistakes in measuring (Fig. 1).

In the dryer, three data-loggers were placed through the first check window on the first (upper) belt, two of them approx. 0.5 m far from the left and right dryer wall and one in the middle (Fig. 2).

The advantage of data-loggers compared to fixed sensors in a dryer is that they pass together with hops through the dryer, continuously recording the entire drying process. The following graphs are based on the average values received from the employed data-loggers.

Fig. 1. – Inserting a data-logger into a protective sieve

Hop samples were being taken throughout the process of drying, following a pre-determined schedule, and then were submitted to a laboratory analysis. The analysis allowed for identification of the hop storage index HSI, the content of alpha bitter acids, and the hop sample moisture content was also determined.

The first sample was always fresh green hops taken immediately after picking. Other samples were taken at check window points (Fig. 3) by individual belts, three samples from each belt. Last samples were taken prior to and after the conditioning, and one more sample prior to baling.

Fig. 2. – Deployment of data-loggers to dryer width

In Stekník as well as in Velká Bystřice the monitored hops were mainly of the Saaz hop variety. The hop moisture content was determined in the laboratory dryer of the Hop Research Institute Co., Ltd, Žatec with forced air circulation according to the EBC 7.2 method. The HSI hop storage index was determined using the EBC 7.13 conventional spectrophotometric method from a toluene hop extract. The content of alpha bitter acids was measured by liquid chromatography according to the HPLC EBC 7.7 method (KROFTA, 2008; WEIHRAUCH ET AL., 2010). Tables and graphs were created reflecting the results of the hop sample laboratory analyses.

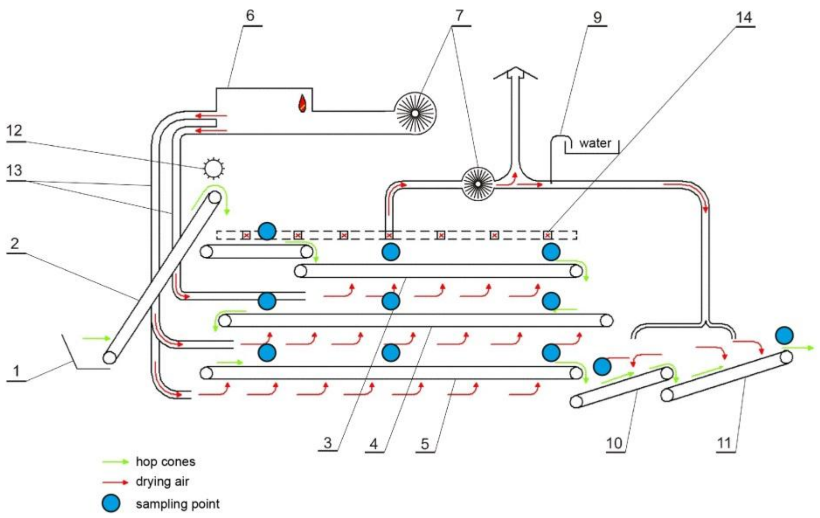

Fig. 3. – Scheme of the belt dryer with indicated sampling points
1 - hopper, 2 - inclined wire mesh conveyor, 3(4,5) - upper (middle, lower) drying wire mesh conveyor, 6 – hot-air aggregate, 7,8 - fan, 9 – water management, 10(11) - first (second) wire mesh conveyor of the conditioning chamber, 12 – straightening roll, 13 - distribution air pipes, 14 - suction openings

RESULTSAND DISCUSSION

The Research Farm in Stekník of the Hop Research Institute Co., Ltd., Žatec

The graph in Fig. 4 clearly shows that the whole drying process is recorded when measured continuously. Around the 90th minute the temperature dropped and the relative humidity increased due to the dryer failure and following forced interruption of operation.

Fig. 5 presents an example of one measurement carried out with samples from a laboratory dryer. Besides hop moisture content, the graph also depicts the hop storage index HSI progresses. The graph in Fig. 6 confirms the previously stated progress of the hop moisture content dependency on hop passage through the dryer. A conclusion can be drawn that hops are dried to approx. 10% of moisture content already at the end of the second belt. The laboratory analyses also indicate that only minimum changes occur both in alpha bitter acids and the HSI after the hops have passed through the belt dryer.

Agrospol Velká Bystřice Ltd.

Data-loggers enabled measuring of the Saaz hop variety in both dryers. This measurement was very problematic, for due to a low yield the drying continuity was often interrupted and the belt dryers were put out of operation many times.

In both dryers the ambient environment was measured only on the third belt and in conditioning. The resulting values are to be found in Fig. 6 and 7. Both measurements confirmed that hops are already dried on the third belt and are unnecessarily over-dried, which means wasting of energy expended to heat the drying air.

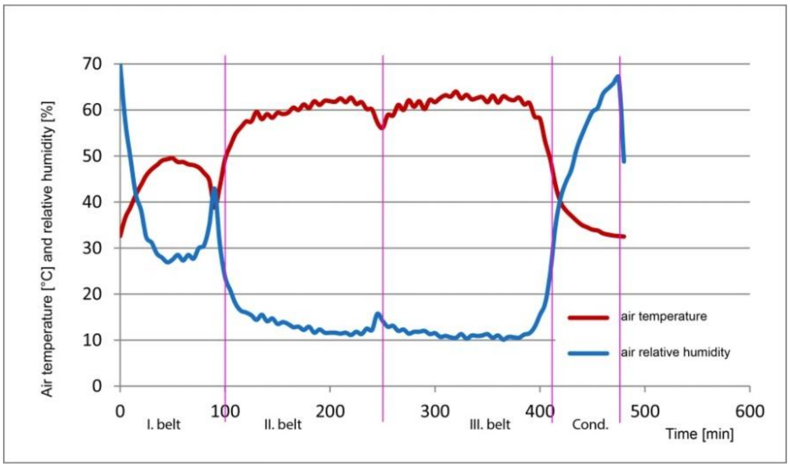

Fig. 4. – Air temperature and relative humidity of the Saaz hop variety measured by means of data-loggers

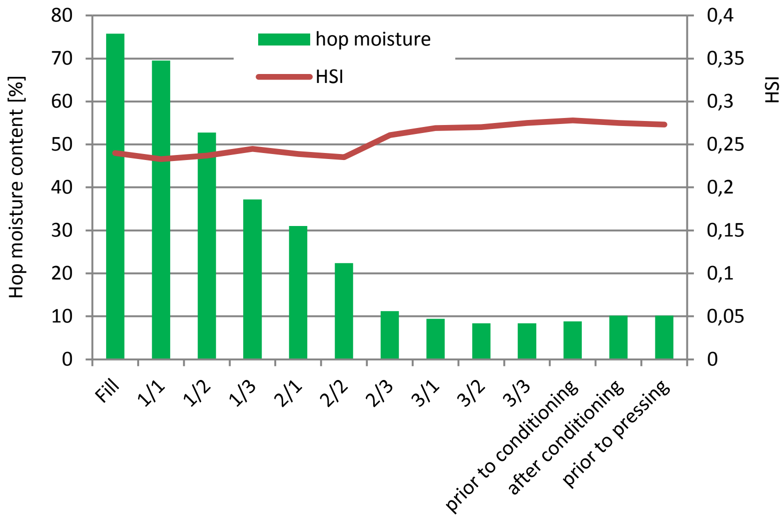

Fig. 5. – Progress of the hop moisture content and HSI with samples of the Saaz hop variety(1/1 – 1st belt and 1st window…)

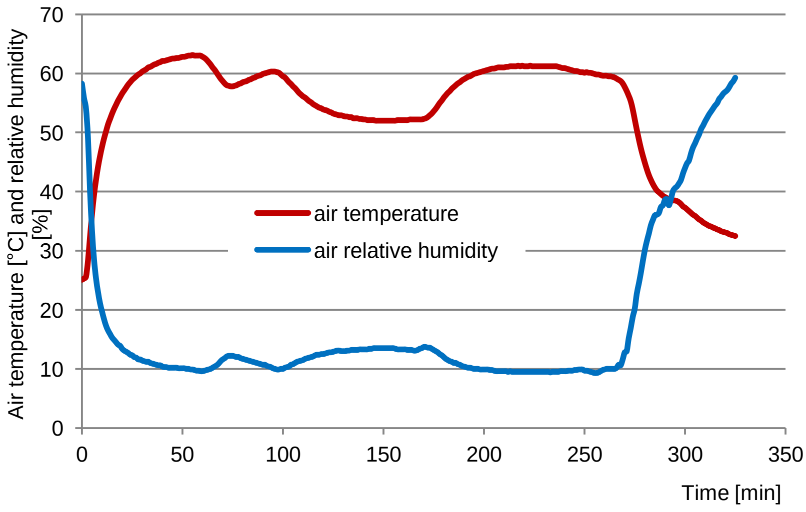

Fig. 6. – Air temperature and relative humidity with the Saaz hop variety measured by means of data-loggers in the PSCH 750 belt dryer

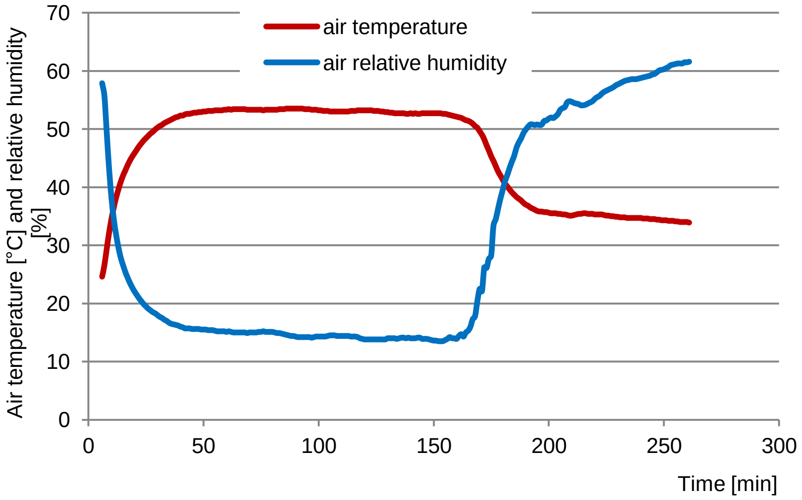

Fig. 7. – Air temperature and relative humidity with the Saaz hop variety measured by means of data-loggers in the PSCH 900 belt dryer

In the plant of Agrospol Velká Bystřice Ltd. samples were taken in both belt dryers when drying the Saaz hop variety.

Examples from the individual measurements are given in Fig. 8 and 9. Besides hop moisture contents, the graphs also illustrate the hop storage index HSI progresses.

The graphs in Fig. 8 and 9 (Velká Bystřice) show similar progress to the graph in Fig. 5 (Stekník), which suggests the same sub-conclusion.

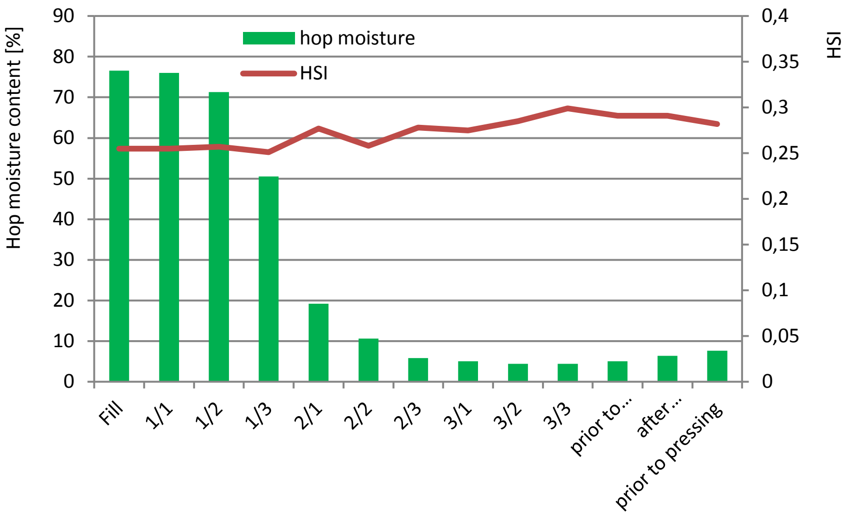

Fig. 8. – Progress in the hop moisture content and HSI with the Saaz hop variety samples in the PSCH 750 belt dryer

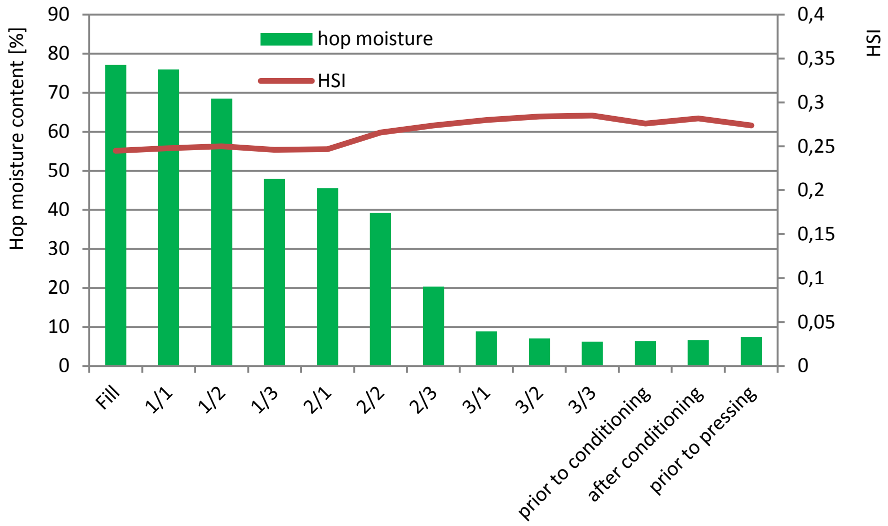

Fig. 9. – Progress in the hop moisture content and HSI with the Saaz hop variety samples in the PSCH 900 belt dryer

CONCLUSIONS

The progress of drying in the operating belt dryers showed that hops are practically dry (10 ± 2.0 % of moisture content) already at the end of the second belt, or possibly at the beginning of the third belt (Stekník). Hop drying in the belt dryers in Velká Bystřice proved that hops are considerably over-dried (4 to 8 % of moisture content) and are subsequently adjusted to the final moisture content of 8-10 %. According to the company staff this state is intentional, working as prevention against the occurrence of nests of moist hops, which occurs on irregular basis when drying hops with high initial moisture content. The causes of such state (nest occurrence) should be examined in greater detail in the next project solution. Over-drying results in extensive hop cone shattering, rendering the manipulation with hops for further processing more difficult and leading to larger losses in the lupulin content.

The reports from travels to important hop-growing areas in the USA, Germany and China provided by hop experts showed that in these countries hops have been dried and processed in a similar way, therefore we may assume similar outputs from the measurement. Foreign research centres do not deal with the given issues, which is the reason why there are no comparable results available for possible discussion.

As indicated in the above, there is great room for improvement in the whole drying process, both in terms of energy and the quality of the final hop product. A complex innovation in the hop drying process in the current belt dryers is very much needed and logically we may assume savings for heating medium and electric energy, resulting from shortening the drying time, increasing the capacity of the facility, and shortening the harvest time. In case of the concept of low-temperature drying no energetic savings can be expected, but the main economic benefit will lie in increasing quality of the product which the hop growers will realise at higher prices.

ACKNOWLEDGEMENTS

This paper was created with the contribution of the Czech Ministry of Agriculture as a part of NAZV n° QJ1510004 research project. In the project solution, besides CULS Prague, are involved: Hop Research Institute Co., Ltd., Žatec, Chmelařství, cooperative Žatec, Rakochmel, Ltd., Kolešovice and Agrospol Velká Bystřice Ltd.

REFERENCES

1. DOE, P. E., MENARY, R. C.: Optimization of the Hop Drying Process with Respect to Alpha Acid Content. In: J. Agric. Engng Res. 24, 1979: pp. 233-248.
2. HANOUSEK, B., RYBKA, A., BERNÁŠEK, K.: Hodnocení práce česačky chmele PT 30/15 a sušení chmele v pásové a komorových sušárnách v r. 2007. Ekonomicko-technologický seminář k problematice pěstování chmele 27. 2. 2008. Hop Research Institute Co., Ltd., 2008: pp. 43-61 (In Czech).
3. HENDERSON, S. M.: Equilibrium Moisture ContentofHops. J. Agric. Engng Res. 1, 1973: pp. 55-58.

4. HENDERSON, S. M., MILLER, G. E.: Hop Drying - Unique Problems and Some Solutions. In: J. Agric. Engng Res. 17, 1972: pp. 281-287.
5. HOFMANN, R., WEBER, S., RETTBERG, S.: Optimization of the Hop Kilning Proces to Improve Energy Efficiency and Recover Hop Oils. Brewing Science, March/April, 66, 2013: pp. 23-30.
6. JECH, J., ARTIM, J., ANGELOVIČ, M., ANGELOVIČOVÁ, M., BERNÁŠEK, K., HONZÍK, I., KRČÁLOVÁ, E., KVÍZ, Z., MAREČEK, J., POLÁK, P., PONIČAN, J., RUŽBARSKÝ, J., RYBKA, A., SLOBODA, A., SOSNOWSKI, S., SYPULA, M., ŽITŇÁK, M.: Stroje prerastlinnú výrobu 3 - Stroje a zariadenia na pozberovú úpravu rostlinných materiálov a na ich skladovanie. Profi Press s.r.o. Prague-Czech Republic, 2011 (In Czech and Slovak).
7. KIENINGER, H., FORSTER, A.: Brauwiss. 26, 1973: pp. 214-217.
8. KIRCHMEIER, H., RODEL, G., DEMMEL, M.: Verfahren zur Abtrennung von Drahtstucken bei der Hopfenernte. Landtechnik, 60(3), 2005: pp.148-149 (In German).
9. KROFTA, K.: Hodnocení kvality chmele. Metodika pro praxi. Hop Research Institute Co., Ltd., 2008: 50 p. (In Czech).
10. PODSEDNÍK, J.: Hop harvesting technology in the Czech Republic 1996-2000. Proceedings of the Technical Commission I.H.G.C. of the XLVIIIth International Hop Growers Congress. Canterbury- England. Agros Žatec-Czech Republic, 2001: 9 p.
11. RYBÁČEK, V.: Hop production. Development in Crop Science, 16. Elsevier, Amsterdam-Niederland and SZN, Prague-Czech Republic, 1991.
12. SRIVASTAVA, A. K., GOERING, C. E., ROHRBACH, R. P., BUCKMASTER, D. R.: Engineering Principles of Agricultural Machines. ASABE, 2nd Edition, Michigan, USA, 2006.
13. WEIHRAUCH, F., BAUMGARTNER, A., FELSL, M., KAMMHUBER, K., KNEIDL, J., LUTZ, A., NEUHO, BUCKL, E., PETZINA, C., SPERR, B., WEIHRAUCH, S., WYSCHKON, B.: The influence of aphid infestation during the hop growing season on the quality of harvested cones. Programme, EBC Hop Symposium 2010, Wolnzach (Bavaria), 29, 12.-14. Sept. 2010.

Corresponding author:
doc. Ing. Adolf Rybka, CSc., Department of Agricultural Machines, Faculty of Engineering, Czech University of Life Sciences Prague, Kamýcká 129, Praha 6, Prague, 16521,Czech Republic, phone: +420 22438 3121, e-mail: rybka@tf.czu.cz

VERIFICATION OF THE FUNCTIONALITY OF THE DIAGNOSTIC OF A SYSTEM WITH MANY ATTENUATION ELEMENTS

J. Řezníčková, K. Řasová

Department of Rehabilitation Medicine, Third faculty of medicine, Charles University and Faculty Hospital Královské Vinohrady, Czech Republic

Abstract
When carrying out a vibration analysis of a composite system, the point is mainly determining stiffness and attenuation between individual elements. The TVS method deals with this analysis in case that the elements are arranged linearly and oscillations predominate in one direction only. The frequency region analyzed by this system is between 5 and 180 Hz. The system consists of one vibrator, one strain gauge, and twenty accelerometers which are attached by means of double-sided adhesive tape to the analyzed structure. In this structural arrangement, also the precise location of the sensors and the actual values of the variable properties of the measured system make a difference to a certain extent. The content of this article is the verification of the TVS method for two basic methodology requirements, repeatability for an identical sample and resolution for two different samples, i.e. we determine the extent to which minor variations of the state of the measured system and small variations in the position of the sensor locations influence the results obtained using the TVS method.

Key words: attenuation, stiffness, diagnostics, verification of function.

INTRODUCTION

Although many works deal with oscillations of backbone elements, KELLER ET AL. (2010) and RAMIREZ ET AL. (2013), for example, this is usually the measurement of oscillations in such situation where the measured person actively makes a movement. The authors then get into such situation where the difficult definability of external stimuli leads to problems when interpreting the results. The closest measurement which is already made fairly as standard in the USA is the measurement of impedance (the applied force simultaneously with the acceleration caused) on the body of one vertebra. The method is applied also therapeutically in such a way that a frequency scan is used to find the resonance maximum of the vertebra concerned and vibration excitation is then applied to it. We do not know about any other complex investigative method which is carried out in such situation where the patient is inactive and thus the data are not made non-transparent. A part of our team has been dealing with the TVS method since 2003 and has published some preliminary results, comparing, for example, changes in the mechanical parameters of the spine while driving a car or while doing exercise (ZEMAN AND ZABLOUDILOVÁ, 2007).

The functional disorders of the musculoskeletal system are one of the most common causes of musculoskeletal pains. The functional disorders of the thoracic spine include faulty, impaired posture in this area (Fig. 1) and also a change in the method of making various routine movements (a change in the locomotive stereotype) and the reduction or limitation of the mobility of the thoracic spin (VÉLE, 1997).

It follows from the methodology that every method must be repeatable, i.e. that we have to obtain similar results when making more measurements on the same object. The second basic requirement is that we have to be able to tell two different objects apart. We try to verify both of these methodological requirements for the TVS method (JELEN ET AL., 2010). For this purpose, a series of experiments was conducted and two objects were measured in the following mode during this series.

The aim of this work is thus primarily verifying the stability of the results, and whether particular people are recognisable (distinguishable) with the aid of correlation coefficient, i.e. without use of any interpretation model.

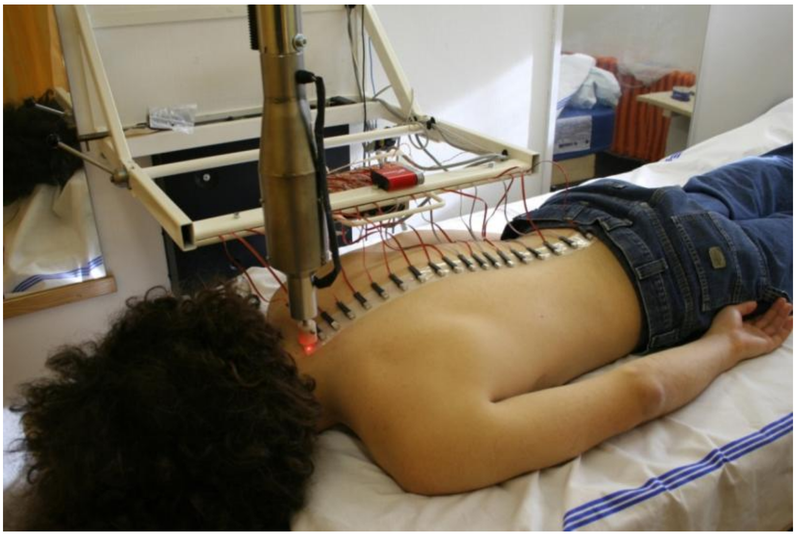

Fig. 1. – Measurement using the TVS method

MATERIALS AND METHODS

When the spin is excited using the Transfer Vibration through Spine method (TVS), see Fig. 1, the passive transmission of vibrations excited from the stimulated vertebra to the adjacent vertebrae and, for lower frequencies, a neuromuscular response occur. Sensing and evaluating the acceleration of vertebrae C7-S1 give us valuable information not only about the state of the intervertebral joints in the body, discs, ligaments, and adjacent musculature, but also about the functioning of the postural mechanism in individual vertebral segments (ZEMAN, 2006).

Twenty accelerometers were placed on the spine of a person lying prone. Each of them was attached to one vertebra from C7 to S1. An impactor was put on vertebra C7 and then L5. Mechanical pulses in the shape of a Gaussian curve with a half-width of 10 ms acted on the excited vertebra with a peak force of 10 N (JELEN ET AL., 2012). As a result of this impact the spine started to move in a specific way. As the excited vibrations of the spine resulting from such impact have amplitude in the order of tens of micrometers, the movement was not measured directly, but the position was obtained by double integration of the measured acceleration (PANSKÁ ET AL., 2012).

After placing one of the objects in the test device, two measurements were made in sequence immediately without reattaching the sensors, which thus remained in the same places. Comparing the results of the two measurements, we are able to recognize the extent to which the micro variation of the system state between these measurements will influence the results obtained. After making these two measurements, we do the same thing on the second object. Comparing the results obtained in the case of the first object and the second object, we are able to determine whether the results enable us to tell the objects apart. After taking a pair of measurement on the second object, we return to the first object and make two measurements immediately in sequence again. However, it is basically necessary to reattach the sensors between the first measurement series on the first object and the second measurement series on the second object. Comparing the series thus gives us the opportunity to assess the extent to which the results measured depend on the position of the sensors. Now we make the second series of measurement also on the second object for the same reason. Then the third series on the first object and on the second object follows.

The evaluation takes place as follows: only the phase and the amplitude of the frequency just excited are determined using the signal measured by the accelerometers. As the frequency changes continuously from the lowest to the highest and back while measurement is made and this process is repeated three times, the spin is always measured six times at a frequency concerned. When evaluating, we always consider the average of the six values thus obtained, the ratio between the vertebra excited by amplitude, and the amplitude of the vertebra tested to be the result. This takes place for all measured frequencies, which gives us a spectrum of the transmission of vibrations from the exciting vertebra to the tested vertebra. Transmissions from vertebra C7 to vertebrae Th3 Th5, Th7, Th10, L2, and L4 were evaluated for this contribution. These calculations were made for the series of measurement on two probands described above.

The spectra obtained were compared as follows. Firstly, the coefficient of determination among all the obtained spectra for the vertebra concerned was determined, i.e. both for repeated measurements on the same volunteer and among the volunteers themselves. Secondly, the Shapiro-Wilk test of normality for the difference between the spectral values and the measurements compared was also carried out for all combinations. If the differences between the spectra have a normal distribution, it can be assumed that they consist of random influences only and not of systematic influences. The more the distribution of this difference is distant from the normal Gaussian distribution, the more the signal of the measurements compared changes systematically.

RESULTS AND DISCUSSION

Tab. 1. – Gives the coefficients of determination among all measurements made

	1x1	**2x2**	**1x2**	**1x1***	**2x2***	**2x2***
Th3	0.21	0.19	0.13	0.32	0.34	0.83
Th5	0.11	0.07	0.05	0.00	0.02	0.23
Th7	0.13	0.08	0.07	0.25	0.05	0.17
Th10	0.21	0.19	0.13	0.32	0.34	0.83
L2	0.14	0.08	0.07	0.09	0.02	0.08
L4	0.18	0.12	0.10	0.30	0.28	0.03

Here we can see that the coefficients of determination are always the smallest ones among any comparisons of the volunteers between each other. The second volunteer tested has coefficients of determination a little higher compared with its measurements, but the first volunteer is more similar to him himself. This comparison shows that the average coefficients of determination enable us to identify which measurement belongs to which of the probands. This meets the methodological requirements for the repeatability and sensitivity of measurement.

Tab. 2. – Shows the mean values of the Shapiro-Wilk test among all the measured results

	1x1	**2x2**	**1x2**	**1x1***	**2x2***	**2x2***
Th3	0.63	0.68	0.62	0.15	0.72	0.62
Th5	0.58	0.69	0.63	0.21	0.86	0.55
Th7	0.61	0.67	0.64	0.43	0.73	0.39
Th10	0.48	0.39	0.46	0.17	0.88	0.16
L2	0.68	0.63	0.66	0.55	0.80	0.52
L4	0.40	0.56	0.50	0.36	0.76	0.51

As the extreme p-value for all the cases mentioned is 10^{-6}, it is evident that the normality of the differential spectrum can be rejected in all cases. Using the values of the coefficients given in the table, it is nevertheless possible to assume relatively which differential spectra have their distribution of values more similar to a normal distribution than other. As you can see, it is found out for all the vertebrae that the differential spectrum calculated among the volunteers is the closest to a random distribution. A little less random distribution is for comparing the proband with him himself in the case of the first proband and the least random distribution is in the case of the second proband. The same results can also be surprisingly achieved using the Kolmogorov-Smirnov test of normality. These comparisons show that a systematic difference is mainly among the spectra of the volunteers, while individual measurements on the same volunteer show differences more corresponding with a Gaussian distribution.

According to the result of this experiment it seems that the results of earlier works are also consistent. E.g. for the work of KAMP ET AL. (2014) the point is confirmation of the results for the truck driver.

CONCLUSIONS

The purpose of this study was to evaluate the extent to which it is possible to rely on the uniqueness and, at the same time, on the repeatability of the spectra obtained using TVS. Volunteers of a similar phenotype and geomorphologic features were deliberately chosen for repeated measurements. Despite the high spectral similarity, it was shown that the mutual spectral similarity between the volunteers was always lower and less random than when repeated measurements on the same volunteer were compared.

REFERENCES

1. JELEN, K., KLOUČKOVÁ, K., ZEMAN, J., KUBOVÝ, P., FANTA, O.: Changes in attenuation characteristics of axial system of pregnant drivers detected by the TVS method. Neuroendocrinology letters, 33, 4, 2012: 101-107.
2. JELEN, K., ZEMAN, J., KUBOVÝ, P., DRAHORÁDOVÁ, R., HOLUB, T.: Limit Loading Processes and their Reflection in Intevertebral Dynamics. Brno: Tribun EU, 2010.
3. KAMP, K., BILLICH, R., JELEN, K., ZEMAN, J.: The influence of hypokinesis. Acta Universitatis Carolinae Kinanthropologica, Vol. 50, January 2014. pp 28-36. ISSN 1212-1428.
4. PANSKÁ, Š., KLOUČKOVÁ, K., ZEMAN, J., MAREŠOVSKÝ, L., JELEN, K.: Mechanical Loading And Aging Of A Human Axial System: Identification Of Connective Tissues Changes By The Means Of The Tvs Method. In: AGEING 2012, 26. October 2012, Prague, pp. 100 – 108, Prague, Czech Republic.
5. ZEMAN, J., ZABLOUDILOVÁ, P.: Identification of changes of transfer function of mechanical vibrations of human spine after car driving. 2007.
6. ZEMAN, J.: The Intervertebral Disc Energy Transfer. In: Czech Society of Biomechanics - Charles University in Prague: Biomechanics, Biofluidics and Alternative Biomaterial Substitutions, pp. 73-74. Prague, Charles University in Prague 2006.
7. KELLER, T. S., COLLOCA, CH. J., FUHR, A. W.: In Vivo Transient Vibration Assessment of the Normal Human Thoracolumbar Spine, Journal of Manipulative and Physiological Therapeutics, 2000, v. 23/8.
8. MORGADO RAMIREZ, D. Z., STRIKE, S., LEE, R. Y. W.: Measurement of transmission of vibration through the human spine using skin-mounted inertial sensors, Medical Engineering & Physics, 2013, v. 35.
9. VÉLE, F.: Kineziologie pro klinickou praxi. Praha, Grada, 1997.

Corresponding author:

Jitka Řezníčková, Department of Rehabilitation Medicine, Third faculty of medicine, Charles University and Faculty Hospital Královské Vinohrady, Šrobárova 50, 100 34 Praha 10, Czech Republic, e-mail: reznickovajitus@centrum.cz

ESTABLISHMENT OF A POWER FARMING SYSTEM IN AN UPLAND FIELD CONVERTED FROM PADDY FIELD– GREEN SOYBEAN GROWTH AND YIELDS IN AN UPLAND FIELD DURING THE FIRST YEAR AFTER CONVERSION FROM PADDY FIELD CULTIVATION

M. Sato, D. Tanabe, M. Katahira, M. Natsuga

Yamagata University, 1-23, Wakabamachi, Tsuruoka , Yamagata, 998-8555, Japan

Abstract

This study assessed power farming and a new cropping system for vegetable cultivation in an upland field converted from a paddy field with improved drainage. We investigated green soybean cultivation and examined soil physical properties, work capabilities of rotary tilling and ridge-making implements, and green soybean growth and yield. Field experiments were conducted at two small paddy fields: Blocks A (2.0 a) and B (2.0 a) at the Yamagata Field Science Center Takasaka Farm, Faculty of Agriculture, Yamagata University. Block A had an outer open ditch only. Block B had an outer open ditch with a mole drain. The green soybean cultivar "Yuagari-musume" was seeded on May 14, 2015. We investigated soil physical properties (saturated hydraulic conductivity, plastic limit, pF1.8 water content, and upland index), work accuracy (theoretical work rate, pulverization rate, and ridge shape), and green soybean growth and yield. The open ditch and mole drain in gray lowland soil improved soil physical properties somewhat. Both fields had high pulverization rates and good soil water contents at the plastic limit with up-cut rotary tilling. However, the mole drain might have adverse effects during low rain fall years because water from the converted rice fields might drain out.

Key words: paddy-upland rotation, open field vegetable, green soybean, soil physical properties, power farming system.

INTRODUCTION

Yamagata Prefecture in Japan is famous as a paddy rice production area. Furthermore, that paddy field area on the Sea of Japan side of the country has many fields that have heavy clay soil with poor drainage. Nevertheless, Yamagata Prefecture has cultivated upland field crops positively to make effective use of paddy fields. Upland fields converted from paddy fields of Yamagata Prefecture usually grow soybeans. However, many area farmers have demanded introduction of garden crop cultivation, which is highly profitable, to improve land productivity. Garden crop cultivation on upland fields converted from paddy fields should introduce a work system to improve soil physical properties including drainage, air conductivity, and the pulverization rate. A work system of paddy fields with poor drainage in Japan has usually made open ditches and under-drains. Recently, soy bean cultivation in Japan has been introducing rotary tilling and ridge-making work systems (HOSOKAWA, 2004) to mitigate wet injury. Efforts to promote garden crop cultivation on upland fields converted from paddy fields should consider adoption of cropping systems that are suited to rural areas (HOSOKAWA, 2002). This study was undertaken to assess a power farming and new cropping system for cultivating vegetables in an upland field converted from a paddy field with improved drainage. We used green soybean as the first year crop of an upland field converted from a paddy field. We investigated soil physical properties, work capabilities of rotary tilling, ridge-making implements, and green soybean growth and yields.

MATERIALS AND METHODS

Test fields and test blocks

Field experiments were conducted in two small paddy fields, Block A (2.0 a) and B (2.0 a), at Yamagata Field Science Center Takasaka Farm, Faculty of Agriculture, Yamagata University. Block A had an outer open ditch only. Block B had an outer open ditch with a mole drain (Fig. 1).

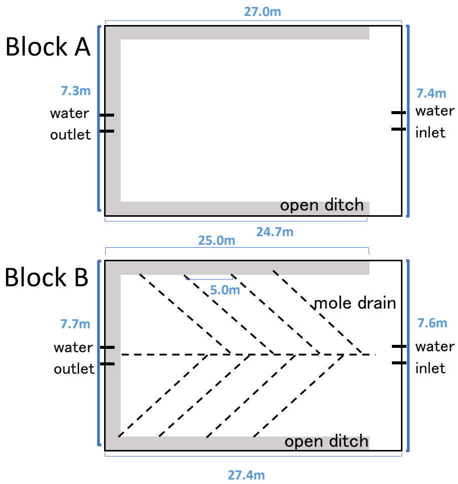

Fig. 1. – Open ditch and mole drain placement in test fields

Machine components

We made an open ditch using a tractor (AT-410, 30.9 kW; Iseki Co. Ltd.) with an attached screw auger type ditcher (OM-310; Matsuyama Co. Ltd.) on October 27, 2014. We made a mole drain at block B using a tractor (AT-410, 30.9 kW; Iseki Co. Ltd.) with an attached mole drainer (PD-110; Iseki Co. Ltd.) on November 8, 2014. Open ditches were set with ditch bottom width of 15–19 cm (S. D.:1.0 cm), ditch top width of 30–35 cm (S. D.:2.0 cm), and ditch depth of 26–38 cm (S. D.:3.5 cm). We constructed eight mole drains, four mole drains at one side, which were made for a 5 m interval from the drain side to the spout side. Each mole drain was connected to the open ditch. We sowed green soybeans using a rotary tilling and a ridge-making work system that comprised a tractor (KL31ZC, 22.8 kW; Kubota Corp.), up-cut rotary (APU1610H; Matsuyama Co. Ltd.), and sowing machine (AFRG-2S; Yazaki Co. Ltd.) (Fig. 2).

Fig. 2. – Schematic diagram of the rotary tilling and ridge-making work system

Cultivation outline

We used the medium-harvest-type green soybean cultivar "Yuagari-musume". Seed preparation was done using insecticide (Cruiser-MAXX; Syngenta). Basal fertilizing was 2 t/ 10 a for manure and 4 kg-N/ 10 a for chemical fertilizer (N-P_2O_5:K_2O=12:16:14) before sowing on all field areas. The sowing machine setting was 75 cm for inter-row space and 20 cm for hill space, sown in 6 rows with 2 seeds per hill on May 14, 2015.

Investigation contents

We investigated soil physical properties before drainage and before sowing, in addition to sowing work accuracy, growth, and yield of green soybeans. The investigated soil physical properties were saturated hydraulic conductivity ($cm.s^{-1}$), plastic limit water content, and the pF1.8 water content. These were investigated using the cylinder core (50 mm diameter, 51 mm height, 100 mL volume), which were extracted from soil (0–5 cm area) after removal of soil surface and organic matter. We obtained these data from three sampling points which had diagonal lines of a field, and equalized each datum. Therefore, we calculated the upland index according to the following formula (1).

Upland index = Plastic limit water content / pF1.8 water content (1)

The theoretical work rate was calculated using advanced work time for an average of three times. Sowing work accuracy was affected by the pulverization rate and ridge shape, which included the ridge bottom width, ridge top width, and ridge height. We investigated the germination rate to measure hill space on 4 rows, which were except outside rows each test blocks at 13 days after sowing. To assess the growth of green soybeans, we investigated the plant height, the number of nodes and branches, and the leaf color measured by SPAD 502 at three times, for four test points of 2.4 m length in each test block. We investigated yields for green soybeans at each test point.

RESULTS AND DISCUSSION

Soil physical properties of upland fields converted from paddy fields

Soil physical property of upland fields converted from paddy fields are presented in Tab. 1. Plastic limit water contents were 27.4% before drainage in October, 2014 and 30.6% after drainage in April, 2015 at test block A, and 28.8–30.8% at test block B. PF1.8 water contents were 0.38–0.41 in test block A, and 0.38–0.38 at test block B. Saturated hydraulic conductivity was -6, which was a multiplier only, after drainage for each test block. However, before sowing, they were -6 ‐ -7 in test block A and -4 ‐ -7 in test block B, which had little difference from test block A. Upland indexes were 0.71–0.74 in test block A, and 0.77–0.81 at test block B. These values were not significantly different for the respective test blocks and sampling times. An upland field converted from paddy fields was reported for the plastic limit water contents, non-plastic deformation of soil aggregate, with few deviations to improve drainage as the pF1.8 water content decreased. The paddy field of Takasaka, which was classified on gray lowland soil, had better drainage than the heavy clay paddy field. Therefore, that field had 0.71–0.77 at the upland indexes before drainage. The mole drain had little effect of decreasing the pF1.8 moisture contents.

Tab. 1. – Soil physical properties of the respective test blocks

Test blocks	Sampling season	Plastic limit water contents (%)	PF1.8 water contents	Saturated hydraulic conductivity (cm sec^{-1})	Upland indexes
A	2014/10	27.4	0.38	-6	0.71
	2015/4	30.6	0.41	-6～-7	0.74
B	2014/10	28.8	0.38	-6	0.77
	2015/4	30.8	0.38	-4～-7	0.81

Theoretical work rate and work accuracy

Theoretical work rates of tilling and ridging were, respectively, 0.70 h/ 10 a in test block A and 0.75 h/ 10 a in test block B. These values were not significantly different. Pulverization rates were 88.0% in test block A and 82.7% in test block B. These values were not significantly different (Tab. 2). Using up-cut rotary showed 80% over the pulverization rate at each test block of converted first year. Upland field of tilling and ridging showed ready pulverization such that it had about 0.3 at moisture content, which was near the plastic limit water content value at each test block.

Tab. 2. – Theoretical work rate and pulverization rate of tilling and ridging

Test blocks	Theoretical work rates (h 10a^{-1})	Pulverization rates (%)	Moisture content
A	0.70	88.0	0.30
B	0.75	82.7	0.29

Ridge shapes of test block A were 64.4 cm at the ridge bottom width, 33.7 cm at the ridge top width, and 18.5 cm at ridge height. Ridge shapes of test block B were 64.9 cm at the ridge bottom width, 36.0 cm at the ridge top width, and 17.8 cm at ridge height (Figs. 3 and 4). The ridge exhibited the same shape at each test; it was not significantly different. In addition, Hosokawa reported that up-cut rotary tilling and ridge-making work was 30–35 cm at the ridge top width and 15–20 cm at the ridge height (HOSOKAWA, 2004). Results showed good tilling and ridge-making work accuracy such that our study has the same ridge top width and height as those of Hosokawa's results.

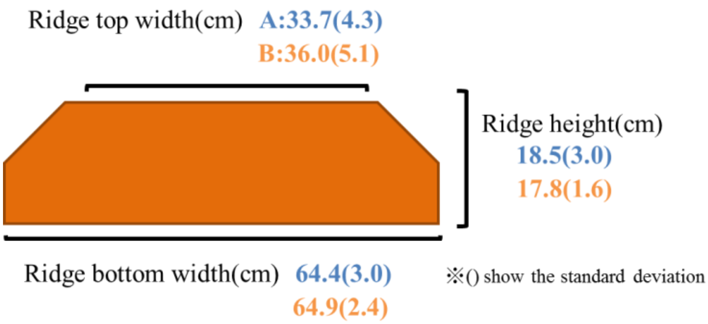

Fig. 3. – Schematic diagram showing ridge shapes

Fig. 4. – Field conditions after tilling and ridge-making work

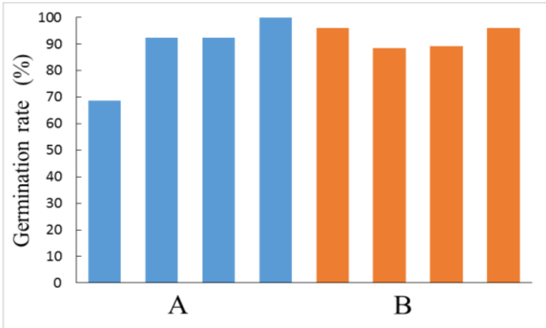

Fig. 5. – Germination rates of respective test blocks

Germination rate and growth of green soybean

The germination rates are shown in Fig. 5. Germination rates were 69–100% in test block A and 88–96% at test block B. Germination rates were 88% over at average values of each test block to attain a high pulverization rate and good water contents for green soy beans. Although test blocks A and B were found to have no significant difference, test block A might have some effect on the germination rate because of the difference of drainage to decrease the germination rate in a part of test block A.

Growth from the first stage to the flowering stage of green soybean is shown on Tab. 3. Plant heights were 10.9–26.8 cm in test block A and 11.9–29.6 cm in test block B. Numbers of nodes were 5.1–10.6 in test block A and 5.3–10.2 in test block B. Numbers of branches were 0–2.5 in test block A and 0.3–2.3 in test block B. Leaf colors were 30.0–31.7 in test block A and 31.7–32.9 in test block B. Growth of green soybean was not so much different for test fields, as shown in Fig. 6. However, test block B, which had the same plant height and number of nodes as test block A, had a longer interval length of nodes than test block A as well as increased plant density with much more leaf growth in the field. Consequently, test block B, which had a mole drain, supported better growth at the first stage than test block B.

Tab. 3. – Green soybean growth at respective test blocks

Day after seeding	Test blocks	Plant height (cm)	Number of nodes	Number of branches	Leaf color (SPAD)
33	A	10.9	5.1	0.0	30.0
	B	11.9	5.3	0.3	28.9
42	A	15.8	8.0	0.8	35.6
	B	16.7	7.9	1.2	36.8
53	A	26.8	10.6	2.5	31.7
	B	29.6	10.2	2.3	32.9

Green soybean yield

Yields of green soybean were 1173 kg/ 10 a in test block A and 747 kg/ 10 a in test block B (Tab. 4). Results demonstrated that drainage had no effect in this year that constituted a significant difference in any test block. This year had slight annual rainfall of 194 mm. Therefore, because of the low amount of rainfall, conditions of green soybean cultivation of this year were insufficient to test mitigation of wet damage introduced by tilling and ridge-making work system. To improve drainage, we reduced the amount of field water capacity, which decreased the green soybean yield in test block B, making it unable to accumulate the necessary water for vegetables.

Fig. 6. – Field conditions of harvest time (August 5, 2015: 80 days after sowing)

Tab. 4. – Yield and yield components

Test blocks	Planting density per square meter	Number of petiole per one	Number of pods per petiole	Pod weight per pod (g)	Rate of number of effective pods (%)	Yields (kg 10a^{-1})
A	13.3	23.4	2.8	2	68.2	1173.3
B	14.3	23.3	2.1	1.8	59.7	747.8

CONCLUSIONS

Although the upland field converted to a paddy field in its first year was able to show slightly decrease pF1.8 water content, that field showed small effects by which the upland index was over 0.8, with an increased range of saturated hydraulic conductivity. The tilling and ridge-making work system achieved good work accuracy with high pulverizing capability by up-cut rotary and good water contents at tilling time. In years with slight rainfall, the introduced mole drain and tilling and ride-making work system might induce water shortages at the flowering stage because of the decreased field water capacity amount.

REFERENCES

1. HOSOKAWA, H.: Rotary Tilling and Ridge-making Implement of Soybean for avoiding Wet Injury in Clay Upland Field Converted from a Paddy Field, Journal of the Japanese Society of Agricultural Machinery and Food Engineers, 66(5), 2004: 14–16.
2. HOSOKAWA, H.: The establishment of crop rotation technology combining upland crops and vegetables in Hokuriku heavy clay upland field converted from paddy field with a heavy snow area, Journal of the Japanese Society of Agricultural Machinery and Food Engineers, 64(5), 2002: 9–13.

Corresponding author:

Mai Sato, Yamagata University, 1-23, Wakabamachi, Tsuruok , Yamagata, 998-8555, Japan

THE TEMPERATURE RESPONSE OF MAMMALS TO A STEP CHANGE OF THE EXTERNAL TEMPERATURE

J. Sedláček, J. Zeman

Department of Physics, Faculty of Engineering, Czech University of Life Sciences Prague, Czech Republic

Abstract
Our paper deals with the description of reaction of warm-blooded animals to changes in temperature. A complex regulation mechanism is started during the changes in temperature, which is aimed at stabilisation of the basal temperature of an animal. This process is called PID controller. The process leads to gradual changes in the surface temperature of an animal. The course of changes in temperature over time is recorded during the experiments described below. During certain amount of time, which is introduced here as the relaxation time, changes in temperature end almost entirely. The change in temperature of a certain part of an animal body is determined by each animal. The time which is needed to this change in temperature is also determined. As it become apparent, both these figures depend on animal species and also on the size and the sign of change in the external temperature. So the paper shows the methodology for data, which describes the thermoregulatory process. The experiment was executed on a llama of Vicugna pacos – alpaca and on a sheep of Clun Forest. By comparing the results of the experiment for the animals mentioned above we came to the clear conclusion. The speed of thermoregulation of the measured llama is much higher than the speed of thermoregulation of the measured sheep.

Key words: thermoregulation, warm blooded animals, PID controller, relaxation time.

INTRODUCTION

The thermoregulation of the warm blooded animals, which stabilises the basal temperature, is a very complex process. The thermoregulation consists of chemical as well as mechanical actions, which are directed by nervous and lymphatic systems. In the long-term changes are involved also hormones. It seems that during the short-term changes, the temperature of the peripheral parts of a body is regulated primarily mechanically. We will show one example. When the information about hypothermia of a certain peripheral part of a body below critical temperature t_c = 21.3 °C reaches the brain, the flow of blood through this limb is stopped almost immediately. It is the consequence of the constriction of the blood vessels. From this moment on, no blood flows into the limb and for this reason no heat is brought there and also no new substances (ATP) from which the heat can be created. The limb becomes insensitive without inflow of blood, because tactile cells do not have required energy and oxygen, which are needed to the creation of a neural excitation. The same applies to the activity of the muscular and temperature sensory cells. The movement of the hypothermic parts of limbs is possible only in a passive way, e. g. by pulling tendons, which originates outside the hypothermic parts of the body. After the warming of the hypothermic part of a limb with the help of external heat, the blood vessels dilate again. The “warm” blood flows into the limb rapidly. At the same time, the cold blood is ejected out of the limb into the body, which may cause a thermal shock. In any case, it leads to the rapid decrease in temperature. It is obvious, that the description of such complicated process is very difficult with using only few parameters. For that reason, we concentrated on the purely phenomenological description of changes in the external temperature of the limb. Our aim in this phase of the research was to compile a sufficiently general mathematical description, which characterizes the temperature reaction of animal to a step change of the external temperature with the help of several parameters. In accord with the description of the activity of PID controller, we are introducing only two parameters which primarily describe its features. The introduction following two parameters is expedient and for basic description sufficient. 1. The finite change of the temperature in the infinite time, which takes place on the surface of the limb, during a step change of the external temperature by 10 °C. The temperature change over time takes place approximately exponentially. Therefore we used the power coefficient of this exponential curve as the second parameter, which describes the thermoregulatory process, which is caused by the temperature jump of the surroundings.

MATERIALS AND METHODS

The temperature of the animal was stabilised in a lee outdoor enclosure during several hours. After that the surface temperature of the animal was measured by a thermographic camera (We used the camera TiR-01 the Fluke brand.). In the case of examination of the furred parts of an animals body, it was necessary to pull fur apart in order the skin could be seen. The animal was brought into the heated stable after taking a picture. The current temperature was measured by using a thermographic camera always at the same spot on the surface of the animal. Taking pictures was carried out by using software Smart View 3.0 periodically every 30 seconds. The measurement was ended after stabilization of body temperature of the animal. The animal stayed in the heated stable five hours and then was brought in the lee outdoor enclosure again. Here, other measurement was carried out by the same procedure.

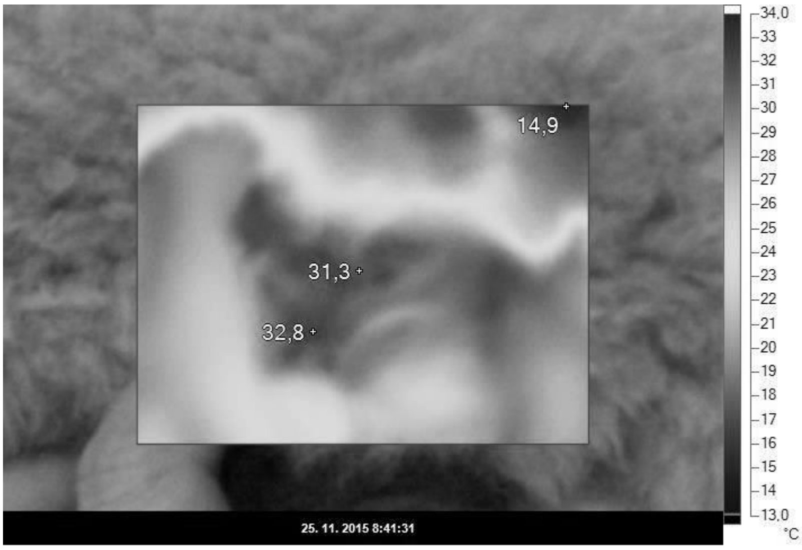

Fig. 1. – Llama after the transition from the outdoor enclosure to the stable

For the sake of completeness, we had to determine the temperature and the humidity of the surroundings, both in the cold and in the warm zone. It was done by using anemometer Testo 410-2. The time series of the temperatures was fitted with the suitable exponential curve with using the least squares method. We have used the Solver tool of the program MS Excel 2010 for this purpose – see MOŠNA (2010). In this way the following parameters were ascertained: the temperature change Δt and the relaxation time τ. The calculation was made as follows. We calculated the functional values for the functions (1) and (2) in the times of measurements, which were exactly deducted from the dating of the respective image.

$$\zeta(t) = \zeta_1 + |\Delta\zeta_1| e^{-\frac{t}{\tau_1}}, \tag{1}$$

$\zeta(t)$ – the approximated temperature of the limb of the animal,

ζ_1 – the initial value of the temperature of the animal at the start of the increase of temperature,

$\Delta\zeta_1$ – the temperature difference, of which increases the temperature of the animal during the measurement,

t – the time,

τ_1 – the relaxation time of the temperature increase.

$$\zeta(t) = \zeta_2 - |\Delta\zeta_2| e^{-\frac{t}{\tau_2}}, \tag{2}$$

$\zeta(t)$ – the approximated temperature of the limb of the animal,

ζ_2 – the initial value of the temperature of the animal at the start of the decrease of temperature,

$\Delta\zeta_2$ – the temperature difference, of which decreases the temperature of the animal during the measurement,

t – the time,

τ_2 – the relaxation time of the temperature decrease.

We calculated the sum of squared differences of the measured and the approximated values. We found the coefficients ζ_i, $\Delta\zeta_i$ and τ_i. with the Solver tool. The coefficients of such values, for which the sum of squared differences is minimal. We calculated the mean square deviation for $\Delta\zeta_i$ coefficients using the relationship (3).

$$s(i) = \sqrt{\frac{\sum_{j=1}^{N} \left(\zeta_i(j) - \zeta_i'(j)\right)^2}{N(N-1)}}\,, \qquad (3)$$

$s(i)$ – the mean square deviation for the increase or the decrease of temperature,

$\zeta_i(j)$ – the approximated temperature in time j,

$\zeta_i'(j)$ – the measured temperature in time j,

N – the number of measurement.

There is a connection between the coefficient of the temperature reaction of the animal and the temperature change of the surroundings. Therefore we introduced the relative temperature coefficient by relationship (4), which specifies the animal.

$$\alpha_i = \frac{\Delta\zeta_i}{\zeta_1^a - \zeta_2^a}\,, \qquad (4)$$

ζ_1^a – the air temperature before measurement,

ζ_2^a – the air temperature during measurement.

To verify the functionality of the method, we tested animals of llama and sheep. They were adults in both cases.

RESULTS

The conditions of the measurement are stated in the Tab. 1. The determined values of the coefficients of the equations (1) and (2) are shown in the Tab. 2.

Tab. 1. – The conditions of the measurement

Measured animal	Llama		Sheep	
i	1	2	1	2
ζ_i^a (°C)	15.2	1.9	14.9	2.3
Air humidity (%)	42.2	74.3	50.2	76.4
Wind speed (m/s)	0	1.6	0	1.8

Tab. 2. – The determined values of the coefficients of the equations (1) and (2)

Measured animal	Llama		Sheep	
i	1	2	1	2
ζ_i (°C)	31.2	32.3	33.1	34.8
$\Delta\zeta_i$ (°C)	4.4	-3.1	5.6	-1.7
α_i	0.33	-0.23	0.44	-0.13
τ (min)	7.5	6.1	18.7	12.8

The measured temperature dependences and their approximation by the equations (1) and (2) are stated in the Fig. 2 – 5.

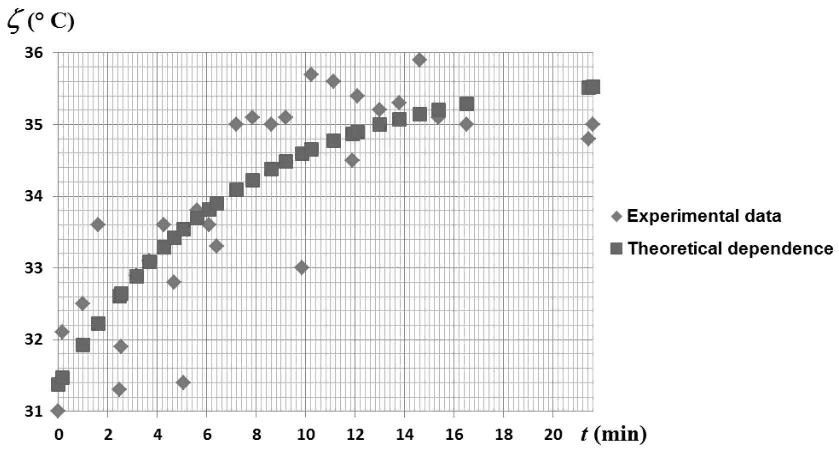

Fig. 2. – The increase of the body temperature of llama after the transfer out of the outdoor enclosure into the heated stable

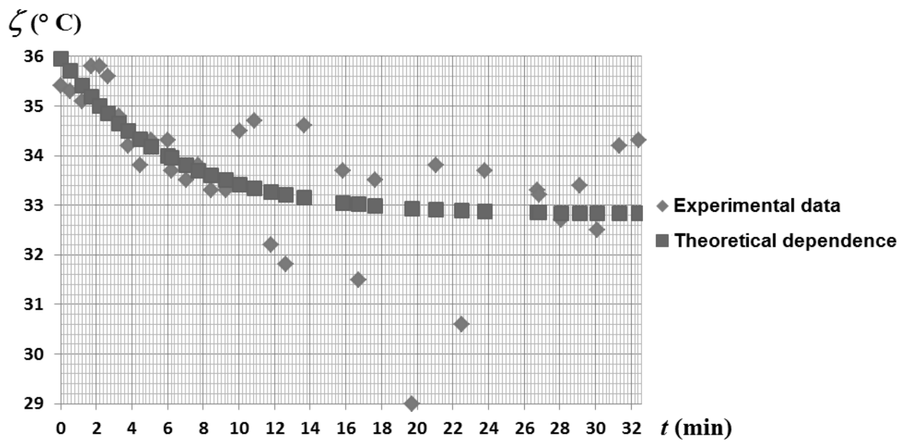

Fig. 3. – The decrease of the body temperature of llama after the transfer out of the heated stable into the outdoor enclosure

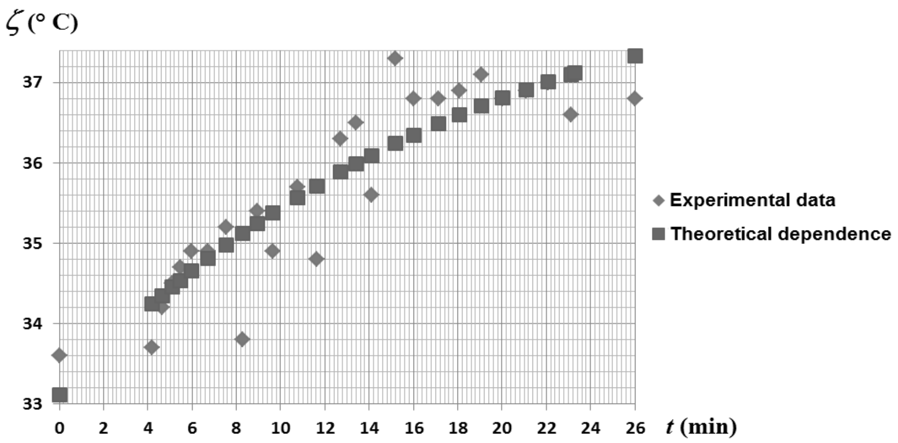

Fig. 4. – The increase of the body temperature of sheep after the transfer out of the outdoor enclosure into the heated stable

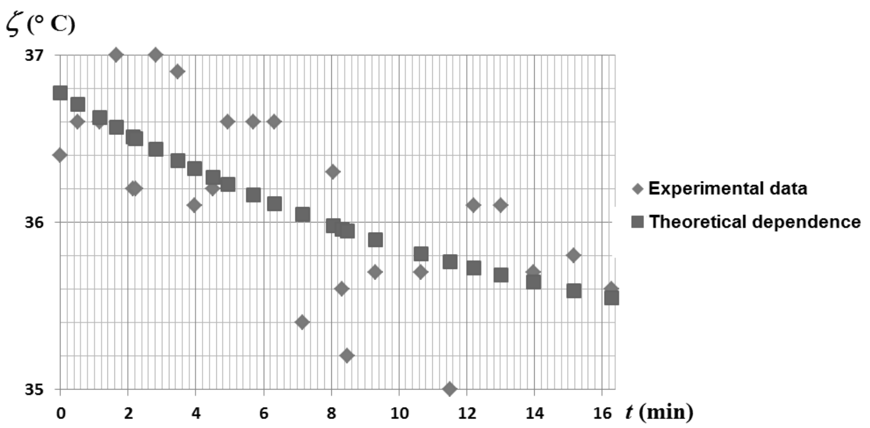

Fig. 5. – The decrease of the body temperature of sheep after the transfer out of the heated stable into the outdoor enclosure

DISCUSSION

Fig. 1 – 5 confirm our assumption that the basic features of the temperature changes of the animal in response to a step change in the external temperature can be broadly characterized by equations (1) and (2). Thus proving that the temperature differences $\Delta\zeta_i$ and the relaxation times τ, whose real values are shown in the Tab. 2, are suitable characteristics of the temperature reaction of the animals. The variance of measured

values for the increase of temperature (see Fig. 2 and 4) is always smaller than for the decrease of temperature (see Fig. 3 and 5). Determined parameters in Tab. 2 show that their values differ for different kinds of animals significantly and therefore they fulfill the necessary condition of the applicability of the proposed method. (i.e. the ability to distinguish between two different objects using obtained parameters.)

CONCLUSIONS

We managed to establish a methodology for the determination of basic thermoregulatory parameters of animals. We have verified that the data obtained as described above are applicable to our way of evaluation and determination of parameters: temperature difference $\Delta\zeta_i$ and relaxation times τ_i for the increase and the decrease of temperature. The measurements were executed for both of these processes on a llama of Vicugna pacos – alpaca and on a sheep of Clun Forest. We determined for these animals: Relaxation times are in llama 7.5 minutes and in sheep 18.5 minutes, for the positive change of the temperature (i.e. transition from cold place to warm place). Relaxation times are in llama 6.1 minutes and in sheep 12.8 minutes, for the negative change of the temperature (i.e. transition from warm place to cold place). During a step change of the external temperature by 10 °C, we observed the following facts. The temperature changes of the peripheral parts of a body are in llama 4.4 °C and in sheep 5.6 °C, for the positive change of the temperature. The temperature changes of the peripheral parts of a body are in llama 3.1 °C and in sheep 1.7 °C, for the negative change of the temperature. The relative temperature coefficients for our llama are: 0.33 – in the case of the temperature increase and -0.23 – in the case of the temperature decrease. The relative temperature coefficients for our sheep are: 0.44 – in the case of the temperature increase and -0.13 – in the case of the temperature decrease. We see the causes of differences of thermoregulation between both animals in these facts: 1) The larger percentage of the subcutaneous fat of sheep. 2) The dissimilarity of environment, where both animals usually live. The environment, where llama usually lives, is typically colder; with more pronounced temperature fluctuations, which requires to respond faster. Regarding the dissimilarity of the fur quality of both animals, it is a fact, that the llama fur isolates better than the sheep fur. This reduces the speed of the llama thermoregulation somewhat. It means, if llama had the same fur like a sheep, the relaxation time of llama would be even lower, than we measured in our experiment.

REFERENCES

1. CORREA, P. N., CORREA, A. N.: Transiently Induced Hyperthermia in Humans Exposed to a Controlled Orac Environment (online). Experimental Aetherometry, 2007, series 2, vol. 4, p. 1-27. Available at: http://www.aetherometry.com/Electronic_Publications/Science/AS2-33/AS2-33.php.
2. HIEBERT, S. M., NOVERAL, J.: Are chicken embryos endotherms or ectotherms? A laboratory exercise integrating concepts in thermoregulation and metabolism (online). Advances in Physiology Education, 2007, vol. 31, no. 1, p. 97-109. ISSN 1522-1229. Available at: http://advan.physiology.org/content/31/1/97.
3. MORRISON, S. F., NAKAMURA, K., MADDEN, C. J: Central control of thermogenesis in mammals (online). Experimental Physiology, 2008, vol. 93, issue 7, p. 773-797. ISSN 1469-445X. Available at: http://onlinelibrary.wiley.com/doi/10.1113/expphysiol.2007.041848/full.
4. MOŠNA, F.: Statistical data processing on PC (online). Faculty of Education, Charles University, Prague, 2010, 54 p. ISBN ISBN 978-80-7290-448-8. Available at: https://sites.google.com/site/projektalmamater/seminare/statistika (in Czech).
5. Temperature Monitoring and Perioperative Thermoregulation. (online). Cleveland Clinic. Center for Continuing Education. Available at: http://www.clevelandclinicmeded.com/online/casebased/outcomesresearch/temperature/content3.htm.

Corresponding author:

RNDr. Jan Sedláček, PhD., Department of Physics, Faculty of Engineering, Czech University of Life Sciences Prague, Kamycka 129, Praha 6, 165 21 Prague, phone: +420 22438 3286, e-mail: sedlacek@tf.czu.cz

SEMI-CRAWLER TRACTOR EFFECTIVENESS FOR LASER LEVELING

H. Shindo [1], M. Saito [1], S. Keiji[1], S. Konno[2], M. Katahira[2]

[1]*Akita Prefectural Agricultural Experiment Station, 34-1, Genhachizawa, Yuwaaikawa, Akita, 010-1231, Japan*
[2]*Yamagata University, 1-23, Wakabamachi, Tsuruoka, Yamagata, 998-8555, Japan*

Abstract
Field leveling of paddy fields in Japan is worsening because of the introduction of large block fields and paddy-upland rotation. Field leveling is increasing in importance to support crop cultivation. Therefore, we investigated the influence of fuel consumption and the effectiveness of laser leveling work in large paddy fields comparing full-crawler tractors and semi-crawlers. Laser leveling work conducted by a laser leveler mounted on a semi-crawler tractor can shorten the total work time by decreasing the amount of reverse work and reverse distance compared to a full-crawler tractor. In addition, a semi-crawler tractor can decrease fuel consumption by decreasing the reverse distance. To decrease the fuel consumption and working time, field conditions should be examined before leveling. Work plans must be made to take a short working distance.

Key words: semi-crawler tractor, laser leveling, work time, work distance, fuel consumption, paddy field.

INTRODUCTION

Field leveling of paddy fields in Japan is becoming worse because of the introduction of large block fields and paddy-upland rotation. Therefore, the importance of field leveling has been growing considering its influence on crop cultivation (SHINDO ET AL., 2014). Laser leveling machines attached to tractors have been introduced for field leveling in Japan (KIMURA ET AL., 1999). This work is usually done by a full-crawler type tractor with low ground pressure because it requires strong traction force. Although full-crawler type tractors have high engine power, their work accuracy of turning movement presents a few difficulties. In recent years, semi-crawler tractors with both good steering performance and traction force have been introduced to paddy fields in Japan. Therefore, we investigated the influence of fuel consumption and the effectiveness of laser leveling in large paddy fields to compare full-crawler tractors and semi-crawler tractors.

MATERIALS AND METHODS

1) Test location

We conducted tests at a farmer's paddy field of Akita city in Japan (No. 1 field), at a paddy field at the Akita Agricultural Experiment Station (No. 2 field), and at a farmer's paddy field of Daisen city in Japan (No. 3 field) during 2012–2013. Field profiles were 1 ha (200×50 m) at Akita city fields (Nos. 1, 2), 76 a (152×50 m), and 70 a (140×50 m) at Daisen city field (No. 3).

2) Machine components

We used semi-crawler tractor (HMT transmission, EG105, 77.2 kW; Yanmar Co. Ltd.). Additionally, we used a full-crawler tractor (HST transmission, CT1010, 74.2 kW; Yanmar Co. Ltd.), which had same engine as the semi-crawler tractor and a full-crawler tractor (HST transmission, MK-140S, 103 kW; Morooka Co. Ltd.). Furthermore, we used direct mount type laser levelers of two types (LL4000 – 4 m work width, LL5000 – 5 m work width; Sugano Farm Machinery Mfg. Co. Ltd.) (Fig. 1).

3) Work system of laser leveling

We ploughed the fields using a laser plough (12 inch, 8 bottoms LCPQY128H; Sugano Farm Machinery Mfg. Co. Ltd.) to a set depth of 11–13 cm before laser leveling. Then we performed leveling using a direct mount type laser leveler. The aiming difference of elevation was set to ± 2.5 cm.

Fig. 1. – Test tractors (Left: Semi-crawler Tractor (EG105), Center: Full-crawler Tractor A (CT1010), Right: Full-crawler Tractor B (MK-140))

Test and investigation contents

1) Test blocks

We had laser leveling work at each field at test area Nos. 1–3 using a semi-crawler tractor and a full-crawler tractor to obtain each work rate and field properties by tractors of different types. We designate the Semi-crawler tractor Block as the Sc block and the Full-crawler tractor block as the Fc block. Tab. 1 shows the settings of test blocks and field properties, tractor types, and work width of the laser leveler.

Tab. 1. – Test block components

Test area Nos.	Test Blocks	Tractor Types	Tractor Power kW	Work width of leveler m	Field profiles Long side m	Field profiles Short side m	Field profiles Area ha	Investigation day d-m-y
No.1	Sc	Semi-crawler	77.2	4	200	50	1	21-Apr-12
	Fc	Full-crawler B	103.0	5	200	50	1	20-Apr-12
No.2	Sc	Semi-crawler	77.2	4	200	50	1	24-Apr-13
	Fc	Full-crawler A	74.2	4	200	50	1	23-Apr-13
No.3	Sc	Semi-crawler	77.2	4	152	50	0.76	08-Oct-13
	Fc	Full-crawler A	74.2	4	140	50	0.70	07-Oct-13

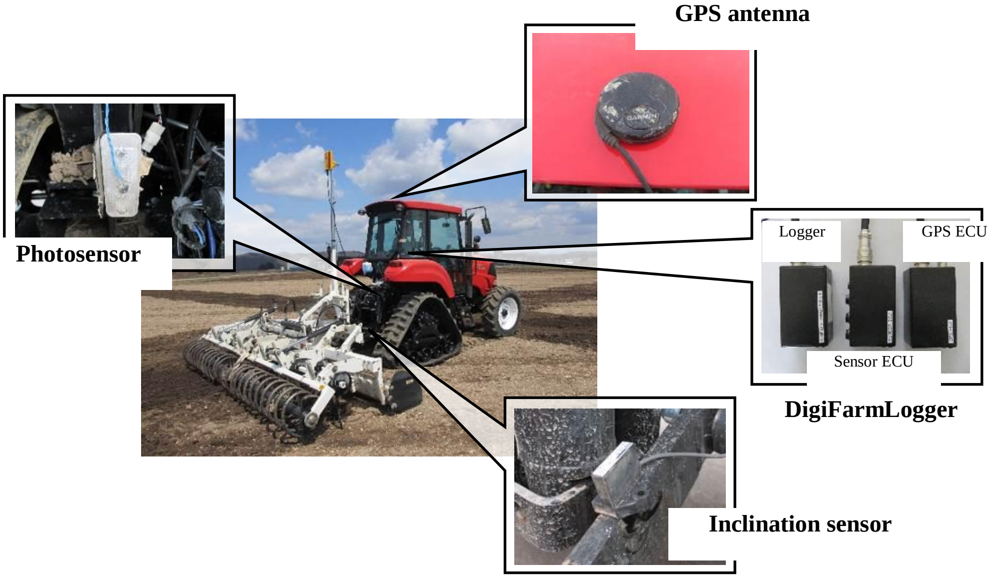

Fig. 2. – Semi-crawler tractor and DigiFarmLogger

2) Investigation contents

Working information of laser leveling was obtained using a farm work information data logger (DFL, DigiFarmLogger (OOMINE ET AL., 2011); Kimura kouyou kougei) attached on a tractor (Fig. 2). That data logger, which comprises a GPS antenna, an inclination sensor attached on a lower link and a photosensor attached on the back lamp, can record the work speed, coordinates, and up-down of the working device continuously. Therefore, we analyzed the work speed, forward-reverse operations and work performance using the data logger system. The tractor fuel consumption was measured using a fuel flow meter (DE-FL; Banzai Racing) attached on the tractor for each test field. We measured the degree of land leveling to divide 40 meshes (250 m^2 (25×10 m)) at No. 1–2 fields of 1 ha area, 30 meshes (253 m^2 (25.3×10 m) at Sc block, and 233 m^2 (23.3×10 m) at Fc block) at No. 3 test field. The paddy field level was measured using a laser surveying machine (LaserEye; Laserplane) at five points per mesh. The measuring points were 200 points at No. 1-2 fields, and were 150 points at the No. 3 field.

RESULTS AND DISCUSSION

(1) Degree of field leveling

Tab. 2 presents paddy field levels before and after leveling. The paddy field levels before leveling on No. 1 field were max 73.8 mm - min - 48.2 mm (σ=21.0) at the Sc block, and max 51.9 mm -- min - 84.1 mm (σ=23.9) at the Fc block. Each test block had the same levels to have about 78% of ± 25 mm points. The paddy field levels after leveling on No. 1 field were max 16.4 mm -- min -18.6 mm (σ=6.6) at the Sc block, and max 13.4 -- min -20.7 mm (σ=6.9) at the Sc block. All measured points of both test blocks were less than ±25 mm. The paddy field level before leveling work on No. 2 field was max 31.2 - min -65.8 mm (σ=21.0) at the Sc block, and max 35.0 mm -- min - 78.0 mm (σ=17.4) at the Fc block. Each test block had the same level to have about 85% of ± 25 mm points. The paddy field level after leveling work on the No. 2 field was max 24.5 mm -- min -44.5 mm (σ=13.2) at the Sc block, and max 23.2 mm -- min - 39.8 mm (σ=12.6) at the Fc block. Both test blocks had more than 96% of ± 25 mm points. The paddy field level after leveling work on the No. 3 field was σ=10.4 at the Sc block, and σ=10.4 at the Fc block. The rate of ± 25 mm points was 84% at the Sc block, and 99% at the Fc block. Consequently, these test results show that No. 1 and 2 fields reached same degree of laser leveling.

Tab. 2. – Paddy field levels before and after laser leveling work

Test area Nos.	Test Blocks	Laser leveling	Measuring points	Max mm	Min mm	Median mm	σ	Level mm	Rate of point (%) > 25mm	< -25mm	-25~ 25mm
No.1	Sc	Before	200	73.8	-48.2	-0.7	21.0	122.0	11.5	10	78.5
		After	200	16.4	-18.6	-0.6	6.6	35.0	0	0	100
	Fc	Before	200	51.9	-84.1	4.4	23.9	136.0	8	14	78
		After	200	13.4	-20.7	-0.1	6.9	34.0	0	0	100
No.2	Sc	Before	200	31.2	-65.8	4.2	18.3	48.5	4.0	11.5	84.5
		After	200	24.5	-44.5	1.0	13.2	34.5	0.0	3.5	96.5
	Fc	Before	200	35.0	-78.0	2.0	17.4	56.5	4.5	8.5	87.0
		After	200	23.2	-39.8	1.7	12.6	31.5	0.0	4.0	96.0
No.3	Sc	Before	150	33.3	-70.7	1.3	19.0	52.0	6.7	8.7	84.7
		After	150	30.1	-37.9	0.1	17.1	34.0	6.0	10.0	84.0
	Fc	Before	150	48.1	-49.9	2.1	16.3	49.0	2.7	10.0	87.3
		After	150	23.2	-28.8	0.2	10.4	26.0	0.0	1.3	98.7

Paddy field levels was calculated an average value of measuring points as 0 level.
Laser leveling at No. 3: The Sc block of Daisen field could not be finished because of rain.

(2) Work time and work components

The work time and components of laser leveling are presented in Tab. 3 and Fig. 3. Work times were, respectively, 6.54 and 6.83 h/ha at the Sc block and Fc block on the No. 1 field. The semi-crawler tractor had shorter work time, in spite of the small work width of laser leveler and also lower engine power than the full-crawler tractor. Regarding work components, each tractor had the same total work time for advance work. However, the amount of reverse work of the Sc block was 194 times, which were much fewer than that of the Fc block. The amount of reverse work per total work time was also much less than that of the Fc block. The respective work times of the Sc and Fc blocks in No. 2 test field were 5.51 and 6.87 h/ha. The Sc block was shorter than the other blocks. Total work time of the advance work was equivalent at the Sc and Fc blocks, but the amount of reverse work of the Sc block was 189 times, which was much smaller than that of the Fc block. The amount of reverse work per total work time was also smaller than that of the Fc block. The amount of reverse work of Sc block in the No. 3 test field was also smaller than that of the Fc block, as well as other test fields. Amounts of reverse work per total work time were also small compared to the Fc block. Laser leveling of paddy field which had long side ridge over 200 m was showed that full-crawler tractor decreased work rate to increase rate of reverse and advance turn (TAKEUCHI ET AL., 2002). So, we got same results, too. These results demonstrate that a semi-crawler tractor has shorter work time by decreasing the amount of reverse work because of better steering performance than that of the full-crawler tractor.

Tab. 3. – Work time and work components

Test area Nos.	Test Blocks	Area	Total work time	Work components				Amount of reverse		Work speed		
				Advance work	Advance turn	Reverse	Stop and others			Ave.	Advance	Reverse
		ha	h	h	h	h	h	Times	Times/h	m/s	m/s	m/s
No.1	Sc	1	6.54	3.89	0.37	1.90	0.38	194	29.7	2.1	2.0	2.1
	Fc	1	6.83	3.95	0.34	2.02	0.52	296	43.3	2.0	1.9	2.4
No.2	Sc	1	5.51	3.05	0.21	1.21	1.03	189	34.3	1.2	1.3	0.9
	Fc	1	6.87	3.78	0.36	1.68	1.06	292	42.5	1.3	1.3	1.5
No.3	Sc	0.76	2.05	1.54	0.12	0.20	0.19	60	29.3	2.0	2.1	1.3
	Fc	0.70	6.36	3.34	0.35	2.03	0.64	304	47.8	1.6	1.5	1.7
	Fc*	0.70	2.05	1.22	0.12	0.56	0.16	95	46.4	1.6	1.5	1.7

Fc* indicates the data for only 2.05 hours from work start at test area NO.3.

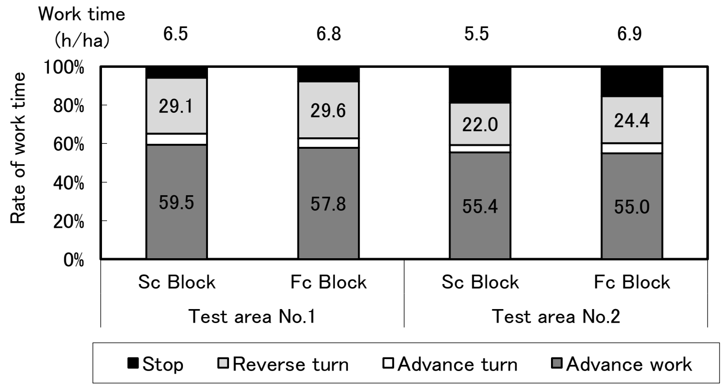

Fig. 3. – Work time components

(3) Total work distance and fuel consumption

The total work distance and components, and fuel consumption of laser leveling are presented in Tab. 4 and Fig. 4. Total work distances of Sc blocks in No. 1 and 2 test fields were, respectively, 45.5 and 19.0 km/ha, which were shorter than that of the Fc block. Each reverse work distance was shorter in these test fields and the amount of reverse work was smaller. Therefore, the rate of reverse work distance per total work distance was also smaller, which suggests that the semi-crawler tractor has shorter reverse distance when turning because it has a smaller turning radius. To increase work rate of laser leveling was shown that full-crawler tractor should have shorten reverse and advance turn time increase work speed to get in next operation, quickly (ONODERA ET AL., 2002). However, semi-crawler tractor could improve work rate to decrease reverse distance.

The fuel consumption of the Sc block in No. 1 and No. 2 test fields were 70.9 and 52.3 l/ha. These were smaller at 26% and 34% than in the Fc block. The fuel consumption per total work distance of No. 2 and No. 3 test fields in which full-crawler tractor and semi-crawler tractor with same type of engine were compared showed equivalent values. That is true because the semi-crawler tractor decreased fuel consumption by its shorter total work distance. To reduce the fuel consumption with laser leveling work, a semi-crawler tractor with a small turning radius can be useful to take short work distances. Setting a working plan for shorter total working distances is also effective.

Tab. 4. - Total working distance and fuel consumption

Test area Nos.	Test Blocks	Area	Work distances		Distance components Advance	Reverse		Fuel consumption			
		ha	km	km/ha	km	km	m/times	L	L/ha	L/h	L/km
No.1	Sc	1	45.5	45.5	30.8	14.7	75.8	70.9	70.9	10.9	1.6
	Fc	1	46.4	46.4	28.9	17.5	59.0	95.4	95.4	14.0	2.1
No.2	Sc	1	19.0	19.0	15.1	3.9	20.6	52.3	52.3	9.3	2.7
	Fc	1	27.8	27.8	19.0	8.8	30.2	79.6	79.6	11.1	2.9
No.3	Sc	0.76	13.6	17.9	12.7	0.9	15.5	24.8	32.6	12.1	1.8
	Fc	0.70	32.9	47.0	20.5	12.4	40.9	62.1	88.6	9.8	1.9
	Fc*	0.70	10.6	15.1	7.1	3.4	36.0	–	–	–	–

Fc* indicates the data for only 2.05 hours from work start at test area NO.3.

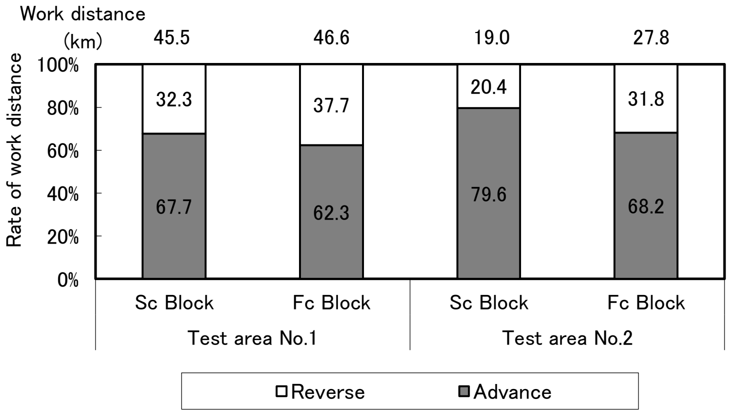

Fig. 4 – Rate of total working distance

CONCLUSIONS

Laser leveling using a laser leveler mounted on a semi-crawler tractor can reduce the total work time by decreasing the amount of reverse work and reverse distance compared to those of a full-crawler tractor. In addition, a semi-crawler tractor can decrease fuel consumption by decreasing the reverse distance. To decrease fuel consumption and the working time, field conditions should be examined before leveling. Working plans should be made to reduce working distances.

REFERENCES

1. KIMURA, S., IMAZONO, S., YAJI, Y.: Development of Labor Saving Operation Technique by Making Large Scale Paddy Field and Direct Seeding Cultivation of Rice in Tohoku District (Part 2). －Development of Technique for Automatic precision Laser-Levelling System－. , Japanese Journal of Farm Work Research 34(2), 1999: 113-121.
2. OOMINE, M., SUGIURA, R.: Development of Farm Working Data Recording System “Digi Farm Logger”. , Farming Mechanization 3116, 2011: 23-27.
3. SHINDO, H., SAITO, M., SASAKI, K.: Effect of Unevenness in a Paddy Field on the Plant Growth in Direct Seeding Cultivation of Rice., Tohoku Branch Report of The Japanese Society of Agricultural Machinery and Food Engineers 61, 2014: 11-14.
4. TAKEUSHI, H., SEKIGUCHI, K., KITAGAWA, I., TAKENAKA, H.: Repuirement for Field Leveling Using Lazer Leveler Machine on Direct Seeding Culture of Paddy Rice. , Bulletin of Hokkaido Pref. Agri. Exp. Stn. 83, 2002: 55-58.
5. ONODERA, T., TSURUTA, M., OSARI, H.: Leveling Rice Paddies Using a Laser Land Leveler When Tilling. , Trans of JAIDRE 219, 2002: 1-8.

Corresponding author:

Hayato Shindo, Akita Prefectural Agricultural Experiment Station, 34-1, Genhachizawa, Yuwaaikawa, Akita, 010-1231, Japan

SOLAR ENERGY OPPORTUNITIES FOR INDONESIA AGRICULTURAL SYSTEMS

R. Sigalingging[1], J. W. Ch. Sigalingging[2], D. Herák[3]

[1]Universitas of Sumatera Utara, Faculty of Agriculture, Department of Mechanical Engineering, Prof. A. Sofyan No. 3 Kampus USU, Medan-20155, Indonesia Republic
[2]The Agency for Meteorology, Climatology and Geophysics of the Republic of Indonesia (BMKG), Deputy of Instrumentation, Calibration, Engineering and Communication Networking, MKKuG Database Management Sub Division, Angkasa I No. 2 Kemayoran, Central Jakarta-10720, Indonesia Republic
[3]Department of Mechanical Engineering, Czech University of Life Sciences Prague, Czech Republic

Abstract
Indonesia has huge agricultural products, which have to process into other products. Energy efficiency and energy conservation have to ameliorate so that amount of energy demand and cost can be reduced in food processing. Global irradiation data was measured by Eppley Pyranometer with coordinates 100.32^o E, 0.20^o S at 864.5meters of the sea-level surface while Indonesia agricultural products data were provided by Indonesian ministry of agriculture. The result shows that total mean global irradiation is between 2,111.9 – 2,427.53 W/m^2/year while to convert paddy into rice, the energy needed was between 30,054 – 32,586 TWh/year which is about 20 times more than total potential of grid-connected PV in Indonesia. This indicates Indonesia agricultural systems probably have the greatest solar energy potential because it is a tropical country and located in the equator line.

Key words: solar energy, renewable energy, agricultural systems, potential, Indonesia.

INTRODUCTION

Improving energy efficiency and energy conservation in Indonesia agriculture are essential to reduce energy demand and therefore reduce cost. Improving energy efficiency, and thus reducing reliance on fossil fuels, will further reduce greenhouse gas emissions. Application of renewable energy especially solar energy can be used for food production and storage (water pumping for crop production and for cattle, electric livestock fences, aeration pumps for fish and shrimp farms, egg incubators, refrigeration for storage, ice-making for storage), food processing (meat and fish drying, plant/seaweed drying, spice drying, cereal grain processing, coconut fiber processing, grain mills, lighting for processing plants), materials processing (rubber drying, sawmills, silk production, silkworm rearing, textile dyeing) and so forth (ROTA ET AL., 2012).

Indonesia is a tropical country and located in the equator line, the country has abundant potential of solar energy. Indonesia government's targets of electricity production from solar energy are 640 MW in 2020 (PLN, 2015) while the target of the government policy regarding national energy supply is to achieve the optimum energy mix in the year of 2025 (PRESIDENTIAL REGULATION NO 5/2006). The government has also been developing photovoltaic (PV) as shown in Fig. 1 and projected to reduce the PV cell cost from \$5/W in 2025 (PLN, 2014). Therefore, this is an opportunity to use in agricultural areas.

Some of related solar technologies already developed in Indonesia such as solar cooker, solar dryer etc. have also been produced locally. But, still abundant of resource of solar energy needs to be utilized using mature and developed technologies. Research in this field is very challenging especially in the small scale electricity generation for rural areas. On the other hand, Solar energy systems have low maintenance costs, and the fuel is free once the higher initial cost of the system is recovered through subsidies and energy savings (from reduced or avoided energy costs). According to the first USDA On-Farm Energy Production Survey, solar panels have been the most prominent way to produce on-farm renewable energy (USDA, 2011). Agriculture hosted some of the first terrestrial photovoltaic (PV) applications of solar energy, as it found uses for solar in remote locations around ranches and farms. Early on, solar electric made economic sense for a number of low power agricultural needs when running utility lines to a specific location was either not possible or too expensive. Therefore, farmers will not lose the chance to get profit for their land. The objective of this study is to show and describe the potential of application solar energy in Indonesia agricultural systems so the new technologies can be developed in future.

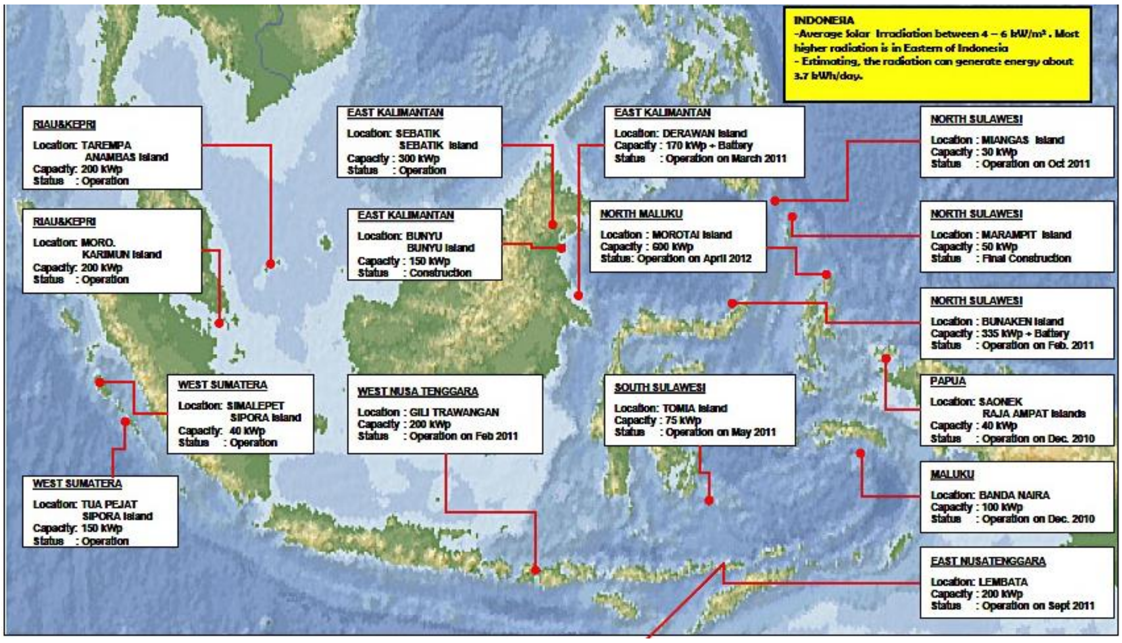

Fig. 1. – Solar PV developed by PLN (2012)

MATERIALS AND METHODS

Global irradiation data was measured by Eppley Pyranometer with coordinates 100.32° E, 0.20° S at 864.5 meters of the sea-level surface while Indonesia agricultural products data was provided by Indonesian ministry of agriculture, which was collected from www.aplikasi.pertanian.go.id. The mean global irradiation was calculated for every month based on daily measurement and the energy demand of agricultural products was calculated based on specific energy consumption.

RESULTS AND DISCUSSION

Based on the daily data collected for 4 years, the monthly mean global irradiation was calculated (Tab. 1), and average global irradiation is displayed (Fig. 2). Tab. 1 shows that the total mean global irradiation is between 2,111.9 – 2,427.53 W/m^2/year. This indicates Indonesia agricultural systems probably have the greatest solar energy potential because it is a tropical country and located in the equator line. Therefore, the country has an abundant potential of solar energy.

According to NASA's data, Indonesia areas get a quite intense of solar irradiation with the average daily irradiation approximately around 5.86 kWh/m^2. The daily average solar irradiation for each month over a period of 22 years between 1983 and 2005 is shown in Fig. 3. Therefore, Indonesia happens to be ideal sites for solar energy production and utilization because of its geographical locations. The solar energy production and utilization in agricultural areas can broadly be categorized into solar photovoltaic (PV) technologies, which convert the sun's energy into electrical energy, and solar thermal technologies. VELDHUIS AND REINDERS (2013) reported that total potential of grid-connected PV in Indonesia was 1100 GWp (Giga Watt Peak) and generating about 1492 TWh, based on current population size and land availability while total potential based on taking restrictions of the present electricity demand during daytime and a minimal base load of conventional power systems was about 27 GWp and generating about 37 TWh/year.

On the other hand, Indonesia agricultural products as shown Tab. 2, which have to be processed, needed huge amount of energy as shown in Tab. 3. The potency solar energy as described above can be applied.

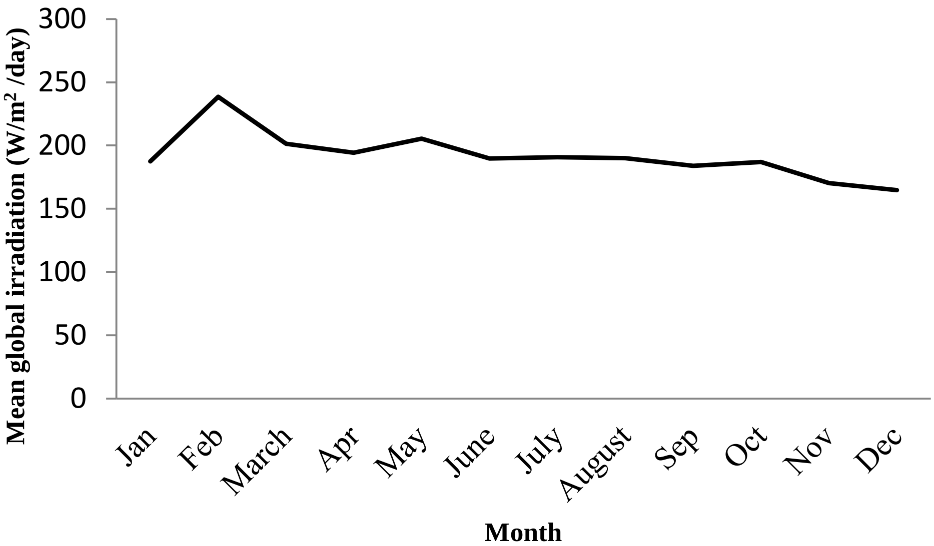

Fig. 2. – Monthly average global irradiation in Indonesia for 4 years

Tab. 1. – Monthly Mean global irradiation in Sumatera island during for 4 years

Month	Mean Global irradiation (W/m^2)			
	2009	2010	2011	2012
Jan	191.22	183.69	178.6	196.62
Feb	195.9	347.58	227.92	182.87
March	219.33	199.43	194.46	192.04
Apr	196.8	192.25	189.46	198.53
May	231.06	192.05	210.85	187.43
June	194.8	190.87	188.46	185.25
July	199.84	173.11	209.99	180.13
August	196.49	200.39	188.7	174.89
Sep	199.62	206.54	173.28	156.83
Oct	197.01	200.51	204.66	146.06
Nov	193.76	158.2	162.28	167.19
Dec	169.47	182.91	162.63	144.06
Sum	2385.3	2427.53	2291.29	2111.9

Tab. 3 shows that the energy needed to convert paddy into rice was between 30,054 – 32,586 TWh/year which is about 20 times more than total potential of grid-connected PV in Indonesia as predicted by VELDHUIS AND REINDERS (2013). According to AHIDUZZAMAN AND ISLAM (2009) the primary energy consumption for mechanical drying was found to be 1,540 MJ/ton of paddy dried to reduce moisture level from 32 % to 14 % under an hot air temperature range of 65 – 130°C. The specific energy consumption was 6.25 MJ/kg of water evaporated from the grain. The electrical energy consumption was found to be 29.26 kWh/ton of paddy processed by a 2 ton per hour capacity modern mill. The milling machinery needs higher electrical load for its several operation viz. pre-cleaning, shelling, separation, grading, polishing, etc. Therefore, it needs mix renewable energy such thermal energy and biomass energy for paddy process because rice is mainly of daily food for Indonesian people.

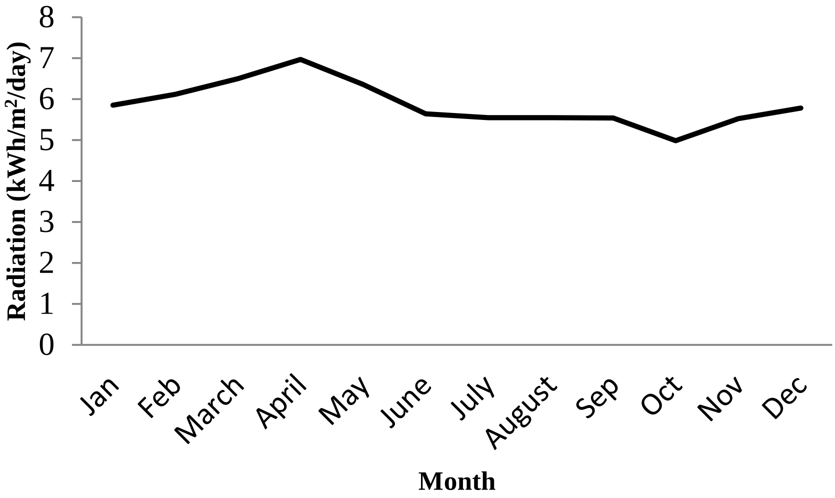

Fig. 3. – Monthly average radiation in Indonesia for 4 years

Energy demand to convert cassava into gari, starch, and flour was between 1.9 – 2.1 TWh. JEKAYINFA AND OLAJIDE (2007); WANG (2009) reported that energy consumption including electrical energy, thermal energy, and labor energy for production of gari, starch, and flour of cassava using efficient and high-capacity processing machines were 0.291, 0.305, and 0.316 MJ/kg, respectively.

Tab. 2. – Indonesian agricultural products at national level

Agricultural products	Production (Ton)			
	2010	2011	2012	2013
Paddy	66 469 394	65 756 904	69 056 126	71 297 709
Corn	18 327 636	17 643 250	19 387 022	18 511 853
Soybean	907 031	851 286	843 153	779 992
Cassava	23 918 118	24 044 025	24 177 372	23 936 921
Palm oil	4 391 624	4 619 308	5 203 104	5 556 401
Coffee	686 921	638 647	691 163	675 915
Tea	156 604	150 776	145 575	145 460
Cacao	837 918	712 231	740 513	720 862

On the other hand, the total energy consumption for drying raw soybean was 1.19 MJ/kg and the electricity generated is used to supply almost all of electricity requirements for palm oil mill, which is estimated to be about 14.36 kWh/ton of FFB (SAMPATTAGUL ET AL., 2011) while to reduce the moisture level from 27 to 13 % in 1 kg corn, an input of 205 kcal fossil energy must be expended (PIMENTEL, 2008). Based on these, energy demand was calculated to produce CPO and to remove moisture level of corn as shown in Tab. 3.

For tea production, A I T (2002) reported that Orthodax tea production, the withering and rolling processes consume more energy (7 kWh/kg) while for cut, tear and curl (CTC) process consume much electrical energy (0.4-0.7 kWh/kg made tea). In this process can use thermal energy for withering and drying process. The ratio consumes both thermal and electrical energy at the ration of 18:15. Drying and freezing processes consume energy 6 MJ to remove 1 kg of water product and 0.3 kWh electricity (1 MJ) to process 1 kg of food products at -20°C, depending on temperature and pressure. In addition, BUNDSCHUH AND CHEN (2014) reported sprinkler irrigation consumed around 10-20 GJ/ha/year of electricity or diesel fuel for pumping water. Pumping water, drying and freezing processes are universal needs for Indonesia agriculture and the use of PV power is a natural choice. Agricultural watering needs are usually the greatest during sunnier dry periods when more water can be pumped with a solar energy system. PV water-pumping systems are simple, reliable, and low maintenance. Larger PV water pumping systems with all balance-of-system components, including the pump, can be installed for under $10 per Watt.

Tab. 3. – Energy demand of Indonesian agriculture to convert products into other products at national level

Agricultural products	Energy Demand (TWh)				Product
	2010	2011	2012	2013	
Paddy	30.379	30.054	31.561	32.586	rice
Corn	4.367	4.204	4.619	4.411	drying
Soybean	3.754	3.523	3.490	3.228	soybean production per ha
	0.300	0.281	0.279	0.258	drying
Cassava	1.933	1.944	1.954	1.935	gari
	2.026	2.037	2.048	2.028	starch
	2.100	2.111	2.122	2.101	flour
Palm oil	0.063	0.066	0.075	0.080	CPO
Coffee	3.244	3.016	3.264	3.192	drying
	0.332	0.308	0.334	0.326	non-roasted
	0.480	0.446	0.483	0.472	roasted
Tea	0.783	0.754	0.728	0.727	CTC
Cacao	1.486	1.263	1.313	1.278	product

CONCLUSIONS

For many agricultural needs, solar energy provides a good alternative for Indonesia agriculture. Indonesia has an abundant potential of solar energy, it indicates from the total mean global irradiation is between 2,111.9 – 2,427.53 W/m^2/year and the average daily irradiation was approximately 5.86 kWh/m^2. Modern, well-designed, simple-to-maintain, and cost-effective solar systems can provide energy that is needed when and where it is needed. Distributed generation, backup in the case of utility grid outage, and net metering present further opportunities for grid-connected solar energy use in agricultural settings in Indonesia.

REFERENCES

1. AHIDUZZAMAN, M. – ISLAM, A. K. M.: Energy utilization and environmental aspects of rice processing industries in Bangladesh. Energies, 2, 2009: 134–149.
2. ASIAN INSTITUTE OF TECHNOLOGY (AIT): Small and medium scale Industries in Asia: energy and environment, tea sector. School of Environment, Resources and Development, Pathumthani, Thailand, 2002.
3. BUNDSCHUN, J. – CHEN, G.: Sustainable energy solutions in agriculture. 8th vol., CRC Press, Taylor & Francis Group, New York, 2014.
4. JEKAYINFA, S.O. AND OLAJIDE, J.O.: Analysis of energy usage in the production of three selected cassava-based foods in Nigeria. Journal of Food Engineering, 82, 2007: 217–226.
5. LYNN, P.A.: Electricity from sunlight. 2nd ed., Collingwood, Australia, Lendlinks 2003.
6. NASA: Atmospheric science data. Available at: https://eosweb.larc.nasa.gov/sse/. Accessed 22 April 2016.
7. PIMENTEL, D., PEMINTEL, M.H.: Food, energy, and society. 3rd ed., CRC Press, Taylor & Francis Group, New York, 2008.
8. PLN: RE Deployment strategies to lower generation cost in isolated grids; renewable energy opportunities from remote Indonesia, 2014.
9. PLN: Power generation and renewable energy, roadmap and opportunities, 2015.
10. ROTA, A., SEHGAL, A., SPERANDINI, S.: Livestock and renewable energy. The International Fund for Agricultural Development (IFAD), Rome, Italy, 2012.
11. SAMPATTAGUL, S., NUTONGKAEW, P., KIATSIRIROAT, T.: Life cycle assessment of palm oil biodiesel production in Thailand. Int. Journal of Renewable Energy, 6, 2011: 1–14.
12. USDA: Solar Energy use in U.S. Agriculture overview and policy issues, 2011. Available at: http://www.usda.gov/oce/reports/energy/Web_SolarEnergy_combined.pdf . Accessed 23 April 2016.
13. VELDHUIS, A.J., REINDERS, A.H.M.E: Reviewing the potential and cost-effectiveness of grid-connected solar PV in Indonesia on a provincial level. Renewable and Sustainable Energy Reviews, 27, 2013: 315–324.
14. WANG, L.: Energy efficiency and management in food processing facilities. CRC Press Taylor & Francis Group, New York, 2009.

Corresponding author:

Riswanti Sigalingging, Department of Mechanical Engineering Faculty of Agriculture, Universitas of Sumatera Utara, Kamýcká 129, Praha 6, Prague, 16521, Indonesia Republic, e-mail: riswanti@usu.ac.id

PERFORMANCE ANALYSES OF SOLAR ADSORPTION REFRIGERATION SYSTEM USING INDONESIAN ACTIVATED CARBON AND METHANOL AS WORKING PAIR

T. B. Sitorus[1], F. H. Napitupulu[1], H. Ambarita[1], T. G. Manik[1]

Department of Mechanical Engineering, Universitas of Sumatera Utara, Jl. Almamater Kampus USU Medan - 20155 Indonesia

Abstract

This study aimed to analyse the performance of a solar adsorption refrigerator using granular activated carbon of coconut shell made in Indonesia and methanol as working pair. The experiments carried out with varying weather conditions. The type of collector were the flat plate with an area of 0.25 m^2. In this research, the maximum value of the COP obtained is 0.1276 when daily global irradiance is 3.918 kWh/m^2 and the minimum value obtained is 0.0830 when daily global irradiance is 2.681 kWh/m^2. The maximum value of SCP obtained is 0.0189 kW/kg and the minimum value obtained is 0.0185 kW/kg. The best adsorption result was the cooling process of water from temperature of 27.90°C to 4.09°C, where the heat extracted from water in the cold box to lower its temperature about 450.01 kJ.

Key words: solar adsorption refrigerator, Indonesian activated carbon, performance analyses.

INTRODUCTION

Indonesia has abundant potential of solar energy because its location is on the equator line between 6°N and 11°N latitudes and in between 95 °E and 141°E longitudes. Most of the Indonesian area gets enough radiation with the average of the solar radiation intensity falling on the surface of the earth Indonesia is 4 kWh/m^2. Based on clear sky conditions that total solar energy in Indonesian archipelagos can range from 16000 to 18000 kJ/m^2/day, according to measurements and predictions (HANDAYANI, 2012; AMBARITA, 2016). One of solar energy utilization for refrigeration system is adsorption refrigerator. The solar powered solid adsorption refrigeration system is the most promising technology with low cost, simple manufacture, maintenance requirements and environmentally friendly. Keep in mind that, researches about solar adsorption refrigerator are still rarein Indonesia. The main objective of this research is to obtain performance of adsorption refrigerator driven by solar energy. This study use granular activated carbon of coconut shell made in local as an adsorbent because the ability to absorb methanol is 300 ml/kg (AMBARITA, 2014). As noted, the activated carbon and methanol seem to be the suitable pair in terms of higher COP and less expensive than other pairs so far in a solid adsorption refrigeration cycle (CRITOPH, 1988).

There are four main working pairs commonly used in solar adsorption refrigerator, namely activated carbon - methanol, zeolite - water, silica gel - water and activated carbon - ammonia (IOAN ET AL., 2015). The application of adsorption refrigeration cycle can be divided into three categories for the room air conditioner (8°C-15°C), for refrigeration of food and vaccine storage (0°C-8°C) and for the purpose of freezing ice and condensation (< 0°C) (FAN, 2007). The physical adsorbents commonly used in adsorption refrigerator are activated carbon, silica gel and zeolite (ANYANWU, 2003). There are two main parameters to evaluate the performance of adsorption refrigeration namely the coefficient of performance (COP) and specific cooling power (SCP). The amount of cooling achieved by a refrigerator per unit of heat supplied is usually given by the COP. The COP valueof the intermittent adsorption refrigerator varies from 0.15 to 0.35 with heat source temperature 60°C-165°C (ZEYGHAMI ET AL., 2015). The COP value of adsorption refrigerator driven by solar energy can be obtained using the equation (JI ET AL., 2014; PARASH ET AL., 2016):

$$COP = \frac{(Q_{cool} - Q_{c-e})}{\int i_{(t)}\, dt} \tag{1}$$

Where i(t) is solar radiation intensity (W/m^2). The cooling effect can be expressed as:

$$Q_{cool} = \Delta x \, . \, m_a \, . \, L \tag{2}$$

and

$$\Delta x = x_{bd} - x_{ad} \tag{3}$$

where m_a is adsorbent mass inside the collector, L is the latent heat of vaporization, x_{bd} is the adsorption capacity before desorption and x_{ad} is the adsorption capacity after desorption. The energy used to cool down the refrigerant liquid from condensing temperature to evaporation temperature can be written as:

$$Q_{c-e} = \int m_a \; \Delta x \; C_{pm} \; dt \qquad (4)$$

where C_{pm} is the specific heat of the refrigerant. Meanwhile, the specific cooling power is the cooling capacity for each kilogram of adsorbent mass can be calculated from equation (WANG ET AL., 2009):

$$SCP = \frac{W_L}{m_a} \qquad (5)$$

where m_a is adsorbent mass inside the collector (kg). And the cooling power (kW) is

$$W_L = \frac{(m_i \; x \; L_w) + (m_i \; x \; c_{pw} \; x \; T_{wa}) - (m_i \; x \; cp_i \; x \; T_i)}{t_c} \qquad (6)$$

where m_i is ice mass (kg), L_w is latent heat of water (kJ/kg), T_{wa} is water temperature (°C), $T_i$is ice temperature (°C), $t_c$is cycle time (second), cp_i is the specific heat of ice (kJ/kg°C) and $cp_w$is the specific heat of water (kJ/kg°C).Thus the aim of this study is to analyse the performance of a solar adsorption refrigerator using granular activated carbon of coconut shell made in Indonesia and methanol as working pair.

MATERIALS AND METHODS

The adsorbent used in this study was ordinary granular activated carbon of coconut shell produced in Sumatera Utara province of Indonesia with grain size 1-3 mm of 6.5 kg shown in Fig. 1. Methanol as refrigerant of 3 litres and water as a medium that was cooled of 4.5 litres.

Fig. 1. – Granular activated carbon of Indonesia

The prototype of solar adsorption refrigerator has been fabricated and used in experiments. The refrigerator consists of three main components, namely collector, condenser and evaporator. The collector was made of stainless steel with plate thickness 2 mm. Two plain glasses cover with thickness of 3 mm separated by a 2 cm air gap were used as transparent covers to prevent the heat loss from the top. The collector contains 6.5 kg of adsorbent then mixed with 15 of the bolts of stainless steel. The bolts of stainless steel with diameter 0.016 m and length 0.05 m, which was aimed to allow a good transfer of heat in the adsorbent. The collector area of 0.25 m^2 and oriented Eastward with tilt angle of 30°. The flat plate collector type was used in this research because easily manufactured and they were commonly used in solar adsorption refrigeration systems (UMAIR ET AL., 2014; SOTERIS, 2009). The collector was isolated using insulating materials, namely wood (20 mm), styrofoam (30 mm), and rockwool (40 mm) as shown in the Fig. 2.

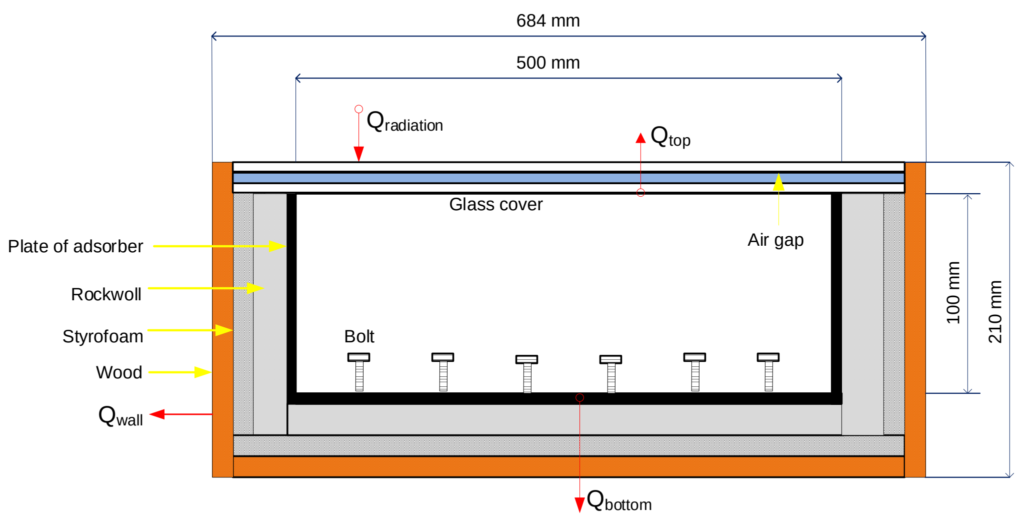

Fig. 2. – The cross section of collector

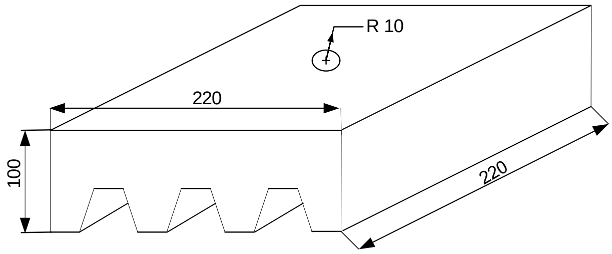

Fig. 3. – Sketch of the evaporator (mm)

The evaporator with heat exchange area of 0.19 m^2 which filled refrigerant of 3 litres was immersed in a cold box. The cold box was filled with water of 4.5 litres and isolated with styrofoam and rockwool. The connections of the collector - condenser - evaporator were flexible tubes with a diameter of 20 mm. The photograph of solar adsorption refrigerator and schematic of refrigerator with measurement systems as shown Fig. 4.

(a)

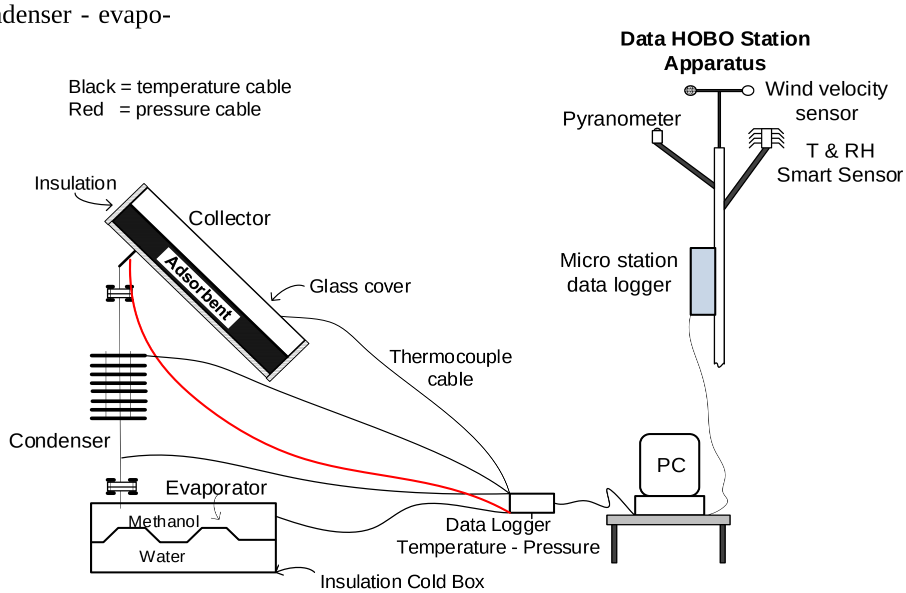

(b)

Fig. 4. – (a) Photograph of refrigerator; (b) schematic of refrigerator with measurement systems

The solar adsorption refrigerator was connected to a data acquisition system, Agilent 3497A through the thermocouples which were placed on the components refrigerator. Temperatures were measured using J type thermocouples with an accuracy of ±0.4%. A HOBO micro station data logger was used to record weather conditions such as solar radiation intensity, ambient temperature, relative humidity and wind speed. A Pace XR5 type P1600-vac-150 data logger with an accuracy ±2% installed on the solar adsorption refrigerator to measure the operating pressure that occurs in solar refrigerator. The measurements were made every one minute. The experimental procedure can be described as follows. Collector heating process until desorption was done by using solar energy and lasts about 9 hours from 08.00 WIB - 17.00 WIB local time. As a note, western Indonesian time or WIB is used in Medan city for local time. When heating-desorption process was completed, then conducted vacuum process around 30 minutes. This process aims to remove the air containing water vapor still present in the adsorbent. The next stage was the filling of liquid refrigerant into the evaporator through a channel that has been made. Furthermore the adsorption process occurred starting from the afternoon. The experiments of solar refrigerator performance were carried out from 08.00 WIB until 08.00 WIB the next day during seven experiments. The experiments had been carried out on location in Medan city, Indonesia in May 2016 with geographic coordinate 3°35’ North - 98°40’ East and altitude about 37.5 meters above sea level.

RESULTS AND DISCUSSION

Tab. 1 shows the weather condition during experiments. The maximum value of solar radiation total during the experiments is 3.918 kWh /m^2 of the fourth experiment and the minimum value occurred on the third experiment is 2.681 kWh /m^2. It also shows the solar radiation time in one experiment ranged from 12.10 - 12.31 hours/day. Solar radiation began to appear from 06.22 WIB until 06.25 WIB during experiments. The distinction of solar radiation total was influenced by the state of the sky such as clear, cloudy and rain with bright.

Tab. 1. – The weather condition during experiments

May 2016 Date	Experiment	Mean Ambient Temperature (°C)	Mean Relative Humidity (%)	Mean Wind Speed (m/s)	Solar Radiation Time (hours/ day)	Solar Radiation Total (kWh/m^2)
1 - 2	1	28.76	83.45	1.06	12.15	2.746
2 - 3	2	28.29	86.44	0.47	12.30	3.042
3 - 4	3	28.10	89.05	0.29	12.13	2.681
4 - 5	4	29.10	82.78	1.17	12.28	3.918
5 - 6	5	30.08	81.09	1.02	12.17	3.874
6 - 7	6	28.06	86.56	0.53	12.31	3.036
7 - 8	7	28.76	83.63	1.69	12.10	3.095

Fig. 5 shows the fluctuations of solar radiation intensity during 24 hours in which the maximum radiation occurs on the second experiment 988.10 W/m^2 at 12.10 WIB. Based on experimental data, that the maximum solar radiation generally occurs at 11.54 WIB - 13.25 WIB and maximum air temperature at 12.41 WIB - 14.45 WIB.

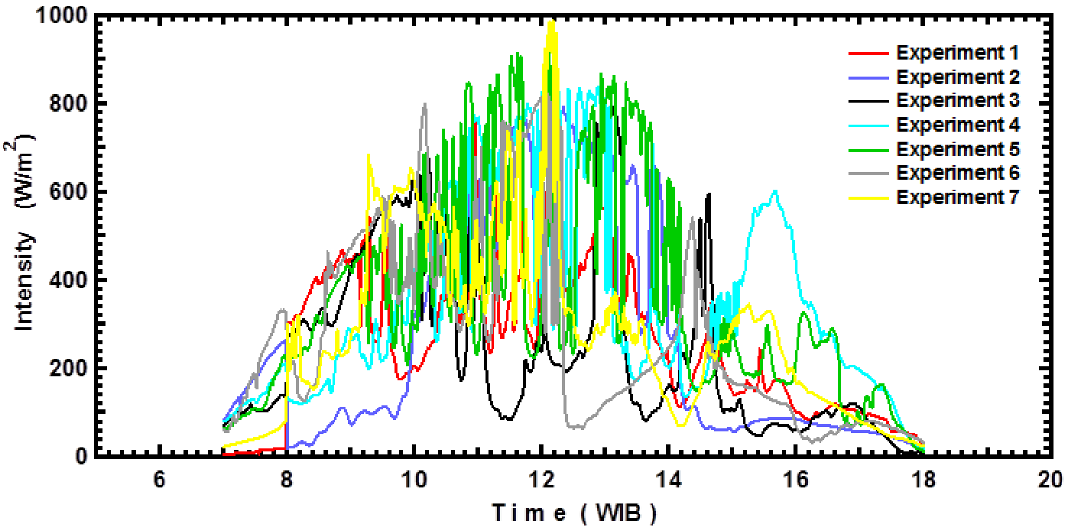

Fig. 5. – Solar radiation during experiments

Fig. 6 shows the typical intensity of solar radiation measurement and theoretical on the fourth experiment. It was used the assumption of clear sky conditions on theoretical calculations. The maximum solar radiation is 930.9 W/m^2 at 12.00 WIB in theoretical calculation and the maximum solar radiation measurement is 841.9 W/m^2 on fourth experiment.

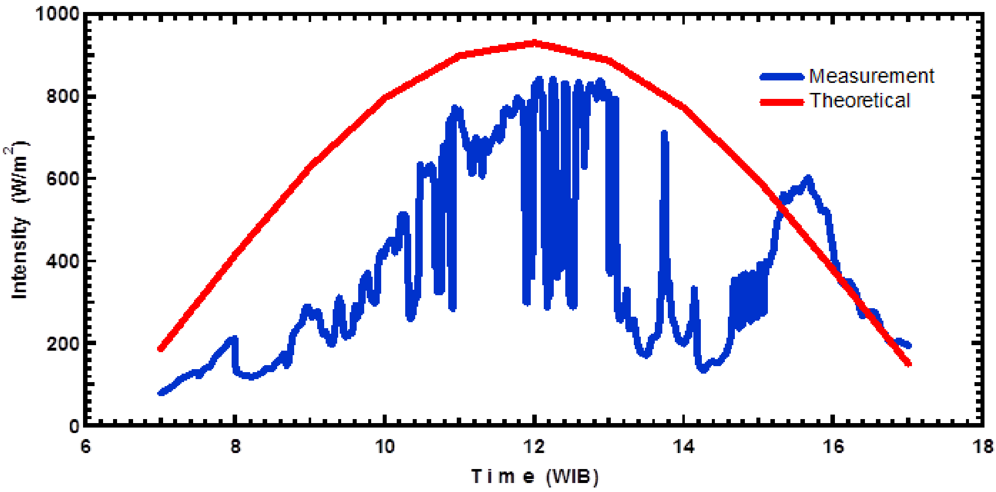

Fig. 6. – Intensity measurement and theoretical on the fourth experiment

The measurement solar radiation way below the theoretical calculation because of the cloud obstruct the beam radiation. In general, the measurement solar radiation agrees well with theoretical calculation. Fig. 7 shows the effect of solar radiation intensity on the component temperature of the first experiment. The experimental data demonstrate that the generation time lasts about nine hours through the day and the cooling process up to adsorption process lasts about fifteen hours. The variations in the collector temperature followed the solar radiation pattern which depends on the solar radiation level. The maximum collector temperature can be achieved was 100.63°C when desorption. From this experiment also show that the higher the solar radiation total will lead to lower the evaporator temperature and this due to the increasing of desorbed refrigerant from adsorbent. This experiment was also carried out measurements of operating pressure that occur in the solar adsorption refrigerator. The measurement results showed the operating pressure of refrigerator varied from 0.0521 bar to 0.3314 bar.

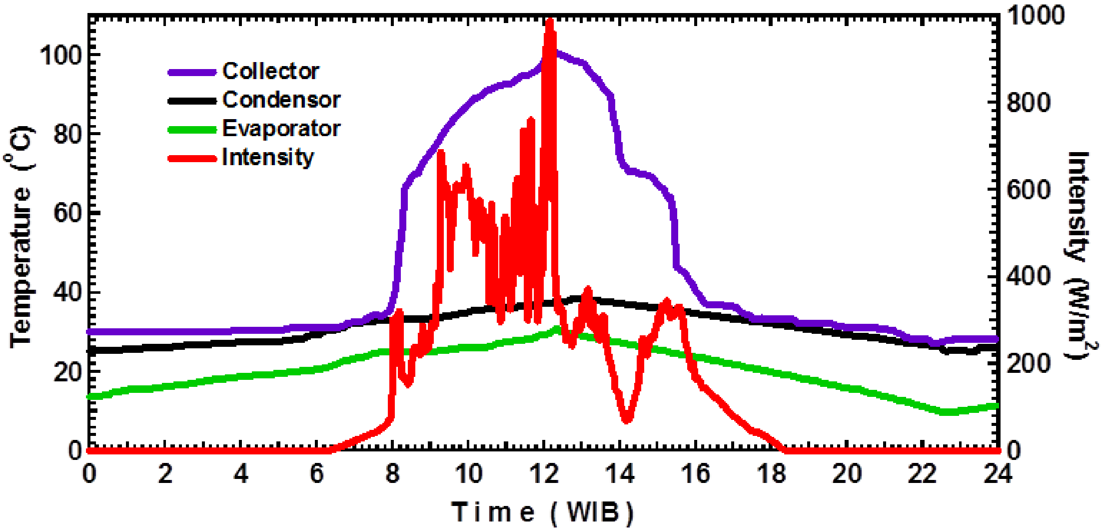

Fig. 7. – The effect of intensity of solar radiation on the component temperature

To analyze the working process of this solar adsorption refrigerator was used pressure - temperature diagram. Fig. 8 shows the actual P-T diagram of seventh experiment, which was representing the working process of solar adsorption refrigerator. The heating process starts from point A at 08.00 WIB local time where the adsorbent was at a low temperature and low pressure. The A-B process was a heating process that followed desorption process B-C takes place on the noon in which the collector receives heat energy so that the collector temperature increases and followed by pressure increasing. The desorption process makes the collector temperature increase until it reaches maximum temperature of 100.63°C when solar radiation maximum was 988.10 W/m^2 at 12.10 WIB local time and followed by pressure increasing to 0.3314 bar that causes refrigerant vapor. In the condenser, the refrigerant vapor was changed to liquid and heat was dissipated to the surroundings. The condensate flows by gravity into the evaporator. During the cooling process C - D and followed adsorption process D-A, the collector is cooled to near ambient temperature, thus reducing the pressure of the entire system. Because the collector continues to release heat during the process of natural convection, the collector undergoes decreasing temperature until it reaches the minimum temperature of 25.08°C at 02.00 WIB and followed by decreasing of pressure that causes refrigerant vapor. In order to evaporate, the refrigerant adsorbs heat from the water around the evaporator as much as the latent heat of vaporization of refrigerant. The cycle was said to be intermittent because the adsorption process happens only during the night.

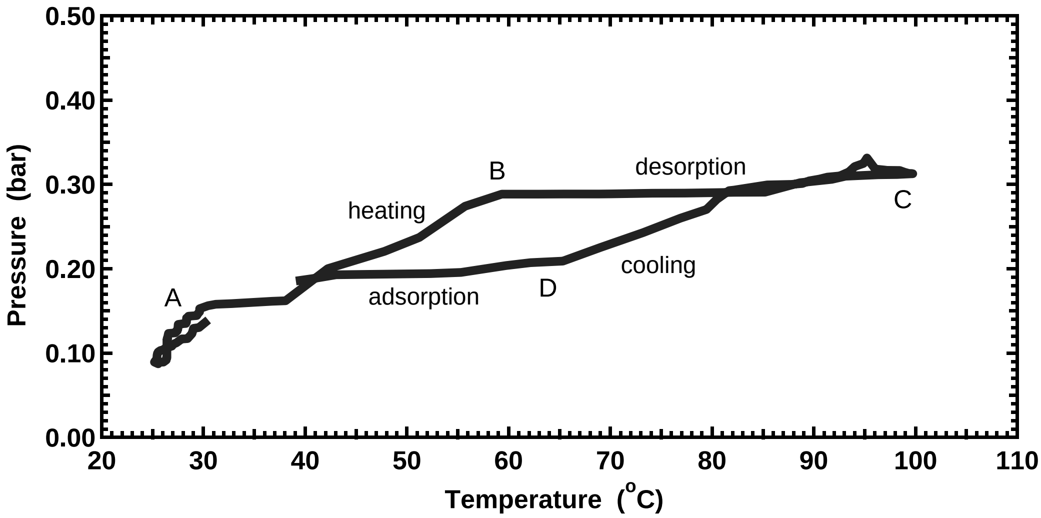

Fig. 8. – The actual P - T diagram of seventh experiment

Tab. 3. – The water temperature and the cooling produced during experiments

Experiment	The actual cooling produced (kJ)	Water temperature (°C)	
		Max	Min
1	302.97	25.76	14.73
2	349.84	26.28	12.77
3	294.84	25.44	14.84
4	547.34	27.90	4.09
5	503.87	27.76	6.10
6	336.23	25.94	13.15
7	399.17	27.16	11.04

Tab. 3 shows conditions of water temperature and the actual cooling produced during experiments.

The minimum water temperature that can be achieved in these experiments during the adsorption process is 4.09°C-14.84°C with a heat source of temperature range 81.02-100.63°C. The total incident global solar energy to the collector area ranging 2412.61 kJ-3525.86 kJ and the actual useful cooling produced was the heat extracted from water in the cold box to lower its temperature of about 200.34 kJ-450.01 kJ during experiments.

Fig. 9 shows the values of COP and SCP obtained during experiments. It appears that the fluctuating value of the COP was always followed by the value of SCP. From the experimental data on this solar refrigerator showed the coefficient of performance to be in the range 0.0830-0.1276 when the solar energy total lies between 9.65 MJ/m^{2}and 14.10 MJ/m^2. The cooling capacity for each kilogram of adsorbent mass or SCP obtained ranging 0.0185 kW/kg - 0.0189 kW/kg. Based on the analysis carried out, the main parameters that affect the performance of a solar adsorption refrigerator were solar radiation total, collector performance and the process of vacuum. The heat received by the collector was eventuality not optimum and also required improving the cooling of the collector. As noted, the solar adsorption refrigerator that uses methanol have normal operating pressure ranges from 0.02 bar-0.2 bar (ERIC, 1998; WANG ET AL., 2009; ZEYGHAMI ET AL., 2015). And the operating pressure of the refrigerator under test was obtained about 0.0521 bar-0.3314 bar. This condition means that the operating pressure of adsorption refrigerator being tested has not fulfilled as expected. This was mainly caused by a vacuum process that is still not optimal, which resulting the presence of unwanted gases in refrigerator.

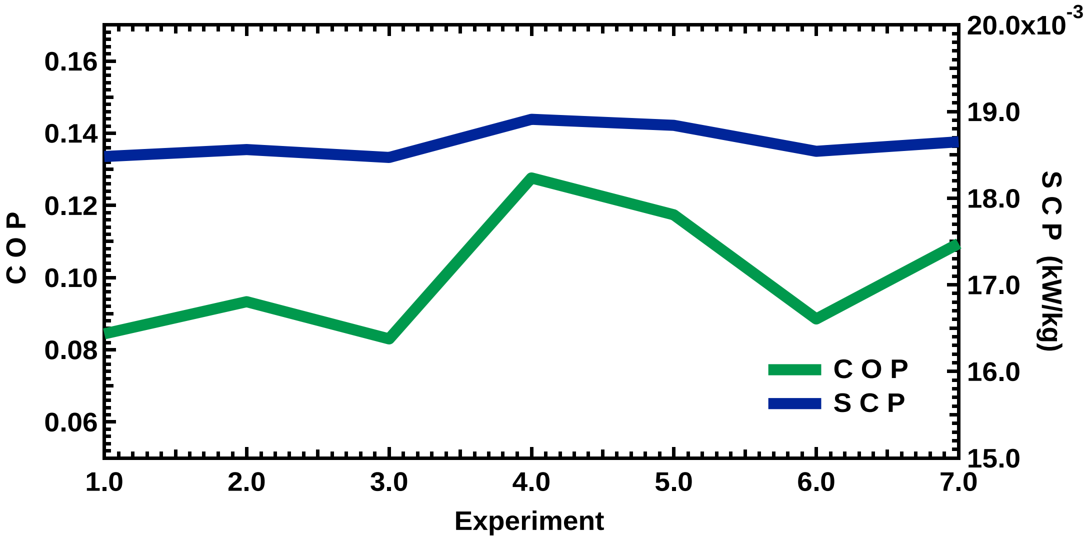

Fig. 9. – The valuesof COPandSCPobtained during experiments

The presence of unwanted gases affects the cycle of thermodynamics, and operating pressure of refrigerator (HANDAYANI, 2012; AMBARITA, 2016). As we know, the average micropore size of the adsorbent was able of adsorbing not only refrigerant, but also unwanted gases such as leaked air. It was thought that the unwanted gases occupy a part of the adsobent microporous surface otherwise available for refrigerant. The presence of unwanted gases that have much higher saturated pressure than refrigerant at the same temperature would destroy the vacuum and diminish the performance of the solar adsorption refrigerator (ERIC, 1998; PARASH ET AL., 2016). The refrigerant adsorbed by adsorbent is less than without the presence of unwanted gases. The unwanted gases desorbed earlier than the refrigerant, making more adsorbent microporesavailable for adsorption of refrigerant during the heating process. The operating pressure would keep increasing as the collector temperature increased because the unwanted gases could not be condensed. Consequently, when there were unwanted gases in the system, a higher maximum collector temperature would be needed to generate the same amount of refrigerant as without the presence of unwanted gases. The desorbed refrigerant would be less than before if the maximum collector temperature was the same.

Tab. 4 shows the collector efficiency, which obtained during experiments. The maximum collector efficiency obtained was 51.46% when maximum solar radiation was 998.10 W/m^2. With statistical function was obtained correlation of weather conditions on the collector efficiency.

Tab. 4. – Collector efficiency during experiments

Experiment	Maximum Solar Radiation (W/m^2)	Ambient Temperature (°C)	Relative Humidity (%)	Wind Speed (m/s)	Collector Efficiency
1	770.60	31.94	69.9	1.53	0.3464
2	793.10	33.13	68.3	1.62	0.4075
3	791.90	34.89	65.3	1.51	0.3932
4	841.90	35.10	63.0	1.33	0.4788
5	948.10	33.97	66.8	0.92	0.4903
6	824.40	32.79	67.4	1.57	0.4196
7	988.10	34.47	61.2	1.07	0.5146

Tab. 5. – Correlation of weather parameters on efficiency collector

Data	Maximum radiation	Ambient temperature	Relative humidity	Wind speed	Collector efficiency
Maximum radiation	1				
Ambient temperature	0.418	1			
Relative humidity	-0.649	-0.837	1		
Wind speed	-0.917	-0.443	0.521	1	
Collector efficiency	0.903	0.642	-0.788	-0.818	1

Tab. 5 shows that there was a significant correlation between collector efficiency to solar radiation intensity 0.903. In addition, also examined the effect of weather on the collector efficiency by using multiple regression analysis. And obtained the coefficient of determination (R^2) is 0.905, it means that the effect of weather conditions on the collector efficiency about 90,5%. Tab. 6 shows the correlation of the daily global irradiance received by collector against the minimum temperature of water and the value of the COP. It was obvious that the correlation of daily global irradiance against with the minimum temperature of water in the cold box and the value of COP namely -0.986 and 0.880 respectively. It states that the greater the daily global irradiance received by the collector, the lower the temperature of the cold water produced and the greater the COP value obtained.

Tab. 6. – Correlation of daily global irradiance on the water temperature and COP

Parameter	Minimum water temperature	Daily global irradiance	COP
Minimum water temperature	1		
Daily global irradiance	-0.986	1	
COP	-0.939	0.880	1

CONCLUSIONS

The performance of adsorption refrigeration driven by solar energy with granular activated carbon-methanol as working pair has been studied. The performance is influenced by the main parameter, namely solar radiation total, collector efficiency, and vacuum process. Experimental results showed that the working pair system can deliver evaporator temperature of about 2.81°C-13.61°C. It is clear that granular activated carbon of coconut shell produced in Sumatera Utara province of Indonesia with methanol as working pair can produce the cooling effect in a solar adsorption refrigerator with a heat source of temperature range of 81.02°C and 100.63°C.

ACKNOWLEDGEMENTS

The authors wish to acknowledge Professor Hideki Kawai from Department of Mechanical Systems of Engineering, Muroran Institute of Technology, Japan for his helpful comments during the research period.

REFERENCES

1. AMBARITA, H.: The adsorption capacity of activated carbon and activated alumina as adsorbent against refrigerants in adsorption cycle. Proceedings of the National Seminar, Mechanical Engineering - University of Indonesia (SNTTM XIII), Jakarta, 15 - 16 October, 2014.
2. AMBARITA, H., KAWAI, H.: Experimental study on solar-powered adsorption refrigeration cycle with activated alumina and activated carbon as adsorbent. Case Studies in Thermal Engineering vol 7, 2016: 36 - 46.
3. ANYANWU, E.E.: Review of solid adsorption solar refrigerator I: an overview of the refrigeration cycle. Energy Conversion and Management vol 44, 2003: 301-312.
4. CRITOPH, E.R.: Performance limitations of adsorption cycles for solar cooling. Solar Energy vol 41, 1988: 21 - 31.
5. ERIC, H., J.: A Study of Thermal Decomposition of Methanol In Solar Powered Adsorption Refrigeration Systems. Solar Energy vol. 62, No. 5, 1998: 325-329.
6. FAN, Y.: Review of solar adsorption technologies - Development and Applications. Renewable and Sustainable Energy Reviews vol 11, 2007: 1758 – 1775.
7. HANDAYANI, A. N.: Potency of Solar Energy Applications in Indonesia. International Journal of Renewable Energy Development vol 1 (2), 2012: 33-38.
8. IOAN, S., CALIN, S.: General review of solar-powered closed sorption refrigeration system”. Energy Conversion and Management vol 105, 2015: 403 - 422.
9. JI, X., LI, M., FAN, J., ZHANG, P., LUO, B., WANG, L.: Structure optimization and performance experiments of a solar-powered finned-tube adsorption refrigeration system. Applied Energy vol 113, 2014: 1293-1300.
10. PARASH, G., PRASHANT, B., ARVIND, M., AMEENUR, S. R. : Adsorption refrigeration technology - An overview of theory and its solar energy applications. Renewable and Sustainable Energy Reviews vol 53, 2016: 1389-1410.
11. SOTERIS, K.: Solar Energy Engineering Proccess and Systems. 1st ed., Cyprus University of Technology 2009.
12. UMAIR, M., AKISAWA, A., UEDA, Y.: Performance Evaluation of a Solar Adsorption Refrigeration System with a Wing Type Compound Parabolic Concentrator. Energies vol 7, 2014: 1448-1466.
13. WANG, W. L., WANG., WANG, Z.R., OLIVEIRA G.R.: A review on adsorption working pairs for refrigeration. Renewable and Sustainable Energy Reviews vol 13, 2009: 421-432.
14. ZEYGHAMI, M., YOGI GOSWAMI, D., STEFANAKOS, E.: A review of solar thermo-mechanical refrigeration and cooling methods. Renewable and Sustainable Energy Reviews vol 51, 2015: 1428-1445.

Corresponding author:

Tulus Burhanuddin Sitorus, Department of Mechanical Engineering, ST.MT.,University of Sumatera Utara, Jl. Dr. T. Mansyur No. 5, Medan, Indonesia, 20155, e-mail: tburhanudin@yahoo.com

RELATIONSHIP BETWEEN THE MEDULLA AND THE DIAMETER OF FERRET HAIRS

M. Skřontová[1], L. Šimková[2], K. Jelen[2]

[1]*Department of Anatomy and Biomechanics, Faculty of Physical Education and Sport, Charles University in Prague, Czech Republic*
[2]*Department of Anatomy and Biomechanics, Faculty of Physical Education and Sport, Charles University in Prague, Czech Republic*

Abstract
The content of this article is a possible explanation of the hair anisotropy, causing the dependence of modulus of elasticity on a hair diameter, which was described in earlier works. The diameter of the medulla part was histologically observed using 27 hairs of 9 different ferrets (*Putorius putorius furo*). The tearing curve was determined for the hairs measured in this way and used to determine material parameters. A linear dependence of medulla thickness on hair diameter was found out, which means a quadratic decrease in the effective cross section of the hair diameter because the modulus of elasticity of the medulla part is lower by two orders than the modulus of elasticity of the cortex. This relationship explains to a considerable extent also the conclusions for the guinea pig (*Cavia porcellus*) hair and the human hairs expressed earlier. At the same time, it is the medulla part what is responsible for the thermal insulation properties of the hair and its description can thus be used when constructing models of materials made of these fibres for their possible industrial applications.

Key words: modulus of elasticity, cross section, guinea pig.

INTRODUCTION

The work focuses on more detailed research on the mechanical properties of animal hairs, especially from the coats of ferrets.

The coat, which is a characteristic of mammals, provides thermal insulation, allows sensory perception, and acts as protection against chemical, physical or microbial damage to the skin (MILLER ET AL., 2012). In the case of animals we can find three types of hairs which produce hair follicles. The primary hair consists of long guard hairs which create the top coat. Each guard hair always grows from its own follicle, but in some cases more hairs can grow from one follicle. The muscles attached to the root of each long hair enable to straighten the hairs. There is also a secondary hair cluster in each guard hair follicle. These secondary hairs include the undercoat. The undercoat function is to provide warmth and protection. Tactile whiskers and eyelashes are the third type of hairs. This type is adjusted to serve as a tactile sensor (ELDREDGE ET AL., 2007).

The hair is embedded in a hair bulb, which is on a fibrous papilla with nourishing blood vessels. The root of the hair is placed in a hair follicle. The hair bulb is connected to a small smooth muscle, which acts as a righting muscle. The hair can be divided into two parts – root and loose hair. The hair root is the part of the hair that is located in the hair follicle under the skin. The loose hair protrudes from the skin (MARTÍNEK, VACEK, 2009).

The hair follicle is composed of five main parts, namely a dermal papilla, which is a group of cells forming a structure right below the follicle, a matrix located around the papilla, which consists of a group of epithelial cells, in which pigment, a hair , and inner and outer cases can be found. The hair itself can be divided into three parts – medulla, cortex and cuticle. The pith (medulla) is the inner part, which consists of longitudinal rows of rectangular cells (PATERSON, 2008). The cortex is the main component of the hair and consists of keratinized cells which are spindle-shaped and flat in shape (MARTÍNEK, VACEK, 2009). Cells containing pigment, melanin, are located here (PATERSON, 2008). Air filled cavities are created in the cells with age and cause the grey to white colour of the hair (MARTÍNEK, VACEK, 2009). The cuticle is the outer layer of the flattened and keratinized cells (PATERSON, 2008). The cells are different in shape and arrangement. They are completely transparent and colourless (have no pigment). They are imbricate and their free edges are oriented to the tip of the hair (MARTÍNEK, VACEK, 2009). The basic motive of this work is to explain why it appears to be decreasing modulus of elasticity with a diameter of hair. An estimate based on the average thickness of the medulla is to be determined dependence of modulus of elasticity on the diameter of the hair.

MATERIALS AND METHODS

In addition to the hair length and thickness, the mechanical properties of hairs are also dependent on the environment, especially on the temperature and relative humidity, in which the samples are examined.

The samples of hairs were taken from 9 ferrets with different lengths of the hair. The most commonly bred ferrets include ferrets with a standard hair length (i.e. shorthaired), followed by angora ferrets (i.e. longhaired). The third type of hair length, polangora, is created by crossbreeding these two types. Samples were cut by a sharp pair of scissors close to the skin surface in the same area, i.e. on the withers.

The diameter (Fig. 1) of each sample was determined using an optical microscope equipped with a digital camera. The diameter was measured 15 times on the first 3 cm of the sample. Always three hairs taken from each animal examined were measured. The overall diameter for a sample concerned was calculated using the values measured in this way. In the case of most samples, it was possible to measure the internal diameter, i.e. the portion of medulla to the overall hair diameter. We obtained two types of diameter in this way and used them for calculations using the software for processing load curve data obtained from the deformation machine because after the diameters were measured, all hairs examined were clamped in the jaws of a Deform type 2 tearing machine and tightened at a speed of 2 mm/min until the breakage itself of the sample. The Deform type 2 tearing machine used by us is suitable for measuring small and slow changes in biological materials. With the tensometer range of up to 20 N and special jaws for measuring fibres, it enables both to determine a classic tearing curve and to measure relaxation or cyclic loading.

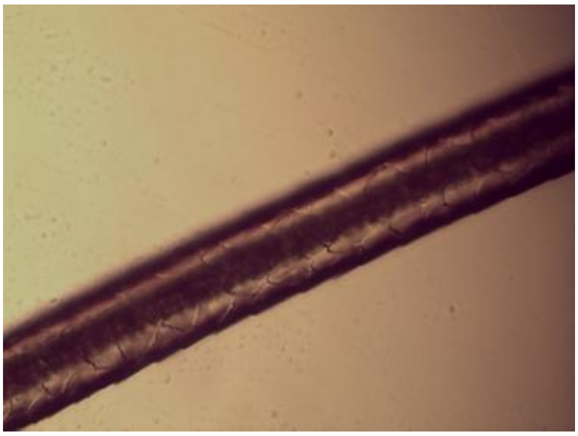

Fig. 1. – A photograph of a hair where its lightness, i.e. the portion of the medulla to the overall diameter of the hair, is clearly visible

The makeing photography for the purpose of comparability analyzes DEEDRICK AND KOCH (2004), SKŘONTOVÁ ET AL. (2016).

RESULTS AND DISCUSSION

The measurement results are clearly arranged in the form of the table and the graphs below.

Tab. 1 gives the average values of the mechanical and material parameters determined using the tearing curves of the ferret hairs. Each of the means or standard deviations was determined using 14 measurements. The table gives both the values calculated classically, with the measured full diameter of the samples, and the values with the reduced diameter, i.e. after deducting the cross section of the medulla part.

Tab. 1. – The average values of the mechanical parameters of the ferret hairs determined by us

	D [μm]	**E [MPa]**	**$\sigma_{0.05}$ [MPa]**	**$\sigma_{0.2}$ [MPa]**	**σ_t [MPa]**	**σ_t' [MPa]**	**ε_t [ ]**	**ε_t' [ ]**	**W [mJ]**	**W_A [MJ/m^3]**	**w_e [MJ/m^3]**
$\bar{x}$	349	64	1.00	0.91	2.25	2.76	0.22	0.20	0.47	0.37	0.012
$\bar{s}_x$	67	23	0.57	0.57	0.72	0.90	0.10	0.08	0.21	0.20	0.014
$\bar{x}^*$	284	92	1.58	1.45	3.27	3.97	0.21	0.19	0.46	0.51	0.020
$\bar{s}_{x^*}$	43	35	1.11	1.10	1.01	1.23	0.10	0.08	0.20	0.26	0.022

Glossary to Tab. 1: $\bar{x}$ – arithmetic average of not reduced quantities; $\bar{s}_x$ – average standard deviation of the not reduced quantities; $\bar{x}^*$- arithmetical average of the reduced quantities; $\bar{s}_{x^*}$ - average standard deviation of the reduced quantities; E' [MPa] – actual modulus of elasticity; $\sigma_{0,05}$[MPa] – limit of linearity, or so-called limit of elasticity; $\sigma_{0,2}$ [MPa] – yield point; σ_t[MPa] – fracture stress; σ_t' [MPa] – actual fracture stress; □$_t$ [ ] – elongation; □$_t'$[ ] – actual relative ultimate elongation; W [mJ] – total mechanical work required for breaking the material; W_A [MJ/m^3] – tensile toughness, the amount of energy required for breaking the material related to the initial tensile volume; w_e[MJ/m^3] – resilience, the amount of energy in a unit of volume of the material concerned loaded with tensile □$_{0.05}$.

Only not reduced values can be found in literature, e.g. ŠIMKOVÁ ET AL. (2013) or SKŘONTOVÁ ET AL. (2015), and if the material parameters are stated in the works, they generally correspond with the data given here. Some parameters such as resilience or elongation, total mechanical work, or tensile toughness are published newly here. Also reduced parameters determined for the hairs of the ferrets with deducted medulla part cannot be found in literature.

Fig. 2 shows the dependence of the modulus of elasticity of the hairs with no correction. The full diameter is therefore used for calculations here as if the entire profile of the hair is exclusively cortex. As a matter of interest, also the power parameter was released when searching for the function; however, it turned out that the experimentally determined dependence is almost perfectly hyperbolic and the power parameter is very close to minus one.

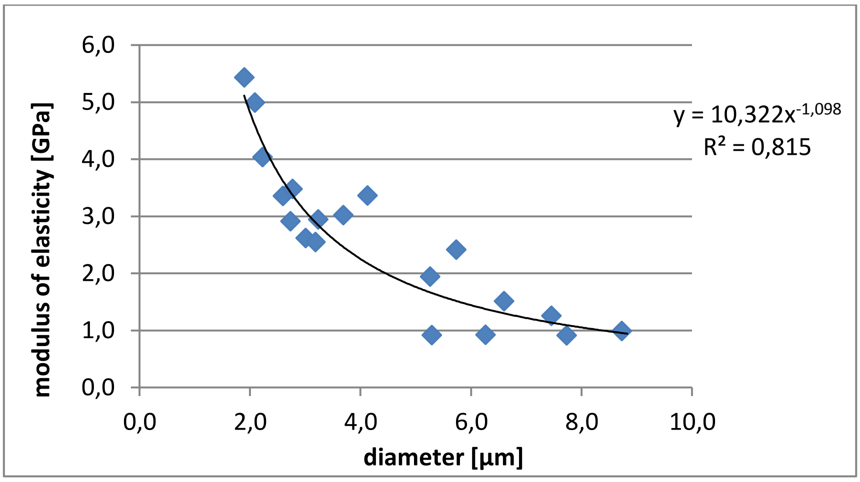

Fig. 2. – Dependence of modulus of elasticity on the diameter of individual hairs

As we can see in Fig. 3, a linear equation can be successfully put on the dependence of medulla diameter on hair diameter. Therefore, we can write the formula $m = 0.7\ D - 21$, where m – diameter of the medulla and D – diameter of the hair. This relation enables us to conclude that hairs less than 20 µm thick will not have medulla at all. This result is new and we have not yet succeeded in finding any similar result in literature. However size of medulla depending on age is observed among black people (ABOAGYE ET AL., 2014; LONGIA, 1966).

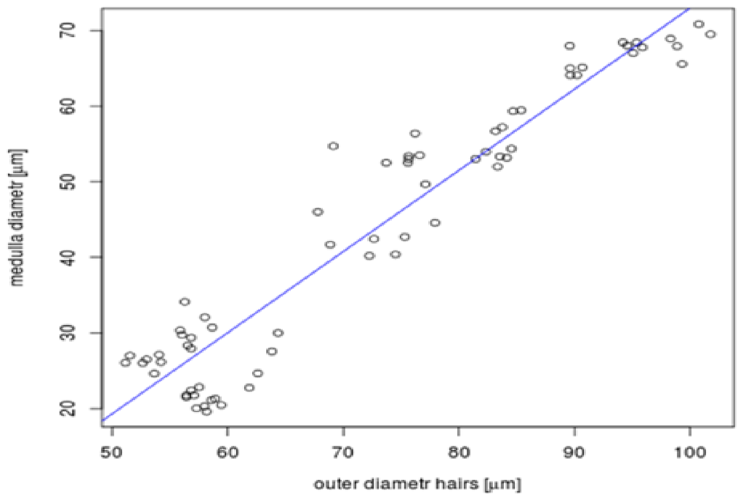

Fig. 3. – The graph shows that the dependence of the diameter of the medulla part is approximately proportional to the overall diameter of the medulla ferret hair

The portion of cortex to medulla can be seen in Fig. 4. According to this graph, it is clear that the most frequent values are found in the range of 0.7 to 0.75. This parameter is very specific for various animal species and can be used to identify an animal by hair. This range for ferrets corresponds with HICKS (1977) and LUNGU ET AL. (2007).

Fig. 5 shows the dependence of the determined modulus of elasticity calculated in the usual way, where a hair is regarded as isotropic material despite its great anisotropy, and at the same time the values of the same hairs calculated for the cross section of the cortex only, which is the main support part of the hair. We can see that only a small part of the dependence of module on hair diameter remains unexplained.

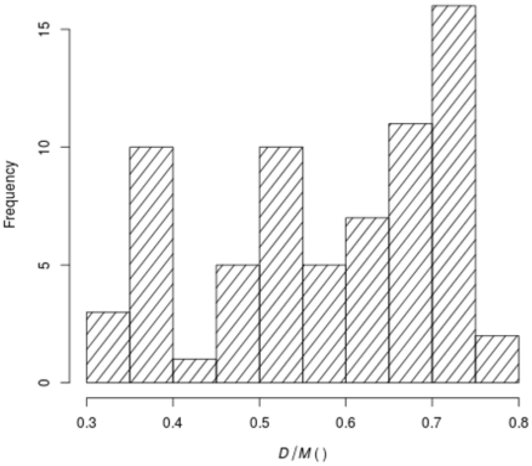

Fig. 4. – Histogram with the ratios of the diameters of ferret hairs and the diameters of their medulla parts shows the greatest occurrence in the 65-75 % region, i.e. the medulla diameter is most frequently 65-75 % or 42-56 % of the cross section of the ferret hair.

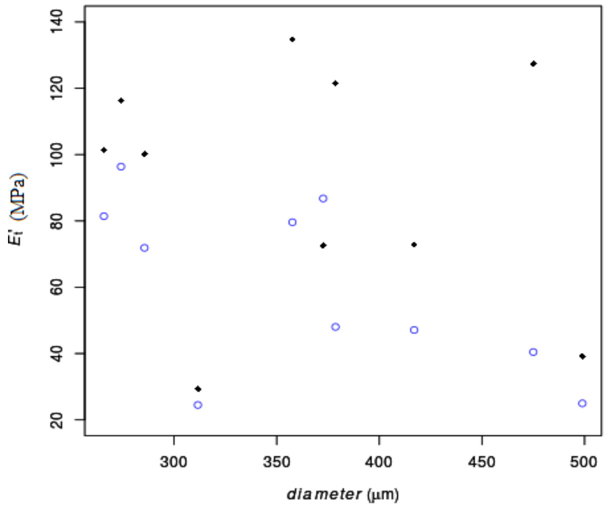

Fig. 5. - Dependence of modulus of elasticity (E_t') on hair diameter.

CONCLUSIONS

Making the current measurement of the medulla part of a hair and determining the tearing curve for the same hairs, we largely succeeded in explaining the previously published dependence of the modulus of elasticity on the cross section of the hair. We succeeded in showing that the dependence of medulla thickness on hair thickness is linear. At the same time, this means that the dependence of the medulla part of the cross section of the hair on the diameter of the hair is quadratic in general. Due to the inclusion of this correction in the calculation of the hair material parameters, the previously determined dependence of the modulus of elasticity on the hair diameter, for example, was explained to a large extent. As the diameter of a hair can be influenced by the breeding method, for example, also the resulting mechanical properties of the coat can be influenced according to these results.

ACKNOWLEDGEMENTS.

This project has been co-financed from the GAUK 884214, SVV 2016-260346.

REFERENCES

1. ABOAGYE, B., AHENKORAH, J., HOTTOR, B., ADDAI, F.: Comparative Characteristics Of Black And Grey Chest And Selected Facial Hairs In Negroid Males. The Internet Journal of Biological Anthropology, 2014: vol. 7, no. 1.
2. DEEDRICK, D. W., KOCH, S. L.: Microscopy of Hair Part II: A Practical Guide and Manual for Animal Hairs. Forensic Science Communications (online), 2004: vol. 6, no. 3.
3. ELDREDGE, D. M., CARLSON, L. D., CARLSON, D. G., GIFFIN, J. M.: Dog Owner's Home Veterinary handbook. Wiley, New Jersey, 2007.
4. HICKS, J. W.: Microscopy of hairs, A Practical Guide and Manual, 1977.
5. LONGIA, H. S.: Increase in medullary index of human hair with passage of time. J. Crim. L. Criminology and Police Sci., vol. 57, 1966: p. 221 – 222.

6. LUNGU, A., RECORDATI, C., FERRAZZI, V., GALLAZZI, D.: Image analysis of animal hair: Morphological features useful in forensic veterinary medicine. Lucrări Ştiinłifice Medicină Veterinară, vol. XL, Timişoara, 2007: 439 – 446.
7. MARTÍNEK, J., VACEK, Z.: Histological atlas. Grada Publishing, Prague, 2009 (in Czech).
8. MILLER, W. H., GRIFFIN, C. E., CAMPBELL, K. L.: Muller and Kirk's Small Animal Dermatology, 7th edition, Saunders-Elsevier, St. Louis, 2012.
9. PATERSON, S.: Manual of Skin Diseases of the Dog and Cat. Blackwell Publishing, Chichester – West Sussex, 2008.
10. SKŘONTOVÁ, M., ŠIMKOVÁ, L., JELEN, K., CHALUPA, B., ZEMAN, J.: Viscoelastic Parameters of Mammalian Hair, In: 21st Congress of the European Society of Biomechanics ESB 2015, Published by Czech Technical University in Prague, 5 – 8 July 2015, Prague, Czech Republic, p. 503.
11. SKŘONTOVÁ, M., ZEMAN, J., ŠIMKOVÁ, L., JELEN, K.: Influence of pregnancy on the shape and thickness of a hair. In: Experimental and Computational Methods in engineering EVM 2016, Published by Department of Machinery and Mechanics, Faculty of Production Technology and Management, University Jana Evangelisty Purkyně Ústí nad Labem, 2 – 3 June 2016, Ústí nad Labem, Czech Republic, (in Czech).
12. ŠIMKOVÁ, L., SKŘONTOVÁ, M., JELEN, K., CHALUPA, B.: Determination of different animal species hair viscoelastic. In: 5th International Conference Trends in Agricultural Engineering TAE 2013, Published by Czech University of Life Sciences Prague, 3 – 6 September 2013, Prague, Czech Republic, p. 590 – 594.

Corresponding author:
Marie Škrontová, Department of Anatomy and Biomechanics, Faculty of Physical Education and Sport, Charles University in Prague, José Martího 269/31, 162 52 - Praha 6 – Veleslavín, phone: +420-736605076, e-mail: skrontova.m@seznam.cz

ASSESSMENT OF LINSEED HARVEST EFFICIENCY

J. Souček

Research Institute of Agricultural Engineering, Prague, p. r. i. Czech republic

Abstract
The change in variety composition in favour of oil-varieties of flax brought about even a change in harvest practices in favour of combine harvesters. Post- harvest residues, mainly in the form of stalks, are usable material from the technical and energy point of view. The most often used form is pressing into the form of bales. In cases, when the material obtained in this way cannot be rationally used, the carried out operations will have a negative effect on overall costs expended to crop growing. The subject of realized research was to determine parameters of different types of flax stalk processing into the form of bales and compare them to the alternative of their crushing and incorporation into the soil. The experiments were carried out at the following varieties: Recital, Oural, Amon, Flanders and Baikal. Levelized costs for harvest fluctuated in a wide range 461 CZK/t up to 3,420 CZK/t.

Key words: flax, energy consumption, bioenergy, harvest costs, combine harvester, pressing.

INTRODUCTION

Flax is a traditional crop of the Czech rural areas. In the past the flax fibre varieties were dominated on the Czech fields. Flax was perceived primarily as a technical crop, but it had also significance as a part of food and in crop rotation as well. According to ČANDOVÁ ET AL. (2011) the sown areas of flax have been gradually decreased since 1992. Currently the main application area for the use of flax is food production. That is why there are grown in the Czech Republic at the present time only oil varieties of flax.

The change of varietal composition and method of final use brought about also the change in method of harvest. During the harvest of fiber varieties the emphasis was put on assurance of quality and usable length of stem. To the harvest there were used the flax pullers. In the conditions of the Central Europe there were by NEUBAUER ET AL. (1989) most frequently used the trailed types of flax pullers integrated with wheeled tractor.

With the growing of oil-varieties there has been gradually abandoned the harvesting method using the flax puller and the flax is harvested in more effective way by means of combine harvesters. Nowadays, the primary product is by CHAUHANET ET AL. (2009) and BJELKOVÁ ET AL. (2012) flax seed, which is usable in food industry and other fields. The flax stem can be used to the production of short fibre, but in the practice it is used as a rule in energy production or, where it is possible, incorporated into the soil. Other possibility is an industrial use, for example in paper production. For the mentioned kinds of use there are not an obstacle shorter length of harvested stem, which enables a reduction of mass flow through the threshing mechanism and elimination of risk of its blockage. At very short length of stem, and therefore low yield, itis however its processing less profitable.

The harvest of flax by means of combine harvester is according SOUČEK AND BLAŽEJ (2012) effective, but put increased demands on the state of crop stand .It is also necessary the quality and uniform desiccation by FROMET (1993) and PRAŽAN ET AL. (2015) and low water content at the time of harvest by NILSSON (2005).

The aim of described research is to determine the effect of different technology of stalks harvest and cultivated variety on harvests efficiency.

MATERIALS AND METHODS

During the research there were determined the yields of individual parts of five linseed varieties as well as energy and exploitation parameters of harvest operations. All the data were obtained by measuring in operational and pilot plant conditions. The studied varieties were: Recital, Oural, Amon, Flanders and Baikal. The yields of individual parts of plants have been determined within the pilot plant experiment in site of Lukavec. Parameters of harvest were laid down by measuring in pilot plant and operational conditions in sites Lukavec, Morkovice, Šumperk, Loštice, Bludov a Bohutín.

In order to evaluate and compare the crop stands were harvested by combine harvester (Wintersteiger) and residual stalks were harvested and processed in four variants:

- 1-by pressing into round bales (CASE JX 1100 U + KRONE VARIO PACK Multi-cut 1500)
- 2- by pressing into gigant square bales (Massey Ferguson 8460 + Hesston 4880)
- 3- by pressing into small square bales (ZETOR 5211 + CLAAS Markant 50)
- 4- stem was disintegrated during the harvest by crusher connected to combine harvester and subsequently incorporated into the soil by disc harrows (CASE 7230 + FARMET4,6 m).

Harvest losses ranged around 5%. During the harvest there wasn´t harvested a part of plants comprising the root and part of stem attributable to the stubble (about 15 cm).

The yield of individual parts of plants was determined by conversion from gravimetrically specified quantity of dry matter in average sample. This average sample was established for all varieties from the results of cultivation trials lasting for 5 years in order to reduce the risk of their influencing by weather.

The specific energy obtained were determined from yield and calorific value of individual parts of linseed selected varieties.

$$Q_{i\,ha}^{t} = n_{i\,part} . Q_{i\,part}^{t} \quad \text{(MJ)} \qquad (1)$$

where: n_{ipart} yield of analysed part (t/ha)

$Q_{i\,part}^{t}$ calorific value of analysed part (MJ/kg)

Exploitation parameters of operations were determined by means of time record and the GPS. The consumption of diesel fuel was determined by means of flow meter built into the energy device, possibly by method of full tank.

Into the values of consumption of diesel fuel and need of work there is included the transport distance, which was for all of variants 2,5 km.

Consumed energy W_e was determined as total consumed direct energy W_{sp} (consumed in form of diesel fuel) related to the yield.

$$W_{sp} = m_{pal} . Q_{i\,pal}^{t} \quad \text{(MJ)} \qquad (2)$$

where: m_{pal} weight of consumed fuel (kg)

$Q_{i\,pal}^{t}$ calorific value of consumed fuel (MJ/kg)

$$W_e = \frac{W_{sp}}{m_s} \quad \text{(MJ/t)} \qquad (3)$$

where: m_s weight of processed dry material (t)

Levelized costs for particular alternatives of harvest were determined on the basis of measured values by calculation in expert system Agrotekis, which is as expert system freely available on the website www.vuzt.eu. The calculation of levelized costs comes from total costs, which are determined as the sum of fixed and variable costs:

$$N_C = N_f + N_v \quad \text{(CZK)} \qquad (4)$$

where: N_f fixed costs (CZK)

N_v variable costs (CZK)

Levelized costs were determined by calculation as unit costs:

$$N_j = \frac{N_C}{n_j} \quad \text{(CZK/t)} \qquad (5)$$

where: n_j yield (t)

Obtained data were evaluated by ANOVA, using the PC software Statistica CZ v12.

RESULTSAND DISCUSSION

All the varieties were harvested by combine harvester Wintersteiger Seed Universal after previous desiccation of crop stand by the Roundup. The yields of individual parts of monitored varieties of harvested plants are illustrated on the Fig. 1.

For the harvest of flax stem there were selected the alternatives with pressing into the round bales, large square bales, small square bales and the alternative without harvest with crushing in the course of harvest and subsequent incorporation into the soil by disc harrows. Thus, there were available for comparison 4 alternatives of harvest.

On the Fig. 2 there are shown values of specific consumed energy and need of work related to1 hectare of crop stand.

At conversion of consumed direct energy in form of diesel fuel on yields of selected varieties of flax it is possible to express specific energy consumed to 1 tonne of weight. For better comparison the values were related to 1 tonne of harvested seed. The values converted into dry matter are shown graphically on the Fig. 3.

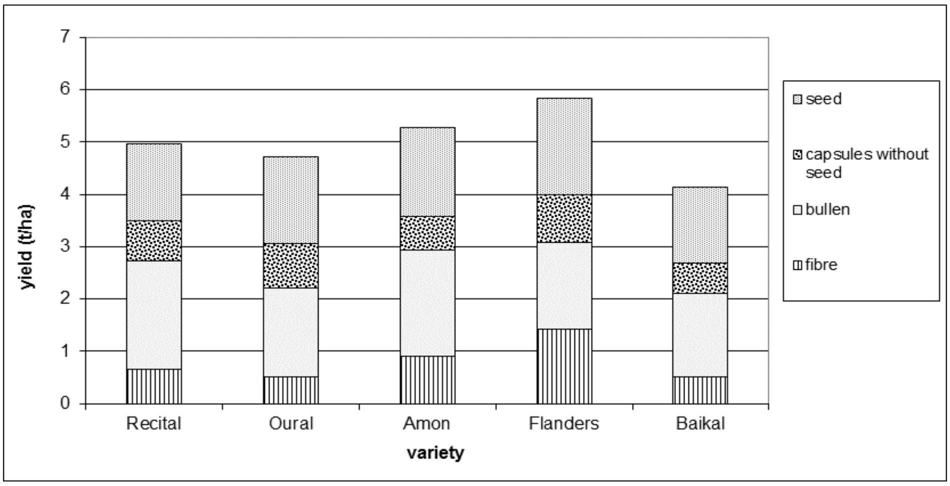

Fig. 1. – Yield of individual parts of linseed selected varieties during the harvest by combine harvester (site of Lukavec, given in dry matter)

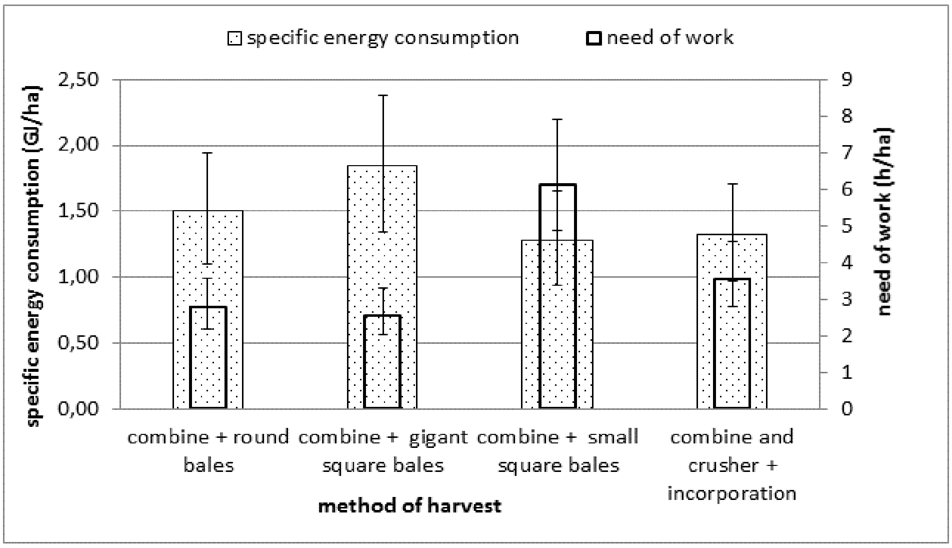

Fig. 2. – Specific consumed energy and need of work destined for harvest of selected alternatives of harvest

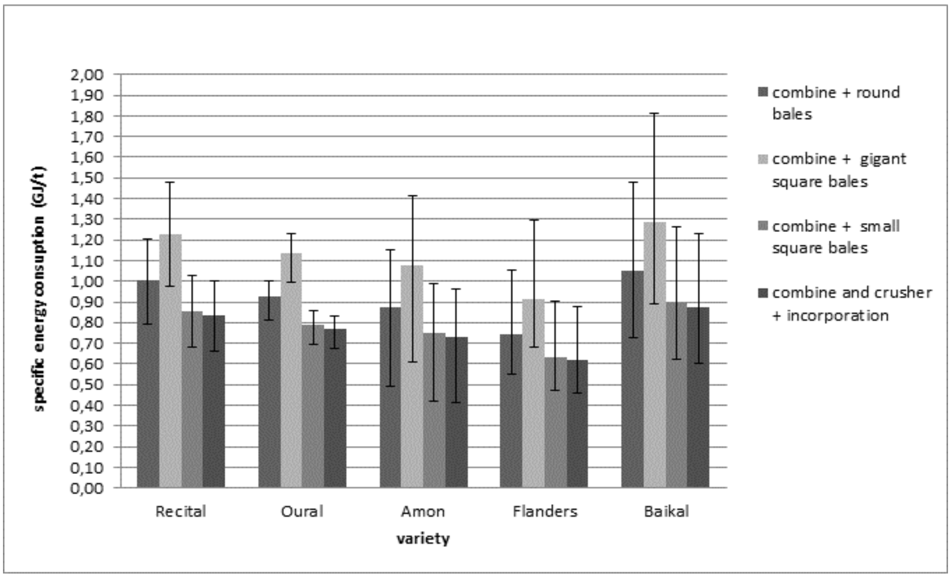

Fig. 3. – Specific consumed energy for evaluated harvest alternatives of linseed selected varieties related to 1 tonne of seed

In case of harvest of flax stem in form of bales there is a real possibility of its material or energy use. In order to quantify the energy contained in obtained mass of linseed there were gained the data by means of analytical analyses of with drawed samples and their yield. Average yields of individual parts of plants are graphically shown on the Fig. 1. The results of analyses of these parts of plants are shown in the Tab. 1.

Tab. 1. – Average results of analysis of individual parts of linseed

	combustion heat	calorific value	ash	carbon	nitrogen
	(MJ/kg)	(MJ/kg)	(%)	(%)	(%)
seed	26.76	18.07	3.99	48.01	2.86
capsules	18.92	12.28	3.95	48.03	0.82
bullen	18.24	11.77	1.96	49.02	0.77
fibre	16.73	10.65	4.60	47.70	0.79
roots	17.97	11.57	6.32	46.84	0.50

The calorific value, basic energy indicator, is the highest in the seed, however the seed isn´t used to the energy purposes. The calorific value is mainly influenced by analytic composition and by water content.
The amount of specific energy obtained by individual parts of plant sis shown on the Fig. 4.The values were obtained by conversion of calorific value into the yield per hectare of cultivated area. These values range from 44 up to 63 GJ/ha.
The specific energy obtained during the harvest with use of combine harvester ranged from 43 up to 63 GJ/ha.
In order to evaluate the technology it is important to know economic point of view. As the main indicator for particular alternatives of technological processes at selected varieties there were calculated levelized costs related to 1 tonne of produced dry matter of material. These levelized costs were calculated from real costs for operation of machinery, depreciations of machinery wage costs and material costs (fuel, lubricants, preparations for desiccation of crop stand etc.).
In case of utilization of harvested post-harvest residues it would be possible to reduce the costs for harvest of seeds to the values shown in the graph on Fig. 5 (alternative with harvest of flax stem). The costs are mentioned in comparison with alternative with crushing and subsequent incorporation of flax stems into the soil by disc plough -harrow.

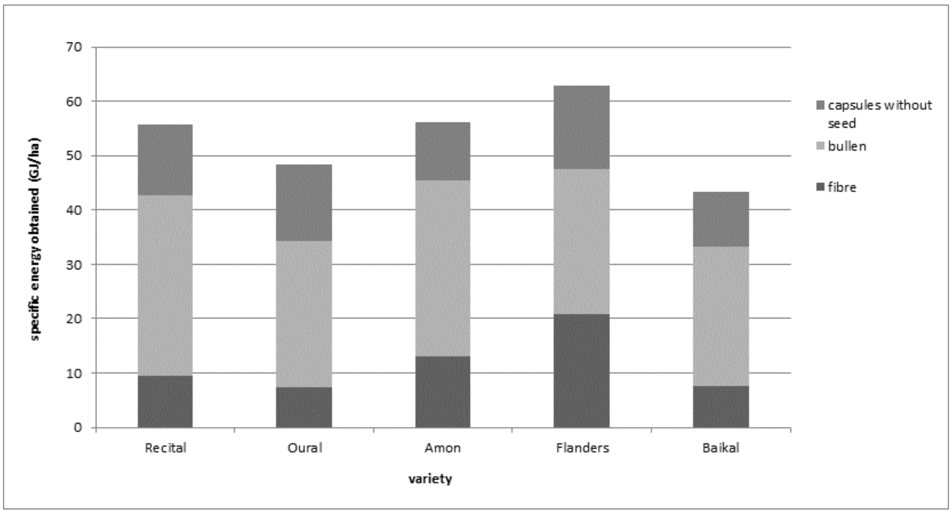

Fig. 4. – Calorific value and dry matter content of samples of linseed selected varieties–the whole plants

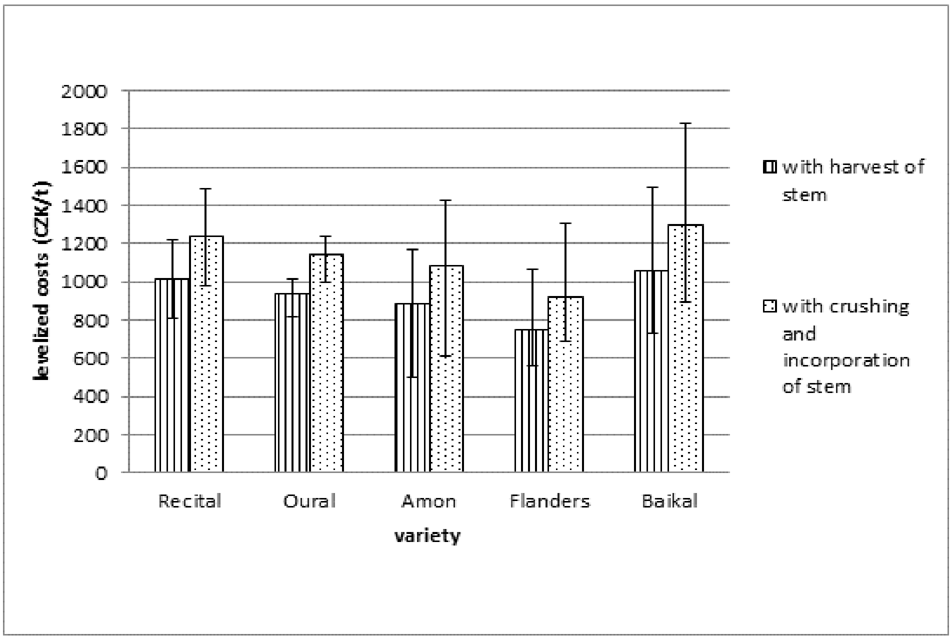

Fig. 5. – Levelized costs for harvest of seeds of linseed selected varieties after deduction of costs for harvest of flax stem (related to the weight of dry matter of harvested seed)

Levelized costs for harvest of flax stem reach the values shown in graph on the Fig. 6.
However, at the present time the flax stem is in practice the commodity, which is marketable only with difficulties, therefore the levelized costs are often expressed as the total costs for harvest related to the yield of seed. Values of levelized costs expressed by this way for all variants are shown in graph on the Fig. 7. In these data there are included all the costs originated in connection with harvest and transport to the storage site (it was taken into account the distance of 2,5 km).

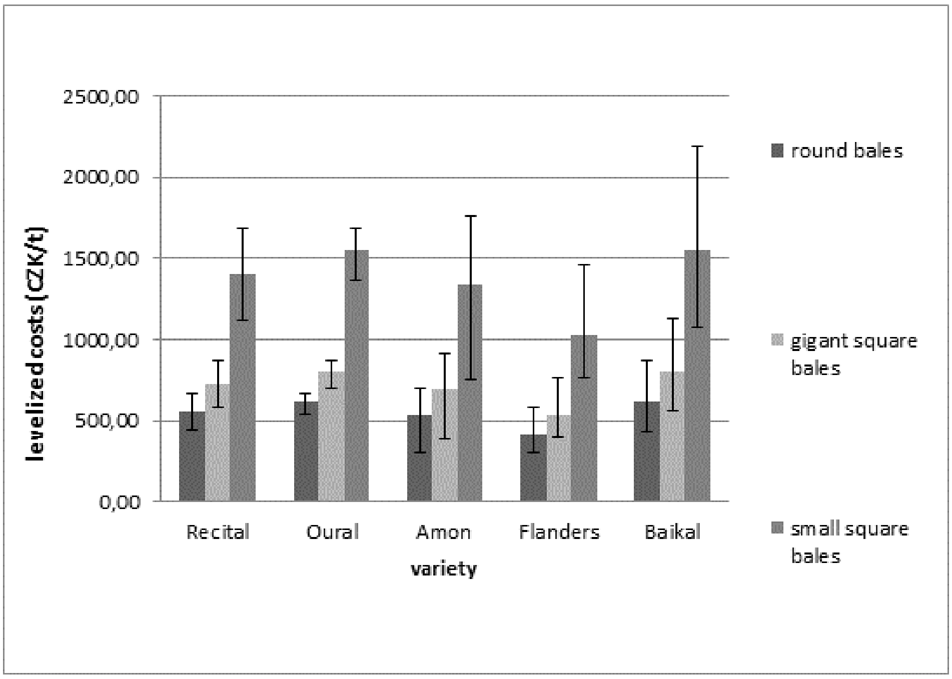

Fig. 6. – Levelized costs for harvest of flax stem of linseed selected varieties (related to the weight of dry matter of harvested flax stem)

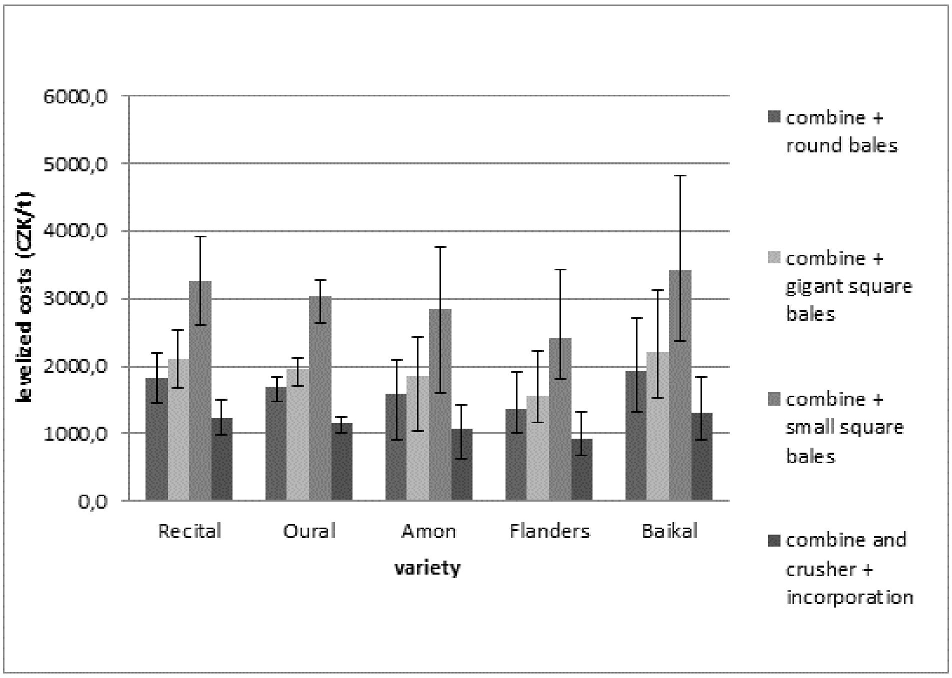

Fig. 7. – Levelized costs for seeds production of selected varieties of linseed (related to the weight of dry matter of seed, including harvesting of stem)

Within the pilot plant experiments there were evaluated five varieties of linseed. There were the following varieties: Recital, Oural, Amon, Flanders and Baikal. From the yield point of view it was achieved in trial site Lukavec the best results in case of the variety Flanders (2.02 t/ha seed, 3.47 t/ha stem), the worst result was reached at the variety Baikal (1.43 t/ha seed, 2.31 t/ha stem).

Specific consumed energy calculated from the consumption of diesel fuel range from 1.28 GJ/ha (pressing of small square bales) up to 1.84 GJ/ha (pressing of giant square bales).From energy consumption point of view the technology of flax stem pressing into the small square bale sis more efficient, than crushing and incorporation of this flax stem into the soil.

The calorific value of plant parts used for energy production at water content up to 20% ranged from 10.65 up to 12.28 MJ/kg, which are the values comparable to the work of ČANDOVÁ ET AL. (2009). Energy, which can be obtained in the form of post-harvest residues (stem + empty capsules) at monitored varieties in case of monitored varieties from 43 GJ/ha (Baikal variety) up to 63 GJ/ha (Flanders variety).

The share of delivered direct energy makes 2 - 4% of obtained energy.

From the obtained results it is obvious, that the amount of levelized costs for harvest of flax seed in case of placing of flax stem on market range for particular varieties from 751 CZK/t of dry matter (Flanders) up to 1.061 CZK/t of dry matter (Baikal). In case of crushing and incorporation of flax stem into the soil by disc plough-harrow the costs increased by 20-25% and range from 919 CZK/t of dry matter up to 1.298 CZK/t of dry matter.

Levelized costs for the harvest of flax stem are therefore in the wide range. Under the given yields of flax stem the lowest levelized costs were achieved in case of harvest using the round bales (410 CZK/t up to 619 CZK/t). At pressing into the large square bales the levelized costs were higher and ranged from 534 CZK/t up to 807 CZK/t. The highest costs from 1.031 CZK/t up to 1.557 CZK/t were determined in case of pressing into the small square bales. The comparison of results from the varietal point of view the lowest costs were determined at Flanders variety, on the contrary the highest costs in case of Oural variety. It was mainly caused by the yield of flax stem, which was the highest at Flanders variety and the lowest at Oural variety.

In practice the linseed growers are very often forced to harvest the flax stem from field also in case, that they haven´t any use for it. The reason can be for example a difficult way of its incorporation into the soil, unsuitability of its presence in soil for the subsequent crops or elimination of excessive occurrence of pests. In these cases it is necessary to express the levelized costs as the total costs for harvest of seed and stem expressed only for quantity of seed. Also in this case the lowest costs were determined at variant with pressing into round bales. These costs range from 1.353 up to 1.911 CZK/t. The costs are higher at pressing into giant square bales (1.566 up to 2.213 CZK/t) and the highest costs were determined at pressing into small square bales (2.422 up to 3.420 CZK/t). The lowest levelizedcosts were in this case again at Flanders variety a the highest ones at Baikal variety.

From the obtained results it is obvious, that efficiency of harvest can significantly influence the whole economy of linseed growing. Apart from the timeliness of harvest by NILSSON (2005) with previous quality desiccation by FROMET (1993), PRAŽAN ET AL. (2015) it is also important right choice of variety suitable for climatic conditions of certain locality and used harvest machinery.

CONCLUSIONS

The growing of linseed has its importance thanks to the production of dieteticly valuable and comprehensively usable flaxseed and stem, which can be utilized as the technical and energy feedstock. The linseed has also its importance for creation of crop rotation and soil protection. There is often mentioned its significance in relation to the area of organic farming and decontamination of infested soils.

Within the pilot plant experiments there were evaluated five varieties of linseed. From the yield point of view it was achieved in trial site Lukavec the best results in case of the variety Flanders, the worst result was reached at the variety Baikal. Levelized costs for the harvest of flax stem are in the wide range. In practice the linseed growers are very often forced to harvest the flax stem from field also in case, that they haven´t any use for it.

If it is suitable or necessary to harvest the flax stem, the most efficient method is pressing into the small round bales, eventually into giant square bales. Pressing into small square bales is from the energy point of view less demanding, but owing to very low performance, very costly.

In cases, when it isn´t probable a possibility of rational use of post-harvest residues and their incorporation into the soil don´t hinder subsequent cultivation operations it is suitable their disintegration by means of a crusher connected to combine harvester and subsequent incorporation into the soil. The advantage of this solution is possibility to connect operations of seed harvest and soil tillage.

ACKNOWLEDGEMENTS

This article can be worked out thanks to the project of long- term development of Research Institute of Agricultural Engineering p.r.i. no. RO0616 and project NAZV no. QI92A143.

REFERENCES

1. BJELKOVA, M., NOZKOVA, J., FATRCOVA-SRAMKOVA, K., TEJKLOVA, E.: Comparisons of lin seed (Linumusitatissimum L.) genotypes with respect to the content of polyunsaturated fatty acids, CHEMICAL PAPERS, 66(10), 2012: p. 972 – 976. ISSN: 0366-6352.
2. ČANDOVÁ, D., SOUČEK, J., VACEK, O.: Properties of flax from energy recovery point of view (CZ), Agritech Science, 3 (3), 2009: p. 1-5. ISSN 1802-8942.
3. FROMET, MA.: Effect of desiccants on seedyield and plant dry matter in linseed, Linum-Usitatissimum, Annals of applied Biology, 122, 1993: p. 100 – 101.
4. CHAUHAN, M. P., SINGH, S., SINGHA. K.: Post Harvest Uses of Linseed, J HumEcol, 28(3), 2009: p. 217-219.
5. NEUBAUER, K. ET AL.: Machines for crop production (CZ), SZN, Praha, 1989. ISBN 80-209-0075-6.
6. NILSSON, D. B.: Svennerstedt, and C. Wretfors, ‘Adsorption Equilibrium Moisture Contents of Flax Straw, Hemp Stalks and Reed Canary Grass’, Biosystems Engineering, 91 (2005), 35–43 <http://dx.doi.org/10.1016/j.biosystemseng.2005.02.010>
7. PRAŽAN, R., ČEDÍK, J., SOUČEK, J., GERNDTOVÁ, I.: Swing booms with large working widths (CZ), Agritech Science, 9 (2), 2015: p. 1-5. ISSN 1802-8942.
8. SOUČEK, J., BLAŽEJ, D.: Linseed harvests parameters depending on the state of cutting mechanism. Research in Agricultural Engineering 58 (2), 2012: p. 46-49. ISSN 1212-9151.

Corresponding author:

Ing. Jiří Souček, Ph.D., Research Institute of Agricultural Engineering, Prague, p. r. i, Czech Republic

THE EFFECT OF PARTICLES SIZES ON THE DENSITY AND POROSITY OF THE MATERIAL

A. Świetochowski, A. Lisowski, M. Dąbrowska-Salwin

Department of Agricultural and Forest Engineering, Faculty of Production Engineering, Warsaw University of Life Sciences, Poland

Abstract
The aim of the study was to determine the specific and bulk density and the porosity of the shredded material from Miscanthus according to its particle sizes distribution. The moisture content of the plants was 20%. For the purpose of evaluation of cut particle size distributions a sieve separator was used with a horizontal sieve oscillation and research methodology in accordance with the requirements of ANSI/ASAE S424.1, compatible with the European standard PN-EN 15149-1. It was found that the bulk and specific density and porosity of the shredded material from Miscanthus were depended on its particles size. In the tested range, the Miscanthus particles has a minimal porosity (approx. 90%) and a maximum bulk density (75 $kg \cdot m^{-3}$) at sizes 6 − 8mm. The highest specific density 910 $kg \cdot m^{-3}$ was obtained for the finest tested particles (approx. 0,8 mm).

Key words: biomass, cut, compression, density, porosity.

INTRODUCTION

Physical properties such as bulk, specific density and porosity are important to understand the quality of feedstock delivered to the biorefinery or for co-firing plants. LAM ET AL. (2008) indicated that bulk density is a major physical property in designing the logistic systems for biomass handling. They concluded that biomass material is dependent on size, shape, moisture content, individual particle density and surface characteristics. Physical properties such as bulk density also have an impact on storage requirements, sizing of the material handling systems and on the final conversion process (MCKENDRY, 2002). The study of RYU ET AL. (2006) on the effect of bulk density on combustion characteristics of biomass indicated that ignition front speed is inversely proportional to bulk density.

LANG ET AL. (1993), and SOKHANSANJ AND LANG (1996) indicated that bulk density of biomass is dependent on material composition, particle shape and size, specific density, and moisture content. The bulk density depends on the packing of the material, namely on the granulometric composition of the particles (KOWALSKA AND LENART, 2003). ANDREJKO (2005) noted that the particle size and its variation may effect on the increasing or decreasing the specific density, depending on the type of material.

One of the main purposes of the compaction process studies is the influence of the material characteristics on the quality of the agglomerated product. Because of that the knowledge of the material properties is necessary to ensure the minimum energy consumption during the agglomeration process (SOKHANSANJ ET AL., 2005). Compaction of the shredded materials of high bulk density increases efficiency and allows to obtain a higher density of the agglomerates what is involved with less displaced air and consequently requires less pressure compaction. Similar as in the case of agglomerates density, the increase in bulk density reduces the energy demand (OBIDZIŃSKI, 2005). The raw materials with a low bulk density cause their irregular feeding and disruptions in the pellets production. This leads to an increase in demand to supply the raw material to feeding the system of matrix and compacting rolls to maintain the required level of the production (LARSON ET AL., 2008).

The aim of the study was to determine the specific and bulk density and the porosity of the shredded material from Miscanthus according to its particle size distribution.

MATERIALS AND METHODS

Miscanthus plants were harvested by a trailed forage harvester Z374 from plots at the Experimental Station in Skierniewice, which belongs to the Warsaw University of Life Sciences. The chopping unit of the forage harvester was equipped with 5 knives. The cutting disc rotational speed amounted to 1000 rpm. The set working parameters allowed for a cutting frequency at 83 Hz and a theoretical length of chopped plant material particles of 8.8 mm (LISOWSKI AND ŚWIĘTOCHOWSKI, 2014).

For the purpose of evaluation of cut particle size distributions a sieve separator was used with a horizontal sieve oscillation and research methodology in accordance with the requirements of ANSI/ASAE S424.1 (ASABE STANDARDS, 2011A), compatible with the European standard PN-EN 15149-1 (PN-EN 15149-1, 2011).

Moisture content (wet basis) was determined in accordance with the ASAE S358.2 standard (ASABE STANDARDS, 2011B). During harvesting and separation the moisture content of the cut Miscanthus material amounted to 20.9 % and 20 %.

Methodology of the investigations included determination of bulk and specific density and porosity of the cut material. The bulk density of the cut plant material was determined by twice repeated weighing of empty container (of 10 dm^3 volume) and container with a sample, on electronic scales with accuracy of 0.1 g.

$$\rho_L = \frac{m - m_n}{V} \tag{1}$$

where: ρ_L – bulk density of shredded plant material, $kg \cdot m^{-3}$; m – mass of container with material, kg; m_n – mass of container, kg; V – volume of container, m^3.

Particle density of the milled material was measured using a gas stereopycnometer (Quantachrome Instruments, Boynton Beach, USA) by measuring the pressure difference when a known quantity of helium under pressure is allowed to flow from a previously known reference volume (V_A) into a sample cell (Vc) containing the cut material. The real volume of the sample (Vp) was calculated from Eq. (2). The particle density of the sample was its mass divided by Vp and was expressed in $kg \cdot m^{-3}$. Each measurement was repeated three times on the same sample.

$$V_P = V_C + \frac{V_A}{1 - \left(\frac{p_1}{p_2}\right)} \tag{2}$$

where: V_P – volume of investigated material, m^3; V_C – volume of measuring chamber, m^3; V_A – volume of datum chamber, m^3; p_1 – pressure in measuring chamber, MPa; p_2 – pressure in the datum chamber, MPa.

The plant material specific density was determined from the dependence:

$$\rho = \frac{m}{V_P} \tag{3}$$

Porosity of the investigated material was calculated on the basis of bulk and specific density:

$$\varepsilon_L = 100\left(1 - \frac{\rho_L}{\rho}\right) \tag{4}$$

where: ε_L – porosity of the material, %; ρ_L – bulk density, $kg \cdot m^{-3}$; ρ – specific density, $kg \cdot m^{-3}$.

Data analysis was carried out using Statistica v.12 computer program, with application of variance analysis procedure and Duncan test.

RESULTS AND DISCUSSION

Particle size distribution of the Miscanthus cut material was characterized by right-sided skewness (skewness coefficient was 1.6) and was relatively leptokurtic (steep), with a kurtosis coefficient of 0.9 (Fig. 1). Particle size geometric mean values of the cut Miscanthus material was 10.47 mm, whereas the dimensionless standard deviation of these averages amounted to 1.86.

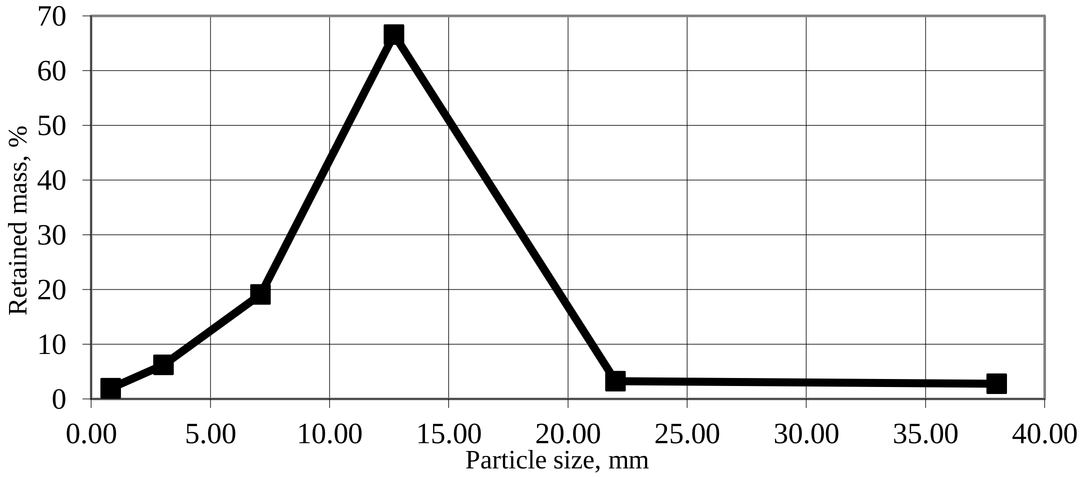

Fig. 1. – Particle size distribution of cut Miscanthus material

On the basis of the results of the analysis of variance (Tab. 1) it could be state, that the material fragmentation had statistically significant influence on values differentiation of its bulk density ($F_{v1=4,v2=45}$=712.1, at p<0.0001), specific density ($F_{v1=4,v2=45}$=488.7, at p<0.0001) and porosity ($F_{v1=4,v2=45}$=485.0, at p<0.0001).

Tab. 1. – The results of the analysis of variance of the particle size affecting on bulk density - ρ_L, specific density - ρ and porosity of the material - ε_L

Parameter	Source	Sum of squares	Degree of freedom	Mean square	Test F	p-value
Bulk density, ρ_L	Particle size	10153.1	4	2538.3	712.1	<0.0001
	Error	160.4	45	3.6		
Specific density, ρ	Particle size	495233	4	123808	488.7	<0.0001
	Error	11400	45	253		
Porosity of the material, ε_L	Particle size	169.7	4	42.4	485.0	<0.0001
	Error	3.9	45	0.1		

From the detailed analysis of the mean values by Duncan test (Tab. 2) results that for the bulk and specific density of the Miscanthus material were created five separate homogenous groups. The highest bulk density (76.78 kg·m^{-3}) had the material of the average value of particles length of 7.1 mm, means sizes close to these given by SAMSON ET L. (2005) as the best to the briquettes production. However, the lowest bulk density had the material of the highest (22 mm) and the lowest (0.82 mm) tested fragmentation amounted to 32.52 and 48.53 kg·m^{-3}, respectively. In the case of specific density of the cut material of Miscanthus, with increasing fragmentation of the material was followed its growth from 600 kg·m^{-3} for particles of the average length of 22 mm to over 900 kg·m^{-3} for particles of 0.82 mm. The specific density of the Miscanthus material in the form of mixture of all fractions, measured by LISOWSKI ET AL. (2011) was approximately 720 kg·m^{-3}.

Tab. 2. – The results of the analysis of Duncan test for the mean values of the bulk and specific density and the porosity

Bulk density							Specific density							Porosity of the material				
Geometric mean, mm	ρ_L, kg·m^{-3}	Homogenous group					Geometric mean, mm	ρ, kg·m^{-3}	Homogenous group					Geometric mean, mm	ε_L, %	Homogenous group		
22	32.52	x					22	600.2	x					7.1	89.58	x		
0.82	48.53		x				12.7	714.4		x				12.7	92.72		x	
12.7	51.96			x			7.1	736.8			x			3.04	92.74		x	
3.04	56.14				x		3.04	774.2				x		22	94.58			x
7.1	76.78					x	0.82	908.4					x	0.82	94.66			x

On the basis of the previous inference, the nonlinear regression models for bulk and specific density and porosity were developed (Tab. 3). All of the models are characterized by the high rate (R from 0.948 to 0.977). The graphic interpretation of these models were presented on the Fig. 2, 3 and 4.

Tab. 3. – Analysis of regression for bulk density, specific density and porosity of the material

Parameter	ρ_L				ρ				ε_L			
	estimate	error	t-value	p-value	estimate	error	t-value	p-value	estimate	error	t-value	p-value
b_0	35.98	2.00	17.93	<0.001	946.4	9.32	101.5	<0.001	96.62	0.247	390.9	<0.001
$b_1(x)$	12.43	1.02	12.15	<0.001	-64.6	4.75	-13.60	<0.001	-2.12	0.126	-16.84	<0.001
$b_2(x^2)$	-1.27	0.117	-10.80	<0.001	5.70	0.547	10.42	<0.001	0.208	0.014	14.40	<0.001
$b_3(x^3)$	0.031	0.003	9.16	<0.001	-0.158	0.016	-9.81	<0.001	-0.005	<0.001	-12.39	<0.001
Equation	$\rho_L = b_0 + b_1x + b_2x^2 + b_3x^3$				$\rho = b_0 + b_1x + b_2x^2 + b_3x^3$				$\varepsilon_L = b_0 + b_1x + b_2x^2 + b_3x^3$			
R	0.948				0.977				0,953			

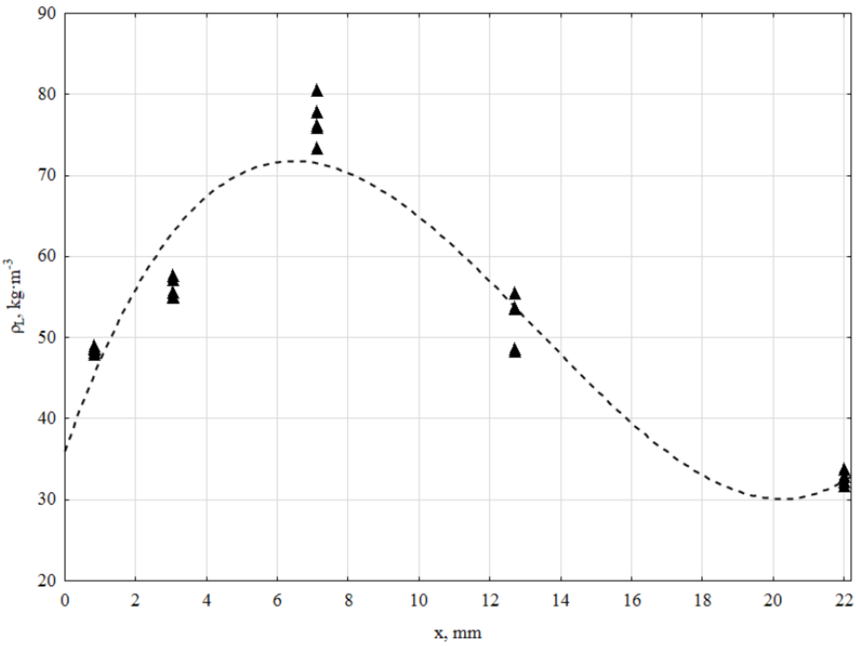

Fig. 2. – Effect of geometric mean of particle length on bulk density of shredded biomass

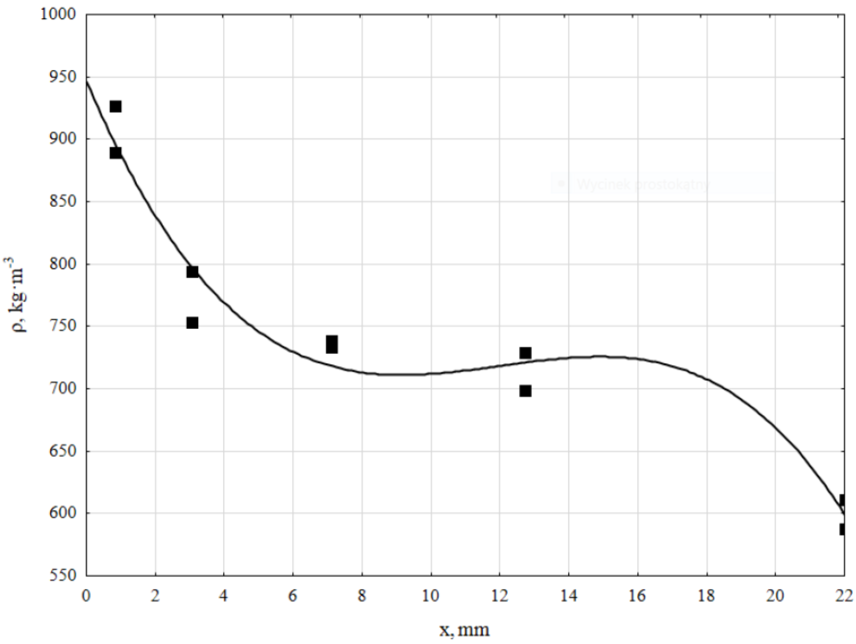

Fig. 3. – Effect of geometric mean of particle length on specific density of shredded biomass

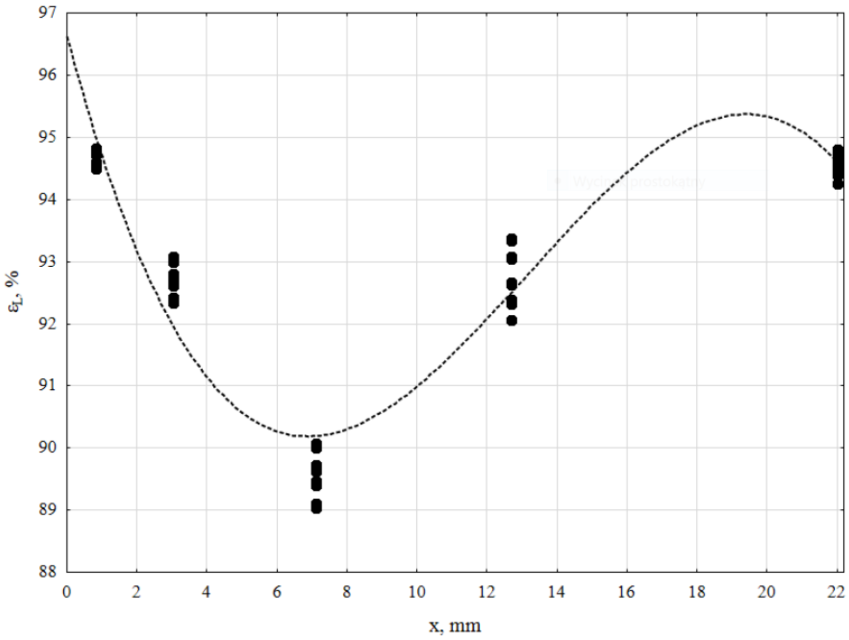

Fig. 4. – Effect of geometric mean of particle length on porosity of material of shredded biomass

The waveforms of dependence of bulk and specific density and porosity from the degree of fragmentation were differentiate. In the range of optimal material fragmentation needed to briquettes production (6-8 mm rating by SAMSON ET AL., 2005), the shredded Miscanthus material had the highest bulk density and the lowest porosity.

Recommended by MANI ET ALL (2003) mixture dedicated to production of pellets with particles dimensions not higher than 3.2 mm has the highest specific density of the material (780 – 900 kg·m^{-3}). The specific density values of this material were higher than the material for briquettes (700 – 950 kg·m^{-3}), which results that the formed fuel made of these plants in the form of pellets or briquettes should meets the requirements of density for this type of products. Presented results indicate on one of the reasons of higher density of pellets than of briquettes.

MIAO ET AL. (2011) reported that bulk density values of ground Miscanthus, switchgrass, and willow decreased with increase in the aperture size of the milling screens. The increase in tapped bulk density values of the biomass for all the sizes in the present study corroborated the observations of LAM ET AL. (2008).

CONCLUSIONS

1. The bulk and specific density and the porosity of the shredded material from Miscanthus were depended on its particle sizes.
2. In the tested range, the Miscanthus particles has a minimal porosity (approx. 90%) and a maximum bulk density (75 kg·m^{-3}) at sizes 6 – 8 mm.

The highest specific density 910 kg·m^{-3} was obtained for the finest tested particles (approx. 0,8 mm).

REFERENCES

1. ANDREJKO D.: The impact of moisture content and particle sizes on the density of loose plant raw materials. Agr. Eng., 11(71), 2005: 9–17 (In Polish).
2. ASABE STANDARDS: Method of determining and expressing particle size of chopped forage materials by screening ANSI/ASAE S424.1. 2011. In: ASABE Standards 2011a, ASABE, St. Joseph, MI, USA, 791–794.
3. ASABE STANDARDS: Moisture measurement – forages ASABE S358.2 (R2008). In: ASABE Standards 2011b, ASABE, St. Joseph, MI, USA, 781.
4. KOWALSKA, J., LENART, A.: The impact of the agglomeration on the general properties of multicomponent food in powder. Acta Sci. Pol. Tech. Ali., 2(2), 2003: 127–36 (In Polish).
5. LAM, P.S., SOKHANSANJ, S., BI, X., LIM, C.J., NAIMI, L.J., HOQUE, M.: Bulk density of wet and dry wheat straw and switchgrass particles. Appl Eng Agric., 24(3), 2008: 351–358.
6. LARSSON, S.H., THYREL, M., GELADI, P., LESTANDER, T.A.: High quality biofuel pellet production from pre-compacted low density raw materials. Bioresource Technol., 99(15), 2008: 7176–7182.

7. LANG, W., SOKHANSANJ, S., SOSULSKI, F.W.: Bulk volume shrinkage during drying of wheat and canola. J. Food Process. Eng.,16(4), 1993: 305–14.
8. LISOWSKI, A., ŚWIETOCHOWSKI, A.: Mechanical durability of pellets and briquettes made from a Miscanthus mixture without and with the separation of long particles. Bioenergy and other renewable energy technologies and systems 1, 2014: 93 – 100.
9. LISOWSKI, A., ŚWIĘTOCHOWSKI, A., LENART, A., SZULC, K.: Density and porosity of the cut and ground material of energy plants. Ann. Warsaw Agr. U. SGGW – AR, Agr., 58, 2011: 21–28.
10. MANI, S., TABIL, L.G., SOKHANSANJ, S.: An Overview of Compaction of Biomass Grinds. Powder Handling and Processing, 15(3), 2003: 160–168.
11. MIAO, Z., GRIFT, T.E., HANSEN, A.C., TING, K.C.: Energy requirement for comminution of biomass in relation to particle physical properties. Ind. Crop Prod., 33, 2011: 504–513.
12. MCKENDRY, P.: Energy production from biomass (part 1): overview of biomass. Bioresource Technol., 83(1), 2002: 37-46.
13. OBIDZIŃSKI, S.: The granulation of plant materials in the ring working system of the granulator. Doctoral dissertation. Białystok Technical University, Białystok, 2005. (In Polish).
14. PN-EN 15149-1:2011. Solid biofuels – Determination of grains size distribution – Part 1: Method of oscillatory sieving with sieves of 3.15 mm or higher aperture. (In Polish).
15. RYU, C., YANG, Y.B., BHOR, A., YATES, N.E., SHARIFI, V.N., SWITENBANK, J.: Effect of fuel properties on biomass combustion: part 1. Experiments-fuel type, equivalence ratio, and particle size. Fuel, 85(7-8), 2006: 1039–1046.
16. SAMSON, R., MANI, S., BODDEY, R., SOKHANSANJ, S., QUESADA, D., URQUIAGA, S., REIS, V., LEM, C.H., CARPIO, C.: The potential of C4 perennial grasses for developing a global bio-heat industry. Critical Reviews in Plant Sciences, 24(5–6), 2005: 461–495.
17. SOKHANSANJ, S., LANG, W.: Prediction of kernel and bulk volume of wheat and canola during adsorption and desorption. J. Agr. Eng. Res., 63(2), 1996: 129–136.
18. SOKHANSANJ, S., MANI, S., BI, X., ZAINI, P., TABIL, L.: Binderless pelletization of biomass. ASAE Paper No. 056061. ASAE, 2950 Niles Road, St. Joseph, MI 49085-9659 USA. 2005.

Corresponding author:
Adam Swietochowski, Department of Agricultural and Forest Engineering, Faculty of Production Engineering, Warsaw University of Life Sciences, Nowoursynowska Street 166, 02-787 Warsaw, Poland

MICRO-TOMOGRAPHY ANALYSIS OF THE FAILURES IN GLASS FIBER REINFORCED PLASTIC

M. Syrovátková, M. Kolínová, M. Petrů

Institut of Nanomaterials, Advanced Technologies and Innovation, Technical University of Liberec, Czech Republic

Abstract

Computer micro tomography is one of the methods that are used for displaying the structural arrangement of small parts or internal structure of materials (composites). Micro tomograph uses different continuous absorption and dispersion component to detect the internal structure the composites. Computer programs to create the images in 2D and 3D projection also allow mathematical analysis of the individual components. The subject of the article is the analysis the internal structure of the composite reinforced with glass fibers and thermoplastic matrix using software micro CT tomograph.

Key words: glass fiber, failure, micro tomograph, composite, porosity.

INTRODUCTION

Requirements for basic mechanical properties of engineering materials are reduce weight, good stiffness, strength and toughness. Most of the industrial materials are treated as homogeneous and isotropic; they are the basis for the most common technical applications. The composite is a multiphase material consisting of the continuous phase and dispersion. Continuous phase - the matrix may be metallic, ceramic, plastic or special. Dispersion - reinforcement may be fiber or particle. Fiber dispersion is continuous or in different lengths (GAY, SUONG, 2007; SUTCLIFE ET AL., 2012). The fibers are mainly used glass, carbon, basalt lesser extent. Recently, experiments with fibers based on natural (vegetable and animal origin) (GAY, SUONG, 2007). Type of reinforcement definite the arrangement of the fibers in the composite. Unidirectional oriented reinforcing fibers are continuous, infinite and oriented in one direction; ideally tense (AGARWAL ET AL., 2006, REQUENA ET AL., 2009). Properties of lamina in the direction of orientation the fibers are the best. The weave fabric is composed of two layers which are oriented towards the perpendicular direction, the fibers are interlaced. Lamina properties are in the directions of fiber orientation similar. Multiaxial knitted fabric with the desired number of oriented layers has the advantage that the fiber layers are not interconnected, and the fibers in the individual layers are oriented in one direction only. Matrix selected in accordance with the sizing of fibers and composites manufacturing technology have affected the occurrence failures in the internal structure. Mechanical stress leads to crack initiation and irreversible damage to composite structures (GAY, SUONG, 2007). This article describing of measurement with computer micro tomography (CT) as one of the methods that are used for displaying the structural arrangement of small parts or internal structure of materials (composites). Non-Destructive Testing (NDT) is a set of procedures and methods based on physical phenomena, through which it is possible to identify, locate and quantify the defect in the product without damage or destruction. In practice, it uses six basic NDT methods; These include visual inspection (VT), capillary penetration method (PT), the ultrasonic method (UT), radiographic methods (RT), magnetic powder method (MT), the method of eddy current (ET) and the method of acoustic emission (AT) (KARBHARI, 2013). Each method has different physical nature, requires a different approach, hardware and software. Radiographic method uses ionizing radiation to display an object, its internal structure, the separation of its constituents on principle the different radiation absorption and display internal failures. Current radiographic methods processing the image using computer technology; it enables much larger possibilities in image processing and evaluation of the data obtained (HARARA, 2008). The subject of the article is the analysis the internal structure of the composite reinforced with glass fibers and thermoplastic matrix using software micro CT tomograph. We use tomograph for the porosity calculation, quantify failures and for calculation of their distribution.

MATERIALS AND METHODS

Computed tomography (CT) is an advanced method. The device is able to non-destructively analysis and visualization the structure, high-quality 3D visualization and analysis of internal structures (BAKALOVÁ ET AL., 2014, PETRŮ ET AL., 2015).

Computer tomograph Sky Scan1272 (Fig.1) uses different X-ray absorption of individual components of the material. For analysis was chosen purposely defective sample of composite material reinforced with fiberglass. The sample is composed of three layers of unidirectional fibers; layers are not interconnected. The matrix is a thermoplastic resin. Air bubbles were predicted between the individual layers. The aim of the experiment was to identify failures by using computer software; to determine the amount and distribution the failures by 3D analysis, realized 2D analysis and create 3D model (SALABERGER ET AL., 2011). Parameters (conditions) of scanning glass fiber reinforced composite are shown in Tab. 1.

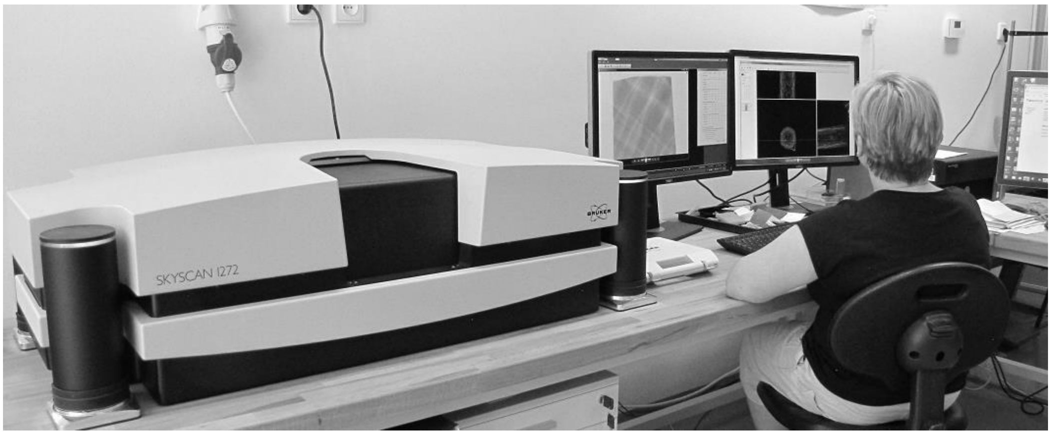

Fig. 1. – High-Resolution X-Ray Microtomograph Skyscan 1272 ; Institute for Nanomaterials, Advanced Technologies and Innovation, TU in Liberec

Tab. 1. – Scan parameters

Sample	GF
Source voltage (kV)	80
Number of rows and columns (pixel)	1640 x 2450
Scaled image pixel size (µm)	5
Exposure (ms)	1085
Rotation step (°)	0.2
Averaging	3
Filter	no filter

Reconstruction of dataset followed after scanning. Special software for the micro CT continues operates of dataset. The program DataViewer displays reconstructed results as a slice-by-slice movie or as three orthogonal sections (Fig. 2). 3D visualization of the sample in program CTVox showed the same material in 3D image (Fig.3a), the failures found in the sample are marked in red Fig.3b). CTAn allows accurate and detailed study of micro-CT results for morphometry and densitometry. The special software counts of porosity: identification of air pores, the calculation of the total volume of pores, their size and distribution, calculation of the volume fraction of open and closed pores. The calculation result is given in percentage of volume of the selected part of the sample. Monitored fiber-reinforced composite is defective. It contains a large amount of air bubbles. For their identification, calculation of volume fraction and distribution of defects was used calculation of porosity by using the software CTAn. Analysis of the sample was performed three times under the same conditions and only the number of slices differed, i.e. the volume of the select part of sample. The result was evaluated by a comparative method. It was performed 2D analysis. The result of this method is the porosity of the each slice of GFRP. CTVol uses surface trangulated models from CTAn and provides a virtual 3D viewing environment, flexible and rich features, to give you a wide range of options for 3D presentation of micro-CT results.

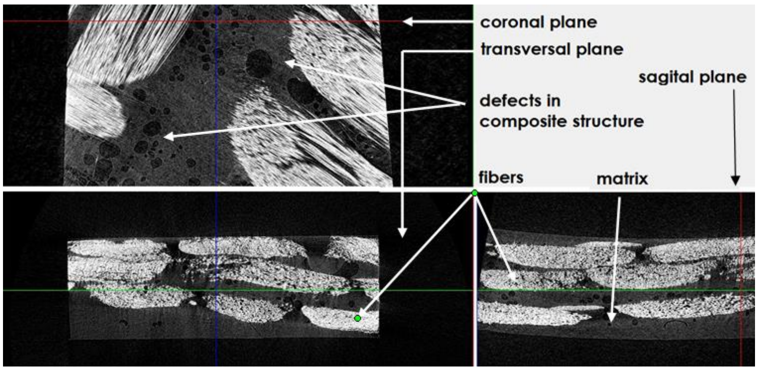

Fig. 2. – Software DataViewer – reconstructed results of composite sample in three orthogonal sections

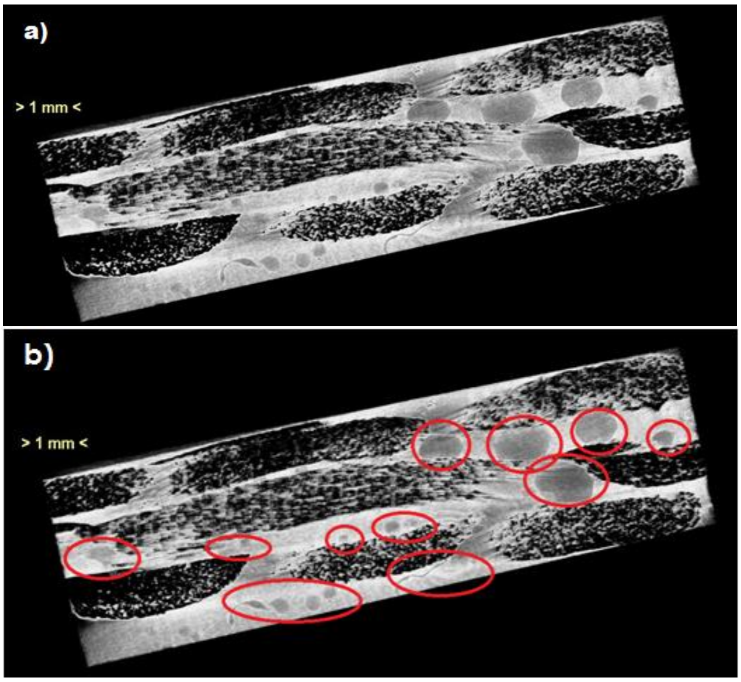

Fig. 3. – Software CTVox – 3Dvisualization of composite sample; a) internal structure of sample; b) failures in the internal structure of sample

RESULTS AND DISCUSSION

To determine the porosity of the fiber-reinforced composite using the CT is not necessary to know their characteristics. The value of porosity is not dependent on the shape and distribution of the pores (as with other methods). For application of CT for determining porosity is the most accurate and reproducible detection of interface between air and other materials - reinforcement and matrix (KASTNER ET AL., 2010). Micro tomography is used as a nondestructive method for determining the distribution of dispersed particles of the composite material (KASTNER ET AL., 2012), and search for defects (Scott A. E., et al). Ct analysis can be used also for the characterization of damage mechanisms in fiber composites (SALABERGER ET AL., 2012). For the experiment was selected composite in which has been supposed very numerous occurrences of defects of different sizes. The selected parameters of the three measurements are summarized in Tab. 2. Average of volume defects (air bubbles) is 29.45 % in the researched sample volume. The result was compared with the porosity (the occurrence frequency of defects) composite with the same properties and composition without the expected defects. Average of porosity was measured and calculated 10.21%, the difference is about 20% (Fig.4). It means approximately a third of the volume of the selected sample. The total porosity values are completed by a percentage of open and closed porosity values. The graph on Fig.5 shows the distribution of the pores (in this case defects - air bubbles) and comparison of results of individual intervals. The 2D analysis of porosity was performed on 900 slices. The interval of porosity was for all slices from 24.8 to 38.8%. The arithmetic average of 2D porosity is 27.7%. The result is graphically interpreted on the Fig.6.Virtual 3D viewing of the sample (Fig.7) and results of the calculation of the 3D porosity were used for visualization of pores (defects) in the program CTVol.

Setting the correct thresholding between the air and the other components of the composite has not been verified by another method.

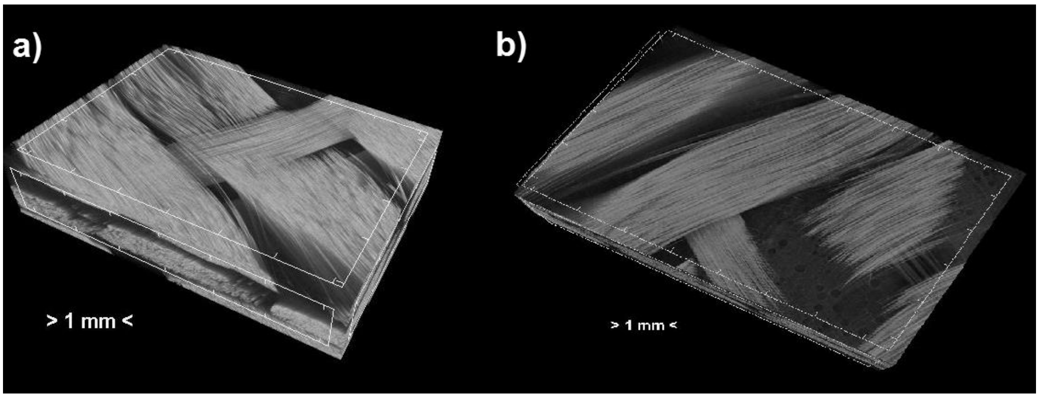

Fig. 4. – Comparison of samples: a) 10% of failures, b) 30% of failures

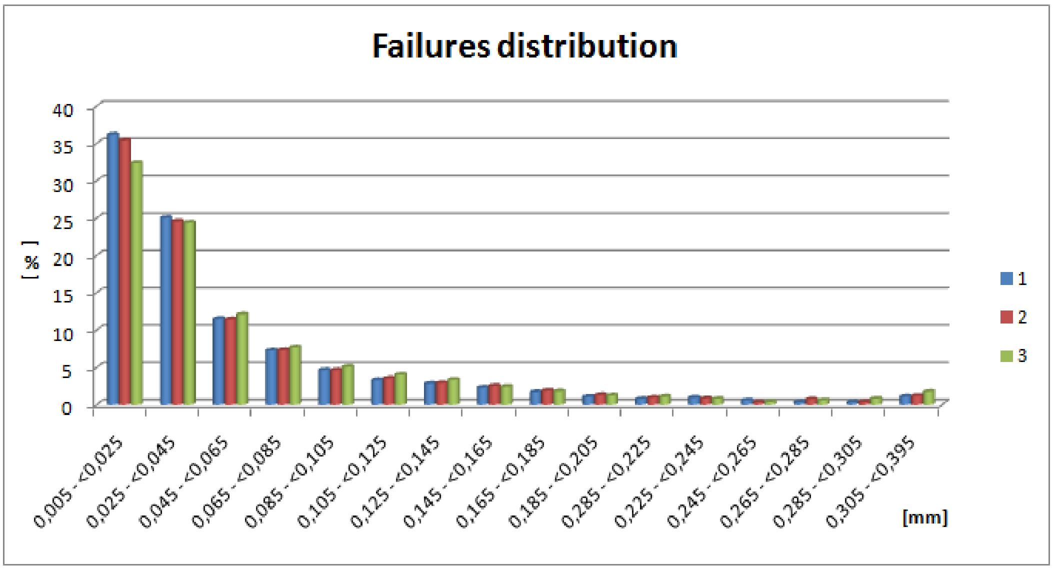

Fig. 5. – Graph of structure separation (failures distribution)

Tab. 2. – 3D analysis of structure GFRP

	Number of layers	Object volume	Open porosity [%]	Closed porosity [%]	Total porosity [%]	Degree of anisotrophy
1	701	54.86463	27.60	1.45	28.65	0.363
2	601	51.35300	27.52	1.43	28.56	0.368
3	651	56.18543	30.28	1.23	31.13	0.362
Average			28.47	1.37	29.45	0.364

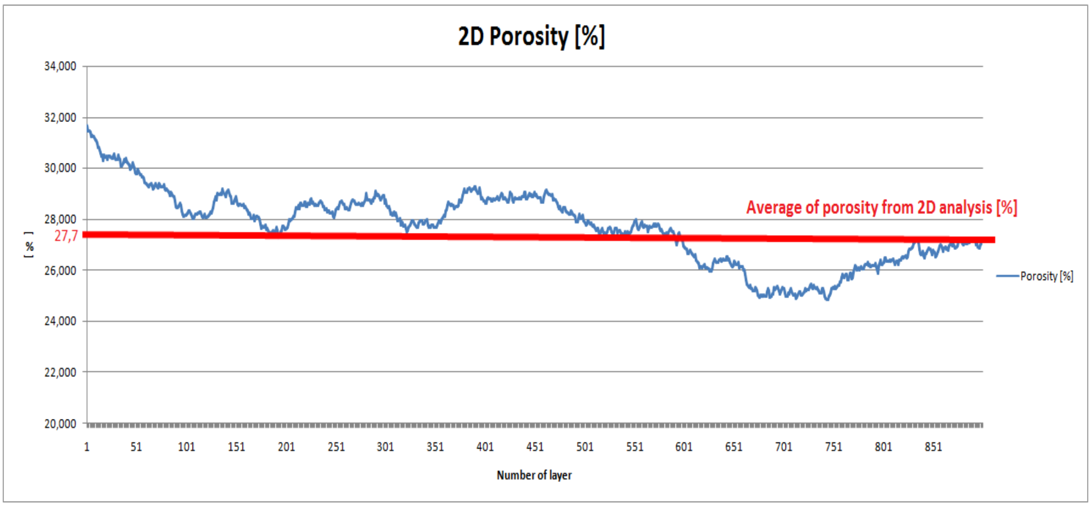

Fig. 6. – 2D porosity single slices

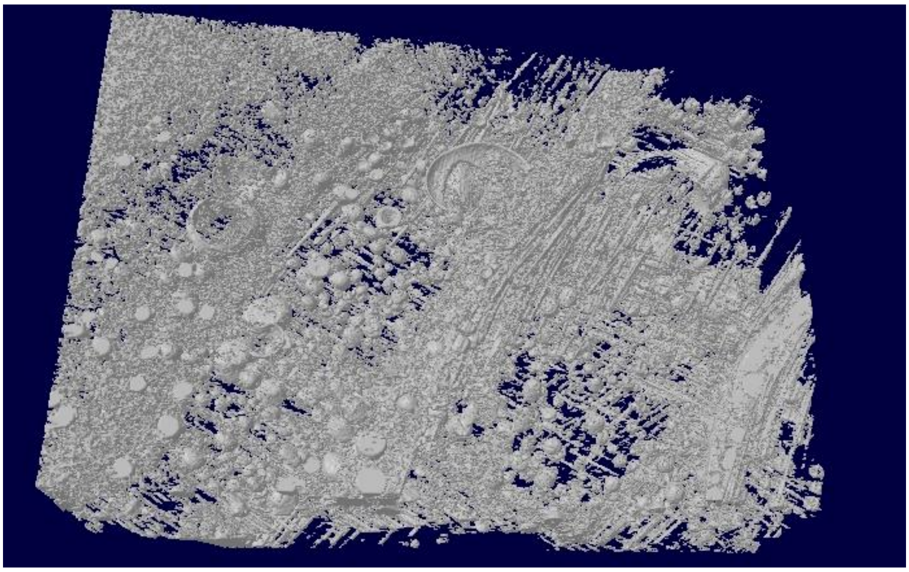

Fig. 7. – Virtual 3D viewing of the pores (failures) in CTVol program

CONCLUSIONS

Computer micro tomography is one of non-destructive methods of examining the internal structure of multi component materials. By using the programs that are part of the equipment micro tomograph is possible to visualize, simulate and implement calculations corre-sponded the properties of individual components. Calculating porosity was used for identifying and quantifying defects in glass fiber reinforced compo-site. The resulting porosity, respectively, the volume fraction of defects has a value of 29, 45%. It was visu-alized virtual 3D viewing of the pores (Fig.5). Setting the correct resolution of interface between the pores (defects - air bubbles) and matrix has proven very important. The visualization showed air bubbles (round objects on Fig.5) and minor micro cracks in the close proximity to the fibers. These micro defects copy fibers tightly and create the impression that the fibers are displayed in the model. The biggest defects are not displayed in the all volume. The degree of anisotrophy approaches 0, the structure is isotropic means properties of this material are the same in all directions.

ACKNOWLEDGEMENTS

The results of this project No. LO1201 were obtained through the financial support of the Ministry of Education, Youth and Sports in the framework of the targeted support of the “National Programme for Sustainability I”.

REFERENCES

1. AGARWAL, B. D., BROUTMAN, L. J., CHANDRASHEKHARA,: Analysis and Performance of Fiber Composites, 3rd Edition, 2006, pp. 576. ISBN: 978-0-471-26891-8.
2. BAKALOVA, T., KOLÍNOVÁ, M., LOUDA, P.: Micro CT Analysis of Geopolymer Composites. Manufacturing technology, 1st edition, Ústí nad Labem: Faculty of Production Technology and Management, 14 (4), 2014, pp. 505 – 510.
3. GAY, D., SUONG V. HOA: Composite materials (second edition). CRC Press Taylor & Francis Group, 2007, ISBN 978-1-4200-4519-2
4. HARARA, W.: Digital radiography for industry. 17th World Conference on Nondestructive Testing, 25-28 Oct 2008, Shanghai, China
5. KARBHARI, W. M.: Non-Destructive Evaluation (NDE) of Polymer Matrix Composites. Woodhead Publishing Limited, 2013, ISBN978-0-85709-344-8
6. KASTNER, J., PLANK, B., SALABERGER, D., SEKELJA, J.: Defect and Porosity Determination of Fibre Reinforced Polymers by X-ray Computed Tomography. 2nd International Symposium on NDT in Aerospace, 2010, Hamburg.
7. KASTNER, J., PLANK, B., SALABERGER, D.: High resolution X-ray computed tomography of fibre- and particle-filled polymers. 18th World Conference on Nondestructive Testing, 16-20 April 2012, Durban, South Africa
8. PETRŮ, M. – SYROVÁTKOVÁ, M. – KOLÍNOVÁ, M., NOVÁK, O.: X-ray microtomograph detection of internal defects for a UD prepreg composite. Materials Science Forum vol. 818, 2015, pp. 295-298
9. REQUENA, G. ET AL.: 3D-Quantification of the distribution of continuous fibers in unidirectionally reinforced composites. Composites Part A: Applied Science and Manufacturing, 40 (2), 2009, pp. 152-163.
10. SALABERGER, D., KANNAPPAN, K. A., KASTNER, J., REUSSNER, J., AUINGER, T.: Evaluation of computed tomography data from fibre reinforced polymers to determine fibre length distribution. International Polymer Processing, 2011, 26 (3), p. 283-291.
11. SALABERGER, D., ARIKAN, M., PAIER,T., KASTNER, J.: Characterization of damage mechanisms in glass fibre reinforced polymers using X-ray computed tomography. 11th European Conference on Non-Destructive Testing (ECNDT 2014), October 6-10, 2014, Prague, Czech Republic.
12. SCOTT, A. E., CLINCH, M., HEPPLES, W., KALANTZIS, N., SINCLAIR, I., SPEARING, S. M.: Advanced Micro-Mechanical Analysis of Highly Loaded Hybrid Composite Structures. Available on: http://www.iccm-central.org.
13. SUTCLIFFE, M. P. F., LEMANSKI, S. L., SCOTT A. E.: Measurement of fibre waviness in industrial composite components. *Composites Science and Technology*, 72.16, 2012, pp. 2016-2023.

Corresponding author:

Martina Syrovátková, Institut of Nanomaterials, Advanced Technologies and Innovation, Technical University of Liberec, Studentská 2, 461 17 Liberec 1, Czech Republic

RESULTS OF FOURTEEN-YEAR MONITORING OF TECHNOLOGICAL AND ECONOMIC PARAMETERS OF OILSEED RAPE PRODUCTION IN SELECTED FARM BUSINESSES

O. Šařec, P. Šařec

Department of Machinery Utilization, Faculty of Engineering, Czech University of Life Sciences Prague, Czech Republic

Abstract

Since the year 2001, field trials focused on technological and economic comparison of conventional and reduced-tillage technologies of soil cultivation and drilling of oilseed rape have been carried out in around 40 farm businesses located in all of the districts of the Czech Republic. Average seed yields didn't prove any significant difference between traditional technologies comprising ploughing and reduced tillage technologies. The same can be said about the difference with respect to the sowed varieties (hybrid and traditional), to the application of organic fertilisers, and to the fertilisation during sowing. The results were influenced by an uneven location of trial fields into the individual production areas. With respect to seed yields and costs per production unit, the production area most suitable for winter rape production proved still to be the potatoes one, in opposite to the corn production area as the worst one. Over the fourteen-year time, the average unit production costs attained by reduced-tillage technology were by 232 CZK.ha^{-1}, i.e. by 4.1 %, lower compared to those gained by conventional technology. The highest differences in favor of reduced-tillage technology were demonstrated on heavier soils.

Key words: winter oilseed rape, conventional technology, reduced tillage, costs, fuel consumption.

INTRODUCTION

Conservation tillage is primarily used as a means to protect soils from erosion and compaction, to conserve soil moisture and to reduce production costs (HOLLAND, 2004). Soil erosion is, also in Europe, a major environmental problem. Recent estimates put the total soil loss from agricultural land in Europe between 3 and 40 t.ha^{-1}.yr^{-1} (VERHEIJEN ET AL., 2009). In the intensive agricultural systems generally used in Europe, the effects of erosion on crop yields mainly occur due to the reduction of the amount of water the soil can store and make available to plants. If soil depth is sufficient, yield losses may be very small as the nutrient losses due to erosion can be compensated for by the increased application of fertilizers (BAKKER ET AL., 2004, 2007). However, the implementation of conservation agriculture and conservation tillage is clearly lagging in Europe in comparison to other continents (HOLLAND, 2004; LAHMAR, 2010; WAUTERS ET AL., 2010).

Over the last three decades, there has been considerable research on the effects of conservation tillage on crop yield in many areas in Europe. Often, detailed reports were published both on the economic and environmental effects of conservation agriculture (e.g. LOPEZ AND ARRUE, 1997; TEBRÜGGE AND BÖHRNSEN, 1997). However, the evidence from different studies often seems contradictory and is therefore difficult to interpret (e.g. CANTERO-MARTINEZ ET AL., 2003; LOPEZ AND ARRUE, 1997). This is to be expected: both the agro-environmental conditions as well as the type of conservation tillage applied vary greatly between individual studies. The recent study of MADARÁSZ ET.AL (2016) however suggested that over the ten trial years, tillage type was a more important factor in the question of yields than the highly variable climate of the studied years. During the first three years of technological changeover to conservation tillage, a decrease of 8.7% was measured, respective to ploughing tillage. However, the next seven years brought a 12.7% increase of conservation-tillage yields of all the crops grown.

According to the analysis of 563 observations carried out by VAN DEN PUTTE ET AL. (2010), no significant yield effect of soil tillage practices was observed for fodder maize, potatoes, sugar beet and spring cereals. Only for grain maize and winter cereals a significant yield reduction occurred under conservation agriculture.

When choosing tillage technology, it is necessary to respect agricultural and ecological conditions. At large, the most suitable conditions for tillage depth and intensity reduction are on medium-textured soils with higher natural fertility in drier conditions of maize and beet production regions (PROCHÁZKOVÁ AND DOVRTĚL, 2000; HORÁK ET AL., 2007).

Reduced-tillage technology of soil cultivation and stand establishment are often applied to heavy-textured soils, where soil environment frequently impede quality stand establishment using conventional soil cultivation technology including ploughing. In such case, reduced-tillage technology is practically the only way of stand establishment. Replacing ploughing with a shallow soil loosening followed by sowing using no-till drills is a suitable alternative (HŮLA AND PROCHÁZKOVÁ, ET AL., 2008). BEDNÁŘ ET AL. (2013) suggests a decrease in sowings and the number of plants per m^2 (35 and fewer), and an increase in between-the rows spacing (to 37.5 cm) which has a positive influence on the decrease of competition among individual oilseed rape plants.

A comparison of the different components of the total costs revealed that reduced-tillage required larger machinery and herbicide costs, but these costs were largely offset by reduced operating costs (SANCHEZ-GIRON ET AL., 2004, 2007). In various other studies, it was concluded that slightly lower crop yields can be offset by the reduced fuel inputs and labour consumption (BONCIARELLI AND ARCHETTI, 2000; GEMTOS ET AL., 1998; TEBRÜGGE, 2000). However, this may be dependent on local situation and farm-specific properties such as farm size (SANCHEZ-GIRON ET AL., 2007), cropping system, etc.

MATERIALS AND METHODS

Around 40 agricultural businesses growing winter oilseed rape in various production areas were chosen in the Czech Republic where different production technologies were monitored. At least one field was monitored in every business. Especially the following values were monitored:

• The nature of individual fields (area, type of soil cultivation, previous crop, the usage of crop residues, last application of organic fertilizers);

• The nature of soil (in particular bulk density - evaluated with the so called Kopecky sampling rollers for soil moisture constant determination, humidity, the degree of compactness – penetration resistance measurement by a penometer);

• The nature of crop (yield, the number of plants per m^2, the weight of roots, hybrid / line variety);

• The data on conducted work operations (machinery, fuel and labour consumption, costs and other supplementary information).

After the completion of terrain experiments there was evaluation of the obtained data and information, economic evaluation of the efficacy of money spent (with every business the amount of expenses spent was evaluated compared to the achieved seed yield and the technology used for cropstand establishment), setting conclusions with a subsequent proposal for a suitable technology for effective growing of winter oilseed rape.

RESULTS AND DISCUSSION

During six production years starting in 2001/02, trials were set up in 507 fields located in all of the districts of the Czech Republic. Reduced-tillage technology of oilseed rape growing was employed in 282 cases, conventional in 225 cases only, partly because during the monitored period, some of the farm businesses changed their technology from conventional to reduced-tillage.

The most frequent tillage procedures within the reduced-tillage technology consisted of two soil cultivations, followed in some cases by a seedbed preparation. Within the conventional technology, the most frequent tillage procedures consisted of stubble cultivation followed by ploughing, and seedbed preparation done once or twice.

Disc cultivators prevailed within conventional technologies, whereas within the reduced-tillage technologies, where two stubble cultivations were common, tine cultivators were more frequent, particularly for the second cultivation.

Prior to oilseed rape sowing, manure was applied mainly in forage and potatoes production areas (30 %, resp. 36 %, of the cases) compared to lower frequencies of cereal, beet and maize production areas (only 16 %, 10 %, resp. 6 % of the cases).

Tab. 1. – Average oilseed rape yields and frequencies of cases according to the tillage technology other criteria over the whole monitored period of fourteen years

	Tillage Technology				Aggregate	
	Reduced		Conventional			
	Yield ($t.ha^{-1}$)	Frequency	Yield ($t.ha^{-1}$)	Frequency	Yield ($t.ha^{-1}$)	Frequency
Production Area						
Forage	3.45	32	3.62	12	**3.49**	**44**
Potato	4.18	12	3.81	65	**3.87**	**77**
Cereal	3.56	90	3.50	46	**3.54**	**136**
Beet	3.90	132	3.73	102	**3.83**	**234**
Maize	3.33	16	—	—	**3.33**	**16**
Variety						
Conventional	3.64	116	3.61	84	**3.63**	**200**
Hybrid	3.80	164	3.77	133	**3.78**	**297**
Mixed	2.33	2	3.58	8	**3.33**	**10**
Organic Fertilisers						
No	3.69	209	3.69	125	**3.69**	**334**
Yes	3.82	73	3.71	100	**3.76**	**173**
Fertilizers at Sowing						
No	3.70	166	3.69	220	**3.70**	**386**
Yes	3.76	116	4.07	5	**3.77**	**121**
Aggregate	**3.72**	**282**	**3.70**	**225**	**3.71**	**507**

Over the period of fourteen production years, the average oilseed rape yield of all 507 fields was 3.71 $t.ha^{-1}$. Tab. 1 shows average rape yields according to several criteria. Reduced-tillage technology reached average yield matching almost exactly the one attained by conventional technology.

Concerning regionalization, the highest average yield demonstrated potatoes production area, followed by beet production area, while maize production area, where only reduced-tillage technology was used, proved inferior results. In all of the production areas except the forage one, average rape yield attained by reduced-tillage technology surpassed the one produced using conventional technology.

The average yield of more expensive hybrid varieties surpassed by 4.3 % the one given by conventional varieties. If organic fertilizers those were applied, the average yield attained by merely 1.8 % higher value. With fertilizer application during rape sowing, which was mainly the case of reduced-tillage technology, the average yield exceeded the yield produced when no fertilizers were applied while sowing by 2.1 %. Relatively small frequencies and uneven distribution of cases in individual categories may have influenced the results.

Among technological and economic indicators, the following were monitored or calculated (see Tab. 2): length of vegetative period, fuel consumption, labour consumption, machinery, material and total costs, and unit costs per ton of production.

With respect to the tillage technologies, the average fuel consumption of the reduced-tillage technology was by 20.6 % lower than the one of the conventional technology, and the labour consumption was lower by 24.3 %. The difference may be stressed by an uneven distribution of organic fertilizer application between the groups. If it is applied, the fuel consumption will rise in average by 28.8 %. The same can be stated about the total costs that were also lower with the reduced-tillage technology, namely by 5.1 %. From that, machinery costs were lower by 11.9 %, material costs by merely 1.3 %. Together with the slightly higher rape yield, the reduced-tillage technology costs per ton of production were by 232 $CZK.t^{-1}$, i.e. by 4.1 %, lower than using conventional technology. The potatoes production area demonstrated the lowest unit costs per ton of production, mainly thanks to its highest average rape yield. Evaluation of the results according to the other criteria, such as organic fertilizer application etc., is only informative due to uneven distribution of cases in individual categories.

Tab. 2. – Average duration of vegetative period, fuel and labour consumption, averages of individual cost components, and average costs per ton of oilseed rape production according to the tillage technology and other criteria over the whole monitored period

	Veget. period (days)	Consumption		Average costs			
		Fuel ($l.ha^{-1}$)	Labour ($hrs.ha^{-1}$)	Machinery ($Kč.ha^{-1}$)	Material ($Kč.ha^{-1}$)	Total ($Kč.ha^{-1}$)	Unit. ($Kč.t^{-1}$)
Tillage Technology							
Reduced	345	71.58	3.70	6 052.25	12 713.45	18 900.81	5 401.98
Conventional	343	90.11	4.89	6 872.26	12 879.57	19 918.94	5 633.59
Production Area							
Forage	359	90.21	5.40	6 419.52	12 513.23	19 214.57	5 686.99
Potato	351	89.67	5.06	6 798.45	12 743.63	19 735.59	5 229.29
Cereal	348	75.88	3.88	6 174.94	11 522.29	17 781.05	5 346.03
Beet	338	77.62	3.97	6 455.41	13 519.77	20 129.89	5 583.55
Maize	334	68.99	3.63	6 043.58	13 787.19	19 880.77	6 526.41
Variety							
Conventional	345	77.06	3.98	6 231.17	11 731.87	18 109.54	5 360.00
Hybrid	344	81.38	4.38	6 545.96	13 508.28	20 203.06	5 593.47
Mixed	332	87.89	4.57	6 261.10	12 476.24	18 957.34	5 765.54
Organic Fertilisers							
No	343	69.97	3.58	5 998.56	11 957.51	18 150.97	5 223.28
Yes	347	98.79	5.48	7 222.41	14 388.94	21 672.62	6 048.22
Fertilizers at Sowing							
No	343	83.11	4.46	6 588.50	12 851.77	19 590.79	5 579.84
Yes	348	69.25	3.47	5 866.39	12 581.09	18 592.94	5 265.28
Aggregate	**344**	**79.80**	**4.23**	**6 416.16**	**12 787.17**	**19 352.64**	**5 504.77**

The fuel and labour consumption as well as the value of costs were influenced by organic fertilizer application. With respect to similar average yields, the unit cost per ton of production exceeded by 15.8 % the average of the cases where no organic fertilizers were applied. Average length of vegetative period did not vary much except for production areas. It was longer with production areas located at higher altitudes.

With respect to the costs per unit of production (Fig. 1), the best results were reached in potato production area with reduced-tillage followed by conventional tillage there, and in cereal production area with both conventional and reduced-tillage technologies. Beet production area with reduced-tillage showed also very good results, namely in recent years.

Concerning average yields, statistical analysis showed no significant differences with regard to the tillage technology, organic fertilizer application, or fertilizer application at sowing, and to rape variety. Production area was the only exception where significant differences were demonstrated between the average rape yields of cereal and beet (Turkey HSD; p = 0.0097) and cereal and potatoes production areas (Turkey HSD; p = 0.0382). The trials thus correspond only partly with what MADARÁSZ ET.AL (2016) proved, i.e. by 12.6 % significantly higher rape yield of conservation compared to ploughing technology over ten-year period. One reason might be the monitoring and operational character of the trials, another one the differences in local climatic and other conditions.

Concerning technological and economic indicators from the viewpoint of tillage technology and organic fertilizer application, fuel and labour consumptions, and machinery costs proved statistically significant differences. Material, total, and unit costs differed significantly only with respect to organic fertilizer application. The conclusion of SANCHEZ-GIRON ET AL. (2004, 2007) on higher herbicide costs of reduced-tillage was thus not confirmed, as was the one on lower machinery costs. Decrease in fuel and labour consumption (BONCIARELLI AND ARCHETTI, 2000; GEMTOS ET AL., 1998; TEBRÜGGE, 2000) was validated entirely.

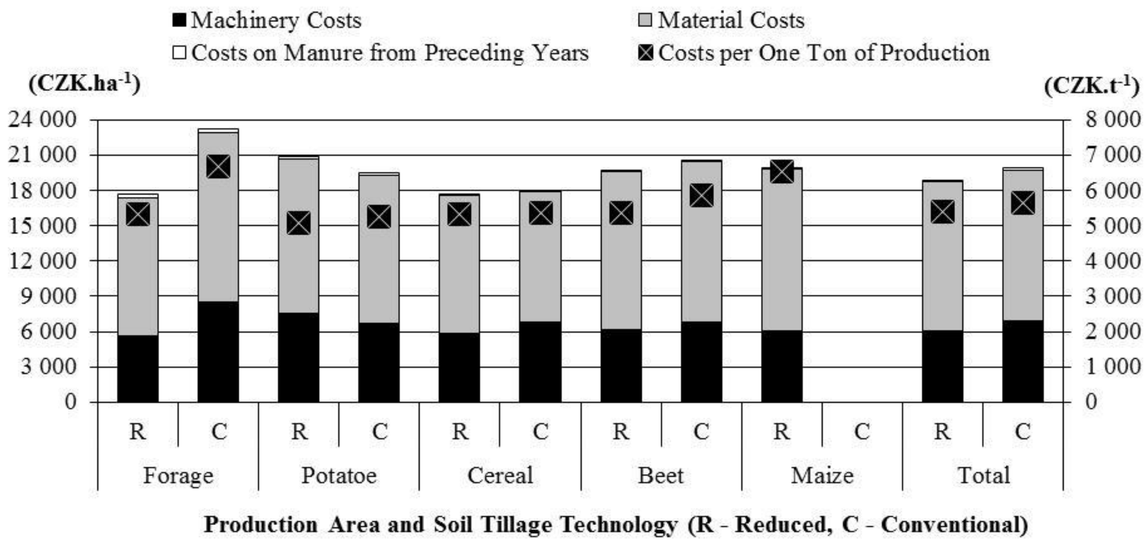

Fig. 1. – Raph of average machinery, material and total costs, and costs per one ton of produced rapeseed with respect to the production area and soil tillage technology over the period of fourteen production years from 2001/02 to 2014/15

CONCLUSIONS

The average fuel consumption of the reduced-tillage technology was by 20.6% lower than that of the conventional technology, the overall labour consumption again lower by 24.3 %. The total costs were again lower by 5.1 %. Yields reached by reduced-tillage were slightly higher, i.e. by 0.6 %, and thus the unit costs lower by 4.1 %. The potatoes production area proved to be the most favourable in terms of oilseed rape yields. Beet production area demonstrated also good results, namely over the recent years.

From the point of view of rape yield, of economics as well as of labour and fuel consumption, the reduced-tillage technology proved to be an adequate alternative to the conventional technology.

ACKNOWLEDGEMENT

The paper was created with institutional support for long-term conceptual development VÚZT, v.v.i. RO0614 and with the grant support CLUS – 2016: 31190/1312/3116 "Effect of cutting tool shape on air flow in working area of mulcher with vertical axis of rotation."

REFERENCES

1. BAKKER, M. M., GOVERS, G., ROUNSEVELL, M. D. A.: The crop productivity-erosion relationship: an analysis based on experimental work. Catena, 57, 2004: p. 55–76.
2. BAKKER, M. M., GOVERS, G., JONES, R. A., ROUNSEVELL, M.D.A.: The effect of soil erosion on Europe's crop yields. Ecosystems, 10, 2007: p. 1209–1219.
3. BEDNÁŘ, V., ŠAŘEC, O., ŠAŘEC, P.: New trends in cropstand establishment of winter oilseed rape. In 5th International Conference Trends in Agricultural Engineering 2013, 3-6 September 2013, Prague: Czech University of Life Sciences Prague, 2013: p. 76-80.
4. BONCIARELLI, F., ARCHETTI, R.: Energy saving through reduction of soil tillage. In: 15th ISTRO Conference, Fort Worth, TX, USA, July 2000.
5. CANTERO-MARTINEZ, C., ANGAS, P., LAMPURLANES, J.: Growth, yield and water productivity of barley (hordeum vulgare l.) affected by tillage and N fertilization in Mediterranean semiarid, rainfed conditions of Spain. Field Crops Research, 84, 2003: p. 341–357.
6. GEMTOS, T. A., GALANOPOULOU, S., KAVALARIS, C.: Wheat establishment after cotton with minimal tillage. European Journal of Agronomy, 8, 1998: p. 137–147.
7. HOLLAND, J.: The environmental consequences of adopting conservation tillage in Europe: reviewing the evidence. Agriculture Ecosystems and Environment, 103, 2004: p. 1–25.
8. HORÁK, L., ŠAŘEC, P., VOZKA P.: Porovnání klasického a půdoochranného způsobu založení porostu pšenice ozimé. Agromanuál, 2007, vol. 2, no. 8, p. 56-59 ISSN 1801-7673. (in Czech).
9. HŮLA, J., PROCHÁZKOVÁ, B.: Minimalizace zpracování půdy et al. Prague: Profi Press, 2008 (in Czech).
10. LAHMAR, R.: Adoption of conservation agriculture in Europe lessons of the KASSA project. Land Use Policy, 27, 2010: p. 4–10.
11. LOPEZ, M., ARRUE, J.: Growth, yield and water use efficiency of winter barley in response to conservation tillage in a semi-arid region of Spain. Soil and Tillage Research, 1997, 44, p. 35–54.

12. MADARÁSZ, B., JUHOS, K., RUSZKICZAY-RÜDIGER, Z., BENKE, S., JAKAB, G., SZALAI, Z.: Conservation tillage vs. conventional tillage: long-term effects on yields in continental, sub-humid Central Europe, Hungary. International Journal of Agricultural Sustainability, 2016, 3 March: 1-20 (in press)
13. PROCHÁZKOVÁ, B., DOVRTĚL, J.: Vliv různého zpracování půdy na výnosy ozimé pšenice. Plant Production, 2000, 10/46, p. 437 – 442. (in Czech)
14. SANCHEZ-GIRON, V., SERRANO, A., HERNANZ, J., NAVARRETE, L.: Economic assessment of three long-term tillage systems for rainfed cereal and legume production in semiarid central Spain. Soil and Tillage Research, 2004, 78, p. 35–44.
15. SANCHEZ-GIRON, V., SERRANO, A., SUAREZ, M., HERNANZ, J., NAVARRETE, L.: Economics of reduced tillage for cereal and legume production on rainfed farm enterprises of different sizes in semiarid conditions. Soil and Tillage Research, 2007, 95, p. 149–160.
16. TEBRÜGGE, F.: Long-term no-tillage as a tool to protect the environment, results of 20 year field trials on different kinds of soil in different crop rotations. In: 15th ISTRO Conference, Fort Worth, TX, USA, July 2000.
17. TEBRÜGGE, F., BÖHRNSEN, A.: Crop yields and economic aspects of no-tillage compared to plough tillage: results of long-term soil tillage field experiments in Germany. Experience with the applicability of no-tillage crop production in the West European countries. In: Proceedings of the EC-Workshop IV, Giessen. Wissenschaftlicher Fachverlag, Boigneville, France, May 12–14 1997.
18. VAN DEN PUTTE, A. ET AL.: Assessing the effect of soil tillage on crop growth: A meta-regression analysis on European crop yields under conservation agriculture. European Journal of Agronomy, 2010, 33, p. 231-241.
19. VERHEIJEN, F.G.A. ET AL.: Tolerable versus actual soil erosion rates in Europe. Earth-Science Reviews, 2009, 94, p. 23–38.
20. WAUTERS, E., BIELDERS, C., POESEN, J., GOVERS, G., MATHIJS, E.: Adoption of soil conservation practices in Belgium: an examination of the theory of planned behaviour in the agri-environmental domain. Land Use Policy, 2010, 27, p. 86–94.

Corresponding author:
doc. Ing. Petr Šařec, Ph.D., Department of machinery utilization, Faculty of Engineering, Czech University of Life Sciences Prague, Kamýcká 129, Praha 6, Prague, 16521, Czech Republic, phone: +420224383147, e-mail: psarec@tf.czu.cz

INFLUENCE OF BIOLOGICAL TRANSFORMATION OF ORGANIC MATTER ON IMPROVEMENT OF WATER INFILTRATION ABILITY OF MODAL LUVISOL

P. Šařec[1], P. Novák[2]

[1]*Department of Machinery Utilization, Faculty of Engineering, Czech University of Life Sciences Prague, Czech Republic*
[2]*Department of Agricultural Machines, Faculty of Engineering, Czech University of Life Sciences Prague, Czech Republic*

Abstract
Low level of soil carbon is one of the major soil issues in the Czech Republic. It results from a decrease in livestock production and from other factors too. Farmyard manure application is one of the ways to rectify this condition. The manure can be supplemented by biological transformation's activators of organic matter. The aim of paper is to verify the effect of fermented farmyard manure and of substances for soil amendment on the change of physical, physical-chemical and biological soil properties, on organic matter fixation, on improvement of water infiltration and retention, and on reduction of soil erosion susceptibility. In this respect, field trials have been established at locality Lázně Bělohrad in the North of Bohemia. Operational trial consists of six variants and is conceived as multi-annual. As the biological transformation's activator, PRP sol agent has been used. In order to verify the effect, soil infiltration abilities have been measured using a ring infiltrometer with a diameter of 0.15 meters. Cone index has been another measured item provided by the registration penetrometer. Soil physical properties have been evaluated using Kopecky's cylinders and subsequently analysed in the laboratories of the CULS Prague. The measurements proved favourable effect of the activator on the decomposition of soil organic matter with resulting change in soil properties. It can be assumed that the effect is going to be gradual and the verification should be carried out also in following trial years.

Key words: activator of organic matter, manure application, soil properties, water infiltration.

INTRODUCTION

Threat to fertility of agricultural land in the Czech Republic is growing. This is due to several factors. This mainly concerns water erosion, which threatens more than half the agricultural land in the Czech Republic (HŮLA & KOVAŘÍČEK., 2010). A related fact is the problem of soil compaction. The soil compaction affects soil physical properties, for example increases soil bulk density which leads to a reduction of soil water infiltration rate (CHYBA ET AL., 2014). Combination of these adverse effects leads to soil erosion and may affect overall crop yields. Low level of soil carbon is one of the reasons related to those events (GUTU ET AL., 2015). This degradation indicator is caused by the decrease of livestock production and wrong cultivation of land.

Recently, there is a turn in conditions. Organic matter is applied to the soil as manure, compost and waste from biogas power plants. Decomposition of organic matter in soils with low levels of carbon may constitute a problem (AMES ET AL., 1984). This status can be improved with the use of activators of organic matter. The activators can have several forms. They may be used separately, or as a special fertilizer seed inoculation (DELČA & STERE, 2013). The studies of activators of organic matter are often focused on the impact on crop yield and soil environment. LESTINGI ET AL. (2007) reported beneficial effect of activators on root system of wheat, corn, sorghum and setaria that caused morphological changes in root starting immediately after germination. LESTINGI ET AL. (2009) also confirmed the positive effect in their further study where they showed a beneficial effect on alfalfa. DELČA & STERE (2013) reported that bacterial density increased significantly following the administration of specific fertilizers (activators). Classic fertilizers did not have any positive effect on microbial density values, which were more or less similar to those reported for the control.

Frequent use of the activators is the utilization of sewage sludge for compost production. PAZDA ET AL. (2005) used activators for the decomposition of wood chips and rice husk in the compost. Effect of the use of activators on soil properties is relatively unexplored phenomenon. Impact can be mainly expected on the physical and chemical properties of soil. KROULÍK ET AL. (2011) suggested a beneficial effect of incorporation of organic matter on the physical properties of soil, on water infiltration into the soil and on partial elimination the consequences of soil compaction after the tracks. It can be also assumed that changes in soil properties will be reflected in the long term rather than immediately after application.

MATERIALS AND METHODS

A field trial was established to demonstrate the influence of the activators of organic matter. The establishment of the experiment occurred in 2014 after the wheat harvest. A field trial has been designed to 6 basic variants.The land is located in Lázně Bělohrad in North of Bohemia (GPS N 50°27.253', E 15°34.208'). The topography is gently sloping, facing southwest, altitude is 360 m above see level. Soil type on the location Lázně Bělohrad is modal luvisol. The content of particles < 0.01 mm: 30% weight (depth 0-0.3 m). The trial plot was divided into individual variants where fertilizer application was carried according to plan and autumn plowing to a depth of 0.25 m was implemented. The fertilizers used were manure (breeding cattle) and NPK 15-15-15 (Lovofert, the Czech Republic). The soil activator used was PRP Sol (PRP Technologies, France). PRP Sol is formed by a matrix of calcium and magnesium carbonate, and mineral elements. Activator of the biological transformation of manure was PRP Fix (PRP Technologies, France). PRP Fix is a granular mixture of mineral salts and carbonates. It was added directly into the bedding. The variants differed by fertilizers used. Dosage of manure was 50 $t.ha^{-1}$, of PRP Sol 200 $kg.ha^{-1}$, and of NPK 200 $kg.ha^{-1}$. Both PRP Fix and PRP Sol activators should not be taken as fertilizer. They are ment to improve conditions for the transformation of organic matter. Fertilization of individual variants is shown in Tab. 1.

The soil was prepared by seedbed combinator during the spring. Maize was sown on all variants. In May 2015 after germination of maize, measurements were taken (after BBCH 10). There were three basic methods of measurement. Soil infiltration abilities have been measured using a ring infiltrometer with a diameter of 0.15 m. The method used was simplified falling-head (BAGARELLO ET AL., 2004). BAGARELLO ET AL. (2006) converts infiltration into saturated hydraulic conductivity. Infiltrometer was poured into a known amount of water and soak time was measured (20 repetitions on each variant).

Tab. 1. – Fertilization of individual variants of field trial

Variant	Fertilization
1	Manure+Fix+Sol
2	Manure+Fix
3	Manure+Sol
4	Manure
5	NPK+Sol
6	NPK - control

Cone index has been another measured item provided by the registration penetrometer. PN-10 penetrometer with cone having an angle 30° (area of 100 mm^2) was used. Soil physical properties have been evaluated using Kopecky’s cylinders with volume 100 cm^3 and subsequently analysed in the laboratories of the CULS Prague. Moisture was measured by Theta Probe (Delta Devices). Yield measurement was carried out in September 2015. Samples were taken and analyzed subsequently in the laboratories of the CULS Prague. Data were processed by the programmes MS Excel (MICROSOFT CORP., USA) and Statistica 12 (STATSOFT INC.,USA).

RESULTS AND DISCUSSION

Fig. 1 is a graph of saturated hydraulic conductivity. There are noticeable differences among each of the variants. These are however lower than the initial forecast. This is probably due to the short exposure of activators and applied manure. It is not possible to clearly demonstrate a beneficial effect of activators on saturated hydraulic conductivity. Even favorable impact of manure application on this parameter cannot be proven.

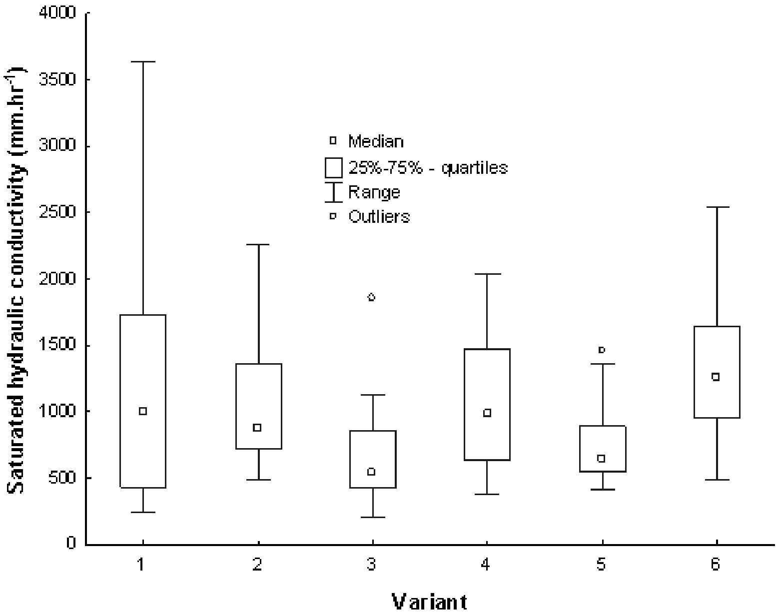

Fig. 1. – Saturated hydraulic conductivity of all the variants at Lázně Bělohrad in May, 2015

The graph outcomes are confirmed by the results of Fisher's LSD test (see Tab. 2). It is possible to find some statistically significant differences among the variants. It is not possible though to establish a causal link between the differences and configuration options. This is probably due to the light-textured soil of the trial plot. Saturated hydraulic conductivity in all variants has reached very high levels. Subsoil beneath the topsoil drained water quickly into the lower layers. Subsoil probably contains a lot of sand particles and low levels of organic carbon. These conclusions correspond to the change of moisture on the soil surface after measurement (see Tab 3). Measurements may have been affected by precision of manure application. In general, the experiment is placed on a very permeable soil.

Tab. 2. – Results of Fisher LSD test (homogenous groups) of saturated hydraulic conductivity at Lázně Bělohrad in May, 2015

Variant	Average ($mm.hr^{-1}$)	1	2	3
3	669.94			****
5	761.69		****	****
4	1065.26	****	****	
2	1091.86	****	****	
1	1175.08	****		
6	1317.04	****		

Tab. 3. – Moisture on the surface beforfe and after saturated hydraulic conductivity measurement at Lázně Bělohrad in May, 2015

Moisture on the surface (% vol.)						
Variant	**1**	**2**	**3**	**4**	**5**	**6**
Before measurement	11.9	11.8	13.0	12.2	11.9	13.1
After measurement	42.1	42.8	43.8	41.8	42.3	41.5

Tab. 4 shows the values of bulk density of the soil in three depths. These figures confirm the initial hypothesis, i.e. the apparent beneficial effects of manure in the soil, but also improved effect using activators of organic matter. From these results, a decrease of density of the soil in relation to the application of manure can be discern. The results suggest beneficial effect of the activators in terms of incorporation of organic matter. Bulk density values are low within all the variats, which influenced the saturated hydraulic conductivity.

Tab. 4. – Bulk density at Lázně Bělohrad in May, 2015

Variant	**1**	**2**	**3**	**4**	**5**	**6**
Depth (m)			**Bulk density (g.cm^{-3})**			
0.05-0.1	1.35	1.46	1.33	1.33	1.53	1.55
0.1-0.15	1.51	1.47	1.46	1.35	1.53	1.50
0.15-0.2	1.55	1.52	1.55	1.37	1.60	1.61

Fig. 2 demonstrates cone index values of individual variants. The graph shows a similar pattern of cone index, depending on the depth. At a depth of about 0.24 m, a sharp increase in cone index may be seen. This interface is caused by the respective depth of tillage (loosening). This phenomenon could also affect the measurement of saturated hydraulic conductivity. Cone index values in 2015 were more affected by the previous way of farming on the land prior to the fertilization and the use of activators. Simultaneously, cone index values showed absence of compacted layers that could affect the conditions of water infiltration into the soil.

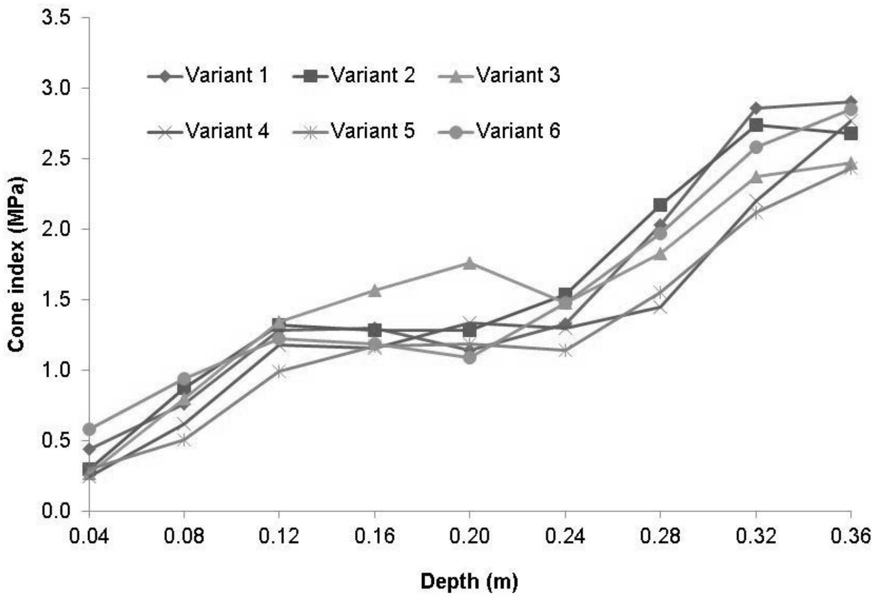

Fig. 2. – Cone index of all variants at Lázně Bělohrad in May, 2015

Tab. 5 shows the basic indicators of the yield of maize in 2015. The differences are mostly below the threshold of statistical significance. Trend of the values showed positive influence of manure fertilization and use of activators to plants. The highest yield was achieved by the variant 1, which used manure as well as both activators. Lowest yield was recorded in the variant 6, which was fertilized with NPK only. In dry summer conditions of 2015, higher water retention in the soil due to increased organic carbon content probably helped. Plant water supply had a direct impact on the yield of maize. The impact could be caused by the gradual mineralization of organic matter and increasing nutrient uptake by plants.

Tab. 5. – Yield parameters at Lázně Bělohrad in September, 2015

Variant	Dry matter (whole plants) (%)	Yield at given dry matter ($t.ha^{-1}$)	Yield (conversion to 38% dry matter) ($t.ha^{-1}$)
1	38.7	34.5	35.2
2	39.2	32.5	33.5
3	38.9	33	33.8
4	37.1	32.8	32.0
5	39.7	30.5	31.8
6	41.4	27.6	30.1
Average	**39.2**	**31.8**	**32.7**

Initial research assumptions were confirmed only partially. Variations in the values of saturated hydraulic conductivity were minimal. This is contrary to many other studies. HŮLA & KOVAŘÍČEK (2010) emphasize the beneficial effect of organic matter to infiltration of water into the soil. Conversely BAGARELLO ET AL. (2006) reported the difficulty of measuring saturated hydraulic conductivity on light soils. At high levels of conductivity, the effects of soil tillage, fertilization or the influence of cultivated crops cannot be clearly demonstrated. Measurement was certainly affected by the short duration of the experiment. It can be assumed that the effect is going to be gradual and the verification should be carried out also in following trial years. The necessity of exploration of the long-term effects also emphasizes FERRI ET AL. (2004). Changing soil structure is always a long-term issue. Application of organic matter and activators was done only a few months before the measurement. It confirmed the conclusions drawn by FERRI ET AL. (2004) about great differences in the decomposition of organic matter in the soil by various influences. This is also confirmed by DELČA & STERE (2013). PAZDA ET AL. (2005) emphasizes the need to support bacterial activities for decomposition of organic matter. LESTINGI ET AL. (2009) also mention the risk for bacterial activity caused by agricultural activities.

The practical impact of the use of an activator should lead to increase in crop yield. The presented results are consistent with the conclusions of LESTINGI ET AL. (2007) about the yield and quality composition of triticale. Similar effect can be expected even on other crops. Overall, the effects of activators of organic matter are among the less explored topics. In connection with changing composition of organic fertilizer (fewer manure and slurry but more compost and waste from biogas plants), the increased importance of activators of organic matter can be expected.

CONCLUSIONS

So far, the work has been unable to clearly demonstrate the beneficial effect of activators of organic matter on parameters of water infiltration into the soil. This is probably due to the short duration of the experiment. Another possibility is the influence of soil parameters of the selected plot to the measurement. Especially light soil infiltration parameters are always strong, even without further intervention. For future measurements, it will be convenient to use other methods. A brilliant blue dye tracer method looks perrspective in this respect.

During the measurement of physical properties of soil, favorable effect on the bulk density of the soil could be observed. However, this was not confirmed by the cone index values measured. The yield results again suggest a beneficial effect of activators of organic matter in order to improve the soil environment. It may also be due to prolonged action of an activator in the soil for other several months. It will be necessary to see the influence of activators on yield of more common crops with different root systems than the maize. Again, the necessity of long-term examination of the effects of activators of organic matter should be emphasized. Research needs to be validated in more locations in order to eliminate the influence of the local environment.

ACKNOWLEDGEMENT

This work was supported by Research Project of the Technology Agency of the Czech Republic no. TA04021390 and by the project of CULS Prague IGA No. 2015:31180/1312/3116.

REFERENCES

1. AMES, R. N., REID, C. P. P., INGHAM, E. R.: Rhisosphere bacterial population responses to root colonization by a vesicular-arbuscular mycorrhizal fungus. New Phytologist, 96, 1984: 555–563.
2. BAGARELLO, V., IOVINO, M., ELRICK, D.: A Simplified Falling-Head Technique for Rapid Determination of Field-Saturated Hydraulic Conductivity. Soil Science Society of America Journal, 68, 2004: 66-73.
3. BAGARELLO, V., ELRICK, D. E., IOVINO, M., SGROI, A.: A laboratory analysis of falling head infiltration procedures for estimating the hydraulic conductivity of soils. Geoderma, 135, 2006: 322-334.
4. CHYBA, J., KROULÍK, M., KRIŠTOF, K., MISIEWICZ, P., CHANEY, K.: Influence of soil compaction by farm machinery and livestock on water infiltration rate on grassland. Agronomy Research, 12, 2014: 59-64.
5. DELČA, E, STERE I.: Influence of chemical fertilizers and biofertilizers on the dynamics of some microbial groups (heterotrophic bacteria, free nitrogen-fixing bacteria) in chernozem soil of Dobrogea (Cumpăna, Valu lui Traian). Romanian Agriculture Research, 30 , 2013: 219-223.
6. FERRI, C. M., STRITZLER, N. P., PAGELLA, J. H.: Nitrogen fertilization on rye pasture: Effect on forage chemical composition, voluntary intake, digestibility and rumen degradation. Journal of Agronomy and Crop Science, 190, 2004: 347-354.
7. GUTU, D., HŮLA, J., KOVAŘÍČEK, P., NOVÁK, P.: The influence of a system with permanent traffic lanes on physical properties of soil, soil tillage quality and surface water runoff. Agronomy Research, 13, 2015: 63-72.
8. HŮLA, J., KOVAŘÍČEK, P.: Water infiltration into soil and surface water runoff in maize growing by three cultivation technologies. In: Trends in Agricultural Engineering. 7-10 September 2010, Prague: Czech University of Life Sciences Prague, 232-235.
9. KROULÍK, M., KVÍZ, Z., KUMHÁLA, F., HŮLA, J., LOCH, T.: Procedures of soil farming allowing reduction of compaction. Precision Agriculture, 12, 2011: 317-333.
10. LESTINGI, A., BOVERA, F., PICCOLO, V., CONVERTINI, G., MONTEMURRO, F.: Effects of compost organic amendments on chemical composition and in vitro digestibility of alfalfa (Medicago sativa L.). Ital Journal Animal Science, 8, 2009: 201–209.
11. LESTINGI, A., DE GIORGIO, D., MONTEMURRO, F., CONVERTINI, G., LAUDADIO, V.: Effects of bio-activators on yield and quality composition of triticale forage as an animal food resource. Journal of Food, Agriculture and Environment, 5, 2007: 164–171.
12. PASDA, N., LIMTONG, P., OLIVER, R., MONTANGE, D., PANICHSAKPATANA, S.: Influence of bulking agents and microbial activator on thermophilic aerobic transformation of sewage sludge. Environmental Technology, 26, 2005:1127-1135.

Corresponding author:

doc. Ing. Petr Šařec, Ph.D., Department of Machinery Utilization, Faculty of Engineering, Czech University of Life Sciences Prague, Kamýcká 129, Praha 6, Prague, 16521, Czech Republic, phone: +420 22438 3147, e-mail: psarec@tf.czu.cz

GROUND MASSIF AS A HEAT SOURCE FOR HEAT PUMP

M. Šeďová

Department of Mechanical Engineering, Faculty of Engineering, Czech University of Life Sciences Prague, Czech Republic

Abstract
The article is describing ground massif as a heat source for heat pump. In the ground massif is stored a horizontal heat exchanger. The heat pump is used for cold water warming and a heating of the administration building. The aim of the research is to analyse the influence of the heat exchanger on the ground massif temperature while extracting heat energy at the beginning and during the heating season 2014 – 2015. Temperatures are measured near the exchanger and on a reference lot in a burial depth of the heat exchanger. In the article are described subsurface temperatures in a depth of 0.2 m also. The energy potential of the ground massif was evaluated using the differences of temperatures of the ground massif in the area of the heat exchanger at the beginning and the end of the heating season.

Key words: ground massif, heat source, heating season, Slinky heat exchanger.

INTRODUCTION

We live in a time when the use of alternative energy sources gets more and more into the foreground. Heat pumps are devices that can effectively use these resources. It can draw a heat from land, air and water, but it can also utilize a secondary heat. These heat sources for heat pump evaporators are used in both residential and civil construction and in agriculture. They can be used for heating of stables for breeding sows with piglets, fattening of broiler chickens to heat water for technological purposes, drying crops, etc.

In South Korea at the Seoul National University the cost of heating greenhouses was solved (HA ET AL., 2011). At the Saint Mary's University in Canada and at the Hokkaido University in Japan the issue of heating water in production ponds, grain drying and pasteurization of milk has been addressed (TARNAWSKI ET AL., 2009). At the Geriz University and at the Ege University in Turkey a usage of gas engine driven heat pump during drying of medicinal and aromatic plants was verified (GUNGOR ET AL., 2011).

Heat pumps ground - water use two sources of low potential heat energy which is drawn by heat exchangers. There are called rock massif and ground massif (ground massif is the rock to a depth of 2 m). Exchangers are installed vertically or horizontally. It consists of polyethylene pipes of different diameters and lengths. This depends mainly on the required performance.

Vertical heat exchangers are using the internal performance of the Earth using polyethylene pipe in the shape of "U" in which a cooling medium is flowing (PETRÁŠ, 2008). The space in the borehole around the pipes is filled with a suitable material to provide good contact between the pipe and the massif and to reduce thermal resistance (FLORIDES & KALORIGOU, 2007).

Horizontal heat exchangers are mainly using thermal energy that is naturally accumulated in the surface ground massif as a result of the incident solar radiation (PETRÁŠ, 2008). With horizontal exchanger the flow of heat is used. Heat comes from above and it is received by upper layer of the Earth from direct and indirect solar energy (radiation, rain, etc.). 98% of the energy draws horizontal heat exchanger from a layer of ground massif that is above it. Only 2% of the energy is taken from the ground massif under the exchanger. This heat exchanger can be considered as a sizable solar collector with low efficiency, which is complemented by a huge heat accumulator (surface) with an annual cycle of charging and discharging.

The aim is to analyze the temperature changes of the ground massif with Slinky heat exchanger in consecutive heating season. Another aim to determine whether the ground massif is able to regenerate sufficiently out of heating season and whether a stable energy source for heat pumps.

MATERIALS AND METHODS

Experimental measurements were carried out in Prague – Dolní Měcholupy within the company Veskom spol. sr.o. The altitude of Prague is 258 m. In this area the average temperature during the heating season is

4°C and the outside temperature for calculation is considered -12°C. The measurement of 5 vertical heat exchangers is taking place there, as well as 1 horizontal exchanger and 1 Slinky exchanger. Overall 9 vertical heat exchangers, 2 horizontal exchangers and 2 Slinky heat exchangers are the heat source for heat pumps which are used for water heating and heating of administration building with floor age of 1,480 m^2. Exchangers were put into operation in August 2008.

Slinky was made of pipes PE 100RC 32 x 2.9 mm. This heat exchanger is installed at a depth of 1.5 m. Its total length is 200 m and it is formed by 53 loops. It is not stored in the bed of sand. The ground massif to a depth of 2 m is dark brown sandy-clay loam. In the heat exchanger a cooling liquid mixture of 33% ethanol and 67% water is used. Fig. 1 shows in placement scheme of sensors that measure the temperature of the ground massif.

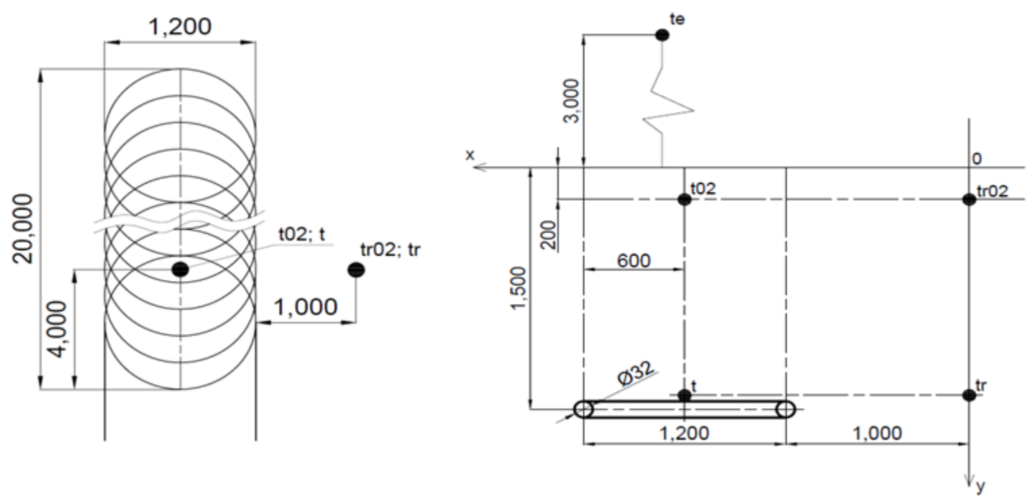

Fig. 1. – Scheme of Slinky heat exchanger and placement of temperature sensors

Designation of the temperature sensors is as follows:
t – temperature sensor located at a depth of 1.5 m in the vicinity of the heat exchanger [°C]
t_r – reference temperature sensor located 1.0 m from the heat exchanger at a depth of 1.5 m [°C]
t_{02} – temperature sensor located at a depth of 0.2 m above the heat exchanger [°C]
t_{r02} – reference temperature sensor located 1.0 m from the heat exchanger at a depth of 0.2 m [°C]
t_e – sensor ambient temperature located at a height of 3.0 m above the surface [°C]
Temperatures of the ground massif and the ambient air are recorded from 1 March 2011 every 15 minutes.

RESULTS AND DISCUSSION

Czech legislation states that heating season lasts from 1 September to 31 May of the following year. Supply of thermal energy is initiated in heating season, when the average daily temperature of outside air in the relevant locality is below 13°C in two consecutive days and the evolution of the weather cannot be expected to increase the temperature above 13°C for the following day.
The average daily air temperature t_{ed} is calculated according to the Eq. 1.

$$t_{ed} = 0.25 \cdot (t_7 + t_{14} + 2 \cdot t_{21}). \text{ [°C]} \quad (1)$$

where: t_7 – temperature at 7:00 a.m. [°C]; t_{14} – temperature at 2:00 p.m. [°C];
t_{21} – temperature at 9:00 p.m. [°C]
The average daily air temperature and temperatures of ground massif at about 3 p.m. in the period from 1 September 2014 to 31 May 2015 are shown in Fig. 2.

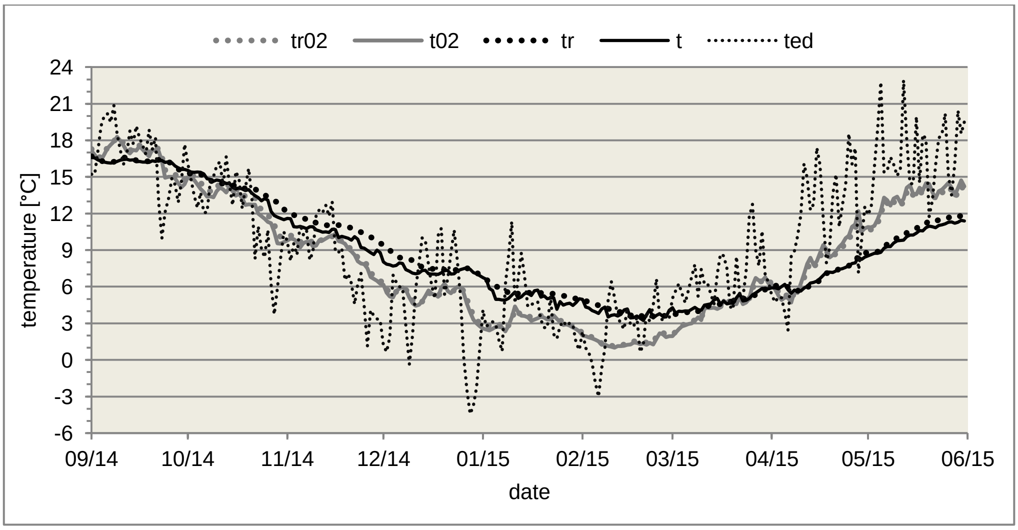

Fig. 2. – Course of the temperatures in the heating season 2014 - 2015

There is only a slight delay of the temperature course of t_{02} at the depth of 0.2 m with respect to air temperatures above the ground massif. A higher delay and a slight reaction to the ambient air temperature were seen for the temperature t at a depth of 1.5 m. The generally known fact that due to a low value of the coefficient of thermal conductivity of the ground massif and a high specific heat capacity, the amplitudes of temperature changes of the ground massif decrease with the depth of the ground massif when compared to the air temperature above its surface, is valid even during the transfer of the heat flow from the ground massif by the installed heat exchanger. The temperature of the ground massif t_{02} at a depth of 0.2 m above the heat exchanger is influenced particularly by the temperature and speed of the surrounding air, the intensity of incident solar radiation, and falls of rain and snow (NEUBERGER ET AL., 2014).

The temperature course of t_{ed} shows that the heating season 2014–2015 lasted from 21 October 2014 to 2 May 2015. In this time period the temperature of the ground massif t gradually decreased from 14.07°C to the minimum value of 2.77°C. This minimum temperature was recorded at 2 a.m. on 20 February 2015. The Eq. 2 in this period is as follows:

$$t = 2\cdot10^{-6}\cdot d^{3} + 9\cdot10^{-5}\cdot d^{2} - 11.49\cdot10^{-2}\cdot d + 13.15. \quad (R^2=0.973) \quad [°C] \quad (2)$$

where: d – number of days from the beginning of the heating season 2014–2015, i.e. from 21 October 2014.

The maximum temperature difference between the temperature t_r which was measured 1.0 m from the heat exchanger at a depth of 1.5 m and the temperature at a depth of 1.5 m in the vicinity of the heat exchanger t was recorded 1 December 2014 with a value of 2.02 K. During the heating season 2013 - 2014 the lowest temperature of the ground massif t was measured 5 February 2014 (ŠEĎOVÁ ET AL., 2015). In the season 2014–2015 was this temperature recorded 28 March 2015.

The Eq. 3 of the reference temperature of the ground massif at a depth of 1.5 m t_r has following forms:

$$t_r = 3\cdot10^{-6}\cdot d^3 - 1\cdot10^{-4}\cdot d^2 - 10.74\cdot10^{-2}\cdot d + 13.81. \quad (R^2=0.986) \quad [°C] \quad (3)$$

where: d – number of days from the beginning of the heating season 2014–2015, i.e. from 21 October 2014.

Fig. 2 shows a gradual increase of the temperature of the ground massif t and the reference temperature t_r in the period from 3 May to 31 May 2015. Eq. 4 and Eq. 5 in this time period are as follows:

$$t = 1\cdot10^{-4}\cdot d^3 - 8.1\cdot10^{-3}\cdot d^2 + 23.52\cdot10^{-2}\cdot d + 8.30. \quad (R^2=0.962) \quad [°C] \quad (4)$$

$$t_r = 1\cdot10^{-4}\cdot d^3 - 7.1\cdot10^{-3}\cdot d^2 + 24.57\cdot10^{-2}\cdot d + 8.43. \quad (R^2=0.970) \quad [°C] \quad (5)$$

where: d – number of days from 3 May 2015.

In this time period the temperature of the ground massif t gradually increased from 8.65°C to 11.73°C.

The energy potential of the ground massif was evaluated from temperature differences of the ground massif in the vicinity of the Slinky heat exchanger Δt at the beginning and at the end of the heating season. Tab. 1.and Tab. 2. show temperature differences at the beginning and at the end of five consecutive heating seasons.

Tab. 1. – Temperature differences of the ground massif at the beginning of heating season

Start of rating season	Date	t[°C]	Δt[K]
2010 - 2011	30 August 2011	18.40	
			-0.94
2011 - 2012	30 August 2012	17.46	
			0.2
2012 - 2013	30 August 2013	17.66	
			-0.72
2013 - 2014	30 August 2014	16.87	
			-0.27
2014 - 2015	30 August 2015	16.60	

Tab. 2. – Temperature differences of the ground massif at the end of heating season

End of rating season	Date	t[°C]	Δt[K]
2010 - 2011	1 May 2011	9.8	
			-1.04
2011 - 2012	1 May 2012	8.4	
			-0.37
2012 - 2013	1 May 2013	7.67	
			1.69
2013 - 2014	1 May 2014	9.36	
			-0.82
2014 - 2015	1 May 2015	8.54	

Temperature differences of the ground massif at the beginning and at the end of heating seasons are within the range of measurement accuracy. These temperature differences shows that ground massif with Slinky heat exchanger, under the climatic conditions and the quantity of heat, can be considered as a stable energy source for heat pumps.

CONCLUSIONS

The course of temperature t_{ed} shows that the heating season 2014 - 2015 lasted from 21 October to 2 May 2015.

During this time period temperatures of the ground massif at a depth of 1.5 m were higher than temperatures of the ground massif at a depth of 0.2 m. After this time period the situation is reversed. Temperatures of the ground massif at the depth of 0.2 m react to changes of air temperatures.

The temperature of the ground massif t and the reference temperature of the ground massif t_r are described by Eqs. (2) to (5).

Temperature differences Δt at the beginning and at the end of heating seasons (Tab. 1., Tab. 2.) did not exceed 2 K.

The measurement results show that the highest temperatures of ground massif at the depth of 1.5 m are achieved in mid-August. In the regeneration period of Slinky heat exchanger before the heating season 2014 - 2015 it occurred 13 August 2014.

From results of temperature in the ground massif t at the beginning and at the end of each heating season the ground massif has sufficient potential energy and can be considered as a stable energy source for heat pumps.

REFERENCES

1. FLORIDES, G., KALORIGOU, S.: Ground Heat Exchangers: A Review of Systems, Models and Applications. Renewable Energy, 32, 2007: 2461–2478.
2. GUNGOR, A., ERBAY, Z., HEPBASLI, A.: Exergoeconomic Analyses of a Gas Engine Driven Heat Pump Drier and Food Drying Process. Applied Energy, 88, 2011: 2677–2684.
3. HA, T., LEE, I. ., HWANG, H., HONG, S., SEO, I., BITOG, J. P.: Development of an Assessment Model for Greenhouse Using Geothermal Heat Pump System. In: American Society of Agricultural and Biological Engineers Annual International Meeting 2011. pp. 2105–2114, Louisville, Kentacky, USA.
4. NEUBERGER, P., ADAMOVSKÝ, R., ŠEĎOVÁ, M.:Temperatures and Heat Flows in a Soil Enclosing a Slinky Horizontal Heat Exchanger. Energies, 7, 2014: 972–987.
5. PETRÁŠ, D.: Low-temperature heating and renewable energy. JAGA group, Bratislava, 2008 (in Czech).
6. ŠEĎOVÁ, M., NEUBERGER, P., ADAMOVSKÝ, R.:Measurement and analysis of temperature changes of ground massif with Slinky heat exchanger. Agronomy Research, 13, 2015: 533 - 538.
7. TARNAWSKI, V., LEONG, W. H., MOMOSE, T., HAMADA, Y.:Analysis of Ground Source Heat Pumps with Horizontal Ground Heat Exchangers for Northern Japan. Renewable Energy, 34, 2009: 127–134.

Corresponding author:

Ing. Michaela Šeďová, Department of Mechanical Engineering, Faculty of Engineering, Czech University of Life Sciences Prague, Kamýcká 129, Praha 6, Prague, 16521, Czech Republic, phone: +420 22438 3174, e-mail: sedova@tf.czu.cz

EQUIPMENT FOR TESTING STABLE FLOOD DEFENSES

L. Ševčík

Technical university in Liberec, Liberec, Czech Republic

Abstract
Issues of the impactor testing flood defenses in this contribution. By impactor will be tested stationary and mobile barriers. They are mechanical deformation test. Standard is a log impactor - weighing 400 kg, a diameter 400 mm and approximately 4 m long. Log alludes by force 2 m/s to the flood barrier. Impact must not lead to instability barriers. The aim is to propose smaller device with the same effects.

Key words: velocity, pneumatic piston, devices, flow rate.

INTRODUCTION

The following figure shows the arrangement of the experiment. The cylinder piston impactor was fitted with a load cell resistance to water immersion. Furthermore, among the wooden headboard of the impactor and the fixed bracket cable was stretched the distance measurement. Pressure compressor air was 0.6 MPa.

Due to the detection of real properties of the air motor was carried out measuring the speed of ejection of the piston rod of the engine and its force effect on a floating log (APPROVAL STANDARD FOR FLOOD ABATEMENT EQUIPMENT, 2013).

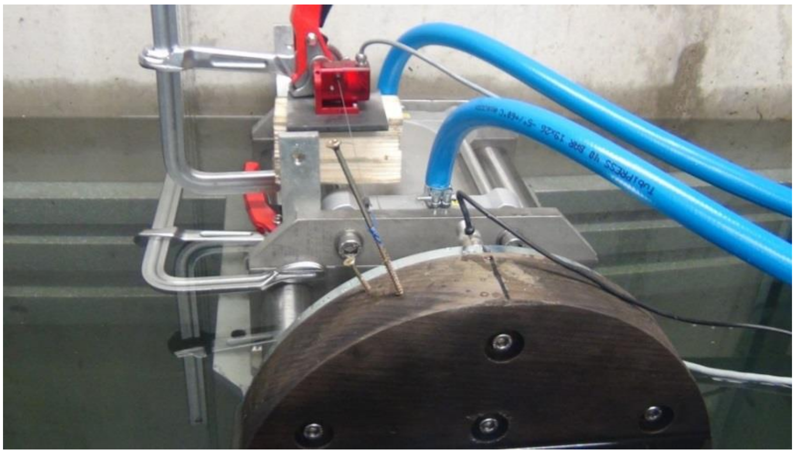

Fig. 1. – Front view of the experiment

Used sensors are in Fig. 1:
- Wire position sensor for sensing position of a piston engine.
- Force transducer to the piston engine to determine the forces acting on the piston log.

The calculations:
- Real time was calculated velocity of the piston engine logs and the derivative signals from the sensors to their position (calculated speed signals exhibit noise generated by a mathematical derivative transaction on real measured signal) (MUTTRAY, OUMERACI, 2005).

Measuring the speed of eject impactor

The air pressure was vented to air cylinder impactor. Impactor was ejected against a flood inhibition. Measurements were carried out forces, piston extension and the calculated energy, see Fig. 2.

Measured values:
- Ejecting piston speed 0.25 m/s.
- Maximum force 25 kN.
- The maximum amount of deformation flood defenses.

If we start from the equality impact energy timber in standing water, we arrive at the value of the strain energy:

$$E = \frac{1}{2}mv^2 \text{ given} \tfrac{1}{2}\ 400\ kg\ 2\ m/s2\ get\ 800J. \tag{1}$$

Energy of cylinder:

$$E_{cylinder} = \frac{1}{4}\pi d^2 \int_0^{E\max} p(z)dz \text{ given} \qquad (2)$$

diameter 200x200x3,14 / 4 of 1 MPa (max. Pressure) = 0.125 maximum stroke 3925 J.

So that, in terms of energy it is enough and it can reduce by the pressure. If we neglect the effect of speed on the deformation, so we could cylinder attached to the wall, shoot the strength and track and stop when we reach 800 J (MALCANGIO ET AL., 2011). In conclusion, the piston is of sufficient strength, but does not have the necessary speed.

The measurement result was insufficient velocity impactor, 10 times less than required. The speed can be increase by next possibilities- by changing the pneumatic diagram or by different mechanism.

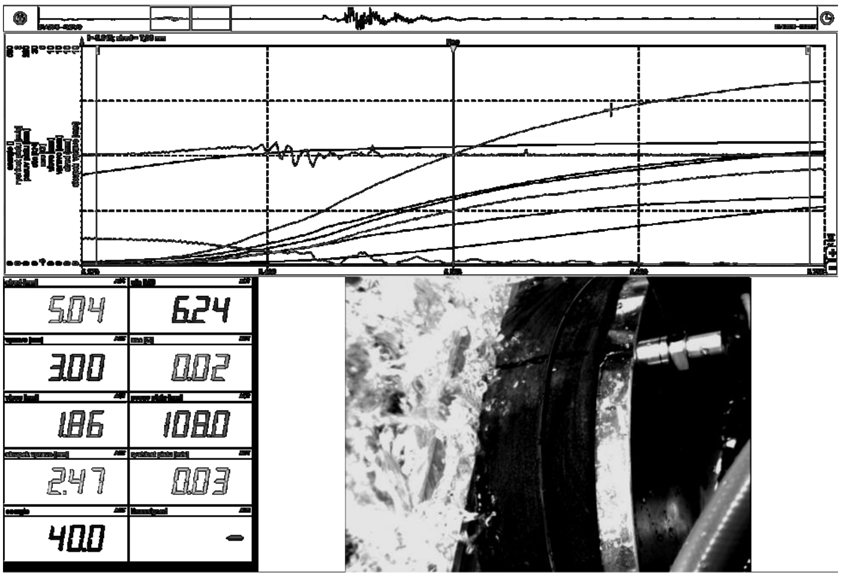

Fig. 2. – Measurement results

Optimization of pneumatic schema

Was designed pneumatics schematic diagram of impactor see. Fig. 3. Small the flow of air caused inadequate speed ejection piston.

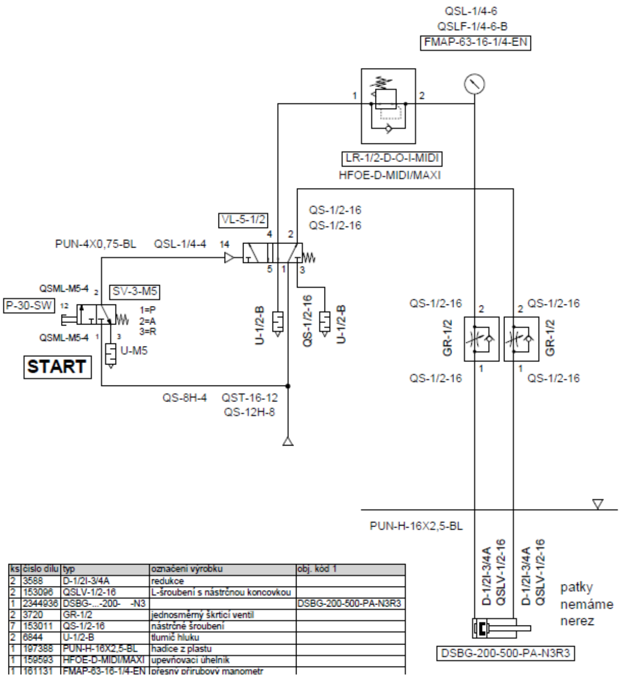

ks	číslo dílu	typ	označení výrobku	obj. kód 1
2	3588	D-1/2I-3/4A	redukce	
2	153096	QSLV-1/2-16	L-šroubení s nástrčnou koncovkou	
1	2344936	DSBG-...-200- -N3		DSBG-200-500-PA-N3R3
2	3720	GR-1/2	jednosměrný škrticí ventil	
7	153011	QS-1/2-16	nástrčné šroubení	
2	6844	U-1/2-B	tlumič hluku	
1	197388	PUN-H-16X2,5-BL	hadice z plastu	
1	159593	HFOE-D-MIDI/MAXI	upevňovací úhelník	
1	161131	FMAP-63-16-1/4-EN	přesný přírubový manometr	

Fig. 3. – Pneumatic schema of impactor

Given the small space in the canal was a cylinder -200-500 impactor DSBG indicated in the diagram changed to cylinder-DSBG 200-125, with smaller stroke. From the measurement showed that the pressure in the cylinder is only 0,08 MPa and in the reservoir of the compressor was 0.6 MPa, 7.5 times smaller. The pneumatic cylinder is designed to 1 MPa, a pressure in the cylinder could 12.5x increase the. The result is insufficiently oversized and intake air into the cylinder. To reduce air resistance was eliminated throttle valve, truncated tube 16 mm minimum. The result - the rate unchanged, has been calculated feed rate of the piston rod. For the simulation was used valve MFH-3-3 / 4 (thread ¾ ")

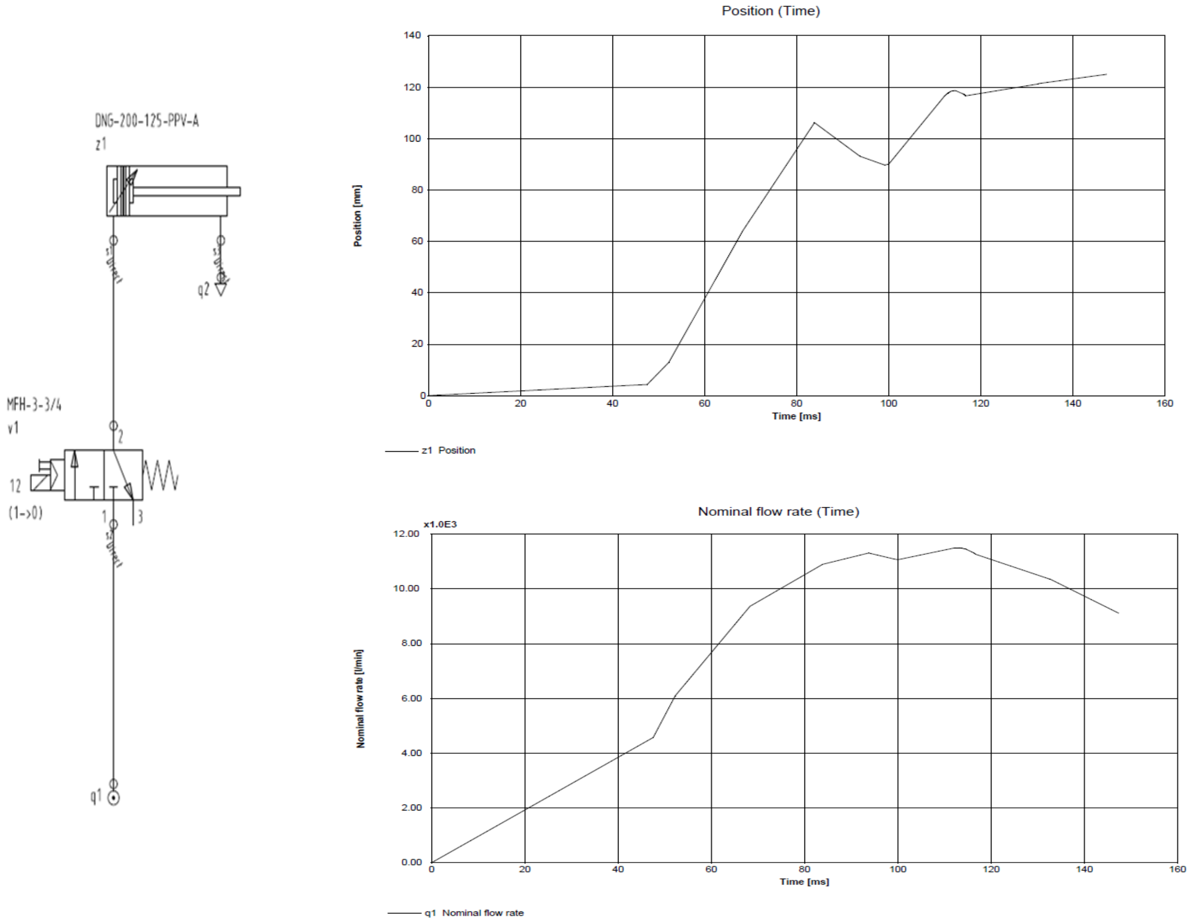

Fig. 4. – Pneumatic scheme without air tank, position of piston, nominal flow rate

VL-5-15 To reach 2 m/s and a stroke of 125 mm will need to get to time moving from one extreme position to the other in 62,5 ms at a constant speed 2 m/s. Unfortunately, even with this valve resulting value (total time crossing) is based on 150 ms.

Simulations are two, without an air tank (see Fig. 4) and without air tank (see Fig. 5). But theresults are the same, the total time is 150 ms. There is still instability, starting at the stroke traveled about 90 mm. The speed is so great that it cannot roll vented and leads to bounce back. The flow rates are enormous, 12 tis nl / min. (Norm liter). NB. Calculation counts load 10 kg.

A calculated 12000 norm liter per minute is the value of the required volume of air (at atmospheric pressure) per minute. The equations (P * V) / T = const. (Pressure 0 absolute value, a pressure of 6 bar - we calculate 7 bar), T - the temperature is neglected because it is still the same. The cylinder is 200 mm diameter, 125 mm stroke, about 4 liters need for filling (6-bar pressure!) 7bar * 4 l = 1 bar * V (standard liters) V = 28 nl

This value is required for the cylinder.

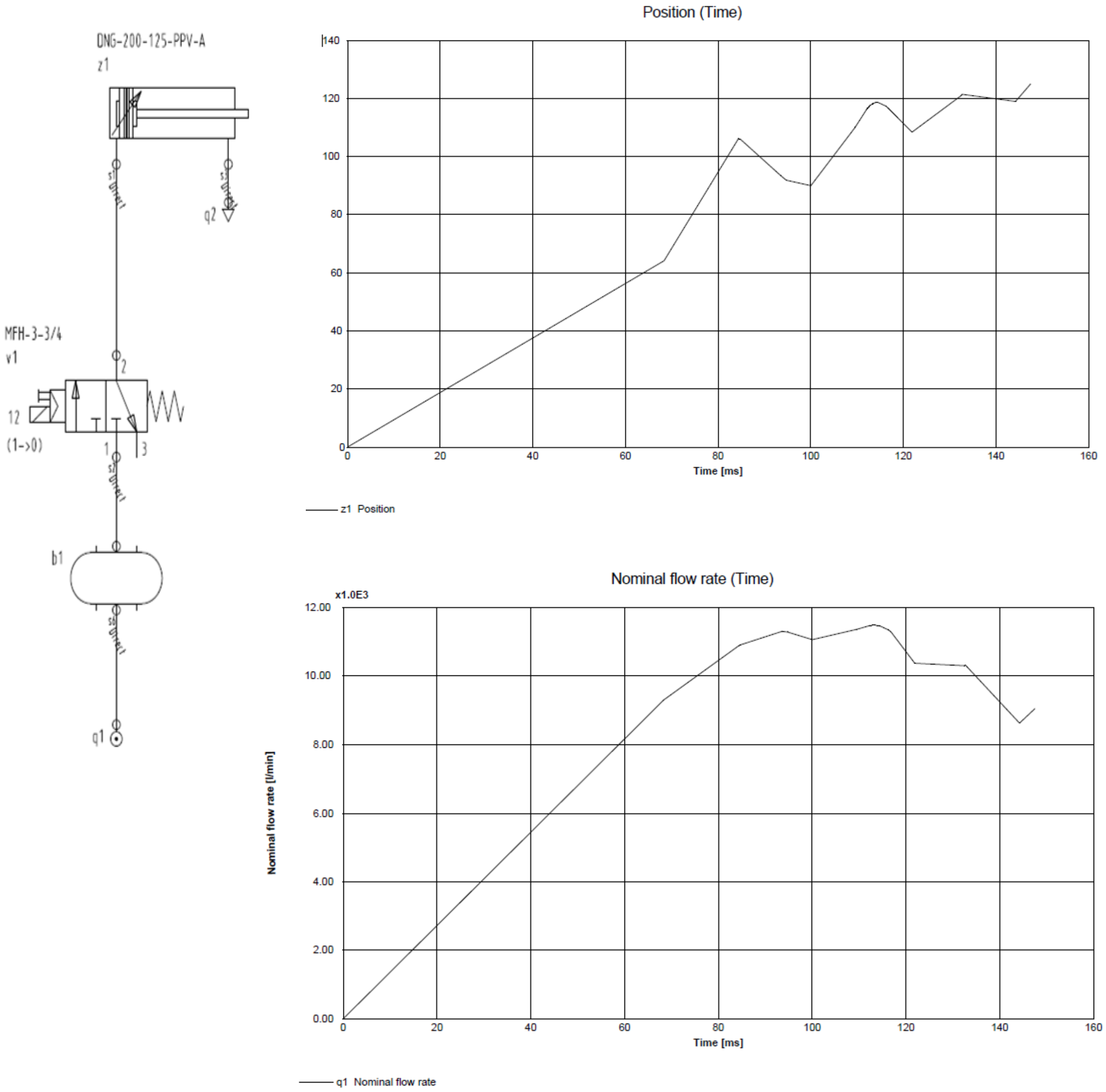

Fig. 5. – Pneumatic scheme with air tank, position of piston, nominal flow rate

Now it depends for what time I need him to fill. The required time, thus 62,5 ms, then the corresponding flow rate:

28 nl / 0.0625 s = 448 nl / s = approx. 26,9 tis nl/min.

As a control I can take the needed time from the graph, i.e. 150 ms. Then it comes out there about 12000 nl / min as a simulation.

Practically, it would be good to use a pressure tank. It should have a greater capacity. We need four liters of pressurized air. From a small pressure vessels would quickly "escaped air" and would dramatically reduce the pressure cylinder would rapidly "fade".

It can conclude that in these conditions it is not possible to achieve the speed of 2 m/s by available pneumatic elements.

Ejection mechanism

Detention brake pressurizing and releasing causes certain effects "air gun" (see Fig. 6 left). Certainly it will be more dynamic than the classic start valve. Bounce-back is prevented, while ensuring adequate exhaust from the second chamber at the price enlarges the hole in the cylinder cover.

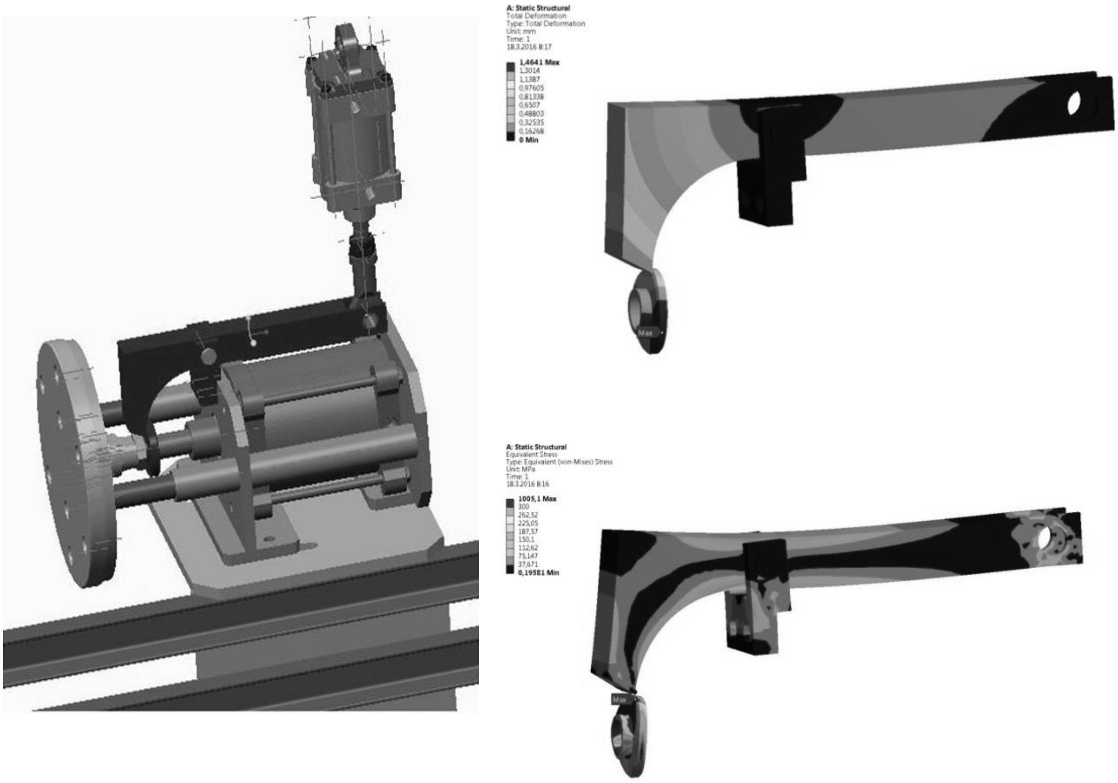

Fig. 6. – 3D model, stress and deformation ejection mechanism

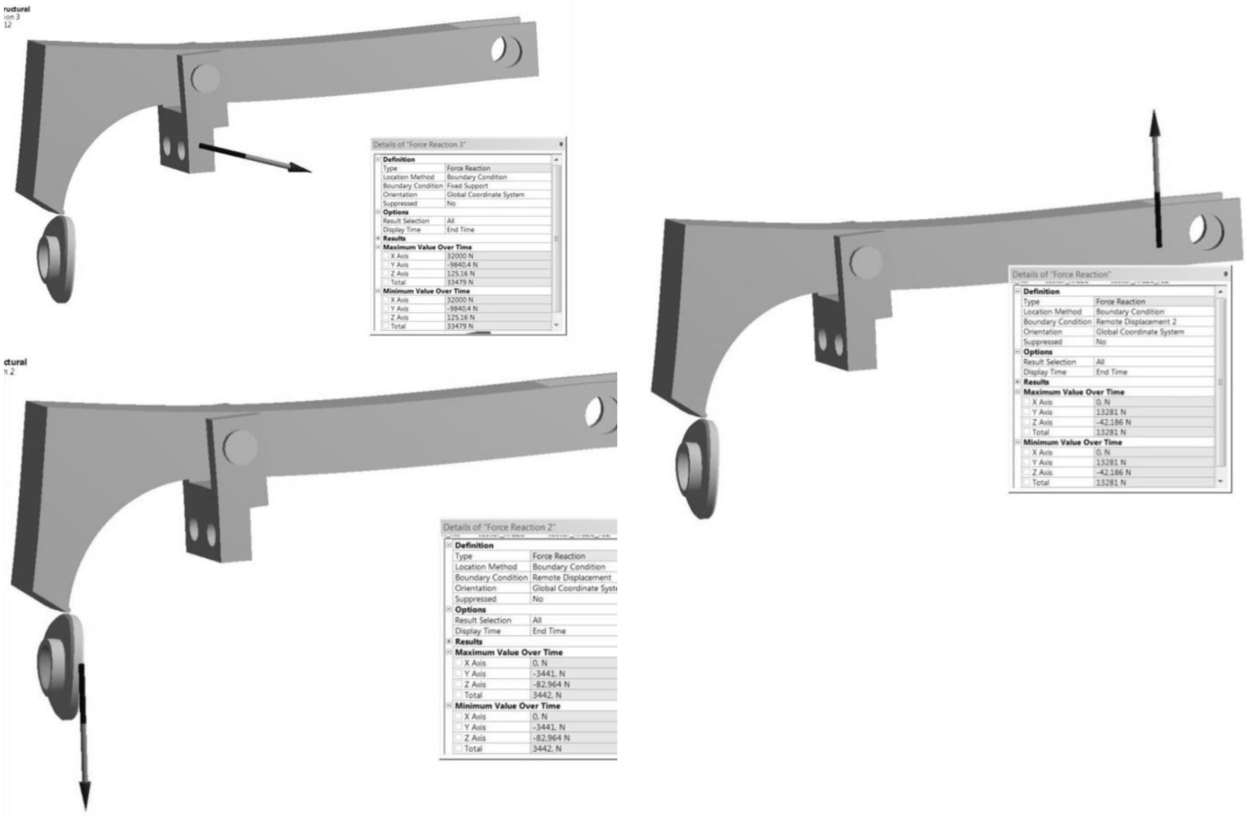

Fig. 7. – Strength for unlocking, power saving in the frame, the contact force between the lever and the ring disarming

The piston rod of the main pneumatic cylinder impactor is attached with special ring. The ring is hooked with armed release lever. At the other end of this lever is unlocking pneumatic cylinder. In the case of pushed back will be shut before the pressurized piston. The aim was to design this mechanism. Calculation of stress and strain (see Fig. 6 left) was made in ANSYS. Deformation of the lever reaches value 1.4 mm, and contact stress of about 1000 MPa. A calculation of the contact forces see. Fig. 7. Forces were derived from FEM analysis.

It was calculated to force unlocking mechanism with a friction coefficient of 0.2. Further reactions in storage and contact force, force vectors refer to Fig. 7.

CONCLUSIONS

Proposal was made of impact testing equipment for stationary and mobile flood barriers. Due to the layout of the channel was designed pneumatic cylinder of diameter 200 mm and a stroke 125. When the pressure is 10 bar the impactor has 3 times more energy than is required in the tests. But impactor does not have required speed. In this contribution was optimized pneumatic schema. The optimization is only three-time increase impact speed. And therefore was designed ejection mechanism. Its properties must be verified in practice yet.

ACKNOWLEDGEMENTS

The results of this project VI20152018005 were obtained with co-funding from the Ministry of the Interior of the Czech republic as part of targeted support from the project "Vývoj proti povodňových systémů pro zvýšení ochrany obyvatelstva a infrastruktury".

REFERENCES

1. FM GLOBAL: Approval Standard for Flood Abatement Equipment, Class Number 2510, FM APPROVALS LLC. 2013: Available at: . [https://www.fmglobal.com/assets/pdf/fmapprovals/2510.pdf].
2. MUTTRAY, M., OUMERACI, H.: Theoretical and experimental study on wave damping inside a rubble mound break water. Coast. Eng. 52 (8), 2005: p. 709–725.
3. D. MALCANGIO, M., TORRESI, G., PASCAZIO AND PETRILLO, A.F.: Numerical Simulations of Water Wave Propagation by Volume of Fluid Approach, 34th IAHR World Congress - Balance and Uncertainty 26 June - 1 July 2011, Brisbane, Australia.

Corresponding author:
Ladislav Ševčík, Technical University in Liberec, Czech Republic, Studentská 2, Liberec 46117

LOW-CYCLIC FATIGUE OF ADHESIVE BONDS REINFORCED WITH FIBRES

V. Šleger, M. Müller, J. Zavrtálek

Faculty of Engineering, Czech University of Life Sciences, Prague, Czech Republic

Abstract

The paper deals with a testing of a low-cyclic fatigue of single-lap bonds reinforced with a textile waste from a process of tyres recycling. The aim of the experiment is to clarify a fatigue behaviour (low-cyclic fatigue tests) of joints adhesive bonded with a two-component structural adhesive filled with the textile waste from the process of tyres recycling applied on the structural carbon steel S235J0. The aim of the research was to evaluate a service life of the adhesive bond in terms of its fatigue stressing at a low-cyclic shear test (30 % and 60 % from a reference value of a maximum force). The number of cycles was 200, 500 and 1000. Adding of the filler in the form of the Polyamide PA microfibers from the textile waste showed in a positive way. The adhesive bond strength was increased of 6 % to 11 %.

Key words: number of cycles, Quasi-static load, structural adhesive, textile waste, tyres recycling.

INTRODUCTION

A production process differs in various industrial branches, however, it has usually one common element – a creation of the bond. The adhesive bonding technology is a prospective method of connecting different materials (MÜLLER, VALÁŠEK 2013A; MÜLLER 2011).

A research on factors influencing mechanical properties of the adhesive bond is important for a successful application of adhesive bonds. The adhesive bond fatigue is a significant factor in terms of the practical application (MÜLLER, 2015A; MÜLLER ET AL., 2013; MÜLLER, VALÁŠEK, 2013B; MESSLER 2004).

Adhesive bonds are expected to retain a significant proportion of their load bearing capacity for the entire duration of the service life of the bonded structure. Service conditions can often involve an exposure to the cyclic fatigue, which is possibly the most destructive form of a mechanical loading. The fatigue damage is an irreversible process that can occur at relatively low stress levels due to the presence of high peel and shear stresses at the overlap edges. These stresses reduce both the static strength and fatigue life of bonded structures (BROUGHTON ET AL., 1999).

A particular issue with the integrity of adhesive bonds is the presence of cracks and flaws in the manufactured adhesive bond. The presence of these defects, at least at some scale, appears inevitably and the propagation of such cracks/flaws has the potential to affect the service life of the adhesive bonds and even to cause a catastrophic failure of bonded structures in the service (HAFIZ ET AL., 2010). Hence, a better understanding of the crack propagation behaviour under realistic types of combined service loading is an important aspect of evaluating the potential performance of adhesive bonds (KELLY, 2006; HAFIZ ET AL., 2010).

Adding the suitable filler into an adhesive (a matrix) decreases a price, or it improves mechanical properties of the adhesive bond (VALÁŠEK, MÜLLER, 2015). The filler is based on both a primary raw-material, as well as the waste. In recent years, ways for efficient use of the waste from the tyres recycling have been searching (MÜLLER, 2015B; FANG ET AL., 2000; FERREIRA ET AL.; 2013). A rubber granulate, a metal waste and a textile waste come into being from the mechanical process of the waste tyres recycling (KNAPČÍKOVÁ ET AL., 2014; ACEVEDO ET AL., 2015; MÜLLER, NOVÁK, 2015). The rubber granulate is used in the area of the tyres recycling at the present. The rubber granulate is effectively used in various products. However, we cannot forget other parts of the tyre, e.g. the textile fibres (TARANU ET AL., 2013; MÜLLER, 2015B; FANG ET AL., 2000; FERREIRA ET AL., 2013). Fibres are used for a large variety of applications. Textiles, nonwovens as well as fibre reinforced composite materials are commonly used in daily life and in technical applications (BARTL ET AL., 2015).

Results of a thermal analysis of the waste fibres show that the fibres are of polyamide. After the process of tyres shredding two main types of fibres can be identified: a fibre and a microfibre. In the first case, the fibres maintain their original form (cord), while the microfibers are a consequence of different stages in the shredding process (PARRES ET AL., 2009).

The aim of the research was to set a possible utilization of the cleaned textile waste from the process of the tyres recycling in an area of the polymeric composite systems determined as a filled adhesive. The microfibres from the shredding process of the tyres were used within the research. The aim of experiments is to clarify the fatigue behaviour (low-cyclic fatigue tests) of the bond adhesive bonded with the two-component structural adhesive filled with the textile waste from the process of tyres recycling applied on the structural carbon steel S235J0. The aim of the research was to evaluate the service life of the adhesive bond in terms of its fatigue stressing at the low-cyclic shear test.

MATERIALS AND METHODS

A great proportion of impurities in a form of the rubber granulate was removed from the textile waste used for experiments. This material was used as the filler for a production of the polymeric composite material. The cleaning of the textile microfibres from the rubber particles was performed by a fluid cleaning in a firm which provided the tested filler.

The subject of performed experiments was the polymeric composite, whose continuous phase was in a form of a two-component epoxy adhesive (CHS Epoxy 1200) and a discontinuous phase (reinforcing particles) in a form of Polyamide PA microfibres (the textile waste from the process of tyres recycling).

The concentration of the filler in the matrix is indicated by the wt. fraction of the filler. The determination of the concentration of the sub-components was expressed using a weight relative to 100 g of the matrix (the two-component adhesive). The filler was added into the matrix CHS Epoxy 1200 (two-component reactoplastics resin) in the ratio of 2 g and 4 g to 100 g of matrix. Weight ratios were chosen with a respect to a practical application when the filler is mixed mainly on the basis of weight ratios.

The basis of adhesive bonds laboratory testing was the determination of the tensile lap-shear strength of rigid-to-rigid bonded assemblies according to the standard ČSN EN 1465 (Equivalent is BS 1465).

Laboratory tests were performed using the standardized test specimens made according to the standard ČSN EN 1465 (dimensions 100 ± 0.25 x 25 ± 0.25 x 1.5 ± 0.1 mm and lapped length of 12.5 ± 0.25 mm) from the carbon steel S235J0.

The surface treatment is essential not only in the area of the adhesive bonding technology (MÜLLER, 2014; NOVÁK, 2012; HOLEŠOVSKÝ ET AL., 2012; DOBRÁNSKÝ ET AL., 2015; DOBRÁNSKÝ ET AL., 2014). The surface determined for the bonding was mechanically and chemically treated. The mechanical treatment consisted in a grit blasting of the bonded area by the Garnet MESH 80. The chemical cleaning consisted in removing impurities in a bath of Acetone.

Subsequently, the mixture of the adhesive was prepared by mixing of a part A (a resin) and a part B (a hardener) in a given ratio. The filler was added in the required ratio after mixing parts A and B.

Then, the adhesive was evenly applied on one bonded surface. The adhesive bonds were fixed with a weight of 750 g after applying second bonded part. The adhesive bonds were left for 7 days in the laboratory before the destructive testing. The reason was reaching the full strength of the adhesive bond and a minimization of the influence of the secondary hardening. Adhesive bonds hardened at the laboratory temperature 22 °C ± 2 °C.

Shims of the same thickness as the bonded material were adhesive bonded to the edges of the adhesive bonds after ending the hardening process. The reason was an elimination of the bending moment at the destructive testing of the adhesive bonds.

Laboratory tests were performed using the universal tensile strength testing machine LABTest 5.50ST (a sensing unit AST type KAF 50 kN, an evaluating software Test&Motion). The failure type according to ISO 10365 was determined at the adhesive bonds.

Five test specimens were tested in each series. The reference value of the adhesive bond strength was determined for each tested adhesive according to the standard ČSN EN 1465. The upper and lower limits for low-cyclic tests were calculated from the average value.

The test specimens were cyclically loaded in a such way the loading tension pulsated between the minimum value determined from the reference strength of the adhesive bond (i.e. 5 %) and chosen percentage value 30 % or 60 % from the reference strength of the adhesive bond with 0 g filler.

The loading speed at the static test of the adhesive bond strength was always set as $1\ mm \cdot min^{-1}$. The loading speed at the cyclic testing was always set as $30\ mm \cdot min^{-1}$. In the case that the adhesive bond was not destructive damaged after 200, 500 and 1000 cycles, the adhesive bond was subsequently broken, i.e. the testing machine developed force by the speed $1\ mm \cdot min^{-1}$ as long as the test specimens were broken.

Fracture surfaces and an adhesive bond cut was examined with SEM (scanning electron microscopy) using a microscope MIRA 3 TESCAN (the fracture surfaces were dusted with gold) and Stereoscopic microscope Arsenal.

The results of measuring were statistically analysed. Statistical hypotheses were also tested at measured sets of data by means of the program STATISTICA. A validity of the zero hypothesis (H_0) shows that there is no statistically significant difference ($p > 0.05$) among tested sets of data. On the contrary, the hypothesis H_1 denies the zero hypotheses and it says that there is a statistically significant difference among tested sets of data or dependence among variables ($p < 0.05$).

RESULTS AND DISCUSSION

A width of the microfiber was 24.38 ± 6.02 μm. A similar mean of the microfibers 29.67 ± 2.3 μm was ascertained also by PARRES ET AL. (2009). The length of the microfibre was very variable – 2424.63 ± 1805.86 μm. PARRES ET AL. (2009) also state very variable length.

A good wettability between the adhesive and the adhesive bonded material (Fig. 1) was proved using the electron microscopy within the experimental research.

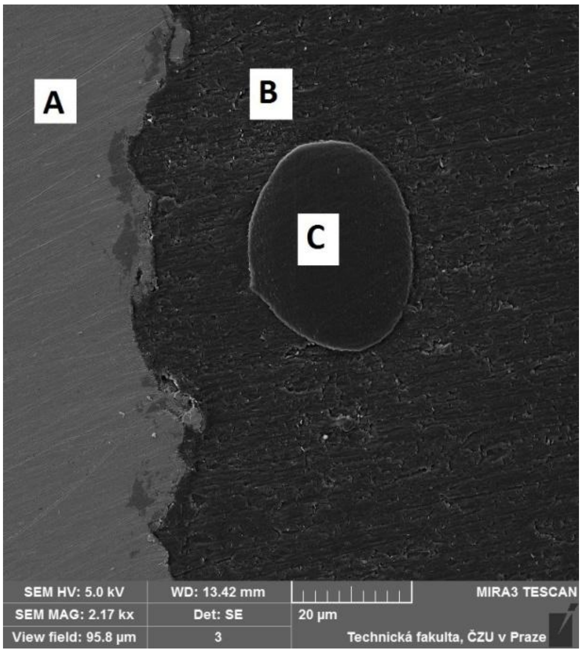

Fig. 1. – SEM images of adhesive bond cut: A - adherent S235J0, B – matrix CHS Lepox 1200 (two-component epoxy), C - microfibres of Polyamide PA from textile waste from process of tyres recycling

The surface roughness of the adhesive bonded material S235J0 after the mechanical treatment by a grit blasting was in the direction parallel to the loading force at the destructive testing of the adhesive bonds Ra 1.96 ± 0.17 μm, Rz 12.23 ± 1.31 μm.

The strength of the adhesive bond without the filler was 10.5 ± 1.4 MPa. Adding 2 g (11.1 ± 0.5 MPa) and 4 g (11.6 ± 1.0 MPa) of the filler increased the adhesive bond strength ca. of 6 % to 11 %. Adding the filler in the form of Polyamide PA microfibres from the textile waste from the process of tyres recycling showed in a positive way.

A type of a fracture surface changed after adding of the filler. The fracture surface of the matrix (the adhesive) was of the adhesive type. At the adhesive bonds (adhesive bonded with the composite system) the fracture surface was of the adhesive type. Results of the adhesive bond strength are visible from Fig. 2, 3 and 4.

It is possible to say in terms of the statistical testing of the influence of different filler concentrations that the concentrations are statistically homogeneous groups. The hypothesis H_0 was certified, i.e. there is no difference in the adhesive bond strength in the significance level 0.05 among single concentrations 0 g, 2 g and 4 g of the filler in the form of the Polyamide PA microfibres from the textile waste from the process of tyres recycling. The statistical comparison (T-test, $\alpha = 0.05$) of the influence of increasing filler concentration on the adhesive bond strength is presented in Tab. 1. It is evident from the statistical comparison of the values that increasing concentration of the filler did not statistically influence the adhesive bond strength.

It is possible to say in terms of the statistical testing of the influence of various numbers of cycles on the adhesive bond strength that the cycles are statistically homogeneous groups. The hypothesis H_0 was certified, i.e. there is no difference in the adhesive bond strength in the significance level 0.05 among single number of cycles (0, 200, 500 and 1000).

The statistical comparison (T-test, $\alpha = 0.05$) of the influence of the number of cycles on the adhesive bond strength is presented in Tab. 2. It is evident from the statistical comparison of the values presented in Fig. 2, 3 and 4 that the number of cycles does not statistically influence the adhesive bond strength.

Also a minimum difference between 30 % and 60 % of the loading from the reference value of the adhesive bond strength is obvious from the results. The average difference in the adhesive bond strength did not exceed 13 %.

Tab. 1. – Statistical comparison of influence of filler concentration on adhesive bond strength (T-test)

Loading from reference value of adhesive bond strength (%)	Number of cycles (-)	H_0: (p>0.05)
100	0	0.3259
60	200	0.2790
60	500	0.4609
60	1000	0.2973
30	200	0.3230
30	500	0.4396
30	1000	0.2922

Symbol O and C mean the outer part of root and the central part of root, respectively

Tab. 2. – Statistical comparison of influence of filler concentration and number of cycles on adhesive bond strength (T-test)

Loading from reference value of adhesive bond strength (%)	Filler concentration (g)	H_0: (p>0.05)
30	0	0.1553
30	2	0.3773
30	4	0.7025
60	0	0.2291
60	2	0.8335
60	4	0.1663

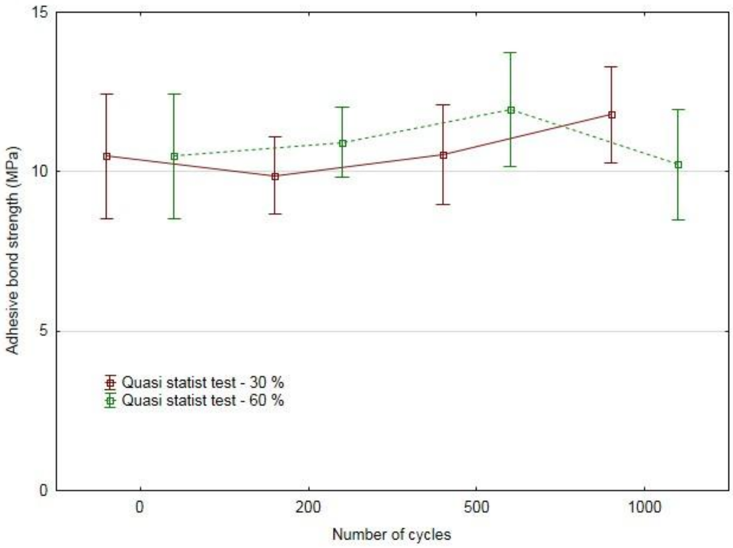

Fig. 2. – Influence of low-cyclic fatigue on adhesive bond strength (adhesive bonds with 0 g of filler)

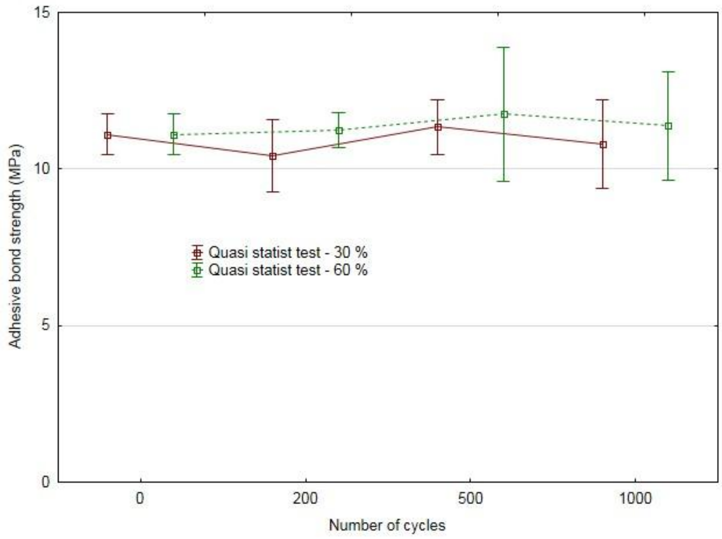

Fig. 3. – Influence of low-cyclic fatigue on adhesive bond strength (adhesive bonds with 2 g of filler)

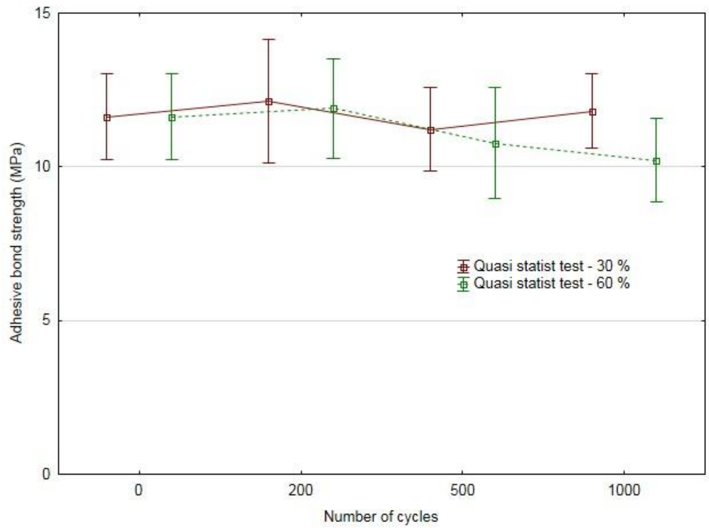

Fig. 4. – Influence of low-cyclic fatigue on adhesive bond strength (adhesive bonds with 4 g of filler)

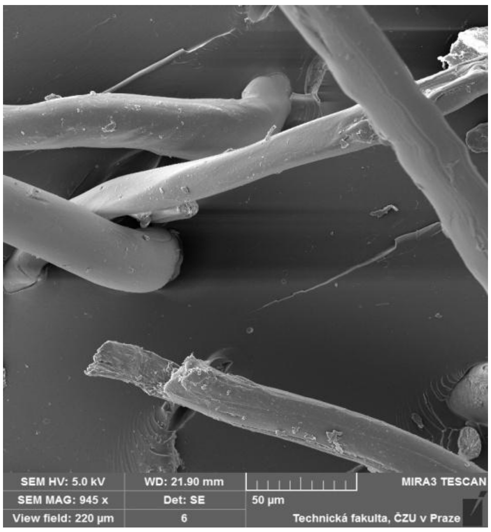

Fig. 5. – Fracture surface of sample (filler: microfibres of Polyamide PA from the textile waste from the process of tyres recycling 2 g: 100 g matrix, good wetting of filler with resin, uneven distribution of filler, secondary electrons)

A strong interaction between the adhesive and particles is evident (Fig. 1). When applying the filler into the resin, the wetting of the filler with the matrix is very important (JÄCKEL, SCHEIBNER, 1991). Results of the experiment also show the irregular stratification of filler microparticles in the matrix (Fig. 5).

CHANG AND YEIH (2001) proved in their experiments that the irregular shape of the filler ensured good interaction between the matrix and the filler. Microfibres of a regular cross-section were used as the filler within the experiment (Fig. 1). The assumption about a negative influence of the filler on the adhesive bond tensile strength was not confirmed (CHO ET AL., 2006). The course of the testing is visible from a diagram of the low-cyclic test. Fig. 6 presents the low-cyclic test at 60 %, which is finished after reaching 200 cycles by the destruction of the adhesive bond.

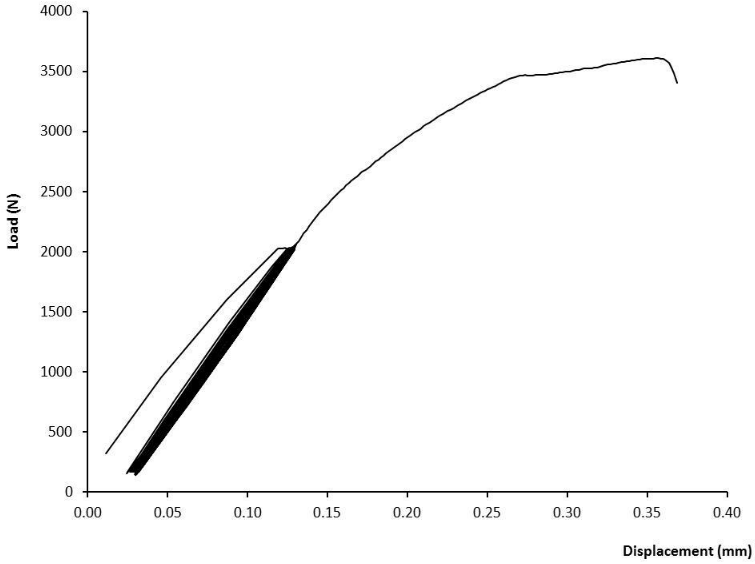

Fig. 6. – Low-cyclic test (60 %, 200 cycles, filler 4 g)

Fig. 7 presents the low-cyclic test at 60 %, which is finished after reaching 500 cycles by the destruction of the adhesive bond. A so called cyclic reinforcement occurred at some bonds after finishing the cycling. This entails an increase of the loading force after the end of the cycling.

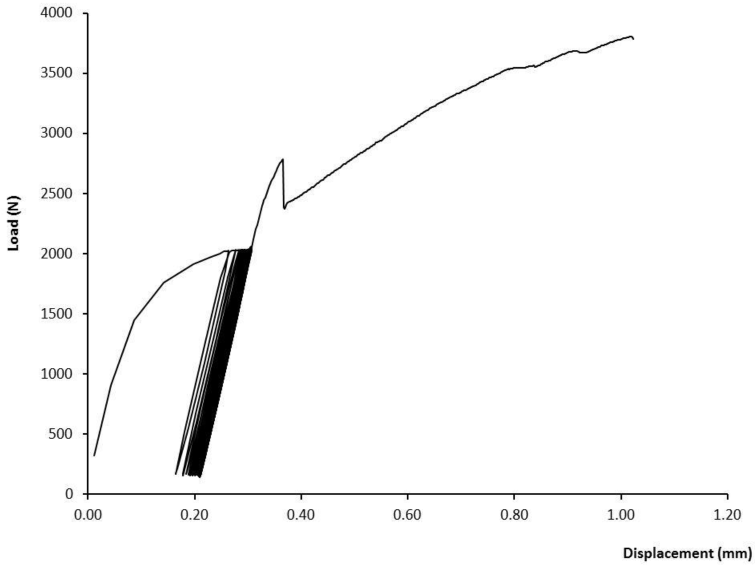

Fig. 7. – Low-cyclic test (60 %, 500 cycles, filler 0 g)

The experiment results did not confirm the assumption that the repeated cyclic loading with high value (i.e. e.g. 60 % (BROUGHTON ET AL., 1999; ŠLEGER, MÜLLER, 2015) of the reference strength of the adhesive bond) can lead to the premature failure of the adhesive bond in a relative short number of cycles. A cause can be a cumulative effect of the cyclic shear loading (ŠLEGER, MÜLLER, 2015).

CONCLUSIONS

Following conclusions can be deduced from performed experiments:

- The influence of the low-cyclic tests on the change of the fracture surface was not proved.
- The microfibres of Polyamide PA from the textile waste from the process of tyres recycling are of good wettability with the matrix.
- Adding the filler in the form of Polyamide PA from the textile waste from the process of tyres recycling showed in a positive way. It came to the increase of 6 % to 11 % of the adhesive bond strength.

It is possible to say in terms of the statistical testing of the influence of various filler concentrations and number of cycles that they both are statistically homogeneous groups, i.e. they do not influence the adhesive bond strength.

Acknowledgement

Supported by Internal grant agency of Faculty of Engineering, Czech University of Life Sciences Prague (Research on mechanical properties of multi-component polymer systems during their preparation, processing and application, 2016:31140/1312/3109).

REFERENCES

1. ACEVEDO, B., FERNÁNDEZ, A. M., BARRIOCANAL, C.: Identification of polymers in waste tyre reinforcing fibre by thermal analysis and pyrolysis. *Journal of Analytical and Applied Pyrolysis*, 111, 2015: 224-232.
2. BARTL, A., HAKL, A., MIHALYI, B., WISTUBA, M., MARINI, I.: Recycling of fibres materials. Process Safety and Environmetal Protection. *Trans. IChemE*, 83, 2015: 351-358.
3. BROUGHTON, W. R., MERA, R. D., HINOPOULOS, G.: Cyclic Fatigue Testing of Adhesive Joints, Test Method Assessment. Project PAJ3 - Combined Cyclic Loading and Hostile Environments 1996-1999, Report No 8, Centre for Materials Measurement & Technology, National Physical Laboratory, Teddington, 1999: 34 pp.
4. CHANG, J. J., YEIH. W. CH.: The effect of particle shape on bond strength improvement of epoxy particle coating composites. *Journal of Marine Science and Technology*, 9, 2001: 153-160.
5. CHO, J., JOSHI, M. S., SUN, C. T.: Effect of inclusion size on mechanical properties of polymeric composites with micro and nanoparticles. *Composites Science and Technology*, 66, 2006: 1941-1952.
6. DOBRÁNSKÝ, J., BARON, P., KOČIŠKO, M., VOJNOVÁ, E.: Monitoring of the influence of moisture content in thermoplastic granulate on rheological properties of material. *Applied Mechanics and Materials*. 616, 2014: 207-215.
7. DOBRÁNSKÝ, J., BARON, P., KOČIŠKO, M., BĚHÁLEK, L., VOJNOVÁ, E.: Solving depressions formed during production of plastic molding. *Metalurgija*, 54(3), 2015: 496-498.
8. FANG, Y., ZHAN, M., WANG, Y.: The status of recycling of waste rubber. *Materials and Design*. 22(2), 2000: 123-127.
9. FERREIRA, C. T., PEREZ, C. A. B., HIRAYAMA, D., SARON, C.: Recycling of polyamide (PA) from scrap tires as composites and blends. *Journal of Environmental Chemical Engineering*. 1, 2013: 762-767.
10. HAFIZ, T. A., ABDEL WAHAB, M. M., CROCOMBE, A. D., SMITH, P. A.: Mixed-mode fracture of adhesively bonded metallic joints under quasi-static loading. *Engineering Fracture Mechanics*, 77, 2010: 3434-3445.
11. HOLEŠOVSKÝ, F., NÁPRSTKOVÁ, N., NOVÁK, M.: GICS for grinding process optimization. *Manufacturing technology*. 12, 2012: 22-26.
12. JÄCKEL, M., SCHEIBNER, W.: Boundary layer induced modification of thermal and mechanical properties of epoxy resin composites. *Cryogenics*, 31(4), 1991: 269-272.
13. KELLY, G.: Quasi-static strength and fatigue life of hybrid (bonded/bolted) composite single-lap joints. *Composite Structures* 72, 2006: 119-129.
14. KNAPČÍKOVÁ, L., MONKA, P., HLOCH, S.: Composite Materials Reinforced with Fabric from Used Tyres. *Journal of Manufacturing and Industrial Engineering*. 12(3-4), 2014: 20-24.
15. MESSLER, R., W.: Joining of materials and structures from pragmatic process to enabling technology. Burlington, Elsevier, 2004: 816 pp.
16. MÜLLER, M.: Influence of surface integrity on bonding process. *Research in Agricultural Engineering*, 57, 2011: 153-162.
17. MÜLLER, M., HERÁK, D., VALÁŠEK, P.: Degradation limits of bonding technology depending on destinations Europe, Indonesia. *Tehnicki Vjesnik-Technical Gazette*, 20(4), 2013: 571-575.
18. MÜLLER, M., VALÁŠEK, P.: Comparison of variables influence on adhesive bonds strength calculations. *Manufacturing Technology*, 13(2), 2013a: 205-210.
19. MÜLLER, M., VALÁŠEK, P.: Influence of liquid contaminants on strength of adhesive bond on basic of two-component epoxy adhesive. In: *5th International Conference on Trends in Agricultural Engineering 2013*, Prague, Czech University of Life Sciences Prague, 2013b: pp. 441-445.
20. MÜLLER, M.: Setting of causes of adhesive bonds destruction by means of optical analysis. *Manufacturing Technology*, 14, 2014: 371-375.
21. MÜLLER, M.: Research on surface treatment of alloy AlCu4Mg adhesive bonded with structural single-component epoxy adhesives. *Manufacturing Technology*, 15(4), 2015a: 629-633.
22. MÜLLER, M.: Hybrid composite materials on basis of reactoplastic matrix reinforced with textile fibres from process of tyres recyclation. *Agronomy Research*, 13(3), 2015b: 700-708.
23. MÜLLER, M., NOVÁK, P.: Researches of liquid contaminants influence on change of hardness of agricultural tyre tread. *Research in Agricultural Engineering*, 61(1), 2015: 14-20.
24. NOVÁK, M.: Surfaces with high precision of roughness after grinding. *Manufacturing technology*. 12, 2012: 66 -70.
25. PARRES, F., CRESPO-AMORÓS, J. E., NADAL-GISBERT,

A.: Mechanical properties analysis of plaster reinforced with fiber and microfiber obtained from shredded tires. *Construction and Building Materials*, 23, 2009: 3182-3188.
26. ŠLEGER, V., MÜLLER, M.: Quasi Static Tests of Adhesive Bonds of Alloy AlCu4Mg. *Manufacturing Technology*, 15(4), 2015: 694-698.
27. TARANU, N., BANU, D., OPRISAN, G., BUDESCU, M., BEJAN, L.: Strengthening of thin reinforced concrete slabs with composite strips. *Romanian Journal of Materials,* 43(1), 2013: 3-13.
28. VALÁŠEK, P., MÜLLER, M.: Abrasive wear in three-phase waste-based polymeric particle composites. *Tehnicki Vjesnik-Technical Gazette,* 12(2), 2015: 257-262.

Corresponding author:
doc. Ing. Vladimír Šleger, CSc., Department of Mechanical Engineering, Faculty of Engineering, Czech University of Life Sciences Prague, Kamýcká 129, Praha 6, Prague, 16521, Czech Republic, phone: +420 22438 3173, e-mail: sleger@tf.czu.cz

SOLAR ENERGY CONVERSION IN PLANT LEAF STOMATA AS LEAF TEMPERATURE CHANGES

T. Ūksas, R. Čingienė, V. Kučinskas, A. Sirvydas

Aleksandras Stulginskis University, Lithuania

Abstract

The Sun provides energy to the Earth in the form of rays which is used by plants for biomass development. Biomass developed by plants can only release such amount of energy which matches the amount of solar radiation energy absorbed by plants in the biomass production process. The process of CO_2 assimilation involves complex biological and physical processes of energy exchange. The article presents information on how the plant uses changing thermal factors and processes in the habitat for intensifying the assimilation process. It analyses the processes of plant energy exchange stimulating the consumption of environmental carbon dioxide and at the same time the increase of biomass and the reduction of environmental air pollution. It has been found that in sunshine a thermal stomata engine (the biological prototype of heat engine) works in a plant leaf and generates mechanical energy at the expense of heat. The article presents the thermodynamic processes and cycle of the plant leaf stomata engine. Mechanical energy developed in a plant leaf is used to intensify the process of assimilation by activating leaf energy and gas exchange with the environment.

Key words: plant energy exchange, thermal processes, plant leaf temperature.

INTRODUCTION

The Sun provides energy to the Earth in the form of rays. Theoretically, the utilisation rate of the solar energy absorbed by plants for the production of organic matter could represent around 20 to 25 % (ŠLAPAKAUSKAS, 2006; ІЛЬКУН, 1967). In practice, only around 2 % of the absorbed solar energy is used for photosynthesis. Visible light absorbed by plants accounts for 80 to 85 %, light reflected by them – 10 % and light conducted through leaves – 5 to 10 % (FITTER, HAY, 2002; ŠLAPAKAUSKAS ET AL., 2008). The share of the absorbed solar energy representing 96 to 98 % in the plant leaf is converted into energy in the form of heat. Due to a small mass and biologically limited maximum temperature (58 °C) STAŠAUSKAITĖ (1995) and LEVITT (1980) of their tissues thin plant leaves are not able to accumulate released heat. Therefore, the solar energy transformed into heat in plant leaves has to be released, in the form of heat and water vapour, to the environment as a metabolite. Heat released to the environment from energy exchange between the plant and the environment is of little value (low temperature) and non-concentrated and is, therefore, not used for further transformation in technological-energy processes. Plant energy exchange together with the process of assimilation form an important nature's generative and regenerative system by creating conditions for the existence of life on Earth (MARTIN AND HENRICHS, 2010).

In the course of its development the plant has adapted, to the maximum extent, to the natural conditions of its habitat. By their anatomic structure plant organs of different biological purpose have accommodated as far as possible to the biological and environmental physical factors inside them making it possible to use all available driving forces for the plant's vital function. The plant uses wind and gravitational forces which are created around it by temperature, humidity and gas concentration gradients. Heat conversion processes take place in plant leaf stomata transforming the thermal energy of low potential into mechanical energy. The mechanical energy generated in a plant leaf is used as a driving force to prevent friction caused by leaf gas exchange with the environment and intensify the processes of exchange, necessary for the process of assimilation in daylight (SIRVYDAS ET AL., 2011).

An analysis of thermal processes taking place in the conversion of the solar energy into mechanical one in a plant leaf at changing plant leaf temperature is presented here.

MATERIALS AND METHODS

The work employed the method of the balance of energies in a plant. The temperature of a plant growing in natural environmental conditions was measured by thermocouple temperature sensors made of Cu-

CuNi (copper-constantan) wires, 0.05 mm in diameter. To maintain the same resistance of the sensors, only wires of equal length were used. The measurements were recorded with an instrument ALMEMO 2590-9 having a microprocessor data processing and accumulation system. Temperatures were recorded by necessity taking a maximum of 100 measurements per second. This enabled us to observe short-term dynamic processes of temperature changes. Temperature sensors for all temperature measurements were used in observance of the requirements to be met by temperature measurements (in respect of the plant and its environment) (СИРВИДАС AND ЮШКА, 1973; SIRVYDAS ET AL., 2006).

Research object – thermal-thermodynamic processes taking place in a plant leaf during the process of CO_2 assimilation. The physical processes of metabolism and energy exchange occurring in the plant are directly related with the plant's vital processes. To maintain the plant's vital processes, the physical processes responsible for the plant's energy-mass exchange must satisfy assimilation needs in daylight and bio-energy needs during hours of darkness. Processes taking place in the plant leaf ↔ environment exchange system can only be analysed after the structure of a plant leaf and the processes (physical and biological) occurring inside it have been examined. While carrying out the analysis of literature it has become observed that physical processes taking place in the plant leaf have been insufficiently examined (ŠLAPAKAUSKAS AND DUCHOVSKIS, 2008; NOBEL, 2001; NEW AP BIOLOGY CURRICULUM UNITS, 2013).

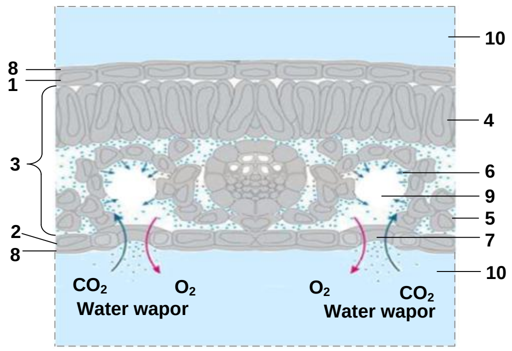

Fig. 1. – Chart of plant leaf anatomic structure and gas exchange (CO_2, O_2, H_2O vapour) with the environment. 1 – upper epidermis, 2 – lower epidermis, 3 – mesophyll, 4 – palisade tissue, 5 – spongy tissue, 6 – system of gas channels, 7 – stoma opening, 8 – cuticle 9 – gaseous environment in the spongy tissue of a leaf, 10 – ambient air surrounding the leaf

While analysing the structure of a plant leaf section we have noticed that the upper and lower surfaces are covered by upper epidermis 1 and lower 2 epidermis, respectively (Fig. 1). The thickness of leaves exposed to bright light and exposed to shadow differs (e.g. the leaves of beach (*Fagus sylvatica*) are 210–90 µm thick. The primary leaf tissue between epidermis laminae is mesophyll 3 which is responsible for the process of assimilation. The mesophyll consists of two layers – palisade tissue 4 and spongy tissue 5. The palisade tissue (palisade parenchyma) is a tissue best adapted for photosynthesis. More than 80 % of chloroplasts in a leaf (conducting the process of assimilation) occur in the palisade tissue, in the upper layer of mesophyll (DAGYS ET AL., 1974)The thickness of this layer accounts for a mere 30 % of the leave thickness.

Large intercellular spaces form among the cells of spongy parenchyma making a gas exchange system of stomata 7 and mini-, macro- and nano-channels 6. The intercellular spaces occupy a large surface area of mesophyll cells by which they come into direct contact with air circulating in the gas exchange system. That surface is called the internal surface of a leaf. The leaf external to internal surface ratio in the plants of different ecological groups is not the same. It is known that the internal leaf surface of plants exposed to shadow (heliophobic plants) is by 6.8 – 9 times, that of mesophytes by 11.0-20.0 times, and that of leaves exposed to bright light is by 17.2 to 31.3 times larger than their external surface. Hence, having a big surface of contact with air mesophyll cells can absorb carbon dioxide from it. Since on both sides a leaf is covered by the epidermis with the cuticle which nearly does not allow water vapour and gas to pass through, air and carbon dioxide enter the leaf through stomata (ŠLAPAKAUSKAS AND DUCHOVSKIS, 2008; NOBEL, 2001; DAGYS ET AL., 1974).

A leaf area unit contains a large number of stomata: from 23 to 400 in 1 mm^2. They are very small. In leaves of different plants the area of stoma opening varies between 0.17 and 239 μm^2, and the total area of their openings accounts for 0.52-5.28 % of the leaf surface. Nevertheless, about 90 to 95 % of CO_2 gets into a leaf through stomata and hardly 5 to 10 % spread through the epidermis or cuticle (ŠLAPAKAUSKAS AND DUCHOVSKIS, 2008; NOBEL, 2001; DAGYS ET AL., 1974). The literature analysing the anatomic structure of the spongy mesophyll of a plant leaf presents very different charts of water vapour movement and carbon dioxide entry into a plant leaf through stomata (ŠLAPAKAUSKAS AND

DUCHOVSKIS, 2008; KEITH, 2000; NEW AP BIOLOGY CURRICULUM UNITS, 2013). It is clear, however, that together with ambient air CO_2 enters the spongy tissue of a leaf through open plant leaf stomata, and plant metabolites (O_2 and water vapour) are released to the environment through them. Many charts show that each stoma is responsible for its own system of gas exchange. In our opinion, the most precise and comprehensive system of leaf gas exchange related to the anatomic structure of a leaf is presented in Fig. 2.

The anatomic structure of a plant leaf with mini-, macro- and nano-channels and physiological processes occurring therein is relevant to all fields of live nature and technological sciences (ŠLAPAKAUSKAS AND DUCHOVSKIS, 2008; SIRVYDAS ET AL., 2011; SAJITH ET AL., 2011). Recently, little attention has been devoted to the examination of thermal-thermodynamic processes taking place in plant leaf channels-cavities and the opportunity to transform their heat into mechanical energy (SIRVYDAS ET AL., 2011; SIRVYDAS ET AL., 2013). A CO_2 gas mass from the ambient air is moving in the direction of a plant leaf surface in the air layer surrounding the leaf. Heat, H_2O vapour and O_2 also move in the same surface air layer of a plant leaf, in the opposite direction though. Hence, two very complex flows of opposite directions simultaneously form on the plant leaf surface.

RESULTS AND DISCUSSION

Experimental investigations show that air temperature around plants in sunshine is changing (Fig. 2).We observed fluctuations in plant leaf temperature (Fig. 3)and temperature difference (Fig. 4) in natural environmental conditions in sunshine. We have found that temperature changes in a plant leaf and ambient air depend on a number of energy exchange and environmental processes which are described in publications (SIRVYDAS ET AL., 2010; SIRVYDAS ET AL., 2011).

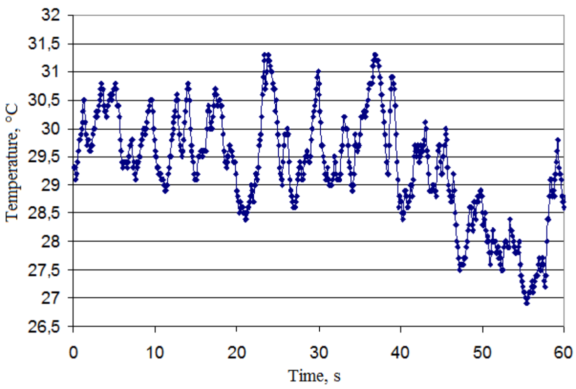

Fig. 2. – Fluctuations in air temperature around a plant in natural environmental conditions in sunshine. Wind speed v_{vid} = 1.1 m/s.

Biological processes taking place inside a plant leaf depend on plant tissue temperature. As the data of investigation show, the temperature of the plant leaf and of the air around it is continually changing during the sunny period of the day. During a long period of its development the plant has accommodated as far as possible to environmental factors using them for its vital functions. It is advisable to analyse the impact of change in plant leaf and ambient temperature (as a thermal factor) on the process of assimilation which is responsible for the existence of life on Earth.

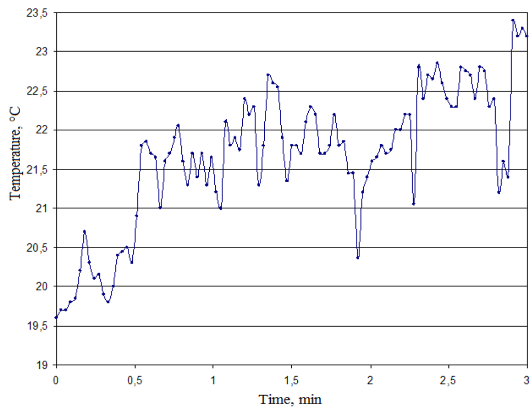

Fig. 3. – Fluctuations in air temperature around a plant in natural environmental conditions in sunshine. Wind speed $v_{vid.}$ = 5.3 m/s.

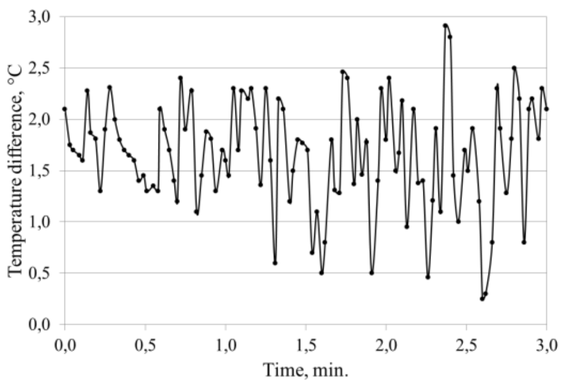

Fig. 4. – Change in the difference of temperature between a plant leaf and the environment in natural environmental conditions in sunshine

All biological and energy transformation processes occurring in a plant leaf depend on the local temperature of a plant leaf. The local temperature of a plant leaf is the result of the local balance of energies in the plant leaf. In general, during the sunny period of the day as leaf exposure with regard to the Sun changes, the plant leaf receives pulsating radiation energy flow Q_{rad} (SIRVYDAS ET AL., 2010). Due to the vertical and horizontal movement of airflows of changing temperature the plant leaf is affected by pulsating convective heat flowQ_{convec}. Pulsating heat flows Q_{rad} and Q_{convec}. will cause the pulsations of accumulated heat flow Q_{accum}. in a plant leaf. In this case of plant leaf energy exchange we can use the following equation for the balance of energies in a plant leaf:

$$\pm Q_{acum} \pm Q_{rad} \pm Q_{convec} = 0 \qquad (1)$$

The pulsating process of heat accumulation will cause temperature pulsations in plant tissues by value Δt. The pulsating temperature of plant leaf tissues in gas cavities (mini-, macro- and nano-cavities, channels) will generate respective thermodynamic processes. The thermodynamic processes in plant leaf cavities may participate in the transformation of heat into mechanical energy if the following conditions of the second law of thermodynamics are satisfied:

1. The process of heat conversion into mechanical work requires processes of periodically changing nature. This condition has been satisfied as plant leaf temperature is changing in sunshine. The temperature of the plant leaf and air around it is continually changing in sunshine (SIRVYDAS ET AL., 2011).
2. Heat sources of different temperatures have to participate in the process of heat conversion into mechanical energy. During the sunny period of the day this condition is satisfied. The solar radiation energy absorbed by plant leaves and the ambient air surrounding them are two heat sources of different temperature participating in energy exchange in plant leaves.

While analysing processes in plant leaf cavities we can see that when plant leaf temperature drops, the process of heat release to the environment takes place. During this process gas volume in leaf cavities decreases. This leads to the forced intake of ambient air into the gas cavities of a leaf. When plant leaf temperature rises, the process of heat supply to a leaf takes place. During this process temperature and pressure in the gas cavities of a plant leaf increase. The process of gas expansion takes place. Part of gas present in the cavities of a plant leaf is released to the environment through leaf stomata. As changes in plant leaf temperature repeat, processes recur and the cycle begins all over again. That means that a biological prototype of the thermal engine exists in a plant leaf which creates, for the account of heat, mechanical energy for gas movement through stomata and for the destruction of parietal layers (of heat and mass exchange) on a leaf surface. It works in sunshine. Mechanical energy developed in a plant leaf is used to intensify the process of assimilation by activating gas exchange with the environment.

As regards the transformation of heat energy into mechanical energy, we usually assume that a mechanical engine of a certain structure is required for that purpose. However, there are engines which produce mechanical energy by a gas flow. The potential energy of pressure is converted into kinetic one, while the latter – into mechanical work. Technically, the transformation of potential energy to kinetic energy occurs in special tubes (de Laval nozzles). The combination of plant leaf cavities, channels and stomata is very similar to the design and operating principles of a rocket (jet) engine.

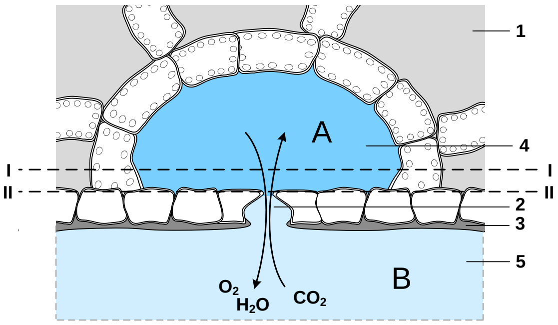

Fig. 5. – Chart showing the system of the gas cavities (mini, macro and nano), channels and stomata of a plant leaf. A – cavity in a plant leaf; B – ambient environment of a plant leaf; I–I, II–II – outside positions of alleged membrane. 1 – spongy tissue, 2 – stoma opening, 3 – cuticle 4 – gas environment in the spongy tissue of a leaf, 5 – ambient air in leaf surroundings

Energy transformations in a plant leaf are possible only during the sunny period of the day in the presence of leaf temperature pulsations. It is difficult to accurately describe the thermodynamic processes of heat transformation to mechanical energy in a plant leaf and to form a thermodynamic cycle. This is because a plant leaf is a live organism of the plant in which complex biological and physical processes are taking place simultaneously. The environment as well as biological (assimilation) processes and their intensity have an impact on the progress of physical processes in leaf cavities, channels and stomata, the biological mechanism of stomatal guard cells manifests itself. Therefore, to understand physical processes taking place in the gaseous cavities of a leaf they need to be idealised and charted as is often done in thermodynamics.

A chart of the gas cavities and channels of a plant leaf is presented in Fig. 5 for the purpose of analysing thermodynamic processes taking place in them and the operating principle of the thermal engine working in a plant leaf.

For the thermodynamic analysis of cycles the assumption is made that the same amount of air (absolutely dry in this case) in the gas cavities of a plant leaf is used in the cycle. To analyse thermodynamic processes taking place in leaf cavities an alleged membrane dividing the analysed gas cavity volume in a plant leaf into to two parts is used. In the course of thermodynamic processes in cavity A air mass remains constant. Its volume may change depending on pressure and temperature. Cavity B has contact with ambient air through a stoma channel. As volume A changes, ambient air enters cavity B through the leaf stoma or is released into the environment through it. (Fig. 1). In the case of constant energy exchange when plant leaf temperature is the highest air volume in cavity A (Fig. 1) will be maximum and in cavity B – minimum (cavity B = 0). At this moment pressure in the leaf cavity is equal to ambient air pressure and the alleged membrane will be in position II–II.

Point 1 represents the thermodynamic state of the air in cavity A in the coordinate system *pv* (pressure–volume) (Fig. 6). In point 1 the volume of cavity A is maximum and pressure *p* equals the atmospheric pressure.

As the temperature of the plant leaf drops pressure in cavity A decreases and vacuum forms. Pressure in environment B exceeds pressure in plant leaf cavity system A. Due to the formed difference in pressures ambient air enters the plant leaf cavity through the stoma moving the alleged membrane from position II–II to position I–I. When ambient air enters cavity B vacuum in cavity A does not reach the maximum value but is maintained at a certain constant level $p_2 = const$, which depends on the size of the leaf cavity and the hydraulic resistance of the leaf stoma channel. Depending on occurring biological processes the plant leaf may change the dimensions of the stoma channel (in this aspect biological channels have an advantage over static energy transformation channels used in technologies). Therefore, as temperature in cavity A drops (during the cooling process), the pressure difference between cavity A and the ambient environment remains constant ($p_1 - p_2 = const$), the volume of cavity A decreases. When the minimum temperature is reached in cavity A (point 3) the compression process in the cavity of the plant leaf continues due to higher pressure in the ambient environment. It is a polytropic compression process. It continues as long as pressure in cavity A becomes the same as pressure in the ambient environment (point 4).

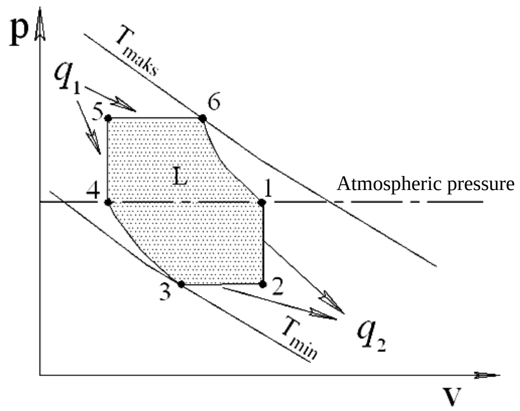

Fig. 6. - The thermodynamic cycle of the thermal engine working in the plant leaf gas system in the *pv* (pressure *p*, volume *v*) coordinate system. L – area of the cycle; 1, 2, 3, 4, 5, 6 – characteristic points of thermodynamic states describing the parameters of plant leaf cavities (explanation is in the text)

At the end of adiabatic compression (without heat exchange with the environment in process 3-4) volume in plant leaf cavity A reaches the minimum value. The alleged membrane reaches the outside position of minimum volume I–I.

As plant leaf temperature rises (solar energy is absorbed) pressure in plant leaf cavity A increases reaching the maximum value in point 5. As temperature in cavity A continues to increase, the difference in pressures in cavity A and ambient environment remains constant $p_5 - p_4 = const$. The Volume of cavity A increases pushing the alleged membrane towards position II–II. When the maximum temperature is reached (point 6), higher pressure in plant leaf cavities A leads to the polytropic expansion process as pressure drops to continue until the pressures reach the balance in point 1. At the end of polytropic expansion (in process 6–1) leaf cavity volume reaches the maximum value in point 1. The alleged membrane reaches the outside position of maximum volume II–II.

The cycle is completed and returns to the initial position. A new wave of plant leaf temperature change will repeat the aforesaid cycle in the gas system of a plant leaf.

Processes taking place in plant leaf gas cavities are charted. That facilitates an investigation aimed at proving that the heat engine of mini-micro sizes producing mechanical energy is present in the system of plant leaf gas cavities during the sunny period of the day. Although real processes occurring during this cycle deviate from the theoretical processes discussed above, the fact that such an engine does exist in the plant leaf has been explained. Basing on the laws of thermodynamics we may state that mechanical work L performed by the processes of gas exchange in a plant leaf during the sunny period of the day is represented in the *p-v* (pressure– volume) coordinate system by cycle area 1–2–3–4–5–6–1 (Fig. 6.).

This article presents the thermodynamic analysis of the world's smallest heat engine working in a live plant leaf during the sunny period of the day. The number of engines in 1 mm^2 matches the number of stomata in the system of plant leaf gas exchange (up to 400).

CONCLUSIONS

1. In sunshine, as the temperature of plant leaf tissues changes, thermal parameters in the gas cavities of a leaf change, which leads to respective thermodynamic processes.

2. In sunshine, a thermal stomata engine (the biological prototype of a heat engine) works in a plant leaf and generates mechanical energy at the expense of heat.

3. Mechanical energy developed in the plant leaf intensifies the process of assimilation by activating leaf energy and gas exchange with the environment.

4. Plant energy exchange together with the process of assimilation form an important nature's generative and regenerative system by creating conditions for the existence of life on Earth.

REFERENCES

1. ŠLAPAKAUSKAS, V.: Augalųekofiziologija. Lietuva, Kaunas 2006.
2. ІЛЬКУН,Г.М.: Енергетичнийбалансрослин. УкраинаКиев 1967.
3. FITTER, A., HAY, R.: Environmental physiology of Plants. Academic press. 2002.
4. ŠLAPAKAUSKAS, V., DUCHOVSKIS, P.: Augalųproduktyvumas. Lietuva 2008.
5. STAŠAUSKAITĖ, S.: Augalųvystymosifiziologija. Lietuva, Vilnius 1995.
6. ELLWAGNER, T., BINGHAM, JR., CHAPELL, S.: We and Tolin SA. Cytological effects of ultra-high temperatures on Corn. Weed Sciennce, 1973: pp. 299-303.
7. LEVITT, J.: Response of plants on environmental stresses. Academic Press. New York 1980.
8. MARTIN, J., HENRICHS, T.: The European environment. *European Environment* Agency. 2010.
9. SIRVYDAS, A., KERPAUSKAS, P., KUČINSKAS, V.: Augalųenerginėapykaita. Lietuvos Žemės Ūkio Universitetas. Lietuva, Akademija 2011: pp. 22.
10. СИРВИДАС, А., ЮШКА, В.: Измерениетемпературырастений в микроклиматических и физиологическихисследованиях. Лит. НИИ лесногохоз-ва. Каунас, 1973: 34 с.
11. SIRVYDAS, A., KERPAUSKAS, P., NADZEIKIENĖ, J., STEPANAS, A., TEREŠČIUK, V. S.: Temperature measurements in research of thermal weed extermination. Proceedings of the international conference Development of agricultural technologies and technical means in ecological and energetic aspects. Lithuania. Raudondvaris. No.11, 2006: pp. 321-331.
12. NOBEL, P. S.: Physiological and Environmental Plant physiology. *Academic press*. 1991: 635 p.
13. KEITH, A., MOTT AND THOMAS, N, BUCKLEY.: Patchy stomatal conductance: emergent collective behaviour of stomata. *Trends in plant science*. 2000: pp. 258-262.
14. GAS EXCHANGE IN PLANTS: Available at: http://www.cartage.org.lb/en/themes/sciences/botanicalsciences/photosynthesis/ GasExchange/GasExchange.htm.
15. COLORADO STATE UNIVERSITY: CMG garden notes. Available at: http://www.ext.colostate.edu/mg/Gardennotes/144.html.
16. NEW AP BIOLOGY CURRICULUM UNITS: 2013. Available at: http://supercoolandawesome.blogspot.com/2013/05/gas-exchange-in-aquatic-and-terrestrial.html.
17. DAGYS, J., BLUZMANAS, P., BORUSAS, V., ŠLAPAKAUSKAS ,V.: Augalųfiziologija. Lietuva, Vilnius 1974.
18. SAJITH, V., HARIDAS, D., SOBHAN, C. B.: Reddy Convective heat transfer studies in macro and mini channels. International Journal of Thermal Sciences. 2011: pp 239-249.
19. SIRVYDAS, A., NADZEIKIENĖ , J., KERPAUSKAS, P., ŪKSAS, T.: The principle of heat conversion into mechanical work. *Mechanika*. 2013: pp 358 – 362.
20. SIRVYDAS, A., KUČINSKAS, V., KERPAUSKAS, P., NADZEIKIENĖ, J., KUSTA, A.: Solar radiation energy pulsations in a plant leaf. Journal of Environmental Engineering and landscape management. 2010: pp. 188-195.
21. SIRVYDAS, A., KUČINSKAS, V., KERPAUSKAS, P., NADZEIKIENĖ, J.: Theoretical modeling of temperature pulsations in plant leaf which are caused by leaf swing with respect to the sun. Journal of Environmental Engineering and landscape management. 2011: pp. 251–259.

Corresponding author:

Tomas Ūksas.Aleksandras Stulginskis University, Faculty of Agricultural Engineering, Institute of Energy and Biotechnology Engineering., Studentu 15, LT-53361 Akademija, Kaunasm phone. +37037 75 22 19, e-mail: acikuraci@gmail.com

ESTIMATION OF SOIL PENETRATION RESISTANCE USING GENERALIZED REGRESSION NEURAL NETWORKING

İ. Ünal[1], Ö. Kabas[1], S. Çetin[1], M. Topakci[2]

[1]*Akdeniz University, Vocational School of Technical Science, Antalya, Turkiye*
[2]*Department of Agricultural Machinery and Technologies Engineering, Faculty of Agriculture, Akdeniz University, Antalya, Turkiye*

Abstract
Soil compaction is a major problem affecting negatively the soil physical, chemical and biological properties and impedes plant root growth. Soil penetration resistance values should be collected from many points of the production area to determine the effects of these problems on plant growth. Soil penetration value collection from large production areas is time-consuming and tedious application for researchers. Also, the number of measurement points to what extent will be sufficient to evaluation on whole production area is not clear. To eliminate this ambiguity, soil penetration values of the unmeasured points should be estimated to evaluate the whole area. Artificial neural networks are one of the most popular mathematical computing and modelling method used to estimate unknown data values with known data values. In this study, we collected 1603 samples of geographical position and soil penetration value from 40 cm depth within the 20 ha field. From the 1603 values, 24% records were selected for testing and the remaining 76% records were used for educating and validating. Soil penetration values of the unmeasured points were estimated using Generalized Regression Neural Network (GRNN) method in Matlab. In addition to mean squared error (MSE), root mean square error (RMSE), mean absolute error (MAE) and R^2 has been also used for evaluation of prediction accuracy on GRNN method. The results showed very good agreement between the predicted and the measured real values of soil penetration resistance.

Key words: artificial neural networks, estimation, soil penetration resistance, GRNN.

INTRODUCTION

The tractors, tillage tools and the machine systems which are used in the agricultural production can cause field traffic. Especially today's machines such as powerful tractors, combine harvesters etc. which are becoming heavier because of their additional attached equipment, have become a reason for high level of soil compaction observed in agricultural fields. Another reason for soil compaction is tillage in non-suitable terms of the soil. In addition to these external effects, natural effects such as excessive rainfall and drought can also be a reason for high levels of soil compaction (PORTERFIELD ET AL., 1986; TEKIN ET AL., 2008).

Soil compaction can be defined as a function of the specific weight and humidity of the soil. During compaction, soil particles get closer each other and a diminishing of the entrapped air is seen. As a result; an increase is seen for soil bulk density and soil penetration resistance (CARRARA ET AL., 2007; RAPER, 2005). Soil compaction has also a negative effect on the physical, chemical and biological properties of the soil. This negative effect limits roots growth and the plants cannot complete their growth properly. Hence, less yield and economic losses are seen. In addition to this, the machines, which are operating on the compacted soil need extra energy (AL-ADAWI ET AL., 1996; ADAMCHUK ET AL., 2003). Therefore, the determination of the soil penetration resistance level is quite important for sustainable production, yield and conservation of the farmland. It also has a place in the precision farming approach, which promises that the field performance could be tracked, mapped and analyzed down to the square meter level so that farmers can know how well or poorly each part of a field is producing (TEKIN, 2010).

Agriculture sector plays major role directly or indirectly in improving economy of developing countries. Sustainable and competitive agricultural production can be made by using electronic and computer technology. Also, information, data or knowledge is one of the most importing factors for the precision agriculture technology. To make the right decisions in agriculture production, we should collect more data from large production areas. But, data collection process such as soil penetration data is time-consuming and tedious application for researchers. For this reason, researchers can use estimation techniques. In this context, the use of Artificial Neural Networks (ANN) can be considered an alternative approach for predicting soil penetration resistance. ANN have been employed to solve many problems in agriculture (ERZIN ET AL., 2010; KIM AND GILLEY, 2008). VARELLA ET AL. (2002) used ANN for the determination of land cover from digital images. KHAZAEI AND DANESHMANDI (2007) used ANN to model the drying kinetics of sesame seeds. They concluded that the ANN technique presented better results than traditional mathematical modeling. SARMADIAN ET AL. (2009) used ANN to model soil properties, and the results were better than the multivariate regression analysis, showing the effectiveness of the ANN technique. Recently, TRIGUI ET AL. (2011) used ANN model to predict sugar diffusivity as a function of date variety, temperature and diffusion period.

Artificial neural networks have been used to estimate parameters on different soil science struggles, like vegetation cover (KIMES ET AL., 1998; BUENDÍA ET AL., 2002; MENA AND MONTECINOS, 2006; BOCCO ET AL., 2007), soil hydrodynamics (MANETA AND SCHNABEL, 2003; RUBIO, 2005), soil erosion hydrodynamics (MAS ET AL., 2002), underground water contamination (REBOLLEDO ET AL., 2002; RODRÍGUEZ, 2009; GARCÍA ET AL., 2010), however there are few reports on variables related to mechanical properties of the soil. HALGUIN ET. ALL (2011) reported that the elaboration of an Artificial Neural Network for the estimation of soil penetration resistance at different depths, considering as influential variables humidity, density, static load, and inflate pressure. The best estimation results were obtained at a depth of 20-30 cm. BAYAT ET AL. (2007) were compared neural networks, linear and nonlinear regression techniques to model penetration resistance. The results further showed that ANN models performed better than nonlinear regression models. ABREQUIE ET AL. (2014) were evaluate in short-term the impact of different tillage systems in organic farming (traditional tillage to superficial tillage without reversal) on soil resistance to penetration. The results showed very good agreement between the predicted and the desired values of soil resistance (R^2 = 0.98). The objective of the present research is to estimate soil penetration resistance values for unmeasured points on farm land using generalized regression neural networking.

MATERIALS AND METHODS

Experiment field and soil

The field experiments using the system were carried out in agricultural research area of Akdeniz University. The experimental field is 20 ha in size. The research area is located approximately 20 km from Antalya between the coordinates of 30.84 E and 36.94 N. The soil type is clay-loam and consists of 41% sand, 26% silt, 33% clay. Content of organic matter was 1.3%. Soil bulk density, water content and soil resistance values were determined as 1.32 g/cm^3, 7.5%, and 1.45 MPa at a depth between 0 and 20 cm, and 1.38 g/cm^3, 8.9%, 1.89 MPa at a depth between 20 and 40 cm, respectively.

Data collection

The horizontal penetrometer was used in this study. It was developed in our previous study (TOPAKCI ET AL., 2010). The designed system was connected to a Massey Ferguson 3095D four-wheeled tractor (Fig. 1). During the experiments, some small variations were seen in the tractor speed, even though care was taken to keep the tractor speed at a constant value to avoid any negative effect of speed changes on the penetration resistance. The experiments were carried out in a field shortly after a wheat harvest and measurement values of 40 cm operation depth and 15 m linear intervals were obtained. Much research indicates that the depth of the hard pan is mostly between 30 and 60 cm. The depth of 40 cm has been chosen as working depth to get data on the hard pan level of the field. The average speed of 2.39 km h^{-1} was calculated according to data from the GPS receiver. Forward speeds of 1.80 km h^{-1} and 2.96 km h^{-1} were determined as the minimum and maximum values, respectively. The time interval for the entire measurement was set to 1 second and 1816 data points were stored in the database.

Generalized Regression Neural Networks

In the literature, the fundamentals of the GRNN can be obtained from SPECHT (1991); NADARAYA (1964) KERNEL REGRESSION, TSOUKALAS AND UHRIG (1997), also SCHIOLER AND HARTMANN (1992). A diagrammatic of the GRNN is given in Fig. 2. A general regression neural network (GRNN) does not require an iterative training procedure. It can approximate any arbitrary function between input and output vectors, drawing the function estimate directly from the training data. Furthermore, it is consistent; that is, as the training set size becomes large, the estimation error approaches zero, with only mild restrictions on the function. The GRNN is used for estimation of continuous variables, as in standard regression techniques (NESIL ET AL., 2011).

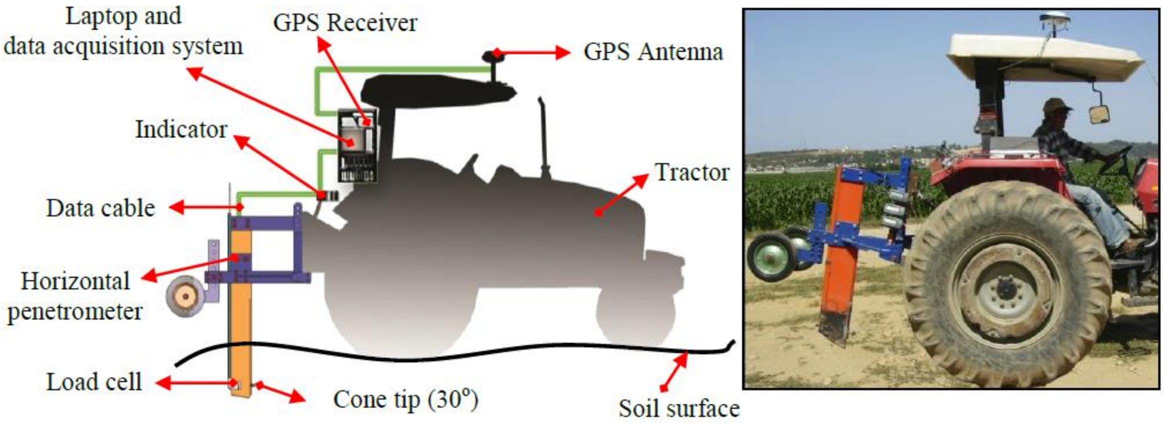

Fig. 1. – Horizontal penetrometer

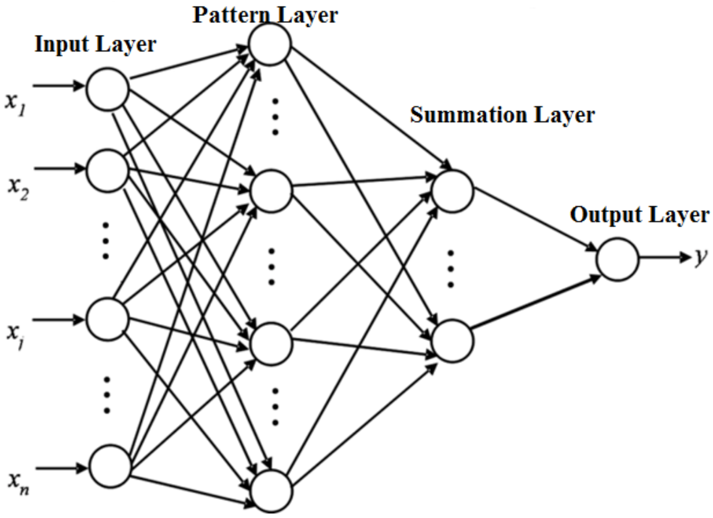

Fig. 2. – General structure of GRNN

A GRNN consists of four layers: input layer, pattern layer, summation layer and output layer. The number of input units in input layer depends on the total number of the observation parameters. The first layer is connected to the pattern layer and in this layer each neuron presents a training pattern and its output. The pattern layer is connected to the summation layer. The summation layer has two different types of summation, which are a single division unit and summation units. The summation and output layer together perform a normalization of output set. In training of network, radial basis and linear activation functions are used in hidden and output layers. Each pattern layer unit is connected to the two neurons in the summation layer, S and D summation neurons. S summation neuron computes the sum of weighted responses of the pattern layer. On the other hand, D summation neuron is used to calculate un-weighted outputs of pattern neurons. The output layer merely divides the output of each S-summation neuron by that of each D-summation neuron, yielding the predicted value Yi to an unknown input vector x as Equation 1 and 2 (JANG ET AL., 1997);

$$Y^i = \frac{\sum_{i=1}^{n} y_i.exp - D(x, x_i)}{\sum_{i=1}^{n} exp - D(x, x_i)} \qquad (1)$$

$$D(x, x_i) = \sum_{k=1}^{m} (\frac{x_k - x_{ik}}{\sigma})^2 \qquad (2)$$

y_i is the weight connection between the i_{th} neuron in the pattern layer and the S-summation neuron, n is the number of the training patterns, D is the Gaussian function, m is the number of elements of an input vector, x_k and x_{ik} are the j_{th} element of x and x_i, respectively, σ is the spread parameter, whose optimal value is determined experimentally.

GRNN performance evaluation

The performance of the artificial neural network during its training and validation steps, can be evaluated using diverse techniques, such as root mean squared error RMSE, sum of squares of error SSE, mean error ratio MER, mean square error MSE, R2 correlation factor (GOYAL AND GOYAL, 2011). We used MSE

(Equation 3), RMSE (Equation 4) and MAE (Equation 5) values for statistical analyze which were calculated as:

$$MSE = \sum_{t=1}^{N} \left(\frac{Y_t - O_t}{T} \right)^2 \tag{3}$$

$$RMSE = \sqrt{\frac{1}{T} \left[\sum_{t=1}^{N} \left(\frac{Y_t - O_t}{Y_t} \right)^2 \right]} \tag{4}$$

$$MAE = \frac{1}{T} \sum_{t=1}^{N} |Y_+ - O_T| \tag{5}$$

where, Y_t is the expected exit, O_t is the obtained exit, T is the number of records, and N is the number of neurons in the pattern layer.

GRNN development

For this study, every second, we transiently collected GPS data and soil penetration value on study field by the using horizontal penetrometer. We collected 1603 GPS data and penetration value from 13 linear lines. First three and last three lines were used extrapolation process of estimating for GRNN. Middle three lines were used interpolation process of estimating for GRNN. In order to obtain the optimum amount of training data, three different types of training data set are created: (1) extrapolation data set (EXT 1); (2) interpolation data set (INT 1); and (3) extrapolation data set (EXT 2). The rest data is used for the validation of the corresponding models. Data collection map is given in Fig. 3. Numbers of training and test data sets are given in Tab. 1.

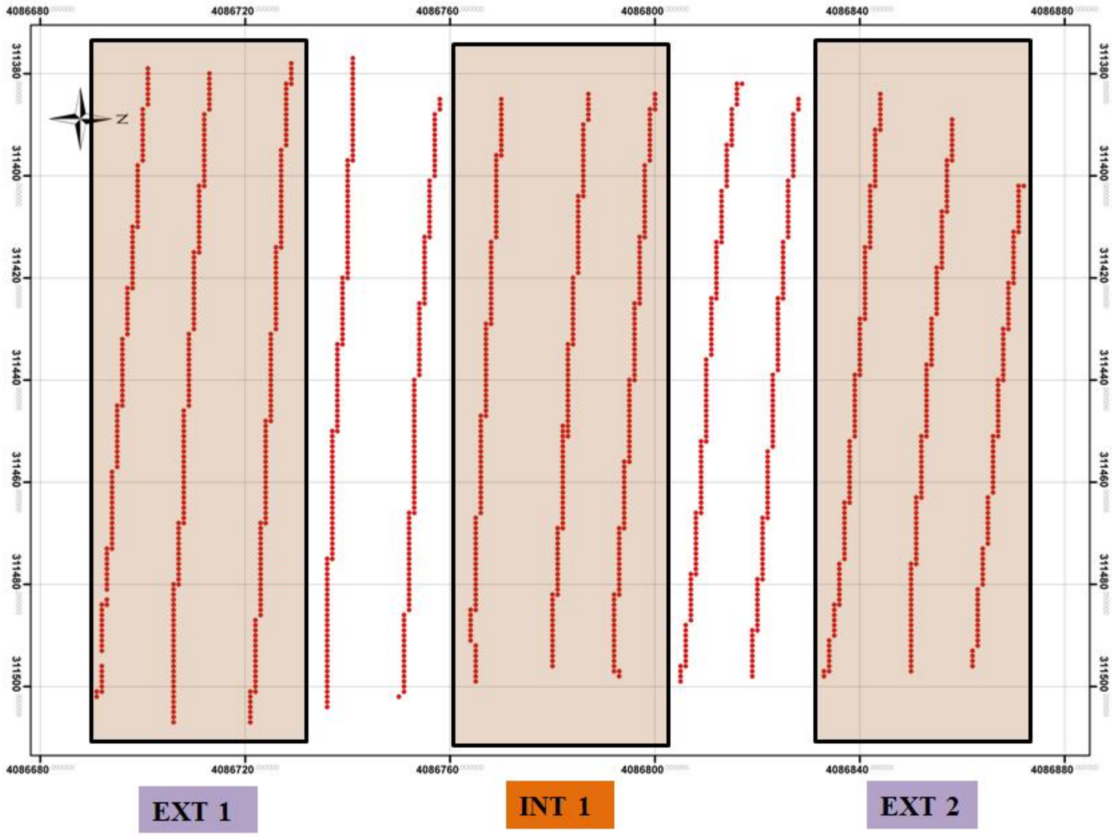

Fig. 3. – Data collection map

Tab. 1. – Numbers of training and test data sets

	Test	Educating
EXT 1	401	1202
INT 1	361	1242
EXT 2	340	1263

RESULTS AND DISCUSSION

In this study, we compared the real and the estimated soil penetration data using GRNN method. For comparison process, we used the RMSE and MSE values. EXT 1 process result is given graphically in Fig. 4. INT 1 process result is given graphically in Fig. 5. EXT 2 process result is given graphically in Fig. 6. The Error Analysis of Extrapolation and Interpolation Performances of the GRNN method are given in Tab. 2.

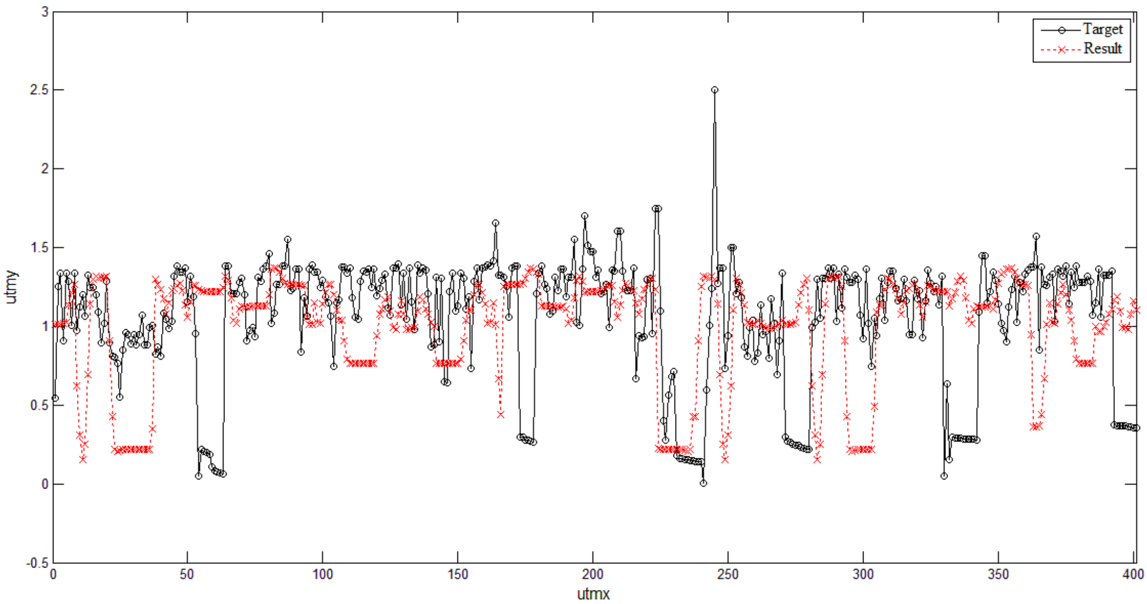

Fig. 4. – EXT 1 process result

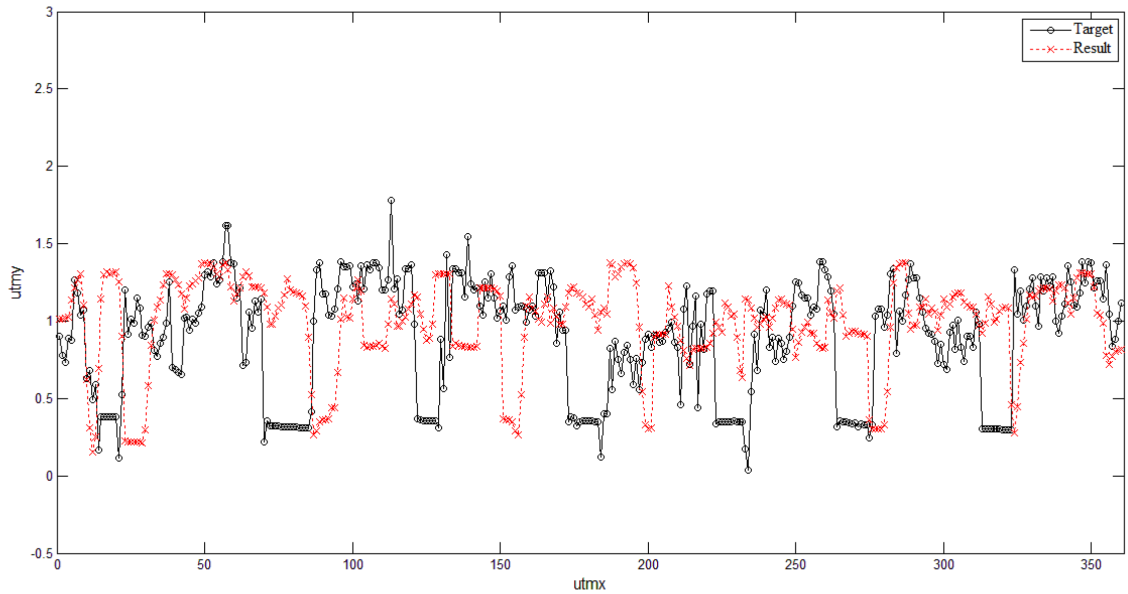

Fig. 5. – INT 1 process result

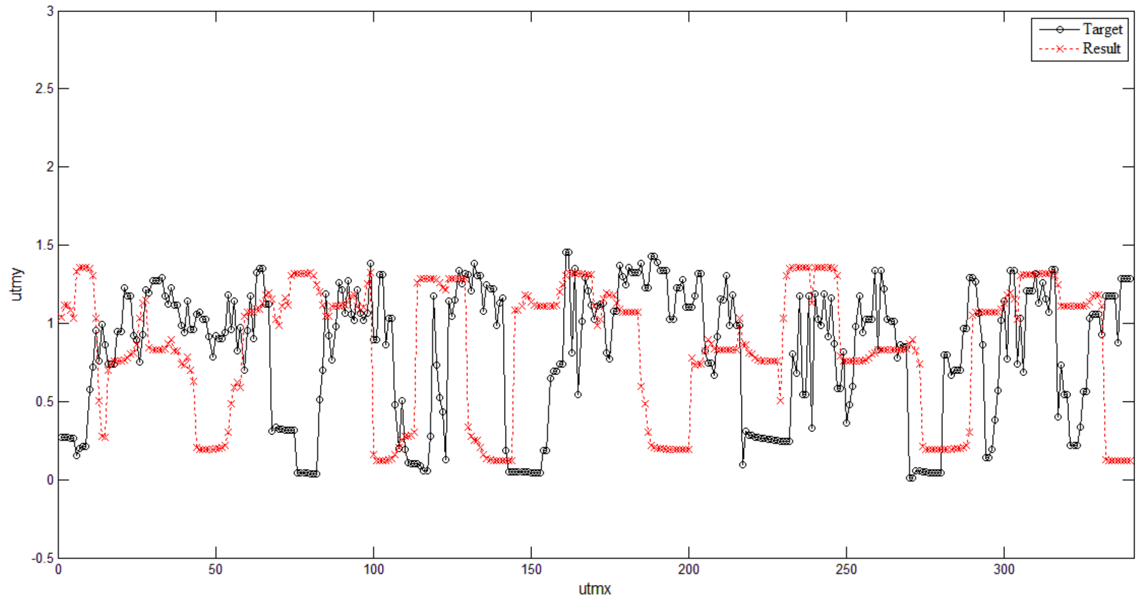

Fig. 6. – EXT 2 process result

Tab. 2. – The Error Analysis of Extrapolation and Interpolation Performances of the GRNN

σ = 1	**EXT 1**	**INT 1**	**EXT 2**
MSE	0.2443	0.2506	0.4092
RMSE	0.4943	0.5006	0.6397
MAE	0.4007	0.372	0.5136
R^2	0.847	0.905	0.831

As it can be seen in Tab. 2, and Fig. 4–6 generally GRNN method that used in this article are very successful for prediction of soil penetration resistance. During the data collection process on study field, horizontal penetrometer was taken out from soil by the reason of some problems. As it can be seen in Fig. 4-6, analyze results were negatively affected by the soil penetration resistance values between 0 and 0.5 MPa. When this soil resistance values is removed from test dataset, MSE, RMSE and MAE values can be move towards the 0.

KRUPP AND GRIFFIN (2006), a general regression neural network (GRNN) was developed for predicting soil composition from CPT (Cone Penetration Test) data. Measured values of cone resistance and sleeve friction obtained from CPT soundings, together with grain-size distribution results of soil samples retrieved from adjacent standard penetration test boreholes, were used to train and test the network. Researchers reported that the profiles of soil composition estimated by the GRNN generally compare very well with the actual grain-size distribution profiles, and overall the neural network had an 86% success rate at classifying soils as coarse grained or fine grained. CAI ET AL. (2015) were analyzed relationship between CPTU (Piezocone Penetration Test) parameters and soil types and strata, and was designed the structure of a general regression neural network (GRNN) for soil classification and soil strata identification. Researchers reported that the GRNN-based model was found to be correlating well for the 87% of the cases with the USCS classification system results. SANTOS ET AL. (2012) were to perform an analysis of the soil penetration resistance behavior measured from the cone index under different levels of bulk density and water content using statistical analyses, specifically regression analysis and ANN (Artificial Neural Networking) modeling. The regression analysis presented a determination coefficient of 0.92 and an RMSE of 0.951, and the ANN modeling presented a determination coefficient of 0.98 and an RMSE of 0.084. Researchers reported that the ANN modeling presented better results than the mathematical model obtained from regression analysis.

In this study, we compared real and predicted soil penetration resistance values by using regression analysis. The results of the regression analysis show that the predicted soil penetration resistance values was indeed positively correlated with real values (EXT1=0.847, INT1=0.905 and EXT2=0.831).

CONCLUSIONS

In this study, the possibility to use artificial neural networks on the prediction of soil penetrance resistance was explored. The results of the study show that using new artificial neural networks with better predictions is an important contribution to research and professional application of soil science. Soil penetration value collection from large production areas is time-consuming and tedious application for researchers. The option of using a prediction tool saves time and costs on experimental execution. In this paper, we used GRNN method for estimating soil penetration values. Compared with the other neural networks, GRNN has a relatively simple and static structure.

ACKNOWLEDGEMENTS

This work was supported by The Scientific Research Projects Coordination Unit of Akdeniz University.

REFERENCES

1. ABROUGUI, K., CHEHAIBI, S., LOUVET, J. N., HANNACHI, C., DESTAIN, M. F.: Soil Structure and the Effect of Tillage Systems. Bulletin UASVM Agriculture. 69, 2012: 11-16.
2. ADAMCHUK, V. I., SKOTNIKOV, A. V., SPEICHINGER, J. D., KOCHER, M. F.: Instrumentation System for Variable Depth Tillage. In Proceedings of ASAE Annual International Meeting, 27–30 July 2003, Las Vegas, NV, USA.
3. AL-ADAWI, S. S., REEDER, R. C.: Compaction and subsoiling effects on corn and soybean yields and soil physical properties. Trans. ASAE, 39, 1996: 1641-1649.
4. BAYAT, H., NEYSHABOURI, M. R., HAJABBASI, M. A., MAHBOUBI, A. A., MOSADDEGHI, M. R.: Comparing neural networks, linear and nonlinear regression techniques to model penetration resistance. Turkish Journal of Agricultural Forestry, 32, 2008: 1–9.
5. BOCCO, M., OBANDO, G., SAYAGO, S., WILLINGTON, E.: Neural network models for land cover classification from satellite images. Agric. Téc. 2007, 67(4):414 - 421.
6. BUENDÍA, E., VARGAS, E., LEYVA, A., TERRAZAS, S.: Aplicación de redes neuronales artificiales y técnicas SIG para la predicción de coberturas fo-restales. Serie Ciencias Forestales y del Medio Ambiente. Rev. Chapingo, 8 (1), 2002:31 - 37.
7. CAI, G., LIU, S., PUPPALA, A. and TONG, L.: "Identification of Soil Strata Based on General Regression Neural Network Model From CPTU Data." Marine Georesources & Geotechnology, 33, 2015: 229-238.
8. CARRARA, M., CASTRIGNANÒ, A., COMPARETTI, A., FEBO, P., ORLANDO, S.: Mapping of penetrometer resistance in relation to tractor traffic using multivariate geostatistics. Geoderma, 142, 2007: 294-307.
9. ERZIN Y., RAO B. H., PATEL A., GUMASTE S. D., SINGH, D. N.: Artificial neural network models for predicting electrical resistivity of soils from thermal resistivity. Int J Therm Sci, 49(1), 2010: 118-130.
10. GARCÍA, I., RODRÍGUEZ, J. G., LÓPEZ, F., TENORIO, Y. M.: Transporte de contaminantes en aguas subterráneas mediante redes neuronales artificiales. Inf. Tecnol, 21(5), 2010:79 - 86.
11. GOYAL, S., GOYAL, G. K.: Cascade and feed-forward backpropagation artificial neural network models for prediction of sensory quality of instant coffee flavoured sterilized drink. Can. J. Artif. In-tell. Machine Learn. Pattern Recog., 2(6), 2011:78 - 82.
12. HOLGUÍN, N. J. V., SALCEDO, L. O. G., WILL, A. L. E.: Prediction of soils penetration strength using artificial neural networks. Acta Agronómica, 60(3), 2011: 251-260.
13. JANG, J. S. R., SUN, C. T., MIZUTANI, E.: Neuro-fuzzy and soft computing: a computational approach to learning and machine intelligence. Prentice Hall, Upper Saddle River, New Jersey, USA, 1997.
14. KHAZAEI J., DANESHMANDI S.: Modeling of thinlayer drying kinetics of sesame seeds: mathematical and neural networks modeling. International Agrophysics. 21(1), 2007: 335-348.
15. KIM M., GILLEY J. E.: Artificial neural network estimation of soil erosion and nutrient concentration in runoff from land application areas. Comput Electron Agr, 64(2), 2008: 268-275.
16. KIMES, D. S., NELSON, R. F., MANRY, M. T., FUNK, A. K.: Attributes of neural networks for ex-tracting continuous vegetation variables from opti-cal and radar measurements. Intern. J. Remote Sensing, 19(14), 1998: 639 - 2663.
17. KURUP, P., GRIFFIN, E.: Prediction of soil composition from CPT data using general regression neural network. Journal of Computing in Civil Engineering, 20(4), 2006: 281–289.
18. MANETA, M., SCHNABEL, S.: Aplicación de redes neuronales artificiales para determinar la distribución espacial de la humedad del suelo en una pequeña cuenca de drenaje: estudios prelimi-nares. Estudios de la Zona no Saturada del Suelo, 6, 2003: 295 - 304.
19. MAS, J. F., PUIG, H., PALACIO, J. L., SOSA, A.: Modelado del proceso de deforestación en una región del sureste de México. Memorias del II Seminario Latinoamericano de Geografía Física, Julio, 2002, pp. 24-27, Maracaibo, Venezuela (CD-ROM).
20. MENA, C., MONTECINOS, R.: Comparación de redes neuronales y regresión lineal para estimar productividad de sitio en plantaciones forestales, utilizando geomática. Bosque, 27(1), 2006:35 - 43.
21. NADARAYA, E.A.: On estimating regression, Theory Probab. Appl. 1964, 10: 186–190.
22. NESIL, S., GÜNEŞ, F., ÖZKAYA, U., TURETKEN, B.: Generalized Regression Neural Network Based Phase Characterization Of A Reflectarray Employing Minkowski Element Of Variable Size. XXXth URSI General Assembly and Scientific Symposium, 13 - 20 August 2011, Istanbul, Turkey.
23. PORTERFIELD, J. W., CARPENTER, T. G.: Soil compaction: an index of potential compaction for agricultural tires. Trans. ASAE, 29, 1986: 917-922.
24. RAPER, R.L.: Agricultural traffic impacts on soil. J. Terramech., 42, 2005: 259-280.
25. REBOLLEDO, F. J., OBREGÓN, N., DUARTE, C.: Ecohidroinformática: un nuevo paradigma para la gestión inteligente de los recursos hídricos. XXVIII Congreso

Internacional de Ingeniería Sani-taria y Ambiental, 27-31 Octubre 2002, Cancún, México.

26. RODRÍGUEZ, J. G.: Pronóstico de la migración de contaminantes en aguas subterráneas median-te redes neuronales artificiales [Ph.D. thesis.]. en In-geniería Ambiental. Instituto Politécnico Nacional. México, 2009, 129 p.
27. RUBIO, C.: Hidrodinámica de los suelos de un área de montaña media mediterránea sometida a cambios de uso y cubierta [Ph.D. thesis.]. en Ciencias del Suelo. Universidad Autónoma de Barcelona, Barcelona, España, 2005, 194 p.
28. SANTOS, FL., MENDES DE JESUS, VA. AND VALENTE, DSM.: Modeling of soil penetration resistance using statistical analyses and artificial neural networks. Acta Scientiarum, 34(2), 2012: 219-224.
29. SARMADIAN F., MEHRJARDI T., AKBARZADEH A.: Modeling of some soil properties using artificial neural network and multivariate regression in Gorgan province, north of Iran. Australian Journal of Basic and Applied Sciences. 3(1), 2009: 323-329.
30. SCHIOLER, H., HARTMANN, U.: Mapping neural network derived from the Parzen window estimator. Neural Netw. 5(6), 1992: 359–372
31. SPECHT, D. F.: A General Regression Neural Network. Ieee T Neural Networ, 2(6), 1991: 568-576.
32. TEKIN, A. B.: Variable rate fertilizer application in Turkish wheat agriculture: Economic assessment. AJAR, 5, 2010: 647-652.
33. TEKIN, E., KUL, B., OKURSOY, R.: Sensing and 3D mapping of soil compaction. Sensors, 8, 2008: 3447-3459.
34. TOPAKCI, M., UNAL, I., CANAKCI, M., CELIK, H. K., KARAYEL, D.: Design of a Horizontal Penetrometer for Meas uring On-the-Go Soil Resistance. Sensors. 10, 2010: 9337-9348.
35. TRIGUI, M., GABSI, K., EL AMRI, I., HELAL, A., BARRINGTON, S.: Modular feed forward networks to predict sugar diffusivity from date pulp Part I. Model validation. Int J Food Prop, 14, 2011: 356-370.
36. TSOUKALAS, L. H., UHRIG, R. E.: Fuzzy and Neural Ap-proache in Engineering. New York, John Wiley and Sons Inc., 1997.
37. VARELLA, C. A., PINTO, F. A., QUEIROZ, D. M., SENA, D. G.: Determinação da cobertura do solo poranálise de imagensdigitais e redesneurais. Revista Brasileira de Engenharia Agrícola e Ambiental. 6(2), 2002: 225-229.

Corresponding author:

İlker ÜNAL, Akdeniz University, Vocational School of Technical Science, Antalya, Turkiye, e-mail: ilkerunal@akdeniz.edu.tr

INFLUENCE OF DIFFERENT METHODS OF BIO-PREPARATION USE ON CUTTING CHARACTERISTICS OF WINTER WHEAT RESIDUES

K. Vaitauskienė, E. Šarauskis, V. Naujokienė, A. Jasinskas

Aleksandras Stulginskis University, Lithuania

Abstract

The objective of this work is to establish the influence of different bio-preparation use on cutting characteristics of winter wheat residues. According to the first method the winter wheat crop was sprayed with bio-preparations ("Amalgerol", "Azofit" and their combination) in spring after plant vegetation had renewed. The influence of different bio-preparations on cutting characteristics was investigated and compared with the control. According to the second method bio-preparation "Azofit" was sprayed on plant residues right after winter wheat harvesting. It was investigated how cutting characteristics of plant residues varied in 1, 2 or 3 weeks. The cutting investigation results were compared with the results of cutting winter wheat residues left on the soil surface under natural conditions. Experimental research of physical-mechanical properties of plant residues were carried out at the Institute of Agricultural Engineering and Safety of Aleksandras Stulginskis University, using an experimental research machine "Instron 5960".

The experimental research results indicate that the time of bio-preparation use and impact duration have influence on plant residue cutting force. According to the first method, having sprayed winter wheat with different bio-preparations in spring it was established that after harvesting winter wheat residues required 5 % ("Amalgerol") and 37 % ("Azofit", and "Azofit" and "Amalgerol" combination) stronger force compared with the winter wheat residues without using bio-preparations in the control application. According to the second method, having sprayed plant residues with bio-preparation "Azofit" actually after harvesting in autumn it was established that following three weeks of bio-preparation duration, the force of plant residue cutting decreased significantly (about 28 %) compared with the control application.

Key words: winter wheat, plant residues, bio-preparation, cutting, knife.

INTRODUCTION

With the increasing popularity of no-till agriculture an increasing number of problems arise with plant residues left on the soil surface. Because of their mechanical, biological and other characteristics, plant residues interfere with quality operation of tillage and drilling machinery (ARVIDSSON, 2010, VAITAUSKIENĖ ET AL., 2015, ŠARAUSKIS ET AL., 2012). Therefore, research investigations to establish plant residue cutting characteristics are relevant for the quality of soil tillage and sowing technological processes, manufacture of agricultural machinery and selection of its working parts (HEMMATIAN ET AL., 2012).

Researchers from different countries (HEMMATIAN ET AL., 2012, LINKE, 1998, TAVAKOLI ET AL., 2009, ŠARAUSKIS ET AL., 2013) have noticed that the force required to cut or break plant residues depended on the plant species, stem diameter, plant length, moisture, cell structure and elasticity. The design and technological parameters of working parts have great importance for the ability to cut or break through plant residues (LIU ET AL., 2007, 2010). Canadian researchers established that a coulter with disks of 360 mm diameter and 2 mm thickness, while penetrating 60 or 70 mm into the soil, cut approximately 80 % of the straw on the soil surface, and the remaining 20 % of the straw was pressed into the soil. A larger disc coulter with 460 mm diameter and 4 mm thickness disks cut approximately 95 % of straw while penetrating 60 or 70 mm into the soil. A disc coulter with even larger disks (600 mm diameter and 4.5 mm thickness) cut only approximately 20 % of straw while penetrating 55 mm into the soil. The investigations established that more straw was cut with an increase of penetration depth (KUSHWAHA ET AL., 1983; KUSHWAHA ET AL., 1986).

Iranian researchers state that a greater force is required to cut a rice stem with greater stem cross-sectional area. In addition, the rice stem (moisture content 80 %) cutting force depends on the cutting speed as well. Increasing the cutting speed from 0.6 m s^{-1} to 1.5 m s^{-1} when knife sharpness of 35° cutting force reduces the by about 40 % (TABATABAEE AND BORGHEIE, 2006). Moreover, other Iranian researchers propose as well that the plant residue cutting force depends on the cutting speed. On the contrary, increasing the cutting speed from 0.3 to 0.9 m s^{-1} the force required to cut a sugarcane stem (moisture content 78 %) increased by about 3 % (HEMMATIAN ET AL., 2012).

In addition, very important is the period during which plant residues are left on the soil surface after harvesting. The force required to break overwintered winter wheat straw is about 3.2-fold lower than the force required to break the straw of winter wheat harvested fresh in autumn. The breaking force for overwintered spring barley straw decreases approximately by about 34% compared with the autumn straw (ŠARAUSKIS ET AL., 2013). Long periods deteriorate the mechanical characteristics of plant residues, however, an opportunity is not always provided for waiting until the plant residue mechanical characteristics, which influence the technological processes of the working parts of tillage and drilling machinery, are weakened under natural conditions. Very often, several weeks after crop harvesting, new plants are already being drilled. The application of no-till and strip-till results in the plant residues from the previous harvest being left on the soil surface, which directly influences the operation process of working parts. Because plant residues left on the surface for a short time can maintain strong mechanical characteristics, disc coulters may fail to cut through or break them. In such cases plant residues will be pressed into the notches. To prevent this, it is necessary to speed up the processes of plant residue mineralization and the associated mechanical weakening. To activate such processes, different biological preparations are being introduced rapidly. The functions performed by biological preparations have great direct and indirect impacts on the growth and quality of crops, the spreading of pests in the soil and plant residues, the distribution of diseases, the rates of nutrient circulation in the soil, the receptivity of soil to water and the consistency of its ecological productivity. They also affect the stability of agroecosystems and the resistance to abiotic environmental factors and stress (BRUSSAARD ET AL., 2007). Biological preparations create a distinctive agricultural culture and ensure long-term and stable fertility of field plants, while maintaining clean environment without causing damage to people (AHMADI, 2010; BRUSSA ARD ET AL., 2007).

These biological preparations are most often used as nutrients for the soil and plants. Plants sprayed with the solution of such preparations can assimilate mineral materials better, grow more vigorously and the productivity of plants increases (DEWAR, 2006; JAKIENĖ ANDLIAKAS, 2013). The biological preparation consists of nitrogen-fixing stem bacteria Acotobactervinelandii and biologically active materials affecting the structure of plant residues. Therefore, the mineralization of plant residues is activated on the soil surface, and at the same time, the nitrogen-fixing bacteria perform the function of speeding up the processes of plant residue decomposition and the weakening of the mechanical characteristics of the residues (AHMADI, 2010; HOLTZE ET AL., 2008; JAKIENĖ, 2011; VAITAUSKIENĖ, 2015).

RAUCKIS (2012) states that the plant residues left on the soil surface, soil before drilling and plants in the beginning of vegetation are recommended to spray with the solution of biological preparation “Azofit” or “Amalgerol”. Thus plant residuesmineralisation is faster, nutrients present in plant residues are released sooner and soil aeration as well as soil and seed contact are improved. Due to organic colloid formation soil temperature increases (±2°C) and this reason determines faster and more uniform germination of seeds.

There have been some investigations carried out on the use of biological preparations in different agronomical aspects, however, the impact of biopreparations on the mechanical properties of plant residues depending on the methods of use has not been established.

MATERIALS AND METHODS

Establishing of Cutting Forces

The experimental research was conducted in the Laboratory of the Institute of Agricultural Machinery, Mechanics and Safety Engineering, Aleksandras Stulginskis University. The plant residue cutting forces were determined using an experimental machine for testing low force–mechanical properties “Instron 5960” (Fig. 1) with software “Bluehill”.

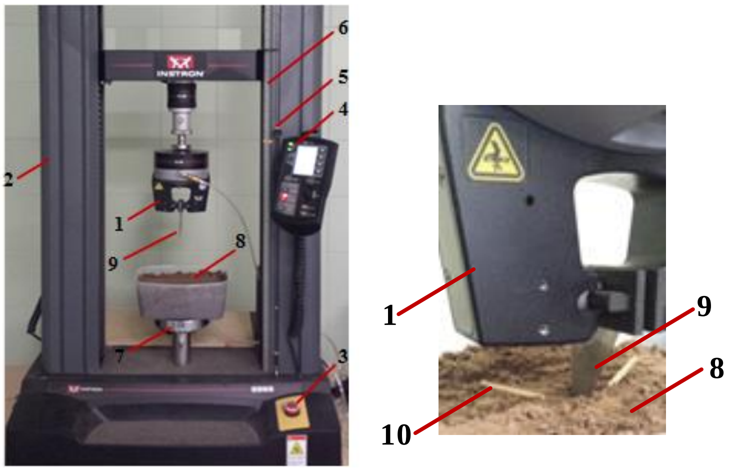

(a) (b)

Fig. 1. – Equipment for testing force–mechanical characteristics of materials "Instron 5960": a) machine ready for investigating cutting forces of plant residues: 1 – knife fixing clamp; 2 – frame; 3 – emergency shutdown button; 4 – control panel; 5 – movement limit stop; 6 – measuring scale; 7 – base; 8 – container with soil; 9 – cutting knife; 10 – experimental sample; b) sliding-cutting simulating a disc coulter with serrated cutting edge

The plant residue cutting investigations were performed by a knife with the edge of 0.4 mm in width, 4 mm in length and penetration depth – up to 70 mm (Fig. 1, b). The knife edge was sharpened at an angle of 30º. To obtain the most natural conditions possible, the experiments were conducted with the residues in contact with the soil. Light loam soil with moisture content of 15.0±1.3 % and penetration resistance of approximately 1.0±0.06 MPa was used for the experiments. Such soil penetration resistance corresponds to no-till conditions (CANNELL, 1985). In order to improve the quality of cutting plant residues, the disc coulters with serrated edges are often used in no-till equipment (BIANCHINI ET AL., 2008; ŠARAUSKIS ET AL., 2013A). For this purpose, another way of cutting plant residues with the knife positioned at an angle of 60º (Fig. 1, b) was investigated, the cutting of plant residues in the indentation of the disc coulter edge was simulated. Thus, a sliding process of cutting plant residues was performed.

In this study, the rate of knife movement was 20 mm·min^{-1}. After each plant residue cutting experiment, the soil was densified over, and the penetration resistance and moisture content were measured by an Eijkelkamppenetrologger with 3 replications to ensure uniform physico-mechanical soil characteristics and experimental conditions.

Sample Properties

Winter wheat residues were investigated as this crop is most widely cultivated for industrial purposes in Lithuanian and other Baltic countries. According to the first method 4 applications were installed. In application 1 winter wheat plots were sprayed with bio-preparation "Azofit" at a spraying rate of 1.0 l. ha^{-1}, in application 2 "Amalgerol" was used at a spraying rate of 4.0 l ha^{-1} and in application 3 – "Azofit" (1.0 l·ha^{-1}) and "Amalgerol" (4.0 l. ha^{-1}) combination. The spraying was carried out in spring – on 4 April 2015. An additional application (control) was installed to compare investigation results, in which no bio-preparations were used. During the same year right after harvesting the investigations of the cutting force of winter wheat residues were conducted.

The experimental research according to the second method was carried out in two applications. Application 1 was a control one: after harvesting winter wheat its residues were left on the soil surface under natural climatic conditions. In application 2 plant residues were sprayed with bio-preparation "Azofit" at a spraying rate of 1.0 l ha^{-1}.

Biological preparations were mixed with 200 l of water. The area of sprayed plots was less than 1 ha, therefore, the rate of biological preparations was adjusted accordingly. Having evaluated the fact that in agriculture after harvesting in autumn there is no much time left before sowing of new crops, a 3 week period was chosen for the experimental research according to the second method, during which the investigations were conducted once a week every seven days. At the start, initial experimental investigations were conducted to establish characteristics of the forces required to cut plant residues. The samples of plant residues collected (100 mm in length, 4 mm in diameter on average, uncrushed) were weighed and dried in a desiccator at 105ºC as recommended by many researchers (SILVA–FERNANDES ET AL., 2015; WOOD ET AL., 2014). When the plant residues reached air-dried mass (approximately 24 hrs) their moisture contents were calculated. The experiments on cutting plant residues were conducted with 5 replications. Randomized sample taking of plant residues from five different spots of each plot was performed. Assuming that it is complicated to maintain uniform moisture content of different plant residues under natural climatic conditions, the plant residue moisture content was measured during each investigation of cutting characteristics.

Statistical Data Analysis

The data obtained during the experimental research were analysed by dispersion (ANOVA) analysis method using Excel software. The arithmetic means, their standard deviations and intervals of confidence were determined with the probability level ($P<0.05$) respectively. Significant differences between the investigated data options were established by calculating the honestly significant difference HSD at 0.05 probability by Tukey's HSD method (TARAKANOVAS AND RAUDONIUS, 2003). In the pictures, the letters indicate significant differences between the factors. Common letters indicate no significant difference.

RESULTS AND DISCUSSION

The force required to cut through plant residues is a very important technological indicator in agriculture, which demonstrates how easily machinery working parts cuts or fails to cut plant residues. The experiments assessed the efficiency of biological preparations in facilitating the winter wheat residues using the angled knife.

According to the first method moisture content of the winter wheat residues analysed was 6 % on average and according to the second method – it was 30 % on average (Tab. 1).

Tab. 1. – Geometric means and moisture content of plant residues during experimental research period

Plant residue (method)	Diameter mm	Length mm	Moisture content % 0 (start)	After 1 week	After 2 weeks	After 3 weeks
Winter wheat (method 1)	4±0.5	100±2.5	6±0.9			
Winter wheat (method 2)	4±0.4	100±2.6	30±1.2	34±2.5	30±2.1	25±1.7

The cutting process of winter wheat residues as well as the residues of other plants on the soil surface depends highly on the physical and mechanical characteristics of the soil and the plant residues. The penetration resistance of the soil surface and the moisture content of plant residues are of the utmost importance. If the soil penetration resistance is not sufficient and the plant residues are of high moisture content, the residues are most often left uncut because they would only be pressed into the soil by a coulter. To cut through plant residues, the penetration resistance of the soil has to be higher than the normal stresses of plant residues (KUSHWAHA ET AL., 1986; LINKE, 1998; ŠARAUSKIS ET AL., 2005). 1.0 MPa penetration resistance of soil was used in this experimental research, which most often corresponds to no-till and strip-till conditions on the light loam soils and it was sufficient to cut through the plant residues in all cases of the experiments. This resistance, however, was too low for winter wheat residues with high moisture content to be cut through.

During the experiments according to the first method it was established that the use of biological preparations "Amalgerol", "Azofit" and their combination resulted in significantly stronger force for cutting winter wheat residues (approximately 7 N) compared with the control application. In other cases significant differences were not established (Fig. 2 a). The same experiments established how the depth of knife penetration into soil varies (Fig. 2 b) until plant residues are cut through. Though cutting through winter wheat residues affected by biological preparations required the force which was significantly different in certain cases, plant residues were cut through when the knife penetrated the soil at similar depths (24 mm on average). There were no significant differences between the applications examined.

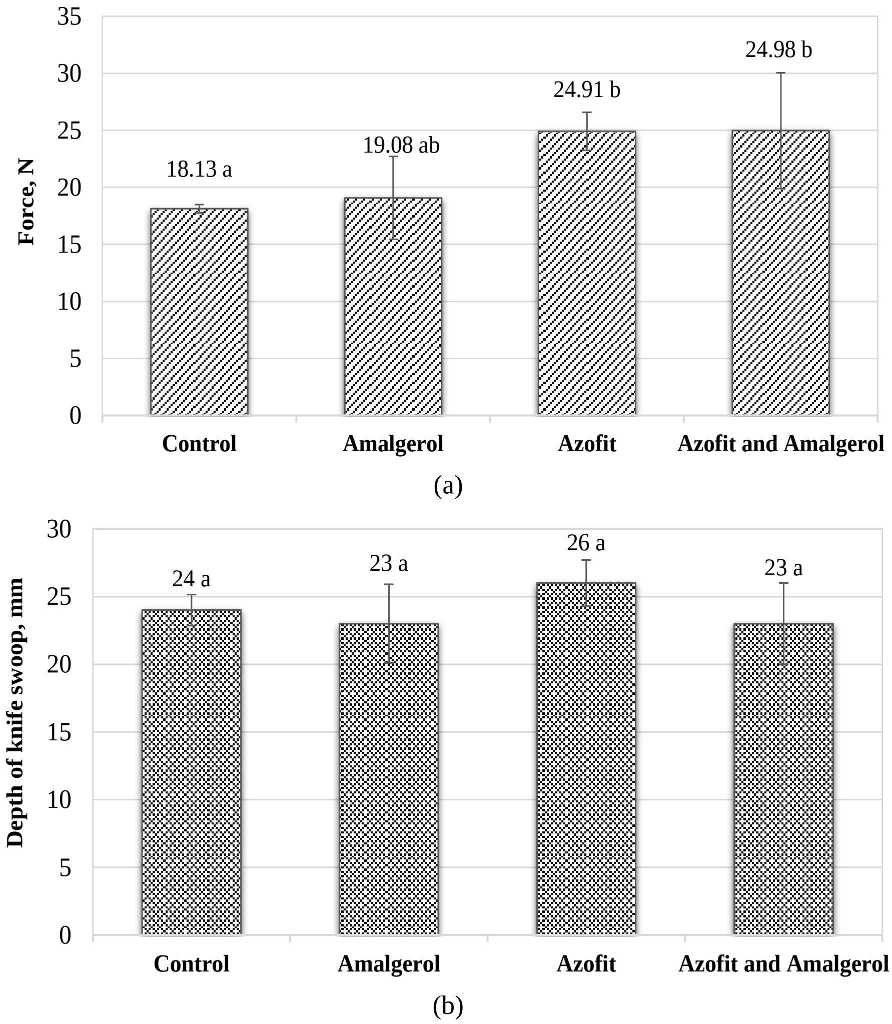

Fig. 2. – Influence of biological preparations on cutting force (a) of winter wheat residues and depth of knife swoop (b)

The research results achieved by using the first method indicate that spraying of winter wheat crop in spring with biological preparations can entail strengthening of plant mechanical characteristics and such plants can resist unfavorable meteorological conditions during vegetation more easily.

The second method helps to achieve a different objective – biological preparation spraying on plant residues speeds up the processes of plant residue mineralization and weakens the mechanical characteristics of the residues to reduce their negative influence on the working parts of soil tillage and drilling equipment as much as possible. The experimental research established the influence of biological preparation "Azofit" on cutting through winter wheat residues. The comparison of the cutting forces applied on the spring rapeseed residues treated and untreated with biological preparation "Azofit" established that significantly lower force was required after the three week biological treatment (Fig. 3). In other cases there were no significant differences among the applications analysed.

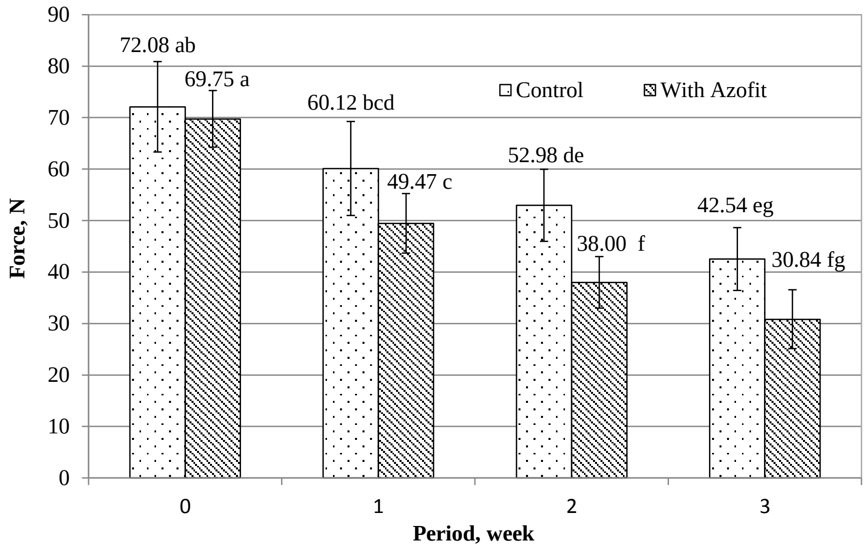

Fig. 3. – Influence of biological preparation and its action period on cutting force of winter wheat residues

In summarizing the experimental results, we can state that the biological preparation use has influence on the force of cutting winter wheat residues. In trying to achieve fast plant residue decomposition after harvest it is expedient to treat plant residues with some biological preparation. This fact has to be emphasized as in such way the use of biological preparation can both intensify the processes of plant residue decomposition and weaken residue mechanical characteristics. Rapid breakdown of the mechanical characteristics of plant residues is of key importance in applying no-till and strip-till technologies, where the impact of plant residues on the quality of drilling is very high. If plant residues are not removed from a seed-drilling notch, seeds can be left unincorporated or incorporated into plant residues. In such cases, seed germination can fail and plant development can be retarded.

CONCLUSIONS

It was established that the use of bio-preparations "Amalgerol", "Azofit" or their combination in spring results in strengthening of mechanical characteristics of winter wheat residues. A stronger plant residue cutting force (approximately by 5 % with "Amalgerol") and (about 37 % with "Azofit", and "Azofit" and "Amalgerol" combination) was achieved compared with the control application.

The experiments established that the use of bio-preparations "Amalgerol", "Azofit" or their combination had no substantial influence on the cutting depth through winter wheat residues. In all cases analysed, plant residues were cut through, when the knife penetrated the soil at similar depths (24 mm onaverage).

It is of key importance in no-till and strip-till technologies that the plant residues left on the soil surface do not prevent the working parts of tillage and drilling machinery from performing their functions well. The force required to cut through plant residues is a very important technological indicator of how easily the working parts of no-till and strip-till machinery cut or fail to cut plant residues. The application of "Azofit" biological preparation reduces the force needed to cut through the winter wheat residues. After three weeks of biological preparation impact it was established that the difference was substantial (approximately 28 %).

REFERENCES

1. AHMADI, M.: Effect of zinc and nitrogen fertilizer rates on yield and yield components of oilseed rape (Brassica napus L.). American–Eurasian J. of Agric. and Environ. Sci. 7, 2010: 259–264.
2. ARVIDSSON, J.: Energy use efficiency in different tillage systems for winter wheat on a clay and silt loam in Sweden. Eur. J. Agron. 33 (3), 2010: 250–256.
3. BIANCHINI, A., MAGALHAES, P.S.G.: Evaluation of coulters for cutting suggar cane residue in a soil bin. Biosyst. Eng. 100, 2008: 370–375.
4. BRUSSAARD, L., DE RUITER, P.C., BROWN, G.: Soil biodiversity for agricultural sustainability. Agricultural. Ecosyst. & Environ. 121, 2007: 233–244.
5. CANNELL, R.Q.: REDUCEDTILLAGE IN NORTH–WESTEUROPE: a review. Soil and Tillage Res. 5 (2), 1985: 129–177.
6. DEWAR, A.M., MAY, M.J., WAIWOD, I.P.: A novel approach to

the use of genetically modified herbicide tolerant crops for environmental benefit. Proceeding of the Royal Society: Biological Sci. 270, 2006: 335–340.
7. HEMMATIAN, R., NAJAFI G., HOSSEINZADEH, B., TAVAKOLI HASHJIN, T., KHOSHTAGHAZA, M.H.: Experimental and theoretical investigation of the effects of moisture content and internodes position on shearing characteristics of sugar cane stems. J. of Agric. Sci. and Technol. 14, 2012: 963–974.
8. HOLTZE, M.S., SORENSEN, S.R., SORENSEN, J., AAMAD, J.: Microbial degradation of the benzonitrile herbicides dichlobenil, bromoxynil and ioxynil in soil and subsurface environments— insights into degradation pathways, persistent metabolites and involved degrader organisms. Environ. Pollut. 154, 2008: 155–168.
9. JAKIENĖ, E.: Effect of biological products on sugar–beet crop. Zemes ukio mokslai, 18, 2011: 64–71.
10. JAKIENĖ, E., LIAKAS, V.: Effect of the biological preparations Azofit and Amalgerol on sugar beet seeding. The sixth international scientific conference Rural development proceedings. Akademija. 6, 2013.
11. KUSHWAHA, R.L., VAISHNAV, A.S., ZOERB, G.C.: Shear strength of wheat straw. Can. Agricu. Eng. 25, 1983: 163–167.
12. KUSHWAHA, R.L., VAISHNAV, A.S., ZOBERG, G.C.: Soil bin evaluation of disc coutlers under no – till crop residue conditions. Trans. of ASAE, 29, 1986: 40–44.
13. LINKE, C.: Direktsaat – eine Bestandsaufnahme unter besonderer Berücksichtigung technischer, agronomischer und ökonomischer Aspekte. Dissertation – Hohenheim. 1998. p. 482.
14. LIU, J., CHEN, Y., KUSHWAHA, R.L.: Effect of tillage speed and straw length on soil and straw movement by a sweep. Soil and Tillage Res. 109, 2010: vol. 109: 9–17.
15. LIU, J., CHEN, Y., LOBB, D.A., KUSHWAHA, R.L.: Soil–straw–tillage tool interaction: field and soil bin study using one and three sweeps. Can. Biosyst. Eng. 47, 2007: 2.1–2.6.
16. RAUCKIS, V.: Conference „Amalgerol 2012“. 2012. <http://www.kustodija.lt/lt/info/394/Konferencijos+Amalgerol+2012+atgarsiai>.
17. SILVA-FERNANDES, T., DUARTE, L.C., CARVALHEIRO, F.; MARQUES, S., LOUREIRO–DIAS, M.C., FONSECA, C., GIRIO, F.: Biorefining strategy for maximal monosaccharide recovery from three different feedstocks: Eucalyptus residues, wheat straw and olive three pruning. Biores. Tec. 183, 2015: 203–212.
18. ŠARAUSKIS, E., BURAGIENE, S., ROMANECKAS, K., SAKALAUSKAS, A., JASINSKAS, A., VAICIUKEVICIUS, E., KARAYEL, D.: Working time, fuel consumption and economic analysis of different tillage and sowing systems in lithuania. Proceedings of 11th International Scientific Conference “Engineering for Rural Development”, May 24–25, Jelgava, Latvia 2012: pp. 52–59.
19. ŠARAUSKIS, E., KÖLLER, K., BUTKUS, V.: Research on technological parameters to determine the design factors of direct drilling coulters for sugar beets. Lanbauforschung Volkenrode, 3, 2005: 171–180.
20. ŠARAUSKIS, E., MASILIONYTĖ, L., ANDRIUŠIS, A., JAKŠTAS, A.: The force needed for breaking and cutting of winter wheat and spring barley straw. Zemdirbyste Agric. 100 (3), 2013: 269–276.
21. ŠARAUSKIS, E., MASILIONYTE, L., ROMANECKAS, K., KRIAUCIUNIENE, Z., JASINSKAS, A.: The effect of the disc coulters forms and speed ratios on cutting of crop residues in no–tillage system. Bulg. J. of Agric. 19 (3), 2013a: 620–624.
22. TABATABAEE, K.R., BORGHEIE, A.: Measuring the Static and Dynamic Cutting Force of Stem for Iranian Rice Varieties. J. of Agric. Sci. Tech. 8, 2006: 193–198.Science, 19 (3) 2013: 620–624.
23. TARAKANOVAS, P., RAUDONIUS, S.: The program package “Selekcija” for processing statistical data. Akademija, Kedainiai. 2003: p. 56.
24. TAVAKOLI, H., MOHTASEBI, S.S., JAFARI, A.: Effects of moisture content, internode position and loading rate on the bending characteristics of barley straw. Res. in Agric. Eng. 2009, vol. 55, no. 2, p. 45–51.
25. VAITAUSKIENĖ, K., ŠARAUSKIS, E., NAUJOKIENĖ, V., LIAKAS, V.: The influence of free-living nitrogen-fixing bacteria on the mechanical characteristics of different plant residues under no-till and strip-till conditions. Soil and tillage Res. 154, 2015: 91-102.
26. WOOD, I.P., ELLISTON, A., COLLINS, S.R.A., WILSON, D., BANCROFT, I., WALDRON, K.W.: Steam explosion of oilseed rape straw: Establishing key determinants of saccharification efficiency. Biores. Tech.162, 2014: 175–183.

Corresponding author:
Lect. dr. Kristina Vaitauskienė, Institute of Agricultural Engineering and Safety, Faculty of Agricultural Engineering, Aleksandras Stulginskis university, Lithuania, Studentu str. 15b, LT-53362,Akademija, Kaunas district, Lithuania, phone: +37037752357, e-mail: kristina.vaitauskiene@asu.lt

TWO-BODY ABRASION OF FE-BASED PARTICLE EPOXY COMPOSITES - EXPERIMENTAL APPROACH

P. Valášek[1], A. Ruggiero[2], R. D'Amato[3], J. Machado[4]

[1]*Department of Material Science and Manufacturing Technology Faculty of Engineering, Prague, Czech University of Life Sciences Prague, Czech Republic*
[2]*Department of Industrial Engineering, University of Salerno, Salerno, Italy*
[3]*Departamento de Ingeniería Mecánica, Universidad Politecnica de Madrid, Madrid, Spain*
[4]*Department of Mechanical Engineering, University of Minho, Guimarães, Portugal*

Abstract

It is possible to efficiently change the mechanical characteristics of polymer materials and simultaneously optimize its cost via micro particle fillers. Inclusion of hard inorganics particles on the basis of metal powders mostly leads to increase of hardness and wear resistance of polymers. These properties can be used in many application areas, for example in agriculture. Optimization of adhesive and cohesive characteristic is possible with these fillers under certain conditions. This paper describes the possibility of filling the reactoplastics represented with epoxy resin filled with hard inorganic powder on the Fe-basis, when the wear resistance and fundamental adhesive characteristics are evaluated. Inclusion of Fe-based powder led to increased resistance against to two-body abrasion of 69% while the adhesive characteristics stayed preserved.

Key words: adhesion, metal powder, strength, wear.

INTRODUCTION

The inclusion of inorganics fillers into the polymer matrix creates the composite system. It is possible to define these systems as polymer particle composites. It is possible to utilize inherent corrosion resistance of polymer particle composites in combination with their excellent mechanical properties and low density in various industry areas (PERREUX AND SURI, 1997). Polymer matrix can by created by reactoplastic or thermoplastic. Reactoplastics have a wide spread in the area of experimental description of composite behavior – they have excellent mechanical properties and the preparation of experiment does not require complicated technological equipment comparing to thermoplastics. Moreover, many reactoplastics, as an epoxy resin for instance, are used in the area of structural adhesive bonding, where the fillers can play a significant factor in optimization (MÜLLER ET AL., 2008; VALÁŠEK AND MÜLLER, 2015; RUGGIERO ET AL., 2015B).

Utilization of aluminium powder in the shape of spherical particles (smaller than 50 µm) for description of shear characteristics on the aluminium sheets is described by KAHRAMANA ET AL. (2008), who state, that even though the finite element analysis shows higher stresses at the adhesive-metal substrate interface, actual failure occurs within the adhesive indicating that the strength of adhesion to the metal substrate surface is stronger than the strength of the adhesive itself. For optimization of the adhesive strength of the joints can be used also different particle on the metal basis. (KILIK AND DAVIES, 1989).

KAVAK AND ALTAN (2012) for example state, Sn-Pb powder. OHSAKO AND YOSHIZAWA (2011) state that it is possible to use the inorganics particles for optimization on the interface – interaction between composite system and adherent to whom the system is applied. This interaction is as important as the ability of matrices to wet the particles, thus mutual semi phase interaction (ZHAI ET AL., 2006).

It is possible to use also hard inorganic particles on the Fe-basis for optimization of plastics matrices (GUNGOR, 2007; GAO ET AL., 2016). GUNGOR (2006) states the comparison of Fe/HDPE composite with the mechanical properties of unfilled HDPE, Fe filled polymer composites showed lower yield and tensile strength, % elongation, and Izod impact strength, while the modulus of elasticity and hardness of the composites were higher than those of HDPE. Interesting possibility of usage ferrite particles are their magnetics properties, which can be according to FULCOA ET AL. (2016) used in polymer matrices in the combination with different kinds of fillers, for example with fibers (ZOIS ET AL., 2003).

TIAN ET AL. (2014) also use Fe-Si particles in the interaction with epoxy resin to optimize magnetic properties of matrix with different temperatures (-60°-

140 °C), but at the same time they state, that impact strength of Fe-Si/epoxy composites increases with increasing the Fe-Si content.

Presence of hard inorganic particles in polymer material increases wear resistance (RUGGIERO ET AL., 2015A). Morphology of particles ranks among significant parameters, which effect the adhesion between filler and the used resin – CHENG ET AL. (2002) state as the most important parameter the roughness of particles and they say that important is also the shape of particles and also their size (LAU ET AL., 2006). Filled reactoplastic in form of so called liquid metals is possible to use for renovation of functional parts of machines and equipment (VALÁŠEK ET AL., 2015).

This experiment has as objective to describe the resistance of particle composite on the basis of Fe-based powder and epoxy resin (Fe-based/Epoxy) to two-body abrasion. Description of adhesive characteristic is important from the viewpoint of interaction of composite and surface to which is the system applied. Remaining mechanical properties and picture analysis of fracture areas are shown to clarify the behavior of composite.

MATERIALS AND METHODS

Special technological procedure (such as vacuum) has not been used for the preparation of composite mixtures. Procedure of preparation was chosen with respect to minimization of resulting price of composite and with respect to practise where the composites – liquid metals – determined for renovation of machine parts are applied straight on the renovated area.

Two-component epoxy resin Glue Epox Rapid was used. The particles on the Fe basis were mechanically mixed into the resin. Composites were prepared with different volume percentage of filler because of determination of effect of particle inclusion on mechanical properties as: 5%, 10%, 15%, 20% and 25%.

For optical and chemical analysis of Fe-based powder and optical analysis of fracture areas was used electron microscope - SEM - (Tescan Mira 3 GXM) equipped with an energy dispersive X-ray on the surface of each sample using vacuum coating (Quorum Q150R ES) which scan system (Oxford X-MaxN). For analysis of adherent surface was used fluorescence confocal microscope (Axio Imager Zeiss LSM 800).

The two-body abrasion was tested on a rotating cylindrical drum device with the abrasive cloth of the different grain size (P120, P220 and P400 - Al_2O_3 grains) according to the standard CSN 62 1466. The testing specimen is in the contact with the abrasive cloth and it covers the distance of 60 m. During one drum turn of 360° it is provoked the testing specimen left above the abrasive cloth surface. Consequent impact of the testing specimen simulates the concussion. The pressure force is 10 N. The mean of the testing specimens was 15.5 ± 0.1 mm and their height was 20.0 ± 0.1 mm. The mass decreases were measured on analytic scales weighing on 0.1 mg. The volume decreases were calculated on the basis of the found out volume and the density of the composite systems. The highest temperature value observed in the interface of the testing sample and the abrasive cloth was recorded by thermal camera. The hardness of test specimens was measured by the method Shore D (CSN EN ISO 868).

Adhesion characteristics were assessed on aluminium adherents with a thickness of 1.5 mm in accordance with the standard CSN EN 1465. The surfaces of aluminium sheets were blasted using the synthetic corundum (Al_2O_3) of the fraction F80 under the angle of 90°. Then the surface was cleaned and degreased using perchlorethylene and prepared to the composite application. Adequate surface treatment of adherents is required before applying resins (VALÁŠEK AND MÜLLER, 2014). The lapping was according to the standard 12.5 ± 0.25 mm (see Fig. 1).

For statistical comparison the T-test and ANOVA were used when the zero hypothesis H_0 ($p > 0.05$) states an agreement of the statistical sets of data.

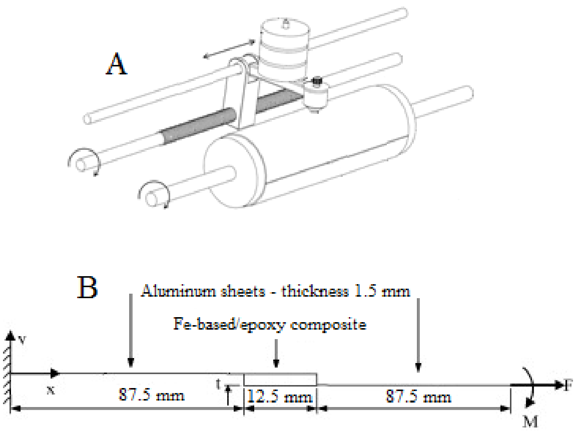

Fig. 1. – a) Schema of equipment for two-body abrasive wear testing, b) Model of lap-shear testing

RESULTS

Specification of fillers (particles) before application into the matrix, i.e. determination of chemical content and morphology of particles, is essential from the point of view of understanding the semi phase interaction. Specific chemical composition of particles was determined experimentally by the Oxford X-MaxN EDS system, resolution at 5.9 keV – 124 eV (Fe 98.2%, see Fig. 2).

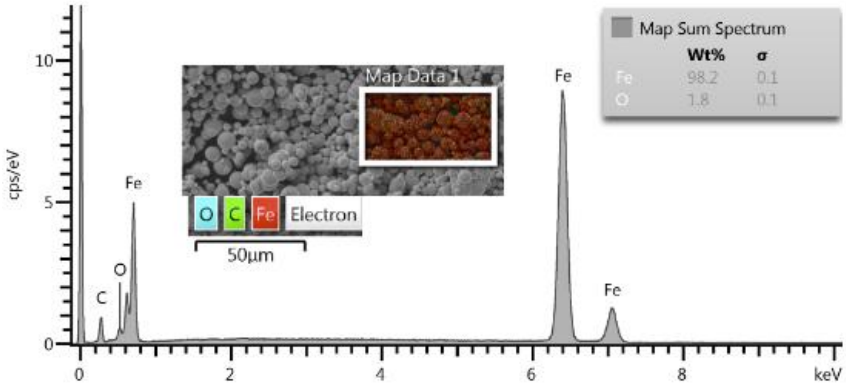

Fig. 2. – Results of EDS particle analysis of Fe-based powder

Powdery density of Fe-based powder is from 3.0 to 5.0 g·cm^{-3}, pycnometrics density 7.0 g·cm^{-3}. Perfect wetting of filler with resin (1.15 g·cm^{-3}) is considered when preparing the composite systems, therefore the pycnometrics density is used for calculations (theoretical density). Dimension of particles was determined via optical analysis (see histogram Fig. 3-a). Particles evinced the spherical shape, see image from electronic microscope (Fig. 3-b).

Among significant qualitative factors of composite systems ranks the porosity *P*, which calculation follows from the comparison of theoretical and real density of composite. Higher porosity shows the excessive presence of air bubbles or bad distribution of the filler (see Tab. 1). Another mechanical property which can be in correlation with assessed wear resistance is hardness (see Tab. 1) - stated properties were assessed on testing samples for resistance to abrasive wear, hardness was assessed in their sedimented parts. Presence of Fe-based powder in epoxy resin increased the hardness according to Shore D from the value 89.63 ± 1.06 (0%) up to value 93.42 ± 1.32 (25%).

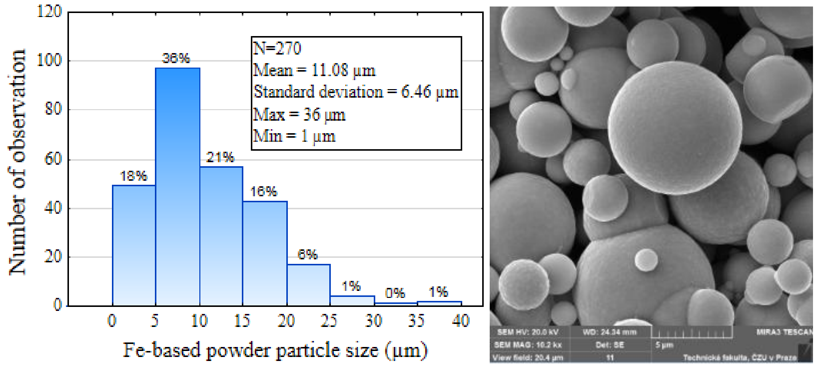

Fig. 3. – a) Histogram (left), b) Spherical Fe-based particles (right)

Tab. 1. – Density, porosity and hardness

Properties	0%	5%	10%	15%	20%	25%
Theoretical density (g·cm^{-3})	1.15	1.44	1.71	2.03	2.32	2.61
Porosity (%)	0	5.6	6.5	4.9	6.0	7.3
Hardness Shore D (-)	89.63	91.05	91.13	92.65	92.62	93.42
Standard deviation (-)	1.06	1.70	1.14	0.91	1.47	1.32
Variation coeficient (%)	1.2	1.9	1.3	1.0	1.6	1.4

The fluorescence confocal microscope Axio Imager Zeiss LSM 800, objective with magnification 10x and numerical aperture 0.45 was used for description of surface of aluminium sheets before application of composite system (see Fig. 4). Significant parameters of roughness measured by described procedure states Tab. 2 according to standard ISO 25178.

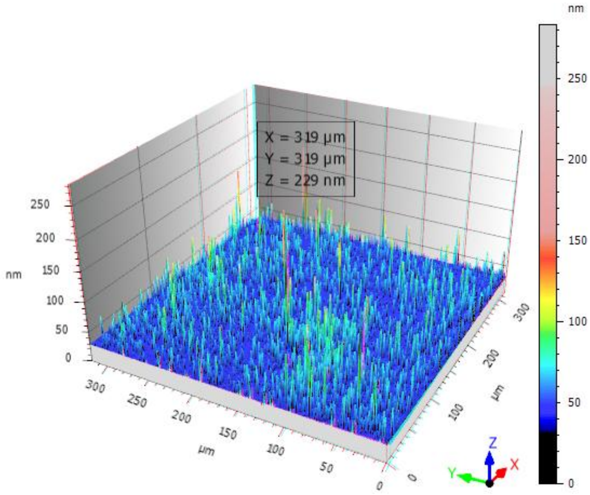

Fig. 4. – Topography of surface of Al sheet before application of composite

Tab. 2. – Roughness parameters (ISO 25178)

Properties	Mean	SD	Min	Max
Arithmetical mean height of the surface Sa (nm)	16.6	13.9	1.89	42.6
Maximum height of the surface Sz (nm)	255	0.53	251	255
Maximum height of valleys Sv (nm)	12.1	11.6	1.0	36.0
Maximum height of peaks Sp (nm)	243	11.6	219	254
Root mean square height of the surface Sq (nm)	28.7	19.3	6.10	61.5

Fig. 5 a, b and c represents the cut of the bonded joint via SEM analysis. Very good wetting in the interface of composite system and adherent is visible in the cut of the joints. Good interaction of particular phases and whole composite system with adherent is crucial for corresponding mechanical properties.

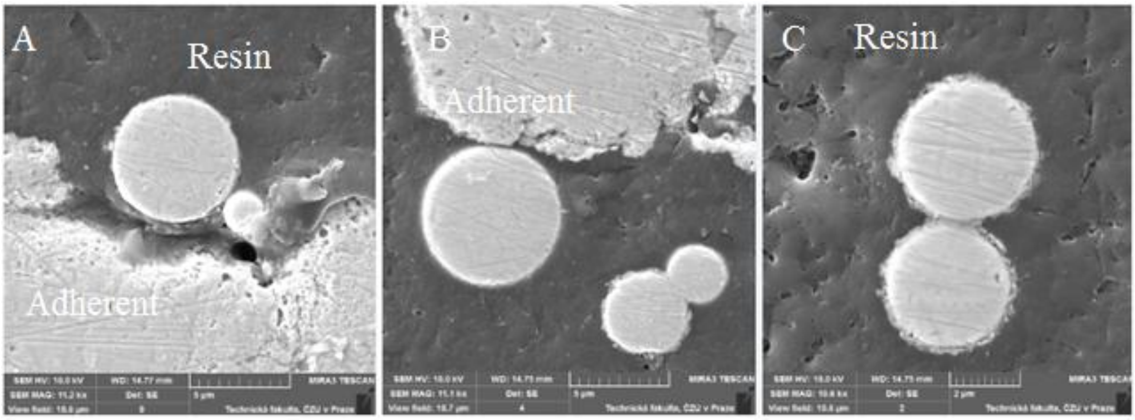

Fig. 5. – Cut of the bonded joint (SEM): a - Wetting with presence of bubble, b - Perfect wetting of adherent and particles, c - Wetting of particles

Resin without filler reached shear strength 8.82 ± 0.44 MPa on the aluminium adherent. From statistical analysis provided with T-test is possible to confirm the null hypothesis H_0: $\mu1=\mu2$ up to concentration of filler 15% ($p > 0.06$). It is possible to state that increased concentration of filler in the resin (20 and 25%) led to statistically decrease of values in shear strength.

Arrangement of particles of Fe-based powder in the composite system on the cohesive fracture is pictured via SEM analysis on Fig. 6 a, b and c. Good mutual interaction between particles of Fe-based powder and used epoxy resin is visible from the images.

Tab. 3. – Lap-shear tensile strength

Properties	0%	5%	10%	15%	20%	25%
Shear strength (MPa)	8.82	8.19	8.03	7.98	7.58	7.60
Standard deviation (MPa)	0.44	0.50	0.80	0.72	0.55	0.77
Variation coeficient (%)	5.0	6.1	10.0	9.0	7.2	10.1
T-test (*p*) compared with 0% (-)	1	0.06	0.08	0.06	0.00	0.00

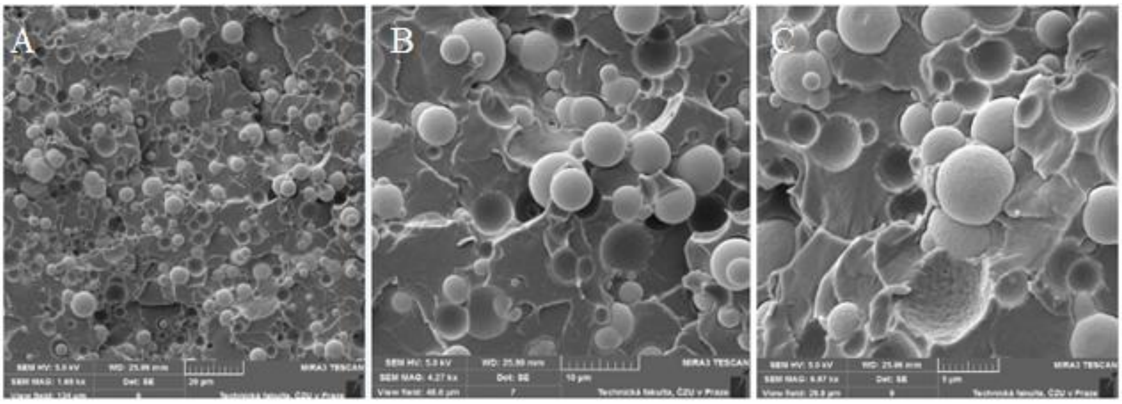

Fig. 6. – Analysis of cohesive fracture (SEM): a) MAG 1.68 kx, b) MAG 4.27 kx, c) MAG. 6.97 kx

Results of resistance to two-body abrasion shows Fig. 7-a, from the graph is visible that presence of Fe-based powder increased the ability of the system to resist to two-body abrasion. Volume losses of unfilled resin corresponded to 0.631 ± 0.009 cm^3 (P120), 0.367 ± 0.004 cm^3 (P220) and 0.213 ± 0.003 cm^3 (P400). During the test of resistance to abrasive wear was measured temperature of testing sample via thermal camera, the temperature did not exceed 41.4 °C (Fig. 7-b).

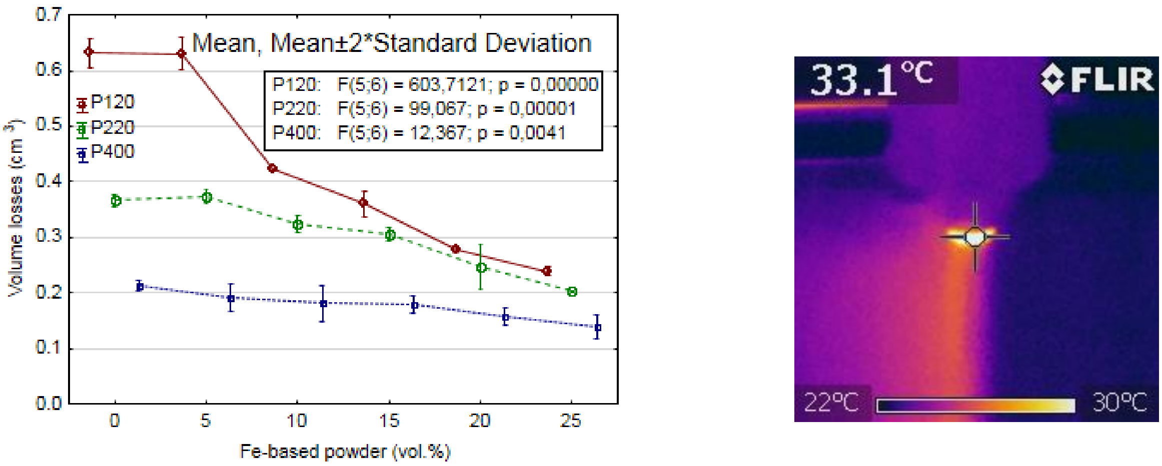

Fig. 7 – Resistance to two-body abrasion: a) Results (left), b) Image from thermal camera: course of the test (right)

DISCUSSION

Chosen technological procedure of preparation of composites without using the vacuum follows from the practical requirements, i.e. simple and fast application on the functional surfaces, however this procedure has an impact on demonstrable presence of pores in the material (on an average 6%). High porosity negatively affects the assessed mechanical properties, limitation of porosity can lead to optimization of monitored characteristics. On the scale of Shore D was the increase of hardness by inclusion of Fe-based powder about 2.6% and it was in compliance with conclusions of many authors (SATAPATHY AND BIJWE, 2002; VALASEK ET AL., 2015) who describe the inclusion of hard inorganic microparticles into the polymers. Resistance to abrasive wear increased with increasing amount of filler in the matrix, which is in compliance with many authors (SATAPATHY AND BIJWE, 2007; XUE QUNJI AND WANG QUIHA, 1997), who used hard inorganic particles on the basis of corundum, silicon carbide or powder on the metal basis to increase the resistance of polymers. Ability to increase the resistance to abrasion was the most manifested on cloth with bigger abrasive grains (P120), where the volume losses decreased up to 62% (for cloth P220 was decrease 45% and for cloth P400 was decrease 34%). In the interval with concentration of Fe-based powder in resin 5-15% was not statistically significant decrease of values of shear strength, there was a decrease of values of shear strength max. 15% with higher concentration of the filler.

CONCLUSIONS

Described composite systems preserve adhesive properties assessed via shear strength with inclusion of Fe-based powder up to 15%. There is a slight decrease of this characteristic from this concentration. Inclusion of Fe-based powder increased the hardness and wear resistance. Described properties correspond to requirements of filled polymers used for renovation of functional areas of machines and equipment – there is an increase of resistance to abrasive wear with preservation of adhesive characteristic. Abrasive wear ranks among the most represented kinds of wear in the area of agriculture.

REFERENCES

1. FULCOA, A.P.P., MELO, J.D.D., PASKOCIMAS, C.A., MACHADO, F.L.D.A., RODRIGUES, A.R.: Magnetic properties of polymer matrix composites with embedded ferrite particles. Ndt&E Int., 77, 2016: 42–48.
2. GAO, G., LI, Y., CHEN, Y.: Dynamic response for porous epoxy resin matrix composites filled with iron powder at different strain rates and constitutive relationships. Mech Adv Mater Struc., 23(7), 2016: 811–818.
3. GUNGOR, A.: Mechanical properties of iron powder filled high density polyethylene composites. Materials and Design, 28(3), 2007: 1027–1030.
4. GUNGOR, A.: The physical and mechanical properties of polymer composites filled with Fe powder. Journal of Applied Polymer Science, 99, 2006: 2438–2442.
5. Cheng, W. – Dunn, P.F. – Brach, R.M.: Surface roughness effects on microparticle adhesion. J Adhesion, 78(11), 2002: 929–965.
6. KAHRAMANA, R., MEHMET, S., BEKIR Y.: Influence of adhesive thickness and filler content on the mechanical performance of aluminum single-lap joints bonded with aluminum powder filled epoxy adhesive. J Mater Process Tech., 205, 2008: 183–189.
7. KAVAK, N., ALTAN, E.: Influence of filler amount and content on the mechanical performance of joints bonded with metal powder filled adhesive. In: 15th International Conference on Advances in Materials and Processing Technologies, Wollongong, 773–774, 2012, pp. 226–233, NSW, Australia.
8. KILIK, R., DAVIES, R.: Mechanical properties of adhesive filled with metal powders. Int J Adhes Adhes., 9(4), 1989: 224–228.
9. LAU, K.T., GU, C., HUI, D.: A critical review on nanotube and nanotube/nanoclay related polymer composite materials. Compos Part B-Eng., 37, 2006: 425–436.
10. MÜLLER, M., ET AL.: Optimization of surface treatment parameters in adhesive bonding technology. In: 7th International Scientific Conference - Engineering for Rural Development, 2008, pp. 214–219, Latvia University of Agriculture, Jelgava.
11. OHSAKO, F., YOSHIZAWA, K.: Molecular theory of adhesion of metal/epoxy resin interface. Kobunshi Ronbunshu, 68(2), 2011: 72–80.
12. PERREUX, D., SURI, C.: A study of the coupling between the phenomena of water absorption and damage in glass/epoxy composite pipes. Compos Sci Technol., 57, 1997: 1403–1413.
13. RUGGIERO, A., ET AL.: Friction and wear behaviors of Al/Epoxy composites during reciprocating sliding tests. Manufacturing Technology, 15(4), 2015a: 684–689.
14. RUGGIERO, A., MEROLA, M., CARLONE, P., ARCHODOULAKI, V. M.: Tribo-mechanical characterization of reinforced epoxy resin under dry and lubricated contact conditions. Compos Part B: Eng., 79, 2015b: 595–603.
15. SATAPATHY, B.K., BIJWE, J.: Analysis of simultaneous influence of operating variables on abrasive wear of phenolic composites. Wear, 253 2002: 787–794.
16. TIAN, J., ET AL.: Impact and magnetic properties of magnetic Fe-Si/epoxy composites. Fuhe Cailiao Xuebao/Acta Materiae Compositae Sinica, 31(1), 2014: 1–8.
17. VALASEK, P., MÜLLER, M.: Abrasive wear in three-phase waste-based polymeric particle composites. Teh Vjesn., 22(2), 2015: 257–262.
18. VALASEK, P., MULLER, M., SERGEJ, H.: Recycling of corundum particles – two-body abrasive wear of polymeric composites based on waste. Teh Vjesn., 22(3), 2015: 567–572.
19. VALASEK, P., MULLER, M.: Application of wear-resistant polymeric particle composites in construction of ploughing body. Listy Cukrov Repar., 130, 2014: 284–288.
20. XUE, Q., WANG, Q.: Wear mechanisms of polyetheretherketone composites filled with various kinds of SiC. Wear, 213 1997: 54–58.
21. ZHAI, L., LING, G., LI, J., WANG, Y.: The effect of nanoparticles on the adhesion of epoxy adhesive. Mater Lett., 60(25-26), 2006: 3031–3033.
22. ZOIS, H., APEKIS, L., MAMUNYA, Y.P.: Structure-electrical properties relationships of polymer composites filled with Fe-powder.Macromolecular Symposia, 194, 2003: 351–359.

Corresponding author:

doc. Ing. Martin Valášek, Ph.D., Department of Material Science and Manufacturing Technology, Faculty of Engineering, Czech University of Life Sciences Prague, Kamýcká 129, Praha 6, Prague, 16521, Czech Republic, phone: +420 22438 3262, e-mail: valasekp@tf.czu.cz

TOOLS FOR EVALUATION OF WEED COMPETITIVENNESS OF WHEAT

O. Vlášek, P. Konvalina, K. Suchý, B. Machková

Faculty of Agriculture, University of South Bohemia in České Budějovice, Czech Republic

Abstract

This study is concentrated on the testing of methods of weed competitiveness evaluation. There were used simple scoring methods (tuft shape, the length of the plant) and compared with indirect methods based on LAI (SunScan Devices - Canopy Analysis Sytem) and soil coverage evaluation (multispectral image data analyzes by software MultiSpecW32). When evaluating parameter LAI, there were positive correlations with the length of the plant in all stages of measuring (BBCH 33-36, 55, 69). When assessing ground cover vegetation in BBCH 29, there were possitive correlation with the length of plants in all stages of the evaluation (BBCH 33-36, 55, 69). After evaluating the characters contributing to the weed competitiveness of varieties, we can´t find variety with the highest weed competitiveness. But the results of our experiment shown that tools based on LAI and soil coverage measurements could be use for proposal of varieties with better weed competitiveness.

Key words: methods of evaluation, wheat, weed competitiveness.

INTRODUCTION

Weed plants are one of the main factors limiting the level of agricultural yield (ANDREW ET AL., 2015). In comparison with pests and diseases, weeds have the potential to incur the greatest yield loss, through competition with the crop and decreasing yield quality, and can, therefore, incur high costs of control (OERKE, 2006). Because of the availability of herbicides in the last 50 years, the natural competitiveness of field crops to weeds has been overlooked (LAMMERTS VAN BUEREN, 2002). Application of herbicides have also significant environmental impact. While i.e. the volume of greenhouse gases emissions caused by the application of pesticides has decreased during the time (MOUDRÝ ET AL., 2013A), and is currently on low values (MOUDRÝ ET AL., 2013B; MOUDRÝ ET AL., 2013C), the ecotoxicity of pesticides is often high.

Many cultural control methods may be employed by farmers to reduce weed populations, including delayed drilling, increased seed rate and rotational ploughing (LUTMAN ET AL., 2013). Competitive cultivars are a potentially attractive option in comparison, because they do not incur any additional costs (ANDREW ET AL., 2015). Cereal cultivars having a high degree of crop competitive ability, especially against aggressive weeds, are highly beneficial in organic farming as well as in other farming systems that aim to limit the use of herbicides (HOAD ET AL, 2008; MASON ET AL., 1990). Morphological, physiological, and biochemical traits are thought to control plant competitiveness. A competitive crop ideotype for spring wheat should include taller plants, with fast early season growth, early maturity, and increeased fertile tiller number (MASON ET AL., 1990; KÖPKE 2005; KRUEPL ET AL 2006).

Early interest in competitive cultivar traits mainly focussed on maximum canopy height. Although the advantages of plant height in terms of shading weeds are clear, it cannot, alone, explain variation in competitive ability (ANDREW ET AL., 2015). Early vigour of a cultivar is related to crop establishment and the rate at which aboveground material is produced and has been correlated with morphological leaf traits such as leaf area in the earliest phases of growth (REBETZKE & RICHARDS, 1999). Tillering capacity in wheat contributed to suppression of dry matter production in mixed flora assemblages (KORRES & FROUD- WILLIAMS, 2002). In wheat, leaf area index at early growth phases was associated with suppression (HUEL & HUCL, 1996; HOAD ET AL., 2006; HANSEN ET AL., 2008).

The competitiveness against weed is not targeted by breeding of modern wheat cultivars (KONVALINA ET AL., 2014). We cannot consider the newly bred plants are naturally competitive to weed plants, because it has not confronted any important competitive weed plant during the breeding process (LAMMERTS VAN BUEREN, 2002).

Methods for determination of the ability to suppress weeds must be practical and stable enough to be employed in the breeding selective process and in the evaluation of new lines and cultivars. Selection of the ability to suppress weeds can be made at weeded plots directly, or, according to BERTHOLDSSON (2005), it can be made indirectly – by selection of characteristics (features) related to the competitiveness.

This study aims to verify practical possibilities for the employment of modern methods, which are based on a detailed analysis of image, or a measurement of leaf area. We can study natural wheat competitiveness against weeds by using these methods and techniques. This work partly aims to evaluate correlations of the above-mentioned methods with classical evaluation techniques, which are based on evaluation of particular morphological characteristics.

MATERIALS AND METHODS

Eight spring wheat varieties (Anabel, Astrid, Dafne, Izzy, Quintus, KW Scirocco, SG – S833 – 11, and SW Kadrilj) were grown on the test plots in České Budějovice and Zvíkov. The experiment was carried out in compliance with organic farming standards.

Characteristic of the test plot in České Budějovice is as follows: altitude of 385 metres above sea level, grain-growing region, land type – sand and earth, gley brown soil. Beans (Faba vulgaris) as forgoing crops. Harrowing (protection against weeds) was carried out once a growing season.

Characteristic of the test plot in Zvíkov is as follows: altitude of 485 metres above sea level, grain-growing region, land type – earth, brown soil. Mixture of legumes and cereals as a forgoing crop. Harrowing (protection against weeds) was carried out once a growing season.

Evaluating the wheat competitiveness against weeds, we studied the following characteristics:

- Tuft shape (the methodology reference) in BBCH 29;
- Length of plants (the methodology reference) measured in three different periods (BBCH 33–36, BBCH 51–55, BBCH 69);
- Flag leaf position (the methodology reference) in BBCH 51–55;
- Vegetation cover was measured with the MultiSpecW32 software instrument during the periods of BBCH 29 and BBCH 33–36;
- LAI analysis was carried out with the SunScan (Canopy Analysis System) instrument during three different periods (BBCH 33–36, BBCH 51–55, BBCH 59).

The statistical data analysis was carried out with the STATISTICA 9.1 (StatSoft, Inc. USA) program. We used the analysis of variance (ANOVA) in order to evaluate an impact of the locality, variety or both on every assessed characteristic. Tukey HSD test was carried out as well. We measured average figures of every variety at both stations. We also measures average figures of every characteristic at both stations. Correlations were employed there; they showed closeness strength) of relations between the variables.

RESULTS AND DISCUSSION

Official variety tests do not deal with the competitiveness of cereals against weeds. Some of the recommended characteristics are evaluated there, they are not interpreted anyway (their relation to the competitiveness against weeds is not interpreted there). This is e.g. the length of plant (HOAD ET AL., 2006). Therefore, our article aims to describe relations (correlations) between the individual characteristics that influence the competitiveness against weeds. At the same time, we have to tell genetically determined characteristics apart. We have to tell characteristics influencing the environment apart as well.

Tab. 1 shows the results of analysis of variance for every factor. The results have shown the length of plant is influenced by the locality (it was strongly influenced in every measured and tested case). Varieties of cereals with long stalks are much more competitive than varieties with short stalks (CUDNEY ET AL., 1991). The other way around, the tuft shape and the position of flag leaf were influenced by the variety, not the locality in our tests (see Tab. 2). The vegetation cover rate was strongly influenced by the locality in our tests. It is one of the most significant characteristics for the competitiveness against weeds (LEMERLE ET AL., 1996).

Tab. 1. – Analysis of factor influence (ANOVA**)**

Factor	DF	LAI BBCH 36		LAI BBCH 49		LAI BBCH 55		Plant length BBCH 33-36		Plant length BBCH 55		Plant length BBCH 69	
		MS	%	MS	%	MS	%	MS	%	MS	%	MS	%
Variety (1)	7	1.7178	16.2***	0.694	1.63ns	1.20	1.91***	48	16.2**	74	0.26***	470	1.87***
Locality (2)	1	7.6002	71.7***	38.07	89.5***	60.30	96.0***	31827	71.7***	28203	99.6***	2456	97.82***
1x2	7	0.9226	8.7*	3.171	7.46***	1.070	1.70***	31	8.69*	38	0.13**	76	0.30**
Eror	176	0.389	-	0.595	-	0.268	-	13	-	11	-	27	-
Note: P < 0.05; **P < 0.01; P < 0.001; ns - no significant													

Tab. 2. – Analysis of factor influence (ANOVA)

Factor	DF	Uncovered soil BBCH 29		Uncovered soil BBCH 33-36		Soil coverage BBCH 29		Soil coverage BBCH 33-36		Tuft shape		Flag leaf position	
		MS	%	MS	%	MS	%	MS	%	MS	%	MS	%
Variety (1)	7	152	5***	111	6***	152	5***	111	6***	44.1	88**	46**	87
Locality (2)	1	2860	93***	1604	89***	2869	93***	1604	89***	3.0	6**	0**	0
1x2	7	74	2**	80	5***	75	2**	80	5***	3.0	6**	7**	12
Eror	176	21	-	18	-	21	-	18	-	0.0	-	0	-
Note: P < 0.05; **P < 0.01; P < 0.001; ns - no significant													

Tab. 3. – Variety evaluation results I

Variety	LAI BBCH 36	LAI BBCH 49	LAI BBCH 55	Plant length BBCH 33-36	Plant length BBCH 55	Plant length BBCH 69
Anabel	1.76±15.1ab	2.66±13.9a	3.13±11.5a	35.25±15.0a	47.67±13.9a	74.25±11.5a
Astrid	1.95±12.8ab	3.05±11.9a	3.39±14.3ab	32.83±12.8a	52.58±11.9a	81.63±14.3ab
Dafne	2.24±14.2ab	2.86±10.4a	3.14±12.1ab	33.83±14.2a	51.29±10.4a	81.20±12.1ab
Izzy	2.33±13.0b	2.91±12.5a	3.51±11.3ab	34.66±13.0a	52.79±12.5a	88.70±11.3b
Quintus	1.66±15.3a	3.00±13.0a	3.83±10.1b	33.20±15.3a	51.37±13.0a	78.33±10.1ab
KW Scirocco	1.73±11.7a	2.97±13.5a	3.40±14.1ab	37.17±11.7a	50.71±13.5a	84.29±14.1ab
SW Kad-rilj	1.68±13.0a	2.90±12.9a	3.27±12.7ab	33.25±13.6a	53.25±13.8a	84.75±14.4ab
SG S 833	2.12±13.6ab	3.26±13.8a	3.34±14.4ab	34.38±13.0a	50.63±12.9a	79.50±12.7ab
Note: Statistically different at P < 0,05 (Tukey HSD test).						

Tab. 3 and 4 show the results of evaluated parameters of every tested variety. The results have shown a considerable variability of characteristics among tested varieties. We can choose a variety which has more preferable characteristic in more likely to be competitive against weeds.

Tab. 4. – Variety evaluation results II

Variety	Uncovered soil BBCH 29	Uncovered soil BBCH 33-36	Soil coverage BBCH 29	Soil coverage BBCH 33 - 36	Tuft shape BBCH 29	Flag leaf position BBCH 55
Anabel	42.02±7.3ab	32.89±5.5ab	57.98±7.9ab	67.11±5.6ab	3.00±0.0a	5.00±0.0b
Astrid	40.58±5.3a	29.75±3.8b	59.42±5.3a	70.25±3.8b	3.00±0.0a	3.00±0.0a
Dafne	39.14±6.7a	31.80±5.5ab	60.86±6.7a	68.20±5.5ab	5.00±0.0b	3.00±0.0a
Izzy	46.83±.4b	36.01±3.4a	53.17±5.4b	63.98±3.4a	1.00±0.0c	3.00±0.0a
Quintus	43.83±4.7ab	33.46±5.6ab	56.17±4.7ab	66.53±5.6ab	5.00±0.0b	5.00±0.0b
KW Scirocco	40.69±5.5a	34.99±6.0a	59.31±5.5a	65.01±6.0a	3.00±0.0a	5.00±0.0b
SW Kadrilj	40.78±6.3a	33.99±3.0ab	59.22±6.3a	66.01±3.0ab	3.00±1.0d	3.00±0.0a
SG S 833	44.20±6.8ab	360.3±7.8a	55.85±6.9ab	63.96±7.8a	3.00±0.0a	7.00±1.0c
Note: Statistically different at P < 0,05 (Tukey HSD test).						

Assessing the practical employment of the weed competitiveness evaluation methods and techniques, we carried out and assessed the correlation analysis (see Tab. 5). Measuring the leaf area index (LAI) in BBCH 49, we found positive correlations with the length of plant in every measured period (BBCH 33–36, 55, 69). LAI is one of the main factors that influence the competitiveness to weeds (Huel and Hucl, 1996). The length of plant we measured in BBCH 33–36, 55 and 69, correlated with the leaf area LAI (BBCH 55). The length of plant in BBCH 55 related obviously to the length of plant in BBCH 33–36 and BBCH 69. We also found a correlation between the vegetation cover in BBCH 29 and the length of plant in BBCH 33–36, 55 and 69. LAI figures in BBCH 55 correlated with the vegetation cover in BBCH 33–36. We found a correlation in every stage of evaluation. Such a finding has been supported by NEUHOFF ET AL. (2005) who also say that the total LAI correlates to the vegetation cover. Crop stands with well-established photosynthetic apparatus are more likely to reach higher LAI values, even in later stages of growth. The other way around, plants with smaller leaf area in early stages of growth do not reach larger leaf area or higher yield rate during the rest of the growing season either (DREWS ET AL., 2004).

Tab. 5. – Correlation analysis

Parameter	Mean	SD	LAI BBCH 33-36	LAI BBCH 49	LAI BBCH 55	Plant length BBCH 33- 36	Plant length BBCH 55	Plant length BBCH 69	Uncovered soil BBCH 29	Uncovered soil BBCH 33 -36	Soil coverage BBCH 29	Soil coverage BBCH 33-36	Tuft shape BBCH 29	Flag leaf position BBCH 55
LAI BBCH 36	1.93	0.702												
LAI BBCH 49	2.95	0.943	0.13*											
LAI BBCH 55	3.38	0.803	0.25*	0.34*										
Plant length BBCH 36	34.32	13.47	0.25*	0.46*	0.68*									
Plant length BBCH 55	51.29	12.72	0.27*	0.47*	0.69*	0.95*								
Plant length BBCH 69	81.58	13.15	0.27*	0.44*	0.61*	0.88*	0.92*							
Uncovered soil BBCH 29	42.26	6.523	-0.10*	-0.24*	-0.36*	-0.55*	-0.52*	-0.47*						
Uncovered soil BBCH 33 -36	33.65	5.615	-0.12*	-0.19*	-0.40*	-0.46*	-0.49*	-0.41*	0.58*					
Soil coverage BBCH 29	57.73	6.527	0.10*	0.25*	0.36*	0.55*	0.52*	0.47*	-1.00*	-0.58*				
Soil coverage BBCH 33-36	66.38	5.615	0.12*	0.19*	0.40*	0.46*	0.49*	0.41*	-0.58*	-1.00*	0.58*			
Tuft shape	3.13	1.320	-0.11^{ns}	0.01^{ns}	-0.01^{ns}	-0.11^{ns}	-0.13^{ns}	-0.26*	-0.12^{ns}	-0.12^{ns}	0.12^{ns}	0.12^{ns}		
Flag leaf position	4.25	1.396	-0.15*	0.97^{ns}	0.06^{ns}	0.06^{ns}	-0.07^{ns}	-0.13^{ns}	0.01^{ns}	0.11^{ns}	-0.01^{ns}	-0.11^{ns}	0.19*	
Note: *Statistically significant. ^{ns}Not significant														

CONCLUSIONS

This study was concentrated on the evaluation of competitive ability of spring wheat varieties by selected characteristics affecting competitiveness against weeds. It also included the practical verification of image analysis methods and LAI index measurement that were employed and the natural wheat competitiveness against weeds was tested and assessed. The results have shown close correlations between the above-mentioned methods and the classical evaluation of characteristics, which is based on a plant morphology. If the cereal variety testing includes the weed competitiveness testing in the future, a combination of methods will be employable there – the plant morphology and the (crop stand) vegetation cover.

ACKNOWLEDGEMENT

This work was supported by the research project No. NAZV QJ1310072 of the National Agency for Agricultural Research of the Ministry of Agriculture of the Czech Republic and the University of South Bohemia in České Budějovice (project No. GAJU 094/2016/Z).

REFERENCES

1. IKS, A., STORKEY J., SPARKES D.: A review of the potential for competitive cereal cultivars as a tool in integrated weed management. Weed Res. 55, 2015: 239–248.
2. BERTHOLDSSON, N. O.: Early vigour and alleopathy – Two useful Traits for enhanced barley and beat competitiveness against weeds, Weed Res. 45, 2005: 94-102.
3. CUDNEY, D.W., JORDAN, L. S., HALL, A. E.: Effect of wild oat (*Avena fatua*) infestations on light interception and growth rate of wheat (*Triticum aestivum)*, Weed Sci. 39, 1991: 175-179.
4. DREWS, S. D., NEUHOFF – KÖPKE, U.: Optimizing fading ability of winter beat stand as a method of weed control, J. Plant Dis. Prot. 19, 2004: 545-552.
5. HANSEN, P. K., KRISTENSEN, K., WILLAS, J. A weed suppressive index for spring barley (Hordeum vulgare) varieties. Weed Res. 48, 2008: 225–236.
6. HOAD, S. P., DAVIES, D. H. K., TOPP, C. F. E.: How to select varieties for organic farming: science and practice. In: ATKINS, C., BALL, B., DAVIES, D. H. K., REES, R., RUSSELL, G., STOCKDALE, E. A., WATSON, C. A., WALKER, R., YOUNIE, D.: What Will Organic Farming Deliver? Aspects of Applied Biology, pp. 117–120. Association of Applied Biologists, Warwick, UK. 2006.
7. HOAD, S., TOPP, C., DAVIES, K.: Selection of cereals for weed suppression in organic agriculture: a method based on cultivar sensitivity to weed growth. Euphytica 163, 2008: 355–366.
8. HUEL, D. G., HUCL, P.: Genotypic variation for competitive ability in spring wheat. Plant Breed. 115, 1996: 325–329.
9. KONVALINA, P., STEHNO, Z., CAPOUCHOVÁ, I., ZECHNER, E., BERGER, S., GRAUSGRUBER, H., JANOVSKÁ, D., MOUDRY, J.: Differences in grain/straw ratio, protein content and yieldin landraces and modern varieties of different wheat species under organic farming. Euphytica 199, 2014: 31-40
10. KÖPKE, U.: Crop ideotypes for organic cereal cropping systems. In: LAMMERTS VAN BUEREN, E. T., ØSTERGÅRD, H. (Eds.): Proceedings of the COST SUSVAR/ECO-PB Workshop on Organic plant Breeding Strategies and the use of Molecular Markers, pp. 13-16. Louis Bolk Institute, Driebergen, Netherlands, 2005.
11. KORRES, N. E., FROUD-WILLIAMS, R. J.: Effects of winter wheat cultivars and seed rate on the biological characteristics of naturally occurring weed flora. Weed Res. 42, 2002: 417–428.
12. KRUEPL, C., HOAD, S., DAVIES, K., BERTHOLDSSON, N. O., PAOLINI, R.: Weed competitivness. In: DONNER, D., OSMAN, A. (Eds.): Handbook cereal variety testing for organic low input agriculture. COST860-SUSVAR, pp. W1-W16, Risø National Laboratory, Denmark, 2006.
13. LAMMERTS VAN BUEREN, E. T. (ET AL).: Ecological concepts in organic farming and their consequences for an organic crop ideotype. In: LAMMERTS VAN BUEREN, E. T.: Organic plant breeding and propagation: concepts and strategies, [Ph.D. thesis.]. Wageningen University, Wageningen, The Netherlands, 2002: pp. 38-61.
14. LEMERLE, D., VERBEEK, B., COUSENS, R. D., COOMBES, N. E.: The potential for selecting wheat varieties strongly competitive against weeds. Weed Res. 36, 1996: 505–513.
15. MARTIN, R. J., FELTON, W. L.: Effect of crop-rotation, tillage practice, and herbicides on the population-dynamic of wild oats in wheat. Aust. J. Exp. Agr. 33, 1993: 159-165.
16. MOUDRÝ, J. JR., JELÍNKOVÁ, Z., PLCH, R., MOUDRÝ, J., KONVALINA, P., HYPŠLER, R.: The emissions of greenhouse gases produced during growing and processing of wheat products in the Czech Republic. J. Food, Agric. Environ. 11 (1) 2013a: 1133-1136.
17. MOUDRÝ, J. JR., JELÍNKOVÁ, Z., MOUDRÝ, J., BERNAS, J., KOPECKÝ, M., KONVALINA, P.: Influence of farming systems on production of greenhouse gas emission within cultivation selected crops. J. Food Agric. Environ. 11 (3-4), 2013b: 1015-1018.
18. MOUDRÝ, J. JR., JELÍNKOVÁ, Z., JAREŠOVÁ, M., PLCH, R., MOUDRÝ, J., KONVALINA, P.: Assessing greenhouse gas emissions from potato production and processing in the Czech Republic. Outlook Agric. 42, 2013c: 179-183.
19. MURPHY, K., DAWSON, J., JONES, S. S.: Relationship among phenotypic growth traits, yield and weed suppression in spring wheat landraces and modern cultivars. Field Crops Res. 105, 2008: 107-115.
20. NEUHOFF, D., HOAD, S., KÖPKE, U., DAVIES, K., GAWRONSKI, S. GAWRONSKA, H., DREWS, S., JUROSZEK, P., LUCAS BUENO, C., ZANOLI R.: Strategies of Weed Control in Organic Farming,(WECOF), Final Report ofthe FP5 European Combined Project,[online]. [cit 2015-09-15]. Available: http://www.wecof.ini-bonn.de.
21. OERKE, E. C.: Crop losses to pests. World J. Agric. Sci. 144, 2006: 31–43.
22. REBETZKE, G. J., RICHARDS, R. A.: Genetic improvement of early vigour in wheat. Aust. J. Agric. Res. 50, 1999: 291–301.

Corresponding author:

Ondřej Vlášek, Faculty of Agriculture, University of South Bohemia in České Budějovice, Studentská 1668, 37001 České Budějovice, Czech Republic

MEASUREMENT OF PRESSURE DISTRIBUTION IN KNEE JOINT REPLACEMENT

J. Volf[1], V. Novák[1], V. Ryzhenko[1], D. Novák[2]

[1]Faculty of Engineering, Czech University of Life Sciences Prague, Czech Republic
[2]Faculty of Natural Sciences, Matej Bel University Banská Bystrica, Slovakia

Abstract
The paper describes the measurement procedure of pressure distribution in knee arthroplasty and it verifies the accuracy of mathematical model of the pressure in the artificial joint. First it briefly presents the composition of the artificial joint. Then it describes in detail the measurement procedure, i.e. the measuring machine, which simulates a human step cycle, and the layout and type of used sensors. Finally, the measured pressure data are compared with those from the mathematical model and its accuracy is evaluated.

Key words: sensor, transducer, pressure distribution, biomechanics, knee joint replacement, knee arthoplasty.

INTRODUCTION

In some specific or particularly serious cases of impairment of human knee joint it is necessary to perform a total replacement of the joint with an artificial one – the knee arthoplasty. In order to maintain the functionality of the leg, the replacement should meet the kinematical requirements on a healthy joint, and – as an implanted part of human's body – it should exhibit excellent reliability to avoid repeating interventions into the body of the patient, for more detail see ZACH ET AL. (2004).

A titanium plate is attached onto the tibia bone; on the top of this plate is fixed a polymer-based layer with cut u-shape groove, into which fits in the third steel part that is attached to the femur bone. The polymer layer is necessary to prevent a direct contact between two metallic parts of the artificial joint and to enable reasonable friction between them. As the polymer part is especially susceptible to mechanical wear, the aim of the study is to check the pressure distribution in the contact layer and to compare the results with calculated theoretical values, according to mathematical model by ZHU AND CHEN (2004), and to determine the places with highest load and its magnitude.

MATERIALS AND METHODS

The artificial replacement joint, see Fig. 1, consists of following parts, as marked at the picture:

(1) femoral component
(2) tibial plateau
(3) basis of tibial component
(4) spindle of tibial component
(5) compensatory support
(6) compensatory support

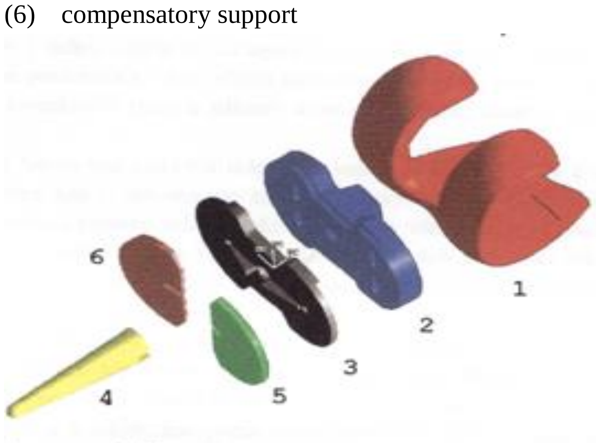

Fig. 1. – The structure of artificial knee replacement

Different materials are used for various components of knee arthroplasty. The femoral component is made of metal material (mostly cobalt alloy – Vitalium), tibial component is made of the same material, too, but contact area (tibial plateau) is from ultra high molecular polyethylene (UHMWPE).

New femoral components from oxide ceramic (Zirconium dioxide ZrO_2 and Alluminium dioxide AlO_2) are being developed. Metal materials are used because of their strength and elasticity, but they are not abrasion-proof and their life-cycle is shorter. Ceramic materials are bioinert and exhibit good friction characteristic; however, their disadvantage enhanced is fragility. Ceramic femoral component has different geometric parameters. We use combination of metal femoral component, i.e. UHMWPE tibial plateau and metal tibial component.

The geometric model of knee replacement was created by finite element method. Detailed description of this method is commented by DONÁT (1997). This mathematical model corresponds as much as possible the real knee joint. The geometric model was formulated in CAD system EDS/Unigraphics, developed by firm Walter, a.s. Prague. Theoretic results were obtained in system ABAQUS. The mathematic model of pressure distribution was created only for femoral component (upper part) and tibial plateau (lower part), which are depicted from another point of view in Fig. 2.

Fig. 2. – Femoral component and tibial plateau

Some simulations of pressure distribution in knee joint deal with a physiologic knee, i.e. with a complete knee with muscles and fibrous apparatus. We use a simplified model of knee replacement which doesn't comprehend lattice ligaments and the pressure distribution is slightly different according to KONVIČKOVÁ (2000). This simplified model is created for first verifying study. We used only stress of tibia-femoral contact area with pressure, which corresponds ca. 2.5 times average body weight. We suppose this about 70 kg, corresponding with force about 1 800 N.

Within the experiment, we used semiconductor strain gages. Although they exhibit significant dependency of electrical resistance on the temperature and a nonlinear dependency of the measured resistance on the deformation, we consider the negatives being compensated by their accuracy and stress-fatigue resistance. The temperature error may be compensated by small thermometers. We use monocrystalline semiconductor strain gages with N conductivity, which exhibits more linear dependency on press deformation, length of 2 mm from producer VTS Zlín, Czech Republic. These strain gages were developed specially for our workplace, further details about biomechanical measurements in VOLF (2002).

The sensor placement in human knee joint isn't simple, because the sensor must fulfill several conditions. The main condition is, that sensor mustn't influence the surface shape of knee components. If sensor changes geometry of tibial plateau, it would change also the contact areas and thus contact pressures, as by MOOTANAH (2006) and ANDERSON ET AL. (2006).

According to the mathematical model the maximal stress values are not in geometric minimum, but they are shifted. Thus sensors are allocated at four places in supposed maximal pressure area – see Fig. 3, (A) – (D). Because the sensors mustn't change the surface shape of knee components, they are placed in special holes with 3 mm diameter that are bored into the tibial plateau from below, which is demonstrated in Fig. 4. The number of holes is limited in order not to influence the tension course within the material.

Fig. 3. – Placement of the sensors

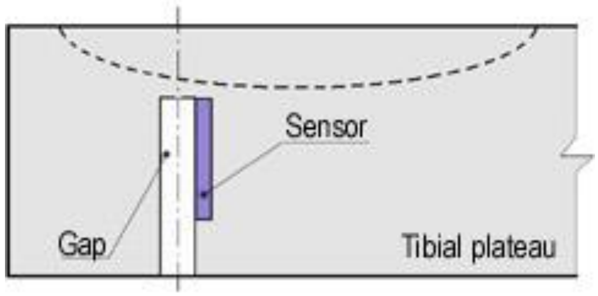

Fig. 4. – Hole in tibial plateau with sensor placement

The sensors are fixed in these gaps; placement of sensor is parallel with axis of gap. The gaps' depth is limited by elastic area of UHMWPE material of tibialplateau, the bottom of the hole may not be closer than 3 mm to the contact surface of the tibial plateau with the femoral component. After fixing into the hole the sensors are covered by silicone. One hole contains in addition a thermometer to compensate the temperature error of the semiconductor.

The measurements were performed on a movement simulator, a PLC controlled machine, which models the movements of a human knee joint. We performed the measurements according to norm ISO 14243-3:2004(E) that prescribes exactly the movements of individual parts of the joint in relation to each other, in order to simulate accurately the movement of a natural knee joint, further details about the simulation by Zhu and Chen (1999). This device is placed in the biomechanics laboratory of Czech Technical University, Faculty of Machine Engineering in Prague. The device with the artificial joint is depicted in Fig. 5.

Fig. 5. – Knee movement simulator and artificial joint

RESULTS AND DISCUSSION

Calculated values according to the mathematical model by ZHU AND CHEN (2004) exhibit no significant differences in stress distribution between individual replacement materials. The stress is concentrated into two nodes, as may be seen in Fig. 3. Maximal intensity of contact stress is 8.23 MPa with metal femoral component and 8.19 MPa with ceramic femoral component. Contact stress is much more less than value of limit stress for UHMWPE. This material has limit stress 13 MPa. Maximal values of reduced stress on tibial plateau is 7.05 MPa for both metal and ceramic femoral component. Maximal values of reduced stress are 5.73 MPa for metal and 7.35 MPa for ceramic femoral component. According to calculations, the limit stress values of replacement materials are not exceeded. The calculated pressure distribution is represented graphically in Fig. 6.

The machine simulated one human step so that we could measure the pressure in dependency on the flexion of the joint in determined angles from 0° to 25° in 5° steps. The results are depicted graphically in Fig. 7 – gap B and Fig. 8 – gap D. The pressure was measured increasing and decreasing of acting force in range 0 – 1 730 N on knee replacement for determined angles.

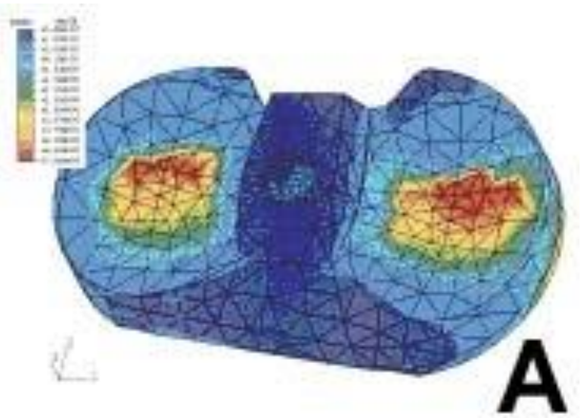

Fig. 6. – Calculated pressure distribution in artificial knee replacement

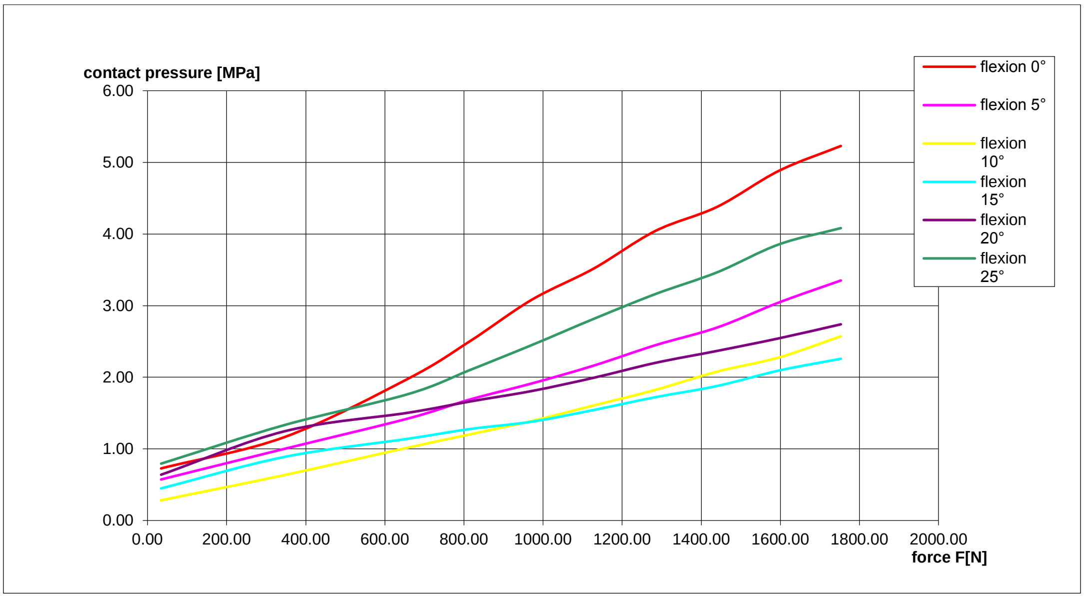

Fig. 7. – Contact pressure, gap B

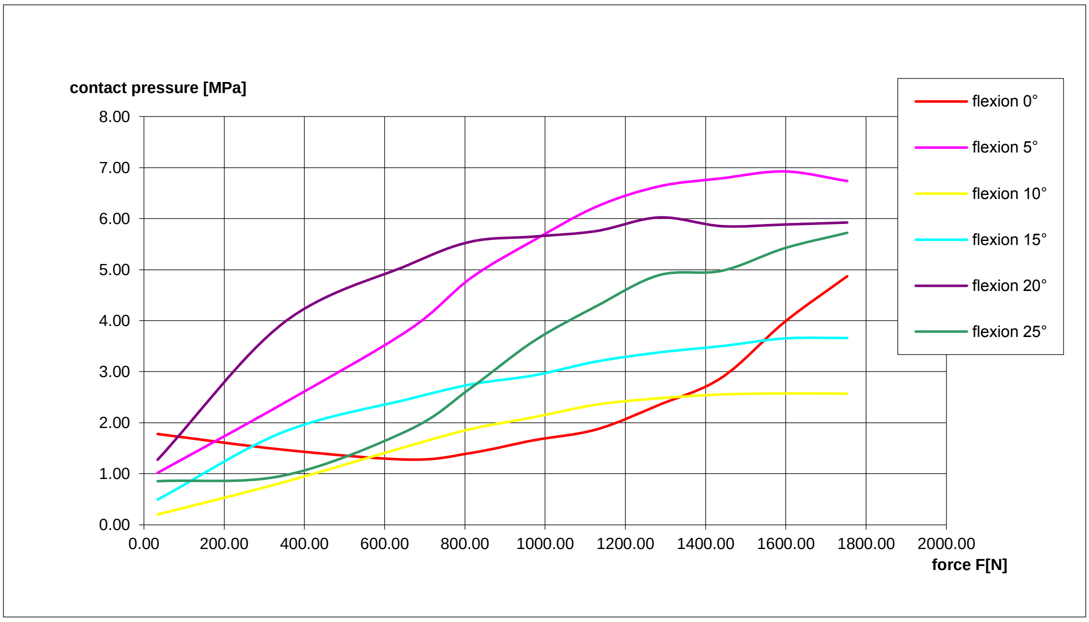

Fig. 8. – Contact pressure, gap D

The precedent figure represents the contact pressure values in knee arthroplasty for six defined flexion values (angles 0° to 25°) in dependency on the load force. The pressure increases quasi-linear with force in the contact point B, but the dependency on the flexion degree cannot be determined; the two highest pressure values (for maximum load) are obtained for the flexion 0° and 25°. The contact point D exhibits significant different course of the pressure with increasing load. Given the flexion 0°, the contact pressure slightly decreases, then it increases significantly. By the other flexion degrees, the contact pressure increases with the load, however, some curves reach their local maximum. Such irregularities of pressure dependency process in knee replacement are given by the geometry of contact areas, which affects significantly the pressure distribution.

Some hysteresis of deformation process by loading and unloading was found out in calibration. This is caused by material properties of UHWPE, from which the plateau is produced. This hysteresis can by substituted by average value without significant influence on the next measurements.

The subject of pressure distribution in knee joint was reflected by ZHU AND CHEN (1999, 2004), who created a mathematical model of pressure distribution in a knee joint. Calculations of the pressure distribution basing on the model are provided by DONÁT (1997) and ZACH ET AL. (2004). We verified the calculations by previously mentioned authors with the actually measured values. The comparison of the calculated and measured pressure values in points B and D is shown in Tab. 1., values are given for the flexion 0° - according to the mathematical model.

Tab. 1. – Calculated and measured pressure values in points B and D

	Gap B	Gap D
calculated value	6.7 MPa	5.1 MPa
measured value	5.3 MPa	4.8 MPa

The measured data in the respective points correspond with the calculated ones. However, it has to be pointed out, that an exact conformity and a direct comparison of the values are not possible. The maximal load obtained by the movement simulator is limited due to simulator's construction to 1 730 N and the pressure values calculated by the mathematical model base on the force of 2 300 N. An extrapolation of the measured force is not possible due the irregular shape of the curve (i.e. nonlinear dependency of the pressure on the applied force, mainly at the point D, see Fig. 8, which is given by slight rotation of the joint surfaces). The maximal pressure values reached up to 5.3 MPa (gap B) and 6.9 MPa (gap D). These values are way below the limit of the material, which is 13 MPa. These values are in correspondence with the mathematical model given above. Hereby we proved that the mathematical model describes accurately the load of knee arthroplasty and that such mathematical model can be used to design artificial joints. We further conclude that no one of the sensors exhibited unexpected or unacceptable pressure peak that could endanger the functionality of the artificial joint.

CONCLUSIONS

The aim of our work was to verify the mathematical model of pressure distribution in an artificial knee replacement. We modelled the real movement of the knee joint according to norm ISO 14243-3:2004(E) in the simulating machine. To measure the pressure, we used semiconductor strain gages placed in holes bored in tibial plateau component in the artificial joint. We conclude that the contact stress values correspond with the calculated ones, without any unpredicted deviations, so that we verified the mathematical model to be useful and accurate by designing artificial joints.

ACKNOWLEDGEMENT

The measurements were carried out within the IGA project No. 31200/1312/3118 of the Faculty of Engineering, Czech University of Life Sciences in Prague.

REFERENCES

1. ANDERSON, I. A., LIM, K.: Force Measurement. In: Wiley Encyclopedia of Biomedical Engineering, 2006.
2. DONÁT, A.: The Calculation of Contacts Pressures by Knee Joint Replacement [Diploma thesis]. Prague, Czech Technical University, 1997 (in Czech).
3. KONVIČKOVÁ, S., VALENTA, J.: Biomechanics of humans' joints and their replacements. Vienala, Prague, 2000 (in Czech).
4. MOOTANAH, R.: Pressure Sensors. In: Wiley Encyclopedia of Biomedical Engineering, pp. 1-16, 2006.
5. VOLF, J. ET AL.: System for Measurement of Static and Dynamic Pressure Distribution in Biomechanics. In: Automa, vol. 11/2002, pp. 17-19, 2002.
6. ZACH, L., KONVIČKOVÁ, S., RŮŽIČKA, P.: MKP Model of Knee Arthoplasty – Pressure Analysis (in Czech). In: WAM 2004, Prague, Czech Technical University, 2004.
7. ZHU, Y., CHEN, J. X.: 3D Knee Modeling and Biomechanical Simulation. In: Computer in Science Engineering, pp. 82-87, 1999.
8. ZHU, Y., CHEN, J. X.: Simulation and Visualization of Knee Joint Contact using Deformable Model. In: The Fourth International Conference on Computer and Information Technology 2004, 2004.

Corresponding author:

prof. Ing. Jaromír Volf, DrSc., Department of Electrical Engineering and Automation, Faculty of Engineering, Czech University of Life Sciences Prague, Kamýcká 129, Praha 6, Prague, 16521, Czech Republic, phone: +420 22438 3203, e-mail: volf@tf.czu.cz

DETERMINATION OF LOADING CHARACTERISTICS OF A GENERATOR FOR A BLADELESS TURBINE

Z. Vondrášek, L. Dlabal

Department of Electrical Engineering and Automation, Faculty of Engineering, Czech University of Life Sciences Prague, Czech Republic

Abstract

The article summarises the results of experimental measurements on an electricity generator performed on the SETUR DVE 120, a commercially available set equipped with a bladeless turbine. Generator loading characteristics were compiled from the measured data. The measurements were performed in a closed hydraulic testing circuit in a laboratory of the Department of Mechanical Engineering, Faculty of Engineering, Czech University of Life Sciences in Prague. The first part of this article describes the measuring station, the measuring method and determination of operating, technical and other associated parameters. The following part deals with the verification of the machine type (synchronous), determination of the number of the generator's pole pairs and its loading characteristics. The loading characteristics describe the dependence of the line voltage on the phase current or on the electrical output power. Knowledge of the operating characteristics is needed for the efficient utilisation of a small hydro-electric set.

Key words: line voltage, electric current, generator speeds.

INTRODUCTION

Climate change is resulting in numerous unknown effects. Many questions are being raised, especially concerning threats to agriculture. The issue of watering crops is of particular interest in this respect (KUCHAR, 2011). Rural areas on the world frequently struggle with a lack of water for irrigation systems or a complete absence of mains electricity. Reports state that around 1.6 billion people live in rural areas without access to electricity (IEA, 2006; LAHIMER, 2012). This number will not fall unless there are solutions available, especially for less-developed countries. Electrification and computerization of the private activities of people increases the rate (phones, cameras, PC's) and the demands on the availability of electrical power. Using the energetic potential of small water streams by means of a micro-turbine is a possible solution in some cases. This alternative is becoming very attractive in the field of local renewable energy sources for electricity generation (BHUSAL 2007). The newly developed bladeless turbine is one such. In order to operate and utilise a bladeless-turbine-based energy source efficiently, knowledge of its functionality is necessary. For this reason, both the turbine and its generator are currently subject to further investigation.

The aim study was to analyse the parameters measured at the generator for turbine and to determine its loading characteristics. Electricity from the SETUR DVE 120 equipment is generated by a synchronous generator with permanent magnets. These electrical units feature a relatively high efficiency and a high momentum density (GIERAS, 2010; HÖLL, 2014). The weak point of these generators operated with uncontrolled rectifiers is their inability to control their output voltage, which depends not only on the running speed and on the generator's momentary electrical output, but also on the unit's current operating temperature (HÖLL, 2014). On the other hand, their ability to operate in 'island mode' is a significant strength, supporting the versatility of their application (POLÁK, 2013). This strength is enabled by the already mentioned permanent magnets.

MATERIALS AND METHODS

The operating measurements were performed on a synchronous generator in a laboratory of the Department of Mechanical Engineering, Faculty of Engineering, Czech University of Life Sciences in Prague. The measurements of this generator (Fig. 1) were performed using a measuring electrical circuit.

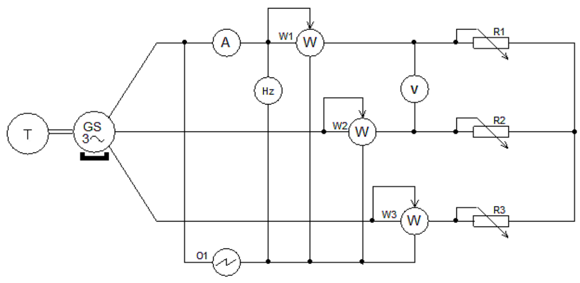

Fig. 1. – Electrical circuit for synchronous generator measuring

T – turbine, GS – synchronous generator, A – ammeter, W – wattmeter(W1, W2, W3), V – voltmeter, Hz – electronic frequency meter,O1 – oscilloscope, R1, R2, R3 – loading rheostats

A bladeless turbine (T) was the source of mechanical energy for the generator. The generated electricity flowed in a three-phase system through a wattmeter (W1, W2, and W3) into an electrical load formed by a rheostat (R1, R2 and R3) in each phase. The generator was loaded symmetrically in all phases during measuring. Generator speeds were controlled by amounts of water running through the turbine, reflecting the generator loading by active resistance (island-type loading).

The line voltage had to be measured with a voltmeter (V) to determine the loading characteristics. The phase current was measured with an ammeter. The measured values of the line voltage and the phase current were also used for correct setting of the measuring range in all the wattmeters. An oscilloscope (O1) was used for determining the voltage/time behaviour. The frequency within the electrical system was measured by an electronic frequency meter (Hz). The frequency measurements confirmed that the generator was synchronous. Further text comments on the procedure for this finding.

Determination of Generator Operating and Technical Parameters

Verification of whether the generator was synchronous was carried out at several generator speeds n. If the electrical system frequency f grows linearly with speed, the generator is synchronous. Then the number of pole pairs p was determined from the following formula (1): (HÖLL, 2014)

$$p = 60 \cdot \frac{f}{n} \qquad (-) \qquad (1)$$

The set's total output power P_{el} under a symmetrical load can be calculated by the following formula (2): (Polák 2015)

$$P_{el} = P_1 + P_2 + P_3 \qquad (W) \qquad (2)$$

where: P_1, P_2 and P_3 are output powers of individual phases of generator

The main criteria characterising an alternator are control and loading characteristics. As the alternator is excited by permanent magnets, the control characteristics cannot easily be found. The measured parameters are used for compiling the loading characteristics, i.e. the dependence of the voltage U_{sd} at terminals on the loading electrical (stator) current I - at a constant generator speed n, frequency f and power factor cos φ. These characteristics are sometimes termed external.

The generator fed a resistance load during measuring. The power factor was cos φ = 1 throughout the measuring. (GAMPA, 2016)

RESULTS AND DISCUSSION

The determination of operating and technical parameters confirmed that the unit was synchronous. This conclusion was based on the electrical system frequency being dependent on the generator speed. It is obvious from Fig. 2 that the electrical system frequency grows linearly with growing generator speed.

It was calculated by means of formula (1) that there were 10 pairs of poles in the synchronous generator, i.e. it was a 20-pole unit.

Loading characteristics were compiled for the synchronous generator (Fig. 3). Curves were drawn for selected generator speeds. It is clear on first sight that the curve lines rather presented a linear decrease with growing load. The growing generator load increased the electrical (stator) current and decreased the line voltage.

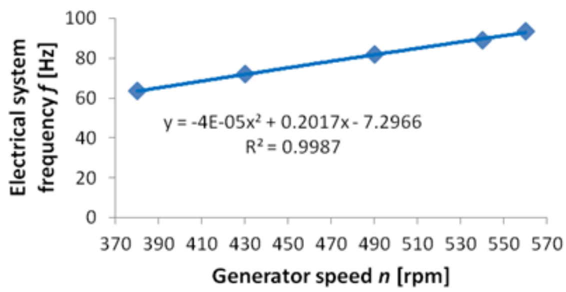

Fig. 2. – Electrical systém frequency – generator speed relationship

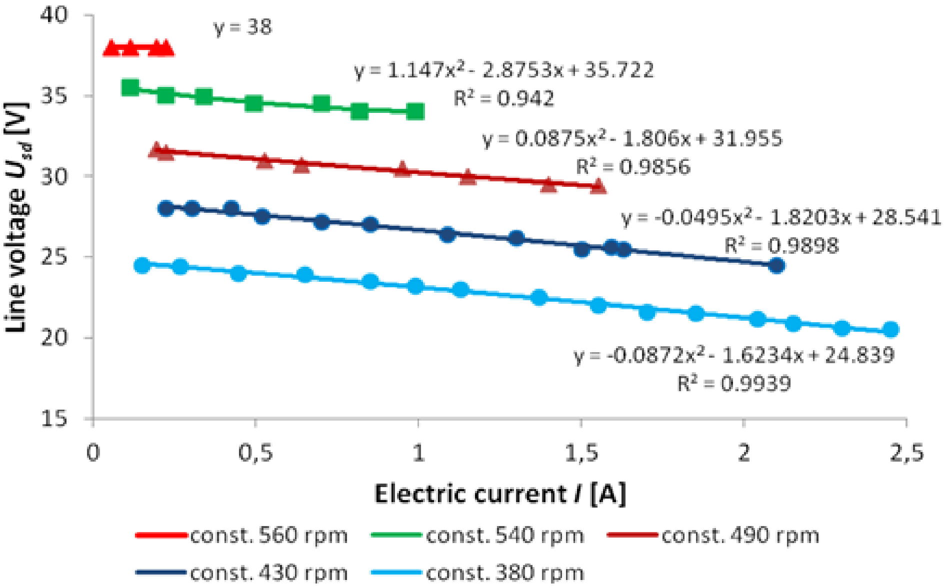

Fig. 3. – Generator loading characteristics – line voltage dependence on the electric current

POLÁK (2013) mentions the possibility of using sets DVE 120 to charge the batteries, but without additional experimental findings. Fig. 3 shows a relatively high dependence of the electrical line voltage U_{sd} on generator speed n, or used electrical current I. An individual stabiliser would be needed to eliminate voltage changes for a particular appliance.

Fig. 3 presents somewhat difficult to read characteristics for n = 560 rpm. For that reason Fig. 4 shows these characteristics in detail. When the generator was gradually loaded at this speed, its line voltage remained virtually unaltered, reaching 38 V.

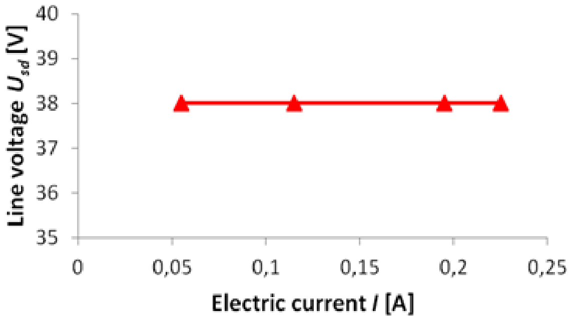

Fig. 4. – Generator loading characteristics for n = 560 rpm

The line voltage behaviour over time was determined with an oscilloscope (Fig. 5). At the same time the generator's electrical system frequency was recorded by means of an electronic frequency meter.

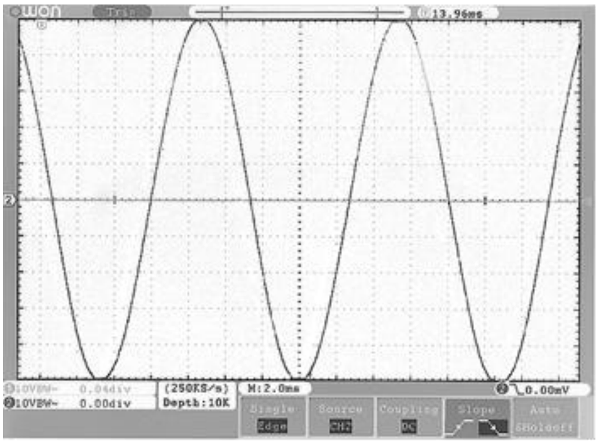

Fig. 5. – The line voltage U_{sd} behaviour at a generator speed n = 560 rpm and an electrical system frequency of f = 93.3 Hz

To summarise, the electrical system frequency was f = 93.3 Hz and the line voltage amplitude $U_{sd;max}$ = 53.5 V at a generator speed of n = 560 rpm and an effective voltage of U_{ef} = 38 V – as measured by a voltmeter.

The dependence of the line voltage on the electrical power (Fig. 6) further documents the applicability of this generator. The loading characteristics (at constant speed) featured a linear voltage decrease with increasing load. The curve lines had rather a slightly negatively-logarithmic shape at lower speeds.

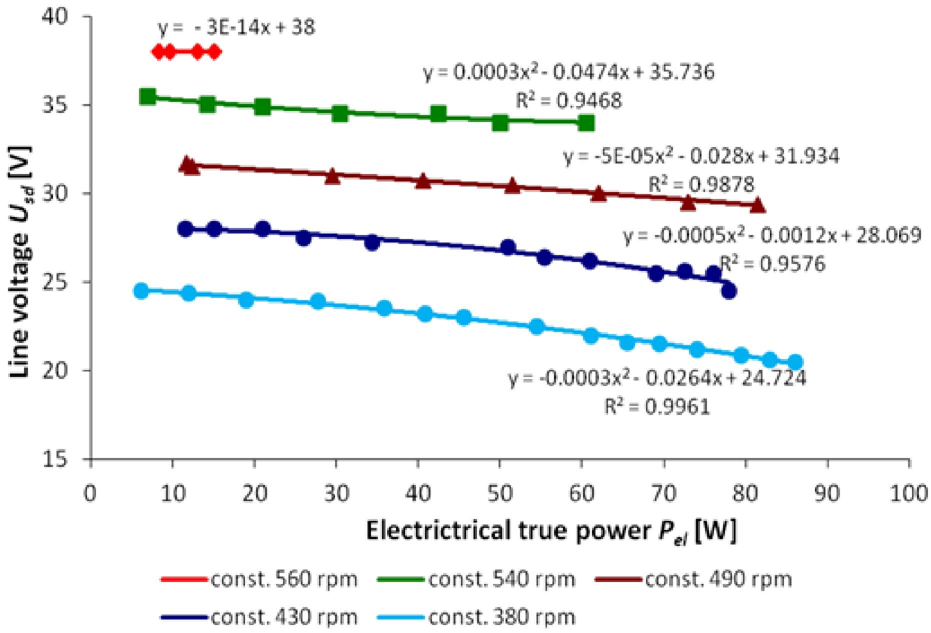

Fig. 6. – Generator loading characteristics – line voltage dependence on the electrical true power

CONCLUSIONS

The objective of the experiment was to determine the operating and technical parameters of a generator linked to a bladeless turbine. The measured values of the generator's peripheral parameters were influenced by the mechanical power supplied by the bladeless turbine. The process found that the DVE 120 set contained a synchronous generator with 10 pole pairs, i.e. it was a 20-pole unit. The output line voltage changed linearly with changing current (decreasing with growing loads) in the set's operating mode. Line voltages generated clear sinusoids, free of any visible deformations. When the synchronous generator (speed of 560 rpm) load was reduced, the electrical system frequency was $f = 93.3$ Hz, which corresponded to a line voltage amplitude $U_{sd;max} = 53.5$ V at an effective voltage of $U_{ef} = 38$ V – as measured by a voltmeter. The generator was operated at different additional speeds, which corresponded with values of line voltage $U_{sd} = 34 \div 35.5$ V, electrical current $I = 0.115 \div 0.99$ A and maximum overall electrical true power of $P_{el} = 60.5$ W achieved at a generator speed of $n = 540$ rpm; of line voltage $U_{sd} = 29.4 \div 31.7$ V, electrical current $I = 0.195 \div 1.55$ A and maximum overall electrical true power of $P_{el} = 81.4$ W achieved at a generator speed of $n = 490$ rpm; of line voltage $U_{sd} = 24.5 \div 28$ V, electrical current $I = 0.225 \div 2.1$ A and maximum overall electrical true power of $P_{el} = 78$ W achieved at a generator speed of $n = 430$ rpm and of line voltage $U_{sd} = 20.5 \div 24.5$ V, electrical current $I = 0.15 \div 2.45$ A and maximum overall electrical true power of $P_{el} = 86$ W achieved at a generator speed of $n = 380$ rpm.

Based on the determined loading characteristics, we can now predict the generator's electrical output parameters when working together with a bladeless turbine under various local conditions. If the generator is operated in conjunction with the above turbine, the characteristics of such a water turbine need to be known – work is still underway to clarify these.

The DVE 120 set is equipped with a bladeless turbine and a generator featuring permanent magnets. It is therefore suitable for electricity generation in "island mode", i.e. independent of electrical infrastructure.

The speed of the set changes with the current offtake in island operation as well as the output current frequency and voltage. This feature is inconvenient for appliances fed by an alternating current system. Output current rectification seems to be more beneficial. Such a set is suitable for charging rechargeable batteries.

ACKNOWLEDGEMENT

This work has been supported by the Internal Grant Agency of the Faculty of Engineering, Czech University of Life Sciences Prague, Project 2014:31130/1312/3114 (Determination of bladeless turbine operating characteristics from the user's perspective).

REFERENCES

1. BHUSAL, P., ZAHND, A., ELOHOLMA, M., HALONEN, L.: Energy efficient innovative lighting and energy supply solutions in developing countries. International Review of Electrical Engineering (I.R.E.E.), 2007: pp. 665 - 670.
2. GIERAS, J. F.: Permanent magnet motor technology. 3rd edition. New York: CRC Press. 2010: ISBN 978-1-4200-6440-7.
3. HÖLL, J., WILDA, L.: PM generator s různým počtempólů a typem vinutí pro použití v manipulační technice. Elektrorevue, Volume 16, Issue 2, April 2014: pp. 100 - 104. ISSN 1213-1539.
4. IEA, I. E. A.: World Energy Outlook 2006. Paris, France, November 2006: pp. 567.
5. KUCHAR, L., IWAŃSKI, S.: Rainfall Simulation for the Prediction of Crop Irrigation in Future Climate. Infrastrukturai Ekologia Terenów Wiejskich. 2011: Nr 2011/05.
6. LAHIMER, A. A., ALGHOUL, M. A., SOPIAN, K., ET AL.: Research and development aspects of pico-hydro power. Renewable and Sustainable Energy Reviews, Volume 16, Issue 8, October 2012: pp. 5861 - 5878. ISSN 1364-0321.
7. POLÁK M., ET AL.: Bezlopatková miniturbína. Praha: Nakladatelství ČVUT, 2013: pp. 57 - 59. ISBN 978-80-01-05233-4.
8. POLÁK, M., DLABAL, L.: Operating characteristics of a bladeless turbine for irrigation purposes. Soil and Water Research, Volume 10, Issue 4, December 2015: pp. 278 - 283.
9. GAMPA S. R., DAS D.: Optimum placement of shunt capacitors in a radial distribution system for substation power factor improvement using fuzzy GA method, International Journal of Electrical Power & Energy Systems, Volume 77, May 2016: pp. 314 - 326, ISSN 0142-0615.

Corresponding author:

Ing. Zbyněk Vondrášek, Ph.D., Department of Electrical Engineering and Automation, Faculty of Engineering, Czech University of Life Sciences Prague, Kamýcká 129, Praha 6, Prague, 16521, Czech Republic, phone: +420 22438 3194, e-mail: vondrasek@tf.czu.cz

RELIABILITY OF SECURITY SYSTEM INTEGRATION FROM THE PERSPECTIVE OF THE INTEGRATION SOLUTION

Z. Votruba

Department of Technological Equipment of Buildings, Faculty of Engineering, Czech University of Life Sciences Prague, Czech Republic

Abstract

This work deals with the issue of security system integration for so-called "intelligent buildings". It does not deal with the entire problematic which is rather wide, but it strives to answer the basic issue whether it is possible to consider such integration from the perspective of reliability parameters of integrated systems without reducing reliability of the security (or other alarm) system itself. Based on the gained findings, performed measurements and tests I have processed statistics and statistical verification of the statement included in the evaluated hypothesis. Actual trends in the alarm system integration are subsequently evaluated based on the obtained data and conclusions. Factors limiting the alarm system integration are also assessed, mainly as regards reliability of the integrated system and its parts. On the basis of theoretical calculations, experimental measurements and modelling premises are defined regarding the features of partial systems and their possible integration.

The basis of my work is verification of the base hypothesis whether an integration of a security (or any alarm) system does not reduce security and reliability of the partial systems in such extent that it will prevent their integration.

Testing of this hypothesis was performed on the basis of long-term measurements of integrated and non-integrated security systems. These results were statistically processed so that the key hypothesis could be verified or rejected and unambiguous conclusions formulated.

The author of this work does not discus legislative or normative terms of the alarm system integration.

Key words: IH&AS, security system, integration, reliability.

INTRODUCTION

Reliability of security systems is a basic parameter affecting the system use and also functioning. As concerns security systems (as well as any other alarm systems), the system reliability definition is traditionally slightly different than in the case of other systems or mechanical components. This definition is based on the definitions prescribed by the applicable industrial standard (e.g. CSN EN 50 131-1) and also especially on the overall conception of the security system (ADELI, 2008). As regards these systems, the system reliability is defined not only as the system ability to carry out the prescribed activity but also the probability of the system activation in the event of an emergency situation. We are therefore also talking about the so-called probability to overcome the system. This probability indeed changes depending on time, with regard to various abilities and on the basis of the system regular operation or climatic and other effects that cannot be deterministically described. Therefore a neuron self-learning model is an ideal tool for such system simulation. This issue, however, is not the base of this work. Security system reliability is regularly derived from the system security class related to the level of "ability" of the applicable system saboteur. The aforementioned standard relatively accurately defines 4 basic security classes. As regards the definition of reliability of the security system itself compared to a security system integrated within a larger complex, definitions of the following terms are more important:

- Probability of detection (Pd)
- Nuisance Alarm Rate (NAR)
- False Alarm Rate (FAR)
- Probability of overcoming (Vd)(ALTHOFF, 2001)

The probability of detection (Pd) corresponds to the probability of presence or movement of the violator in the area secured by the relevant detector or detection system (detection zone). This probability can differ. In general the Nuisance Alarm Rate (NAR) grows when the probability increases and under certain conditions the False Alarm Rate (FAR) increases as well. It is provided in the interval from 0 to 1 and differs for various detectors. As regards standard security systems as a whole, this value ranges for security classes 2 to 3 from 0.85 to 0.92. The project quality, its implementation and regular servicing significantly affect this value.

The Nuisance Alarm Rate (NAR) is defined as the rate of nuisance alarms caused due to circumstances that can be considered as non-risk and to which the detector is basically sensible (e.g. weather conditions, movement of animals or vegetation etc.). The summary of such rates of the individual detectors can be aggregated for the entire system. The valid NAR value for the security system in security class 2 and 3 is defined by the maximum value of 1 alarm per 168 hours (per week). A too high value is a clear indicator of an erroneous project.

The False Alarm Rate (FAR) is the rate of invalid alarms caused without any clear external reason, most frequently due to circuit noises, defective electronic parts or other detector defects. It is usually provided as the number of alarms in a single detection zone per a certain time unit. With a standard security system the rate value of 1 alarm per 8,760 to 17,520 hours (according to the security class) is considered as the limit value. A high value in this case refers to an erroneous installation, poor-quality product or inappropriate service.

Probability of overcoming (Vd) is the probability with which the violator can overcome the detection technology without causing an alarm. It is most frequently done be overcoming the detection zone for example by climbing over, digging out or bridging or by using of the technical limits of the particular detection technology. According to the used technologies the values of this probability range from 0.01 to 0.2 (again in line with the security class and the type of the used system). In this case the project quality and the way of its implementation play a significant role (BOJANOVSKÝ, 2008).

The aforementioned indicators were used as base parameters on the basis of which the formulated hypothesis H0: Security system integration to other systems will not reduce security and reliability of the security system was verified. Even though standard CSN CLC/TS 50398:2009 allows for such degradation under certain circumstances!

MATERIALS AND METHODS

It is probably impossible to define a single universal test for the assessment of reliability of various ways of integration. It is possible to evaluate the overall reliability of individual integration tools, but we have to use another way of testing for each of them. Therefore we used the following methodology:

a) Integration by means of integration relays (PGM): in this case the test is performed on real objects under regular operation [1]. Sufficient operating time without integration and with integration is significant in this case. On the basis of the statistically assessed results of diagnostic signals (NAR, FAR and Vd – see above) evaluation of unambiguity of the operation difference before and after integration is performed. Selection of comparable actual high-quality installations with good operation service is significant for the aforesaid test (LIAN ET AL., 2014).

b) Security system integration by means of the EIB/KNX protocol in a higher-grade interconnected system (AULICKÝ ET AL., 2008). In this case, with regard to the smaller number of available installations, the tests were performed under laboratory conditions. Similar security systems were selected to enable comparison with the previous integration type. Testing was performed both at the physical level (verification of the information transfer from an alarm security and emergency system (ASES) to a PC by means of the KNX data using the Wireshark software) and at the application level (by means of the Loxone software) (HEŘMAN ET AL., 2008).

c) Integration by means of the CIB industrial bus of Teco a.s. was also tested mainly by laboratory means, although in this case one test was performed at an actually operated integrated system also comprising a security system. The test methodology fully complied with the way of testing according to variant of integration b). The Wireshark program was used to verify physical communication between ASES and the testing PC; a mosaic tool for the bus programming also comprising performance testing algorithms was used at the application level.

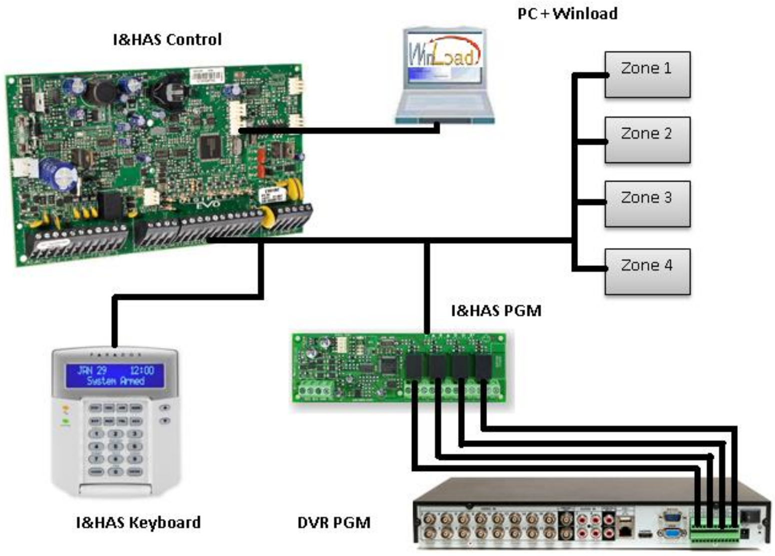

Fig. 1. – Arrangement diagram for PMG testing model according to method a)

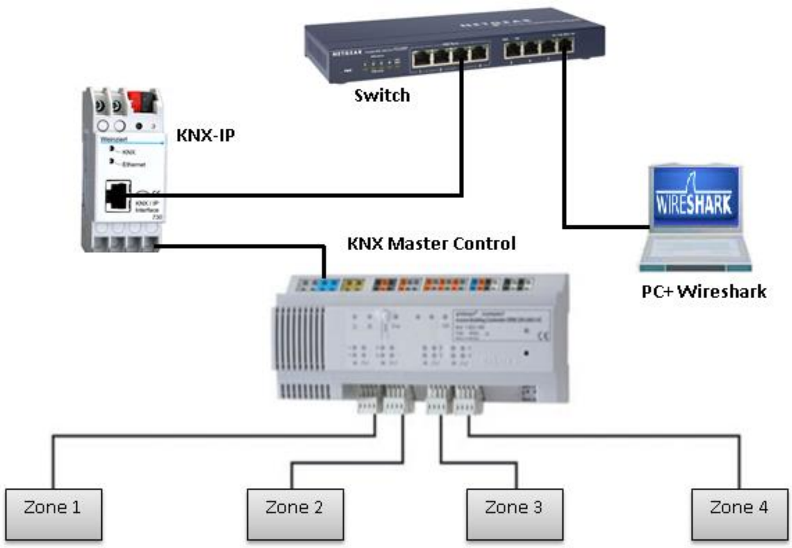

Fig. 2. – Arrangement diagram for KNX testing model according to method b)

Upon testing a set of values gained before integration was compared by means of the given method (reliability indicators NAR and VAR together with a subjective assessment of the possible change in Vd). With view to the differing numbers of measurements the parametric Student t-test or its variant, i.e. the two selection t-test was used because the base set mean value is unknown and only 2 sample data sets are compared. The following zero hypothesis is therefore tested: H0: $\mu 1 = \mu 2$.

With regard to the measurement characteristics and the requirement for testing we used a so-called "non-pair test".

The following calculation of sample characteristics was performed for the samples:

1st sample (number of members: n_1): $\bar{x}_1$, S1

2nd sample (number of members: n_2): $\bar{x}_2$, S2

As the tested samples can come from groups with the same/differing variance of the monitored characteristic value, it is necessary to first test the variance difference of both samples (a zero hypothesis, H0: $\sigma_1^2 = \sigma 2^2$) by means of the F-test.

F = greater variance (S_1^2, S_2^2) / smaller variance (S_1^2, S_2^2)

with sample variances:

$$s_1^2 = \frac{\sum x_i^2 - \frac{(\sum x_i)^2}{n_1}}{n_1 - 1} \qquad (1)$$

$$s_2^2 = \frac{\sum x_i^2 - \frac{(\sum x_i)^2}{n_2}}{n_2 - 1} \qquad (2)$$

To search the tabular critical values for the F-test it is necessary to determine the degrees of freedom for the numerator of the greater and smaller variance.

If F ≤ $F_{0.975}$, i.e. H0 applies: $\sigma_1^2 = \sigma 2^2$ (both samples therefore come from populations with an equal variance); the non-pair t-test is used to test the difference in mean values for equal variances:

$$t = \frac{\left|\overline{x_1} - \overline{x_2}\right|}{\sqrt{\frac{(n_1 - 1) \times s_1^2 + (n_2 - 1) \times s_2^2}{n_2 + n_1 - 2} \times \frac{n_1 + n_2}{n_1 \times n_2}}} \qquad (3)$$

If F > $F_{0.975}$, i.e. H0 does not apply: $\sigma_1^2 = \sigma 2^2$ (both samples therefore come from populations with a differing variance); the non-pair t-test is used to test the difference in mean values for differing variances:

$$t = \frac{\left|\overline{x_1} - \overline{x_2}\right|}{\sqrt{\frac{s_1^2}{n_1} + \frac{s_2^1}{n_2}}} \qquad (4)$$

Excel functions (F.TEST and T.TEST) were used for the aforesaid calculations.

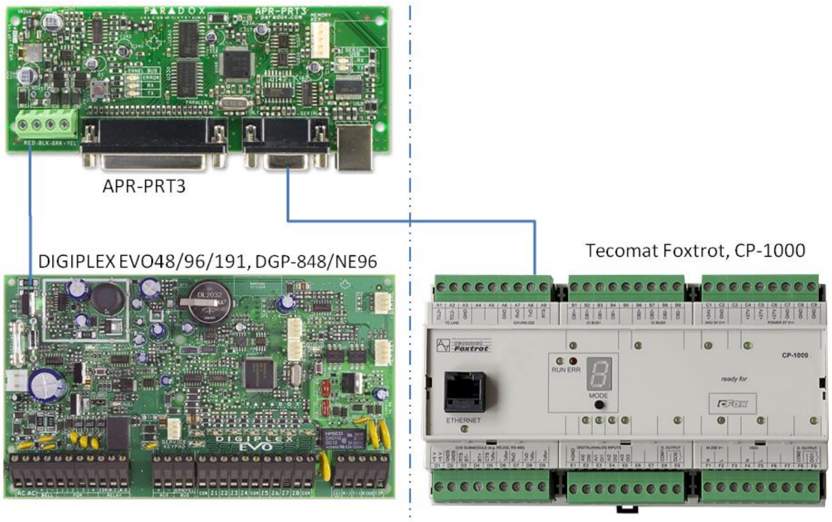

Fig. 3. – Arrangement diagram for CIB testing model according to method c)

RESULTSAND DISCUSSION

Input data for the integration testing by means of the program relay of an ASES switchboard was read from 3 different security switchboards in various operations. The age of all systems ranged from 3 to 5 years. Different times before integration rather showed as more difficult for statistic processing than as the relevant impact on the testing result.

Tab. 1. – System critical events

	System 1		System 2		System 3	
	before	after	before	after	before	after
Number of operation days (since integration)	236	628	120	142	411	123
Ratio of nuisance alarms	0.8%	1.2%	2.1%	2.0%	1.3%	2.6%
Ratio of false alarms	0.3%	0.1%	0.4%	0.5 %	0.2%	2.1%
Ratio of critical system defects	0.2%	0.5%	0.2%	0.1%	0.1%	0.7%
Ratio of critical user defects	1.4%	0.3%	4.0%	2.7%	3.2%	3.8%

***Note:** the term “**before**” means before the integration date, the term “**after**” means operation after the integration date (also applies in the following tables)*

Tab. 2. – Hypothesis testing results

	System 1		System 2		System 3	
	before	after	before	after	before	after
average	0.0321	0.0187	0.0571	0.0911	0.1029	0.1108
standard deviation	0.1797	0.1178	0.355	0.1897	0.3287	0.2211
variance	0.0751	0.0385	0.2871	0.0887	0.2245	0.0871
F test significance	5E-36 p <0.05		1,28E-30 p <0.05		0,0150 p <0.05	
t test significance	0,1635 p <0.05		0,3052 p <0.05		0,8096 p <0.05	
Conclusion	at the given significance level H_0 was confirmed		at the given significance level H_0 was confirmed		at the given significance level H_0 was confirmed	

It is obvious from the performed measurements and statistic processing that integration carried out by means of program outputs/inputs in alarm systems does not cause reducing of reliability and the individual systems do not affect each other significantly from the statistical perspective. The rate of alarms (both nuisance and false), operators' errors and critical errors did not show any difference before integration and after it. It is an interesting aspect that the ratio of false alarms compared to the standard (FAR) was basically exceeded 2 times in all three systems, independent of the level of integration.

This provides obvious information regarding the quality of the project or its implementation (or service).

When testing integration by means of the KNX bus (according to variant b) of our methodology) the testing took place in two stages. First, one main line was connected to the bone KNX bus and a message transfer test were carried out (a status change at the ASES switchboard). Subsequently the 4 main lines were interconnected and statuses were read from all the lines. The test results are provided in the following Tab. 3.

It is obvious that the test results with the KNX bus confirmed the preliminary assumption that the KNX bus will show unreliable communication with more main lines. Testing of the base hypothesis is therefore quite unambiguous (VOTRUBA ET AL., 2011).

Tab. 3. – Reliability of transfer of changed ASES status by the KNX bus

	1 main line		4 main lines	
	to ASES	to PC	to ASES	to PC
Number of operating hours	64	64	52	52
Number of changes	7658	7,653	6240	4,187
Number of lost changes	0	5	0	2,053
Number of lost changes in %	0	0.0653	0	32.9

Tab. 4. – Hypothesis testing results

	1 main line	4 main lines
F test significance	0.04781 p <0.05	0.5741 p <0.05
t test significance	0.01874 p <0.05	0.1501 p <0.05
Conclusion	at the given significance level H_0 was confirmed	at the given significance level H_0 was confirmed

The aforementioned result was subsequently also confirmed by testing at the application level using the Loxone tool that confirmed the problems of the KNX bus upon packet collisions between the particular main lines. With view to the unambiguous result at the transfer level, no other result analysis at the application level was carried out.
Using of the CIB bus does not have such tradition world-wide as using of the KNX bus; however this method is quite well-known and frequently used in the Czech Republic. Therefore the test results for the integration tendency are quite significant. The test was performed similarly as in the case of the KNX bus testing, i.e. first with a single ASES switchboard per bus and subsequently with 4 switchboards (each at an independent branch). The results are summarized in the following table.
With view to the gained results statistical processing could not have been performed correctly – the standard deviation and variance have zero values or range close to zero. Surprisingly, reliability of the changed transfer by means of the CIB bus was thus evidenced.

Tab. 5. – Reliability of transfer of a changed ASES status by the CIB bus

	1 main branch		4 main branches	
	to ASES	to PC	to ASES	to PC
Number of operating hours	75	75	68	68
Number of changes	9,000	9,000	8,150	8,148
Number of lost changes	0	0	0	2
Number of lost changes in %	0	0	0	0.025

DISCUSSION

Although the aforementioned results are a significant simplification, they provide a certain notion which direction to follow in the integration tendencies concerning alarm systems for so-called intelligent buildings.
Integration by means of PGM is applicable in practice for up to approximately 20 – 30 statuses; in case of a greater number an insolvable logical problem occurs, which cannot be resolved within the ASES system logic. It however concerns one of the simplest and most effective ways of integration for small and medium systems. It was confirmed in a quite extensive test that despite some conditions provided in the literature this way is not problematic as regards reduction of the ASES system reliability.
According to the tests, integration by means of the KNX bus is also suitable for smaller and medium installations or for installations with a single main line. It is surprising because it was anticipated that KNX buses would be a good solution for the largest integration systems. It however appears that there is a problem with the power supply of elements, which is a chronic issue with KNX buses, together with irregular “unambiguity” of some users within the bus, even in the direct line. It is due to the use of the CSMA/CA (Carrier Sense Multiple Access with Collision Avoidance) method as a tool preventing limitation of the number of collisions at a common bus (ANTTIROIKO ET AL., 2013). If two users transmit at the same time, the telegram whose bit sequence reads log 0 earlier shall be preferred. This procedure is quite frequently used for the communication technique but it has one great problem. The described regulation only functions at the line level. If a KNX bus is divided into more lines (which is a frequent case with larger installations), this method fails and the telegram is lost without such loss identification. If a participant tries to send the telegram more than three times but fails to get it through (due to the communication load or the set communication priority), the user may “drop out” off the communication for a certain period (which actually happened in the course of practical testing). Such drop out lasted up to several seconds and in some cases manual restarting was necessary. This was probably the reason for the quite frequent failure of the status transfer as described in the test (KNX, 2008).
In both cases the CIB bus showed almost perfect reliability (it is suspected that failures in the second part of the test were caused rather by an error in the test than in the bus). This result is quite surprising and it is most probably caused by the communication centralization. Unlike KNX, CIB does not use a decentralization model (KLABAN, 2008). Communication is controlled by a central PLC automatic machine with quite good control of the elements accessing the bus. Using of the bus (system) for integration therefore has

a great potential as regards security and reliability of information transfer to the bus.

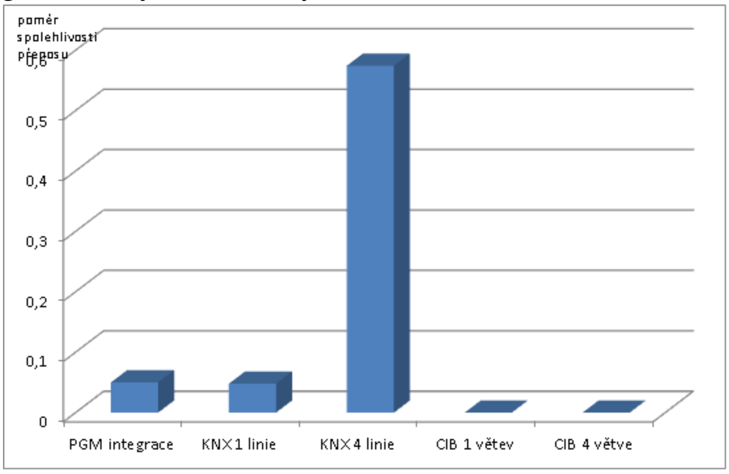

Fig. 4. – Comparative reliability values of alarm information transfer at various integration platforms

CONCLUSIONS

The partial conclusions of our three tests were described in the previous chapter. It can be generally claimed that on the basis of the performed tests we can reasonably claim that integration by means of PGM is a suitable tool for integration mainly for smaller integrated systems also comprising security systems. To the contrary, using of the most widely spread industrial bus is quite problematic for extensive systems and it cannot be recommended for the security system integration, mainly if a greater number of lines is used. The CIB bus represents a high quality way of integration, mainly for medium systems. It uses its control units to ensure quality and reliable transfer of the status information from security systems.

The author is aware that the aforementioned tests are not sufficient for all possible ways of using industrial buses as integration tools for alarm systems; they however provide a certain notion, and based on the tests the author seeks to create another way of integration at a new level, i.e. integration by means of a neuron module using the self-learning principles of neuron networks (VOTRUBA, 2016; ZHOU ET AL., 2013).

Tab. 6. – Summary of results in a table form

Technology integration	Key positive characteristics	Key negative characteristics
PGM	• price • simplicity • reliability • universal use	• only for smaller systems • problematical expandability • reduced user comfort
KNX/EIB	• expandability • large producers • extensive systems • distributed solution	• higher price • incomplete compatibility • errors in transfer (collisions) • insufficient power supply solution • problematic changes in configuration and programming
CIB	• expandability in the Czech Republic and compatibility with other solutions • proprietary preparation for alarm integration • extensive systems • clear programming	• higher price • server solution • unsolved module locking • insufficient power supply solution

Tab. 7 - Suitability of the integration technology application according to size

Technology integration	Small integration *(1 – 15 statuses)*	Medium integration *(10 – 200 statuses)*	Extensive integration *(100 and more statuses)*
PGM	80%	20%	0%
KNX/EIB	2%	80%	12%
CIB	5%	15%	80%

REFERENCES

1. ADELI, H.: Smart structures and building automation in the 21(st) century, 25th International Symposium on Automation and Robotics in Construction Location: Vilnius, LITHUANIA Date: JUN 26-29, 2008.
2. ALTHOFF, J.: Preface. In Safety of Modern Systems. Congress Documentation Saarbruecken 2001. Cologne : TŰV- Verlag GmbH, 2001, p. 5-6. ISBN 3-8249-0659-7.
3. ANTTIROIKO, A.,V., VALKAMA, P., BAILEY, S.J.: Smart cities in the new service economy: building platforms for smart services. AI and Society, 2013, p. 1-12, ISSN 0951-5666.
4. AULICKÝ, V., ET AL.: Smart buildings and ecological construction. Praha, Publishing house Dr. Josef Raabe, s.r.o, 2008. 280 s. ISBN 1803-4322.
5. BOJANOVSKÝ, J.: Smart buildings - „Control, safety and information systems in modern buildings“, SECURITY Magazine, December 2008.
6. HEŘMAN, J., ET AL.: Electrical and telecommunication installations. Praha: Verlag Dashöfer, 2008. ISSN 1803-0475.
7. KLABAN J.,Inels and bus CIB – Modern smart wiring system, Automa, 12/2008, p. 28 – 31.
8. KNX SYSTEM ARCHITECTURE. Konnex association, 2008. Available at:http://www.knx.org/_ leadmin/downloads/03 - KNX Standard/KNX Standard Public Documents/KNX System Architecture.pdf. (cit. 2015-10-5)
9. LIAN, K., HSIAO, S., SUNG, T.: Smart home safety handwriting pattern recognition with innovative technology, Computers and Electrical Engineering, Volume 40, Issue 4, May 2014, p 1123-1142
10. VOTRUBA, Z.: Integration of protective systems within the project "SMART buildings", 2016, dissertation, Prague CUA
11. VOTRUBA, Z., KOTEK, T., HART, J.: Universal interconnection protective systems in intelligent building project. Security magazine. 2011, č. 2, ISSN 1210-8723.
12. ZHOU, Q., ZHANG, Z., CUI, F.: Research on the integrated control teaching system of building based on fieldbus, Applied Mechanics and Materials 278-280 , 2013, pp. 1952-1955, ISSN 1660-9336.

Corresponding author:

Ing. Zdeněk Votruba, Ph.D., Department of Technological Equipment of Buildings, Faculty of Engineering, Czech University of Life Sciences Prague, Kamýcká 129, Praha 6, Prague, 16521, Czech Republic, phone: +420 22438 3149, e-mail: votruba@tf.czu.cz

DYNAMIC VISCOSITY AND POUR POINT OF HYDRAULIC OILS

V. Vozárová, A. Petrović, J. Csillag, M. Božiková, Ľ. Híreš, M. Valach

Department of Physics, Faculty of Engineering, Slovak University of Agriculture in Nitra, Slovak Republic

Abstract

This article presents the experimental results of dynamic viscosity and pour point of three hydraulic oil OSO S 46 AGIP samples – new oil and two used oils. Measurements were made under laboratory conditions with laboratory viscometer DV2T fy Brookfield. Examination of the dynamic viscosity in the temperature interval from 25°C to 90°C was made. The exponential dependency of viscosity on the temperature for the each sample was obtained in accordance with Arrhenius equation. Monitoring of pour point was provided by differential scanning calorimetry (DSC) this method gives information on thermal effects in the sample subjected to the temperature programme was realised in the temperature range from 20°C to the temperature of -45°C by using differential scanning calorimeter DSC 1 Mettler Toledo. It was determined that temperature of freezing (pour point) of used oil samples is lower than new oil sample.

Key words: hydraulic oil, dynamic viscosity, pour point.

INTRODUCTION

At the present time, hydrostatic systems are widely dispersed in the industry. It provides the various types of motions. The power transmission is realized by hydraulic fluid. Hydraulic fluid needs service and observation of operating parameters (Hujo et al., 2012). Today time offers us various kinds of industrial fluids. Hydraulics, which is used in transport and handling equipment, for its operation need the working medium - liquid in its hydrostatic systems (Kosiba et al., 2013). The testing of hydraulic systems is important for the design of new types of devices, the research of biodegradable fluid properties and their impact on the technical condition of hydraulic components (Hujo et al., 2015). Hydraulic systems are widely used in the executive mechanisms, road and construction machinery, agricultural and forestry equipment, as well as in many other areas. Development of existing hydraulic components is focused at increasing the transmitted power, reduction of energy consumption, minimize environmental pollution and increase technical lifetime and reliability (Jablonický et al., 2012). Hydraulic fluid in the hydraulic system have multiple functions, in addition to energy transfer, universal oils must lubricate, dissipate heat and be compatible with the seal material and metal materials of the system components (Majdan, 2014; Tkáč et al., 2010). The transmission of hydrostatic pressure and the use of hydrodynamic principle requires perfect medium. Each liquid has its own characteristics, which have different impact on the various elements of the hydraulic system of working equipment. Fluid must meet all the conditions, which are occur during the operation of hydraulic systems.

Physical properties such as viscosity and temperature interval of thermal stability are very important factors of bio-lubricants or bio-fuels which influence the possibilities of their use in agricultural machinery. Physical properties of bio-oil, bio-diesel and bio-ethanol were investigated by several authors, e.g. Valach et al., 2015; Vozárová et al., 2015; Hlaváč et al., 2014; Hlaváč and Božiková, 2014 and others.

This work is part of analysis of the physico-chemical properties of sampled hydraulic fluids with evaluation of changes in hydraulic fluids, which are used in hydraulic presses at lines number 46 and 47 of DS Smith Worldwide ™ Dispenser manufacturing plant.

MATERIALS AND METHODS

Temperature dependence of viscosity – viscosity as one of the most important rheological parameters is defined as the resistance of a fluid to flow. Viscosity of most of the liquids decreases with increasing temperature according to Arrhenius equation (Figura and Teixeira, 2007):

$$\eta = \eta_0 e^{\frac{E_A}{RT}}, \tag{1}$$

where η is, dynamic viscosity (Pa.s), η_0 is reference value of dynamic viscosity (Pa.s), E_A is activation energy (J/mol), R is gas constant (J/K.mol) and T is absolute temperature (K). Present data have been obtained from measurements performed on laboratory viscometer DV2T fy Brookfield. The experiments have been performed with use of ULA (0) spindle.

Monitoring of pour point by differential scanning calorimetry (DSC) - differential scanning calorimetry or DSC is a thermo-analytical technique which monitors heat effects associated with phase transitions and chemical reactions as a function of temperature, at pre-defined speed of heating (cooling), with assuming that both materials – sample and reference are under the same conditions (HAINES, 1995).

RESULTS AND DISCUSSION

Measuring of three samples dynamic viscosity of hydraulic oil OSO S 46 Agip 46, as a function of temperature, has been considered. First sample was new (Fig. 1). The others were used oils in two different press lines: press line No. 46 – sample 1, and press line No. 47 – sample 2 (Figs. 2 and 3). The procedure of sample preparation for viscosity measurements corresponded to a typical sampling procedure. The adequate volume (20 ml) of oil was put into the apparatus cuvette. The viscosity data were obtained in temperature range from 25°C to 90°C. Temperature of the sample was adjusted by the device automatically. The measured values of dynamic viscosity were saved in a table form. Based on these values, dynamic viscosity – temperature charts were plotted.

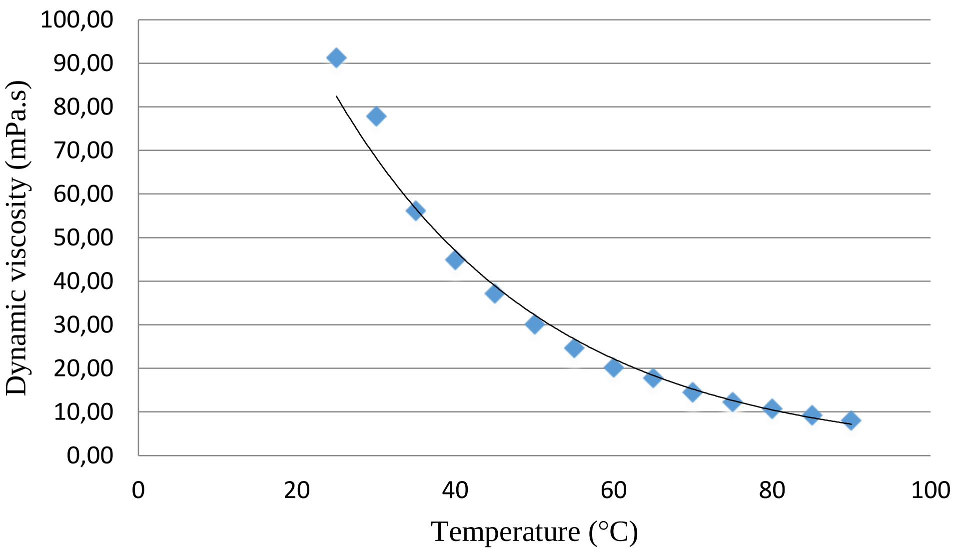

Fig. 1. – Temperature dependent viscosity of OSO S 46 AGIP hydraulic oil – new oil sample

The operating temperature in press lines, from which the samples of the oil were taken, is 50°C, so the most attention has been paid what happens with the viscosity at that temperature. It is possible to observe from Figs. 1-3 that dynamic viscosity of hydraulic oils is decreasing exponentially with increasing of temperature, what was expected and corresponds with conclusions reported in literature (VALACH ET AL., 2015; VOZÁROVÁ ET AL., 2015; HLAVÁČ ET AL., 2014; HLAVÁČ AND BOŽIKOVÁ, 2014; TRÁVNÍČEK ET AL., 2013; SEVERA ET AL., 2012). Regression equations and determination coefficients for individual samples are in the Tab. 1. As it can be seen from the dependencies for all samples, the development is characterized by the curve very well. The determination coefficients for all the samples are very high, which also confirms strong exponentially decreasing dependence.

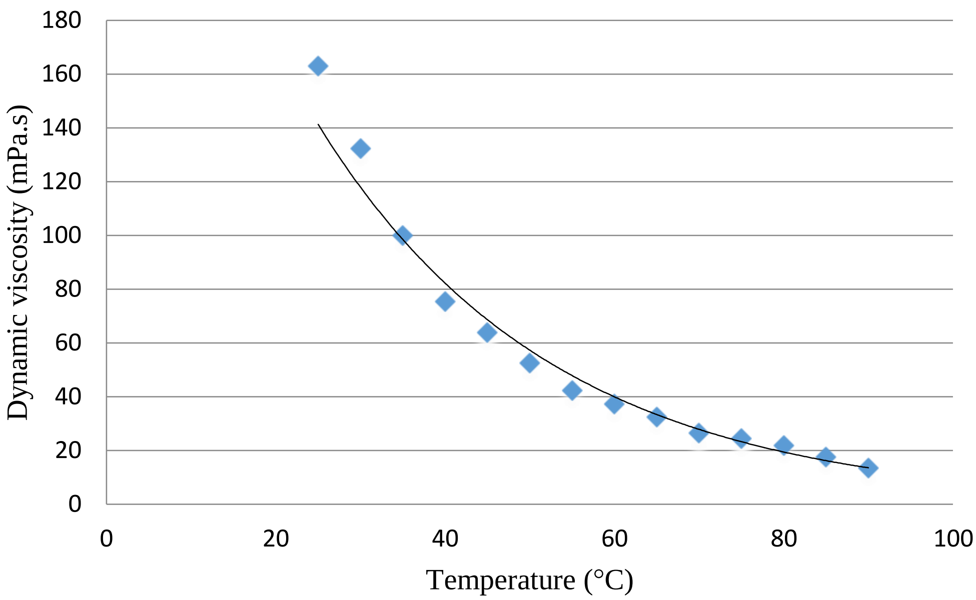

Fig. 2. – Temperature dependent viscosity of OSO S 46 AGIP hydraulic oil – used oil sample 1

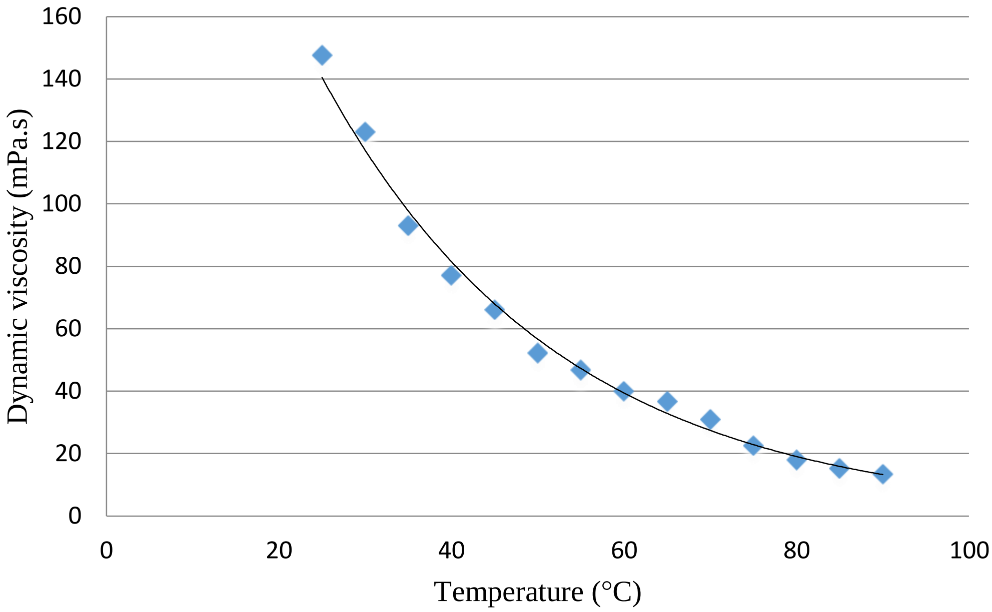

Fig. 3. – Temperature dependent viscosity of OSO S 46 AGIP hydraulic oil – used oil sample 2

Tab. 1. – Determination coefficients and regression equations

Sample	Regression equation	Determination coefficient R^2
New oil	$y = 210.6e^{-0.038x}$	0.9910
OSO S 46 AGIP 46	$y = 348.48e^{-0,036x}$	0.9867
OSO S 46 AGIP 47	$y = 348.34e^{-0,036x}$	0.9933

For monitoring of pour point of oils (phase transition of oil components) by DSC method was used device DSC 1 (Mettler Toledo). Samples of hydraulic oil OSO S 46 Agip with weight (11-13) mg were hermetically sealed in aluminium crucibles and thermally treated at the speed of heating (cooling) 2 K/min in the temperature range from 20°C to the temperature of -45°C. The measurement was carried out in an inert, dynamic atmosphere of N_2. As a result we got a DSC thermogram, which was evaluated in STARe software (Fig. 4).

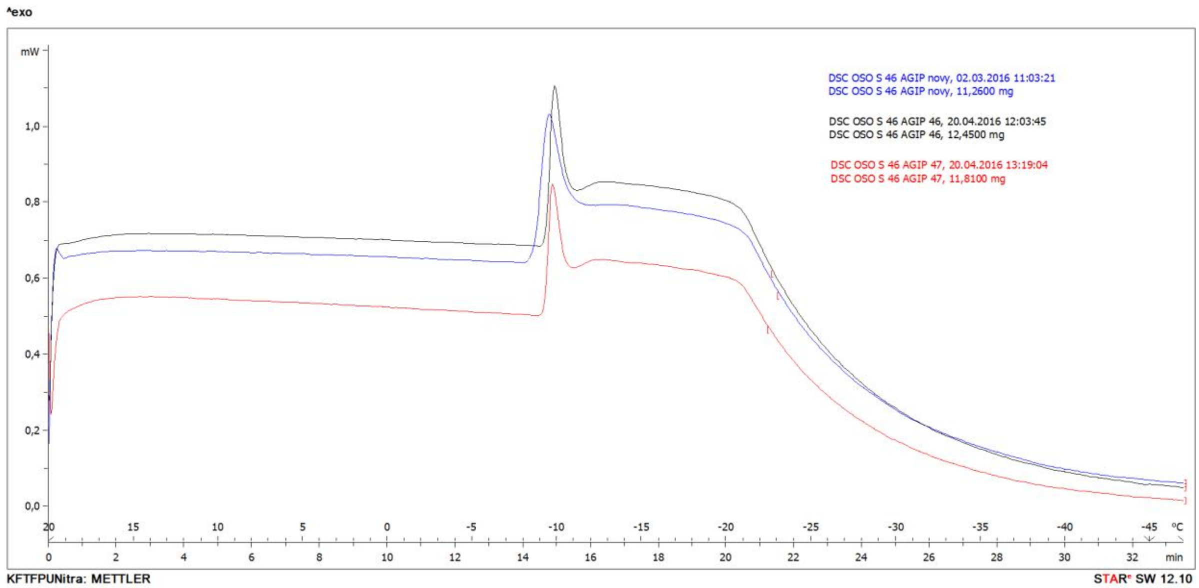

Fig. 4. – Pour point monitoring by DSC method of OSO S 46 Agip hydraulic oil – new and used oil samples

In the process of oil freezing and in the case of a new oil sample, we observed exothermal peak at the temperature -9.51 °C. This point is defined as a freezing point and temperature is nearly equal to the melting point (depending on the material purity). Since oil is an amorphous matter, the pour point takes place not only in one point, but in the range of temperatures which shows the graph (onset at -8.73 °C and endset -10.87 °C). In the case of oil from press line No. 46 (sample 1), the temperature of peak was -9.84 °C (onset at -9.39 °C and endset -10.65 °C). In the sample, where was used oil from press line No. 47 (sample 2), the temperature of exothermal peak was -9.71 °C (onset at -9.32 °C and endset -10.53 °C).

As it can be seen from the graph, there is a small difference between new sample and used samples of hydraulic oil in the view of pour point. The experiment shows that the new sample has higher temperature of pour point. Interesting fact is that new sample has wider interval of freezing. On the contrary, used samples have narrower interval of solidification, which is probably result of two years of continuous work of press lines using the same hydraulic oil.

CONCLUSIONS

Our results of pour point are significantly different as indicated by producer. The pour point introduced in the specifications of the producer is -27 °C. This difference may be caused by several factors (incorrect data of producer, inappropriate storage conditions or other unknown factors, for example thermal history). It should be experimentally verified in the next research. Press lines are located in halls with temperatures above zero, so this difference in temperature between the information from the producer and the measured values is not so significant in the case of using oil in hydraulic systems. But this information should be taken into account, in the case of the storage of oil, because the warehouse is not heated, practically oils are exposed to the outside temperature. If the winter temperatures are below -10°C, it may change the characteristics of the oil.

It can be concluded that knowledge of viscosity behaviour of a hydraulic oil as a function of temperature is of great importance, especially when considering running efficiency and performance of press line. Consequently, its function can be sensitive to the viscosity characteristics of the oil. Viscosity influences the oil's ability to flow through the hydraulic system, therefore affects the pressure required to push the oil sufficiently to develop the necessary flow. The rate of oil flow is important to the life of the hydraulic system. Dynamic viscosity of hydraulic oils is decreasing exponentially with increasing of temperature in accordance with theory (Arrhenius equation) and other authors (WAN NIK ET AL., 2005; VALACH ET AL., 2015; VOZÁROVÁ ET AL., 2015; HLAVÁČ ET AL., 2014; HLAVÁČ AND BOŽIKOVÁ, 2014; SEVERA ET AL., 2012). Viscosity results are also in accordance with results of ferrographic analysis that showed no metal particles. All samples of hydraulic oils were clean, they probably content no particles (neither non-metal), which should change viscosity of used oils. Our results are part of the analysis of hydraulic oils needed for correct operation of pressing equipment guarantee.

ACKNOWLEDGEMENTS

This work was co-funded by European Community under project no 26220220180: Building Research Centre „AgroBioTech“ and it was also supported by the project of Scientific Grant Agency of Slovak Republic (VEGA) under No. 1/0854/14 and 1/0337/15.

REFERENCES

1. FIGURA, L. O., TEIXEIRA, A. A.: Food physics, Physical properties - measurement and applications. USA: Springer. 2007: 550 p.
2. HAINES, P. J.: Thermal Methods of Analysis, Blackie Academic & Professional, London 1995.
3. HLAVÁČ, P., BOŽIKOVÁ, M., PRESOVÁ, R.: Temperature relations of selected engine oils dynamic viscosity. Acta technologica agriculturae., 17, 2014: 104 – 107.
4. HLAVÁČ, P., BOŽIKOVÁ, M.: Effect of Temperature on Dynamic Viscosity and Activation Energy of Milk and Acidophilus Milk. Advanced Materials Research. 1059, 2014: 53 – 59.
5. HUJO, Ľ., KANGALOV, P. G., KOSIBA, J.: Laboratory test devices for evaluating the lifetime of tractor hydraulic components: (proceedings, methods and applications). 1st ed. Ruse: University "Angel Kanchev" of Ruse, 2015: 69 p.
6. HUJO, Ľ., KOSIBA, J., JABLONICKÝ, J., TULÍK, J.: Load characteristics of three-point tractor linkage. In Naučni trudove: zemedelska technika i technologii, agrarni nauki i veterinarna medicina, remont i nadeždnosť: zemedelska technika i technologii, agrarnye nauki i veterinarnaja medicina, remont i nadežnosť. 51 (1.1), 2012: 172-176.
7. KOSIBA, J., TKÁČ, Z., HUJO, Ľ., STANČÍK, B., ŠTULAJTER, I.: The operation of agricultural tractor with universal ecological oil. Research in Agricultural Engineering, 59, 2013: 27–33.
8. MAJDAN, R., TKÁČ, Z., STANČÍK, B., ABRAHÁM, R., ŠTULAJTER, I., ŠEVČÍK, P., RÁŠO, M.: Elimination of ecological fluids contamination in agricultural tractors. Research in agricultural engineering. 60 (1), 2014: 9-15.
9. SEVERA, L., KUMBÁR, V., BUCHAR, J., ČORŇÁK, Š., GLOS, J., HLAVÁČ, P., ČUPERA J.: On the engineering flow properties of used and new engine oils. Applications of physical research in engineering: The renewable energy sources and physical properties of selected industrial materials. Nitra: Slovak University of Agriculture. 2012.
10. TKÁČ, Z., MAJDAN, R., DRABANT, Š., ABRAHÁM, R., VOZÁROVÁ, V., JABLONICKÝ, J.: Hodnotenie vlastností hydraulických kvapalín na základe skúšok s použitím hydrogenerátora (Performance evaluation of hydraulic fluids based on tests using hydraulic generator). Nitra, Slovenská poľnohospodárska univerzita. 2010.
11. TRÁVNÍČEK, P., VALACH, M., HLAVÁČOVÁ, Z., MAREČEK, J., VÍTĚZ, T., JUNGA, P.: Selected physical properties of liquid biofuels. Research in Agricultural Engineering. 59, 2013: 121-127.
12. VALACH, M., HÍREŠ, L., KANGALOV, P.: Biofuels and Biolubricants in Agricultural Machinery. Ruse, University of Ruse. 2015.
13. VOZÁROVÁ, V., KARDJILOVA, K., HÍREŠ, L., VALACH, M., WOLLNER, A.: Temperature Dependence of Dynamic Viscosity and DSC Analysis of the Plantohyd samples. Journal of Central European Agriculture, 16, 2015: 221-230.
14. WAN NIK, W. B., ANI, F. N., MASJUKI, H. H., ENG GIAP, S. G.: Rheology of bio-edible oils according to several rheological models and its potential as hydraulic fluid. Industrial Crops and Products, 22, 2005: 249-255.

Corresponding author:

Vlasta Vozárová, Department of Physics, Faculty of Engineering, Slovak University of Agriculture in Nitra, Slovak Republic

A REVIEW OF MUNICIPAL SOLID WASTE MANAGEMENT IN INDONESIA

M. Wasserbauer, D. Herák

Department of Mechanical Engineering, Faculty of Engineering, Czech University of Life Sciences Prague, Czech Republic

Abstract

The article is focused on the description of situation of Municipal Solid Waste Management in Indonesia from the perspective of the law and regulations as well as supporting governmental programs and with regard to the potential business in the near future. It was found that waste management in Indonesia is regulated by the following laws: Law Concerning Environmental Management; Waste Law regarding waste management; Presidential refers to energy, sustainability and environment protection and gives to all levels of Government responsibility for energy conservation; Presidential Regulations includes the targets for an energy mix by 2020. The government of Indonesia have also implemented some follow up programs such as: PROPER, a business performance-rating program is an alternative policy instrument to encourage compliance by companies; ADIPURA is a program for cities in Indonesia which succeed in maintaining the sanitation and environment management.

Key words: PROPER, ADIPURA, law, act, regulation, energy, strategy, government.

INTRODUCTION

The main factor influencing the waste production is the population of Indonesia, its growth and density. Indonesia is the most populous country in Southeast Asia with the total population amounting were 255 587 718 in 2012 with annual growth around 1.49 %. The population growth will bring problems faced by the government (KIS-KATOS & SPARROW, 2015A; LEHKONEN & HEIMONEN, 2015; LIU & YAMAUCHI, 2014). In 2010 the average waste produced in Indonesia was about 200 000 tons per day and the production is rapidly increasing (APRILIA, TEZUKA, & SPAARGAREN, 2013; S M KERSTENS, LEUSBROCK, & ZEEMAN, 2015; S.M. KERSTENS, SPILLER, LEUSBROCK, & ZEEMAN, 2016). Indonesian cities are facing serious issues concerning municipal solid waste (MSW). The issues occurred in all steps of waste management such as storage, collection, transferring, transportation, treatment, with the end point in the landfills. Problems are appearing not only with the waste from the households, but also from industrial processes. In a 2009 study conducted by the Bandung Institute of Technology's Centre for Research for Energy Policy (LPPM 2008), it was reported that 16.4 % or approximately 1.15 million tons of scheduled industrial waste generated annually goes unmanaged. Composition of MSW is as follows: household waste 48%, market waste 24%, commercial waste 9%, street and public facilities 5% and others 14%.From these facts it is evident that municipal solid waste management plays key role in development of the Indonesian cities as well as industrial areas and it is integral part of several supported programs initialised by new government of Indonesian president Joko Widodo. From the point of view of the import of municipal solid waste technologies to Indonesia it is currently supported by the fact that based on the stable economic growth Moody´s Investors Service raised Indonesian investment rating to Baa3 (NACIRI, 2015). This value represents Indonesia as the best country of investment evaluation from financial crisis during years 1997 and 1998. Another rating company, Standard & Poor´s raised investment rating of Indonesia to BB. This company also raised long-term rating of Indonesian rupiah to BB+ (HASPOLAT, 2015). In accordance with current Indonesian investment rating, some Czech financial institutions - ČRB and EGAP decided to change territorial risk qualification of Indonesia from category 5 to category 4 (BINH, 2015; RICHTER, 2015). For comparison of investment ratings, similar rating values are currently assigned to Turkey (KRIYANTONO, 2015; MOELIODIHARDJO, SOEMARDI, BRODJONEGORO, & HATAKENAKA, 2012; NIJMAN, 2015; RACHMAN, RIANSE, MUSARUDDIN, & PASOLON, 2015; RUDITO, 2014; SINGH & SETIAWAN, 2013; SIRINGORINGO, MARGIANTI, KOWANDA, & SAPTARIANI, 2013; WIHANTORO, LOWE, COOPER, & MANOCHIN, 2015). Therefore the aim of this study is to describe situation of Municipal Solid Waste Management in Indonesia from the perspective of the law and regulations as well as supporting governmental programs and with regard to the potential business in the near future.

MATERIALS AND METHODS

Primary data was collected from Ministry of Energy and Mineral Resources (Indonesia), Directorate General of Renewable Energy and Energy Conservation (Indonesia), United Nations Centre for Regional Development (Indonesia), Cleansing Department of Jakarta Province (Indonesia), World Bank (Indonesia), CekIndo (Indonesia) in period from 2010 until 2016. Methods used for the data collection varied according to the target groups, semi structured personal interviews, focus group discussions and analysis of internal documents were the most frequent. Most beginnings and termination parts of the interviews were informal, and many insights were obtained during casual conversations. Secondary data was gained by analysis of published materials of Statistical office of Indonesia (Badan Pusat Statistik Indonesia), analysis of law and regulations of Indonesia (Penelitan Hukum Indonesia) and by analysis of presidential directives (Direktif President RI).

RESULTS AND DISCUSSION

Waste management in Indonesia is regulated by the following laws:

1. Law Concerning Environmental Management No. 32 of 2009

It sets a mandatory utilization framework in the transportation, industrial, commercial and power generation sectors for biodiesel, bioethanol and bio-oil from 2009 to 2025

2. Waste Law No.18/2008 regarding waste management

According to Law No. 18/2008, waste generation must be minimized from the source to reduce the burden of waste transport and disposal. The law also highlights the importance of community in undertaking measures for waste reduction to minimize the burden of management and treatment. However, as these initiatives are still voluntary, not many communities are willing to apply the initiative. As the follow up of waste law no. 18/2008, the Ministry of Environment release waste law no. 81/2012. There are 3 main important issued in this law which are the first is starting in the year of 2013, every government regency/town have to change the open dumping system in landfill to be environment friendly. Second, in the industries business (producer, importer, distributor, retailer, etc) along with the government have to realize the application of extended producer responsibility in waste management. And the third is the administrator of the residential area, industries area, commercial area, public facilities, special facilities, and other facilities, have to sort, collect, and manage the waste in each area (APRILIA ET AL., 2013; S M KERSTENS ET AL., 2015; S.M. KERSTENS ET AL., 2016; KIS-KATOS & SPARROW, 2015B).

3. Presidential Law No. 30 2007 refers to energy, sustainability and environment protection and gives to all levels of Government (central and regional) responsibility for energy conservation.

4. Presidential Regulations No. 5 2006 include the targets for an energy mix by 2020 which includes at least 15 % of national energy consumption to be generated from renewable energy, including biofuel, geothermal and other renewable sources.

Despite the available local regulations, the enforcement is still low. To implement the waste law No. 18/2008 regarding waste management, the Ministry of Environment formulated 3 drafts of regulations including waste minimization, waste handling and waste specific management (LAW ACT, 2008). From these drafts, the Ministry of Environment forms the program to handle the waste management called 3R - reduce, reuse and recycle. Since 2007, the 3R program was initiated in 33 provinces as pilot subject of segregation, composing and recycling in about 300 locations in 2010. By 2014, it is expected that the implementation of 3R program will reduce the amount of disposed waste to landfill by 20% (GARCGIA, AFSAH, & STERNER, 2009).

Based on the 3R program, the government in their efforts to improve the waste management practices implemented some follow up programs such as:

1. PROPER, a business performance-rating program is an alternative policy instrument to encourage compliance by companies (Fig. 1; Fig. 2). PROPER is aimed to:

• Improve compliance of companies in environmental environment;

• Improve commitment of stakeholder in creating environment sustainability;

• Improve sustainable environment management performance;

• Increase awareness of business player to comply with environment legislation;

• Reinforce principles: reuse, recycle and recovery in waste management (3R).

2. ADIPURA is a program for cities in Indonesia which succeed in maintaining the sanitation and envi-

ronment management. The strategies for the implementation of Adipura program are:
• To motivate local government by providing incentive and awards;
• To motivate the competition among local government;
• To apply local specific of each area with their own specific trademark.

GOLD	For businesses/activities that have successfully perform environmental management effort and achieved satisfactory result.
GREEN	For businesses/activities that have perform environmental management effort and achieve better result set forth in the regulation requirements.
BLUE	For businesses/activities that have perform environmental management effort, and have achieved the minimum standard of regulation requirements.
BLUE MINUS	For businesses/activities that have performed environmental management effort, but have not achieved the minimum standard of regulation requirements.
RED	For businesses/activities have performed environmental management effort, but have achieved a part of the minimum standard of requirement as regulated.
RED MINUS	For businesses/activities have performed environmental management effort, but have achieved a small part of the minimum standard of requirement as regulated.
BLACK	For businesses/activities that does not perform environmental management effort significantly.

Fig. 1. – Colour indicator and colour specification in PROPER program

The already published research (GARCIA ET AL., 2009) supported the fact that foreign owned companies were more sensitive to the PROPER program and worked hard to meet the criterion of the ranking to ensure a good standing in the rankings each year (Fig. 2). One would expect the foreign owned and large local firms sensitive to achieving a good rating to also focus on the evolving criterion for PROPER; including waste management aspects. Companies embracing the newly introduced criterion on 3R alternatives for management of waste stand a chance to be rewarded with a desirable rating should they also fulfil all other requirements (WIBOWO & GIESSEN, 2015). Municipal Solid Waste (MSW) handling based on 3R program looks as shown on the figure. The majority of the waste was collected (69%), another part was buried (10%), composted & recycled (7%), burned (5%), or remained unmanaged (10%) (SME, 2008). In 2010, the Directorate General for New and Renewable Energy and Energy Conservation was established under the Ministry of Energy and Mineral Resources to promote demand-side energy management (conservation) and sustainable supply-side energy management (diversification away from fossil fuel sources). The National Energy Council secretary general, Hadi Purnomo, said that with the rise in fuel consumption and a decline in fossil energy reserves, renewable energy must be utililized and stop export of gas and coal, which can be used as alternatives to oil (which is imported since 2006). One of the strategies to produce more energy from renewable sources is to start using biofuel, which should contribute to the energy production mix by 5 % in 2025, according to the National Energy Strategy. Municipal Solid Waste (MSW) handling based on 3R program looks as shown on the figure. The majority of the waste was collected (69%), another part was buried (10%), composted & recycled (7%), burned (5%), or remained unmanaged (10%) (SME, 2008). In 2010, the Directorate General for New and Renewable Energy and Energy Conservation was established under the Ministry of Energy and Mineral Resources to promote demand-side energy management (conservation) and sustainable supply-side energy management (diversification away from fossil fuel sources). The National Energy Council secretary general, Hadi Purnomo, said that with the rise in fuel consumption and a decline in fossil energy reserves, renewable energy must be utilized and stop export of gas and coal, which can be used as alternatives to oil (which is imported since 2006). One of the strategies to produce more energy from renewable sources is to start using biofuel, which should contribute to the energy production mix by 5 % in 2025, according to the National Energy Strategy.

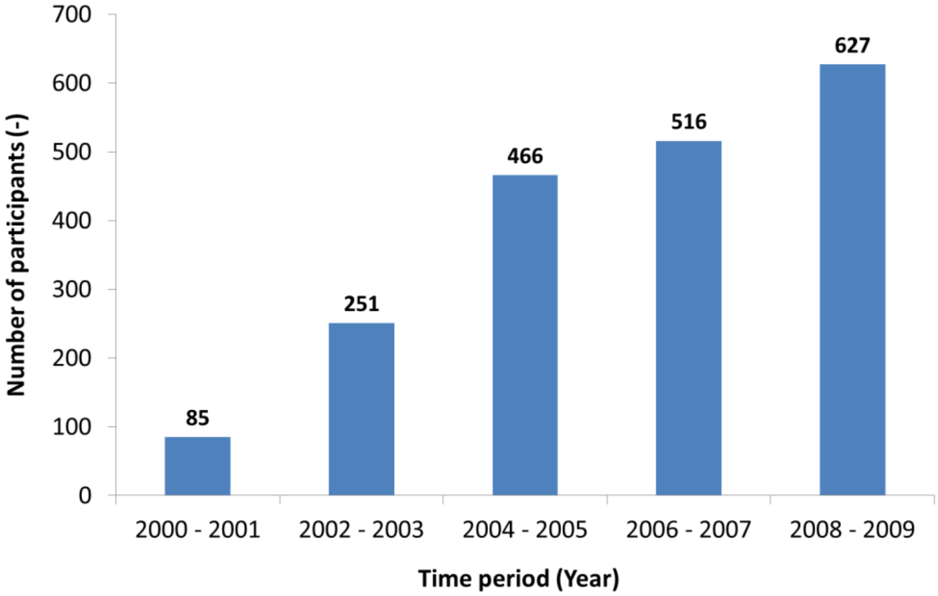

Fig. 2. – Number of Companies Participating in PROPER program

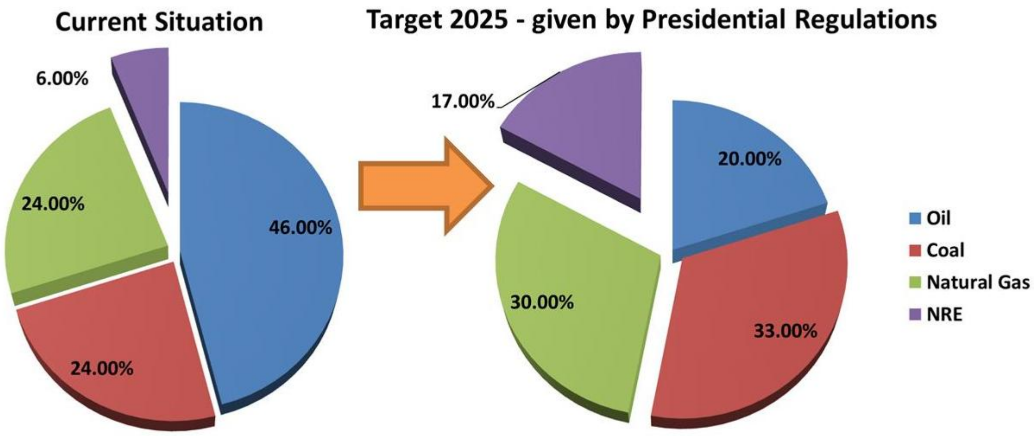

Fig. 3. – National Energy Strategy

Data from the Energy and Mineral Resources Ministry show that currently only 5 % of energy supplies in the country come from new and renewable energy (APRILIA ET AL., 2013; S M KERSTENS ET AL., 2015; S.M. KERSTENS ET AL., 2016). The energy sector ranks as the second biggest emitter after the forestry sector, which accounts for 65 % of total carbon emissions (BPS, 2014; BPS, 2015). Emissions from the energy sector are projected to continue to grow. Arief Heru Kuncoro, the ministry's new renewable energy and energy conservation director general said "The energy sector may become the largest emitter. We still have more renewable energy potentials, such as geothermal, micro hydro and biomass, as well as solar and wind." To reduce greenhouse emissions, the ministry plans to increase the share of new and renewable energy to about 17 % by 2025 from the current 5 % (SINGH & SETIAWAN, 2013) (Fig. 3). In Indonesia only a small portion of solid waste is recycled, in spite of the existence of a relatively large market for used products made from recycled materials, such as plastics, glass bottles, scrap paper and scrap metal. This view is difficult to substantiate since recycling is done mainly by the informal private sector, especially scavengers, itinerant buyers, and garbage truck helpers. It occurs at four points: the household level, during collection, at temporary transfer points and at the final disposal site. In all councils and municipalities, the scavengers play an important role within the system, where they reduce as much as 15% of the total waste generated daily, even though their activities generally interfere with the safe and efficient operation of the sites. Given the high content of compostable materials, solid waste composting was started in 1991 and it reached the maximum capacity of 24.2 tons/day in 2000 at 14 composting facilities using windrow systems. At the time of writing, there are only around four composting facilities in operation, including a new one at the landfill site with a design capacity of about 50 tons/day. As is common with other parts of the overall MSW system, a lack of strategic development for composting has led to poor performance. Problems that have been encountered but not solved include:

• Lack of market development;

• Lack of environmental guidelines to deal with odours, rodents and other environmental impacts;

• Contaminated feedstock;

• Insufficient provision of space to operate and expand;

• Lack of quality control by untrained staff.

More important is the lack of community participation in any initiative and poor local government management, especially in providing tool kits and guidance on how to make a better compost product at household and community level. It is clear that an insignificant reduction in the quantity of waste going to final disposal through recycling and composting or other means is not only due to collection problems, but also lack of commitment to introduce an appropriate system that fits with the characteristics of the waste and the community. To change this, a completely different approach is advocated. The Ministry of Finance set Law No 101/PMK.04/2007 which gives exception for the import duty for materials and equipment use to prevent environment pollution. This duty exception is given for industrial companies or waste management companies. No import duty or tax for importing EWA aerobic fermenter is therefore currently known.

CONCLUSIONS

Indonesia is the fourth most populous country in the world, currently reaching 250 millions inhabitants with its prospective to hit 450 million by 2045 if the trend did not change. It is one of the most protected markets in the world, together with countries like China, Russia or Brazil. Indonesia is on its way to stable democracy. Indonesia regained its investment ratings Baa3 by Moody´s and BBB- by Fitch lost during the Asian financial crisis in 1998. The GDP growth is topping 6 % already since 2007 with the only exception in 2009.

Waste management in Indonesia is regulated by the following laws: 1. Law Concerning Environmental Management No. 32 of 2009; 2. Waste Law No.18/2008 regarding waste management; 3. Presidential Law No. 30 2007 refers to energy, sustainability and environment protection and gives to all levels of Government (central and regional) responsibility for energy conservation.; 4. Presidential Regulations No. 5 2006 includes the targets for an energy mix by 2020 which includes at least 15 % of national energy consumption to be generated from renewable energy.

Based on the 3R program, the government in their efforts to improve the waste management practices implemented some follow up programs such as:

1. PROPER, a business performance-rating program is an alternative policy instrument to encourage compliance by companies.

2. ADIPURA is a program for cities in Indonesia which succeed in maintaining the sanitation and environment management.

Industrial areas are still open for possible future participation of Czech exporters in energetics, infrastructure and environmental technologies and it is supported by The Ministry of Finance which set Law No 101/PMK.04/2007 that gives exception for the import duty for materials and equipment use to prevent environment pollution.

ACKNOWLEDGEMENTS

This study has been supported by Integral Grant Agency of Faculty of Engineering, Czech University of Life Sciences Prague, grant number: 2016: 31130/ 1312/ 3106.

REFERENCES

1. Aprilia, A., Tezuka, T., &Spaargaren, G.: Inorganic and Hazardous Solid Waste Management: Current Status and Challenges for Indonesia. Procedia Environmental Sciences, 17, 2013: 640–647.
2. Binh, D.: Study On The Credit Guarantee System: The Case Of The V4 Countries. Challenges in Economic and Technological Development, University of Miskoloc, 2015: 24 - 33.
3. Garcia, J. H., Afsah, S., & Sterner, T.: Which Firms are More Sensitive to Public Disclosure Schemes for Pollution Control? Evidence from Indonesia's PROPER Program. Environmental and Resource Economics, 42(2), 2009: 151–168.
4. Haspolat, F. B.: Analysis of Moody's Sovereign Credit Ratings: Criticisms Towards Rating Agencies Are Still Valid? Procedia Economics and Finance, 30, 2015: 283–293.

5. KERSTENS, S. M., LEUSBROCK, I., & ZEEMAN, G.: Feasibility analysis of wastewater and solid waste systems for application in Indonesia. The Science of the Total Environment, 530-531, 2015: 53–65.
6. KERSTENS, S. M., SPILLER, M., LEUSBROCK, I., & ZEEMAN, G.: A new approach to nationwide sanitation planning for developing countries: Case study of Indonesia. Science of The Total Environment, 550, 2016: 676–689.
7. KIS-KATOS, K., & SPARROW, R.: Poverty, labor markets and trade liberalization in Indonesia. Journal of Development Economics, 117, 2015a: 94–106.
8. KIS-KATOS, K., & SPARROW, R.: Poverty, labor markets and trade liberalization in Indonesia. Journal of Development Economics, 117, 2015b: 94–106.
9. KRIYANTONO, R.: Public Relations and Corporate Social Responsibility in Mandatory Approach Era in Indonesia. Procedia - Social and Behavioral Sciences, 211, 2015: 320–327.
10. LEHKONEN, H., & HEIMONEN, K.: Democracy, political risks and stock market performance. Journal of International Money and Finance, 59, 2015: 77–99.
11. LIU, Y., & YAMAUCHI, F.: Population density, migration, and the returns to human capital and land: Insights from Indonesia. Food Policy, 48, 2014: 182–193.
12. MOELIODIHARDJO, B. Y., SOEMARDI, B. W., BRODJONEGORO, S. S., & HATAKENAKA, S.: University, Industry, and Government Partnership: Its Present and Future Challenges in Indonesia. Procedia - Social and Behavioral Sciences, 52, 2012: 307–316.
13. NACIRI, A.: Credit Rating Governance: Global Credit Gatekeepers. 2015.
14. NIJMAN, V.: CITES-listings, EU eel trade bans and the increase of export of tropical eels out of Indonesia. Marine Policy, 58, 2015: 36–41.
15. RACHMAN, A., RIANSE, U., MUSARUDDIN, M., & PASOLON, Y.: The Potential of Delivering Clean Locally Available Limitless Rice Husk Energy in the Celebes Island Indonesia. Energy Procedia, 79, 2015: 55–60.
16. RICHTER, S.: Export Promotion Framework of the Czech Republic. Central European Business Review. 2015.
17. RUDITO, B.: The Improvement of Community Economy as Impact of Corporate Social Responsibility Program: A Case Study in Pengalengan, Bandung, West Java, Indonesia. Procedia - Social and Behavioral Sciences, 164, 2014: 471–476.
18. SINGH, R., & SETIAWAN, A. D.: Biomass energy policies and strategies: Harvesting potential in India and Indonesia. Renewable and Sustainable Energy Reviews, 22, 2013: 332–345.
19. SIRINGORINGO, H., MARGIANTI, E. S., KOWANDA, A., & SAPTARIANI, T.: Shopping Behavior of Indonesian Consumer Towards Imported Products. Procedia - Social and Behavioral Sciences, 81, 2013: 411–415.
20. WIBOWO, A., & GIESSEN, L.: Absolute and relative power gains among state agencies in forest-related land use politics: The Ministry of Forestry and its competitors in the REDD+ Programme and the One Map Policy in Indonesia. Land Use Policy, 49, 2015: 131–141.
21. WIHANTORO, Y., LOWE, A., COOPER, S., & MANOCHIN, M.: Bureaucratic reform in post-Asian Crisis Indonesia: The Directorate General of Tax. Critical Perspectives on Accounting, 31, 2015: 44–63.
22. LPPM: Indonesian - German Environmental Program, Centre for Research on Energy Policy.Institute Technology Bandung, "Report prepared for Public -Private-Partnership to establish National Guidelines for waste co-processing", Jakarta, 2009.
23. BPS: Environmental Care Behavior Indicators. Badam Pusat Statistik Indonesia, Jakarta, 2014.
24. BPS: Captive Power Statistics. BadamPusatStatistik Indonesia, Jakarta, 2015.
25. SME: Indonesian domestic solid waste statistic,State ministry of Environment, Jakarta, 2008.
26. LAW ACT: Waste Management Law of 2008 (No. 18/2008), Jakarta, 2008.

Corresponding author:
Ing. Michal Wasserbauer, Department of Mechanical Engineering, Faculty of Engineering, Czech University of Life Sciences Prague, Kamýcká 129, Praha 6, Prague, 16521, Czech Republic, phone: +420 22438 3181, e-mail: wasserbauer@tf.czu.cz

EFFECT OF LOADING POSITION AND STORAGE DURATION ON THE MECHANICAL PROPERTIES OF ABATE FETEL PEAR VARIETY

E. Yesiloglu[1] , D. Yildirim[2] , Y. B. Oztekin[1]

[1]*Ondokuz Mayis University, Faculty of Agriculture, Department of Agricultural Machinery*
[2]*Black Sea Agricultural Research Institute, Samsun-Turkey*

Abstract
In the study, the mechanical properties of Abbate Fetel pear have been examined in terms of storage time and loadingposition. The experiments were conducted in two stages; the first experiment was carried out immediately after the harvest and the second experiment was carried out after 30 days in cold storage. The mechanic properties of the pear fruit such as rupture force, deformation, rupture energy and firmness have been examined on the fruit's bloom side, lateral side and stem side. Furthermore, the size, sphericity, mass, amount of soluble solids and volume of the pear fruit have been determined. The relationship between the sides of the fruit and firmness has been found as statistically significant (P<0.001). The maximum firmness value has been found at the stem side, while the lowest firmness value has been found at the bloom side. The lowest rupture energy value of the pear fruit has been determined to be needed at the bloom side.

Key words: pear; mechanical properties; rupture force; rupture energy; firmness.

INTRODUCTION

Biological materials are exposed to mechanic effects in almost all processes from sowing or planting to the time they are offered to the consumer. These effects may be in the form of static or dynamic forces. The sizes, implementation time, structure of the force or type of implementation are mainly effective in the biological material's responses to these forces.

The mechanical deformations occurring in the fruits may be at significant levels during the implementations including cleaning, sorting, grading, packaging, transport and distribution that are harvest and post-harvest operations.

The biological materials that are under static or dynamic loading typically exhibit certain behaviors depending on their structural features. These behaviors emerge as yield or rupture. The implemented pushing force causes biological material to shorten, while the pulling force causes elongation. With the help of force-deformation curve, it is possible to determine modulus of elasticity of the material, biological yield limit, rupture point, and the values related to force-deformation and energy emerging at these points (ALAYUNT, 2000).

There are two important points on the force-deformation curve. These are biological yield point and rupture point. Biological yield point is the point on the curve at which the force decreases or remains constant with increasing deformation. This point indicates the cellular ruptures and it is used in determining the product's sensitivity to damage. The cell is not damaged before this point. The rupture point is the point at which the material ruptures, cracks or deteriorates under loading. After the rupture point, the force decreases rapidly with increasing deformation. The volume of the material/product deteriorates and its resistance to the force decreases; the maximum rupture point is obtained at this point. (MOHSENIN, 1970)

The mechanical properties of biological materials contain the resistance parameters of the product. These properties are determined by analyzing the force-deformation curve related to the product.

The mechanical damages on the fruits cause loss of quality. The pear fruit is among the fruits that are sensitive to different types of mechanical damages that may occur at harvest or post-harvest period. It is necessary to know the mechanical properties of the pear fruit in order to reduce the mechanical damages/losses that occur at harvest and post-harvest period.

When the harvested fruits and vegetables are stored in appropriate conditions, they retaintheir fresh qualifications significantly for a while. The cold storage provides different storage conditions according to the type of product. Depending on the cold storage conditions, certain changes may occur in the properties of the fruits stored at such an environment. For this reason, it is of importance to determine the mechanical properties of the fruites that are stored in cold storage.

In this study, the mechanical properties of the pear fruite, which is among the fresh fruits that is of commercially importance for Turkey, have been examined in terms of static load effect immediately after the harvest at room temperature and after 30 days in cold storage conditions.

The pear is the common name of the edible fruits of several tree and shrub species of genus Pyrus that is classified under the subfamily of Maloideae that belongs to the family of Rosaceae. Following apple and grapefruit, the pear constitutes the third major temperate fruit. The most of the cultivated forms of the genus *Pyruscommunis* L. (Pear) are grown in Anatolia. There are over 5000 varieties of pear in the world. In Turkey, which has so many different ecological conditions, it is reported that 640 varieties of pear are cultivated on a regional and local basis (ÖZAYDIN AND ÖZÇELIK, 2014).

According to the recent data, world pear production is approximately 24 million tons annually. Turkey ranks fifth in terms of production quantity of pear (ANONYMOUS, 2014).

The pear fruit contains K, Ca, Mg, S and Fe elements that have an important role in human nutrition to a large extent.

EMADI ET AL., (2011) examined the physical and mechanical properties of Tabrizi peach variety. The mean of physical properties including mass, volume, dimensions (big, medium and small diameters), arithmetic mean diameter, sphericity and density were respectively found to be 137.37 g, 107.37 cm, 61.1 mm, 60.29 mm, 59.21 mm, 60.14 mm, 96.05% and 1.24 g/cm. The mean of mechanical properties including stiffness of peach, without and with peel, were respectively found as 11.35 and 15.31 N. Linear relationships were respectively found between mass and volume, mass and three orthogonal diameters, volume and three orthogonal diameters, stiffness without peel and geometric mean diameter, also stiffness with peel and geometric mean diameter with correlation coefficients of 0.625, 0.743, 0.63, 0.872 and 0.897.

WASALA ET AL., (2012) examined the physical and mechanical properties of Seeni, Embul and Kolikuttu varieties of banana. The moisture content, linear dimensions of bunches and fruits, sphericity and aspect ratio of fruits, bulk density and true density, coefficient of static friction and the angle of repose on different surfaces such as wood, steel and Styrofoam, and fruit firmness were measured for the abovementioned three cultivars at the harvest maturity. The average bunch length of the banana cultivars Embul and Kolikuttu were higher than those of Seeni. The geometrical mean diameters of Embul and Kolikuttu fruits were also higher than Seeni (p0.05). The bulk density of fruits and hands were higher than those of the whole bunch. The lowest coefficient of static friction was on Styrofoam and the highest was on a wooden surface. There was no significant difference in terms of the firmness of mature green banana fruits between the cultivars ($p>0.05$).

MATERIALS AND METHODS

The Abate Fetel pears used in the research were harvested by hand from the SAMMEY fruit production farm in Samsun Province in October 2015, the commercial harvest period. The harvested pears were stored at 1°C storage temperature and 90% relative humidity for 30 days. Before the measurements, the pear fruits were held in at 21±2°C temperature to reach ambient temperature for 1 h.

The Abate Fetel that originated in France was found in 1866. It can be immediately distinguished with its large and conical fruit with a too long neck. Its rind is thin and partly rusty; its color is dark yellow when the fruit is mature. The fruit is quite juicy and aromatic with its white flesh that has a hard texture and sweet flavor; it is a highly qualified fruit (ANONYMOUS, 2010).

The pear fruits were cleaned from dust, dirt, twigs and impurities before commncing the experiments. The pear size measurements were carried out with a digital calliper having an accuracy of 0.01 mm in term of the major, intermediate and minor diameters.

Using the determined axis measurements, arithmetical mean diameter (D_a), geometric mean diameter (D_g) and sphericity values were calculated by the following equations (where; L major diameter, mm; W intermediate diameter, mm; T minor diameter, mm) (Fig. 1) (MOHSENIN, 1980, 1970; MILANI ET AL., 2007).

$$D_a = (L + W + T)/3 \quad (1)$$

$$D_g = (LWT)^{1/3} \quad (2)$$

$$\phi = \frac{(LWT)^{1/3}}{L} \quad (3)$$

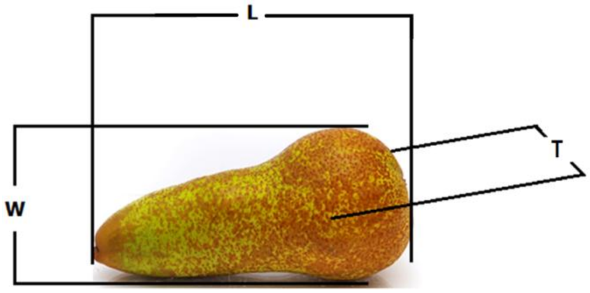

Fig. 1. – Sizes of pear fruit

Geometric mean diameter values and the following equation were utilized in determining the surface area (MOHSENIN, 1980).

$$S = \pi D_g^2 \tag{4}$$

At this equation;
S: Surface area (mm^2)
Dg: Geometric mean diameter (mm).
The volume of the pear (*V*) was calculated by the following equation (MOHSENIN, 1980):

$$V = \frac{\pi}{6}(LWT) \tag{5}$$

The content of the total soluble solid (TSS) was determined using Atago Pocket and PAL-1(Japan) digital refractometer.
The mechanical properties of pear fruit were determined using LLoyd (Lloyd Instrument LRX Plus, Lloyd Instruments Ltd, An AMATEK Company) biological material tester. The device is composed of a platform to hold the sample, a movable member, a unit providing movement and a data processing unit (Fig. 2). The data processing unit has a load cell with 100 N capacity and a computer with NEXYGEN Plus software to which the data is transferred. During the experiments, a 8-mm diameter probe was connected to the moving part and load was applied to the blossom side, lateral side and stem side of the pear fruit at the press rate of 20 mm/min (GARCIA ET AL., 1995).

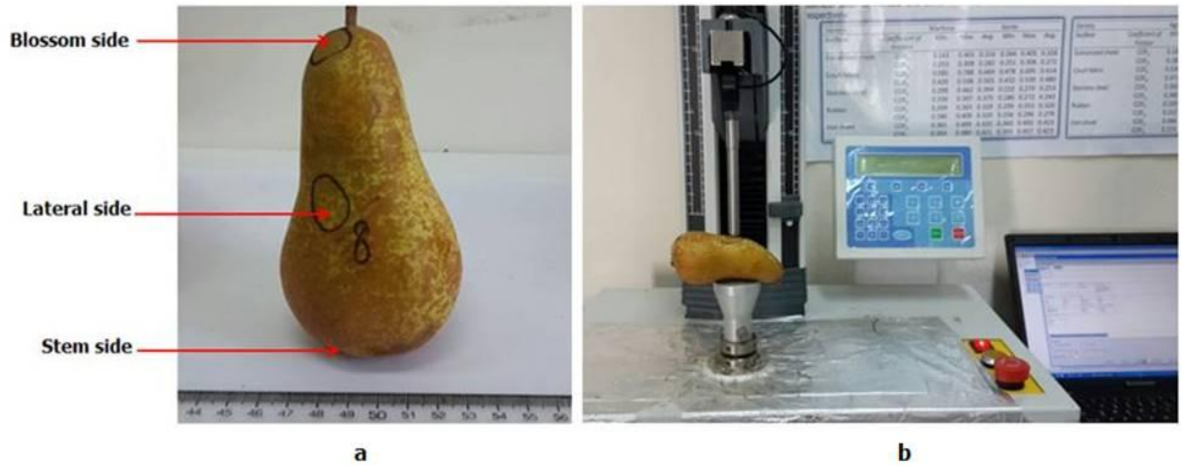

Fig. 2. – a - Representation of the three axes and three perpendicular dimensions of pear, **b -** Lloyd Instrument universal testing machine

The force-deformation curve was plotted based on the values obtained from the load cell by means of the software program. The peak (A) of the force-deformation curve was determined as rupture force (Fig. 3). The rupture energy was determined by calculating the area under the force-deformation curve. The software saves the obtained values into a data file. The experiments were conducted in 10 replicates.

Firmness was calculated by dividing the rupture force by dividing the deformation to the rupture point (YURTLU AND YESILOGLU, 2012).
The value of all the measured properties is summarized in Tab. 1. The length ranged from 113.58 to 130.56 mm; the width ranged from 55.04 to 65.06 mm; and the thickness ranged from 53.69 to 60.50 mm. The geometric mean diameter ranged from 70.08 to 77.54 mm.

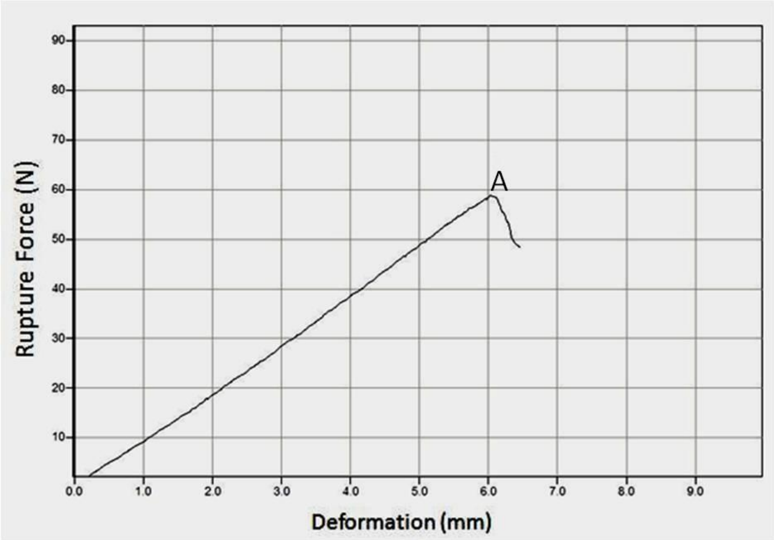

Fig. 3. – Force-deformation curve of pear fruit

RESULTS AND DISCUSSION

Mean, minimum and maximum values together with standard deviations of some physical properties of Abbate Fetel pears are listed in Tab. 1.

Tab. 1. – Physical properties and standard deviation of pear

Pear dimension, mm	*Major diameter (L)*	122.93±5.05
	Intermediate diameter (W)	59.72±3.44
	Minor diameter (T)	57.46±2.01
Average diameter, mm	*Arithmetic mean (L+W+T)/3*	80.03±2.83
	Geometric mean $(LWT)^{1/3}$	74.95±2.61
	Sphericity (%)	0.61±0.02
	Surface area, mm^2	17671.37±1219.82
	Mass (g)	206.99±16.41
	Water soluble dry matter (%)	12.89±1.31
	Volume (mm^3)	229180.6±21671.97

According to research results, the values of the rupture force, deformation and firmness have been observed to increase after the pear fruits were stored for 30 days. The effect of the storage time on the firmness property of the pear fruit has been found statistically significant ($P<0.05$).

Tab. 2 shows the means and statistical values of the mechanical properties resulting from the load applied to the three sides of the pear fruit depending on the storage time.

According to research results, the values related to the rupture force, deformation, rupture energy and firmness respectively ranged between 15.2- 59.26 N; 2.16-6.88 mm; 0.036- 0.26 J; and 4.15- 10.29 N/mm.

The relationship between pear locations and firmness has been found statistically significant ($P<0.001$). The maximum firmness value was found at the stem side, while the lowest firmness value was found at bloom side of the pear fruit.

Tab. 2. – Measurement parameters and some statistical values

Storage Time	Pear locations	Rupture Force (N)	Deformation (mm)	Rupture Energy (J)	Firmness (N/mm)
1 day	B	31.17±11.03	4.59±1.35	0.102±0.04	6.78±0.99
	L	39.51±8.77	4.85±1.06	0.145±0.06	8.12±0.19
	S	42.68±8.98	4.69±0.88	0.152±0.05	9.07±0.33
30 days	B	32.59±7.85	4.86±0.98	0.104±0.05	7.09±0.54
	L	41.18±7.80	4.84±0.94	0.147±0.04	8.52±0.31
	S	48.04±5.49	5.10±0.66	0.157±0.04	9.43±0.44
Means					
1 day		37.79±10.74	4.71±1.11	0.14±0.05	7.99±1.14
30 days		40.59±9.47	4.84±0.86	0.13±0.05	8.34±1.08
	B	31.89^{a}±9.69	4.59^{a}±1.19	0.102^{a}±0.04	6.94^{a}±0.83
	L	40.31^{b}±8.14	4.84^{a}±0.98	0.144^{b}±0.05	8.31^{b}±0.32
	S	45.36^{c}±7.75	4.89^{a}±0.78	0.153^{b}±0.05	9.25^{c}±0.42
P values					
Pear locations		<0.001	0.590	<0.001	<0.001
Storage Time		0.217	0.626	0.742	<0.05

CONCLUSIONS

It has been found that the length (L) of the pear fruit ranged between 113.26 and 130.56; its width (W) ranged between 55.04 and 663.64; and its thickness (T) ranged between 53.69 and 59.81 mm. The fruit's sphericity value ranged between 0.58% and 0.64%; the mass value ranged between 175.66 and 234.94 g; the amount of soluble solids ranged between 10.8% and 15.3%; and its volume value ranged between 180192.1 and 265959 mm^3.

According to the results of the experiments, the stem side of the pear fruit is the area that is mostly ruptured. The lowest rupture energy value of the pear fruit has been determined to be needed at the bloom side.

REFERENCES

1. ALAYUNT, F.N.:. Physical properties of biological materials. ege university, publication of faculty of agriculture No. 541, Izmir, Turkey, ISBN: 975-483-464-4. 2000.
2. ANONYMOUS: FAOSTAT production data [online]. 2014 Available at: http://faostat3.fao.org/faostatgateway/go/to/download/Q/QV/E
3. EMADİ, B., ABOLGHASEMİ, R., AGHKHANİ, MH., TOOSİ, T.: Physical and Mechanical Properties of Peach. WorldAppliedSciencesJournal12 (1), 2011: 119-122.
4. GARCIA JLL., M. RUIZ-ALTISENT Y P. BARREIRO: Factors influencing apple and pear physical properties and bruise susceptibility. J.Agric.Eng.Res. (in press); AGENG 1995: p 94-G-062 Milano.
5. HAZBAVİ, E., KHOSHTAGHAZA, M.H., MOSTAAN, A., BANAKAR, A.: Effect of storage duration on some physical properties of date palm (cv. Stamaran). Journal of the Saudi Society of Agricultural Sciences. 14, 2015: 140–146.
6. MOHSENİN, N.N.: Physical properties of plant and animal material. Gordon and Breach. New York 1970.
7. MOHSENİN, N. N.: Physical properties of plant and animal material. Gordon and Breach Science Publishers Inc., New York, USA 1980.
8. ÖZAYDIN, A.G., ÖZÇELİK, S.: Effect of oven drying on some physiochemical properties of ankara pear. Academic Food Journal. 12(4), 2014:17-26.
9. ÖZAYDIN, A.G., ÖZÇELİK, S.: Different Drying Conditions on Quality of Microbiologic Investigation of the Effects of Some Major Pear Varieties. Fruit Science. ISSN: 2148-0036. 3(1) 2016: 37-44.
10. WASALA, W.M.C.B., DHARMASENA, D.A.N., DİSSANAYAKE, T.M.R., THİLAKARATHNE, B.M.K.S.: Physical and mechanical properties of three commercially grown banana (Musa acuminata Colla) cultivars in Sri Lanka - Tropical Agricultural Research V24(1) 2012: 42-53.
11. YURTLU, Y. B., YEŞİLOĞLU, E.: Mechanical behaviour and split resistance of chestnut under compressive loading. Journal of Agricultural Sciences 17(4) 2011: 337-346.

Corresponding author:

ElÇİn YEŞİLOĞLU, Ph.D., Department of Agricultural Machinery, Faculty of Agriculture, Ondokuz Mayis University, Turkey

EVALUATING THE SOIL MOISTURE CONTENT THROUGH DIFFERENT INTERPOLATION METHODS

D. Yıldırım[1], B. Cemek[2], A. Ünlükara[3]

[1]*Black Sea Agricultural Research Institute, Irrigation and Land Reclamation Unit, Samsun, Turkey*
[2]*Department of Agricultural Structures and Irrigation, Faculty of Agriculturem, Ondokuz Mayıs University, Samsun, Turkey*
[3]*Department of Biosystems Engineering, Seyrani Faculty of Agriculture, Erciyes University, Kayseri, Turkey*

Abstract
Water is vital for the plant growth. An adequate amount of soil moisture content is required in order to increase plant growth and yield. The spatial distribution can be determined using different methods for different depths of soil moisture content. In this study the spatial distribution is created at four different soil depths (30, 60, 90 and 120 cm) using deterministic and stochastic methods. In order to determine the most appropriate methods, Root Mean Square Error (RMSE) and Mean Absolute Error (MAE) values were compared between the methods. The lowest RMSE (11.296) and MAE (7.821) values were obtained for 0-30 cm depth of soil moisture content by Ordinary Kriging method. As for the depth of 30-60 cm, the lowest RMSE (13.682) and MAE (8.444) values were obtained through Inverse Distance Weight (IDW). As for the depth of 60-90 cm, the lowest RMSE (17.767) and MAE (11.473) values were obtained through the Radial Basis Function (RBF). As for the depth of 90-120 cm, the lowest RMSE (20.24) and MAE (14.18) values were obtained through the IDW method. The soil moisture content maps have been prepared for 0-30 cm, 30-60 cm, 60-90 cm and 90-120 cm soil depths based on these methods.

Key words: interpolation methods, Ordinary Kriging, radial basis function, inverse distance weight, soil moisture.

INTRODUCTION

The soils can vary as a result of natural soil formation and the effects of the human activities on different spatial and temporal scales. A source of information including the basic information such as soil, physiography, climate, vegetation, soil moisture content and land use is needed to develop the planning strategies to ensure sustainable use of agricultural lands as well as to carry out modelling of the environmental topics. The change to occur should be monitored in temporal and spatial terms in order to determine, map and plan the changes of soil characteristics of agricultural lands and to make these characteristics efficient and sustainable. Soil variability is frequently seen as a result of the data obtained from soil survey, soil and plant tests and product yield. However, assuming that their lands are homogeneous, most of the farmers implement homogeneous soil and plant management throughout all the land. As a result of these practices, excessive or insufficient practices are implemented in certain parts of the lands. This situation leads to an increase in the cost, decrease in net economic gain and unnecessary energy use as well as pollution in surface and ground waters (CASTRIGNANO ET AL., 2000).

Today, land use is more intensive and there is a need for a more precise evaluation of the distribution and behaviors of the soil as a result of that. Users want to know the amount and kinds of the variability of the soil mapping units in order to make their management decisions accurately within confidence limits. For example, it is essential to know the mean values of the mapping units within certain confidence limits. In addition, the information about the structure of the spatial variability can be forecasted through mapping units (NORDT ET AL., 1991). Depending on the soil variability, the use of geo-statistical methods has been more widespread rather than the traditional methods including different approaches in order to make these forecasts.

In parallel with the developments in computer technology, Geo-statistics is a technique that allows generalizing land properties using the relationships between the parameters by spending much less time, laboring and money (WARRICK ET AL., 1986; ZHANG ET AL., 1995). The concept of geo-statistics generally refers to the stochastic methods used for determining and forecasting the distinctive characteristics of the spatially referenced data.

Traditional statistics assumes that the variability in soil is random and it does not have a spatial correlation; the samples to be taken from each point of the land are independent. It uses the parameters such arithmetic mean, standard deviation and variation coefficient by calculating from the samples. The samples taken from the points that are close to each other are similar compared to the samples taken from distant points. In modelling studies (water flow modelling and non-point source (uncertain) pollution studies, etc.), intensive terrain data are needed for the verification of the models. In this type of use, the soil data, which are spatially variable in the soil in an area, layer or volume, should be grouped, processed, averaged or transformed to a scale that can reveal the similarities and differences in soil properties. The information about the spatial variable components of the soil is required to perform such groupings within the confidence limits to an extent (YOUNG ET AL., 1998; ROGOWSKI AND WOLF, 1994; BROWN AND HUDDLESTON, 1991).

DING ET AL. (2011) also used IDW, Ordinary Kriging and Spline methods in order to determine the distribution of soil moisture content. The distribution of soil moisture was determined by each method and Ordinary Kriging method was determined to be more appropriate for the spatial distribution upon comparing the lowest RMSE values of each method. ARSLAN ET AL. (2011) evaluated the spatial distribution of the exchangeable sodium percentage using different interpolation methods and they determined Simple Kriging as the best interpolation method.

The study has been conducted in a 6-decare area. The moisture distributions have been mapped by means of geostatistical techniques for different soil depths (30 cm, 60 cm, 90 cm and 120 cm) and soil moisture distributions have been determined for different layers. Geostatistical techniques can be used to obtain and map the soil properties.

MATERIALS AND METHODS

Vezirköprü District of Samsun Province is geographically situated between 41° 00’ – 41° 19’ North latitudes and 35° 48’ – 35° 01’ East longitudes. The long annual average highest temperatures have been respectively recorded as 29.8 °C (July) and 30.7 °C (August). The average precipitation has been recorded as 520 mm based on the average of long years; April and May are the rainy months (Tab. 1). The study area is about 6.5 decares. The soil moisture content in the field has been measured by neutron gauge device through the 40 accesstubes placed on certain points. The access tubes were placed at 120-cm depth and soil moisture content has been measured at every 30 cm (0-30, 30-60, 60-90 and 90-120 cm). The tubes have been placed in the study area as shown in Fig. 1. A system has been established based on the precipitation in this experimental area. In this system, the rainwater is stored under the soil. The area has not been irrigated during the experiment and melon and watermelon have been cultivated. An experimental area has been formed to examine the effects of precipitation on the changes of soil moisture content and crop yield. The experimental subjects have been placed in parallel to the levelling curves and an accesstube has been placed in each subject in order to determine soil moisture content. Thanks to this system, the effects of precipitation on the changes of soil moisture content have been examined at different depths (0-30 cm, 30-60 cm, 60-90 cm and 90-120 cm). As a result of the study, soil moisture maps have been drawn using the interpolation methods at the depths of 0-30 cm, 30-60 cm, 60-90 cm and 90-120 cm. The interpolation methods used in this study are stochastic (Ordinary Kriging and CoKriging) and deterministic (IDW and RBF) methods.

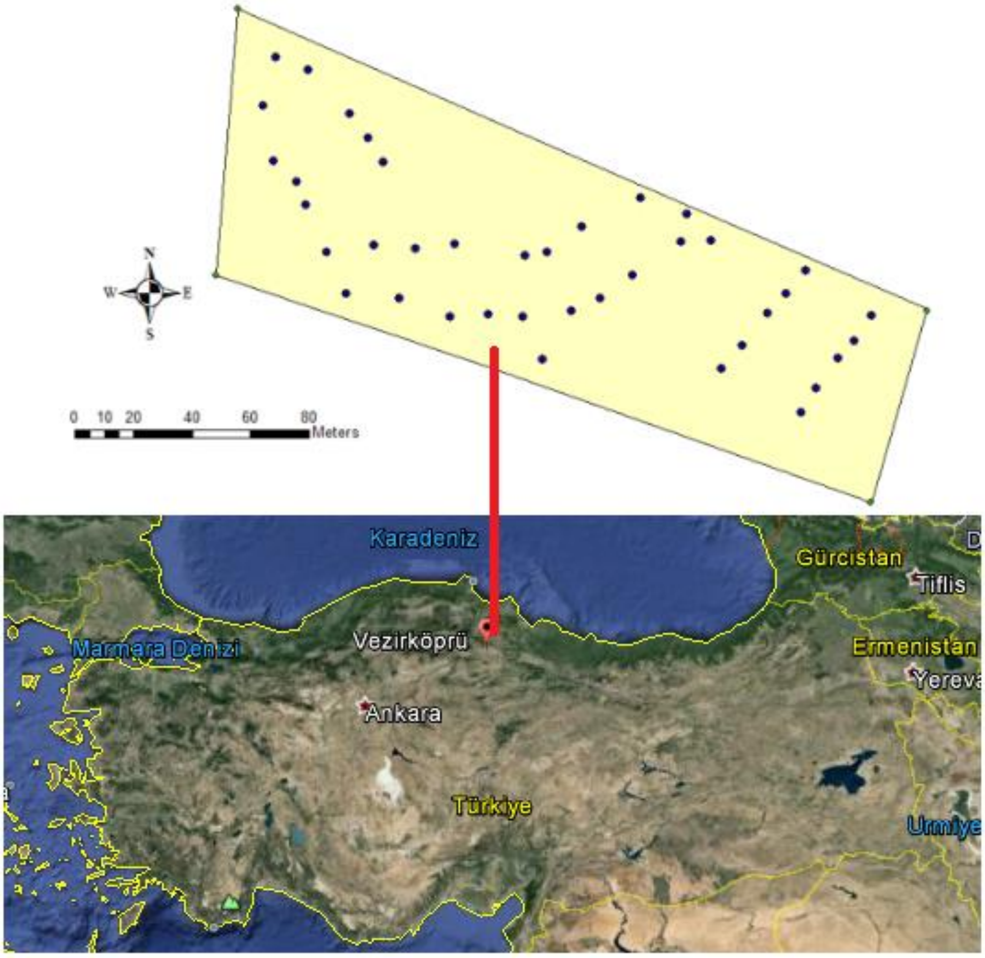

Fig. 1. – Study Area and Sample Points

Tab. 1. – Some of the long average annual climate parameters in Vezirköprü District

Meteorological Data	Months											
	Jan.	**Feb.**	**March**	**April**	**May**	**June**	**July**	**August**	**Sept.**	**Oct.**	**Nov.**	**Dec.**
Average Temp. (°C)	2.1	3.4	7.5	12.2	16	19.7	22.1	22.5	18.9	13.8	7.6	3.6
Highest Temp. Avr. (°C)	13.4	16.9	21	22.4	25.4	27	29.8	30.7	27.1	22.1	17.2	16
Lowest Temp. Avr. (°C)	-7.7	-8.8	-5.8	2.8	4.8	12.3	14.6	16	9.6	4.1	-0.8	-8.1
Relative Humidity Avr. (%)	75.5	70.5	64.1	63.5	63.8	61.7	56.6	55.5	57.7	65.1	74.1	76.3
Total Precipitation Avr. (mm)	36.5	31.7	37.3	56.7	72	65.8	30.5	22.1	23.2	52	46.2	46.2

Interpolation Methods

Today in Geographical Information Systems (GIS), the spatial interpolation methods are used to interpret the data collected from the points whose coordinates are known. There are two different interpolation methods in literature; these are stochastic and deterministic interpolation methods (ISAAKS AND SRIVASTAVA, 1989; ESRI, 2003). Stochastic methods process the data taking into consideration both mathematical and statistical functions to reveal the uncertainty and errors in forecasting. The stochastic methods also called as geo-statistical methods are basically known as Kriging. Kriging is an interpolation method that takes the spatial changes (variograms) into consideration. Kriging is used as an overall definition for the lowest generalized squared regression algorithms that form the basis of DenieKrige's studies (WEBSTER AND OLIVER, 2001). All Kriging predictors are derived from the following equation.

$$\hat{Z}(x_o) - \mu = \sum_{i=1}^{n} \lambda_i [Z(x_i) - \mu(x_o)] \tag{1}$$

μ given in the equation is a known constant average that is assumed as constant throughout the whole area and calculated as the average of the data (WACKERNAGEL, 2003). λ_i refers to Kriging weighting and it is dependent on the size of search window and the number of the samples determined to use in calculating n. $\mu(x_o)$ denotes the average of the samples in the search window. Kriging methods are subcategorized as Ordinary Kriging (OK), Block Kriging (BK), Disjunctive Kriging (DK), Universal Kriging (UK), Indicator Kriging (IK), and CoKriging (CoK). The traditional statistical methods are unable to provide information about the spatial relationship of the sampled points in a given area. CoKriging method is based on using detailed and incomplete secondary data and considering prominently the spatial cross-correlation between the primary and secondary variables (GOOVAERTS, 1999). It is used to estimate a variable by means of the other variable that are related to each other (eg: bulk density of the soil and soil moisture content). IDW, RBF and Kriging are the most commonly used interpolation methods (SUN ET AL., 2009). IDW is based on the distance from a point with an unknown value to the point with the known value by means of an unprejudiced weight matrix using the following equation

$$Z = \left[\sum_{i=1}^{n} \left(Z_i / d_i^m \right) / \sum_{i=1}^{n} \left(1 / d_i^m \right) \right] \tag{2}$$

where Z is the estimated value, Zi is the measured sample value at point i, di is the distance between Z and Zi, and m is the weighting power that defines the rate at which weights fall off with d_i, with a typical m value of 1–5 (KESHAVARZI AND SARMADIAN, 2012). RBF methods are radial-based methods and the features of the interpolated surfaces precisely pass through the data points and they have the lowest curves. The RBF method contains different functions for the forecasted surfaces. These functions are Completely Regularized Spline (CRS), Spline with Tension (ST), Thinplate Spline (TPS), Multiquadratik (M) and Inverse Multiquadratic (IM) (XIE ET AL., 2011).

The traditional statistical methods do not provide exactly accurate results since they make estimations based on the sampled points in a given area irrespective of the spatial dependence (MULLA AND MC BRATNEY, 2001). In the current study, four different interpolation methods have been used to determine the soil moisture distribution. The soil moisture data has been tested to see whether it has a normal distribution at different depths or not. In the current study, the spatial distribution of the soil moisture for 4 depths have been determined according to the most appropriate method using IDW and RBF of the deterministic methods and Ordinary (second order) Kriging and CoKriging of the geostatistic methods. In CoKriging method, the height has been used as the second variable to determine the effect of the second variable. The sequence followed in the study is shown in Fig. 2.

Evaluation of the Methods

The samples taken from a total of 40 points were measured using neutron gauge device. The soil moisture content values related to the depths of 0-30 cm, 30-60 cm, 60-90 cm and 90-120 cm have been used to evaluate the results of the most appropriate interpolation model. Different comparison techniques are used to determine the relationship between the measured and forecasted values. There are different comparison methods in literature to investigate the relationship between the measured and estimated values of soil moisture content and to choose the most appropriate model providing the results that are the closest to the measured values. Root mean square error (RMSE) and mean absolute error (MAE) are among the most widely used parameters. The model providing the lowest RMSE and MAE values has been chosen as the most appropriate model based on the equations 3 and 4.

$$RMSE = \sqrt{\frac{\sum_{i=1}^{m} (yi - Oi)^2}{n}} \tag{3}$$

$$MAE = \left| \frac{\sum_{i=1}^{n} \left(y_i - O_i \right)}{n} \right| \tag{4}$$

where n is the number of the tested data, Oi is the forecasted precipitation data and yi is the measured precipitation data.

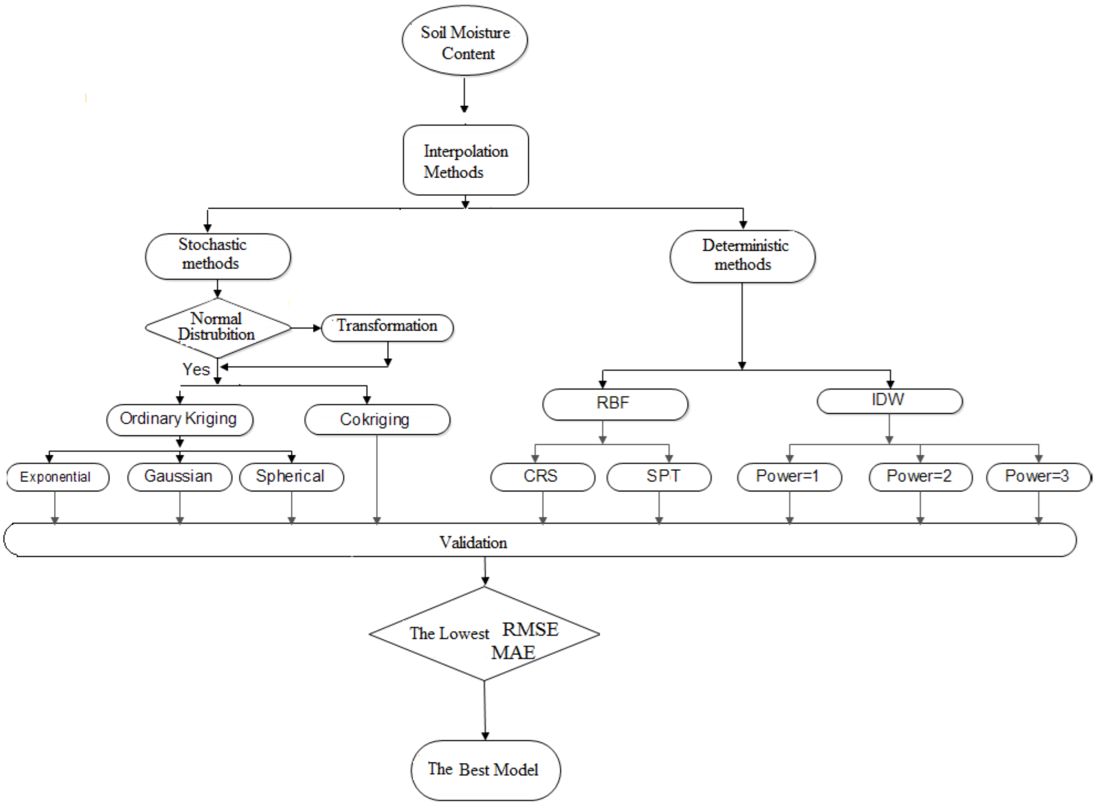

Fig. 2. – Flowchart of the interpolation methods used for the spatial distribution of soil moisture content

RESULTS AND DISCUSSION

In the current study, the soil moisture value has been determined at the depths of 0-30 cm, 30-60 cm, 60-90 cm and 90-120 cm. The soil depth maps have been drawn using deterministic and stochastic methods. The descriptive statistical values of the soil moisture content measured for each depth are shown in Fig. 2. The CV values of the soil moisture at the depths of 0-30 cm and 30-60 cm have been found lower than 15 (10.7 and 13.8) and they are categorized as "less variable". The soil moisture has a moderate variability (CV value between 15 and 35) at 60-90 cm and 90-120 cm depths. It has been found that the skewness values of the 4 depths do not have normal distribution; so, logarithmic distribution has been ensured performing transformation. Skewness value of the dataset is considered normal up to 0.5. When the skewness value is between 0.5 and 1, square root transformation is performed; however, when it is greater than 1, logarithmic transformation is performed. With these two transformation methods, the data can have a normal distribution (WEBSTER, 2001). Logarithmic transformation is performed to make data distribution closer to normal, to linearize the non-linear relationship and to decrease the heterogeneity and extreme/deviation values of the variances.

Comparison of the Interpolation Methods

In the current study, 8 different combinations of Ordinary Kriging (second-order), CoKriging, IDW, RBF interpolation methods have been used. Exponential, Gaussian and Spherical models have been tested in Ordinary Kriging method that is a stochastic method. As for the deterministic methods, three different weight powers have been tested for IDW and two different functions have been tested for RBF. 10 classifications have been used for soil moisture distribution. RMSE and MAE values have been evaluated for each method. The most accurate mapping method has been chosen between the deterministic and stochastic methods based on the lowest RMSE and MAE values. The lowest RMSE and MAE values were respectively obtained from Gaussian model (Ordinary Kriging), power 1 variogram (IDW), RBF method and power 1 variogram (IDW) for the depths of 0-30 cm, 30-60 cm, 60-90 cm and 90-120 cm. It has been determined that the most accurate mapping can be done based on these methods. The results of these methods are listed in Tab. 3. The spatial distribution maps of the soil moisture at different depths are shown in Fig. 3 based on the best methods.

Tab. 2. – Basic statistical results for all data

Depth	Highest	Lowest	Mean	Standard Dev.	CV	Kurtosis	Skewness
0-30	122.82	64.37	109.70	11.81	10.77	5.42	-2.05
30-60	123.01	52.18	104.61	14.48	13.84	5.36	-2.20
60-90	136.83	45.20	108.15	19.49	18.02	3.51	-1.69
90-120	141.81	28.82	113.11	21.07	18.63	5.67	-1.84

Tab. 3. – Results of the soil moisture at four depths based on different interpolation methods

	OK-G		IDW-1		RBF-ST		CoK-Spherical	
	RMSE	MAE	RMSE	MAE	RMSE	MAE	RMSE	MAE
0-30	11.296	7.821	11.506	7.923	11.938	8.055	11.35	7.919
30-60	13.813	8.709	13.682	8.444	13.98	8.742	13.823	8.631
60-90	21.695	13.97	17.846	11.653	17.767	11.473	18.557	12.728
90-120	21.06	14.6	20.24	14.18	20.46	13.92	21.223	14.468

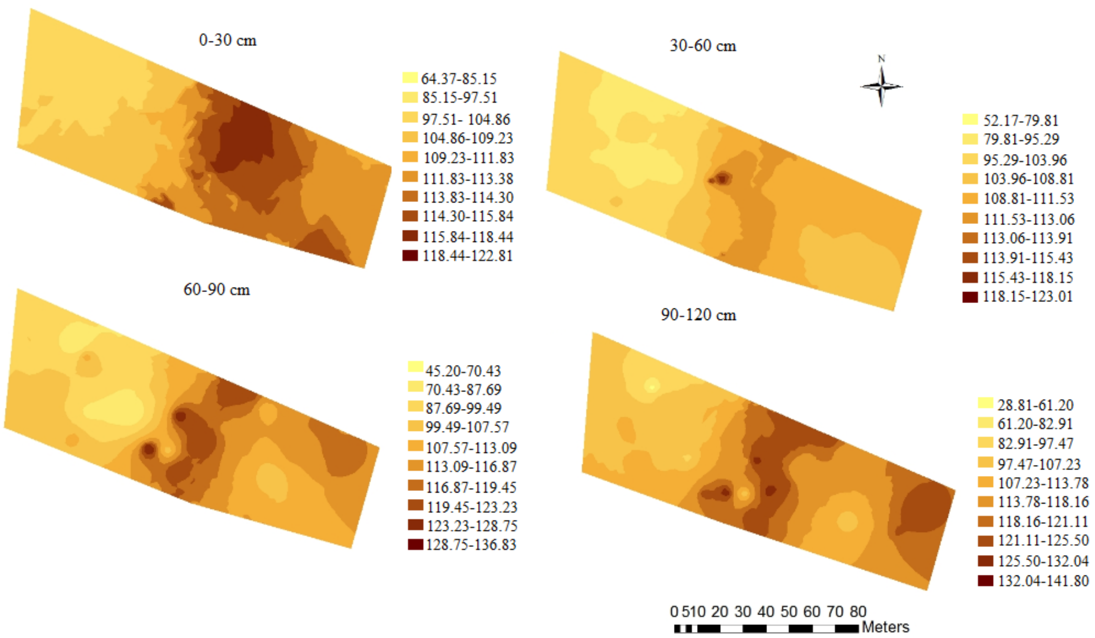

Fig. 3. – Spatial distribution maps of the soil moisture content at different depths

CONCLUSIONS

When compared, the lowest RMSE and MAE values have been respectively obtained from Gaussian model (Ordinary Kriging), power 1 variogram (IDW), RBF method and power 1 variogram (IDW) for the depths of 0-30 cm, 30-60 cm, 60-90 cm and 90-120 cm. The most accurate mapping has been done based on these methods. Cross-validation method has been performed to determine the best method. It has been seen that other methods provided similar results. In the current study, different results have been reached for each depth. Therefore, in the studies on soil properties and climate data, determining the most appropriate interpolation method and screening the distribution according to this method are considered to provide more accurate results in order to determine the spatial distribution properties of the soil moisture content from which the point data are obtained. Planning the agricultural production and hence the irrigation time is very difficult in the areas where the soil moisture content are not determined by depth. Therefore, it is important to produce and use the spatial distribution maps properly by means of these techniques. Especially, different interpolation methods are used to estimate the spatial distribution of the soil moisture content in the complex terrains in the catchment areas. XUELING ET AL. (2013) examined the appropriateness of different interpolation methods (Ordinary Kriging, IDW, linear regression, regression Kriging) in forecasting the soil moisture throughout the soil profile (1 m) based on 153 samples taken from the Loess Plateau of China. As a result, they found that there are significant differences between each method in terms of homogenous lands. It has been found that Environmental impact factors have discontinuous spatial dependence in Ordinary Kriging and IDW models and the soil moisture in the homogeneous terrains of the small basins has poor spatial predictive value. The spatial distribution of soil moisture cannot be sufficiently characterized by means of the direct measurements in the practical implementations; therefore, it is necessary to create new observation points and determine the best interpolation method for them. Most of the hydrological practices can affect the soil moisture and existence of different variations for soil moisture samples can lead to complicated results (PERRY AND NIEMANN, 2008). Before determining the soil parameters from which the point data are obtained and mapping the spatial distribution of the values related to soil properties, it is considered to have better results by firstly determining the most appropriate interpolation method and then interpreting the results based on the spatial distributions using this method. With this study, the spatial distributions of the soil moisture content have been determined at different soil depths and it has been found that the changes in soil moisture content can be spatially determined. As a result, this study is expected to be a guide for the further studies.

REFERENCES

1. ARSLAN, H., CEMEK, B., GÜLER, M., YILDIRIM, D.: Değişebilir Sodyum Yüzdesinin (ESP) Konumsal Dağılımının Farklı Enterpolasyon Yöntemleriile Değerlendirilmesi. II. Ulusal Sulamave Tarımsal Yapılar Sempozyumu. 24-25. Mayıs, 505-512., 2012: İzmir.
2. BROWN, R.B., HUDDLESTON, J.H.: Presentation of Statistics Data on Map Units to The User. In Spatial Variabilities of Soil And Landform. SSSA Special Pub.No:28, 1991: pp 127-147.
3. DING, Y., WANG, Y., MIAO, Q.: Research on the spatial interpolation methods of soil moisture based on GIS, International Conferences on Information Science and Technology, Jiansu, China, 2011: March 26-28.
4. ESRI: Using Arcview GIS. Environmental System Research Institute.Inc.:Redlans, Calif., 2003.
5. GOOVAERTS, P.: Using elevation to aid the geostatistical mapping of rainfall erosivity. Catena, 34, 1999: 227-242.
6. ISAAKS, E.H., SRIVASTAVA, R.M.: An Introduction toApplied Geostatistics. Oxford Uni. Press, Inc. New York, 1989, 561 pp.
7. KESHAVARZI, A., SARMADIANI, A.: Mapping of spatial distribution of soil salinity and alkalinity in a semi-aridregion. Annals of Warsaw University of Life Sciences Land Reclamation, 44(1), 2012: 3–14.
8. MULLA, D.J., MCBRATNEY, A.B.: Soil Spatial Variability, Handbook of soil science, CRS Pres., 2001.
9. NORDT, L.C., JACOB, J.S., WILDING, L.P.: Quantifying Map Unit Composition for Quality Control in Soil Survery.p., 1991, 183-197 In: Spatial Variabilities of Soil and Landforms. Editors: Mausbach, M.J. And Wilding, L.P. Soil Sci. Soc. of America, Inc, Madison Wisconsin, USA.
10. PERRY, M.A., NIEMANN, J.D.: Generation of soil moisture patterns at the catchment scale by EOF interpolation. Hydrol. Earth Syst. Sci., 12, 2008: 39-53.
11. ROGOWSKI, A. S., WOLF, K.J.: Incoporation Variability into Soil Map Unit Delineation. Soil Sci. Soc. Am. J., 58, 1994:163-174.
12. SUN, Y., KANG, S., LI, F: Comparison of interpolation methods for depth to ground water and its temporal and spatial variations in the Minqinoas is of North West China. Environmental Modelling& Software, 24, 2009: 1163–1170. Tsanis,
13. YOUNG, F.J., HAMMER, R.D., WILLIAMS, F.: Evaluating Central Tendency and Variance of Soil Properties within Map Units. Soil Sci. Soc. Am.J., 62, 1998: 1640-1646.
14. WARRICK, A.W., MYERS, D.E., NIELSEN, D.R.: Geostatistical Methods Applied to Soil Science, In: Methods of Soil Analysis, Part I. Physical and Mineralojical Methods, ASA and SSSA Agronomy Monografh no:9(2nded)., 1986: pp. 53-82, Madison.
15. WACKERNAGEL, H.,: Multivariate Geostatistics: An Introduction with Applications. Springer, Berlin, 2003: 387 pp.
16. WEBSTER, R., OLIVER, M.: Geostatistics for environmental Science. John Wiley and Sons, Ltd, Ch,chester, 2001: 271 pp.
17. WEBSTER, R.: Statistics To Support Soil Research And Their Presentation. European journal of Soil Science, 52, June 2001: 331-340.
18. XIE,Y., CHEN, T., LEI, M., YANG, J.: Spatial distribution of soil heavy metal pollution estimated by different interpolation methods: accuracy and uncertainty analysis. Chemosphere, 82, 2011: 468–476.
19. ZHANG, R., RAHMAN, S., VANCE, G.F., MUNN, L.C.: Geostatistical Analysis of Trace Elements In Soil and Plants, Soil Science, 159(6), 1995: pp. 383-390.

Corresponding author:

Demet Yıldırım, Black Sea Agricultural Research Institute, Irrigation and Land Reclamation Unit, Samsun, Turkey

INNOVATIVE CONSTRUCTIONS OF CUTTING AND GRINDING ASSEMBLIES OF AGRICULTURAL MACHINERY

M. Zastempowski, A. Bochat

Institute of Machine Operation and Transport, Faculty of Mechanical Engineering, UTP University of Science and Technology in Bydgoszcz, Poland

Abstract

This article presents construction of the shear and drum cutting assemblies, as well as the beater shredders which have been commonly used in agrarian machines designed for acquiring or processing material for consumption, fodder and power purposes. Due to the fact of high demand for these working assemblies' power, their new constructional solution has been suggested. Results of experimental studies (bench testing) driving, among the others, to determination of the demand for power at the time of plant materials' cutting and shredding, have also been discussed.

Key words: materials' cutting, materials' shredding, working assemblies of farm machines, drum cutting assembly, shear cutting assembly, beater shredder.

INTRODUCTION

Cutting and shredding assemblies are very important working assemblies of farm machines designed for harvesting and processing of plant material for consumption, fodder or power purposes. According to DULCET AT AL. (2006), the harvested plant material may be further effectively processed and stored. The following machines are equipped with cutting and shredding assemblies: mowing machines, chaff cutters, combine harvesters and all types of shredders. The specific character of their construction and the principles of their operation result, among the others, from the fact that the cutting or shredding process realized by them, concerns plant materials the structure of which is non-homogeneous, and their physio-mechanical properties have not been thoroughly identified.

One of the very important ways of lowering the costs of food, fodder or biomass production is, among the others, reduction of outlays needed for obtaining material for its production. It may be achieved by designing machines, which shall be characterized by low working processes' energy consumption. In case of machines for harvesting and shredding materials like cereals or green fodders, it concerns among the others, the cutting and shredding processes realized by them.

At the Faculty of Mechanical Engineering of the University of Science and Technology in Bydgoszcz, there are being conducted continuous activities aiming at developing of new constructional solutions of the machines' working assemblies. At present, new constructions of working assemblies of agricultural machines, with particular consideration of cutting and shredding assemblies, are being designed, the effect of which are the new shear-finger, drum cutting assembly's constructions and the beater shredder.

MATERIALS AND METHODS

The shear-finger cutting assembly is the basic cutting unit occurring in many agricultural machines, in which cutting elements with crosscut edges participate directly in the process of stalks' or stems' cutting process.

The essence of the traditional construction of the shear-finger cutting assembly consists in the fact that the assembly consists in a movable cutter bar and an immovable finger bar. Fingers tapering towards the front facilitating material's partitioning into portions are fastened to the finger bar. Then, material is cut with the use of scissors fastened to the cutter bar performing the back and forth motion. The side fingers' edges or finger liners fastened to them act as the crosscut edge. Correct contact of the knives to finger liners is guaranteed by buttons screwed down to the finger bar. The exemplary diagram of the shear-finger cutting assembly is presented in Fig. 1. and in Fig. 2 its selected construction in a view is shown.

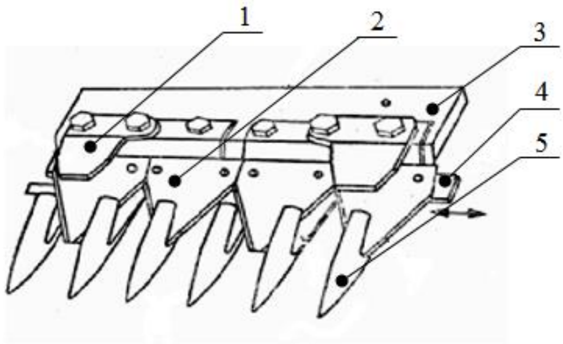

Fig. 1. – Diagram of the shear-finger cutting assembly (KANAFOJSKI, KARWOWSKI, 1980):
1- cutter bar's button, 2 - knife, 3 - finger bar, 4 - cutter bar, 5 – finger

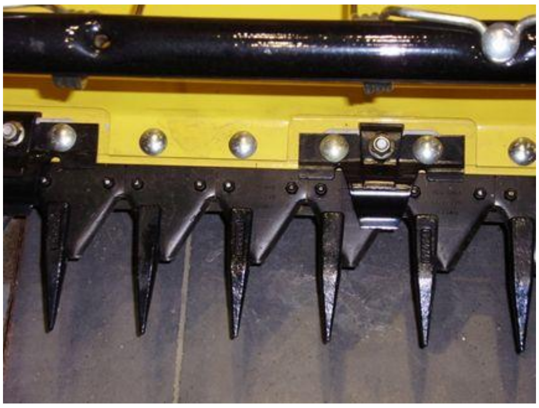

Fig. 2. – Shear-finger cutting assembly of New Holland (own study)

In spite of extensive spreading of agrarian machines equipped with shear-finger cutting assemblies, their construction has not changed considerably for a longer period of time, and in a commonly available, up-dated literature, one may find their single and only conceptual new construction's solutions presented by GUARNIERI AT AL. (2007). Relatively, high energy's consumption is the disadvantage and inconvenience of the existing and commonly used shear-finger cutting assemblies.

Experimental studies conducted by the authors show, that the resistance to dead movement of the cutting assembly has a significant share in the cutting process's power consumption, and the increase of demand for the power in working motion at the time of plant material's cutting amounts only to approx. 10%, what was described by ZASTEMPOWSKI (2010). That drove the authors to construct and to patent the new shear-finger cutting assembly's construction.

The essence of the shear-finger cutting assembly's new construction (Fig. 3) is characterized by the fact, that in place of standard slide buttons, there have been used innovative buttons (of new construction) having an opening in which a roller fastened on a pivot has been inserted. Additionally, a cutter bar of a decreased crosswise section has been used, and the fingers' surfaces that the cutter bar mate with, were subject to the process of electroplating. These processes are to make it possible to lower the demand for power necessary to overcome the friction forces in the cutting assembly's dead movement.

Changes of that type have an important impact on the decrease of the friction forces and inertial forces, what directly translates into the decrease of demand for the shear-finger cutting assembly's power.

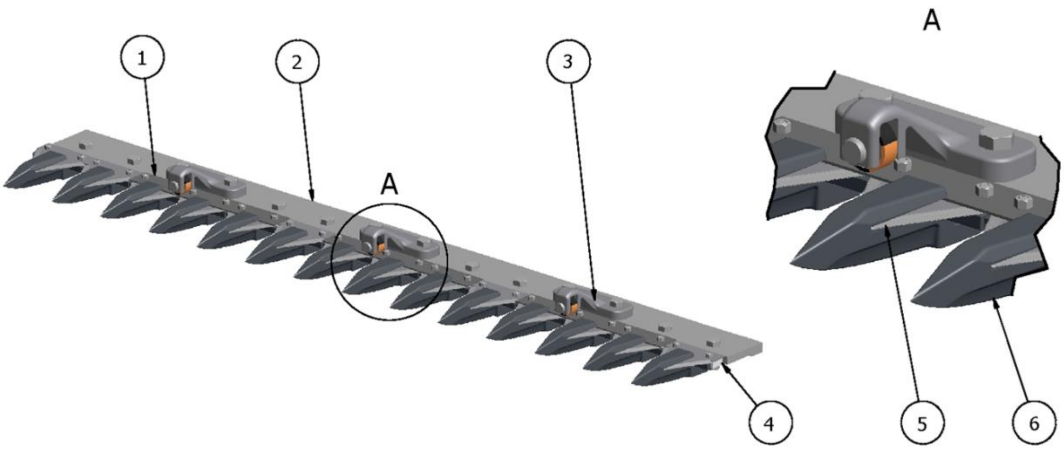

Fig. 3. – New construction of the shear-finger cutting assembly (own study): 1 - tool insert, 2 - finger bar, 3 - button, 4 - cutter bar, 5 - knife, 6 - finger

Calculations of the value of forces acting in the working system and the demand for power on the basis of the calculation tool developed on the basis of own calculation models as well as models presented in literature have been conducted. Calculations were conducted for a traditional construction of a shear-finger cutting assembly for which the demand for power amounts to 15.81 kW and for a new construction of a cutting assembly for which the demand for power amounts to 11.76 kW. ZASTEMPOWSKI AND BOCHAT (2012) wrote on that. The calculations unequivocally prove, that the offered new construction of the shear-finger cutting assembly, due to lower power demand, is characterized by higher functioning effectiveness.

The drum cutting assembly constitutes a basic operating assembly of self-propelled straw cutters, attached or stationary. The task of a drum cutting assembly is cutting of plant material (stalks or stems) into parts (chaff) of determined length.

Application of an assembly of that type in straw cutters makes it possible to obtain the required level of material's shredding. The exemplary construction of the drum cutting assembly is presented in Fig. 4.

Cutting drums may have an open or closed construction. A drum of open construction consists of a shaft on which discs with openings are embedded. Cutter holders are fastened to these discs. Cutting knives are fastened in tool posts. The knives, depending on a drum's construction, may be straight or bended along the screw line, and moreover we can distinguish solid and sectional knives. The cutting drum is positioned in the side plates of the chaff cutter.

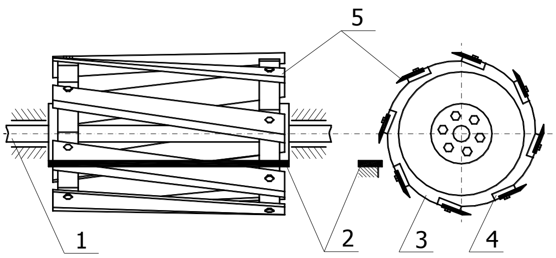

Fig. 4. – Cutting drum of the chaff cutter (BOCHAT, 2010):
1- cutting drum's shaft, 2 - crosscut Edge called shear bar, 3 - cutting drum's disc, 4 - cutter holder, 5 - cutting knife

However, in a cutting drum of a closed construction, on the shaft instead of several discs there is fastened construction in the form of a closed roller on side surface of which there are arranged brackets with cutting discs fastened to them.

In Fig. 5 there is presented the cutting drum of New Holland.

Fig. 5. – Cutting drum of the chaff cutter of New Holland (NEW HOLLAND)

The rules of the drum cutting assembly's operation consist in the fact, that the rotary movement of a cutting drum results in dislocating of cutting knives with them. Knives moving in respect of the immovable shear bar cause, in the first phase – squeeze – pressing of the plant material's layer, and its cutting through in the second stage.

Supplying material between the knife's blade and the counter cutter takes place through the rotational motion of feeding-squeezing rollers, which preliminarily form and thicken the material.

In spite of big popularization of agrarian chaff cutters equipped with drum cutting assemblies, constructions of their cutting assembiles have not been changed lately. From the balance of power (Sankey'a) consumed by a chaff cutter with a drum cutting assembly it results, that the power collected by the cutting assembly clearly predominates over the powers consumed by the remaining working assemblies and amounts to 75-80% , already presented by BOCHAT AND KORPAL (2013). Looking for more energy effective constructional solutions of the drum cutting assembly cutting plant material into chaff, a new design of the cutting assembly has been developed, patented and constructed at the Faculty of Mechanical Engineering WIM UTP.

The essence of the new cutting drum's construction lies in the fact, that it consists of a drive shaft and three discs where the central one has a bigger diameter as compared to the side ones. Knives of blades straight or bended along the screw line in the V arrangement are screwed directly to the discs (Fig. 6). Such construction of a drum makes it possible to cut the material in a diagonally slant manner, the effect of which there should be a considerable lowering of energy consumption of the cutting assembly's operation.

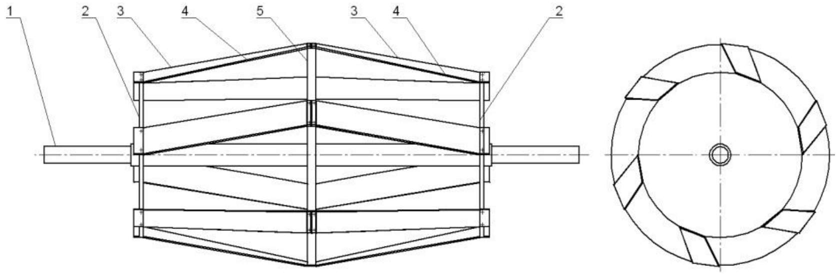

Fig. 6. – New construction of the cutting drum (own study): 1 - shaft, 2 - external discs, 3 - knives, 4 - knives' cutting edges, 5 - central disc

Shredding of cereals' grains is one of the main technological operations performed in the farm-food industry and on farms. Out from may types of shredders, that is: plate grain mills, roller mills, crushing mills and beater shredders, from the point of shredding effectiveness the beater shredders have found the widest application , described by BOCHAT AND WESOŁOWSKI (2009, 2010), DMITREWSKI (1992), KAPUR AT AL.(1990), OBIDZIŃSKI AND HEJFT (2000), OPIELAK (2000), FLIZIKOWSKI AT AL. (2015) AND TOMPOROWSKI AND FLIZIKOWSKI (2013).

However, the present design solutions of the beater shredders are characterised by big shredding energy consumption, as a result of what it is necessary to use power transmission systems of big horsepowers for their power transmission, what has already been described by DMITREWSKI, (1992) and MAGDALINOVIĆ (1989).

The basic elements of a typical beater shredded are a rotor with stiffly fixed beaters, a sieve or a shredder's sieves, a shredding plate or plates and a supporting structure with power transmission system. Low efficiency as compared to energy consumption is a defect and inconvenience of known, traditional design solutions of beater shredders, what has been earlier presented by BOCHAT AND WESOŁOWSKI (2009), KAPUR AT AL. (1990). Most of all it is determined by a rotor's construction, where beaters have the shape of rectangular plates. As the effect of it, under the influence of beaters' strokes, particles of material start moving along the lines similar to a circle. They form a thin layer rotating along an internal perimeter of a shredding chamber what causes that, in spite of sometimes insufficient shredding degree, material has been circulating quite a long time before it goes through the openings in sieves. In Fig. 7a there is presented the traditional rotor of a beater shredder in isometric view.

The essence of a new design lies in the fact, that the working assembly of the shredder consists of the disc rotor embedded on a shaft to which self-aligning beaters are fastened. The beaters have the shape of plates in the form of a circular sector of the obtuse angle of at least 35°, while the beater's fixing hole lies on the circular sector's axis of symmetry close to its arch basis. Such a construction of a beater shredder's rotor causes, that the particles of the shredded material hit by beaters do not move along circular path and do not create a rotating ring, but they move more or less radially with reference to sieves and hit them immediately. It results quicker going of material through the openings in sieves. In Fig. 7b there is presented a new construction of a beater shredder's rotor in isometric view. The presented new design solution of the beater shredder is the subject matter of patent of the RP no 173497 (BOCHAT A.).

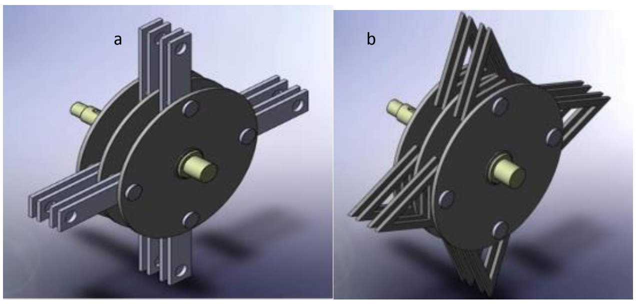

Fig. 7. – The isometric view of the beater shredder's rotor (own study): a - traditional design solution of the rotor (α=0°), b - new design solution of the rotor with beaters in the shape of a circular sector (α=45°)

RESULTS AND DISCUSSION

At the Faculty of Mechanical Engineering of UTP in Bydgoszcz there are also conducted experimental tests concerning the process of cutting with shear-finger cutting assembly. One of the tests' purpose was to determine the total cutting operation $\boldsymbol{L_c}$ performed by the cutter bar.

Determination of dependency was attempted:

$$L_c = f(v_{n\,śr}, v_m). \quad (1)$$

Rye straw (winter rye: Dańkowskie Złote) was the material used for the tests. That material was chosen due to its farming commonness at the territory of Poland.

In order to perform the tests concerning the cutting process with the use of a shear-finger cutting assembly, the authors have designed and constructed a test bed composed of the following elements: a mowing machine ZO34 equipped with a shear-finger cutting assembly fastened on an adjustable frame bearer, feeder of material to be cut, equipped with a pneumatic drive system, power system for power transmission and the cutting assembly's speed control, equipment for the measurement of the turning moment and the rotational speed, equipment for the measurement of the fed material's speed. While designing of the test bed, care was taken of the possibility to change the angle of inclination of the cutting assembly with reference to the cut plants. The general view of the test bed is presented in Fig. 8. The structure of the test bed for examining of the power outlays, reflects the process of plant material cutting conducted in real field conditions, and the additional options of parameters' adjustment and positioning allow for comprehensive tests for different plant materials.

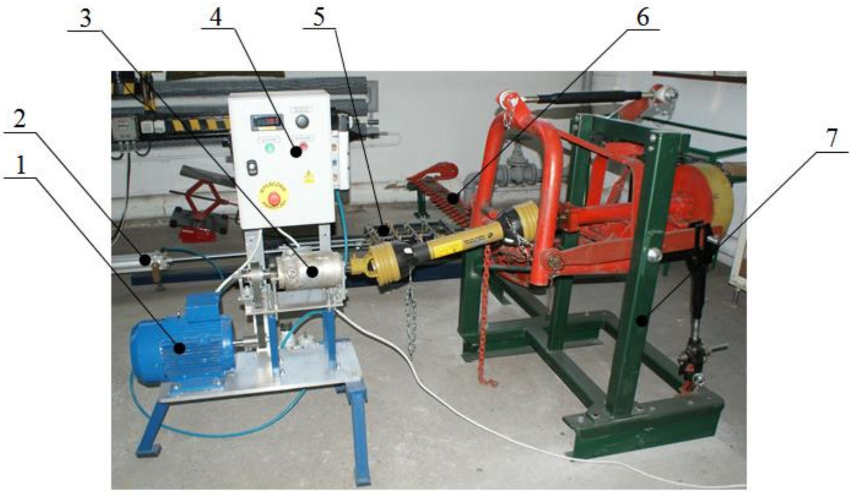

Fig. 8. – Station for examinations of the cutting process with the shear-finger cutting assembly [own study]: 1 - electric motor, 2 - compressed-air engine, 3 - torque measuring shaft, 4 - control and adjustment system, 5 - feeder of material to be cut, 6-mowing machine's cutter bar, 7 - frame bearer with TUZ

In the test bed presented in Fig. 8, the power transmission of the cutter bar's mowing machine is from the electric motor via the power take-off's shaft and the mowing machine's belt transmission. The electric system makes stepless cutter bar's speed adjustment possible. However, the truck's power transmission with material to be cut is realized via the air-operated servo-motor with a system providing constant feeding speed with an opportunity of its smooth change.

As a result of the conducted stand surveys, the total cutting operation of the stalks series L_c (for a single stroke of the cutter bar) depending on the cutter bar's speed $v_{n\,śr}$ and the speed of feeding material to be cut v_m have been determined.

The exemplary results from the conducted surveys are presented in Fig. 9.

From the conducted experimental surveys it results, that the speed of the cutter bar of the cutting assembly and the feeding speed of material to be cut have an important impact on energy consumption of the cutting process of stalk plants performed with the shear-finger cutting assembly.

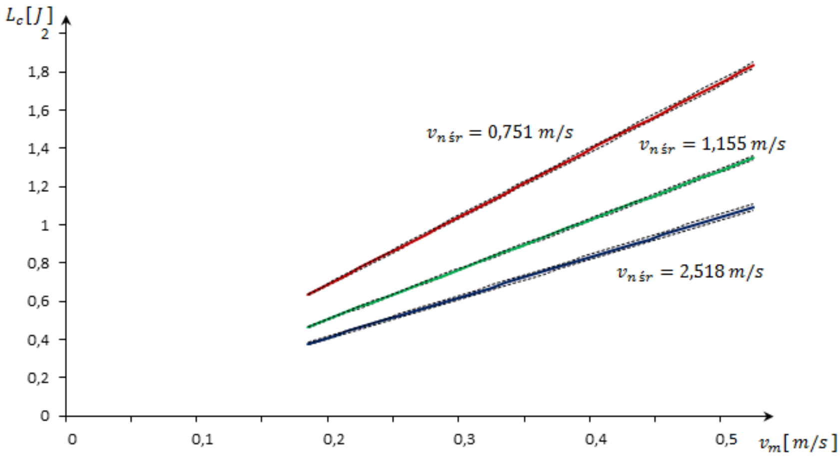

Fig. 9. – Confidence intervals for regression function [own study]

The maximum value of cutting operation $L_c = 1.784$ J was received for the cutter bar's speed $v_{n\,śr} = 0.751$ m/s and the speed of feeding material to be cut $v_m = 0.50$ m/s. However, the lowest value of cutting operation $L_c = 0.330$ J was received for the cutter bar's speed $v_{n\,śr} = 2.58$ m/s and the speed of feeding material to be cut $v_m = 0.18$ m/s. The cutting operation of the single stalk for the accepted speed configurations $v_{n\,śr}$ and v_m amounted respectively to: $L_{cj} = 0.1829$ J and $L_{cj} = 0.3532$ J. Authors of the article have also drawn up the mathematical model of the cutting process, presented by ZASTEMPOWSKI AND BOCHAT (2014).

At the Faculty of Mechanical Engineering of the University of Science and Technology in Bydgoszcz there are also conducted experimental surveys concerning the process of cutting with the drum cutting assembly. During these surveys, there was determined the impact of the selected design features and parameters of a drum cutting assembly on its performance characteristics and the assessment of the possibilities of application of an alternative construction of the drum cutting assembly conducting skew cutting.

Rye straw (winter rye: Dańkowskie Złote) and rape's stalks were used as the material to be cut in the surveys. Material designed for the surveys was selected due to its cultivation's universality at the territory of Poland and its designation for fodder's purposes and, subsequently rape's straw as the energetic material in briquettes' production.

For the purposes of conducting of the surveys concerning the process of cutting with the use of the drum cutting assembly, a second test stand was constructed, which makes it possible to conduct crosswise as well as diagonally slant cutting.

That stand consists of a drum cutting assembly and the measurement devices consisting of: torque measuring shaft with a measuring instrument and a PC control unit of a notebook's type. A test stand is characterised by the fact that it is possible to test cutting assemblies which cut perpendicularly with reference to the feed of the layer cut, and cutting at angle with reference to the direction of the layer's movement. Moreover, it is possible to receive different pressing degrees of the plant material layers which is to be cut.

With the help of the mentioned test stand, it is possible to determine:

- the unit cutting resistance $\boldsymbol{p_c}$,
- the unit cutting operation referred to the area of the cutting surface $\boldsymbol{L_{jS}}$,
- the unit cutting operation referred to the mass of the cut material $\boldsymbol{L_{jm}}$,
- efficiency of the cutting assembly ***W.***

The general view of the test stand is presented in Fig. 10. At the test stand, the drive of the cutting drum's assembly and the assembly of feeding-squeezing rollers is from two independent electric motors via a belt transmission with a cogbelt. In both the cases, there is an option of an independent, stepless adjustment of rotational speed.

The test bed has been equipped with a torque measuring shaft of the measurement range up to 200 Nm, which makes it possible to measure the turning moment on the shaft propelling the cutting drum. It makes it possible to measure energy consumption of the performed process of plant material's cutting into chaff. While designing of the bed, attention was also paid to make it possible to change the positioning of knives' inclination for both the constructional solutions of the cutting drum.

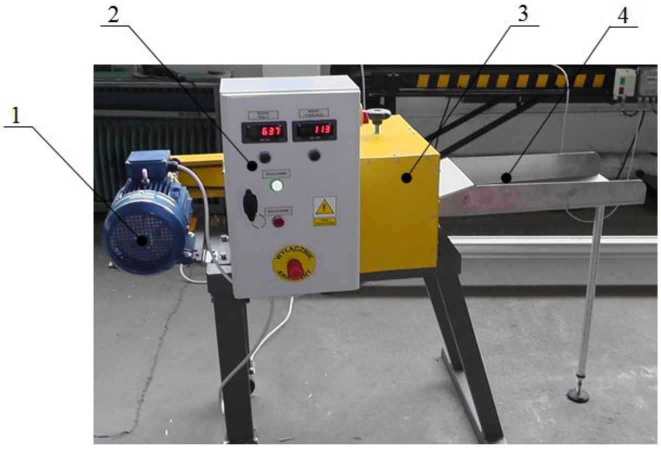

Fig. 10. – Test bed for surveys of the process of cutting with the drum cutting assembly – front view (own study): 1- electric motor with belt transmission, 2 - feed-control system, 3 - feeding-squeezing rollers, 4 - charging gutter

The structure of the test bed for energy inputs' studying reflects the process of plant material's cutting into chaff performed in real field conditions, and additional parameters' adjustment and setpoint options make it possible to conduct comprehensive surveys for different types of plant materials.

The selected results of preliminary studies are presented in Fig. 11 where graphically the influence of the material's feeding angle θ on the unit value of cutting resistance p_c for a determined cutting speed v_c. and the material's compacting degree h/h_o, what has been described by BŁASZCZYK (2009).

The conducted experimental studies show unequivocally, that the considerable impact on capacity, energy-consumption of the cutting process with the drum cutting assembly and non-uniformity of the length of the obtained chaff there have: the type of the cutting drum's construction, cutting speed and the cutting material's compacting degree.

It results from the conducted experimental studies, that: application of the cutting drum of new generation as compared to a traditional solution for straw cutting, shall contribute to the increase of the process's efficiency from 5 to 8 %, and in case of new construction of the cutting drum the impact of the degree of material's pressing shall not cause any substantial changes in the cutting process's efficiency. Application of the new construction's cutting drum as compared to the traditional solution, shall contribute to a considerable decrease of the unit energy's consumption (for 25%), together with the increase of the cut material's pressing degree the unit energy's consumption for the material's cutting increases more or less linearly.

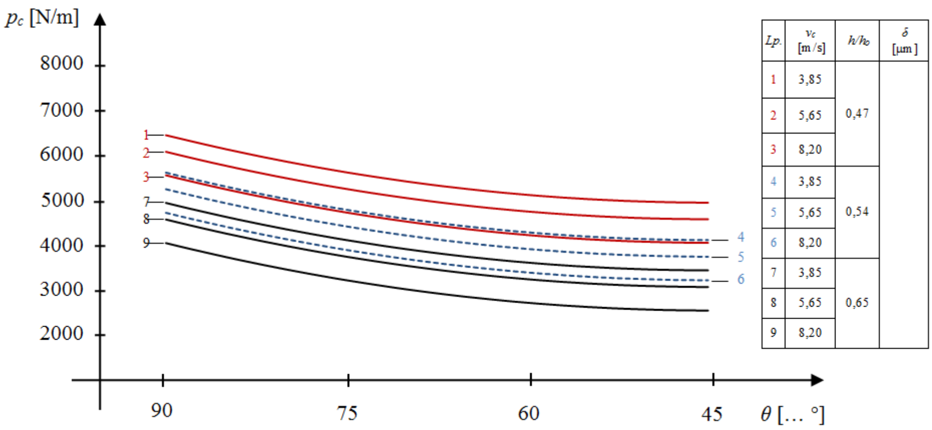

Fig. 11. – Influence of the material's feeding angle θ on the unit value of rye straw's cutting resistance p_c for the cutting speed value v_c, degree of compacting h/h_o and thickness of the blade δ included in the table attached to the diagram (BŁASZCZYK, 2009).

It concerns both constructions of cutting drums, for both the constructions of cutting drums together with the increase of the cutting tangential velocity the degree of chaff length's non-uniformity decreases more or less linearly.

At the Faculty of Mechanical Engineering of UTP in Bydgoszcz there are also conducted experimental surveys concerning the process of material shredding aiming at determination of the shredding process's effectiveness.

For the purposes of the surveys realization, a test stand the view of which is presented in Fig. 12, has been designed and constructed.

A test stand consists of a modified beater shredder type WIR RB-1.3, equipped for the tests with a traditional working assembly of new prototype rotor's designs together with the control-measuring apparatus in the form of the system of electric motor's steering providing fluent rotor's rotations and torque measuring shaft's adjustment for loading's measurement on the rotor's shaft.

Within the frames of the experiment, the triticale's grain was shredded (winter triticale Krakowiak). This material was selected for the surveys because of its cultivation universality and its designation for fodder purposes.

In order to determine shredding effectiveness, the following factors have been assumed to determine:

- shredder's capacity ***W***,
- unit power consumption $\boldsymbol{E_j}$,
- share of individual fractions in shredded material ***X***.

Selected results of tests presented in Fig. 13.

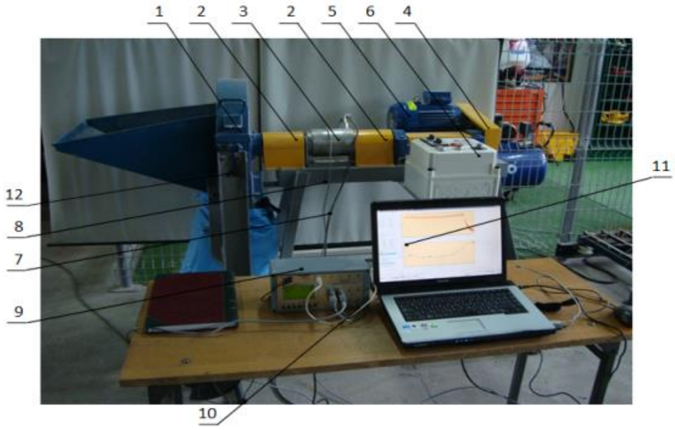

Fig. 12. – View of the test stand (own study): 1 - a modified beater shredder type WIR RB-1.3, 2 - elastic jaw clutch Poly-Norm, 3 - torque measuring shaft with revolution counter type MIR 20, 4 - belt transmission, 5 - electric motor 7 kW, 380 V, 6 - control box with frequency converter Lenze SMD, 7 - transmission conductor of turning moment, 8 - transmission conductor of rotational speed, 9 - two-channel measuring device MW2006-4, 10 - transmission conductor type USB, 11 - computer system with data registration software PP203 and the author's calculation program RB01, 12 - supporting construction.

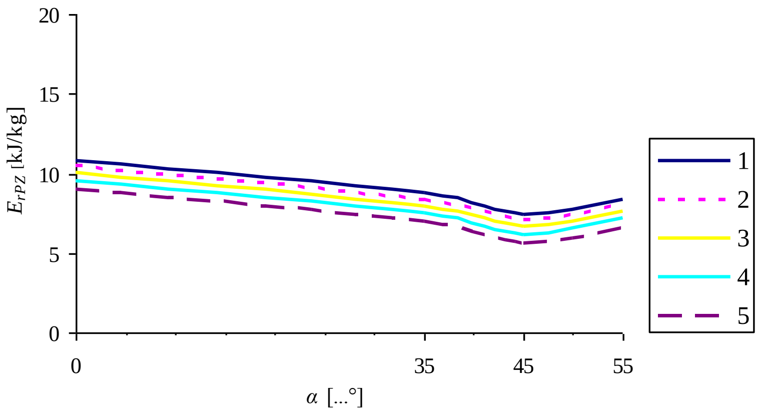

Fig. 13. – Impact of the beaters' angle on the unit power consumption during triticale's shredding for the peripheral speed value of beaters' ends v, beater's gap s = 15 mm and the diameter of openings in sieves d = 5 mm (ZASTEMPOWSKI AT AL., 2015)

It results from the conducted experimental studies, that the following ones have substantial impact on the shredder's output and the unit power consumption as well as the contents of fraction in shredded grains of triticale cereals: the constructional form of a beater assembly, beaters' angle, peripheral speed of beaters' endings, diameter of openings in sieves, beater's gap.

Application in the beater shredder's of a new construction of the rotor equipped with beaters in the shape of a circular sector, resulted in the increase of the shredder's capacity from 11 to 32% and the decrease of the unit power's consumption for shredding from 14 to 46% as compared to traditional constructional rotor's solutions.

Application of a new construction of the beater shredder's rotor, equipped with beaters in the shape of a circular sector, results in the decrease of the dust fraction in shredded cereal, as compared to the traditional design solution.

Application of beaters of the angle α=45° influences:

– the decrease of the dust fraction content from 7.26 to 7.75%,
– the decrease of the fine fraction content from 8.58 to 9.23%,
– the increase of the coarse fraction content from 16.33 to 16.49%;

The conducted analysis of shredding effectiveness has proved, that in case of triticale, application of beaters of the shape of circular sector α=45° , beater gap of the value of $s = 10$ mm and sieves of the openings' diameter $d = 5$ mm is the most effective design solution of the beater assembly.

CONCLUSIONS

New design modification developed at the Faculty of Mechanical Engineering of the University of Science and Technology in Bydgoszcz of the working assemblies of machines and equipment commonly used in agriculture, in food industry and while acquiring materials for power purposes at the time of biomass production are presented in this article.

The exemplary results of tests performed at author's test beds have been discussed. All the new designs of working assemblies presented in the article, influence reduction of power's demand during the process of plant material's cutting or shredding. Application of the above discussed constructions may contribute to lowering of the costs of production of food, fodders or power materials' of biomass type.

REFERENCES

1. BŁASZCZYK, M.: The impact of the design features of the cutting drum for the characteristics of the utility cut plant materials. (Polish language). Dissertation. Faculty of Mechanical Engineering UTP in Bydgoszcz, 2009.
2. BOCHAT, A.: Theory and design of cutting units of agricultural machinery. (Polish language). Publishing House UTP in Bydgoszcz, 2010.
3. BOCHAT, A., KORPAL, K.: Research issues of cutting layers of anisotropic material. (Polish language). Inż. Ap. Chem. 52, No. 2, 2013: 51-53.
4. BOCHAT, A., WESOŁOWSKI, L.: Analysis of design solutions of grinders beater in terms of the efficiency of their operation. (Polish language). Inż. Ap. Chem. 2010, 49, No. 5: 22-23.
5. BOCHAT, A., WESOŁOWSKI, L.: The new design team working of hammer mill. (Polish language). Inż. Ap. Chem. 48, No. 2, 2009: 25-26.
6. DMITREWSKI, J.: Theory and design of agricultural machinery. (Polish language). PWRiL, Warszawa, 1992.
7. DULCET, E., KASZKOWIAK, J., BOROWSKI, S., MIKOLAJCZAK, J.: Effects of microbiological additive on baled wet hay. Biosystems engineering, 95(3), 2006: 379-384.
8. FLIZIKOWSKI, J., SADKIEWICZ, J., TOMPOROWSKI, A.: Characteristics usable six-grained cylindrical grinding of raw materials for chemical and food industry. (Polish language). Przemysł Chemiczny 94/1 (2015), DOI: 10.15199/62.2015.1.9.
9. GUARNIERI, A., MAGLIONI, C., MOLARI, G.: Dynamic analysis of reciprocating single-blade cutter bars. Trans. of ASABE, 50(3), 2007: 755-764.
10. KANAFOJSKI, CZ., KARWOWSKI T.: Theory and design of agricultural machinery. (Polish language). TOM II. PWRiL, Warszawa, 1980.
11. KAPUR, P. C., SCHOENERT, K., FURSTENAU, D. W.: Energy-size relationship for breakage of single particles inarigidly mounted roll mill. International Journal of Mineral Processing. No. 29, 1990.
12. MAGDALINOVIĆ, N.: A procedure for rapid determination of the Bond work index. International Journal of Mineral Processing. No. 13, 1989.
13. OBIDZIŃSKI, S., HEJFT R.: Impact of speed of the chopper working on energy consumption of the grinding process. (Polish language). Scientific Papers of Opole University of Technology, 2000.
14. OPIELAK, M.: Selected problems of grinding materials in the food industry. (Polish language). Publishing House Agricultural University in Lublin, 2000.
15. WESOŁOWSKI L., BOCHAT A.: Attempts to model grinding granular materials through hammer mill. Inż. Ap. Chem. 49, No. 5, 2010: 127-129
16. TOMPOROWSKI A., FLIZIKOWSKI J.: The characteristics of movement of multi-disc grinder grain biomass. (Polish language). Przemysł chemiczny 92/4(2013), Warszawa 2013: 498-503.
17. ZASTEMPOWSKI M., BOCHAT A.: Selected aspects of the design of energy-efficient construction scissor-finger-cutting. (Polish language). Journal Research and Applications in Agricultural Engineering, 57(4), 2012: 212-216.

18. ZASTEMPOWSKI M.: Assessment of the efficiency of the scissor-finger-cutting unit on chosen example mowers. (Polish language). Inż. Ap. Chem. 2010, 49, No. 5: 144-145
19. ZASTEMPOWSKI, M., BOCHAT, A., WESOŁOWSKI, L.: A comparative study of new and traditional designs of hammer mill. Trans. of the ASABE, 58(3), 2015: 585-596.
20. ZASTEMPOWSKI, M., BOCHAT, A.: Modeling of cutting process by the shear-finger cutting block. (Polish language). Applied Engineering in Agricultural, 30(3), 2014: 347-353.
21. Advertising materials of company New Holland.

Corresponding author:

Marcin Zastempowski, Institute of Machine Operation and Transport, Faculty of Mechanical Engineering, UTP University of Science and Technology in Bydgoszcz, ul. Prof. S. Kaliskiego 7, 85-789 Bydgoszcz, Poland, phone: +485 2340 8208, e-mail: zastemp@utp.edu.pl

INFLUENCE OF APPLICATION OF ORGANIC MATTER AND ITS ACTIVATORS ON SOIL-TILLAGE IMPLEMENT DRAFT ON MODAL LUVISOL

N. Žemličková, P. Šařec

Department of Machinery Utilization, Faculty of Engineering, Czech University of Life Sciences Prague, Czech Republic

Abstract

The article discusses the results of measurement of soil physical properties and implement draft that has been done within field trial established at Lázně Bělohrad in the North of Bohemia in the year 2014. Different variants of treatment with substances for soil (PRP Sol) and manure (PRP Fix) amendment and with cattle manure were examined in terms of their influence on several parameters including energy demand for soil tillage. In the first stage, soil physical property, i.e. cone index, was measured. The results indicated that at soil upper layer, cone index within some of the trial variants dropped and on the contrary within other variants increased relative to control with no apparent pattern of treatment. Subsequently, draft of chosen tillage implements was measured in order to assess potential decrease in energy demand of treated variants. There was a minor 0.38% increase in relative aggregate unit draft after manure, and soil and manure activators' application compared to the control. The unit draft remained practically unchanged relative to the control within one variant, decreased within two variants, and increased within another two variants. The latter two were the variants where the most treatments were accomplished. It could be therefore assumed that higher number of machinery passes may have resulted in the increased implement draft. The assumed benefits of manure and manure and soil activators may not have had time to take effect.

Key words: draft, activator of organic matter, manure application, soil properties.

INTRODUCTION

Since 2014, field trials have been carried out in order to verify the influence of application of fermented farmyard manures and substances for soil amendment (activators of organic matter) on the changes of physical, physical-chemical and biological soil characteristics, organic matter fixation, improvement of parameters of infiltration and water retention, decrease of soil erosion risks, and decrease of energy demand for soil tillage.

Soil compaction is one of the soil properties in question. It leads to loss in crop yield, since the compaction prevents plants' root system to penetrate through to deeper soil layers to reach water / nutrients. Soil compaction has also negative impact on the environment (BALL ET AL., 1999; CHYBA ET AL., 2014) due to the reduced ability of the soil to absorb water. CHYBA ET AL. (2014) verified significantly higher water infiltration rate in the non-compacted soil than in the compacted soil.

Soil compaction primarily affects the physical properties of soil, either in the short or long term. For example at higher soil moisture levels, passes of farm machinery can lead to excessive soil compaction. The results of VERO ET AL. (2012) indicate that higher soil moisture deficits (SMD) at the time of machinery trafficking resulted in smaller changes to soil characteristics and more rapid recovery from surface deformation than when trafficking occurred at lower SMD. According to the results OF AHMADI AND GHAUR (2015), gradual increase in soil water content generally resulted in an increase in soil bulk density after tractor wheeling. The negative effect of soil compaction is manifested through increased bulk density, soil cone index, and other variables. This all leads to reduction in porosity, hydraulic soil properties, stability and other variables (ALAKUKKU, 1996). All these parameters are connected together and influence crop yields. CELIK ET AL. (2010) confirmed organic applications to significantly lower the soil bulk density and penetration resistance.

Effect of the use of substances for soil amendment (activators) on soil properties is a relatively unexplored phenomenon. Impact can be mainly expected on the physical and chemical properties of soil. KROULÍK ET AL. (2011) suggested a beneficial effect of incorporation of organic matter on the physical properties of soil, on water infiltration into the soil and on partial elimination of the consequences of soil compaction beneath the tracks. It can be also assumed that changes in soil properties will be reflected in the long term rather than immediately after application. According to PODHRÁZSKÁ ET AL. (2012), repeated conventional tillage and application of PRP Sol did not demonstrate any improvement in soil physical properties (density, porosity, soil compaction, reduced water content in soil).

Another factor that influences the variables mentioned is soil structure and soil aeration. If the soil is loosened, water capacity is higher compared to the untilled soil (EKWUE AND HARRILAL, 2010). Each soil structure has its own typical values of bulk density, porosity, hydraulic characteristics and other variables. For example, sandy-loam soils have higher cumulative infiltration rate than clay-loam soils, the lowest values are observed in turn with clay soils (EKWUE AND HARRILAL, 2010).

For the evaluation of soil compaction, values of soil density and penetration measurements are commonly used. Penetration measurement is also known as the cone index, i.e. the value of soil resistance against a cone of known dimensions (angle and area). Measurement of cone index has advantages over measurements of density in a simple data acquisition from the entire soil depth (limited by penetrometer depth range), the process of penetration measurements can also be automated (RAPER, 2005).

In terms of economy and operation, energy demand of soil tillage is one of the crucial elements. Tillage is the base operation in agricultural systems and its energy consumption represents a considerable portion of the energy consumed in crop production (LARSON AND CLYMA, 1995). McLaughlin et al. (2002), LIANG ET AL. (2013) and PELTRE ET AL. (2015) reported manure amendments to have significant effect on reduction in tillage implement draft. Prolonged application and higher rates brought advanced reduction.

The purpose of this study was to verify any changes in draft required for tillage after several years of treatment with substances for soil amendment and with fermented farmyard manure.

MATERIALS AND METHODS

In 2014, field trials examining effects of substances for soil amendment and fermented manure were established. In 2014, the draft measurements were done on 14th October after the wheat harvest. Silage maize was grown in the field afterwards, and the measurements were completed on 15th September 2015 after its harvest. The trial field was located near Lázně Bělohrad in North of Bohemia (GPS N 50°27.253', E 15°34.208'; altitude: 410 m). The topography was gently sloping, facing southwest. Soil type on the location Lázně Bělohrad was modal luvisol. Soil texture in the field was silt loam. The content of clay particles under 0.01 mm was 30 % of weight at the depth from 0 to 0.3 m. Some selected soil properties at the beginning of the experiment are presented in Tab. 1.

The trial plot was a 180 meters wide and 550 meters long rectangle selected to be homogenous and to avoid headland. It was divided lengthwise into six 30 meters wide and 550 meters long variants where fertilizer application was carried out according to a plan. The plots' spatial distribution had to be simple due to an operational nature of the experiment. The fertilizers used were cattle manure and NPK 15-15-15 (Lovofert). As the soil activator, PRP Sol (PRP Technologies) was applied during stubble cultivation. PRP Sol is formed by a matrix of calcium and magnesium carbonate, and mineral elements. As the activator of biological transformation of manure, PRP Fix (PRP Technologies) was applied directly into bedding. PRP Fix is a granular mixture of mineral salts and carbonates. Both activators should not be regarded as fertilizers. They are supposed to improve conditions for the transformation of organic matter.

Fertilization of individual variants is shown in Tab. 2. The variants differed by fertilizers used. Dosage of cattle manure was 50 $t.ha^{-1}$, of PRP Sol 200 $kg.ha^{-1}$, and of NPK 200 $kg.ha^{-1}$. The field was ploughed afterwards. In spring, seedbed preparation was carried out.

In order to assess soil physical properties, cone index measuring method was used. The registered penetrometer PEN 70 developed at the CULS Prague was employed. Moisture was measured by Theta Probe (Delta-T Devices Ltd, UK). Ten measurements of both cone index and soil moisture were taken in a rectangular grid for each trial variant. The draft of selected soil tillage implements was measured by means of the method of drawbar dynamometer with strain gauges S-38 /200 kN/ (LUKAS, the Czech Republic) between two tractors. Data acquisition system NI CompactRIO (National Instruments Corporation, USA) was employed, and its sample rate was set at 0.1 s. Several machinery passes were carried out for each variant. Firstly, the tillage implement was working at a set-up working depth and at a constant speed in order to measure the overall draft of the pulled tractor and implement working. The working depth was verified by its measurement for each pass. Secondly, the measurement was done with implement not working in order to measure the rolling resistance and the force induced by potential field gradient. These were deduced from the overall draft in order to calculate the implement draft. Direction of passes, i.e. downhill and uphill, was therefore taken into account. Trimble Business Center 2.70 (Trimble, USA) was used to assign acquired data to individual trial variants. Data were then processed by the programmes MS Excel (Microsoft Corp., USA) and Statistica 12 (Statsoft Inc., USA). Finally, the measured draft values were compared to the values calculated using ASAE D497.7 standard (ASABE Standards 2011). This standard uses a simplified draft prediction equation:

$$D = F_i \cdot (A + B \cdot S + C \cdot S^2) \cdot W \cdot T \quad \text{(N)} \qquad (1)$$

where D is the implement draft force; F_i is a dimensionless soil texture adjustment parameter with different values for fine, medium and coarse textured soils; A, B and C are machine-specific parameters; S is field speed ($km.hr^{-1}$); W is implement width (m or number of tools); and T is tillage depth (cm).

Tab. 1. – Selected physical and chemical properties of soil at Lázně Bělohrad (13th August, 2014)

	Soil depth (m)	
	0.00 – 0.30	**0.30 – 0.60**
clay (< 0.002 mm) (%)	15	21
silt (0.002 – 0.05 mm) (%)	66	67
very fine sand (0.05 – 0.10 mm) (%)	3	1
fine sand (0.10 – 0.25 mm) (%)	16	11
texture (USDA)	silt loam	silt loam
bulk density ($g.cm^{-3}$)	1.56	1.52
total porosity (%)	41.97	42.64
volumetric moisture (%)	31.50	23.70
humus content (%)	1.81	0.58
pH (H_2O)	6.26	6.23
pH (KCl)	4.99	5.09
CEC – cation exchange capacity ($mmol.kg^{-1}$)	110	120

Tab. 2. – Fertilization of individual variants of field trial at Lázně Bělohrad

Variant	Fertilization
I a	cattle manure with FIX + NPK
II a	cattle manure with FIX + SOL+ NPK
III a	cattle manure+ NPK
IV a	cattle manure + SOL+ NPK
V a	SOL + NPK
VI a	NPK (Control)

RESULTS AND DISCUSSION

Tab. 3 shows the overall average values of the basic physical properties of soils. There was a clear difference in volumetric soil moisture between the two years due to exceptionally dry weather over the whole vegetative period of the year 2015. This clearly increased the values of cone index which depended on soil moisture. Illustrative aggregate values at three different depths are presented in the Tab. 3. Since the climatic conditions were drastically different in both years, more interesting than the absolute values were the relative differences to the control variant VIa.

Year-on-year changes in relative cone index values at upper soil layer are presented in Fig. 1 and 2. The measurements, which results were used in the figures, were carried out in spring, when more uniform distribution of soil moisture was ensured after winter. Cone index of the trial variants remained unchanged or dropped relative to control only in the case of the Variant IIa (cattle manure with FIX + SOL+ NPK) and IIIa (cattle manure + NPK). Cone index of the other variants increased relative to control, with the Variant I even by more than 30 %.

Tab. 3. – The overall averages of soil moisture and cone index, and operating conditions and overall results of measurement of soil tillage implement drafts at Lázně Bělohrad in autumn of 2014 and 2015

	Fall 2014	**Fall 2015**
Soil properties		
vol. moisture at 0.00 – 0.05 m (%)	34.60	7.88
cone index at 0.08 m (10^6 Pa)	1.122	2.000
cone index at 0.12 m (10^6 Pa)	1.378	3.267
cone index at 0.16 m (10^6 Pa)	1.689	4.933
Draft measurement		
tractor	NH T8030	NH T8030
engine power (HP)	310	310
implement	tine cultivator	tine cultivator
implement type	Farmet Hurikán	Farmet Hurikán
working width (m)	2.8 (11 tools)	2.8 (11 tools)
working depth (m)	0.136	0.156
working speed (km.hour^{-1})	9.30	8.09
overall implement draft (N)	34 088	24 291
ASAE predicted draft (N)	21 076	23 147
unit draft (N.m^{-2})	12 174	8 675

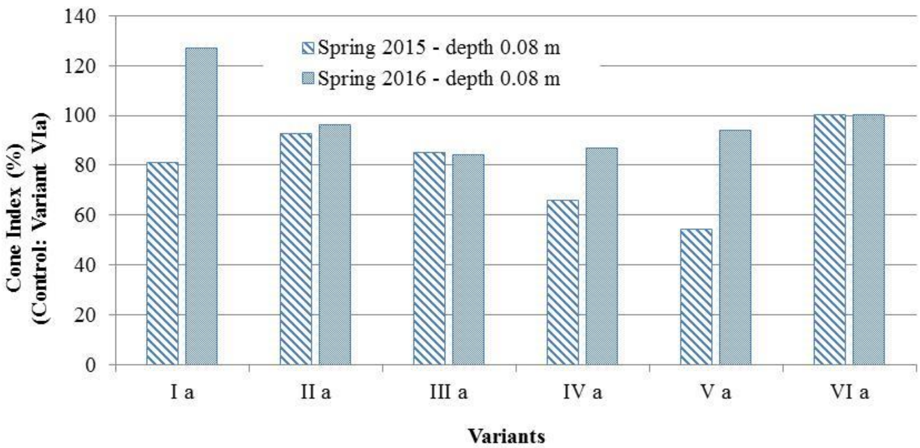

Fig. 1. – Graph comparing relative differences of soil cone index values at the depth of 0.08 m at Lázně Bělohrad in spring 2015 and 2016 (Variant VIa – 100 %)

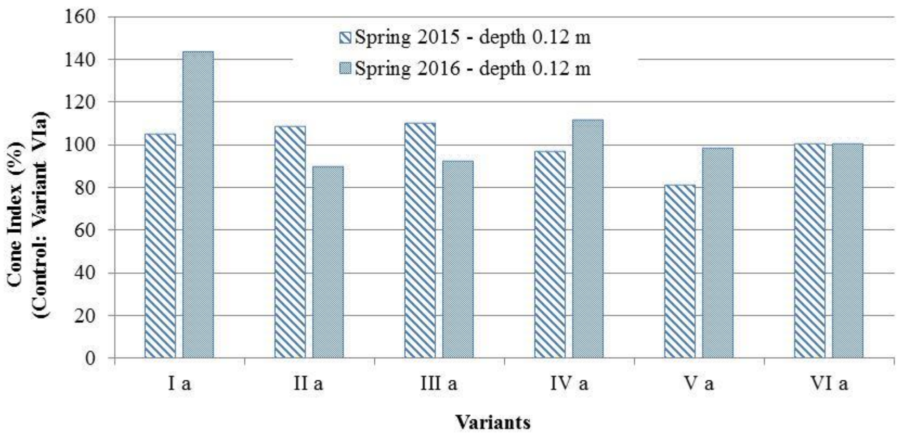

Fig. 2. – Graph comparing relative differences of soil cone index values at the depth of 0.12 m at Lázně Bělohrad in spring 2015 and 2016 (Variant VIa – 100 %)

When measuring draft force (Tab. 3), the same implement was engaged within both measurements. Both overall implement draft values were rather high and surpassed predictions (ASAE D497.7 MAR2011 standard) by 38 % in autumn 2014, and by 5 % in autumn 2015. Nevertheless, the difference still fitted within the ±50% range allowed for by the ASAE standard.

The overall measured implement draft was recalculated to unit draft in order to allow for working width and depth of tillage. Value of aggregate unit draft measured in autumn 2015 dropped substantially compared to the original value, i.e. measured in autumn 2014.

Fig. 3 presents aggregate unit draft values compared to the control. Due to the different climatic and operational conditions, absolute values could not be considered. The ratio of individual measured unit draft values to the average value of the control variant was therefore used for evaluation. There was a minor 0.38% increase in unit draft after manure, and after soil and manure activators. The difference was not statistically significant ($p = 0.65813$).

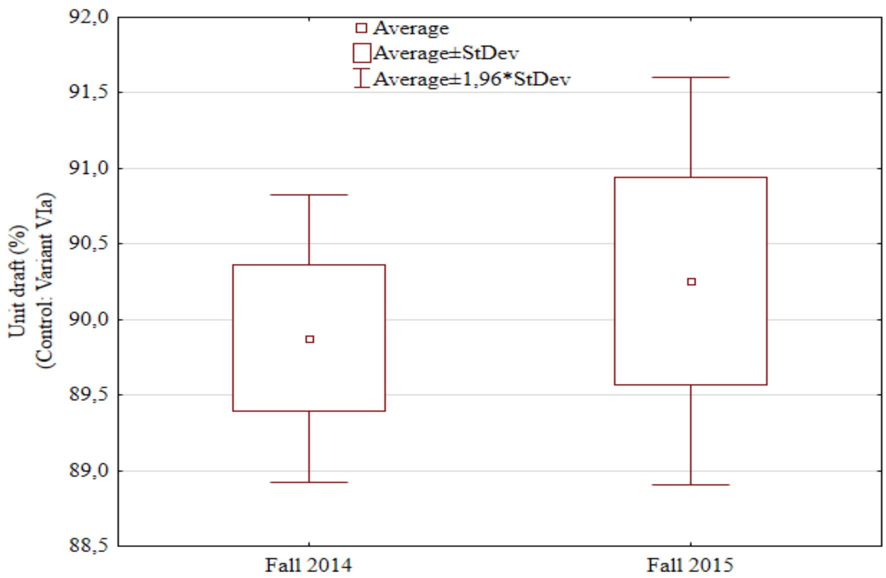

Fig. 3. – Graph comparing relative differences of implement unit draft related to control at Lázně Bělohtad in autumn 2014 and 2015 (control variant VIa excluded)

When taking into account relative differences of individual variants (Fig. 4), the decrease in draft was attained within Variants IIIa (cattle manure+ NPK) and Va (SOL + NPK). Unit draft of the Variant Ia (cattle manure with FIX + NPK) remained similar, and an increase in unit draft was measured within the Variants IIa (cattle manure with FIX + SOL+ NPK) and IVa (cattle manure + SOL+ NPK). The latter two were the variants where the most treatments were accomplished, i.e. application of cattle manure (with and without PRP Fix), of PRP Sol, and of NPK. It could be therefore assumed that higher number of machinery passes may have resulted in the increased implement draft.

Initial research assumptions were not confirmed so far. In opposite to what Celik et al. (2010) suggested, i.e lower penetration resistance, cone index values increased within some of the variants compared to the control. To date, application of PRP Sol has not brought verifiable improvements as well. Findings of Podhrázská et al. (2012) has thus been confirmed so far.

Conclusions of McLaughlin et al. (2002), Liang et al. (2013) and Peltre et al. (2015) on manure application influence on implement draft reduction are not consistent with the trial results. The effects of activators of organic matter are among the less explored topics. In connection with changing composition of organic fertilizer (fewer manure and slurry but more compost and waste from biogas plants), the increased importance of activators of organic matter can be expected. Measurements were certainly affected by a short duration of the experiment. The assumed benefits of manure, and manure and soil activators did not have time to take effect. Instead, the impact of higher number of machinery passes due to their application may have been manifested. With this respect, uncontrolled trespassing during maize harvest may have also influenced the results. It can be assumed that the effect is going to be gradual and the verification should be carried out also in following trial years, when there will be enough data to carry out thorough statistical analysis.

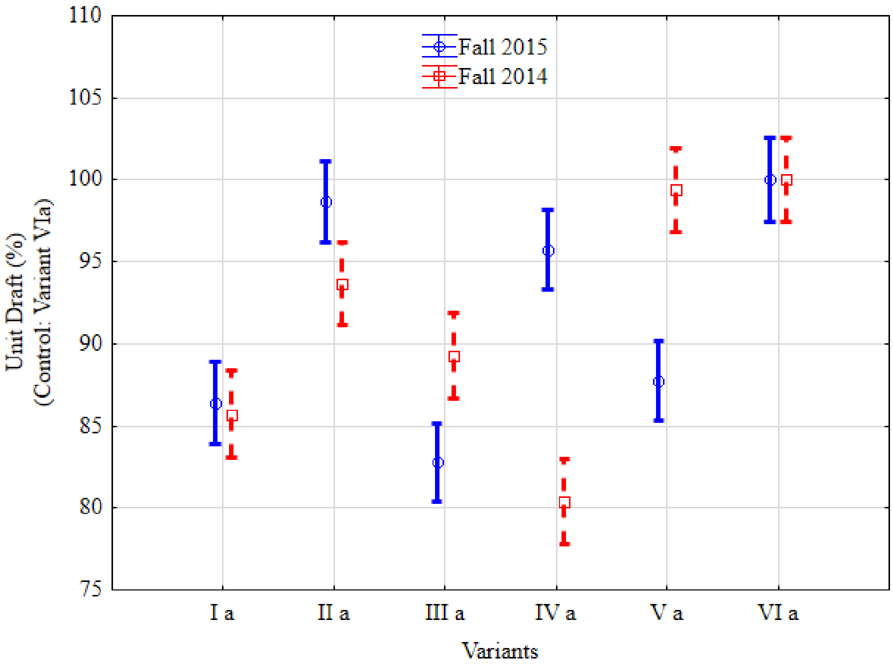

Fig. 4. – Graph comparing relative differences of implement unit draft with respect to individual variants at Lázně Bělohrad in autumn 2014 and 2015 (Variant VIa – 100 %; vertical lines depict 0.95 confidence intervals)

CONCLUSIONS

So far, the work has not proved the beneficial effect of substances for soil (PRP Sol) and manure amendment (PRP Fix) and of cattle manure on soil cone index and on implement draft force reduction. A longer duration of the experiment would though enable to draw more detailed conclusions. At soil upper layer, cone index within some of the trial variants dropped and on the contrary within other variants increased relative to control with no apparent pattern of treatment.

Subsequently, draft of chosen tillage implements was measured. There was a minor 0.38% increase in relative aggregate unit draft after manure, and soil and manure activators' application compared to the control. The unit draft remained practically unchanged relative to the control within one variant, decreased within two variants, and increased within another two variants. The latter two were the variants where the most treatments were accomplished, i.e. application of cattle manure (with and without PRP Fix), of PRP Sol, and of NPK. It could be therefore assumed that higher number of machinery passes may have resulted in the increased implement draft. The assumed benefits of manure and manure and soil activators may not have had time to take effect. Instead, the impact of higher number of machinery passes due to their application may have been manifested.

The necessity of long-term examination of the effects of activators of organic matter should be emphasized. Research needs to be validated in more locations in order to eliminate the influence of the local environment.

ACKNOWLEDGEMENTS

The work was supported by Research Project of the Technology Agency of the Czech Republic no. TA04021390 and by the internal research project of the Faculty of Engineering IGA 2016: 31180/1312/3115.

REFERENCES

1. AHMADI, I., GHAUR, H.: Effects of soil moisture content and tractor wheeling intensity on traffic-induced soil compaction. Journal of Central European Agriculture, 2015, vol. 16, no. 4, pp. 489-502
2. ALAKUKKU L.: Persistence of soil compaction due to high axle load traffic. I. Short-term effects on the properties of clay and organic soils. Soil and Tillage Research, 1996, 37. pp. 211-222
3. ASABE STANDARDS 2011: ASAE D497.7 MAR2011, Agricultural Machinery Management Data. ASABE, St. Joseph, MI, USA
4. BALL, B.C., PARKER, J.P, SCOTT A.: Soil and residue management effects on cropping conditions and nitrous oxide fluxes under controlled traffic in Scotland. Soil & Tillage Research, 1999, 52. pp. 191-201
5. CELIK, I, GUNAL, H., BUDAK, M., AKPINAR, C.: Effects of long-term organic and mineral fertilizers on bulk density and penetration resistance in semi-arid Mediterranean soil conditions. Geoderma, 2010, 160. pp. 236-263
6. CHYBA, J., KROULÍK, M., KRIŠTOF, K., MISIEWICZ, P., CHANEY, K.: Influence of soil compaction by farm machinery and livestock on water infiltration rate on grassland. Agronomy Research, 2014, 12. pp. 59-64
7. EKWUE, E.I., HARRILAL, A.: Effect of soil type, peat, slope, compaction effort and their interactions on infiltration, runoff and raindrop erosion of some Trinidadian soils. Biosystems Engineering, 2010, 105. pp. 112–118
8. KROULÍK, M., KVÍZ, Z., KUMHÁLA, F., HŮLA, J., LOCH, T:. Procedures of soil farming allowing reduction of compaction. Precision Agriculture, 2011, 12. pp. 317-333
9. LARSON, D.L., CLYMA H.E.: Electro-osmosis effectiveness in reducing tillage draft force and energy forces. Transactions of ASAE, 1995, 38: 1281-1288
10. LIANG, A., MCLAUGHLIN, N.B., MA, B.L., GREGORICH, E.G., MORRISON, M.J., BURTT, S.D., PATTERSON, B.S., EVENSON, L.I.: Changes in mouldboard plough draught and tractor fuel consumption on continuous corn after 18 years of organic and inorganic N amendments. Energy, 2013, 52. pp. 89-95
11. MCLAUGHLIN, N.B., GREGORICH, E.G., DWYER, L.M., MA, B.L.: Effect of organic and inorganic soil nitrogen amendments on mouldboard plow draft. Soil & tillage research, 2002, 64. pp. 211-219
12. PELTRE, C., NYORD, T., BRUUN, S., JENSEN, L.S., MAGID, J.: Repeated soil application of organic waste amendments reduces draught force and fuel consumption for soil tillage. Agriculture, Ecosystems and Environment, 2015, 211. pp. 94-101
13. PODHRÁZSKÁ, J., KONEČNÁ, J., KAMENÍČKOVÁ, I., DUMBROVSKÝ, M.: Survey of the impact of PRP SOL subsidiary substance on the hydrophysical properties of soil at cultivation of sugar beet. Listy cukrovarnické a řepařské, 2012, 128. pp. 128-133
14. RAPER R.L.: Agricultural traffic impacts on soil. Journal of Terramechanics, 2005, 42. pp. 259–280
15. VERO S.E., ANTILLE D.L., LALOR S.T.J. & HOLDEN, N.M.: The effect of soil moisture deficit on the susceptibility of soil to compaction as a result of vehicle traffic. In: American Society of Agricultural and Biological Engineers Annual International Meeting 2012. Dallas, TX, United States, ASABE, 2012, Vol. 7, pp. 5419-5434.

Corresponding author:

Ing. Nikola Žemličková, Department of machinery utilization, Faculty of Engineering, Czech University of Life Sciences Prague, Kamýcká 129, Praha 6, Prague, 16521, Czech Republic, e-mail: zemlickovan@tf.czu.cz

MICROCLIMATE IN DRIVERS' CABIN OF COMBINE HARVESTERS

R. Zewdie[1], P. Kic[2]

[1]Department of Vehicles and Ground Transport, Faculty of Engineering, Czech University of Life Sciences Prague, Czech Republic
[2]Department of technological equipment of buildings, Faculty of Engineering, Czech University of Life Sciences Prague, Czech Republic

Abstract
Ergonomically and climatically bearable drivers and operators' cabin correlate thermal comfort. Comfortable drivers and operators are supposed to guarantee better performances. Activity performance in relation to operators' exposure to temperature variety whilst driving was surveyed through measurements the authentic environmental circumstances in the driver's cabin. Cluttering side and windshield are constantly evolving irrespective to the direct solar radiation, which affect the variation of microclimates, especially in hot summer time and eventually cause stress on a driver. For the research implementation, the related data collection of microclimate conditions in driver's cabin in three farm machineries, specifically three combine harvesters of three different brands were monitored. Farm machinery operators' cabin microclimate and heart rate variables relevant data are collected for detail analysis. This research paper is the outcome of the findings.

Key words: heart rate**,** microclimate, safety, stress, thermal comfort.

INTRODUCTION

The comfort of drivers in different climatic conditions, particularly in the driver's space is so far given insufficient attention. A research on thermal comfort and related issues are undervalued. Generally, drivers of all mode of transport system in daily operation are affected by microclimate. Particularly, operators of mobile power equipment like drivers of agricultural machinery, earthmoving machines, and road and highways maintenances machines are exposed to the direct intervention of summer sun exposure, and other inconvenient weather conditions. Microclimate in the driver's cabin significantly affects the human thermal comfort which is one of the core issues of this paper. The cabin environment has an emphasis on thermal comfort not only for reasons of convenience, but also safety.

Radiation temperature, which surrounds the driver in which there would be radiative heat flow between the surface of the body and the surrounding areas. With the increase of humidity partial pressure of water vapor rises, this causes the rate of evaporation of sweat from the body of a driver leading to discomfort. On the contrary, very low humid air, the driver's mucous membranes of the eyes dry and dust formation increases. Air velocity is an important factor that influences suitable temperature inside. High air velocity can cause undesirable cooling of the body; especially during long exposure to the driver causing speed airflow excessively stresses to the organism and the cabin may not be designed for long stays drivers. Recommended values of microclimate in the cabin of the car according to VLK (2003) are: air temperature 18–22 ºC relative humidity 40–60 %; air velocity 0.1 $m.s^{-1}$ at 18 ºC and 0.4 $m·s^{-1}$ at 24 ºC; air exchange per person (clean air) 25-50 $m^3·h^{-1}$ of fresh air; maximum concentration of pollutants 0.17 % of CO_2, 0.01 % of CO and 1 $mg·m^{-3}$ of dust.

Scientific studies have shown the effects of inappropriate working condition on fatigue, which significantly applies to prolonged drivers working hours. Human factors research shows that driver stress is associated with workload and fatigue, and is constructs that can have an impact on overall driver safety. Furthermore, a heart rate variability analysis was particularly applicable for this research as it is a strong indicator of mental stress or workload caused by driving tasks (MULDER, 1992). Numerous researchers used different measurement to assess driver workload under diverse driving conditions. The conclusions made by monitoring physiological based measures support an objective and continuous analysis in a dynamically changing situation (LI ET AL. 2004). Researchers JORNA (1993) and APPARIES ET AL. (1998) came to a conclusion that the relationship between safety and stress depends on the route conditions and work load. Furthermore, measurements of the heart are the most practical for application in the driving domain as it least interferes with driving performance (HARTLEY ET AL., 1994). Specific research has not yet well expended to ensure the mental and physical workload and its impact on farm machine operators.

The objective of the finding is to examine operators engaged on rural, bumpy, uneven, rough pavements, dusty, muddy and stubble farm fields. Frequent steering, reducing speed, monitoring various operations different devices while driving in short intervals, long working hours denote a significant degrade in driver performance. Due all these performances, farm machine operators are exposed to whole body vibration which leads to swift fatigue compared to acceptable and normal operating conditions, surfaces and pavements. In order to fully understand the complexity of the relationship between surface characteristics and driver behaviours, this paper closely examines various yet realistic uneven, rough, up and down drives, turns, breaking and accelerating and other working related conditions, influences of driving behaviours, physical strength of the operators playing a leading role on dimensions of stress. Generally, unexpected events are correlated to impaired driver cognition due to fatigue, stress, or mental workload (LI ET AL., 1995). Therefore, by evaluating stress as a form of distraction, this paper addresses the comfort of farm field surface conditions.

Measurements of driver stress can be objectively captured using physiological measures. Physiological measurements can be used to quantify changes in the body's state (NISKANEN ET AL., 2004). These measurements can include skin conductivity, cardiac, neurological, muscle, and respiratory activity. Many studies have concluded that during periods of increased stress, it tends to be an increase in the values of heart rate and the low to high frequency ratio (SLOAN ET AL., 1994; LEE ET AL., 2007; PARTIN ET AL., 2006; ZHAO ET AL., 2010). Similar research findings published ZEWDIE AND KIC (2015), ZEWDIE AND KIC (2016), shows the impacts of the microclimate conditions in drivers cabin plays a significant role on the stress and changes in heart rate variability. A suitable microclimate is necessary and the systems must ensure a suitable microclimate as it is one of the most important safety features of the vehicles. The driver's cabin features a large flat glass, a small volume of air inside and relatively low heat insulation, resulting in a greater degree of influence on the operating conditions. The objective of this research paper is to investigate presumptions: if the heart rate variance depends on the operational performances and physical conditions of each operators; the air conditioner in the driver's cabin has affects the thermal comfort and affects the quality of microclimate and presents analysis among those measured parameters the influential and significant in terms of thermal comfort to operators.

MATERIALS AND METHODS

The authors performed the research on three farm machines (combine harvesters) drivers cabins of two agricultural enterprises at Eastern and Southern Bohemia farming fields cultivating on areas of nearly 2500 ha each. Three combine harvesters, Claas 450, German brand, air conditioned (AC) and East Bohemian farm enterprise property, Massey Ferguson (AC), UK brand and Fortschritt E 517, East German brand (non AC) both belonging to South Bohemian enterprise with their respective operators were at the disposition for the research performance.

For the heart rate measurement, the authors used the Polar measuring sensors package which is the brand of Kempele, Finland. The operators put on a sensor (Polar RS800CX) around the body and computer device on the wrist of the driver to record the heart rate variability (HRV). The package of the measuring instrument consists of four parts of Polar brand. Data detected (heart rate of the driver of the farm machinery) stored in Polar RS800CX are transformed through infra port to a personal computer for further processing and analysis. The Czech government health protection regulation determines the conditions for the protection of health related to light manual work such as driving under normal operating conditions. Under this regulation, for particular metabolic energy output 81–105 $W \cdot m^{-2}$, the recommended operating temperature is 20 ± 2 °C and relative humidity to be 30–70 %. Thermal state of the internal environment can be described by applying the index of temperature and humidity (THI). This index is widely used to describe the heat stress, and it is also a key indicator of the environmental conditions of stress.

Data on the microclimate conditions in the farm machinery operator's cabin were collected from measurement devices which are installed on the dashboard of the respective farm machinery. The thermal comfort in the space was continuously measured by globe temperature (measured by globe thermometer FPA 805 GTS with operative range from –50 to +200 °C with accuracy ± 0.01 °C and diameter of 0.15 m) together with temperature and humidity of surrounding air measured by sensor FH A646-21 including the temperature sensor NTC type N with operative range from – 30 to + 100 ºC with accuracy ± 0.01 °C, and air humidity by capacitive sensors with operative range from 5 to 98 % with accuracy ± 2 %. The concentration of CO_2 was measured by the sensor FY A600 with operative range 0–0.5 % and accuracy ± 0.01 %. For the sound measurement, a Digital Sound Level Meter (Unitest 93411, produce of BHA GmbH, Klottertal, Germany) with measuring range 30–135 dB, accuracy ± 2 dB and resolution 0.1 dB was applied. All data were measured continuously and stored at intervals of one minute to the measuring instrument ALMEMO 2690–8, which is the product of Ahlborn Mess-und Regelungstechnik GmbH, Holzkirchen, Germany.

This research work and measurements were carried out in July 22, and August 5 to 6, 2015 which were extreme hot summer days. When the research was performed there was a continuous hot climatic condition (the external temperature reached about 35 °C ± 2 °C). The data of CO_2 concentration, the thermal index composed of internal globe temperature t_g, and internal temperature t_i as well as internal relative humidity RH_i are carefully collected for further analysis. The obtained results of microclimate including noises LA (dB) in the cabin and heart rate measurements were processed by Excel software and verified by statistical software Statistica 12 (*ANOVA and TUKEY HSD Test*). Different superscript letters (a, b, c) mean values in common are significantly different from each other in the rows of the table (*ANOVA; Tukey HSD Test; $P \leq 0.05$*), e.g. if there are the same superscript letters in all the rows it means the differences between the values are not statistically significant at the significance level of 0.05.

RESULTS AND DISCUSSION

Principal results of microclimate and heart rate measurements in all three combine harvesters cabin MF, Claas 450 and E 517 are summarized and presented in Tab. 1 which represents the CO_2 pollutant, the thermal index, noise level, relative humidity in operator's cabin and the heart rate of the operators. Tab. 2 shows the statistically significant data obtained for comparison in all three driving cabins. The data are means ± SD. Different letters (a, b, c) in the superscript are the sign of high significant difference (*ANOVA; Tukey HSD Test; $P \leq 0.05$*).

Tab. 1. – Determined microclimate in cabin and noise values, data in the table are means ± SD

Parameter	**Unit**	**MF**	**Claas 450**	**E 517**
CO_2	**(%)**	0.51 ± 0.24^a	0.14 ± 0.05^b	0.05 ± 0.01^c
t_g	**(°C)**	31.0 ± 1.4^a	27.2 ± 3.5^b	41.1 ± 2.1^c
t_i	**(°C)**	24.0 ± 1.7^a	25.3 ± 2.1^b	39.1 ± 1.2^c
RH_i	**(°C)**	23.5 ± 2.7^a	34.0 ± 3.4^b	28.2 ± 1.3^c
LA	**dB**	74.7 ± 5.1^a	80.6 ± 5.2^b	86.6 ± 1.5^c

Tab.2. – Selected detail microclimate comparison parameters

	CO_2 (ppm)			RH_i (%)		
Harvester	**MF**	**Claas 450**	**E 517**	**MF**	**Claas 450**	**E 517**
Average	5,100	1,210	490	23.5	33.8	28.2
Median	5,000	1,280	490	23.7	33.4	28.2
Maximum	9,290	1,840	660	30.4	41.0	30.8
Minimum	1,020	350	350	18.4	24.9	25.3
St. Devia.	2,400	500	100	2.70	3.42	1.30

Tab.3. – Operators heart rates on selected segments, data in the table are means ± SD

		MF	**Claas 450**	**E 517**
Segment		**HR ± SD**	**HR ± SD**	**HR ± SD**
Field ride		93 ± 3.8^a	94 ± 3.8^a	88 ± 4.2^a
Downhill drive		101 ± 5.3^a	109 ± 6.5^a	102 ± 5.1^a
Uphill drive		85 ± 4.1^a	87 ± 3.9^a	94 ± 3.3^a
Stop		96 ± 5.9^a	115 ± 6.0^b	110 ± 5.6^c

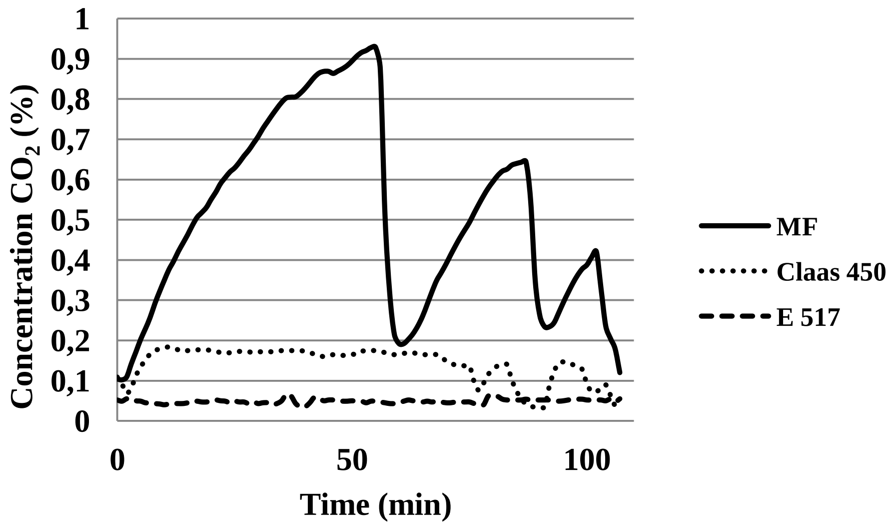

Fig. 1. – Measured concentration of CO_2 in the operators' cabin

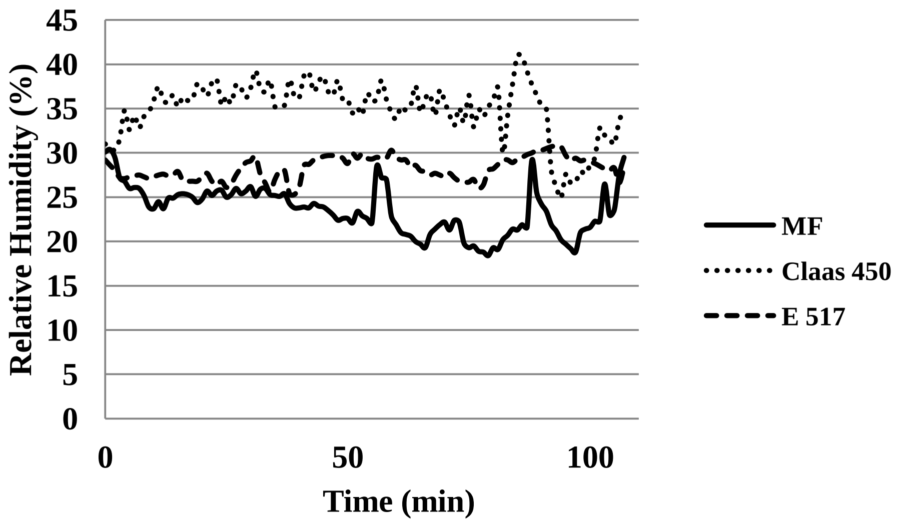

Fig. 2. – Measured relative humidity inside the operators cabin

Based on the result of the measurements Tab. 1 and Tab. 2, in the combine harvester cabin the internal temperatures were different. Tinted glass of the wind shield and side windows of the combine harvester had a noticeable influence in reducing the radiation. Law radiation temperature t_g and internal temperature t_i has been observed on both tinted glass and air conditioned harvesters (t_g = 31.0 °C, t_i = 24.0 °C) in MF harvester cabin and t_g = 27.3 °C, t_i = 25.3 °C in Claas 450 harvester cabin). Strong radiation effect has been observed and measured by globe thermometers t_g on E 517 combine harvester cabin due to clear glass of the wind shield and side windows; i. e. t_g = 41.1 °C and the internal temperature t_i raised to 39.1 °C. This indicates that the influence of solar radiation has increased compared to the internal temperature t_i, which is against regulation in relation to the directive on health supervisor (Government Regulation 361/2007 of Czech Republic, 2007). From the measurements evaluation, the inner temperatures can reduce the influence of solar radiation by adequate ventilation of the operators driving cabin. To maintain the recommended air temperature inside the cabin, operators are recommended to use air conditioning and frequent ventilation.

The results on Tab. 3 demonstrate the changes in heart rate variability on all three farm machine operators depending on the feature of the farm field and their actual performance. On the operator E 517 (22 years old and 75 kg), it is clearly seen that he has the lowest average heart rate (88 ± 4.1) has been registered at the field drive segment. MF (40 years old and 95 kg) and Claas 450 (48 years old 115 kg) operators scored the lowest heart rate on uphill drive (85 ± 4.1 and 87 ± 3.9 respectively). On all operators, the highest heart rate was observed at downhill drive (MF 101 ± 5.5, Claas 450 – 109 ± 6.5, and E 517-102 ± 5.1). At the stop segment, operators E 517 and Claas 450 had defects and frequent telephone calls from their respective despatchers due to pulleys release and malfunctions of the cooling system (E 517) and threshing cylinder (Claas 450). Both scored high heart rate (Claas 450 – 115 ± 6.0 and E 517 – 110 ± 5.6). Significant increase of heart rate was observed at downhill drive and farm field drives on all three operators. The highest heart rate increase of combine harvester operator was registered on a cell phone call from the despatcher related to defects (E 517) by 128 % and operator of Claas 450 due to threshing cylinder defect (131 %). Frequent turns during harvest performance had significant influence to heart rate fluctuations with the increase of 125 % on combine harvester operators by average. A profound increase in heart rate was observed while refilling water to the radiator of harvester E 517 due to the leak of cooling system (130 %). Often pulley failure had factors in the increase in heart rate to the operator E 517 (131 %). Braking performance due to deceleration has played as well significant heart rate value changes (127 %) in average.

CONCLUSIONS

The results on Fig. 1 and Fig. 2 indicate proofs on two hypotheses: the air conditioner in the driver's cabin positively affects the microclimate. If the air conditioner is not functioning as it is expected, it may be hazardous. This has a significant impact on the thermal comfort of the operator (the driver). Maladjustment or non-inspected air conditioner may worsen some parameters of microclimate conditions in the drivers' cabin especially if the blowhole is not properly functioning.

Drivers are recommended to ventilate sufficiently even in colder outdoor conditions to let in the fresh air (O_2) and exhaust the polluted air (CO_2 and odours). Based on the results of the measurement, a maximum pollutant concentration CO_2 (0.929 % = 9,290 ppm) has been observed in harvester operator of MF cabin which is air conditioned. On the fitted function Fig. 1, it is clearly seen the fluctuating curve observed which may be caused due to incorrect function of ventilation or occasional door opening for communication with the truck driver. The obtained result shows that the maximum amount of CO_2 has exceeded fivefold (9,290 ppm); which is hazardous to the operator's health (VLK, 2003). Slight increase of CO_2 concentration was observed in Claas 450 operator's cabin (0.185 = 1,850 ppm) throughout the course of the harvest performance. The maximum tolerable level of concentration of CO_2 has been sustained. In the combine harvester cabin E 517 the CO_2 pollutant level was the least (max. 0.066 % = 660 ppm). Separate propeller ventilator was fixed for additional ventilation due to extreme outside temperature (35 °C) extra to the ventilation set by the manufacturer. This may cause the concentration of CO_2 to the accepted level. The highest concentration of noise was measured in the E 517 harvester's cabin (86.6 ± 1.5°). This could be due to opened ventilation window throughout the course of harvest.

The lowest relative humidity was observed again in the cabin of MF (23.5 %) by average; for a temperature of 18–22 °C recommended relative humidity is 40–60 % (VLK, 2003). The Claas 450 harvester cabin again scored the better value of relative humidity (33.8 %) by average; in harvester E 517 driver's cabin, it was observed a little below the level of the recommended value (28.3 %) by average. From the values measured the authors strongly recommend ventilation in driver's cabin even if the farm machineries are equipped with air condition.

The outcome of this extensive research provides a comprehensive view of the most important parameters related to microclimate problems in drivers or operators encountering in their respective cabins, and analyses the most influential not deeply examined scientific field which are not given adequate consideration.

ACKNOWLEDGEMENTS

The authors are extremely grateful and would like to express thanks to the management, combine harvester operators and all the staff members of AGRO LIBOMŘICE a.s, and Brloh Agricultural Enterprise, who allowed us to carry out the data collection for our research.

REFERENCES

1. APPARIES, R., RINIOLO, T., PORGES, S.: A psychophysiological investigation of the effects of driving longer-combination vehicles. Ergonomics, 41(5), 1998: pp. 581–592.
2. HARTLEY, L., ARNOLD, P., SMYTHE, G., HANSEN, J.: Indicators of fatigue in truck drivers. Applied Ergonomics, 25(3), 1994: pp. 143–156.
3. JORNA, P. G. A. M.: Heart rate and workload variations in actual and simulated flight. Ergonomics, 36(9), 1993: 1043-1054.
4. LEE, H., KIM, J., KIM, Y., BAEK, J., RYU, M., PARK, K.: The relationship between HRV parameters and stressful driving situation in the real road. In: Proceedings of the 6th International Special Topic Conference on Information Technology Applications in Biomedicine, 2007: pp. 198-200.
5. LI, C., ZHENG, C., TA, C.: Detection of ECG characteristic points using wavelet transforms. IEEE Transactions on Biomedical Engineering, 42(1), 1995: pp. 21–28.
6. LI, Z., JIAO, K., CHEN, M., WANG, C.: Reducing the effects of driving fatigue with magnitopuncture stimulation. Accident Analysis & Prevention, 36(4), 2004: pp. 501–505.
7. MATTHEWS, G., DORN, L., HOYES, T. W., DAVIES, R. D., GLENDON, A. I., TAYLOR, R. G.: Driver stress and performance on a driving simulator. Human Factors: The Journal of the Human Factors and Ergonomics Society, 40(1), 1998: 136-149.
8. MULDER, L. J. M.: Measurement and analysis methods of heart rate and respiration for use in applied environments. Biological Psychology, 34, 1992: 205-236.
9. NISKANEN, J., TARVAINEN, M., RANTA-AHO, P., KARJALAINEN, P.: Software for advanced HRV analysis. Computer Methods and Programs in Biomedicine, 76(1), 2004:73-81
10. PARTIN, D., SULTAN, M., THRUSH, C., PRIETO, R., WAGNER, S.: Monitoring driver physiological parameters for improved safety. Society of Automotive Engineers, Report No. 01-1322, 2006.
11. SLOAN R. P., SHAPIRO P. A., BAGIELLA E., BONI S. M., PAIK M., BIGGER J. T., STEINMAN R. C., GORMAN J. M.: Effect of mental stress throughout the day on cardiac autonomic control. Biological Psychology, 37(2), 1994: 89-99.
12. VLK, F.: Stavba motorových vozidel: Osobní automobil, autobusy, nákladní automobily, jizdní soupravy, ergonomika, biomechanika, struktura, kolize, materiály. (Construction of motor vehicles: cars, buses, trucks, trains, ergonomics, biomechanics, structure, collision, materials). Brno: Ser, 2003. (In Czech).
13. ZEWDIE, R., KIC, P.: Selected factors affecting microclimatic conditions in drivers Cabin. In: 14th International Scientific Conference on Engineering for Rural Development. Latvia University of Agriculture, Jelgava, 2015, pp. 61–66.
14. ZEWDIE, R., KIC, P.: Transport route segments and stress effect on drivers. In: Agronomy Research, vol. 14(1), 2016: pp. 269-279.
15. ZEWDIE, R., KIC, P.: Microclimate conditions and stress factors affecting farm machine operators during harvest. In: 15th International Scientific Conference on Engineering for Rural Development. Latvia University of Agriculture, Jelgava, 2016, pp. 20-30.
16. ZHAO, X., FANG, R., XU, S., RONG, J., LIU, X.: Sound as a countermeasure against driving fatigue based on ECG. In: Proceedings of the 10th International Conference of Chinese Transportation Professionals, 2010, pp. 401-413.

Corresponding author:

Dr. Ing. Retta Zewdie, Department of Vehicles and Ground Transport, Faculty of Engineering, Czech University of Life Sciences Prague, Kamýcká 129, Praha 6, Prague, 16521, Czech Republic, phone: +420 22438 3101, e-mail: zewdie@tf.czu.cz

Proceeding of 6th International Conference on Trends in Agricultural Engineering 2016

September 7th 2016 – September 9th 2016

Publisher: Czech University of Life Sciences Prague Kamýcká 129, Prague, Czech Republic
Editor in chief: David Herák
Editors: Rostislav Chotěborský, Stanislav Kovář, Václav Křepčík
Printing house: ZEBRA Media s.r.o.
Number of copies: 150
Number of pages: 749
Issue: First
Year: 2016

All manuscripts in conference proceedings have been reviewed by peer review process

ISBN 978-80-213-2683-5

The authors shall be solely responsible for the technical and linguistic accuracy of the manuscripts

TAE 2016